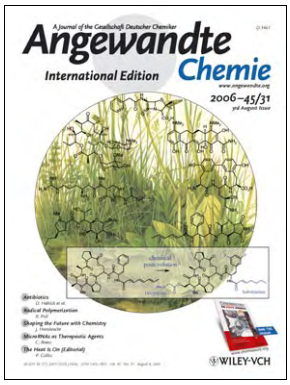
Cover Picture

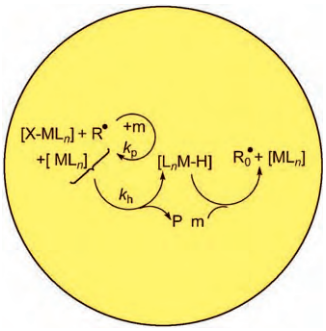


Franz von Nussbaum, Michael Brands, Berthold Hinzen, Stefan Weigand, and Dieter Häbich*

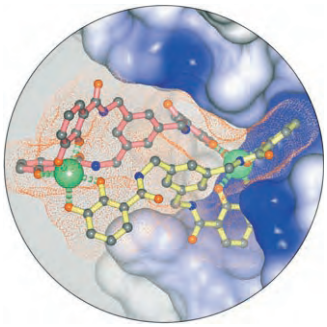
The exceptional often hides within the ordinary. In 1503, Albrecht Dürer saw a complex microcosm concealed in an apparently unimportant piece of turf ("Great Piece of Turf" with courtesy of http://reisserbilder.at). In a similar fashion, chemical postevolution can elicit exceptional properties from known natural products. In their Review on page 5072 ff., Häbich and co-workers analyze the application of this principle on antibiotics.



The Correct Qualifications
In his Essay on page 5052 ff., J. Hambrecht, the CEO of BASF, addresses the need for an open dialogue between universities and the chemical industry to ensure that up-coming chemists are optimally prepared for their future careers.



Radical Polymerization
R. Poli discusses in his minireview on page 5058 ff. how one-electron processes in transition metals are important to the understanding of these radical polymerization reactions.



Bacterial Iron Transport
In their Communication on page 5132 ff., A.-K. Duhme-Klair et al. discuss the dimeric assembly $(CeuE)_2{\cdot}\{Fe(mecam)\}_2$, which reveals interactions between the ferric enterobactin mimic $[\{Fe(mecam)\}_2]^{6-}$ and two periplasmic binding protein molecules (CeuE from *Campylobacter jejuni*).

The Heat Is On ...

DOI: 10.1002/anie.200602672

... for Authors: They have to publish ever more articles in "high-impact" journals just to get their grant proposals taken seriously, to position their departments among the "clusters of excellence", or to push their universities up to "elite" status. These terms stem from the current debate in Germany, but the phenomenon is worldwide—and in some countries there is even a direct incentive: authors are rewarded financially whenever they publish a manuscript in a top journal. However, scrutiny of the quality of each individual manuscript is all too easily neglected: as long as something is found in the right journal, many take it for granted that the article has been sufficiently "evaluated" and can be appropriately "categorized".

... for Referees: An ever-increasing number of articles and grant proposals, for example, for the "clusters of excellence" and "elite universities", must however stand up against peer review—and naturally these proposals first have to be written. Lately, potential referees have been declining to review manuscripts on the grounds that they have to prepare "cluster of excellence" grant proposals! As a result, the best referees are in danger of becoming less available even though the manuscripts they evaluate represent the most important basis for secondary evaluation. The referees for *Angewandte Chemie* are internationally well-distributed (see Figure 1). There are, however, two points that stand out: 1) referees from Germany are more strongly represented than one would expect considering the international authorship; 2) only about 1% of the referees come from China, though about 20% of the manuscripts come from there. Effective immediately, we will also begin drawing on more referees from China. The referee process is quite fast: referee reports arrive on average (!) 13 days after being requested. Such a quick turnaround is especially impressive when one considers that the referees of manuscripts for *Angewandte Chemie* (and other top journals) devote a great deal of effort to their evaluations. This is not to say that deficiencies or errors in manuscripts are never overlooked by the referees and editors of this journal: Corrigenda, Correspondences, and even manuscript retractions also find their way every now and then into *Angewandte Chemie*!

Average turnaround time for referee reports: 13 days

... for Editors: The push for authors to publish in high-impact journals has resulted in a rapid increase in submitted manuscripts at *Angewandte Chemie* (Figure 2), and this growth is not limited to an individual country or region.

On the Rise: Under these circumstances, is the recent increase in Impact Factor (to 9.596) and the Immediacy Index (to 2.109) a blessing or a bane? The trends in these key indices are shown in Figure 3 and 4. One argument that is frequently heard is, "The Impact Factor of *Angewandte Chemie* is only so high because of the Review articles." An inspection of the corresponding journals of the American Chemical Society (ACS) and the Royal Society of Chemistry (RSC) shows that this is not the case. One can easily calculate the Impact Factor of hypothetical journals with a profile very similar to that of *Angewandte Chemie* (Table 1); in view of these figures, we can safely assume that the Impact Factor of *Angewandte Chemie* would be around 9—even without Reviews.

Combined Impact Factors:
JACS + Chem. Rev. 8.116
ChemComm + Chem. Soc. Rev. 4.744

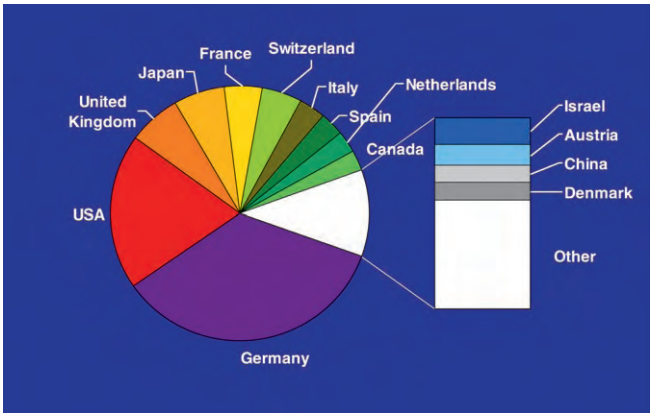


Figure 1. Country of origin of referees for *Angewandte Chemie* 2005.

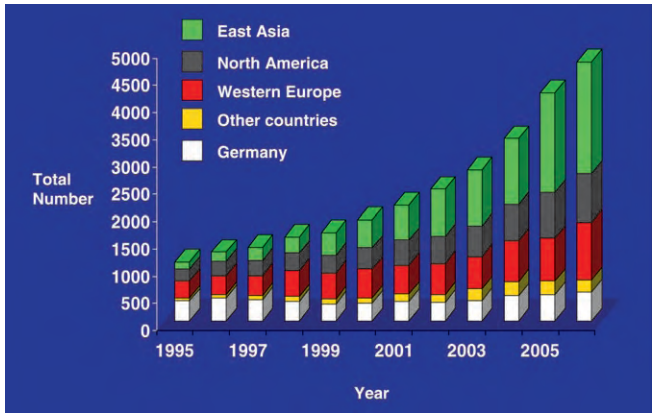


Figure 2. Country or region of origin of Communications since 1995. For 2006, the values have been extrapolated on the basis of the first six months.

© 2006 Wiley-VCH Verlag GmbH & Co. KGaA, Weinheim

Table 1: Comparison of *Angewandte Chemie* with actual and hypothetical (red) journals of the ACS and RSC.

	Number of citations 2003/2004	Number of articles 2003/2004	Impact Factor
J. Am. Chem. Soc.	45 707	6161	7.419
Chem. Rev.	7033	337	20.869
Acc. Chem. Res.	2694	205	13.141
J. Am. Chem. Soc. + *Chem. Rev.*	52 740	6498	8.116
J. Am. Chem. Soc. + *Acc. Chem. Res.*	48 401	6366	7.603
Chem. Commun.	11 907	2690	4.426
Chem. Soc. Rev.	1306	95	13.747
Chem. Commun. + *Chem. Soc. Rev.*	13 213	2785	4.744
Angew. Chem.[a]	22 004	2293	9.596

[a] In 2003/2004 we published 102 Reviews and 37 Minireviews.

Heat Regulation: The rate of rejection increased from 68% in the previous year to 70% in the first four months of 2006. We published about 10% more Communications in the first six months, and we are stepping up our requests to authors to shorten their manuscripts and to make more use of the option of presenting details of their work in the Supporting Information, which is published in electronic format only. For manuscripts that are deemed too specialized or much too long for *Angewandte Chemie* it is also extremely important to assure a smooth transfer to the likewise-prestigious sister journals, which target a more specific audience and/or publish Full Papers.

On the Decline: Where there is pressure, there are also sometimes dishonest tactics: poor citation behavior, multiple publication of the same article, plagiarism to the point of outright fraud—it's all been seen before! However, "where there's danger, a source of salvation is also at hand." The ACS has the "Ethical Guidelines to Publication of Chemical Research" (see http://pubs.acs.org/instruct/ethic.html), and now the European Association for Chemical and Molecular Sciences (EuCheMS) has issued the "Ethical Guidelines for Publication in Journals and Reviews" (see www.euchems.org). Every editor of *Angewandte Chemie* and its sister journals has a copy of these guidelines on their desk—guidelines which rightly begin with guidelines for editors! It is, however, not part of the editors' duties to "bawl out" authors for their misconduct, as one referee recently asked me to do as he wanted to have an author rebuked for an alleged misdeed.

A Boost: The EuCheMS is organizing the First European Chemistry Congress from August 27th to 31st in Budapest (see the announcement on the back cover of this issue as well as www.euchems-budapest2006.hu). The program, which was admirably assembled by a team led by Jean-Marie Lehn and Peter Kündig, promises an excellent conference which will surely give an enormous boost to the European chemistry scene. Highlights of the conference will be the presentations of several Nobel Prize laureates (P. J. Crutzen, J.-M. Lehn, G. A. Olah, K. Wüthrich, A. H. Zewail); moreover, the EuCheMS Lecture will be given (D. Seebach), and for the first time the European Young Chemists Award will be presented. For *Angewandte Chemie*, it is an especially joyful occasion as its Editoral Board Chairman, François Diederich (Figure 5), will receive the August Wilhem von Hofmann Commemorative Medal at the conference. This issue of *Angewandte Chemie* will be distributed in Budapest, and it is thus fitting that it includes an Essay from Jürgen Hambrecht which sheds light on the challenges facing young chemists who are trying to enter the chemical industry—in a world in which even the European perspective is much too narrow. As CEO of BASF (and himself a chemist) Jürgen Hambrecht is predestined as no other to impart his stance on this matter.



Figure 5. François Diederich will receive the August Wilhem von Hofmann Commemorative Medal at the 1st European Chemistry Congress in Budapest.

Moving Forward: With the "1st European Chemistry Congress" Europe

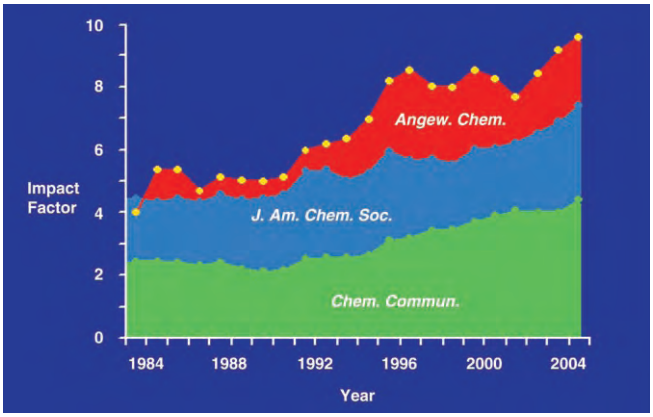


Figure 3. Trends in the Impact Factor (according to the Institute of Scientific Information, Philadelphia, USA) of *Angew. Chem.*, *J. Am. Chem. Soc.*, and *Chem. Commun.* from 1984 to 2005.

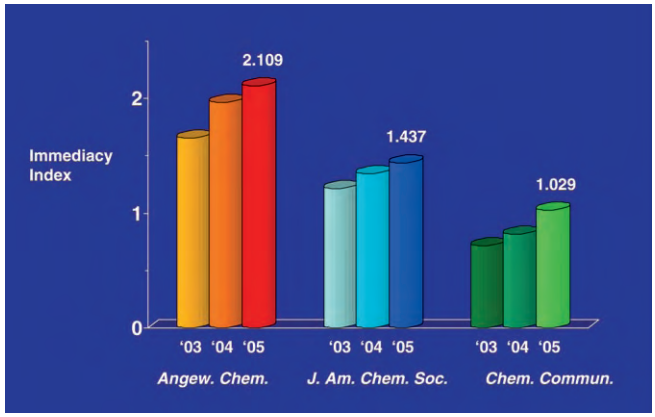
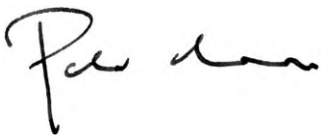


Figure 4. Comparison of Immediacy Indices of *Angewandte Chemie*, *Journal of the American Chemical Society*, and *Chem. Commun.* 2003–2005.

© 2006 Wiley-VCH Verlag GmbH & Co. KGaA, Weinheim



is a late bloomer. America has for a long time held the outstanding ACS Meetings as well as an American Chemical Congress every five years. And Asia already held the 11th Asian Chemical Congress (ACC) in Seoul last year, and the 12th will be held in September 2007 in Kuala Lumpur. By then, *Chemistry—An Asian Journal* will already be one year old, as the first issue has recently appeared! It has surely surpassed the expectations of all the scientific societies and people that were involved with its founding. In line with the demand for an international top journal for Full Papers and Focus Reviews from all areas of chemistry, a solid 60% of accepted manuscripts come from Asia and a further 20% each from America and Europe. Institutional subscribers of *Angewandte Chemie* will receive *Chemistry—An Asian Journal* this year and next year as part of their subscriptions (electronic and printed versions). This complimentary distribution makes a thorough survey of the journal possible for readers and librarians, and it essentially guarantees authors an equally broad readership as in *Angewandte Chemie* itself. The pressure is high to make *Chemistry—An Asian Journal* a success. All signs are positive, and it will perhaps even help a little toward reducing the pressure on other fronts.



Peter Gölitz



Stop the presses! Another bit of good news at the last minute: *ChemMedChem* will be incorporated into MEDLINE/PubMed retroactively from the first issue, which is essential for a journal at the interface of chemistry, biology, and medicine and is sure to give it further momentum. Incidentally, in Issues 7 and 8 of *ChemMedChem* are presented the Nobel Lectures from J. R. Warren and B. J. Marshall, in which they describe in an extraordinarily riveting account their discovery of *Helicobacter pylori*. No less interesting, naturally, are the Nobel Lectures from Y. Chauvin, R. H. Grubbs, and R. R. Schrock in Issue 23 of *Angewandte Chemie*.

© 2006 Wiley-VCH Verlag GmbH & Co. KGaA, Weinheim

VIP The following Communications have been judged by at least two referees to be "very important papers" and will be published online at www.angewandte.org soon:

*J. G. Cordaro, D. Stein, H. Rüegger, H. Grützmacher**
Making the True "CP" Ligand

*N. Shimokhina, A. Bronowska, S. Homans**
Contribution of Ligand Desolvation to Binding Thermodynamics in a Ligand–Protein Interaction

*M. B. Harney, Y. Zhang, L. R. Sita**
Bimolecular Control over Polypropene Stereochemical Microstructure in a Well-Defined Two-State System and a New Fundamental Form: Stereogradient Polypropene

*H. Niu, M. Gao**
Synthesis of Diameter-Tunable CdTe Nanotubes Templated by One-Dimensional Nanowires of Cadmium Thiolate Polymer

*Y. Li, B. S. Lokitz, C. L. McCormick**
Thermally Responsive Vesicles and their Structural "Locking" through Polyelectrolyte Complex Formation

A. Fürstner, C. Nevado, M. Tremblay, C. Chevrier, F. Teplý, C. Aïssa, M. Waser*
Total Synthesis of Iejimalide B

News

Catalysis Research: Prize to Glorius _____ **5044**

Organic Synthesis: Hultzsch awarded _____ **5044**

Materials Chemistry: Schnick honored _____ **5044**

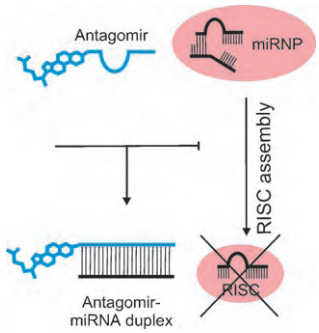
Books

Beyond Oil and Gas: The Methanol Economy — George A. Olah, Alain Goeppert, G. K. Surya Prakash

reviewed by J. O. Metzger _____ **5045**

Highlights

Big things come in small packages: MicroRNAs (miRNAs) are small regulatory RNA molecules in eukaryotes. Altered miRNA expression patterns can be used as a diagnostic tool, for example, in patients with chronic lymphatic leukemia. Also, the inhibition of miRNA function in vivo has been recently achieved by using "antagomirs"—antisense cholesterol conjugates (see scheme; miRNP = miRNA–protein complex, RISC = RNA-induced silencing complex).



Gene Expression

C. Arenz* _____ **5048 – 5050**

MicroRNAs—Future Drug Targets?

Essays

Innovation through communication: What is required of young graduates in chemistry today and how can these skills be developed? An open dialogue between universities and the chemical industry may push innovations and thus lead the way to a successful future.

Science and Industry

J. Hambrecht* _____ **5052 – 5056**

Shaping the Future with Chemistry: What's in Store for Chemistry Graduates in Research and Industry?

© 2006 Wiley-VCH Verlag GmbH & Co. KGaA, Weinheim

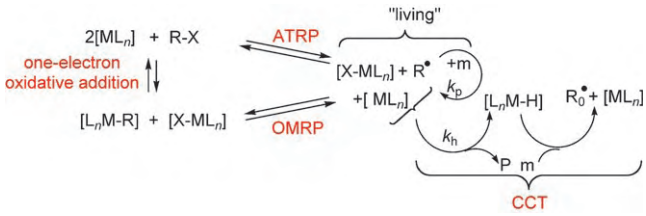
Contents

Minireviews

Controlled Radical Polymerization

R. Poli* ——— **5058 – 5070**

Relationship between One-Electron Transition-Metal Reactivity and Radical Polymerization Processes



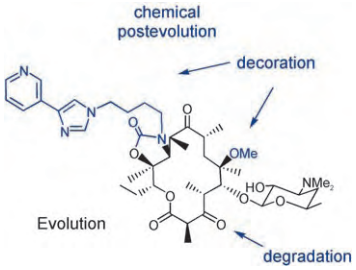
Radical processes: An understanding of one-electron transition-metal reactivity is of fundamental importance for the correct interpretation of experimental results in metal-mediated radical polymerization processes. Thermodynamics and kinetics parameters, the effect of the coordination geometry and spin state of the metal complex, and the properties of the ligand are considered.

Reviews

Antibiotics

F. von Nussbaum, M. Brands, B. Hinzen, S. Weigand, D. Häbich* ——— **5072 – 5130**

Antibacterial Natural Products in Medicinal Chemistry—Exodus or Revival?



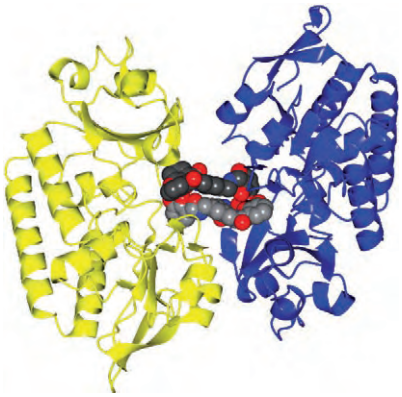
Nature's universe of antibacterial compounds has evolved over millions of years and chemists have exploited this treasure of lead structures for half a century. The β-lactams and the macrolides are outstanding success stories of this era. Today, natural products and basic antibacterial research seem to be "endangered species". Revisiting natural products with modern chemistry and reversed genomics is one option for their revival.

Communications

Iron Complexes

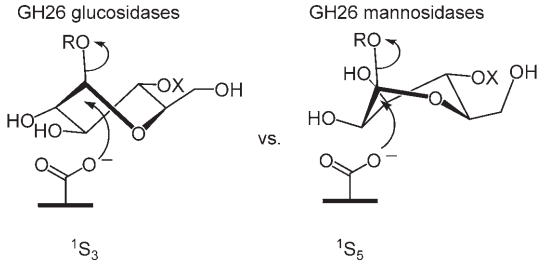
A. Müller, A. J. Wilkinson, K. S. Wilson, A.-K. Duhme-Klair* ——— **5132 – 5136**

An [{Fe(mecam)}$_2$]$^{6-}$ Bridge in the Crystal Structure of a Ferric Enterobactin Binding Protein



Bridging the gap: The dinuclear ferric enterobactin mimic [{Fe(mecam)}$_2$]$^{6-}$ (H$_6$-mecam = 1,3,5-*N*,*N*′,*N*″-tris(2,3-dihydroxybenzoyl)triaminomethylbenzene) is recognized by two periplasmic binding protein molecules (yellow and blue; see structure). The assembly is stabilized through hydrophobic interactions between the ligand backbones of the dinuclear iron complex.

© 2006 Wiley-VCH Verlag GmbH & Co. KGaA, Weinheim

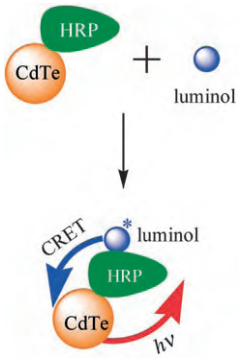


Pick-a-path: A series of enzymatic snapshots along the reaction coordinate of a lichenase (specific for gluco-configured substrates) demonstrates that this enzyme uses a different reaction pathway, featuring a $^1S_3 \rightarrow {}^4H_3 \rightarrow {}^4C_1$ migration, to that previously observed for the closely related mannanases.

Enzyme Models

V. A. Money, N. L. Smith, A. Scaffidi, R. V. Stick, H. J. Gilbert, G. J. Davies* ——— **5136 – 5140**

Substrate Distortion by a Lichenase Highlights the Different Conformational Itineraries Harnessed by Related Glycoside Hydrolases



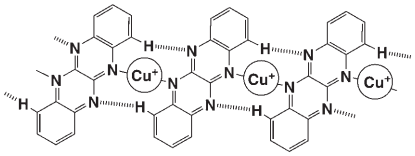
No need to FRET: An efficient chemiluminescence resonance energy transfer (CRET) between luminol and CdTe quantum dots (QDs) is demonstrated. The system is based on horseradish peroxidase (HRP)–QD conjugates and the luminol/hydrogen peroxide chemiluminescence reaction. Multiple QD acceptors with different emission wavelengths can also be used simultaneously. The CRET approach can offer an alternative to fluorescence energy transfer (FRET) investigations.

Energy Transfer

X. Huang, L. Li, H. Qian, C. Dong, J. Ren* ——— **5140 – 5143**

A Resonance Energy Transfer between Chemiluminescent Donors and Luminescent Quantum Dots as Acceptors (CRET)

Molecular conductors: A new, modifiable electron acceptor with a 5,6,11,12-tetraazanaphthacene (TANC) framework was introduced in Cu^I–TANC coordination polymers (see picture). The conduction mechanism of a high-conductivity crystal constructed from these polymers can be described as 1D variable-range hopping based on the disordered F^- ions.

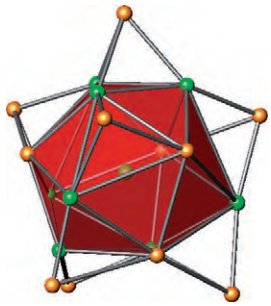


Conducting Materials

M. Tadokoro,* S. Yasuzuka, M. Nakamura, T. Shinoda, T. Tatenuma, M. Mitsumi, Y. Ozawa, K. Toriumi, H. Yoshino, D. Shiomi, K. Sato, T. Takui, T. Mori, K. Murata ——— **5144 – 5147**

A High-Conductivity Crystal Containing a Copper(I) Coordination Polymer Bridged by the Organic Acceptor TANC

A profitable merger: The reaction of K_5Bi_4 with $ZnPh_2$ yields the 20-atom cluster $[Zn@(Zn_8Bi_4)@Bi_7]^{5-}$ (see structure; zinc green, bismuth orange), which consists of a central zinc atom within a Zn_8Bi_4 icosahedron (red) capped by seven bismuth atoms. Extensive amalgamation of the two types of atoms, reminiscent of an alloy, occurs in this intermetalloid cluster.



Cluster Compounds

VIP

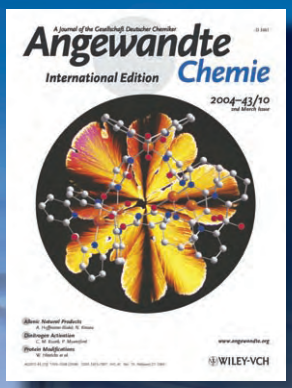
J. M. Goicoechea, S. C. Sevov* ——— **5147 – 5150**

$[Zn_9Bi_{11}]^{5-}$: A Ligand-Free Intermetalloid Cluster

© 2006 Wiley-VCH Verlag GmbH & Co. KGaA, Weinheim

The best in chemistry –

for more than a hundred years



A Journal of the Gesellschaft Deutscher Chemiker

Angewandte
International Edition **Chemie**

www.angewandte.org

1888: ***The beginning of a success story***

Constant Innovations

1962: *First issue of the International Edition*
1976: *Graphical abstracts*
1979: *Cover pictures*
1988: *Centenary of Angewandte*
1989: *Routine use of color*
1991: *New section: Highlights*
1992: *Computerized editorial tracking system*
1995: *Internet service for readers*
1998: *Regular press service; full-text online*
2000: *New section: Essays; EarlyView: Communications available online ahead of the printed version*
2001: *New section: Minireviews*
2002: *Online submission of manuscripts*
2003: *Weekly publication; new section: News; new layout*
2004: *Backfiles (1962-1997); ManuscriptXpress: Online system for authors and referees*



Angewandte's advisors...

Manfred Reetz
Max-Planck-Institut für Kohlenforschung, Mülheim

*» **Angewandte Chemie** is extremely well-balanced in providing various types of information to the academic and industrial chemical community. If you inadvertently miss an issue, the mishap will catch up with you sooner or later. «*

Angewandte Chemie International Edition *is a journal of the German Chemical Society (GDCh)*

GDCh

WILEY InterScience® DISCOVER SOMETHING GREAT

WILEY-VCH

1188104_gu

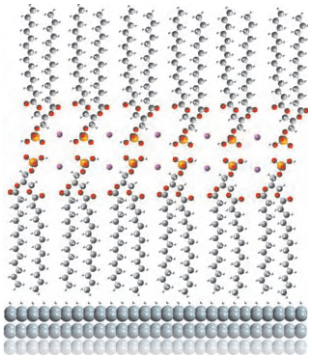
Twists and turns: ZnS nanohelices have been synthesized in high yield by using a simple vapor deposition process. These nanohelices also have Y-shaped branched secondary growths, which always point toward the inside of the helix. The formation of these hierarchical structures is discussed based on structural information.



Nanostructures

D. Moore, Y. Ding,
Z. L. Wang* ——— **5150 – 5154**

Hierarchical Structured Nanohelices of ZnS

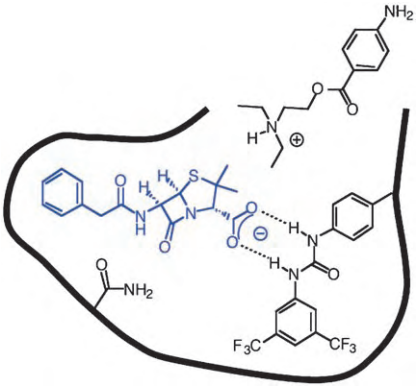


The structure and dynamics of monolayer and bilayer (see picture) phospholipids have been studied with spatiotemporal resolutions by ultrafast electron crystallography. The expansion and restructuring of the chains were observed after a femtosecond temperature jump in the substrate, and a transient structural ordering was revealed. The atomic forces were identified to be coherent in the nonequilibrium state of the assembly.

Molecular Dynamics

S. Chen, M. T. Seidel,
A. H. Zewail* ——— **5154 – 5158**

Ultrafast Electron Crystallography of Phospholipids



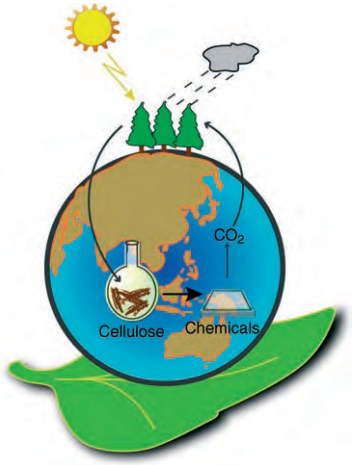
Making a good impression: A molecularly imprinted polymer is prepared against Penicillin G by using a stoichiometric quantity of a urea-based monomer. This polymer displays a high affinity for the template (see picture) and other β-lactam antibiotics, as determined by chromatographic retention factors in high quantities of buffer (90%). Retention values on the nonimprinted polymer were dramatically lower under the same conditions.

Molecular Recognition

J. L. Urraca, A. J. Hall,*
M. C. Moreno-Bondi,
B. Sellergren* ——— **5158 – 5161**

A Stoichiometric Molecularly Imprinted Polymer for the Class-Selective Recognition of Antibiotics in Aqueous Media

Sweetly done: Pt or Ru catalysts supported on inorganic oxides show high activity for the conversion of cellulose into sugar alcohols (mainly sorbitol) in water under hydrogen pressure; furthermore, the catalysts can be recycled over repeated runs. Glucose is produced in low yields, thus suggesting that the Pt (or Ru)/oxide works as a bifunctional catalyst for the hydrolysis of cellulose and subsequent reduction to sugar alcohols.



Biorefinery

A. Fukuoka,* P. L. Dhepe ——— **5161 – 5163**

Catalytic Conversion of Cellulose into Sugar Alcohols

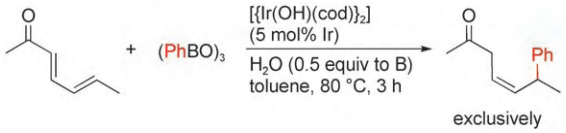
© 2006 Wiley-VCH Verlag GmbH & Co. KGaA, Weinheim

Contents

Regioselectivity

T. Nishimura, Y. Yasuhara, T. Hayashi* ——— 5164 – 5166

Highly Selective 1,6-Addition of Aryl Boronic Acids to α,β,γ,δ-Unsaturated Carbonyl Compounds Catalyzed by an Iridium Complex

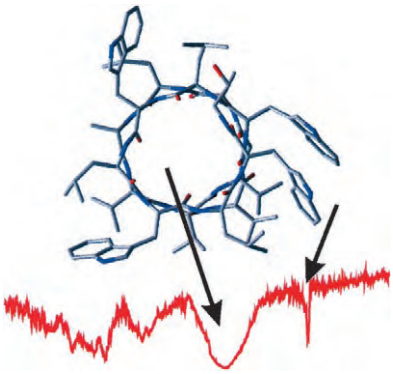


Perfect control: The catalytic 1,6-addition of aryl boronic acids to electron-deficient dienes was realized by use of an iridium catalyst (see scheme). High yields of the corresponding δ-arylated carbonyl compounds were obtained with perfect 1,6-selectivity.

Spectroscopy

A. Abo-Riziq, B. O. Crews, M. P. Callahan, L. Grace, M. S. de Vries* ——— 5166 – 5169

Spectroscopy of Isolated Gramicidin Peptides

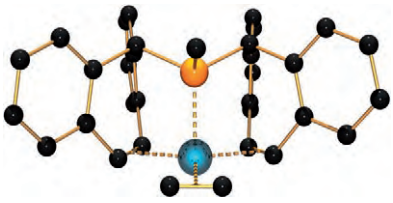


An eye for detail: Double-resonant IR–UV spectroscopy of isolated gramicidin peptides in the gas phase shows evidence for a helical structure, similar to that in the condensed phase. This approach probes local details in isolated molecules, free of interactions.

Rhodium Complexes

D. Ostendorf, C. Landis, H. Grützmacher* ——— 5169 – 5173

Trigonal Pyramids: Alternative Ground-State Structures for Sixteen-Electron Complexes

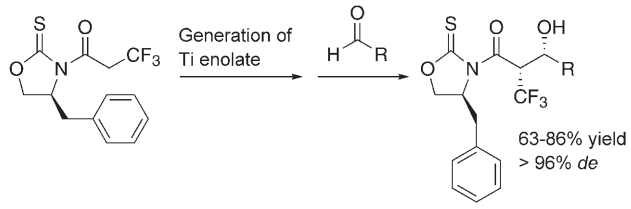


A structural alternative for sixteen-electron ML_4 complexes is the trigonal-pyramidal (TP) form. This has been demonstrated by the preparation of TP complexes of rhodium(I) with three equatorial olefin ligands and one axial silyl ligand (see picture: C black, Rh blue, Si orange).

CF_3-Containing Enolates

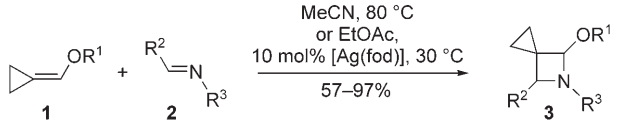
X. Franck,* B. Seon-Meniel, B. Figadère* ——— 5174 – 5176

Highly Diastereoselective Aldol Reaction with α-CF_3-Substituted Enolates



A CF_3 group and a chiral auxiliary are the key features of the Ti enolate used in the aldol reaction shown above. The *syn* aldol is formed in good yields, and defluorination leading to the vinylic CF_2 product is not observed. The aldol product may be used to prepare more elaborate CF_3-containing compounds, for instance, through the corresponding 1,3-diol.

© 2006 Wiley-VCH Verlag GmbH & Co. KGaA, Weinheim



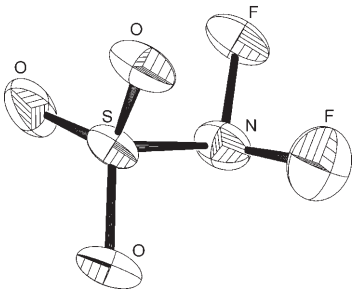
A silver lining: [2+2] Cycloadditions of imines **2** to (alkoxymethylene)cyclopropanes **1** proceed readily at 80 °C and ambient pressure to furnish spirocyclopropanated 2-alkoxyazetidines **3** in good to excellent yields. The same reaction can be brought about at 30 °C in the presence of a catalytic amount of [Ag(fod)] (fod = 6,6,7,7,8,8,8-heptafluoro-2,2-dimethyl-3,5-octanedionato).

Cycloadditions

I. Nakamura,* T. Nemoto, Y. Yamamoto, A. de Meijere _____ **5176 – 5179**

Thermally Induced and Silver-Salt-Catalyzed [2+2] Cycloadditions of Imines to (Alkoxymethylene)cyclopropanes

---



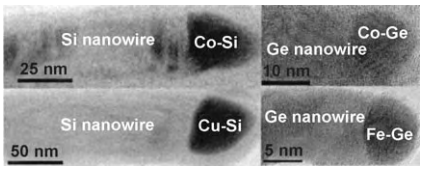
Safe difluoroaminating reagents: Salts of the elusive $SO_3NF_2^-$ ion were prepared by aqueous fluorination of $SO_3NH_2^-$ with F_2. These salts were characterized (see ORTEP of the anion) and shown to be excellent reagents for the preparation of *gem*-bis(difluoroamines). Salts of the intermediate SO_3NHF^- ion were also isolated and characterized.

Fluorinated Substituents

R. Haiges,* R. Wagner, J. A. Boatz, M. Yousufuddin, M. Etzkorn, G. K. S. Prakash, K. O. Christe,* R. D. Chapman,* M. F. Welker, C. B. Kreutzberger _____ **5179 – 5184**

Preparation, Characterization, and Crystal Structures of the SO_3NHF^- and $SO_3NF_2^-$ Ions

---



The top seed: Various metal nanocrystals are studied as crystallization seeds for silicon and germanium nanowires. The wires are grown by decomposing silane or germane reactants in supercritical organic solvents. Co and Ni nanocrystals promote the seeding of high-quality nanowires and catalyze reactant decomposition under the reaction conditions.

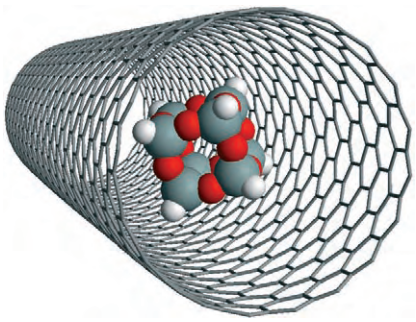
Nanowires

H.-Y. Tuan, D. C. Lee, B. A. Korgel* _____ **5184 – 5187**

Nanocrystal-Mediated Crystallization of Silicon and Germanium Nanowires in Organic Solvents: The Role of Catalysis and Solid-Phase Seeding

---

A spectroscopic probe of nanotube diameter: The strength of the interaction of $H_8Si_8O_{12}$ with the inner walls of carbon nanotubes (see picture) depends on the inner diameter. This, in turn, affects the Si–H stretching frequency, which can be probed by IR spectroscopy.



Carbon Nanotubes

J. Wang, M. K. Kuimova, M. Poliakoff, G. A. D. Briggs, A. N. Khlobystov* _____ **5188 – 5191**

Encapsulation and IR Probing of Cube-Shaped Octasilasesquioxane $H_8Si_8O_{12}$ in Carbon Nanotubes

© 2006 Wiley-VCH Verlag GmbH & Co. KGaA, Weinheim

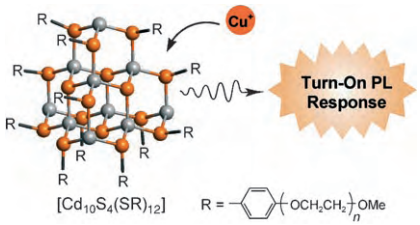
Contents

Copper Sensor

K. Konishi,* T. Hiratani ____ **5191 – 5194**

Turn-On and Selective Luminescence Sensing of Copper Ions by a Water-Soluble $Cd_{10}S_{16}$ Molecular Cluster

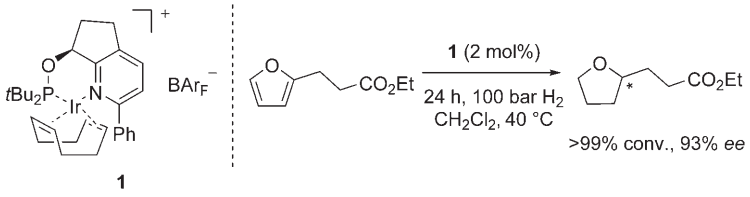
A large turn-on effect in the form of a notable photoluminescence (PL) enhancement was observed for an oligo(ethylene glycol)-appended CdS cluster molecule with a $Cd_{10}S_{16}$ core upon mixing with Cu^{I} in water (see graphic). Analysis by the Job method and size-exclusion chromatography suggested that the turn-on response, which was found to be specific for Cu^{I}, is associated with the formation of a Cu^{I}-containing multicluster network.



Asymmetric Hydrogenation Catalysts

S. Kaiser, S. P. Smidt, A. Pfaltz* _____ **5194 – 5197**

Iridium Catalysts with Bicyclic Pyridine–Phosphinite Ligands: Asymmetric Hydrogenation of Olefins and Furan Derivatives



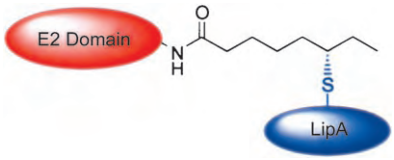
1

Superior bicyclics: Iridium catalysts as **1** derived from pyridine–phosphinite ligands considerably extend the scope of asymmetric hydrogenation. In addition to various unfunctionalized and functionalized olefins, furans, and benzofurans, for which no catalysts were known before, are also hydrogenated with high enantioselectivity (see scheme).

Biosynthesis

P. Douglas, M. Kriek, P. Bryant, P. L. Roach* _____ **5197 – 5199**

Lipoyl Synthase Inserts Sulfur Atoms into an Octanoyl Substrate in a Stepwise Manner

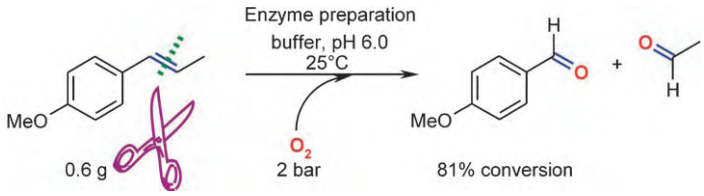


One step at a time: The insertion of the two sulfur atoms found in lipoyl groups requires the enzyme lipoyl synthase (LipA). The order of insertion of the two sulfur groups has been elucidated by spectroscopic characterization of a monothiolated species.

Biocatalytic Alkene Cleavage

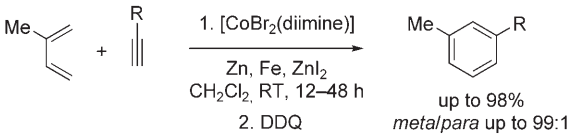
H. Mang, J. Gross, M. Lara, C. Goessler, H. E. Schoemaker, G. M. Guebitz, W. Kroutil* _____ **5201 – 5203**

Biocatalytic Single-Step Alkene Cleavage from Aryl Alkenes: An Enzymatic Equivalent to Reductive Ozonization



O_2 can do: Innocuous molecular oxygen O_2 is the only reagent needed to perform highly chemoselective biocatalytic single-step alkene-cleavage reactions (see scheme). The products are analogous to those of (reductive) ozonization and related metal-based methods. In contrast neither special equipment nor an additional reducing agent is required. The biocatalytic reaction can be performed at ambient temperature. Depending on the substrate, aldehydes or ketones are obtained.

© 2006 Wiley-VCH Verlag GmbH & Co. KGaA, Weinheim



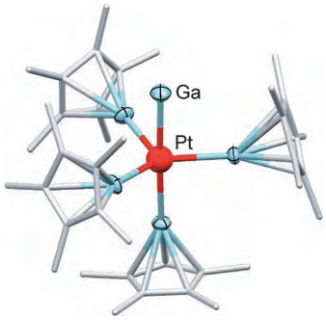
Overcoming the *ortho/para* rule? The regioselectivity of Diels–Alder reactions with neutral electron demand between 1,3-dienes with alkynes can be controlled by simple cobalt diimine complexes so that the *meta*-substituted cycloadducts are generated in good yields and excellent regioselectivity (see scheme; DDQ = 2,3-dichloro-5,6-dicyano-1,4-benzoquinone).

Diels–Alder Reaction

G. Hilt,* J. Janikowski, W. Hess ——— **5204 – 5206**

meta-Directing Cobalt-Catalyzed Diels–Alder Reactions

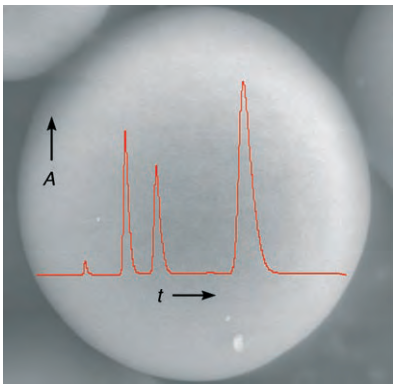
In the buff: The reaction of $[Pt(GaCp^*)_4]$ with the Ga^+ source $[Ga_2Cp^*][BAr^F]$ ($Cp^* = C_5Me_5$; $BAr^F = B\{C_6H_3(3,5\text{-}CF_3)_2\}_4$) leads to the title complex, which exhibits a naked gallium atom coordinated to a platinum center. DFT calculations reveal that the Ga^+ ligand serves as a σ acceptor, and the Pt–Ga bond is additionally supported by strong π interactions.



Metalloid Complexes

B. Buchin, C. Gemel, T. Cadenbach, I. Fernández, G. Frenking,* R. A. Fischer* ——— **5207 – 5210**

"Naked" Ga^+ and In^+ as Pure Acceptor Ligands: Structure and Bonding of $[GaPt(GaCp^*)_4][BAr^F]$



Alternative adsorbents: Spherical particles of a phenylene-bridged periodic mesoporous organosilica material (see picture) are applied in HPLC for the first time. Three test mixtures of up to four components with different polarities can be separated with the new column material.

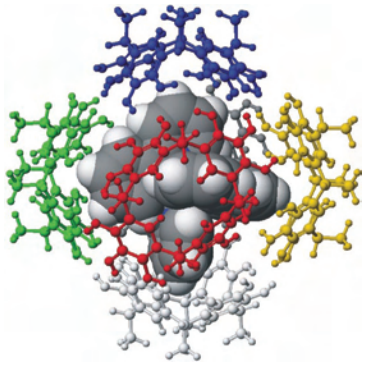
Chromatography

V. Rebbin, R. Schmidt, M. Fröba* ——— **5210 – 5214**

Spherical Particles of Phenylene-Bridged Periodic Mesoporous Organosilica for High-Performance Liquid Chromatography

---

Survival of the fittest: Only those hexameric pyrogallarene and resorcinarene capsules which contain a guest with the right size, shape, and symmetry (see picture) survive the electrospray ionization process that makes them detectable by mass spectrometry. Tandem MS experiments with mass-selected ions provide evidence that the hexamers retain their capsular structure even in the gas phase.



Host–Guest Complexes

N. K. Beyeh, M. Kogej, A. Åhman, K. Rissanen, C. A. Schalley* **5214 – 5218**

Flying Capsules: Mass Spectrometric Detection of Pyrogallarene and Resorcinarene Hexamers

© 2006 Wiley-VCH Verlag GmbH & Co. KGaA, Weinheim

Contents

Protein Modifications

C. Ludwig, M. Pfeiff, U. Linne, H. D. Mootz* ——— **5218 – 5221**

Ligation of a Synthetic Peptide to the N Terminus of a Recombinant Protein Using Semisynthetic Protein *trans*-Splicing



Splice it! An active intein can be reconstituted from a recombinant C-terminal and a short synthetic N-terminal fragment. This allows ligation of a synthetic peptide to the N terminus of a recombinant protein of interest by protein *trans*-splicing and circumvents the requirement for a C-terminal thioester or other reactive groups common to chemical ligation approaches.

Sources

Product and Company Directory

You can start the entry for your company in "Sources" in any issue of *Angewandte Chemie*.

If you would like more information, please do not hesitate to contact us.

Wiley-VCH Verlag – Advertising Department
Tel.: 0 62 01 - 60 65 65
Fax: 0 62 01 - 60 65 50
E-Mail: MSchulz@wiley-vch.de

Service

Keywords ——— *5222*

Authors ——— *5223*

Preview ——— *5225*



For more information on Chemistry—An Asian Journal see www.chemasianj.org

© 2006 Wiley-VCH Verlag GmbH & Co. KGaA, Weinheim



Awarded...

Alfried Krupp Prize to F. Glorius

The Alfried Krupp Prize for young professors goes this year to Frank Glorius (Philipps-Universität Marburg). The prize of €1000000 recognizes his services in research as well as in teaching. Glorius has devoted himself for many years to the development of new concepts in catalysis and their application in organic syntheses. Among others, his contributions include the development of new classes of N-heterocyclic carbenes, the asymmetric hydrogenation of (hetero)arenes, and "conjugated" Umpolung. He recently published a review article in *Angewandte Chemie* on asymmetric heterogeneous catalysis.[1]



F. Glorius

Glorius studied chemistry at the Universität Hannover and the Max-Planck-Institut (MPI) für Kohlenforschung (Coal Research) in Mülheim a.d. Ruhr and completed his PhD in 2000 under the supervision of A. Pfalz at the Universität Basel and the MPI für Kohlenforschung on the topic of chiral bisoxazoline ligands. He spent one year with D. A. Evans at Harvard University, and from 2001 until 2004 was a Liebig Fellow at the MPI für Kohlenforschung and the Universität Dortmund under the guidance of A. Fürstner. Glorius has been a professor of organic chemistry at the Philipps-Universität Marburg since the end of 2004. He received the ORCHEM prize for young scientists in the same year.

K. C. Hultzsch receives Dr. Lieseberg Prize

The Faculty of Chemistry and Geosciences of the University of Heidelberg has awarded Kai Carsten Hultzsch this year's Dr. Lieseberg Prize for his preparative work on asymmetric hydroamination. Asymmetric hydroamination is an atom-efficient method for the addition of amines to unsaturated C–C bonds; the group of Hultzsch has developed highly active and selective rare-earth-metal and lithium catalysts for this process. Already in 2004, an article from Hultzsch appeared in *Angewandte Chemie* on the cyclization hydroamination of aminoalkenes with cationic zirconocene and titanocene catalysts.[2]



K. C. Hultzsch

Kai Carsten Hultzsch studied chemistry at the Johannes-Gutenberg-Universität Mainz, where in 1999 he received his PhD under J. Okuda on the topic of rare-earth-metal complexes as catalysts for the polymerization of non-polar and polar monomers. He subsequently undertook postdoctoral research with R. R. Schrock at the Massachusetts Institute of Technology (MIT) on catalysts for asymmetric ring-closing metathesis. Since 2001 he has led an Emmy-Noether-Nachwuchsgruppe (development group) at the Institut für Organische Chemie in Erlangen. In 2006 he completed his habilitation in organic and organometallic chemistry.

W. Schnick awarded the Horst Dietrich Hardt Prize

This year the Horst Dietrich Hardt Prize from the Naturwissenschaftlich-Technischen Fakultät III der Universität des Saarlandes has been conferred for the first time. The prize will be awarded every three years in recognition of pioneering research in the area of inorganic metal compounds. The first laureate is Wolfgang Schnick, who has developed new luminescent materials that have led, for example, to industrial applications of highly efficient white light-emitting diodes (LEDs). His work is ground-breaking for the production of LEDs for general lighting applications. His latest article in *Angewandte Chemie* reports the first microporous nitridic clathrate $P_4N_4(NH)_4(NH_3)$.[3]



W. Schnick

Wolfgang Schnick studied chemistry in Hannover, where he also received his PhD in 1986 under M. Jansen on alkali metal ozonides. He then spent a year with A. Rabenau at the MPI für Festkörperforschung (solid-state research) in Stuttgart. After stints in Bonn, where he received his habilitation in inorganic chemistry in 1992, and Bayreuth, he is now a professor for inorganic solid-state chemistry at the Ludwig-Maximilians-Universität München. Schnick's services were also recognized by the Bayerischen Akademie der Wissenschaften (Bavarian Academy of Sciences and Humanities), which admitted him this year as a member.

[1] M. Heitbaum, F. Glorius, I. Escher, *Angew. Chem.* **2006**, *118*, 4850; *Angew. Chem. Int. Ed.* **2006**, *45*, 4732.

[2] D. V. Gribkov, K. C. Hultzsch, *Angew. Chem.* **2004**, *116*, 5659; *Angew. Chem. Int. Ed.* **2004**, *43*, 5542.

[3] F. Karau, W. Schnick, *Angew. Chem.* **2006**, *118*, 4617; *Angew. Chem. Int. Ed.* **2006**, *45*, 4505.

DOI: 10.1002/anie.200602752

InterScience
© 2006 Wiley-VCH Verlag GmbH & Co. KGaA, Weinheim

Gene Expression

DOI: 10.1002/anie.200601537

MicroRNAs—Future Drug Targets?**

*Christoph Arenz**

Keywords:
antisense agents · bioconjugates · gene expression · microRNA · RNA

A growing body of evidence suggests that gene regulation in eukaryotes takes place to a large extent on the RNA level.[1] A group of endogenous regulatory RNA molecules, the so-called microRNAs (miRNAs), are being intensively examined by biologists and physicians. These small RNA molecules are not only believed to be involved in the regulation of nearly 30% of all human genes[2] but an ever-increasing amount of data points towards a connection between specific changes in miRNA expression patterns and various diseases.

MicroRNAs are formed in the cell nucleus from so-called primary microRNAs (pri-miRNAs, Figure 1). These transcripts can be produced either autonomously under the control of a specific promoter or from the intron of a protein-encoding primary transcript through RNA polymerase II. One or more precursor miRNAs (pre-miRNAs) are then formed by cleavage of the pri-miRNAs by the ribonuclease Drosha. These pre-miRNAs are made up of 70–80 nucleotides and exhibit a typical hairpin conformation. The pre-miRNAs are transported out of the nucleus into the cytosol by the protein exportin 5. In the cytosol, the ribonuclease Dicer then nucleolytically cleaves both strands of the helical stem. The resulting miRNA is an approximately 21-nucleotide double-stranded RNA that typically contains 5′-monophosphates and a two-nucleotide overhang on each of the 3′ ends.

The miRNAs show many similarities to short interfering RNAs (siRNAs), which are already well-known in the context of RNA interference. However, the double-stranded siRNAs are normally perfectly self-complementary, whereas the hairpin miRNAs typically exhibit one or more bulges or loops, leading to only partial complementarity of the strands. The mature miRNAs recruit various proteins to build a miRNA–ribonucleoprotein complex (miRNP) that unwinds the double-stranded miRNA, thus forming the so-called RNA-induced silencing complex (RISC). In comparison to siRNAs, whose perfect complementarity to the respective target mRNAs leads to degradation of the said mRNA, miRNAs are not perfectly complementary to the corresponding mRNAs. The miRNA RISC binds mRNA molecules primarily within the 3′-untranslated region (3′-UTR). This partially complementary binding typically results in translational repression of many different mRNAs.

Many questions, however, remain unanswered in the area of gene regulation by miRNAs. For example, the number of miRNAs in various organisms has still not been fully determined. Presently, more than 320 validated human miRNAs are known, although some estimates report as many as 400 to 1000 different miRNAs in humans.[3] With a few exceptions, the identity and even the number of genes that are regulated by the respective miRNAs are unknown. The fact that the first miRNAs discovered are involved in early development through regulation of proliferation, differentiation, and programmed cell death (apoptosis) raised the suspicion among biologists early on that these substances might play a role in cancer genesis. Recently, several reports have addressed altered expression patterns in miRNAs that correlate with various types of cancer, such as liver cell carcinoma and thyroid and lung cancers.[4] Such disease-associated changes in the miRNA expression patterns are often very specific, thus opening up new opportunities for medical diagnostics.

Croce et al. recently reported an association between miRNA expression patterns and different diagnostic and prognostic factors for chronic lymphatic leukemia (CLL).[5] CLL is the most common type of blood cancer in western industrial nations.[6] The course of this disease varies strongly from patient to patient: While some patients may require early treatment, others go often more than ten years after first diagnosis before the disease reaches the stage where therapeutic treatment becomes necessary. Different clinical markers, such as ZAP-70 (Zeta-associated protein, 70 kDa), a protein tyrosine kinase, can be used to determine a patient's prognosis (good/bad) or to assess the need for an initial treatment. By using microchips specially made for human miRNAs,[7] a CLL-specific alteration in the expression of 13 (out of 190 tested) miRNAs could be identified. From this group of miRNAs, nine were found to be overexpressed in those patients with the more aggressive variant of CLL, for whom there was only a short interval between diagnosis and initial treatment. For those patients that had a longer interval, however, no overexpression of the nine miRNAs was seen. In the course of this study, the question as to whether the altered expression levels of

[*] Prof. Dr. C. Arenz
Institut für Chemie
Humboldt-Universität zu Berlin
Brook-Taylor-Strasse 2
12489 Berlin (Germany)
Fax: (+49) 30-2093-6947
E-mail:
christoph.arenz@chemie.hu-berlin.de

[**] The author thanks the Fonds der Chemischen Industrie and the Innovationsfond der Humboldt-Universität zu Berlin for financial support.

InterScience
© 2006 Wiley-VCH Verlag GmbH & Co. KGaA, Weinheim

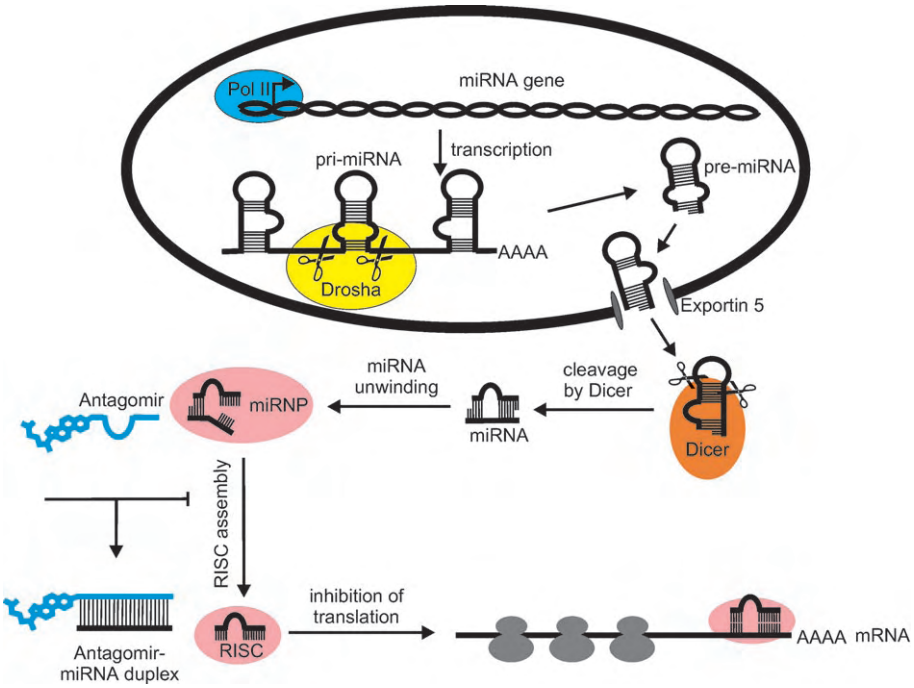


Figure 1. Formation, maturation, and action of microRNAs (simplified). The antagomirs hybridize with the mature miRNAs, thus blocking the silencing effect of the corresponding mRNAs.

the miRNAs were the cause of the CLL could not be answered.

The evidence is steadily increasing, however, that at least some miRNAs play an important role in the development and progression of various cancers. As an example, two recent reports examine the *miR-17-92* gene, which is located within a chromosomal section that is amplified in B-cell lymphomas. It was shown that the respective miRNAs, when compared to healthy cells, are indeed upregulated in this form of cancer. Moreover, viral overexpression of *miR-17-92* in combination with overexpressed c-Myc protein leads to a significant acceleration in the formation of B-cell lymphomas in a mouse model.[8] Particularly interesting in connection with these results is the discovery that the c-Myc transcription factor, which is known to be oncogenic at high concentrations, apparently drives the transcription of the *miR-17-92* cluster.[9]

The vast number of reports indicating the role of miRNAs in connection with diseases such as diabetes, neurological disorders, and cancer automatically raises the question whether these insights could be used for the development of novel therapeutic strategies. As many cancers are accompanied by low levels of miRNA, the administration of metabolic-stabilized miRNA analogues as a cancer therapy is currently being explored.[10] In the opposite case, however, where diseases are characterized by increased levels of particular miRNAs, the inhibition of miRNA function might be preferable. Such is the case with LNA antisense oligonucleotides, which were successfully applied to specifically inhibit the function of miRNAs in *Drosophila melanogaster* cells.[11]

In a recently published study, Krützfeldt et al. were able to silence the function of specific miRNAs in living mice upon administering specially developed antisense agents.[12] Injection of these so-called antagomirs into the tail veins of the mice led in each case to a specific reduction of four different miRNAs in all organs tested, with the exception of the brain. A closer biochemical examination of the mice treated with antagomir-122 showed that above all, levels of mRNAs containing recognition sequences for the corresponding miRNA-122 in their 3′-UTRs (ca. 360 mRNAs) were increased by a factor of at least 1.4. On the basis of a previously performed bioinformatical analysis it was expected that several genes involved in cholesterol metabolism would be influenced by miRNA-122. Indeed, the injection of 240 mg kg^{-1} of the antagomir led to a 40% reduction of HMG-CoA reductase, the rate-limiting enzyme in cholesterol biosynthesis, as well as to the reduction of the plasma cholesterol level by a similar extent.

These antagomirs are 2′-*O*-methyl-oligoribonucleotides that contain a phosphorthioate backbone and a cholesterol moiety at the 3′ end.[13] Such modifications facilitate not only the entrance of the nucleic acid mimetics to the various tissues and cells but also lead to a drastic increase in the biological half-life of the substances. Using such modified antisense molecules, but not in the case of simple antisense RNA, degradation of the corresponding miRNA-122 was seen even after more than 20 days. Interestingly, in addition to the aforementioned overexpression of mRNAs, a downregulation of nearly as many mRNAs occurred. The authors speculate that through a degradation of miRNA-122, an upregulation of repressor proteins might occur, leading to inhibition of the expression of the corresponding effector genes.

The first in vivo study with agents specific for miRNAs has shown the "proof of principle" of this concept. The effects of the antagomirs on the protein level, however, were only examined for a few enzymes connected with

 © 2006 Wiley-VCH Verlag GmbH & Co. KGaA, Weinheim

cholesterol metabolism. The physiological effect of a complete and prolonged degradation of miRNA-122 is in the end relatively small. It could be that miRNAs are responsible for a fine-tuning rather than a turning on/off of associated genes. Thus, the question still remains open as to whether miRNAs are truly suitable target structures for therapeutic intervention in humans.

[1] Review: E. Wienholds, R. H. Plasterk, *FEBS Lett.* **2005**, *579*, 5911 – 5922.

[2] B. P. Lewis, C. B. Burge, D. P. Bartel, *Cell* **2005**, *120*, 15 – 20.

[3] E. Berezikov, V. Guryev, J. van de Belt, E. Wienholds, R. H. Plasterk, E. Cuppen, *Cell* **2005**, *120*, 21 – 24.

[4] Selected examples: a) S. Volinia, G. A. Calin, C. G. Liu, S. Ambs, A. Cimmino, F. Petrocca, R. Visone, M. Iorio, C. Roldo, M. Ferracin, R. L. Prueitt, N. Yanaihara, G. Lanza, A. Scarpa, A. Vecchione, M. Negrini, C. C. Harris, C. M. Croce, *Proc. Natl. Acad. Sci. USA* **2006**, *103*, 2257 – 2261; b) N. Yanaihara, N. Caplen, E. Bowman, M. Seike, K. Kumamoto, M. Yi, R. M. Stephens, A. Okamoto, J. Yokota, T. Tanaka, G. A. Calin, C. G. Liu, C. M. Croce, C. C. Harris, *Cancer Cell* **2006**, *9*, 189 – 198; c) Y. Murakami, T. Yasuda, K. Saigo, T. Urashima, H. Toyoda, T. Okanoue, K. Shimotohno, *Oncogene* **2006**, *25*, 2537 – 2545; d) P. Pallante, R. Visone, M. Ferracin, A. Ferraro, M. T. Berlingieri, G. Troncone, G. Chiappetta, C. G. Liu, M. Santoro, M. Negrini, C. M. Croce, A. Fusco, *Endocr.-Relat. Cancer* **2006**, *13*, 497 – 508.

[5] G. A. Calin, M. Ferracin, A. Cimmino, G. Di Leva, M. Shimizu, S. E. Wojcik, M. V. Iorio, R. Visone, N. I. Sever, M. Fabbri, R. Iuliano, T. Palumbo, F. Pichiorri, C. Roldo, R. Garzon, C. Sevignani, L. Rassenti, H. Alder, S. Volinia, C. G. Liu, T. J. Kipps, M. Negrini, C. M. Croce, *N. Engl. J. Med.* **2005**, *353*, 1793 – 1801.

[6] M. J. Keating, N. Chiorazzi, B. Messmer, R. N. Damle, S. L. Allen, K. R. Rai, M. Ferrarini, T. J. Kipps, *Hematology* **2003**, *8*, 153 – 175.

[7] C. G. Liu, G. A. Calin, B. Meloon, N. Gamliel, C. Sevignani, M. Ferracin, C. D. Dumitru, M. Shimizu, S. Zupo, M. Dono, H. Alder, F. Bullrich, M. Negrini, C. M. Croce, *Proc. Natl. Acad. Sci. USA* **2004**, *101*, 9740 – 9744.

[8] L. He, J. M. Thomson, M. T. Hemann, E. Hernando-Monge, D. Mu, S. Goodson, S. Powers, C. Cordon-Cardo, S. W. Lowe, G. J. Hannon, S. M. Hammond, *Nature* **2005**, *435*, 828 – 833.

[9] K. A. O'Donnell, E. A. Wentzel, K. I. Zeller, C. V. Dang, J. T. Mendell, *Nature* **2005**, *435*, 839 – 843.

[10] a) F. J. Slack, J. B. Weidhaas, *Future Oncol.* **2006**, *2*, 73 – 82; b) C. M. Croce, G. A. Calin, WO 2004043387, **2004**.

[11] U. A. Orom, S. Kauppinen, A. H. Lund, *Gene* **2006**, *372*, 137 – 141.

[12] J. Krützfeldt, N. Rajewsky, R. Braich, K. G. Rajeev, T. Tuschl, M. Manoharan, M. Stoffel, *Nature* **2005**, *438*, 685 – 689.

[13] M. Manoharan, V. Kesavan, K. G. Rajeev, US 2005107325, **2005**.

 © 2006 Wiley-VCH Verlag GmbH & Co. KGaA, Weinheim

Science and Industry

DOI: 10.1002/anie.200602160

Shaping the Future with Chemistry: What's in Store for Chemistry Graduates in Research and Industry?

*Jürgen Hambrecht**

Keywords:
educational system · innovation · research and development

What kind of outlook do young chemistry graduates have today? What do they expect from industry? What awaits them in the world of industry? And what does the industry expect from them?

It's been thirty years since I myself left the university to join BASF's research community with a PhD in my pocket and plenty of ideas, but plenty of questions on board too. It was an exciting time, and I still enjoy talking to newcomers to our company about what they've seen and done, their prospects, and their dreams for the future.

Chemistry is fascinating. In that respect, it's no different for young scientists today than it was for me back then. Chemistry is fascinating because it makes many things possible that would have been inconceivable not too long ago. Pioneering inventions from the world of chemistry are part and parcel of contemporary everyday life. Just imagine life without plastics, for instance. And the quality of life of future generations depends to a huge extent on innovations being developed in chemical labs today. To put it in a nutshell: We can shape the future with chemistry. The fascination of chemistry and the opportunities it offers has remained with me and inspired me to this day.

Much of this fascination was revealed to me by my own teacher and PhD supervisor, Professor Eugen Müller, who would have celebrated his 100th birthday last November. He personified a type of research scientist that you rarely see today. He was driven by a relentless urge to discover, which took him deep into the furthest realms and most intricate twists of whatever research area he was currently involved in, but he was at the same time a generalist who upheld the Humboldt ideal.

[*] Dr. J. Hambrecht
BASF Aktiengesellschaft
67056 Ludwigshafen (Germany)
E-mail: juergen.hambrecht@basf-ag.de

Does the Future Belong to the Specialists?

Generalists are getting increasingly thin on the ground in today's scientific community. The very term "generalist" has almost a negative connotation: at the end of the day, someone who's good at almost everything is not good enough at any one thing to be able to perform outstanding work in a given area.—At least, you'd be forgiven for thinking so, given the image people have of contemporary science: highly specialized expertise concentrated in a sharply circumscribed specialist area. Everyone neatly tucked into their own little box.

Of course there are important reasons why we have this trend in science today. Certainly the most obvious one is that the body of knowledge in all disciplines has grown enormously, and specialization is the logical result. It would be hard to find a person nowadays who comes even remotely close to knowing everything there is to know about a given area of his or her discipline, organic chemistry for example.

Another reason for the galloping specialization is the phenomenon we all call globalization: capital and knowledge have virtually unlimited mobility and can go almost anywhere in the world at almost any time. The world is changing ever more rapidly as a result, with a commensurate increase in the pace of science and business. Today's new insight is tomorrow's old hat. A measure that promises competitive advantages now may soon be outbid by international rivals. All this adds to the pressure to perform, which in turn promotes a desire to occupy an inviolable position in the competitive environment by acquiring excellence in a specialist niche. Most chemical companies have gone this route; specialization is their response to the consolidation pressures to which the industry is exposed. The target is to ensure profitable growth by enhancing efficiency and by achieving market leadership in well-defined business areas.

There is no question about it, specialization is important and essential for research excellence. Nevertheless, if you concentrate all your attention on a single, sharply defined area, you might end up missing what may be a truly defining moment: the chance to discover something really new.

If you concentrate on a single, sharply defined area, you might miss the chance to discover something really new.

How Does Innovation Come About?

The history of science is full of stories of genuinely new and pioneering discoveries which came about when scientists lifted their nose from their

InterScience
© 2006 Wiley-VCH Verlag GmbH & Co. KGaA, Weinheim

Petri dish long enough to notice things going on elsewhere. Serendipity played a role in many new discoveries. Many of the highest-impact innovations we know of today started out as a failed experiment in terms of what the scientist was originally trying to achieve. And that would have been that, had the inventor not opened his eyes and recognized the opportunities opening up in an area extraneous to what his work had actually been intended to accomplish.

The history of chemistry has a number of highly instructive anecdotes in this regard. One of them has a direct bearing on BASF's success story.[1]

150 years ago, a student called William Henry Perkin in London set out to synthesize the substance quinine, which was in widespread use at the time to treat fevers. Instead, oxidation of impure aniline produced a purple solution. Most of Perkin's fellow students would probably have poured it down the drain. Perkin's curiosity was piqued, however, and he used the solution to try and dye a piece of silk—with success. This moment marked the birth of the dye industry. Synthetic dyes were far and away cheaper than natural dyes, as well as having better properties and a more extensive color range. They revolutionized the entire textile industry. BASF started out more than 140 years ago with aniline dyes. Today it is the world's leading chemical company.

The history of chemistry abounds with similar stories. Nylon and Teflon were chance discoveries which went on to conquer the globe. The famous repeelable "Post-It" notes entered the world as the serendipitous outcome of development work on a new superglue. It took a brilliant idea for a potential use of this actually unwanted by-product, which was so far removed from the originally intended outcome, and an effective marketing concept to bring about the overwhelming success we all know about. All these stories show that the ostensible detours and dead ends encountered in a research project may unearth huge potential, provided, of course, there are creative, open minds around who recognize and realize that potential.



Front page of a BASF price-list from 1896.

Opening Up the Ivory Tower

A scientific discovery on its own is not enough to produce innovation or progress. True innovation occurs only when you apply what has been discovered in the lab, when you—so to speak—translate science into useful everyday applications. This translation work takes place at the science–business interface. The importance of this accomplishment is frequently underrated, especially at our universities.

And yet, innovations are the be-all and end-all as far as our future is concerned. A society can develop and grow only through innovation. Economic growth, prosperity, and a better quality of life for the largest possible number of people can come about and be maintained only through innovation.

That is why it is more important than ever for scientists and the business community to move up closer, talk more to each other, and share ideas. In a world that is evolving ever more rapidly, the connections and interactions we have to cope with are increasingly complex. We are facing vital issues such as securing our global energy supply and feeding a rapidly growing population on this planet. Isolated specialists cooped up in their ivory towers won't find the answers to all these issues. What we need are open minds—minds that recognize how and where disciplines mesh with each other. Minds that come up with new, better solutions as a result. We need diversity. By this I mean diversity of expertise, and I also mean diversity of cultural background.

It is more important than ever for scientists and the business community to move closer together and share ideas.

Cultural diversity in the strict sense is about a mix of nationalities, religious affiliations, and social traditions. Increasing internationalization in research and industry is throwing people together who are from very different cultural and educational backgrounds. They have to be able to get on together; indeed, they have to complement each other in terms of the strengths each one has to contribute. For this reason alone, open-mindedness is an absolute prerequisite for success in science and industry.

Apart from these more general cultural differences, each specialist discipline also has its particular culture. Chemists, biologists, engineers, and IT experts all have their own specialist language and a world view shaped by their particular discipline. If you've ever taken part in an interdisciplinary project, you'll know how many misunderstandings can arise from cultural differ-



Jürgen Hambrecht, born 1946, earned his PhD (1975) in organic chemistry with Eugen Müller at the Eberhard-Karls-Universität Tübingen. He joimed BASF in 1976 as a research chemist in the Polymers Laboratory and subsequently held various leading positions in hte company. In 1997 he was appointed to the Board of Executive Directors and became Chairman in May 2003. From 2003 to 2005 he was President of the German Chemical Industry Association. Since 2003 he has been Vice President of the Federation of German Industries, and from July 2006 he his the Chairman of the Asia-Pacific Committee of German Business.

 © 2006 Wiley-VCH Verlag GmbH & Co. KGaA, Weinheim

ences of these kinds. And yet, not only international collaboration, but cooperation between disciplines is more essential than ever in today's world. The first European Chemical Congress, scheduled to take place in Budapest in August this year, recognizes this fact, and it's an event we're all very excited about.



Examination of genetically engineered rice crops in a laboratory.

Networked Thinking, Lifelong Learning

All research areas that have produced new technologies with major future potential arose at the interface between multiple disciplines. Biotechnology, nanotechnology, new materials development, exploration of new energies and raw material sources, you name it—success in any of these areas depends on whether project team members from very different specialist backgrounds can communicate, work together, and add to each other's strengths.

In science and industry we also need minds and leadership personalities with enough vision to give guidance, provide direction, and weave the individual strands into a coherent pattern. We need personalities who define direction courageously and yet responsibly, but without limiting the thought and research curiosity of the individual. And we need excellent leadership talents now more than ever.

I believe it is absolutely essential for a successful future to promote interdisciplinary, networked thought—in every type of education and training and at every stage. Starting at school, intensifying at university, and continuing after graduation.

Now more than ever, graduates must be willing and able to continuously update and expand their acquired expertise. And now more than ever, any graduate who has just completed training can expect at least once in his or her life to have to acquire an entirely new qualification unrelated to his or her original trade. This situation applied in the past and continues to apply in the present as far as my own professional biography is concerned. The area of research I was first interested in was polymeric by-products of low-molecular-weight organic synthesis processes.[2] My scientific curiosity, expressed in the topic of my PhD thesis, brought me straight into the polymer chemistry division when I joined BASF. Later on, I was involved with very different issues: purchasing and business administration, for instance, and above all management and leadership. Lifelong learning is a must in this day and age. This applies in all professions and disciplines, both for providers of routine services and for highly specialized experts. It applies in particular to all those who intend to or have already assumed leadership responsibilities.

Lifelong learning is a must in this day and age.

Movement in the Education System

The following part deals specifically with changes in the German education system. The concerns and aims are of relevance to all societies. How does the German education system prepare young people to meet all these requirements? I think it probably does a much better job than people give it credit for, despite the public moaning that seems to be reaching another crescendo at the moment. It is right and proper to point out negative trends and deficiencies: the increasing gap between educational elites and people from educationally remote socioeconomic strata, poor integration of migrants, lack of promotion of special talents, university courses that are too long and too inefficient, brain drain to other countries. Measures to promote self-initiative and entrepreneurship also leave a lot to be desired in Germany. There's plenty of room for improvement and reform. Nevertheless, it is counterproductive to slam the German educational system as an unmitigated disaster.

While recognizing that there is plenty than deserves criticism, we must not forget that things have definitely started to change for the better in the German education system. For instance, there is an increased awareness and appreciation of the fact that good education starts early. Children are born with a keen desire to learn and discover, and we need to build on these instincts early on. Industry and business are starting to recognize their responsibilities in this regard and many companies are helping to improve the education of children in this country by sponsoring projects on their own or in cooperation with the public sector. One example of the industry's growing commitment is the Knowledge Factory,[3] a platform combining the activities of a large number of German businesses in a bid to promote education and entrepreneurship. Effective models of cooperation between the private sector and public-sector education institutions are textbook examples of ways to make school a better preparation for life.

Reforms of tertiary education are also up and running. After decades of the notorious complaints about mass universities, inefficient teaching, poor scientific excellence, and loss of international reputation, profound changes are apparent wherever you look. There has been extensive and long-standing public debate on the pros and cons of introducing Bachelor and Master degrees, elite universities, and the forming of excellence clusters. The Association of Donors for the Promotion of Science (Stifterverband für die Deutsche Wissenschaft[4]) was a major catalyst here. Our tertiary education institutions are now taking action, and this is a very welcome development.

The Bachelor/Master system has a number of advantages over the conventional German degree system (comprising a two-year "Vordiplom" (intermediate diploma) which is not an academic qualification but a necessary requirement to commence the three-year "Dip-

 © 2006 Wiley-VCH Verlag GmbH & Co. KGaA, Weinheim

lom"/Master), especially for those studying chemistry. As well as facilitating international comparability and hence offering students better opportunities to gain valuable experience abroad during their course of studies, the Bachelor system is better geared toward accommodating students' individual abilities and career plans. For instance, a student who stops studying after three years in our conventional degree system, for whatever reason, is simply a dropout with no qualifications. In contrast, a student who leaves after the same number of years with a Bachelor degree has a bona fide professional qualification. And all those who wish to obtain further qualifications, either through specialization in the same subject, or by obtaining related university or non-university training, or indeed by switching to a different area for a good reason, can do so under potentially better circumstances.

Good bye, Humboldt?

The prospect of adapting to the Anglo–American university system has prompted moaning and lamentation in many quarters. Critics say the Anglo–American model will make university education too much like school, promote a one-sided, stereotyped focus on a particular discipline, and leave little or no room for the development of individual, personal strengths. They say Germany is turning its back on the Humboldt idea of education, which was once a role model emulated everywhere in the world. Since I made my admiration of the virtues of the generalist like Humboldt very clear at the outset of this Essay, I'd like to say a few brief words on this topic now.

In my research work, as a leader of a globally operating corporation, and also in my private life, I've always seen the truth of a very fundamental principle confirmed: there are no patent remedies. It would be foolish to believe the introduction of the Anglo–American system is going to be a cure-all with a built-in guarantee of improving our tertiary education in Germany. Whether any system succeeds crucially depends on how it is put into practice in the nitty-gritty and how well it is applied in a specific individual case. If students do not benefit from appropriate guidance and continue to receive a poor level of individual supervision from their tutors and lecturers, a Bachelor system will change nothing for the better. If interfacing with other disciplines is not encouraged, for example on the basis of a wider range of options for combining subjects, and if interdisciplinary dialogue does not become an integral part of routine operations and curricula at our institutions of tertiary education, then these institutes will not be better equipped to meet the challenges of the future, no matter what system is employed. If more energy and resources are channeled into a bureaucratic evaluation process than in identifying and promoting young talents, then the quality of our science will not improve.

That is why I believe it is wrong to polarize between the Anglo–American system and the Humboldt ideal. In any case, Humboldt's spirit as good as departed from our German universities years ago. I firmly believe that the introduction of Bachelor and Master degree programs opens up many opportunities to change our tertiary education system for the better.

Talking to Each Other

The incentive and motivation of our young people toward further personal and professional development ultimately depends not on a particular university system or on how stringently knowledge and performance are evaluated. Rather, it depends primarily on the dedication and example set by competent, credible, and empathic teachers. I for my part know no better source of inspiration than personal interaction with a counterpart who provides intellectual and personal stimulation. Facilitating and promoting this should be a cornerstone of the efforts to reform tertiary education in Germany.

Now, and even more so in the future, we need people in industry, in politics, and everywhere in society who are not only at the cutting edge in their particular field, but who are mature and stable personalities with social skills and the willingness and ability to shoulder responsibility. It is therefore a fundamental task of our educational institutions to challenge and encourage our young people in their personal development. It is important now more than ever, in particular for the elites of the future, to exhibit not only professional expertise, but also to contribute open-mindedness, an ability to listen, empathy, and willingness to engage in true dialogue. Because leadership primarily means communication.

The elite require not only professional expertise, but must also contribute open-mindedness to engage in true dialogue. Because leadership primarily means communication.

Innovation and Responsibility

At this juncture I'd like to broach an issue that has to do with poor communication and a lack of openness toward areas beyond the confines of a specialist discipline. Increasing specialization in the sciences has resulted in a growing level of wordlessness and alienation from the public. In the chemical industry in particular we have long been guilty of showing too little of ourselves to the so-called "man in the street". We have failed to communicate the immense benefit of chemistry. People tend to be wary or indeed afraid of what they don't know and don't understand. That is what has given the chemical industry a bad name, and nothing endures as tenaciously as a poor reputation. Our industry has been working for many years to restore this lost faith.[5] Incidentally, this is an area to which universities and university teaching staff could add much more.

Fear of, and hostility to technology are the poorest advisors imaginable when it comes to shaping our future. However, public debate all too often tends to favor those who devote all their efforts to exposing the risks of innovative developments whilst blocking out their opportunities. Of course we have to identify and minimize potential risks in order to prevent damage to human

 © 2006 Wiley-VCH Verlag GmbH & Co. KGaA, Weinheim

health and the environment. This precautionary principle[6] is a paramount concern of the chemical research community and industry in particular. Nevertheless, it would be nonsense to demand one hundred percent exclusion of even the remotest risk, for to do so is a basic scientific impossibility. To compound matters, this kind of nonsensical misinterpretation is a complete reversion of the laudable precautionary principle. Preventing opportunities is every bit as irresponsible as closing your eyes in the face of real threats. Those who misuse the precautionary principle as a zero-risk principle not only risk paralysis and stagnation of today's societies but are also ruining the chances of future generations to achieve a better quality of life.

The well-being of future generations depends on our willingness and ability to produce greater innovation. The European Union, and Germany as part of that union, will be able to keep pace internationally as a location of science and business only if we excel in research and development. The European Council's "Lisbon Strategy" set the target of raising European research and development investment to 3% of the European Union's gross domestic product by 2010. To achieve this target, it is not enough to set aside the necessary financial resources; we also have to rekindle people's interest in and love of innovation and progress.

I would therefore like to close by appealing to all parties with a special responsibility toward the public, whether they are in research and teaching, in universities or industry, in politics or interest groups: We are ambassadors of progress. It is up to all of us to reach out to the public, encourage open dialogue, convincingly plead the case of science and technology and their social benefits, and enlist the support of the largest possible number of people in the mission of shaping our future together.

[1] *Die BASF. Eine Unternehmensgeschichte* (Ed.: W. Abelshauser), C. H. Beck, München, **2002**.

[2] "Notiz zur Umsetzung von 3,4-Diphenyl-1,2-cyclobutendion mit Grignard-Verbindungen": J. Hambrecht, H. Straub, E. Müller, *Chem. Ber.* **1975**, *107*, 3962–3965; "Diin-Reaktion 42. Komplexchemische Synthese substituierter 1,4-Naphthochinone und isoheterokondensierter Benzochinone": J. Hambrecht, E. Müller, *Justus Liebigs Ann. Chem.* **1977**, 387–399.

[3] http://www.wissensfabrik-deutschland.de.

[4] Stifterverband für die Deutsche Wissenschaft, *Vitaler Austausch*, Bericht 05–06, Mai **2006**. http://www.stifterverband.de.

[5] See, for example, the image campaign of VCI "Chemie. Element unseres Lebens." http://www.element-unseres-lebens.de; http://www.vci.de.

[6] See United Nations General Assembly, *Report of the United Nations Conference on Environment and Development*, A/CONF. 151/26 (Vol.I), August 12, **1992**; Commission of the European Communities, *Communication from the Commission on the Precautionary Principle*, Brussels, February 2, **2000**.

 © 2006 Wiley-VCH Verlag GmbH & Co. KGaA, Weinheim

Controlled Radical Polymerization

DOI: 10.1002/anie.200503785

Relationship between One-Electron Transition-Metal Reactivity and Radical Polymerization Processes

*Rinaldo Poli**

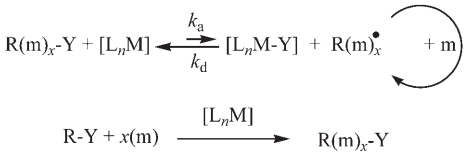
Keywords:
bond energy · oxidative addition · polymerization · radical reactions · transition metals

Controlled radical polymerization has come along in leaps and bounds following the development of efficient transition-metal catalysts for atom-transfer radical polymerization. Another type of controlled radical polymerization process, namely organometallic radical polymerization, uses the reversible formation of metal–carbon bonds. Metals are also implicated in catalytic chain transfer, a process that involves the abstraction of hydrogen atoms. This Minireview discusses the importance of one-electron transition-metal reactivity in metal-mediated controlled radical polymerization processes.

Introduction

Controlled radical polymerization (CRP) is one of the most spectacular advances in polymer chemistry in recent years. Consequently, materials with well-defined features such as architecture, average molecular weight, molecular-weight distribution, and chain-end functions have become accessible through the use of a variety of polar monomers and friendlier polymerization techniques (e.g. unpurified organic solvents, emulsions, etc.). The key requirement to achieve this level of control is to reduce to negligible levels the chances for two propagating radicals to encounter each other and result in irreversible bimolecular terminations. Of the various strategies employed to date, atom-transfer radical polymerization (ATRP) has attracted the greatest attention since it was first reported in 1995 by Wang and Matyjaszewski[1] and Sawamoto and co-workers.[2]

In ATRP, a transition-metal complex acts as a regulator of the concentration of radicals by reversibly transferring a halogen atom to the active radical, thereby transforming it into a halogen-terminated dormant species, without being incorporated itself into the polymer chain. Therefore, the metal complex acts merely as a catalyst and can potentially be recovered and recycled. The overall process can be described as a catalyzed sequential insertion of a certain (controlled) number of monomer (m) units into the carbon–halogen bond of a suitable alkyl halide initiator (see Scheme 1) and considered as a natural extension of the metal-catalyzed atom-transfer radical addition (ATRA).[3] The catalyst $[L_nM]$ activates the dormant species $R(m)_x$–Y by accepting its terminal halogen atom, Y, and generates the active radical $R(m)_x^{\bullet}$ and an oxidized complex $[L_nM–Y]$. The latter complex is related to the catalyst by an atom transfer, which results in a difference of one electron in the metal electronic configuration.

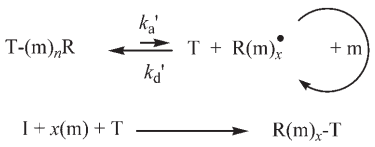


Scheme 1. Mechanism of atom-transfer radical polymerization (ATRP). R = alkyl; m = monomer; Y = halogen atom; $[L_nM]$ = catalyst (L = ligand, M = metal).

Before the fundamental principles of ATRP were uncovered, however, transition-metal complexes had already been shown to control the concentration of radical species and thereby allow controlled chain growth in radical polymerization processes. The method is a particular example of the general concept of reversible addition–cleavage (see Scheme 2), in which a radical initiator I produces R• as a primary radical, as with classical free radical polymerization, while T is a reversible spin trap, namely a species that forms relatively labile bonds with the propagating radical. As T remains bound to the chain end in the polymer product, it is not a catalytic species. This procedure was first introduced by

[*] Prof. R. Poli
Laboratoire de Chimie de Coordination
CNRS UPR 8241
205 Route de Narbonne
31077 Toulouse cedex (France)
Fax: (+33) 5-6155-3003
E-mail: poli@lcc-toulouse.fr

InterScience
© 2006 Wiley-VCH Verlag GmbH & Co. KGaA, Weinheim



Scheme 2. Mechanism of reversible addition–cleavage polymerization. T = reversible spin trap; I = initiator.

Otsu and Tazaki using the trityl radical as spin trap[4] and was subsequently developed with nitroxide radicals (nitroxide-mediated polymerization (NMP)). A stable but labile T–R compound may also be used as initiator, for example, an alkoxyamine for NMP.

Wayland et al. extended this method to transition-metal complexes as spin traps, demonstrating the ability of Co porphyrin complexes to control the polymerization of acrylates.[5] In this case, the concentration of radicals is controlled by the reversible homolytic cleavage of the metal–carbon bond, a process that is closely related to the mechanism of action of vitamin B_{12}.[6] This reversible step, like the atom-transfer step in ATRP, is also a one-electron process. This reversible addition–cleavage methodology has also been termed "stable free radical polymerization" (SFRP) based on the notion that the spin trap T is often a stable radical, for example, a nitroxide radical or a metalloradical. However, this is not strictly a requirement and, as we shall see later, other species such as diamagnetic complexes and also complexes with triplet, quartet, and higher spin states may equally well assure this function. Besides NMP, other specially coined terms have also been used for specific reversible addition–cleavage processes, for example, CMRP for cobalt-mediated radical polymerization.[7]

Herein, we focus our attention on the reversible addition–cleavage phenomenon with T being a generic metal complex, and thus refer to this process as an organometallic radical polymerization (OMRP) because it involves the reversible cleavage of a metal–carbon bond. Another important method for controlling radical polymerization is reversible addition–fragmentation chain transfer (RAFT), in which the trapping function is exerted by dithioesters.[8,9] The latter methodology, however, combines the reversible addition–cleavage with degenerative transfer.[10] All of the above-mentioned methods differ in the nature of the moderator and the mechanism by which a dormant species is produced, but the consumption of the monomer always occurs through the same radical intermediates.

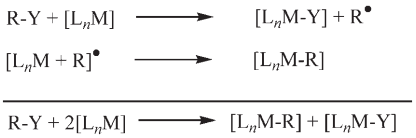
This Minireview describes the two fundamental one-electron processes involving transition metals, namely ATRP (Scheme 1) and OMRP (Scheme 2, T = transition-metal complex), as well as other one-electron processes that relate to controlled radical polymerization, and brings together established concepts of transition-metal coordination chemistry and the more recent notions of metal-mediated controlled radical polymerization.



Rinaldo Poli obtained his PhD at the Scuola Normale Superiore, Pisa, in 1985. After a postdoctoral stay at Texas A&M University (1985–87), he joined the University of Maryland, College Park, where he was promoted to full professor in 1995. He joined the Université de Bourgogne in France in 1996, and in 2003 he moved to Toulouse, where he currently teaches at the Ecole National Supérieur des Ingénieurs en Arts Chimiques et Technologiques and leads a research group at the Laboratoire de Chimie de Coordination. His research interests encompass various aspects of transition-metal chemistry, including aqueous organometallic chemistry and catalysis, and controlled radical polymerization.

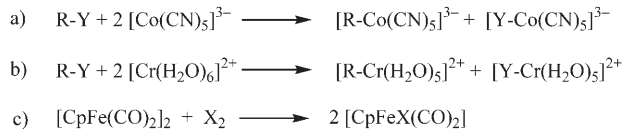
One-Electron Reactivity of Transition-Metal Complexes

In transition-metal chemistry and particularly in organometallic chemistry, studies of chemical reactivity are mostly focused on two-electron processes, such as ligand exchange, migratory insertion, and oxidative addition, because of their close relevance to a variety of catalytic processes. However, one-electron reactivity also plays a crucial role in many catalytic and stoichiometric reactions.[11] An important example is the one-electron oxidative addition of alkyl halides (Scheme 3), whereby one molecule of substrate splits homolytically to deliver the halogen atom to one metal complex molecule, and the alkyl radical to a second one. This process is favored when the metal can expand its electron count and coordination number by only one unit.



Scheme 3. One-electron oxidative addition process of alkyl halides in transition-metal chemistry.

A seminal example involves the pentacyanocobaltate(II) ion, $[Co(CN)_5]^{3-}$, which yields a 1:1 mixture of $[Y\text{-}Co(CN)_5]^{3-}$ and $[R\text{-}Co(CN)_5]^{3-}$ (Scheme 4a).[12] Another example is the reaction of alkyl halides with aqueous Cr^{2+} (Scheme 4b), providing access to $[R\text{-}Cr(H_2O)_5]^{2+}$, one of the earliest examples of stable alkyl derivatives of an open-shell transition metal, together with $[Y\text{-}Cr(H_2O)_5]^{2+}$.[13] This reaction is quite general for complexes of Cr^{II} and is a key process in the



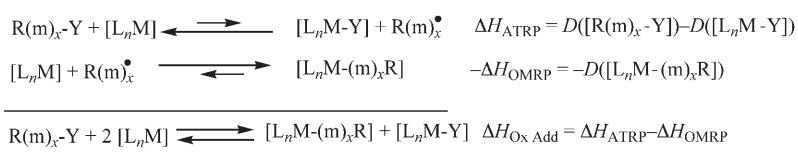
Scheme 4. Examples of one-electron oxidative addition processes. X = Cl, Br, I.

 © 2006 Wiley-VCH Verlag GmbH & Co. KGaA, Weinheim

Nozaki–Hiyama–Kishi reaction[14,15]—a reaction that is catalytic in chromium[16] and used in modern organic synthesis.

The reaction shown in Scheme 4c is also an example of one-electron oxidative addition, although its intimate mechanism seems to involve two-electron processes.[17] The $[CpFe(CO)_2]_2$ complex does not react spontaneously with alkyl halides, but this process may also be relevant in controlled radical polymerization (see below). The mechanism of the one-electron oxidative addition reaction of alkyl halides has been quite firmly established as involving first the abstraction of a halogen atom, followed by capture of the residual organic radical by the second transition-metal complex molecule (Scheme 3).[18,19] The reactivity of organic radicals with transition-metal complexes has also been extensively investigated by Kochi,[20] Espenson,[21,22] and Meyerstein and coworkers.[23,24] The reason for the first event to be the formation of M–Y, rather than that of M–R, is related to the greater homolytic bond strength of the M–Y bond relative to the M–R bond. Thus, if we consider the process to ideally take place by homolytic rupture of the R–Y bond to yield R$^\bullet$ and Y$^\bullet$, the unsaturated metal complex finds a greater thermochemical advantage to form a bond with Y first. Note that the two steps of this process correspond to the two equilibria needed to accomplish a metal-mediated radical polymerization (ATRP and OMRP, respectively).

It is quite ironic that coordination chemists, who have known and understood the mechanism of this reaction for such a long time, have not realized its potential for controlled organic synthesis (ATRA) or polymerization (ATRP and/or OMRP). Conversely, the polymer scientists who have exploited ATRP to such a sophisticated degree do not seem to have fully explored its limitations in terms of the constraints imposed by the one-electron oxidative addition process. We shall explore these limits herein.



Scheme 5. Interplay of ATRP and OMRP equilibria in controlled radical polymerization processes. D = bond-dissociation energy.

Consideration of Bond-Dissociation Energies in One-Electron Processes

The concepts developed in this section are a logical deduction from generally accepted considerations and reasonable assumptions. They allow the rationalization of a wealth of experimental facts, as will be shown from hereon in. We start from the observation, from a phenomenological point of view, that an OMRP process in which the organometallic complex is devoid of halogen atoms cannot enter the ATRP equilibrium, as is the case, for instance, for the Co porphyrin system. Unless halogen atoms are present in the coordination sphere, an OMRP is therefore uncontaminated by ATRP activation/deactivation equilibria. For systems that are set up under ATRP conditions, however, the situation may be more complicated. An analysis may be carried out using a variant of Scheme 3, in which the active radical has already inserted a certain number, x, of monomer molecules (see Scheme 5). Once $[ML_n]$ has accepted the halogen atom and generated the active radical R(m)$_x^\bullet$ (Scheme 5, first equilibrium), the latter may form the R(m)$_x$–Y dormant species upon encountering the $[Y–ML_n]$ spin trap. On the other hand, the propagating radical may also encounter a second $[ML_n]$ molecule, leading to R(m)$_x$–ML_n, the OMRP dormant species (Scheme 5, second equilibrium). Thus, an ATRP process may be contaminated by the OMRP activation/deactivation equilibrium and ultimately by the one-electron oxidative addition process.

To understand all the possibilities and limitations, it is useful to consider the thermochemistry of the two equilibria in terms of the homolytic bond-dissociation energies (D). The OMRP equilibrium is simply the homolytic rupture of the metal–carbon bond, thus $\Delta H_{OMRP} = D([L_nM–(m)_xR])$. The ATRP equilibrium formally involves the homolytic rupture of the R(m)$_x$–Y bond and the formation of the Y–ML_n bond, therefore $\Delta H_{ATRP} = D(R(m)_x–Y) – D([L_nM–Y])$.

From the point of view of an OMRP system, as it is uncontaminated by ATRP its capability to control the radical polymerization is simply related to $D([L_nM–(m)_xR])$. Thus, if the metal–carbon bond is too weak, the $[ML_n]$ species has insufficient ability to trap the radicals and the resulting OMRP equilibrium leads to too high a concentration of radicals, which translates into a significant proportion of bimolecular terminations and to an uncontrolled process. If, at the other extreme, the R(m)$_x$–ML_n bond is too strong (namely, the equilibrium is displaced towards the dormant species), no significant amount of radicals will be generated and polymerization does not take place. Finally, when the bond strength is *just right*, a controlled polymerization will take place (see Figure 1). This discussion is valid, of course, when there are no halogens in the system, thus no radical trapping by the ATRP equilibrium may occur.

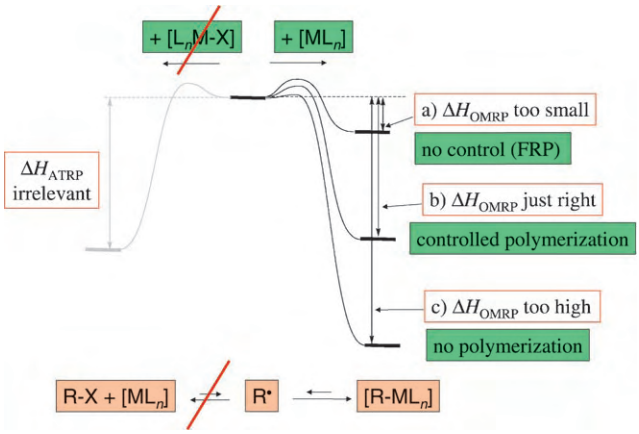


Figure 1. Effect of $\Delta H_{OMRP} = D([R(m)_x–ML_n])$ values in organometallic radical polymerization (OMRP).

© 2006 Wiley-VCH Verlag GmbH & Co. KGaA, Weinheim

As to the meaning of "just right", it is clear that more than a single value of the metal–carbon bond-dissociation energy will be suitable for a controlled radical polymerization process. Intuitively, a stronger bond will lead to a lower concentration of radicals at equilibrium and therefore to a slower polymerization but at the same time to a better control. However, the so-called "persistent radical effect"[25] ensures that a controlled process will also occur when the system generates a rather high amount of free radicals initially, because the spin trap, $[ML_n]$, is stable and will accumulate in the system following the initial disappearance of the reactive radicals caused by the irreversible terminations. The result is a self-regulation of the OMRP equilibrium. This observation also serves to alert us about the importance of the dynamic radical concentration, that is, the equilibrium position, which depends on the free energy and not on the enthalpy. Thus, looking merely at the thermochemistry is insufficient. In fact, the concentration of other species (e.g. $[ML_n]$, which accumulates because of the irreversible terminations) is not the only factor that plays an important role; the reaction entropy also affects the ability of the system to control the polymerization. As the OMRP spin-trapping reaction is clearly characterized by a negative reaction entropy, the value of the bond-dissociation energy for $R(m)_x{-}ML_n$ overestimates the stability of the OMRP dormant species.

If we now look at a system that is set up under ATRP conditions, the outcome depends first of all on the value of ΔH_{ATRP}. If this enthalpy difference is too small, too large, or just right, the amount of free radicals generated by the atom-transfer process will correspondingly be too large, too small, or just right (note that the ATRP equilibrium involves the same number of molecules on both sides, and thus $\Delta S_{ATRP} \approx 0$ or $\Delta G_{ATRP} \approx \Delta H_{ATRP}$). However, in this case we also need to consider the effect of the coupled OMRP equilibrium. As the ATRP equilibrium will generally be shifted toward the combination of ATRP catalyst $[ML_n]$ (which is also the OMRP spin trap) and dormant species R–Y, a fair concentration of OMRP spin trap will be available. The simplest case to examine is that in which ΔH_{ATRP} is too large (Figure 2). As the amount of radicals at equilibrium will be too small, there will be essentially no polymerization. Under these conditions, the value of ΔH_{OMRP} is irrelevant.

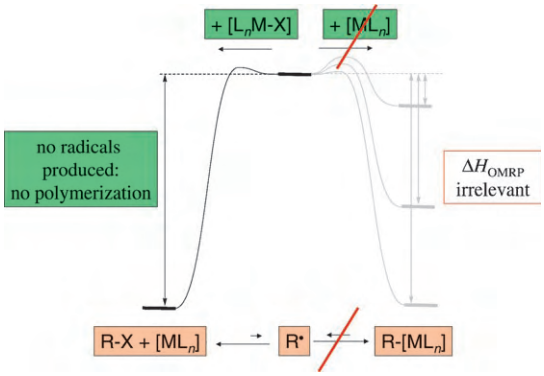


Figure 2. Possible pathways in ATRP when ΔH_{ATRP} is too large.

Under the opposite circumstances, that is, if ΔH_{ATRP} is too small, the free radicals will not be efficiently trapped and the only possible regulation of their concentration may be provided by the OMRP equilibrium (see Figure 3). If ΔH_{OMRP}

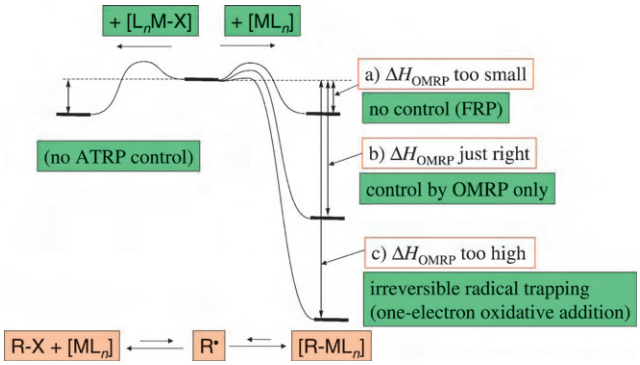


Figure 3. Possible pathways in ATRP when ΔH_{ATRP} is too small.

is also too small (case a), no efficient trapping is possible and the polymerization will be uncontrolled. If, at the opposite extreme (case c), ΔH_{OMRP} is too large, all radicals generated by the ATRP equilibrium will be irreversibly trapped by the OMRP equilibrium. The overall result is an irreversible one-electron oxidative addition and no polymer is formed. Finally, if ΔH_{OMRP} is just right (case b), a controlled polymerization will take place. Note, however, that the control is ensured by the OMRP equilibrium, even though the system is set up under ATRP conditions.

The thermochemistry of the overall one-electron oxidative addition ($\Delta H_{Ox\,Add}$, Scheme 5) favors the combination of oxidized complexes. Therefore, when the ATRP process is set up starting from a 1:1 ratio of $[ML_n]$/R–Y, as is often the chosen stoichiometry, the resulting polymer will contain a 1:1 mixture of $[ML_n]$- and Y-end-functionalized chains. However, only one half of the $[ML_n]$ complex exerts its regulating function—the polymer-chain-capping complex, by the OMRP mechanism—because the other half is sequestered in the $[L_nM{-}Y]$ complex, a poor spin trap for the ATRP mechanism.

Finally, we need to examine the situation in which ΔH_{ATRP} is just right (see Figure 4). The meaning of "just right" is

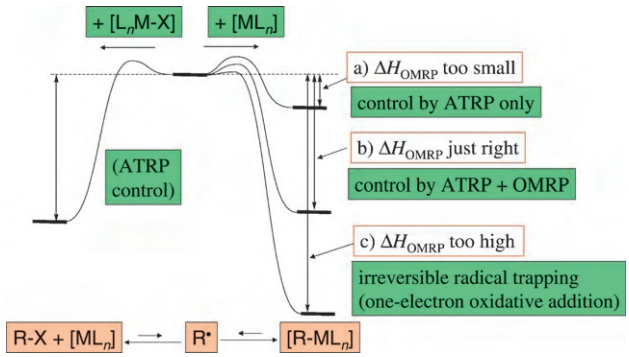


Figure 4. Possible pathways in ATRP when ΔH_{ATRP} is just right.

 © 2006 Wiley-VCH Verlag GmbH & Co. KGaA, Weinheim

identical here to the OMRP situation examined above; that is, the persistent radical effect operates in this case too. Under these circumstances, in the limiting situation where ΔH_{OMRP} is too small (case a) there is no efficient trapping of the active radical by the ATRP catalyst to yield the organometallic dormant species. However, trapping still takes place by the oxidized $[L_nM{-}Y]$ complex to yield the halogen-capped dormant species $R(m)_x{-}Y$, and therefore a controlled polymerization process takes place. This case refers to a pure ATRP process. When ΔH_{OMRP} is also just right (case b), both trapping events will occur simultaneously. In this case, the polymerization will be controlled and the two mechanisms, ATRP and OMRP, will cooperate. A better control (and a slower polymerization) is expected relative to the case where ΔH_{OMRP} is too small, because the OMRP equilibrium contributes to further lower the concentration of propagating radicals. Finally, when ΔH_{OMRP} is too large (case c), trapping by $[ML_n]$ will be irreversible. Therefore, even though the ATRP equilibrium is suitably placed to provide a controlled polymerization process, no polymerization will be possible and the reagents will lead quantitatively to the products of the one-electron oxidative addition.

The bond energy criteria elaborated above illustrate the thermochemical conditions required to achieve a controlled radical polymerization by either (or both) mechanisms. However, note that these conditions are necessary but not sufficient to ensure that the polymerization is well controlled; a crucial kinetic condition must also be considered, namely that the trapping rates must be fast relative to the propagation rates (i.e. a low energy for the transition states leading to the dormant species).

Interplay of ATRP and OMRP

The conditions examined in Figure 4 are important for radical polymerizations carried out under ATRP conditions. Generally, it is implicitly assumed that ΔH_{OMRP} is small (case a) as the vast majority of ATRP studies that report new catalysts only make reference to a mechanistic scheme such as that shown in Scheme 1. Very few studies have explicitly challenged this assumption, asking the specific question of whether the ATRP catalyst could generate an organometallic dormant species. One such example is the interaction of Cu^I complexes with the growing radical chains of polystyrene and poly(methyl acrylate). It was found that CuBr/4,4′-di-5-nonyl-2,2′-bipyridine and CuOTf/4,4′-di-*tert*-butyl-2,2′-bipyridine systems (OTf = trifluoromethanesulfonate) have no effect on the rate of polymerization of styrene (e.g. initiated by the thermal decomposition of azobis(isobutyronitrile) (AIBN)) but significantly slow down the rate of polymerization of methyl acrylate (MA).[26] This finding shows that there is a reversible interaction between the propagating methyl acrylate derived radicals (but not those derived from styrene) and the Cu^I metal center. However, Matyjaszewski and Woodworth noted that the interactions are very weak and neither improve the control of molecular weight and polydispersity nor affect tacticities, which are the same as in conventional free radical polymerization without copper complexes. They concluded that control in ATRP does not originate from interactions of growing radicals with copper complexes but in the reversible transfer of halogen atoms. However, the same situation may not be valid in other cases. We were the first to report a system that controls the radical polymerization of styrene under both ATRP and OMRP conditions.[27] The system in question is $[CpMoCl_2L_2]$, a cyclopentadienylmolybdenum(III) system in which L_2 is bis(diphenylphosphino)ethane (dppe), $(PMe_3)_2$, or η^4-butadiene. We later observed the same phenomenon when L_2 was ArN=CH−CH=NAr (Ar = 2,6-diisopropylphenyl).[28] As the Mo^{III} complex can reversibly trap the propagating radical under OMRP conditions and as its concentration remains high under ATRP conditions, it is evident that both trapping mechanisms occur simultaneously (case b, Figure 4).

The $[CpMoCl_2L_2]$ complexes contain halogen atoms in the coordination sphere, therefore, after trapping the propagating radical to form a $[CpL_2Cl_2Mo{-}(m)_xR]$ dormant species, the latter could act, in turn, as an ATRP spin trap. If this happens, a mixture of $R(m)_x{-}Cl$ and a new molecule, a Mo^{III}-capped polymer chain $[R(m)_x{-}MoClL_2Cp]$, would form; that is, the OMRP system would operate through the ATRP mechanism. However, analyses of the resulting polymer by ^1H NMR spectroscopy and MALDI-TOF mass spectrometry revealed no chlorinated end-functions in that particular case.[27] It can be imagined that transfer of a Cl atom from a sterically encumbered $[R(m)_x{-}MoClL_2Cp]$ complex to the propagating radical (itself a sterically hindered molecule) may be an unfavorable process relative to trapping by the less encumbered and more mobile $[CpMoCl_2L_2]$. Whether this phenomenon is true in general, however, is not known, and the possible contamination by ATRP for a system set up under OMRP conditions, when the organometallic dormant species contains a halogen atom, should always be considered as a possibility.

It is now pertinent to question whether other metal catalysts might display the same phenomenon of ATRP/OMRP dual control. A wide range of transition-metal complexes have been reported to control the radical polymerization of various monomers under typical ATRP conditions. These include $Ti^{III}X_3$ (X = Cl, Br),[29] $[ReO_2I(PPh_3)_2]$,[30] a variety of Fe^{II} coordination compounds,[31–34] $[RuCl_2(PPh_3)_3]$,[2] $[OsCl_2(PPh_3)_3]$,[35] $Co(O_2C_7F_{15})_2$,[36] $[RhCl(PPh_3)_3]$,[37] $[Ni(PPh_3)_4]$,[38] $[Ni\{o,o'\text{-}(Me_2NCH_2)_2C_6H_3\}Br]$,[39] $Pd(OAc)_2/PPh_3$,[40] and $SmCl_2$/lactic acid.[41] For the particular case of $[Cp_2TiCl]$, it has been proposed that both ATRP and OMRP processes take place contemporarily; the reactions are carried out under "reverse" ATRP conditions by thermally decomposing AIBN in the presence of $[Cp_2TiCl_2]$.[42,43] A related system, involving a $[Cp_2TiCl]$-induced oxirane ring opening as the initiation process, also seems to involve the reversible formation of a Ti^{IV}-capped dormant species.[44,45] The latter system is interesting because the initiation step is an ATRP-like activation that yields $[Cp_2(Cl)Ti{-}OCH_2CH_2^{\bullet}]$; however, the process is irreversible because of the high homolytic strength of the $Ti^{IV}{-}O$ bond as a result of the oxophilic character of titanium. The controlling function is assured by an OMRP-type trapping process by additional $[Cp_2TiCl]$.

© 2006 Wiley-VCH Verlag GmbH & Co. KGaA, Weinheim

Of the numerous reports of ATRP using Fe^{II} systems, to the best of our knowledge none of these addresses the possibility of simultaneous OMRP control through the formation of organometallic Fe^{III} dormant species. On the other hand, alkyl derivatives of Fe^{III} have been described, although they are relatively unstable compounds. For instance, Kochi has shown that the one-electron oxidation of stable $[Et_2Fe(bpy)_2]$ yields $[Et_2Fe(bpy)_2]^+$ (bpy = 2,2′-bipyridyl), which then decomposes in a variety of ways including through Fe–C bond homolysis.[46] Also, [(porphyrin)Fe^{III}-(alkyl)] systems[47,48] were shown to readily undergo Fe–C bond homolysis.[49] The generation of Fe^{III} alkyl species was recently suggested as an event leading to catalytic chain transfer (CCT; this phenomenon will be discussed later on).[50]

To the best of our knowledge, the capability of $[RuCl_2(PPh_3)_3]$ to trap radicals has also not been considered.[51] Quite recently, the osmium complex $[OsCl_2(PPh_3)_3]$ was shown to effectively control, like our $[CpMoCl_2L_2]$ system, the radical polymerization of styrene under both ATRP and OMRP conditions.[35] Moreover, the reactions carried out under OMRP conditions did not reveal any chlorinated end-groups, whereas those carried out under ATRP conditions did not reveal any osmium-containing end-groups. As with our $[CpMoCl_2L_2]$ complexes, the $[OsCl_2(PPh_3)_3]$-controlled polymerization set up under OMRP conditions does not appear to be contaminated by the ATRP process, whereas the polymerization set up under ATRP conditions must necessarily feature the OMRP trapping process. However, the system is energetically more stable as the sum of the Os^{II} catalyst plus the halogen-capped dormant species, leading to a polymer product capped only by halogen atoms under ATRP conditions. A given Os^{III}–C bond is certainly expected to be stronger in a homolytic sense than the corresponding Ru^{III}–C bond, but it would be interesting to establish whether Ru^{II} complexes display efficient trapping of propagating radicals.

Until recently, Co^{II} complexes had been proven effective only as OMRP spin traps and as chain-transfer catalysts (see below). However, it was recently reported that cobalt(II) perfluorooctanoate can control the polymerization of styrene initiated by (1-bromoethyl)benzene (BEB) under typical ATRP conditions.[36] The efficiency of the same system was also reported under typical OMRP conditions (thermal decomposition of AIBN), although the authors incorrectly termed this process as "reverse ATRP"; in fact, no halogen is present, other than that of the $CoCl_2$ precursor, which is transformed to $Co(O_2CC_7F_{15})_2$ in situ by reaction with sodium perfluorooctanoate). Therefore, a question remains as to whether the process with $Co(O_2CC_7F_{15})_2$/BEB system involves a combination of ATRP and OMRP (case b, Figure 4) or is a pure OMRP (case b, Figure 3). Weiser and Muelhaupt reported the presence of halogen end-groups (from NMR studies) and the absence of cobalt (by atomic absorption spectroscopy), suggesting formation of the ATRP dormant species (apparently, even for the polymer obtained under OMRP conditions). However, the evidence is not compelling because the polymer was treated with HCl-containing methanol before analysis.

Another recent study reported the use of $CoCl_2$/Me_6tren (Me_6tren = tris(2-dimethylaminoethyl)amine) to control the polymerizations of styrene and methyl methacrylate (MMA) under typical ATRP conditions with ethyl 2-bromoisobutyrate (2-EiBBr) as initiator, although the resulting polymers showed high polydispersities (1.6–1.8).[52] There was no mention of possible OMRP trapping therein, and the characterization of the chain-end functions (again, only by NMR spectroscopy) is not unambiguous. Interestingly, the control of these processes was improved by the addition of a few percent of $FeBr_3$ or $CuBr_2$. Under these conditions, an Fe^{II}/Fe^{III}- or Cu^{I}/Cu^{II}-based ATRP mechanism apparently becomes operational. It was proposed that the higher oxidation state Fe or Cu complex traps more efficiently the growing radical chain and then is reoxidized by the Co^{III}/Me_6tren species. Thus, the process would remain controlled by the Co^{II}/Co^{III} pair through an ATRP mechanism. However, amine-supported low-spin Co^{III} complexes are not strong oxidants[53,54] and the redox equilibria shown in Scheme 6 are likely shifted toward the Co^{III} species and the more-active Fe^{II} or Cu^{I} catalyst. It then appears that the improved control upon addition of $FeBr_3$ or $CuBr_2$ likely originates from a switch to an Fe^{II}/Fe^{III} or Cu^{I}/Cu^{II} ATRP mechanism.

$$FeBr_2/Me_6tren + CoCl_2Br/Me_6tren \rightleftharpoons FeBr_3/Me_6tren + CoCl_2/Me_6tren$$

$$CuBr/Me_6tren + CoCl_2Br/Me_6tren \rightleftharpoons CuBr_2/Me_6tren + CoCl_2/Me_6tren$$

Scheme 6. Redox equilibria between different ATRP catalysts. Me_6tren = tris(2-dimethylaminoethyl)amine.

The Effect of Irreversible Radical Trapping on Initiator Efficiencies

The situation corresponding to case c in Figure 3 and Figure 4 merits further analysis. The considerations that are discussed here are valid for any process in which the propagating radical is trapped irreversibly by any reaction, but not necessarily leading to the irreversible formation of a metal–carbon bond. Specifically, the propagating radical may also bind irreversibly to one of the ligands. As we concluded earlier, under these circumstances no polymerization should result; however, this is only true provided that the reaction products of the radical-trapping reaction do not involve themselves in radical-controlling equilibria. Note that the one-electron oxidative addition reaction is characterized by a $[ML_n]$/R–Y stoichiometry of 2:1 (Scheme 3). However, most ATRP processes are set up with a 1:1 stoichiometry, under the assumption that only the atom-transfer equilibrium of Scheme 1 is operative (i.e., the first step of Scheme 3). Under these conditions, and if the reaction leads to the oxidative addition products $[L_nM–Y]$ and $[L_nM–R]$ (or any other product of radical trapping), then 50% of the alkyl halide that was initially present remains unconsumed. At this point, a controlled polymerization may still take place if the $[L_nM–Y]$ molecule or the $[L_nM–R]$ molecule, or both, has the ability to function as an ATRP catalyst. The initiator efficiency (f) will be reduced, to $f = 0.5$ for this particular example of 1:1 stoichiometry.

© 2006 Wiley-VCH Verlag GmbH & Co. KGaA, Weinheim

The initiator efficiency is readily determined experimentally from the ratio of the theoretical and experimental molecular weights. When only half of the initiator molecules give rise to growing polymer chains, the number-average molecular weight for the polymer isolated at any given monomer conversion will be twice that calculated if the initiator had 100% efficiency. There are several reports of unusually low initiator efficiencies, with no satisfactory interpretation offered. In some cases initiator efficiency values are not mentioned, but low values are calculated by taking the ratio of the expected and the experimentally observed number-average molecular weights. We reported a few systems that are characterized by quite low initiator efficiencies, for instance, $f = 0.55$ for the styrene polymerization process shown in Figure 5.[55] A similar behavior is observed for the analogous polymerization of methyl acrylate using the same catalyst ($f = 0.6$).

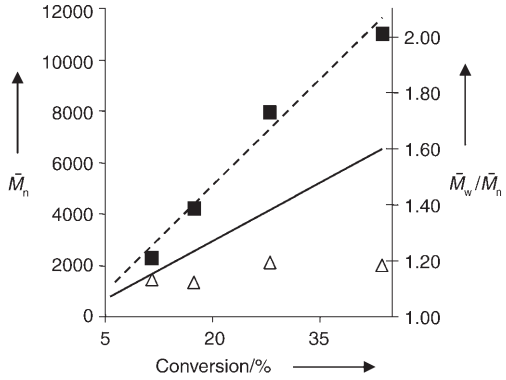


Figure 5. Experimental (squares) and theoretical (solid line) number-average molecular weights (M_n) for the polymerization of styrene under ATRP conditions: [$CpMoCl_2$(*i*PrNCHCHN*i*Pr)]/Al(O*i*Pr)$_3$/MeCHICOOEt in toluene solution (30% v/v) at 90°C. The polydispersity index ($\bar{M}_w/\bar{M}_n$) is shown as triangles.[55]

There are two main reasons for low initiator efficiencies: The first of these is related to a slow rate of activation relative to the rate of propagation. Under these circumstances, only a fraction of initiator molecules is activated at a particular time and will grow at a regular rate, while another fraction has not yet been activated. This behavior results in a broad polydispersity. However, with time all the initiator molecules will eventually be activated and the efficiency factor f will tend to one (see Figure 6a). The second reason behind low initiator efficiencies is a slow deactivation of the propagating radicals, for example, a small value of k_d in Scheme 1. In this case, the concentration of propagating radicals builds up to higher levels, inducing a significant amount of bimolecular terminations. This behavior also results in a broad molecular-weight distribution. In this case, the corresponding amount of initiator molecules is lost irreversibly and the initiator efficiency factor remains low throughout the polymerization process. However, the persistent radical effect will set in sooner or later, bringing the process back under control, and the polydispersity will decrease with an increase in conversion (see Figure 6b). Clearly, the process represented in Figure 5

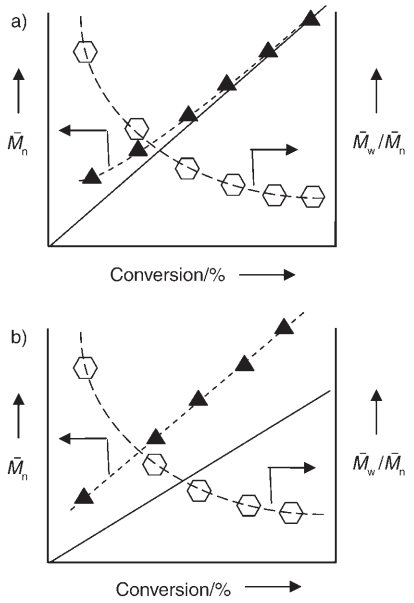


Figure 6. Typical evolution of molecular weight (triangles) and polydispersity (hexagons) when the initiator efficiency (f) is low: a) slow initiation rate; b) slow deactivation rate. The straight line represents the theoretical M_n for a living process ($f = 1$).

does not belong to either of these situations because the distribution is already rather narrow ($\bar{M}_w/\bar{M}_n < 1.2$) at the beginning of the polymerization and does not decrease further.

The hypothesis that an irreversible one-electron oxidative addition reduces the initiator efficiency when using [$CpMoCl_2$(*i*PrNCHCHN*i*Pr)] as the ATRP catalyst is proven by the following observations:[56] a) The MA/[$CpMoCl_2$(*i*PrNCHCHN*i*Pr)]/AIBN system, typical OMRP conditions, leads to no polymer whatsoever, proving that all radicals generated by the initiator are irreversibly trapped by the metal complex. b) Whereas the MA/[$CpMoCl_2$(*i*PrNCHCHN*i*Pr)]/MeCHICOOEt system (140:1:1; 30% in toluene), typical ATRP conditions, yields PMA with an initiator efficiency of 0.6 (see above), the corresponding system with a stoichiometry of 154:1:0.5 does not yield any polymer. However, after the addition of one further equivalent of MeCHICOOEt (1.5 equiv overall), polymerization starts in a controlled fashion and the experimental molecular weights are close to but slightly smaller than the theoretical values (calculated on the basis of only the equivalent of initiator added later; see Figure 7). As polymerization still takes place after one half of the initiator is irreversibly neutralized by [$CpMoCl_2$(*i*PrNCHCHN*i*Pr)], it means that the products of this irreversible reaction must themselves act as ATRP catalysts, generating polymer by the activation of the residual initiator.

The notion that the irreversible radical trapping may involve a ligand rather than the metal center itself is illustrated by a recent report on the activity of cobaltocene ([Cp_2Co]) in the ATRP of MMA initiated by $Me_2CBrCOOEt$.[57] On the basis of well-established organometallic chemistry, Wang et al. proposed the transformations described in Scheme 7. However, they reported an efficiency

© 2006 Wiley-VCH Verlag GmbH & Co. KGaA, Weinheim

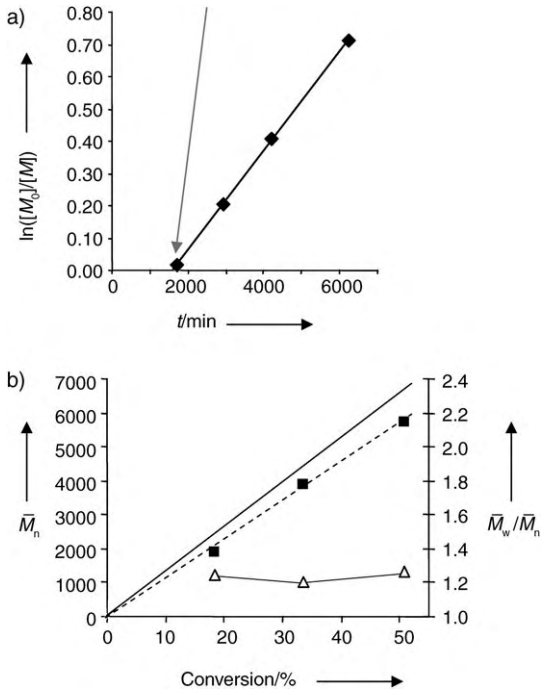
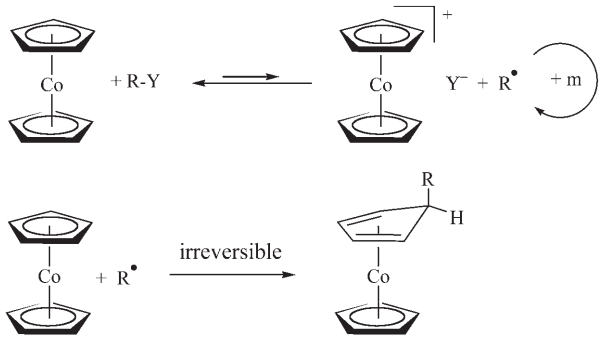


Figure 7. a) Kinetics as a function of time, and b) evolution of the molecular weight (squares) and polydispersity index (triangles) as a function of conversion, for a poly(methacrylate) (PMA) obtained in toluene (30% v/v) at 80°C with MA/[$CpMoCl_2$(*i*PrNCHCHN*i*Pr)]/Al-(O*i*Pr)$_3$ (MA/Mo/Al = 154:1:1). MeCHICOOEt was used as the initiator, 0.5 equivalents initially, followed by an additional 1 equivalent after approximately 1800 min (30 h; indicated with the gray arrow). The straight solid line in part (b) represents the theoretical M_n for a living process ($f = 1$).[56]

factor as low as $f = 0.25$ for a Co/RBr ratio of 1:1. Such a low value cannot be consistent with the suite of events described in Scheme 7, for which a minimum value of $f = 0.5$ should be observed for this particular stoichiometry and, moreover, under the assumption that one of the two products is an active ATRP catalyst. Furthermore, this scheme includes the hypothesis that the outer-sphere oxidation product $[Cp_2Co]^+Br^-$ is an efficient radical trap. Other studies, however, showed that outer-sphere complexes are less efficient radical traps in ATRP.[58,59] On the basis of other known organometallic chemistry of cobalt, this very low



Scheme 7. Proposed mechanism for the cobaltocene-catalyzed ATRP of methyl methacrylate (MMA).

efficiency factor may be rationalized by imagining that an additional fraction of available initiator further oxidatively adds to the Co^I product of Scheme 7 to yield Co^{II} and/or Co^{III} products, which could then operate as ATRP catalysts. Indeed, $[CpCo(\mu\text{-}Y)]_2$ and $[CpCoX(\mu\text{-}Y)]_2$ (X, Y = one-electron ligand) complexes have been described.[60] On the other hand, the $[Cp_2Co]^+Br^-$ system may well be an inactive complex. Various tests could further probe the mechanism of this reaction, for instance, through the use of $[Cp_2Co]^+Br^-$ under "reverse" ATRP conditions.

Extension to "Difficult" Monomers

A current challenge of CRP is to control the radical polymerization of monomers that generate more reactive radicals, such as vinyl acetate, vinyl chloride, vinylidene chloride, and ethylene. Much effort has been devoted to the ATRP method, but success has remained limited. The reason why these monomers are not easily controlled by ATRP is evident on the basis of the thermochemical considerations developed above and from the bond-dissociation energy values obtained for model R–Y molecules (see Table 1).[61]

Table 1: Computed (BP86/6–31G**) bond-dissociation energies (D) of representative R–Y molecules as propagating radical models for the monomers shown.[a]

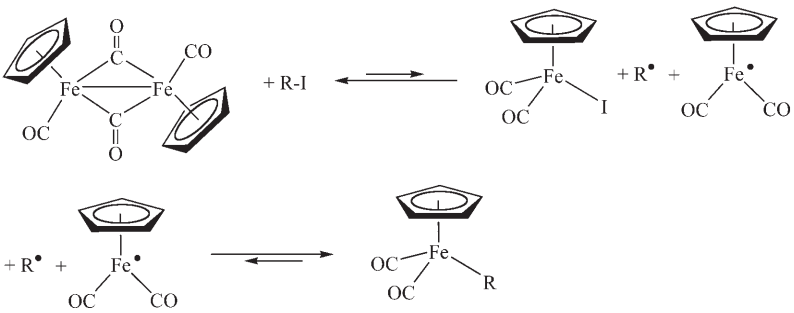
R	D [kcal mol^{-1}]		Monomer
	Y = Cl	Y = Br	
CH_3CH_2	83.1	73.1	ethylene
$CH_3CH(OCH_3)$	82.2	73.3	vinyl ether
$CH_3CH(O_2CCH_3)$	79.5	69.5	vinyl acetate
$CH_3CH(Cl)$	76.0	66.0	vinyl chloride
$CH_3CH(COCH_3)$	71.0	62.9	vinyl ketone
$CH_3CH(CO_2CH_3)$	69.9	61.4	methyl acrylate
$CH_3CH(Ph)$	68.5	59.9	styrene
$(CH_3)_2C(CO_2CH_3)$	66.9	58.9	methyl methacrylate
$CH_3CH(CN)$	65.9	57.2	acrylonitrile

[a] Values taken from Reference [61].

These molecules may be considered as models of propagating radicals derived from the monomers indicated. Thus, relatively stabilized radicals such as those of styrene and methyl acrylate form weaker bonds with halogen atoms, whereas more reactive radicals such as those of vinyl chloride, vinyl acetate, or ethylene form stronger bonds. As $\Delta H_{ATRP} = D(R\text{–}Y) - D([L_nM\text{–}Y])$ and the second term is constant for a given catalyst/halogen combination, the more reactive radicals will lead to more difficult activations for a given catalyst. The difference between styrene and vinyl acetate, for example, is close to 10 kcal mol^{-1} for both Cl and Br derivatives. Clearly, these two monomers cannot be controlled by the same metal system. The bond-dissociation energies of alkyl bromides are 8–10 kcal mol^{-1} weaker than those of the corresponding alkyl chlorides, but a similar differential is expected for the L_nM–Y bonds, thus a change of halogen is not expected to provide a great variation of ΔH_{ATRP}.

© 2006 Wiley-VCH Verlag GmbH & Co. KGaA, Weinheim

A suitable solution may be found by changing other factors in the catalytic metal complex, such as the ligands, the metal oxidation state, or the type of metal. DFT calculations on model complexes have shown that the bond-dissociation energy for M–Y decreases upon increasing the oxidation state, whereas it is much less dependent on the nature of two-electron (L-type) ligands.[27] Therefore, the radical polymerization of more difficult monomers may become controllable by using lower-oxidation-state catalysts. In this respect, the ubiquitous Cu^{I} system is rather limited, whereas more possibilities may exist for other metals such as Ti, Mo, and Re. However, the effect of the coordination geometry, electronic configuration, and spin state of one-electron (X-type) ligands has not yet been studied in detail. Another useful argument is that bond-dissociation energy values usually increase within a group in the order 3d < 4d < 5d. Thus, more-difficult monomers may be controlled by changing the metal to a heavier congener (e.g. Mo to W, or Ru to Os). Useful information may be anticipated by systematic studies in these areas.



Scheme 8. Oxidative addition of alkyl halides to $[CpFe(CO)_2]_2$.

There is, however, a potential problem with this approach. As M is changed to strengthen the M–Y bond, the M–R bond will strengthen too. Therefore, while ΔH_{ATRP} is displaced toward a suitable range ΔH_{OMRP} will correspondingly increase, and this increase may render the radical-trapping process irreversible and lead to the products of one-electron oxidative addition. This negative effect may be somewhat attenuated by working on the ligand steric properties. Indeed, as propagating radicals occupy a larger cone angle in the metal coordination sphere relative to the halogen atoms, the bond-dissociation energy for $[L_nM–(m)_xR]$ is expected to be more sensitive to the steric bulk of the ligand than that for $[L_nM–Y]$. Thus, the selection of a sterically more encumbering ligand shell, perhaps in combination with lower oxidation states or with heavier metals, may hold some promise for matching the required ΔH_{ATRP} value while maintaining a relatively low ΔH_{OMRP} value when using reactive propagating radicals.

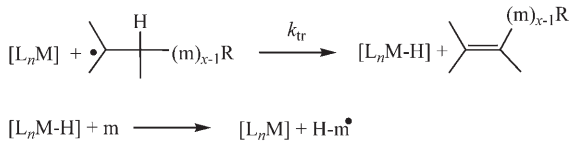
Sawamoto and co-workers showed that the radical polymerization of vinyl acetate (VAc) could be controlled by $[CpFe(CO)_2]_2$ in the presence of the iodide initiators $Me_2C(I)COOEt$ or $MeCH(I)OCOCH_3$, and $Al(OiPr)_3$ as co-catalyst in anisole at 60 °C.[62] As the system involved an Fe^{I} catalyst, it was therefore expected to form stronger bonds with I (leading to Fe^{II}–I) relative to Fe^{II} (leading to Fe^{III}–I). Also, as the catalyst is a relatively unencumbered system, it is possible to envisage the formation of relatively strong Fe^{II}–alkyl bonds. Furthermore, the metal–metal-bonded dinuclear catalyst imposes the formation of the 17-electron and highly reactive $[CpFe(CO)_2]$ metalloradical in the proximity of the propagating radical. It seems logical that a one-electron oxidative addition process should occur to yield a mixture of $[Cp(CO)_2FeI]$ and $[Cp(CO)_2Fe–(VAc)_xR]$ (see Scheme 8). Indeed, stable alkyl derivatives such as $[CpFe(CO)_2Et]$ are well known.[63,64] The experimental evidence that the initiator efficiency factor is close to unity and that the isolated polymer contains iodo end-groups shows that the equilibrium for one-electron oxidative addition lies on the side of $[CpFe(CO)_2]_2$ and $R(VAc)_xI$. This behavior is as expected; oxidative addition of alkyl halides to $[CpFe(CO)_2]_2$ have not been reported. However, the control mechanism could involve the active participation of the OMRP-type trapping process (case b, Figure 4). This hypothesis could be easily checked by carrying out a radical polymerization under OMRP conditions, for example, from a suitable presynthesized $[CpFe(CO)_2R]$ complex such as $[CpFe(CO)_2\{CH(Ph)CH_3\}]$[65,66] or from $[CpFe(CO)_2]_2$ and a radical initiator.

The best way to regulate the concentration of free radicals for highly reactive propagating radicals, however, is through the OMRP equilibrium. As discussed above, the OMRP activation relies only on the bond-dissociation energy of the metal–carbon bond in the organometallic dormant species. It is always possible in principle to design a metal complex, through an intelligent selection of ligands, metal centers, and oxidation state, to give an organometallic dormant species with $D([L_nM–(m)_xR]) = \Delta H_{OMRP}$ in a suitable range for any monomer, as the OMRP equilibrium is not contaminated by other coupled equilibria (at least not in the absence of halogen atoms in the coordination sphere). In this respect, it is pertinent to mention the controlled polymerization of vinyl acetate by this technique using $[Co(acac)_2]$ as spin trap (acac = acetylacetonate).[7] This system is in contrast to other Co^{II} systems (e.g. with porphyrins or Schiff bases as ligands), which irreversibly trap the propagating radicals of VAc (ΔH_{OMRP} too high) but control the polymerization of acrylates. Conversely, while the ΔH_{OMRP} value for $[(acac)_2Co–(m)_xR]$ is just right for VAc as monomer (m), it is too small for methyl acrylate and thus leads to an uncontrolled process. There appears to be greater promise for the development of new controlled radical processes of the "difficult" monomers in OMRP than in ATRP. The difficulty associated with the formation of metal-capped polymers may be surmounted by subsequent transformations, which may allow the recovery and recycling of the metal complex. Indeed, this is the case for $[Co(acac)_2]$-capped PVAc, which may be converted into an R_2NO-capped polymer and $[Co(acac)_2]$ by treatment with stable nitroxides.[67]

© 2006 Wiley-VCH Verlag GmbH & Co. KGaA, Weinheim

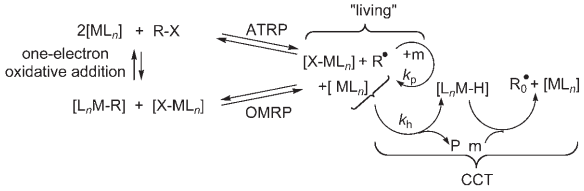
The Intervention of Catalytic Chain Transfer (CCT)

Catalyzed chain transfer is another phenomenon that is intimately related to the presence of transition metals that undergo one-electron processes. Chain transfer can be catalyzed through the abstraction by $[ML_n]$ of a β-hydrogen atom from the propagating radical to yield a hydride complex, $[L_nM{-}H]$, and a "dead" polymer chain with an unsaturated end-group (see Scheme 9).[68]



Scheme 9. Mechanism of catalyzed chain transfer (CCT).

This phenomenon has practical relevance because it gives access to macromonomers with a controlled average molecular weight. Thus, considerable effort is devoted to the search of ML_n systems that exhibit high transfer rate constants (k_{tr} in Scheme 9) for a number of industrial applications.[69] However, this phenomenon interferes with the chain growth process when "pseudo-living" polymerizations are sought through ATRP or OMRP methods. To resume, an $[L_nM]$ complex apt to increase both its electron count and its coordination number by one unit has the potential to simultaneously exert three functions: catalyst for ATRP, spin trap in OMRP, and radical chain-transfer catalyst. Our above-mentioned study of the $[CpMoCl_2L_2]$ systems in the controlled polymerization of styrene highlighted for the first time the interplay of these three functions.[27] This phenomenon can be integrated in a general scheme that encompasses the metal-mediated generation of radicals and regulation of concentration, the living chain growth, the chain transfer, and the one-electron oxidative addition (Scheme 10).



Scheme 10. A global scheme for the metal-mediated generation of radicals and one-electron processes.

An interesting consideration concerns the conditions that are most appropriate for the manifestation of CCT. On the basis of the general energetic schemes in Figure 1 and Figure 4, the equilibrium concentration of the potential chain-transfer catalyst will be low under OMRP conditions (the equilibrium is largely shifted toward the organometallic dormant species), whereas it will be high under ATRP conditions (the equilibrium is largely shifted toward $[ML_n]$ and the halogenated dormant species). The latter condition is valid provided that the OMRP trapping process does not predominate. Thus, we can conclude that CCT is favored under two circumstances, namely a) under OMRP conditions, when ΔH_{OMRP} is too small, (case a, Figure 1) and b) under ATRP conditions, provided that the OMRP trapping process is not too important (e.g. case a, Figure 4). The most efficient catalytic processes are those carried out under OMRP conditions with $[ML_n]$ complexes that form very weak metal–carbon bonds, because the concentration of the free radicals and the catalyst may be relatively high at the same time. On the other hand, under ATRP conditions the concentration of $[ML_n]$ may be high but that of the free radical is kept low by the ATRP (and possibly also the OMRP) activation/deactivation equilibrium. The most active catalysts appear to be those based on cobaloximes, containing no halogen ligands in the system.[70,71] Catalytic activity, however, has also been shown for other systems such as $[(C_5R_5)Cr(CO)_3]$ (R = H, Me, Ph), $[Cp^*Fe(CO)_2]$ and heavier analogues, the tris(pyrazolyl)borato (Tp) derivatives $[TpMo(CO)_3]$ and $[Tp^*Mo(CO)_3]$,[72–74] and certain Fe diimine systems.[75]

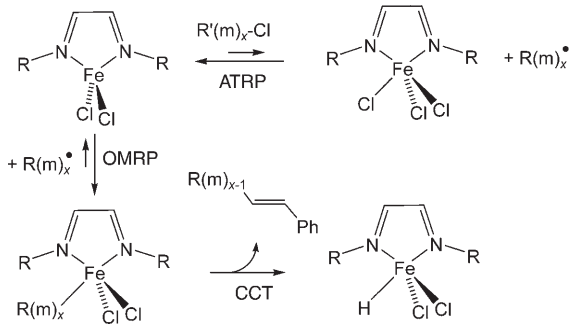
The relative ability of a transition-metal complex to abstract a β-hydrogen atom and to form a M–C bond depends on the propagating radical. Certain radicals have a greater propensity than others to transfer a hydrogen atom. For a given radical though, the type of metal complex affects the relative trapping/transfer ratio in ways that are not yet completely understood. Steric effects have a greater impact on the formation of the organometallic dormant species than on the hydrogen-atom-transfer process that yields the hydride intermediate. Another potential side reaction consuming the chain-transfer catalyst and equally disfavored by a greater steric encumbrance is the dimerization of $[ML_n]$. Recent studies by Tang and Norton on $[(C_5R_5)Cr(CO)_3]$-type catalysts showed that steric bulk enhances CCT activity by disfavoring the dimerization to M–M and the formation of M–R in favor of the hydrogen-atom-transfer reaction.[74]

A recent study in our laboratory showed that the complexes $[MoX_3(PMe_3)_3]$ (X = Cl, I) display different trapping abilities for free radicals generated under OMRP conditions. The trichloride complex significantly slows down the AIBN-initiated radical polymerization of styrene (though the observed molecular weight and $\bar{M}_w/\bar{M}_n$ are typical of an uncontrolled process), whereas the triiodide complex has essentially no effect.[76] This behavior is attributed to the greater steric bulk of the three iodide ligands relative to the corresponding number of chlorides. Consequently, when the polymerization is carried out under ATRP conditions—$[MoX_3(PMe_3)_3]$ and an alkyl halide initiator—the equilibrium concentration of $[MoX_3(PMe_3)_3]$ during the polymerization process will be greater for X = I than for X = Cl. This difference can rationalize the experimental observation of "living" growth in the case of the trichloride and CCT in the case of the triiodide. Incidentally, the $[MoX_3(PMe_3)_3]$ complexes are not stable free radicals but instead contain three unpaired electrons (spin quartet state).

An intriguing new pathway for CCT was recently proposed, apparently associated to changes in spin state. Four-coordinate Fe^{II} complexes of the type $[FeCl_2(RN{=}CHCH{=}$

© 2006 Wiley-VCH Verlag GmbH & Co. KGaA, Weinheim

NR)] control the polymerization of styrene under ATRP conditions. However, whereas derivatives with alkyl R groups yield "living" chain growth, those with aryl R groups yield CCT.[77,78] This phenomenon correlates with the spin state of the atom-transfer product, the Fe^{III} complex [$FeCl_3$(RN=CHCH=NR)] ($S = 5/2$ for R = alkyl; $S = 3/2$ for R = aryl). Gibson and co-workers propose that the same preference for relative spin state holds for the organometallic dormant species, whose formation would then be preferentially observed for the aryl-substituted complexes. Both Hartree–Fock calculations and the experimentally observed greater stability (higher decomposition temperature) of the aryl-substituted [$FeCl_2(CH_2Ph)$(RN=CHCH=NR)] complexes support this view. The organometallic dormant species would then lead to chain transfer through a β-hydride elimination process (Scheme 11). Thus, this particular metal complex



Scheme 11. A proposed CCT pathway involving β-hydride elimination.

system appears to function by a combination of one-electron and two-electron processes, suitably orchestrated by the spin state. In this variant of the CCT mechanism, the catalytic ability is not related to the weakness of the M–R bond but rather to the availability of open coordination sites positioned *cis* to the M–R function which induce the β-hydride elimination process. The β-hydride elimination is mechanistically related to the olefin insertion into M–H and M–R bonds, that is, the key step of olefin coordination polymerization. The completion of both olefin coordination/insertion and homolytic bond cleavage by using the same metal complex may open up new doors in polymer chemistry.

In another study, we found that complexes [$CpMoCl_2(PMe_3)_2$] and [$CpMoCl_2$(dppe)] lead to a "living" polystyrene chain growth under ATRP conditions, whereas the very similar complex [$CpMoCl_2(\eta^4\text{-}C_4H_6)$], under identical conditions, leads to CCT.[27] However, we observed a "living" polymer growth (no CCT) with all three complexes when working under OMRP conditions. This observation could be explained by invoking a lower concentration of the chain-transfer catalyst under OMRP conditions. However, the different outcome of the different systems under ATRP conditions may not be so straightforward to explain. The rationalization we put forward in our original report was based on a greater steric impediment in the β-hydrogen transfer process for the more encumbered phosphine complexes. However, this impediment should be stronger for the formation of the organometallic dormant species, yet there is control in all cases under OMRP conditions, showing that the metal–carbon bond is strong enough and forms rapidly for all systems. If the steric factor is important for the generation of the organometallic dormant species, then ΔH_{OMRP} should be smaller for the bulkier phosphine system and result in a greater concentration of chain-transfer catalyst, which is inconsistent with the experimental result. A CCT mechanism involving β-hydride elimination, as for the above-mentioned Fe system (Scheme 11), also appears unsuitable because in that case more CCT should be observed under OMRP conditions, contrary to the experimental results. We have not yet a complete understanding of the key parameters that regulate chain-transfer versus radical-trapping processes.

Conclusions and Outlook

A thorough understanding of one-electron transition-metal reactivity is of fundamental importance for the correct interpretation of experimental results in metal-mediated radical polymerization processes. A variety of situations may result, depending on the thermodynamic parameters of the two fundamental steps of the one-electron oxidative addition process (Scheme 5) and on the kinetics of the catalyzed chain transfer (Scheme 9). The two fundamental steps of the one-electron oxidative addition correspond to the activation/deactivation equilibria of the two different metal-mediated controlled radical polymerization processes, ATRP and OMRP. These depend, from a thermochemical point of view, on the homolytic bond dissociation energies of three bonds: the L_nM–Y bond of the ATRP spin trap, the $R(m)_x$–Y bond of the ATRP dormant species, and the $R(m)_x$–ML_n bond of the OMRP dormant species. Knowledge of these three bond dissociation energies for a given system is essential to predict whether it will lead to an uncontrolled polymerization, to an irreversible one-electron oxidative addition, to no polymerization at all, or to a controlled polymerization. In the latter case, it is then possible to predict whether the control will be insured solely by the ATRP activation/deactivation equilibrium or solely by the analogous OMRP equilibrium, or by a combination of both. The interplay of the two equilibria, accompanied by an irreversibility of the OMRP-type radical-trapping process, may lead to low initiator efficiency factors (f), provided the oxidative addition products are themselves active ATRP catalysts. We have explored the necessary conditions to achieve the controlled polymerization of monomers that produce more-reactive radicals. A greater flexibility in terms of the radical controlling equilibrium position is provided under OMRP conditions by systems devoid of halogen atoms, although a drawback of this method is the necessary post-polymerization treatment to remove the metal from the chain ends. Finally, we have explored the conditions that regulate the extent of metal-catalyzed chain transfer, although a complete understanding of the parameters that regulate the relative extent of OMRP trapping and chain-transfer events is still lacking.

Radical processes mediated by transition-metal complexes will certainly continue to be investigated in the future.

© 2006 Wiley-VCH Verlag GmbH & Co. KGaA, Weinheim

These processes require complexes that can increase both their electronic configuration and their coordination number by one unit—a condition that, given an appropriate coordination sphere (steric and electronic properties of the ligands, coordination geometry, and spin state), can be satisfied for many different metals in a variety of different oxidation states. Further advances in this area will require a better understanding of how such parameters as ligand properties independently affect the three basic bond-dissociation energies and the rate of β-hydrogen transfer.

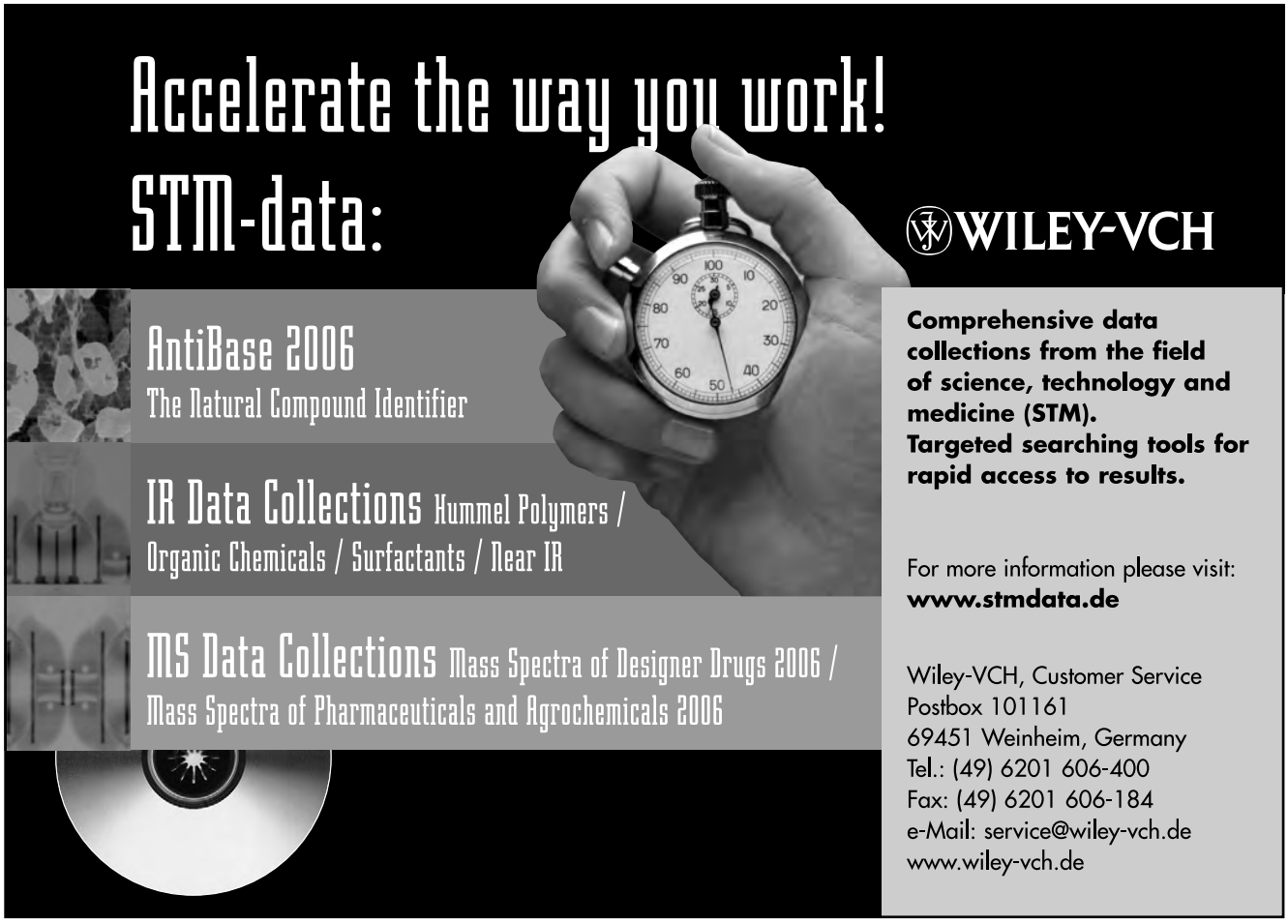
I am grateful to the polymer chemists who have sparked my interest in controlled radical polymerization (Yves Gnanou and Jerome Claverie) and those with whom I have had fruitful collaborations (Krzysztof Matyjaszewski and Dave Haddleton), as well as the students and postdoctoral fellows who have invested their time in my laboratory in this research area (Erwan Le Grognec, François Stoffelbach, Sébastien Maria, and José Mata). Funding provided by the CNRS, the Conseil Régional de Bourgogne, and the ANR (NT05-2_42140) is also gratefully acknowledged. Theoretical calculations carried out in our group were made possible by grants of computing time by the CINES (Montpellier) and CALMIP (Toulouse).

Received: October 26, 2005
Published online: July 4, 2006

[1] J.-S. Wang, K. Matyjaszewski, *J. Am. Chem. Soc.* **1995**, *117*, 5614 – 5615.
[2] M. Kato, M. Kamigaito, M. Sawamoto, T. Higashimura, *Macromolecules* **1995**, *28*, 1721 – 1723.
[3] D. P. Curran, *Synthesis* **1988**, 417 – 439.
[4] T. Otsu, T. Tazaki, *Polym. Bull.* **1986**, *16*, 277 – 284.
[5] B. Wayland, G. Poszmick, S. Mukerjee, *J. Am. Chem. Soc.* **1994**, *116*, 7943 – 7944.
[6] T.-T. Tsou, M. Loots, J. Halpern, *J. Am. Chem. Soc.* **1982**, *104*, 623 – 624.
[7] A. Debuigne, J. R. Caille, R. Jérôme, *Angew. Chem.* **2005**, *117*, 1125 – 1128; *Angew. Chem. Int. Ed.* **2005**, *44*, 1101 – 1104.
[8] J. Chiefari, Y. K. Chong, F. Ercole, J. Krstina, J. Jeffery, T. P. T. Le, R. T. A. Mayadunne, G. F. Meijs, C. L. Moad, G. Moad, E. Rizzardo, S. H. Thang, *Macromolecules* **1998**, *31*, 5559 – 5562.
[9] R. T. A. Mayadunne, E. Rizzardo, J. Chiefari, J. Krstina, G. Moad, A. Postma, S. H. Thang, *Macromolecules* **2000**, *33*, 243 – 245.
[10] S. G. Gaynor, J. S. Wang, K. Matyjaszewski, *Macromolecules* **1995**, *28*, 8051 – 8056.
[11] K. M. Smith, *Organometallics* **2005**, *24*, 778 – 784.
[12] J. Halpern, J. P. Maher, *J. Am. Chem. Soc.* **1964**, *86*, 2311.
[13] F. A. L. Anet, E. Leblanc, *J. Am. Chem. Soc.* **1957**, *79*, 2649 – 2650.
[14] Y. Okude, S. Hirano, T. Hiyama, H. Nozaki, *J. Am. Chem. Soc.* **1977**, *99*, 3179 – 3181.
[15] H. Jin, J. Uenishi, W. J. Christ, Y. Kishi, *J. Am. Chem. Soc.* **1986**, *108*, 5644 – 5646.
[16] A. Fürstner, N. Shi, *J. Am. Chem. Soc.* **1996**, *118*, 12349 – 12357.
[17] R. J. Haines, A. L. Du Preez, *J. Am. Chem. Soc.* **1969**, *91*, 769 – 770.
[18] J. Halpern, J. P. Maher, *J. Am. Chem. Soc.* **1965**, *87*, 5361 – 5366.
[19] J. Halpern, *Acc. Chem. Res.* **1970**, *3*, 386 – 392.
[20] J. K. Kochi, *Acc. Chem. Res.* **1974**, *7*, 351 – 360.
[21] J. H. Espenson, *Adv. Inorg. Bioinorg. Mech.* **1982**, *1*, 1 – 63.
[22] J. H. Espenson, *Acc. Chem. Res.* **1992**, *25*, 222 – 227.
[23] R. Van Eldik, D. Meyerstein, *Acc. Chem. Res.* **2000**, *33*, 207 – 214.
[24] A. Masarwa, D. Meyerstein, *Adv. Inorg. Chem.* **2004**, *55*, 271 – 313.
[25] H. Fischer, *Macromolecules* **1997**, *30*, 5666 – 5672.
[26] K. Matyjaszewski, B. E. Woodworth, *Macromolecules* **1998**, *31*, 4718 – 4723.
[27] E. Le Grognec, J. Claverie, R. Poli, *J. Am. Chem. Soc.* **2001**, *123*, 9513 – 9524.
[28] F. Stoffelbach, R. Poli, P. Richard, *J. Organomet. Chem.* **2002**, *663*, 269 – 276.
[29] Y. Kabachii, S. Kochev, L. Bronstein, I. Blagodatskikh, P. Valetsky, *Polym. Bull.* **2003**, *50*, 271 – 278.
[30] Y. Kotani, M. Kamigaito, M. Sawamoto, *Macromolecules* **1999**, *32*, 2420 – 2424.
[31] K. Matyjaszewski, M. Wei, J. Xia, N. E. McDermott, *Macromolecules* **1997**, *30*, 8161 – 8164.
[32] T. Ando, M. Kamigaito, M. Sawamoto, *Macromolecules* **1997**, *30*, 4507 – 4510.
[33] V. C. Gibson, R. K. O'Reilly, W. Reed, D. F. Wass, A. J. P. White, D. J. Williams, *Chem. Commun.* **2002**, 1850 – 1851.
[34] R. K. O'Reilly, V. C. Gibson, A. J. P. White, D. J. Williams, *J. Am. Chem. Soc.* **2003**, *125*, 8450 – 8451.
[35] W. A. Braunecker, Y. Itami, K. Matyjaszewski, *Macromolecules* **2005**, *38*, 9402 – 9404.
[36] M.-S. Weiser, R. Muelhaupt, *J. Polym. Sci. Part A* **2005**, *43*, 3804 – 3813.
[37] G. Moineau, C. Granel, P. Dubois, R. Jérôme, P. Teyssié, *Macromolecules* **1998**, *31*, 542 – 544.
[38] H. Uegaki, M. Kamigaito, M. Sawamoto, *J. Polym. Sci. Part A* **1999**, *37*, 3003 – 3009.
[39] C. Granel, P. Dubois, R. Jérôme, P. Teyssié, *Macromolecules* **1996**, *29*, 8576 – 8582.
[40] P. Lecomte, I. Draiper, P. Dubois, P. Teyssié, R. Jérôme, *Macromolecules* **1997**, *30*, 7631 – 7633.
[41] Y. B. Xiong, L. Fan, Z. Q. Shen, *Chem. J. Chin. Univ. (Chin.)* **2005**, *26*, 2153 – 2156.
[42] D. Grishin, L. Semyonycheva, E. Telegina, A. Smirnov, V. Nevodchikov, *Russ. Chem. Bull.* **2003**, *52*, 505 – 507.
[43] D. F. Grishin, S. K. Ignatov, A. A. Shchepalov, A. G. Razuvaev, *Appl. Organomet. Chem.* **2004**, *18*, 271 – 276.
[44] A. D. Asandei, I. W. Moran, *J. Am. Chem. Soc.* **2004**, *126*, 15932 – 15933.
[45] A. D. Asandei, G. Saha, *Macromol. Rapid Commun.* **2005**, *26*, 626 – 631.
[46] W. Lau, J. C. Huffman, J. K. Kochi, *Organometallics* **1982**, *1*, 155 – 169.
[47] D. A. Clarke, D. Dolphin, R. Grigg, A. W. Johnson, H. A. Pinnock, *J. Chem. Soc. C* **1968**, 881 – 885.
[48] C. Floriani, F. Calderazzo, *J. Chem. Soc. A* **1971**, 3665 – 3669.
[49] R. D. Arasasingham, A. L. Balch, C. R. Cornman, L. Latos-Grazynski, *J. Am. Chem. Soc.* **1989**, *111*, 4357 – 4363.
[50] R. K. O'Reilly, V. C. Gibson, A. J. P. White, D. J. Williams, *Polyhedron* **2004**, *23*, 2921 – 2928.
[51] M. Kamigaito, T. Ando, M. Sawamoto, *Chem. Rev.* **2001**, *101*, 3689 – 3745.
[52] Z. H. Li, Y. M. Zhang, M. Z. Xue, L. Zhou, Y. G. Liu, *J. Polym. Sci. Part A* **2005**, *43*, 5207 – 5216.
[53] J. E. Huheey, E. A. Keiter, R. L. Keiter, *Inorganic Chemistry. Principles of Structure and Reactivity*, 4th ed., Harper & Row, New York, **1993**.
[54] P. A. Rock, *Inorg. Chem.* **1968**, *7*, 837 – 840.
[55] F. Stoffelbach, D. M. Haddleton, R. Poli, *Eur. Polym. J.* **2003**, *39*, 2099 – 2105.
[56] F. Stoffelbach, R. Poli, P. Richard, unpublished results.
[57] B. Wang, Y. Zhuang, X. Luo, S. Xu, X. Zhou, *Macromolecules* **2003**, *36*, 9684 – 9686.
[58] K. Matyjaszewski, J. H. Xia, *Chem. Rev.* **2001**, *101*, 2921 – 2990.

 © 2006 Wiley-VCH Verlag GmbH & Co. KGaA, Weinheim

[59] X. S. Wang, S. P. Armes, *Macromolecules* **2000**, *33*, 6640 – 6647.
[60] R. Poli, *Chem. Rev.* **1991**, *91*, 509 – 551.
[61] M. B. Gillies, K. Matyjaszewski, P.-O. Norrby, T. Pintauer, R. Poli, P. Richard, *Macromolecules* **2003**, *36*, 8551 – 8559.
[62] M. Wakioka, K. Y. Baek, T. Ando, M. Kamigaito, M. Sawamoto, *Macromolecules* **2002**, *35*, 330 – 333.
[63] M. L. H. Green, P. L. I. Nagy, *J. Organomet. Chem.* **1963**, *1*, 58 – 69.
[64] A. Davison, J. A. McCleverty, G. Wilkinson, *J. Chem. Soc.* **1963**, 1133 – 1138.
[65] T. Y. Orlova, V. N. Setkina, D. N. Kursanov, *J. Organomet. Chem.* **1977**, *136*, 371 – 373.
[66] L. J. Dizikes, A. Wojcicki, *J. Am. Chem. Soc.* **1977**, *99*, 5295 – 5303.
[67] A. Debuigne, J.-R. Caille, R. Jérôme, *Macromolecules* **2005**, *38*, 5452 – 5458.
[68] N. S. Enikolopyan, B. R. Smirnov, G. V. Ponomarev, I. M. Belgovskii, *J. Polym. Sci. Part A* **1981**, *19*, 879 – 889.
[69] A. A. Gridnev, S. D. Ittel, *Chem. Rev.* **2001**, *101*, 3611 – 3659.
[70] A. A. Gridnev, *Vysokomol. Soedin. Ser. A* **1989**, *31*, 2153 – 2159.
[71] K. J. Abbey, G. M. Carlson, M. J. Masola, D. Trumbo, *Polym. Mater. Sci. Eng.* **1986**, *55*, 235 – 238.
[72] G. P. Abramo, J. R. Norton, *Macromolecules* **2000**, *33*, 2790 – 2792.
[73] L. Tang, E. Papish, G. Abramo, J. Norton, M. Baik, R. Friesner, A. Rappe, *J. Am. Chem. Soc.* **2003**, *125*, 10093 – 10102.
[74] L. Tang, J. Norton, *Macromolecules* **2004**, *37*, 241 – 243.
[75] V. C. Gibson, R. K. O'Reilly, D. F. Wass, A. J. P. White, D. J. Williams, *Macromolecules* **2003**, *36*, 2591 – 2593.
[76] S. Maria, F. Stoffelbach, J. Mata, J.-C. Daran, P. Richard, R. Poli, *J. Am. Chem. Soc.* **2005**, *127*, 5946 – 5956.
[77] V. C. Gibson, R. K. O'Reilly, H. S. Rzepa, M. P. Shaver, *Polym. Prepr. Am. Chem. Soc. Div. Polym. Chem.* **2005**, *46*, 160 – 161.
[78] M. P. Shaver, L. E. N. Allan, H. S. Rzepa, V. C. Gibson, *Angew. Chem.* **2006**, *118*, 1263 – 1266; *Angew. Chem. Int. Ed.* **2006**, *45*, 1241 – 1244.



© 2006 Wiley-VCH Verlag GmbH & Co. KGaA, Weinheim

Antibiotics

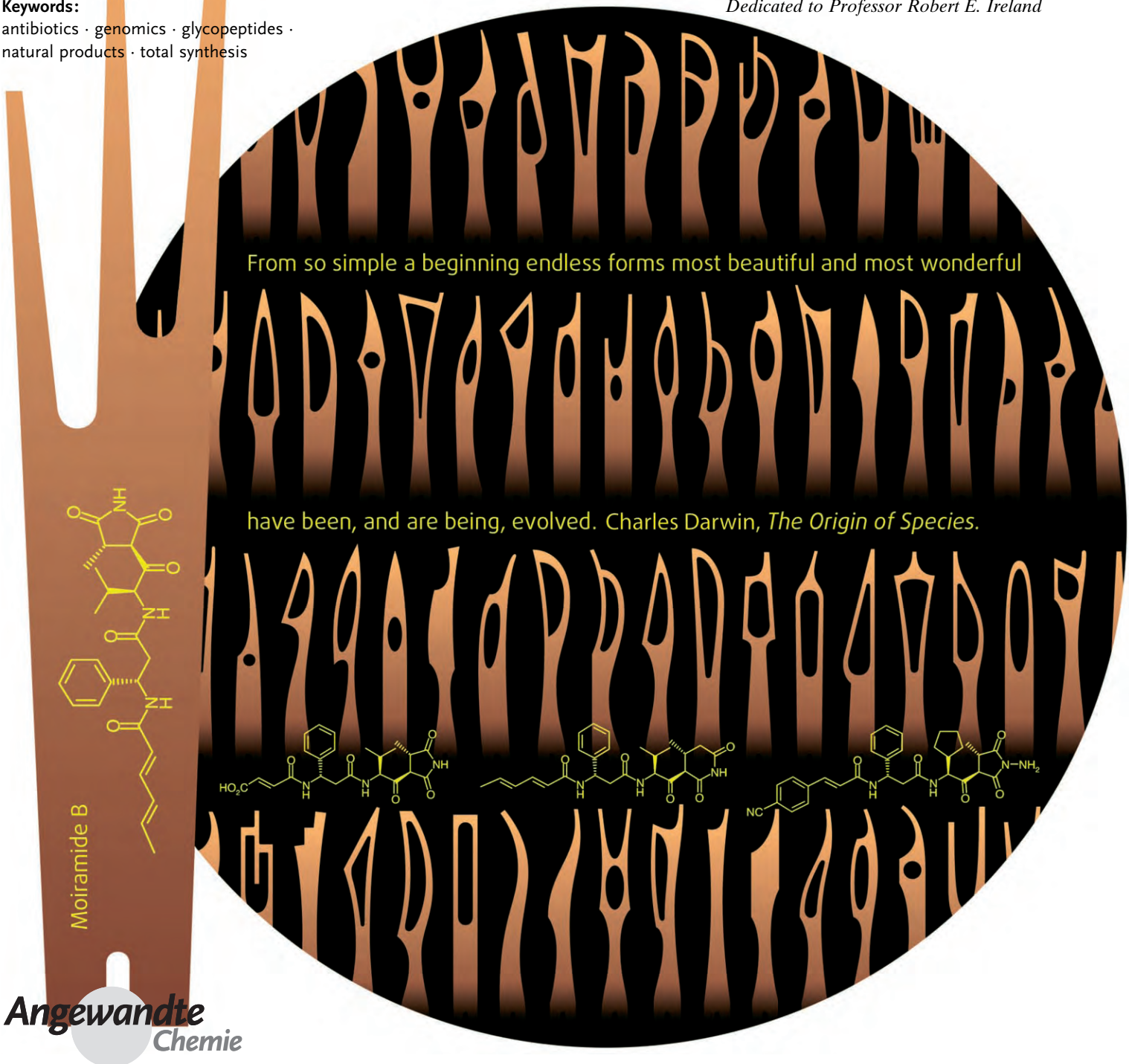
DOI: 10.1002/anie.200600350

Antibacterial Natural Products in Medicinal Chemistry—Exodus or Revival?

*Franz von Nussbaum, Michael Brands, Berthold Hinzen, Stefan Weigand, and Dieter Häbich**

Keywords:
antibiotics · genomics · glycopeptides · natural products · total synthesis

Dedicated to Professor Robert E. Ireland



© 2006 Wiley-VCH Verlag GmbH & Co. KGaA, Weinheim

To create a drug, nature's blueprints often have to be improved through semisynthesis or total synthesis (chemical postevolution). Selected contributions from industrial and academic groups highlight the arduous but rewarding path from natural products to drugs. Principle modification types for natural products are discussed herein, such as decoration, substitution, and degradation. The biological, chemical, and socioeconomic environments of antibacterial research are dealt with in context. Natural products, many from soil organisms, have provided the majority of lead structures for marketed anti-infectives. Surprisingly, numerous "old" classes of antibacterial natural products have never been intensively explored by medicinal chemists. Nevertheless, research on antibacterial natural products is flagging. Apparently, the "old fashioned" natural products no longer fit into modern drug discovery. The handling of natural products is cumbersome, requiring nonstandardized workflows and extended timelines. Revisiting natural products with modern chemistry and target-finding tools from biology (reversed genomics) is one option for their revival.

From the Contents

1. Introduction	5073
2. Scope and Focus of this Article	5076
3. Novel, Effective, and Safe Antibiotics are Urgently Needed	5077
4. Antibacterials, an Arduous Marketplace	5078
5. Biological Targets and Chemical Leads	5079
6. Chemical Postevolution of Antibacterial Natural Products	5084
7. β-Lactam Antibiotics	5090
8. Macrolide and Ketolide Antibiotics	5094
9. Lincosamides	5096
10. Furanomycin, a Lead with Insufficient Potential	5099
11. Pyrrolidinedione Antibacterials	5100
12. Tetrahydropyrimidinone Antibiotics	5102
13. Biphenomycins	5106
14. Tuberactinomycins and Capreomycins	5108
15. Glycopeptide Antibiotics	5110
16. Lysobactins	5114
17. Enopeptin Depsipeptide Antibiotics	5116
18. Summary and Conclusion	5118
19. Abbreviations	5119

1. Introduction

All industrialized societies rely on the pharmaceutical industry's ability to address their inherent medical needs. With infectious diseases, this trust is nourished by the ready supply of a plethora of marketed antibiotics for the immediate treatment of routine or life-threatening bacterial infections.[1] Indeed, the research and development of antibacterial agents during the last century has been a chronicle of success, whereby all parties thrived. Since the introduction of the first sulfonamides and penicillins in 1935 and 1940 (Figure 1), the once marked mortality rate associated with bacterial infec-

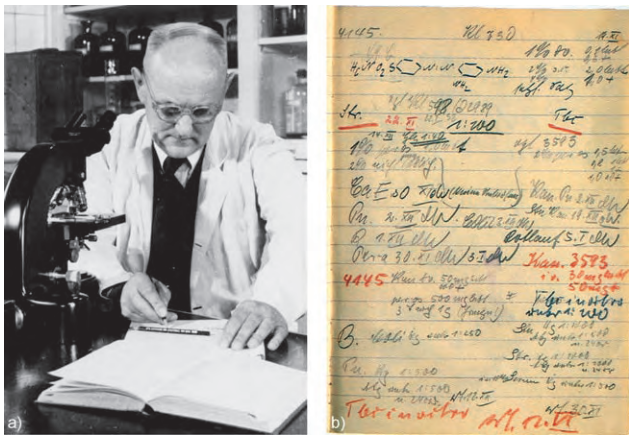


Figure 1. a) Nobel laureate, pioneer of antibacterial therapy, and inventor of the sulfonamides, Gerhard Domagk (1895–1964), with his most important working tool. Under the microscope he studied the effect of different chemicals on bacteria. b) Page from Domagk's laboratory notebook describing the exceptional activity of azo dye D 4145 on streptococci. D 4145, launched in 1935 as "prontosil", was a diazo prodrug of the active component 4-aminophenylsulfonamide that was marketed in 1936 under the name "prontalbin". At the outset, antibacterial chemotherapy stemmed from synthetic dyes rather than natural products. Essential principles of chemotherapy have been worked out with the sulfonamides.

[*] Dr. F. von Nussbaum, Dr. M. Brands, Dr. B. Hinzen, Dr. S. Weigand, Dr. D. Häbich
Bayer HealthCare AG
Medicinal Chemistry Europe
42096 Wuppertal (Germany)
Fax: (+49) 202-36-5461
E-mail: dieter.haebich@bayerhealthcare.com

© 2006 Wiley-VCH Verlag GmbH & Co. KGaA, Weinheim

tions experienced a remarkable downturn.[2] Antibiotics[3] have saved millions of lives and eased patients' suffering.

Many of the antibacterial agents were natural products or potent semisynthetic variations thereof (Table 1).[4–7] Improved subclasses followed, such as the cephalosporins and carbapenems or, recently, the ketolides and glycylcyclines. As a whole, they have served as structural scaffolds for extensive medicinal-chemistry programs in virtually every major pharmaceutical company.

By the early 1970's, the existing therapies were seen as adequate and the need for new antibiotics began to be questioned.[8] Waning public interest and health measures as well as—with a time lag—declining industrial support for antibacterial research were the consequences of that fallacious consensus. After an innovation gap of several decades, an oxazolidinone (linezolid)[9] and a lipopeptide (daptomycin)[10,11] were the first truly new chemical entities (NCEs) to be launched.

Today, infectious diseases are the second major cause of death worldwide and the third leading cause of death in developed countries (Table 2).[12] In the US, bacteria are the most common cause of infection-related death.[13] Antibiotics are no longer effective in all cases, and treatment options for certain microorganisms have become increasingly scarce.[14] Former last-resort drugs have become the first-line therapy. "Resistance threatens to turn back the clock" and is rapidly



From left to right: B. Hinzen, F. von Nussbaum, D. Häbich, M. Brands, S. Weigand (Photograph P. Voits).

Franz von Nussbaum, born in Frankfurt/Main, studied chemistry at the University of Munich, where he received his PhD in the research group of Prof. W. Steglich (1998). After a postdoctoral Feodor-Lynen fellowship with Prof. S. D. Danishefsky at Columbia University (1999–2000), he joined Central Research at Bayer AG, Leverkusen. Since 2002 he has been working as a medicinal chemist for Bayer HealthCare AG in Wuppertal. The optimization of bioactive natural products is a central theme of his research interest.

Michael Brands, born in Duisburg in 1966, studied chemistry at the Universities of Münster and Bochum/MPI für Kohlenforschung, where he received his PhD in 1993 in the group of Prof. H. Butenschön. After a postdoctoral stay in the group of Prof. W. Oppolzer at the University of Geneva (1993–1995), he joined the pharmaceutical division of Bayer AG as a medicinal chemist. Since April 2006 he has been a Director of Medicinal Chemistry, responsible for the chemical drug-discovery activities in the therapeutic areas of diabetes and heart failure.

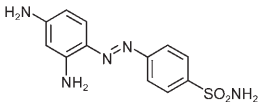
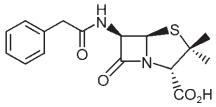
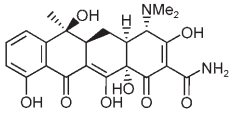
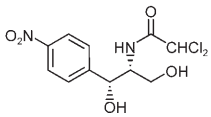
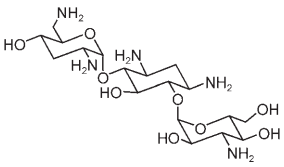
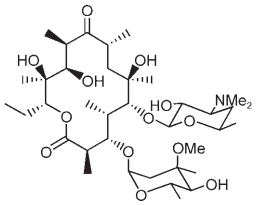
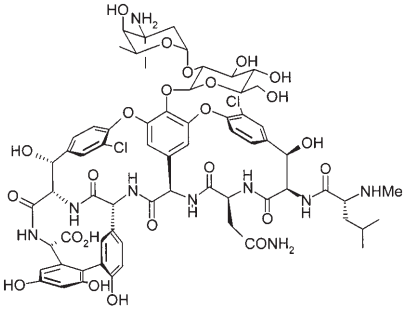
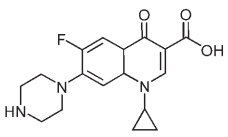
Berthold Hinzen was born in Cologne, Germany, in 1967. He studied Chemistry in Basel and obtained his PhD with Prof. F. Diederich at the ETH in Zürich, Switzerland (1996). After a postdoctoral fellowship in Prof. Steven Ley's group in Cambridge, UK, he joined Bayer AG in Wuppertal in 1998 as a medicinal chemist. Since 2004 he has been a Director of Medicinal Chemistry, responsible for the chemical drug-discovery activities in the therapeutic area thrombosis.

Stefan Weigand, born in 1969, studied chemistry at the Universities of Würzburg and Göttingen, where he received his PhD in 1997 in the group of Prof. R. Brückner. After a postdoctoral Feodor-Lynen fellowship under the guidance of Prof. B. M. Trost at Stanford University (1997–1998), he joined the pharmaceutical division of Bayer AG as a medicinal chemist. Since May 2005 he has been working as a group leader in cancer research at Roche Diagnostics GmbH in Penzberg.

Dieter Häbich, born in Stuttgart, studied chemistry at the University of Stuttgart, where he received his PhD in the group of Prof. F. X. Effenberger in 1977. After a postdoctoral NATO-research fellowship with Prof. R. E. Ireland at California Institute of Technology in Pasadena, USA (1979–1980), he joined Bayer AG, Wuppertal as a medicinal chemist. In 1991 he became a Director of Medicinal Chemistry and has been responsible for chemical anti-infective research in the areas of antibacterials, antimycotics, and antivirals.

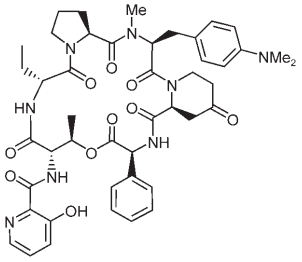
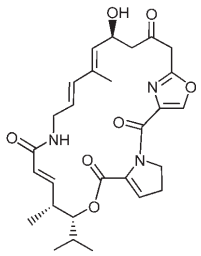
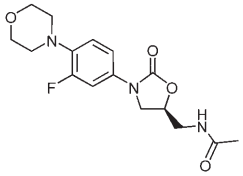
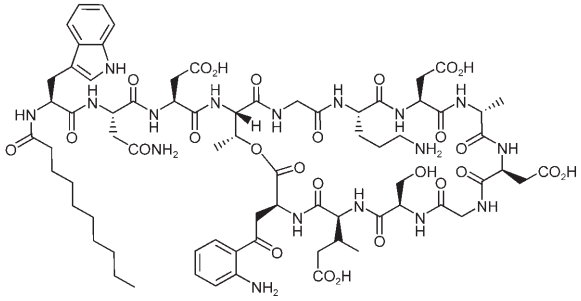
 © 2006 Wiley-VCH Verlag GmbH & Co. KGaA, Weinheim

Table 1: Introduction of new antibacterial classes for human therapy.

Year	Class	Target	Example	Structure
1935	sulfonamides (synthetic)	folate pathway	prontosil	 **1**
1940	β-lactams	cell wall	penicillin G	 **2**
1949	polyketides	protein biosynthesis	tetracycline	 **3**
1949	phenylpropanoids	protein biosynthesis	chloramphenicol	 **4**
1950	aminoglycosides	protein biosynthesis	tobramycin	 **5**
1952	macrolides	protein biosynthesis	erythromycin A	 **6**
1958	glycopeptides	cell wall	vancomycin	 **7**
1962	quinolones (synthetic)	DNA replication	ciprofloxacin	 **8**

© 2006 Wiley-VCH Verlag GmbH & Co. KGaA, Weinheim

Table 1: (Continued)

Year	Class	Target	Example	Structure
1962	streptogramins	protein biosynthesis	pristinamycin ($I_A + II_A$)	 **9**  **10**
...				
2000	oxazolidinones (synthetic)	protein biosynthesis	linezolid	 **11**
2003	lipopeptides	bacterial membrane	daptomycin	 **12**

spreading, particularly in hospitals, where antibiotics are heavily used.[15] The ability of bacteria to evade any form of established therapy has become apparent and pathogens resistant to one or more antibiotics are emerging and spreading worldwide.[16] Development of resistance is inevitably the result of antibiotic use and ultimately limits the efficacy and life span of every antibiotic. Although correct antibiotic use will slow down resistance, it will not prevent it: only the persistent discovery and development of new drugs can keep this problem in check. Nonetheless, more and more pharmaceutical companies are curtailing or exiting the antibacterial field and the pipeline for new antibiotics is running dry. "Bad Bugs, No Drugs", the call for action by the Infectious Disease Society of America (IDSA), places this desperate situation in the limelight.[17] The evolving crisis[18] results from a combination of scientific, economic, and regulatory causes. Despite tremendous technological advances in combinatorial chemistry, genomics, and high-throughput screening (HTS), companies large and small have been unsuccessful in identifying new and valid antibacterial agents. Furthermore, the pharmaceutical industry faces considerable fiscal and political challenges and its traditional virtues of individuality, commitment to science, and cultural and ethical standards are thought to be in danger, in particular with regard to the antibacterial field.[19] The dilapidation of antibacterial drug discovery and development in combination with a growing proportion of elderly and immuno-compromised patients and an increasing risk of acquiring infections caused by resistant bacteria, could culminate in a global public-health crisis and catapult physicians back to the pre-antibiotic days.[17]

2. Scope and Focus of this Article

This review focuses on selected contributions by medicinal chemistry to synthethic modifications of antibiotics through de novo or semisynthesis, rather than on unaltered pure natural-product drugs. The Sections were selected according to structural characteristics and encompass established classes such as the β-lactam antibiotics, novel candidates in clinical development, as well as the prospects of antibacterial natural products as lead structures. Many aspects of the traditional classes have been thoroughly studied and competently reviewed in numerous articles and books, and even attempting to compile a comprehensive

 © 2006 Wiley-VCH Verlag GmbH & Co. KGaA, Weinheim

Table 2: Key bacterial pathogens and associated infectious diseases.

Pathogen	Infectious Disease
Staphylococcus aureus	skin and wound infection, abscess, bacteremia, nosocomial pneumonia, endocarditis, toxic shock syndrome
Streptococcus pneumoniae	upper respiratory infection, pneumonia, otitis, sinusitis, meningitis
Streptococcus pyogenes	pharyngitis, tonsillitis, skin and soft-tissue infection, scarlet fever
Enterococcus faecalis	bacteremia, endocarditis, urinary-tract infection, peritonitis
Enterococcus faecium	bacteremia, endocarditis, peritonitis
Escherichia coli	bacteremia, urinary-tract and gastrointestinal infection
Klebsiella pneumoniae	hospital-acquired pneumonia, bacteremia
Proteus spp.	urinary-tract infection
Haemophilus influenzae	respiratory infection, otitis, sinusitis, meningitis
Moraxella catarrhalis	respiratory infection
Pseudomonas aeruginosa	nosocomial pneumonia, burn infection, bacteremia
Acinetobacter spp.	pneumonia in immuno-compromised patients
Mycobacterium tuberculosis	tuberculosis

documentation would far exceed the scope of this review. Thus, there is no claim to completeness and some important innovations such as the aminoglycosides, the tetracyclines[20] and glycylcyclines,[21] or the peptide deformylase inhibitors[22] were deliberately omitted. The intention of the present article is to call attention to the promising prospects of antibacterial natural products as up-to-date lead structures for medicinal chemistry and guideposts for novel targets, pioneering the way to future therapies. We wish to alert researchers and decision makers to realistically assess society's urgent medical need for a sustainable supply of effective and safe antibiotics. New ideas and solutions are needed that encourage, facilitate, and support this endeavor. There is no long-term alternative to antibacterial research.

3. Novel, Effective, and Safe Antibiotics are Urgently Needed

More and more bacterial infections evade standard treatment and are difficult if not impossible to treat. Resistance to multiple antibiotics[23] is spreading throughout the world and the number of reports on therapy failures and rising treatment costs is growing, especially in the hospital environment[11,24] (Table 3). Extensive, sometimes inappropriate use of antibiotics, inadequate hygiene (even in modern hospitals), cosmopolitan travel, the increasing aging and immunocompromised population, and the lack of rapid diagnostics have fueled this problem.

Table 3: Prevalence of resistance in hospital-acquired infections, US 2004.[42]

Antibiotic	Pathogen	Resistance [%]
methicillin	*S. aureus*	59.5
	coagulase-negative staphylococci	89.1
vancomycin	enterococci	28.5
cephalosporins 3rd generation	*Enterobacter* spp.	31.1
	P. aeruginosa	31.9
	E. coli	5.8
	K. pneumoniae	20.6
imipenem	*P. aeruginosa*	21.4
quinolones	*P. aeruginosa*	29.5

The presence of an antibiotic exerts an evolutionary pressure on the microbial population and selects resistant organisms. Bacteria can evade the lethal effects of antibiotics through several mechanisms,[25,26] for example, by alteration of the target (proteins),[27] enzymatic deactivation of the antibacterial drug,[28] restricted antibiotic penetration,[29] and increased efflux.[30] Mobile genetic elements that might accelerate the spread of resistance have become a serious threat as well (plasmides).[31] Resistance among Gram-positive bacteria has been primarily encountered in nosocomial infections in intensive care units (ICU), but is now also observed in community-acquired infections[32] that eventually require hospitalization. Gram-positive pathogens, such as methicillin-resistant *Staphylococcus aureus* (MRSA),[33,34] vancomycin-resistant enterococci (VRE),[35] and penicillin-resistant *Streptococcus pneumoniae* (PRSP),[36–38] are the most prominent pathogens in this respect. Methicillin-resistant *Staphylococcus epidermidis* (MRSE) is advancing quickly.[39] Regardless of their historic titles, MRSA, VRE, etc., they have all acquired resistance to multiple antibiotic classes, often already during the 1990's.[40] This development, in tandem with the emergence of new bacterial pathogens, such as *Acinetobacter* and *Legionella* species or coagulase negative staphylococci,[41] clearly calls for new antibiotics without cross-resistance to currently used drugs.

In many cases vancomycin, quinupristin/dalfopristin, or linezolid provide the last option for responsive therapy and determine if a patient lives or dies. Therefore, the observation of clinical strains with reduced vancomycin susceptibility (VISA),[43] increased glycopeptide resistance in enterococci, and the first reports on cases of high-level vancomycin resistance in *S. aureus* (VRSA)[44] are of considerable

 © 2006 Wiley-VCH Verlag GmbH & Co. KGaA, Weinheim

concern.[45] Staphylococci resistant to quinupristin/dalfopristin and linezolid are emerging.[46] In July 2004, the Infectious Disease Society of America (IDSA) reported[17] that "about two million people acquire bacterial infections in US hospitals each year, and 90000 die as a result. About 70% of those infections are resistant to at least one drug. The trends toward increasing numbers of infections and increasing drug resistance show no sign of abating. Resistant pathogens lead to higher health-care costs because they often require more-expensive drugs and extended hospital stays. The total cost to US society is nearly $5 billion annually."

The evolution of resistance in ICU patients in US hospitals (but also in Europe) is alarming.[47] Seven years ago, only half of the *S. aureus* isolated from ICU patients in US hospitals were multiresistant (MRSA). Driven by prevailing use, the corresponding MRSA proportion in Japan has been even higher.[48] Meanwhile, physicians also face significant worldwide resistance problems with Gram-negative pathogens,[30e,49] in particular with *Pseudomonas aeruginosa* (HAP, cSSTI), *Escherichia coli* (cUTI, IAI), enterobacteriaceae with extended spectrum β-lactamases, and some *Klebsiella* species.[50] Furthermore, multiresistant variants of *Mycobacterium tuberculosis* demand new and more-effective drugs against tuberculosis, the most widespread and persistent infection worldwide.[51–55] About 1.9 billion people are estimated to carry *M. tuberculosis*! At the 44th Interscience Conference on Antimicrobial Agents and Chemotherapy (ICAAC),[56,57] the pre-eminent forum for current issues on antibiotic resistance, clinical development, and antibacterial discovery programs, the infectious disease community has expressed serious concerns that more untreatable pathogens may develop. Antimicrobial resistance is contributing to detrimental clinical results and increased health-care expenditures.[47] It has become evident that there is an urgent need for novel antibacterial drugs without cross-resistance to antibiotics in use, more initiatives to foster the responsible and appropriate use of antibiotics,[58] and better infection control measures. As "dead bugs don't mutate", bactericidal rather than bacteriostatic agents have been recommended as resistance breakers.[59] Frequently, high-dose therapy with antibacterial drug combinations is the method of choice to suppress breakthroughs of resistance. In addition, the use of pharmacodynamic models[60] can help to minimize resistance for the patients benefit.

4. Antibacterials, an Arduous Marketplace

With over 200 marketed drugs, antibacterials represent a well-developed area with a high therapeutic standard. Currently it costs about US$ 800 million and often takes more than a decade to bring a new drug to the market.[61] These tremendous expenditures and the increasing complexity of drug discovery and development have caused an industry-wide research and development shift away from acute infectious diseases (short-course therapy) towards more-profitable chronic illnesses (long-term treatment). Without doubt, fast and effective antibacterials represent one of medicine's major achievements! However, from a marketing standpoint, efficient antibiotics are the worst sort of drug as they cure the disease usually within a few days and thus eliminate their own need (auto-obsolence). Thus, overall treatment costs are often low. This results in less revenue per patient and is commercially less attractive than some of the chronic disease states in which products are prescribed over years or lifelong once an initial diagnosis is made. The commercial success of "chronic drugs" along with the "auto-obsolence of antibacterials"[62] has tempted many companies to preferentially invest into areas such as hyperlipidaemia, hypertension, dementia, mood disorders, pain, asthma, rheumatoid arthritis, or obesity.[63]

Investment in antibacterial discovery and development is flagging in big pharmaceutical companies. Abbott, Aventis, Bristol-Myers Squibb, Eli Lilly, GlaxoSmithKline, Proctor & Gamble, Hoffmann-La Roche, and Wyeth have left the field or are downsizing, while Bayer and others are about to follow. Several adverse factors have played a role in weakening this essential therapeutic area:[15,18,64] resistance limits the life span of every antibiotic, thereby fundamentally threatening the investment. However, resistance alone is not the only reason why interest in antibacterials has waned; the dynamics of the pharmaceutical market are also a contributory factor. Increasing fragmentation of the market, recent patent expiry of blockbuster drugs, and the growing regulatory hurdles for the clinical evaluation of new antibiotics are also to be held responsible.[65] The demand for blockbuster drugs[63] pressures large companies to focus on safe broad-spectrum antibacterials for extensive use. At the same time, the call for more-limited use of broad-spectrum agents discourages the first-line treatment with new antibiotics and reduces their expected sales.[66]

In all, activities have shifted away from big pharmaceutical companies to smaller biotechnology or specialty firms. These biotech companies concentrate more on novel small-spectrum or niche products that are commercially less viable for big pharmaceutical companies. In addition, biotech has taken up and successfully progressed products such as daptomycin,[10,11] which was initially put aside by their more powerful partners. Yet, most of the biotech companies cannot bear the significant costs of large-scale clinical trials on their own.[67]

Still, antibacterials have an advantage. The development of antibiotics has been benefited from highly predictive animal models, with above-average clinical success rate of about 17% (average 11%). In contrast to other therapeutic areas in which lack of efficacy often is the major cause of attrition in the clinic, the toxicology, clinical safety, and commercial aspects are most critical for an antibiotic.[68]

The number of antibacterials approved by the US Food and Drug Administration (FDA) decreased by more than half over the last two decades (Figure 2) and only 6 of 506 "new molecular entities" in development were antibacterial agents.[62] In 2002, out of 89 new drugs, no new antibiotics were approved.

According to commercial analysts,[70] antibacterial companies are currently facing significant hurdles in maintaining product revenue levels and, in particular, large companies face the prospect of leaner times. Some of their most

 © 2006 Wiley-VCH Verlag GmbH & Co. KGaA, Weinheim

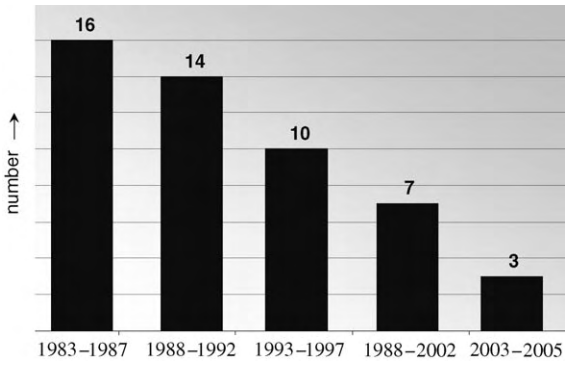


Figure 2. New antibacterial agents approved in the US.[62]

profitable drugs such as amoxycillin/clavulanic acid and ciprofloxacin have gone off-patent, allowing other companies to sell cheaper generic versions of them. Generic competition, drug resistance, and increased regulatory scrutiny have placed great pressure on antibacterial profit margins. Shareholder value interests increasingly frame research and development investment strategies and stagnating growth induces lower commercial attention. As a result, many analysts and managers cultivate a wary view of the prospects of the antibacterial market.[63] Indeed, in comparison to other areas, the antibacterial market remained relatively flat in recent times and Datamonitor[70] predicts an average growth rate of merely 1.4% for the year 2010. The number of antibacterial blockbusters is expected to decrease and the hospital sector will be dominated by specialist products. Activity against resistant isolates, shorter treatment courses, the possibility to switch from i.v. to oral application, cost, and improved side-effect profile are driving the hospital sector in which the fastest growing indications are expected to be respiratory tract infections (RTI; 6.2% of 2002 sales), urinary tract infections (UTI; 4.9%), and skin and soft tissue infections (SSTI; 4.9%).[70] On the other hand, antibiotics represent the third largest pharmaceutical drug market segment with global sales of US$ 25782 million (Table 4), a third of which is spent on parenteral (i.v.) hospital antibiotics. Despite the poor growth rates, the overall antibacterial market is still attractive.

Table 4: Top 10 antibacterial companies by global sales of antibiotics in 2004 (Source: Wood Mackenzie[69]).

Rank	Company	US$ million
1	Pfizer	2938
2	GlaxoSmithKline	2425
3	Abbott	1657
4	Bayer	1346
5	Johnson & Johnson	1295
6	Hoffmann-La Roche	1142
7	Wyeth	846
8	Merck & Co.	704
9	Daiichi	687
10	Shionogi	678
Others		12064
Total		**25782**

5. Biological Targets and Chemical Leads

5.1. Natural Products as Antibacterial Lead Structures[71]—Coevolution of Targets and Inhibitors

Less than 1% of all known organic compounds are natural products; 99% are synthetica. Despite this extreme situation, more than a third of all drug sales (1981–2004) were based on natural products or the "intellectual DNA" behind them.[4] Natural products did not only contribute to drug discovery as chemical lead structures but also served as guideposts to—pharmaceutically unexplored but evolutionary validated—targets and modes of action that could subsequently be explored with synthetic mimetics.[72]

Structural diversity and complexity within natural products is unique and easily dwarfs synthetica. The functional complexity found in natural products will never be invented de novo in a chemistry laboratory. Natural products present unique ring architectures (vancomycin, stephacidin B) and complex molecular pharmacophores (erythromycin, epothilone). Their sphere of action ranges from small-molecule binding (cycloserine, salicylic acid) to quasi supramolecular interactions (ramoplanin, palytoxin). Many natural pharmacophores are more like molecular machines (β-lactams, mitomycin C) than static binders and are often flanked with recognition domains that can selectively trigger a "warhead" within target proximity (calicheamicin). Binding to the molecular target may even craft a higher-order interaction, as found for the pore-forming nisin/lipid II complex. Many natural products do not attack a single enzyme, but rather a whole enzyme family (β-lactams/penicillin-binding proteins (PBPs)), and can even have multiple modes of action (vancomycin, inhibition of transpeptidases and transglycosylation). Interestingly, this natural multiple-target approach contrasts with the HTS-governed "single-target dogma" of the current drug-discovery processes.

The extraordinary success of natural products as guideposts to new drugs is most obvious in antibacterials.[6] Here, more than other indications, the reliance on natural-product lead structures has remained the most-successful route to discovering clinically relevant therapeutics.[73–75] Over 75% of new chemical entities (NCEs) submitted between 1984 and 2004 were based on natural-product lead structures.[4] Only 21% of antibacterial NCEs had a pure synthetic history,[4] for example, the oxazolidinones, which originally stemmed from a Du Pont company screening hit.

From an evolutionary point of view, it is not surprising that natural products are promising lead structures especially for antibacterial drugs.[76] Microorganisms, in particular fungi, but also bacteria (actinomycetes), successfully fostered their armamentarium against bacterial competitors for millions of years. Antibiotics were vital weapons in the persistent fight for space and resources. Microorganisms evolved sustainable strategies to modulate competitors and aggressors, based on the coevolution of their secondary metabolites with the corresponding targets in bacteria. Molecules that kill their bacterial neighbors or prohibit their replication have coevolved with their microbial producers and their defense strategies (resistance). In vitro potency, self-tolerability, and

 © 2006 Wiley-VCH Verlag GmbH & Co. KGaA, Weinheim

biosynthetic effort have been key selectors within the evolution of antibacterials. To exert an effect, most of these antibiotics must penetrate bacterial membranes[77] and attack at least one adversarial molecular target. Clearly, controlling bacterial resistance was a major challenge for microbial producers of antibacterial metabolites. In general, antibiotics are the products of nonessential secondary metabolic pathways that are switched on when required. Structural adaptation within bioactive secondary metabolites relies on the evolution of biosynthetic pathways, that is, the evolution of the biosynthesis machinery on a genetic level (gene duplication, gene shuffling). A strong interest in these evolutionary processes has evolved recently:[78,79] the modification of known biosynthetic pathways (combinatorial biosynthesis, metabolic engineering) or the discovery of silent biosynthetic gene clusters, which possibly hold the, genetically encrypted,[80] instructions for the synthesis of unexplored natural products (metabolome mining) that can't be produced from classical fermentation approaches.[81]

The concept of "privileged structures"[82] is another way to explain the high success rate of natural products within diverse therapeutic areas, not only within antibiotics. Structural analogy between enzymes of utterly different biological function and divergent peptide sequence is based on folding types and domain families that are common in the whole proteome and seems to explain the "cross-talk" of natural-product leads in "uncommon" therapeutic areas. This concept is especially useful for rationalizing the behavior of natural products within therapeutic areas that are not correlated to the original ecological purposes of secondary metabolites.[83] Therefore, it does indeed make sense to screen antibacterial natural products against a central-nervous-system target

Statistical investigations also have been employed to help explain the high success rate[4] of natural products versus synthetica in drug discovery. So far, no clear rules could be extracted from this work. It seems that the structural secret to success, incorporated in natural products, cannot be easily disclosed by statistical means, that is, by simply counting chemical functionalities, rings, and chiral centers or looking at physicochemical parameters such as membrane affinity, polar surface area, pK_a, etc. The biological relevance of natural products in medicinal chemistry is apparently not based on a general physicochemical or structural master plan, but on the fact that every single secondary metabolite has been evolutionary engineered within a complex network of biological interdependencies. However, modern search methods (data mining) have extracted some trends that distinguish synthetica from natural products and indicate a certain structural complementarity in both substance pools.[84,85] Statistically, natural products have higher molecular weights, higher counts of hydroxy groups, and higher polarity than "average" synthetica.

5.2. The "Classical" Approach—From Bug to Drug

Antibacterial activity is assessed in MIC tests that determine the lowest concentration of a substance required to completely inhibit bacterial growth over an 18–24 h period. MIC testing and other microbiological in vitro procedures[86] have been enormously helpful in the search for promising structural scaffolds to initiate programs.[87] Medicinal chemists optimized compound stability, potency, antibacterial spectrum, and selectivity along with pharmacological properties. To date, all established antibacterial classes have been identified by using MIC whole-cell assays.[88] Animal models[89,90] that reflect antibacterial activity and are predictive for clinical situations have traditionally complemented this "classical approach", whereas microbial pharmacodynamics,[60] which link drug exposure and potency to microbiological or clinical effect for a specific pathogen, have increasingly gained importance (see Section 6.1). Although, cytotoxicity is easily monitored with standard in vitro models, setting up animal models for the assessment of systemic toxicity is elaborate and expensive. In general, the throughput of animal models is low and thus only selected lead candidates are examined.

Extensive use of antibiotics exerts evolutionary pressure on microbial populations and selects resistant bacteria. To keep pace with microbial resistance, the classical approach of pharmaceutical companies has, for decades, been to investigate incremental structural variations of established antibacterial classes. In this way, many classes have been advanced towards their third- and fourth-generation forms, and it is an open question as to how many more generations can follow before a class will loose its efficiency.

The majority of marketed antibiotics inhibit or deregulate the biosynthesis of bacterial macromolecules through a mere handful of clinically validated modes of action, that is, target areas (Table 5). For example, β-lactam antibiotics, glycopeptides, and fosphomycin inhibit bacterial cell-wall biosynthesis (Figure 3), whereas lipopeptides and cationic peptides, such as polymyxins, disrupt membrane integrity. The folate coenzyme biosynthetic pathway is blocked by trimethoprim and sulfonamides, novobiocin and the quinolones inhibit bacterial DNA replication, and rifampicin obstructs transcription (RNA-synthesis).[91] Inhibition of bacterial protein synthesis (translation) by selectively blocking the ribosome[92] is a very common target area.[93–95] Many structurally diverse classes of antibiotics, such as the streptogramins,[96] tetracyclines,[20]

Table 5: Estimated number of essential broad-spectrum genes/targets.

Target area	Essential genes	Established antibiotic classes
DNA replication	20	3
divisome	8	0
transcription	6	1
translation	58	8
fatty acid biosynthesis	12	0
cell-wall biosynthesis	17	3
nucleotide biosynthesis	9	0
coenzyme biosynthesis	6	2
secretion	5	0
Total	**141**	**17**

 © 2006 Wiley-VCH Verlag GmbH & Co. KGaA, Weinheim

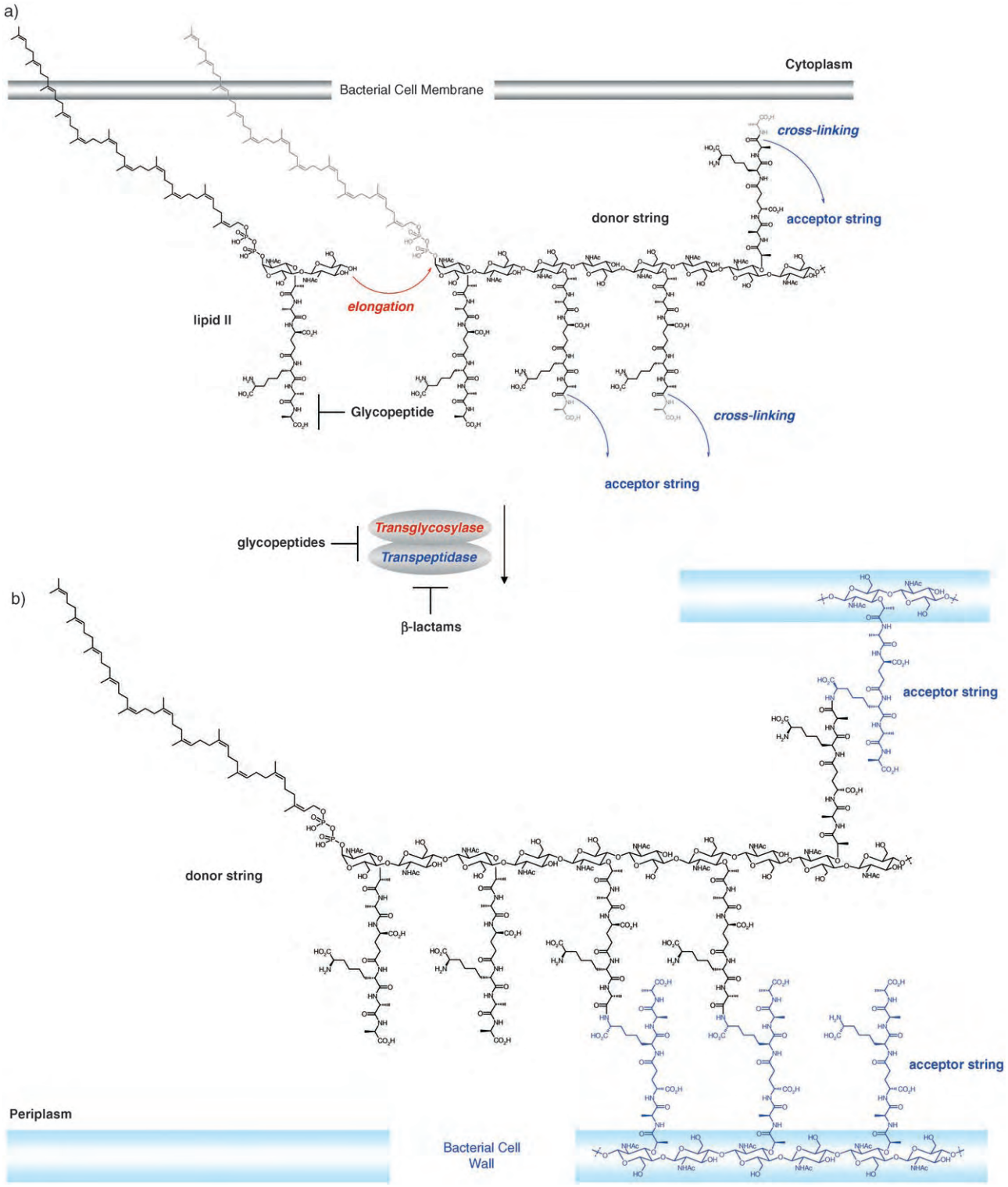


Figure 3. Peptidoglycan biosynthesis from a chemists point of view. An idealized scheme for the Gram-negative bacterium *E. coli* is depicted—the chemical structure of peptidoglycan varies amongst different bacteria. a) Lipid II (the next monomer) is attached to a nascent, growing peptidoglycan string in the elongating transglycosylation step (red). Both, the monomer and the growing chain navigate in the bacterial membrane with their C_{55} lipid tail. In the cross-linking transpeptidation step, the donor peptidoglycan string grasps for available acceptor stings (blue). b) The resulting peptidoglycan (or murein) sacculus is a flexible and enormously stable macromolecular meshwork that defines the shape of the bacterial cell and protects the microorganism against its high internal osmotic pressure. Different antibiotics interfere with these concluding steps of the bacterial cell-wall synthesis: glycopeptide antibiotics bind to the D-Ala-D-Ala terminus of Lipid II and barricade the action of bacterial transglycosylases and transpeptidases. β-Lactams inhibit transpeptidases.

 © 2006 Wiley-VCH Verlag GmbH & Co. KGaA, Weinheim

macrolides, lincosamides, aminoglycosides,[97] and chloramphenicol all work through this mode of action, albeit by interacting with distinct subunits[98] or at different steps of this complex process (Figure 4). Traditionally, the mode of action of an antibacterial agent was investigated and elucidated after its discovery and sometimes long after its introduction into clinical therapy. With penicillin, it took almost half a century for its molecular targets, the penicillin-binding proteins (PBPs), to be identified.[99] Drug discovery processes in the pharmaceutical industry underwent dramatic changes (genomics revolution)[100] thanks to new computational methods and the remarkable advances in high-throughput technologies in screening, combinatorial chemistry, and genomics. Turning away from traditional approaches and established antibacterial classes, scientists and executives swiftly envisaged a revolutionary potential in the identification and pursuance of novel biological targets.

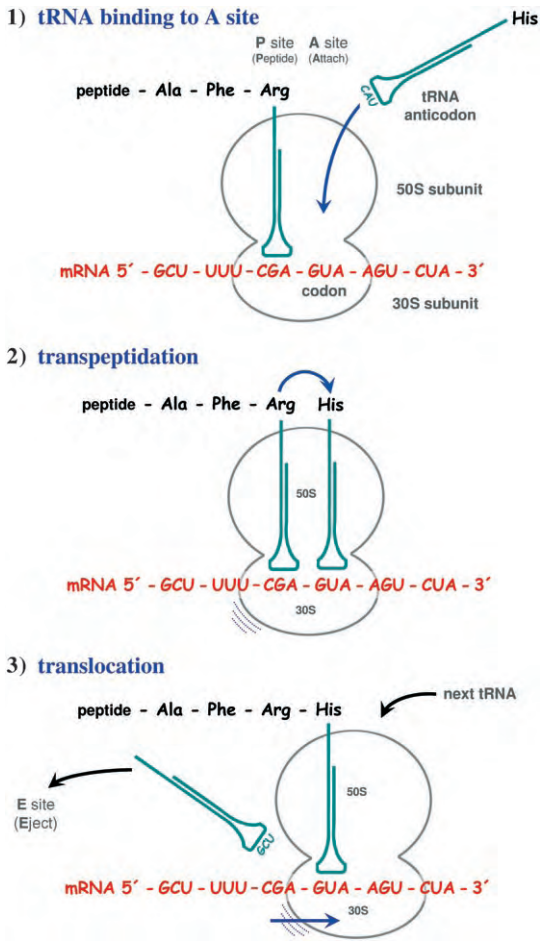


Figure 4. The bacterial ribosome, composed of a 30S and a 50S subunit, is the apparatus for protein synthesis. The ribosome moves along a messenger RNA (mRNA) template and "translates" the successive codons (triplets of nucleotides code for specific amino acids) into a growing peptide chain in three schematic steps: 1) Binding: A transfer RNA (tRNA) loaded with an amino acid (His) binds to the acceptor (**A**) site by complementary base pairing (anticodon). 2) Transpeptidation: The tRNA in the peptidyl (**P**) site is discharged by transfering the growing peptide chain to the His on the tRNA in the **A** site. 3) Translocation: The ribosome advances to the next codon on the mRNA. The new **A** site is, therefore, free for the next tRNA and the empty tRNA is ejected (**E** site). Different inhibitors of bacterial protein synthesis interact at different steps or with distinct subunits of this complex process: tetracyclines compete with the tRNA for **A** site binding, aminoglycosides cause misreading of the mRNA code and incorporation of incorrect amino acids into the peptide, chloramphenicol and tetrahydropyrimidinone antibiotics block transpeptidation, and macrolides/ketolides inhibit translocation. Many antibiotics act by binding into and physically obstructing the peptide exit tunnel of the ribosome.

5.3. The "Target-Based" Approach—From Target to Lead

The growing information on bacterial genetics, initiated by the first report on the complete bacterial genome sequence of *Haemophilus influenzae* in 1995[101] along with novel tools for gene-expression profiling[102] and proteomics,[103] boosted the new paradigm of functional genomics not only in antibacterial drug discovery.[104,105] The exponentially growing delivery of further prokaryotic whole-genome sequences[106] all of a sudden revealed a plethora of so far unexploited bacterial targets waiting to be mined.[107] However, identifying valid targets from genomic sequences is not trivial, and the selection of the right targets for screening compound libraries has become a vital decision in all areas of pharmaceutical research.[108–111] Today, knowing the mode of action and the molecular target of a novel antibacterial is considered a prerequisite for a project. Only with this information can a good in vitro/in vivo screening workflow be established in the interest of a rational structure–activity relationship (SAR; the medicanal chemist's roadmap for optimizing potency and selectivity).

The target-based approach has offered new opportunities, but the process of target validation is multifaceted and often associated with uncertainty. A valid antibacterial target[107,112] must be conserved across a broad range of medically relevant pathogens (spectrum) and either absent or sufficiently different in mammals (selectivity).[113] It must be essential,[112,114,115] screenable,[116] and druggable[117,118] and must avoid potential cross-resistance to marketed antibiotics. Any new antibacterial must produce a low frequency of resistance. Approximately 10 % of all microbial genes are thought to be essential for bacterial growth in vitro (Table 5),[119,120] however, proving a target's in vivo essentiality can be quite complex.[121] After passing all these requirements, a fair number of broad-spectrum antibacterial targets remain that exceed the number of targets addressed by established antibiotics.

Proteins, derived from gene sequences that fulfill these criteria, are selected as targets and used for establishing HTS[122,123] to scan compound libraries. In a HTS, the effect of a great number of compounds on the enzymatic activity[105] or on genetically engineered whole cells[124] is monitored. Active compounds, identified as "hits" are rescreened to afford a set of "confirmed hits" which is investigated in secondary assays, for example, to confirm the mode of action and to perform resistance analyses. Confirmed hits are clustered, prioritized, and preliminary SARs are extracted from the screening data. A clear SAR is the medicinal chemist's roadmap for optimizing potency and selectivity on the basis of target activity (IC_{50}), MIC, and, if available, target protein struc-

 © 2006 Wiley-VCH Verlag GmbH & Co. KGaA, Weinheim

ture.[125,126] At the same time, the chemical purity of the hits is checked and often they are resynthesized and their eligibility is discussed before they qualify as lead structures for focused chemistry programs that aim at improving not just the effect, but also the pharmacological profile (e.g. serum half-life, tissue distribution, and solubility).

In principle, the exact target of a drug candidate, stemming from a single-target screen, is known. However, for many successful antibacterial classes such as the β-lactams, glycopeptides, or quinolones, the real mode of action is multifaceted and cannot be reduced to the simple interaction with a single target.[127] Indeed, the "one-target-one-disease" philosophy and the scope of "monotarget medicine" clearly has its limitations.[128] Despite sophisticated genetic strategies and techniques, no new clinical antibacterials have been identified through these HTS-based processes.[129,100,130] Past HTS approaches across industry have suffered from target and assay diversity and low hit-to-lead success rates.[107] In the hope of developing more "first-in-class drugs", research activities were shifted from classical targets and "priviledged" structural scaffolds to new target and non-natural product leads.

Yet, drugs that target novel mechanisms generally have a significantly higher risk of failure and have added little value when compared with drugs that are based on known targets.[131] In their critical analysis: "Antibiotics: where did we go wrong?" Overby and Barrett speak of the "seduction of genomics and forgetting how to make a drug".[18b] Indeed, target-based approaches have primarily concentrated on target activity and have produced potent inhibitors that were often unable to penetrate bacterial cell walls, thus being devoid of antibacterial activity. Yet, attaining and enhancing antibacterial activity requires an enormous medicinal-chemistry effort and, even for novel structures with MIC, it is extremely difficult to immediately match activity, spectrum, and tolerability of the established classes' advanced-generation agents. Consequently, companies, large and small, have been unsuccessful in identifying new and valid antibacterial agents through target-based approaches. The shift to target-based drug discovery could be a contributing factor to the decline in productivity of the pharmaceutical industry.[132] For antibacterial drug discovery, however, this approach has ultimately failed and needs to be modified or replaced to achieve a closing of the productivity gap.[133] A risk-balanced portfolio requires that this process be supplemented with precedented targets, me-toos, or the reversed-genomics approach.

5.4. The "Reversed-Genomics" Approach—From Active Structure to Lead

Identifying and selecting a viable lead structure is the key to success. Inadequate lead quality was a prominent reason for the failure of many previous discovery programs. For the generation of a lead structure, the reversed-genomics (RG) approach provides a powerful and efficient complementary alternative to the target-based approach (Figure 5). It starts with an active antibacterial compound that exhibits MIC and for which the target and mode of action are not yet known. Modern molecular biology offers excellent techniques to rapidly identify and validate unknown target areas and molecular targets.[86,100,134,135] Bacteria respond to adverse environmental conditions such as heat, starvation, or the presence of an antibiotic by activating stress-dependent regulatory networks. The stress response triggered by an antibiotic relates to its mode of action and can be monitored by various RG techniques, such as: 1) the incorporation of specific radio-labeled precursor molecules, 2) transcriptome analysis, 3) proteome analysis, and 4) FTIR spectroscopy. Such standard tools can be complemented with specific assays for metabolic pathways, enzyme tests, and resistant mutants. Nonpathogenic *Bacillus subtilis* has served as an ideal model organism for proteomics and expression profiling.[135,136] It is one of the best-studied bacteria and is closely related to clinically relevant Gram-positive pathogens.[137–140]

1) Precursor incorporation: A fast method for identifying the mode of action of an antibacterial compound is to examine its effect on the key bacterial macromolecular biosyntheses in the presence of specific radio-labeled precursor molecules in whole cells (Figure 6). Radiolabel incorporation indicates which of the four key processes, protein biosynthesis or the synthesis of DNA, RNA, or cell wall, shows the greatest reaction to the agent, whereas nonselective compounds tend to block several pathways simultaneously.[142,143] This assay serves as a guidepost for more detailed studies.

2) Transcriptome analysis: Inhibition of a specific target by an antibiotic induces characteristic changes in the microorganism's global expression profile, resulting in up- or down-regulation of certain genes. The transcriptional activity of all genes encoded in a bacterial genome can be monitored at the same time and studied by expression profiling techniques (transcriptome analysis) that are based on DNA microarrays. Such profiles, when compared to the reference profiles of established antibiotics, are characteristic for the mode of

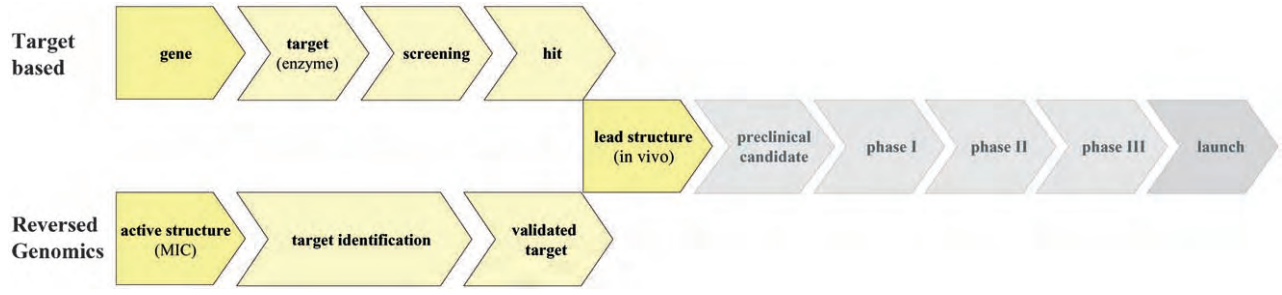


Figure 5. Target-based and reversed-genomics approaches are complementary drug-discovery processes for antibacterial lead-structure generation.

© 2006 Wiley-VCH Verlag GmbH & Co. KGaA, Weinheim

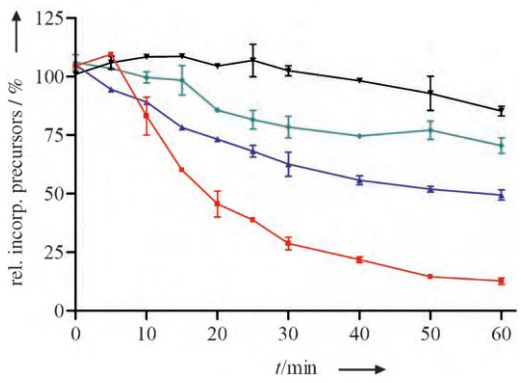


Figure 6. Precursor incorporation: The effect of tetrahydropyrimidinone antibiotic **13** on the principal bacterial biosyntheses pathways of *S. aureus* in the presence of specific radiolabeled precursor molecules was examined. Radiolabel incorporation kinetics indicated which of the four key processes—protein biosynthesis/[^{14}C]leucine (red), synthesis of DNA/[^{14}C]thymidine (blue), RNA/[^{14}C]uridine (black), or cell wall/*N*-acetyl [^{14}C]glucosamine (green)—shows the greatest reaction to the agent. For example, **13** preferentially inhibited protein biosynthesis.[141]

action of an antibacterial agent. Transcriptome analysis has proven to be an efficient tool for tracking a novel agent's mode of action and to elucidate its target.[142,138,144] With an appropriate set of reference antibiotics at hand, compounds with an analogous mode of action can rapidly be identified.

3) Proteome analysis: Changes in gene expression of bacterial pathogens after treatment with antibiotics can also be studied by quantifying proteins, typically by separating cellular proteins by using two-dimensional gel electrophoresis (Figure 7).[136] This method allows the detection of changes at the translation level, that is, protein variants and modifications. Proteome analysis has successfully been used in classifying the mode of action of novel antibacterials[136] as well as for target validation.[145]

4) FTIR spectroscopy: Infrared spectra (IR) of entire bacteria can be used to obtain further insight. When bacteria are treated with antibiotics, characteristic changes in absorption occur. Monitoring these changes by FTIR reveals the principal modes of action.[146,147]

These RG techniques complement each other and all together provide a powerful and efficient platform for lead structure identification and validation. In our experience over the last decade with both the target-based HTS and the RG approaches, the latter, in particular when used to examine natural products, had a significantly higher success rate in generating novel and valid antibacterial leads. Nevertheless, we expect that a well-balanced combination of all these technologies, along with new ideas and efforts, will eventually illuminate the way to valid lead structures and novel antibacterial agents.

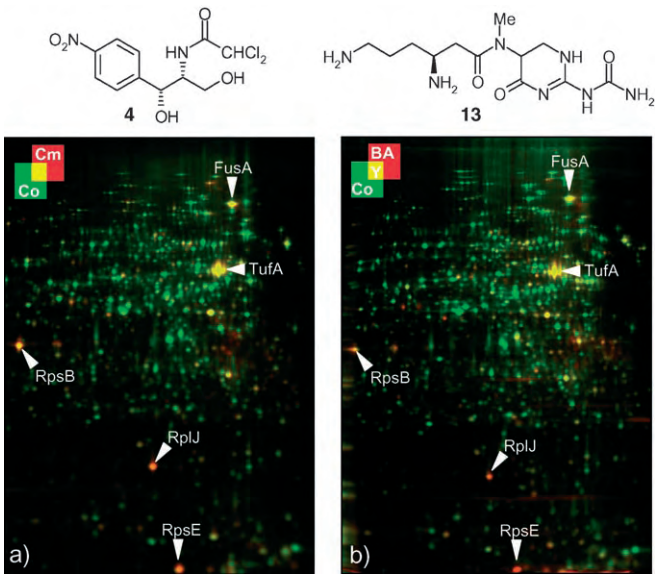


Figure 7. Proteome analysis is a valuable tool for classifying the mode of action of novel antibacterials in the pathogen. Changes in gene expression can be studied by separating and quantifying cellular proteins by using two-dimensional gel electrophoresis. Although each antibiotic shows an individual protein expression profile, overlaps in the expression of marker proteins (arrows) indicate a similar mode of action. By comparing its profile with the profile of chloramphenicol (**4**), **13** was found to be a peptidyl-transferase inhibitor.[136]

6. Chemical Postevolution of Antibacterial Natural Products

In the current environment of the pharmaceutical industry, natural-product chemists often feel like Neanderthal men,[148] not fitting into the paradigm of modern drug discovery. Natural-product chemistry is stigmatized as being old fashioned, expensive, ineffective, and incompatible with modern drug-discovery processes.

6.1. Natural-Product-Derived Antibacterials are Different from Other Drugs

Antibacterial drugs differ from "other drugs" in many aspects (Table 6). Empirical rules (Lipinski et al.),[149] found in medicinal chemistry, are often irrelevant for antibacterials, in particular for those derived from natural products (macrolides, glycopeptides). Many antibacterial drugs have to satisfy the requirements for parenteral and oral administration, a highly demanding task for any drug.

Antimicrobial "chemotherapy" is based on Paul Ehrlich's principle of "selective toxicity". Antibacterial drugs inhibit the growth of bacteria (bacteriostatic) or even better kill them (bactericidal). The treatment goal is the fast eradication of bacteria in cooperation with the immune system. The fact that antibacterial therapy is a "killing discipline" has many implications for the physicochemical and pharmacological profile of antibacterial drugs.

Targets: In many therapeutic areas, the partial modulation of a single target is sufficient. Yet, for antibacterial therapy, complete inhibition of multiple targets is normal. Essential bacterial biosynthetic pathways have to be blocked completely. Inhibition of multiple targets will increase the in vitro potency and minimize the development of resistance. A variety of large natural products exerts multiple modes of action (vancomycin). They act like "pharmacophore chame-

 © 2006 Wiley-VCH Verlag GmbH & Co. KGaA, Weinheim

Table 6: Natural-product-derived antibacterials versus "other" drugs. Empirical rules of thumb.

	Topic	Antibacterials	Other drugs *(Lipinski etc.)*
Target/ Mode of Action		multiple targets; multivalent; block target	single target; selective; modulate target
Structure		complex; multiple pharmacophores	simple; single pharmacophore
Physicochemistry	M_w [g mol^{-1}]	> 500	< 500
	log MA (pH 7.5)	< 3 (parenteral) < 5 (oral)	< 5
	rotatable bonds	> 10	< 10
	H donors	> 5 (parenteral)	< 5
	H acceptors	> 10	< 10
	solubility [g L^{-1}]	> 0.5–2	< 1
Pharmacokinetics	dose	often high	often low
	protein binding [%]	critical	less critical

leons". Indeed, antibacterial drugs tend to have high molecular weights and "repellently" complex structures.

Physicochemistry: The polarity window of antibacterials is defined by solubility requirements and penetration phenomena. In Gram-negative bacteria, porins are essential for uptake and often represent an entry barrier for too-lipophilic molecules.[77] For parenteral drugs, a high solubility in aqueous media is a must (0.5–2 g L^{-1} or even higher). Consequently, parenteral antibacterials have to be polar (log MA < 3). On the other hand, too-polar molecules do not sufficiently penetrate through the cytoplasmic membrane of bacteria.[150] Yet, polar drugs may be concentrated in bacteria through specific transport mechanisms. Passive diffusion through the membrane is not mandatory in this case. Efflux and influx phenomena also have to do with polarity. Bacterial multidrug transporters pump out amphiphilic and lipophilic compounds to a higher degree than hydrophilic molecules. To achieve efficacy in vivo, a compound needs to show substantial passive absorption from the gut into the blood stream, which is determined by adequate aqueous solubility and moderate lipophilicity.[151] Owing to these polarity requirements, many combinatorial libraries are not "antibiotic-like". In this respect, free OH and NH groups are "endangered species" as they entice combinatorial chemists to derivatize them. Indeed, standard combinatorial libraries preferentially were built within the lipophilic rather than in the polar range.

Pharmacokinetics/Pharmacodynamics: Bacterial pathogens can colonize every part of the human body. However, many infections are localized (blood stream, skin, respiratory or urinary tract). The time course of free-drug concentration at the site of infection (time versus concentration) is determined by pharmacokinetics (V_{SS}, $t_{1/2}$, AUC, f_U). Protein binding of antibacterials should not be too high (< 90 %) as only the free drug can act on the target (fraction unbound, f_U > 10 %).[152]

The killing effect of a specific drug concentration depends on its pharmacodynamics (concentration versus antibacterial effect). Only an appropriate time course of drug concentration leads to clinical efficacy. This special time course of drug concentration is the "driver of efficacy" and is further described by the pharmacokinetic/pharmacodynamic index (PK/PD; time versus antibacterial effect)[153,60] that may differ significantly between antibacterial drugs. For example, the PK/PD index of most β-lactams is "time over MIC". Sufficient killing of bacteria is only achieved if the β-lactam concentration remains above the MIC at the site of infection for ≈ 40 % of the treatment time (≈ 9 h day^{-1}).

Dose: In contrast to most other therapeutic areas, very high doses are necessary to attain sufficient drug concentrations in the infected tissue. For example, up to 36 g of penicillin G or 4 g of erythromycin may be given daily to patients with severe infections.[154] Only excellent tolerability will allow for such dosage regimens. As expected, drugs addressing bacterial targets that are absent in mammals (peptidoglycan) have a higher chance to exhibit an outstanding therapeutic index. These drugs will not show a mechanism-based toxicity. However, they may have other toxicity issues (nephro- and ototoxicity of aminoglycosides, QT interval prolongation of the heart, or phototoxicity of quinolones).

6.2. Are Natural Products Good Drugs?

Many natural products are a good starting point for medicinal chemistry. Yet, only a few "pure" natural products fulfill the complex property profile of a pharmaceutical drug (daptomycin, erythromycin, penicillin G, tetracycline, vancomycin).[73,74] Though the medicinal chemist and the "antibacterial microbe" both have the common goal to control bacterial pathogens, a drug has to match additional physicochemical, pharmacological, toxicological, and technical requirements that have not been selectors within the evolution of antibacterial secondary metabolites.

Typical limitations of natural-product leads are limited chemical stability or low solubility, which especially hamper the development of parenteral drugs. In addition, the intellectual property situation is often less clear in unmodified natural products. Many natural products are complex structures with a high molecular weight. "Heavy" structures break Lipinski's rules[149] and will most likely exhibit no absorption from the gut into the blood, therefore impeding oral formulation. Furthermore, complex structures look expensive for technical development. A narrow antibacterial spectrum of the natural-product lead might be the result of low target affinity but often has to do with physicochemical limitations (membrane affinity window) or efflux phenomena that affect transmembrane transport in certain pathogens (spectrum gap). Some natural antibiotics do not show sufficient in vitro potency in standard models (MIC) owing to high protein binding (low F_U) or adhesion phenomena within the test system. Unfavorable pharmacokinetic parameters in animals or humans, such as low half-life in the body ($t_{1/2}$), high clearance of the drug (C_L), low metabolic stability, low

© 2006 Wiley-VCH Verlag GmbH & Co. KGaA, Weinheim

exposure (AUC), or insufficient distribution into infected tissue (V_{SS}), might result in a total lack of in vivo efficacy. Tolerability is one of the big issues of natural antibacterial lead structures. For example, tetracyclines exhibit pronounced phototoxicity, and the use of aminoglycosides is complicated by nephrotoxicity as well as irreversible ototoxicity.

A serious chemistry program will only be initiated if the natural screening hit can be "validated" with further SAR data points. Only a validated hit has the potential to fulfill the criteria for a new lead structure. Combinatorial libraries often yield hit clusters including preliminary SAR data, whereas, natural products only yield solitary hits (singletons), thereby providing no further information. At this point, the synthesis of new congeners is a prerequisite for preliminary SAR information. Usually, chemists will decide to evaluate a hit cluster (synthetica) rather than a singleton (natural-product hit).

6.3. Natural Evolution versus Chemical Postevolution—Orthogonality in Substructure Space

Natural products arise from natural evolutionary processes. In a similar way, a medicinal chemist also shapes the structure of natural templates in an evolutionary optimization process (chemical postevolution). Within learning cycles, successive generations of lead-structure variants of the original natural products evolve. Favorable attributes are passed on to the next generation, unfavorable properties are discarded. Individual mutations are mixed in each generation and tested for their compatibility. Permutation of properties from male and female individuals (sex) is a key strategy in natural evolution, whereas the structural combination of distinct chemical leads is crucial for success in medicinal chemistry (additive SAR).

Obviously, natural selection and chemical postevolution do not have exactly the same objectives. However, many properties of a molecule play an important role during both the process of natural evolution and the process of chemical optimization. In both processes, individual parameters such as target affinity, solubility, and cytotoxicity variably contribute to the "fitness" of a specific molecule. Nature continues to design highly complex pharmacophores from scratch by the everlasting interplay of mutation and selection over vast periods of time. With a rather limited palette of building blocks—acetate, propionate, mevalonate, shikimate, amino acids—nature creates surprisingly manifold structures. Evolutionary change in natural products stems from mutations in the corresponding biosynthesis genes. Structural diversity is driven by the rearrangement of modular biosynthesis genes (polyketides) and a refinement toolbox that is typically applied within the late stage biogenesis (oxidation, methylation, condensation).

Rolling out of new starting materials was a rare event within evolution. Truly novel starting materials required a fundamental changeover of the biosynthetic machinery that has evolved over millions of years. Presumably, the coevolution of proteins and natural products was another reason for nature's evolutionary focus on a few mainstream biosynthetic pathways to primary and secondary metabolites. Hence, a remarkable substructural conservatism results. In most natural products, the skilled eye can discover the same substructural motives time and time again. Indeed, the impressive macroscopic diversity of natural products is composed from a fairly narrow set of substructural motives.

In general, a medicinal chemist can easily evade nature's rigid biosynthetic pathways. Ordinary structural elements are virtually inaccessible for natural producers (*tert*-butyloxy, fluoroaryl, most heterocycles), and switching starting materials is a common method towards diversity. Complementary to nature, the medicinal chemist can explore additional substructural space: in a sense, chemical postevolution of natural products is orthogonal to natural structural evolution. Within a short time, medicinal chemistry can explore white spots in structural space (and biological activity) that have never been touched by microorganisms, fungi, plants, and animals over the entire period of evolution.

6.4. Chemical Postevolution—Improving Nature's Blueprints

Medicinal chemistry has the challenging task of simultaneously optimizing the natural-product lead structure for in vitro potency, in vivo efficacy, low toxicity, druglike physicochemical properties, and good pharmacokinetics (chemical postevolution). This multidisciplinary effort intertwines chemistry, microbiology, pharmacology, and toxicology. SAR, structure–toxicity relationships (STRs), and a basic understanding of pharmacokinetics are established in learning cycles (test sequences) and are based on biological data from the individually designed "screening cascade". Most natural hits in antibacterials have been picked because they show satisfactory in vitro potency (MIC). Now, medicinal chemistry is used to induce into the structure additional properties, such as solubility or tolerability, without losing its intrinsic antibacterial activity.

In the industrial research environment—governed by project timelines—it is especially difficult to work with complex natural products. Only a real commitment to the lead will prevent a medicinal chemist from sidestepping towards "easier" small molecules that are amenable to efficient parallel synthesis and guarantee the production of more test compounds. Sometimes natural-product leads are hastily judged to be not optimizable owing to a steep SAR (few potent derivatives) or a SAR that parallels STR (potent derivatives are toxic). Often this has to do with limited diversity of the available derivatives rather than with insufficient lead potential. In these particular cases, the chemical methodology does not really capture the lead structure (core variations), but plasters the pharmacophores with lipophilic residues (limitations of the template concept).

Despite a common prejudice, it is possible to increase the innate antibacterial activity of natural products in the laboratory even though the natural product has been evolutionarily optimized for antibacterial activity[155] over millions of years.

 © 2006 Wiley-VCH Verlag GmbH & Co. KGaA, Weinheim

6.5. How to Get Starting Material?

A natural-product chemist working with natural products often works with very limited amounts of material. Substance supply is the key challenge for most natural-product chemistry programs in the pharmaceutical industry. Typically, the natural-product screening hit is only available in minor amounts (mg range) in the initial project phase. Only few projects can afford to bring up further "starting material" (the natural product) through total synthesis without losing too much time and resources (see below). Cooperation with dedicated academic groups may help to assure material supply in time (de novo synthesis).

Regularly, fermentation is the most efficient source of the natural-product starting material. Still, not every natural-product screening hit can be easily obtained through biotechnological means. Many producer strains are not available or cannot be grown in culture (mycorrhiza fungi). Other organisms grow well, but the biosynthesis of antibiotic secondary metabolites cannot be elicidated under culture conditions. Only dedicated expert groups guarantee reproducible fermentation conditions that are a prerequisite for technical development and production on a large scale.

6.6. The Modest Life of De Novo Synthesis in Industry

Only de novo synthesis—and not semisynthesis—provides the most manifold options for broad structural variation that can fully assess a lead structure's potential (Table 7). Various natural products have been explored through total synthesis, and peptidic structures and structures of intermediate complexity seem to be especially suitable for this approach in industry. For example, in the carbapenem area, de novo synthesis has played a key role in chemical optimization and technical development. However, for complex structures with high molecular weights, de novo synthesis tends to be expensive and slow. The highest hurdle for the de novo synthesis of complex molecules is the phase of technical development. A "good" drug candidate may be found in research by means of de novo synthesis, but if there is no practical semisynthetic entry for development, this compound might never be produced on a technical scale. Therefore, not many medicinal-chemistry programs in antibacterials dealing with complex natural-product leads can afford the "luxury" of establishing SARs based on de novo synthesis within the exploratory project phase. Indeed, the medicinal potential of many "old", but complex, classes has not yet been fully assessed by means of de novo synthesis. Not a single purely synthetic glycopeptide, tetracycline, aminoglycoside, or rifampicin has ever reached the clinic. Although total syntheses have been described for these molecules, no comprehensive SAR/STR has been established to date. From a chemist's structural perspective these classes are not "old" at all! Serious de novo synthetic explorations would most likely yield novel drug candidates.

De novo synthesis has demonstrated its impact in some therapeutic areas (antitumor, antiviral). The "cost-effective" de novo solid-phase synthesis of enfuvirtide, an anti-HIV peptide composed of 36 amino acids, in 106 steps is most impressive.[156] Recent masterpieces in the chemistry of epothilones,[157] ecteinascidin 743, and discodermolide demonstrated that it is indeed possible, when academia and industry cooperate, to employ complex de novo syntheses in the development of new drugs.

Table 7: Perception of de novo synthesis and semisynthesis of antibacterial natural products.

	De novo synthesis	Semisynthesis
perception	total synthesis, art in organic chemistry—"create"	derivatization, tool for organic chemistry—"fix problems"
literature	uncountable	underrepresented (scattered in patents)
timelines	slow	fast
mandatory supply with natural-product lead compound	only small amounts of reference material needed	larger quantities of "starting material" crucial (fermentation and isolation)
structure–activity relationship	global and comprehensive	locally restricted
biology of products	bioactivity "guaranteed"	mostly inactive congeners
disadvantage	long synthetic routes	selectivity issues (handle a minefield of functionality)
advantage	controlled selectivity (orthogonal protecting groups)	short synthetic routes
experience with functional natural product	in the last synthetic step	all the time
technical development	"cost of goods" critical	proven economic significance

6.7. Semisynthesis is Key in Industry

Semisynthesis can only address a limited chemical space of the natural-product lead structure. But it is fast and apparently straightforward. In practice, semisynthesis is the method of choice for lead optimization in the exploratory project phase with complex natural products. Experience and today's analytical techniques (HPLC, LC-ESI-MS, NMR spectroscopy) allow for reactions in the 100-μg scale for initial SAR studies even with complex molecules (microderivatization). Preliminary in vitro testing can be done with less than 1 mg of material (MIC, cytotoxicity). Also in late-stage industrial development (kg scale), semisynthesis is often the common logical consequence of structural complexity, timelines, and "cost of goods" estimates. Many marketed antibacterial drugs are semisynthetic congeners of natural products, and are obtained from the chemical refinement of

© 2006 Wiley-VCH Verlag GmbH & Co. KGaA, Weinheim

fermentation products (oritavancin, tigecyclin,[21] telithromycin, rifampicin).[4]

6.8. The Modest Life of Semisynthesis in Academia

Derivatization chemistry is still under-represented in chemical literature despite its unrivalled importance for the drug discovery process. Although the chemical literature thrives on total syntheses, only few organic chemists from academia seem to be attracted by the semisynthetic elaboration of complex natural products. In the early 20th century, pioneers like Willstätter and Robinson groped their way through the constitution of complex alkaloids by doing decoration and degradation reactions.[158] Today, derivatization is regarded to be a simple tool for fixing problems in structure elucidation when spectroscopy alone cannot do the job (Mosher ester for NMR spectroscopy, persilylation for GC analysis, and heavy atoms for X-ray analysis).

Only total synthesis, which creates complex matter from scratch or thought, is cherished as "art in chemistry". Yet, derivatization of complex natural products is a highly demanding scientific task that can only be accomplished with state-of-the-art chemistry and analytics. When looking at the target molecule, the derivatization chemist is confronted with a minefield of unprotected functionality at a stage of high complexity. Every chemical operation planned may be spoiled by selectivity issues. Conversely, in total synthesis, troublesome functionalities are blocked with orthogonal protecting groups from the very beginning when it is still at a stage of low complexity. Typically, de novo synthesis deals with the real natural product only in the last, often redeeming, step. Throughout total synthesis, protecting groups block the natural chemical functionality that is important for biological activity. In contrast, during semisynthesis, most chemical experience is gained with the total and accordingly functional structure, as it has been invented by nature for target interaction. In this way, the medicinal chemist learns about the architecture and intrinsic reactivities of a natural-product lead that cannot be deduced by just looking at the Lewis structure or by working with (protected) fragments.

When starting the total synthesis of a natural antibiotic, bioactivity is often guaranteed for target molecules that come from literature. Instead, many semisynthetic analogues of natural products are inactive and not appreciated. In general, total syntheses towards natural products are published in high-impact journals, whereas semisynthesized natural-product analogues and mimetics face higher hurdles. The risk to explore the unpublishable is high in semisynthesis and the exploration of natural-product congeners.

6.9. Principle Types of Structural Modification—What is the best strategy?

Natural products may be tailored in a direct fashion by chemical derivatization (structural modification). Furthermore, formal products of structural modification may be obtained through de novo synthesis. The success of a natural-product chemistry program strongly depends on the chosen concept of modification. We differentiate three principle types of structural modification: 1) decorating modification (attach), 2) degrading modification (cut out), and 3) substituting modification (cut out and reattach). Various synthetic congeners of natural products are intermediate cases that have been obtained by combinations of several modification types. For example, telithromycin is obtained by degrading and decorating modification of the natural product erythromycin. There is no defined border between modification products and mimetics of natural-product lead structures (see Table 8).

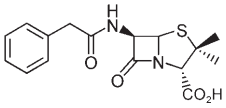
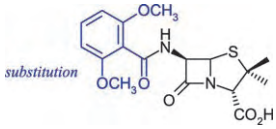
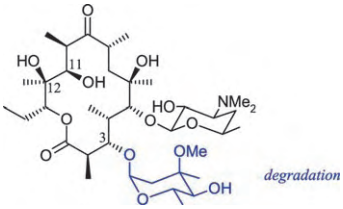
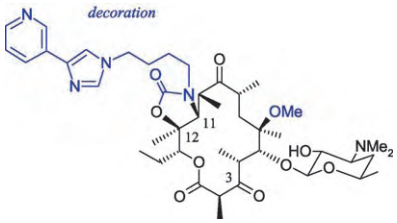
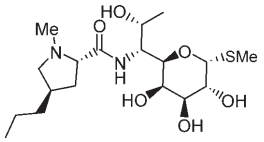
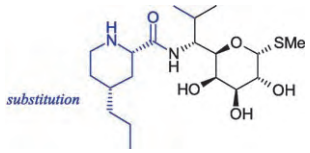
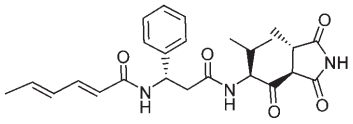
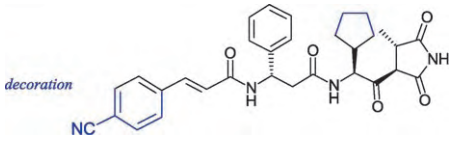
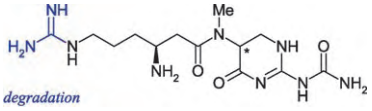
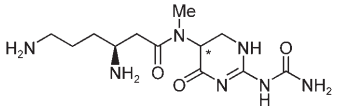
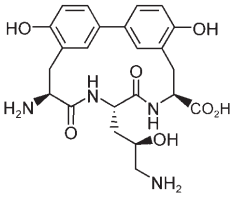
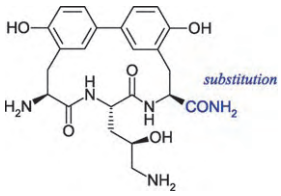
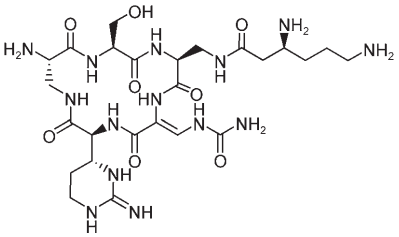
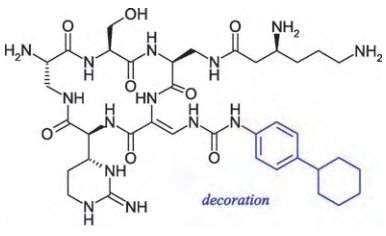
Decorating modification is the most popular form of structural modification in medicinal chemistry, especially in semisynthesis. Functional groups presented by the "natural-product template" are used as anchors to attach additional, non-natural residues. Reductive alkylations, acylations, PEGylations,[159] and hydrogenations are "classical" reaction types of decorating derivatization. For example, various glycopeptides from the vancomycin series have been decorated with lipophilic biphenyl residues (oritavancin) through reductive alkylation, leading to a modified mode of action. Solubility may be increased by adding charged residues. Usually, regio- and chemoselectivity is a serious issue when decorating complex structures as they present a whole ensemble of, naturally free, functional groups. In these cases, the laborious handling of protecting groups is a prerequisite for sufficient chemical selectivity and acceptable yields. With smaller natural products, decorating derivatization often fails to yield bioactive congeners for a different reason:[160] the few functional groups present are important for target interaction and decorating the molecule merely results in the futile masking of pharmacophores. This kind of chemical "baroquization" has stigmatized many natural products as being nonoptimizable.

Substituting modification allows a deeper exploration of the natural-product lead. This is an especially powerful methodology in semisynthesis. In a first move, parts of the molecule are cut out by chemical means. Then, the gap is filled by reattachment of bioisosteric building blocks, mimetic structures, or abiotic constructs. This strategy has several major advantages: not only are peripheral functional groups of the chemical lead addressed, but even core modifications of the carbon skeleton are possible. Whether critical biological parameters can be tuned is assessed on the basis of a complete, but locally restricted, SAR map. Substituting derivatization is more tempting than decoration as a thorough understanding of reactivity within the natural-product lead is crucial. When selective degradation reactions are unavailable, de novo synthesis is the way to advance. For decades, penicillins have proven the high potential of substituting derivatization.

Degrading modification is successful when structurally defined toxophores or labile groups that are not simultaneously pharmacophores can be cut out of the molecule by chemical means. Unfavorable parts of the natural-product lead, not important for target interaction, may be degraded to obtain a drug of higher stability (ramoplanin aglycon) or lower structural complexity. However, chemoselectivity prob-

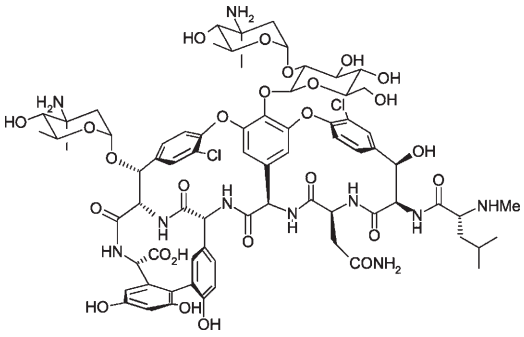
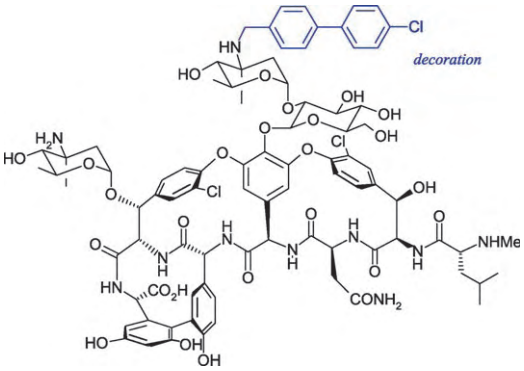
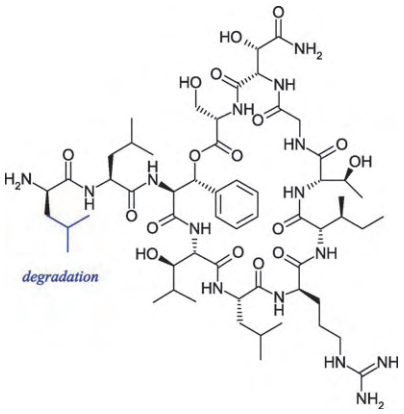
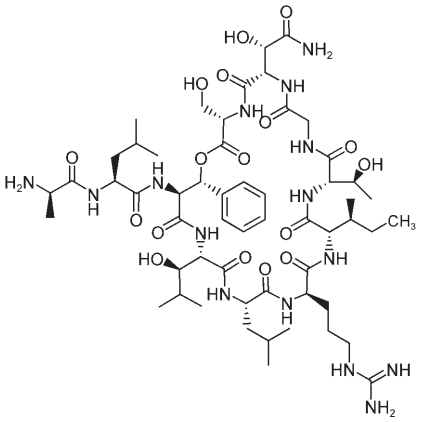
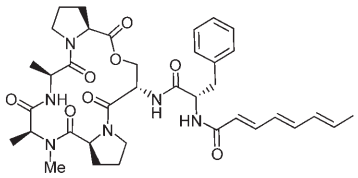
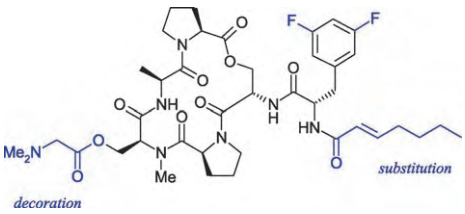
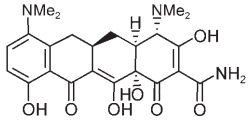
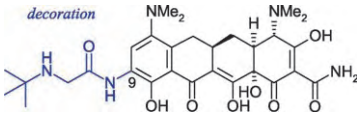
 © 2006 Wiley-VCH Verlag GmbH & Co. KGaA, Weinheim

Table 8: Modification of natural-product lead structures through semisynthesis and de novo synthesis. Type and site of modification (blue) and progress achieved.

Natural-product lead structure	Synthetic congener	Type	Progress
 penicillin G (**2**)	 methicillin (**14**)	substituting modification through semisynthesis, mutasynthesis, and de novo synthesis	increased stability
 erythromycin A (**6**)	 telithromycin (**15**)	degrading and decorating modification; degradation of cladinose; decoration of C11/C12 and C6 area	new binding mode, low cross-resistance with erythromycin, stability in acidic medium
 lincomycin (**16**)	 VIC-105555 (**17**)	substituting modification through semisynthesis	reduced resistance induction
 moiramide B (**18**)	 **19**	decorating modification via de novo synthesis	improved potency and stability
 TAN-1057A/B (**20**)	 **13**	degrading modification of the toxophore through de novo synthesis	reduced toxicity
 biphenomycin B (**21**)	 **22**	substituting modification through semisynthesis and de novo synthesis	improved antibacterial spectrum
 capreomycin 1 A (**23**)	 **24** ($R^1 = OH$)	decorating modification through semisynthesis	improved antibacterial spectrum and potency

© 2006 Wiley-VCH Verlag GmbH & Co. KGaA, Weinheim

Table 8: (Continued)

Natural-product lead structure	Synthetic congener	Type	Progress
 chloroeremomycin (**25**)	 oritavancin (**26**)	decorating modification through semi-synthesis	additional mode of action, extended antibacterial spectrum
 lysobactin (**27**)	 [D-Ala^1]lysobactin (**28**)	degrading modification within the linear segment through semi-synthesis; Edman degradation	preliminary SAR
 A 54556 B (**29**)	 **30**	decorating and substituting modification through de novo synthesis	improved stability, solubility, and potency
 minocycline (**31**)	 tigecycline (**32**)	decorating modification through semi-synthesis	beat resistance by better binding to ribosome

lems often thwart "direct" semisynthetic degradation. In many cases, de novo synthesis is the method of choice for truncated derivatives of natural products. For example, as a result of guanidine degradation, **13** showed significantly reduced toxicity with respect to the natural-product lead TAN-1057 (**20**, Section 12). Yet, **13** was obtained by de novo synthesis and is just a formal degradation product of **20**.

7. β-Lactam Antibiotics

The β-lactam group of antibiotics was the first class of antibacterial natural products introduced as a therapeutic treatment of bacterial infections. Today, more than 75 years after Fleming's discovery of penicillin from cultures of *Penicillium notatum*,[161] this group still includes the clinically most-widely-used agents and accounts for about half of all antibacterial drugs prescribed (Figure 8).

 © 2006 Wiley-VCH Verlag GmbH & Co. KGaA, Weinheim

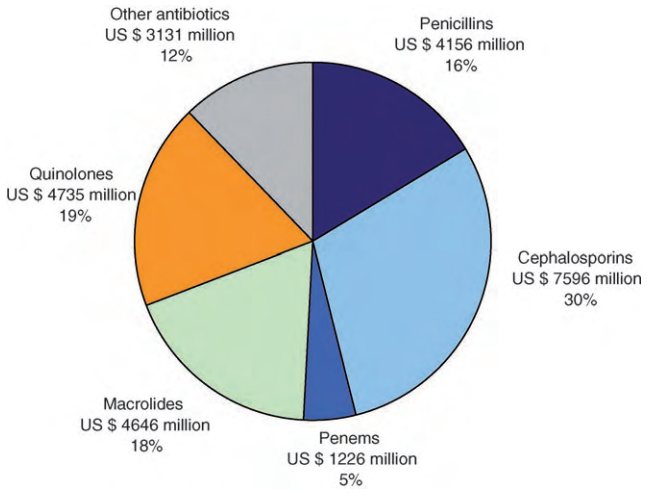
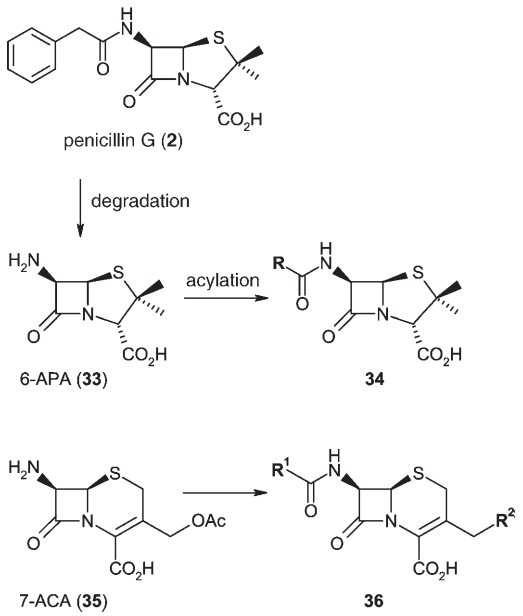


Figure 8. Global sales of the major antibacterial classes in 2004 (from Wood Mackenzie[69]).



Scheme 1. Semisynthetic modifications of building blocks 6-APA (**33**) and 7-ACA (**35**) through a substituting-derivatization strategy.

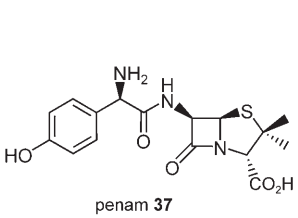
Owing to their broad antibacterial spectrum, their clinical efficacy, and their excellent safety profile, β-lactam antibiotics have been one of the preeminent areas of pharmaceutical drug discovery. Their compact structural density, along with their sensitivity, has provided a challenging "playground" for generations of medicinal chemists that has not lost its attractiveness even now. All β-lactam antibiotics share a common structural element, the four-membered azetidinone or β-lactam ring, their pivotal reference mark and center of action. In most antibiotics, this central β-lactam ring is fused to a second five- or six-membered ring system. In the biosynthetic multistep process to form penicillins and cephalosporins, nature employs L-valine, L-cysteine, and L-α-aminoadipic acid. With the the help of a modular nonribosomal peptide synthetase for the construction of an intermediate tripeptide that is oxidatively converted into the primary penicillin, isopenicillin N, by isopenicillin N synthetase.[162] Natural penicillin G (**2**), the first therapeutic antibiotic and lead structure of this class, still had a few critical features that needed improvement, for example, narrow antibacterial spectrum, instability in acidic (stomach) and basic (intestine) environments, limited solubility, pronounced sensitivity to hydrolysis by bacterial penicillase enzymes, and fast clearance from the body. Additional biosynthetic studies afforded the first orally applicable β-lactam antibiotic, penicillin V,[163] which has improved activity against staphylococci and better stability towards acids. However, not until the key building blocks 6-aminopenicillanic acid (6-APA, **33**)[164] and 7-amino cephalosporanic acid (7-ACA, **35**)[165] became readily available from high producing strains of *Penicillium chrysogenum*[164] by enzymatic cleavage of penicillin G (**2**) with penicillin acylase[166] or chemical synthesis, respectively, did medicinal chemists enter the infinite game of semisynthetic variations (Scheme 1).

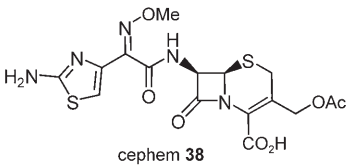
For about thirty years, penicillins (penams) **37**[167] and cephalosporins (cephems) **38**[167–169] remained the sole examples of β-lactam antibiotics. During a booming search and discovery period during the 1970s and 1980s, many related subgroups, such as the monobactams (aztreonam, **39**),[170] oxacephems (moxalactam, **40**),[167,171] carbacephems (loracarbef, **41**),[172] oxapenams (clavulanic acid, **42**),[173] penems (faropenem, **43**),[173a,174] carbapenems (imipenem, **44**),[170,175] and oxapenems (AM-112, **45**),[176] were discovered from microbes or were obtained by synthetic efforts. Endless structural variations of these β-lactam scaffolds provided derivatives with increased potency and improved physicochemical and pharmacokinetic profiles.[168] Many aspects and subgroups of this important research area have been extensively reviewed,[177] and therefore, only a few selected examples, issues, and references can be mentioned herein.

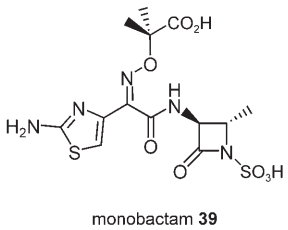
β-Lactam antibiotics inhibit bacterial growth by interacting with PBPs, enzymes that are normally involved in the terminal transpeptidation (cross-linking) steps of bacterial cell-wall biosynthesis.[178] The historic term penicillin-binding protein demonstrates how a class of antibiotics can serve to detect new targets (target fishing) and increase the understanding of biological processes. The enzymes mistake β-lactam antibiotics for the C-terminal L-Lys-D-Ala-D-Ala end of peptide chains yet to be cross-linked. Their active-site serine opens the β-lactam ring and blocks the PBP enzyme by forming an inert acyl enzyme intermediate.[179] As a result, well-defined peptidoglycan cross-linking damages occur that eventually kill susceptible microbes and in most cases lead to complete destruction of the bacterial cell by autolysins, bacterial cell-wall autolytic enzymes.[180]

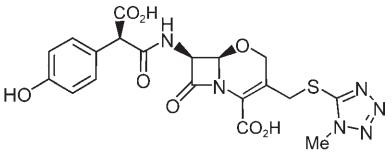
The peptidoglycan (or murein) sacculus is a flexible and enormously stable macromolecular meshwork that defines the shape of the bacterial cell and protects the microorganism against its high internal osmotic pressure.[181] The chemical structure of peptidoglycan varies among different bacteria. In most bacteria, peptidoglycan consists of strings of alternating β-1,4-linked *N*-acetyl-glucosamine and *N*-acetyl-muramic acids that are cross-linked by short peptide chains (Figure 3).[182] Peptidoglycan and related biosynthetic path-

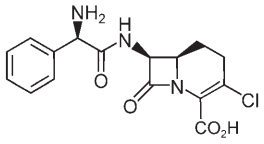
 © 2006 Wiley-VCH Verlag GmbH & Co. KGaA, Weinheim

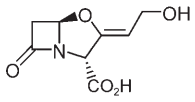

penam **37**

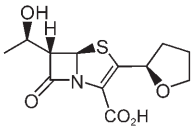

cephem **38**

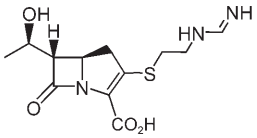

monobactam **39**

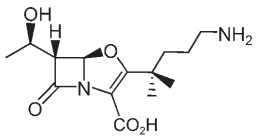

oxacephem **40**


carbacephem **41**


oxapenam **42**


penem **43**


carbapenem **44**

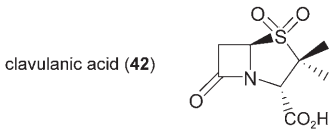

oxapenem **45**

marketed β-lactamase inhibitors, such as sulbactam (**46**)[177d] and tazobactam (**47**),[192] are not effective against class C enzymes. Most β-lactamase inhibitors are bad PBP binders and are themselves almost devoid of antibacterial activity.

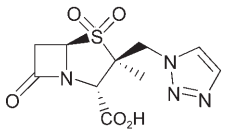
The stability of cephalosporins towards β-lactamases and the expansion of their antibacterial spectrum has been gradually improved during their chemical postevolution. Based on their efficacy and activity profile rather than on their structure, they have been grouped into four generations.[169] First-generation cephems, although active against Gram-positive staphylococci and streptococci, have only moderate activity against Gram-negative bacteria that do not produce β-lactamases. These Gram-negative limitations

ways do not exist in mammals. Therefore, β-lactam antibiotics, in general, have excellent safety profiles and often are the agents of choice for pediatric use. Furthermore, peptidoglycans or parts thereof warn our body about intruding bacteria and trigger an immune response.

The distinct activity of various β-lactam antibiotics arises from a combination of their different affinities to PBPs, their stability towards degrading β-lactamase enzymes, and differences in their physicochemical properties. These key features or combinations thereof also play a dominant role in the development of resistance. Resistance to β-lactam antibiotics can be caused by various events: An altered PBP, for example, in PRSP, attainment of an additional low-affinity PBP, such as PBP2a in methicillin-resistant *S. aureus* (MRSA),[183] diminished ability to penetrate bacterial cell walls, for example, in strains of *P. aeruginosa* lacking the outer membrane protein OprD (D2 porin),[184] activation of multiple-drug efflux systems, for example, MexAB-OprM in *P. aeruginosa*,[185] and production of β-lactamase enzymes, which inactivate the antibiotic by hydrolyzing its β-lactam ring.[186] Production of β-lactamases, in particular by Gram-negative bacteria is a significant cause of resistance to β-lactam antibiotics. At present, nearly 500 β-lactamases have been described and classified into four classes, A–D.[187] Classes A, C, and D are serine enzymes, whereas class B enzymes are zinc metallo-β-lactamases.[188] In particular, class A and also class C enzymes are of clinical relevance, but resistance in the other classes is on the rise. One successful therapeutic strategy has been to administer a β-lactamase inhibitor together with an antibiotic.[189] Augmentin, the combination of the β-lactamase inhibitor clavulanic acid (**42**) with amoxycillin (**37**), may serve as a representative and commercially unbeaten example.[190] Clavulanic acid (**42**), obtained from *Streptomyces clavuligerus*, remains one of the rare examples of an unaltered natural β-lactam that is used in therapy.[191] However, **42** and other


clavulanic acid (**42**)

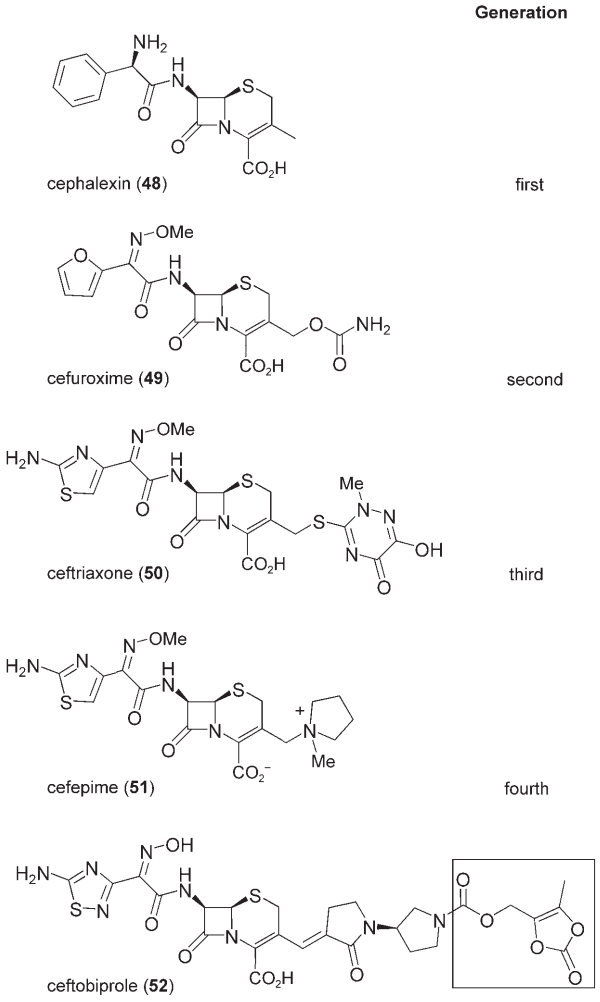
sulbactam (**46**)


tazobactam (**47**)

have been improved in subsequent generations, albeit at the expense of their ability to cope with Gram-positive pathogens. In particular, the efficient and safe third-generation cephems, such as cefotaxime, cefixime, ceftibuten, and ceftriaxone (**50**), have been widely used in patients. Compared to earlier generations, fourth-generation cephalosporins, cefepime (**51**), and cefpirome, cover an extended Gram-negative antibacterial spectrum including multiple-drug-resistant *Enterobacter* and *Klebsiella* species.

Recently, a new group of so-called *anti*-MRSA-cephalosporins[193] has been added. In addition to the coverage of a Gram-negative spectrum comparable to third-generation drugs, the members of this group exhibit an extended Gram-positive spectrum, including, for the first time, useful activity against methicillin-resistant staphylococci. Ceftobiprole (BAL5788, **52**), the most-advanced representative, has recently completed phase-II clinical studies in patients with complicated skin and skin-structure infections (cSSSI).[169] Only cephalexin (**48**) is small and lipophilic enough to be orally available. All other examples are parenteral drugs. To achieve oral availability of large polar cephems, ester prodrugs, for example, cefuroxime axetil, have commonly been used.[194] After absorption from the gastrointestinal tract, the ester groups are rapidly cleaved and the active parent drug is released. In a different prodrug approach, the *N*-terminal carbamate function in **52** (see box) has been

 © 2006 Wiley-VCH Verlag GmbH & Co. KGaA, Weinheim

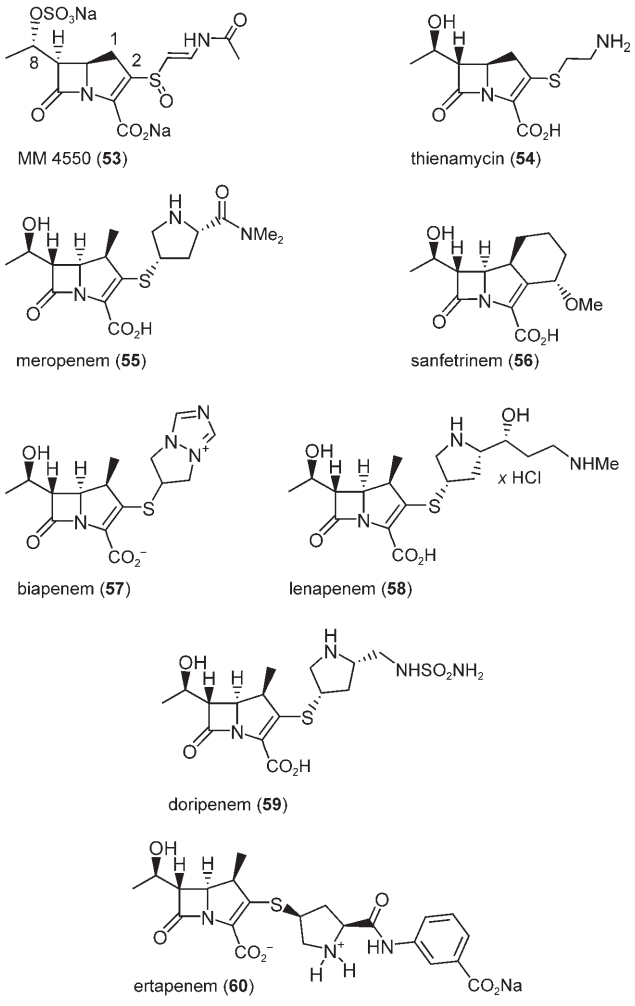


employed to achieve sufficient solubility for parenteral application of the active parent cephem BAL-9141.[169]

The carbapenems[175,177e] qualify as "first-line agents" for the treatment of severe nosocomial infections because of their excellent antibacterial activity, their very broad spectrum of activity, and their stability to most clinically relevant serine β-lactamases. Olivanic acids, such as MM 4550 (**53**)[195] and thienamycin (**54**)[196] were the first examples of this subgroup. The olivanic acids, discovered during a screening program for β-lactamase inhibitors from *Streptomyces olivaceus*, were *cis*-substited β-lactams that, in addition to their ability to inhibit β-lactamases, also exhibited broad-spectrum antibacterial activity.[197] However, they were too unstable for clinical application.

The first carbapenem introduced into clinical therapy was imipenem (**44**), the *N*-formimidoyl derivative of **54**, another highly unstable natural antibiotic with a free terminal amino group and a *trans*-substited β-lactam ring. Its *trans*-β-lactam substitution and 8*R* rather than 8*S* stereochemistry improved antibacterial activity without sacrificing the stability to β-lactamases. Thienamycin (**54**) was isolated from cultures of *Streptomyces cattleya* during a soil-screening program for inhibitors of peptidoglycan synthesis[198] and shortly after, its first total synthesis was reported.[199] Imipenem's basic amidino group is protonated at physiological pH, rendering it more stable than the natural antibiotic **54**. These pioneering works have served as a starting shot for numerous companies and academic groups to enter carbapenem research programs in the 1980s. In contrast to other β-lactams, carbapenems are stable to most clinically relevant β-lactamases.[200] In general, only class B and D enzymes are able to inactivate them.[201] However, besides creating stable and potent derivatives of sensitive natural products, a fair share of additional problems were waiting to be solved by medicinal chemists. As **44** was hydrolyzed in vivo by human renal dehydropeptidase I, it had to be administered as a 1:1 combination with the dehydropeptidase inhibitor cilastatin to prevent inactivation of the antibiotic.[202]

Panipenem, the next carbapenem to be approved in Japan, suffered from the same drawback, and likewise required coadministration of a dehydropeptidase I inhibitor, betamipron.[203] The medicinal chemists next goal was to combine excellent broad-spectrum activity with chemical and enzymatic stability in one single molecule. This was achieved with meropenem (**55**), the first clinical carbapenem with a β-methyl group in position 1.[204] 1-β-Methyl substitution rendered carbapenems stable to hydrolytic degradation by renal dehydropeptidase I, a discovery that was immediately taken

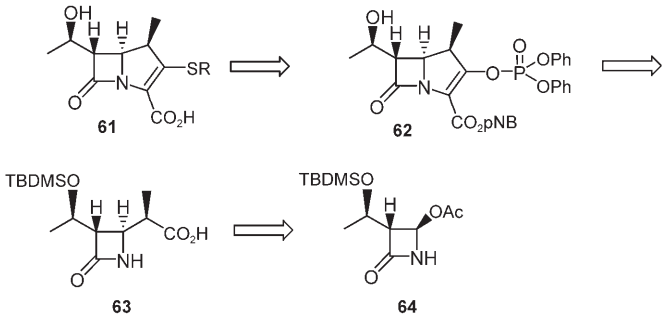


 © 2006 Wiley-VCH Verlag GmbH & Co. KGaA, Weinheim

up and explored through related structural variations. For example, the 1-β-methyl group could also be part of a third fused ring, revealing novel tricyclic "tribactams" or "trinems" such as sanfetrinem (GV 104326, **56**).[205]

Nevertheless, most structural exploration efforts focused on modification of the 2-position. Further parenteral carbapenems, such as biapenem (L-627, **57**),[206] lenapenem (BO-2727, **58**),[207] doripenem (S-4661, **59**),[208] ertapenem (MK-826, **60**),[209] and others,[175] followed in a fascinating process of chemical postevolution. Ertapenem (**60**), a parenteral 1-β-methyl carbapenem with a longer serum half-life (once daily) than **44** and **55** may serve as an example for a drug with a distinct pharmacokinetic improvement.[209b]

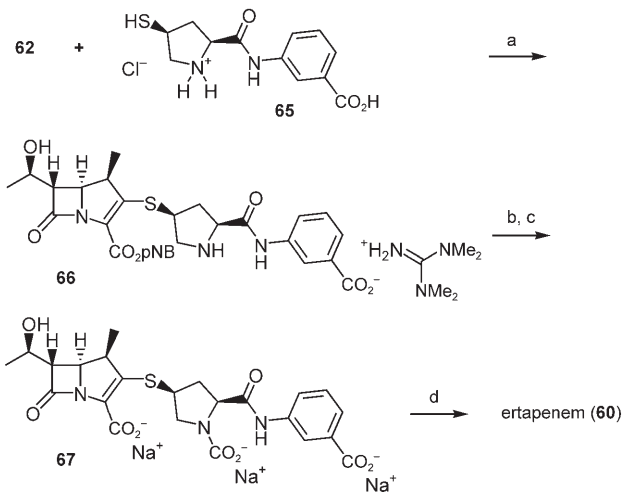
Technically, carbapenem antibiotics have been produced by de novo syntheses rather than by fermentation processes. The synthetic access to 1-β-methyl carbapenems was pioneered by chemists in the Merck company who, by their retrosynthetic concept, defined 4-nitrobenzyl-protected 1-β-methyl carbapenem enolphosphate **62**, carboxyethyl-azetidinone **63**, and acetoxy azetidinone **64** as key building blocks (Scheme 2).[210] Many synthetic pathways toward these crucial intermediates have been elaborated since.[211] Today, they are commercially available on a large scale, in particular from Japanese companies.



Scheme 2. Retrosynthesis of 1-β-methyl carbapenems.[210]

Ertapenem's chiral thiol side chain **65** has been obtained in an efficient one-pot synthesis amenable for large-scale production.[212] Coupling of enol phosphate **62** with unprotected thiol **65** to afford ertapenem sodium (**60**) proved to be delicate owing to the presence of acidic and basic functions. Nonetheless, Merck chemists devised an efficient reaction that minimized the use of protecting groups[213] and employed tetramethylguanidine as a base. The use of carbon dioxide during the hydrogenolysis of the 4-nitrobenzyl ester at pH 8 enabled transient protection of the pyrrolidine as sodium carbamate. Ion-pair extraction and crystallization under mild conditions concluded this challenging task (Scheme 3).

Sensitive β-lactam intermediates and products often require particularly mild synthetic methods.[214] As a "principle", reactions that work with β-lactams seem to work with almost any other structure, but not vice versa! Nevertheless, the very favorable clinical experiences with marketed carbapenems have rewarded medicinal chemists for many challenging syntheses and difficulties during development. β-Lactam antibiotics continue to be one of the most important



Scheme 3. The Merck synthesis of ertapenem (MK-0826, **60**), a novel carbapenem approved in 2001.[213] Reagents and conditions: a) tetramethylguanidine, *N*-ethylpyrrolidone, −40 °C, 3 h; b) H_2, 5% Pd/C, CO_2, pH 8, below 15 °C; c) $(PhO)_2P(O)OH$, 50% NaOH, isoamyl alcohol; d) 1-propanol, below −5 °C, pH 5.5.

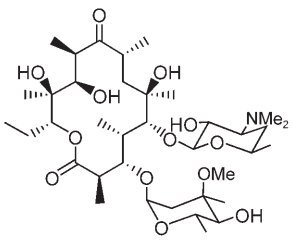
classes in antibacterial research and development. Their efficacy and compatibility has allowed their broad therapeutic application in the community and in hospital environments including on children and elderly patients.

8. Macrolide and Ketolide Antibiotics

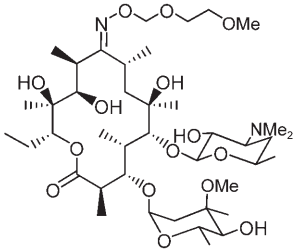
Macrolide antibiotics, a subgroup of the polyketide natural products, are an important class of therapeutic agents that act against community-acquired respiratory infections such as community-acquired pneumonia (CAP), acute bacterial exacerbations of chronic bronchitis, acute sinusitis, otitis media, and tonsillitis/pharyngitis.[215,216] *Streptococcus pneumoniae*, *Streptococcus pyogenes*, *Haemophilus influenzae*, and *Moraxella catarrhalis* are the predominant pathogens involved in this diseased state. Despite their bacteriostatic mode of action, macrolides account for about 20% of all the antibiotics prescribed. Macrolides have a unique distribution with very high concentrations in lung tissue. Many aspects of the macrolides have been thoroughly studied and competently reviewed in numerous articles[217] and books.[215,218] Herein, we intend to focus on a few selected contributions by medicinal chemistry.

Erythromycin A (**6**), the prototype and ancestor of the macrolide family, was first isolated from *Streptomyces erythreus* discovered in a soil sample taken from the Philippine Archipelago by scientists from the company Lilly in 1952.[219] The structure of **6**, the major and most important component produced during fermentation along with its congeners erythromycin B and C, was subsequently elucidated[220,221] and its absolute configuration was established by NMR spectroscopy studies[222] and X-ray crystallographic analysis.[223] Immediately, its complex structure with two unusual sugars, L-cladinose and D-desosamine, attached to a 14-membered lactone ring with 10 asymmetric centers, attracted

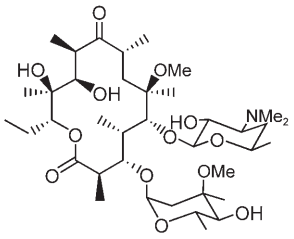
 © 2006 Wiley-VCH Verlag GmbH & Co. KGaA, Weinheim



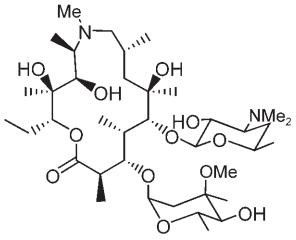
erythromycin A (**6**)



roxithromycin (**68**)



clarithromycin (**69**)



azithromycin (**70**)

the synthetic chemists' attention and resulted in one of the milestones in synthetic chemistry: Corey's total synthesis of erythronolide A in 1979[224] and Woodward's asymmetric total synthesis of **6** in 1981.[225]

Despite the creation of the principle tools for macrolide de novo synthesis, semisynthesis has been economically more viable and has remained the basis for all marketed macrolide (and ketolide) antibiotics to date.

In many respects, polyketide biosynthesis,[226] with erythromycin as the best-studied example,[227] resembles the biosynthesis of fatty acids. Macrolide antibiotics are derived from successive condensations of acetate, propionate, and butyrate building blocks put together with the help of modular polyketide synthases.[226,228] The resulting linear acyl chains cyclize through lactonization, and the final modification of the backbone proceeds in a highly controlled fashion. The modular organization of the underlying structural genes has facillitated the alteration of the structure of complex polyketides in a predicted manner and enabled an increase in molecular diversity through combinatorial biosynthesis.[229,78]

Macrolide antibiotics block bacterial protein biosynthesis by binding to the 23S ribosomal RNA of the 50S subunit and interfere with the elongation of nascent peptide chains during translation.[230] The crystal structure of the 50S ribosomal subunit of *Deinococcus radiodurans* alone and cocrystallized with erythromycin and other macrolides has been elucidated and revealed how these antibiotics work.[231] Located in domain V, near the peptidyl transferase site, macrolide antibiotics obstruct the peptide exit tunnel without affecting peptidyl transferase activity.

Erythromycin A (**6**), which helps against the major respiratory pathogens, is considered safe and is widely prescribed for children. However, it is stalled by a limited antibacterial spectrum and limited stability in acidic medium, therefore resulting in poor bioavailability and a number of side effects such as gastrointestinal motility, proarrhythmic action, and inhibition of drug metabolism.[232] Therefore, for decades enormous efforts have been made to obtain natural and semisynthetic erythromycin derivatives with more favorable profiles. The second-generation macrolide antibiotics, roxithromycin (**68**),[233] clarithromycin (**69**),[234] and azithromycin (**70**),[235] have gradually replaced **6** owing to their broader spectrum of activity, enhanced activity, improved physicochemical and pharmacokinetic profile, and attenuated side effects.[236]

However, similar to **6**, the second-generation variants also have poor activity against macrolide resistant pathogens. Macrolide resistance in Gram-positive bacteria[237] arises from several mechanisms: 1) decrease of intracellular macrolide concentration by efflux pumps such as *msr*(A) in staphylococci[238] and *mef*(A) in streptococci;[239] 2) methylation of the 23S ribosomal RNA at position A2058 by ribosomal methylases encoded by *erm* genes that obstructs binding of macrolides, lincosamides, and streptogramin B and causes MLS_B cross-resistance;[240] 3) esterase-mediated cleavage and inactivation of the macrocyclic lactone ring;[241] and 4) sporadic ribosome mutations.

Fueled by the prevalence of erythromycin resistance, the sustained efforts to discover new and potent structural subgroups within the macrolide family have led to the rediscovery of the ketolide antibiotics. Ketolides[242] are derived from 14-membered macrolides by removal of L-cladinose under acidic conditions and selective oxidation of the resulting 3-hydroxy group to the corresponding carbonyl group. Although the 3-keto motif has been known from weak natural antibiotics, such as picromycin,[243] for many years, the presence of L-cladinose was erroneously regarded as a crucial structural element for antibacterial activity. Thus, its far-reaching consequences only became apparent with the first semisynthetic ketolide RU-64004 (HMR 3004, **71**) synthesized by chemists at Roussel Uclaf.[244] Essentially, this prototype ketolide was stable in acidic media, showed good intracellular penetration, and demonstrated potent activity against erythromycin A resistant and penicillin-resistant streptococci and *H. influenzae*. Furthermore, it was found not to induce the MLS_B resistance phenotype.

Systematic exploration of the SAR options of the ketolide backbone unveiled various novel ketolide series with potent activity and an improved pharmacokinetic profile:[245–247] generally, the exchange of L-cladinose with a carbonyl function at C3 increased activity against resistant strains with Mef-mediated efflux and erm methyltransferase. Introduction of a C2 fluoro group substituent enhanced activity and improved the pharmacokinetics. A C11/12 cyclic carbamate group enhanced the activity against susceptible and resistant strains by stabilizing the ketolide conformation, and the hetero-aryl groups were responsible for improved activity against erm methylase mediated resistance owing to additional interaction and enhanced affinity for methylated ribosomes.[244] Structural modifications of the crucial heterocyclic moiety were systematically investigated and telithromycin (**15**, HMR 3647, Sanofi Aventis),[248] cethromycin (**72**, ABT-773, Abbott),[249] and subsequently the 6,11-*O*-bridged

 © 2006 Wiley-VCH Verlag GmbH & Co. KGaA, Weinheim

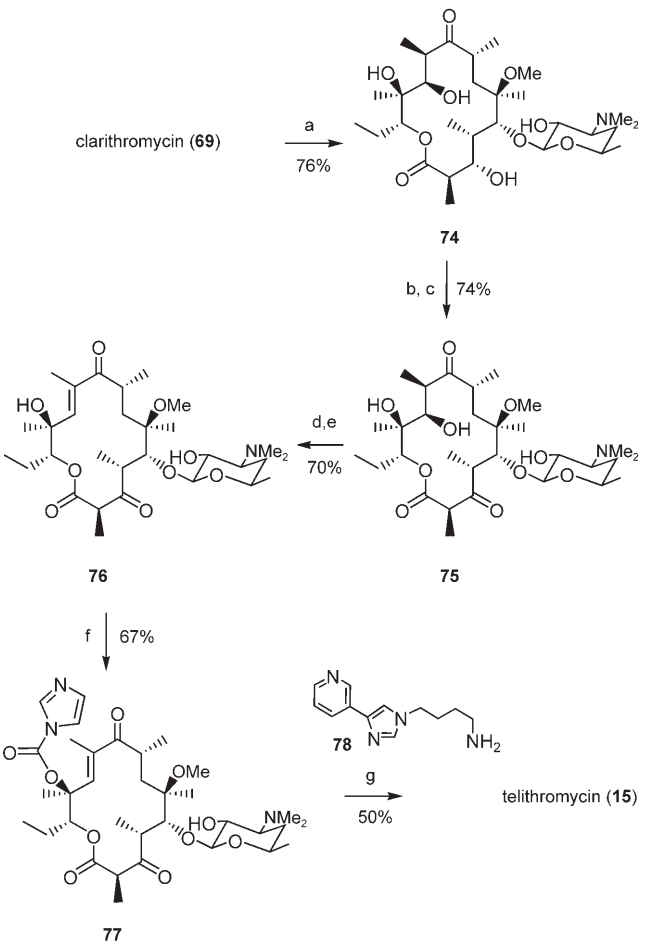
oxime ketolide EP-013420 (**73**, Enanta)[250] emerged as the leading compounds.

Typically, the ketolide telithromycin (**15**) was synthesized from 6-*O*-methylerythromycin (clarithromycin, **69**) in eight steps (Scheme 4):[244b,248,251] hydrolytic cleavage of L-cladinose under acidic conditions and modified Pfitzner-Moffat[252] oxidation of the resulting 3-hydroxy group afforded ketolide **75** that was selectively mesylated and eliminated to give enone **76**. Reaction of the corresponding acylimidazolyl derivative **77** with the primary amine **78** after stereoselective intramolecular Michael addition provided the cyclic carbamate **15**.

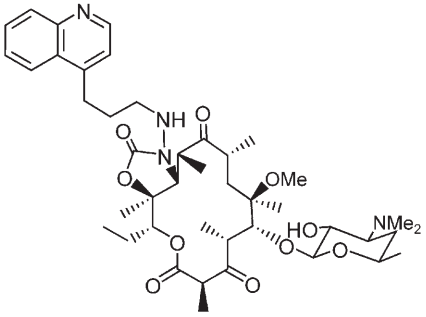
Telithromycin (**15**) was the first ketolide to be approved in Europe (2001), Japan (2003), and in the US (2004) for the once-daily oral treatment of respiratory tract infections such as acute exacerbation of chronic bronchitis due to *S. pneumoniae*, *H. influenzae*, and *M. catarrhalis*, acute bacterial sinusitis, and mild-to-moderate CAP, including infections caused by multidrug-resistant *S. pneumoniae*. The development of **72** was suspended during phase III clinical studies whereas **73** is currently in phase II trials. However, all ketolides lack activity against *E. coli* and constitutively MLS_B-resistant strains of *S. aureus* (Table 9).

The in vivo efficacy of **15** in acute murine infection models caused by erythromycin-sensitive Gram-positive cocci was comparable to **69**, but clearly superior against erythromycin-resistant strains (Table 10).

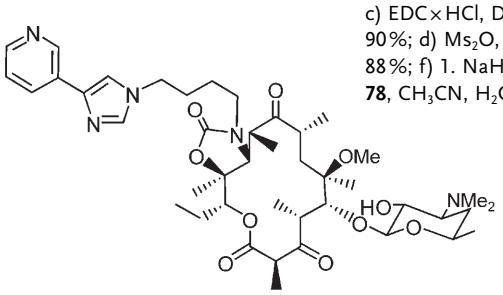
The main challenges for the uptake of a ketolide in the market will be its differentiation from other classes such as macrolides, fluoroquinolones, and β-lactam antibiotics that currently dominate the RTI segment. Approval for pediatrics and the development of a parenteral formulation could expand its promising market potential.[248c]



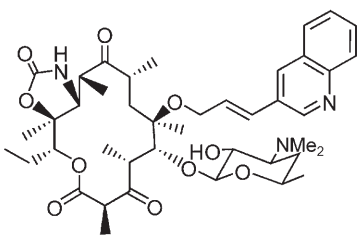
Scheme 4. Semisynthesis of telithromycin (**15**) from clarithromycin (**69**).[244b,248,251] Reagents and conditions: a) 1. 12 N HCl, H_2O, 2 h, RT; 2. NH_4OH pH 8, 76%; b) Ac_2O, K_2CO_3, acetone, 20 h, RT, 82%; c) EDC×HCl, DMSO, CH_2Cl_2, pyridinium trifluoroacetate, 4 h, RT, 90%; d) Ms_2O, pyridine, 5 h, RT, 79%; e) DBU, acetone, 20 h, RT, 88%; f) 1. NaH, DMF, CDI, −10°C, 1 h; 2. H_2O, 0°C, 67%; g) amine **78**, CH_3CN, H_2O, 60°C, 50%.



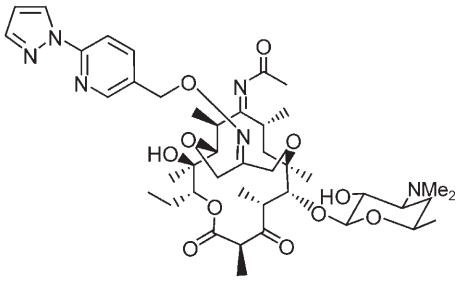
RU-64004 (**71**)



telithromycin (**15**)



cethromycin (**72**)



EP-013420 (**73**)

9. Lincosamides

Lincomycin (**16**) and and its semisynthetic congener clindamycin (**79**) were introduced into clinical medicine as oral

© 2006 Wiley-VCH Verlag GmbH & Co. KGaA, Weinheim

Table 9: Antibacterial activity in vitro of macrolide clarithromycin (**69**) versus ketolide telithromycin (**15**), MIC [$\mu g\,mL^{-1}$].[248]

	S. aureus[a]	*S. aureus*[b]	*S. aureus*[c]	*S. pneum.*[a]	*S. pneum.*[b]	*S. pneum.*[c]	*H. infl.*
69	0.3	40	40	0.04	40	40	5
15	0.04	0.08	40	0.02	0.02	0.15	1.2

[a] Erythromycin susceptible. [b] Inducibly erythromycin resistant. [c] Constitutively erythromycin resistant.

Table 10: Efficacy in vivo of macrolide clarithromycin (**69**) versus ketolide telithromycin (**15**), ED_{50} [$mg\,kg^{-1}$].[248]

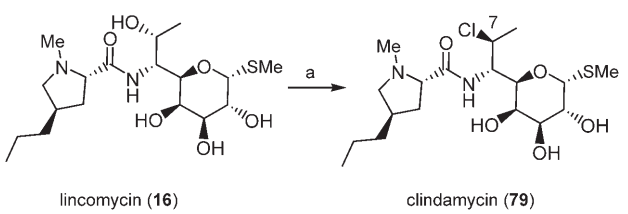
	S. aureus[a]	*S. aureus*[b]	*S. aureus*[c]	*S. pneum.*[a]	*S. pneum.*[b]	*S. pneum.*[c]	*H. infl.*
69	6	55	n.d.[d]	7.5	>50	>50	120
15	10	4.5	n.d.[d]	1	4	0.15	57

[a] Erythromycin susceptible. [b] Inducibly erythromycin resistant. [c] Constitutively erythromycin resistant. [d] n.d. = not done.

antibiotics in 1960 and 1969, respectively.[253] Extensions for parenteral applications followed shortly after. These low-molecular-weight antibacterials exhibit a spectrum similar to that of the macrolides, including activity against most Gram-positive organisms and the anaerobes, but not the Gram-negatives and enterococci.[254] The use of lincomycin **16** and clindamycin **79** strongly declined after a period of extensive application against severe staphylococcal sepsis, anaerobic infections and, in combination with other antibiotics, severe intra-abdominal or opportunistic sepsis.[255] Today, their use is mainly limited to topical applications. The relegation of both drugs from first-line antibiotics to niche products can be attributed to their limited antibacterial spectrum, the emergence of resistance, and mainly to a severe side effect of this class, the development of pseudomembraneous colitis in some patients.[256] This side effect is caused by *Clostridium difficile,* which is not covered by the antibacterial spectrum of lincosamides. Consequently, closure of this spectrum gap would be desirable.

Clindamycin (**79**)[257,258] is a semisynthetic derivative of the natural product lincomycin (**16**), which is produced by fermentation of *Streptomyces lincolnensis*,[259] (Scheme 5). This transformation is remarkable as one secondary alcohol is transformed selectively in the presence of three others. Selective transformations of polyfunctional natural products to generate SAR data are important tools for chemical postevolution. Maintaining a similar, favorable acute-toxicity profile, **79** is about two- to fourfold more potent than its parent **16** (Table 11).[261]

Both drugs, **16** and **79**, demonstrated favorable pharmacokinetics in laboratory animals and humans,[262,263] with excellent bioavailability and penetration into relevant tissues. Their solubility and stability in solution allowed for oral and parenteral application as well, but their relatively short half-life (2–4 h) required twice-daily (peroral) or even three-times-daily (i.v.) dosing. Thus, an improved pharmacokinetic profile, which would allow once-daily dosing, would be highly desirable for novel lincosamides.



Scheme 5. Synthesis of clindamycin (**79**) from the natural product lincomycin (**16**).[260] Reagents and conditions: a) *N*-chlorosuccinimide, PPh_3, THF, reflux, 18 h, 84%.

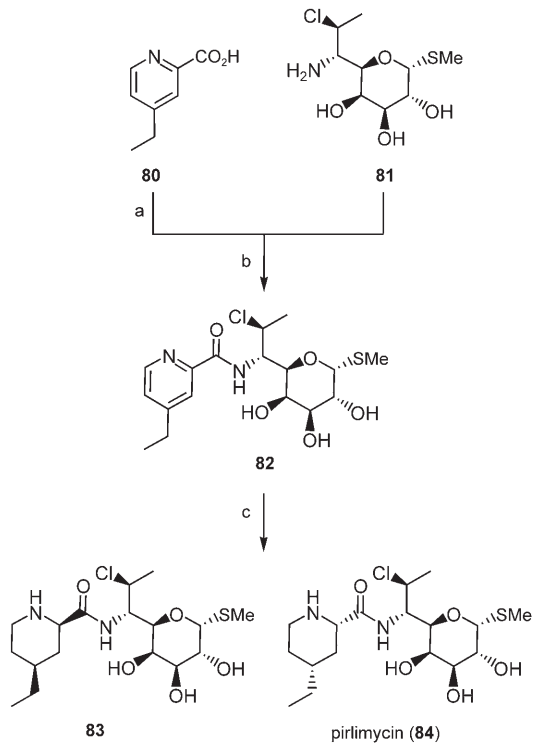
Table 11: Antibacterial activity in vitro of lincomycin (**16**) and clindamycin (**79**), MIC [$\mu g\,mL^{-1}$].

Organism	Lincomycin (**16**)	Clindamycin (**79**)
S. aureus	0.5	0.125
S. hemolyticus	0.25	0.125
S. viridans	0.25	0.064
B. subtilis	32	1
E. coli	1000	64
K. pneumoniae	125	8

Lincosamides exert their antibacterial activity by binding to the ribosome and inhibiting bacterial protein synthesis. Specifically, macrolides, lincosamides, and streptogramin B type antibiotics bind to adjacent sites on the 50S ribosomal subunit. X-ray crystal structures of the complexes of the bacterial ribosome with these antibiotics have been solved.[264,265] Not surprisingly, resistance development of **79** is similar to the macrolides owing to a similar binding mode. Yet, the rate of resistance development for **79** is lower than that for erythromycin. Resistance occurs mainly by methylation of A2058 on 23S rRNA (erm methyltransferase), which reduces the binding affinity of lincosamides and macrolides to the ribosomal target. It may be speculated that resistance may be overcome, in analogy to the ketolides, with derivatives that bind slightly differently. Finding second-generation lincosamides with an extended antibacterial spectrum (including enterococci-, MRSA-, and clindamycin-resistant strains), an improved side-effect profile (coverage of *C. difficile* to prohibit pseudomembraneous colitis), and superior pharmacokinetics (once-daily dosing) remains a rewarding goal.

Semisynthetic pirlimycin (**84**, Scheme 6), prepared at Upjohn with a substituting derivatization strategy,[266] showed some of the desired characteristics. Dosed intraperitoneally, the 50% lethal dose (LD_{50}) for **84** in mice was 600 $mg\,kg^{-1}$, clearly superior to clindamycin (300 $mg\,kg^{-1}$). Furthermore, structural changes in **84**, lacking the metabolically labile *N*-methyl group of **79**, significantly improved the

 © 2006 Wiley-VCH Verlag GmbH & Co. KGaA, Weinheim



Scheme 6. Upjohn's synthesis of pirlimycin (**84**) through substituting derivatization. Reagents and conditions: a) isobutyl chloroformate, Et_3N, CH_3CN, 10 °C, 1 h; b) **81**, acetone, H_2O, 25 °C, 18 h; c) MeOH, H_2O, 1 N HCl, PtO_2, H_2 (50 psi), 25 °C, 18 h; separation of diastereomers, 40% of **84**.

pharmacokinetic behavior resulting in higher plasma levels and a prolonged half-life. Although **79** and **84** covered an almost identical in vitro antibacterial spectrum, the latter was 2–20-times more potent in various animal infection models, most likely owing to an improved pharmacokinetic profile.[266] But, as with all lincosamides, pirlimycin (**84**) was still inactive against enterococci and no improvement in resistance development or activity against resistant strains could be achieved (Table 12).[267] Based on these limitations, the development of pirlimycin (**84**) was not warranted for use in humans—it has been marketed for veterinary use.

Several methods for semisynthetic modification of lincomycin (**16**) and clindamycin (**79**) have been reported[268] in addition to the methodology developed during total synthesis

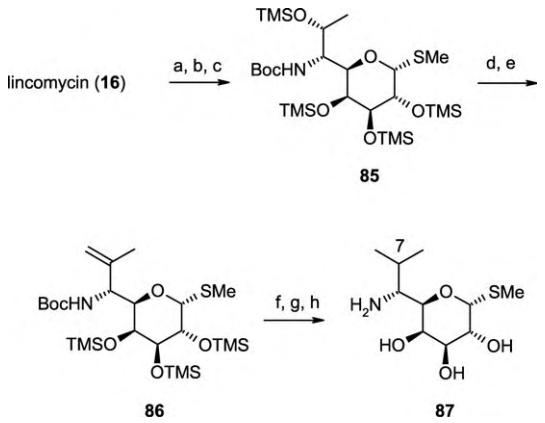
Table 12: Antibacterial activity in vitro of clindamycin (**79**) and pirlimycin (**84**), MIC_{90} [$\mu g\,mL^{-1}$].

Organism	Clindamycin (**79**)	Pirlimycin (**84**)
S. aureus[a]	0.125	0.5
S. aureus[b]	>16	>16
S. pyogenes	0.06	0.5
S. pneumoniae[c]	0.25	0.5
S. pneumoniae[d]	16	>16
S. viridans	0.06	0.5

[a] MSSA, methicillin-susceptible *S. aureus*. [b] MRSA, methicillin-resistant *S. aureus*. [c] PSSP, penicillin-susceptible *S. pneumoniae*. [d] PRSP, penicillin-resistant *S. pneumoniae*.

of the natural product.[269] However, none of these efforts led to significantly improved derivatives until Vicuron initiated a research program for second-generation lincosamides. Substitution of the 7-hydroxy group function by a methyl group in conjunction with novel amides resulted in the discovery of VIC-105404 (**90**)[270] and VIC-105555 (**17**).[271] The latter has been rapidly progressed into preclinical development.

Starting from **16**, 7-methylthiolincosamine (**87**) was obtained in eight steps (Scheme 7). Hydrazinolytic cleavage



Scheme 7. Synthesis of 7-methylthiolincosamine (**87**). Reagents and conditions: a) $N_2H_4{\cdot}H_2O$; b) $(Boc)_2O$, Et_3N, MeOH; c) BSTFA, Et_3N, DMF; d) DMSO, $(COCl)_2$, Et_3N, CH_2Cl_2, $-70\rightarrow-40$ °C; e) $PPh_3Me^+Br^-$, *t*BuOK; f) Dowex H^+, MeOH; g) H_2 (65 psi), Pd/C; h) TFA/H_2O (9:1).

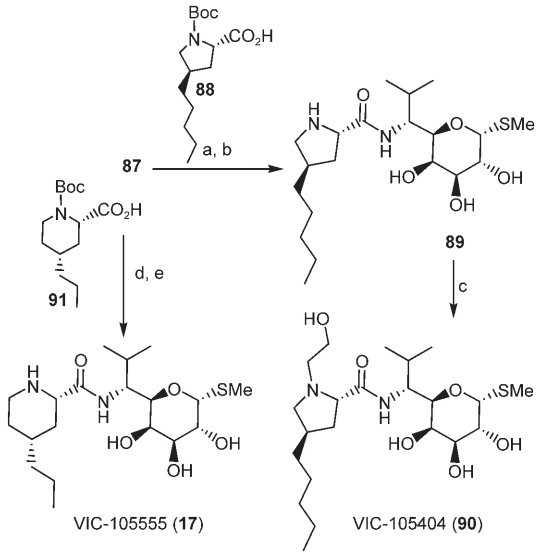
of the amide followed by a selective Swern-type oxidation, Wittig olefination, and subsequent catalytic reduction of the methylene group were the key reactions in this transformation. Coupling of **87** with proline **88** followed by *tert*-butoxycarbonyl (Boc) deprotection and subsequent N-alkylation of **89** with oxirane gave VIC-105404 (**90**). Similar operations led to VIC-105555 (**17**, Scheme 8).

Compared with clindamycin (**79**), **17** displayed improved in vitro activity against enterococci and selected anaerobes, especially *C. difficile* (Table 13),[271,272] and showed superior efficacy in systemic-infection animal models.[273–275]

In rats, **17** had a longer half-life (3.72 versus 1.10 h), a larger volume of distribution (10.7 versus 4.54 $L\,kg^{-1}$), and a lower clearance (2.39 versus 4.46 $L\,h^{-1}\,kg^{-1}$)) than **79**. VIC-105555 (**17**) was stable in liver microsomes of all species and showed lower serum binding than **79**. Data from animals and allometric species scaling predicted a favorable human pharmacokinetic profile for **17**, which could eventually allow for once-daily dosing.[276] Despite the similar structure, comparable in vitro profile, and the same binding mode as clindamycin (**79**),[277] it did not seem possible to create mutants of *E. faecalis* resistant to **17** by serial passaging. However, mutants carrying an A2058 mutation by methylation on the 23S rRNA (erm methyltransferase) were still resistant to **17** (MIC > 256 $\mu g\,mL^{-1}$).[278]

It will be interesting to see whether the in vitro and in vivo improvements achieved for **17** will translate into a clinical

 © 2006 Wiley-VCH Verlag GmbH & Co. KGaA, Weinheim



Scheme 8. Vicuron's synthesis of VIC-105555 (**17**) and VIC-105404 (**90**) from 7-methylthiolincosamine (**87**). Reagents and conditions: a) **88**, HBTU, Et_3N; b) TFA/H_2O (9:1); c) oxirane, Et_3N; d) **91**, HBTU, Et_3N; e) TFA/H_2O (9:1).

Table 13: Antibacterial activity in vitro of clindamycin (**79**) and VIC-105555 (**17**), MIC [$\mu g\,mL^{-1}$].[272]

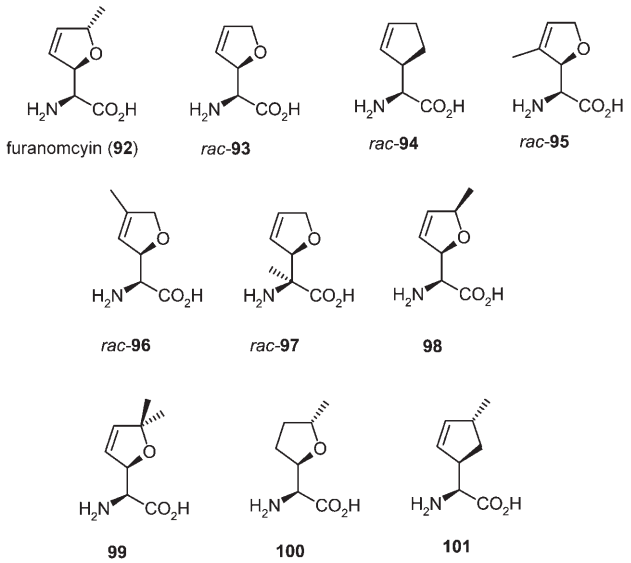
Organism	Clindamycin (**79**)	VIC-105555 (**17**)
S. pneumoniae	≤ 0.25	≤ 0.016–0.03
S. aureus	≤ 0.06–0.12	0.12–0.5
E. faecium	0.12 to >8	0.12 to >32
E. faecalis	8 to >8	0.5–1
B. fragilis	0.5–2	0.25–2
C. difficile	2–16	0.12–1

benefit. Second-generation lincosamides should allow successful treatment of infections by enterococci and offer a superior side-effect profile.

10. Furanomycin, a Lead with Insufficient Potential

With a molecular weight of 157 $g\,mol^{-1}$, L-(+)-furanomycin (**92**) is one of the smallest antibacterial natural products reported. This unusual α-amino acid was isolated by Katagiri et al. in 1967 from the fermentation broth of *Streptomyces threomyceticus L-803* (ATCC 15795)[279] and shown to inhibit the growth of bacteria such as *M. tuberculosis*, *E. coli*, *B. subtilis*, and some *Shigella*- and *Salmonella* species in the μM range. Its initially assigned absolute configuration was revised unambiguously to (+)-(α*S*,2*R*,5*S*) through syntheses starting from D-glucose,[280] and by an X-ray crystal-structure analysis of the *N*-acetyl derivative.[281]

Labeling experiments indicated that furanomycin biosynthesis proceeds through a polyketide pathway starting from two acetates and one propionate.[282] Analogous to the polyether antibiotics, its cyclic ether functionality stems from molecular oxygen that is introduced through epoxidation and intramolecular epoxide opening.[283] Furanomycin is accepted as a substrate by isoleucyl aminoacyl–tRNA synthetase and its antibacterial activity results from a substitution for isoleucine during the bacterial protein translation.[284] Therefore, the antibacterial activity of **92** is antagonized by isoleucine.[279] Furanomycin hampers the formation of isoleucyl–tRNA in *E. coli*, whereas other aminoacyl–tRNAs are not affected.[285] Aminoacyl–tRNA synthetases are essential in all living organisms[286] and have attracted considerable interest as novel targets in bacterial protein synthesis.[287] For **92**, no literature report on in vivo activity was found, but with pseudomonic acid,[288] a marketed antibiotic with a similar mode of action, a proof of concept existed. Besides antibacterial activity in vitro and in vivo,[289] **92** combined drug-like features,[290] such as polarity, sufficient solubility, and moderate structural complexity, which rendered it attractive to medicinal chemists. Several synthetic approaches towards **92** have been developed, some of which consist of up to 20 steps. Many syntheses have started from carbohydrates such as D-glucose,[280] D-ribose,[291] D-glucosamine,[292] L-xylose,[293] and D-mannitol.[294] Other approaches have used dimethyl L-tartrate,[295] serine,[296] glycine,[297] or furanes[280b,285b,298] as starting materials. In particular, approaches starting from amino acids were captivating as with six to seven steps they were short and flexible enough to rapidly access isomers and close congeners for evaluation of the SAR.



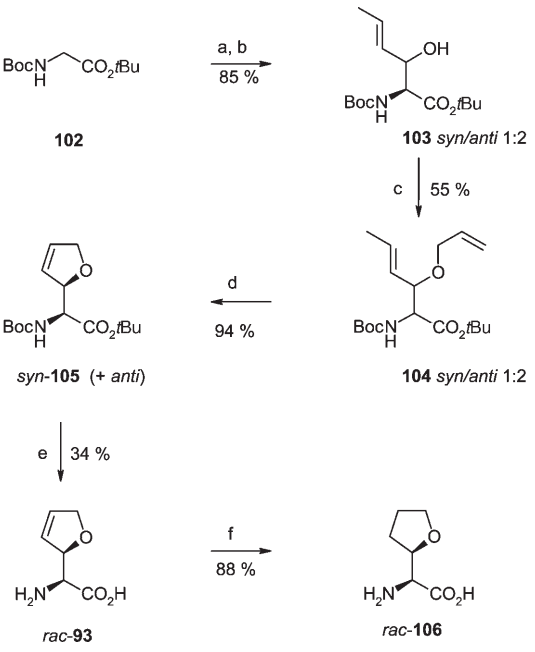
First of all, it was important to learn which structural parts in furanomycin were essential for activity and which parts could be removed or modified. Since norfuranomycin had been reported to exhibit antibacterial activity (MIC) against some Gram-negative bacteria,[298] straightforward protocols towards derivatives of **92** were envisaged. To gain rapid insight into SARs, control of diasteroselectivity was considered more important than controlling the absolute configuration. Ring-closing metathesis was used for the construction of the dihydrofurane ring. The required precursor **104**, accessible through *O*-allylation of β-hydroxyamino acid **103**,

 © 2006 Wiley-VCH Verlag GmbH & Co. KGaA, Weinheim

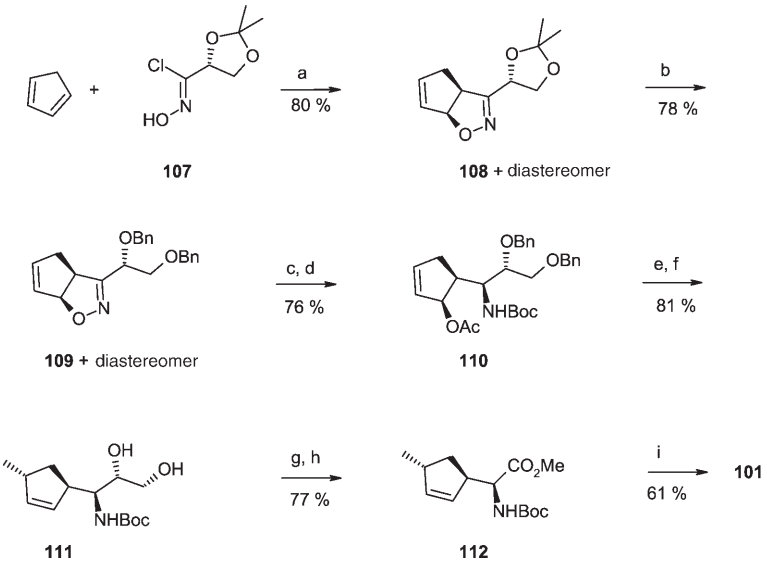
which was generated by aldol addition of an α,β-unsaturated aldehyde to the glycine ester **102** (Scheme 9).[297]

The effect of shifting the methyl group to various positions of the core structure was then investigated. The basic set of structures to probe the SAR was complemented by the α-*S*,2*R*,5*R* diastereomer 5′-*epi*-furanomycin (**98**), 5′-methylfuranomycin (**99**), and L-(+)-dihydrofuranomycin (**100**), as well as the carba analogue of the natural antibiotic **101**. These chiral congeners were prepared by 1,3-dipolar cycloaddition of glyceronitrile oxide as a chiral glycine equivalent[299] to either 2-methylfuran[294,300] or cyclopentadiene (Scheme 10).[301]

Unfortunately, the structural requirements of isoleucyl aminoacyl–tRNA synthetase for furanomycin-like substrates proved to be quite strict. A very tight SAR was observed and all of the synthetic isomers and derivatives of the natural antibiotic demonstrated no or clearly inferior MICs against a panel of selected Gram-positive and Gram-negative wild-type pathogens including *S. aureus* and *E. coli*. Only L-(+)-dihydrofuranomycin (**100**) showed borderline MIC (32–64 μg mL^{-1}) against *S. aureus* and the chiral carba analogue **101** exhibited weak antibacterial activity (4 μg mL^{-1}) against an efflux-pump-deficient *E. coli*. In summary, furanomycin harbored insufficient lead potential and was not a valid starting point for a drug-discovery program.



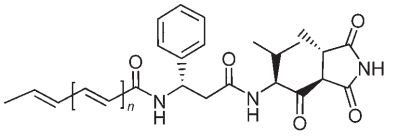
Scheme 9. Kazmaier's synthesis of norfuranomycin derivatives through ring-closing metathesis.[297] Reagents and conditions: a) 1. LDA (2.5 equiv), THF, −78 °C; 2. $TiCl(OiPr)_3$ (1.5 equiv); b) methacrolein (3 equiv), THF, −78 °C, 3 h, 85 %; c) allyl ethyl carbonate (1.5 equiv), $[\{(allyl)PdCl\}_2]$ (2.5 mol %), PPh_3 (11 mol %), THF, 50 °C, 3 d, 55 %; d) $[(Cy_3P)_2Cl_2Ru{=}CHPh]$ (2.5 mol %), CH_2Cl_2, 40 °C, 16 h, 94 %; e) 4 M HCl/dioxane, 4 h, 0 °C, 34 %; f) H_2, Pd/C, CH_3OH, 12 h, RT, 88 %.



Scheme 10. Jäger and co-workers's synthesis of the chiral carba analogoue **101** of natural L-(+)-furanomycin (**92**).[301] Reagents and conditions: a) NEt_3 (1.2. equiv), Et_2O; b) TFA (1. 3 %), MeOH, H_2O; 2. BnBr, NaH; c) 1. $LiAlH_4$, Et_2O; 2. Boc_2O, dioxane, H_2O; d) Ac_2O, DMAP, pyridine; e) MeMgBr, CuCN, Et_2O, −20 C; f) Na, NH_3(liquid), THF −78 °C; g) $Pb(OAc)_4$, CH_2Cl_2, −20 °C; h) 1. $NaClO_2$, CH_3CN, *t*BuOH, H_2O, 2-methyl-2-butene, NaH_2PO_4, −20 °C; 2. CH_2N_2, Et_2O; i) 1. 90 % TFA; 2. NaOH, $NaHCO_3$, H_2O, THF.

11. Pyrrolidinedione Antibacterials

The natural peptide antibiotic andrimid (**113**) was first isolated by Komura and co-workers in 1987 from cultures of a symbiont of the brown planthopper *Nilaparvata lugens*.[302] Some years later, **113** and related new metabolites, moiramides A–C, were also discovered in a marine isolate of *Pseudomonas fluorescens* obtained from a tunicate collected in Moira Sound at Prince of Wales Island, Alaska.[303]



andrimid, *n* = 2 (**113**)
moiramide B, *n* = 1 (**18**)

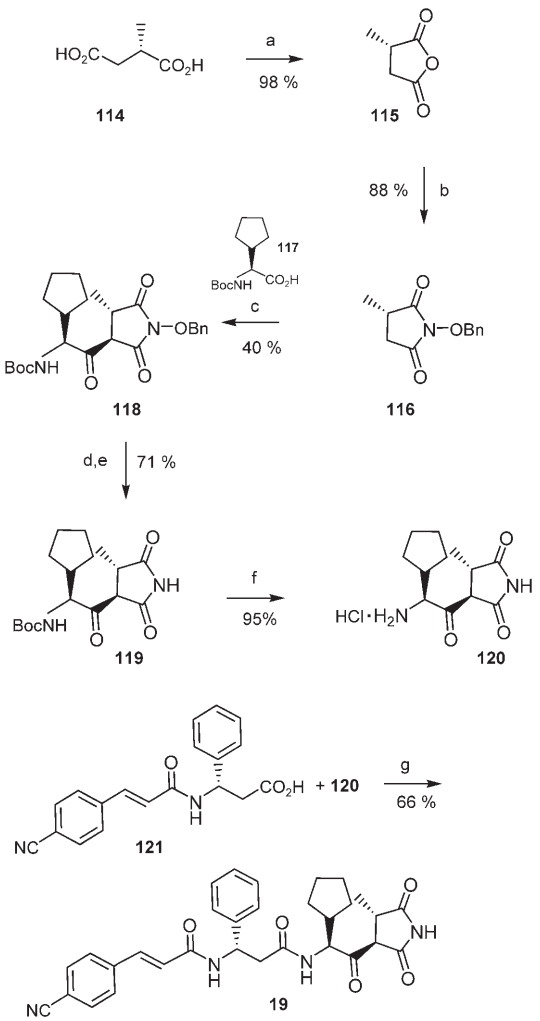
The linear structure of these metabolites was elucidated by spectroscopic means[302,303] and was shown to contain four characteristic elements: a pyrrolidinedione head group, a valine derived β-ketoamide, a (*S*)-β-phenylalanine part, and a *N*-terminal polyunsaturated fatty acid. Isotope incorporation experiments revealed that nature constructs the essential right-hand part from valine, glycine, and acetate units.[303,304] Notably, metabolites **113** and **18** exhibited good in vitro antibacterial activity against MRSA. Various diastereoselective and asymmetric total syntheses of **113** and **18** have been described[304,305] and allowed for ready access to these antibiotics. Subsequently, these methods also served as a basis for

 © 2006 Wiley-VCH Verlag GmbH & Co. KGaA, Weinheim

structural variation and evaluation of the potential of these lead structures in our laboratories.[306,307]

However, before starting a medicinal-chemistry program, it had to be clarified whether the pyrrolidinedione antibiotics act through an essential mode of action. In profiling **113** and **18**, their published biological activity could be endorsed, however, a reported effect on RNA synthesis[308] could not be confirmed by precursor incorporation studies.[309,310] Application of various RG techniques (see Section 5.4) led to the identification of the molecular target:[144,309,311] pyrrolidinedione antibiotics exert their effect by inhibiting the first committed step in bacterial fatty acid biosynthesis, a reaction catalyzed by the carboxyltransferase subunit of the multimeric bacterial enzyme acetyl-CoA carboxylase.[309] For most living organisms, fatty acid biosynthesis is a vital metabolic process, but the pathways in bacteria[312] and mammals[313] are different. Acetyl-CoA carboxylase is essential for microbial growth and is broadly conserved amongst bacteria.[310] No potent inhibitors of bacterial acetyl-CoA carboxylase were known and overall, this enzyme seemed to be an appealing target for future broad-spectrum antibacterials. Acting through an essential target, covering a broad spectrum of Gram-positive and Gram-negative bacteria, demonstrating low resistance induction, and showing a low rate of spontaneous development of resistance, natural pyrrolidinedione antibiotics **113** and **18** proved to be attractive lead structures but were far from being useful drugs. Several parameters, such as potency, chemical and metabolic stability, solubility, and drug–drug interaction needed to be improved by a medicinal-chemistry program.

Synthesis of novel pyrrolidinedione antibacterials was achieved by adapting pathways described in the literature (Scheme 11).[304,305] Dehydration of (*S*)-(−)-methylsuccinic acid (**114**) with acetyl chloride afforded methylsuccinic anhydride **115**, which was treated with *O*-benzyl hydroxylamine in the presence of *N*,*N*′-carbonyldiimidazole (CDI) to yield (*S*)-2-methyl-*N*-benzyloxy succinimide (**116**). *N*-Boc-protected (2*S*)-cyclopentyl glycine, prepared according to Andersson and co-workers,[314] was activated with CDI in THF, added to **116**, and the solution was slowly added to a solution of lithium hexamethyldisilazide (LiHMDS) in THF at low temperature to produce β-ketoamide **118**. Under the reaction conditions, *trans*-**118** was predominantly formed from an equilibrium mixture of the *cis*-, *trans*-, and enolic forms. Removal of the *N*-benzyloxy group to give acyl succinimide **119** was achieved by hydrogenolysis and subsequent treatment of the *N*-hydroxy intermediate with 2′-bromoacetophenone and triethylamine.[315] Deprotection of **119** under acidic conditions yielded the primary amine **120**, which was reacted with *N*-Acyl-(*S*)-β-phenylalanine (**121**) under standard peptide-coupling conditions to afford pyrrolidinedione antibacterial **19**, a formal double-decoration product of natural **18**. Alternatively, **19** and congeners could be obtained from **120** by a stepwise procedure in about 60% overall yield: coupling with *N*-Boc-(*S*)-β-phenylalanine, Boc removal under acidic conditions, and reaction of the resulting primary amine with the corresponding cinnamic acid under standard coupling conditions.[306]



Scheme 11. Synthetic route used to explore pyrrolidinedione structural variations and the SAR.[306] Reagents and conditions: a) CH_3COCl, 4 h, 60 °C, 98%; b) *O*-benzyl hydroxylamine, CDI, CH_2Cl_2, 12 h, RT, 88%; c) 1. *N*-Boc-(2*S*)-cyclopentyl glycine (**117**), CDI, THF; 2. LiHMDS, THF, 15 min, −65 °C; 3. conc. aqueous NH_4Cl, −65 °C→RT, 40%; d) H_2, Pd/C (10%), EtOH, 1 h, RT; e) 2′-bromoacetophenone, Et_3N, cat. DMAP, CH_3CN, 20 h, RT; f) 4 N HCl in 1,4-dioxane, 2 h, RT, 95%; g) HATU, iPr_2EtN, CH_2Cl_2, DMF, 10 h, 0 °C→RT, 66%.

Through this route, and also by solid-phase synthesis starting with polymer bound (*S*)-β-phenylalanine, a broad variety of pyrrolidinedione antibacterials became readily available.[306,307] Broad structural variations were tolerated at the fatty acid side chain without adversely affecting target activity. Inhibitory values (IC_{50}) remained in the nM range for the *E. coli* and *S. aureus* acetyl-CoA carboxylase enzymes with polar and lipophilic side chains as well (Table 14).

Apparently, the side chain was not involved in key interactions with the enzyme and could be used for tuning the physicochemical profile. On the other hand, the nature of the side chain had a significant influence on antibacterial activity (MIC). Comparing compounds **122** and **123** demonstrated that despite excellent target activity of **122** and the benefit of a polar substituent for other parameters, such as

 © 2006 Wiley-VCH Verlag GmbH & Co. KGaA, Weinheim

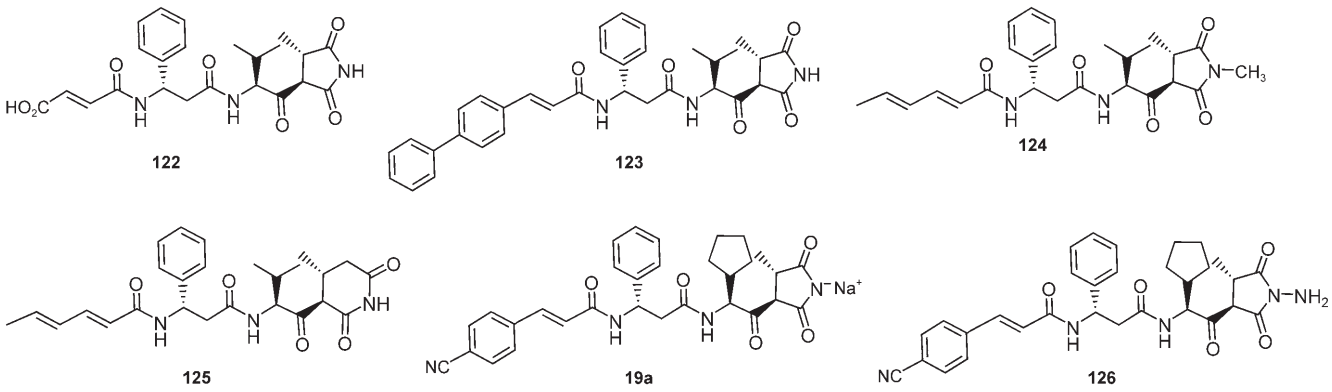


Table 14: Inhibitory values (IC_{50} [nM]) against carboxyltransferase (AccAD subunits), and in vitro antibacterial activity (MIC [$\mu g\,mL^{-1}$]) of pyrrolidinedione antibacterials.

	IC_{50}		MIC			
	E. coli	*S. aureus*	*E. coli*[a]	*E. coli*[b]	*S. aureus*	*S. pneum.*
113	13	305	32	>64	8	8
18	6	96	4	32	8	32
19	4	44	1	32	0.03	1
122	2	317	>64	>64	>64	>64
123	37	540	>64	>64	2	16
124	25	211	16	>64	16	>64
126	2	33	0.5	16	0.01	0.25

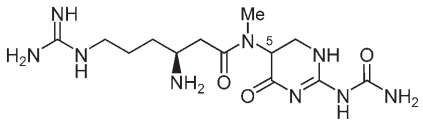
[a] Efflux-pump deletion strain. [b] Wild type.

solubility, reasonable lipophilicity was required for penetration into bacterial cells and for good MIC values. Replacing the (*S*)-β-phenylalanine by non-aromatic β-amino acids led to a loss in activity. On the other hand, significant improvement of antibacterial activity could be achieved by varying the lead's β-ketoamide part, for example, by replacing (*S*)-valine with (2*S*)-cyclopentyl glycine, whereas aromatic amino acids in this position rendered the molecule inactive.

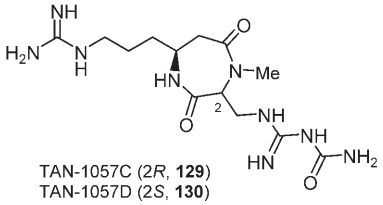
The pyrrolidinedione head group was thought to mimic the transition state of the carboxyltransferase reaction as it was most sensitive towards structural variations. In comparision to moiramide B (**18**), its *N*-methyl derivative **124** suffered from a two- to fourfold decrease in activity, yet the corresponding hydrazide was at least equipotent, whereas the piperidinedione congener **125** was inactive. These studies also confirmed the importance of the 4-(*S*)-methyl head-group substituent for efficient target interaction.[306] Sufficient water solubility for parenteral application ($>5\,g\,L^{-1}$) was achieved by preparing the corresponding pyrrolidinedione sodium salts, for example, **19a**, which were generally employed in murine infection models. Thus, parenteral treatment of lethal *S. aureus* infections in mice with single doses of **19a** ($50\,mg\,kg^{-1}$) or **126** ($25\,mg\,kg^{-1}$), resulted in 100% survival.[316] With the synthetic pyrrolidinedione antibacterials **19** and **126**, which are readily available in multi-gram scale, many critical properties of the natural antibiotics **113** and **18** could be ameliorated. Systematic exploration of the SAR will help to improve potency to evaluate the full potential of these attractive lead structures.

12. Tetrahydropyrimidinone Antibiotics

A structurally unique group of novel antibiotics was isolated from *Flexibacter* species found in soil samples collected in the Nachi mountain area in the Wakayama Prefecture in Japan. First published in a patent application,[317] scientists from Takeda disclosed the structure of these novel antibiotics in 1993 and denoted them as TAN-1057A–D (**127**–**130**).[318] The epimeric tetrahydropyrimidinone antibiotics TAN-1057A/B (**127**/**128**) were isolated from *Flexibacter* sp. PK-74, whereas the epimeric dioxo diazepans TAN 1057C/D (**129**/**130**) resulted from *Flexibacter* sp. PK-176.



TAN-1057A (5*S*, **127**)
TAN-1057B (5*R*, **128**)



TAN-1057C (2*R*, **129**)
TAN-1057D (2*S*, **130**)

The structure of **127**/**128** was elucidated through a combination of spectroscopic studies and degradation experiments yielding primarily (*S*)-β-homoarginine and α-*N*-methyl-2,3-diamino propionic acid. The constitution of TAN-1057C/D (**129**/**130**) was determined from their spectroscopic data as well as on the observation that **129**, upon treatment with base, was rapidly converted into a mixture of **127** and **128**. Owing to the instability of **129** and **130**, total synthetic endeavors and medicinal-chemistry optimization have concentrated on **127** and **128**.

The antibacterial activity, in particular of TAN1057A (**127**), was characterized in detail.[319] Although its in vitro MIC values against Gram-positive organisms such as *S. aureus* and *S. pneumoniae* were mediocre under standard conditions

 © 2006 Wiley-VCH Verlag GmbH & Co. KGaA, Weinheim

(6.25–12.5 μg mL^{-1}), the compound was reported to exhibit in vivo efficacy superior to vancomycin and imipenem in a murine *S. aureus* sepsis model.

From incorporation studies with [^{14}C]leucine, it was concluded that TAN-1057A/B (**127**/**128**) acted by blocking bacterial protein biosynthesis,[319] and, in detailed studies, **127**/**128** was found to inhibit bacterial growth through binding to the 50S subunit of ribosomes.[320] Dissection of the translational apparatus revealed an effect on protein biosynthesis by inhibition of the peptidyl transferase step.[321] This target was independently confirmed by using proteomics technologies for **13**, a "degraded" analogue of TAN-1057A/B (**127**/**128**) with improved tolerability.[136] swelling and impairment of the cell wall was the macroscopic effect of **13** on the growth of *S. aureus* (Figure 9). Competition experiments with other antibiotics, inhibiting peptidyl transferase, revealed a unique binding site for **127**/**128**.[321] Consequently, *S. aureus* subtypes selected for **127**/**128** resistance did not show cross-resistance to a panel of known inhibitors of bacterial translation.[322] Natural **127**/**128** showed a comparable, nonspecific inhibitory activity in cell-free translation assays derived from prokaryotes and eukaryotes,[321] which could be the reason for the natural product's high acute toxicity in mice (LD_{50} 50 mg kg^{-1} i.v.).[318] Thus, **127**/**128** itself was far from being an appropriate clinical drug candidate, yet, its potent in vivo activity against *S. aureus* rendered it an attractive lead structure. Furthermore, its pronounced solubility was well suited for parenteral application.

A total synthesis of the natural product TAN-1057A/B (**127**/**128**) was thought to offer the structural flexibility needed for accessing analogues with improved properties. Despite manageable complexity, its structure and properties harbored some synthetic challenges: the peptide bond between the β-homoarginine side chain and the pyrimidinone heterocycle was difficult to form owing to steric hindrance and low nucleophilicity of the amino component **139**. Synthesis of the heterocycle itself was conceivable from a corresponding 2,3-diamino propionic acid precursor in which the congestion of functional groups rendered the orchestration of reaction centers and protective groups into a strategic exercise. The C5 stereogenic center of the heterocycle was prone to epimerization and it was known from the Takeda group that the heterocyclic component was sensitive towards strongly basic or acidic conditions. Consequently, harsh conditions, particularly during the final steps of the synthesis, had to be avoided. Three different total syntheses[323–325] of the diasteromeric mixture of TAN-1057A/B (**127**/**128**) and one stereoselective synthesis[326] resulting in the pure diastereomer **127** have been completed.

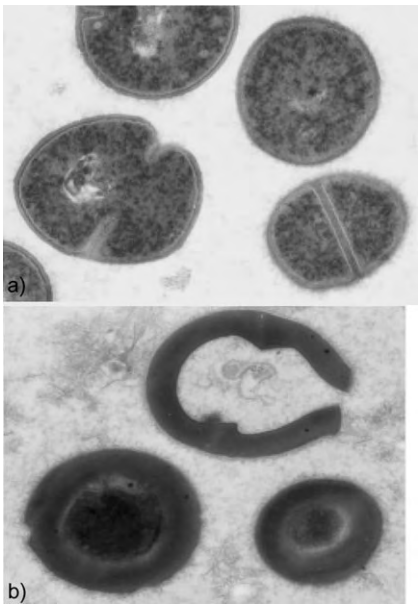
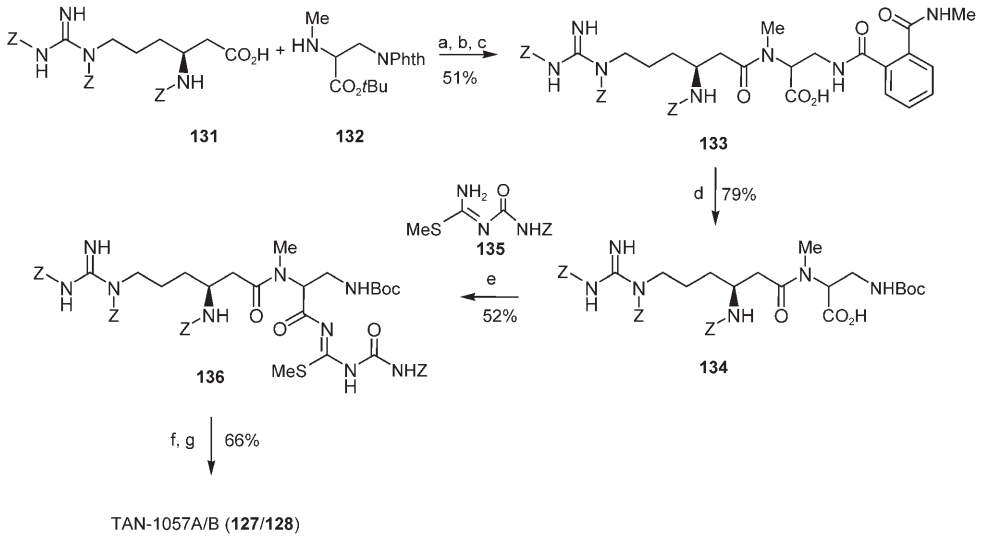


Figure 9. Action of **13** on *S. aureus*: Swelling and impairment of the bacterial cell wall. Electron micrograph a) before and b) after treatment with **13** (2 μg mL^{-1}) for 4 h.

Yuan and Williams' synthesis of **127**/**128**[323] was published first and employed a rather linear sequence (Scheme 12). Triple-protected β-homoarginine **131** was coupled to the 2,3-diamino propionic acid derivative **132** as an open-chain precursor of the pyrimidinone heterocycle, thus avoiding difficulties with the peptide formation. After three protecting-group manipulations, isothiurea derivative **135** was coupled with the carboxylic acid moiety in **134**, setting the stage for ring closure after removal of the Boc group. In the final step, all four Z protecting groups were removed concomitantly through hydrogenation under mild conditions. The

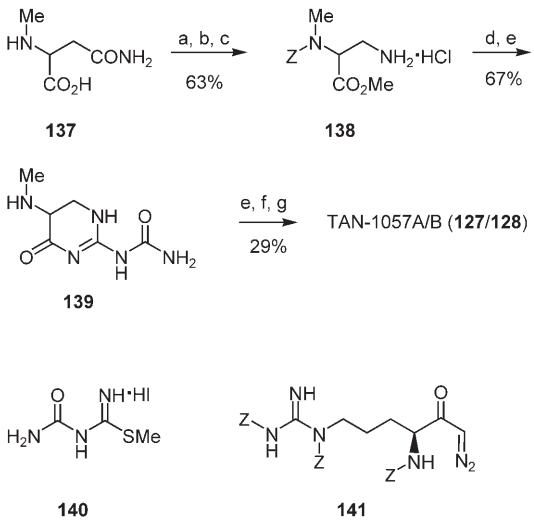


Scheme 12. Yuan and Williams' synthesis of TAN-1057A/B (**127**/**128**).[323] Reagents and conditions: a) BOPCl, 16 h, 55%; b) CH_3NH_2, MeOH, 5 min.; c) TFA/anisole 25:1, 0°C→RT, 1 h, 93% (2 steps); d) Boc_2O, Et_3N, water/dioxane 1:1, 16 h; e) EDC, DMAP, CH_2Cl_2, 16 h, 52%; f) TFA/anisole 10:1, 15 min., evaporation; then NEt_3, THF, 10 min, 67%; g) $PdCl_2$, H_2, MeOH/CH_2Cl_2 2:1, 99%.

© 2006 Wiley-VCH Verlag GmbH & Co. KGaA, Weinheim

longest linear sequence comprised twelve steps, including five steps for the preparation of **132** starting from L-*N*-Z-asparagine. Originally, an enantioselective synthesis was planned by using **132** as a homochiral building block. However, epimerization under various conditions hampered this synthetic route. Yuan and Williams also completed the total synthesis of the seven-membered congeners TAN-1057C/D (**129**/**130**).[323]

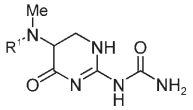
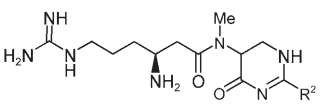
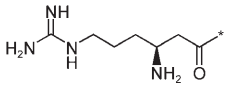
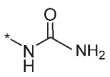
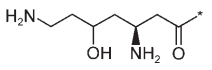
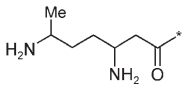
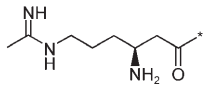
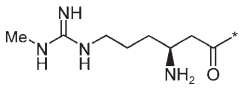
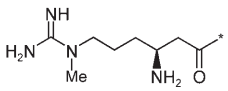
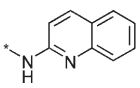
The more-convergent synthesis of de Meijere, Belov, and co-workers (Scheme 13) was published shortly after.[324] The racemic asparagine derivative **137** was prepared through a Michael addition of methylamine to maleamide. After protection, the 2,3-diamino propionic acid motif was included through a Hofmann rearrangement. Ring formation was successfully accomplished in a single step by employing the isothiurea building block **140**. The originally reported, moderate yield of 35% could be subsequently doubled by the reaction conditions (changing the solvent from isopropanol to acetonitrile, decreasing the temperature, and increasing the reaction time).[326] The crucial peptide bond formation was accomplished by irradiation of the β-homoarginine precursor **141** in the presence of the deprotected amino pyrimidinone **139**, which reacted with the ketene product of the Wolff rearrangement. Final triple deprotection gave TAN-1057A/B (**127**/**128**).



Scheme 13. De Meijere, Belov and co-workers's synthesis of TAN-1057A/B (**127**/**128**).[324] Reagents and conditions: a) $PhCH_2OCOCl$, aq. NaOH, 3 h, 88%; b) $PhI(OCOCF_3)_2$, pyridine, DMF/water 1:1, 4 h, 74%; c) MeOH, $SOCl_2$, −20 °C→RT, 24 h, 97%; d) **140**, NaOAc, MeCN, 55 °C, 70%;[326] e) H_2, 10% Pd/C, DMA, 24 h, 96%; f) **141**, *hν*, DMA, 2 h, 30%; g) $PdCl_2$, H_2, MeOH, 99%.

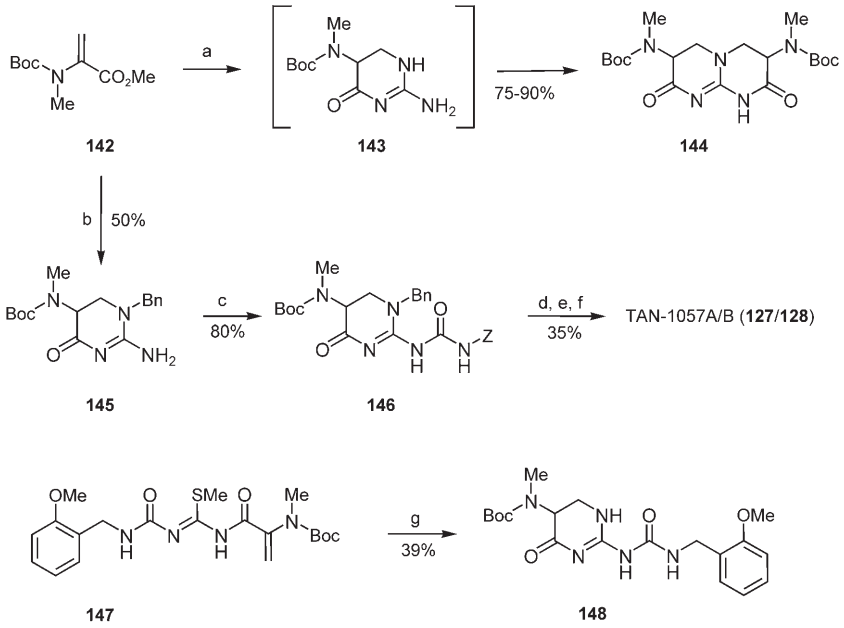
With eight steps, the synthesis by de Meijere, Belov, and co-workers was short and offered a practical access to **127**/**128**. The key building block **139** became available on a large scale in six steps and with a minimum of protecting group manipulation as the free amino group of **140** did not interfere with the cyclization reaction. This synthetic route was successfully employed to generate numerous different analogues (Table 15). Furthermore, careful optimization of the reaction conditions along this synthetic route resulted in the first enantioselective total synthesis of TAN-1057A (**127**).[326]

Table 15: Antibacterial activity in vitro of western derivatives with de novo synthesized β-amino acid side chains[330,334,336] and eastern variations of the urea,[325,328,334] MIC *S. aureus* [μg mL^{-1}].

		MIC			MIC
127/128		0.25	**127/128**		0.25
152		0.4	**157**		64
153		0.4	**158**		8
154		0.2	**159**		0.4
155		0.8	**160**		0.05
156		0.025	**161**		0.1

In the original approach, de Meijere, Belov, and co-workers envisaged the synthesis of **127**/**128** by addition of the guanidino moiety, hidden in the ureido pyrimidinone, to dehydro alanine **142** (Scheme 14).[324] Yet, addition did not stop after one Michael addition/ring closure, but rather triggered a tandem sequence forming the bicyclic derivative **144**. The second Michael addition could be suppressed by protecting one of the guanidino nitrogens as has been shown in different approaches: Ganesan and Lin[327] formed the guanidino function in situ from an elaborated dehydroalanine precursor **147** and scientists from Gilead used *N*-benzyl-protected guanidine in a Michael-addition approach yielding the intermediate **145**.[325] After incorporation of the urea moiety, the intermediate **146** was converted into the natural product **127**/**128** by using a modification of the original conditions by de Meijere, Belov, and co-workers [324] in 7 steps and 12% overall yield.

 © 2006 Wiley-VCH Verlag GmbH & Co. KGaA, Weinheim

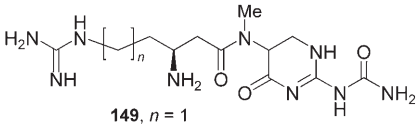


Scheme 14. Synthetic approaches to intermediates **144**,[324] **148**,[327] and natural product TAN-1057A/B (**127**/**128**)[327] by using dehydroalanine precursors. Reagents and conditions: a) Guanidine, *i*PrOH, 48 h; b) *N*-benzyl guanidine (TFA salt), K_2CO_3, *i*PrOH, RT, 16 h, then 50 °C, 4 h; c) Z-NCO, THF, 16 h; d) TFA, CH_2Cl_2; e) **131**, $AgClO_4$, NEt_3, DMF; f) $PdCl_2$, Pd/C, H_2, MeOH; g) 2 M NH_3 in MeOH, 20 h.

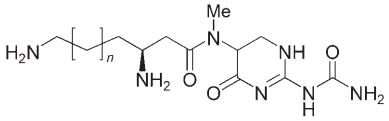
the formation of pyrrolidines and piperidines. By using β-amino acids synthesized de-novo,[330,334,335] further side-chain SAR trends were explored (Table 15). Incorporation of heterocycles, such as thiazoles or isoxazoles, deleted anti-staphylococcal activity.[334] Small groups, such as carbonyl, hydroxy (**152**), or methyl (**153**), were tolerated but the resulting antibiotics did not exhibit improved properties relative to **127**/**128**. Distinct variations of the original guanidine through an amidine group (**154**) or the methyl guanidines (**155** and **156**) led to compounds with high activity against stapylococci, which in the case of **156**, was accompanied with activity against pneumococci (Table 16).

The only variation so far reported for the dihydro pyrimidinone heterocycle was that of the N1-methylated derivative, which was inactive against staphyloccoci.[325] As methylation of the proximal NH function of the adjacent urea group led to inactive compounds (**157**, Table 15),[325] it seemed that the urea needed to be locked by a hydrogen bond (through the NH group of the ring) in a rigid conformation. Interestingly, the urea motif could be mimicked by various heterocycles such as pyrimidine **159**, pyridine **160**, and amino quinoline **161**.[334]

The different routes to **127**/**128** enabled structural variations in all parts of the molecule. One goal, pursued independently by scientists from the University of Colorado, Gilead, and Bayer, was to reduce the acute toxicity of the natural antibiotic while maintaining its excellent activity. The plan was to create a small-spectrum antibiotic that covered the spectrum gaps of established drugs such as imipenem. Both, the ω-guanidino group and the β-amino function were essential for activity against staphylococci.[328] A shift of the β-amino group to the α-position, maintaining the overall chain length, was not tolerated.[329] A systematic investigation revealed that reducing the distance between the amino and the guanidino group (**149**) was detrimental for activity, whereas the insertion of an additional methylene group (**150**) was tolerated.[330] The replacement of the ω-guanidino function by a ω-amino-group in **13** and **151** clearly improved tolerability. In this novel series, both, the *S* configuration and the β-amino position represented an optimum (Table 17).[330,331]



149, *n* = 1
150, *n* = 3



13, *n* = 1
151, *n* = 2

Table 16: Antibacterial activity in vitro of TAN-1057A/B (**127**/**128**) analogues, MIC [μg mL^{-1}].

	S. aureus	*S. epidermidis*	*E. faecium*	*E. faecalis*	*S. pneumoniae*
127/128	0.25	0.25	2	>16	16
151	0.25	0.125	0.25	64	32
156	0.025	0.125	2	64	4
160	0.05	0.25	2	>64	2

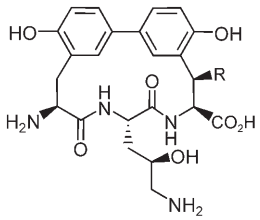
The amino acid components for the optimization program were readily available, for example, by Arndt–Eistert chain elongation. To explore the SAR options in the side chain, for derivatives of **13** and **151**, the synthesis of novel β-lysine or β-homolysine derivatives became important.[332] Surprisingly little was known about this field.[333] A reason for the lack of de novo synthetic methods for β-lysine and β-homolysines might lie in the 1,4- and 1,5-relationship between the ω-amino center and the β-amino group, which is prone to side reactions, such as

These optimization efforts resulted in compounds superior to the natural antibiotic **127**/**128** (Table 16, Table 17). Both, in vitro potency and in vivo efficacy of **151** were maintained, whereas it was more efficient in blocking protein biosynthesis in prokaryotes than in eukaryotes (Table 17).

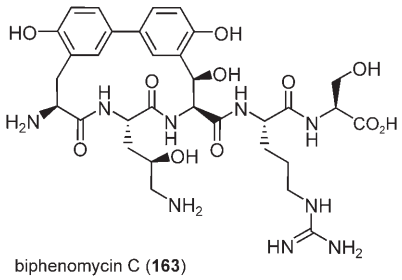
 © 2006 Wiley-VCH Verlag GmbH & Co. KGaA, Weinheim

This was reflected in an improved cytotoxicity profile and clearly improved tolerability. β-Homolysine **151** was tolerated in i.v doses of up to 150 mg kg^{-1} in mice and fulfilled the profile of a small-spectrum problem solver; a similar profile was achieved with β-lysine **13**. With **156** and **160**, the spectrum of in vitro antibacterial activity could be considerably broadened to include pneumococci, however, at the expense of the tolerability and therapeutic index. Thus, neither **156** nor **160** were suitable for clinical development.

The attractive antibacterial properties and the structure of natural antibiotics TAN-1057A/B (**127**/**128**) evoked the attention of several synthetic research groups. Systematic SAR exploration required novel routes to β-lysine and β-homolysine derivatives. The synthetic pyrimidinone antibiotics **13** and **151**, readily accessible on a large scale, exhibited improved cytotoxicity and tolerability while retaining eminent potency of the natural product. In this case, formal degradation of the natural product—through de novo synthesis—led to congeners with superior tolerability.



biphenomycin A, R = OH (**162**)
biphenomycin B, R = H (**21**)



biphenomycin C (**163**)

Table 17: Biological properties of TAN-1057A/B (**127**/**128**) analogues.

	S. aureus sepsis ED_{100} [mg kg^{-1}][a]	Translation prokaryotes IC_{50} [μM]	Translation eukaryotes IC_{50} [μM]	Cytotoxicity EC_{50} [μg mL^{-1}]
127/128	0.25	0.3	0.17	0.25
151	0.25	0.5	2.8	6
156	≤0.5	0.06	n.d.[b]	n.d.[b]
160	1	n.d.[b]	0.07	n.d.[b]

[a] 100% survival after parenteral administration of the given dose in mice. [b] n.d. = not done.

13. Biphenomycins

In 1967, a group from Lederle Laboratories reported the isolation of LL-AF283α, an antibiotic with unusual biological properties obtained from the fermentation of *S. filipinensis*.[337,338] Later, in 1991, Borders and co-workers[339] found that LL-AF283α was identical to the peptide antibiotic biphenomycin A (WS-43708A), which was reported by scientists from Fujisawa in 1984.[340,341,342] Biphenomycins displayed a structurally unique architecture with a cyclic tripeptide containing a biphenyl moiety in a 15-membered ring. The absolute stereochemistry of biphenomycin A (**162**) and its known congeners, biphenomycin B (**21**) and C (**163**),[343] was determined.[344,345]

The in vitro activity of biphenomycin A (**162**) was virtually limited to *Cornybacterium xerosis*. Growth of other bacteria, such as *S. aureus*, *E. coli*, or *S. pyogenes*, was not affected up to 200 μg mL^{-1} using agar-well diffusion or agar-dilution MIC assays. However, **162** was highly effective in vivo in a murine sepsis model. Administered subcutaneously, **162** protected mice, from an otherwise lethal infection, against *S. aureus* Smith (ED_{90} 1 mg kg^{-1}) and was five-times more effective than vancomycin in the same experiment.[337] The reason for this discrepancy between in vivo and in vitro activity has remained unclear. MIC values seemed to be strongly influenced by the test conditions.[337,341] Any in vitro antibacterial activity was completely suppressed with complex media (e.g. Mueller–Hinton agar), yet, with semisynthetic media, MICs could be measured for Gram-positive bacteria, but not for their Gram-negative counterparts.[341] Furthermore, it appeared that highly resistant mutants were selected on first exposure of **162**, which pointed to an unfavorable resistance profile.[339] On the other hand, these mutants showed no cross-resistance to established antibiotics, such as vancomycin, tetracycline, ampicillin, or erythromycin. Biphenomycin A (**162**) was well tolerated after oral dosing of up to 640 mg kg^{-1}.[337]

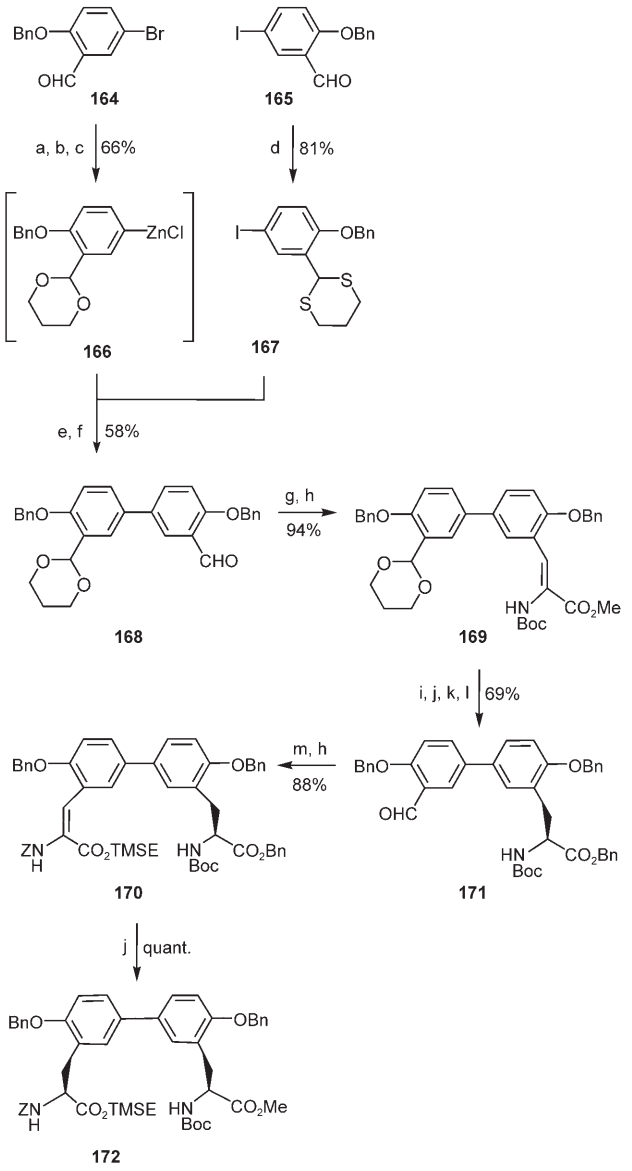
With interesting in vivo efficacy, good tolerability, and no cross-resistance to marketed antibiotics, the biphenomycins represented an attractive starting point for an optimization program in medicinal chemistry. On the other hand, the lack of in vitro activity, the questionable resistance behavior, and the unknown target posed barriers which had to be overcome. Conditional to solving these issues was the availability of a total synthesis which would allow rapid structural modification of selected parts of the molecule.

The first total synthesis of biphenomycin B (**21**) was published by Schmidt et al.[346] in 1991. Its sequence consisted of 1) synthesis of (*S*,*S*)-isotyrosine (**172**), 2) formation of an *ansa*-tripeptide (**174**), 3) macrocyclization, and 4) removal of protecting groups (Scheme 15 and Scheme 16).

Key steps of the synthesis of orthogonally protected (*S*,*S*)-isotyrosine were the Pd-catalyzed coupling of the zinc compound **166** with aryl iodide **167** followed by the sequential introduction of the dehydroamino acids **169** and **170**. The initially formed *E*/*Z* mixtures of **169** and **170** were isomerized with triethylamine on carbon to the respective *Z* compounds. These *Z* alkenes set the stage for the enantioselective hydrogenation that proceeds with >99% *ee* to yield **171** and **172**, respectively.

After Boc deprotection, **172** was coupled with (2*S*,4*R*)-hydroxyornithine (**173**), which was obtained from mannitol.[347] Alternative approaches to differently protected

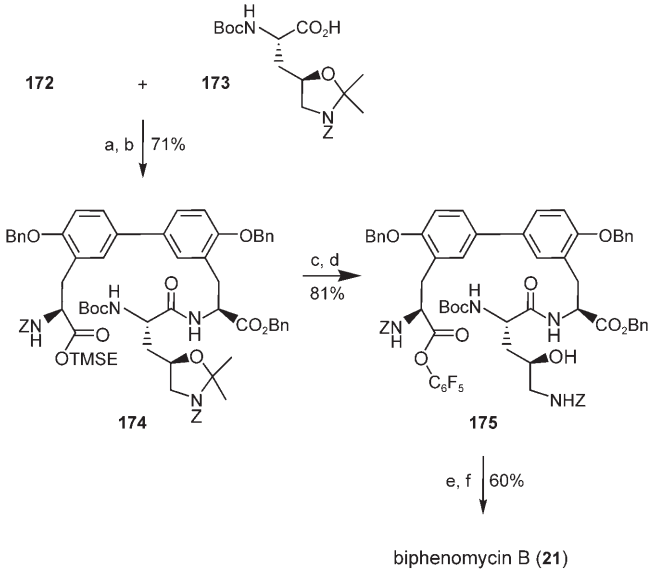
 © 2006 Wiley-VCH Verlag GmbH & Co. KGaA, Weinheim



Scheme 15. The synthesis by Schmidt et al. of (*S*,*S*)-isotyrosine (**172**).[346] Reagents and conditions: a) propane-1,3-diol, $BF_3{\cdot}Et_2O$, toluene, reflux, 4 h; b) Mg, THF, reflux, 3 h; c) $ZnCl_2$, THF, reflux, 1 h; d) propane-1,3-dithiol, $BF_3{\cdot}Et_2O$, toluene, reflux, 4 h; e) $[PdCl_2(PPh_3)_2]$, iBu_2AlH, RT, 3 h; f) NBS, 2,6-lutidine, CH_3CN, H_2O, 0 °C, 5 min; g) methyl *N*-*tert*-butoxycarbonyl(dimethoxyphosphoryl)glycinate, LiCl, DBU, CH_3CN, RT, 1 h; h) NEt_3, C, EtOH/$CHCl_3$ (1:1), RT, 2 d; i) LiOH, H_2O, dioxane, RT, 12 h; j) [Rh(cod)dipamp)]BF_4, H_2, MeOH, RT, 72 h; k) BnOH, DCC, DMAP, ethyl acetate, −15 to 20 °C, 12 h; l) PPTS, acetone, H_2O, reflux, 6 h; m) *N*-benzyloxycarbonyl(dimethoxyphosphoryl)glycine trimethylsilyl ester, LiCl, DBU, CH_3CN, RT, 2 h.

hydroxyornithine derivatives have been reported.[348] Manipulation of protecting groups and activation of the carboxy moiety as a pentafluorophenyl ester **175** (for the macrocylization) proceeded with excellent yields in a biphasic system under high-dilution conditions. Thus, **21** was obtained after simultaneous removal of five protecting groups in the final step (Scheme 16).

Overall, this route delivered the desired natural product in 22 steps with excellent optical purity in 9% overall yield



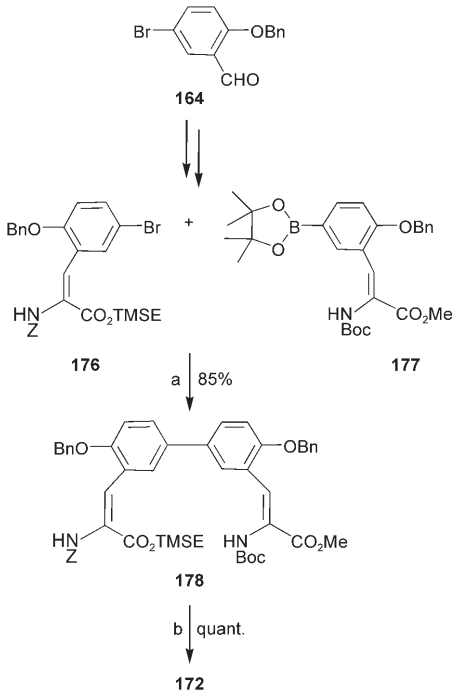
Scheme 16. Schmidt's total synthesis of biphenomycin B (**21**).[346] Reagents and conditions: a) HCl, dioxane, 20 °C, 2 h; b) EDC, HOBt, CH_2Cl_2, −15→20 °C, 14 h; c) AcOH/H_2O (9:1), 50 °C, 7 h; d) Bu_4NF, DMF, RT, 1 h, C_6F_5OH, EDC, CH_2Cl_2, −15→20 °C, 14 h; e) HCl, dioxane/CH_2Cl_2 (1:1), 0 °C, evaporation, $CHCl_3$, $NaHCO_3$, 20 °C, 5 min; f) trimethylsilyl trifluoromethanesulfonate, thioanisole, TFA, RT, 30 min.

starting from the appropriately substituted benzaldehyde derivatives (Scheme 15). Following his approach to biphenomycin B, Schmidt et al. also completed the synthesis of biphenomycin A (**162**) with some modifications in the preparation of the isotyrosine.[349,350] More-recent approaches by Paintner et al.[351] and others[352–354] were based on Schmidt's synthesis with modifications in the construction of the enantiopure isotyrosine. Thus, various methods for the construction of the biaryl have been successfully applied, including Stille, Suzuki, and oxidative cross-couplings with $VOCl_3$.

However, besides the total synthesis of natural biphenomycin A and B, neither derivatives nor close analogues thereof had been prepared. A first series of simplified amide and ester derivatives, including derivatizations at the peptide backbone have been reported recently.[355,356] The number of steps to the desired analogues of the natural product has been reduced significantly compared with the original sequence. Thus, biphenomycin B analogues have been prepared in 16 steps starting from benzaldehyde **164** through a Suzuki–Miyaura coupling[357] and subsequent double asymmetric hydrogenation (Scheme 17).[358,359] This route gave access to the same intermediate **172** as in the synthesis by Schmidt et al.. Intermediate **172** was obtained as a single diastereomer with complete stereocontrol (*ee* > 99%). Furthermore, the overall yield and feasibility of the synthesis has been improved by optimization of the macrocylization protocol and the final removal of the protecting groups.

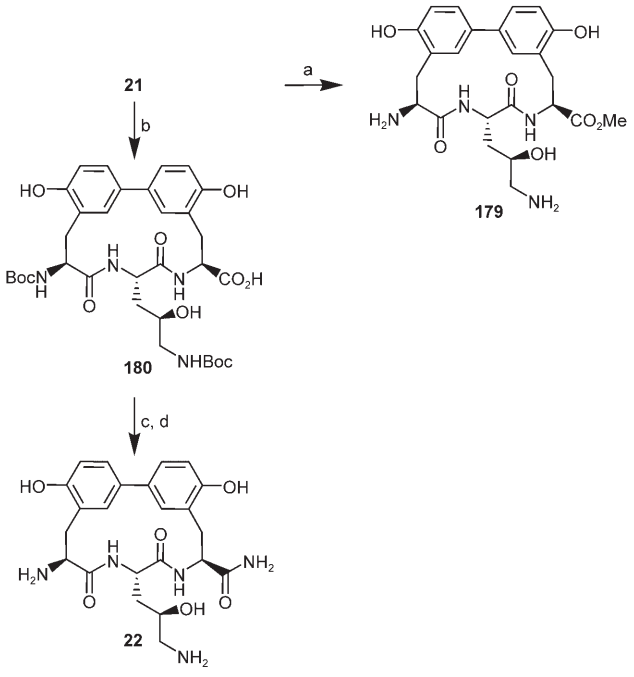
The biphenomycin analogues obtained by this methodology could be selectively derivatized by either direct esterification or amide formation through 1) Boc protection

 © 2006 Wiley-VCH Verlag GmbH & Co. KGaA, Weinheim



Scheme 17. Bayer's large-scale approach to hydroxydiisotyrosine **172**.[358] Reagents and conditions: a) Bis(diphenylphosphanyl)ferrocenpalladium(II)chloride, Cs_2CO_3, 1-methyl-2-pyrrolidon, H_2O, 50 °C, 10 h, 85 %; b) H_2 (3 bar), (*S,S*)-Et-DuPhos-Rh (1.5 %), EtOH/dioxane (1:1), RT, 3 d, quant., > 99 % *de*, > 99 % *ee*.

of the free amino groups, followed by 2) amide formation of the terminal carboxy group and, 3) acid-catalyzed Boc deprotection (Scheme 18). This approach led to novel con-



Scheme 18. Derivatization of biphenomycin B (**21**). Reagents and conditions: a) 4 M HCl in dioxane, MeOH, RT, 24 h, 97 %; b) di-(*tert*-butyl)-dicarbonate, H_2O, Na_2CO_3, MeOH, 0 °C→RT, 12 h, 83 %; c) $Na_2S_2O_4$, iPr_2NEt, NH_4Cl, HATU, DMF, 4 h, RT, 52 %; d) 4 M HCl in dioxane, RT, 30 min, 97 %.

Table 18: Antibacterial activity in vitro of **179** and **22** against Gram-positive pathogens, MIC [$\mu g\,mL^{-1}$].

	S. aureus	*S. aureus*	*E. faecalis*	*B. catarrhalis*
22	1.5	0.2	1	1
179	0.1	0.05	3	1

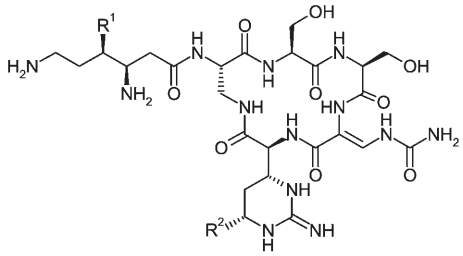
generers of biphenomycin B (**21**) that have improved in vitro activity (Table 18).[355,356,360]

Although both the biphenomycins and vancomycin possess a biphenyl group, no evidence for binding of **162** to the cell-wall analogue of *N*-Ac-D-Ala-D-Ala exists.[344] Instead, bacterial protein biosynthesis seemed to be the target of this novel class of antibacterials.[356]

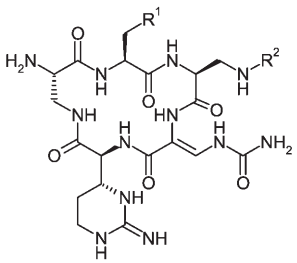
In summary, efficient pathways for the de novo synthesis of biphenomycins have been established and are paving the way to novel congeners (substituting derivatization) with improved in vitro activity and further insight into the molecular target of these novel antibacterials.

14. Tuberactinomycins and Capreomycins

The tuberactinomycin family of antibiotics consists of the closely related cyclic homopentapeptides tuberactinomycins and capreomycins. Viomycin (tuberactinomycin B, **182**), discovered in 1951,[361,362] was marketed by Ciba and Pfizer as a tuberculostatic agent in the 1960s. The capreomycins were isolated from the fermentation of *Streptomyces capreolus* as a four-component mixture, with **23** and **185** as the major and **186** and **187** as the minor compounds.[363] Both subclasses exhibit good activity against *Mycobacteria* including multidrug-resistant strains, but have only limited activity against other species.[364]



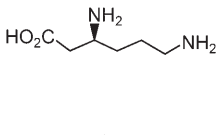
tuberactinomycin A, R^1 = OH, R^2 = OH (**181**)
tuberactinomycin B, R^1 = H, R^2 = OH (**182**, viomycin)
tuberactinomycin N, R^1 = OH, R^2 = H (**183**)
tuberactinomycin O, R^1 = H, R^2 = H (**184**)



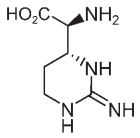
capreomycin IA, R^1 = OH, R^2 = β-lysyl (**23**)
capreomycin IB, R^1 = H, R^2 = β-lysyl (**185**)
capreomycin IIA, R^1 = OH, R^2 = H (**186**)
capreomycin IIB, R^1 = H, R^2 = H (**187**)

 © 2006 Wiley-VCH Verlag GmbH & Co. KGaA, Weinheim

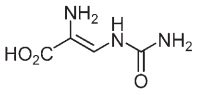
The nonproteinogenic amino acids, β-lysine (**188**), (2*S*,3*R*)-capreomycidine (**189**), and β-ureidodehydroalanine (**190**)—contained in the peptide backbone—complicated the structural elucidation of this class. The original structural



β-lysine (**188**)



(2*S*,3*R*)-capreomycidine (**189**)



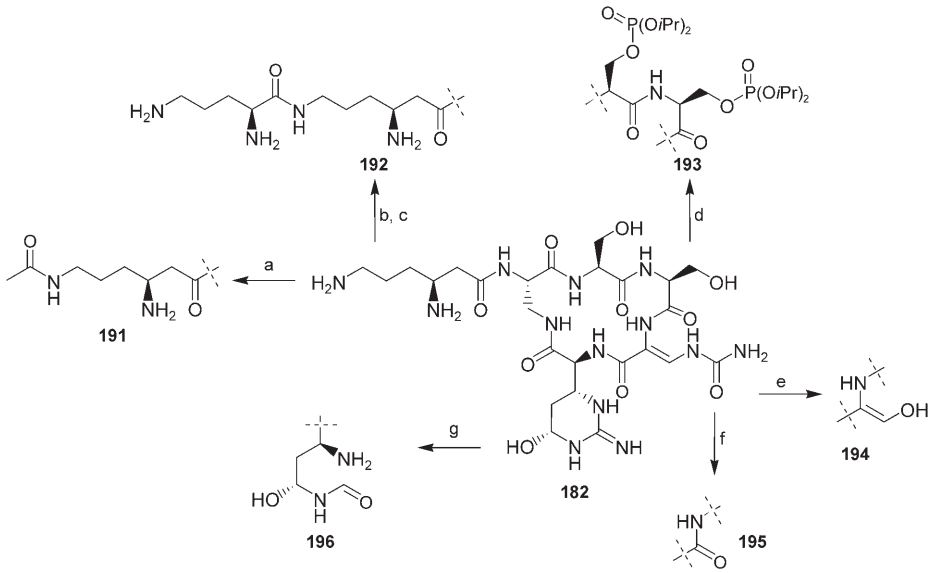
β-ureidodehydroalanine (**190**)

proposal[365] for capreomycin IB (**185**), was later revised by Shiba and co-workers.[366] Concurrently, several papers were published with proposed partial structures[367] or suggestions for the complete constitution of the tuberactinomycins (especially viomycin).[368–370] However, the correct structures were not determined until the X-ray crystal structure for tuberactinomycin O[371] (**184**) was resolved, and subsequently the structure of viomycin (**182**) was established.[372]

The activity of the tuberactinomycin family of antibiotics is limited mainly to Mycobacteria such as *Mycobacterium tuberculosis* or *Mycobacterium kansasii* (MIC 2–20 $\mu g\,mL^{-1}$).[373,374] They exert their antibiotic activity as potent inhibitors of the translation step of prokaryotic protein biosynthesis by inhibiting both the initiation and elongation steps. A detailed report on the interaction of tuberactinomycins at the target level illustrated how these compounds interacted with RNA.[375] When tested against a panel of *M. tuberculosis* strains in vitro, capreomycins compared favorably with streptomycin, cycloserine, and kanamycin.[376] No cross-resistance of tuberactinomycins with kanamycin, lividomycin, or paronomycin was observed.[377] Development of resistance in vitro seemed to be slow, especially when compared with kanamycin.[373] The in vivo efficacy of these compounds was low after oral dosing, but good after subcutaneous administration in experimental murine tuberculosis models.[373] Although tuberactinomycins were not devoid of toxicological problems, their toxicity profile after i.v. and peroral administration was quite favorable.[378] Overall, these biological features warranted further evaluation of this class for their clinical use as antituberculosis agents.

The early commercialization of viomycin (**182**) triggered intense research activities around these antimicrobials in academia and industry. Initial biological studies were often performed with mixtures of tuberactinomycins (**181**–**184**) or capreomycins (**23, 185**–**187**). Then, based on the studies of Gould and co-workers[379,380] on the biosynthesis of capreomycins, selective fermentation processes were developed.[381,382] Furthermore, several total syntheses enabled the selective access to viomycin (**182**),[383] tuberactinomycin N (**183**),[384] tuberactinomycin O (**184**),[385] and capreomycin.[366d] Despite the broad methodic arsenal to elucidate the SAR of tuberactinomycin-like antibiotics by total synthesis, most derivatives prepared for biological testing have been obtained through fermentation and semisynthesis. The first hints for the structural requirements necessary to produce activity against Mycobacteria were obtained from blocking specific functional groups in viomycin (**182**; Scheme 19).[386] Thus, the acetylation of the terminal amino group (**191**)[387] or both amino groups of β-lysine (not shown) led to a complete loss in activity (MIC *Mycobacterium* sp 607: 1.6 $\mu g\,mL^{-1}$ (**182**) versus $>400\ \mu g\,mL^{-1}$ (**191**)).[388] Acylation with uncharged or acidic amino acids at the same position also produced inactive compounds, whereas introduction of a basic amino acid (**192**) maintained the original MIC.[389] Similarly, blocking of the serine hydroxy groups, as in **193**, left the activity unchanged.[386] Surprisingly, hydrolysis of the urea functionality, which was regarded as one of the pharmacophores of this class, produced **194** with comparable in vitro activity as observed for viomycin (**182**; MIC *Mycobacterium* sp 607: 1.6 $\mu g\,mL^{-1}$ versus 3.1 $\mu g\,mL^{-1}$, for **182** and **194**, respectively).[386] Oxidation of **182** yielded the inactive bisamide **195**.[390] Finally, reductive opening of the capreomycidine ring of **182** led to a complete loss in activity (**196**).[391]

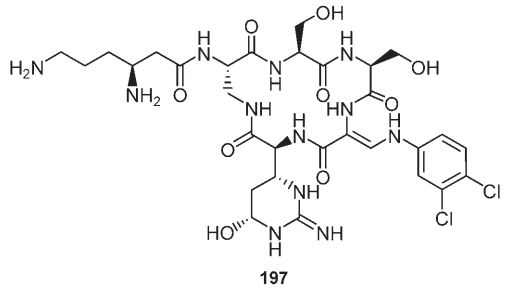
Similar modifications have been performed with tuberactinomycin N (**183**),[392–394] tuberactinomycin O (**184**),[395] and capreomycins.[396] However, none of these efforts resulted in a significantly improved activity against Mycobacteria or an extension of the antibacterial spectrum.



Scheme 19. Semisynthetic modification of viomycin (**182**). Reagents and conditions: a) *N*-acetoxy succinimide, Et_3N, carbonate buffer solution, dioxane, 1 h; b) *Z*-D-Orn(Z)-OSuc, Et_3N, carbonate buffer solution, THF, 0 °C, 12 h; c) H_2, Pd, DMF; e) hydrolysis; f) $KMnO_4$ (oxidation); g) $NaBH_4$ (reduction).

© 2006 Wiley-VCH Verlag GmbH & Co. KGaA, Weinheim

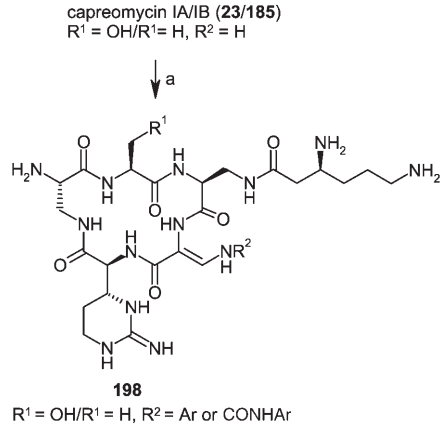
Driven by the widespread emergence of bacterial resistance, Pfizer initiated a HTS against *Pasteurella haemolytica* with the goal to discover novel leads for both animal and human infections.[397] The 3,4-dichlorophenylamino analogue **197** of viomycin (**182**), discovered by this approach, exhibited



197

good MICs against the animal pathogens *P. multocida* and *P. haemolytica*, but only mediocre activity against other bacteria (Table 19). However, further variation of the substituted ureido analogues of capreomycin IA/IB (mixture of **23** and **185**) yielded novel compounds with activities against several multidrug-resistant Gram-positive pathogens and Gram-negative *E. coli* (Scheme 20).[398]

Further to their in vitro potency, these compounds were also efficacious in murine infection models. For example, **201** exhibited an ED_{50} of 3 mg kg^{-1} (subcutaneous application) against MRSA and VRE. Starting from substituted urea **24**, guanidine **202** was obtained in 36% yield (Scheme 21).[399] Irrespective of this substantial change in basicity of the terminal amine in **202** compared with **24**, both compounds exhibited the same antibacterial spectrum against all tested Gram-positive strains.

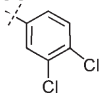
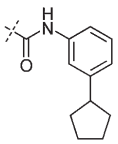
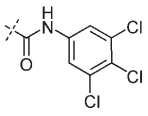
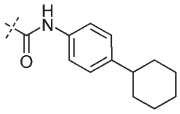


Scheme 20. Synthesis of the ureido derivatives of capreomycin IA/IB (**23**/**185**). Reagents and conditions: a) aniline or phenyl urea, 2 N HCl, dioxane, 65 °C, 4 h–12 h.

Treatment of viomycin (**182**) in trifluoroacetic acid with nucleophiles generated the respective Pictet–Spengler-like derivatives at the hydroxy group of viomycin with undetermined stereochemistry (Scheme 22).[400] Arylation or introduction of a sulfonamide group at C19 did not improve activity, whereas carbamate and urea substitution at this position were found to be more potent than the parent antibiotic (Table 20).

By using de novo synthesis, Pfizer scientists could significantly expand the antibacterial spectrum of tuberactinomycin-like antibiotics from *Mycobacterium*-only to Gram-positive pathogens, including multiresistant strains. Yet, despite proven in vitro and in vivo potency of the novel analogues, no further clinical development in this class has been reported to date.

Table 19: Antibacterial activity in vitro of ureido derivatives of capreomycin IA/IB (**23**/**185**), MIC [μg mL^{-1}].

	R^2 (in **198**)	*P. multocida*	*E. coli*	MRSA	*E. faecium*	*E. faecalis*
23/**185**	$CONH_2$	50	200	100	>1000	>1000
197	[a]	0.78	12.5	12.5	50	25
199		0.39	6.25	0.78	25	12.5
200		0.39	12.5	3.12	3.12	3.12
201		0.2	6.25	0.78	3.12	1.56
24		n.d.[b]	n.d.[b]	1.56	3.12	3.12

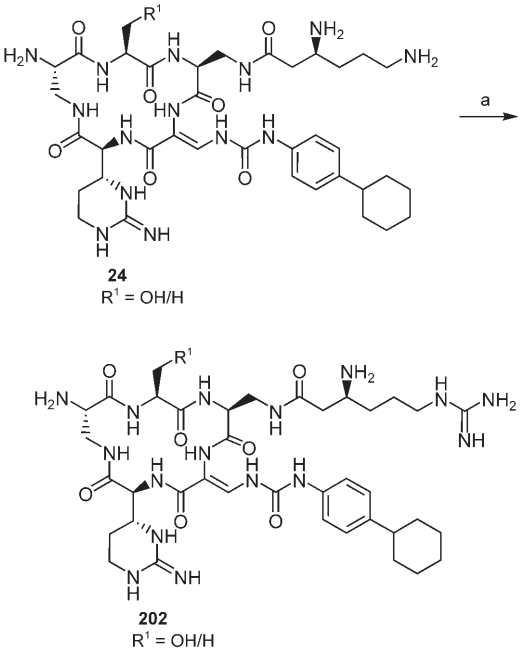
[a] See formula in text. [b] n.d. = not done.

15. Glycopeptide Antibiotics

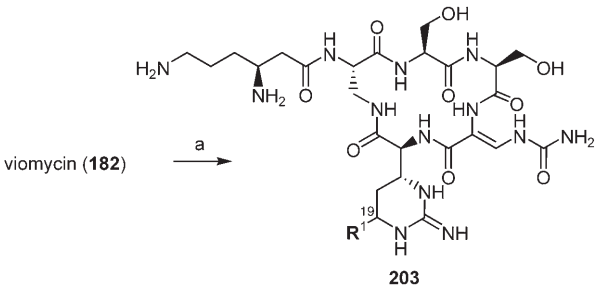
Owing to the lack of cross-resistance to other antibacterial drugs, the glycopeptide antibiotics[401] have become first-line drugs for the (parenteral) treatment of life-threatening multiresistant infections by Gram-positive bacteria in many hospitals. Vancomycin (**7**, Figure 10), the first glycopeptide antibiotic introduced into clinical practice in 1959,[402] was isolated from *Streptomyces orientalis* (now *Amycolatopsis orientalis*) from soil samples by Lilly scientists in the mid 1950s.[403] The elucidation of its complex structure took years and required several attempts and revisions until it could unequivocally be assigned in the early 1980s.[404,405]

Although related congeners have been used as growth promoters for livestock, teicoplanin (**208**) is the only additional member of this class that is available for human use, albeit not in the US. Both drugs

 © 2006 Wiley-VCH Verlag GmbH & Co. KGaA, Weinheim

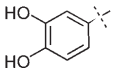
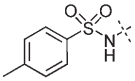
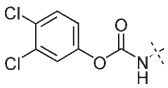
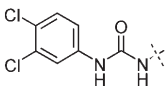


Scheme 21. N Terminal modification of capreomycin derivative **24**. Reagents and conditions: a) methyl imidothiocarbamate, H_2O, pH 10.7, RT, 7 d, 36%.



Scheme 22. C19 modifications of viomycin (**182**). Reagents and conditions: a) nucleophile (1,2-dihydroxybenzene, 4-methylsulfonamide, 3,4-dichlorophenylcarbamate, or 3,4-dichlorophenylurea), TFA, RT, 15 h.

Table 20: Antibacterial activity in vitro of C19 derivatives of viomycin (**182**), MIC [$\mu g\,mL^{-1}$].

	R^1	*P. multocida*	*E. coli*	MRSA
182	HO	200	200	n.d.[a]
204		200	200	n.d.[a]
205		200	200	n.d.[a]
206		6.25	25	3.12
207		1.56	6.25	25

[a] n.d. = not done.

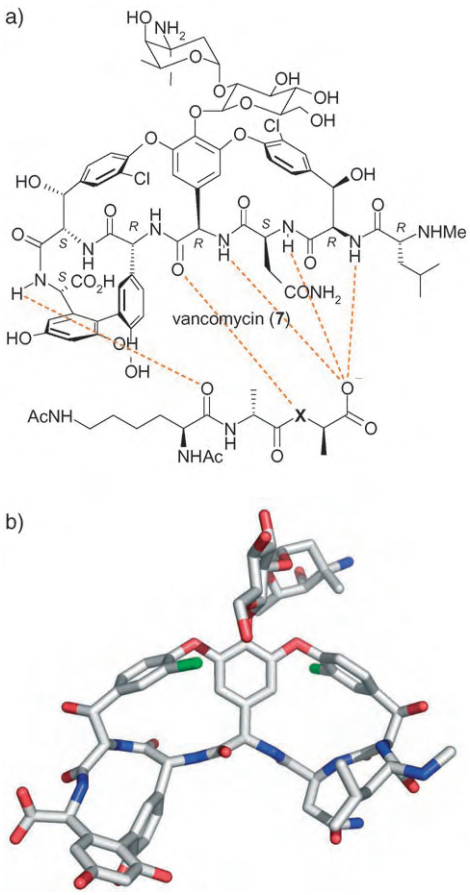


Figure 10. a) Hydrogen bonding between vancomycin (**7**) and the L-Lys-D-Ala-D-Ala (X = NH) peptidoglycan precursor terminus model peptide.[416b] In the resistance phenotypes VanA and VanB, the molecular recognition site D-Ala-D-Ala (X = NH) of the peptidoglycan precursor strands is replaced by a D-Ala-D-lactate terminus (X = O). b) The X-ray crystal structure of vancomycin illustrates its rigid concave shape[417a]

are unaltered natural antibiotics of the large dalbaheptide group that is produced by various actinomycetes.[406] Their common structural element is a linear heptapeptide backbone (configuration *R*,*R*,*S*,*R*,*R*,*S*,*S*) in which some aromatic amino acid residues are cross-linked (biphenyl and diphenylether motives) and build a rigid concave shape. For years, total syntheses of vancomycin's complex structure presented an enormous challenge for the foremost synthetic groups.[407] It is particularly informative to compare the successful synthetic strategies of Evans et al.,[408] Nicolaou et al.,[409] and Boger et al.[410] with nature's biosynthetic route to glycopeptides.[411,412] In contrast with the chemists, micorganisms assemble the complete linear heptapeptide (nonribosomal peptide synthetases) before oxidative (enzymatic) cross-linking of the side chains. With about 35 steps, the biosynthetic route to **7** remains considerably shorter than any de novo synthesis.

Glycopeptide antibiotics inhibit bacterial cell-wall biosynthesis by recognizing and strongly binding to the L-Lys-D-Ala-D-Ala termini of peptidoglycan precursor strands at the external side of the membrane. In this way, transpeptidases are prevented from executing their cross-linking job.[413–415]

 © 2006 Wiley-VCH Verlag GmbH & Co. KGaA, Weinheim

NMR spectroscopic[416] and X-ray crystal[417] studies demonstrated that evolution has saliently shaped the rigid antibiotic cavity for tight binding to its target through five specific hydrogen bonds in a stoichiometric complex (Figure 10). The blocking of transpeptidases indirectly also affects transglycosylase action.

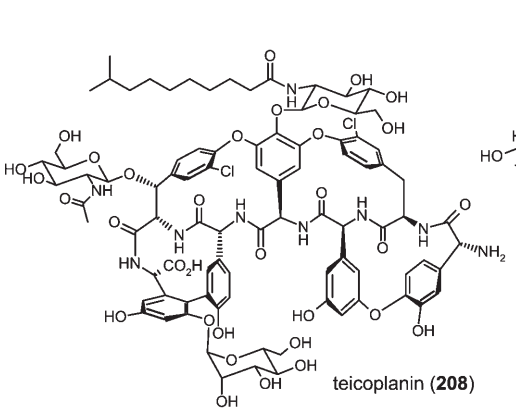
Glycopeptide antibiotics are restricted to treating Gram-positive infections as they cannot penetrate the outer membrane of Gram-negative bacteria. With the rise of MRSA infections in hospitals, vancomycin (**7**) became the antibiotic of last resort but, owing to its frequent use, resistant Gram-positive pathogens, in particular vancomycin-resistant enterococci (VRE) have emerged and worryingly spread.[418] By 2003, more than half of the clinical VRE isolates in the US had become resistant to glycopeptides.[35] In the main resistance phenotypes (VanA and VanB), the molecular recognition site D-Ala-D-Ala (X = NH) of the peptidoglycan precursor strands is replaced by a D-Ala-D-lactate terminus (X = O).[419] This "simple" amide to ester replacement at the peptidoglycan terminus, that is, the loss of a single hydrogen bond ($C^{1.4}$-carbonyl to X = O) and concomitant creation of a destabilizing lone pair/lone pair interaction between the ligand and antibiotic notably results in a 1000-fold decrease in binding affinity and a dramatic loss in antibacterial activity (MIC).[420]

In a spectacular example of chemical postevolution, Boger and co-workers have selectively omitted the "disturbing" $C^{1.4}$-carbonyl functionality (Figure 10). Their fully synthetic $C^{1.4}$-deoxo congener of vancomycin exhibited enhanced affinity for the D-Ala-D-lactate terminus (no repulsive interaction) leading to restored antibacterial activity against resistant pathogens.[421] Some glycopeptide antibiotics tend to form homodimers that bind much tighter to the peptidoglycan termini than the corresponding monomers.[413] The emergence of vancomycin-resistant enterococci and staphylococci[422] has encouraged the search for new (lipo)glycopeptides with improved pharmacokinetic and pharmacodynamic properties and activities towards resistant strains.[414,423,424]

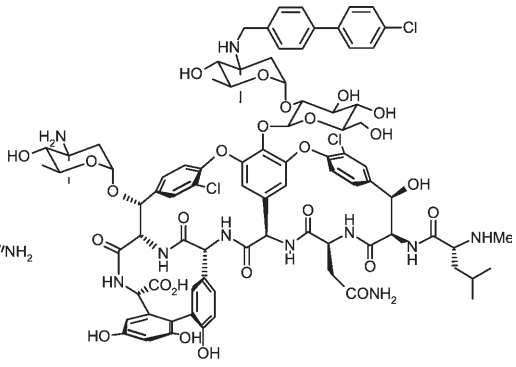
Despite successful total syntheses and available innovative synthetic methods, fermentation and subsequent semisynthetic variation of natural glycopeptide scaffolds has been the prevalent way to explore SARs[423] and the only practicable route to bulk production of clinical candidates. Novel, resistance-breaking glycopeptides possess structural elements that promote dimerization and membrane anchoring. Dimerization causes tighter binding of ligands terminating in D-Ala-D-lactate,[425] whereas lipophilic side chains endorse anchoring in the cytoplasmic membrane, thereby helping to position the antibiotic close to its target and eventually also disturb the bacterial-membrane integrity. These effects have stimulated chemists to prepare covalent vancomycin dimers.[426] Lipophilic side chains can restore activity against VRE while maintaining the effectiveness against MRSA.[427]

The presence of specific sugars is of vital importance for glycopeptide activity; aglycones are uniformly less active. An additional amino sugar at residue 6 and aromatic chlorine substituents promote favorable dimerization, and substitution of the free carboxylate function by basic carboxamides increases the activity against staphylococci. On the other hand, most efforts to change the natural heptapeptide backbones resulted in reduced activity.[406]

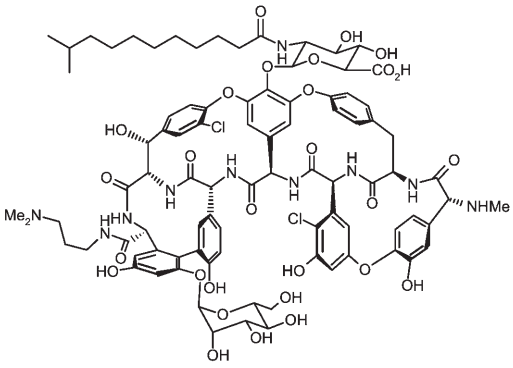
Three semisynthetic second-generation drugs, oritavancin (LY-333328, **26**),[428,415] dalbavancin (BI-397, **209**),[429] and telavancin (TD-6424, **210**),[430] have been advanced to clinical development[431] and have provided insight into how medicinal-chemistry programs work. Oritavancin (**26**) is the 4′-chlorobiphenylmethyl derivative of the natural vancomycin analogue chloroeremomycin (**25**). The spectrum of **26** covers VRE, MRSA, and to some extent also glycopeptide-intermediate *S. aureus* (GISA). Its bactericidal action and half-life allow for once-daily administration. Dalbavancin (**209**) has a



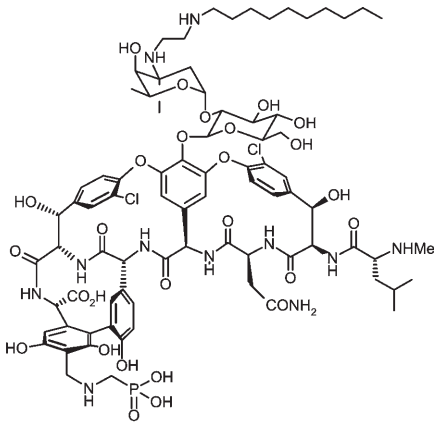
teicoplanin (**208**)



oritavancin (**26**)



dalbavancin (**209**)



telavancin (**210**)

 © 2006 Wiley-VCH Verlag GmbH & Co. KGaA, Weinheim

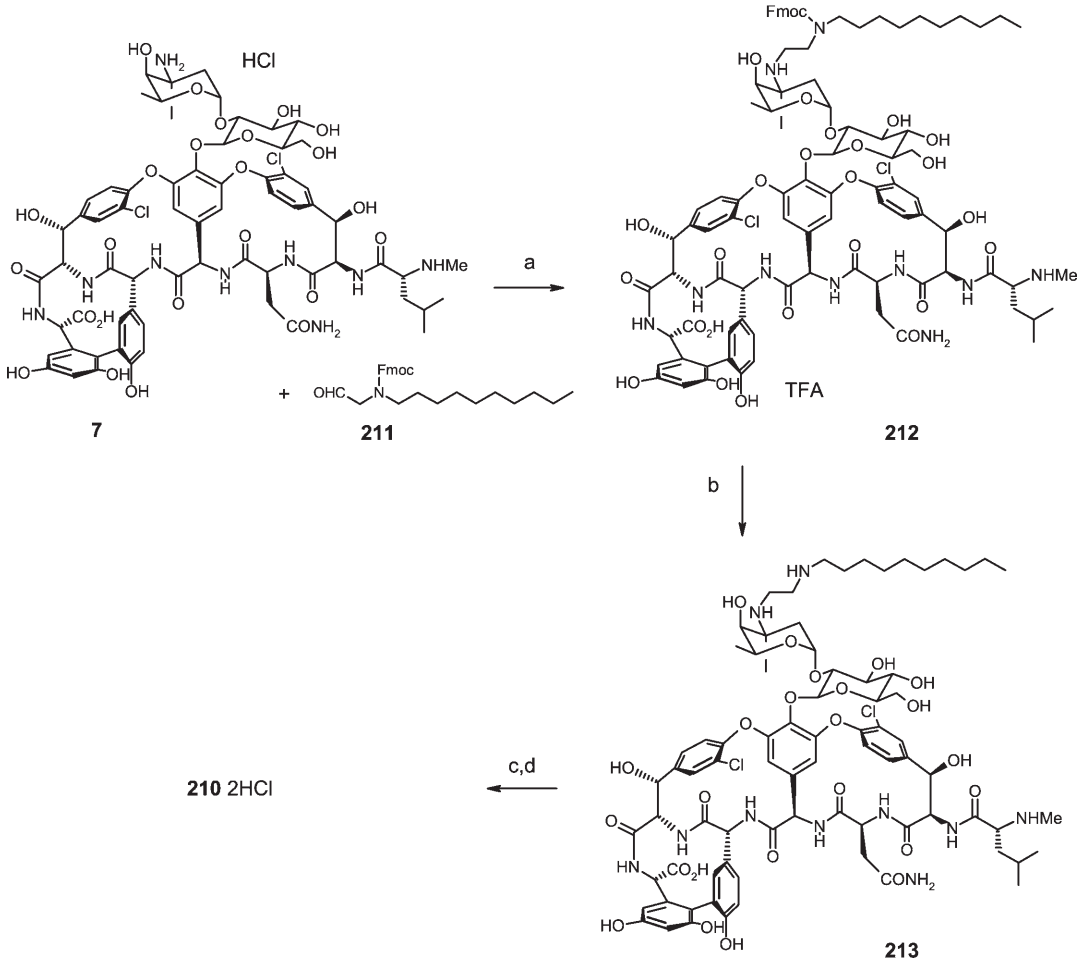
similar spectrum but is not active against VRE of the VanA-resistance genotype (Table 21). Owing to its prolonged retention in the body (half-life 174 h), one administration per week seems sufficient.

The discovery of telavancin (**210**),[432] the youngest and most promising congener, encapsulates the essential aspects of a successful glycopeptide optimization: in search of glycopeptides with improved in vitro activity, Theravance chemists prepared *N*-decylaminovancomycin (**213**, Scheme 23), the MIC of which was superior or at least equipotent to **7**. As expected, the introduction of the lipophilic substituent restored activity against enterococci regardless of their susceptibility while maintaining activity against MRSA and VISA. However, although increased lipophilicity improved in vitro activity, at the same time it negatively influenced physicochemicistry and absorption, distribution, metabolism, and excretion (ADME) properties: in contrast to **7**, **213** was poorly excreted from urine and showed an unfavorable tissue distribution in rats. To counterbalance lipophilicity and distribution properties, the supplementary addition of different hydrophilic groups was explored. Indeed, compounds with negatively charged polar groups exhibited increased urinary excretion and reduced accumulation in the liver and kidney while maintaining the improved in vitro profile. As a result of these studies, the lipoglycopeptide antibiotic **210** was selected for development.[430] It demonstrated potent in vitro activity against clinically relevant aerobic[433] and anaerobic[434] Gram-positive bacteria without cross-resistance to comparative drugs, showed rapid bactericidal action, and effected its activity through multiple modes of action (inhibition of peptidoglycan

Table 21: Antibacterial activity in vitro of glycopeptides vancomycin (**7**), oritavancin (**26**), dalbavancin (**209**), and telavancin (**210**), MIC_{90} [$\mu g\,mL^{-1}$].[430a]

	7	26	209	210
MSSA[a]	1	1	0.25	1
MRSA[b]	4	1	0.25	1
VRSA[c]	32	0.25	1	0.5
S. pneumoniae	0.5	0.008	0.06	0.008
Enterococcus spp. VanB	128	1	1	2
Enterococcus spp. VanA	>128	4	128	8

[a] Methicillin-susceptible *S. aureus*; [b] Methicillin-resistant *S. aureus;* [c] Vancomycin-resistant *S. aureus*.



Scheme 23. Theravance's semisynthesis of telavancin hydrochloride (**210**) from vancomycin hydrochloride.[430] Reagents and conditions: a) iPr_2NEt, DMF, 6–8 h, RT, MeOH, TFA, 15 min RT, borane-*tert*-butylamine complex, 2 h, RT; b) *tert*-butylamine, 40 °C, 7 h; c) (aminomethyl)phosphonic acid, CH_3CN, 20–30 °C, 15 min; iPr_2NEt, 1 h, RT, aqueous CH_2O, −7 °C, 12 h; 3 N HCl, pH 2.59, −5 °C; EtOH, 5 °C, 3 h; d) Amberlite XAD chromatography, CH_3CN, H_2O, HCl.

 © 2006 Wiley-VCH Verlag GmbH & Co. KGaA, Weinheim

synthesis and perturbation of bacterial cell membrane potential and permeability).[435] In vivo pharmacodynamics in various animal models[436] as well as pharmacokinetics and tolerability in healthy subjects suggested an effective once-daily therapy.[437]

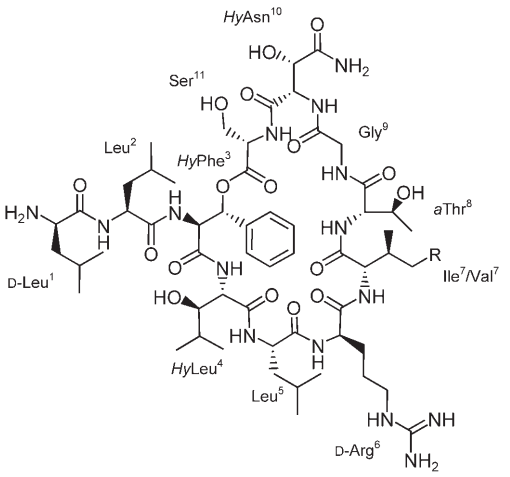
Telavancin (**210**) has been prepared from vancomycin hydrochloride and other commercially available starting materials through a three-stage process (Scheme 23):[438,439] selective reductive alkylation of **7** with *N*-Fmoc-*N*-decylaminoacetaldehyde (**211**) by means of borane-*tert*-butylamine complex followed by treatment with methanol and trifluoroacetic acid afforded the Fmoc-protected intermediate **212**. The Fmoc group of **212** was removed with *tert*-butylamine in DMF to yield *N*-decylaminovancomycin (**213**) in one pot. Mass spectrometric analysis confirmed that reductive alkylation selectively occurred at the vancosamine nitrogen and not at the N terminus of the peptide backbone. Mannich condensation with (aminomethyl)phosphonic acid and aqueous formaldehyde produced crude **210**, which was purified by Amberlite XAD chromatography to yield pure telavancin hydrochloride. The original procedure[432] has been continuously modified and optimized for production.[430]

Through chemical postevolution, the new, semisynthetic glycopeptide antibiotics, in particular oritavancin (**26**) and telavancin (**210**), have achieved significant technical progress over their established natural congeners in terms of activity against resistant strains and pharmacokinetic and pharmacodynamic properties. It will be interesting to learn to what extend these favorable profiles will be reflected in cure rates during advanced clinical trials. If approved, these compounds could become valuable drugs for the treatment of severe infections with multiresistant pathogens.

16. Lysobactins

The lysobactins are good examples of structurally exciting antibacterial natural products that are not the result of expeditions to remote tropical habitats, but were detected in urban soil organisms. Lysobactin (**27**) was isolated from the fermentation broth of *Lysobacter* sp. SC-14076 (ATCC 53042) by scientists from Squibb.[440,441]

The lysobactin strain was obtained from a leaf-litter sample found in the historic Washington Crossing State Park, US. Independently, scientists from Shionogi reported on katanosins A and B, which originate from a soil bacterium found in Katano City, Japan.[442] The producer strain PBJ-5356 was described as related to the genus *Cytophaga*, but not as *Lysobacter* sp.. Surprisingly, katanosin B later turned out to be identical to **27**.[443] Recently, katanosin A (**214**) has also been found to be a minor metabolite of the *Lysobacter* ATCC 53042 strain.[444] Most likely **27** and **214** belong to the armamentarium of their bacterial producers. Correspondingly, lytic attack of other microorganisms was the name-giving characteristic for the genus *Lysobacter*.[445] From a chemotaxonomic point of view it is surprising to find special secondary metabolites such as **27** and **214** being biosynthesized within two different phyla such as Proteobacteria (*Lysobacter*) and Bacteroidetes (*Cytophaga*).



lysobactin, R = CH_3 (**27**, ≡ katanosin B)

katanosin A, R = H (**214**)

The biosynthesis of bacterial cell walls appears to be the primary target area of lysobactin antibiotics.[441,442] Both **27** and **214** inhibited consumption of the cell-wall precursor [^{14}C]GlcNAc, a very good indicator for interference with the peptidoglycan biosynthesis (Figure 3). Most likely, inhibition of peptidoglycan formation is induced by the binding of lysobactin to lipid intermediates (not through binding to biosynthetic enzymes) that occur as biosynthetic precursors downstream of the muramyl pentapeptide. Lysobactin antibiotics seem to have a mode of action that is different from vancomycin (**7**).[446]

Lysobactin (**27**) and katanosin A (**214**) are highly active against Gram-positive bacteria, such as staphylococci or enterococci. In these pathogens submicromolar MIC values were obtained that were often superior to vancomycin.[440,442,447] The excellent antibacterial in vitro activity of **27** and **214** was maintained in vancomycin-resistant enterococci. Promising therapeutic in vivo efficacy could be demonstrated in a systemic murine *S. aureus* infection model (ED_{50} 1.8 mg kg^{-1} i.v., CFU ≈ 10^5).[442]

The primary structure of lysobactin (**27**) was elucidated in an elegant interplay of spectroscopic methodology and enzymatic degradation reactions.[448] Lysobactin has a "lariat structure" that consists of the dipeptidic "linear segment" (D-Leu^1-Leu^2) and the nonadepsipeptidic "cyclic segment" (*Hy*Phe^3-*Hy*Leu^4-Leu^5-D-Arg^6-Ile^7-*a*Thr^8-Gly^9-*Hy*Asn^{10}-Ser^{11}). So far, the secondary solution structure of **27** has not been fully elucidated.[449] The high content of nonproteinogenic amino acids[450] clearly hints at a nonribosomal biosynthesis.[451] The remarkable hydrolytic stability of all amide bonds towards proteases and peptidases may be regarded as the result of an evolutionary optimization that lead to a cyclic structure with a high content of β-hydroxylated as well as non-natural D-configurated amino acids. These structural motifs, cyclic, β-hydroxylated, and D-configurated, are often encountered in depsipeptidic and peptidic secondary metabolites. This opposes the common prejudice of the non-drugability of peptide structures owing to their low proteolytic stability.

 © 2006 Wiley-VCH Verlag GmbH & Co. KGaA, Weinheim

However, in lysobactin (**27**) the lactone linkage is prone to hydrolysis.[448]

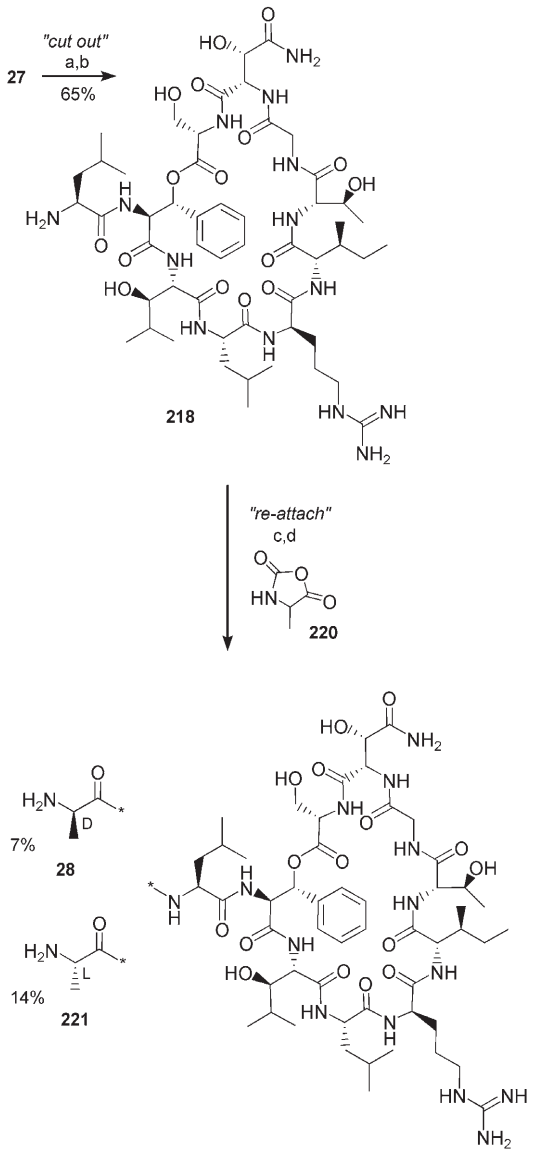
So far, a total synthesis of lysobactin (**27**) has not been published. Expected challenges are the synthesis of *threo*-β-hydroxyasparagine, the generation and conservation of the lactone function (in the presence of four hydroxy groups), and the crucial macrocyclization. Cardillo and co-workers,[452,453] Lectka and co-workers,[454] VanNieuwenhze and co-workers,[455] and Palomo et al.[456–458] started tackling the synthetic challenges of the lysobactin target molecule. Egner and Bradley[459] already reported on the solid-phase synthesis of a close lysobactin congener **217** (Scheme 24), however, no biological data have been published for **217**.

In the complex class of lysobactin antibiotics, semisynthesis was again the faster way to set up preliminary SARs. The Edman elaboration of the natural product allowed for selective modification of lysobactin at amino acid position 1 through a substituting-derivatization strategy (cut out and reattach; Scheme 25).[444,447] Reacylation of **218** showed that the N-terminal D-Leu[1] played a crucial role for the biological activity of lysobactin antibiotics. The N-terminal amino acid seems to be a prerequisite for activity, consequently, the Edman degradation product **218** turned out to be inactive. N Capping with a D-configured amino acid at position 1 (as in the natural product) appeared to be beneficial for in vitro activity (**28** versus **221**; Table 22).[447]

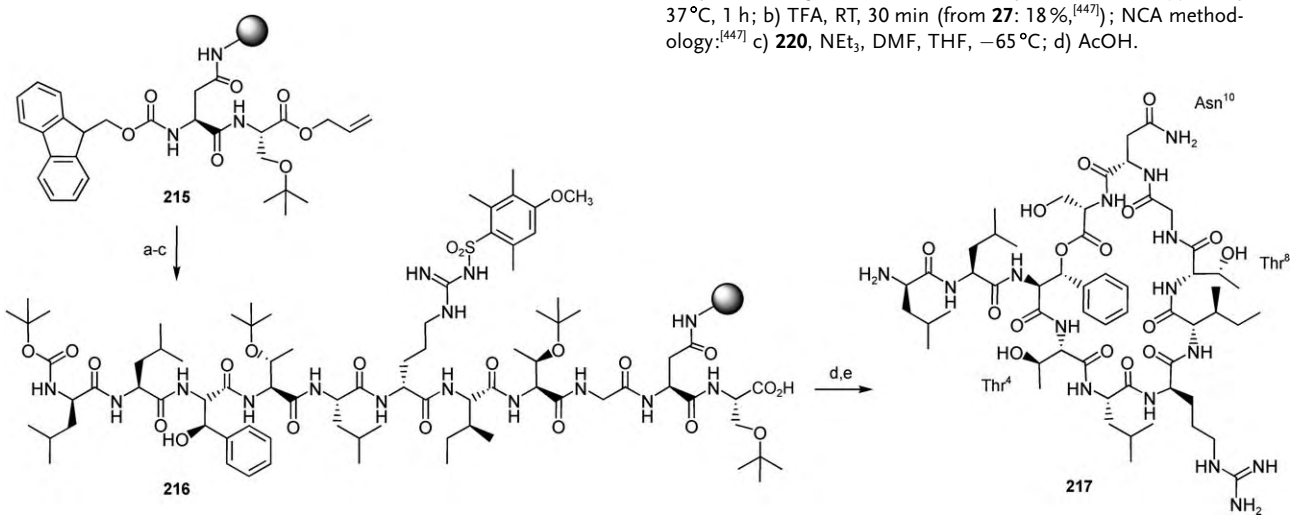
The lysobactins are interesting antibacterial lead structures with promising in vitro activity and in vivo efficacy. So far, knowledge about this class is based on the natural

Table 22: Antibacterial activity in vitro of lysobactin antibiotics against Gram-positive pathogens, MIC [$\mu g\,mL^{-1}$].[447]

	S. aureus	*E. faecalis*
27	0.2	0.8
218	100	50
28	0.4	1.6
221	3.1	6.3



Scheme 25. Squibb's single Edman degradation (substituting modification).[444,447] Reagents and conditions: a) excess PhNCS, pyridine/H_2O, 37 °C, 1 h; b) TFA, RT, 30 min (from **27**: 18%,[447]); NCA methodology:[447] c) **220**, NEt_3, DMF, THF, −65 °C; d) AcOH.



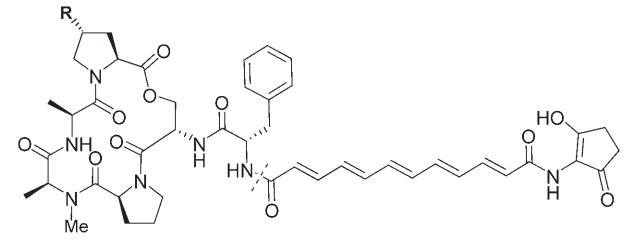
Scheme 24. Bradley's solid-phase synthesis of the lysobactin congener **217** through macrolactonization.[459] Reagents and conditions: a) Fmoc peptide synthesis, 6×DIC/HOBt couplings, CH_2Cl_2; b) Fmoc peptide synthesis, 3×EEDQ couplings, CH_2Cl_2; c) Pd^0; d) DIC, HOBt, DMAP, CH_2Cl_2, 37 °C, 12 h; e) TFA/iPr_3SiH/H_2O (95:2.5:2.5), 4 h (overall yield 15.6%).

 © 2006 Wiley-VCH Verlag GmbH & Co. KGaA, Weinheim

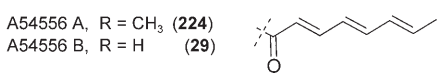
products **27** and **214** and some semisynthetic Edman derivatives. A preliminary SAR could be established for the amino acid position 1 within the linear segment. Further work has to be done for a real assessment of this interesting class.

17. Enopeptin Depsipeptide Antibiotics

Natural depsipeptides have a definite therapeutic potential as antibacterial agents and for various other indications.[460] Two depsipeptides from which the family name was derived, enopeptin A (**222**) and B (**223**), were isolated in 1991 from a culture broth of *Streptomyces* sp. RK-1051, found in a soil sample collected in Tsuruoka City, Japan.[461] Their structure, elucidated by chemical and spectroscopic means, consisted of a 16-membered lactone ring made up of five (*S*)-amino acids and a lipophilic polyene side chain attached to the serine N terminus.[462,463] Both their antimicrobial activity against Gram-positive bacteria and some Gram-negative membrane-defective mutants and their unique structural components evoked the chemists' interest in their total synthesis.[464] Almost a decade earlier, scientists from the company Eli Lilly described the isolation of a similar depsipeptide antibiotic A54556, a complex of eight depsipeptidic factors A–H, which was produced by aerobic fermentation of *Streptomyces hawaiiensis* (NRRL 15010).[465]



enopeptin A, R = CH_3 (**222**)
enopeptin B, R = H (**223**)



A54556 A, R = CH_3 (**224**)
A54556 B, R = H (**29**)

The complex A54556 and its separated factors exhibited interesting activity against penicillin-resistant staphylococci and streptococci inducing detailed investigations in our laboratories. As the original patent had been abandoned, producer strains and compounds were free for use and allowed repetition of the original experiments. Structural elucidation of the separated factors revealed that in constrast to reported results,[465] in our hands, the correct constitution of factor A corresponded to enopeptin depsipeptide **224**. Mode of action studies with *B. subtilis* demonstrated impaired bacterial cell division and induction of filamentation (Figure 11). By RG techniques, it could be shown that lead structures **224** and **29** inhibited bacterial growth by binding to ClpP (caseine lytic protease).[467,466] To protect the bacterial cell, ClpP is tightly regulated and requires a Clp–ATPase and accessory proteins for activation. Binding of **224** or **29** to ClpP eliminates the protection and triggers the ClpP core, which is

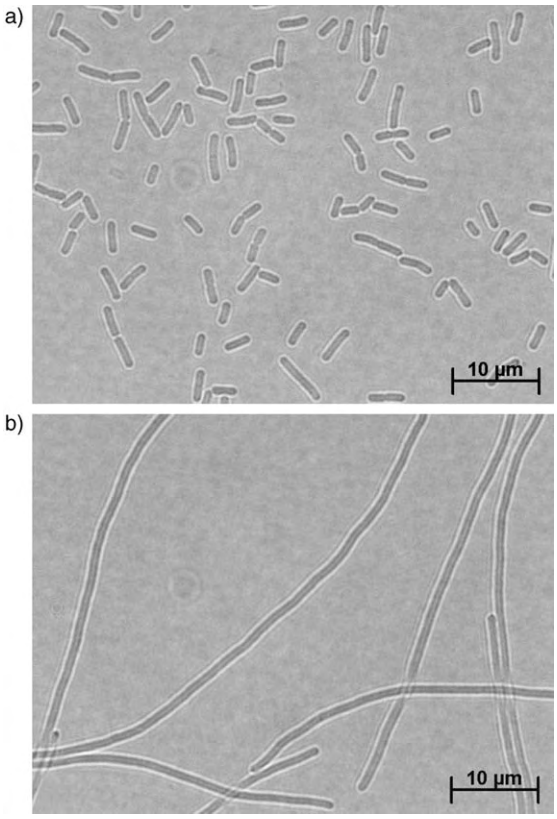


Figure 11. Action of **224** on *B. subtilis*: impaired cell division and induction of filamentation. Electron micrograph a) before and b) after treatment with **224** (0.4 μg mL^{-1}) for 5 h.[467]

then capable of proteolytic degradation in the absence of the regulatory Clp-ATPases. The consequence is uncontrolled proteolysis resulting in inhibition of bacterial cell division and finally cell death. Owing to this unprecedented mechanism of action, **224** and **29** were devoid of cross-resistance for all antibiotics on the market or in clinical development.[467]

On the other hand, the natural products suffered from various deficiencies that needed improval to assess the full potential of this class. Despite promising in vitro activity against enterococci and streptococci, natural enopeptin depsipeptide antibiotics **224** and **29** exhibited only moderate in vitro potency against staphylococci and were inactive against Gram-negative bacteria (Table 23). Both lead structures were not effective in vivo in standard lethal bacterial infection models in mice and their ADME profile was critical. Their chemical stability proved to be rather limited, their solubility was insufficient for parenteral application, and they were rapidly cleared from the body. Under these premises, an optimization program needed rational guidance and profited from a thorough understanding of the lead conformation based on X-ray crystal structure analysis of the synthetic congener **225** (Figure 12).[468]

Crystallization of **225** from aqueous acetonitrile gave solvent-free crystals. Acyldepsipeptide **225** adopted a conformation in which the lipophilic side chain was fixed by two hydrogen bonds to the top of the macrolactone ring. One NH···OC hydrogen bond (2.1 Å) was located between the NH

 © 2006 Wiley-VCH Verlag GmbH & Co. KGaA, Weinheim

Table 23: Antibacterial activity in vitro of natural and synthetic enopeptin antibiotics against Gram-positive pathogens, MIC [$\mu g\,mL^{-1}$].

	S. aureus	*S. pneumoniae*	*E. faecium*	*E. faecalis*
224	8	0.5	1	1
29	16	1	2	2
231	>64	>64	>64	>64
232	1	0.25	≤0.125	0.125
233	0.5	≤0.125	≤0.125	0.125
234	8	2	2	1
235	1	≤0.125	≤0.125	≤0.125
236	<0.125	≤0.125	≤0.125	≤0.125
237	0.25	≤0.125	≤0.125	≤0.125
30	0.5	≤0.125	≤0.125	≤0.125

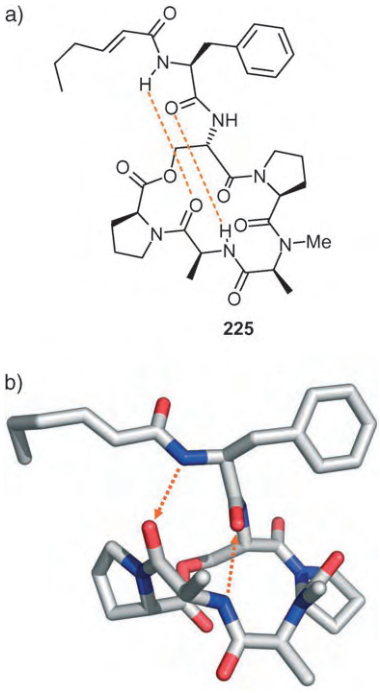
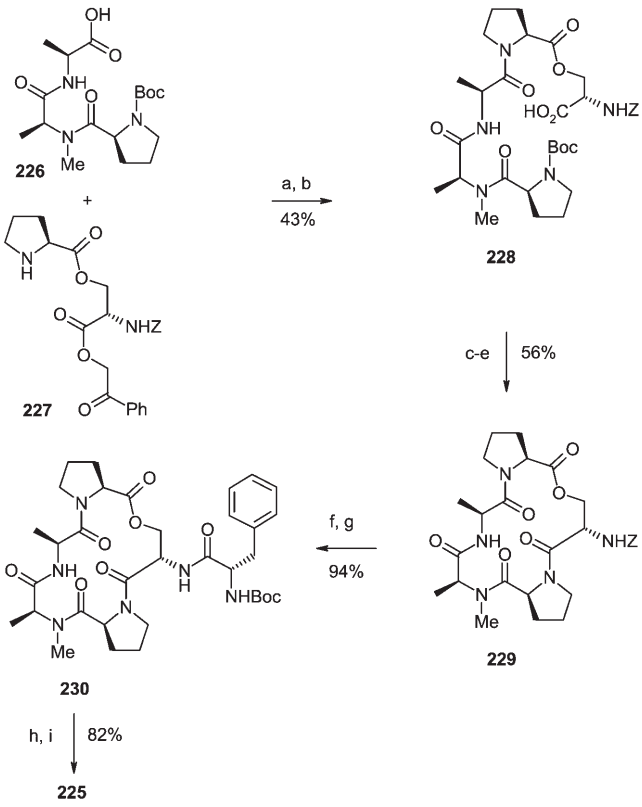


Figure 12. X-ray crystal structure of synthetic enopeptin **225**. The lipophilic side chain is fixed by two hydrogen bonds to the top of the macrocyclic core.[468]



Scheme 26. Synthesis of novel enopeptin analogues.[469] Reagents and conditions: a) CH_2Cl_2, HOBt, TBTU, iPr_2EtN, 0°C→RT, 79%; b) $AcOH/H_2O$ (9:1), Zn, 2 h, RT, 54%; c) CH_2Cl_2, pentafluorophenol, EDC, 0°C→RT, 18 h; d) 4 N HCl in dioxane, 1 h, RT; e) CH_2Cl_2, H_2O, $NaHCO_3$, RT, 56%; f) MeOH, aqueous HCl, H_2 (1 bar), Pd/C, 97%; g) *N*-Boc-phenylalanine, DMF, HATU, iPr_2EtN, RT, 97%; h) CH_2Cl_2, TFA/H_2O (9:1), 45 min, RT, quant.; i) 2-hexenoic acid, DMF, HATU, iPr_2EtN, 82%.

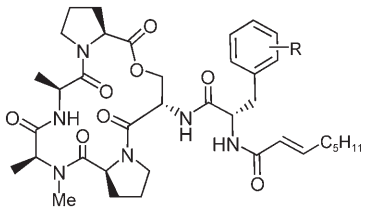
group of phenylalanine and the carbonyl function of alanine, a second hydrogen bond (2.0 Å) was found between the alanine NH and the phenylalanine carbonyl. To preserve this active conformation, the medicinal chemists concentrated their structural variations on those parts of the molecule that were not involved in hydrogen bonding: *N*-methylalanine, proline in the upper portion of the structure, and the aryl and alkyl residues in the side chain (Scheme 26). The total synthesis by Schmidt et al. of enopeptin B[464] served as a basis for the synthesis of novel enopeptin analogues and for elaborating the enopeptin depsipeptide SAR.[469]

The synthesis proceeded by coupling tripeptide **226** with the ester **227** through standard peptide chemistry. Linear pentapeptolid **228** was cyclized to macrolactone **229** according to the pentafluorophenyl ester method by Schmidt et al..[470] The cyclization process may have thrived on a favored conformation of precursor **228**, which was preshaped by the hydrogen bond pattern that defined the ultimate conformation of the target macrocycle **229**. Removal of the Z protecting group and attachment of the phenylalanine side chain afforded the intermediate **230**. Acidic cleavage of the Boc group and coupling to hexenoic acid produced the desired enopeptin analogue **225**.

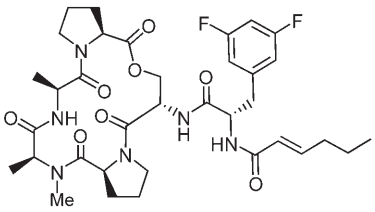
Starting from intermediate **230**, the side chain SAR (Table 23) was explored by substituting modification of the natural triene C8 acyl group. *E* configurated α,β-unsaturation proved to be crucial for biological activity, whereas additional double bonds were dispensable. Heptenoic acid side chains represented an optimum in length and lipophilicity and the corresponding analogues showed significantly improved chemical stability. To enhance solubility in water, polar functions were incorporated into the side chain, however, these efforts resulted in completely inactive congeners. Introduction of fluoro substituents in positions 3 and 5 of the side chain phenylalanine considerably improved activity against *S. aureus*, whereas an additional fluorine in position 4 was deleterious (**231**–**234**). Replacing the phenyl ring by a pyridyl or a cyclohexyl residue was not tolerated.

Substituting modifications in upper proline were demanding for chemistry. In this case, the natural 4-(*R*)-methyl

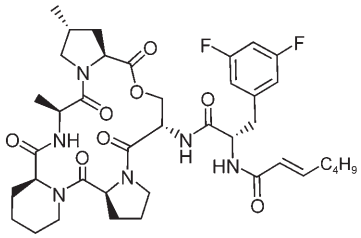
 © 2006 Wiley-VCH Verlag GmbH & Co. KGaA, Weinheim



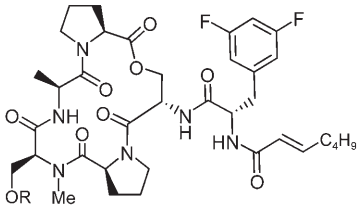
231 R = H **233** R = 3,5-F_2
232 R = 3-F **234** R = 3,4,5-F_3



235



236



237 R = H
30 R = CO-CH_2NMe_2

substituent seemed to be the optimum. Increasing its size (ethyl, methoxy) or changing its position (4- to 3-substitution) clearly reduced antibacterial activity. For the natural *N*-methylalanine, *N*-alkyl substitution was indeed essential as removal of the *N*-methyl group yielded inactive depsipeptides. Replacing *N*-methylalanine by *N*-methylglycine was not tolerated, but incorporation of rigid cyclic amino acids afforded potent congeners: synthetic acyldepsipeptide **236** showed an impressive biological profile in vitro and in vivo. MIC values against Gram-positive pathogens were in the range of established antibiotics (Table 23), no cross-resistance was observed, and potency was retained with multiresistant clinical isolates. Intraperitoneal treatment of lethal *E. faecalis* infections in mice with a single doses of of **236** (0.5 mg kg^{-1}) resulted in 100% survival.[467] Finally, *N*-methylalanine in the variable lower part of the macrocycle was replaced with *N*-methylserine (compound **237**) to provide a handle for increased aqueous solubility. The corresponding exocyclic *N*,*N*-dimethylglycine ester **30** exhibited sufficient aqueous solubility to allow parenteral application while retaining excellent antibacterial activity. Indeed, medicinal chemists competently corrected inherent deficiencies (stability, solubility, potency) of natural enopeptin depsipeptide antibiotics (chemical postevolution). In this project, efficient de novo synthesis rather than a fermentative/semisynthetic approach has been used to systematically explore the potential of the natural-product lead structures **224** and **29**.

18. Summary and Conclusion

Accepting and defining the new socioeconomic environment for antibacterial research: Bacterial infections increasingly evade standard treatment as resistance to multiple antibiotics is spreading throughout the world. Reports on therapy failures and rising treatment costs are omnipresent, especially in the hospital environment. Resistant pathogens lead to higher health-care expenditures owing to extended hospital stays and expensive drugs. Yet, resistance is inevitably the result of antibiotic use and therefore limits the efficacy and life span of every antibiotic. There is an urgent medical need for a sustainable supply of new, effective, and safe antibacterial drugs without cross-resistance to currently used antibiotics. On the other hand, investment in antibacterial discovery and development is flagging and many big pharmaceutical companies have exited the field. Generic competition, drug resistance, and increased regulatory scrutiny have placed greater pressure on antibacterial profit margins. Indeed, efficient antibiotics eliminate their own need by rapidly curing the disease (auto-obsolence). As shareholder-value interests increasingly frame research and development investment strategies, the commercial success of drugs against chronic diseases has tempted many companies to preferentially invest into "chronic drugs" rather than into "short-term antibacterials". Moreover, industry has not delivered novel and valid antibacterial agents of late. Attempts to exploit novel antibacterial targets have been disappointing and the "one-target-one-disease" approach has been unsuccessful for this area. For antibacterial drug discovery, the high-throughput-screening approach has failed and needs to be modified or replaced to help close the productivity gap. Only the persistent discovery and development of novel resistance-breaking antibacterial lead structures will guarantee future therapy. New ideas and solutions are needed that facilitate and support this endeavor.

Reshaping of the research strategy and finding new ways of funding: A revision of the mainstream scientific approaches together with pharma-political consensus solutions to increase economic chances and commercial viability of novel antibacterials will help to avoid future "preantibiotic" scenarios. Public–private partnerships for antibacterial research and development (as for HIV, tuberculosis, and malaria) should be explored. Processes need to be improved by bringing key experts from academia, clinicians, regulators, and the pharmaceutical industry together. Some visionary biotech enterprises have already revitalized the field of antibacterial research and natural-product exploration with great success (AnalytiCon, Basilea, Cubist, Kosan, Replidyne, Vicuron, etc.). Incentives for antibiotics in relation to chronic and life-style drugs would help to convince decision makers to reinvest into antibacterial research and development: intellectual-property extension for priority antibiotics (wild card) that open up a new class (first in class), restoration of patent time lost during review, and streamlining clinical studies by allowing fast-track reviews, and the use of surrogate markers are some of the points for discussion. Increasing harmonization between regulatory authorities in different countries or even global approval criteria remain wishes for the future. Better infection control measures, monitoring of resistance and initiatives that foster the responsible and appropriate use of antibiotics will help to prolong the life span of established antibacterials and to retain public acceptance for antibiotic therapy.

 © 2006 Wiley-VCH Verlag GmbH & Co. KGaA, Weinheim

Exploitation of contemporary scientific methodology for natural-product research: Medicinal chemistry provides the tools (semisynthesis, de novo synthesis) for the iterative optimization of natural products to obtain patentable drug molecules with improved pharmacokinetic, physicochemical, and toxicological properties (chemical postevolution). The diligent selection of natural antibiotic lead structures for medicinal-chemistry programs and guideposts for valid targets can reveal pathways to future therapies (reversed genomics). In silico modeling of the binding of these privileged structures to their targets allows the conception of less-complex molecules with improved properties that can serve as scaffolds for medicinal and combinatorial chemistry. With the exception of some β-lactam antibiotics, only the semisynthesis of congeners of antibacterial natural products has gained economic importance to date.

Revisiting "old" antibacterial classes and clinically validated targets: Even within known natural antibiotics, a dormant value of structural diversity has not been explored. Many "old" classes have never been thoroughly assessed by de novo synthesis and only partial SAR information is available on their backbone structures. Clearly, more could be done, in this case, to fully exploit the weapons against bacteria that are already in our possession. The clinically validated modes of action of the established antibacterial classes should not be neglected. New technologies, such as combinatorial biosynthesis, can create attractive novel natural products or provide (improved) congeners of known antibiotics. However, the benefit of these elaborate techniques for industrial antibacterial research has not yet been proven. It is currently not clear whether combinatorial approaches in biosynthesis will allow for a rationally directed and sufficiently diverse chemical postevolution that is needed to transform natural products into drugs.

Continuing natural-product research in the interest of patients: The demand on pharmaceutical companies to meet their business objectives and the demand for cost containment is forcing industry to think of efficient solutions. Under these premises, the last decade has been difficult for natural-product research. Although the idea that antibacterial research is feasible without natural products is widespread today, the past decades have taught us the opposite. As the resistance pendulum strikes back, there is no alternative to antibacterial research with natural products. Indeed, it might be hubris to assume that mankind can dispense with nature's universal knowledge on antibiotics. Natural scaffolds contain the key to bacterial vulnerability.

19. Abbreviations

ADME(T)	Absorption, Distribution, Metabolism, Excretion, (Toxicity)
AUC	area under the curve (pharmacokinetic parameter)
Boc	*tert*-butoxycarbonyl
BOPCl	(1-benzotriazolyl)oxy tris(dimethylamino)-phosphonium chloride
BSTFA	*N*,*O*-bis(trimethylsilyl)trifluoroacetamide
CAP	community-acquired pneumonia
CDI	*N*,*N*′-carbonyl diimidazole
CFU	colony-forming units
ClpP	caseine lytic protease
CNS	central nervous system
COD	1,5-cyclooctadiene
cSSSI	complicated skin and skin structure infections
cSSTI	complicated skin and soft tissue infections
cUTI	complicated urinary tract infection
DBU	1,8-diazabicyclo[5.4.0]undec-7-ene
DCC	dicyclohexyl carbodiimide
DIC	*N*,*N*-diisopropylcarbodiimide
DIPAMP	1,2-ethylene bis[(2-methoxyphenyl)phenyl-phosphane]
DMA	*N*,*N*-dimethylacetamide
DMAP	4-dimethylaminopyridine
DMF	*N*,*N*-dimethylformamide
DMSO	dimethyl sulfoxide
ED	effective dose
EDC	1-ethyl-3-(3-dimethylaminopropyl)carbo-diimide
EEDQ	2-ethoxy-*N*-ethoxycarbonyl-1,2-dihydro-quinoline
(*S*,*S*)-Et-DuPhos-Rh	(+)-1,2-bis[(2*S*,5*S*)-2,5-diethylphospholano]benzene(cyclooctadiene)rhodium(I) trifluormethanesulfonate
FCS	fetal calf serum
FDA	US Food and Drug Administration
Fmoc	9-fluorenylmethoxycarbonyl
f_U	fraction unbound (pharmacokinetic parameter)
GISA	glycopeptide-intermediate *Staphylococcus aureus*
HAP	hospital-acquired pneumonia
HATU	*O*-(7-azabenzotriazol-1-yl)-*N*,*N*,*N*′,*N*′-tetramethyluronium hexafluorophosphate
HBTU	benzotriazol-1-yl-*N*-tetramethyl-uronium hexafluorophosphate
HOBt	1-hydroxy 1*H*-benzotriazole
HMDS	1,1,1,3,3,3-hexamethyldisilazane
HTS	high-throughput screen(ing)
IAI	intra-abdominal infections
ICAAC	interscience conference on antimicrobial agents and chemotherapy
ICU	intensive-care unit
IC_{50}	inhibitory concentration 50%
IDSA	infectious disease society of america
i.v.	intravenous (parenteral)
i.p.	intraperitoneal (application)
LDA	lithium diisopropylamide
MA	membrane affinity (descriptor for lipophilicity)
MDRSP	multidrug resistant *Streptococcus pneumoniae*
MIC	minimal inhibitory concentration
MLS_B resistance	macrolide, lincosamide, streptogramine B resistance

© 2006 Wiley-VCH Verlag GmbH & Co. KGaA, Weinheim

MRSA	methicillin-resistant *Staphylococcus aureus*
MRSE	methicillin-resistant *Staphylococcus epidermidis*
MSSA	methicillin-susceptible *S. aureus*
Ms	mesyl
NBS	*N*-bromosuccinimide
NCE	new chemical entity
PBP	penicillin-binding protein
Phth	phthaloyl
PK	pharmacokinetics
pNB	*p*-nitrobenzyl
p.o.	peroral (application)
PPTS	pyridinium *p*-toluene sulfonate
PRSP	penicillin-resistant *Streptococcus pneumoniae*
PSSP	penicillin-susceptible *S. pneumoniae*
QT	electrophysiological heart parameter
RG	reversed genomics
RTI	respiratory-tract infection
SAR	structure–activity relationship
s.c.	subcutaneous (application)
SSTI	skin and soft tissue infections
STR	structure–toxicity relationship
TBDMS	*tert*-butyldimethylsilyl
TBTU	benzotriazol-1-yl-*N*-tetramethyluronium tetrafluoroborate
TFA	trifluoroacetic acid
THF	tetrahydrofuran
TMSE	trimethylsilylethyl
$t_{1/2}$	serum half-life (pharmacokinetic parameter)
UTI	urinary-tract infection
VISA	vancomycin-intermediate *Staphylococcus aureus*
VRSA	vancomycin-resistant *Staphylococcus aureus*
VRE	vancomycin-resistant *Enterococcus faecium*
V_{SS}	volume of distribution (pharmacokinetic parameter)
Z	benzyloxycarbonyl (protecting group)

Over the years, cooperation with numerous synthetic academic groups has provided a fruitful basis for our antibacterial research platform in medicinal chemistry. In particular, we would like to thank T. Bach, V. N. Belov, S. Bräse, R. Brückner, A. Fürstner, G. Helmchen, V. Jäger, U. Kazmaier, A. Kirschning, A. de Meijere, K. C. Nicolaou, and J. Pietruszka for their valuable and enthusiastic contributions. Furthermore, we would like to express our gratitude to E. Redpath (Wood Mackenzie) and H. G. Rohbeck for providing data on antibiotic sales and competitor analyses. We are grateful to N. Griebenow for stimulating discussions on the concept of chemical postevolution and to A. Hillisch for his advice in computational chemistry. This article would not have been possible without the dedicated work and scientific insight of our valued colleagues H. Brötz-Oesterhelt, N. Brunner, S. Bartel, Y. Cancho-Grande, R. Endermann, K. Ehlert, M. Es-Sayed, C. Freiberg, C. Fürstner, R. Gahlmann, M. Gehling, R. Grosser, T. Henkel, I. Knezevic, J. Krüger, H. Labischinski, T. Lampe, H.-G. Lerchen, H. Meier, M. Michels, B. Newton, H. Paulsen, J. Pohlmann, S. Raddatz, J. Ragot, G. Schiffer, A. Schumacher, S. Seip, M. Stadler, N. Svenstrup, J. Telser, and K. Ziegelbauer. For inspiring discussions of the manuscript, we are indebted to A. Mullen, R. Süssmuth, and S. Wegener. The referees gave us many valid comments and thoughts with their great expertise in this field. Finally, we would like to thank H. Rübsamen-Waigmann, H. Haning, and H. Wild for their constant support of our endeavors in natural-product chemistry. H Reichel (www.daxo.de) has designed the frontispage "the evolution of the daxophone" and font "FF daxline pro regular".

Received: January 26, 2006

[1] Historically, "antibiotics" stood for natural products and their derivatives, whereas "antibacterials" meant synthetic compounds, see, for example: L. Silver, K. Bostian, *Eur. J. Clin. Microbiol. Infect. Dis.* **1990**, *9*, 455 – 461.
[2] S. Rachakonda, L. Cartee, *Curr. Med. Chem.* **2004**, *11*, 775 – 793.
[3] C. Walsh, *Antibiotics, actions, origins, resistance*, 1. Aufl., ASM, Washington, DC, **2003**.
[4] D. J. Newman, G. M. Cragg, K. M. Snader, *J. Nat. Prod.* **2003**, *66*, 1022 – 1037.
[5] H. Labischinski, *J. Med. Microbiol.* **2001**, *291*, 317 – 318.
[6] C. Walsh, *Nat. Rev. Microbiol.* **2003**, *1*, 65 – 70.
[7] I. Chopra, L. Hesse, A. J. O'Neil, *J. Appl. Microbiol.* **2002**, *92*, 4S-15S.
[8] The US Surgeon General W. H. Stewart is reported to have commented that "the book on infectious diseases could now be closed".[2]
[9] M. R. Barbachyn, C. W. Ford, *Angew. Chem.* **2003**, *115*, 2056 – 2144; *Angew. Chem. Int. Ed.* **2003**, *42*, 2010 – 2023.
[10] A. Raja, J. LaBonte, J. Lebbos, P. Kirkpatrick, *Nat. Rev. Drug Discovery* **2003**, *2*, 943 – 944.
[11] J. D. Alder, *Drugs Today* **2005**, *41*, 81 – 90.
[12] a) World health organisation (WHO) Geneva, *World Health Report-2002*, **2002**; b) C. Nathan, *Nature* **2004**, *431*, 899 – 902.
[13] R. W. Pinner, S. M. Teutsch, L. Simonsen, *J. Am. Med. Assoc.* **1996**, *275*, 189 – 193.
[14] R. P. Wenzel, M. B. Edmont, *N. Engl. J. Med.* **2000**, *343*, 1961 – 1963.
[15] M. Leeb, *Nature* **2004**, *431*, 892 – 893.
[16] N. M. Clark, E. Hershberger, M. J. Zervosc, J. P. Lynch, *Curr. Opin. Crit. Care* **2003**, *9*, 403 – 412.
[17] Infectious disease society of America (IDSA): http://www.idsociety.org.
[18] a) S. J. Projan, *Curr. Opin. Microbiol.* **2003**, *6*, 427 – 430; b) K. M. Overbye, J. F. Barrett, *Drug Discovery Today* **2005**, *10*, 45 – 52; c) A. F. Boggs, *Expert Opin. Ther. Pat.* **2003**, *13*, 1107 – 1112.
[19] J. Drews, *Drug Discovery Today* **2003**, *8*, 411 – 420.
[20] a) I. Chopra, M. Roberts, *Microbiol. Mol. Biol. Rev.* **2001**, *65*, 232 – 260; b) M. G. Charest, C. D. Lerner, J. D. Brubaker, D. R. Siegel, A. G. Myers, *Science* **2005**, *308*, 367 – 368.
[21] a) G. A. Pankey, *J. Antimicrob. Chemother.* **2005**, *56*, 470 – 480; b) E. Rubinstein, D. Vaughan, *Drugs* **2005**, *65*, 1317 – 1336.
[22] D. Chen, Z. Yuan, *Expert Opin. Invest. Drugs* **2005**, *14*, 1107 – 1116.
[23] a) F. M. Walsh, S. G. Amyes, *Curr. Opin. Microbiol.* **2004**, *7*, 439 – 444; b) D. M. Livermore, *Clin. Infect. Dis.* **2003**, *36* (Suppl. 1), S11 – S23.

 © 2006 Wiley-VCH Verlag GmbH & Co. KGaA, Weinheim

[24] a) S. Solomon, T. Horant, M. Andrus, J. Edwards, S. Fridkin, J. Koganti, G. Peavy, J. Tolson, *Am. J. Infect. Control* **2003**, *31*, 481 – 498; b) J. Müller-Jung, Kreative Keime im Krankenhaus, *Frankfurter Allgemeine Zeitung*, 11.4.**2006**, S. 10.
[25] C. Walsh, *Nature* **2000**, *406*, 775 – 781.
[26] G. D. Wright, *Curr. Opin. Chem. Biol.* **2003**, *7*, 563 – 569.
[27] R. Hakenbeck, T. Grebe, D. Zahner, J. B. Stock, *Mol. Microbiol.* **1999**, *33*, 673 – 678.
[28] G. D. Wright, *Curr. Opin. Microbiol.* **1999**, *2*, 499 – 503.
[29] P. A. Lambert, *J. Appl. Microbiol. Symp. Suppl.* **2002**, *92*, 46S-54S.
[30] a) X. Z. Li, H. Nikaido, *Drugs* **2004**, *64*, 159 – 204; b) K. S. McKeegan, M. I. Borges-Walmsley, A. R. Walmsley, *Curr. Opin. Pharmacol.* **2004**, *4*, 479 – 486; c) M. L. Nelson, *Curr. Med. Chem. Anti-Cancer Agents* **2002**, *1*, 35 – 54; d) G. W. Kaatz, *Expert Opin. Emerging Drugs* **2002**, *7*, 223 – 233; e) P. Wiggins, *Expert Opin. Invest. Drugs* **2004**, *13*, 889 – 902.
[31] B. Gonzáles-Zorn, T. Teshager, M. Casas, M. C. Porrero, M. A. Moreno, P. Courvalin, L. Domínguez, *Emerging Infect. Dis.* **2005**, *11*, 954 – 956.
[32] E. A. Eady, J. H. Cove, *Curr. Opin. Infect. Dis.* **2003**, *16*, 103 – 124.
[33] J. F. Barrett, *Expert Opin. Ther. Targets* **2004**, *8*, 515 – 519.
[34] C. D. Salgado, B. M. Farr, D. P. Calfee, *Clin. Infect. Dis.* **2003**, *36*, 131 – 139.
[35] L. M. Deshpande, G. J. Moet, D. J. Biedenbach, R. N. Jones, *44th Interscience Conference on Antimicrobial Agents and Chemotherapy*, Washington, DC, USA, **2004**, abstract C2-1360 (SENTRY antimicrobial surveillance program).
[36] C. G. Whitney, M. M. Farley, J. Hadler, L. H. Harrison, C. Lexau, A. Reingold, L. Lefkowitz, P. R. Cieslak, M. Cetron, E. R. Zell, J. H. Jorgensen, A. Schuchat, *N. Engl. J. Med.* **2000**, *343*, 1917 – 1924.
[37] K. A. Gordon, D. J. Biedenbach, R. N. Jones, *Diagn. Microbiol. Infect. Dis.* **2003**, *46*, 285 – 289.
[38] R. Reinert, S. Jenkins, D. Farrell, M. Patel, *44th Interscience Conference on Antimicrobial Agents and Chemotherapy*, Washington, DC, USA, **2004**, abstract C2-833 (PROTEKT antimicrobial surveillance program).
[39] S. K. Bouchillon, D. J. Hoban, J. L. Johnson, *Int. J. Antimicrob. Agents* **2004**, *23*, 181 – 196.
[40] a) J. Davies, *Science* **1994**, *264*, 375 – 382; b) T. M. File, Jr., *Chest* **1999**, *115* (Suppl. 3), 3S-8S; c) O. Cars, *Drugs* **1997**, *54* (Suppl. 6), 4 – 10.
[41] G. L. Archer, M. W. Climo, *Antimicrob. Agents Chemother.* **1994**, *38*, 2231 – 2237.
[42] National Nosocomial Infections Surveillance System, CDC: http://www.cdc.gov/ncidod/dhqp/nnis_pubs.html.
[43] K. Hiramatsu, H. Hanaki, T. Ino, *J. Antimicrob. Chemother.* **1997**, *40*, 135 – 146.
[44] a) K. Hiramatsu, K. Okuma, X. X. Ma, M. Yamamoto, S. Hori, M. Kapi, *Curr. Opin. Infect. Dis.* **2002**, *15*, 407 – 413; b) L. M. Weigel, D. B. Clewell, S. R. Gill, N. C. Clark, L. K. McDougal, S. E. Flannagan, J. F. Kolonay, J. Shetty, G. E. Killgore, F. C. Tenover, *Science* **2003**, *302*, 1569 – 1571.
[45] A. M. Bal, I. M. Gould, *Expert Opin. Pharmacother.* **2005**, *6*, 2257 – 2269.
[46] M. Baysallar, A. Kilic, H. Aydogan, F. Cilly, L. Doganci, *Int. J. Antimicrob. Agents* **2004**, *23*, 510 – 512.
[47] C. A. DeRyke, D. Maglio, D. P. Nicolau, *Expert Opin. Pharmacother.* **2005**, *6*, 873 – 889.
[48] K. Hiramatsu, N. Aritaka, H. Hanaki, S. Kawasaki, Y. Hosoda, S. Hori, Y. Fukuchi, I. Kobayashi, *Lancet* **1997**, *350*, 1670 – 1673.
[49] G. J. Moet, M. G. Stilwell, D. J. Biedenbach, R. N. Jones, *44th Interscience Conference on Antimicrobial Agents and Chemotherapy*, Washington, DC, **2004**, USA, abstract C2-1707 (SENTRY antimicrobial surveillance program).
[50] a) European antimicrobial resistance surveillance system (EARSS): http://www.earss.rivm.nl; b) Resistance surveillance project of the British society for antimicrobial chemotherapy (BSAC): http://www.bsacsurv.org; c) D. J. Hoban, D. J. Biedenbach, A. H. Mutnick, R. N. Jones, *Microbiol. Infect. Dis.* **2003**, *45*, 279 – 285.
[51] D. M. Morens, G. K. Folkers, A. S. Fauci, *Nature* **2004**, *430*, 242 – 249.
[52] D. A. Mitchison, *Am. J. Respir. Crit. Care Med.* **2005**, *171*, 699 – 706.
[53] J. K. Borchardt, *Drug News & Perspect.* **2002**, *15*, 535 – 542.
[54] S. Kumari, V. J. Ram, *Drugs Today* **2004**, *40*, 487 – 500.
[55] J. B. Nachega, R. E. Chaisson, *Clin. Infect. Dis.* **2003**, *36* (Suppl. 1), S24-S30.
[56] Interscience conference on antimicrobial agents and chemotherapy: http://www.icaac.org.
[57] M. N. Alekshun, *Expert Opin. Invest. Drugs* **2005**, *14*, 93 – 99.
[58] a) LIBRA, an initiative of Bayer HealthCare AG to foster the worldwide, responsible and appropriate use of antibiotics: http://www.librainitiative.com/life/en/index.html; b) Alliance for the prudent use of antibiotics: http://www.tufts.edu/med/apua/index.html.
[59] C. W. Stratton, *Emerging Infect. Dis.* **2003**, *9*, 10 – 16.
[60] G. L. Drusano, *Nat. Rev. Microbiol.* **2004**, *2*, 289 – 300.
[61] a) J. A. DiMasi, R. W. Hansen, H. G. Grabowski, *J. Health. Econ.* **2003**, *22*, 151 – 185; b) J. E. Calfee, *Nature* **2004**, *429*, 807: M. Goozner, *The $800 Million Pill: The Truth Behind the Cost of New Drugs*, University of California Press **2004**; c) J. M. Reichert, *Nat. Rev. Drug Discovery* **2003**, *2*, 695 – 702.
[62] B. Spellberg, J. H. Powers, E. P. Brass, L. G. Miller, J. E. Edwards, *Clin. Infect. Dis.* **2004**, *38*, 1279 – 1286.
[63] R. F. Service, *Science* **2004**, *303*, 1796 – 1799.
[64] D. M. Shlaes, R. C. Moellering, Jr., *Clin. Infect. Dis.* **2000**, *34*, 420 – 422.
[65] a) C. J. Thomson, *Curr. Opin. Microbiol.* **2004**, *7*, 445 – 450; b) R. P. Wenzel, *N. Engl. J. Med.* **2004**, *351*, 523 – 526; c) D. N. Gilbert, J. E. Edwards, Jr., *Clin. Infect Dis.* **2002**, *35*, 215 – 216.
[66] J. H. Powers, *Curr. Opin. Infect. Dis.* **2003**, *16*, 547 – 551.
[67] I. Kola, J. Landis, *Nat. Rev. Drug Discovery* **2004**, *3*,711 – 715.
[68] D. J. Hoban, *Clin. Cornerstone* **2003**, (Suppl. 3), S12 – S20.
[69] Wood Mackenzie's Productview: http://www.woodmac.com/pharmabiotech.
[70] L. Harris, Analyst Datamonitor, *Superbugs and Superdrugs—6th Annual SMI Conference*, London, March, 1 – 2, **2004**; Datamonitor website: http://www.datamonitor.com.
[71] General aspects of natural-product chemistry, such as isolation, purification, and structure elucidation shall not be discussed herein. These topics have been reviewed elsewhere, for example, J. A. Leeds, E. K. Schmitt, P. Krastel, *Expert Opin. Invest. Drugs* **2006**, *15*, 211 – 226.
[72] a) A. M. Rouhi, *Chem. Eng. News* **2003**, *81*, 77 – 91; b) L. F. Tietze, S. Chandrasekhar, H. P. Bell, *Angew. Chem.* **2003**, *115*, 4128 – 4160; *Angew. Chem. Int. Ed.* **2003**, *42*, 3996 – 4028.
[73] M. S. Butler, *J. Nat. Prod.* **2004**, *67*, 2141 – 2153.
[74] M. S. Butler, *Nat. Prod. Rep.* **2005**, *22*, 162 – 195.
[75] F. E. Koehn, G. T. Carter, *Nat. Rev. Drug Discovery* **2005**, *4*, 206 – 220.
[76] R. D. Firn, C. G. Jones, *Nat. Prod. Rep.* **2003**, *20*, 382 – 391.
[77] H. Nikaido, *Microbiol. Mol. Biol. Rev.* **2003**, *67*, 593 – 656.
[78] H. B. Bode, R. Müller, *Angew. Chem.* **2005**, *117*, 6988 – 7007; *Angew. Chem. Int. Ed.* **2005**, *44*, 6828 – 6846.
[79] S. Weist, R. D. Süssmuth, *Appl. Microbiol. Biotechnol.* **2005**, *68*, 141 – 150.
[80] In certain cases, it is possible to guess the structure of polyketides from the genetic code of the biosynthesis modules.
[81] N. Perić-Concha, P. F. Long, *Drug Discovery Today* **2003**, *8*, 1078 – 1084.

 © 2006 Wiley-VCH Verlag GmbH & Co. KGaA, Weinheim

[82] R. Breinbauer, I. R. Vetter, H. Waldmann, *Angew. Chem.* **2002**, *114*, 3002 – 3015; *Angew. Chem. Int. Ed.* **2002**, *41*, 2878 – 2890.
[83] M. A. Koch, A. Schuffenhauer, M. Scheck, S. Wetzel, M. Casaulta, A. Odermatt, P. Ertl, H. Waldmann, *Proc. Natl. Acad. Sci. USA* **2005**, *102*, 17272 – 17277.
[84] T. Henkel, R. M. Brunne, H. Müller, F. Reichel, *Angew. Chem.* **1999**, *111*, 688 – 691; *Angew. Chem. Int. Ed.* **1999**, *38*, 643 – 647.
[85] M. Feher, J. M. Schmidt, *J. Chem. Inf. Comput. Sci.* **2003**, *43*, 218 – 227.
[86] A. J. O'Neill, I. Chopra, *Expert Opin. Invest. Drugs* **2004**, *7*, 1237 – 1244.
[87] L. Silver, K. Bostian, *Eur. J. Clin. Microbiol.* **1990**, *13*, 1045 – 1063.
[88] H. Breithaupt, *Nat. Biotechnol.* **1999**, *17*, 1165 – 1169.
[89] *Handbook of Animal Models of Infection* (Eds.: O. Zak, M. A. Sande), Academic Press, San Diego, USA, **1999**.
[90] J. D. Alder, *Current Pharm. Design* **1997**, *3*, 143 – 158.
[91] F. Parenti, G. Lancini in A *ntibiotics and Chemotherapy*, 7th ed. (Eds.: F. O'Grady, H. P. Lambert, R. G. Finch, D. Greenwood), Churchill Livingstone, New York, NY, **1997**, pp. 453 – 459.
[92] D. N. Wilson, K. H. Nierhaus, *Angew. Chem.* **2003**, *115*, 3586 – 3610; *Angew. Chem. Int. Ed.* **2003**, *42*, 3464 – 3468.
[93] V. Ramakrishnan, *Cell* **2002**, *108*, 557 – 572.
[94] I. Chopra, *Expert Opin. Invest. Drugs* **1998**, *7*, 1237 – 1244.
[95] D. J. C. Knowles, N. Foloppe, N. B. Matassova, A. I. H. Murchie, *Curr. Opin. Pharmacol.* **2002**, *2*, 501 – 506.
[96] E. Bacqué, J.-C. Barrière, N. Berthaud, *Curr. Med. Chem. Anti-Cancer Agents* **2005**, *4*, 185 – 217.
[97] A. Coates, Y.-M. Hu, R. Bax, C. Page, *Nat. Rev. Drug Discovery* **2002**, *1*, 895 – 910.
[98] A. P. Carter, W. M. Clemons, D. E. Brodersen, R. J. Morgan-Warren, B. T. Wimberly, V. Ramakrishnan, *Nature* **2000**, *407*, 340 – 348.
[99] B. G. Spratt, *Proc. Natl. Acad. Sci. USA* **1975**, *72*, 2999 – 3003.
[100] L. Miesel, J. Greene, T. A. Black, *Nat. Rev. Genet.* **2003**, *4*, 442 – 456.
[101] R. D. Fleischmann et al., *Science* **1995**, *269*, 496 – 512.
[102] M. Chee, R. Yang, E. Hubbell, A. Berno, X. C. Huang, D. Stern, J. Winkler, D. J. Lockhart, M. S. Morris, S. P. A. Fodor, *Science* **1996**, *274*, 610 – 614.
[103] a) A. Shevchenko, O. N. Jensen, A. V. Podtelejnikov, F. Sagliocco, M. Wilm, O. Vorm, P. Mortensen, A. Shevchenko, H. Boucherie, M. Mann, *Proc. Natl. Acad. Sci. USA* **1996**, *93*, 14440 – 14445; b) W. W. Zhang, *Pharmacogenomics* **2005**, *6*, 555 – 562.
[104] S. R. Waterman, *Am. J. PharmacoEconomics* **2001**, *1*, 263 – 269.
[105] D. McDevitt, M. Rosenberg, *Trends Microbiol.* **2001**, *9*, 611 – 617.
[106] Up until May 2006, only 279 bacterial gene sequences have been deciphered The Institute for Genomic Research (TIGR); http://www.tigr.org.
[107] S. J. Projan, *Curr. Opin. Pharmacol.* **2002**, *2*, 513 – 522.
[108] A. D. Roses, D. K. Burns, S. Chissoe, L. Middleton, P. St. Jean, *Drug Discovery Today* **2005**, *10*, 177 – 189.
[109] C. J. Zheng, L. Y. Han, C. W. Yap, B. Xie, Y. Z. Chen, *Drug News & Perspect.* **2005**, *18*, 109 – 127.
[110] P. D. Jackson, J. J. Harrington, *Drug Discovery Today* **2005**, *10*, 53 – 60.
[111] U. A. K. Betz, *Drug Discovery Today* **2005**, *10*, 1057 – 1063.
[112] S. A. Haney, L. E. Alksne, P. M. Dunman, E. Murphy, S. J. Projan, *Curr. Pharm. Des.* **2002**, *8*, 1099 – 1118.
[113] Some valid antibacterial targets are indeed present in humans but they are nonessential (mitochondrial peptide deformylase, PDF).
[114] A target, essential for growth or viability of a microorganism.
[115] F. Arigoni, F. Talabot, M. Peisch, M. D. Edgerton, E. Meldrum, E. Allet, R. Fish, T. Jamotte, M.-L. Curchod, H. Loferer, *Nat. Biotechnol.* **1998**, *16*, 851 – 856.
[116] Literature evidence or positive experience with a HTS format for a related target exists.
[117] Literature evidence or positive experience with a target class or lead structure for a closely related target exists. Preferentially a target with a single interaction site so that a high probability for identifying a potent low-molecular-weight inhibitor is gained.
[118] Y. Sugiyama, *Drug Discovery Today* **2005**, *10*, 1577 – 1579.
[119] C. J. Tomson, E. Power, H. Ruebsamen-Waigmann, H. Labischinski, *Curr. Opin. Microbiol.* **2004**, *7*, 445 – 450.
[120] A. F. Chalker, R. D. Lunsford, *Pharmacol. Ther.* **2002**, *95*, 1 – 20.
[121] D. J. Payne, *Drug News & Perspect.* **2004**, *17*, 187 – 194.
[122] J. R. Broach, J. Thorner, *Nature* **1996**, *384*, 14 – 18.
[123] P. Gribbon, A. Sewing, *Drug Discovery Today* **2005**, *10*, 17 – 22.
[124] G. J. R. Zaman, *Drug Discovery Today* **2004**, *9*, 828 – 830.
[125] a) Three-dimensional structural information on target proteins is helpful for target validation and chemical optimization strategies. Conservation of the active site over a range of pathogens enhances the chance to find a broad-spectrum inhibitor; b) J. J. Barker, *Drug Discovery Today* **2006**, *11*, 391 – 404; c) L. O. Haustedt, C. Mang, K. Siems, H. Schiewe, *Curr. Opin. Drug Discovery Dev.* **2006**, *9*, im Druck.
[126] M. B. Schmid, *Trends Microbiol.* **2002**, *10*, 27 – 31.
[127] C. P. Gray, W. Keck in *Microbial Genomics and Drug Discovery* (Eds.: T. J. Dougherty, S. J. Projan), Marcel Dekker, New York, USA, **2003**.
[128] C. G. Wermuth, *Drug Discovery Today* **2004**, *9*, 826 – 827.
[129] A. S. Waller, J. M. Clements, *Curr. Opin. Drug Discovery Dev.* **2002**, *5*, 785 – 792.
[130] In our opinion, it is not clear whether the peptide deformylase inhibitors, sometimes claimed as the first novel class from genomics efforts to enter clinical trials, do not stem from a reversed-genomics approach based on the natural antibiotic actinonin.
[131] P. Ma, R. Zemmel, *Nat. Rev. Drug Discovery* **2002**, *1*, 571 – 572.
[132] a) F. Sams-Dodd, *Drug Discovery Today* **2005**, *10*, 139 – 147; b) E. F. Schmid, D. A. Smith, *Drug Discovery Today* **2005**, *10*, 1031 – 1039.
[133] S. Carney, *Drug Discovery Today* **2005**, *10*, 1011 – 1013.
[134] G. H. Cassel, J. Mekalanos, *J. Am. Med. Assoc.* **2001**, *285*, 601 – 605.
[135] C. Freiberg, H. Brötz, H. Labischinski, *Curr. Opin. Microbiol.* **2004**, *7*, 451 – 459.
[136] J. E. Bandow, H. Brötz, L. I. O. Leichert, H. Labischinski, M. Hecker, *Antimicrob. Agents Chemother.* **2003**, *47*, 948 – 955.
[137] K. Buttner, J. Bernhardt, C. Scharf, R. Schmid, U. Mader, C. Eymann, H. Antelmann, A. Volker, U. Volker, M. Hecker, *Electrophoresis* **2001**, *22*, 2908 – 2935.
[138] B. Hutter, C. Schaab, S. Albrecht, M. Borgmann, N. A. Brunner, C. Freiberg, K. Ziegelbauer, C. O. Rock, I. Ivanov, H. Loferer, *Antimicrob. Agents Chemother.* **2004**, *48*, 2838 – 2844.
[139] H. P. Fischer, N. A. Brunner, B. Wieland, J. Paquette, L. Macko, K. Ziegelbauer, C. Freiberg, *Genome Res.* **2004**, *14*, 90 – 98.
[140] M. Gebauer, *Drug Discovery Today* **2004**, *9*, 915 – 917.
[141] G. Schiffer, unpublished work.
[142] D. J. Payne et al., *Antimicrob. Agents Chemother.* **2002**, *46*, 3118 – 3124.
[143] C. Freiberg, N. A. Brunner, G. Schiffer, T. Lampe, J. Pohlmann, M. Brands, M. Raabe, D. Häbich, K. Ziegelbauer, *J. Biol. Chem.* **2004**, *279*, 26066 – 26073.
[144] C. Freiberg, H. P. Fischer, N. A. Brunner, *Antimicrob. Agents Chemother.* **2005**, *49*, 749 – 759.

 © 2006 Wiley-VCH Verlag GmbH & Co. KGaA, Weinheim

[145] D. Beyer, H.-P. Kroll, R. Endermann, G. Schiffer, S. Siegel, M. Bauser, J. Pohlmann, M. Brands, K. Ziegelbauer, D. Häbich, C. Eymann, H. Brötz-Oesterhelt, *Antimicrob. Agents Chemother.* **2004**, *48*, 525 – 532.
[146] N. N. Kaderbhai, D. I. Broadhurst, D. I. Ellis, R. Goodacre, D. B. Kell, *Comp. Funct. Genomics* **2003**, 4, 376 – 391.
[147] H. Labischinski, G. Schiffer, J. Schmitt, T. Udelhoven (Synthon KG), WO 03042406, **2003** [*Chem. Abstr.* **2003**, 138, 381718].
[148] The fossilized remains of a skeleton of the Neanderthal man were discovered in 1856 in the Feldhofer cave 10 miles away from the Bayer Pharmaceutical Research Center Wuppertal.
[149] C. A. Lipinski, F. Lombardo, B. W. Dominy, P. J. Feeney, *Adv. Drug Delivery Rev.* **1997**, *23*, 3 – 25.
[150] H. Nikaido, *Semin. Cell Dev. Biol.* **2001**, *12*, 215 – 223.
[151] R. S. DeWitte, *Curr. Drug Discovery* **2002**, 19 – 22: "It is much easier for greasy compounds to have high binding affinity in vitro than for their more-soluble analogues."
[152] a) E. L. Schuck, H. Derendorf, *Expert Rev. Anti-Infect. Ther.* **2005**, *3*, 361 – 373; b) Some complex antibiotics with excellent efficacy show surprisingly high protein binding in blood plasma (daptomycin, f_U 8 %).
[153] D. Andes, W. A. Craig, *Int. J. Antimicrob. Agents* **2002**, *19*, 261 – 268.
[154] a) B. R. Meyers, *Antimicrobial Therapy Guide*, 16th ed., Antimicrobial Prescribing, Newtown, USA, **2004**; b) H. A. Dieterich, E. Mutschler, *Antiinfektiva*, WVG, Stuttgart, **1998**.
[155] Besides antibacterial acitivity, stability, (self)tolerability, biosynthetic effort, and resistance induction within the target organism are important parameters that also define the value of a secondary metabolite for a producing organism.
[156] B. L. Bray, *Nat. Rev. Drug Discovery* **2003**, *2*, 587 – 593.
[157] a) A. Rivkin, T.-C. Chou, S. J. Danishefsky, *Angew. Chem.* **2005**, *117*, 2898 – 2910; *Angew. Chem. Int. Ed.* **2005**, *44*, 2838 – 2850; b) K. C. Nicolaou, B. A. Pratt, S. Arseniyadis, M. Wartmann, A. O'Brate, P. Giannakakou, *ChemMedChem* **2006**, *1*, 41 – 44; c) F. Cachoux, T. Isarno, M. Wartmann, K.-H. Altmann, *Angew. Chem.* **2005**, *117*, 7636 – 7640; *Angew. Chem. Int. Ed.* **2005**, *44*, 7469 – 7473.
[158] E. Winterstein, G. Trier, *Die Alkaloide*, **1910**, Gebr. Bornträger, Berlin.
[159] J. Li, W. J. Kao, *Biomacromolecules* **2003**, *4*, 1055 – 1067.
[160] F. von Nussbaum, R. Hanke, T. Fahrig, J. Benet Buchholz, *Eur. J. Org. Chem.* **2004**, 2783 – 2790.
[161] a) A. Fleming, *Br. J. Exp. Pathol.* **1929**, *10*, 226 – 236; b) P. I. Lerner, *N. Engl. J. Med.* **2004**, *351*, 524.
[162] a) M. Habeck, *Drug Discovery Today* **2002**, *7*, 1109 – 1110; b) C. J. Schofield, J. E. Baldwin, M. F. Byford, I. Clifton, J. Hajdu, C. Hensgens, P. Roach, *Curr. Opin. Struct. Biol.* **1997**, *7*, 857 – 864.
[163] a) G. A. Glister, A. Grainger, *Analyst* **1950**, *75*, 310; b) K. Bauer, W. Kaufmann, *Naturwissenschaften* **1960**, *47*, 469.
[164] F. R. Batchelor, F. P. Doyle, J. W. C. Nayler, G. N. Rolinson, *Nature* **1959**, *183*, 256 – 258.
[165] R. B. Morin, B. G. Jackson, E. G. Flynn, R. W. Roeske, *J. Am. Chem. Soc.* **1962**, *84*, 3400 – 3401.
[166] W. Kaufmann, K. Bauer, *Naturwissenschaften* **1960**, *47*, 474.
[167] G. S. Singh, *Mini-Rev. Med. Chem.* **2004**, *4*, 93 – 109.
[168] A. Bryskier, *J. Antibiot.* **2000**, *53*, 1028 – 1037.
[169] M. G. P. Page, *Expert Opin. Invest. Drugs* **2004**, *13*, 973 – 985.
[170] a) A. Imada, K. Kitano, K. Kintaka, M. Muroi, M. Asai, *Nature* **1981**, *289*, 590 – 591; b) G. S. Singh, *Mini-Rev. Med. Chem.* **2004**, *4*, 69 – 92.
[171] L. D. Cama, B. G. Christensen, *J. Am. Chem. Soc.* **1974**, *96*, 7582 – 7584.
[172] a) D. A. Evans, E. B. Sjogren, *Tetrahedron Lett.* **1985**, *26*, 3787 – 3790; b) J. W. Misner, J. W. Fisher, J. P. Gardner, S. W. Pedersen, K. L. Trinkle, B. G. Jackson, T. Y. Zhang, *Tetrahedron Lett.* **2003**, *44*, 5991 – 5993.
[173] a) T. T. Howarth, A. G. Brown, T. J. King, *J. Chem. Soc. Chem. Commun.* **1976**, 266 – 267; b) D. Häbich, P. Naab, K. Metzger, *Tetrahedron Lett.* **1983**, 2559 – 2562; c) A. Dalhoff, C. J. Thomson, *Chemotherapy* **2003**, *49*, 105 – 120.
[174] J. M. T. Hamilton-Miller, *Pharmacotherapy* **2003**, *23*, 1497 – 1507.
[175] G. Bonfiglio, G. Russo, G. Nicoletti, *Expert Opin. Invest. Drugs* **2002**, *11*, 529 – 544.
[176] a) A. J. Eglington, *J. Chem. Soc. Chem. Commun.* **1977**, 720; b) H. Wild, W. Hartwig, *Synthesis* **1999**, 1099 – 1103; c) I. N. Simpson, C. J. Urch, G. Hagen, R. Albrecht, B. Sprinkart, H. R. Pfaendler, *J. Antibiot.* **2003**, 56, 838 – 847.
[177] a) O. K. Kim, J. Fung-Tomc, *Expert Opin. Ther. Pat.* **2001**, *11*, 1267 – 1276; b) J. R. Hwu, K. S. Ethiraj, G. H. Hakimelahi, *Mini-Rev. Med. Chem.* **2003**, *3*, 305 – 313; c) A. R. White, C. Kaye, J. Poupard, R. Pypstra, G. Woodnutt, B. Wynne, *J. Antimicrob. Chemother.* **2004**, *53* (Suppl. 1) I3-I20; d) C. Acuna, X. Rabasseda, *Drugs Today* **2001**, *37*, 193 – 210; e) D. Andreotti, S. Biondi, *Curr. Opin. Anti-Infect. Invest. Drugs* **2000**, *2*, 133 – 139; f) G. Cornaglia, *Clin. Microbiol. Infect.* **2000**, *6* (Suppl. 3), 41 – 45; g) J. Q. Del Rosso, *Cutis* **2003**, *71*, 153 – 157; h) A. Novelli, S. Conti, M. I. Cassetta, S. Fallani, *Clin. Microbiol. Infect.* **2000**, *6* (Suppl. 3), 50 – 52.
[178] a) H. Labischinski, *Med. Microbiol. Immunol.* **1992**, *181*, 241 – 265; b) J. M. Ghuysen, *Trends Microbiol.* **1994**, *2*, 372 – 380.
[179] J. V. Höltje, *Microbiol. Mol. Biol. Rev.* **1998**, *62*, 181 – 203.
[180] K. Lewis, *Microbiol. Mol. Biol. Rev.* **2000**, *64*, 503 – 524.
[181] W. Vollmer, J. V. Höltje, *J. Bacteriol.* **2004**, *186*, 5978 – 5987.
[182] a) P. Welzel, *Chem. Rev.* **2005**, *105*, 4610 – 4660; b) T. D. H. Bugg, C. T. Walsh, *Nat. Prod. Rep.* **1992**, *9*, 199 – 215; c) K. H. Schleifer, O. Kandler, *Bacteriol. Rev.* **1972**, *36*, 407 – 477; d) M. J. Spencelayh, Y. Cheng, R. J. Bushby, T. D. H. Bugg, J. Li, P. J. F. Henderson, J. O'Reilly, S. D. Evans, *Angew. Chem.* **2006**, *118*, 2165 – 2170; *Angew. Chem. Int. Ed.* **2006**, *45*, 2111 – 2116.
[183] D. Lim, N. C. J. Strynadka, *Nat. Struct. Biol.* **2002**, *9*, 870 – 876.
[184] a) J. Trias, J. Dufresne, R. C. Levesque, H. Nikaido, *Antimicrob. Agents Chemother.* **1989**, *33*, 1201 – 1206; b) J. Trias, H. Nikaido, *Antimicrob. Agents Chemother.* **1990**, *34*, 52 – 57.
[185] a) R. Srikumar, C. J. Paul, K. Poole, *J. Bacteriol.* **2000**, *182*, 1410 – 1414; b) X. S. Li, L. Zhang, K. Poole, *J. Antimicrob. Chemother.* **2000**, *45*, 433 – 436.
[186] a) J. F. Fisher, S. O. Meroueh, S. Mobashery, *Chem. Rev.* **2005**, *105*, 395 – 424; b) T. D. Gootz, *Expert Rev. Anti-Infect. Ther.* **2004**, *2*, 317 – 327.
[187] a) http://www.lahey.org/studies; b) K. Bush, *Clin. Infect. Dis.* **2001**, *32*,1085 – 1089.
[188] J. Spencer, T. R. Walsh, *Angew. Chem.* **2006**, *118*, 1038 – 1042; *Angew. Chem. Int. Ed.* **2006**, *45*, 1022 – 1026.
[189] a) R. G. Micetich, S. M. Salama, S. N. Maiti, A. V. N. Reddy, R. Singh, *Curr. Med. Chem. Anti-Infect. Agents* **2002**, *1*, 193 – 213; b) V. P. Sandanayaka, A. S. Prashad, *Curr. Med. Chem.* **2002**, *9*, 1145 – 1165.
[190] A. R. White, C. Kaye, J. Poupard, R. Pypstra, G. Woodnutt, B. Wynne, *J. Antimicrob. Chemother.* **2004**, *53* (Suppl. 1), I3 – I20.
[191] A. G. Brown, D. F. Corbett, J. Goodacre, J. B. Harbridge, T. T. Howarth, R. J. Ponsford, I. Stirling, T. J. King, *J. Chem. Soc. Perkin Trans. 1* **1984**, 635 – 650.
[192] C. M. Perry, A. Markham, *Drugs* **1999**, *57*, 805 – 843.
[193] D. M. Springer, *Curr. Med. Chem. Anti-Infect. Agents* **2002**, *1*, 269 – 279.
[194] M. Miauchi, T. Hirota, K. Fujimoto, J. Ide, *Chem. Pharm. Bull.* **1989**, *37*, 3272 – 3276.
[195] a) A. G. Brown, D. Butterworth, M. Cole, G. Hanscomb, J. D. Hood, C. Reading, *J. Antibiot.* **1976**, *29*, 295 – 304; b) J. D.

 © 2006 Wiley-VCH Verlag GmbH & Co. KGaA, Weinheim

Hood, S. J. Box, M. S. Verall, *J. Antibiot.* **1979**, *32*, 295 – 304; c) M. J. Basker, *J. Antimicrob. Chemother.* **1982**, *10*, 4 – 7.
[196] a) J. S. Kahan, F. M. Kahan, E. O. Stapley, R. T. Goegelman, S. Hernandez (Merck & Co., Inc., USA), US 3950357, **1976** [*Chem. Abstr.* **1976**, *85*, 92190]; b) G. Albers-Schoenberg, B. H. Arison, O. D. Hensens, J. Hirshfield, K. Hoogsteen, E. A. Kaczka, R. E. Rhodes, J. S. Kahan, F. M. Kahan, R. W. Ratcliffe, E. Walton, L. J. Ruswinkle, R. B. Morin, B. G. Christensen, *J. Am. Chem. Soc.* **1978**, *100*, 6491 – 6499; c) J. S. Kahan, H. Kropp, J. G. Sundelof, J. Birnbaum, *J. Antimicrob. Chemother.* **1983**, *12* (Suppl. D), 1 – 35.
[197] M. J. Basker, R. J. Boon, P. A. Hunter, *J. Antibiot.* **1980**, *33*, 878 – 884.
[198] J. S. Kahan, F. M. Kahan, R. Goegelman, S. A. Currie, M. Jackson, E. O. Stapley, T. W. Miller, A. K. Miller, D. Hendlin, S. Mochales, S. Hernandez, H. D. Woodruff, J. Birnbaum, *J. Antibiot.* **1979**, *32*, 1 – 12.
[199] D. B. R. Johnston, S. M. Schmitt, F. A. Bouffard, B. G. Christensen, *J. Am. Chem. Soc.* **1978**, *100*, 313 – 315.
[200] B. M. Beadle, B. K. Shoichert, *Antimicrob. Agents Chemother.* **2002**, *46*, 3978 – 3980.
[201] D. M. Livermore, N. Woodford, *Curr. Opin. Microbiol.* **2000**, *3*, 489 – 495.
[202] H. Kropp, J. G. Sundelof, R. Hajdu, F. M. Kahan, *Antimicrob. Agents Chemother.* **1982**, *22*, 62 – 70.
[203] H. Takahagi, T. Hirota, Y. Matsushita, S. Muramatsu, M. Tanaka, E. Matsuo, *Chemotherapy* **1991**, *39* (Suppl. 3), 236 – 241.
[204] M. Fukusawa, Y. Sumita, E. T. Harabe, T. Tanio, H. Nouda, T. Kohzuki, T. Okuda, H. Matsumura, M. Sunagawa, *Antimicrob. Agents Chemother.* **1992**, *36*, 1577 – 1579.
[205] a) R. Wise, J. M. Andrews, N. Brenwald, *Antimicrob. Agents Chemother.* **1996**, *40*, 1248 – 1253; b) F. Sifaoui, E. Varon, M.-D. Kitzis, L. Gutmann, *Antimicrob. Agents Chemother.* **1998**, *42*, 173 – 175.
[206] P. J. Petersen, N. V. Jacobus, W. J. Weiss, R. T. Testa, *Antimicrob. Agents Chemother.* **1991**, *35*, 203 – 207.
[207] S. Nakagawa, T. Hashizume, K. Matsuda, M. Sanada, O. Okamoto, H. Fukatsu, N. Tanaka, *Antimicrob. Agents Chemother.* **1993**, 37, 2756 – 2759.
[208] Y. Iso, T. Irie, Y. Nishino, K. Motokawa, Y. Nishitani, *J. Antibiot.* **1996**, 49, 199 – 209.
[209] a) C. J. Gill, J. J. Jackson, L. S. Gerckens, B. A. Pelak, R. K. Thompson, J. G. Sundelof, H. Kropp, H. Rosen, *Antimicrob. Agents Chemother.* **1998**, *42*, 1996 – 2001; b) H. M. Wexler, *J. Antimicrob. Chemother.* **2004**, *53* (Suppl. 2), ii11 – ii21.
[210] D. H. Shih, F. Baker, L. Cama, B. G. Christensen, *Heterocycles* **1984**, *21*, 29 – 40.
[211] A. H. Berks, *Tetrahedron* **1996**, *52*, 331 – 375.
[212] K. M. J. Brands, R. B. Jobson, K. M. Conrad, J. M. Williams, B. Pipik, M. Cameron, A. J. Davies, P. G. Houghton, M. S. Ashwood, I. F. Cottrell, R. A. Reamer, D. J. Kennedy, U.-H. Dolling, P. J. Reider, *J. Org. Chem.* **2002**, *67*, 4771 – 4776.
[213] a) J. M. Williams, K. M. J. Brands, K. M. Conrad, B. Pipik, K. A. Savary, F.-R. Tsay, P. G. Houghton, R. T. Skerlj, R. B. Jobson, G. Marchesini, *226th ACS National Meeting*, New York, Sept. 7 – 11, **2003**, abstract orgn. 73; b) K. M. J. Brands, R. Cvetovich, L. S. Crocker, M. D. Ward, A. J. Mahajan, R. M. Wenslow, J. M. Williams, D. R. Sidler, E. S. Fisher, R. B. Jobson, C. Orella (Merck & Co., Inc., USA), WO 03026572, **2003** [*Chem. Abstr.* **2003**, *138*, 261606].
[214] H. Wild in *The Organic Chemistry of β-Lactams*, (Hrsg.: G. I. Georg), 1. Aufl., VCH, New York, **1993**, S. 1 – 119.
[215] *Macrolides: Chemistry, Pharmacology and Clinical Uses* (Hrsg.: A. J. Bryskier, J.-P. Butzler, H. C. Neu, P. M. Tulkens), Arnette Blackwell, Paris, **1993**.
[216] A. K. Wierzbowski, D. J. Hoban, T. Hisanaga, M. Decorby, G. G. Zhanel, *Curr. Infect. Dis. Rep.* **2005**, *7*, 175 – 184.
[217] a) Y. J. Wu, *Curr. Pharm. Des.* **2000**, *6*, 181 – 223; b) D. T. Chu, *Med. Res. Rev.* **1999**, *19*, 497 – 520; c) A. Bryskier, *Expert Opin. Invest. Drugs* **1999**, *8*, 1171 – 1194; d) A. Bryskier, *Expert Opin. Invest. Drugs* **1997**, *6*, 1697 – 1709.
[218] *New Macrolides, Azalides and Streptogramins in Clinical Practice* (Eds.: H. C. Neu, L. S. Young, S. H. Zinner, J. F. Acar), Marcel Dekker, New York, NY, **1995**.
[219] J. M. McGuire, R. L. Bunch, R. C. Andersen, H. E. Boaz, E. H. Flynn, H. M. Powell, J. W. Smith, *Antibiot. Chemother.* **1952**, *2*, 281 – 283.
[220] E. H. Flynn, M. V. Sigal, Jr., P. F. Wiley, K. Gerzon, *J. Am. Chem. Soc.* **1954**, *76*, 3121 – 3131.
[221] P. F. Wiley, K. Gerzon, E. H. Flynn, M. V. Sigal, Jr., O. Weaver, U. C. Quarck, R. R. Chauvette, R. Monahan, *J. Am. Chem. Soc.* **1957**, *79*, 6062 – 6070.
[222] W. Hofheinz, H. Grisebach, *Chem. Ber.* **1963**, *96*, 2867 – 2869.
[223] D. R. Harris, S. G. McGeachin, H. H. Mills, *Tetrahedron Lett.* **1965**, 679 – 685.
[224] E. J. Corey, P. B. Hopkins, S. K. S. Yoo, K. P. Nambiar, J. R. Falck, *J. Am. Chem. Soc.* **1979**, *101*, 7131 – 7134.
[225] R. B. Woodward et al., *J. Am. Chem. Soc.* **1981**, *103*, 3215 – 3217.
[226] L. Katz, *Chem. Rev.* **1997**, *97*, 2557 – 2575.
[227] J. S. Tuan, J. M. Weber, M. J. Staver, J. O. Leung, S. Donadio, L. Katz, *Gene* **1990**, *90*, 21 – 29.
[228] A. J. Birch, *Science* **1967**, *156*, 202 – 206.
[229] D. E. Cane, *Chem. Rev.* **1997**, *97*, 2463 – 2464.
[230] L. H. Hansen, P. Mauvais, S. Douthwaite, *Mol. Microbiol.* **1999**, *31*, 623 – 631.
[231] a) J. Harms, F. Schluenzen, R. Zarivach, A. Bashan, S. Gat, I. Agmon, H. Bartels, F. Fransceschi, A. Yonath, *Cell* **2001**, *107*, 679 – 688; b) F. Schluenzen, R. Zarivach, J. Harms, A. Bashan, A. Tocilj, R. Albrecht, A. Yonath, F. Fransceschi, *Nature* **2001**, *413*, 814 – 821.
[232] E. Abu-Gharbieh, V. Vasina, E. Poluzzi, F. De Ponti, *Pharmacol. Res.* **2004**, *50*, 211 – 222.
[233] J.-F. Chantot, A. J. Bryskier, J.-C. Gasc, *J. Antibiot.* **1986**, *39*, 660 – 668.
[234] a) S. Morimoto, Y. Takahashi, Y. Watanabe, S. Omura, *J. Antibiot.* **1984**, *37*, 187 – 189; b) S. Morimoto, Y. Takahashi, T. Adachi, T. Nagate, Y. Watanabe, *J. Antibiot.* **1990**, *43*, 286 – 294.
[235] a) J. A. Retsema, A. E. Girard, W. Schekly, M. Manousos, M. R. Anderson, G. M. Bright, R. J. Borovoy, L. A. Brennan, R. Mason, *Antimicrob. Agents Chemother.* **1987**, *31*, 1939 – 1947; b) S. Djokic, G. Kobrehel, G. Lazavreski, *J. Antibiot.* **1987**, *40*, 1006 – 1015.
[236] J. M. Blondeau, *Expert Opin. Pharmacother.* **2002**, *3*, 1131 – 1151.
[237] a) F. J. Baquero, *J. Chemother.* **1999**, *11*, 35 – 43; b) G. W. Amsden, *J. Antimicrob. Chemother.* **1999**, *44*, 1 – 6.
[238] E. D. Milton, C. L. Hewitt, C. R. Harwood, *FEMS Microbiol. Lett.* **1992**, *76*, 141 – 147.
[239] a) A. Tait-Kamrath, J. Clancy, M. Cronan, F. Dib-Hajj, L. Wondrack, W. Yuan, J. Sutcliffe, *Antimicrob. Agents Chemother.* **1997**, *41*, 2251 – 2255; b) G. V. Doern, K. P. Heilmann, H. K. Huynh, P. R. Rhomberg, S. L. Coffman, A. B. Brueggemann, *Antimicrob. Agents Chemother.* **2001**, *45*, 1721 – 1729.
[240] M. C. Roberts, J. Sutcliffe, P. Courvalin, L. B. Jensen, J. Rood, H. Seppala, *Antimicrob. Agents Chemother.* **1999**, *43*, 2823 – 2830.
[241] L. Wondrack, M. Massa, B. V. Yang, J. Sutcliffe, *Antimicrob. Agents Chemother.* **1996**, *40*, 992 – 998.
[242] G. G. Zhanel, M. Walters, A. Noreddin, L. M. Vercaigne, A. Wierzbowski, J. M. Embil, A. S. Gin, S. Douthwaite, D. J. Hoban, *Drugs* **2002**, *62*, 1771 – 1804.

 © 2006 Wiley-VCH Verlag GmbH & Co. KGaA, Weinheim

[243] H. Muxfeldt, S. Shrader, P. Hansen, H. Brockmann, *J. Am. Chem. Soc.* **1968**, *90*, 4748 – 4749.

[244] a) C. Agouridas, Y. Benedetti, A. Denis, O. Le Martret, J.-F. Chantot, *35th Interscience Conference on Antimicrobial Agents and Chemotherapy*, San Francisco, USA, **1995**, abstract F-157; b) C. Agouridas, A. Denis, J. M. Auger, Y. Benedetti, A. Bonnefoy, F. Bretin, J.-F. Chantot, A. Dussarat, C. Fromentin, S. G. D'Ambrières, S. Lachaud, P. Laurin, O. Le Martret, V. Loyau, N. Tessot, *J. Med. Chem.* **1998**, *41*, 4080 – 4100.

[245] Y.-J. Wu, W.-G. Su, *Curr. Med. Chem.* **2001**, *8*, 1727 – 1758.

[246] A. M. Nilius, Z. Ma, *Curr. Opin. Pharmacol.* **2002**, *2*, 1 – 8.

[247] R. F. Keyes, J. J. Carter, E. E. Englund, M. M. Daly, G. G. Stone, A. M. Nilius, Z. Ma, *J. Med. Chem.* **2003**, *46*, 1795 – 1798.

[248] a) A. Denis, C. Agouridas, J.-M. Auger, Y. Benedetti, A. Bonnefoy, F. Bretin, J.-F. Chantot, A. Dussarat, C. Fromentin, S. G. D'Ambrières, S. Lachaud, P. Laurin, O. Le Martret, V. Loyau, N. Tessot, J.-M. Pejac, S. Perron, *Bioorg. Med. Chem. Lett.* **1999**, *9*, 3075 – 3080; b) Y.-Q. Xiong, T. P. Le, *Drugs Today* **2001**, *37*, 617 – 628; c) A. Raja, J. Lebbos, P. Kirkpatrick, *Nat. Rev. Drug Discovery* **2004**, *3*, 733 – 734.

[249] a) Y. S. Or, R. F. Clark, S. Wang, D. T. Chu, A. M. Nilius, R. K. Flamm, M. Mitten, P. Ewing, J. Alder, Z. Ma, *J. Med. Chem.* **2000**, *43*, 1045 – 1049; b) Z. Ma, R. F. Clark, A. Brazzale, S. Wang, M. J. Rupp, L. Li, G. Griesgraber, S. Zhang, H. Yong, L. T. Phan, P. A. Nemoto, D. T. Chu, J. J. Plattner, X. Zhang, P. Zhong, Z. Cao, A. M. Nilius, V. D. Shortridge, R. Flamm, M. Mitten, J. Meulbroek, P. Ewing, J. Alder, Y. S. Or, *J. Med. Chem.* **2001**, *44*, 4137 – 4156; c) D. J. Plata, M. R. Leanna, M. Rasmussen, M. A. McLaughlin, S. L. Condon, F. A. J. Kerdesky, S. A. King, M. J. Peterson, E. J. Stoner, S. J. Wittenberger, *Tetrahedron* **2004**, *60*, 10171 – 10180.

[250] a) B. Scorneaux, A. Arya, A. Polemeropoulos, L. F. Han, K. Amsler, A. Sonderfan, G. Wang, Y. Wang, Y. Peng, G. Xu, H. Kim, T. Lien, L. Phan, Y. S. Or, *43rd Interscience Conference on Antimicrobial Agents and Chemotherapy*, Chicago, Illinois, USA, **2003**, abstract F-1191; b) G. Wang, D. Niu, Y.-L. Qiu, L. T. Phan, Z. Chen, A. Polemeropoulos, Y. S. Or, *Org. Lett.* **2004**, *6*, 4455 – 4458.

[251] A. Graul, J. Castaner, *Drugs Future* **1998**, *23*, 591 – 597.

[252] K. E. Pfitzner, J. G. Moffatt, *J. Am. Chem. Soc.* **1965**, *87*, 5661 – 5670.

[253] I. Phillips, *J. Antimicrob. Chemother.* **1981**, *7* (Suppl. A), 11 – 18.

[254] D. A. Leigh, *J. Antimicrob. Chemother.* **1981**, *7* (Suppl. A), 3 – 9.

[255] A. P. Ball, *J. Antimicrob. Chemother.* **1981**, *7* (Suppl. A), 81 – 84.

[256] a) L. E. Cohen, C. J. McNeil, R. F. Wells, *J. Am. Med. Assoc.* **1973**, *223*, 1379 – 1380; b) S. P. Borriello, H. E. Larsen, *J. Antimicrob. Chemother.* **1981**, *7* (Suppl. A), 53 – 62.

[257] R. D. Birkenmeyer (Upjohn), US 3435025, **1969** [*Chem. Abstr.* **1969**, *71*, 81696x].

[258] R. D. Birkenmeyer, F. Kagan, *J. Med. Chem.* **1970**, *13*, 616 – 619.

[259] D. J. Mason, A. Dietz, C. Deboer, *Antimicrob. Agents Chemother.* **1962**, 554 – 559.

[260] K. Bowden, G. P. Stevens, *J. Serb. Chem. Soc.* **2000**, *65*, 691 – 694.

[261] B. J. Magerlein, R. D. Birkenmeyer, F. Kagan, *Antimicrob. Agents Chemother.* **1966**, 727 – 736.

[262] C. Lewis, H. W. Clapp, J. E. Grady, *Antimicrob. Agents Chemother.* **1962**, 570 – 582.

[263] C. Lewis, K. F. Stern, J. E. Grady, *Antimicrob. Agents Chemother.* **1964**, 13 – 17.

[264] J. Poehlsgaard, S. Douthwaite, *Curr. Opin. Invest. Drugs* **2003**, *4*, 140 – 148.

[265] F. Schlünzen, R. Zarviach, J. Harms, A. Bashan, A. Tocilj, R. Albrecht, A. Yonath, F. Franceschi, *Nature* **2001**, *413*, 814 – 821.

[266] R. D. Birkenmeyer, S. J. Kroll, C. Lewis, K. F. Stern, G. E. Zurenko, *J. Med. Chem.* **1984**, *27*, 216 – 223.

[267] a) V. I. Ahonkhai, C. E. Cherubin, M. A. Shulman, M. Jhargoo, U. Bancroft, *Antimicrob. Agents Chemother.* **1982**, *21*, 902 – 905; b) M. E. Evans, L. S. Patterson, C. W. Stratton, *Antimicrob. Agents Chemother.* **1982**, *22*, 334 – 335; c) S. M. Hussain Qadri, M. R. Karim, D. J. Flournoy, *J. Antibiot.* **1983**, *36*, 42 – 46.

[268] a) A. A. Sinkula, W. Morozowich, E. L. Rowe, *J. Pharm. Sci.* **1973**, *62*, 1107 – 1111; b) F. LeGoffic, *J. Antimicrob. Chemother.* **1985**, *16* (Suppl. A), 13 – 21; c) F. Sztaricskai, Z. Dinya, G. Batta, A. Macsarai, M. Hollosi, Z. Majer, R. Masuma, S. Omura, *J. Antibiot.* **1973**, *50*, 866 – 873; d) J. Gonda, E. Zavacka, M. Budesinsky, I. Cisarova, J. Podlaha, *Tetrahedron Lett.* **2000**, *41*, 525 – 529.

[269] a) B. J. Maegerlein, *Tetrahedron Lett.* **1970**, 33 – 36; b) B. J. Maegerlein, *J. Med. Chem.* **1972**, *15*, 1255 – 1259; c) E. R. Larson, S. Danishefsky, *J. Am. Chem. Soc.* **1983**, *105*, 6715 – 6716; d) S. Knapp, P. J. Kukkola, *J. Org. Chem.* **1990**, *55*, 1632 – 1636.

[270] J. G. Lewis, A. E. Atuegbu, T. Chen, S. A. Kumar, D. V. Patel, C. J. Hackbarth, R. Asano, C. Wu, W. Wang, Z. Yuan, J. Trias, R. J. White, M. F. Gordeev, *44th Interscience Conference on Antimicrobial Agents and Chemotherapy*, Washington, DC, USA, **2004**, abstract F-1388.

[271] J. G. Lewis, S. Gu, S. A. Kumar, T. Chen, H. O'Dowd, D. V. Patel, C. J. Hackbarth, R. Asano, C. Park, L. Blais, C. Wu, Z. Yuan, J. Trias, R. J. White, M. F. Gordeev, *44th Interscience Conference on Antimicrobial Agents and Chemotherapy*, Washington, DC, USA, **2004**, abstract F-1389.

[272] R. N. Jones, H. S. Sader, T. R. Fritsche, *45th Interscience Conference on Antimicrobial Agents and Chemotherapy*, Washington, DC, USA, **2005**, abstract F-2040.

[273] C. Park, J. Blais, S. Lopez, M. Gomez, R. Rossi, G. Candiani, D. Jabs, A. Kubo, M. Maniar, P. Margolis, C. Hackbarth, J. Lewis, M. Gorgeev, R. White, J. Trias, *44th Interscience Conference on Antimicrobial Agents and Chemotherapy*, Washington, DC, USA, **2004**, abstract F-1392.

[274] J. Blais, C. Hackbarth, J. Lewis, R. White, J. Trias, *44th Interscience Conference on Antimicrobial Agents and Chemotherapy*, Washington, DC, USA, **2004**, abstract F-1393.

[275] D. Jabes, G. Candiani, R. Rossi, S. Riva, M. Feroggio, L. Colombo, F. Garofalo, J. Lewis, J. Trias, *44th Interscience Conference on Antimicrobial Agents and Chemotherapy*, Washington, DC, USA, **2004**, abstract F-1394.

[276] a) V. Tembe, D. Chen, L. Scott, S. Mukadam, G. Withers, Z. Yuan, J. Lewis, M. Gordeev, M. Buckwalter, J. Dowell, R. White, J. Trias, *44th Interscience Conference on Antimicrobial Agents and Chemotherapy*, Washington, DC, USA, **2004**, abstract F-1395; b) V. Tembe, D. Chen, L. Scott, P. Bani-Hashemi, P. Vadiveloo, J. Lewis, M. Gordeev, Z. Yuan, R. White, J. Trias, *44th Interscience Conference on Antimicrobial Agents and Chemotherapy*, Washington, DC, USA, **2004**, abstract F-1396.

[277] P. S. Margolis, M. M. Maniar, C. Wu, W. Wang, J. Lewis, M. Gordeev, Z. Yuan, R. White, J. Trias, *44th Interscience Conference on Antimicrobial Agents and Chemotherapy*, Washington, DC, USA, **2004**, abstract F-1390.

[278] J. Blais, C. Park, M. Maniar, P. Margolis, N. Rafanan, A. Kubo, S. Lopez, M. M. Gomez, C. Hackbarth, J. Lewis, M. Gordeev, R. White, J. Trias, *44th Interscience Conference on Antimicrobial Agents and Chemotherapy*, Washington, DC, USA, **2004**, abstract F-1391.

[279] K. Katagiri, K. Tori, Y. Kimura, T. Yoshida, T. Nagasaki, H. Minato, *J. Med. Chem.* **1967**, *10*, 1149 – 1154.

[280] a) M. M. Joullié, P. C. Wang, J. E. Semple, *J. Am. Chem. Soc.* **1980**, *102*, 887 – 889; b) J. E. Semple, P. C. Wang, Z. Lysenko, M. M. Joullié, *J. Am. Chem. Soc.* **1980**, *102*, 7505 – 7510.

[281] M. Shiro, H. Nakai, K. Tori, J. Nishikawa, Y. Yashimura, K. Katagiri, *J. Chem. Soc. Chem. Commun.* **1980**, 375.

 © 2006 Wiley-VCH Verlag GmbH & Co. KGaA, Weinheim

[282] R. J. Parry, H. P. Buu, *J. Am. Chem. Soc.* **1983**, *105*, 7446 – 7447.
[283] R. J. Parry, R. Turakhia, H. P. Buu, *J. Am. Chem. Soc.* **1988**, *110*, 4035 – 4036.
[284] T. Kohno, D. Kohda, M. Haruki, S. Yokoyama, *J. Biol. Chem.* **1990**, *265*, 6931 – 6935.
[285] a) K. Tanaka, M. Tomaki, S. Watanabe, *Biochim. Biophys. Acta* **1969**, *195*, 244 245; b) T. Masamune, M. Ono, *Chem. Lett.* **1975**, 625 – 626.
[286] J. R. Brown, W. F. Doolittle, *Proc. Natl. Acad. Sci. USA* **1995**, *92*, 2441 – 2445.
[287] a) J. Pohlmann, *Drugs Future* **2004**, *29*, 243 – 251; b) S. Kim, S. W. Lee, E. C. Choi, S. Y. Choi, *Appl. Microbiol. Biotechnol.* **2003**, *61*, 278 – 288; c) J. Tao, P. Schimmel, *Expert Opin. Invest. Drugs* **2000**, *9*, 1767 – 1775.
[288] a) A. T. Fuller, G. Mellows, M. Woolford, G. T. Banks, K. D. Barrow, E. B. Chain, *Nature* **1971**, *234*, 416 – 417; b) P. Brown, D. J. Best, N. J. Broon, R. Cassels, P. J. O'Hanlon, T. J. Mitchel, N. F. Osborne, J. M. Wilson, *J. Med. Chem.* **1997**, *40*, 3563 – 3570.
[289] L-(+)-furanomycin, obtained by total synthesis (see reference [294]) exhibited an MIC of 2 – 4 $\mu g\,mL^{-1}$ against *S. aureus* and *E. coli* and complete survival $ED_{100} < 50\,mg\,kg^{-1}$ i.p. in a murine *S. aureus* infection model. (R. Endermann, Bayer HealthCare AG, unpublished results).
[290] a) J. R. Proudfoot, *Bioorg. Med. Chem. Lett.* **2002**, *12*, 1647 – 1650; b) I. Muegge, *Med. Res. Reviews*, **2003**, *23*, 302 – 321; c) T. Wunberg, M. Hendrix, A. Hillisch, M. Lobell, H. Meier, C. Schmeck, H. Wild, B. Hinzen, *Drug Discovery Today* **2006**, *11*, 175 – 180.
[291] M. J. Robins, J. M. R. Parker, *Can. J. Chem.* **1983**, *61*, 317 – 322.
[292] S. Y. Chen, M. M. Joullié, *J. Org. Chem.* **1984**, *49*, 1769 – 1772.
[293] J. Zhang, D. L. J. Clive, *J. Org. Chem.* **1999**, *64*, 1754 – 1757.
[294] P. J. Zimmermann, I. Blanarikova, V. Jäger, *Angew. Chem.* **2000**, *112*, 936 – 938; *Angew. Chem. Int. Ed.* **2000**, *39*, 910 – 912.
[295] S. H. Kang, S. B. Lee, *Chem. Commun.* **1998**, 761 – 762.
[296] M. P. Van Brunt, R. F. Standaert, *Org. Lett.* **2000**, *2*, 705 – 708.
[297] U. Kazmaier, S. Pähler, R. Endermann, D. Häbich, H.-P. Kroll, B. Riedl, *Bioorg. Med. Chem.* **2002**, *10*, 3905 – 3913.
[298] H. R. Divanford, Z. Lysenko, J. E. Semple, P.-C. Wang, M. M. Joullié, *Heterocycles* **1981**, *16*, 1975 – 1985.
[299] R. Müller, T. Leibold, M. Pätzel, V. Jäger, *Angew. Chem.* **1994**, *106*, 1305 – 1308; *Angew. Chem. Int. Ed. Engl.* **1994**, *33*, 1295 – 1298.
[300] P. J. Zimmermann, J.-Y. Lee, I. Hlobilova (neé Blanarikova), R. Endermann, D. Häbich, V. Jäger, *Eur. J. Org. Chem.* **2005**, *16*, 3450 – 3460.
[301] J.-Y. Lee, G. Schiffer, V. Jäger, *Org. Lett.* **2005**, *7*, 2317 – 2320.
[302] A. Fredenhagen, S. Y. Tamura, P. T. M. Kenny, H. Komura, Y. Naya, K. Nakanishi, *J. Am. Chem. Soc.* **1987**, *109*, 4409 – 4411.
[303] J. Needham, M. T. Kelly, M. Ishige, R. A. Andersen, *J. Org. Chem.* **1994**, *59*, 2058 – 2063.
[304] W. McWorther, A. Fredenhagen, K. Nakanishi, H. Komura, *J. Chem. Soc. Chem. Commun.* **1989**, 299 – 301.
[305] a) A. V. Rama Rao, A. K. Singh, C. V. N. S. Varaprasad, *Tetrahedron Lett.* **1991**, *32*, 4393 – 4396; b) D. J. Dixon, S. G. Davies, *J. Chem. Soc. Chem. Commun.* **1996**, 1797 – 1798; c) S. G. Davies, D. J. Dixon, *J. Chem. Soc. Perkin Trans. 1* **1998**, 2635 – 2643.
[306] J. Pohlmann, T. Lampe, M. Shimada, P. G. Nell, J. Pernerstorfer, N. Svenstrup, N. A. Brunner, G. Schiffer, C. Freiberg, *Bioorg. Med. Chem. Lett.* **2005**, *15*, 1189 – 1192.
[307] a) N. Brunner, C. Freiberg, T. Lampe, B. Newton, M. Otteneder, J. Pernerstorfer, J. Pohlmann, G. Schiffer, M. Shimada, N. Svenstrup, R. Endermann, P. G. Nell (Bayer HealthCare AG), WO 04113290, **2004** [*Chem. Abstr.* **2004**, *142*, 56673]; b) N. Brunner, C. Freiberg, T. Lampe, B. Newton, M. Otteneder, J. Pernerstorfer, J. Pohlmann, G. Schiffer, M. Shimada, N. Svenstrup, R. Endermann, P. G. Nell (Bayer HealthCare AG), WO 03091212, **2003** [*Chem. Abstr.* **2003**, *139*, 350943].
[308] M. P. Singh, M. J. Mroczenski-Wildey, D. A. Steinberg, R. J. Andersen, W. M. Maiese, M. Greenstein, *J. Antibiot.* **1997**, *50*, 270 – 273.
[309] C. Freiberg, N. A. Brunner, G. Schiffer, T. Lampe, J. Pohlmann, M. Brands, M. Raabe, D. Häbich, K. Ziegelbauer, *J. Biol. Chem.* **2004**, *279*, 26066 – 26073.
[310] M. S. Davis, J. Solbiati, J. E. Cronan, Jr., *J. Biol. Chem.* **2000**, *275*, 28593 – 28598.
[311] C. Freiberg, *BIOspektrum* **2005**, *11*, 180 – 182.
[312] C. O. Rock, J. E. Cronan, *Biochim. Biophys. Acta* **1996**, *1302*, 1 – 16.
[313] S. S. Chirala. W. Y. Huang, A. Jayakumar, K. Sakai, S. J. Wakil, *Proc. Natl. Acad. Sci. USA* **1997**, *94*, 5588 – 5593.
[314] D. A. Alonso, S. K. Bertilsson, S. Y. Johnsson, S. J. M. Nordin, M. J. Södergren, P. G. Andersson, *J. Org. Chem.* **1999**, *64*, 2276 – 2280.
[315] a) P. Consonni, D. Favara, A. Omodei-Salé, G. Bartolini, A. Ricci, *J. Chem. Soc. Perkin Trans. 2* **1983**, 967 – 973; b) S. Robin, J. Zhu, H. Galons, C. Pham-Huy, J. R. Claude, A. Tomas, B. Voissant, *Tetrahedron: Asymmetry* **1995**, *6*, 1249 – 1252.
[316] C. Freiberg, J. Pohlmann, P. G. Nell, R. Endermann, J. Schuhmacher, B. Newton, M. Otteneder, T. Lampe, D. Häbich, K. Ziegelbauer, *Antimicrob. Agents Chemother.*, submitted.
[317] H. Ono, Y. Funabashi, S. Harada, EP 339596, **1989** [*Chem. Abstr.* **1990**, *113*, 38896].
[318] Y. Funabashi, S. Tsubotani, K. Koyama, N. Katayama, S. Harada, *Tetrahedron* **1993**, *49*, 13 – 28.
[319] N. Katayama, S. Fukusumi, Y. Funabashi, T. Iwahi, H. Ono, *J. Antibiot.* **1993**, *46*, 606 – 613.
[320] W. S. Champney, J. Pelt, C. L. Tober, *Curr. Microbiol.* **2001**, *43*, 340 – 345.
[321] N. Böddeker, G. Bahador, C. Gibbs, E. Mabery, J. Wolf, L. Xu, J. Watson, *RNA* **2002**, *8*, 1120 – 1128.
[322] E. Limburg, R. Gahlmann, H. P. Kroll, D. Beyer, *Antimicrob. Agents Chemother.* **2004**, *48*, 619 – 622.
[323] C. Yuan, R. M. Williams, *J. Am. Chem. Soc.* **1997**, *119*, 11777 – 11784.
[324] V. V. Sokolov, S. I. Kozhushkov, V. N. Belov, M. Es-Sayed, A. de Meijere, *Eur. J. Org. Chem.* **1998**, 777 – 783.
[325] L. Zhang, L. Xu, C. U. Kim, *Tetrahedron Lett.* **2003**, *44*, 5871 – 5873.
[326] V. N. Belov, M. Brands, S. Raddatz, J. Krüger, S. Nikolskaya, V. Sokolov, A. de Meijere, *Tetrahedron* **2004**, *60*, 7579 – 7589.
[327] P. Lin, A. Ganesan, *Synthesis* **2000**, 2127 – 2130.
[328] R. M. Williams, C. Yuan, V. J. Lee, S. Chamberland, *J. Antibiot.* **1998**, *51*, 189 – 201.
[329] Y. Cancho Grande, R. Endermann, R. Gahlmann, J. Krüger, S. Raddatz, M. Brands, *Drugs Future* **2002**, *27* (Suppl. A: XVIIth Int. Symp. on Medicinal Chemistry Barcelona/Spain), C79.
[330] M. Brands, R. Endermann, R. Gahlmann, J. Krüger, S. Raddatz, *Bioorg. Med. Chem. Lett.* **2003**, *13*, 241 – 245.
[331] M. Brands, M. Es-Sayed, D. Häbich, S. Raddatz, J. Krüger, R. Endermann, R. Gahlmann, H. P. Kroll, H. U. Geschke, A. de Meijere, V. N. Belov, V. Sokolov, S. Kozhushkov, M. Kordes, WO 00/012484, **2000** [*Chem. Abstr.* **2000**, *137*, 47208].
[332] a) P. Spiteller, F. von Nussbaum, β- *Amino Acids in Natural Products* in *Enantioselective Synthesis of* β-*Amino Acids* (Eds.: V. Soloshonok, E. Juaristi), 2nd ed., Wiley, New Jersey, **2005**, pp. 19 – 91; b) F. von Nussbaum, P. Spiteller, β-*Amino Acids in Nature* in *Highlights in Bioorganic Chemistry—Methods and Applications* (Eds.: C. Schmuck, H. Wennemers), Wiley-VCH, Weinheim, **2004**, pp. 63 – 89.
[333] For the synthesis of β-amino acids, see: a) S. Abele, D. Seebach, *Eur. J. Org. Chem.* **2000**, 1 – 15; b) E. Juaristi, *Enantioselective*

 © 2006 Wiley-VCH Verlag GmbH & Co. KGaA, Weinheim

Synthesis of β-Amino Acids, Wiley-VCH, Weinheim, **1997**; c) A. Kuhl, M. G. Hahn, M. Dumić, J. Mittendorf, *Amino Acids* **2005**, *29*, 89 – 100.

[334] M. Brands, Y. Cancho Grande, R. Endermann, R. Gahlmann, J. Krüger, S. Raddatz, *Bioorg. Med. Chem. Lett.* **2003**, *13*, 2641 – 2645.

[335] N. Aguilar, J. Krüger, *Molecules* **2002**, 7, 469 – 474.

[336] M. Brands, R. Endermann, R. Gahlmann, J. Krüger, S. Raddatz, J. Stoltefuß, V. N. Belov, S. Nizamov, V. N. Sokolov, A. de Meijere, *J. Med. Chem.* **2002**, *45*, 4246 – 4253.

[337] J. H. Martin, L. A. Mitscher, P. Shu, J. N. Porter, N. Bohonos, S. E. DeVoe, E. L. Patterson, *Antimicrob. Agents Chemother.* **1967**, 422 – 425.

[338] J. H. Martin, J. N. Porter, L. A. Mitscher (Lederle Pharm.), US 3,452,136, **1969** [*Chem. Abstr.* **1969**, *71*, 59640].

[339] C. C. Chang, G. O. Morton, J. C. James, M. M. Siegel, N. A. Kuck, R. T. Testa, D. B. Borders, *J. Antibiot.* **1991**, *44*, 674 – 677.

[340] K. Umehara, M. Ezaki, M. Iwami, M. Yameshita, S. Hashimoto, T. Komori, I. Uchida, M. Hashimoto, Y. Mine, M. Khosaka, H. Aoki, H. Imanaka, *24th Interscience Conference on Antimicrobial Agents and Chemotherapy* **1984**, abstracts 1141 and 292.

[341] M. Ezaki, M. Iwami, M. Yameshita, S. Hashimoto, T. Komori, K. Umehara, Y. Mine, M. Khosaka, H. Aoki, H. Imanaka, *J. Antibiot.* **1985**, *38*, 1453 – 1461.

[342] I. Uchida, N. Shigematsu, M. Ezaki, M. Hashimoto, H. Aoki, H. Imanaka, *J. Antibiot.* **1985**, *38*, 1462 – 1468.

[343] M. Ezaki, N. Shigematsu, M. Yamashita, T. Komori, K. Umehara, H. Imanaka, *J. Antibiot.* **1993**, *46*, 135 – 140.

[344] R. Kannan, D. H. Williams, *J. Org. Chem.* **1987**, *52*, 5435 – 5437.

[345] a) F. K. Brown, J. C. Hempel, J. S. Dixon, S. Amato, L. Mueller, P. W. Jeffs, *J. Am. Chem. Soc.* **1989**, *111*, 7328 – 7333; b) L. Feliu, M. Planas, *Int. J. Pept. Res. Ther.* **2005**, *11*, 53 – 97.

[346] U. Schmidt, R. Meyer, V. Leitenberger, A. Lieberknecht, H. Griesser, *J. Chem. Soc. Chem. Commun.* **1991**, 275 – 277; For previous work, see: U. Schmidt, R. Meyer, V. Leitenberger, A. Lieberknecht, *Angew. Chem.* **1989**, *101*, 946 – 948; *Angew. Chem. Int. Ed. Engl.* **1989**, *28*, 929 – 931.

[347] U. Schmidt, R. Meyer, V. Leitenberger, F. Stäbler, A. Lieberknecht, *Synthesis* **1991**, 409 – 413.

[348] a) J. Rudolph, F. Hannig, H. Theis, R. Wischnat, *Org. Lett.* **2001**, *3*, 3153 – 3155; b) J. Rudolph, F. Hannig (Bayer AG), WO 02102764, **2002** [*Chem. Abstr.* **2002**, *138*, 39541]; c) R. Lepine, A.-C. Carbonelle, J. Zhu, *Synlett* **2003**, 1455 – 1458; d) F. F. Paintner, L. Allmendinger, G. Bauschke, P. Klemann, *Org. Lett.* **2005**, *7*, 1423 – 1426.

[349] U. Schmidt, V. Leitenberger, R. Meyer, H. Griesser, *J. Chem. Soc. Chem. Commun.* **1992**, 951 – 953.

[350] U. Schmidt, V. Leitenberger, H. Griesser, J. Schmidt, R. Meyer, *Synthesis* **1992**, 1248 – 1254.

[351] F. F. Paintner, K. Görler, W. Voelter, *Synlett* **2003**, 522 – 526.

[352] A. G. Brown, M. J. Crimmin, P. D. Edwards, *J. Chem. Soc. Perkin Trans. 1* **1992**, 123 – 130.

[353] A. G. Brown, P. D. Edwards, *Tetrahedron Lett.* **1990**, *31*, 6581 – 6584.

[354] R. Lepine, J. Zhu, *Org. Lett.* **2005**, *7*, 2981 – 2984.

[355] T. Lampe, I. Adelt, D. Beyer, N. Brunner, R. Endermann, K. Ehlert, H.-P. Kroll, F. von Nussbaum, S. Raddatz, J. Rudolph, G. Schiffer, A. Schumacher, Y. Cancho-Grande, M. Michels, S. Weigand (Bayer HealthCare AG), WO 106480, **2003** [*Chem. Abstr.* **2003**, *140*, 59934].

[356] T. Lampe, I. Adelt, D. Beyer, N. Brunner, R. Endermann, K. Ehlert, H.-P. Kroll, F. von Nussbaum, S. Raddatz, J. Rudolph, G. Schiffer, A. Schumacher, Y. Cancho-Grande, M. Michels, S. Weigand (Bayer HealthCare AG), WO 012816, **2004** [*Chem. Abstr.* **2004**, *140*, 164239].

[357] N. Miyaura, A. Suzuki, *Chem. Rev.* **1995**, *95*, 2457 – 2483.

[358] T. Lampe, I. Adelt, D. Beyer, N. Brunner, R. Endermann, K. Ehlert, H.-P. Kroll, F. von Nussbaum, S. Raddatz, J. Rudolph, G. Schiffer, A. Schumacher, Y. Cancho-Grande, M. Michels, S. Weigand (Bayer HealthCare AG), WO 033129, **2005** [*Chem. Abstr.* **2005**, *142*, 411656].

[359] For a similar aproach using a double asymmetric hydrogenation, see: A.-S. Carlström, T. Frejd, *J. Chem. Soc. Chem. Commun.* **1991**, 1216 – 1217.

[360] T. J. Dougherty, T. V. Magee, *Expert Opin. Ther. Pat.* **2005**, *15*, 1409 – 1421.

[361] A. C. Finlay, G. L. Hobby, F. A. Hochstein, T. M. Lees, T. F. Lenert, J. A. Means, S. Y. Pan, P. P. Regna, J. B. Routein, B. A. Sobin, K. B. Tate, J. H. Kane, *Am. Rev. Tuberc.* **1951**, *63*, 1 – 3.

[362] W. S. Marsh, R. L. Mayer, R. P. Mull, C. R. Scholz, R. W. Townley (Ciba), US Patent 2,633,445, **1953** [*Chem. Abstr.* **1953**, *47*, 8974c].

[363] E. B. Herr, Jr., M. E. Henry, G. E. Pittenger, C. E. Higgens, *Proc. Indian Acad. Sci.* **1960**, *69*, 134.

[364] E. B. Herr, Jr., M. O. Redstone, *Ann. N. Y. Acad. Sci.* **1966**, *135*, 940 – 946.

[365] B. W. Bycroft, D. Cameron, L. R. Croft, A. Hassanali-Walji, A. W. Johnson, T. Web, *Nature* **1971**, *231*, 301 – 302.

[366] a) T. Shiba, S. Nomoto, T. Teshima, T. Wakamiya, *Tetrahedron Lett.* **1976**, *17*, 3907 – 3910; b) T. Shiba, S. Nomoto, T. Wakamiya, *Experientia* **1976**, *26*, 1109 – 1111; c) S. Nomoto, T. Teshima, T. Wakamiya, T. Shiba, *J. Antibiot.* **1977**, *30*, 955 – 959; d) S. Nomoto, T. Teshima, T. Wakamiya, T. Shiba, *Tetrahedron* **1978**, *34*, 921 – 927.

[367] a) J. H. Bowie, D. A. Cox, A. W. Johnson, G. Thomas, *Tetrahedron Lett.* **1964**, 3305 – 3308; b) J. R. Dyer, C. K. Kellogg, R. F. Nassar, W. E. Streetman, *Tetrahedron Lett.* **1965**, 585 – 592; c) B. W. Bycroft, D. Cameron, L. R. Croft, A. W. Johnson, T. Webb, P. Coggon, *Tetrahedron Lett.* **1968**, 2925 – 2930; d) B. W. Bycroft, L. R. Croft, A. W. Johnson, T. Webb, *J. Antibiot.* **1969**, *22*, 133 – 134; e) B. W. Bycroft, D. Cameron, A. Hassanali-Walji, A. W. Johnson, *Tetrahedron Lett.* **1969**, 2539 – 2541; f) B. W. Bycroft, D. Cameron, A. W. Johnson, T. Webb, *J. Chem. Soc. Perkin Trans. 1* **1972**, 820 – 827; g) B. W. Bycroft, D. Cameron, L. R. Croft, A. Hassanali-Walji, A. W. Johnson, T. Webb, *J. Chem. Soc. Perkin Trans. 1* **1972**, 827 – 834.

[368] T. Kitagawa, Y. Sawada, T. Miuea, T. Ozasa, H. Taniyama, *Tetrahedron Lett.* **1968**, 109 – 113.

[369] L. Lechowski, *Tetrahedron Lett.* **1969**, 479 – 482.

[370] B. W. Bycroft, D. Cameron, L. R. Croft, A. Hassanali-Walji, A. W. Johnson, T. Webb, *Experientia* **1971**, *27*, 501 – 503.

[371] H. Yoshioka, T. Aoki, H. Goko, K. Nakatsu, T. Noda, H. Sakakibara, T. Take, A. Nagata, J. Abe, T. Wakamiya, T. Shiba, T. Kaneko, *Tetrahedron Lett.* **1971**, 2043 – 2046.

[372] T. Noda, T. Take, A. Nagata, T. Wakamiya, T. Shiba, *J. Antibiot.* **1972**, *25*, 427 – 428.

[373] W. B. Sutton, R. S. Gordee, W. E. Wick, L. V. Stanfield, *Ann. N. Y. Acad. Sci.* **1966**, *135*, 947 – 959.

[374] A. Nagata, T. Ando, R. Izumi, H. Sakakibara, T. Take, K. Hayano, J.-N. Abe, *J. Antibiot.* **1968**, *21*, 681 – 786.

[375] H. Wank, J. Rogers, J. Davies, R. Schroeder, *J. Mol. Biol.* **1994**, *236*, 1001 – 1010.

[376] H. R. Black, R. S. Griffith, J. F. Brickler, *Antimicrob. Agents Chemother.* **1963**, *161*, 522 – 529.

[377] M. Tsukamura, S. Mizuno, *J. Gen. Microbiol.* **1975**, *88*, 269 – 274.

[378] J. S. Welles, P. N. Harris, R. M. Small, H. M. Worth, R. C. Anderson, *Ann. N. Y. Acad. Sci.* **1966**, *135*, 960 – 973.

[379] M. Wang, S. J. Gould, *J. Org. Chem.* **1992**, *57*, 5176 – 5180.

[380] S. J. Gould, D. A. Minott, *J. Org. Chem.* **1992**, *57*, 5214 – 5217.

[381] M. S. Brown, A. E. Doro, H. A. I. McArthur, B. K. Morse, T. K. Murphy, R. G. Wax, *J. Antibiot.* **1997**, *50*, 696 – 700.

 © 2006 Wiley-VCH Verlag GmbH & Co. KGaA, Weinheim

[382] B. K. Morse, M. S. Bown, J. W. Gagne, H. A. I. McArthur, E. L. McCormick, T. K. Murphy, M. T. Narrol, D. A. Perry, A. A. Smogowicz, R. G. Wax, J. W. Wong, *J. Antibiot.* **1997**, *50*, 698 – 700.
[383] T. Teshima, S. Nomoto, T. Wakamiya, T. Shiba, *Tetrahedron Lett.* **1976**, 2343 – 2346.
[384] T. Shiba, T. Ando, T. Teshima, *J. Antibiot.* **1979**, *32*, 1078 – 1079.
[385] T. Teshima, S. Nomoto, T. Wakamiya, T. Shiba, *J. Antibiot.* **1977**, *30*, 1073 – 1079.
[386] T. Kitagawa, T. Miura, S. Tanaka, H. Taniyama, *J. Antibiot.* **1972**, *25*, 429 – 431.
[387] T. Kitagawa, T. Miura, M. Takaishi, H. Taniyama, *Chem. Pharm. Bull.* **1975**, *23*, 2123 – 2127.
[388] T. Kitagawa, T. Miura, H. Taniyama, *Chem. Pharm. Bull.* **1972**, *20*, 2176 – 2184.
[389] T. Kitagawa, T. Miura, C. Takaishi, H. Taniyama, *Chem. Pharm. Bull.* **1976**, *24*, 1324 – 1330.
[390] T. Kitagawa, T. Miura, Y. Sawade, K. Fujiwara, R. Ito, H. Taniyama, *Chem. Pharm. Bull.* **1974**, *22*, 1827 – 1834.
[391] T. Kitagawa, T. Miura, S. Tanaka, H. Taniyama, *J. Antibiot.* **1973**, *26*, 528 – 531.
[392] T. Yamada, T. Teshima, T. Shiba, *Antimicrob. Agents Chemother.* **1981**, *20*, 834 – 836.
[393] S. Nomot, T. Shiba, *J. Antibiot.* **1977**, *30*, 1008 – 1011.
[394] T. Wakamiya, T. Teshima, H. Sakakibara, K. Fukukawa, T. Shiba, *Bull. Chem. Soc. Jpn.* **1977**, *50*, 1984 – 1989.
[395] T. Teshima, S. Nomoto, T. Wakamiya, T. Shiba, *Bull. Chem. Soc. Jpn.* **1977**, *50*, 3372 – 3380.
[396] S. Nomoto, T. Shiba, *Bull. Chem. Soc. Jpn.* **1979**, *52*, 1709 – 1715.
[397] J. P. Dirlam et al., *Bioorg. Med. Chem. Lett.* **1997**, *7*, 1139 – 1144.
[398] L. J. L. Norcia, A. M. Silvia, J. P. Dirlam, R. C. Schnur, J. M. Bergeron, J. A. Retsema, S. F. Hayashi, *J. Antibiot.* **1999**, *52*, 1007 – 1016.
[399] R. G. Linde II, N. C. Birsner, R. Y. Chandrasekaran, J. Clancy, R. J. Howe, J. P. Lyssikatos, C. P. MacLelland, T. V. Magee, J. W. Petitpas, J. P. Rainville, W.-G. Su, C. B. Vu, D. A. Whipple, *Bioorg. Med. Chem. Lett.* **1997**, *7*, 1149 – 1152.
[400] J. P. Lyssikatos, S.-P. Chang, J. P. Dirlam, S. M. Finegan, A. E. Girard, S. F. Hayashi, D. P. Larson, A. S. Lee, R. G. Linde II, C. P. MacLelland, J. W. Petitpas, S. B. Seibel, C. B. Vu, *Bioorg. Med. Chem. Lett.* **1997**, *7*, 1145 – 1148.
[401] K. C. Nicolaou, C. N. C. Boddy, S. Bräse, N. Winssinger, *Angew. Chem.* **1999**, *111*, 2230 – 2287; *Angew. Chem. Int. Ed.* **1999**, *38*, 2097 – 2152.
[402] A. A. Dutton, P. C. Elmes, *Br. Med. J.* **1959**, *1*, 1144 – 1149.
[403] M. H. McCormick, J. M. McGuire, G. E. Pittenger, R. C. Pittenger, W. M. Stark, *Antibiot. Annu.* **1955–1956**, *3*, 606 – 611.
[404] M. P. Williamson, D. H. Williams, *J. Am. Chem. Soc.* **1981**, *103*, 6580 – 6585.
[405] C. M. Harris, T. M. Harris, *J. Am. Chem. Soc.* **1982**, *104*, 4293 – 4295.
[406] A. Malabarba, T. I. Nicas, R. C. Thompson, *Med. Res. Rev.* **1997**, *17*, 69 – 137.
[407] a) A. J. Zhang, K. Burgess, *Angew. Chem.* **1999**, *111*, 666 – 669; *Angew. Chem. Int. Ed.* **1999**, *38*, 634 – 636; b) L. H. Thoresen, K. Burgess in *Organic Syntheses Highlights V* (Eds.: H.-G. Schmalz, T. Wirth), Wiley-VCH, Weinheim, **2003**, pp. 297 – 306.
[408] a) D. A. Evans, M. R. Wood, B. W. Trotter, T. I. Richardson, J. C. Barrow, J. L. Katz, *Angew. Chem.* **1998**, *110*, 2864 – 2868; *Angew. Chem. Int. Ed.* **1998**, *37*, 2700 – 2704; b) D. A. Evans, C. J. Dinsmore, P. S. Watson, M. R. Wood, T. I. Richardson, B. W. Trotter, *Angew. Chem.* **1998**, *110*, 2868 – 2872; *Angew. Chem. Int. Ed.* **1998**, *37*, 2704 – 2708.
[409] a) K. C. Nicolaou, M. Takayanagi, N. F. Jain, S. Natajaran, A. E. Koumbis, T. Bando, J. M. Ramanjulu, *Angew. Chem.* **1998**, *110*, 2881 – 2883; *Angew. Chem. Int. Ed.* **1998**, *37*, 2717 – 2719; b) K. C. Nicolaou, H. J. Mitchell, N. F. Jain, N. Winssinger, R. Hughes, T. Bando, *Angew. Chem.* **1999**, *111*, 253 – 255; *Angew. Chem. Int. Ed.* **1999**, *38*, 240 – 244.
[410] a) D. L. Boger, S. Miyazaki, S. H. Kim, J. H. Wu, O. Loiseleur, S. L. Castle, *J. Am. Chem. Soc.* **1999**, *121*, 3226 – 3227; b) D. L. Boger, S. Miyazaki, S. H. Kim, J. H. Wu, S. L. Castle, O. Loiseleur, Q. Jin, *J. Am. Chem. Soc.* **1999**, *121*, 10004 – 10011.
[411] B. K. Hubbard, C. T. Walsh, *Angew. Chem.* **2003**, *115*, 752 – 789; *Angew. Chem. Int. Ed.* **2003**, *42*, 730 – 765.
[412] R. D. Süssmuth, W. Wohlleben, *Appl. Microbiol. Biotechnol.* **2004**, *63*, 344 – 350.
[413] a) G. M. Sheldrick, P. G. Jones, O. Kennard, D. H. Williams, G. A. Smith, *Nature*, **1978**, *271*, 223 – 225; b) D. H. Williams, B. Bardsley, *Angew. Chem.* **1999**, *111*, 1264 – 1286; *Angew. Chem. Int. Ed.* **1999**, *38*, 1172 – 1193.
[414] D. Kahne, C. Leimkuhler, W. Lu, C. Walsh, *Chem. Rev.* **2005**, *105*, 425 – 448.
[415] N. E. Allen, T. I. Nicas, *FEMS Microbiol. Rev.* **2003**, *26*, 511 – 532.
[416] a) J. R. Kalman, D. H. Williams, *J. Am. Chem. Soc.* **1980**, *102*, 906 – 912; b) D. H. Williams, M. P. Williamson, D. W. Butcher, S. J. Hammond, *J. Am. Chem. Soc.* **1983**, *105*, 1332 – 1339.
[417] a) M. Schäfer, T. R. Schneider, G. M. Sheldrick, *Structure* **1996**, *4*, 1509 – 1515; b) P. J. Loll, R. Miller, C. M. Weeks, P. H. Axelsen, *Chem. Biol.* **1998**, *5*, 293 – 298.
[418] a) M. J. Bonten, R. Willems, R. A. Weinstein, *Lancet Infect. Dis.* **2001**, *1*, 314 – 325; b) R. Patel, *J. Antimicrob. Chemother.* **2003**, *51* (Suppl. S3), iii13 – iii21.
[419] C. T. Walsh, S. L. Fisher, I. S. Park, M. Prahad, Z. Wu, *Chem. Biol.* **1996**, *3*, 21 – 28.
[420] a) T. D. Bugg, G. D. Wright, S. Dukta-Mahlen, M. Arthur, P. Courvalin, C. T. Walsh, *Biochemistry* **1991**, *30*, 10408 – 10415; b) C. C. McComas, B. M. Crowley, D. L. Boger, *J. Am. Chem. Soc.* **2003**, *125*, 9314 – 9315.
[421] B. M. Crowley, D. L. Boger, *J. Am. Chem. Soc.* **2006**, *128*, 2885 – 2892.
[422] I. G. Boneca, G. Chiosis, *Expert Opin. Ther. Targets* **2003**, *7*, 311 – 328.
[423] F. Van Bambeke, Y. Van Laethem, P. Courvalin, P. M. Tulkens, *Drugs* **2004**, *64*, 913 – 936.
[424] M. N. Preobrazhenskaya, E. N. Olsufyeva, *Expert Opin. Ther. Pat.* **2004**, *14*, 141 – 173.
[425] J. P. Mackay, U. Gerhard, D. A. Beauregard, M. S. Westwell, M. S. Searle, D. H. Williams, *J. Am. Chem. Soc.* **1994**, *116*, 4581 – 4590.
[426] a) U. N. Sundram, J. H. Griffin, T. I. Nicas, *J. Am. Chem. Soc.* **1996**, *118*, 13107 – 13108; b) K. C. Nicolaou, R. Hughes, S. Y. Cho, N. Winssinger, C. Smethurst, H. Labischinski, R. Endermann, *Angew. Chem.* **2000**, *112*, 3981 – 3986; *Angew. Chem. Int. Ed.* **2000**, *39*, 3823 – 3828.
[427] R. Nagarajan, *J. Antibiot.* **1993**, *46*, 1181 – 1195.
[428] a) R. D. G. Cooper, N. J. Snider, M. J. Zweifel, M. A. Staszak, S. C. Wilkie, T. I. Nicas, D. L. Mullen, T. F. Butler, M. J. Rodriguez, B. E. Huff, R. C. Thompson, *J. Antibiot.* **1996**, *49*, 575 – 581; b) J. F. Barrett, *Curr. Opin. Invest. Drugs* **2001**, *2*, 1039 – 1044; c) S. M. Bhavnani, J. S. Owen, J. S. Loutit, S. B. Porter, P. G. Ambrose, *Pharmacology* **2004**, *50*, 95 – 102.
[429] a) A. Malabarba, S. Donadio, *Drugs Future* **1999**, *24*, 839 – 846; b) G. Candiani, M. Abbondi, M. Borgonovi, G. Romanò, F. Parenti, *J. Antimicrob. Chemother.* **1999**, *44*, 179 – 192; c) A. Malabarba, A. Ciabatti, *Curr. Med. Chem.* **2001**, *8*, 1759 – 1773; d) M. Steiert, F.-J. Schmitz, *Curr. Opin. Invest. Drugs* **2002**, *3*, 229 – 233.
[430] a) J. L. Pace, J. K. Judice, *Curr. Opin. Invest. Drugs* **2005**, *6*, 216 – 225; b) L. A. Sorbera, J. Castaner, *Drugs Future* **2004**, *29*, 1211 – 1219; c) J. K. Judice, J. L. Pace, *Bioorg. Med. Chem. Lett.* **2003**, *13*, 4165 – 4168.

 © 2006 Wiley-VCH Verlag GmbH & Co. KGaA, Weinheim

[431] F. Van Bambeke, *Curr. Opin. Pharmacol.* **2004**, *4*, 471 – 478.
[432] M. R. Leadbetter, S. M. Adams, B. Bazzini, P. R. Fatheree, D. E. Karr, K. M. Krause, B. M. Lam, M. S. Linsell, M. B. Nodwell, J. L. Pace, K. Quast, J. P. Shaw, E. Soriano, S. G. Trapp, J. D. Villena, T. X. Wu, B. G. Christensen, J. K. Judice, *J. Antibiot.* **2004**, *57*, 326 – 336.
[433] A. King, I, Phillips, K. Kaniga, *J. Antimicrob. Chemother.* **2004**, *53*, 797 – 803.
[434] E. J. C. Goldstein, D. M. Citron, C. V. Merriam, Y. A. Warren, K. L. Tyrrell, H. T. Fernandez, *Antimicrob. Agents Chemother.* **2004**, *48*, 2149 – 2152.
[435] D. L. Higgins, R. Chang, D. V. Debabov, J. Leung, T. Wu, K. M. Krause, E. Sandvik, J. M. Hubbard, K. Kaniga, D. E. Schmidt Jr., Q. Gao, R. T. Cass, D. E. Karr, B. M. Benton, P. P. Humphrey, *Antimicrob. Agents Chemother.* **2005**, *49*, 1127 – 1134.
[436] S. S. Hedge, N. Reyes, T. Wiens, N. Vanasse, R. Skinner, J. McCullough, K. Kaniga, J. Pace, R. Thomas, J.-P. Shaw, G. Obedencio, J. K. Judice, *Antimicrob. Agents Chemother.* **2004**, *48*, 3043 – 3050.
[437] J. P. Shaw, J. Seroogy, K. Kaniga, D. L. Higgins, M. Kitt, S. Barriere, *Antimicrob. Agents Chemother.* **2005**, *49*, 195 – 201.
[438] M. Leadbetter, M. Linsell, J. Lee, J. Liu (Theravance Inc.), WO 03029270, **2003** [*Chem. Abstr.* **2003**, *138*, 287982].
[439] D. Schmidt, Jr., J. D. Sganga (Theravance Inc.), WO 03018608, **2003** [*Chem. Abstr.* **2003**, *138*, 221851].
[440] J. O'Sullivan, J. E. McCullough, A. A. Tymiak, D. R. Kirsch, W. H. Trejo, P. A. Prinicipe, *J. Antibiot.* **1988**, *41*, 1740 – 1744.
[441] D. P. Bonner, J. O'Sullivan, S. K. Tanaka, J. M. Clark, R. R. Whitney, *J. Antibiot.* **1988**, *41*, 1745 – 1751.
[442] J. I. Shoji, H. Hinoo, K. Matsumoto, T. Hattori, T. Yoshida, S. Matsuura, E. Kondo, *J. Antibiot.* **1988**, *41*, 713 – 718.
[443] T. Kato, H. Hinoo, Y. Terui, J. Kikuchi, J. I. Shoji, *J. Antibiot.* **1988**, *41*, 719 – 725; Erratum: T. Kato, H. Hinoo, Y. Terui, J. Kikuchi, J. I. Shoji, *J. Antibiot.* **1989**, *42*, C-2.
[444] a) F. von Nussbaum, N. Brunner, S. Anlauf, R. Endermann, C. Fürstner, E. Hartmann, J. Koebberling, J. Ragot, G. Schiffer, J. Schuhmacher, N. Svenstrup, J. Telser, M.-A. Brüning (Bayer HealthCare AG), WO 04099239, **2004** [*Chem. Abstr.* **2004**, *141*, 423388]; b) F. von Nussbaum, N. Brunner, R. Endermann, C. Fürstner, E. Hartmann, J. Ragot, G. Schiffer, J. Schuhmacher, N. Svenstrup, J. Telser, S. Anlauf, M.-A. Brüning (Bayer HealthCare AG), WO 06042653, **2006** [*Chem. Abstr.* **2006**, 388744]; c) F. von Nussbaum, N. Brunner, R. Endermann, C. Fürstner, E. Hartmann, J. Ragot, G. Schiffer, J. Schuhmacher, N. Svenstrup, J. Telser, S. Anlauf, M.-A. Brüning (Bayer HealthCare AG), WO 06042654, **2006** [*Chem. Abstr.* **2006**, 388745].
[445] P. Christensen, F. D. Cook, *Int. J. Syst. Bacteriol.* **1978**, *28*, 367 – 393.
[446] a) H. Maki, K. Miura, Y. Yamano, *Antimicrob. Agents Chemother.* **2001**, *45*, 1823 – 1827; b) E. Breukink, B. de Kruijff, *Nat. Rev. Drug Discovery* **2006**, *5*, 321 – 333.
[447] A. A. Tymiak, D. R. Kirsch, J. O'Sullivan, J. E. McCullough (E. R. Squibb & Sons, Inc.), US 4754018, **1988** [*Chem. Abstr.* **1990**, *112*, 75294].
[448] A. A. Tymiak, T. J. McCormick, S. E. Unger, *J. Org. Chem.* **1989**, *54*, 1149 – 1157.
[449] a) N. H. Andersen, X. Lai, P. K. Hammen, T. M. Marschner, *NMR Applications in Biopolymers* (Eds.: J. W. Finley), Plenum, New York, **1990**, pp. 95 – 134; b) The first single crystal X-ray structure of lysobactin has been achieved: Bayer HealthCare AG, unpublished results.
[450] "Unnatural amino acids" are not found in nature. "Nonproteinogenic amino acids" are not found in peptides derived from the ribosomal protein biosynthesis. They may be building blocks or substructures in secondary metabolites, such as nonribosomal peptides or alkaloids.
[451] F. Bernhard, G. Demel, K. Soltani, H. V. Döhren, V. Blinov, *DNA Sequence* **1996**, *6*, 319 – 330.
[452] S. Armaroli, G. Cardillo, L. Gentilucci, M. Gianotti, A. Tolomelli, *Org. Lett.* **2000**, *2*, 1105 – 1107.
[453] G. Cardillo, S. Fabbroni, L. Gentilucci, R. Perciaccante, A. Tolomelli, *Komppa Centenary Symposium – 100 Years of Natural Product Synthesis*, Helsinki, Finland, **2003**, Poster ORGN843.
[454] A. M. Hafez, T. Dudding, T. R. Wagerle, M. H. Shah, A. E. Taggi, T. Lectka, *J. Org. Chem.* **2003**, *68*, 5819 – 5825.
[455] A. Guzman-Martinez, R. B. Lamer, M. S. VanNieuwenhze, *229th ACS National Meeting*, *San Diego*, *CA*, March 13 – 17, **2005**.
[456] C. Palomo, M. Oiarbide, I. Ganboa, J. I. Miranda, *Tetrahedron Lett.* **2001**, *42*, 8955 – 8957.
[457] C. Palomo, J. M. Aizpurua, I. Ganboa, M. Oiarbide, *Pure Appl. Chem.* **2000**, *72*, 1763 – 1768.
[458] C. Palomo, J. M. Aizpurua, I. Ganboa, B. Odriozola, E. Maneiro, J. I. Miranda, R. Urchegui, *Chem. Commun.* **1996**, 161 – 162.
[459] B. J. Egner, M. Bradley, *Tetrahedron* **1997**, *53*, 14021 – 14030.
[460] Review: C. E. Ballard, H. Yu, B. Wang, *Curr. Med. Chem.* **2002**, *9*, 471 – 498.
[461] H. Osada, T. Yano, H. Koshino, K. Isono, *J. Antibiot.* **1991**, *44*, 1463 – 1466.
[462] H. Koshino, H. Osada, T. Yano, J. Uzawa, K. Isono, *Tetrahedron Lett.* **1991**, *32*, 7707 – 7710.
[463] J.-J. Young, L.-J. Jung, W.-T. Liu, S.-N. Ho, L.-R. Chang, Y.-C. Tsai, R. Bhaskaran, C. Yu, *J. Antibiot.* **1994**, *47*, 922 – 931.
[464] U. Schmidt, K. Neumann, A. Schumacher, S. Weinbrenner, *Angew. Chem.* **1997**, *109*, 1152 – 1154; *Angew. Chem. Int. Ed. Engl.* **1997**, *36*, 1110 – 1112.
[465] K. H. Michel, R. E. Kastner (Eli Lilly and Company), US 4492650, **1985**, [*Chem. Abstr.* **1985**, *102*, 130459].
[466] a) M. R. Maurizi, M. W. Thompson, S. K. Singh, S. H. Kim, *Methods Enzymol.* **1994**, *244*, 314 – 331; b) J. Wang, J. A. Hartling, J. M. Flanagan, *Cell* **1997**, *91*, 447 – 457.
[467] a) H. Brötz-Oesterhelt, D. Beyer, H.-P. Kroll, R. Endermann, C. Ladel, W. Schroeder, B. Hinzen, S. Raddatz, H. Paulsen, K. Henninger, J. E. Bandow, H. G. Sahl, H. Labischinski, *Nat. Med.* **2005**, *11*, 1082 – 1087; b) B. Hinzen, S. Raddatz, H. Paulsen, T. Lampe, A. Schumacher, D. Häbich, V. Hellwig, J. Benet-Buchholz, R. Endermann, H. Labischinski, H. Brötz-Oesterhelt, *ChemMedChem* **2006**, *1*, 689 – 693.
[468] J. Benet Buchholz, Bayer AG, unpublished results.
[469] B. Hinzen, H. Brötz, R. Endermann, K. Henninger, H. Paulsen, S. Raddatz, T. Lampe, V. Hellwig, A. Schumacher (Bayer AG), WO 03024996, **2003**, [*Chem. Abstr.* **2003**, *138*, 271978].
[470] U. Schmidt, A. Lieberknecht, H. Griesser, J. Talbiersky, *J. Org. Chem.* **1982**, *47*, 3261 – 3264.

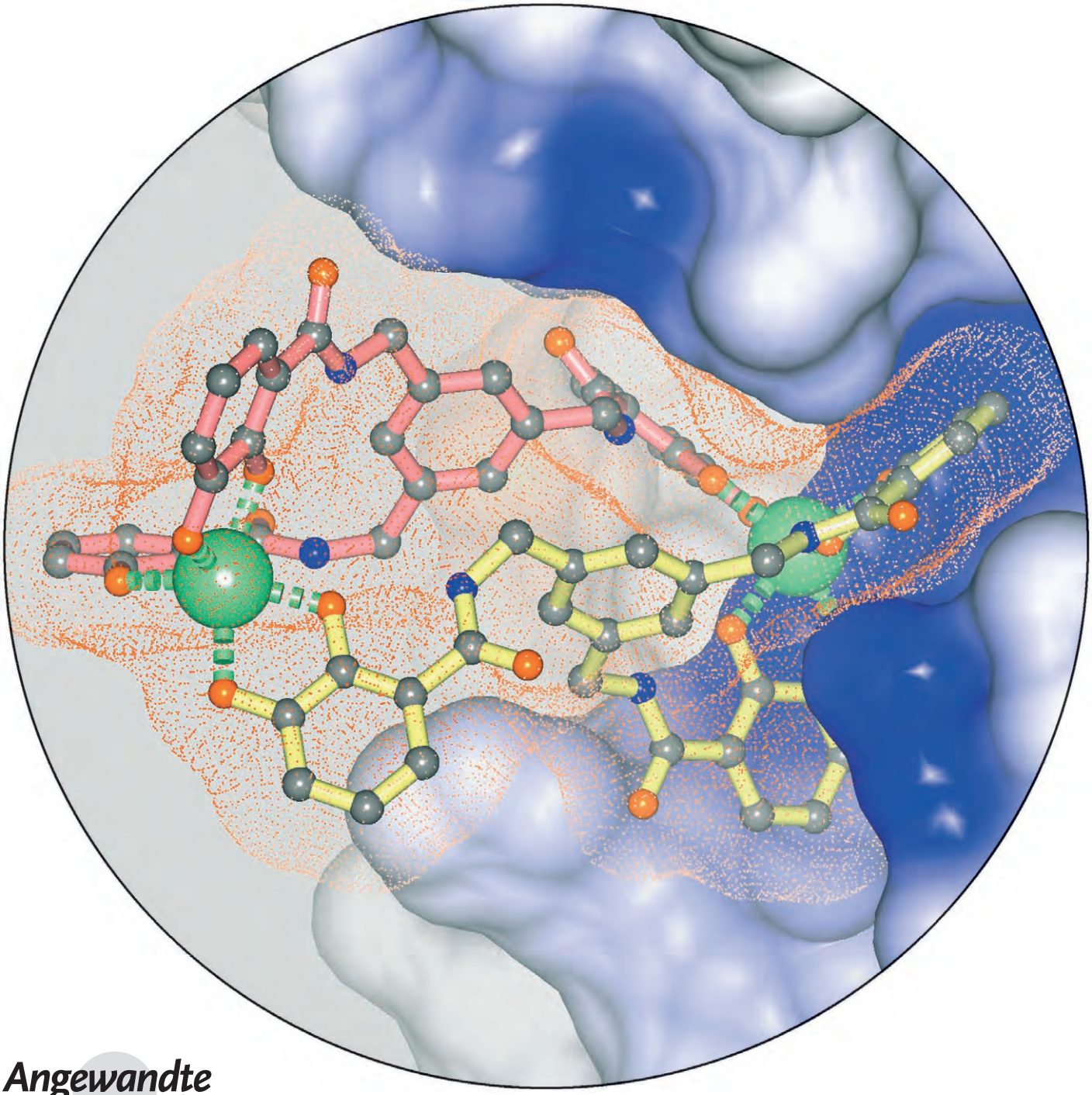
 © 2006 Wiley-VCH Verlag GmbH & Co. KGaA, Weinheim

Iron Complexes

DOI: 10.1002/anie.200601198

An $[\{Fe(mecam)\}_2]^{6-}$ Bridge in the Crystal Structure of a Ferric Enterobactin Binding Protein**

*Axel Müller, Anthony J. Wilkinson, Keith S. Wilson, and Anne-K. Duhme-Klair**



WILEY InterScience DISCOVER SOMETHING GREAT

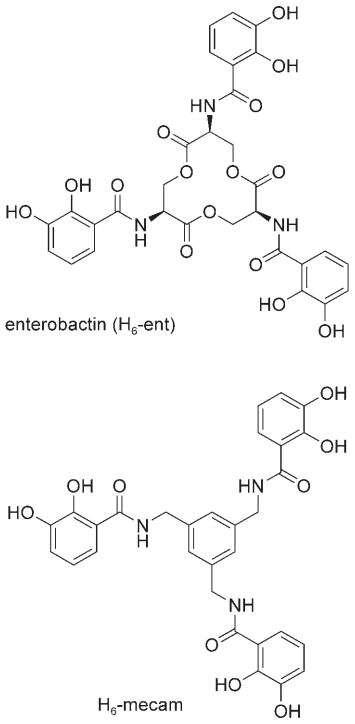
© 2006 Wiley-VCH Verlag GmbH & Co. KGaA, Weinheim

The control of self-assembly processes through noncovalent interactions is of immense importance in the area of bio-inspired supramolecular chemistry.[1] In particular, the exploration of interstrand π interactions to determine the nuclearity of helical metal complexes is currently attracting a lot of attention.[2,3] Here we present the crystal structure of the periplasmic ferric enterobactin binding protein CeuE of *Campylobacter jejuni* bound to Λ,Λ-[{Fe(mecam)}$_2$]$^{6-}$ (H_6-mecam = 1,3,5-*N*,*N*′,*N*″-tris(2,3-dihydroxybenzoyl)triaminomethylbenzene), which represents an intriguing example of a dinuclear ferric enterobactin mimic that is recognized stereoselectively by two identical protein molecules. The assembly is stabilized through hydrophobic interactions between the mesitylene spacers in the ligand backbone of the dinuclear iron complex.

C. jejuni is a leading cause of acute bacterial gastroenteritis. It is commensal in poultry, cattle, and swine and is normally transmitted to humans via contaminated poultry products or drinking water. To colonize the intestine of the host successfully, *C. jejuni* has to compete with other bacteria for essential nutrients, such as Fe.[4] To acquire Fe, *C. jejuni* uses a high-affinity uptake system, which relies on siderophores.[5] To maximize its chances of survival, *C. jejuni* takes advantage of several external siderophores adventitiously, including enterobactin (Scheme 1), the highly effective tris(catecholamide) siderophore of *Escherichia coli*.[6]

Enterobactin binds Fe^{III} with extremely high affinity ($\log\beta = 49$).[7] In Gram-negative bacteria, the Fe–enterobactin complex is recognized by a cell surface receptor protein[8] and transported into the periplasm, where it is captured by a periplasmic binding protein, CeuE in *C. jejuni*. The periplasmic ferric siderophore binding protein delivers the Fe–enterobactin complex to the inner membrane transporter for translocation into the cytoplasm.

As one of the most powerful iron chelators known, enterobactin has inspired the development of a range of synthetic tris(catecholamide) ligands, such as H_6-mecam[9] (Scheme 1). Like enterobactin, H_6-mecam relies on three catecholamide "arms" to chelate Fe^{III}, but the mesitylene backbone of H_6-mecam is hydrophobic and achiral while the tris(L-serine) backbone of enterobactin is hydrophilic and chiral. As H_6-mecam is easier to synthesize and more stable than the hydrolytically labile triester enterobactin, it has been used extensively to study various aspects of bacterial iron transport.[10,11] Ferric enterobactin and ferric mecam complexes, however, have so far eluded detailed structural characterization owing to their paramagnetism and the lack of good-quality single crystals. Crystal structures of Fe-tris(catecholamide) complexes are surprisingly rare, and a search of the Cambridge Structural Database revealed only one example, [Fe(trencam)]$^{3-}$,[12] in which the three Fe-binding catecholamides are attached to a triaminotriethylamine (tren) backbone.



Scheme 1. Enterobactin and its mimic, H_6-mecam.

Here, we determined the crystal structure of the periplasmic ferric enterobactin binding protein CeuE from *C. jejuni* in complex with ferric mecam. This structure is the first of a ferric mecam complex and the first to reveal the interactions of a periplasmic catecholamide siderophore receptor protein with its substrate (Figure 1). Remarkably, the siderophore mimic forms an [{Fe(mecam)}$_2$]$^{6-}$ dimer, which bridges a pair of CeuE molecules. This is a genuine bridge, as there are no protein–protein interactions in the (CeuE)$_2$-{Fe(mecam)}$_2$ assembly.

In the assembly, the two CeuE molecules are nearly identical and have bilobate structures characteristic of periplasmic binding proteins.[13] Each [Fe(catecholate)$_3$]$^{3-}$ recognition site of the central [{Fe(mecam)}$_2$]$^{6-}$ complex resides in a binding cleft between two α/β domains. The catecholate oxygen atoms interact with the positively charged sidechains of Arg117, Arg204, and Arg248, which balance the charge of the [Fe(catecholate)$_3$]$^{3-}$ unit (Figure 2). Although not apparent from the sequence, the overall structure of CeuE is very similar to that of FhuD, the periplasmic hydroxamate siderophore binding protein of *E. coli*.[14] In contrast to FhuD, the domain interface in CeuE is hydrophillic and selective for ferric catecholates, which are negatively charged.

[*] A. Müller, Prof. A. J. Wilkinson, Prof. K. S. Wilson, Dr. A.-K. Duhme-Klair
Department of Chemistry
University of York
York, YO10 5DD (UK)
Fax: (+44) 1904-432-587
E-mail: akd1@york.ac.uk

[**] This work was supported by EU SPINE (contract no. QLG2-CT-2002-00988). We thank the ESRF Grenoble for data collection and the EPSRC National Mass Spectrometry Service Centre in Swansea for measurements, as well as Prof. P. H. Walton, Prof. R. N. Perutz, Dr. A. Leech, J. Thompson, and H. Niblock for advice and/or experimental assistance. H_6-mecam = 1,3,5-*N*,*N*′,*N*″-tris(2,3-dihydroxybenzoyl)triaminomethylbenzene.

 © 2006 Wiley-VCH Verlag GmbH & Co. KGaA, Weinheim



Figure 1. Ribbon representation of two CeuE molecules bound to the $[\{Fe(mecam)\}_2]^{6-}$ dimer, which is highlighted in space-fill representation with the carbon atoms of the two $mecam^{6-}$ ligands distinguished by shading.

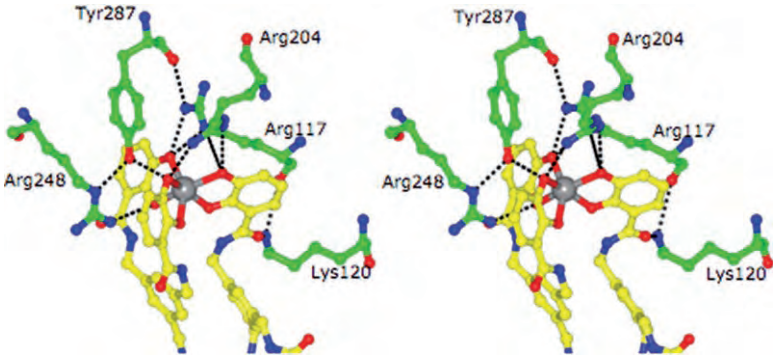


Figure 2. Stereoview showing the interactions of the binding pocket of CeuE (C green) with the $[Fe(catecholate)_3]^{3-}$ unit (C yellow, Fe gray).

Each iron atom in $[\{Fe(mecam)\}_2]^{6-}$ is coordinated by four oxygen donors from one mecam moiety and two from the other to result in a distorted octahedral coordination geometry (Figure 3). The Fe–O distances range from 1.9 to 2.2 Å. If we consider the resolution of the structure (2.4 Å), then these distances are in agreement with the distances found in $[Fe(trencam)]^{3-}$ (1.99 and 2.03 Å).[12] In the dimer, the aromatic rings of the two mecam backbones are nearly coplanar with an interplanar angle of 15°. The rings are significantly offset with one of the δ^+ methylene carbon atoms positioned over the center of the π electrons of the other ring—a geometry commonly observed in π-stacked systems.[15] The distance of 3.9 Å between the center of the aromatic ring and the methylene carbon atom indicates significant hydrophobic interactions.[15] Consequently, dimer formation appears to be favored by the hydrophobic nature of the mesitylene spacer of mecam, a structural feature of the mimic that is not present in enterobactin.

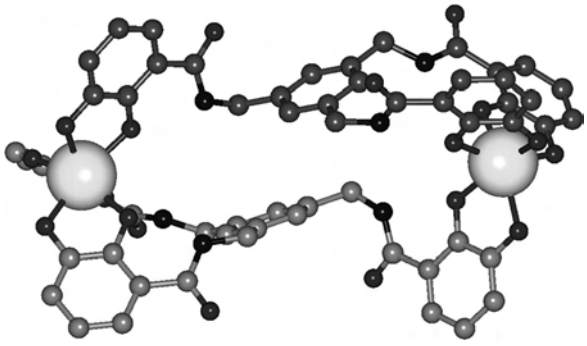


Figure 3. Ball-and-stick representation of the $[\{Fe(mecam)\}_2]^{6-}$ complex. Carbon atoms of the two $mecam^{6-}$ ligands are distinguished by shading, while hydrogen atoms are not shown.

In enterobactin, the conformation of the tris(serine) backbone would favor the hexadentate encapsulation of a single metal ion, a phenomenon that has been termed ligand predisposition.[16] Evidence for the mononuclear structure of $[Fe(ent)]^{3-}$ was obtained in vitro from NMR spectroscopic studies on the corresponding diamagnetic Ga^{III} complex,[17] crystallographic insights from the V^{IV} complex,[18] and MM3 calculations.[19]

In contrast to the tris(serine) and tren backbones, the aromatic spacer in mecam is planar and should allow the ligand to bind Fe^{III} in the form of a 1:1 or 2:2 complex or to form even larger aggregates. The immediate coordination environment of the Fe center is formally identical in these species. Information on the nuclearity of the Fe^{III} or Ga^{III} complexes formed by mecam in the absence of protein is not available in the literature. ^2H NMR spectroscopic studies on a mecam analogue with CD_3 groups in the 4-position of the catechol rings showed that upon Fe^{III} binding, only one paramagnetically shifted resonance was observed for the three CD_3 groups above pH 10,[20] indicating the formation of a C_3-symmetrical complex with equivalent catechol rings under these conditions. This result is consistent with the formation of a mononuclear complex, but also with a homochiral tetrahedral 4:4 complex[21b] or a mixture of different species in dynamic equilibrium on the NMR timescale.

In the presence of CeuE, dimerization to give $[\{Fe(mecam)\}_2]^{6-}$ is favored by hydrophobic interactions between the two spacer units which appear to outweigh the resulting sixfold negative charge of the metal complex, at least in forming the $(CeuE)_2$-$\{Fe(mecam)\}_2$ assembly, where the negative charge is countered by the protein, which minimizes the electrostatic repulsion in the dimer. A similar dependence of the nuclearity of metal complexes on spacer geometry and electrostatic effects is well documented for bis(catecholamide) complexes.[21] As these tetradentate ligands are unable to saturate the six coordination sites of Fe^{III} in a 1:1 complex, the formation of dinuclear triple-stranded $[Fe_2L_3]^{6-}$ helicates[22] or even tetrahedral $[Fe_4L_6]^{12-}$ clusters[21b] is observed. Which structure predominates depends on the type of spacer used.[21] If the geometrical constraints of the spacer are not unequivocal, mixtures of species are obtained and additional stabilizing effects, such as interactions with cationic guests,[23] π stacking,[2] solvent, and temperature,[24] determine the nuclearity.

 © 2006 Wiley-VCH Verlag GmbH & Co. KGaA, Weinheim

Interestingly, in contrast to enterobactin, mecam delivers very little Fe to the cytoplasm. Instead, the Fe–mecam complex accumulates in the periplasmic space.[25] Assuming that Fe–mecam dimerizes in the presence of CeuE in the periplasm as it does in the crystals described here, the formation of dimeric assemblies could explain the lack of further transport. The concentration of about 0.5 mM of CeuE-Fe-mecam used in the crystallization procedure lies within the typical concentration range of substrate-bound binding proteins found in the periplasmic space.[13] Alternatively, the lack of further transport could be attributed to the protonation of one of the *meta*-hydroxy oxygen atoms in the Fe–mecam complex[20] ($\log K_{FeHmecam} = 7.08$) in the slightly acidic periplasm, preventing transport across the inner membrane, as previously suggested.[25]

Another remarkable feature of the structure of the $(CeuE)_2$-$\{Fe(mecam)\}_2$ assembly is the chirality of the Fe centers. Both $[Fe(catecholate)_3]^{3-}$ recognition sites in the crystal structure of $[\{Fe(mecam)\}_2]^{6-}$ have the same chirality (Λ), resulting in a helical structure of the complex. This preference for the Λ configuration is retained in solution, as indicated by the circular dichroism (CD) spectrum in the region of the ligand-to-metal charge-transfer bands (Figure 4). A negative band around 450 nm and a positive band around 560 nm are characteristic of a tris(catecholamide) complex with Λ chirality.[26] As mecam is achiral and there are no direct contacts between the two CeuE molecules that could induce a helical twist in the complex, this preference results from interactions with the substrate-binding pocket of the protein.

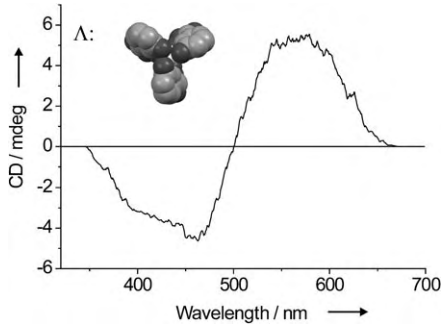


Figure 4. CD spectrum of the $(CeuE)_2$·$\{Fe(mecam)\}_2$ complex in buffer at pH 7.7. Inset: space-fill representation of the $[Fe(catecholate)_3]^{3-}$ unit illustrating the Λ configuration.

In contrast, the iron–enterobactin complex has been shown to adopt a Δ configuration induced by the chirality of the tris(L-serine) backbone. Correspondingly, the CD spectrum of the ferric enterobactin complex shows a positive band around 420 nm and a negative band at 530 nm.[26] According to reported experimental evidence,[17–19,26] ferric enterobactin is a mononuclear complex with Δ configuration in vitro, but it cannot be entirely excluded that ferric enterobactin may change configuration or even dimerize in the presence of a periplasmic binding protein. That ferric enterobactin can change configuration upon binding to a protein is evident from the crystal structure of the adduct between $[Fe(ent)]^{3-}$ and the lipocalin protein NGAL, in which the conformation of the Fe–tris(catecholamide) unit is Λ (PDB code 1L6M). It should be mentioned though that in the structure the chiral tris(L-serine) backbone was partially degraded.[27]

In conclusion, we have determined the crystal structure of a dimeric $(CeuE)_2$-$\{Fe(mecam)\}_2$ assembly that reveals interactions between the periplasmic binding protein CeuE of *C. jejuni* and a ferric enterobactin mimic, $[\{Fe(mecam)\}_2]^{6-}$. The protein induces Λ chirality at the Fe centers and balances the negative charge of the complex. The mesitylene spacer in the backbone of mecam, which differentiates the mimic from enterobactin, gives rise to hydrophobic interactions that favor the formation of the dimeric assembly. These results emphasize the importance of the backbone structure and chirality in the design of siderophore mimics.

Experimental Section

H_6-mecam was synthesized according to a reported procedure.[9b] M.p.: 129–133 °C; ^{1}H NMR (400 MHz, [D$_6$]DMSO): $\delta = 4.46$ (d, 6H, $J = 6$ Hz, CH_2-NH), 6.66 (t, 3H, $J = 8$ Hz, ArH-cat), 6.75 (dd, 3H, $J = 1$ Hz, 8 Hz, ArH-cat), 7.19 (s, 3H, ArH-mes), 7.29 (dd, 3H, $J = 1$ Hz, 8 Hz, ArH-cat), 9.38 ppm (t, 3H, $J = 6$ Hz, NH); ESI-MS (MeOH): *m/z* (%): 572.1 (100) $[M-H]^-$; elemental analysis (%) calcd for $C_{30}H_{27}N_3O_9 \cdot 0.5\,H_2O$: C 61.85, H 4.84, N 7.21; found: C 61.48, H 4.86, N 7.14.

The Fe^{III} complex of mecam was prepared by adding a solution of H_6-mecam (23 mg, 0.04 mmol) in methanol (1.25 mL) to a solution of $FeCl_3 \cdot 6\,H_2O$ (11 mg, 0.04 mmol) in H_2O (250 μL). The resulting dark purple solution was evaporated to dryness to afford a purple powder. ESI-MS (MeOH, apparent pH 3): *m/z* (%): 625.1 (100) $[M+2H]^-$, 647.1 (60) $[M+H+Na]^-$. HR ESI-MS: *m/z* calcd for $C_{30}H_{22}N_3O_9FeNa$: 647.0609; found: 647.0615. The absorption spectrum at pH 8 matched the one previously reported.[9b]

The crystal structure of $[\{Fe(mecam)\}_2]^{6-}$·$(CeuE)_2$ was refined against an X-ray data set, which is 92% complete to 2.4-Å spacing and consists of 23425 unique reflections. The model has a working *R* factor of 0.17, a free *R* factor of 0.25, $rms_{bond} = 0.019$, and $rms_{angle} = 1.6°$. There are no Ramachandran outliers. Figures were generated with CCP4mg.[28] The atomic coordinates and X-ray crystal structure factor data have been deposited in the Protein Data Bank with the accession code 2chu. Details of protein expression, X-ray data collection, and refinement can be found in this deposition.

Received: March 26, 2006
Revised: May 15, 2006

Keywords: iron · N,O ligands · proteins · self-assembly · siderophores

[1] D. N. Reinhoudt, M. Crego-Calama, *Science* **2002**, *295*, 2403–2407.
[2] L. J. Childs, M. Pascu, A. J. Clarke, N. W. Alcock, M. J. Hannon, *Chem. Eur. J.* **2004**, *10*, 4291–4300.
[3] N. W. Alcock, G. Clarkson, P. B. Glover, G. A. Lawrance, P. Moore, M. Napitupulu, *Dalton Trans.* **2005**, 518–527.
[4] A. H. M. van Vliet, J. M. Ketley, S. F. Park, C. W. Penn, *FEMS Microbiol. Rev.* **2002** *26*, 173–186.
[5] Reviews in "Iron Transport and Storage in Microorganisms, Plants and Animals": *Metal Ions in Biological Systems*, *Vol. 35* (Eds.: A. Sigel, H. Sigel), Marcel Dekker, New York, **1999**.
[6] K. Palyada, D. Threadgill, A. Stintzi, *J. Bacteriol.* **2004**, *186*, 4714–4729.

 © 2006 Wiley-VCH Verlag GmbH & Co. KGaA, Weinheim

[7] L. D. Loomis, K. N. Raymond, *Inorg. Chem.* **1991**, *30*, 906 – 911.
[8] S. K. Buchanan, B. S. Smith, L. Venkatramani, D. Xia, L. Esser, M. Palnitkar, R. Chakraborty, D. van der Helm, J. Deisenhofer, *Nat. Struct. Biol.* **1999**, *6*, 56 – 63.
[9] a) M. C. Venuti, W. H. Rastetter, J. B. Neilands, *J. Med. Chem.* **1979**, *22*, 123 – 124; b) F. L. Weitl, K. N. Raymond, *J. Am. Chem. Soc.* **1979**, *101*, 2728 – 2731.
[10] T. J. Brickman, M. A. McIntosh, *J. Biol. Chem.* **1992**, *267*, 12350 – 12355.
[11] D. J. Ecker, L. D. Loomis, M. E. Cass, K. N. Raymond, *J. Am. Chem. Soc.* **1988**, *110*, 2457 – 2464.
[12] T. D. P. Stack, T. B. Karpishin, K. N. Raymond, *J. Am. Chem. Soc.* **1992**, *114*, 1512 – 1514.
[13] A. J. Wilkinson, K. H. G. Verschueren, *ABC Proteins: From Bacteria to Man*, Elsevier, Dordrecht, **2003**, chap. 10, 187 – 207.
[14] T. E. Clarke, S.-Y. Ku, D. R. Dougan, H. H. Vogel, L. W. Tari, *Nat. Struct. Biol.* **2000**, *7*, 297 – 291; T. E. Clarke, V. Braun, G. Winkelmann, L. W. Tari, H. J. Vogel, *J. Biol. Chem.* **2002**, *277*, 13966 – 13972.
[15] C. Janiak, *J. Chem. Soc. Dalton Trans.* **2000**, 3885 – 3896.
[16] Z. Hou, T. D. P. Stack, C. J. Sunderland, K. N. Raymond, *Inorg. Chim. Acta* **1997**, *263*, 341 – 355.
[17] M. Llinas, D. M. Wilson, J. B. Neilands, *Biochemistry* **1973**, *12*, 3836 – 3843.
[18] T. P. Karpishin, T. M. Dewey, K. N. Raymond, *J. Am. Chem. Soc.* **1993**, *115*, 1842 – 1851.
[19] B. P. Hay, D. A. Dixon, R. Vargas, J. Garza, K. N. Raymond, *Inorg. Chem.* **2001**, *40*, 3922 – 3935.
[20] M. E. Cass, T. M. Garrett, K. N. Raymond, *J. Am. Chem. Soc.* **1989**, *111*, 1677.
[21] Reviews: a) M. Albrecht, *Chem. Soc. Rev.* **1998**, *27*, 281 – 287; b) D. L. Caulder, K. N. Raymond, *Acc. Chem. Res.* **1999**, *32*, 975 – 982; c) S. Leininger, B. Olenyuk, P. J. Stang, *Chem. Rev.* **2000**, *100*, 853 – 908; d) M. J. Hannon, L. J. Childs, *Supramol. Chem.* **2004**, *16*, 7 – 22.
[22] E. J. Enemark, T. D. P. Stack, *Inorg. Chem.* **1996**, *35*, 2719 – 2720.
[23] M. Scherer, D. L. Caulder, D. W. Johnson, K. N. Raymond, *Angew. Chem.* **1999**, *111*, 1689 – 1694; *Angew. Chem. Int. Ed.* **1999**, *38*, 1587 – 1592.
[24] A.-K. Duhme, *J. Chem. Soc. Dalton Trans.* **1997**, 773 – 778.
[25] B. Matzanke, E. J. Ecker, T. S. Yang, B. H. Huynh, G. Müller, K. N. Raymond, *J. Bacteriol.* **1986**, *167*, 674 – 680.
[26] T. B. Karpishin, T. D. P. Stack, K. N. Raymond, *J. Am. Chem. Soc.* **1993**, *115*, 6115 – 6125.
[27] D. H. Goetz, M. A. Holmes, N. Borregaard, M. E. Bluhm, K. N. Raymond, R. K. Strong, *Mol. Cell* **2002**, *10*, 1033 – 1043.
[28] E. Potterton, S. McNicholas, E. Krissinel, K. Cowtan, M. Noble, *Acta Crystallogr. Sect. B* **2002**, *58*, 1955 – 1957.

 © 2006 Wiley-VCH Verlag GmbH & Co. KGaA, Weinheim

Enzyme Models

DOI: 10.1002/anie.200600802

Substrate Distortion by a Lichenase Highlights the Different Conformational Itineraries Harnessed by Related Glycoside Hydrolases**

*Victoria A. Money, Nicola L. Smith, Adrian Scaffidi, Robert V. Stick, Harry J. Gilbert, and Gideon J. Davies**

The conformational itineraries, adopted by the more than twenty thousand glycosidases, present an emerging picture that these enzymes adopt a variety of specific reaction pathways.[1] Catalytic itineraries for the enzymatic hydrolysis of glycosides likely feature one of four transition-state pyranoside-ring conformations: one of two classical boats ($B_{2,5}$ and $^{2,5}B$) or one of two half chairs ($^{4}H_{3}$, $^{3}H_{4}$, and/or their closely related envelope forms ^{4}E and ^{3}E).[2] Considerations of the conformational aspects of the transition state are becoming central to the development of specific transition-state mimics both as mechanistic and cellular probes and as therapeutic agents.[3] A central question is raised by these conformational pathways: is the (on-enzyme) transition-state structure dictated solely by the chemistry of the parent glycoside, the topography of the enzyme active centre, or a subtle interplay of both? The glycoside hydrolase family GH26 provides a powerful system to investigate these issues as, although most of its members are β-mannanases,[4] it has recently been shown that select GH26 enzymes are specific for "gluco-configured" substrates, notably β-1,3:β-1,4 mixed-linkage β-glucan lichenan[5] and β-1,3 linked xylan.[6] Herein we present a series of enzymatic snapshots along the reaction coordinate of a family GH26 lichenase from *Clostridium thermocellum*, hereafter named *Ct*Lic26A. The Michaelis complex of this enzyme with unhydrolyzed methylumbelliferyl β-laminaribioside **1** reveals a conformation between $^{1}S_{3}$ (skew) and $^{1,4}B$, whereas the covalent reaction intermediate, trapped through the use of the 1,2-difluoro trisaccharide **2**, is

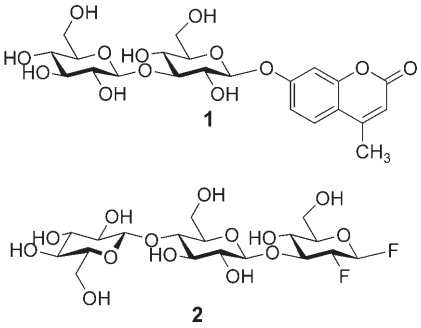
[*] Dr. V. A. Money, Prof. G. J. Davies
York Structural Biology Laboratory
Department of Chemistry
University of York, York YO10 5YW (UK)
Fax: (+44) 1904-328-266
E-mail: davies@ysbl.york.ac.uk
Dr. N. L. Smith, Prof. H. J. Gilbert
Institute for Cell and Molecular Biosciences
University of Newcastle upon Tyne
Newcastle upon Tyne NE2 4HH (UK)
A. Scaffidi, Prof. R. V. Stick
Chemistry M313
School of Biomedical, Biomolecular and Chemical Sciences
The University of Western Australia
35 Stirling Hwy, Crawley WA 6009 (Australia)

[**] This work was supported by the Biotechnology and Biological Sciences Research Council (BBSRC).

Supporting information for this article is available on the WWW under http://www.angewandte.org or from the author.

WILEY InterScience DISCOVER SOMETHING GREAT
© 2006 Wiley-VCH Verlag GmbH & Co. KGaA, Weinheim

found in the $^4C_1$ (chair) conformation. These conformations are in stark contrast to the $^1S_5$ and $^{O}S_2$ conformations observed for the equivalent complexes of the closely related β-mannanases from this family.[4] These observations strongly suggest that individual, even closely related, enzymes harness different conformational itineraries that are necessarily a composite both of enzyme structure and glycoside chemistry.



*Ct*Lic26A is a lichenase whose favored substrates are mixed linkage β-1,3:β-1,4 glucans.[5] Catalysis occurs with net retention of the anomeric configuration through the formation (glycosylation) and subsequent breakdown (deglycosylation) of a covalent glycosyl-enzyme intermediate that is flanked on either side by oxocarbenium-ion-like transition states. Such a reaction demands two essential catalytic groups: a nucleophile and an acid/base that, in this family, are both enzyme-derived carboxylates. The sequence of the enzyme is classified into the glycoside hydrolase (GH) family 26, a family more normally associated with β-mannanases. This classification remained even though the 3D structure[5] has shown it to be a "clan GH-A" enzyme[7] with a characteristic $(\beta/\alpha)_8$ barrel and the signature catalytic constellation of catalytic acid/base and nucleophile on strands β-4 and β-7, respectively. The Michaelis complex of *Ct*Lic26A was trapped by using methylumbelliferyl-β-laminaribioside **1** in conjunction with an inactive enzymatic variant in which the catalytic nucleophile Glu 222 was replaced by glutamine: cocrystallization of Glu 222 Gln *Ct*Lic26A with **1** afforded the Michaelis complex with the X-ray structure solved to 1.4 Å resolution. Similarly, preincubation of the acid/base Glu 109 Ala mutant of *Ct*Lic26A with the 1,2-difluoro trisaccharide **2**, followed by crystallization, allowed crystallographic observation of the trapped 2-fluoroglycosyl enzyme intermediate, which was also observed at a resolution of 1.4 Å.

The structure of the Michaelis complex clearly reveals the unhydrolyzed substrate, at full occupancy, distorted into an approximate $^1S_3$ conformation with an axial leaving group, fulfilling the stereoelectronic requirements of an incipient oxocarbenium-ion-like species and with the "nucleophile" poised, in what might be termed a "near-attack conformation",[8] for in-line attack at the anomeric centre, Figure 1. Such a structure is also consistent with the dictates of the antiperiplanar lone-pair hypothesis.[9] Similarly, the covalent glycosyl-enzyme intermediate, stabilized both through the 2-fluoro substituent and by the lack of an appropriate catalytic base for the deglycosylation step, lies in a relaxed $^4C_1$ conformation, Figure 1.

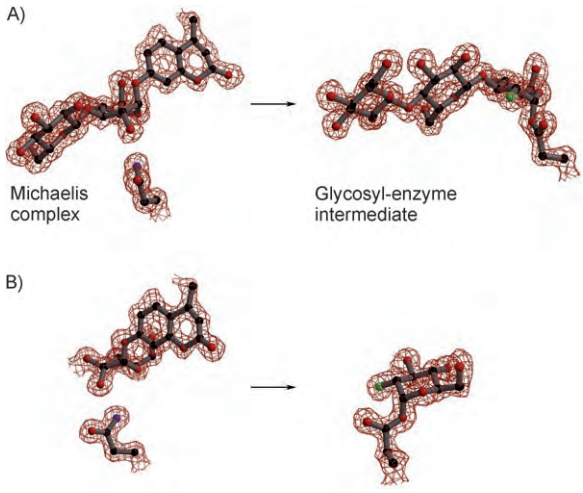
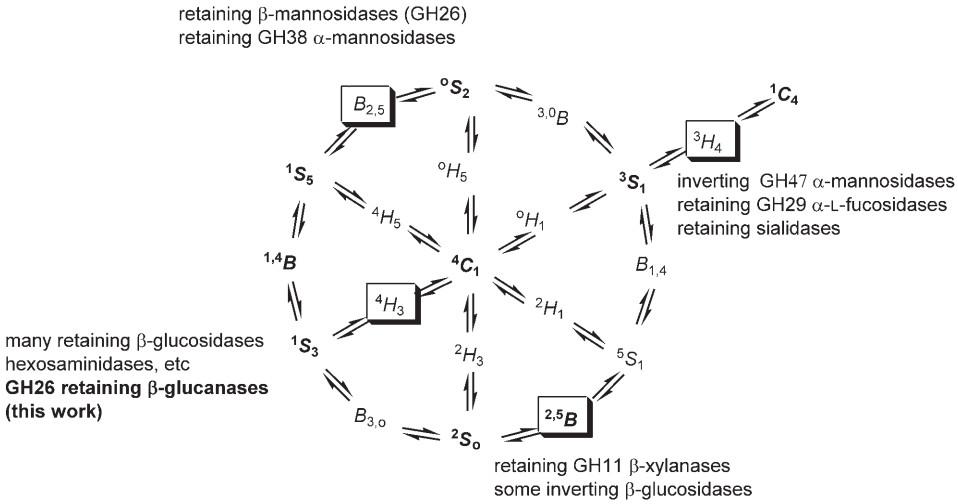


Figure 1. Side-on (A) and end-on (B) views of the trapped Michaelis and glycosyl-enzyme intermediate complexes for *Ct*Lic26A. For the end-on views, only the −1 subsite pyranoside is shown for clarity, together with the methylumbelliferyl group for the Michaelis complex. Electron density shown is a $2F_{obs}-F_{calcd}$ synthesis contoured at approximately 1σ (0.55 electrons/Å^2).

These two structures, representing "snapshots" along the glycosylation reaction coordinate of *Ct*Lic26A, are similar to those observed previously for some GH5 (also Clan GH-A) β-glycosidases active on gluco-configured substrates.[10] They are thus consistent with a $^4H_3$ (or the closely related ^4E) conformation for the transition state, which is flanked by the $^1S_3$ and $^4C_1$ conformations in the classical pyranoside interconversion agenda, Scheme 1. Catalysis is thus likely to occur through a simple "electrophilic migration"[11] of the anomeric carbon along the reaction coordinate. Notably, however, the $^1S_3 \rightarrow {}^4H_3 \rightarrow {}^4C_1$ migration for the family GH26 lichenase is not observed in β-mannoside hydrolysis by β-mannanase *Cj*Man26A (β-mannanase is the predominant activity displayed by GH26 enzymes) from this family.[4]

Previously, X-ray crystallography had been used to take a series of enzymatic "snapshots" along the reaction coordinate of *Cj*Man26A. Observation of an unusual $^1S_5$ conformation for the Michaelis complex of unhydrolyzed substrate suggested that the conformationally adjacent $B_{2,5}$ conformation might be that adopted by the reaction transition state. Subsequent trapping of the covalent reaction intermediate in an $^{O}S_2$ conformation lent strong credence to this proposal as $^1S_5$ and $^{O}S_2$ conformations flank $B_{2,5}$ in the pyranoside interconversion agenda, see Scheme 1. Catalysis is again considered as an "electrophilic migration" of C1, through a $B_{2,5}$ transition state, consistent with the principle of least molecular motion. Furthermore, it was evident that such a transition state for enzymatic mannoside hydrolysis has an additional advantage in that it places O2 pseudoequatorial, therefore relieving unfavorable 1,2 diaxial effects for nucleophilic substitution at the anomeric carbon. Additional evidence for the relevance of the $B_{2,5}$ conformation comes from the observations that D-mannono-1,5-lactone and 5-

 © 2006 Wiley-VCH Verlag GmbH & Co. KGaA, Weinheim



Scheme 1. Pyranoside interconversion itinerary with likely reaction coordinates for the different glycosidases shown. Potential transition states are shown boxed and conformations observed "on-enzyme" in crystal structures are indicated in bold.[1,12] Retaining sialidases are believed to use what equates to the $^{3}S_{1}\rightarrow{}^{3}H_{4}\rightarrow{}^{1}C_{4}$ pathway ($^{5}S_{2}\rightarrow{}^{4}H_{5}\rightarrow{}^{2}C_{5}$).[13]

amino-5-deoxy-D-mannono-1,5-lactam, both sp^2 hybridized at C1, also favor this unusual boat conformation.[14] The proposal of a $^{1}S_{5}\rightarrow B_{2,5}\rightarrow{}^{O}S_{2}$ conformational change for a retaining β-mannanase predicted both that retaining α-mannosidases could utilize a "reverse" conformational agenda ($^{O}S_{2}\rightarrow B_{2,5}\rightarrow{}^{1}S_{5}$) and that these enzyme classes should be inhibited by compounds featuring "pseudoequatorial" groups at C2. Subsequently, the β-linked covalent intermediate for the family of GH38 retaining α-mannosidases has indeed been observed in $^{1}S_{5}$ conformation[15] and likewise, a significant number of compounds with "pseudoequatorial" C2 substituents have been shown to be inhibitors of β-mannosidases.[12,14,16]

One of the important, indeed controversial, aspects of glycosidase catalysis is whether sequence and structurally related enzymes working on different glycoside substrates adopt similar, or markedly different, conformational approaches to catalysis; does the enzyme, the substrate, or a subtle interplay of both dictate the catalytic itinerary and transition-state conformation? Comparison of the family GH26 β-mannanases and lichenses that are specific for manno- and gluco-configured substrates, respectively, in the light of wider work on other glycosidase families, suggests that the conformational agenda adopted is necessarily a subtle interplay of enzyme-structure-derived geometric constraints and the stereoelectronic and steric dictates of the substrate. X-ray crystal structure observations have certainly revealed that structurally, and therefore evolutionarily, related enzymes do not necessarily adopt the same catalytic pathways. The geometry of the substrate alone, however, does not dictate its reaction pathway; there is strong evidence that inverting α-mannosidases (family GH47) instead harness a $^{3}H_{4}$ transition state,[17,18] whereas some inverting β-glucosidases are believed to harness a $^{O}S_{2}\rightarrow{}^{2,5}B$ pathway (for an example, see reference [19]). For β-xylanases, we again see employment of different conformational pathways: GH10 enzymes are believed to perform catalysis through a $^{4}H_{3}$ transition state, whereas structurally-unrelated GH11 enzymes may harness a $^{2,5}B$ conformation,[20] see Scheme 1. Given the increasing number of examples, we propose that structurally related enzymes working on similar substrates are likely to harness the same conformational pathways, but that related enzymes working on chemically different sugars may harness alternative agendas that reflect the chemistry of their substrate.

What then governs the specificity of a clan GH-A enzymes? We have previously commented[4,12] that the interactions around C1 and O2 of enzymes acting on gluco- (including xylose) and manno-configured substrates are extremely similar. This is again the case here. Both GH26 gluco- and manno-specific enzymes display near identical geometry for the catalytic acid, nucleophile, and the O2-interaction residue (histidine in GH26 enzymes, although it is normally asparagine in clan GH-A [7]), see Figure 2 A. The conservation of the O2-interaction geometry strongly sug-

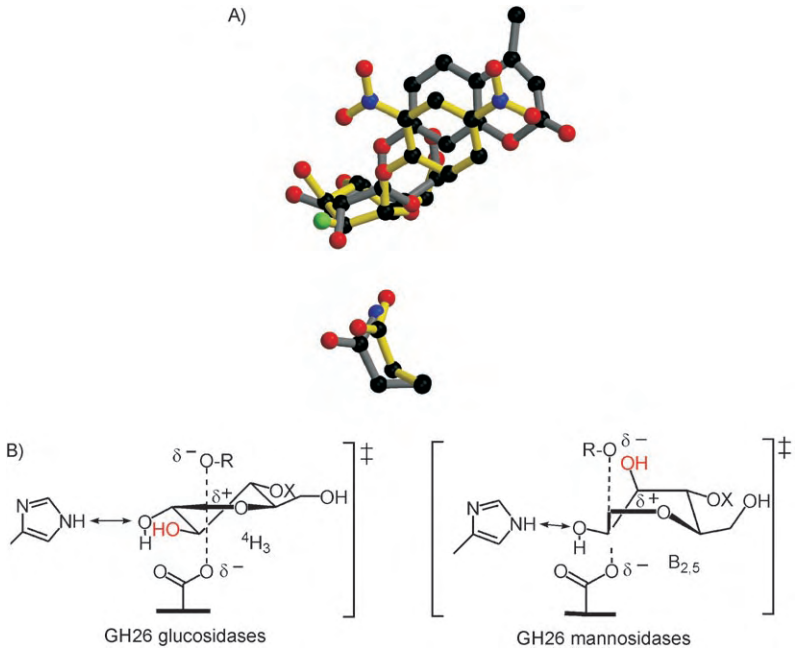


Figure 2. A) Overlap of the "Michaelis" complexes for manno- and gluco-specific enzymes from family GH26 (*Ct*Lic26A, gray; *Cj*Man26A, yellow). B) Comparison of (predicted) $^{4}H_{3}$ and $B_{2,5}$ transition states for glucoside and mannoside hydrolysis by clan GH-A enzymes (O3, discussed in the text below, is indicated in red as a reference).

 © 2006 Wiley-VCH Verlag GmbH & Co. KGaA, Weinheim

gests that O2 lies pseudoequatorial during the hydrolysis of both glucosides and mannosides, again consistent both with $^4H_3$ and $B_{2,5}$ conformations for their respective transition states (Figure 2B) and with the potential for interaction of O2 with the catalytic nucleophile.

The comparison of GH26 gluco- and manno-specific enzymes provides support for an earlier hypothesis that the interactions and environment of O3 contribute to the specificity and reaction coordinate. O3 is the atom whose position differs significantly between $^4H_3$ and $B_{2,5}$ transition states in which O3 lies equatorial in $^4H_3$, but pseudoaxial (and "up") in the latter. Comparison of glucosidases and mannosidases suggested that the O3 interacting residues of these two classes lie in different positions. The requirement for direct hydrogen-bonding groups tethering O3 is less important in the case of *Ct*Lic26A, as O3 is restrained to an equatorial position by virtue of the β-1,3 glycosidic linkage to the adjacent sugar.

The conformation of the reaction transition state is crucial if one is to harness the extremely tight binding of the transition state (resulting from the amazing catalytic proficiency of these enzymes) for specific enzyme inhibition in a therapeutic context. In this light, the inhibition of Golgi α-mannosidases is emerging as a potential anti-cancer target.[21–23] Mannosidase II action is a prerequisite for the action of Golgi β-1,6-*N*-acetylglucosaminyltransferase V (MGAT5). This latter enzyme plays a key role in malignancy and cancer progression, with MGAT5-deficient mice exhibiting suppressed tumor growth and metastasis.[24] The evidence strongly points to retaining α-mannosidases that display the same, but reversed, conformational pathway as the family GH26 retaining β-mannanases. This leads to the possibility of specific, targeted inhibition of clinically relevant enzymes. In this context, a large number of mannosidase inhibitors have been proposed in recent times with amidines,[25] pyridines[26] and isoquinuclidines,[27] and functionalized mannostatin and aminocyclopentitetrol analogues[21] that are notable for their binding to mannosidases.

Herein we have shown that related family GH26 enzymes acting on gluco-configured substrates offer an alternative catalytic pathway, with the flanking snapshots of a Michaelis complex and intermediate suggesting catalysis progress through a $^4H_3$ (or related ^4E) transition state. This work contributes to the evolving landscape of conformational pathways and provides further incentive to develop powerful and specific transition-state mimics as drug candidates for the future. General rules are certainly beginning to emerge. Whether an enzyme is "*exo*" or "*endo*" in activity may also play a significant role. One would predict that *exo*-acting enzymes, in which the glycon sugar is not tethered to an extended oligo- or polysaccharide chain, are able to explore a larger conformational space than *endo*-acting enzymes whose −1 subsite glycon is necessarily restrained by the oligosaccharide chain to which it is linked. The chemistry of the sugar, although important, does not dominate: there is strong evidence for both $B_{2,5}$ and $^3H_4/^3E$ transition states for mannoside hydrolysis and both $^4H_3$ and $^{2,5}B$ for the hydrolysis of gluco-configured substrates. Similarly, the evolutionary origin and structure of the enzyme is not overriding; only subtle changes in the enzyme are observed for GH-A clan enzymes in order for them to favor different conformational pathways for the hydrolysis of mannosides or glucosides.

Experimental Section

Compound **1** was purchased from Sigma-Aldrich. The synthesis of compound **2** will be described shortly. E109A *Ct*Lic26A was prepared, according to reference [5], in the non-His-tagged form that is suitable for ligand-binding studies. Amino acid substitution of the catalytic nucleophile E222 of *Ct*Lic26A to Gln (E222Q) was generated by the QuickChange site-directed mutatgenesis kit (Stratagene) by using pCF1 as template DNA and primers 5′ CCCATCATTATAGCACAGTTTGCATCAGCTGAAATAGGCG 3′ and 5′ CGCCTATTTCAGCTGATGCAAACTGTGCTATAATGATGGG 3′. The plasmid pCF1 (Taylor et al., 2005), which is a recombinant of pET21a, encodes protein *Ct*Lic26As, which does not contain a His tag. *E. coli* strain BL21 (DE3), harboring the recombinant plasmid, was cultured in Luria—Berton (LB) containing ampicillin (50 μg mL^{-1}) at 37 °C to an A_{600} of 0.6, and expression was induced by addition of isopropyl-1-thio-β-D-galactopyranoside to a final concentration of 1.0 mM and incubated for an additional 5 h at 37 °C. *Ct*Lic26A E222Q was purified from material released from osmotic shock by anion-exchange chromatography followed by size-exclusion chromatography.

E109A *Ct*Lic26A was preincubated with powdered **2** and crystallized in ammonium sulfate (0.15 M), polyethylene glycol (PEG) 5 K monomethyl ether (30%; w/v) buffered to pH 6.5 with 100 mM 2-(4-morpholinyl)ethanesulfonic acid (MES). Crystals of E222Q *Ct*Lic26A were obtained in a similar manner with the inclusion of **1** instead of **2**. X-ray crystal data for E109A *Ct*Lic26A with **2** were collected on beamline ID14-4 of the European Synchrotron Radiation Facility (ESRF) to 1.4 Å resolution. Data were processed with MOSFLM from the CCP4[28] suite. The data are 99.8% (98.9) complete with an R_{merge} of 0.053 (0.17), a mean $I/\sigma I$ of 19.3 (8.0), and multiplicity of observation of 4.8 (3.9) (outer resolution shell data in parentheses). For E222Q *Ct*Lic26A with **1** the X-ray diffraction data were collected on ID14-4 at the ESRF and are 99.9% complete with an R_{merge} of 0.047 (0.242), a mean $I/\sigma I$ of 22 (4.3), and a multiplicity of 4.8 (3.5). Both data sets show very low overall B values reflecting well-ordered crystals. The structures were refined with REFMAC[29] (E109A with **2**, final R_{cryst}/R_{free} of 0.15/0.18; E222Q with **1**, final R_{cryst}/R_{free} of 0.15/0.18). Structural figures were drawn with BOBSCRIPT.[30]

A full table of X-ray crystal data and structure quality data is provided in the Supporting Information.

Received: March 1, 2006
Published online: July 5, 2006

Keywords: drug design · enzyme models · glycosides · reaction pathways · transition states

[1] G. J. Davies, V. M.-A. Ducros, A. Varrot, D. L. Zechel, *Biochem. Soc. Trans.* **2003**, *31*, 523.
[2] G. Davies, M. L. Sinnott, S. G. Withers in *Comprehensive Biological Catalysis, Vol. 1* (Ed.: M. L. Sinnott), Academic Press, London, **1997**, p. 119.
[3] A. Vasella, G. Davies, M. Böhm, *Curr. Opin. Chem. Biol.* **2002**, *6*, 619.
[4] V. Ducros, D. L. Zechel, G. N. Murshudov, H. J. Gilbert, L. Szabo, D. Stoll, S. G. Withers, G. J. Davies, *Angew. Chem.* **2002**, *114*, 2948; *Angew. Chem. Int. Ed.* **2002**, *41*, 2824.
[5] E. J. Taylor, A. Goyal, C. I. P. D. Guerreiro, J. A. M. Prates, V. Money, N. Ferry, C. Morland, A. Planas, J. A. Macdonald, R. V.

 © 2006 Wiley-VCH Verlag GmbH & Co. KGaA, Weinheim

Stick, H. J. Gilbert, C. M. G. A. Fontes, G. J. Davies, *J. Biol. Chem.* **2005**, *280*, 32761.
[6] F. Okazaki, Y. Tamaru, S. Hashikawa, Y. T. Li, T. Araki, *J. Bacteriol.* **2002**, *184*, 2399.
[7] B. Henrissat, I. Callebaut, S. Fabrega, P. Lehn, J. P. Mornon, G. Davies, *Proc. Natl. Acad. Sci. USA* **1995**, *92*, 7090.
[8] T. Bruice, *Acc. Chem. Res.* **2002**, *35*, 139.
[9] P. Deslongchamps, *Stereoelectronic Effects in Organic Chemistry*, Pergamon, Oxford, **1983**.
[10] G. J. Davies, L. Mackenzie, A. Varrot, M. Dauter, A. M. Brzozowski, M. Schulein, S. G. Withers, *Biochemistry* **1998**, *37*, 11707.
[11] D. J. Vocadlo, G. J. Davies, R. Laine, S. G. Withers, *Nature* **2001**, *412*, 835.
[12] F. Vincent, T. M. Gloster, J. Macdonald, C. Morland, R. V. Stick, F. M. V. Dias, J. A. M. Prates, C. M. G. A. Fontes, H. J. Gilbert, G. J. Davies, *ChemBioChem* **2004**, *5*, 1596.
[13] M. F. Amaya, A. G. Watts, T. Damager, A. Wehenkel, T. Nguyen, A. Buschiazzo, G. Paris, A. C. Frasch, S. G. Withers, P. M. Alzari, *Structure* **2004**, *12*, 775.
[14] Z. Walaszek, D. Horton, I. Ekiel, *Carbohydr. Res.* **1982**, *106*, 193.
[15] S. Numao, D. A. Kuntz, S. G. Withers, D. R. Rose, *J. Biol. Chem.* **2003**, *278*, 48074.
[16] V. H. Lillelund, H. Z. Liu, X. F. Liang, H. Søhoel, M. Bols, *Org. Biomol. Chem.* **2003**, *1*, 282.
[17] F. Vallée, K. Karaveg, A. Herscovics, K. W. Moremen, P. L. Howell, *J. Biol. Chem.* **2000**, *275*, 41287.
[18] K. Karaveg, A. Siriwardena, W. Tempel, Z. J. Liu, J. Glushka, B. C. Wang, K. W. Moremen, *J. Biol. Chem.* **2005**, *280*, 16197.
[19] A. Varrot, S. Leydier, G. Pell, J. M. Macdonald, R. V. Stick, H. J. Gilbert, G. J. Davies, *J. Biol. Chem.* **2005**, *280*, 20181.
[20] E. Sabini, G. Sulzenbacher, M. Dauter, Z. Dauter, P. L. Jorgensen, M. Schulein, C. Dupont, G. J. Davies, K. S. Wilson, *Chem. Biol.* **1999**, *6*, 483.
[21] B. Li, S. P. Kawatkar, S. George, H. Strachan, R. J. Woods, A. Siriwardena, K. W. Moremen, G. J. Boons, *ChemBioChem* **2004**, *5*, 1220.
[22] N. Shah, D. A. Kuntz, D. R. Rose, *Biochemistry* **2003**, *42*, 13812.
[23] X. Wen, Y. Yuan, D. A. Kuntz, D. R. Rose, B. M. Pinto, *Biochemistry* **2005**, *44*, 6729.
[24] M. Granovsky, J. Fata, J. Pawling, W. J. Muller, R. Khokha, J. W. Dennis, *Nat. Med.* **2000**, *6*, 306.
[25] M.-P. Heck, S. P. Vincent, B. W. Murray, F. Bellamy, C.-H. Wong, C. Mioskowski, *J. Am. Chem. Soc.* **2004**, *126*, 1971.
[26] M. Terinek, A. Vasella, *Helv. Chim. Acta* **2003**, *86*, 3482.
[27] M. Böhm, E. Lorthiois, M. Meyyappan, A. Vasella, *Helv. Chim. Acta* **2003**, *86*, 3818.
[28] Collaborative Computational Project Number 4, *Acta Crystallogr. Sect. D* **1994**, *50*, 760
[29] G. N. Murshudov, A. A. Vagin, E. J. Dodson, *Acta Crystallogr. Sect. D* **1997**, *53*, 240.
[30] R. M. Esnouf, *J. Mol. Graphics Modell.* **1997**, *15*, 132.

 © 2006 Wiley-VCH Verlag GmbH & Co. KGaA, Weinheim

Energy Transfer

DOI: 10.1002/anie.200601196

A Resonance Energy Transfer between Chemiluminescent Donors and Luminescent Quantum-Dots as Acceptors (CRET)**

*Xiangyi Huang, Liang Li, Huifeng Qian, Chaoqing Dong, and Jicun Ren**

Fluorescence resonance energy transfer (FRET) is a powerful technique for probing very small changes in the distance between donor and acceptor fluorophores, and is ideal for the sensitive detection of molecular binding events and changes in protein conformation in response to interactions with a particular target molecule or to changes in the solution environment. In recent years, luminescent semiconductor nanocrystals (also called quantum dots, QDs) have been favorably adopted in the FRET-based studies, such as deriving QD–protein–conjugate configuration,[1] QD–protein sensing assemblies,[2,3] photochromic switching,[4] photodynamic medical therapy,[5] and probing DNA replication and telomerization.[6] This success is due to the unique size-dependent physical and chemical characteristics of QDs. QDs were applied to FRET as both donors[7–10] and acceptors,[11–13] and some of the advantages offered compared to conventional dyes include sharp and symmetrical emission spectra, high quantum yield (QY), good chemical and photo stability, and size-dependent emission-wavelength tunability. Recently, QDs as acceptors were successfully used in bioluminescence resonance energy transfer (BRET).[14]

As with any fluorescence technique, however, photobleaching and autofluorescence limit the usefulness of FRET. Herein we report a resonance energy transfer between chemiluminescent donors and QDs as acceptors, which is called chemiluminescence (CL) resonance energy transfer (CRET), and is similar to BRET.[14–19] CRET involves nonradiative (dipole–dipole) transfer of energy from a chemiluminescent donor to a suitable acceptor molecule. In contrast to FRET, CRET occurs by the oxidation of a luminescent substrate without an excitation source. In our system, we chose the luminol/hydrogen peroxide CL reaction catalyzed by horseradish peroxidase (HRP) because this is one of the most sensitive CL reactions. In capillary electrophoresis with CL detection, the detection limit of HRP was below 10^{-19} mol

[*] X. Huang, L. Li, H. Qian, C. Dong, Prof. Dr. J. Ren
College of Chemistry & Chemical Engineering
Shanghai Jiaotong University
800 Dongchuan Road, Shanghai 200240 (China)
Fax: (+86) 21-5474-1297
E-mail: jicunren@sjtu.edu.cn

[**] This work was financially supported by NSFC (No. 90408014, 20335020), and the Nano-Science Foundation of Shanghai (0452M052, 05M05002). CRET = chemiluminescence resonance energy transfer.

Supporting information for this article is available on the WWW under http://www.angewandte.org or from the author.

WILEY InterScience DISCOVER SOMETHING GREAT
© 2006 Wiley-VCH Verlag GmbH & Co. KGaA, Weinheim

in the presence of *para*-iodophenol (*p*-IP) as an enhancer.[20] And more importantly, the CL spectrum (425–435 nm) of luminol overlaps well with the absorption of the QDs (Figure 1 A). The principle of CRET is illustrated in

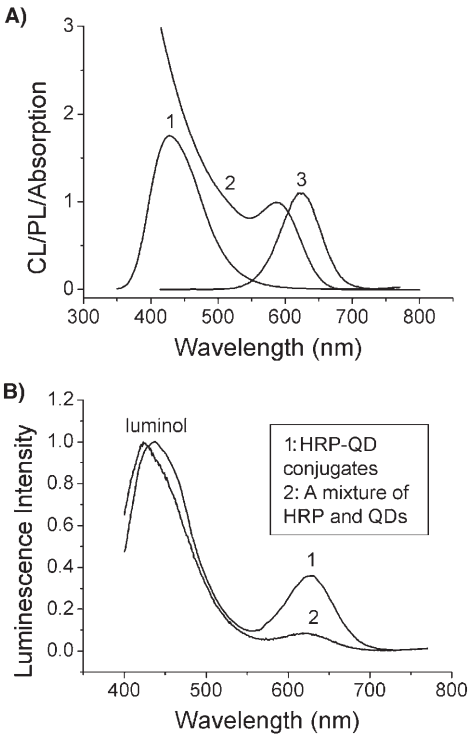
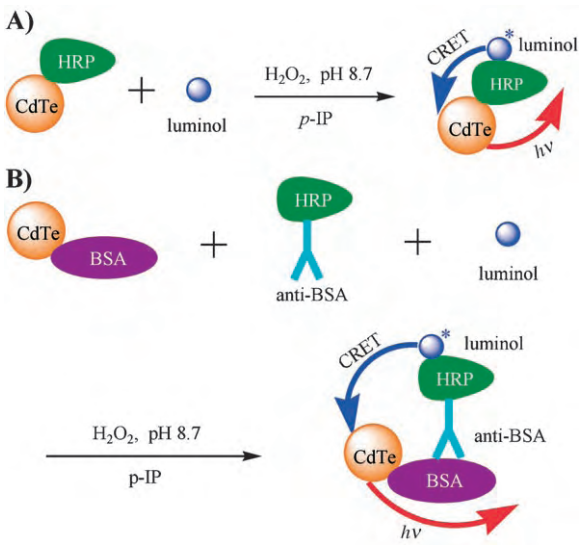


Figure 1. A) The CL of the luminol (1) spectrally overlaps with the absorption of the QDs (2). The diameter of CdTe QDs used is approximately 4 nm, and their emission wavelength is around 622 nm (3); CL = chemiluminescence, and PL = photoluminescence. Luminescence spectra of the QD–HRP-luminol system using luminol as donor and QDs as accepters. B) Comparison of CL spectra of HRP-QDs conjugates and a mixture of HRP and QDs using the QD–HRP-luminol system. CL reaction buffer was 0.05 M sodium borate solution (pH 10.0) containing of 1.0×10^{-4} M luminol, 5.0×10^{-4} M H_2O_2 and 5.0×10^{-4} M *para*-iodophenol. The concentrations of the QD–HRP conjugates are 1×10^{-6} M (HRP). All spectra are normalized.

Scheme 1. In Scheme 1 A, the CL donor, luminol, is not directly linked with the QDs, and the catalyst, HRP, is conjugated to the QDs. HRP can continuously catalyze the luminol/hydrogen peroxide CL reaction. In this system, the QD–HRP conjugates can be used as probes in cell and tissue imaging similar to BRET.[14] In Scheme 1 B, QDs are linked with bovine serum albumin (BSA), and HRP is conjugated with the BSA antibody (anti-BSA). When the anti-BSA–HRP binds to the BSA–QDs, CRET can occur. This system has potential to be used in immunoassay in non-competition and competition modes (see Supporting Information).

In our study, different sized water-soluble CdTe QDs were synthesized in the aqueous phase using the reaction between Cd^{2+} and NaHTe solution in the presence of mercaptopropyl acid (MPA) as a stabilizer[21] and their QYs were measured to be 40–50 %. The MPA-coated CdTe QDs were conveniently conjugated to certain proteins (such as HRP and BSA) using EDC (1-ethyl-3-(3-dimethylaminopropyl) carbodiimide) as a



Scheme 1. A) Schematic illustration of CRET based on luminol donors and HRP-labeled CdTe QD accepters, B) Schematic illustration of CRET for luminol donors and QD accepters based on the immuno-reaction of QD–BSA and anti-BSA–HRP. See text for details.

coupling reagent. The mixtures were purified using ultra-filtration membrane. The QD bioconjugates were characterized by capillary electrophoresis with laser-induced fluorescent detector. Our results showed that ultra-filtration was an effective and simple approach to purify QD–HRP conjugates and the conjugates were stable after being kept for one week (see Supporting Information). The diameter of HRP (M_W = 40 kDa) was estimated to be 35 Å, by using spherical approximation.[22] The hydrodynamic diameter of 622 QD–HRP conjugates and 622 QD (that is, QDs with an emission wave length of 622 nm), measured by fluorescence correlation spectroscopy (FCS),[23] were approximately 8 nm and 4 nm, respectively (see Supporting Information). Each 622 QD–HRP conjugate was estimated to contain one or two copies of immobilized HRP.

We investigated the CRET between luminol and QD bioconjugates in the QD–HRP system and the results obtained are shown in Figure 2. In Figure 2 A, four different sized QDs (with emissions at 557, 587, 622, and 657 nm) were used as acceptors. An efficient CRET between luminol and QD bioconjugate was observed, which looked like FRET. The CRET ratios, determined by dividing the acceptor emission by the donor emission, ranged from 0.22 to 0.32. The small differences of the CRET efficiency among the QDs are attributed to their different donor–accepter distances and quantum yields.

A comparison of CL spectra between HRP–QDs conjugates and a mixture of HRP and QDs (Figure 1 B) shows that the CL intensity ratio of QDs:luminol from the mixture of QDs and HRP was very low (Figure 1 B (2)), which was attributed to the low adsorption of QDs onto HRP. The electropherograms (see Supporting Information) of a mixture of HRP and QDs confirmed that a little of HRP was adsorbed onto QDs in the buffer solution (PBS, 0.01 M) by electrostatic interaction. There is a slight red-shift in luminol emission in

 © 2006 Wiley-VCH Verlag GmbH & Co. KGaA, Weinheim

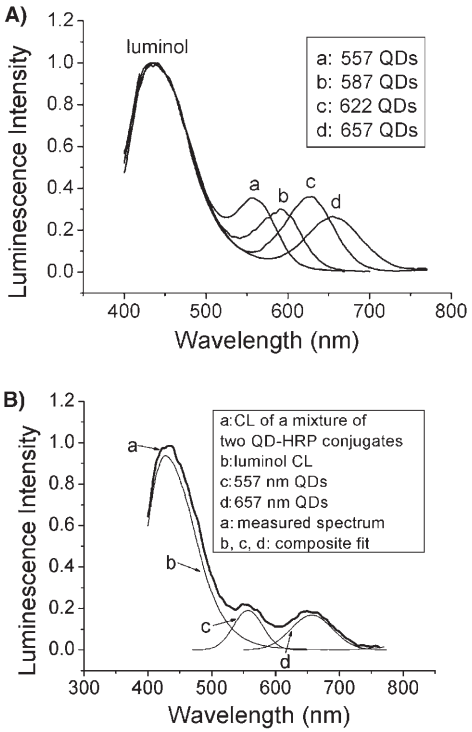


Figure 2. A) CL spectra of the QD–HRP–luminol system using luminol as donor and different sized QDs as accepters. B) CL spectra of the QD–HRP–luminol system using two QD accepters simultaneously. Other conditions are the same as in Figure 1. All spectra are normalized.

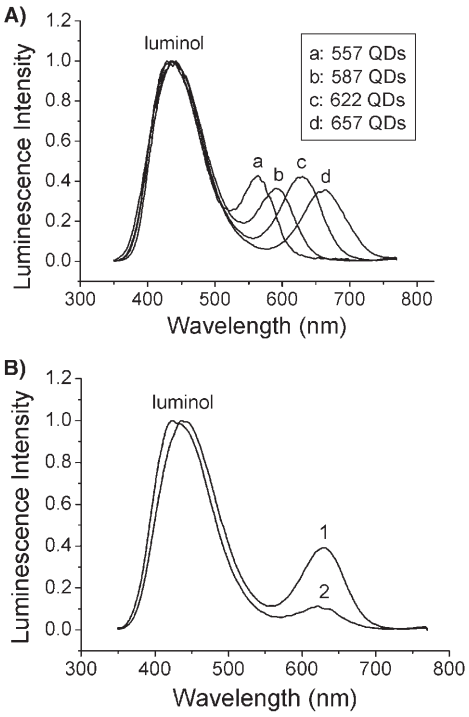


Figure 3. A) CL spectra for the QD–BSA/anti-BSA–HRP/luminol system using multiple QDs accepters interacting with luminol donors, respectively. B) Comparison of CL spectra of the QDs-BSA/anti-BSA–HPR immuno-complex (1) and a mixture of QD–BSA, anti-BSA, and HPR (2). CL reagents are delivered by a syringe to the quartz cuvette which containing QD–BSA/anti-BSA–HRP immuno-complex. Other conditions are the same as in Figure 1. All spectra are normalized.

the CRET experiment (Figure 1 B (1)). This phenomenon is unclear and may be due to the decrease of confinement in one dimension.[24,25]

Furthermore, we also observed the CRET of the luminol donor with two different size QD accepters (557 nm and 657 nm) simultaneously, and the CL spectra are shown in Figure 2 B. This result demonstrated that the multiplexed CRET could be realized similar to the multiplexed FRET.[3]

On the basis of the above results, we attempted to apply CRET to immunoassay based on antigen(BSA)–antibody(anti-BSA IgG) interactions. Immunoglobulin antigen (BSA) was first conjugated to CdTe QDs by electrostatic interaction, while HRP was covalently conjugated to the corresponding antibody (anti-BSA IgG). The mixtures were purified using an ultra-filtration membrane. The purified mixtures were mixed and incubated at 37 °C for 2–4 h. The CL reaction of luminol and hydrogen peroxide was used in the CRET process.

The CL spectra using different sized QDs as accepters are shown in Figure 3 A based on the immuno-interaction. These data illustrate that an efficient CRET between luminol and QD bioconjugates is generated when the anti-BSA–HRP binds to the BSA–QDs. In this system, the CRET ratios ranged from 0.27 to 0.36, which are approximately the same CRET ratios as those of the directly coupled conjugates. The distance between the donor and acceptor of the antibody-sandwiched conjugates is not the simple addition of the sizes of BSA, anti-BSA, and HRP since proteins are folded. However, the distance in the antibody-sandwiched conjugates is still expected to be longer than in the directly coupled conjugates, this longer distance should result in a lower CRET ratio. We attribute the results to a little uncoupled horseradish peroxidase in the purified QD–HRP solution, which thus led to the higher CL intensity of luminol and a lower CRET ratio for the directly coupled conjugate.

Comparisons of CL spectra of QD–BSA/anti-BSA–HRP immuno-complex and the mixture of QD–BSA conjugates and anti-BSA, and HRP are shown in Figure 3 B. The low CL intensity ratio of QDs:luminol from the mixture Figure 3 B (2) was also attributed to the weak adsorption of QDs onto HRP.

In summary, we demonstrated an efficient CRET between luminol and QDs based on HRP–QD conjugates and the immuno-interaction of the QD–BSA and anti-BSA–HRP in the luminol/hydrogen peroxide CL reaction. Further, we showed the potential for the application of multiple QDs acceptors with different emission wavelengths to multiplex analysis. Compared to FRET, CRET experiments are very simple and do not need an exciting light source. Additionally, in our system, the catalyst, HRP (not the CL donor, luminol), was directly linked with the QDs, and can continuously catalyze the CL reaction, which is probably the main reason for an efficient CRET. We anticipate that the CRET will become an attractive alterative method for quantitative bioanalysis, cell, and tissue imaging. CRET has its own limitations, however, and requires an oxidant, H_2O_2. High

 © 2006 Wiley-VCH Verlag GmbH & Co. KGaA, Weinheim

concentration H_2O_2 will quench the fluorescence of QDs. The future work is to develop the special detection system of CRET to enhance the detection sensitivity since the CL collection system of CRET used in this study is inefficient.

Experimental Section

CdTe QDs were prepared using the reaction between Cd^{2+} and NaHTe solution in the presence of MPA as a stabilizer according to the approach described in the ref. [21] Absorption spectra were collected using a Lambda 20 UV/Vis spectrophotometer (Perkin-Elmer). Emission spectra were measured with a Varian Cary spectrometer. The QYs of CdTe QDs are shown in the Supporting Information.

CdTe QDs were conjugated to proteins using EDC as a coupling reagent. First, a reaction mixture containing CdTe QDs (0.1–0.3 mg mL^{-1}), HRP (0.1 mg mL^{-1}), and EDC (0.5 mg mL^{-1}) in pH 7.0 PBS (0.01 M) was prepared and kept at room temperature for 2–4 h. Then the mixture was purified using an ultra-filtration membrane (Micoron YM-50–50 000 NMWL, Millipore, USA) according to the instructions from the manufacture. Finally the purified products were stored in refrigerator at 4 °C.

BSA can facilely conjugate to CdTe QDs by electrostatic attraction. A mixture (a) of QDs (0.1–0.2 mg mL^{-1}) and BSA (0.3 mg mL^{-1}; containing 0.01 M PBS, pH 7.0) was left for 0.5 h at the room temperature. Anti-BSA was conjugated to HRP using EDC as a coupling reagent: A mixture (b) of anti-BSA (0.3–0.5 mg mL^{-1}), HRP (0.1 mg mL^{-1}), and EDC (1.0 mg mL^{-1}; containing 0.01 M PBS, pH 7.0) was left for 2–4 h at room temperature. The mixtures (a) and (b) were purified using ultra-filtration membrane (Micoron YM-100–100 000 NMWL, Millipore, USA). Then, the purified mixtures (a) and (b) were mixed together and incubated at 37 °C for 2–4 h. Finally, the reaction solution was stored in refrigerator at 4 °C.

Fluorescence correlation spectroscopy (FCS)[23] was used to measure the hydrodynamic diameter of QD–HRP conjugates and QDs. A P/ACE MDQ capillary electrophoresis (CE) system (Beckman Coulter Inc., Fullerton, CA, USA) was applied to characterize the QDs conjugates. $Na_2B_4O_7$ solution (0.025 M, pH 8.0) was used as running buffer.

CL spectra were measured with a Varian Cary spectrometer using a 3 mL quartz cuvette (1 cm optical path). Herein, the luminol/hydrogen peroxide CL reaction catalyzed by HRP is adopted, and *para*-iodophenol is acted as an enhancer. The CL reaction buffer consists of sodium borate solution (pH 10.0; 50 mmol L^{-1}; containing 1.0×10^{-4} M luminol, 5.0×10^{-4} M H_2O_2, 5.0×10^{-4} M *para*-iodophenol). 0.5 mL the CL reaction buffer was added to the quartz cuvette containing a given HRP–QDs conjugate or QD–BSA/anti-BSA–HRP immuno-complex (containing 0.01 M PBS, pH 7.0), the pH value of the mixed CL reaction solution was 8.7. CL reactions were initiated, and CL spectra were measured with a Varian Cary spectrometer.

Received: March 26, 2006
Revised: May 8, 2006
Published online: July 7, 2006

Keywords: chemiluminescence · CRET (chemiluminescence resonance energy transfer) · horseradish peroxidase · quantum dots

[1] I. L. Medintz, J. H. Konnert, A. R. Clapp, I. Stanish, M. E. Twigg, H. Mattoussi, J. M. Mauro, J. R. Deschamps, *Proc. Natl. Acad. Sci. USA* **2004**, *101*, 9612–9617.
[2] I. L. Medintz, A. R. Clapp, H. Mattoussi, E. R. Goldman, B. Fisher, J. M. Mauro, *Nat. Mater.* **2003**, *2*, 630–638.
[3] E. R. Goldman, I. L. Medintz, J. L. Whitley, A. Hayhurst, A. R. Clapp, H. T. Uyeda, J. R. Deschamps, M. E. Lassman, H. Mattoussi, *J. Am. Chem. Soc.* **2005**, *127*, 6744–6751.
[4] Y. Wang, Z. Tang, M. A. Correa-Duarte, L. M. Liz-Marzán, N. A. Kotov, *J. Am. Chem. Soc.* **2003**, *125*, 2830–2831.
[5] A. C. S. Samia, X. Chen, C. Burda, *J. Am. Chem. Soc.* **2003**, *125*, 15736–15737.
[6] F. Patolsky, Y. Weizmann, I. Willner, *J. Am. Chem. Soc.* **2002**, *124*, 770–772.
[7] C. R. Kagan, C. B. Murray, M. G. Bawendi, *Phys. Rev. B* **1996**, *54*, 8633–8643.
[8] S. A. Crooker, J. A. Hollingsworth, S. Tretiak, V. I. Klimov, *Phys. Rev. Lett.* **2002**, *89*, 186802.
[9] D. M. Willard, L. L. Carillo, J. Jung, A. Van Orden, *Nano Lett.* **2001**, *1*, 469–474.
[10] A. R. Clapp, I. L. Medintz, J. M. Mauro, B. R. Fisher, M. G. Bawendi, H. Mattoussi, *J. Am. Chem. Soc.* **2004**, *126*, 301–310.
[11] M. Achermann, M. A. Petruska, S. Kos, D. L. Smith, D. D. Koleske, V. I. Klimov, *Nature* **2004**, *429*, 642–646.
[12] A. R. Clapp, I. L. Medintz, B. R. Fisher, G. P. Anderson, H. Mattoussi, *J. Am. Chem. Soc.* **2005**, *127*, 1242–1250.
[13] N. N. Mamedova, N. A. Kotov, A. L. Rogach, J. Studer, *Nano Lett.* **2001**, *1*, 281–286.
[14] M. K. So, C. Xu, A. M. Loening, S. S. Gambhir, J. Rao, *Nat. Biotechnol.* **2006**, *24*, 339–343.
[15] Y. Xu, D. W. Piston, C. H. Johnson, *Proc. Natl. Acad. Sci. USA* **1999**, *96*, 151–156.
[16] S. Angers, A. Salahpour, E. Joly, S. Hilairet, D. Chelsky, M. Dennis, M. Bouvier, *Proc. Natl. Acad. Sci. USA* **2000**, *97*, 3684–3689.
[17] K. A. Eidne, K. M. Kroeger, A. C. Hanyaloglu, *Trends Endocrinol. Metab.* **2002**, *13*, 415–421.
[18] K. D. G. Pfleger, K. A. Eidne, *Nat. Methods* **2006**, *3*, 165–174.
[19] J. Perroy, S. Pontier, P. G. Charest, M. Aubry, M. Bouvier, *Nat. Methods* **2004**, *1*, 203–208.
[20] J. N. Wang, J. C. Ren, *Electrophoresis* **2005**, *26*, 2402–2408.
[21] L. Li, H. F. Qian, J. C. Ren, *J. Lumin.* **2006**, *116*, 59–66.
[22] M. Onda, Y. Lvov, K. Ariga, T. Kunitake, *Biotechnol. Bioeng.* **1996**, *51*, 163–167.
[23] C. Q. Dong, B. Bi, H. F. Qian, J. C. Ren, *Small*, **2006**, *2*, 534–538.
[24] Z. Tang, N. A. Kotov, M. Giersig, *Science* **2002**, *297*, 237–240.
[25] M. Heilemann, P. Tinnefeld, G. S. Mosteiro, M. G. Parajo, N. F. Van Hulst, M. Sauer, *J. Am. Chem. Soc.* **2004**, *126*, 6514–6515.

 © 2006 Wiley-VCH Verlag GmbH & Co. KGaA, Weinheim

Conducting Materials

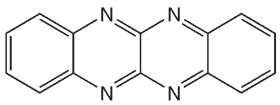
DOI: 10.1002/anie.200600553

A High-Conductivity Crystal Containing a Copper(I) Coordination Polymer Bridged by the Organic Acceptor TANC**

Makoto Tadokoro, Syuma Yasuzuka, Masaharu Nakamura, Takumi Shinoda, Toshinori Tatenuma, Minoru Mitsumi, Yoshiki Ozawa, Koshiro Toriumi, Harukazu Yoshino, Daisuke Shiomi, Kazunobu Sato, Takeji Takui, Takehiko Mori, and Keizo Murata*

Artificial conductors constructed from molecular building blocks can replicate unique low-dimensional electron-transport phenomena depending on the nature of their molecular components.[1] For example, $Cu(DCNQI)_2$ (DCNQI = *N*,*N*′-dicyanoquinodiimine) systems formed from coordination polymers containing alternating 3D linkages between Cu ion donors and organic DCNQI acceptors exhibit an interesting metal–insulator (M–I) transition under high pressure. This behavior is due to the interaction between the localized 3d-electron bands of the Cu ions and the π-electron conductive bands of DCNQI.[2] Therefore, the appropriate combination of donors and acceptors as molecular building blocks, which often form an electron-conducting solid, plays an important role in determining the electron-transport character of a molecular crystal.

Molecules that form high-conductivity molecular solids, particularly organic acceptors, have been limited thus far to cyanoquinoid derivatives such as TCNQ[3] and DCNQI[4] and the metal complex $[M(dmit)_2]$ (dmit = 1,3-dithiole-2-thioxo-4,5-dithiolato).[5] Molecular conductors with various electron-donor frameworks based on heterocyclic structures containing a chalcogen atom such as tetrathiafulvalene (TTF)[6] and tetramethyltetraselenofulvalene (TMTSF)[7] have also been realized, and studies are underway to discover a fundamental molecule with a stable electron-accepting framework to form molecular conductors with a desired transport behavior. Herein, we report a modifiable electron acceptor with 5,6,11,12-tetraazanaphthacene (TANC) as a new fundamental framework and the preparation of a high-conductivity crystal (**1**) from Cu^I–TANC coordination polymers.



TANC

TANC was prepared by modifying a synthetic procedure first reported by Hill.[8] The yellow precipitate obtained from the thermal condensation between *o*-phenylenediamine and oxamide contains 2,2′-bibenzimidazole and 5,11-dihydro-5,6,11,12-tetraazanaphthacene (FFV) in a 3:1 ratio. This mixture was oxidized with PbO_2 in MeCN to give brown crystals of TANC in 20% yield. The cyclic voltammogram of TANC in MeCN exhibits two reversible one-step, one-electron waves in the reverse sweep ($E^1_{1/2} = -0.20$ and $E^2_{1/2} = -0.88$ V vs Ag/AgCl), which means that TANC is a weaker electron acceptor than organic acceptors such as TCNQ and DCNQI that form high-conductivity materials.[9] Unfortunately, TANC cannot be employed as an organic semiconductor with n-type characteristics.

The TANC radical anion can be isolated from an electron disproportionate reaction between FFV and TANC under basic conditions. This compound was obtained as a green precipitate under anaerobic conditions, which immediately turns gray upon exposure to air. The ESR spectrum of the precipitate exhibits a typical anisotropic peak ($g_\perp = 2.011$ and $g_\parallel = 2.0091$) that stabilizes at room temperature (see the Supporting Information).

The high-conductivity crystal **1**, which has the composition $[\{Cu(TANC)\}F_{0.5}]_n$, was obtained from the reaction between TANC and $[Cu(MeCN)_4]BF_4$ in MeOH/MeCN in the form of thin, plate-like, indigo-blue crystals. The presence of half an equivalent of nonstoichiometric F^- ions was determined by X-ray photoelectron spectroscopy (XPS) measurements and quantitative chemical analysis for F^- ions. These F^- ions are generated by the dissociation of BF_4^- anions in the reaction mixture.

Direct electron-conductivity measurements for a single crystal of **1** were performed by the conventional four-probe dc method by varying the temperature (Figure 1). The crystals

[*] Prof. M. Tadokoro, T. Shinoda, T. Tatenuma
Department of Chemistry
Faculty of Science
Tokyo University of Science
Kagurazaka 1-3, Shinjuku-ku, Tokyo 162-8601 (Japan)
Fax: (+81) 3-5228-8714
E-mail: tadokoro@rs.kagu.tus.ac.jp
Dr. M. Mitsumi, Prof. Y. Ozawa, Prof. K. Toriumi
Department of Chemistry
Faculty of Science
Hyogo Prefecture University
Kouto 3-2-1, Kamikouri-cho, Akou-gun 678-1297 (Japan)
Dr. S. Yasuzuka, M. Nakamura, Dr. H. Yoshino, Prof. D. Shiomi, Prof. K. Sato, Prof. T. Takui, Prof. K. Murata
Department of Chemistry and Department of Material Sciences
Graduate School of Science
Osaka City University
Sugimoto 3-3-138, Sumiyoshi-ku, Osaka 558-8585 (Japan)
Prof. T. Mori
Department of Organic Polymeric Materials
Interdisciplinary Graduate School of Science and Engineering
Tokyo Institute Technology
Nagatsuda-cho 4259, Midori-ku, Yokohama 226-8502 (Japan)

[**] This study was supported by a Grant-in-Aid for Scientific Research on Priority Areas (nos. 16041237 and 16038221) and Scientific Research (B) (no. 16350034) from the Ministry of Education, Culture, Science and Technology of Japan. The authors are grateful for time on the BL02B1 beamline of the SPring-8 facility and thank the Analytical Center of Osaka City University for providing the CCD X-ray diffractometer and performing the elemental analysis.
TANC = 5,6,11,12-tetraazanaphthacene.

Supporting Information for this article is available on the WWW under http://www.angewandte.org or from the author.

InterScience
© 2006 Wiley-VCH Verlag GmbH & Co. KGaA, Weinheim

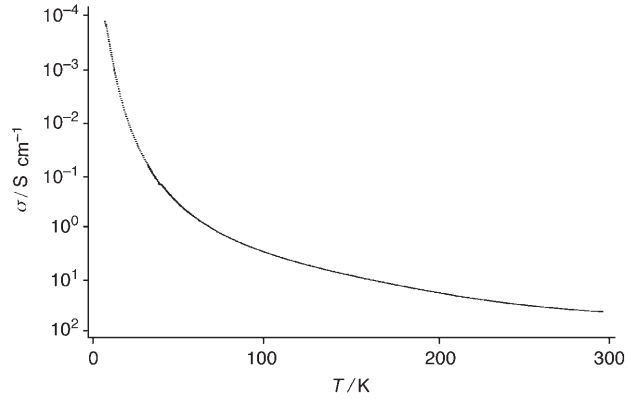


Figure 1. Temperature-dependent conductivity of **1** at ambient pressure using the typical four-probe dc method. The measurement was performed by attaching an Au wire ($\phi = 10$ μm) to the (001) face in a crystal of **1** ($0.78 \times 0.22 \times 0.03$ mm^3).

exhibit a high conductivity of 50 S cm^{-1} along the *a* axis at 300 K, and the conductivity sinks rapidly to 10^{-6} S cm^{-1} at 10 K, with a decrease in temperature. This behavior implies that **1** is a semiconductor at ambient pressure.

An X-ray structure analysis was performed for a platelike single crystal of **1** ($0.41 \times 0.15 \times 0.03$ mm^3).[10] Figure 2a shows a flat-ribbon structure with alternative linkages between the Cu^+ ions and TANC along the *b* axis. Two of the four N atoms in the TANC framework, namely N(1) and N(1)*[1] ("*1": $-x$, $-y$, $-z$), are coordinated to two different Cu^+ ions. The coordination structure around each Cu^+ ion is approximately linear didentate (Cu(1)–N(1) = 1.887(5) Å). The two remaining non-coordinating atoms (N(2) and N(2)*) reinforce the coordination structure through weak C–H···N hydrogen bonds (N(2)···C(2)*[2] = 3.772(9) Å; "*2": $x-1$, $y+1$, z). They

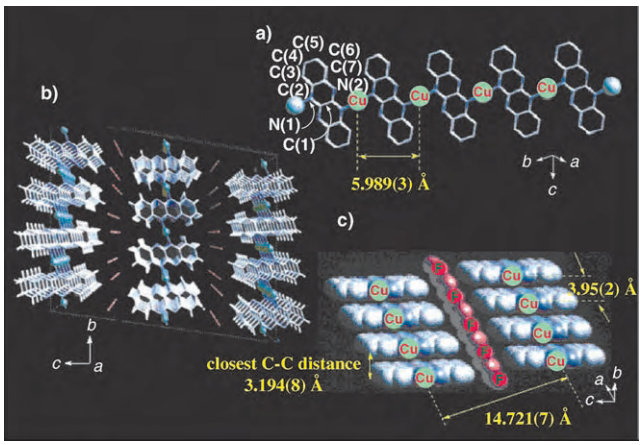


Figure 2. a) The structure of the oblique one-dimensional coordination polymer in **1** with alternating linkages between Cu^+ ions and TANC showing the shortest Cu–Cu distance in the intrapolymer chain (5.989(3) Å); b) the segregated stacking of the coordination polymer along the *a* axis to create two-dimensional stacking layers, which are separated by other layers constructed from disordered F^- ions (pink spheres) along the *c* axis; c) a perspective view along the *a* axis showing the stacking Cu–Cu distances (3.9451(2) Å), the shortest C–C distance (3.19 Å) between the stacking TANC molecules, and the shortest interlayer Cu–Cu stacking distance (14.721(7) Å).

also affect the electron structure of the Cu^+ ion by a weak contact interaction. This interaction originates because the lone-pair electrons of the N(2) and N(2)* atoms are directed toward the Cu^+ ion despite a long noncoordinating distance of 2.853(5) Å between Cu(1) and N(2).

The flat-ribbon structures are arranged in segregated stacks for each fragment of Cu^+ ions and TANC along the *a* axis in **1** to form 2D stacking layers (Figure 2b). The shortest C–C distance between the stacked TANC molecules within the layers is that between C(1) and C(7)*[3] (3.184(9) Å; "*3": $-x$, $-y+1$, $-z$). Few direct Cu–Cu interactions exist between the ribbons in the layer because the shortest Cu(1)–Cu(1)* distance is 3.95(2) Å, which is greater than the total van der Waals radius between two Cu^+ ions. The nonstoichiometric F^- ions are located in the spaces between the layers in a single unit separate the conductive layers along the *c* axis (Figure 2c).

Conductivity anisotropy measurements were performed for **1** at room temperature for the crystal directions (100) and (010) using the Montgomery method.[11] The conductivity, σ_c, is 6.90×10^{-3} S cm^{-1} for the (001) direction, which corresponds to the smallest edge length among the three planes. This value is smaller by four and two orders of magnitude than σ_a (50.0 S cm^{-1} for the (100) direction) and σ_b (0.91 S cm^{-1} for the (010) direction), respectively. This variation occurs due to the alternating layers of F^- ions that disturb the conductivity through the (001) direction, which means that the crystal behaves as an approximate pseudo-1D molecular semiconductor based on the layer stacking along the *ab* plane; the maximum amount of current flows through the 1D stacked TANC arrays along the *a* axis.

This behavior as a 1D molecular conductor can also be explained by extended Hückel calculations based on the crystal structure of **1**.[12] If the Cu atoms are not considered, the LUMO band of the TANC molecules shows the following intermolecular overlaps: 7.1×10^{-3} for the stacking direction of the *a* axis and 0.7×10^{-3} for the interchain direction of the *b* axis. This yields a 1D energy band along the stacking *a* axis with a bandwidth of 0.28 eV and an interchain interaction one-tenth that of the intrachain interaction. The tight-binding approximation of the LUMO band yields a 1D energy band and an open Fermi surface (Figure 3a).

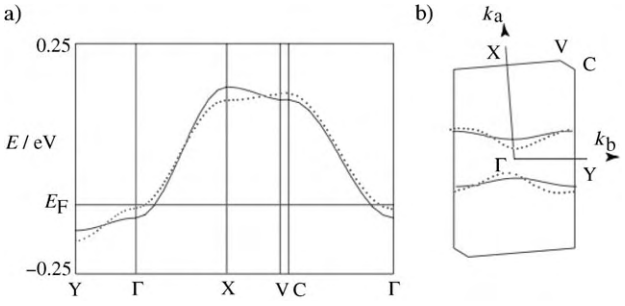


Figure 3. a) The energy dispersion and b) the Fermi surface of a crystal of **1** calculated by the extended Hückel method with a tight-binding approximation. The black line represents the energy band calculated using only the TANC π band and the dotted line represents the energy band obtained by considering the π–d interchain interactions of the hybridization between Cu ions and the TANC LUMO ($t_\perp = 0.01$ eV).

© 2006 Wiley-VCH Verlag GmbH & Co. KGaA, Weinheim

The whole band calculation, including the Cu orbitals, shows that the Cu 3d bands are located around the HOMO band and are completely occupied (Figure 3b). This result is consistent with the existence of only Cu^+ species (absence of Cu^{2+}), as observed by XPS. Furthermore, the nearly temperature-independent spin susceptibility of **1** is regarded as being Pauli-like, which also indicates the absence of Cu^{2+} species. The density of the $S = 1/2$ local spin was estimated to be 1.15% from the Curie tail (see the Supporting Information). Owing to the coordination of the TANC molecules to the Cu atom, the orbital overlap between the TANC LUMO and the Cu orbitals is considerable: 7.5×10^{-3} to the Cu 3d orbitals and 17.3×10^{-3} to the Cu 4p orbitals. However, the hybridization of the Cu 3d orbitals with the TANC LUMO is weak because the 3d levels are located entirely below the LUMO level.

As the Cu 3d orbitals are separated from the LUMO level by more than 1 eV, the Cu 3d–LUMO hybridization yields $t_\perp = 2 \times 0.0752/\Delta = 0.01$ eV for the indirect interchain interaction between the TANC molecules through the Cu atom. These values are similar in order to those for the direct interchain interaction between the TANC molecules and are consistent with the results of the conductivity anisotropy measurements. The tight-binding energy band including this indirect interaction is depicted in Figure 3b, which shows that the 1D band remains essentially unchanged. Therefore, the Cu 3d orbitals do not contribute significantly to the interchain interaction because the Cu atom exists as Cu^+.

Plots of the resistivity against $1/T$ for **1** yield a roughly curved line, which indicates a behavior different from that of a typical thermally excited semiconductor (see the Supporting Information). Therefore, the temperature-dependent resistivity of **1** at high pressure was measured up to approximately 8 GPa by using a cubic anvil apparatus.[13,14] The resistivity increases uniformly until approximately 6.5 GPa, and it decreases slightly at 8 GPa (see the Supporting Information). This variation in the insulating behavior with pressure for **1** is similar to that of Cu–DCNQI systems, which also exhibit an increase in resistivity under high pressure.[15] The sharp decrease in the resistivity above 6.5 GPa at 300 K may be attributed to the enhanced overlap of π orbitals in TANC molecules. However, it is difficult to understand the pressure-enhanced insulating state. The temperature dependence of the resistivity can be well fitted by the variable-range-hopping (VRH) formula even under high pressures,[16] which suggests that the spatially disordered F^- ions play an important role in the electron-transport behavior of **1**. We therefore require a model different from that of the Cu–DCNQI system to understand the pressure-enhanced insulating behavior. The large conductivity anisotropy ($\sigma_a/\sigma_b/\sigma_c \approx 7000{:}117{:}1$) suggests that the energy levels of the Cu 4s and 3d orbitals are significantly higher and lower than that of the TANC LUMO, respectively. Hence, the Cu^+ ions make no contribution to the conduction band. This implies that the hybridization between the Cu 3d orbital and the TANC LUMO is negligible at ambient pressure. The random potential generated by the spatially disordered F^- ions may become stronger upon application of pressure because the distance between the layers with stacked TANC columns and those with disordered F^- ions decreases with an increase in pressure. As a result, the application of pressure may increase the purity of the one-dimensionality and the strength of the random potential as a result of disordered F^- ions. In other words, the 1D VRH is enhanced with an increase in pressure up to 6.5 GPa.

We have reported the preparation of a new high-conductivity crystal **1**, which is constructed from coordination polymers containing Cu^+ ions and novel TANC acceptors. By employing the simple fundamental framework of TANC, it should be possible to convert the crystal structure into that of other analogues and introduce a variety of substituented groups such as a series of TCNQ and DCNQI acceptors. Furthermore, according to the measurements of the temperature-dependent resistivity under high pressure and the conductivity anisotropy, it seems likely that the conduction mechanism of **1** follows the 1D VRH formula based on the disordered F^- ions, which affects the stacking of the TANC columns below 6.5 GPa. It should be possible to establish the mechanism for the decrease in resistivity above 6.5 GPa by preparing other Cu molecular conductors with TANC derivatives.

Experimental Section

1: $[Cu(MeCN)_4]BF_4$ (0.34 g, 1.0 mmol) and TANC (40 mg, 0.17 mmol) were mixed in MeCN (36 mL) and stirred for 10 min. The solution was filtered and divided into 18 × 2-mL portions. MeOH (8 mL) was added to each portion and the mixture was slowly evaporated at room temperature. Deep-blue crystals were deposited from the concentrated solution as thin, platelike rhombuses. Yield: 25.0 mg (50%). Elemental analysis (%) for $C_{14}H_8CuF_{0.5}N_4$: calcd C 55.08, H 2.64, Cu 20.81, F 3.11, N 18.35; found C 55.33, H 2.64, Cu 20.73, F 3.40, N 18.41.

Received: February 10, 2006
Revised: April 24, 2006

Keywords: conducting materials · copper · crystal engineering · high-pressure chemistry · supramolecular chemistry

[1] Special issue on organic conductors: *Chem. Rev.* **2004**, *104*, 4887–5782.
[2] a) R. Kato, *Bull. Chem. Soc. Jpn.* **2000**, *73*, 515; b) M. Tamura, Y. Kashimura, H. Sawa, S. Aonuma, R. Kato, M. Kinoshita, *Solid State Commun.* **1995**, *93*, 585; c) Y. Kashimura, H. Sawa, S. Aonuma, R. Kato, H. Takahashi, N. Mori, *Solid State Commun.* **1995**, *93*, 675.
[3] J. Ferraris, D. O. Cowan, V. Walatka, Jr., J. H. Perlstein, *J. Am. Chem. Soc.* **1973**, *95*, 948.
[4] A. Aumüller, P. Erk, G. Klebe, S. Hünig, J. U. von Schütz, H.-P. Werner, *Angew. Chem.* **1986**, *98*, 759; *Angew. Chem. Int. Ed. Engl.* **1986**, *25*, 740.
[5] L. Brossard, M. Ribault, L. Valade, P. Cassoux, *J. Phys.* **1989**, *50*, 1521.
[6] F. Wudl, R. C. Haddon, E. T. Zellers, F. B. Bramwell, *J. Org. Chem.* **1979**, *44*, 2291.
[7] D. Jerome, A. Mazaud, M. Ribault, K. Bechgaard, *J. Phys. Lett.* **1984**, *39*, 12.
[8] J. H. M. Hill, *J. Org. Chem.* **1963**, *28*, 1931.
[9] A. Aumüller, S. Hünig, *Liebigs Ann. Chem.* **1986**, 142.
[10] Single-crystal data for **1** at 20°C: $C_{14}H_8CuF_{0.5}N_4$, $M_w = 305.29$, triclinic, space group $P\bar{1}$ (no. 2), $a = 3.9521(2)$, $b = 5.989(3)$, $c = 14.721(7)$ Å, $\alpha = 81.29(2)$, $\beta = 85.71(2)$, $\gamma = 84.87(2)°$, $V =$

 © 2006 Wiley-VCH Verlag GmbH & Co. KGaA, Weinheim

342.3(3) Å^3, $Z=1$, $\rho_{calcd}=1.481$ g cm^{-3}, $\mu(Mo_{K\alpha})=15.93$ cm^{-1}. A total of 1459 ($R_{int}=0.039$) independent reflections having $2\theta<54.9°$ were collected. The resulting parameters were refined to converge at R_1 (based on F_o) $=0.074$ for 105 parameters ($I>4.00\sigma(I)$ for $2\theta<54.9°$) on 1193 reflections. Max./min. residual electron density 1.98/−0.58 e Å^{-3}; GOF = 1.64. The data collection for **1** was performed with a computer-controlled Rigaku/MSC Mercury CCD auto-diffractometer using Lorenz-polarization corrections and graphite-monochromated $Mo_{K\alpha}$ radiation ($\lambda=0.71069$ Å). The structures were solved by direct methods with SIR92[17] and full-matrix least-squares (DIRDIF99) refinement.[18] The hydrogen-atom positions were fixed. Further details of the data collection and structure solution of **1** are provided as Supporting Information. CCDC-297950 contains the supplementary crystallographic data for this paper. These data can be obtained free of charge from the Cambridge Crystallographic Data Center via www.ccdc.cam.ac.uk/data request/cif.

[11] H. C. Montgomery, *J. Appl. Phys.* **1971**, *42*, 2971.

[12] T. Mori, A. Kobayashi, Y. Sasaki, H. Kobayashi, G. Saito, H. Inoguchi, *Bull. Chem. Soc. Jpn.* **1984**, *57*, 627.

[13] H. Taniguchi, M. Miyashita, K. Uchiyama, K. Satoh, N. Mori, H. Okamoto, K. Miyagawa, K. Kanoda, M. Hedo, Y. Uwatoko, *J. Phys. Soc. Jpn.* **2003**, *72*, 468.

[14] a) S. Yasuzuka, K. Murata, H. Yoshino, T. Fujimoto, M. Shimotori, M. Nakamura, M. Tadokoro, *J. Phys. Soc. Jpn.* **2005**, *75*, 14704; b) S. Yasuzuka, K. Murata, T. Fujioto, M. Shimotori, K. Yamaya, *J. Phys. Soc. Jpn.* **2005**, *74*, 1782.

[15] a) T. Mori, H. Inokuchi, A. Kobayashi, R. Kato, H. Kobayashi, *Phys. Rev. B* **1988**, *38*, 5913; b) T. Takahashi, K. Kanoda, T. Tamura, K. Hiraki, K. Ikeda, R. Kato, H. Kobayashi, A. Kobayashi, *Synth. Met.* **1993**, *56*, 2281; c) A. Kawamoto, K. Miyagawa, K. Kanoda, *Phys. Rev. B* **1998**, *58*, 1243.

[16] a) N. F. Mott, *Proc. Phys. Soc. London Sect. A* **1949**, *62*, 416; b) N. F. Mott, *Metal–Insulator Transitions*, *2nd ed.*, Taylor and Francis, London, **1990**.

[17] A. Altomare, G. Cascarano, C. Giacovazzo, A. Guagliardi, M. Burla, G. Polidori, M. Camalli, *J. Appl. Crystallogr.* **1994**, *27*, 435.

[18] P. T. Beuskens, G. Admiraal, G. Beurskens, W. P. Bosman, R. de Gelder, R. Israel, J. M. M. Smits, The DIRDIF-99 program system, Technical Report of the Crystallography Laboratory, University of Nijmegen, The Netherlands, **1999**.

 © 2006 Wiley-VCH Verlag GmbH & Co. KGaA, Weinheim

Cluster Compounds

DOI: 10.1002/anie.200601805

$[Zn_9Bi_{11}]^{5-}$: A Ligand-Free Intermetalloid Cluster**

*Jose M. Goicoechea and Slavi C. Sevov**

One of the most important aspects of metal clusters is that they provide a window into the rather ill-defined area of chemistry that lies between isolated molecular species and solid-state compounds with extended structures.[1] Small, cage-like clusters have been relatively well studied and are found to generally follow established rules for electron counting and isolobal relationships.[2] Their structures and bonding are fairly well understood and can be rationalized within the context of these rules. However, this is not the case for large clusters with high nuclearities (more than 12 atoms) and dimensions beyond that of the nanometer. These species lack such a cohesive foundation, and furthermore, many of them seem to disobey traditional electron-counting rules, which ultimately makes the discussion of their structure and bonding very difficult. In addition, only a handful of such clusters have been structurally characterized, most of them limited to the field of precious-metal cluster chemistry.[1b] This scarcity is all the more valid for main-group-element species, for which the first example, $[Al_{77}\{N(SiMe_3)_2\}_{20}]^{2-}$, was isolated by Schnöckel and co-workers only a few years ago.[3] These authors coined the term metalloid cluster for such species in which the metal–metal contacts in the cluster outnumber the metal–ligand contacts, and in which the cluster atoms exhibit close packing, as in bulk metals. More species have been discovered since, and the cluster chemistry of Group 13 has been enriched by the isolation of species with Al_n ($n = 7$, 12, 14, 50, 69) and Ga_m ($m = 9$, 10, 19, 22, 24, 26, 84) metal cores.[4,5]

Similarly, large metal-centered clusters of Group 14 elements have also been extensively studied in recent years. The synthetic approach towards these species involves reactions of nine-atom deltahedral clusters of Group 14 elements, known as Zintl ions, with various transition-metal complexes. Some of the species isolated by this route are: $[Ni(Ni@Ge_9)_2]^{4-}$,[6] $[Pd_2@Ge_{18}]^{4-}$,[7] $[Ni_2Sn_{17}]^{4-}$,[8] $[Ni@Pb_{10}]^{2-}$,[9] $[Pt@Pb_{12}]^{2-}$,[10] and a single cluster of a Group 15 element, $[As@Ni_{12}@As_{20}]^{3-}$.[11] These species are also metalloid clusters, although, as they involve more than one metal, they may be more appropriately referred to as intermetalloid

[*] Dr. J. M. Goicoechea, Prof. S. C. Sevov
Department of Chemistry and Biochemistry
University of Notre Dame
Notre Dame, IN 46556 (USA)
Fax: (+1) 574-631-6652
E-mail: ssevov@nd.edu

[**] We thank the National Science Foundation for financial support of this research (CHE-0446131), and for the purchase of a Bruker APEX II diffractometer (CHE-0443233) and the "Bunch-o-Boxes" cluster (DMR-0079647).

© 2006 Wiley-VCH Verlag GmbH & Co. KGaA, Weinheim

clusters.[12] Nonetheless, the two types of atoms in each of these clusters have two very specific coordination environments; that is, one type of atom centers the cluster, while the other type makes up the cage. Herein, we report the synthesis and structure of a new 20-atom intermetalloid cluster, $[Zn_9Bi_{11}]^{5-}$, with extensive amalgamation of the two types of atoms, as in a true intermetallic compound.

The novel cluster was synthesized during an exploration of the reactivity of ethylenediamine (en) solutions of K_5Bi_4 towards various organometallic compounds, $ZnPh_2$ (Ph = phenyl) in this case, in the presence of 4,7,13,16,21,24-hexaoxa-1,10-diazabicyclo[8.8.8]hexacosane (2,2,2-crypt). The K_5Bi_4 precursor contains tetrameric zigzag $[Bi_4]^{(4+\delta)-}$ oligomers,[13] but its ethylenediamine solutions exhibit double-bonded $[Bi{=}Bi]^{2-}$ dimers and $[Bi_4]^{2-}$ squares,[14,15] which can further fragment upon reaction with transition-metal complexes, as seen in $[Bi_3M_2(CO)_6]^{3-}$ (M = Cr, Mo).[16] A similar reaction carried out with $ZnPh_2$ resulted in the isolation of $[K(2,2,2\text{-crypt})]_5[Zn_9Bi_{11}]\cdot 2\,en\cdot tol$ (tol = toluene), which exhibits naked heterometallic $[Zn_9Bi_{11}]^{5-}$ clusters (Figure 1). Apparently, both phenyl groups at the zinc atoms were "replaced" in this case. This reaction is analogous to the previously studied reactions of deltahedral $[Ge_9]^{4-}$ clusters with EPh_3 (E = Sb, Bi) and $E'Ph_4$ (E′ = Ge, Sn), where one phenyl group is replaced by the cluster, yielding $[Ph_2E\text{-}Ge_9\text{-}EPh_2]^{2-}$ and $[Ph_3E'\text{-}Ge_9\text{-}E'Ph_3]^{2-}$, respectively.[17]

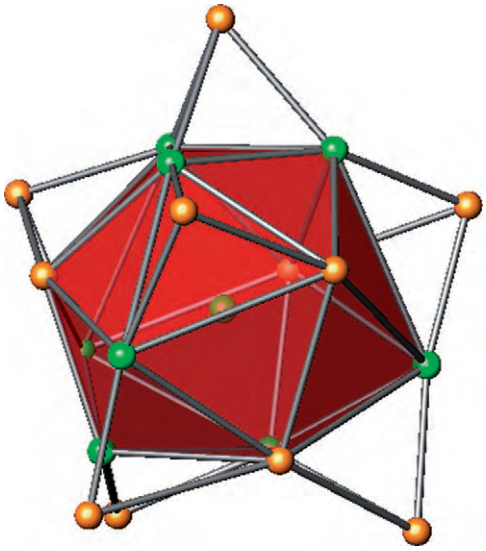


Figure 1. The $[Zn_9Bi_{11}]^{5-}$ cluster: a central zinc atom (green) within a Zn_8Bi_4 icosahedron (red) is capped by seven bismuth atoms (orange), that is, $[Zn@(Zn_8Bi_4)@Bi_7]^{5-}$. Interatomic distances [Å]: Zn_{cen}–Zn_{ico} 2.832(2)–3.594(3), Zn_{cen}–Bi_{ico} 2.822(2)–2.928(2), Zn_{ico}–Bi_{ico} 2.876(2)–3.755(2), Bi_{ico}–Bi_{ico} 3.2051(8), Zn_{ico}–Zn_{ico} 2.894(2)–3.762(2), Bi_{cap}–Zn_{ico} 2.598(1)–2.768(1), Bi_{cap}–Bi_{ico} 3.1072(8)–3.3121(9); the subscripts cen, ico, and cap denote cluster atoms in the central, icosahedral, and capping sites, respectively.

The ligand-free cluster has a central zinc atom which, as in numerous aluminum and gallium metalloid species,[18] is 12-coordinate in an icosahedral environment, albeit a distorted one in this case, owing to the very different atomic radii of zinc and bismuth. The icosahedron consists of eight zinc and four bismuth atoms, that is, Zn_8Bi_4. If not for one of the four bismuth atoms (in the bottom triangle of the icosahedron in Figure 1), it would have a pseudo-threefold axis (vertical in Figure 1 and perpendicular to the page in Figure 2a). Seven of the 20 triangular faces of the icosahedron are capped by bismuth atoms that form a second shell, and the formula of the cluster can be written as $[Zn@(Zn_8Bi_4)@Bi_7]^{5-}$. One of the capping bismuth atoms is along the imaginary threefold axis (top in Figure 1), while the other six are split into two sets of three atoms that are related by the imaginary threefold axis. This arrangement results in a pseudo-threefold axis for the entire cluster, as shown in Figure 2a.

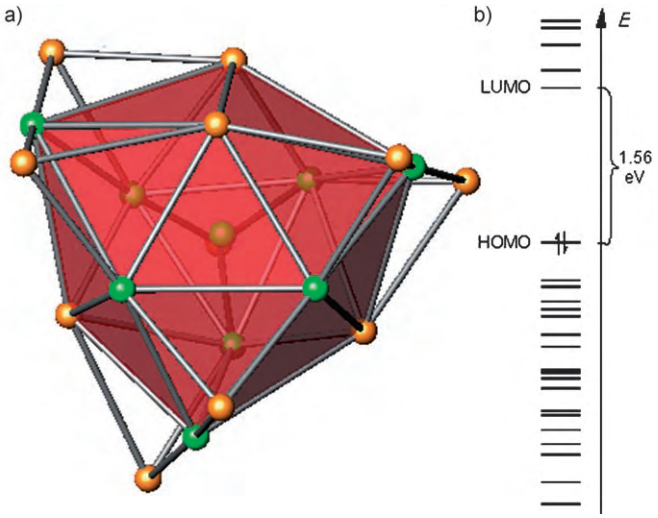


Figure 2. a) View of the $[Zn_9Bi_{11}]^{5-}$ cluster along the pseudo-threefold axis. b) Part of the molecular orbital diagram of $[Zn_9Bi_{11}]^{5-}$; the energy of the HOMO/LUMO gap is indicated.

The "packing" of the atoms in $[Zn_9Bi_{11}]^{5-}$ resembles the distorted cubic close packing (ccp) found in intermetallic compounds and alloys, as well as in some homoatomic metalloid clusters. There are no known zinc–bismuth binary intermetallic phases, which makes comparison of the structure and bonding of the cluster and with those of a bulk material impossible. To our knowledge, no molecular zinc–bismuth species have been reported either. There are, however, several ternary phases with formally anionic zinc–bismuth extended structures, such as $BaZnBi_2$,[19] $Ca_9Zn_4Bi_9$,[20] LiZnBi,[21] and $SrZnBi_2$.[22] The average Zn–Bi distance of 2.840 Å in these compounds compares well with the corresponding distances in $[Zn_9Bi_{11}]^{5-}$ (Figure 1).

Electronically, the Zn_8Bi_4 icosahedron is equivalent to an icosahedron made of 12 atoms of a Group 13 element. Formally, two atoms of the Group 12 element zinc (providing 2 electrons each; total of 4 electrons), and one atom of the Group 15 element bismuth (providing 5 electrons) average as three atoms of a Group 13 element (providing 3 electrons each; total of 9 electrons). Therefore, the Zn_8Bi_4 icosahedron is a heteroatomic version of the homoatomic Al_{12} and Ga_{12} icosahedra, both geometrically and electronically.

Density functional theory (DFT) calculations using the observed geometry and charge of the $[Zn_9Bi_{11}]^{5-}$ cluster

 © 2006 Wiley-VCH Verlag GmbH & Co. KGaA, Weinheim

revealed a gap of 1.56 eV between the highest occupied molecular orbital (HOMO) and the lowest unoccupied molecular orbital (LUMO), with tightly packed molecular orbitals in both the full and empty manifolds (Figure 2b). This orbital distribution indicates a good stability for the cluster and suggests a relative inertness towards both oxidation and reduction. As previously mentioned, rationalization of the bonding and electronic requirements of the homoatomic metalloid clusters has been an elusive goal and an insurmountable obstacle in the majority of cases. The situation is not very different for the heteroatomic intermetalloid cluster $[Zn_9Bi_{11}]^{5-}$, and we can offer only a possible explanation to rationalize the bonding within this species. The bonding in deltahedral closo clusters is accomplished by $2n+2$ delocalized electrons, where n is the number of vertices,[2a] which is 12 in the case of an icosahedron. Furthermore, an additional 2 electrons per vertex are associated with either an exo bond or a lone pair. Thus, the total number of electrons needed for an icosahedron is 50, that is, $(2\times12+2)+2\times12$. The eight zinc and four bismuth atoms of the Zn_8Bi_4 icosahedron provide a total of $8\times2+4\times5=36$ electrons. An additional 2 electrons are provided by the central zinc atom, and 5 more electrons come from the charge of the cluster. This totals 43 electrons, which is 7 electrons short of 50. These 7 electrons must be provided by the seven capping bismuth atoms, which apparently, behave as one-electron ligands to the icosahedron. This hypothesis implies that each bismuth atom keeps its remaining 4 electrons in the form of two lone pairs. While this type of bonding may seem unusual, it is clear from the DFT calculations that this electron count corresponds to a very stable cluster.

The $[Zn_9Bi_{11}]^{5-}$ cluster should be viewed as a part of the small family of "molecular alloys" that have been recently synthesized by similar reactions of Zintl ions with transition-metal reagents.[6–11] This handful of novel species represent intermediates in the eventual generation of intermetallic and alloy-like precipitates. As such, these species can provide important insight into how metal atoms aggregate in solution to initially form metastable clusters, before the ultimate oxidation to form neutral nanoparticles and then bulk solids. The true intermetalloid character of $[Zn_9Bi_{11}]^{5-}$ is expressed in the extensive amalgamation of zinc and bismuth, as would be expected in an eventual zinc–bismuth alloy or intermetallic compound. Such clusters may provide a clue as to what a binary zinc–bismuth phase may look like. Their oxidation may actually lead to metastable intermetallic compounds that are otherwise inaccessible. The discovery of this and other similar species may help develop a greater understanding of this ever-expanding area of chemistry and may lay a stronger foundation for unifying views on the bonding and geometry of metalloid and intermetalloid clusters.

Experimental Section

All manipulations were carried out under an inert atmosphere using standard Schlenk-line and/or glove-box techniques. Ethylenediamine (Acros, 99%) was distilled over sodium metal and stored in a gas-tight ampoule under nitrogen. K_5Bi_4 was synthesized according to a reported procedure.[13] A stoichiometric mixture of the elements (K: 99+%, Strem; Bi: 99.998%, Alfa-Aesar) was heated at 700°C over 2 days, inside a sealed niobium container jacketed in an evacuated fused-silica ampoule. 2,2,2-crypt (Acros, 98%) and $ZnPh_2$ (Strem, 99%) were used as received.

$[K(2,2,2\text{-crypt})]_5[Zn_9Bi_{11}]\cdot2\,en\cdot tol$: K_5Bi_4 (144 mg, 0.139 mmol) and 2,2,2-crypt (242 mg, 0.643 mmol) were weighed out into a test tube inside a glove box and dissolved in ethylenediamine (approximately 3 mL). The resulting dark greenish-blue solution was stirred for 5 min, after which $ZnPh_2$ (36 mg, 0.163 mmol) was added. The reaction mixture was stirred for 2 h, filtered, and the filtrate layered with toluene to allow for crystallization. After several days, very thin black-green plates of $[K(2,2,2\text{-crypt})]_5[Zn_9Bi_{11}]\cdot2\,en\cdot tol$ (estimated yield 5–10%) were obtained, alongside a black amorphous precipitate.

Single-crystal X-ray diffraction data for $[K(2,2,2\text{-crypt})]_5[Zn_9Bi_{11}]\cdot2\,en\cdot tol$ were collected on a Bruker APEX-II diffractometer with a CCD area detector at 100 K with $Mo_{K\alpha}$ radiation. The crystal was selected under Paratone-N oil, mounted on a fiber, and positioned in the cold nitrogen stream on the diffractometer. The structure was solved and refined (on F^2) with the aid of the SHELXTL V6.12 package.[23] Crystal data: $M_r=5177.39$, $P2_1/c$, $a=31.0930(8)$, $b=27.5755(7)$, $c=17.3825(4)$ Å, $\beta=90.869(2)°$, $V=14902.1(6)$ Å^3, $Z=4$, $\rho_{calcd}=2.308$ g cm^{-3}, $\mu(Mo_{K\alpha})=14.557$ cm^{-1}, $R1/wR2=5.38/10.63$% for the observed data. CCDC 606635 contains the supplementary crystallographic data for this paper. These data can be obtained free of charge from the Cambridge Crystallographic Data Centre via www.ccdc.cam.ac.uk/data request/cif.

Single-point DFT calculations were performed on the cluster by employing the atomic positions elucidated by single-crystal X-ray diffraction. The Becke3-parameter hybrid functional[24] with Lee–Yang–Parr correlation[25] (B3LYP) was used in conjunction with the LanL2DZ basis set.[26] Computations were executed with the Gaussian 98 package, revision A.11.3,[27] on Notre Dame's "Bunch-o-Boxes" Beowulf cluster.

Received: May 8, 2006
Revised: May 30, 2006
Published online: July 3, 2006

Keywords: bismuth · cluster compounds · metalloids · zinc · Zintl anions

[1] a) *Metal Clusters in Chemistry* (Eds.: P. Braunstein, L. A. Oro, P. R. Raithby), Wiley-VCH, Weinheim, **1999**; b) *Clusters and Colloids* (Ed.: G. Schmid), VCH, Weinheim, **1994**.
[2] a) K. J. Wade, *Adv. Inorg. Chem. Radiochem.* **1976**, *18*, 1; b) M. Elian, M. M. L. Chen, D. M. P. Mingos, R. Hoffmann, *Inorg. Chem.* **1976**, *15*, 1148; c) R. Hoffmann, *Angew. Chem.* **1982**, *94*, 725; *Angew. Chem. Int. Ed. Engl.* **1982**, *21*, 711.
[3] A. Ecker, E. Weckert, H. Schnökel, *Nature* **1997**, *387*, 379.
[4] a) A. Purath, R. Köppe, H Schnökel, *Angew. Chem.* **1999**, *111*, 3114; *Angew. Chem. Int. Ed.* **1999**, *38*, 2926; b) A. Purath, R. Köppe, H. Schnökel, *Chem. Commun.* **1999**, 1933; c) H. Köhnlein, G. Stösser, E. Baum, E. Möllhausen, U. Huniar, H. Schnökel, *Angew. Chem.* **2000**, *112*, 828; *Angew. Chem. Int. Ed.* **2000**, *39*, 799; d) J. Vollet, J. R. Hartig, H. Schnökel, *Angew. Chem.* **2004**, *116*, 3149; *Angew. Chem. Int. Ed.* **2004**, *43*, 3186; e) H. Köhnlein, A. Purath, C. Klemp, E. Baum, I. Krossing, G. Stösser, H. Schnökel, *Inorg. Chem.* **2001**, *40*, 4830.
[5] a) W. Köstler, G. Linti, *Angew. Chem.* **1997**, *109*, 2758; *Angew. Chem. Int. Ed. Engl.* **1997**, *36*, 2644; b) M. Kehrwald, W. Köstler, A. Rodig, G. Linti, *Organometallics* **2001**, *20*, 860; c) A. Schnepf, G. Stösser, H. Schnökel, *J. Am. Chem. Soc.* **2000**, *122*, 9178; d) A. Schnepf, E. Weckert, G. Linti, H. Schnökel, *Angew. Chem.* **1999**, *111*, 3578; *Angew. Chem. Int. Ed.* **1999**, *38*, 3381; e) G. Linti, A. Rodig, *Chem. Commun.* **2000**, 127; f) J. Steiner, G. Stösser, H.

 © 2006 Wiley-VCH Verlag GmbH & Co. KGaA, Weinheim

Schnökel, *Angew. Chem.* **2004**, *116*, 6712; *Angew. Chem. Int. Ed.* **2004**, *43*, 6549; g) T. Duan, E. Baum, R. Burgert, H. Schnökel, *Angew. Chem.* **2004**, *116*, 5757; *Angew. Chem. Int. Ed.* **2004**, *43*, 3190; h) A. Rodig, G. Linti, *Angew. Chem.* **2000**, *112*, 3076; *Angew. Chem. Int. Ed.* **2000**, *39*, 2952; i) A. Schnepf, H. Schnökel, *Angew. Chem.* **2001**, *113*, 734; *Angew. Chem. Int. Ed.* **2001**, *40*, 712.

[6] J. M. Goicoechea, S. C. Sevov, *Angew. Chem.* **2005**, *117*, 4094; *Angew. Chem. Int. Ed.* **2005**, *44*, 2.

[7] J. M. Goicoechea, S. C. Sevov, *J. Am. Chem. Soc.* **2005**, *127*, 7676.

[8] E. N. Esenturk, J. C. Fettinger, B. W. Eichhorn, *J. Am. Chem. Soc.* **2006**, *128*, 12.

[9] E. N. Esenturk, J. C. Fettinger, B. W. Eichhorn, *Chem. Commun.* **2005**, 247.

[10] E. N. Esenturk, J. C. Fettinger, Y.-F. Lam, B. W. Eichhorn, *Angew. Chem.* **2004**, *116*, 2184; *Angew. Chem. Int. Ed.* **2004**, *43*, 2132.

[11] M. J. Moses, J. C. Fettinger, B. W. Eichhorn, *Science* **2003**, *300*, 778.

[12] T. F. Fässler, S. D. Hoffmann, *Angew. Chem.* **2004**, *116*, 6748; *Angew. Chem. Int. Ed.* **2004**, *43*, 2.

[13] F. Gascoin, S. C. Sevov, *Inorg. Chem.* **2001**, *40*, 5177.

[14] a) L. Xu, S. Bobev, J. El-Bahraoui, S. C. Sevov, *J. Am. Chem. Soc.* **2000**, *122*, 1838; b) T. Hanauer, N. Korber, *Z. Anorg. Allg. Chem.* **2004**, *630*, 2532.

[15] a) A. Cisar, J. D. Corbett, *Inorg. Chem.* **1977**, *16*, 2482; b) A. N. Kuznetsov, T. F. Fässler, *Z. Anorg. Allg. Chem.* **2002**, *628*, 2537.

[16] L. Xu, A. Ugrinov, S. C. Sevov, *J. Am. Chem. Soc.* **2001**, *123*, 4091.

[17] a) A. Ugrinov, S. C. Sevov, *J. Am. Chem. Soc.* **2002**, *124*, 2442; b) A. Ugrinov, S. C. Sevov, *J. Am. Chem. Soc.* **2003**, *125*, 14059; c) A. Ugrinov, S. C. Sevov, *Chem. Eur. J.* **2004**, *10*, 3727.

[18] For recent reviews see: a) A. Schnepf, H. Schöckel, *Angew. Chem.* **2002**, *114*, 3683; *Angew. Chem. Int. Ed.* **2002**, *41*, 3532; b) H. Schnöckel, *Dalton Trans.* **2005**, 3131.

[19] E. Brechtel, G. Cordier, H. Schäfer, *J. Less-Common Met.* **1981**, *79*, 131.

[20] E. Brechtel, G. Cordier, H. Schäfer, *Z. Naturforsch. B* **1979**, *34*, 1229.

[21] C. Tiburtius, H.-U. Schuster, *Z. Naturforsch. B* **1978**, *33*, 35.

[22] G. Cordier, B. Eisenmann, H. Schäfer, *Z. Anorg. Allg. Chem.* **1976**, *426*, 205.

[23] G. M. Scheldrick, Bruker Nonius AXS, Madison, WI, USA, **2001**.

[24] A. D. Becke, *J. Chem. Phys.* **1993**, *98*, 5648.

[25] a) C. Lee, W. Yang, R. G. Parr, *Phys. Rev. B* **1988**, *37*, 785; b) B. Miehlich, A. Savin, H. Stoll, H. Preuss, *Chem. Phys. Lett.* **1989**, *157*, 200.

[26] a) P. J. Hay, W. R. Wadt, *J. Chem. Phys.* **1985**, *82*, 270; b) W. R. Wadt, P. J. Hay, *J. Chem. Phys.* **1985**, *82*, 284; c) P. J. Hay, W. R. Wadt, *J. Chem. Phys.* **1985**, *82*, 299.

[27] M. J. Frisch, G. W. Trucks, H. B. Schlegel, G. E. Scuseria, M. A. Robb, J. R. Cheeseman, V. G. Zakrzewski, J. A. Montgomery Jr., R. E. Stratmann, J. C. Burant, S. Dapprich, J. M. Millam, A. D. Daniels, K. N. Kudin, M. C. Strain, O. Farkas, J. Tomasi, V. Barone, M. Cossi, R. Cammi, B. Mennucci, C. Pomelli, C. Adamo, S. Clifford, J. Ochterski, G. A. Petersson, P. Y. Ayala, Q. Cui, K. Morokuma, N. Rega, P. Salvador, J. J. Dannenberg, D. K. Malick, A. D. Rabuck, K. Raghavachari, J. B. Foresman, J. Cioslowski, J. V. Ortiz, A. G. Baboul, B. B. Stefanov, G. Liu, A. Liashenko, P. Piskorz, I. Komaromi, R. Gomperts, R. L. Martin, D. J. Fox, T. Keith, M. A. Al-Laham, C. Y. Peng, A. Nanayakkara, M. Challacombe, P. M. W. Gill, B. Johnson, W. Chen, M. W. Wong, J. L. Andres, C. Gonzalez, M. Head-Gordon, E. S. Replogle, J. A. Pople, Gaussian, Inc., Pittsburgh, PA, USA, **2002**.

 © 2006 Wiley-VCH Verlag GmbH & Co. KGaA, Weinheim

Nanostructures

DOI: 10.1002/anie.200600429

Hierarchical Structured Nanohelices of ZnS**

*Daniel Moore, Yong Ding, and Zhong Lin Wang**

Wurtzite-structured materials, such as ZnO, ZnS, GaN, and AlN, have an important characteristic: the presence of polar surfaces that result from cation- or anion-terminated atomic planes. Consequently, a series of novel nanostructures, such as nanosprings,[1,2] nanorings,[3–5] nanohelices,[6] and nanobows,[7] have been formed. The mechanism that drives the formation of these novel configurations minimizes the electrostatic-interaction energy of the polar surfaces. As of now, these nanostructures have been mainly observed for ZnO, although nanosprings of wurtzite-structured AlN[5] and rutile-structured SnO_2[3] have also been observed as a result of the same formation mechanism.

ZnS, as another member in the wurtzite family and one of the most important materials in photonics, is a direct wide-band-gap (3.91 eV) semiconductor with a high index of refraction and a high transmittance in the visible range.[8–12] As for one-dimensional nanostructures, ZnS has been synthesized as nanowires, nanobelts, nanotubes, and nanocombs.[9,13–20] Recently, ZnS nanobelts have been doped with manganese, by post-annealing, without changing the crystallography of the ZnS nanobelts.[21] Optically pumped lasing has also been shown in single ZnS nanobelts.[22]

Herein, we report for the first time the high-yielding synthesis of hierarchical structured ZnS nanohelices. The morphology of the ZnS nanohelix is more complex than that observed for ZnO. The mechanism and the process of formation of the hierarchical structure are presented on the basis of the structural information provided by electron microscopy analysis. It is concluded that the hierarchical structure is a combined result of several growth features in the wurtzite ZnS.

The synthesis is based on the vapor deposition process. The as-synthesized samples were analyzed by using X-ray diffraction (XRD) and scanning electron microscopy. The XRD data confirmed that the as-synthesized sample was wurtzite ZnS. Optically, it appears yellow–white and covers the silicon deposition substrate. The synthesized material has a relatively high yield on the substrate and shows a high degree of reproducibility. The deposited material has a dominant morphology, which consists of helices of a ZnS

[*] D. Moore, Dr. Y. Ding, Dr. Z. L. Wang
Department of Materials science and Engineering
Georgia Institute of Technology
Atlanta, GA 30332-0245 (USA)
Fax: (+1) 404-894-8008
E-mail: zhong.wang@mse.gatech.edu

[**] We thank for the support from NSF, the NASA Vehicle Systems Program, Department of Defense Research and Engineering (DDR&E), and the Defense Advanced Research Projects Agency (Award No. N66001-04-1-8903).

WILEY InterScience DISCOVER SOMETHING GREAT
© 2006 Wiley-VCH Verlag GmbH & Co. KGaA, Weinheim

nanobelt. Some scanning electron microscopy (SEM) images of the sample are shown in Figure 1: As can be seen in Figure 1 a, the yield of the helical structures is rather high, and Figure 1 b shows a very long, densely branched nanohelix. The

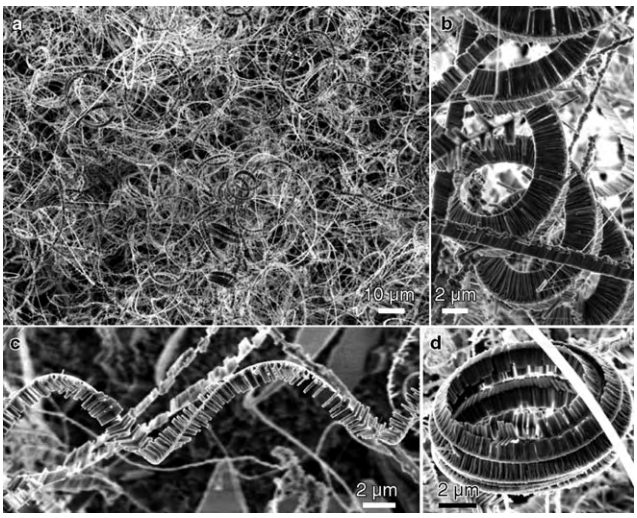


Figure 1. a) Low magnification SEM image that shows the high yield of ZnS nanohelices on the silicon substrate. b) A very long and densely branched nanohelix. c) A more typical moderately branched nanohelix. d) A densely branched nanohelix that has fallen in on itself and loosely formed a ringlike structure.

side branches align well and form an ordered structure along the entire length of the nanohelix. Figure 1 c shows a helix that is long and moderately branched, which is by far the most commonly observed ZnS nanohelix, though the others are common as well. Figure 1 d shows a helix that has curled up into itself to form a ringlike structure.

The nanohelices are made up of two parts: The first is the spine, which coils into a helical shape; the second has Y-shaped branches that all grow to the same size and at the same side of the spine in each nanohelix. The Y-branched structures always grow toward the inside of the helix (Figure 2 a), and they rotate and follow the curled shape of the nanohelix. The Y branches are densely packed to form an aligned and ordered array that follows the coiling geometry of the helix (Figure 2 b).

Statistical data were recorded a wide range of aspects of the helices. The analysis of nearly one hundred separated helices recorded the pitch, radius, and handedness of the helix. No direct relationship was found between pitch and radius, and no preferences towards handedness was noticed (of the helices that could be measured, about 60 % were right-handed and about 40 % left-handed).

The structure of the hierarchical nanohelix was analyzed by transmission electron microscopy (TEM) to understand the formation process. Figure 3 a shows a low-magnification TEM image of a segment of the nanohelix: The Y structure has two V-shaped branches that are rather smooth in shape, but the bottom branch connected to the spine is rather rough, thus possibly indicating some subsequent growth at the side surface (Figure 3 b). Figure 3 c and e are, respectively, a TEM

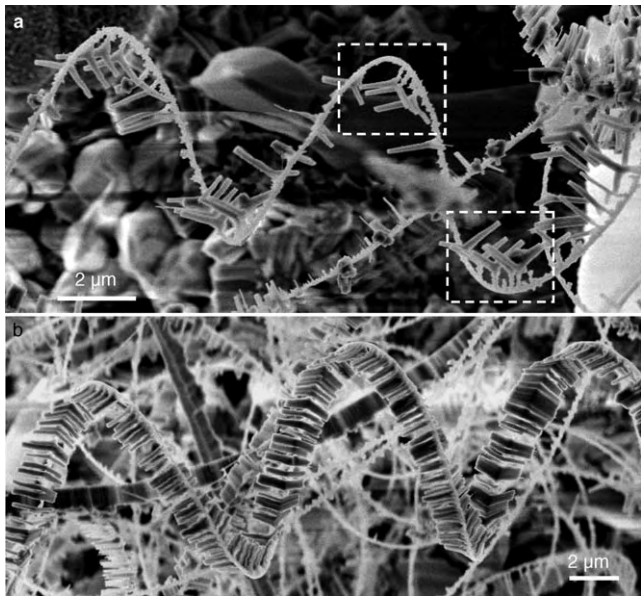


Figure 2. a) A lightly branched nanohelix. The branched secondary growth always grows towards the inside of the helix as seen particularly in the two boxed areas. The nanohelices consist of a spine which coils in a helical shape. On the inner side of the spine there is Y-shaped secondary growth which grows to the same length along an individual nanohelix. b) Another typical, moderately branched nanohelix. The Y-shaped branches always point towards the inside of the coil, regardless of the handedness of the nanohelix, thus suggesting that the inner face is the chemically active Zn-terminated face.

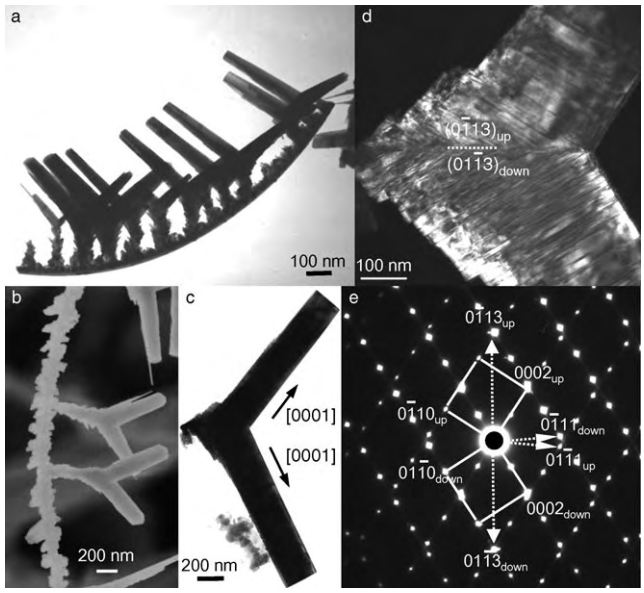


Figure 3. a) A typical TEM image of the ZnS nanohelix. It has been broken as a result of transfer from the silicon deposition substrate to the TEM sample holder. b) An SEM close-up of the secondary Y-shaped branches that grew towards the inside of the helix. The rough growth surface is visible. c) Top-down view of a typical branch growth, its selective-area electron-diffraction (SAED) pattern (e) shows the (0113) twin structure and the growth direction of the branch is along the [0002] direction. d) The dark-field image of the branch growth and the twin plane that reveals a large number of stacking faults, thus indicating a large amount of local strain in the crystal.

 © 2006 Wiley-VCH Verlag GmbH & Co. KGaA, Weinheim

image and the corresponding electron diffraction pattern recorded from the V branches with the incident electron beam perpendicular to the V plane. The V branches have a twin relationship, and the twin plane is $(0\bar{1}13)$, as previously observed for ZnO and CdSe.[23] The diffraction pattern is composed of two sets of diffraction spots that have a symmetrical geometrical layout. The common spot is the twin boundary plane $(0\bar{1}13)$ or $(01\bar{1}3)$. The incident beam direction, for example, the normal direction of the V-branch plane, is $[\bar{2}110]$. This behavior also indicates that the growth direction of the coiling spin is $[\bar{2}110]$. The growth directions of the two branches of the V-shaped structure are [0001]. The stacking faults that lie in the (0001) plane can be clearly seen in the two V branches, which are produced by the structural transformation between wurtzite and the zinc blend,[14] through the dark-field TEM image displayed in Figure 3d.

We next rotated the sample so that it was orientated with one side of the V branches parallel to the electron beam (Figure 4a). The corresponding electron diffraction pattern in

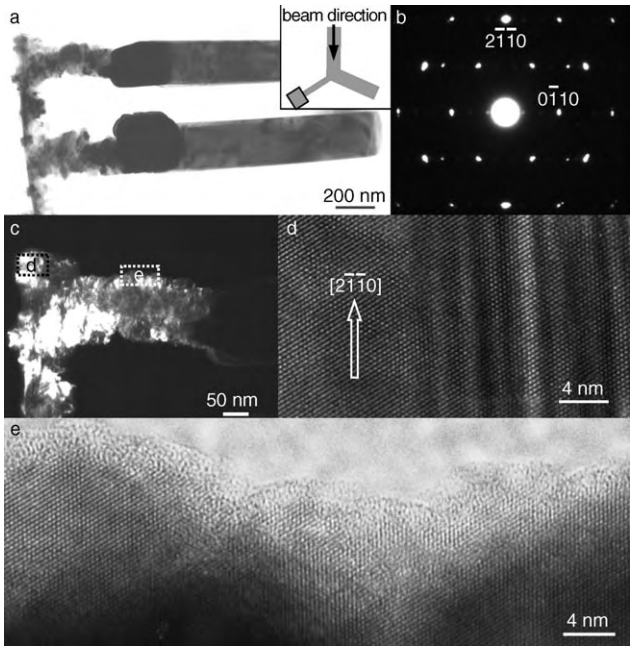


Figure 4. a) A bright-field TEM image with the beam direction along the length of one of the secondary growth branches (inset). b) The SAED pattern of the spine, which shows the growth plane of the spine is the $(2\bar{1}\bar{1}0)$ plane. c) Dark-field image that highlights the growth of the spine and the branched growth. A high-resolution image of d) the spine of the nanohelix and e) the rough secondary growth.

Figure 4b is dominated by the [0001] pattern with some extra spots contributed by the other side branch of the V structure. A dark-field TEM image using one of the diffraction spot shows that the nanohelical spine is a single-crystal piece with one branch of the V structure, although its surface is rough. A high-resolution TEM (HRTEM) image recorded from the selected area d (Figure 4c) clearly display the structure of wurtzite ZnS projected along the *c* axis (Figure 4d). The growth direction of the spine is $[\bar{2}110]$. The HRTEM image (Figure 4e) recorded from the area e (Figure 4c) shows an identical structure as the spine, thus clearly indicating that the bottom branch of the Y structure is a single crystalline piece that belongs to the spine.

The structure of the hierarchical structure can be described as follows (Figure 5a): The spine grows along the

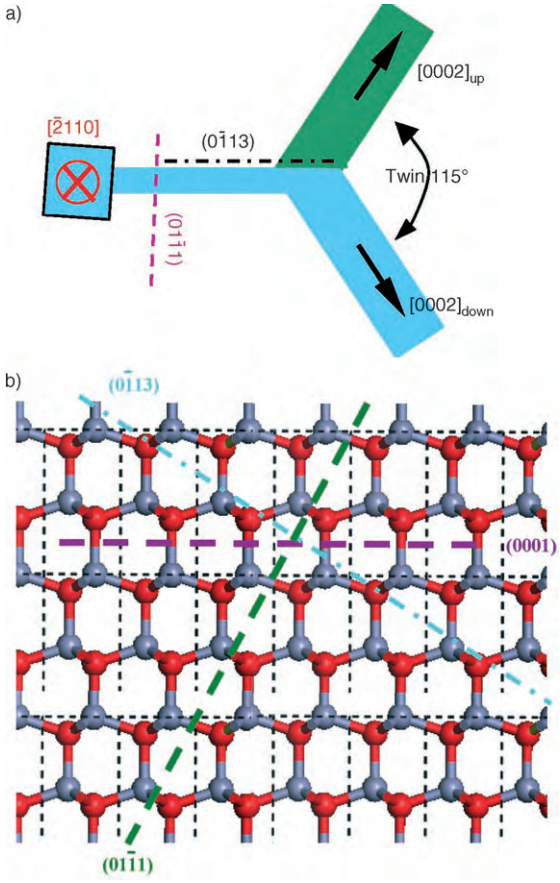


Figure 5. a) A schematic representation of the various planes and growth directions of the nanohelix. The main spine of the nanohelix is oriented along the $(2\bar{1}\bar{1}0)$ plane, with the polar $(01\bar{1}1)$ plane towards the inside of the helix. Off of this polar plane, the secondary growth occurs. b) A projection of the ZnS wurtzite lattice along the $(2\text{-}1\bar{1}0)$ plane that shows the key planes. The {0001} and $\{01\bar{1}1\}$ plane families are polar as they terminate with Zn^{+} and S^{-1} ions. The $\{0\bar{1}13\}$ plane is also shown, as it is the side plane of the initial secondary growth off the nanohelix.

$[\bar{2}110]$ direction, and its side surfaces are defined by $\pm(0\bar{1}13)$ and $\pm(01\bar{1}1)$. The surface is rough because the $\pm(0\bar{1}13)$ are higher energy planes. On the $(01\bar{1}1)$ surface, one branch grows out along $\approx[07\bar{7}4]$, a direction approximately perpendicular to the $(01\bar{1}1)$ plane. Then, a turn in growth direction from $\approx[07\bar{7}4]$ to [0002] leads to the formation of one of the V branches, and a twin growth by sharing the $(01\bar{1}3)$ plane results in the growth of the other branch. This change from the $[07\bar{7}4]$ growth direction to the [0002] direction occurs because of the very high energy associated with growth along the $[07\bar{7}4]$ direction. The direction [0002] is the fastest growth and lowest energy for wurtzite ZnS.

The nature of the $\{01\bar{1}1\}$ and $(0\bar{1}13)$ planes can be understood from the atomic model of ZnS. By projecting

 © 2006 Wiley-VCH Verlag GmbH & Co. KGaA, Weinheim

the structural unit cell along the $[\bar{2}110]$ direction, beside the most typical $\pm(0001)$ polar surfaces that are terminated with zinc and oxygen centers, respectively, the $\pm(01\bar{1}1)$ planes are also polar surfaces (Figure 5b). If $(01\bar{1}1)$ is terminated with zinc cations, the $(0\bar{1}1\bar{1})$ surface is terminated with sulfur anions, thus, the two surfaces will be positively and negatively charged, respectively.

The formation of the hierarchical structure can be separated into two major stages. The first stage is a fast growth of the spine defined by the $\{01\bar{1}1\}$ and $(01\bar{1}3)$ planes. The spine is confined by two oppositely charged zinc-terminated $(01\bar{1}1)$ and sulfur-terminated $(0\bar{1}1\bar{1})$ surfaces, and it can be viewed as a thin plate capacitor with a dipole moment across its width.[2] From our previous study on nanosprings and nanohelices of wurtzite ZnO,[1] the elastic deformation energy is rather small when the thickness of a nanobelt is small; thus, forming a circular structure would reduce the dipole moment of the nanobelt and minimize the energy contributed by the electrostatic interaction from the dipole-polarization and elastic deformation.[4] As a result, the nanobelt coils as the growth proceeds and forms the spine, thus resulting in the formation of a spring or helix with the $(01\bar{1}1)$ polar surface that face inward towards the coiling axis.

On the other hand, we know that the zinc-terminated surface is catalytically active and can induce secondary growth, whereas the sulfur-terminated surface is inert.[13] Thus, the side branches on the zinc-terminated $(01\bar{1}1)$ surface grow out, similar to the growth of the one-sided teeth of the ZnS nanocombs.[14] As described in Figure 5a, a switch and split in growth direction and a formation of a twin form the Y-branched structures. Moreover, the sulfur-terminated $(0\bar{1}1\bar{1})$ surface is inactive and shows no secondary growth. Therefore, the Y branches are aligned on one side of the spine (or nanobelt) and rotate according to the coiling shape of the spine, as observed in Figure 2.

As shown in Figures 1 and 2, the Y branches always point inward to the center. An alternative explanation is that the zinc-terminated $(01\bar{1}1)$ surface may have a larger stress than the sulfur-terminated $(0\bar{1}1\bar{1})$ surface, thus resulting in one-directional bending of the nanobelt. This process can co-contribute to the formation of the nanohelix, which may be a case for ZnS, but our previous study shows that this process is not the dominant for ZnO in the formation of nanosprings.[24]

In summary, hierarchical nanohelices of ZnS are reported for the first time. The nanohelices were synthesized by a vapor deposition process at high yield. The hierarchical nanohelix is formed by a combination of several growth characteristics for the wurtzite structure. The spine is a fast-growing nanobelt that is dominated by the $\pm(01\bar{1}1)$ polar and the $\pm(0\bar{1}13)$ nonpolar surfaces. The presence of polar surfaces results in coiling of the nanobelt to form a helix that minimizes the energy contributed by the polar charges to the surfaces. The difference in surface stress may also contribute to this process. The growth of the nanobelt/spine occurs rather fast. Then, the zinc-terminated $(01\bar{1}1)$ surface initiates the growth of one-sided teeth as a result of self-catalysis, similar to the nanocomb. Along the teeth, a switch in the growth-front plane from $(01\bar{1}1)$ to (0001) to lower the surface energy produces one branch of the Y structure. Finally, a $(0\bar{1}13)$ twin is formed at the switching point of the branch, thus resulting in the growth of the other branch along the [0001] direction, thus finally completing the Y structure. The twin is favorable as a result of the two possible phases of ZnS that coexist in the growth: the wurtzite hexagonal structure and zinc-blend cubic structure. The reported hierarchical nanohelices of ZnS could have novel mechanical, optical, and electrical properties.

Experimental Section

The synthesis of the ZnS nanohelices was carried out by using a simple vapor deposition process. Commercially available ZnS powder (Alfa Aesar, 99.99% purity, metal basis) was placed in the center of a single-zone horizontal tube furnace (Thermolyne 79300), in which the temperature, pressure, atmosphere, and evaporation time were controlled. Single-crystal silicon substrates with 1.5 nm of Au deposited on them with a thermal evaporator were placed "downstream" and at a lower temperature region in the furnace. These were used to collect the deposited material. Using a rotary vacuum pump, the tube was placed under vacuum for several hours to purge oxygen from the chamber. After evacuation to a pressure of about 2×10^{-3} Torr, the temperature in the center of the tube was elevated to 1000 °C at a rate of 50 °C min^{-1}. A N_2 gas flow was introduced into the system at a rate of 50 cm^2 min^{-1}. The inert N_2 gas acted as a carrier for transporting the sublimated vapor to cooler regions within the tube furnace for deposition onto the silicon substrates and also to help increase the pressure. The pressure was allowed to increase to a value of 20 Torr (about 25 mbar). The silicon substrates reached a temperature of about 750 °C. During evaporation, the products were deposited onto the silicon substrates. After maintaining these conditions for 2 h, the nitrogen gas flow was turned off and the products placed under vacuum. At this time, the furnace was allowed to cool to room temperature. The gold particle introduced initially was not found in the grown product, may be as a result of the vaporization of the gold at the early stage of the long growth (2 h).

Received: February 1, 2006
Published online: July 9, 2006

Keywords: chemical vapor deposition · nanohelices · nanostructures · sulfur · zinc

[1] X. Y. Kong, Z. L. Wang, *Nano Lett.* **2003**, *3*, 1625.
[2] R. Yang, Y. Ding, Z. L. Wang, *Nano Lett.* **2004**, *4*, 1309.
[3] R. Yang, Z. L. Wang, *J. Am. Chem. Soc.* **2006**, *128*, 1466.
[4] X. Y. Kong, Y. Ding, R. Yang, Z. L. Wang, *Science* **2004**, *303*, 1348.
[5] J. Duan, S. Yang, H. Liu, J. Gong, H. Huang, X. Zhao, J. Tang, R. Zhang, Y. Du, *J. Cryst. Growth* **2005**, *283*, 291.
[6] P. Gao, Y. Ding, W. Mai, W. Hughes, C. Lao, Z. L. Wang, *Science* **2005**, *309*, 1700.
[7] W. Hughes, Z. L. Wang, *J. Am. Chem. Soc.* **2004**, *126*, 6703.
[8] T. W. Odom, J. Henzie, Y. Babayan, E. C. Greyson, E. S. Kwak, *Talanta* **2005**, *67*, 507.
[9] Y. C. Zhu, Y. Bando, D. F. Xue, D. Golberg, *Adv. Mater.* **2004**, *16*, 831.
[10] R. A. Rosenberg, G. K. Shenoy, F. Heigl, S.-T. Lee, P.-S. G. Kim, X.-T. Zhou, T. K. Sham, *Appl. Phys. Lett.* **2005**, *86*, 263115.
[11] Y. W. Wang, L. D. Zhang, C. H. Liang, G. Z. Wang, X. S. Peng, *Chem. Phys. Lett.* **2002**, *357*, 314.
[12] J. S. Steckel, J. P. Zimmer, S. Coe-Sullivan, N. E. Stott, V. Bulovi, M. G. Bawendi, *Angew. Chem.* **2004**, *116*, 2206; *Angew. Chem. Int. Ed.* **2004**, *43*, 2154.

 © 2006 Wiley-VCH Verlag GmbH & Co. KGaA, Weinheim

[13] D. Moore, C. Ronning, C. Ma, Z. L. Wang, *Chem. Phys. Lett.* **2004**, *385*, 8.
[14] C. Ma, D. Moore, J. Li, Z. L. Wang, *Adv. Mater.* **2003**, *15*, 228.
[15] C. J. Barrelet, Y. Wu, D. C. Bell, C. Lieber, *J. Am. Chem. Soc.* **2003**, *125*, 11498.
[16] P. V. Radovanovic, C. J. Barrelet, S. Gradecak, F. Qian, C. Lieber, *Nano Lett.* **2005**, *5*, 1407.
[17] X. M. Meng, J. Liu, Y. Jiang, W. W. Chen, C. S. Lee, I. Bello, S. T. Lee, *Chem. Phys. Lett.* **2003**, *382*, 434.
[18] Y. Jiang, X. Meng, J. Liu, Z. Xie, C. S. Lee, S.-T. Lee, *Adv. Mater.* **2003**, *15*, 323.
[19] X. Fan, X.-M. Meng, X.-H. Zhang, W.-S. Shi, W.-J. Zhang, J. A. Zapien, C.-S. Lee, S.-T. Lee, *Angew. Chem.* **2006**, *118*, 2630; *Angew. Chem. Int. Ed.* **2006**, *45*, 2568.
[20] J. Hu, Y. Bando, J. Zhan, D. Golberg, *Angew. Chem.* **2004**, *116*, 4706; *Angew. Chem. Int. Ed.* **2004**, *43*, 4606.
[21] Y. Q. Li, J. A. Zapien, Y. Y. Shan, Y. K. Liu, S.-T. Lee, *Appl. Phys. Lett.* **2006**, *88*, 013115.
[22] J. A. Zapien, Y. Jiang, X. M. Meng, W. Chen, F. C. K. Au, Y. Lifshitz, S. T. Lee, *Appl. Phys. Lett.* **2004**, *84*, 1189.
[23] Y. Ding, Z. L. Wang, *J. Phys. Chem. B* **2004**, *108*, 12280.
[24] P. Gao, Z. L. Wang, *Small* **2005**, *1*, 945.

 © 2006 Wiley-VCH Verlag GmbH & Co. KGaA, Weinheim

Molecular Dynamics

DOI: 10.1002/anie.200601778

Ultrafast Electron Crystallography of Phospholipids**

*Songye Chen, Marco T. Seidel, and Ahmed H. Zewail**

We report herein our first study on the structure and dynamics of mono- and bilayer phospholipids, the essential elements of biological membranes, by using ultrafast electron crystallography (UEC).[1,2] The phospholipid was immobilized as a Langmuir–Blodgett film on hydrophilic or hydrophobic silicon substrates. From the diffraction patterns we determined that the dimyristoyl phosphatidic acid (DMPA; Figure 1) molecules were aligned with their aliphatic chains perpendicular to the substrate surface, and resolved the subunit cell -CH_2-CH_2-CH_2- distance to be $c_0 = 2.54$ Å. After a femtosecond temperature jump in the substrate we observed, through changes in the position and intensity of the diffraction, structural dynamics on different time scales: a coherent, non-equilibrium expansion (wave-type) along the aliphatic chains on the picosecond timescale, as well as contraction and restructuring at longer times. Moreover, transient structural ordering was revealed on the ultrashort time scale. For this complex system, UEC allowed us to picture the atomic forces involved in structural dynamics at far-from-equilibrium configurations, whose collective and coherent effects may otherwise be obscured.

The resemblance of both lipid Langmuir films at water surfaces and Langmuir–Blodgett (LB) films to naturally occurring biological membranes means they often serve as model systems for studying membrane structures and properties,[3,4] such as head-group organization and hydration,[5] phase transitions,[6] interactions with membrane proteins,[7,8] and proton diffusion,[9] besides other applications in molecular electronics[10] and biological sensors.[11] Studies on the structure of lipid LB films have mostly been focused on fatty acids and fatty acid salts,[12] but for phospholipids, although more complex and less studied, their structures have been probed by a variety of techniques, including electron diffraction,[13–15] X-ray diffraction,[5,16] infrared spectroscopy,[17,18] scanning tunneling microscopy,[19] and atomic force microscopy.[20]

Structural ultrafast dynamics have not been reported. Ultrafast optical spectroscopy has been used to probe the dynamics of water solvation,[21] and inelastic neutron scattering has enabled the deduction of time scales of collective motions from the dispersion relationships.[22] UEC is well suited for the study of structural changes because of its high sensitivity, low damage at low electron flux,[23] and spatiotemporal resolutions. All experiments were carried out in our UEC apparatus,[2,24] in which the electrons are incident at a grazing angle of $\theta_i = 0$–$5°$ and are scattered by the lipid molecules to form the diffraction patterns in the far field. The scattered electrons are recorded with a low-noise, image-intensified, charge-coupled device (CCD) camera assembly capable of single-electron detection.[23]

The change of the structure was initiated by a femtosecond infrared laser pulse (800 nm, 120 fs, 1 kHz repetition rate) focused onto the sample surface at an incidence angle of 30° and an area of illumination of approximately 1.3 mm^2. Part of this IR beam was frequency tripled (266 nm, ca. 10 nJ) and used to synchronously generate the ultrashort electron pulses (30 keV, $\lambda_{\text{de Broglie}} = 0.07$ Å) through the photoelectric effect. A series of diffraction frames were recorded at a specified time delay by adjusting the time delay between the laser and electron pulses. When combined, these frames give the real-time change of the structure. The time zero was determined in situ.

The lipids are deposited (see Experimental Section) in the so-called Y geometry, that is, head-to-head and tail-to-tail. In the case of a hydrophilic substrate, the first layer is attached to the surface by its hydrophilic head, while for a hydrophobic substrate the attachment is through the hydrophobic tail (see Figure 1B). We used a hydrophilic oxide-terminated silicon-(111) surface for deposition of the monolayer, and a hydrophobic hydrogen-terminated silicon(111) surface for the bilayer (See Experimental Section). Isotherms of the Langmuir film and the transfer ratio at deposition were recorded to ensure the LB films were of high quality. The morphology of

[*] S. Chen, Dr. M. T. Seidel, Prof. Dr. A. H. Zewail
Laboratory for Molecular Sciences, and
Physical Biology Center for Ultrafast Science and Technology
California Institute of Technology
Pasadena, CA 91125 (USA)
Fax: (+1) 626-792-8456
E-mail: zewail@caltech.edu

[**] This work was supported by the National Science Foundation. We thank Prof. J. Heath for the use of his LB facility, E. DeIonno, J.-W. Choi, P. Cao, Dr. Y. Luo, and Dr. H. Yu for advice and discussion on LB films, and the three referees for helpful suggestions.

InterScience © 2006 Wiley-VCH Verlag GmbH & Co. KGaA, Weinheim

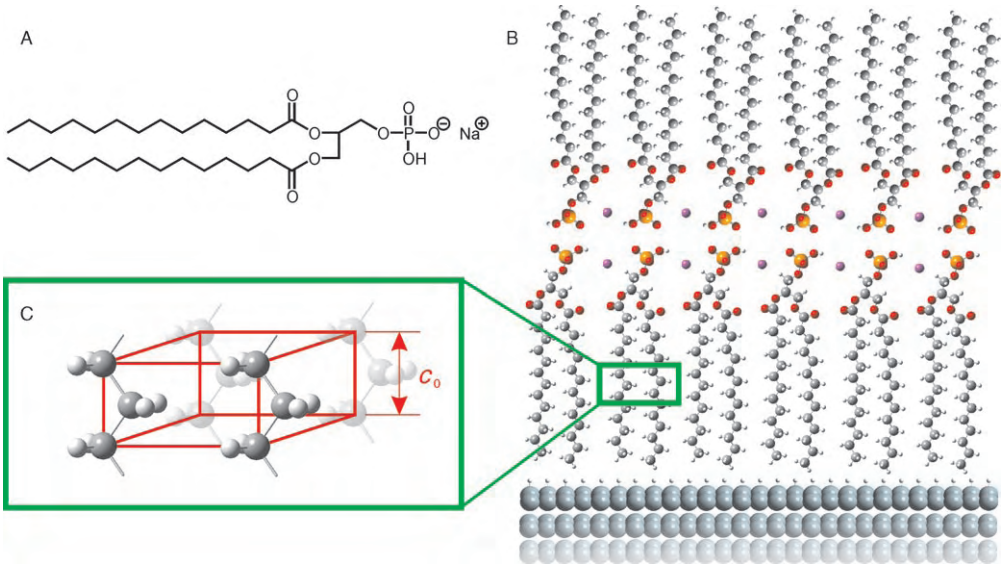


Figure 1. A) A view of the molecular structure, B) the phospholipid DMPA on the substrate, and C) the C_2H_4 subunit cell, with the distance c_0 between the CH_2 groups shown.

the lipids at the air–water interface was monitored with a Brewster angle microscope and no holes or multilayer islands were found. The samples were transferred immediately after deposition into an ultrahigh vacuum (UHV, ca. 10^{-10} Torr), in which all the experiments were carried out. The LB films are stable to electron exposure, as evidenced by the absence of deterioration in the quality of the static diffraction patterns. For a typical pulse of 10^3 electrons at our repetition rate the dosage level is about 10^{-6} electrons s^{-1} Å^{-2}, and for exposure over several hours this translates to about 10^{-2}–10^{-1} electrons Å^{-2}. It is also significant to note that the dosage is provided in a pulsed mode with sufficient time (1 ms) to dissipate the heat.

The electron diffraction recorded here is mainly sensitive to the C_2H_4 subunit of the aliphatic chains[25] as a consequence of the s range covered, where s is the momentum transfer between the incident electron and the scattered electron, that is, $s = kR/L$; $k = 1/\lambda_{\text{de Broglie}}$, R is the distance between a diffraction spot and the main beam position on the screen, and L is the distance between the sample and the screen. The molecular structure of DMPA (Figure 1 A) is similar to that of fatty acids, but with some differences: there are two aliphatic chains instead of one, and there is a different head group. Phospholipids organize in a two-dimensional hexagonal lattice where the aliphatic chains pack parallel to each other and perpendicular to the surface.[13–15,17,18] The structure of the C_2H_4 subunit cell is illustrated in Figure 1 C.

The static diffraction patterns of the monolayers and bilayers (Figure 2 B and C, respectively) are similar. The strongest feature of the patterns is the horizontal (or slightly curved) line, which is labeled by the Miller indices ($hk2$). The diffraction line is basically the composite of Bragg diffractions

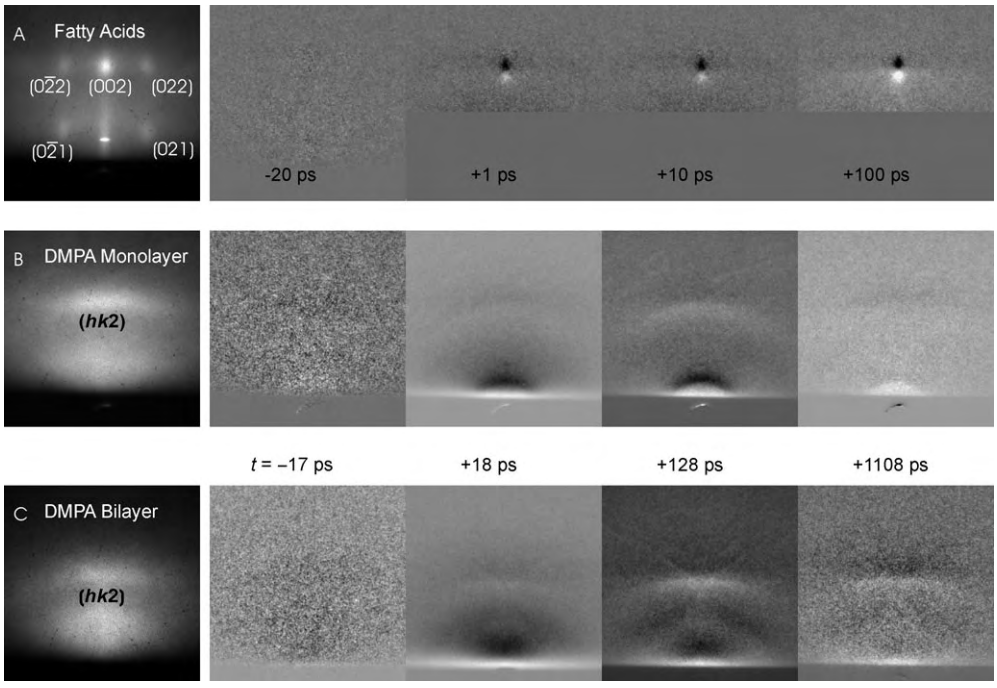


Figure 2. The static diffraction patterns and the diffraction difference patterns of DMPA monolayers, bilayers, and fatty acids on substrates. The diffraction difference patterns of the fatty acid (arachidic acid calcium salt) bilayer are shown with the time delays indicated. For the DMPA molayers and bilayers, the Bragg spots appear as lines on a diffuse background. We note that the diffraction difference patterns at negative times show no features, as expected.

© 2006 Wiley-VCH Verlag GmbH & Co. KGaA, Weinheim

(see Panel A for the fatty acids). The subunit cell parameter c_0 was determined from the *s* value in the vertical direction to be 2.54 Å, which is representative of the -CH_2-CH_2-CH_2- distances, as shown in Figure 1 C. This distance is nearly the same as that determined for the LB films of fatty acids (Figure 2 A). The diffraction line pattern indicates that, although the LB films consist of many crystalline domains, the aliphatic chains are packed parallel to each other. The fact that the diffraction line is oriented parallel to the shadow edge means that the aliphatic chains are aligned nearly perpendicular to the surface. The diffraction patterns in the lower *s* range show diffuse scattering from the different crystalline domains. The diffraction pattern was independent of the electron incidence angle θ_i and the azimuthal angle ϕ, which is consistent with the presence of polycrystalline domains.

The diffraction patterns change significantly following the heating of the substrate with an ultrafast IR laser pulse. This is shown in the frame difference patterns in Figure 2 B and C for the monolayers and bilayers, respectively. Before time zero, that is, when the electron pulse arrives prior to the heating pulse, the diffraction difference patterns are featureless (shown in Figure 2 B and C for $t = -17$ ps). After time zero, the patterns show a change in the (*hk*2) line position—becoming dark at the higher *s* value and bright at the lower *s* value, which indicates a downward movement of the line with time. Shrinkage in the reciprocal space corresponds to an expansion in real space. Therefore, the downward movement of the diffraction line means an increase of the -CH_2-CH_2-CH_2- distances along the aliphatic chains.

To quantify the change in the structure with time, we fitted the (*hk*2) diffraction line in the vertical *s* direction with a Voigt function, thus providing the exact peak center position and integrated intensity at each time point. From the center position, the subunit cell parameter c_0 was obtained, and its change as a function of time is shown in Figure 3 A and B for monolayers and bilayers, respectively. The dynamics of the change is similar for both samples, showing a successive increase in the c_0 value (total ca. 50 ps) and the recovery back (ca. 500 ps) on our time scale. However, the amplitude of the expansion in the monolayer is smaller than in the bilayer by nearly a factor of three. Similar behavior was also observed for fatty acids studied as a function of thickness.[25,26]

For ordered materials we expect the transient intensity change to follow that of the shift Δc_0. By integrating over the vertical *s* range, after careful removal of the background, we obtained the results depicted in Figure 3. The intensity initially drops within about 15 ps after heating with the IR laser, but then increases to even above the static value in approximately 130 ps, and finally recovers back to the initial value at longer times (ca. 400 ps). The initial drop in the intensity is consistent with the disorder induced by the heating pulse. This disorder is typically described by the thermal (incoherent) motion of atoms and can be expressed using standard Debye–Waller factors. However, the subsequent increase in the intensity above the static value indicates the formation of a more-ordered state on the ultrafast time scale and is certainly nonthermal. Comparing the shift and the intensity change with time, we see that when the elongation reaches its maximum, the intensity (toward order) is also at its highest, but the intensity maximum toward disorder occurs at a shorter time. At longer times, the behavior becomes comparable. Similar trends in the intensity behavior were

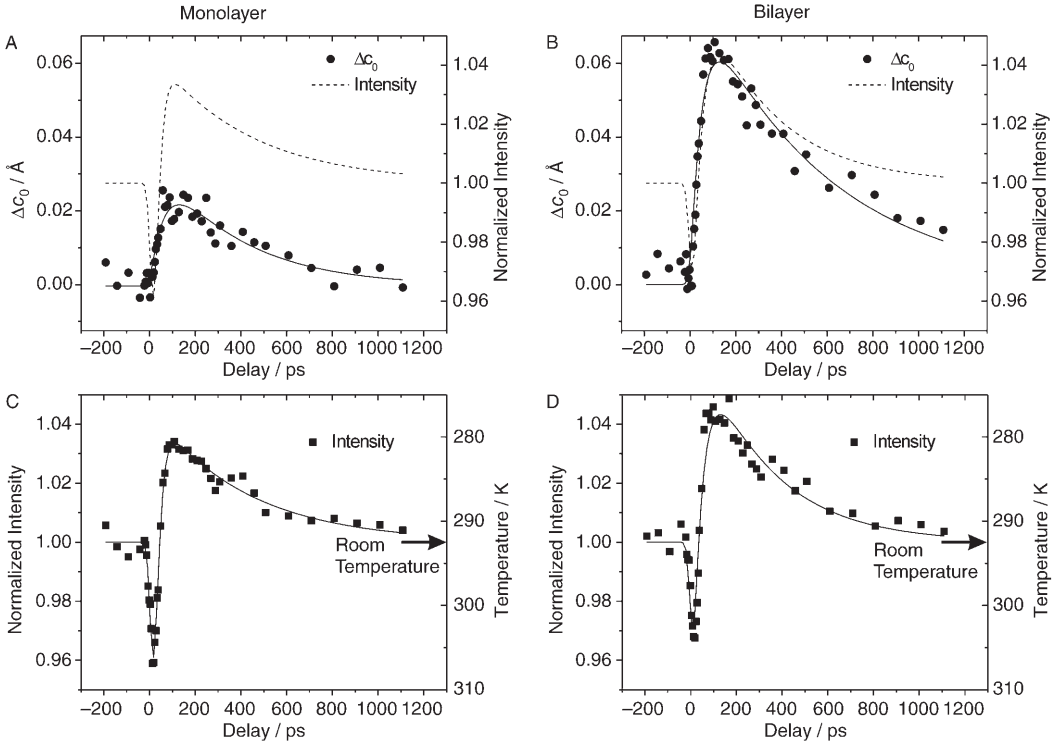


Figure 3. Dynamics of structural change. The axial change Δc_0 and the normalized intensity of the (*hk*2) diffraction line as a function of time for: A) and C) the monolayer, and B) and D) the bilayer of the phospholipid.

 © 2006 Wiley-VCH Verlag GmbH & Co. KGaA, Weinheim

observed for the fatty acids.[26] The width of the diffraction line contains information on changes in the order/disorder of fatty acids, but for phospholipids the signal-to-noise ratio was not sufficiently high to ascertain the significance of the change. We have measured the change in intensity with temperature under steady-state conditions for fatty acids, and if such a change is similar to that of the phospholipids, then the temperature scale in Figure 3C and D would reflect the corresponding equilibrium values. In the simplest model of harmonic chains, a change of 0.02 Å corresponds to a temperature increase of approximately 30 K, in the non-equilibrium regime.

The net change in displacement is determined by the impulsive force (temperature) of the substrate (including coupling) and the maximum value of the extension depends on the elasticity and heat capacity. If heating occurs for an equilibrated system, the change in the value of c_0 with temperature Δc_0 should be independent of the number of C-C-C subunits in the chain, and $\Delta c_0/c_0$ becomes simply α (the thermal expansion coefficient), which is typically very small (10^{-4}–10^{-6}).[27] However, for non-equilibrium dynamics, the impulsive force at short times transmit a large change in the value of Δc_0 as the disturbance (wave-type) accumulates to give the net effect that is dependent on the number of C atoms.[28] Both the observed amplitude of the change and the rise in time are consistent with this non-equilibrium wave-type propagation at ultrashort time and equilibration at much longer times. This picture also explains the dependence on the total length of the chains. Quantification of the total change must take into account the variation in the density of the LB films upon going from single to multiple layers and the nature of the substrate force. It is known that "defects" or holes can be formed when multiple layers are deposited.[29] Moreover, as the effect of the substrate decreases with increasing distance (in this case chain length), some disorder is expected.[30]

The fact that the initial change in intensity (and elongation) occurs within 15 ps and that the distance traveled is approximately 20 Å (for a monolayer) predicts a speed of propagation that is sub-kilometers per second, which is close to the propagation of sound waves (underdamped regime); future experiments will examine this region at different times and temperatures. It will be shown elsewhere[28] that the frequencies of C-C-C motion and force in the diffusive (overdamped) regime have to be unrealistically large. In the underdamped regime, although the force is significant to cause the large change in Δc_0, and coherent propagation is within the chain, the change in the value of Δc_0 relative to that of c_0 is relatively small to preserve the robustness of the Bragg spots throughout the temporal change. However, it is important to point out that for large complex systems the diffraction has features of both "crystalline" and "diffusive" scatterings. The latter gives structural information on the collective motions, which can be examined through cross-terms of Debye–Waller factors.[31] In this regard, the ring(s) apparent at $s \approx 0.3$ Å^{-1} in the diffraction difference patterns should be analyzed for such correlations in the phospholipid, and we shall consider this analysis elsewhere.

The structural dynamics can now be pictured. Since the phospholipids have no resonance absorption at 800 nm, which is the wavelength of the heating IR laser pulse, the energy is absorbed by the substrate. The energy is transferred within a few picoseconds into the substrate lattice (through electron–phonon coupling), which results in an expansion of the substrate lattice.[24,25] On this time scale, the energy is transferred to the adsorbate, where it flows along the aliphatic chains of the DMPA molecules through vibrational motion. The net effect is the elongation of the C_2H_4 subunits. This transport of heat at an early time first induces transient disorder, which causes the intensity of the (*hk*2) diffraction line to drop in the first 15 ps. This result is expected in a Debye–Waller picture, as the degree of inhomogenity along the chains increases with temperature. However, with time, the lipids enter a more ordered state, which manifests itself in an increased diffraction intensity even above the initial value. This effect is achieved by overcoming some energy barrier and through alignment of the aliphatic chains by rotation and other motions, and possibly through transient annealing of the film, which because of defects could have more effect in multiple layers than monolayers. This enhanced structural ordering may be common, even in self-assembly, but it can only be observed[32] in the non-equilibrium state at short times. When the energy dissipates into the substrate, the aliphatic chains of the DMPA molecules begin to contract and restructure toward the initial equilibrium state on the nanosecond time scale. It is known that different phases ("gel" and "liquid") do exist depending on the temperature, and it is interesting that neutron scattering studies give a lifetime of 17 ps for the acoustic phonon excitation in the gel phase.[22]

In conclusion, it has been demonstrated here that monolayer and bilayer phospholipids on hydrophilic and hydrophobic substrates can be studied using UEC. The combined structures (unit cell and orientation) and dynamics (after femtosecond laser heating) are reported, thus providing insights into the nature of atomic motions and energy transfer—coherent versus diffusive—in phospholipids. The transient structural ordering discussed here may be significant to dynamic assembly and collective motions (which occur at short times) in bilayers and possibly membranes. Future work will consider the role of hydration.

Experimental Section

1,2-Dimyristoyl-*sn*-glycero-3-phosphate monosodium salt (dimyristoyl phosphatidic acid, DMPA) was purchased from Aldrich and used without further purification. The lipids were spread from a chloroform/methanol (3:1) solution, and the subphase used was Millipore water containing sodium ions at pH 5.5. The deposition took place in an NIMA Langmuir–Blodgett dipping trough at a dipping pressure of $\pi = 29$ mN m^{-1} and a dipping speed of 1 mm min^{-1}.

Hydrophilic silicon surfaces were prepared just before deposition by cleaning and oxidation with an RCA-1 solution. For the hydrophobic surfaces, subsequent etching of the oxide surface was made in a 40% NH_4F solution for 15–20 min to give the Si(111):H surface.

Received: May 5, 2006

 © 2006 Wiley-VCH Verlag GmbH & Co. KGaA, Weinheim

Keywords: diffraction · Langmuir–Blodgett films · molecular dynamics · phospholipids · surface assembly

[1] J. M. Thomas, *Angew. Chem.* **2004**, *116*, 2658; *Angew. Chem. Int. Ed.* **2004**, *43*, 2606.
[2] F. Vigliotti, S. Chen, C.-Y. Ruan, V. A. Lobastov, A. H. Zewail, *Angew. Chem.* **2004**, *116*, 2759; *Angew. Chem. Int. Ed.* **2004**, *43*, 2705.
[3] G. Roberts, *Langmuir-Blodgett Films*, Plenum, New York, **1990**.
[4] M. C. Petty, *Langmuir-Blodgett Films*, Cambridge University Press, Cambridge, **1996**.
[5] M. Dyck, P. Krüger, M. Lösche, *Phys. Chem. Chem. Phys.* **2005**, *7*, 150.
[6] C. A. Helm, P. Tippmann-Krayer, H. Möhwald, J. Alsnielsen, K. Kjaer, *Biophys. J.* **1991**, *60*, 1457.
[7] I. Fujiwara, M. Ohnishi, J. Seto, *Langmuir* **1992**, *8*, 2219.
[8] M. Subirade, C. Salesse, D. Marion, M. Pezolet, *Biophys. J.* **1995**, *69*, 974.
[9] J. Zhang, P. R. Unwin, *J. Am. Chem. Soc.* **2002**, *124*, 2379.
[10] K. Norgaard, T. Bjornholm, *Chem. Commun.* **2005**, 1812.
[11] A. P. Girard-Egrot, S. Godoy, L. J. Blum, *Adv. Colloid Interface Sci.* **2005**, *116*, 205.
[12] D. K. Schwartz, *Surf. Sci. Rep.* **1997**, *27*, 241.
[13] S. W. Hui, D. F. Parsons, M. Cowden, *Proc. Natl. Acad. Sci. USA* **1974**, *71*, 5068.
[14] L. L. Orekhova, A. Mogilevich, S. V. Orechov, V. V. Klechkovskaya, L. A. Feigin, *Phys. B* **1994**, *198*, 144.
[15] M. Stevens, M. Longo, D. L. Dorset, J. Spence, *Ultramicroscopy* **2002**, *90*, 265.
[16] M. Seul, P. Eisenberger, H. M. McConnell, *Proc. Natl. Acad. Sci. USA* **1983**, *80*, 5795.
[17] B. W. Gregory, R. A. Dluhy, L. A. Bottomley, *J. Phys. Chem.* **1994**, *98*, 1010.
[18] P. Lozano, A. J. Fernández, J. J. Ruiz, L. Camacho, M. T. Martín, E. Muñoz, *J. Phys. Chem. B* **2002**, *106*, 6507.
[19] J. K. H. Hörber, C. A. Lang, T. W. Hänsch, W. M. Heckl, H. Möhwald, *Chem. Phys. Lett.* **1988**, *145*, 151.
[20] J. M. Solletti, M. Botreau, F. Sommer, W. L. Brunat, S. Kasas, T. M. Duc, M. R. Celio, *Langmuir* **1996**, *12*, 5379.
[21] H. Bürsing, D. Ouw, S. Kundu, P. Vöhringer, *Phys. Chem. Chem. Phys.* **2001**, *3*, 2378.
[22] M. C. Rheinstadter, C. Ollinger, G. Fragneto, F. Demmel, T. Salditt, *Phys. Rev. Lett.* **2004**, *93*, 108107.
[23] R. Srinivasan, V. A. Lobastov, C.-Y. Ruan, A. H. Zewail, *Helv. Chim. Acta* **2003**, *86*, 1761.
[24] C.-Y. Ruan, F. Vigliotti, V. A. Lobastov, S. Chen, A. H. Zewail, *Proc. Natl. Acad. Sci. USA* **2004**, *101*, 1123.
[25] S. Chen, M. T. Seidel, A. H. Zewail, *Proc. Natl. Acad. Sci. USA* **2005**, *102*, 8854.
[26] M. T. Seidel, S. Chen, A. H. Zewail, unpublished results.
[27] T. Fukui, M. Sugi, S. Iizima, *Phys. Rev. B* **1980**, *22*, 4898.
[28] J. Tang, A. H. Zewail, unpublished results.
[29] J. B. Peng, G. T. Barnes, I. R. Gentle, *Adv. Colloid Interface Sci.* **2001**, *91*, 163.
[30] C.-Y. Ruan, V. A. Lobastov, F. Vigliotti, S. Chen, A. H. Zewail, *Science* **2004**, *304*, 80.
[31] L. Meinhold, J. C. Smith, *Phys. Rev. Lett.* **2005**, *95*, 218103.
[32] C.-Y. Ruan, D.-S. Yang, A. H. Zewail, *J. Am. Chem. Soc.* **2004**, *126*, 12797.

 © 2006 Wiley-VCH Verlag GmbH & Co. KGaA, Weinheim

Molecular Recognition

DOI: 10.1002/anie.200601636

A Stoichiometric Molecularly Imprinted Polymer for the Class-Selective Recognition of Antibiotics in Aqueous Media**

Javier L. Urraca, Andrew J. Hall, Maria C. Moreno-Bondi, and Börje Sellergren**

Since the introduction of penicillin in 1941, antibiotics have been used effectively in both human and veterinary medicine to fight infectious diseases[1] and, in the latter case, as food additives to promote livestock growth.[2] Antibiotic residues have been observed in aquatic environments, including groundwater, surface water, and tap water, thus raising concern because of both the toxicity of these drugs to aquatic organisms and the emergence of resistant bacterial strains,[3,4] which may impact greatly on the ability of humankind to fight infectious diseases. Also of concern is the presence of antibiotics in meat and dairy products, which can lead to allergic reactions in hypersensitive individuals.[5] Accordingly, the use of antibiotics in veterinary medicine has been restricted or prohibited in some countries,[6] with maximum permitted levels having been defined by both European and North American legislators. Efficient analytical methods are therefore necessary to satisfy the regulatory levels of these compounds in foodstuffs.

In recent years, there has been growing interest in molecularly imprinted polymers (MIPs)[7] and their use as stationary phases for the selective extraction of a variety of molecules, for example, pharmaceuticals, foodstuff components, and pollutants, from a variety of complex matrices, such as blood, urine, and environmental waters.[8] A few reports on the imprinting of antibiotics have appeared,[9–15] with one notable exception:[9] MIPs capable of selectively extracting

[*] Dr. A. J. Hall,[+] Priv.-Doz. B. Sellergren
Institut für Umweltforschung
Universität Dortmund
Otto-Hahn-Strasse 6, 44221 Dortmund (Germany)
Fax: (+49) 231-755-4084
E-mail: andy.hall@sunderland.ac.uk
borje@infu.uni-dortmund.de
Dipl.-Chem. J. L. Urraca, Priv.-Doz. M. C. Moreno-Bondi
Departamento de Química Analítica
Facultad de Ciencias Químicas
Universidad Complutense de Madrid
28040 Madrid (Spain)
[+] Present address:
Institute of Pharmacy, Chemistry and Biomedical Sciences
The University of Sunderland
Wharncliffe Street, Sunderland, SR1 3SD (UK)

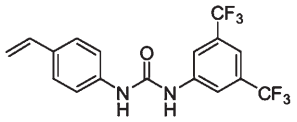
[**] This work was funded in part by the Spanish Ministry of Science and Technology (Project No. BQU2002-04515-C02-01) through a predoctoral grant (J.L.U.).

Supporting information for this article is available on the WWW under http://www.angewandte.org or from the author.

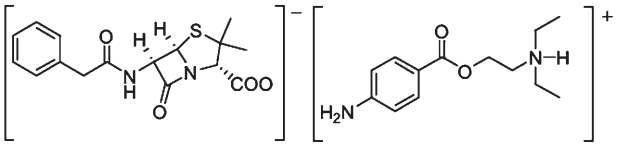
WILEY InterScience DISCOVER SOMETHING GREAT
© 2006 Wiley-VCH Verlag GmbH & Co. KGaA, Weinheim

penicillins from aqueous media have not been reported. This omission is because of the common reliance on the conventional noncovalent imprinting method in which the binding sites are templated through weak-to-medium strength interactions.[7] Typically, only a few percent of the added template give rise to imprinted sites, with the remaining noncomplexed functional monomer contributing to nonspecific binding.

This problem can be overcome by the use of designed "host" monomers capable of stoichiometrically interacting with the template functionalities.[9,16–19] With particular emphasis on the imprinting of oxyanions,[17–19] we report herein our studies on the use of one such monomer **1**, based



1



2P

on the urea motif, in the imprinting of penicillin G as its procaine salt **2P**. The association constant previously reported[19] for the interaction between **1** and tetrabutylammonium benzoate ($K_a = 8800\,\text{M}^{-1}$) in dimethyl sulfoxide (DMSO) should be sufficiently high to promote full complexation of **2P** in the prepolymerization mixture.

The polymers were first tested for their ability to retain the template molecule **2P** and the related salt **2K** (Table 1). We chose to evaluate the materials using mixtures of MeCN and aqueous 2-[4-(2-hydroxyethyl)-1-piperazinyl]ethanesulfonic acid (HEPES) buffer (pH 7.5). This pH value was chosen to ensure deprotonation of the carboxylic acid groups of the analytes, which is necessary for binding to occur to the polymeric urea moieties.

Table 1: Retention behavior of **2P** and **2K** on the imprinted and nonimprinted polymers.

Mobile phase (MeCN/ buffer)	k_{MIP} (**2P**)	k_{NIP} (**2P**)	IF (**2P**)	k_{MIP} (**2K**)	k_{NIP} (**2K**)	IF (**2K**)
100:0	8.3	6.1	1.4	n.e.	18.1	>1.9
95:5	0.41	0.16	2.6	12.0	3.0	4.0
90:10	0.41	0.18	2.3	0.93	0.18	5.2
50:50	0.82	0.41	2.0	0.84	0.18	4.7
10:90	**5.0**	**0.47**	**11**	**6.9**	**0.50**	**14**
0:100	31.8	25.0	1.4	n.e.	29.7	>1.15

Sample volume = 20 μL; analyte concentration = 10 mM (**2P** in MeCN, **2K** in MeCN/water (90:10)); flow rate = 1 mL min^{-1}; column dimensions = 125 × 4.6 mm i.d.; detection at $\lambda = 220$, 265 nm; void volume marker was methanol; n.e. = no elution observed over 60 min. The retention factor (k) and imprinting factor (IF) were calculated as $k = t_R - t_0/t_0$, where t_R is the retention time of the analyte, t_0 the retention time of methanol, and $\text{IF} = k_{MIP}/k_{NIP}$. Results shown are the average of three separate analyte injections.

In pure MeCN, we observe an imprinting effect for the template **2P**, though retention on the MIP is only marginally stronger than on the control nonimprinted polymer (NIP). However, **2K** is very strongly retained on the MIP (no elution within 60 minutes) and shows a higher retention on the NIP than **2P** does. These phenomena are possibly related to mass-transport effects in which the more bulky ion pair **2P** is expected to have greater difficulty in diffusing into the binding sites than the smaller **2K**. This explanation is further supported by the higher imprinting factors (IFs) observed for **2P** at higher buffer contents at which the ion pairs are expected to be fully dissociated.

It should be noted that preliminary HPLC experiments using pure water in place of buffer (results not shown) showed that the retention of **2K** was always dramatically stronger than that of the template **2P**, thus prompting us to use HEPES buffer (pH 7.5) in all further experiments.

The addition of 5% water leads to a dramatic decrease in the retention times for **2P** on both the MIP and NIP, with a similar effect occurring at 10% buffer for **2K**. However, retention on the MIP remains stronger than on the NIP in all cases, thus leading to significant IFs. At 50% aqueous buffer, there is a slight rise in the retention times, with the analytes again more retained on the MIP than on the NIP.

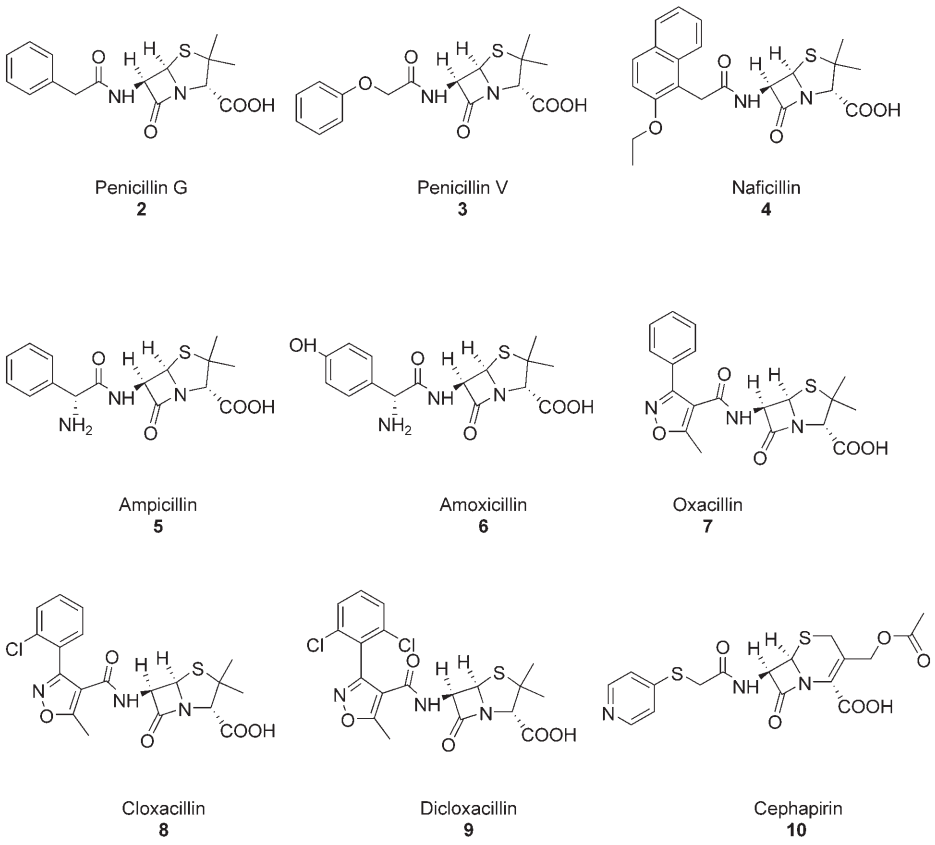
The most interesting observations occur at 90% buffer. Under these conditions, the retention times of the analytes rise significantly on the MIP but, crucially, not on the NIP. It is in this mobile phase that the difference between the recognition properties of the MIP and NIP is most striking, with an IF of >10 for both salts (Table 1). Finally, the retention times climb exponentially in pure aqueous buffer for both the MIP and NIP, although retention on the MIP remains stronger than on the NIP. This retention behavior is commonly observed for MIPs and has been explained by a shift from an electrostatic retention mode in water-poor mobile phases to a hydrophobic mode in water-rich systems in which both modes involve a specific and a nonspecific contribution to the overall retention.[20,9]

We next decided to test the ability of the imprinted polymer to retain other related analytes, namely β-lactam antibiotics **2**–**10**, with the optimal mobile phase as defined by the experiments described above, that is, MeCN/buffer (10:90, v/v).

As can be seen in Figure 1, the retention of all the β-lactam antibiotic analytes on the MIP is rather strong. The template **2P** and the related salt **2K** are the most strongly retained analytes, further supporting the success of the imprinting step. With the exception of amoxicillin (**6**), the MIP appears to contain binding sites principally for the β-lactam carboxylate structure that are capable of accommodating the pendant substituents. Cephapirin (**10**), with a six-membered ring in the β-lactam structure, is the least-well retained of such antibiotics. Finally, the unrelated compound benzoic acid, used as a control analyte, is retained extremely weakly on the imprinted polymer.

In contrast to the retention behaviors shown on the MIP, all analytes are similarly and weakly retained on the control

 © 2006 Wiley-VCH Verlag GmbH & Co. KGaA, Weinheim



zwitterionic analyte **5** shows that this is not a general effect. Instead, we attribute the effects to the existence of complementary binding sites capable of accommodating the β-lactam family of solutes, in which analytes with greater structural similarity to the template molecule display the higher retention factors.

To gain insight into the binding energy and site density of the polymers, we measured the equilibrium binding isotherms for both the imprinted and non-imprinted polymer in the optimum solvent system described above, in which the template is expected to bind strongly to the imprinted polymer (Figure 2). The isotherms showed a good fit to a Langmuir binary site model, thus resulting in two classes of binding sites with largely different binding energies. The resulting parameters gave a maximum binding constant for the MIP of $7800\,\text{M}^{-1}$ and an excess capacity of the MIP over the NIP near the nominal capacity ($112\,\mu\text{mol g}^{-1}$) calculated on the basis of the amount of added template to the prepolymerization mixture. This behavior shows that the matrix urea groups are functional and fully accessible. In the case of the NIP, the high-energy sites have a similar association constant to those of the MIP, although the capacity is much lower, whereas the low-energy sites are weaker and less

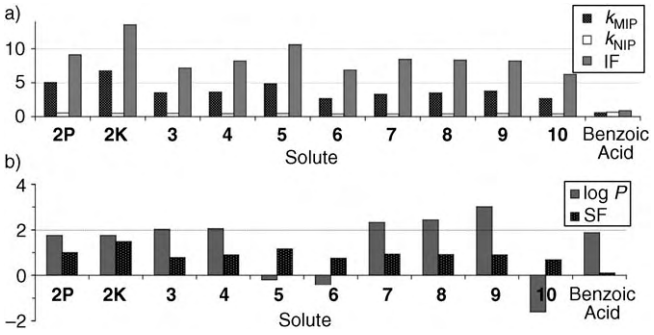


Figure 1. Evaluation of the cross-selectivity of the polymers in terms of a) the retention factors (k) for the MIP, the NIP, and the corresponding imprinting factors (IF) and b) the selectivity factor (SF) and hydrophobicity ($\log P$ values) for the analytes. SF = IF (analyte)/IF (template). Mobile phase = MeCN/HEPES buffer (aq.; pH 7.5; 10:90, v/v), analyte concentration = 1 mM; the void volume marker was methanol. Experimental conditions otherwise as in Table 1.

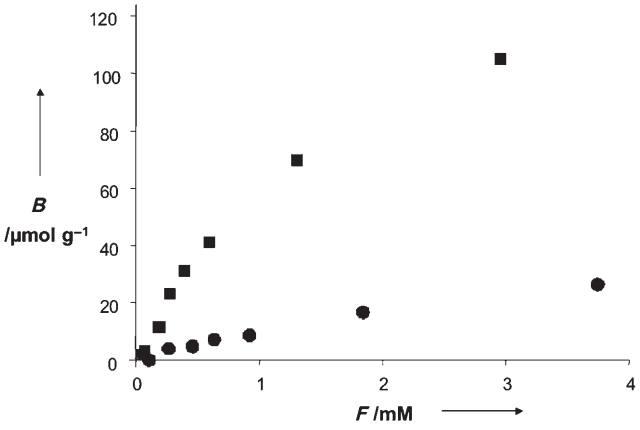


Figure 2. Equilibrium binding isotherms for the uptake of the penicillin G procaine salt by MIP (squares) and NIP (circles) in MeCN/aq. HEPES buffer (pH 7.5; 10:90, v/v). F = concentration of the free solute, B = specific amount of bound solute. The binding constants (K_a) and specific binding capacities (N) were obtained from linear fitting of corresponding Scatchard plots to a Langmuir binary site model. The fitting parameters for the class 1 and 2 sites of the MIP were: 1) $K_a = 7780\,\text{M}^{-1}$, $N = 36.6\,\mu\text{mol g}^{-1}$ ($R^2 = 0.99$); 2) $K_a = 610\,\text{M}^{-1}$, $N = 163\,\mu\text{mol g}^{-1}$ ($R^2 = 0.98$); and for the NIP: 1) $K_a = 7080\,\text{M}^{-1}$, $N = 7.3\,\mu\text{mol g}^{-1}$ ($R^2 = 0.98$); 2) $K_a = 240\,\text{M}^{-1}$, $N = 57.4\,\mu\text{mol g}^{-1}$ ($R^2 = 0.87$). Each data point represents the average of two replicate measurements with a coefficient of variation in the range of 2.7–5.6%.

NIP, again supporting the success of the imprinting step. Attempts were made to correlate the retention data with the physical properties of the analytes used. As is obvious from the lack of correlation between the selectivity factor (SF) and the $\log P$ values shown in Figure 1b,[21] nonspecific hydrophobic retention is not the cause of the enhanced retention observed on the MIP. There appears to be a small trend of increasing retention with increasing $\log P$ values within the series **7**–**9**. However, the retention of the far more hydrophilic

 © 2006 Wiley-VCH Verlag GmbH & Co. KGaA, Weinheim

prevalent than those in the MIP. These results suggest that the differences in retention observed during the chromatographic testing relate more to the number than the binding energy of the high-affinity sites present.

In summary, a stoichiometrically imprinted polymeric receptor for the class-selective recognition of β-lactam antibiotics has been prepared and shown to effectively retain such compounds under predominantly aqueous conditions. We are currently assessing the use of these materials for solid-phase extraction (SPE) in the selective removal of β-lactam antibiotics from environmental water samples and as receptors for fluorescence based assays.

Experimental Section

Polymer preparation: The template **2P** (286 mg, 0.5 mmol), functional monomer **1** (186 mg, 0.5 mmol), methacrylamide (84 mg, 1 mmol), ethylene glycol dimethacrylate (EDMA; 3.8 mL, 20 mmol), and the free radical initiator 2,2′-azo-bis-(2,4-dimethylvaleronitrile) (ABDV; 44 mg, 1 % w/w total monomers) were dissolved in MeCN (5.6 mL). The solution was transferred to a glass tube, cooled to 0 °C, and purged with N_2 for 10 min to remove dissolved oxygen. After purging, the glass tube was sealed and polymerization initiated thermally by placing the tube in a water bath set at 40 °C. Polymerization was allowed to proceed at this temperature for 48 h. The tube was then broken, and the MIP monolith was removed and broken into smaller fragments. The template was removed through sequential washing with MeOH (100 mL), MeOH/0.1 M HCl (9:1, 100 mL), and finally MeOH (100 mL).

Received: April 25, 2006
Published online: July 6, 2006

Keywords: antibiotics · imprinting · molecular recognition · penicillin

[1] A. M. , Johnston, *Int. J. Antimicrob. Agents* **2001**, *18*, 291 – 294.
[2] P. Boerlin, A. Wissing, F. M. Aarestrup, J. Frey, J. Nicolet, *J. Clin. Microbiol.* **2001**, 4193 – 4195.
[3] H. J. Stan, T. H. Heberer, M. Linkerhägner, *Vom Wasser* **1994**, *83*, 57 – 68.
[4] V. H. Smith, F. DeNoyelles, Jr., C. K. Larive, *Environ. Sci. Technol.* **2003**, *37*, 1713 – 1719.
[5] G. Patriarca, C. D'Ambrosio, D. Schiavino, E. Nucera, J. Y. Sun, M. Del Ninno, A. Buonomo, *Int. Arch. Allergy Immunol.* **1999**, *118*, 247 – 250.
[6] B. Hileman, *Chem. Eng. News* **2001**, *79*(8), 47 – 52.
[7] a) C. Alexander, H. S. Andersson, L. I. Andersson, R. J. Ansell, N. Kirsch, I. A. Nicholls, J. O'Mahony, M. J. Whitcombe, *J. Mol. Recognit.* **2006**, *19*, 106 – 180; b) (Ed.: B. Sellergren), *Molecularly Imprinted Polymers: Man-Made Mimics of Antibodies and their Application in Analytical Chemistry.* Techniques and instrumentation in analytical chemistry, Elsevier Science, Amsterdam, Netherlands, **2001**.
[8] F. Lanza, B. Sellergren, *Chromatographia* **2001**, *53*, 599 – 611.
[9] C. Lübke, M. Lübke, M. J. Whitcombe, E. N. Vulfson, *Macromolecules* **2000**, *33*, 5098 – 5105.
[10] J. Cederfur, Y. Pei, M. Zihui, M. Kempe, *J. Comb. Chem.* **2003**, *5*, 67 – 72.
[11] K. Skudar, O. Brüggemann, A. Wittelsberger, O. Ramström, *Anal. Commun.* **1999**, *36*, 327 – 331.
[12] R. Levi, S. McNiven, S. A. Piletsky, S.-H. Cheong, K. Yano, I. Karube, *Anal. Chem.* **1997**, *69*, 2017 – 2021.
[13] M. Senholdt, M. Siemann, K. Mosbach, L. I. Andersson, *Anal. Lett.* **1997**, *30*, 1809 – 1821.
[14] M. Siemann, L. I. Andersson, K. Mosbach, *J. Antibiot.* **1997**, *50*, 89 – 91.
[15] E. Benito-Pena, M. C. Moreno-Bondi, S. Aparicio, G. Orellana, J. Cederfur, M. Kempe, *Anal. Chem.* **2006**, *78*, 2019 – 2027.
[16] G. Wulff, K. Knorr, *Bioseparation* **2002**, *10*, 257 – 276.
[17] A. J. Hall, L. Achilli, P. Manesiotis, M. Quaglia, E. De Lorenzi, B. Sellergren, *J. Org. Chem.* **2003**, *68*, 9132 – 9135.
[18] P. Manesiotis, A. J. Hall, M. Emgenbroich, M. Quaglia, E. De Lorenzi, B. Sellergren, *Chem. Commun.* **2004**, 2278 – 2279.
[19] A. J. Hall, P. Manesiotis, M. Emgenbroich, M. Quaglia, E. De Lorenzi, B. Sellergren, *J. Org. Chem.* **2005**, *70*, 1732 – 1736.
[20] a) C. Dauwe, B. Sellergren, *J. Chromatogr.* **1996**, *753*, 191; b) J. G. Karlsson, L. I. Andersson, I. Nicholls, *Anal. Chim. Acta* **2001**, *435*, 57 – 64.
[21] Log *P* values were calculated using ChemOffice ChemDraw Pro V 9.0.1 software.

 © 2006 Wiley-VCH Verlag GmbH & Co. KGaA, Weinheim

Biorefinery

DOI: 10.1002/anie.200601921

Catalytic Conversion of Cellulose into Sugar Alcohols**

Atsushi Fukuoka and Paresh L. Dhepe*

The production of energy, fuels, and chemicals from renewable biomass is important to prevent global warming by decreasing atmospheric CO_2 generated from the consumption of fossil fuels.[1] Biomass includes various plant components, such as starch and cellulose, that were originally formed by photosynthesis. Starch, a polymer of D-glucose with α-1,4-glycosidic bonds, is soluble in water and a main constituent of corn, rice, potato, and so forth. Attention has been paid to the use of starch to produce fuels and chemicals,[2,3] but starch should primarily be used as a source of food. On the contrary, cellulose is neither soluble in water nor digestible for humans because of its robust structure composed of β-1,4-glycosidic bonds of D-glucose.[4–6] The annual net yield of photosynthesis is 1.8 trillion tons, approximately 40% of which is cellulose.[4]

[*] Prof. A. Fukuoka, Dr. P. L. Dhepe
Catalysis Research Center
Hokkaido University
N-21 W-10, Kita-ku, Sapporo 001-0021 (Japan)
Fax: (+81) 11-706-9110
E-mail: fukuoka@cat.hokudai.ac.jp
Homepage: http://www.cat.hokudai.ac.jp/fukuoka/

[**] This work was supported by CREST, the Japan Science and Technology Agency. We thank Prof. K. Seki for LC–MS analysis, Prof. K. Kuroda for assistance with X-ray fluorescence (XRF), and Dr. S. Inagaki, Dr. S. Yano, Prof. T. Erata, Prof. M. Niwa, and Prof. H. Hattori for helpful discussions.

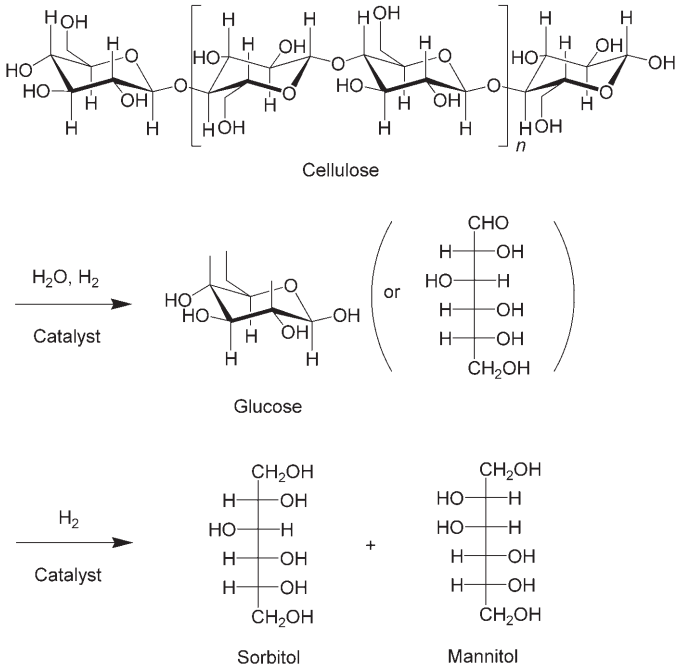
Supporting information for this article is available on the WWW under http://www.angewandte.org or from the author.

© 2006 Wiley-VCH Verlag GmbH & Co. KGaA, Weinheim

This figure shows that cellulose is the most abundant organic compound in nature.

However, the utilization of cellulose has been limited to lumber, fuel, textile, paper, plastics, and so on because cellulose is resistant to degradation. Until now, a great deal of effort has been put toward the degradation of cellulose with enzymes,[4,6] mineral acids,[4,7] bases,[8] and supercritical water.[9] Among the serious drawbacks of these pathways are low activity and/or selectivity, separation of products and catalysts, corrosion hazard, generation of a large amount of neutralization waste, and harsh conditions. Therefore, a new "green" catalytic process is a challenge for the conversion of cellulose to value-added chemicals. In our study of biorefinery with heterogeneous catalysis,[10] we explored the catalytic degradation of cellulose. Herein, we report that supported Pt or Ru catalysts show high activity for the conversion of cellulose into sugar alcohols.

Scheme 1 shows the system studied which includes the hydrolysis of cellulose to glucose and the reduction of glucose



Scheme 1. Catalytic conversion of cellulose into sugar alcohols.

to sorbitol and mannitol. Water was used as the reaction media, and the separation of soluble products and the insoluble catalyst/substrate was readily carried out by filtration. Sorbitol is produced by the hydrogenation of glucose over Raney Ni[3,11] and is used not only as a sweetener but also as a precursor to isosorbide, 1,4-sorbitan, glycols, glycerol, lactic acid, and vitamin C.[3,12] Isosorbide increases the glass-transition point of poly(ethylene terephthalate). Recently, Dumesic and co-workers reported that H_2 for fuel cells[13] and C_{5-6} hydrocarbons[14] can be produced from sorbitol with higher selectivity than from glucose. Mannitol is also a sweetener and a precursor to useful compounds. Accordingly, the production of sorbitol and mannitol from cellulose would be industrially important. The formation of sorbitol from soluble starch was reported in a patent that used Ru catalysts,[15] but no report has shown the catalytic conversion of insoluble cellulose into sugar alcohols.

The catalytic results are summarized in Figure 1, in which the values given in parentheses for the H form of ultrastable Y zeolite (HUSY) are the Si/Al ratios. Pt/γ-Al_2O_3 gave sugar

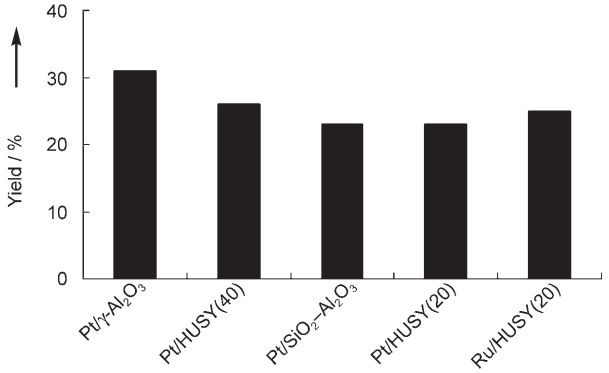


Figure 1. Conversion of cellulose into sugar alcohols by supported metal catalysts. Reaction conditions: cellulose (0.48 g), Pt catalyst (0.21 g), Ru catalyst (0.11 g; Pt, Ru 2.5 wt%), water (60 mL), initial H_2 pressure at RT = 5 MPa, 463 K, 24 h.

alcohols in 31% yield (sorbitol: 25%, mannitol: 6%), and sorbitol was the main product, with a molar ratio of sorbitol/mannitol of 4:1 or higher. The formation of mannitol suggests the epimerization of sorbitol by solid acids. In fact, a small amount of mannitol was formed by using sorbitol as a substrate over the Pt catalysts under the reaction conditions. Among the supported metal catalysts we tested, Pt and Ru catalysts gave high yields of the sugar alcohols, but Pd, Ir, and Ni catalysts showed low activity (see the Supporting Information). The choice of support material was important, with γ-Al_2O_3, HUSY(40), SiO_2–Al_2O_3, and HUSY(20) giving high yields (other supports showed low activity as reported in the Supporting Information). From these results, solid acidity[16] seems to be effective for the catalytic reaction, but the activity does not correspond well with the apparent strength of the acid. It was reported that Ru/HUSY prepared from NaY zeolite (LZY-52) is active in the conversion of starch to sorbitol,[15] but this catalyst showed low activity (0.7% yield) in our reaction of cellulose.

In the optimization of the reaction temperature, the highest yield was observed at 463 K in the range of 443–473 K over Pt/γ-Al_2O_3 (see the Supporting Information). The catalysts were recyclable in repeated runs. After the first run with Pt/γ-Al_2O_3, the catalyst and the remaining cellulose were filtered and washed with water, fresh cellulose and water were added, and the mixture was used for the next run. Similar yields of the sugar alcohols were obtained in up to three cycles (see the Supporting Information). These results indicate that the catalyst is not deactivated in the course of the catalytic runs.

The support materials were also used as catalysts under the conditions that employed H_2 pressure (Figure 2). Only a

 © 2006 Wiley-VCH Verlag GmbH & Co. KGaA, Weinheim

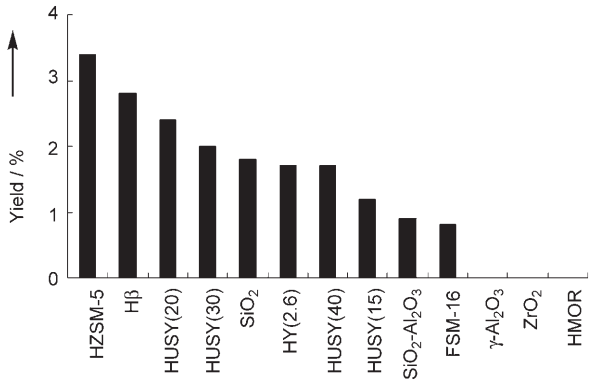


Figure 2. Hydrolysis of cellulose into glucose by support materials. Reaction conditions: cellulose (0.16 g), catalyst (0.068 g), water (20 mL), initial H_2 pressure at RT = 5 MPa, 463 K, 24 h. The yields are based on the number of moles of the initial $C_6H_{10}O_5$ unit in cellulose. HZSM-5 = H form of zeolite Socony mobil, HY = H form of Y zeolite, FSM-16 = folded sheets of mesoporous material, HMOR = H form of moredenite.

small amount of glucose was formed with yields of less than 4%, thus indicating that the metal promotes the hydrolysis of cellulose. Hence, it is suggested that the acid sites for the hydrolysis of cellulose are generated in situ from H_2 in addition to the acidic surface sites intrinsic in the support.[17] In this mechanism, H_2 is dissociatively adsorbed on the metal surface and the hydrogen species reversibly spill over onto the support surface. The acidic sites catalyze the hydrolysis of cellulose to glucose, and the C=O group in glucose is readily reduced by Pt or Ru with H_2 to form sorbitol (Scheme 1). The former hydrolysis is a rate-determining step because the reduction of glucose gave an almost stoichiometric amount of sorbitol over the Pt or Ru catalysts.

The maximum yield was not improved when the reaction was carried out over 72 hours (see the Supporting Information). This finding implies that the further degradation of cellulose was restricted as a result of its robust structure. Previous reports on the hydrolysis of cellulose recognized that the factors that control the conversion of cellulose are crystallinity, degree of polymerization, availability of chain ends, and fraction of accessible bonds.[6] These factors play a significant role in our reactions, in which both substrate and catalyst are solid.

As described above, we have demonstrated for the first time that supported metal catalysts can convert cellulose into sugar alcohols by an environmentally friendly process. This green process opens new opportunities for the use of abundant and inexpensive cellulose as a chemical feedstock with heterogeneous catalysis.

Experimental Section

Support materials and metal precursors are summarized in the Supporting Information. The supports were dried under vacuum (ca. 0.1 Pa) at 423 K for 1 h. Typically, an aqueous solution of $[Pt(H)_2Cl_6]\cdot x\,H_2O$ (5 mL, 15 mg) was added to a mixture of γ-Al_2O_3 (Nishio, A-11, 200 mg) and water (20 mL). The reaction mixture was stirred for 15 h, evaporated to dryness, and dried under vacuum for 24 h. The sample was calcined in O_2 at 673 K for 2 h and reduced in H_2 at 673 K for 2 h to give Pt/γ-Al_2O_3 (Pt 2.5 wt%). Ru/HUSY catalysts were prepared by the various methods given in the Supporting Information.

A typical procedure: cellulose (Merck, Avicel, microcrystalline, 0.16 g), Pt/γ-Al_2O_3 (0.068 g), water (20 mL) and a stirring bar were charged in a stainless-steel autoclave (Taiatsu TPR2, 30 mL). Three-fold scale-up reactions were also performed in an MMJ-100 reactor (OM Lab-Tech). The autoclave was heated at 463 K for 24 h after pressurization with H_2 to 5 MPa at RT. After the reaction, the reaction mixture was centrifuged and the filtered solution was analyzed by HPLC (Shimadzu LC10AT*VP*, RI detector, Shim-pack SPR-Ca column (250 × 7.8 mm), mobile phase: water). Sorbitol and mannitol were characterized by LC–MS (Shimadzu LCMS-2010 A). The yield of sugar alcohols was calculated as follows: yield (%) = (mol of sorbitol and mannitol)/(mol of $C_6H_{10}O_5$ unit in charged cellulose) × 100. Initial ratio of substrate/catalyst (S/C) was 110 (S = mol of $C_6H_{10}O_5$, C = g atom of bulk metal).

Received: May 15, 2006
Published online: July 6, 2006

Keywords: carbohydrates · catalysts · heterogeneous catalysis · reduction · water

[1] D. L. Klass, *Biomass for Renewable Energy, Fuels, and Chemicals*, Academic Press, San Diego, **1998**.
[2] H. Danner, R. Braun, *Chem. Soc. Rev.* **1999**, *28*, 395–405.
[3] US Department of Energy, *Energy Efficiency and Renewable Energy, Top Value Added Chemicals From Biomass, Vol. 1*: "Results of Screening for Potential Candidates from Sugars and Synthesis Gas" http://eereweb.ee.doe.gov/biomass/pdfs/35523.pdf, 2004.
[4] L. T. Fan, M. M. Gharpuray, Y.-H. Lee, *Cellulose Hydrolysis*, Springer, Berlin, **1987**.
[5] H. A. Krässig, *Cellulose—Structure, Accessibility and Reactivity*, Gordon and Breach Science Publishers, Yverdon, **1993**.
[6] Y. P. Zhang, L. R. Lynd, *Biotechnol. Bioeng.* **2004**, *88*, 797–824.
[7] W. S. Mok, M. J. Antal, G. Varhergyi, *Ind. Eng. Chem. Res.* **1992**, *31*, 94–100.
[8] M. Ishida, K. Otsuka, S. Takenaka, I. Yamanaka, *J. Chem. Technol. Biotechnol.* **2005**, *80*, 281–284.
[9] M. Sasaki, Z. Fang, Y. Fukushima, T. Adschiri, K. Arai, *Ind. Eng. Chem. Res.* **2000**, *39*, 2883–2890.
[10] P. L. Dhepe, M. Ohashi, S. Inagaki, M. Ichikawa, A. Fukuoka, *Catal. Lett.* **2005**, *102*, 163–169.
[11] P. Gallezot, P. J. Cerino, B. Blanc, G. Flèche, P. Fuertes, *J. Catal.* **1994**, *146*, 93–102.
[12] P. D. Wulf, W. Soetaert, E. J. Vandamme, *Biotechnol. Bioeng.* **2000**, *69*, 339–343.
[13] G. W. Huber, J. W. Shabaker, J. A. Dumesic, *Science* **2003**, *300*, 2075–2077.
[14] R. R. Davda, J. A. Dumesic, *Chem. Commun.* **2004**, 36–37.
[15] P. Jacobs, H. Hinnekens (Synfina-Oleofina), EP0329923, **1989**.
[16] M. Niwa, K. Suzuki, K. Isamoto, N. Katada, *J. Phys. Chem. B* **2006**, *110*, 264–269.
[17] H. Hattori, T. Shishido, *Catal. Surv. Jpn.* **1997**, *1*, 205–213.

 © 2006 Wiley-VCH Verlag GmbH & Co. KGaA, Weinheim

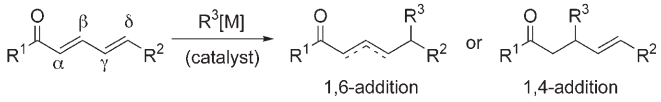
Regioselectivity

DOI: 10.1002/anie.200601719

Highly Selective 1,6-Addition of Aryl Boronic Acids to α,β,γ,δ-Unsaturated Carbonyl Compounds Catalyzed by an Iridium Complex**

*Takahiro Nishimura, Yuichi Yasuhara, and Tamio Hayashi**

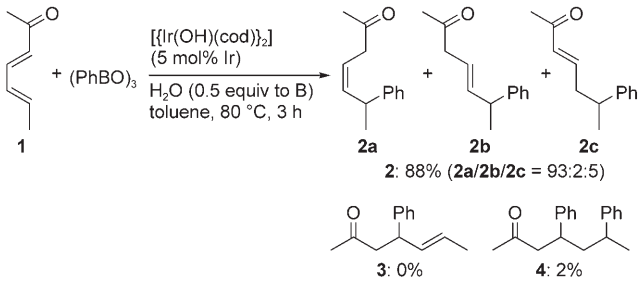
The transition-metal-catalyzed 1,4-addition of organometallic reagents to electron-deficient olefins is one of the most reliable methods for selective C–C bond formation,[1] but, on the contrary, there is considerable difficulty in controlling the regioselectivity of the addition to extended conjugate systems; for example, 1,6- or 1,4-addition to electron-deficient dienes (Scheme 1). In this field of research, in which copper



Scheme 1. 1,6-Addition versus 1,4-addition in α,β,γ,δ-unsaturated carbonyl compounds.

salts have been mainly used as the active catalysts,[1e,2] Fukuhara and Urabe recently reported notable 1,6-selectivity with iron as a catalyst in the addition of aryl Grignard reagents to 2,4-dienoates and -dienamides.[3] Although rhodium-catalyzed conjugate addition has been developing very rapidly,[4] only a few reports have appeared that describe 1,6- or 1,4-selectivity in the addition to electron-deficient dienes.[5,6] High 1,6-selectivity in the rhodium-catalyzed reactions has been reported for a limited combination of substrates: Examples include the addition of aryl zinc reagents to dienones with β-substituents[5] and the addition of aryl and alkenyl boronic acids to δ-unsubstituted dienoates.[6] Herein, we report perfect 1,6-selectivity in the addition of aryl boronic acids to a standard type of α,β,γ,δ-unsaturated carbonyl compound, realized by use of an iridium complex as a catalyst.

During our efforts to realize the 1,6-addition of aryl boronic acids to α,β,γ,δ-unsaturated carbonyl compounds, we found that an iridium complex, [{Ir(OH)(cod)}$_2$] (cod = cyclooctadiene),[7] efficiently catalyzes the addition to simple dienones with perfect 1,6-regioselectivity. Thus, treatment of (3*E*,5*E*)-3,5-heptadien-2-one (**1**) with phenylboroxine (1.0 equiv)[8] in the presence of a catalytic amount of [{Ir(OH)(cod)}$_2$] (5 mol% Ir) and H_2O (0.5 equiv relative to B) in toluene at 80 °C for 3 h gave a mixture of 1,6-adducts, 6-phenylhepten-2-ones **2**,[5] in 88% yield (Scheme 2). The

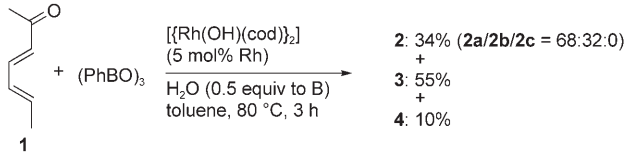


Scheme 2. Iridium-catalyzed 1,6-addition of phenylboronic acid to dienone **1**.

mixture consists of (*Z*)-6-phenyl-4-hepten-2-one (**2a**) as the major isomer (93%), its *E* isomer **2b** (2%), and conjugate ketone **2c** (5%). The formation of the 1,4-addition product **3** was not detected at all under the present reaction conditions. The formation of a small amount of diphenylation product **4** (2%), probably formed by the 1,4-addition of phenylboronic acid to the conjugate ketone **2c**, was also observed.

Although rhodium catalysts have been often used for the addition of aryl metal reagents to electron-deficient alkenes,[4] the iridium catalyst system employed in this addition has not been well demonstrated so far. As a related reaction, Mori and co-workers reported the first example of the iridium-catalyzed addition/elimination reaction of aryl silicon reagents with acrylates to give Mizoroki–Heck-type products.[9] To the best of our knowledge, the present 1,6-addition is the first example of an iridium-catalyzed addition of aryl boronic acids to electron-deficient alkenes or dienes.[10] The unique 1,6-selectivity observed in the iridium-catalyzed addition is made clear by comparison with the result obtained with [{Rh(OH)(cod)}$_2$][11] as a catalyst under the same reaction conditions (Scheme 3). The rhodium-catalyzed reaction gave the 1,4-adduct **3** as the main isomer (55% yield) and a minor amount (34% yield) of 1,6-adducts **2a** and **2b**.

Competition experiments with a 1:1 mixture of dienone **1** and 3-penten-2-one (**5**) gave us insight into the origin of the difference in regioselectivity between the iridium and rhodium catalysts in the addition of phenylboronic acid to the dienone (Scheme 4). Thus, in the reaction of a 1:1 mixture of **1**



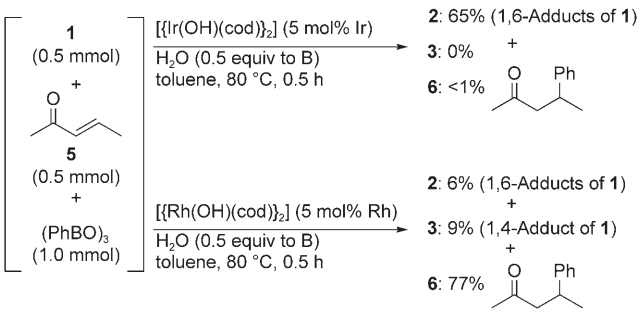
Scheme 3. Rhodium-catalyzed addition of phenylboronic acid to dienone **1**.

[*] Dr. T. Nishimura, Y. Yasuhara, Prof. T. Hayashi
Department of Chemistry
Graduate School of Science
Sakyo, Kyoto 606–8502 (Japan)
Fax: (+81) 75-753-3988
E-mail: thayashi@kuchem.kyoto-u.ac.jp

[**] This work has been supported in part by a Grant-in-Aid for Scientific Research, the Ministry of Education, Culture, Sports, Science and Technology, Japan (Priority Areas "Advanced Molecular Transformations of Carbon Resources").

Supporting information for this article is available on the WWW under http://www.angewandte.org or from the author.

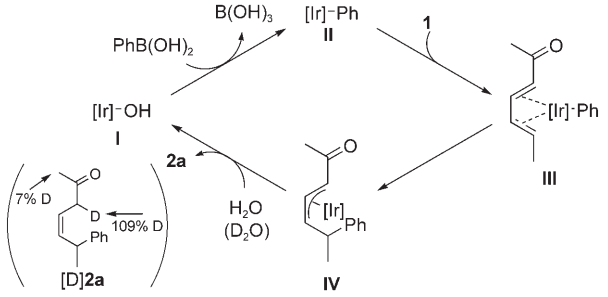
InterScience
© 2006 Wiley-VCH Verlag GmbH & Co. KGaA, Weinheim



Scheme 4. Competitive reaction of dienone **1** and enone **5** with phenylboronic acid in the presence of [{Ir(OH)(cod)}$_2$] or [{Rh(OH)(cod)}$_2$].

and **5** with phenylboronic acid in the presence of [{Ir(OH)-(cod)}$_2$], dienone **1** was consumed exclusively to give the 1,6-adducts **2** (65%), thus leaving enone **5** unreacted. These results indicate that the iridium catalyst has much a stronger reactivity toward the dienone than enone. On the other hand, the competition experiment with [{Rh(OH)(cod)}$_2$] as a catalyst gave a high yield (77%) of 4-phenyl-2-butanone (**6**), which is the 1,4-addition product of enone **5**, and a small amount of **2** (6%) and **3** (9%), the addition products of the dienone **1**.

On the basis of the high reactivity toward the diene moiety and the high *Z* selectivity in the 1,6-addition product, the catalytic cycle of the present iridium-catalyzed reaction is speculated as shown in Scheme 5. Transmetalation of a phenyl



Scheme 5. Proposed catalytic cycle of the iridium-catalyzed 1,6-addition of phenylboronic acid to enone **1**.

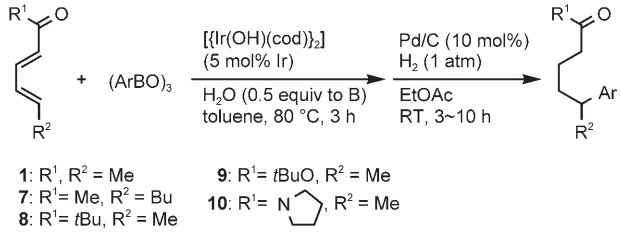
group from the boron to iridium center forms a phenyl–iridium species **II**.[9,12] The coordination of the dienone to the phenyl–iridium complex with a cisoid diene moiety results in the formation of a (η^4-diene)–iridium complex **III**.[13] Insertion of the diene into the phenyl–iridium bond, thus forming π-allyl–iridium moiety **IV**,[14] followed by subsequent hydrolysis with the assistance of phenylboronic acid or boric acid gives the 1,6-addition product **2a** with *Z* configuration and the hydroxo–iridium species **I**. The selective incorporation of deuterium at the α-position in [D]**2a** was observed in the addition to dienone **1** by using D_2O in place of H_2O, which aids the hydrolysis step of π-allyl–iridium complex **IV** and gives **2a**.

The results of the 1,6-addition of aryl boronic acids to α,β,γ,δ-unsaturated carbonyl compounds are summarized in Table 1. The addition products provided by the iridium-catalyzed hydroarylation were subjected to palladium-catalyzed hydrogenation to give saturated ketones (Scheme 6).

Table 1: Iridium-catalyzed 1,6-addition to dienes.[a]

Entry	Diene	Ar	Yield [%][b]
1	**1**	Ph	86 (**11**)[c]
2	**1**	4-MeC_6H_4	82 (**12**)[c]
3	**1**	4-MeOC_6H_4	88 (**13**)[c]
4	**1**	4-$CF_3C_6H_4$	75 (**14**)
5	**1**	4-FC_6H_4	84 (**15**)[c]
6	**1**	2-naphthyl	86 (**16**)
7	**7**	Ph	86 (**17**)
8	**8**	Ph	94 (**18**)
9	**9**	Ph	82 (**19**)
10	**10**	Ph	90 (**20**)

[a] Reaction conditions: [{Ir(OH)(cod)}$_2$] (0.025 mmol Ir), diene (0.50 mmol), $(ArBO)_3$ (0.50 mmol), H_2O (0.75 mmol), toluene (1.0 mL), 80°C, 3 h. After short column chromatography on silica gel, the products were subjected to hydrogenation in the presence of Pd/C (10 mol%) under H_2 (1 atm). [b] Yield of the isolated products. [c] A diarylation product was also obtained in 2% yield in each case.



Scheme 6. Iridium-catalyzed 1,6-addition of aryl boronic acids to electron-deficient dienes.

The reaction of dienone **1** with several aryl boronic acids with electron-donating and -withdrawing substituents on the benzene ring gave the corresponding δ-aryl ketones in high yields (75–88% yields, entries 1–6) after hydrogenation. The 1,4-addition to dienone **1** was not detected in any case. The 1,6-selectivity was also observed in the addition to dienones **7** (R^1 = Me, R^2 = Bu) and **8** (R^1 = *t*Bu, R^2 = Me; entries 7 and 8, respectively). This iridium-catalyzed reaction can be applied to α,β,γ,δ-unsaturated ester **9** and amide **10** to give the corresponding 1,6-addition products in 82 and 90% yield, respectively (entries 9 and 10).

In summary, the catalytic 1,6-addition of aryl boronic acids to electron-deficient dienes was realized by use of an iridium catalyst, which gave high yields of the corresponding δ-arylated carbonyl compounds with perfect 1,6-selectivity.

Experimental Section

(3*E*,5*E*)-3,5-Heptadien-2-one (**1**; 55.1 mg, 0.50 mmol) and H_2O (13.5 μL, 0.75 mmol) were added to a solution of [{Ir(OH)(cod)}$_2$] (8.3 mg, 0.025 mmol Ir) and phenylboroxine (156 mg, 0.50 mmol) in toluene (1.0 mL) at room temperature. The reaction mixture was heated at 80°C for 3 h. After the usual workup, column chromatography on silica gel gave a mixture of the 1,6-addition products. The mixture was hydrogenated in the presence of Pd/C (10 mol% Pd)

 © 2006 Wiley-VCH Verlag GmbH & Co. KGaA, Weinheim

under H_2 (1 atm) in EtOAc (2.0 mL) at room temperature for 3 h to give 6-phenyl-2-heptanone (83.0 mg, 86%).

Received: May 2, 2006
Published online: July 3, 2006

Keywords: 1,6-addition · arylation · boronic acids · iridium · regioselectivity

[1] For recent reviews, see: a) K. Tomioka, Y. Nagaoka in *Comprehensive Asymmetric Catalysis, Vol. 3* (Eds.: E. N. Jacobsen, A. Pfaltz, H. Yamamoto), Springer, Berlin, **1999**, chap. 31.1; b) M. Kanai, M. Shibasaki in *Catalytic Asymmetric Synthesis*, 2nd ed. (Ed.: I. Ojima), Wiley, New York, **2000**, p. 569; c) M. P. Sibi, S. Manyem, *Tetrahedron* **2000**, *56*, 8033; d) N. Krause, A. Hoffmann-Röder, *Synthesis* **2001**, *171*; e) B. H. Lipshutz in *Organometallics in Organic Synthesis. A Manual*, 2nd ed. (Ed.: M. Schlosser), Wiley, Chichester, **2002**, p. 665.

[2] For reviews, see: a) Y. Yamamoto, *Angew. Chem.* **1986**, *98*, 945; *Angew. Chem. Int. Ed. Engl.* **1986**, *25*, 947; b) N. Krause, S. Thorand, *Inorg. Chim. Acta* **1999**, *296*, 1; c) N. Krause, A. Gerold, *Angew. Chem.* **1997**, *109*, 194; *Angew. Chem. Int. Ed. Engl.* **1997**, *36*, 186; for selected recent examples, see: d) H. Wild, L. Born, *Angew. Chem.* **1991**, *103*, 1729; *Angew. Chem. Int. Ed. Engl.* **1991**, *30*, 1685; e) H. Liu, L. M. Gayo, R. W. Sullivan, A. Y. H. Choi, H. W. Moore, *J. Org. Chem.* **1994**, *59*, 3284; f) J. M. O'Reilly, N. Li, W. L. Duax, R. W. Brueggemeier, *J. Med. Chem.* **1995**, *38*, 2842; g) K. Sabbe, C. D'Hallewyn, P. De Clercq, M. Vandewalle, R. Bouillon, A. Verstuyf, *Bioorg. Med. Chem. Lett.* **1996**, *6*, 1697; h) R. K. Dieter, K. Lu, S. E. Velu, *J. Org. Chem.* **2000**, *65*, 8715; i) M. Uerdingen, N. Krause, *Tetrahedron* **2000**, *56*, 2799.

[3] K. Fukuhara, H. Urabe, *Tetrahedron Lett.* **2005**, *46*, 603.

[4] For reviews, see: a) T. Hayashi, *Synlett* **2001**, 879; b) C. Bolm, J. P. Hildebrand, K. Muñiz, N. Hermanns, *Angew. Chem.* **2001**, *113*, 3382; *Angew. Chem. Int. Ed.* **2001**, *40*, 3284; c) K. Fagnou, M. Lautens, *Chem. Rev.* **2003**, *103*, 169; d) T. Hayashi, K. Yamasaki, *Chem. Rev.* **2003**, *103*, 2829; e) T. Hayashi, *Bull. Chem. Soc. Jpn.* **2004**, *77*, 13.

[5] T. Hayashi, S. Yamamoto, N. Tokunaga, *Angew. Chem.* **2005**, *117*, 4296; *Angew. Chem. Int. Ed.* **2005**, *44*, 4224.

[6] G. de la Herrán, C. Murcia, A. G. Csákÿ, *Org. Lett.* **2005**, *7*, 5629.

[7] L. M. Green, D. W. Meek, *Organometallics* **1989**, *8*, 659.

[8] a) Aryl boroxine and water is in a fast equilibrium with aryl boronic acid, see: Y. Tokunaga, H. Ueno, Y. Shimomura, T. Seo, *Heterocycles* **2002**, *57*, 787; b) the use of 0.4 equivalents of phenylboroxine gave 81% yield of the 1,6-addition product **2**, thus indicating that two of the three phenyl groups in phenylboroxine were transferred.

[9] T. Koike, X. Du, T. Sanada, Y. Danda, A. Mori, *Angew. Chem.* **2003**, *115*, 93; *Angew. Chem. Int. Ed.* **2003**, *42*, 89.

[10] For selected recent examples of the iridium-catalyzed carbon–carbon bond-forming reactions, see: the arylation of aldehydes: a) N. Imlinger, M. Mayr, D. Wang, K. Wurst, M. R. Buchmeiser, *Adv. Synth. Catal.* **2004**, *346*, 1836; cycloaddition reactions: b) M. Fabbian, N. Marsich, E. Farnetti, *Inorg. Chim. Acta* **2004**, *357*, 2881; c) T. Shibata, N. Toshida, M. Yamasaki, S. Maekawa, K. Takagi, *Tetrahedron* **2005**, *61*, 9974; d) D. Carmona, M. P. Lamata, F. Viguri, R. Rodriguez, L. A. Oro, F. J. Lahoz, A. I. Balana, T. Tejero, P. Merino, *J. Am. Chem. Soc.* **2005**, *127*, 13386; e) S. Kezuka, S. Tanaka, T. Ohe, Y. Nakaya, R. Takeuchi, *J. Org. Chem.* **2006**, *71*, 543. Allylic alkylations; f) N. Kinoshita, K. H. Marx, K. Tanaka, K. Tsubaki, T. Kawabata, N. Yoshikai, E. Nakamura, K. Fuji, *J. Org. Chem.* **2004**, *69*, 7960; g) A. Alexakis, D. Polet, *Org. Lett.* **2004**, *6*, 3529; h) H. Miyabe, Y. Takemoto, *Synlett* **2005**, 1641; i) T. Graening, J. F. Hartwig, *J. Am. Chem. Soc.* **2005**, *127*, 17192; j) A. Dahnz, G. Helmchen, *Synlett* **2006**, 693; for other reactions: k) Y. Yamazaki, K. Fujita, R. Yamaguchi, *Chem. Lett.* **2004**, *33*, 1316; l) M. Janka, W. He, A. J. Frontier, R. Eisenberg, *J. Am. Chem. Soc.* **2004**, *126*, 6864; m) T. Hirabayashi, S. Sakaguchi, Y. Ishii, *Adv. Synth. Catal.* **2005**, *347*, 872; n) T. Suzuki, T. Matsuo, K. Watanabe, T. Katoh, *Synlett* **2005**, 1453; o) T. Igarashi, T. Inada, T. Sekioka, T. Nakajima, I. Shimizu, *Chem. Lett.* **2005**, *34*, 106; p) V. H. Grant, B. Liu, *Tetrahedron Lett.* **2005**, *46*, 1237; q) I. Kownacki, B. Marciniec, K. Szubert, M. Kubicki, *Organometallics* **2005**, *24*, 6179; r) Y. Masuyama, T. Chiyo, Y. Kurusu, *Synlett* **2005**, 2251; s) M. Banerjee, S. Roy, *J. Mol. Catal. A* **2006**, *246*, 231.

[11] R. Uson, L. A. Oro, J. A. Cabeza, *Inorg. Synth.* **1985**, *23*, 126.

[12] For isolated *ortho*-chelated aryl–iridium complexes, see: A. A. H. van del Zeijden, G. van Koten, R. Luijk, R. A. Nordemann, A. L. Spek, *Organometallics* **1988**, *7*, 1549.

[13] For bis(η^4-diene)aryl–iridium complexes, see: a) J. Müller, H. Menig, *J. Organomet. Chem.* **1980**, *191*, 303; b) J. Müller, C. Friedrich, T. Akhnoukh, K. Qiao, *J. Organomet. Chem.* **1994**, *476*, 93.

[14] For an example of a reaction of [{Ir(OH)(cod)}$_2$] with *i*PrMgBr in the presence of 1,3-pentadiene, which gives (η^3-allyl)(η^4-cod)(η^2-diene)–iridium(I) complex via a hydrido–iridium(I) species, see: J. Müller, W. Hähnlein, H. Menig, J. Pickardt, *J. Organomet. Chem.* **1980**, *197*, 95.

 © 2006 Wiley-VCH Verlag GmbH & Co. KGaA, Weinheim

Spectroscopy

DOI: 10.1002/anie.200601516

Spectroscopy of Isolated Gramicidin Peptides**

*Ali Abo-Riziq, Bridgit O. Crews, Michael P. Callahan, Louis Grace, and Mattanjah S. de Vries**

Many details of intrinsic properties of biomolecules are masked by elements of the biological environment, such as the solvent and intermolecular interactions. Separation of the inter- and intramolecular aspects of biomolecular function requires the study of isolated molecules under solvent-free conditions or with a controlled and limited number of solvent molecules. This can be achieved by gas-phase spectroscopy; however, this approach has been limited to small molecules with masses below a few hundred amu. In 1985 Rizzo et al. reported the first molecular beam experiments with tryptophan[1,2] followed by work on di- and tri-amino acids.[3–5] Ever since, the hope to extend this technique to larger molecules has met with very little success. Although electrospray and

[*] A. Abo-Riziq, B. O. Crews, M. P. Callahan, L. Grace, M. S. de Vries
Department of Chemistry and Biochemistry
University of California
Santa Barbara, CA 93106 (USA)
Fax: (+1) 805-893-4120
E-mail: devries@chem.ucsb.edu

[**] This work was supported by the Donors of the American Chemical Society Petroleum research Fund.

WILEY InterScience DISCOVER SOMETHING GREAT
© 2006 Wiley-VCH Verlag GmbH & Co. KGaA, Weinheim

MALDI have allowed mass spectrometry of very large ionic biomolecules,[6,7] the optical spectroscopy of neutral molecules in the gas phase has been largely restricted to systems with up-to-three residues.[8–12] An exception is a recent report by Bakker et al. on the nonapeptide DSIP (delta-sleep-inducing peptide)[11] with a molecular weight of 849 amu. Herein we report on the first double-resonance IR–UV spectroscopy of isolated gramicidin, a family of 15-residue peptides with molecular weights of 1845–1898 amu. The results are consistent with a secondary structure similar to that in the bulk.

This result shows not only that it is possible to bring these peptides into the gas phase intact but also that they adopt unique structures that reveal details of the intramolecular stabilizing forces. Furthermore, the results show that high-resolution spectroscopy can be performed on these peptides in spite of the large number of internal degrees of freedom. This capability opens the way to molecular-level studies of intermediate-size isolated peptides and of their interactions with individual molecules, such as water, in mass-selected clusters.

This approach employs laser-desorption jet-cooling, followed by double-resonance IR–UV spectroscopy.[13–16] Briefly, we placed biomolecules in the gas phase by pulsed laser desorption, followed by entrainment in a supersonic expansion of argon.[17] We performed electronic spectroscopy in the ultraviolet range of the spectrum by resonance-enhanced two-photon ionization (R2PI). We detected the ions in a TOF-mass spectrometer. We recorded IR spectra by employing an IR "burn" laser pulse, followed after 100 nanoseconds by a UV "probe" laser pulse, which two-photon ionizes through the S1 state. When the IR laser is tuned to a resonance it depletes the ground state, which causes a decrease in the ion signal. In this way, we can record ground-state IR spectra of mass-selected, as well as optically selected molecules and clusters. Furthermore, even when the UV absorption is broad, it is possible to obtain sharp IR spectra with this technique. IR–UV double-resonance spectroscopy is a highly sensitive structural probe because it allows us to measure OH and NH stretch frequencies that shift significantly upon hydrogen bonding.

Gramicidin is a biosynthetic product from *Bacillus brevis* that derives its functionality from forming a monovalent cation-selective channel in the lipid bilayer of targeted cells.[18,19] The channel is built from two peptides back to back, each in a single-stranded right-handed β-helical motif with 6.5 residues per turn. Each peptide is arranged with the carboxylic terminus at an interface of the bilayer and the protected amino terminus buried inside (see Figure 2). As the structure does not rely on a polar solvent, it is possible that the helix persists in the gas phase. Gramicidin consists of a mixture of components that each differ in one residue; Table 1 lists their sequences and formula weights. Figure 1 shows the two-photon ionization mass spectrum of a commercial mixture that is characterized by the parent masses and the absence of fragmentation. By monitoring each of the parent mass peaks as a function of ionization wavelength or hole-burning wavelength, we obtained the spectra of the separate components. The R2PI spectra are broad (not shown) but appear to correlate to one conformer, or a family of closely related conformers, because the double-resonance spectra were identical for all UV probe wavelengths tested. Remarkably, in spite of the large scope of the conformational landscape available to a peptide with up to 15 residues, all peptides in this study appear to adopt a single type of conformation without the aid of a solvent or other element of biology.

Table 1: Sequence of components of gramicidin: HCO–Val–X–Ala–D-Leu–Ala–D-Val–Val–D-Val–Trp–D-Leu–Y–D-Leu–Trp–D-Leu–Trp–$NHCH_2CH_2OH$.

Component	X	Y	M_r [amu]	Average composition
A	Gly	Trp	1880	80–85%
B	Gly	Phe	1845	6–7%
C	Gly	Tyr	1861	5–14%
D	Ala	Trp	1898	1%

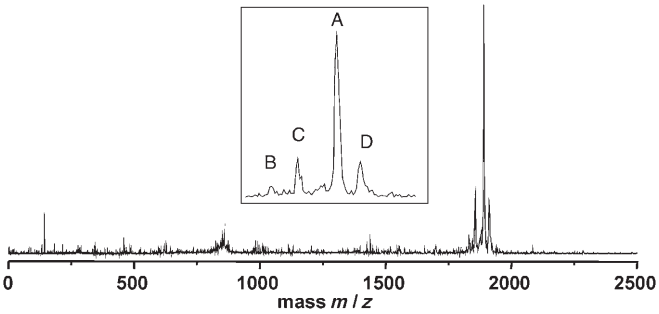


Figure 1. TOF mass spectrum of a gramicidin mixture with its relative abundances listed in Table 1.

Figure 2 shows the IR–UV spectra for each of the four components. Ab initio computations are currently under way to aid in the detailed analysis of these spectra. The structure optimizations, required before vibrational frequencies can be calculated, will take some time for a molecule this size. However, in the absence of such computations, we can already make some observations based on the spectra. The data are all consistent with a helical conformation: free indole NH frequencies are consistent with the tryptophan residing on the outside of the helix as is the free tyrosine OH frequency. Along the backbone, all peptide NH groups are hydrogen bonded leading to an intense broadened and red-shifted peak. The large-amplitude overtone of the NH bending mode at about 3100 cm^{-1} is also indicative of strong NH group hydrogen bonding. Comparison of the spectra of gramicidin A and C demonstrates sequence specificity. The difference between the two sequences is in a single residue, which is a tryptophan (W) in one case and a tyrosine (Y) in the other. The trace for the C form clearly shows the tyrosine OH stretch frequency that is completely absent in trace A.

To gauge the sensitivity of this approach to local structure, Figure 3 compares spectra for three different folding motifs. Figure 4 shows the spectrum of one of these, gramicidin S, in more detail. Its symmetrical β-sheet-type structure leads to pairs of equivalent functions: one pair of free NH_2 (rectangle), two pairs of free NH (solid gray), and two pairs of

 © 2006 Wiley-VCH Verlag GmbH & Co. KGaA, Weinheim

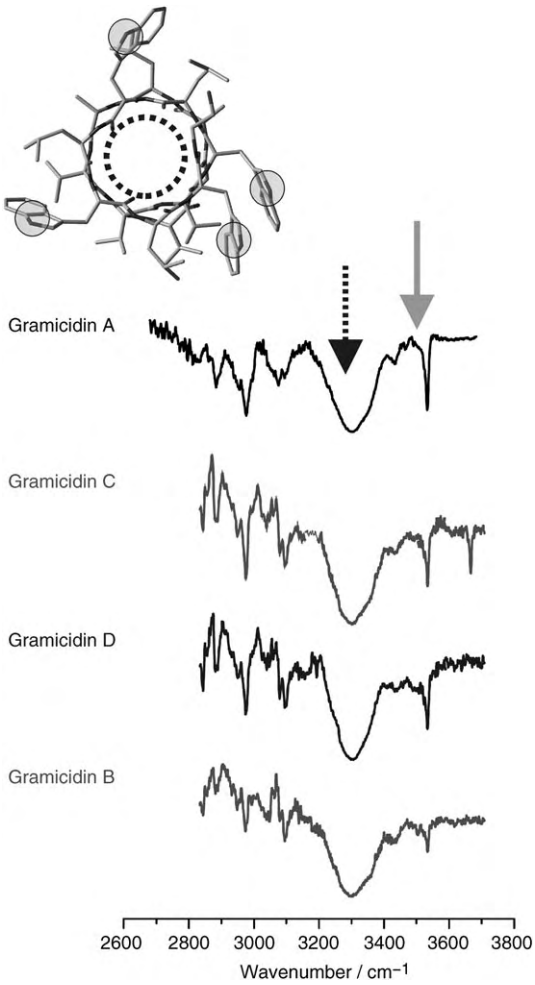


Figure 2. IR–UV double-resonance spectra of gramicidin A–D recorded on the masses of the four components shown in Figure 1. The dotted arrow indicates the wavelength region corresponding to hydrogen bonded NH from the backbone, outlined with a dotted circle in the structure at the top. The gray arrow indicates the wavelength region for free indole NH, outlined with gray circles.

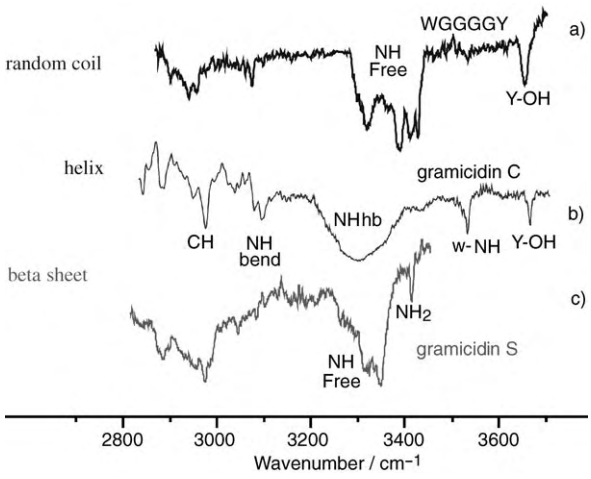


Figure 3. IR–UV double-resonance spectra of three different peptide sequences. The spectra show the distinct response for three different folding motifs. hb = hydrogen bonding.

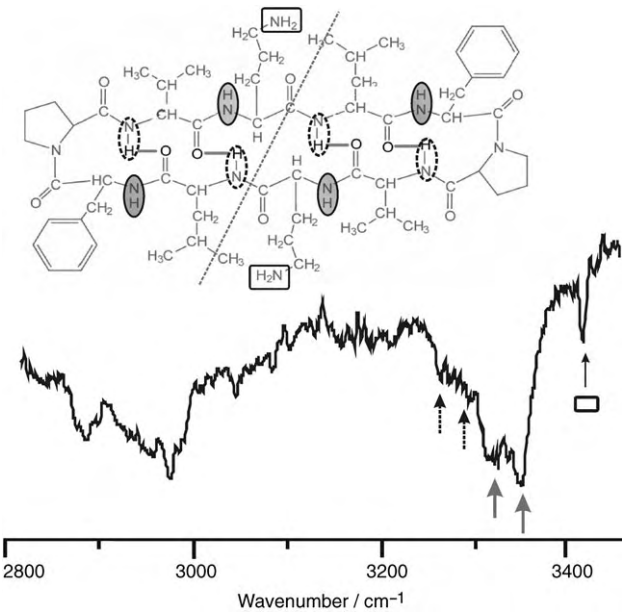


Figure 4. IR–UV double-resonance spectra of gramicidin S recorded on its parent mass. The solid gray arrows indicate the wavelength region corresponding to free or weakly hydrogen bonded NH, dotted black arrows indicate wavelengths for hydrogen bonded NH and the rectangle marks the region for free NH_2. Corresponding moieties in the molecule are marked with the same codes.

hydrogen bonded NH (dotted black). This is consistent with the appearance of the spectrum, which contains the free NH_2 peak as well as structure in the NH peak, which can be interpreted as two shifted and two unshifted peaks. Once again, the secondary structure appears to be maintained in the gas phase in this case. This may be contrasted with the spectrum of WGGGGY in the top trace of Figure 3. Glycine is a helix breaker and thus we would expect this to be a model for a random coil-like structure. Indeed, the NH stretch region is not strongly broadened and shifted as is the case for gramicidin, and the isolated NH frequencies are evident. Furthermore, this spectrum does not show a free indole NH, indicating that the tryptophan is now interacting with other parts of the molecule, rather than being on the outside of a helix. We also obtained the spectra for dimers and trimers of WGGGGY, which show a transition to the bulk spectrum of this compound.

In the analysis of IR spectra of peptides, it is customary to use the amide I and II regions in the mid-IR range, at around 1500 cm^{-1}, for structure analysis. The near-IR region presented herein is usually ignored because, in bulk data, it is insufficiently diagnostic. As can be seen, however, with the increased resolution afforded by the gas phase under jet-cooled conditions, even the near-IR region can be used for structure elucidation. Part of the mid-IR region can also be studied here through the overtones, particularly for the NH bending modes. Preparations are currently under way to perform these same experiments at a free-electron laser facility to access the mid-IR range.[11,20] Traditional analysis relies heavily on deconvolution of overlapping peaks and is based on model peak shapes. The ability to study that same

 © 2006 Wiley-VCH Verlag GmbH & Co. KGaA, Weinheim

region in the gas phase with higher resolution and the ability to study isolated peptides should make this approach significantly more powerful.

The main objective of gas phase spectroscopy is not necessarily structure determination but rather the study of local interactions in isolated molecules. The current results demonstrate that different folding motifs lead to different IR signatures that are much more distinct than what is normally used for structure elucidation by infrared absorption in the condensed phase. The great increase in IR resolution in isolated, cooled peptides opens the way to sensitive probing of local interactions that stabilize folding structures. The mass selectivity in the technique makes it possible to obtain size-dependent cluster spectra. One possible application is the systematic study of mass-selected clusters with water. By following the IR signatures as function of the number of water molecules attached to a peptide, it should be possible to study the role of the solvent at the molecular level.

Received: April 17, 2006
Published online: July 7, 2006

Keywords: gramicidin · IR–UV hole burning · peptide folding · spectroscopy · structure elucidation

[1] T. R. Rizzo, Y. D. Park, D. H. Levy, *J. Am. Chem. Soc.* **1985**, *107*, 277.
[2] T. R. Rizzo, Y. D. Park, L. Peteanu, D. H. Levy, *J. Chem. Phys.* **1985**, *83*, 4819.
[3] J. R. Cable, M. J. Tubergen, D. H. Levy, *J. Am. Chem. Soc.* **1987**, *109*, 6198.
[4] J. R. Cable, M. J. Tubergen, D. H. Levy, *Faraday Discuss. Chem. Soc.* **1988**, *86*, 143.
[5] J. R. Cable, M. J. Tubergen, D. H. Levy, *J. Am. Chem. Soc.* **1988**, *110*, 7349.
[6] J. B. Fenn, M. Mann, C. K. Meng, S. F. Wong, C. M. Whitehouse, *Mass Spectrom. Rev.* **1990**, *9*, 37.
[7] M. Karas, D. Bachmann, U. Bahr, F. Hillenkamp, *Int. J. Mass Spectrom. Ion Processes.* **1987**, *78*, 53.
[8] L. C. Snoek, R. T. Kroemer, M. R. Hockridge, J. P. Simons, *Phys. Chem. Chem. Phys.* **2001**, *3*, 1819.
[9] W. Chin, J. P. Dognon, F. Piuzzi, B. Tardivel, I. Dimicoli, M. Mons, *J. Am. Chem. Soc.* **2005**, *127*, 707.
[10] I. Hünig, K. Kleinermanns, *Phys. Chem. Chem. Phys.* **2004**, *6*, 2650.
[11] J. M. Bakker, C. Plutzer, I. Hunig, T. Haber, I. Compagnon, G. von Helden, G. Meijer, K. Kleinermanns, *ChemPhysChem* **2005**, *6*, 120.
[12] C. Unterberg, A. Gerlach, T. Schrader, M. Gerhards, *J. Chem. Phys.* **2003**, *118*, 8296.
[13] R. H. Page, Y. R. Shen, Y. T. Lee, *J. Chem. Phys.* **1988**, *88*, 5362.
[14] C. Riehn, C. Lahmann, B. Wassermann, B. Brutschy, *Chem. Phys. Lett.* **1992**, *197*, 443.
[15] S. Tanabe, T. Ebata, M. Fujii, N. Mikami, *Chem. Phys. Lett.* **1993**, *215*, 347.
[16] T. S. Zwier, *Annu. Rev. Phys. Chem.* **1996**, *47*, 205.
[17] G. Meijer, M. S. de Vries, H. E. Hunziker, H. R. Wendt, *Appl. Phys. B* **1990**, *51*, 395.
[18] D. A. Langs, *Science* **1988**, *241*, 188.
[19] B. M. Burkhart, R. M. Gassman, D. A. Langs, W. A. Pangborn, W. L. Duax, *Biophys. J.* **1998**, *75*, 2135.
[20] H. Fricke, A. Gerlach, M. Gerhards, *Phys. Chem. Chem. Phys.* **2006**, *8*, 1660.

 © 2006 Wiley-VCH Verlag GmbH & Co. KGaA, Weinheim

Rhodium Complexes

DOI: 10.1002/anie.200601352

Trigonal Pyramids: Alternative Ground-State Structures for Sixteen-Electron Complexes**

*Detlev Ostendorf, Clark Landis, and Hansjörg Grützmacher**

It is widely believed that tetracoordinate complexes of d^8 transition metal centers (Rh^I, Ir^I, Pd^{II}, Pt^{II}, etc.) have a planar structure (P, ideal D_{4h} symmetry) and, indeed, hundreds of examples are known.[1] However, apart from tetrahedral structure T, which is observed for high-spin transition metals from the 4th period,[2] sawhorse (SH, C_{2v}) and trigonal-pyramidal structures (TP, C_{3v}) are alternatives (Scheme 1).[3]



Scheme 1. Planar (P), tetrahedral (T), sawhorse (SH), and trigonal-planar (TP) structures.

The highly reactive transient carbonyls $[M(CO)_4]$ (M = Fe, Ru, Os) have SH structures,[4a–c] as do a few recently isolated Ru^0 and Rh^I complexes, which show remarkable reactivity.[4d–f]

Even computationally, the TP structure has been rarely considered. Pidun and Frenking investigated by DFT methods $[RhX(CO)_3]$ complexes with X = H, HC=O, CH_2OH, and OMe. For $[Rh(HC{=}O)(CO)_3]$, TP is the (slightly) preferred ground-state structure, whereas all other complexes have either a P or an SH form in the global minimum.[5] Within the complementary spherical electron density (CSED) model, Mingos identified SH and TP forms as the next best choices to planar structures for 16-electron complexes of late transition metals.[6] In computations using the orbital ranked symmetry analysis method (ORSAM), Bayse and Hall considered d^8-MH_4 hydrides with SH and TP forms.[7] Proposals for making

[*] Dr. D. Ostendorf, Prof. Dr. H. Grützmacher
Laboratory of Inorganic Chemistry
Department of Chemistry and Applied Biosciences
ETH Zürich
8093 Zürich (Switzerland)
Fax: (+41) 446-331-032
E-mail: gruetzmacher@inorg.chem.ethz.ch
Prof. Dr. C. Landis
Department of Chemistry
University of Wisconsin-Madison
1101 University Ave., Madison, WI 53706 (USA)
E-mail: landis@chem.wisc.edu

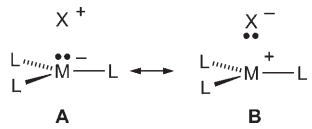
[**] This work was supported by the Swiss National Science Foundation and the ETH Zürich.

Supporting information for this article is available on the WWW under http://www.angewandte.org or from the author.

© 2006 Wiley-VCH Verlag GmbH & Co. KGaA, Weinheim

the TP forms the ground-state structures have not been made. Herein we report the synthesis and isolation of stable compounds that have such a trigonal pyramidal structure.

What ligand set would make the trigonal pyramid the ground-state structure for an ML_4 complex? We reasoned that such a structure might be obtained when the resonance form **A** contributes strongly to the electronic ground state with minimal participation of **B** (Scheme 2).



Scheme 2. Resonance structures **A** and **B** contributing to the electronic ground state of a TP structure.

This case arises when a formally d^{10}-ML_3 donor fragment such as $[Rh(C_2H_4)_3]^-$, which is known to have a trigonal-planar structure,[8] is combined with a cation X^+, most simply a proton or a silyl cation SiH_3^+. Indeed, DFT calculations for $[RhH(C_2H_4)_3]$ and $[Rh(SiH_3)(C_2H_4)_3]$ show that the trigonal-pyramidal form with H or SiH_3 in the apex is significantly more stable than the planar form (Table 1).[9]

Table 1: Calculated relative energies of trigonal-pyramidal (TP) and planar (P) $[RhXL_3]$ complexes.[a]

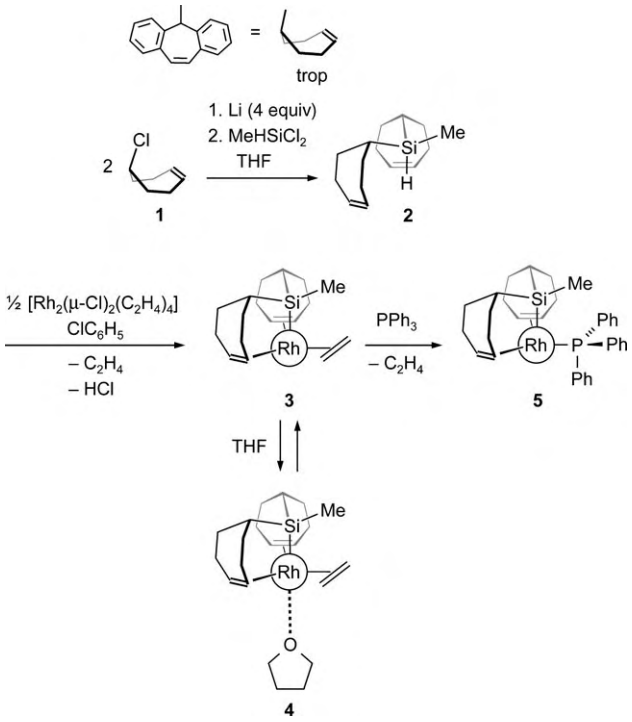
X	L	L′	TP E [kcal mol^{-1}]	P E [kcal mol^{-1}]
H	C_2H_4	C_2H_4	−7.3	0.0
SiH_3	C_2H_4	C_2H_4	−12.6	0.0
SiH_3	C_2H_4	PH_3	−10.6	0.0

[a] B3PW91 functional; 6-31 + G* for non-metal atoms, LANL2DZ at Rh.

Remarkably, even when one π-acceptor C_2H_4 ligand is replaced by a σ-donor PH_3 ligand, the TP form of $[Rh(SiH_3)(PH_3)(C_2H_4)_2]$ is more stable (by about 11 kcal mol^{-1}) than the planar *cis*-$[Rh(SiH_3)(PH_3)(C_2H_4)_2]$ complex.[10]

None of the species in Table 1 is likely be isolated, because insertion of a coordinated C_2H_4 into the Rh–H or Rh–Si bond is expected (Rh^I complexes are efficient catalysts for hydrogenation and hydrosilylation). Therefore we synthesized bis(5*H*-dibenzo[*a*,*d*]cyclohepten-5-yl)methylsilane ($trop_2SiHMe$, **2**), in which this insertion is unlikely to occur because of resulting strain energy in the product.[11] Silane **2** is easily obtained in 85% overall yield from 5-chloro-5*H*-dibenzo[*a*,*d*]cycloheptene (tropCl, **1**), which was first metalated with elemental lithium and then coupled in situ with $MeHSiCl_2$ (Scheme 3).

Note that the rigid conformation of **2** will not allow for a planar structure, but a sawhorse type structure may be obtainable. Silane **2** was treated with 0.5 equiv of $[Rh_2(\mu\text{-}Cl)_2(C_2H_4)_4]$ in chlorobenzene. Ethylene and HCl were liberated, and yellow crystals of $[Rh(trop_2SiMe)(C_2H_4)]\cdot C_6H_5Cl$ (**3**) precipitated in about 70% yield from



Scheme 3. Syntheses of silane **2** and complexes **3**–**5**.

the reaction mixture. When the reaction was performed in THF, or complex **3** was recrystallized from THF, $[Rh(trop_2SiMe)(C_2H_4)(thf)]$ (**4**) was obtained in 70% yield. Finally, when **3** was treated with one equivalent of PPh_3 in THF, ethylene evolved and yellow crystals of $[Rh(trop_2SiMe)(PPh_3)]$ (**5**) were isolated in almost quantitative yield.

Single crystals of **3**, **4**, and **5** were investigated by X-ray diffraction[12] (Figures 1–3). Clearly, **3** has the predicted trigonal-pyramidal structure; the calculated and experimental data agree satisfactorily (see legend to Figure 1). The three coordinated C=C units lie in the basal plane and bind in a trigonal fashion to the Rh atom, which deviates slightly (0.125 Å) from the plane through ct1–ct3 towards the inside of the pyramid (Figure 1b). The ct-Rh-Si angles are close to 90°. In the crystal lattice, one molecule of chlorobenzene lies between two molecules of **3**, but the absence of contacts shorter than 3.63 Å rules out any bonding interaction.

The structural parameters of the core of **4** are very similar to those of **3**. The Rh^I atom deviates by 0.085 Å from the plane through ct1–ct3 (Figure 2). A THF molecule binds loosely to the Rh^I center and completes the trigonal-bipyramidal coordination sphere typical of an 18-electron d^8-ML_5 complex. The very long Rh^I–O distance (2.544 Å) indicates a very weak interaction.

The crystal lattice of the phosphane silanide complex **5** contains no further solvent molecules, and the complex also has the predicted trigonal-pyramidal structure: The sum of the basal bond angles around the rhodium center is 356.6°. Like in **3** and **4**, the angles enclosed by the centroids of the coordinated C=C bonds and the apical Si atom are close to 90°. The ct-Rh-ct angle (129.6°) in **5** is somewhat wider than

 © 2006 Wiley-VCH Verlag GmbH & Co. KGaA, Weinheim

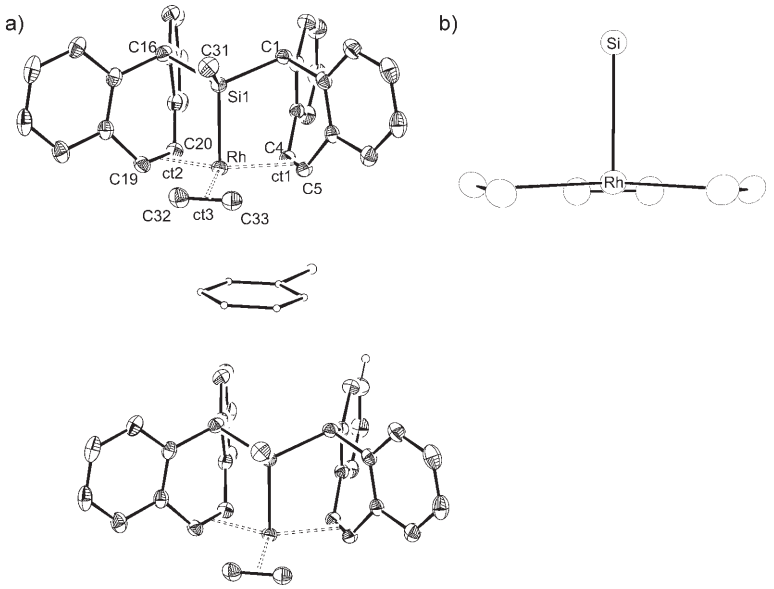


Figure 1. a) Structure of **3**. Hydrogen atoms are omitted for clarity. Thermal ellipsoids are drawn at 30% probability. Bond lengths [Å] and angles [°]: Rh–Si1 2.236(1), Rh1A–Si1A 2.266(2), Rh–C4 2.203(3), Rh–C5 2.217(3), Rh–C19 2.185(3), Rh–C20 2.217(3), Rh–C32 2.222(3), Rh–C33 2.231(3), Rh–ct1 2.095(3), Rh–ct2 2.085(3), Rh–ct3 2.117(3), Si1–C16 1.910(3), Si1–C1 1.912(3), Si1–C31 1.874(3), C4=$C5_{trop}$ 1.405(4), C19=$C20_{trop}$ 1.408(4), C32=C33 1.381(4); ct1-Rh-ct2 125.2(1), ct1-Rh-ct3 115.9(1), ct2-Rh-ct3 117.9(1), ct1-Rh-Si1 91.9(1), ct2-Rh-Si1 91.8(1), ct3-Rh-Si1 96.8(1), C1-Si1-C16 112.6(1), C1-Si1-C31 106.0(1), C31-Si1-C16 105.2(1), C1-Si1-Rh 107.6(1), C16-Si1-Rh 107.9(1), C31-Si1-Rh 117.8(1). ct = centroid of the coordinated C=C bond. Σ(ct-Rh-ct) = 359.0°; Σ(C-Si-C) = 323.7°. b) Plot of the core of **3**. Computed data for [$Rh(SiH_3)(C_2H_4)_3$]: Rh–Si 2.270, Rh–ct1 2.103, Rh–ct2 2.101, Rh–ct3 2.103, Rh–C 2.214–2.217, C=C 1.397; ct-Rh-ct 119.8, Σ(H-Si-H): 320.5°; Σ(ct-Rh-ct) = 359.3°.

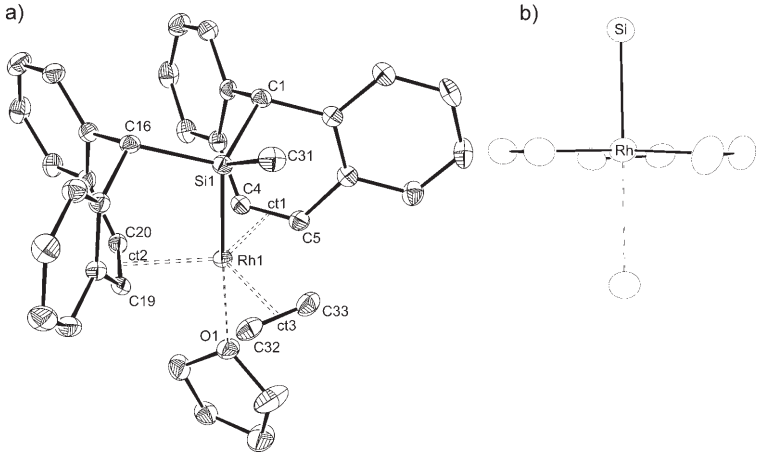


Figure 2. a) Structure of **4**. Hydrogen atoms are omitted for clarity. Thermal ellipsoids are drawn at 30% probability. Bond lengths [Å] and angles [°]: Rh1–Si1 2.243(1), Rh1–O1 2.544(2), Rh1–C4 2.202(2), Rh1–C5 2.192(2), Rh1–C19 2.213(2), Rh1–C20 2.241(2), Rh1–C32 2.211(2), Rh1–C33 2.211(3), Rh1–ct1 2.080(2), Rh1–ct2 2.113(2), Rh1–ct3 2.102(3), Si1–C16 1.911(2), Si1–C1 1.917(2), Si1–C31 1.875(2), C4=$C5_{trop}$ 1.410(3), C19=$C20_{trop}$ 1.410(3), C32=C33 1.373(4); ct1-Rh1-ct2 122.9(1), ct1-Rh1-ct3 119.1(1), ct2-Rh1-ct3 117.5(1), ct1-Rh1-Si1 91.8(1), ct2-Rh1-Si1 91.1(1), ct3-Rh1-Si1 94.2(1), ct1-Rh1-O1 81.6(1), ct2-Rh1-O1 92.0(1), ct3-Rh1-O1 89.7(1), C1-Si1-C16 112.7(1), C1-Si1-C31 104.8(1), C31-Si1-C16 103.4(1), C1-Si1-Rh1 107.7(1), C16-Si1-Rh1 108.5(1), C31-Si1-Rh1 119.9(1). Σ(ct-Rh-ct) = 359.5°; Σ(C-Si-C) = 320.9°. b) Plot of the core of **4**.

those in **3** and **4**, while the ct-Rh-P angles are slightly more acute (111.8, 115.2°). The Rh–Si bonds in **3** (2.236(1) and 2.266(2) Å), **4** (2.243(1) Å), and **5** (2.235(1) Å) are remarkably short, even shorter than the formal Rh=Si bonds in Rh^I silylene complexes.[13a] The Rh–P distance of 2.335(1) Å lies within the upper range of Rh–P bond lengths (ca. 2.26–2.34 Å).[14]

All structural features of the core are well reflected by the computed data for the unconstrained model [$Rh(SiH_3)(PH_3)(C_2H_4)_2$] (see legend to Figure 3). Only the experimentally determined P-Rh-Si angle in **5** (103.4(1)°) is larger than the calculated one (91.1°), certainly due to steric interactions, which can also be made responsible for the larger displacement of the Rh center from the basal plane of 0.220 Å. The acute C38-P1-Rh1 angle (94.9(1)°), which is significantly smaller that the other two C-P-Rh angles (130.4° and 118.0°), is noteworthy. This distortion may indicate a positive hyperconjugative interaction of the P–C σ bond with the empty orbital at the Rh^I center pointing outwards from the basal plane to the missing apical corner of a trigonal-bipyramidal (TBP) structure. Such distortions were also observed for complexes with SH-type structure, in which a P–C σ bond of an apically bonded PR_3 ligand may interact with an unfilled orbital pointing to the missing equatorial site of a TBP structure.[4d,e]

The NMR data of **3** and **5** are compatible with the structures observed in the solid state. In particular, the ^{1}H NOESY spectrum of **5** shows intense cross-peaks for the protons of the SiMe group and the phenyl protons of the PPh_3 ligand indicative of a *cis* arrangement. Such interactions are not expected for a compound in which the PPh_3 group is *trans* to the SiMe group. In the ^{1}H and ^{13}C NMR spectra of all reported compounds, the significant shift of the olefinic CH resonances to lower frequencies (coordination shifts $\Delta\delta_{coord} = \delta_{complex} - \delta_{ligand}$: ^{1}H: approx. −2 ppm, ^{13}C: approx. −60 ppm)[15] indicates significant metal-to-ligand backdonation. However, the inequivalent ^{1}H environments of the coordinated $H_2C{=}CH_2$ molecule in **3** lead to a slightly broadened singlet at room temperature; even at low temperature (183 K) no sharp distinct signals were observed, and this indicates a rather low barrier for rotation around the Rh–ct3 axis.

The NMR data of **3** in CD_2Cl_2 and of the THF complex **4** in [D_8]THF are almost identical. We therefore assume that the equilibrium **3** + THF ⇌ **4** lies far to left and that the interaction of the rhodium center with a fifth ligand in the apical position *trans* to the Si atom is very weak. In particular, the ^{29}Si and ^{103}Rh NMR resonances, which one would expect to respond most sensitively to complexation of an additional fifth

 © 2006 Wiley-VCH Verlag GmbH & Co. KGaA, Weinheim

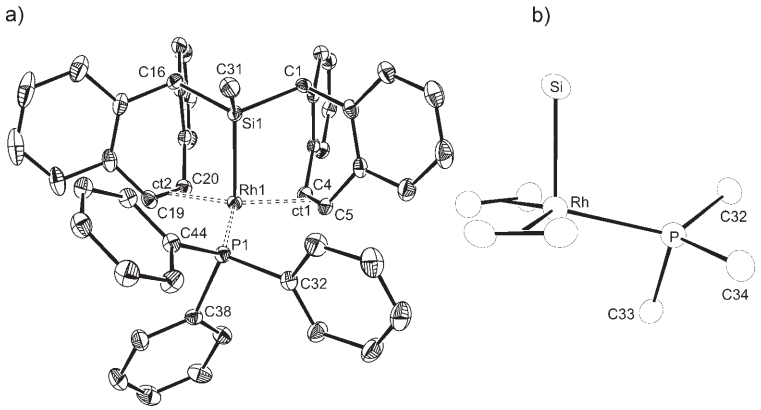


Figure 3. a) Structure of **5**. Hydrogen atoms are omitted for clarity. Thermal ellipsoids are drawn at 30% probability. Bond lengths [Å] and angles [°]: Rh1–Si1 2.235(1), Rh1–C4 2.179(3), Rh1–C5 2.211(3), Rh1–C19 2.182(3), Rh1–C20 2.157(3), Rh1–P1 2.335(1), Rh1–ct1 2.077(3), Rh1–ct2 2.048(3), Si1–C16 1.915(3), Si1–C1 1.906(3), Si1–C31 1.872(3), P1–C32 1.824(3), P1–C38 1.832(3), P1–C44 1.826(3), C4=$C5_{trop}$ 1.420(4), C19=$C20_{trop}$ 1.432(4); ct1-Rh1-ct2 129.6(1), ct1-Rh1-P1 111.8(1), ct2-Rh1-P1 115.2(1), ct1-Rh1-Si1 93.1(1), ct2-Rh1-Si1 93.0(1), P1-Rh1-Si1 103.4(1), C1-Si1-C16 112.2(1), C1-Si1-C31 103.9(1), C31-Si1-C16 106.6(1), C1-Si1-Rh1 105.9(1), C16-Si1-Rh1 106.2(1), C31-Si1-Rh1 122.2(1), Rh1-P1-C32 118.0(1), Rh1-P1-C38 94.9(1), Rh1-P1-C44 130.4(1). Σ(ct-Rh-ct) = 356.6°; Σ(C-Si-C) = 322.7°. b) Plot of the core of **5**. Computed data for $[Rh(SiH_3)(PH_3)(C_2H_4)_2]$ (C_{2v}): Rh–Si 2.279, Rh–P 2.342, Rh–ct 2.051, Rh–C 2.158–2.180, C=C 1.410; P-Rh-Si 91.1, H-P-Rh 2×121.4, H-P-Rh 119.4, ct-Rh-ct 131.0, ct-Rh-P 114.2, Σ(ct-Rh-ct) = 359.5°; Σ(H-Si-H) = 319.4°.

ligand, do not differ much (**3**: $\delta(^{29}Si) = 100.4$, $\delta(^{103}Rh) = -712.6$; **4**: $\delta(^{29}Si) = 97.15$, $\delta(^{103}Rh) = -654.5$]. Furthermore, no cross-peaks between the olefinic protons and α-CH_2 protons of the THF molecule were observed. These observations are in line with predictions made with the CSED model and the general expectations for the *trans* influence: The LUMO of a trigonal-pyramidal d^8-ML_4 complex is rather high in energy and "unavailable" for binding of a nucleophile.[6] Note, however, that planar d^8-ML_4 complexes are even more reluctant to interact with nucleophiles when a distortion from planarity is suppressed. Furthermore, trigonal-bipyramidal d^8-ML_5 complexes, conventionally obtained from planar d^8-ML_4, have the kinetically labile ligand in an equatorial position. Those obtained from TP complexes show lability in the axial position. The remarkable high-frequency shifts of the ^{29}Si NMR resonances in **3**–**5** (ca. +100 ppm vs. −10.4 ppm in **2**) would be formally in accord with a high weight of resonance structure **A** (Scheme 1) but should not be over-interpreted.

Finally, a cyclic voltammogram of **3** in THF with 0.1M $n$$Bu_4NPF_6$ showed one irreversible oxidation wave at +0.6 V and two irreversible reduction waves at −3.1 and −3.3 V versus ferrocenium/ferrocene. This demonstrates the high thermodynamic stability of the neutral molecule with a trigonal-pyramidal structure with respect to its cation and anion, respectively.

Clearly, the trigonal-pyramidal form is a possible ground state structure for d^8-ML_4 complexes. Our investigations indicate that a ligand set composed of at least one very strong (H, SiR_3) and two very weak σ-donor but good π-acceptors (olefins) favors the TP form. A deeper investigation of the electronic structure and factors that stabilize trigonal-pyramidal molecules as well as their potential use as Lewis acids with a well-defined rigid structure[16] is underway.

Experimental Section

All syntheses were performed under an atmosphere of argon by using standard Schlenk techniques. Details of the syntheses and a complete listing of spectroscopic data are given in the Supporting Information.

2: A slight excess of lithium powder (0.310 g, 44.7 mmol) was added to a solution of **1**[17] (5.00 g, 22.1 mmol) in THF (25 mL) at −78 °C. The mixture was stirred for 30 min at 0 °C and for 2 h at room temperature. The resulting deep red solution was added to a solution of dichloromethylsilane (1.26 g, 11.0 mmol) in THF (20 mL) at 0 °C. After stirring overnight, all volatile compounds were evaporated; the residue was taken up in 50 mL of toluene, the suspension filtered, and **2** was isolated from the filtrate as a pale yellow solid which was used without further purification. Yield: 4.07 g (9.5 mmol, 86%). M.p. 58 °C. ^{1}H NMR (500.2 MHz, CD_2Cl_2): $\delta = -0.27$ (d, $^3J_{HH} = 3.6$ Hz, 3H; CH_3), 4.28 (m, 1H; SiH), 6.65 (d, $^3J_{HH} = 11.9$ Hz, 2H; CH_{olefin}), 6.75 ppm (d, $^3J_{HH} = 11.9$ Hz, 2H; CH_{olefin}). ^{13}C NMR (125.8 MHz, CD_2Cl_2): $\delta = -3.20$ (s, 1C; CH_3), 132.69 (s, 2C; CH_{olefin}), 133.09 ppm (s, 2C; CH_{olefin}). ^{29}Si NMR (99.4 MHz, CD_2Cl_2): $\delta = -10.44$ ppm.

3: $[Rh_2(\mu_2\text{-}Cl)_2(C_2H_4)_4]$ (46 mg, 0.117 mmol) and **2** (100 mg, 0.234 mmol) were dissolved in chlorobenzene (1 mL) at 0 °C. After 20 min the color of the reaction mixture had changed from bright orange to brownish yellow. Over 4 d at −20 °C pale yellow crystals of **3** formed. Yield: 109 mg (0.171 mmol, 70%). M.p. > 124 °C (decomp.). ^{1}H NMR (500.2 MHz, CD_2Cl_2): $\delta = -0.93$ (s, 3H; CH_3), 4.72 (d, $^3J_{HH} = 10.5$ Hz, 2H; CH_{olefin}), 4.94 ppm (d, $^3J_{HH} = 10.5$ Hz, 2H; CH_{olefin}). ^{13}C NMR (125.8 MHz, CD_2Cl_2): $\delta = -4.78$ (s, 1C; CH_3), 70.12 (d, $^1J_{RhC} = 6.7$ Hz, 2C; CH_{olefin}), 71.00 (s, 2C; $CH_{ethylene}$), 73.92 ppm (*d*, $^1J_{RhC} = 8.2$ Hz, 2C; CH_{olefin}). ^{29}Si NMR (99.4 MHz, CD_2Cl_2): $\delta = 100.35$ ppm (d, $^1J_{RhSi} = 45.3$ Hz). ^{103}Rh NMR (15.8 MHz, CD_2Cl_2): $\delta = -712.58$ ppm (s).

4: $[Rh_2(\mu_2\text{-}Cl)_2(C_2H_4)_4]$ (46 mg, 0.117 mmol) and **2** (100 mg, 0.234 mmol) were dissolved in THF (1 mL) at room temperature. Gas evolution (C_2H_4) was observed and after 5 min the solution was concentrated to 0.5 mL, shortly warmed to about 40 °C, and cooled to room temperature. Pale yellow crystals of **4** began to precipitate, and the mixture was stored at 7 °C for 10 d. Yield: 70% (103 mg, 0.164 mmol). M.p. > 178 °C (decomp). ^{1}H NMR (500.2 MHz, 263 K, [D_8]THF): $\delta = -1.07$ (s, 3H; CH_3), 3.02 (s, 4H; $CH_{ethylene}$), 4.68 (d, $^3J_{HH} = 10.4$ Hz, 2H; CH_{olefin}), 4.87 ppm (d, $^3J_{HH} = 10.4$ Hz; 2H, CH_{olefin}). ^{13}C NMR (125.8 MHz, 263 K, [D_8]THF): $\delta = -6.26$ (s, 1C; CH_3), 69.46 (d, $^1J_{RhC} = 6.7$ Hz, 2C; $CH_{2,ethylene}$), 69.49 (d, $^1J_{RhC} = 6.7$ Hz, 2C; CH_{olefin}), 72.85 ppm (d, $^1J_{RhC} = 7.9$ Hz, 2C; CH_{olefin}). ^{29}Si NMR (99.4 MHz, [D_8]THF): $\delta = 97.15$ (d, $^1J_{SiRh} = 45.2$ Hz). ^{103}Rh NMR (15.8 MHz, [D_8]THF): $\delta = -654.54$ ppm.

5: **4** (55 mg, 0.087 mmol) was treated with triphenylphosphane (23 mg, 0.088 mmol) in THF (1 mL) at room temperature. Ethylene evolution was observed and after 5 min the solution was layered with hexane (1 mL) and cooled to −15 °C. Yellow crystals of **5** were isolated by filtration and dried in vacuo (67 mg, 0.085 mmol, 97%). M.p. > 161 °C (decomp). ^{1}H NMR (500.2 MHz, [D_8]THF): $\delta = -0.28$ (d, $^4J_{PH} = 2.8$ Hz, 3H; CH_3), 3.86 (m, 2H; CH_{olefin}), 4.29 ppm (m, 2H; CH_{olefin}). ^{13}C NMR (100.6 MHz, [D_8]THF): $\delta = 1.75$ (dd, $^3J_{CP} = 10.6$ Hz, $^2J_{CRh} = 1.5$ Hz, 1C; CH_3), 65.97 (dd, $^1J_{CRh} = 8.6$ Hz, $^2J_{CP} = 4.7$ Hz, 2C; CH_{olefin}), 70.74 ppm (dd, $^1J_{CRh} = 12.6$ Hz, $^2J_{CP} = 9.0$ Hz, 2C; CH_{olefin}). ^{29}Si NMR (79.5 MHz, [D_8]THF): $\delta = 103.68$ (dd, $^1J_{SiRh} = 47.6$ Hz, $^2J_{SiP} = 5.8$ Hz). ^{31}P NMR (161.9 MHz, [D_8]THF): $\delta =$

 © 2006 Wiley-VCH Verlag GmbH & Co. KGaA, Weinheim

30.90 ppm (d, $^1J_{PRh} = 138.6$ Hz). ^{103}Rh NMR (12.6 MHz, [D$_8$]THF): $\delta = -484.14$ ppm (d, $^1J_{PRh} = 139.0$ Hz).

Received: April 5, 2006
Published online: July 7, 2006

Keywords: alkene ligands · density functional calculations · rhodium · Si ligands · silanes

[1] The Cambridge Crystallographic Data Centre (CCDC) cites more than 1600 Rh^{I} complexes with approximately planar structures.

[2] a) For tetrahedral [Co^{I}XL$_3$], see: S. Deblon, L. Liesum, J. Harmer, H. Schönberg, A. Schweiger, H. Grützmacher, *Chem. Eur. J.* **2002**, *8*, 601, and references therein; b) for tetrahedral Ni^{II} complexes, see: C. O. Dietrich-Buchecker, J. Guilhem, J.-M. Kern, C. Pascard, J.-P. Sauvage, *Inorg. Chem.* **1994**, *33*, 3498, and references therein.

[3] We refer to trigonal pyramids as structures in which the angles between the axial and equatorial ligands are equal or close to 90°. Alternatively, they may be described as trigonal bipyramids in which one axial coordination site is vacant. A referee brought to our attention that MS$_3$(L) fragments (M = V, Mo, Fe) with TP structures were observed in transition metal sulfide clusters: a) I. Noda, B. S. Snyder, R. H. Holm, *Inorg. Chem.* **1986**, *25*, 3851; b) E. Nordlander, S. C. Lee, W. C. Cen, Z. Y. Wu, C. R. Natoli, A. Di Cicco, A. Filipponi, B. Hedman, K. O. Hodgson, R. H. Holm, *J. Am. Chem. Soc.* **1993**, *115*, 5549.

[4] a) M. Poliakoff, J. J. Turner, *J. Chem. Soc. Dalton Trans.* **1974**, 2276; b) M = Ru: P. L. Bogdan, E. Weitz, *J. Am. Chem. Soc.* **1989**, *111*, 3163; c) calculations: J. Li, G. Schreckenbach, T. Ziegler, *J. Am. Chem. Soc.* **1995**, *117*, 486. For a general discussion, see: T. A. Albright, J. K. Burdett, M.-H. Whangbo, *Orbital Interactions in Chemistry*, Wiley, **1985**, pp. 360, 404; d) P. Maire, A. Sreekanth, T. Büttner, J. Harmer, I. Gromov, H. Rüegger, F. Breher, A. Schweiger, H. Grützmacher, *Angew. Chem.* **2006**, *118*, 3343; *Angew. Chem. Int. Ed.* **2006**, *45*, 3265; e) P. Maire, T. Büttner, F. Breher, P. Le Floch, H. Grützmacher, *Angew. Chem.* **2005**, *117*, 6477; *Angew. Chem. Int. Ed.* **2005**, *44*, 6318; f) M. Ogasawara, D. Huang, W. E. Streib, J. C. Huffman, N. Gallego-Planas, F. Maseras, O. Eisenstein, K. G. Caulton, *J. Am. Chem. Soc.* **1997**, *119*, 8642, and references therein.

[5] U. Pidun, G. Frenking, *Chem. Eur. J.* **1998**, *4*, 522.

[6] D. M. P. Mingos, *J. Organomet. Chem.* **2004**, *689*, 4420.

[7] C. A. Bayse, M. B. Hall, *J. Am. Chem. Soc.* **1999**, *121*, 1348.

[8] $[Ag(C_2H_4)_3]^+$: I. Krossing, A. Reisinger, *Angew. Chem.* **2003**, *115*, 5903; *Angew. Chem. Int. Ed.* **2003**, *42*, 5725.

[9] All DFT calculations were carried out with the Gaussian 03 set of programs and the B3PW91 functional (for details see Supporting Information). For [Rh(SiH$_3$)(C$_2$H$_4$)$_3$], the isomer with the SiH$_3$ group in the basal plane is less stable by 14 kcal mol^{-1} and corresponds more to an alkyl complex [Rh(CH$_2$CH$_2$SiH$_3$)(C$_2$H$_4$)$_2$], that is, one ethylene ligand has inserted into the Rh–Si bond. For [Rh(SiH$_3$)(PH$_3$)(C$_2$H$_4$)$_2$] no energy minimum for an isomer with a basal SiH$_3$ group was found.

[10] The isomer with the SiH$_3$ and PH$_3$ groups in *trans* positions adopts a SH-type structure which is almost equal in energy to the planar *cis* form ($\Delta E = -0.03$ kcal mol^{-1}).

[11] The synthesis of the related dibenzophosphasemibullvalene was recently reported: J. Geier, G. Frison, H. Grützmacher, *Angew. Chem.* **2003**, *115*, 4085; *Angew. Chem. Int. Ed.* **2003**, *42*, 3955.

[12] Pale yellow, air-sensitive single crystals of **3** were obtained from chlorobenzene solution at −15 °C. Crystal data: C$_{39}$H$_{34}$ClRhSi; monoclinic; space group $P2(1)/c$; $a = 10.6913(5)$, $b = 11.5133(6)$, $c = 24.6594(12)$ Å; $V = 3020.2(3)$ Å^3; $Z = 4$; $\rho_{calcd} = 1.437$ Mg m^{-3}; crystal dimensions $0.36 \times 0.20 \times 0.11$ mm; Bruker SMART Apex diffractometer with CCD area detector; Mo$_{K\alpha}$ radiation ($\lambda = 0.71073$ Å), 200 K, $2\Theta_{max} = 56.56°$; 30672 reflections, 7483 independent ($R_{int} = 0.0249$); direct methods; empirical absorption correction with SADABS (version 2.03); refinement against full matrix (versus F^2) with SHELXTL (version 6.12) and SHELXL-97 (G. M. Sheldrick, Göttingen, 1997); 291 parameters, $R1 = 0.0390$ and $wR2$ (all data) = 0.1107, max./min. residual electron density 0.908/−0.473 e Å^{-3}. All non-hydrogen atoms were refined anisotropically. The contribution of the hydrogen atoms in their calculated positions was included in the refinement by using a riding model. The chlorobenzene units and the units of **3** show an alternating alignment. Furthermore, four percent of the molecules of **3** are disordered about a mirror plane perpendicular to the Rh–Si1 bond (Rh1A–Si1A). The remaining atoms of the disordered molecules overlap with the ligand atoms of the main structure and could therefore not be localized. Pale yellow, air-sensitive single crystals of **4** were obtained from a solution in THF at room temperature. Crystal data: C$_{37}$H$_{37}$OSiRh; orthorhombic; space group $P2(1)2(1)2(1)$; $a = 10.9270(5)$, $b = 12.2839(6)$, $c = 21.6322(10)$ Å; $V = 2903.6(2)$ Å^3; $Z = 4$; $\rho_{calcd} = 1.438$ Mg m^{-3}; crystal dimensions $0.24 \times 0.19 \times 0.15$ mm; Bruker SMART Apex diffractometer with CCD area detector; Mo$_{K\alpha}$ radiation ($\lambda = 0.71073$ Å), 200 K, $2\Theta_{max} = 56.62°$; 30385 reflections, 7220 independent ($R_{int} = 0.0388$); direct methods; refinement against full matrix (versus F^2) with SHELXTL (version 6.12) and SHELXL-97; 362 parameters, $R1 = 0.0280$ and $wR2$ (all data) = 0.0626, max./min. residual electron density 0.930/−0.378 e Å^{-3}. All non-hydrogen atoms were refined anisotropically. The contribution of the hydrogen atoms in their calculated positions was included in the refinement by using a riding model. Yellow, air-sensitive single plates of **5** were obtained from a solution in THF layered with *n*-hexane at 7 °C. Crystal data: C$_{49}$H$_{40}$SiPRh; monoclinic; space group $P2(1)/c$; $a = 17.0615(8)$, $b = 10.3224(5)$, $c = 22.1621(11)$ Å; $V = 3778.5(3)$ Å^3; $Z = 4$; $\rho_{calcd} = 1.390$ Mg m^{-3}; crystal dimensions $0.30 \times 0.22 \times 0.06$ mm; Bruker SMART K1 diffractometer with CCD area detector; Mo$_{K\alpha}$ radiation ($\lambda = 0.71073$ Å), 200 K, $2\Theta_{max} = 52.75°$; 30210 reflections, 7723 independent ($R_{int} = 0.0447$); direct methods; empirical absorption correction with SADABS (version 2.03); refinement against full matrix (versus F^2) with SHELXTL (version 6.12) and SHELXL-97; 476 parameters, $R1 = 0.0327$ and $wR2$ (all data) = 0.0799, max./min. residual electron density 0.754/−0.463 e Å^{-3}. All non-hydrogen atoms were refined anisotropically. The contribution of the hydrogen atoms in their calculated positions was included in the refinement by using a riding model. CCDC-602113 (**3**), -602114 (**4**), and -602115 (**5**) contain the supplementary crystallographic data for this paper. These data can be obtained free of charge from The Cambridge Crystallographic Data Centre via www.ccdc.cam.ac.uk/data_request/cif.

[13] To date, 71 compounds with an Rh–Si bond are listed in the CCDC data base. For recent examples with Rh^{I}–Si bonds, see: a) E. Neumann, A. Pfaltz, *Organometallics* **2005**, *24*, 2008; b) R. Goikhman, M. Aizenberg, Y. Ben-David, L. J. W. Shimon, D. Milstein, *Organometallics* **2002**, *21*, 5060; c) M. Okazaki, S. Ohshitanai, H. Tobita, H. Ogino, *J. Chem. Soc. Dalton Trans.* **2002**, 2061.

[14] F. H. Allen, O. Kennard, D. G. Watson, L. Brammer, A. G. Orpen, *J. Chem. Soc. Perkin Trans. 2* **1987**, S1.

[15] See for comparison: P. Maire, F. Breher, H. Schönberg, H. Grützmacher, *Organometallics* **2005**, *24*, 3207.

[16] Note that most Lewis acids change their structure on complexation of a nucleophile, for instance, from trigonal planar to tetrahedral.

[17] G. Berti, *J. Org. Chem.* **1957**, *22*, 230.

 © 2006 Wiley-VCH Verlag GmbH & Co. KGaA, Weinheim

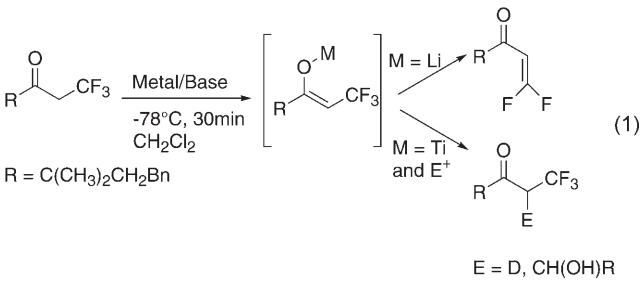
CF_3-Containing Enolates

DOI: 10.1002/anie.200600927

Highly Diastereoselective Aldol Reaction with α-CF_3-Substituted Enolates**

Xavier Franck, Blandine Seon-Meniel, and Bruno Figadère**

Organofluorine compounds have received much attention lately because of their important applications as pharmacologically active products and their unique physical properties.[1] Of the few organofluorine compounds that occur in nature, those bearing a trifluoromethyl group are of particular interest.[1] Although reactions of α-CF_3-substituted enolates appear to be a most attractive way to prepare CF_3-containing compounds, only one example of the use of a Ti enolate in aldol reactions has been reported thus far.[2,3] Indeed, most of α-CF_3 ketone enolates, such as Li enolates, react by defluorination, affording the corresponding α,β-unsaturated β,β-difluoroketones, whereas their titanium enolate counterparts react with aldehydes at −78 °C [Eq. (1)], because of the

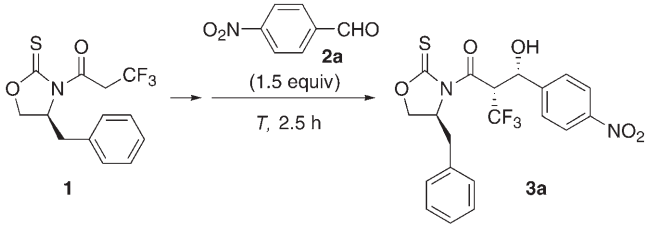


(1)

weaker interaction of titanium with fluorine.[3] These results prompted us to study the reactivity of chiral titanium enolates of α-CF_3 amides, such as (*S*)-*N*-3,3,3-trifluoropropionyl-4-benzyloxazolidine-2-thione (**1**).[4] We report herein that the Ti enolate of a chiral α-CF_3 amide can be generated efficiently, and it reacts with aldehydes in a highly diastereoselective aldol reaction. The CF_3-containing aldols so obtained may then be used as chiral building blocks for the preparation of more elaborate compounds.

The titanium enolates of *N*-propionyl oxazolidine-2-thiones react with achiral aldehydes to provide an alternative and efficient access to Evans or non-Evans *syn* aldols, depending on the type and amount of base used.[5] Thus we first examined the formation of the titanium enolate of the α-CF_3-substituted amide **1**, and its reactivity towards 4-nitrobenzaldehyde (**2a**) (Table 1). The preparation of the required 4-benzyloxazolidine-2-thione was straightforward and followed reported procedures.[6] Quantitative N-acylation was achieved by treatment with 3,3,3-trifluoropropanoic acid in the presence of *N*,*N*′-dicyclohexylcarbodiimide (DCC) and a catalytic amount of 4-dimethylaminopyridine (DMAP) in dichloromethane at 0 °C. Upon addition at −78 °C of nitrobenzaldehyde **2a** to the $TiCl_3$ enolate of **1**, which was prepared in situ (1 equiv of $TiCl_4$ and 2.5 equiv of *N*,*N*,*N*′,*N*′-tetramethylethylenediamine (TMEDA) in CH_2Cl_2 at −78 °C for 20 min), the *syn* aldol product **3a** was obtained in good yield (72 %) and with high diastereoselectivity (> 96 % *de*) (entry 1, Table 1. When the aldehyde **2a** was added at −40 °C or 0 °C, the yields were lower (around 36 % in both cases) but the diastereoselectivity was not affected, and no defluorination was observed (entries 2 and 3, Table 1). When diisopropylethyl amine (DIEA) was used, little or no reaction occurred (entry 4, Table 1). In all cases the *de* values were determined from the crude mixtures by the integration of the ^{19}F NMR signals. Indeed, two doublets in a > 98:2 ratio were observed at $\delta = -63.69$ and −64.54 ppm, corresponding to the nonseparable diastereomers.

Table 1: Formation of the titanium enolate from **1** and its reactivity towards 4-nitrobenzaldehyde (**2a**).[a]



Entry	Amine	*T*	Yield [%]	*de* of *syn* product
1	TMEDA	−78 °C to RT	72	> 96
2	TMEDA	−40 °C	37	> 96
3	TMEDA	0 °C	36	> 96
4	DIEA[b]	−78 °C to RT	0	–

[a] Reaction conditions for generation of the Ti enolate: $TiCl_4$ (1 equiv), amine (2.5 equiv), CH_2Cl_2, −78 °C, 20 min. [b] DIEA (1.1 equiv) and $TiCl_4$ (2 equiv).

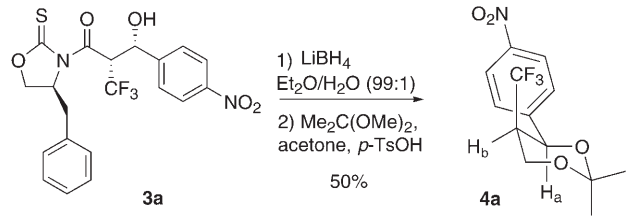
The *syn* relationship of the hydroxy and CF_3 groups in **3a** was determined by ^1H NMR analysis of the corresponding enantiomerically pure acetonide **4a**, which was prepared from aldol **3a** (reduction with $LiBH_4$, followed by treatment with $(CH_3)_2C(OMe)_2$, see Scheme 1) in an unoptimized 50 % overall yield. At this stage, the chiral auxiliary, the (*S*)-5-benzyloxazolidine-2-thione, was easily recovered in 93 % yield. The observed coupling constant between H_a and H_b of

[*] Dr. X. Franck
UMR-CNRS 6014, IRCOF/LHO
Rue Tesniere, 76131 Mont Saint Aignan (France)
E-mail: xavier.franck@insa-rouen.fr
B. Seon-Meniel, Prof. Dr. B. Figadère
Laboratoire de Pharmacognosie, associé au CNRS (BIOCIS)
Université Paris-Sud, Faculté de Pharmacie
Rue Jean-Baptiste Clément
92296 Châtenay-Malabry (France)
Fax: (+33) 146-835-399
E-mail: Bruno.Figadere@cep.u-psud.fr

[**] We thank J. C. Jullian for his help with the NMR experiments, and Prof. R. Hocquemiller for his continued interest in this research.

Supporting information for this article is available on the WWW under http://www.angewandte.org or from the author.

InterScience DISCOVER SOMETHING GREAT
© 2006 Wiley-VCH Verlag GmbH & Co. KGaA, Weinheim

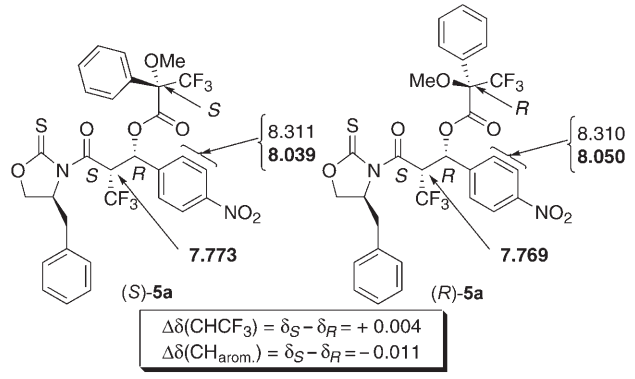


Scheme 1. *p*-TsOH = *p*-toluenesulfonic acid.

the acetonide **4a** was <1 Hz, as expected for an H_{ax},H_{eq} coupling constant in such an acetonide.[7] It is also important to note that the *anti* acetonide with a phenyl group (instead of a 4-nitrophenyl moiety) has already been prepared by a different approach, and showed a different and typical H_{ax},H_{ax} coupling constant of 10 Hz.[8]

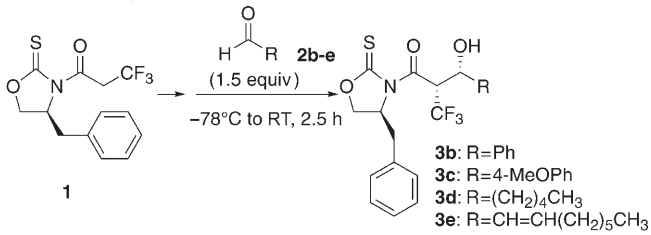
The *syn* diastereoselectivity of the reaction can be rationalized by evoking the formation of the *Z* enolate to give the *syn* aldol via a cyclic transition state, as is usually observed with Ti/amine systems.[9] It is interesting to note that in the case of Ti enolates generated from α-CF_3 ketone, the *anti* aldols are formed as the major products.[3] In our case, we suppose that the affinity of Ti for sulfur is stronger than for fluorine, thus the usual cyclic transition state gives rise to the expected *syn* aldols. At this stage, we may also suppose that the *syn* Evans aldol was produced. In order to confirm this hypothesis, we prepared the Mosher's esters of aldol **3a** directly in an NMR tube.[10] Careful analysis of the differences of the chemical shifts at the positions α and α′ to the carbinol group of esters (*S*)-**5a** and (*R*)-**5a** ($\Delta\delta(CHCF_3)=\delta_S-\delta_R=+0.004$, and $\Delta\delta(CH_{arom})=\delta_S-\delta_R=-0.011$) allowed us to tentatively assign the *R* absolute configuration to the stereogenic center bearing the hydroxy group (because of the rather weak $\Delta\delta(CHCF_3)$ values) (Scheme 2). Then because of the known *syn* relationships, the adjacent stereogenic center bearing the CF_3 group must have the *S* absolute configuration. These 2*S*,3*R* configurations for the newly created stereogenic centers confirm that the *syn* Evans aldol **3a** has been obtained.

We next examined the generalization of this reaction (Table 2). We were pleased to observe that under the same reaction conditions, benzaldehyde (**2b**), and 4-methoxybenzaldehyde (**2c**) gave the expected *syn* aldols **3b** and **3c** in 86 and 85% yields, respectively (entries 2 and 3, Table 2). Again, the diastereoselectivity was excellent and superior to >96% *de*, in both cases. Finally, even aliphatic aldehydes such as pentanal (**2d**) and (*E*)-non-2-en-1-al (**2e**) gave exclusively the *syn* aldols **3d** and **3e** (>96% *de*) in yields of 64 and 63%, respectively (entries 3 and 4, Table 2). The *syn* stereochemistry of the products was secured by NMR analysis of their corresponding enantiomerically pure acetonides. The absolute configuration of aldols **3b–e** is supposed to be 2*S*,3*R* because the same cyclic six-membered transition state may be invoked, and specific rotations of aldols, and of the corresponding acetonides have the same signs (see the Supporting Information).



Scheme 2. Stereochemical assignment based on analysis of the differences of the ^{1}H NMR chemical shifts at the positions α and α′ to the carbinol group of esters (*S*)-**5a** and (*R*)-**5a**.

Table 2: Formation of the titanium enolate from **1** and its reactivity towards aldehydes **2b–e**.[a]



Entry	Aldehyde	Yield [%]	*de* of *syn* product
1	benzaldehyde (**2b**)	86	>96
2	4-methoxybenzaldehyde (**2c**)	85	>96
3	pentanal (**2d**)	63	>96
4	(*E*)-non-2-en-1-al (**2e**)	64	>96

[a] Reaction conditions for generation of the Ti enolate: $TiCl_4$ (1 equiv), TMEDA (2.5 equiv), CH_2Cl_2, −78°C, 20 min.

It is worth noting that under the reaction conditions used we never observed the defluorination reaction leading to the vinylic CF_2 product. This result can be explained by the stability of the $TiCl_3$ enolate of the α-CF_3 amide possessing the oxazolidine-2-thione moiety (vide infra).

We are now studying the scope and limitation of this reaction in our laboratories by varying the type of electrophile that can react with the titanium enolate of **1**. We will also examine reactions with bulkier oxazolidine-2-thiones (such as 5,5-biphenyl-4-benzyloxazolidine-2-thione) in order to study the influence of the steric hindrance of the titanium enolates of the corresponding α-CF_3 amides on the course of the reaction.

In conclusion, the reaction of titanium enolate of the α-CF_3-substituted amide (*S*)-*N*-3,3,3-trifluoropropionyl-4-benzyloxazolidin-2-thione (**1**) with several aldehydes afforded the enantiomerically pure *syn* aldols in good to excellent yields and high diastereoselectivity (>96% *de*). The absolute configuration of aldol **3a** has been determined unambiguously through the Mosher's esters. The absolute configurations of the other aldols have not been determined but are assumed to be identical to those of **3a**. We are currently preparing sugar derivatives to confirm the absolute configuration of the newly created stereogenic centers, especially in the case of aliphatic aldehydes.[11] $LiBH_4$ reduction of the *syn* aldols shoulc provide the corresponding enantiomerically

 © 2006 Wiley-VCH Verlag GmbH & Co. KGaA, Weinheim

pure 1,3-diols and thus open a new access to chiral CF_3-containing compounds. These results show the large scope of such an aldol reaction, and will probably find application in the preparation of pharmacologically active products in the near future.

Received: March 9, 2006
Revised: May 9, 2006
Published online: July 5, 2006

Keywords: aldol reaction · diastereoselectivity · enantioselectivity · titanium · trifluoromethyl group

[1] a) J. P. Begue, D. Bonnet-Delpon, *Chimie Bioorganique et Médicinale du Fluor*-Savoirs Actuels, CNRS and EDP Sciences, Paris, **2005**; b) *Enantiocontrolled Synthesis of Fluoro-organic Compounds* (Ed.: V. A. Soloshonok), Wiley, Chichester, **1999**; c) K. Mikami, Y. Itoh, M. Yamanaka, *Chem. Rev.* **2004**, *104*, 1–16; d) J. A. Ma, D. Cahard, *Chem. Rev.* **2004**, *104*, 6119–6146.
[2] Y. Itoh, M. Yamanaka, K. Mikami, *Org. Lett.* **2003**, *5*, 4807–4809.
[3] Y. Itoh, M. Yamanaka, K. Mikami, *J. Am. Chem. Soc.* **2004**, *126*, 13174–13175.
[4] Prepared by acylation of the corresponding chiral oxazolidin-2-thione; see supplementary material for the spectroscopic data of **1**.
[5] a) M. T. Crimmins, B. W. King, E. A. Tabet, *J. Am. Chem. Soc.* **1997**, *119*, 7883; b) M. T. Crimmins, B. W. King, *J. Am. Chem. Soc.* **1998**, *120*, 9084; c) M. T. Crimmins, K. Chaudhary, *Org. Lett.* **2000**, *2*, 775; d) M. T. Crimmins, B. W. King, E. A. Tabet, K. Chaudhary, *J. Org. Chem.* **2001**, *66*, 894; e) M. T. Crimmins, J. She, *Synlett* **2004**, 1371.
[6] G. Jalce, M. Seck, X. Franck, R. Hocquemiller, B. Figadère, *J. Org. Chem.* **2004**, *69*, 3240–3243, and references herein.
[7] R. M. Silverstein, G. C. Bassler, *Spectrometric Identification of Organic Compounds*, Wiley, New York, **1997**.
[8] T. Sakamoto, K. Takahashi, T. Yamazaki, T. Kitazume, *J. Org. Chem.* **1999**, *64*, 9467–9474.
[9] a) D. A. Evans, J. S. Clark, R. Metternich, V. J. Novack, G. S. Sheppard, *J. Am. Chem. Soc.* **1990**, *112*, 866–868; b) D. A. Evans, F. Urpi, T. C. Somers, J. S. Clark, M. T. Bilodeau, *J. Am. Chem. Soc.* **1990**, *112*, 8215–8216; c) D. A. Evans, D. L. Rieger, M. T. Bilodeau, F. Urpi, *J. Am. Chem. Soc.* **1991**, *113*, 1047–1049; d) J. G. Solsona, P. Romea, F. Urpi, J. Vilarrasa, *Org. Lett.* **2003**, *5*, 519–522; e) C. R. Harrison, *Tetrahedron Lett.* **1987**, *28*, 4135–4138.
[10] a) J. A. Dale, H. S. Mosher, *J. Am. Chem. Soc.* **1968**, *90*, 3732–3738; b) J. A. Dale, H. S. Mosher, *J. Am. Chem. Soc.* **1973**, *95*, 512–519; c) J. A. Dale, D. L. Dull, H. S. Mosher, *J. Org. Chem.* **1969**, *34*, 2543–2549; d) G. R. Sullivan, J. A. Dale, D. L. Dull, H. S. Mosher, *J. Org. Chem.* **1973**, *38*, 2143–2147; e) R. X. Tan, P. R. Jensen, P. G. Williams, W. Fenical, *J. Nat. Prod.* **2004**, *67*, 1374–1382; f) J. M. Seco, E. Quinoa, R. Riguera, *Chem. Rev.* **2004**, *104*, 17–117.
[11] F. Jeannot, G. Gosselin, C. Mathé, *Org. Biomol. Chem.* **2003**, *1*, 2096–2102.

 © 2006 Wiley-VCH Verlag GmbH & Co. KGaA, Weinheim

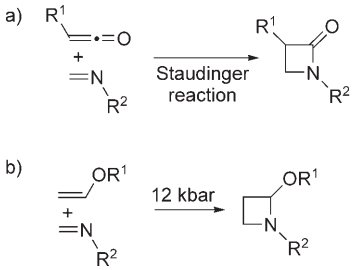
Cycloadditions

DOI: 10.1002/anie.200600961

Thermally Induced and Silver-Salt-Catalyzed [2+2] Cycloadditions of Imines to (Alkoxymethylene)cyclopropanes**

Itaru Nakamura, Tetsuya Nemoto, Yoshinori Yamamoto, and Armin de Meijere*

[2+2] Cycloadditions of imines to carbon–carbon multiple bonds have been widely applied in organic synthesis, as they produce highly useful azetidine derivatives in a single step.[1] [2+2] Cycloadditions of imines to ketenes, originally discovered by Staudinger,[2] provide azetidin-2-ones (β-lactams) (Scheme 1, type a). Recently, allenes[3] and enones[4] were



Scheme 1. [2+2] Cycloadditions of imines to a) ketenes[2] and b) enol ethers.[5]

utilized as substrates for [2+2] cycloadditions with imines. However, cycloadditions of imines to enol ethers (Scheme 1, type b) have rarely been employed; Scheeren and co-workers reported that [2+2] cycloadditions of imines to enol ethers require high pressure (12 kbar).[5] Owing to their ring strain, (alkoxymethylene)cyclopropanes, which are easily accessible and stable at room temperature, ought to be particularly favorable substrates for various cycloadditions;[6] de Meijere et al. reported high-pressure-promoted [4+2] cycloadditions of (alkoxymethylene)cyclopropanes to β,γ-unsaturated α-

[*] Dr. I. Nakamura, T. Nemoto, Prof. Dr. Y. Yamamoto
Department of Chemistry
Graduate School of Science, Tohoku University
Sendai 980-8578 (Japan)
Fax: (+81) 22-795-6784
E-mail: itaru-n@mail.tains.tohoku.ac.jp
Prof. Dr. A. de Meijere
Institut für Organische und Biomolekulare Chemie
Georg-August-Universität Göttingen
Tammannstrasse 2, 37077 Göttingen (Germany)

[**] For one of us (A.d.M.) this is to be counted as Part 129 in the series "Cyclopropyl Building Blocks for Organic Synthesis". Part 128: V. S. Korotkov, O. V. Larionov, A. de Meijere, *Synthesis* **2006**, in press. Part 127: C. Tanguy, A. de Meijere, P. Bertus, J. Szymoniak, O. V. Larionov, A. de Meijere, *Synlett* **2006**, in press.

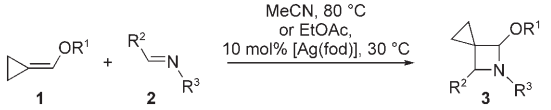
Supporting information for this article is available on the WWW under http://www.angewandte.org or from the author.

WILEY InterScience DISCOVER SOMETHING GREAT
© 2006 Wiley-VCH Verlag GmbH & Co. KGaA, Weinheim

ketoesters.[7] Herein we report our first results concerning [2+2] cycloadditions of imines to (alkoxymethylene)cyclopropanes **1** at ambient pressure.

When (benzyloxymethylene)cyclopropane (**1a**; 1.5 equiv) was heated with *N*-tosylbenzaldimine (**2c**; 1.0 equiv) in acetonitrile at 80 °C for 40 h, the [2+2] cycloadduct 4-benzyloxy-6-phenyl-5-tosyl-5-azaspiro[2.3]hexane (**3ac**) was isolated in 97 % yield, predominantly as the *cis* diastereomer (51:1) (Table 1). The same reaction, but with 1 equivalent of

Table 1: Thermal [2+2] cycloadditions of **2** to (alkoxymethylene)cyclopropanes **1**.



1[a]	R^1	**2**	R^2	R^3	*t* [h]	**3**	Yield [%][b]	*cis*/*trans*[c]
1a	Bn	**2c**	Ph	Ts	40	**3ac**	97[d]	51:1
1a	Bn	**2d**	*p*-$MeOC_6H_4$	Ts	46	**3ad**	82	24:1
1a	Bn	**2e**	*p*-$CF_3C_6H_4$	Ts	6	**3ae**	91	18:1
1a	Bn	**2f**	*t*Bu	Ts	61	**3af**	80	29:1
1a	Bn	**2g**	Ph	Ns	4	**3ag**	92	28:1
1a	Bn	**2h**	Ph	SO_2Ph	32	**3ah**	71	28:1
1b	*n*Bu	**2c**	Ph	Ts	24	**3bc**	80	8:1

[a] In general, **1** (0.3 mmol) was treated with **2** (0.2 mmol). [b] Yields of isolated products. [c] The diastereomeric ratio was determined by ^{1}H NMR spectroscopy. [d] Scale: **1a** (3.0 mmol), **2c** (2.0 mmol); product **3ac** obtained in 68 % yield. Ns = nosyl = *p*-nitrobenzenesulfonyl; Ts = *p*-toluenesulfonic acid.

1a, gave **3ac** in 65 % yield along with recovered **2c** (14 %). The reaction of **1a** with other *N*-tosylarylaldimines **2d** and **2e** produced **3ad** and **3ae** in 82 and 91 % yield, respectively. The *N*-tosylimine of pivaldehyde **2f** also reacted with **1a** to give the corresponding [2+2] cycloadduct **3af** in 80 % yield. With *N*-nosylbenzaldimine (**2g**) and *N*-benzenesulfonylbenzaldimine (**2h**), the corresponding *N*-nosylazetidine **3ag** and *N*-benzenesulfonylazetidine **3ah** were obtained in 92 and 71 % yield, respectively. (*n*-Butoxymethylene)cyclopropane (**1b**) reacted with **2c** smoothly to give **3bc**. The constitutions of the spirocyclopropanated azetidines **3** were confirmed by spectroscopic methods. Furthermore, the structures of both the *cis* and the *trans* isomers of **3ac** were established unambiguously by X-ray crystallographic analyses (Figure 1).[8]

To test the possibility of performing this cycloaddition more efficiently and at lower temperature, several Lewis acidic transition-metal compounds were screened. Among the Lewis acids tested ($AuBr_3$, [Cu(acac)], $Pd(OAc)_2$, $Zn(OTf)_2$, $Sc(OTf)_3$, $Yb(OTf)_3$, AgOTf, [Ag(acac)]), only [Ag(fod)] (fod = 6,6,7,7,8,8,8-heptafluoro-2,2-dimethyl-3,5-octanedionato) exhibited the desired catalytic activity. Thus, the reaction of **1a** (1 equiv) with **2c** (1 equiv) in the presence of [Ag(fod)] (10 mol %) in ethyl acetate at 30 °C proceeded smoothly to give **3ac** in 94 % yield (Table 2, entry 1). At 30 °C in the absence of the silver catalyst, no reaction was observed, and only the starting materials were recovered quantitatively. The choice of solvent turned out to be very important; the reaction proceeded almost equally well in acetone, THF, and CH_2Cl_2, but sluggishly in acetonitrile, toluene, and hexane.

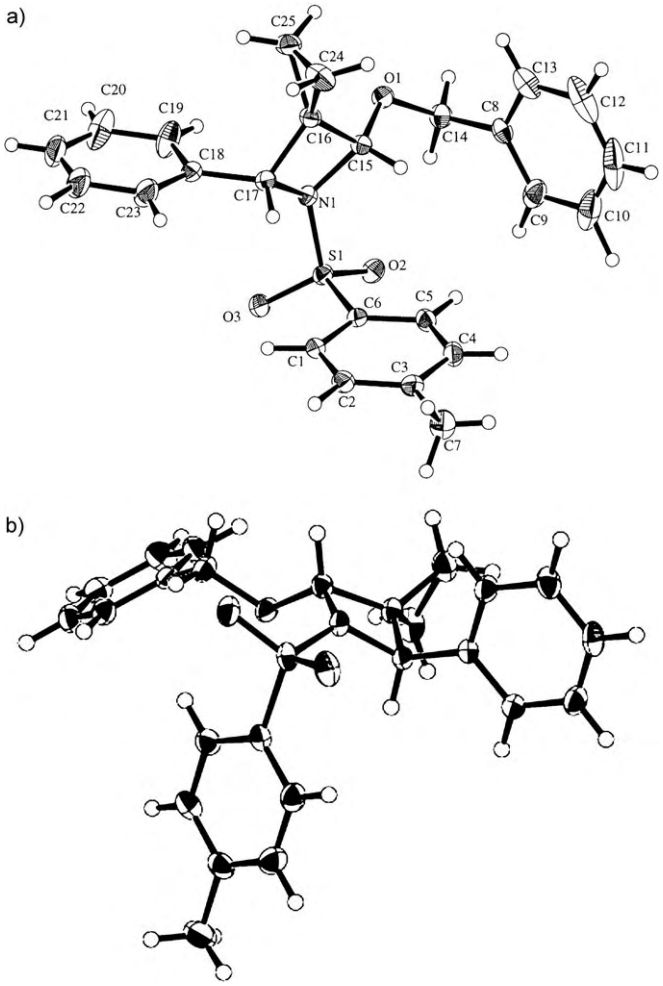


Figure 1. Crystal structures of a) *cis*-**3ac** and b) *trans*-**3ac**. ORTEP representations with thermal ellipsoids set at 50 % probability.[8]

Table 2: Catalyzed versus thermally induced [2+2] cycloadditions of **2** to **1a**.

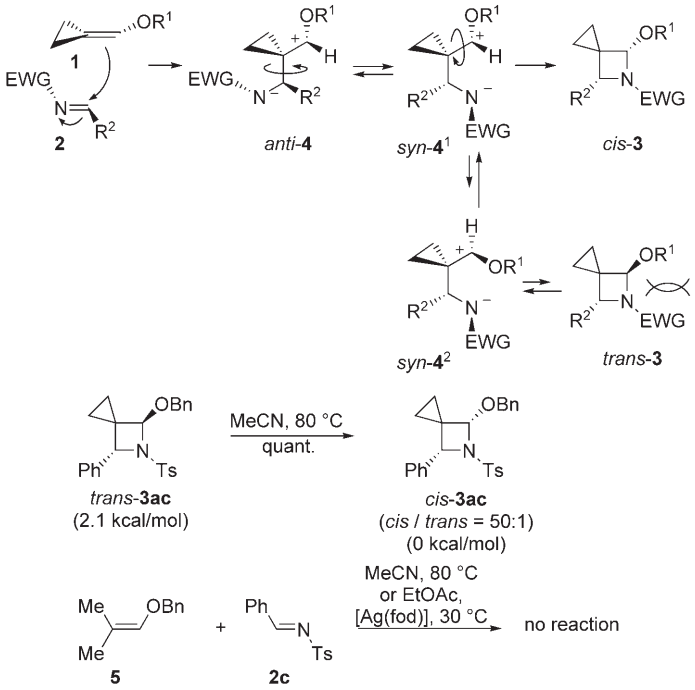
Entry	**2**	R^2	R^3	**3**	Catalytic[a]		Thermal[b]	
					Yield [%][c]	*cis*/*trans*[d]	Yield [%][c]	*cis*/*trans*[d]
1	**2c**	Ph	Ts	**3ac**	94	135:1	97	51:1
2	**2i**	CO_2Et	Ts	**3ai**	45	35:1	57[e]	1.2:1
3	**2j**	Ph	Ms	**3aj**	77	46:1	93	5:1
4	**2k**	4-$CF_3C_6H_4$	Ms	**3ak**	76	48:1	84	4:1

[a] The reaction of **1** (0.3 mmol) and **2** (0.3 mmol) was carried out in the presence of [Ag(fod)] (10 mol %) in ethyl acetate (0.3 mL) at 30 °C. [b] The reaction of **1** (0.3 mmol) and **2** (0.2 mmol) was carried out in acetonitrile (0.1 mL) at 80 °C. [c] Yields of isolated products. [d] The diastereomeric ratio was determined by ^{1}H NMR spectroscopy. [e] The reaction was carried out at 30 °C. Ms = methanesulfonyl.

The catalyzed reaction of the *N*-tosylimine **2i** derived from ethyl glyoxylate produced **3ai** with higher *cis* selectivity than that of the thermal reaction (Table 2, entry 2). The reaction of *N*-mesylbenzaldimines **2j** and **2k** also proceeded with higher *cis* selectivity under the catalytic conditions (Table 2, entries 3 and 4).[9]

 © 2006 Wiley-VCH Verlag GmbH & Co. KGaA, Weinheim

This [2+2] cycloaddition is proposed to proceed in two steps via the well-stabilized 1,4-zwitterion **4**. Initially, nucleophilic attack of the carbon–carbon double bond in **1** on the electrophilic center in the imine **2** would most probably lead to the *anti*-oriented zwitterion *anti*-**4**, which after internal rotation cyclizes to the azetidine *cis*-**3** or *trans*-**3** (Scheme 2).

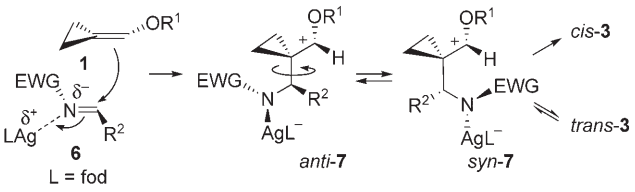


Scheme 2. Mechanism of the thermally induced [2+2] cycloaddition of **1** + **2**. EWG = electron-withdrawing group.

Apparently, this ring closure is reversible, and *cis*-**3** is the thermodynamically more stable isomer, as isolated *trans*-**3ac**, when heated in acetonitrile at 80 °C for 16 h, isomerized virtually completely to *cis*-**3ac**. Under the same conditions, *cis*-**3ac** remained unchanged. The greater stability of *cis*-**3ac** most likely stems from a smaller repulsion between the toluenesulfonyl and the benzyloxy group in the *cis* isomer (see Figure 1). According to DFT calculations at the B3LYP/6-311G level of theory, *cis*-**3ac** is 2.1 kcal mol^{-1} more stable than *trans*-**3ac**. The stabilization of the zwitterionic intermediate **4** by the cyclopropyl group adjacent to the cationic center is essential, as the enol ether **5**, which does not contain a cyclopropane ring, did not react with the *N*-tosylimine **2c**, neither under purely thermal nor under catalytic conditions.[10]

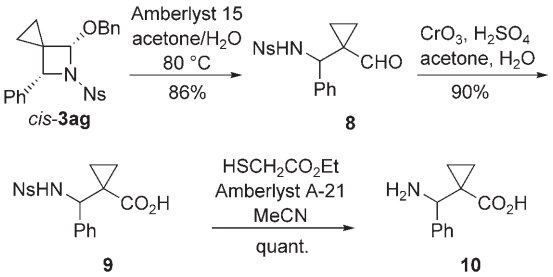
The silver complex certainly acts as a Lewis acid and enhances the electrophilicity of the imine as in **6** (Scheme 3), and C–N bond formation would occur through the silver amide intermediate *syn*-**7**, leading predominantly to the *cis*-**3** isomer.

One of the potential applications of these newly accessible spirocyclopropanated azetidines was demonstrated by the facile three-step conversion of the [2+2] cycloadduct *cis*-**3ag** into the β-phenylalanine analogue **10**. Hydrolysis of *cis*-**3ag** afforded the aldehyde **8** in 90% yield. Jones oxidation of **8**



Scheme 3. Mechanism of the silver-catalyzed [2+2] cycloaddition of **1** + **2**.

and subsequent removal of the nosyl group of **9** gave **10** (Scheme 4).



Scheme 4. Synthesis of α-cyclopropane-modified β-phenylalanine **9**.

Several catalyzed cycloadditions of methylenecyclopropanes to imines have been reported in recent years; [3+2] cycloadditions occur upon palladium-catalyzed reactions of alkylidenecyclopropanes with sulfonylimines[11] and upon Lewis acid catalyzed reactions of arylidenecyclopropanes with tosylimines.[12] Under scandium catalysis, arylidenecyclopropanes react with *N*-phenylimines in a [4+2] cycloaddition.[13] The reactions presented herein are the first examples of [2+2] cycloadditions of imines to methylenecyclopropane derivatives. The readily available 2-alkoxyazetidines offer themselves as versatile building blocks for the synthesis of various other compounds. One such application is preparation of α-cyclopropanated β-amino acids such as **10**, some of which are found in biologically active compounds.[14] It has also been shown that oligopeptides derived from α-cyclopropanated β-amino acids may have interesting secondary structures.[15]

Experimental Section

General procedure: a) Thermal conditions: Substrate **1** (0.3 mmol) was added to a solution of the imine **2** (0.2 mmol) in acetonitrile (0.1 mL) under argon in a Wheaton microreactor. The mixture was stirred at 80 °C for 4–61 h, and the product **3** was purified by column chromatography through silica gel (Fuji Silysia) with hexane/EtOAc/Et_3N (20:1:2) as eluent. b) Catalytic conditions: Substrate **1** (0.3 mmol) was added to a mixture of [Ag(fod)] (12.1 mg, 0.030 mmol) and the imine **2** (0.3 mmol) in ethyl acetate (0.3 mL) under argon in a Wheaton microreactor. The mixture was stirred for 37–42 h and then filtered through a short silica gel (Fuji Silysia) column with EtOAc/Et_3N (10:1) eluent. Purification of the crude product by chromatography through silica gel (Fuji Silysia) with hexane/EtOAc/Et_3N (20:1:2) afforded **3**.

3ac: ^{1}H NMR (400 MHz, $CDCl_3$): δ = 0.05–0.08 (m, 1H), 0.55–0.60 (m, 2H), 0.78–0.82 (m, 1H), 2.39 (s, 3H), 4.84 (dd, J = 84, 12.4 Hz, 2H), 4.85 (s, 1H), 5.50 (s, 1H), 7.20–7.37 (m, 12H), 7.65 ppm

 © 2006 Wiley-VCH Verlag GmbH & Co. KGaA, Weinheim

(d, $J = 8.4$ Hz, 2H); ^{13}C NMR (100 MHz, $CDCl_3$): $\delta = 4.4$, 8.3, 21.6, 29.7, 65.4, 70.6, 92.3, 127.4, 127.6, 127.7, 127.7, 127.9, 128.2, 128.3, 129.4, 135.2, 137.3, 137.7, 143.6 ppm; IR (neat): $\tilde{\nu} = 3062$–2953, 2902, 1596, 1338, 1250, 1115 cm^{-1}; elemental analysis: calcd for $C_{25}H_{25}NO_3S$ (419.54): C 71.57, H 6.01, N 3.34, S 7.64; found: C 71.40, H 6.14, N 3.34, S 7.56; HRMS(EI): m/z calcd for $C_{25}H_{25}NO_3S$: 419.1555; found: 419.1550.

Received: March 11, 2006
Revised: May 1, 2006
Published online: July 6, 2006

Keywords: amino acids · cycloaddition · cyclopropanes · homogeneous catalysis · silver

[1] For a review, see: S. France, A. Weatherwax, A. E. Taggi, T. Lectka, *Acc. Chem. Res.* **2004**, *37*, 592 – 600.
[2] a) H. Staudinger, *Justus Liebigs Ann. Chem.* **1907**, *356*, 51 – 123; for recent reports concerning the Staudinger reaction, see: b) C. Palomo, J. M. Aizpurua, I. Ganboa, M. Oiarbide, *Eur. J. Org. Chem.* **1999**, 3223 – 3235; c) S. France, H. Wack, A. M. Hafez, A. E. Taggi, D. R. Witsil, T. Lectka, *Org. Lett.* **2002**, *4*, 1603 – 1605; d) B. L. Hodous, G. C. Fu, *J. Am. Chem. Soc.* **2002**, *124*, 1578- 1579; e) A. E. Taggi, A. M. Hafez, H. Wack, B. Young, D. Ferraris, T. Lectka, *J. Am. Chem. Soc.* **2002**, *124*, 6626 – 6635.
[3] T. Akiyama, K. Daidouji, K. Fuchibe, *Org. Lett.* **2003**, *5*, 3691 – 3693.
[4] J. A. Townes, M. A. Evans, J. Queffelec, S. J. Taylor, J. P. Morken, *Org. Lett.* **2002**, *4*, 2537 – 2540.
[5] R. W. M. Aben, R. Smit, J. W. Scheeren, *J. Org. Chem.* **1987**, *52*, 365 – 370.
[6] a) A. T. Bottini, L. J. Cabral, *Tetrahedron* **1978**, *34*, 3187 – 3194; b) N. A. Petasis, E. I. Bzowej, *Tetrahedron Lett.* **1993**, *34*, 943 – 946.
[7] A. de Meijere, A. Leonov, T. Heiner, M. Noltemeyer, M. T. Bes, *Eur. J. Org. Chem.* **2003**, *3*, 472 – 478.
[8] CCDC-284945 (*trans*-**3ac**) and CCDC-284946 (*cis*-**3ac**) contain the supplementary crystallographic data for this paper. These data can be obtained free of charge from The Cambridge Crystallographic Data Centre via www.ccdc.cam.ac.uk/data_request/cif.
[9] In a preliminary attempt to induce an asymmetric reaction of **1a** with **2c** with Ag(OTf) and (S)-binap as a chiral catalyst system, the product **3ac** was not obtained all.
[10] a) H. Hart, J. M. Sandri, *J. Am. Chem. Soc.* **1959**, *81*, 320; b) N. C. Deno, H. G. Richey, Jr., J. S. Liu, J. D. Hodge, J. J. Houser, M. J. Wisotsky, *J. Am. Chem. Soc.* **1962**, *84*, 2016; c) D. D. Roberts, R. C. Snyder, Jr., *J. Org. Chem.* **1979**, *44*, 2860 – 2863; d) For a review see: A. de Meijere, *Angew. Chem.* **1979**, *91*, 867 – 884; *Angew. Chem. Int. Ed. Engl.* **1979**, *18*, 809 – 826.
[11] B. H. Oh, I. Nakamura, S. Saito, Y. Yamamoto, *Tetrahedron Lett.* **2001**, *42*, 6203 – 6205.
[12] M. Shi, B. Xu, J.-W. Huang, *Org. Lett.* **2004**, *6*, 1175 – 1178.
[13] a) M. Shi, L.-X. Shao, B. Xu, *Org. Lett.* **2003**, *5*, 579 – 582; b) L. Patient, M. B. Berry, S. J. Coles, M. B. Hursthouse, J. D. Kilburn, *Chem. Commun.* **2003**, 2552 – 2553; c) S. Rajamaki, J. D. Kilburn, *Chem. Commun.* **2005**, 1637 – 1639.
[14] Cf. D. L. Varie, C. Shih, D. A. Hay, S. L. Andis, T. H. Corbett, L. S. Gossett, S. K. Janisse, M. J. Martinelli, E. D. Moher, R. M. Schultz, J. E. Toth, *Bioorg. Med. Chem. Lett.* **1999**, *9*, 369 – 374.
[15] a) D. Seebach, S. Abele, T. Sifferlen, M. Hänggi, S. Gruner, P. Seiler, *Helv. Chim. Acta* **1998**, *81*, 2218 – 2241; b) S. Abele, P. Seiler, D. Seebach, *Helv. Chim. Acta* **1999**, *82*, 1559 – 1571; c) S. Abele, D. Seebach, *Eur. J. Org. Chem.* **2000**, 1 – 15.

 © 2006 Wiley-VCH Verlag GmbH & Co. KGaA, Weinheim

Fluorinated Substituents

DOI: 10.1002/anie.200601020

Preparation, Characterization, and Crystal Structures of the SO_3NHF^- and $SO_3NF_2^-$ Ions**

Ralf Haiges, Ross Wagner, Jerry A. Boatz, Muhammed Yousufuddin, Markus Etzkorn, G. K. Surya Prakash, Karl O. Christe,* Robert D. Chapman,* Mark F. Welker, and Charles B. Kreutzberger*

Dedicated to Dr. Carl Schack on the occasion of his 70th birthday

Recently, a new class of materials having high-energy, *gem*-bis(difluoroamino)-substituted heterocyclic nitroamines, has gained attention for use as high-energy oxidizers: HNFX[1,2] and TNFX[3] have been synthesized under strongly acidic conditions from their corresponding ketone derivatives by using an excess of difluoroamine.[4]

HNF_2 is a shock-sensitive and thermally unstable gaseous compound,[5,6] which can be generated from different precursors, for example, tetrafluorohydrazine,[7] *N*,*N*-difluorourea,[8] *N*,*N*-difluorocarbamates,[9] or trityldifluoroamine.[10] Of these precursors, only trityldifluoroamine is a stable,

[*] Dr. R. Haiges, Dr. R. Wagner, M. Yousufuddin, Dr. M. Etzkorn, Prof. Dr. G. K. S. Prakash, Prof. Dr. K. O. Christe
Loker Research Institute and Department of Chemistry
University of Southern California
Los Angeles, CA 90089-1661 (USA)
Fax: (+1) 213-740-6679
E-mail: haiges@usc.edu
kchriste@usc.edu

Dr. R. D. Chapman
Chemistry Branch (Code 498200D)
Naval Air Warfare Center Weapons Division
1900 N. Knox Rd. Stop 6303
China Lake, CA 93555-6106 (USA)
Fax: (+1) 760-939-1617
E-mail: robert.chapman@navy.mil

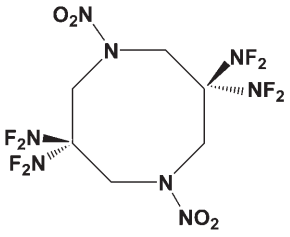
Dr. J. A. Boatz
Space and Missile Propulsion Division
Air Force Research Laboratory (AFRL/PRSP)
10 East Saturn Boulevard, Bldg 8451
Edwards Air Force Base, CA 93524 (USA)

Dr. M. F. Welker, Dr. C. B. Kreutzberger
TPL, Inc.
3921 Academy Parkway North NE
Albuquerque, NM 87109-4416 (USA)

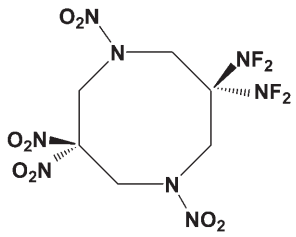
[**] The work at the University of Southern California (USC) was funded by the Air Force Office of Scientific Research, the Office of Naval Research, Lawrence Livermore National Laboratory, and the National Science Foundation, and that at the Naval Air Warfare Center Weapons Division (NAWCWD) and TPL, Inc. was supported by the Office of Naval Research. Portions of this work were previously reported in limited-distribution presentations.[1]

Supporting information for this article is available on the WWW under http://www.angewandte.org or from the author.

 © 2006 Wiley-VCH Verlag GmbH & Co. KGaA, Weinheim



HNFX



TNFX

storable solid. However, it is not useful as a general reagent for the preparation of larger quantities of *gem*-bis(difluoroamines) because its synthesis requires the use of expensive N_2F_4, which is not commercially available and must be prepared from difluoroamine, and of equivalent amounts of mercury in an organic solvent. The use of mercury presents environmental problems, and working with N_2F_4 in an organic solvent can be hazardous. Therefore, it is highly desirable to develop a stable, solid, readily accessible difluoroamine source. Obvious candidates for HNF_2 sources are difluorosulfamate salts. Although the parent free acid $HOSO_2NF_2$ had been known since 1961 and has been widely used as a difluoroaminating reagent,[11,12] no reports could be found on the existence of its salts. Herein, we report the results from two independent studies.

$Na^+SO_3NF_2^-$ was isolated by fluorinating aqueous sulfamic acid at 0 °C, neutralizing the product with concentrated aqueous sodium hydroxide, filtering off the less-soluble sodium fluoride by-product, and drying the neutral solution under vacuum. This process was improved by direct fluorination of $SO_3NH_2^-$ salts with diluted elemental fluorine in aqueous solutions at 0 °C [Eq. (1)].

$$NaSO_3NH_2 + 2\,F_2 \rightarrow NaSO_3NF_2 + 2\,HF \quad (1)$$

The reaction conditions were similar to those previously used for the fluorination of urea,[8a] carbamates,[9a] and sulfamide.[13] The acidic reaction mixture was not stable above approximately 5 °C, and the difluorosulfamate [Eq. (2)] rapidly hydrolyzed upon warming to ambient temperature.

$$SO_3NF_2^- + H_2O \rightarrow SO_3OH^- + HNF_2 \quad (2)$$

The ease of this acid-catalyzed hydrolysis can account for the lack of previous reports of isolated salts of the difluorosulfamate anion. The isolation of difluorosulfamate salts required careful control of the reaction conditions and rapid removal of the water and HF by-product at 0 °C in a vacuum. This method resulted in the isolation of pure, colorless $NaSO_3NF_2$ in 94 % yield.

The dry sodium salt is stable at room temperature but decomposes when exposed to atmospheric moisture. It was stored in the dry argon atmosphere of a glove box for a period of 4 months without showing any sign of decomposition. The identity of the compound was established by the observed material balance, vibrational and multinuclear NMR spectroscopy, electronic structure calculations, and by converting it into $[PNP][SO_3NF_2]\cdot CH_2Cl_2$ (PNP = bis(triphenylphosphoranylidene)ammonium) and determining its crystal structure.

The Raman and IR spectra of solid $NaSO_3NF_2$ are shown in the Supporting Information, and the observed frequencies and intensities are listed in Table 1. They were assigned by comparison with those calculated at the MP2[14] level of theory with the 6-311 + G(d) basis set. Whereas the ^{19}F NMR spectrum of naturally abundant $[^{14}N]NaSO_3NF_2$ in CD_3CN gives only a broad resonance at $\delta = 34$ ppm, the spectrum of an ^{15}N-labeled sample in the same solvent shows a sharp doublet at $\delta = 33.8$ ppm with $^1J(^{19}F\text{-}^{15}N) = 138$ Hz. The ^{15}N NMR spectrum shows a sharp triplet at $\delta = -20.4$ ppm with the same $^1J(^{15}N\text{-}^{19}F)$ coupling constant.

Table 1: Comparison of observed and unscaled calculated MP2/6-311 + G(d) vibrational frequencies (cm^{-1}) and intensities for $SO_3NF_2^-$ in point group C_s.

Mode		Approx. mode description	Observed[a],[e]		Calculated[b]
			IR	Raman	
a′	ν_1	ν_{as} SO_3	1309 vs	1304 [0.8]	1286 (364) [7.2 dp]
	ν_2	ν_s SO_3	1080 s	1089 [10.0]	1051 (59) [38 p]
	ν_3	ν_s NF_2	968 w	997 [4.0] 971 [0.9]	979 (72) [4.4 p]
	ν_4	ν SN	715 m	722 [5.5]	671 (64) [17 p]
	ν_5	δ_{as} SO_3	627 s 617 s	630 [1.1]	601 (140) [0.6 dp]
	ν_6	δ_{sciss} NF_2		526 [2.6]	521 (1.6) [7.3 p]
	ν_7	δ_{sym} SO_3	525 vw		501 (25) [4.6 p]
	ν_8	δ_{rock} SO_3	[c]	337 [4.3]	298 (1.6) [8.6 p]
	ν_9	δ_{wag} NF_2	[c]	264 [1.3]	224 (0.5) [2.4 p]
a″	ν_{10}	ν_{as} SO_3	1284 vs	1267 [0.7]	1282 (362) [7.7 dp]
	ν_{11}	ν_{as} NF_2	869 m	868 [1.6]	829 (75) [2.1 dp]
	ν_{12}	δ_{as} SO_3	532 w	537 [2.0]	532 (35) [3.5 dp]
	ν_{13}	δ_{rock} SO_3	[c]	390 [2.6]	325 (0.8) [0.8 dp]
	ν_{14}	δ_{twist} NF_2	[c]	186 [1.3]	154 (0.02) [6.1 dp]
	ν_{15}	τ S-N	[c]	[d]	37 (0.00) [2.0 dp]

[a] As Na^+ salt. Relative Raman intensities given in brackets. [b] IR intensities given in km mol^{-1} (in parentheses) and Raman intensities given in Å^4 amu^{-1} (in brackets). [c] Not observed, IR spectrum recorded only between 4000 and 400 cm^{-1}. [d] Not observed, Raman spectrum recorded only between 3600 and 80 cm^{-1}. [e] In addition to the listed bands, IR bands at 1627 m, 1209 w, 1184 m, 565 w, and Raman bands at 1618 [0.5], 1321 [0.7], 572 [1.2] cm^{-1} were observed but were not assigned.

Colorless and air-stable $[PNP][SO_3NF_2]$ was obtained by neutralizing the fluorination reaction mixture, adding PNP^+Cl^-, and extracting with methylene chloride [Eq. (3)]. Single crystals of $[PNP][SO_3NF_2]\cdot CH_2Cl_2$ suitable for X-ray crystal structure determination were obtained by recrystallization from CH_2Cl_2.

$$NaSO_3NF_2 + PNP^+Cl^- \rightarrow [PNP][SO_3NF_2] + NaCl \quad (3)$$

$[PNP][SO_3NF_2]\cdot CH_2Cl_2$ crystallizes in the triclinic space group $P\bar{1}$. The X-ray structure analysis reveals the presence of two isolated $[PNP]^+$ and $[SO_3NF_2]^-$ units together with two disordered CH_2Cl_2 molecules in the unit cell (packing diagrams are given in the Supporting Information). The

 © 2006 Wiley-VCH Verlag GmbH & Co. KGaA, Weinheim

closest F···H and O···H contacts between neighboring cations and anions are 2.682 Å and 2.349 Å, respectively. The dimensions of the SO_3N skeleton of the $SO_3NF_2^-$ ion (Figure 1) are more similar to those of sulfamic acid[15] than

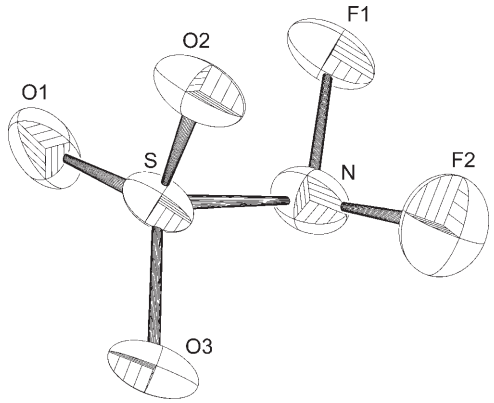


Figure 1. ORTEP drawing of the anion of $[PNP][SO_3NF_2]\cdot CH_2Cl_2$. Thermal ellipsoids are shown at the 50% probability level. Bond lengths [Å] and angles [°]: S–O1 1.428(4), S–O2 1.424(3), S–O3 1.424(3), S–N 1.772(4), F1–N 1.412(5), F2–N 1.463(6); O1-S-O2 114.7(2), O1-S-O3 116.1(2), O2-S-O3 116.8(2), O1-S-N 100.1(2), O2-S-N 106.1(2), O3-S-N 99.3(2), F1-N-F2 99.0(3), F1-N-S 104.5(3), F2-N-S 99.6(3).

to the ones reported for salts with the $SO_3NH_2^-$ ion.[16] Estimations of the double-bond character of the S–N bond are frequently made by comparison of the observed lengths with that predicted from Pauling's covalent radii (1.74 Å)[17] or with the bond length in sulfamic acid (1.772(1) Å).[15b] In the solid state, the latter has the zwitterionic structure $^+NH_3$–SO_3^-, which possesses a formal S–N single bond. The observed S–N bond length in $SO_3NF_2^-$ (1.772(4) Å) is similar to that in sulfamic acid and larger than the typical values found in the $SO_3NH_2^-$ ion (1.64 Å). The S–O bond lengths (1.428(8) Å and 1.424(3) Å)are shorter than the values reported for sulfamates (1.44–1.45 Å)[16] and sulfamic acid (1.438(1) Å, 1.436(1) Å, and 1.435(1) Å).[15b] The average O-S-O and O-S-N angles (115.9° and 101.8°, respectively) are in good agreement with those reported for sulfamic acid.

The marked differences in the S–N and S–O bond lengths between $SO_3NF_2^-$ and $SO_3NH_2^-$ can be readily reconciled by the large difference between the electronegativity values of hydrogen and fluorine. The strongly electron withdrawing fluorine atoms pull some of the negative charge away from the oxygen atoms, thereby increasing the S=O double-bond character and shortening the S–O bonds. By contrast, the electron-donating hydrogen atoms increase the electron density on the nitrogen atom, which passes it on to the S=O bonds. This results in partial N=S double bond character and increased negative charge on the oxygen atoms with concomitant lengthening of the S–O bonds.

When only one equivalent of fluorine was used in the fluorination reaction of $SO_3NH_2^-$, the SO_3NHF^- ion was formed [Eq. (4)].

$$NaSO_3NH_2 + F_2 \rightarrow NaSO_3NHF + HF \quad (4)$$

Colorless and somewhat moisture sensitive $NaSO_3NHF$ was obtained when the acidic reaction mixture was evaporated in a vacuum at 0 °C. The compound was identified and characterized by its vibrational spectra and by its crystal structure as the salt $[PPh_4][SO_3NHF]$. The Raman and IR spectra of $NaSO_3NHF$ are shown in Supporting Information, and the observed frequencies and intensities are listed in Table 2 and were assigned by comparison with those calculated at the MP2[11] level of theory with the 6-311 + G(d) basis set.

Table 2: Comparison of observed and unscaled calculated MP2/6-311 + G(d) vibrational frequencies (cm^{-1}) and intensities for SO_3NHF^- in point group C_1.

Mode	Approx. mode description	Observed[a],[d]		Calculated[b]
		IR	Raman	(IR) [Raman]
ν_1	ν NH	3100 s, br	3000 [1.3]	3481 (2.4) [69]
ν_2	δ_{sciss} HNF	1522 w		1410 (30) [2.8]
ν_3	ν_{as} SO_3	1242 vs	1246 [1.3]	1270 (368) [7.3]
ν_4	ν_{as} SO_3	1213 vs	1225 [1.2]	1240 (401) [7.1]
ν_5	ν_s SO_3/δ_{wag} NH	1064 s	1065 [10.0]	1041 (82) [27]
ν_6	ν_s SO_3/δ_{wag} NH	1021 m	1014 [5.9]	1033 (45) [18]
ν_7	ν NF	863 m	869 [4.3]	923 (38) [14]
ν_8	ν SN	602 s	602 [5.0]	699 (161) [16]
ν_9	δ_{as} SO_3	590 s		584 (66) [4.5]
ν_{10}	δ_{as} SO_3	497 w	466 [2.6]	520 (26) [3.4]
ν_{11}	δ_{sym} SO_3	477 w	445 [3.0]	509 (26) [5.9]
ν_{12}	δ_{rock} SO_3	438 w	424 [3.7]	371 (0.1) [4.7]
ν_{13}	δ_{rock} SO_3	[c]	411 [3.0]	343 (8.1) [2.6]
ν_{14}	δ_{wag} NF	[c]		215 (1.2) [1.1]
ν_{15}	τ S-N	[c]	122 [2.0]	118 (1.9) [0.4]

[a] As Na^+ salt. Relative Raman intensities given in brackets. [b] IR intensities given in km mol^{-1} (in parentheses) and Raman intensities given in $Å^4\,amu^{-1}$ (in brackets). [c] Not observed, IR spectrum recorded only between 4000 and 400 cm^{-1}. [d] In addition to the listed bands, IR bands at 1313 m, 1168 s, 1082 s, 918 m, 897 m, 773 m, 731 s, 617 m and Raman bands at 1168 [1.0], 1153 [1.0], 913 [1.2], 666 [1.0] cm^{-1} were observed but were not assigned.

The $[PPh_4][SO_3NHF]$ salt was obtained by metathesis in the same manner as shown in Equation (3). It crystallizes in the triclinic space group $P\bar{1}$. The X-ray structure analysis reveals the presence of two nonequivalent $[PPh_4]^+$ and $[SO_3NHF]^-$ units (packing diagrams are shown in the Supporting Information). One SO_3NHF^- ion could be refined well, but the SO_3 group of the second ion is disordered. This results in a relatively high R factor of 8.16% for the refined structure. The closest F···H and O···H contacts between neighboring cations and anions are 2.566 Å and 2.373 Å, respectively. The ordered SO_3NHF^- ion is depicted in Figure 2. The observed S–N bond length in SO_3NHF^- (1.694(5) Å) lies between those observed for $SO_3NF_2^-$ (1.772(4) Å) and $SO_3NH_2^-$ (1.64 Å). This situation is in accord with the expectation that the electronic effect of an -NHF group is intermediate between those of an $-NF_2$ and an $-NH_2$ group.

The presence of one hydrogen atom and one fluorine atom attached to the same nitrogen atom was further established by proton and fluorine NMR spectroscopy. The

 © 2006 Wiley-VCH Verlag GmbH & Co. KGaA, Weinheim

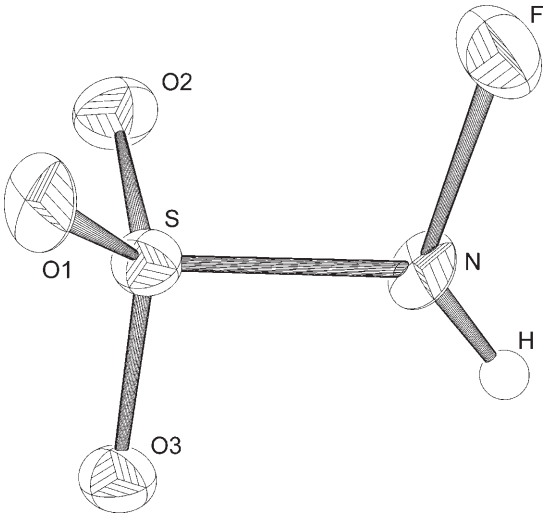


Figure 2. ORTEP drawing of the anion of $[PPh_4][SO_3NHF]$. Thermal ellipsoids are shown at the 50% probability level. Selected bond lengths [Å] and angles [°]: S–O1 1.433(4), S–O2 1.457(4), S–O3 1.447(3), S–N 1.694(5), F1–N 1.474(5), O1–S-O2 114.4(2); O1-S-O3 115.3(2), O2-S-O3 114.1(2), O1-S-N 108.5(2), O2-S-N 104.3(2), O3-S-N 98.0(2), F-N-S 106.4(3).

proton and fluorine spectra showed doublets at $\delta = 8.69$ and -103.0 ppm, respectively, with the same $^2J(^1H\text{-}^{19}F)$ coupling constant (49 Hz).

The utility of $NaSO_3NF_2$ as an alternative source of difluoroamine in organic difluoroamination reactions was demonstrated by the transformation of carbonyl into *gem*-bis(difluoroamino) groups. Qualitative reactions of acetone, cyclohexanone, 3-pentanone, and 1-acetylpiperidin-4-one with the reagent in approximately 100% H_2SO_4 and 30% oleum showed formation of the expected *gem*-bis(difluoroamino)alkane by ^1H, ^{13}C, and ^{19}F NMR spectroscopy. In the case of 1-acetylpiperidin-4-one, only the oxygen atom of the ring-carbonyl group was replaced, whereas the carbonyl oxygen atom of the acetyl group did not react. A quantitative comparison was conducted by using 1,3-dibromoacetone as a model ketone. 1,3-Dibromo-2,2-bis(difluoroamino)propane was formed in 38% yield by using $NaSO_3NF_2$ in anhydrous H_2SO_4 containing approximately 1% SO_3. This compares with a yield of 37% for conventional difluoroamination (HNF_2 in oleum) of 1,3-dibromoacetone.

Experimental Section

Materials and Apparatus (USC): All reactions were carried out in teflon-FEP ampules closed by stainless steel valves or pyrex glass vessels closed by grease-free Kontes glass-teflon valves. Volatile materials were handled in stainless steel/teflon-FEP[18] or pyrex glass vacuum lines. Nonvolatile solids were handled in the dry argon atmosphere of a glove box. Infrared spectra were recorded in the range 4000–400 cm^{-1} on a Midac, M Series, FT-IR spectrometer using KBr pellets. The pellets were prepared inside the glove box using an Econo mini-press (Barnes Engineering Co.) and transferred in a closed container to the spectrometer before placing them quickly into the sample compartment, which was purged with dry nitrogen to minimize exposure to atmospheric moisture and potential hydrolysis of the sample. Raman spectra were recorded on a Bruker Equinox 55 FT-RA spectrometer using a Nd-YAG laser at 1064 nm with power levels of 100–200 mW and pyrex melting-point capillary tubes as sample containers. NMR spectra were recorded unlocked on Bruker AMX 500 and Varian Mercury/VX 400 NMR spectrometers at room temperature. The ^{19}F and ^{15}N NMR spectra were referenced to external samples of $CFCl_3$ and nitromethane, respectively.

The starting materials H_2NSO_3H, H_2SO_4, $[P(C_6H_5)_4]Cl$, [PNP]Cl, NaOH (all Aldrich), $[^{15}N_2]$urea (MSD Isotopes), and fluorine (Air Products and Chemicals Inc.) were used without further purification. Solvents were dried by standard methods and freshly distilled prior to use. $NaSO_3NH_2$ was obtained by neutralization of HSO_3NH_2 with NaOH. $[^{15}N]HSO_3NH_2$ was prepared from $[^{15}N_2]$urea and H_2SO_4 according to a modified literature method.[19]

$NaSO_3NHF$ (USC): A solution of $NaSO_3NH_2$ (0.380 g, 3.19 mmol) in water (4 mL) was placed into a teflon-FEP ampule equipped with a teflon-coated magnetic stirring bar and a teflon gas-inlet tube. After cooling to 0 °C, fluorine (3.19 mmol; 10% v/v in nitrogen) was introduced at a rate of 110 mL min^{-1}. The reaction mixture was pumped to dryness at 0 °C, leaving behind a colorless solid (0.391 g; weight calcd for 3.19 mmol $NaSO_3NHF = 0.437$ g).

$[PPh_4][SO_3NHF]$ (USC): A solution of $NaSO_3NH_2$ (0.695 g, 5.00 mmol) in water (10 mL) was placed into a teflon-FEP ampule equipped with a magnetic stirring bar and a teflon gas-inlet tube. After cooling to 0 °C, fluorine (5.00 mmol; 10% v/v in nitrogen) was introduced at a rate of 110 mL min^{-1}. The reaction mixture was neutralized by adding cold solid $NaHCO_3$ and filtered through a cold porcelain frit. A cold solution of PPh_4Cl (5.00 mmol) in water (50 mL) was added to the clear filtrate. The resulting milky solution was extracted three times with 50 mL of cold CH_2Cl_2. The combined organic phases were dried over $MgSO_4$ and pumped to dryness at ambient temperature, leaving behind a colorless solid (2.039 g; weight calcd for 5.00 mmol $PPh_4SO_3NHF = 2.267$ g). Crystals were grown from a solution in CH_2Cl_2 by slow evaporation of the solvent with a stream of dry nitrogen.

$NaSO_3NF_2$ (USC): A solution of $NaSO_3NH_2$ (0.236 g, 1.98 mmol) in water (7 mL) was placed into a teflon-FEP ampule equipped with a magnetic stirrer and a teflon gas-inlet tube. After cooling to 0 °C, fluorine (10% v/v in nitrogen) was introduced at a rate of 110 mL min^{-1}. After 45 min, the fluorination was discontinued, and the reaction mixture pumped to dryness at 0 °C, leaving behind a colorless solid (0.288 g; weight calcd for 1.98 mmol $NaSO_3NF_2 =$ 0.307 g).

$NaSO_3NF_2$ (TPL): Sulfamic acid (16.42 g, 0.169 mol) was dissolved in H_2O (30 mL), and NaOH (8.1 g, 0.20 mol) was added. Fluorine (10% v/v in nitrogen) was bubbled through the solution at 0 °C. The progress of the fluorination of sulfamate was monitored by ^{19}F NMR spectroscopy of reaction aliquots to observe the conversion of monofluorosulfamate ($\delta = -102.1$ ppm vs. external $CFCl_3$ in $[D_6]$acetone) into difluorosulfamate ($\delta = 36.6$ ppm). After 1.5 h, the fluorination was complete, and the cloudy mixture was neutralized with concentrated aqueous NaOH. The NaF precipitate was removed by filtration. On the basis of its ^{19}F NMR spectrum, the filtrate appeared to be a 96:4 mixture of $NaSO_3NF_2$ and NaF. The viscous filtrate was quickly dried at room temperature in a vacuum desiccator over excess P_2O_5. After 24 h, ^{19}F NMR spectroscopy of the dried solid showed the same $SO_3NF_2^-/F^-$ ratio as the initial filtrate.

$[A][SO_3NF_2]$ (A = PNP, PPh_4, $AsPh_4$) (USC): A solution of $NaSO_3NH_2$ (0.357 g, 3.00 mmol) in water (10 mL) was placed into a teflon-FEP ampule equipped with a magnetic stirring bar and a teflon gas-inlet tube. After cooling to 0 °C, fluorine (10% v/v in nitrogen) was introduced at a rate of 110 mL min^{-1}. After 60 min, the fluorination was discontinued, and the reaction mixture was neutralized by adding cold solid $NaHCO_3$. The reaction mixture was filtered through a cold porcelain frit, and a cold aqueous solution of 3.00 mmol A^+Cl^- was added to the clear filtrate. The resulting milky solution was extracted three times with 10 mL of cold CH_2Cl_2. The combined organic phases were dried over $MgSO_4$ and pumped to

 © 2006 Wiley-VCH Verlag GmbH & Co. KGaA, Weinheim

dryness at ambient temperature, leaving behind colorless solids ($[PPh_4][SO_3NF_2]$: 1.283 g, calcd weight for 3.00 mmol = 1.414 g; $[AsPh_4][SO_3NF_2]$: 1.466 g, calcd weight for 3.00 mmol = 1.543 g; $[PNP][SO_3NF_2]$: 2.071 g, calcd weight for 3.00 mmol = 2.011 g). Crystals were grown from a solution in CH_2Cl_2 by slow evaporation of the solvent with a stream of dry nitrogen.

2,2-Bis(difluoroamino)propane and 1-acetyl-4,4-bis(difluoroamino)piperidine (USC): $NaSO_3NF_2$ (2.5 equiv.) was added in increments at 4 °C to a vigorously stirred mixture of $CDCl_3$ (1.5 mL), 30 % oleum (1.5 mL), and the ketone starting material (1.0 mmol). Immediate gas evolution was observed. After 15 min, the upper organic phase was analyzed by ^{19}F, ^1H, and ^{13}C NMR spectroscopy, showing the formation of the desired *gem*-bis(difluoroamines).

1,3-Dibromo-2,2-bis(difluoroamino)propane (TPL): 1,3-Dibromoacetone (24.72 g, 0.114 mol) was added to a mixture of sodium difluorosulfamate (61 g, ≤ 0.39 mol) in sulfuric acid (310 mL) containing approximately 1 % SO_3 (made from 30 % oleum plus concd H_2SO_4) plus 100 mL dichloromethane. The reaction mixture was stirred for 4 days at 0 °C, quenched in water, neutralized, and extracted with dichloromethane. Removal of the solvent produced 13.2 g of solute, the major constituent of which was 1,3-dibromo-2,2-bis(difluoroamino)propane (38 % crude yield). Three short-path distillations (room temperature at 1–3 Torr) produced material that was > 95 % pure (elemental analysis and ^1H NMR) with residual 1,3-dibromoacetone as the main impurity. ^1H NMR spectroscopy (200 MHz, $CDCl_3$, TMS): $\delta = 3.98$ ppm (quint., 1.25 Hz). $^{13}C\{^1H\}$ NMR spectroscopy ($CDCl_3$): $\delta = 23.75$ (quint., 5.5 Hz), 99 ppm (m). ^{19}F NMR spectroscopy ($CDCl_3$): $\delta = 29.9$ ppm (s). ^1H NMR spectroscopy (C_6D_6): $\delta = 3.24$ ppm (quint., 1.27 Hz). ^{13}C NMR spectroscopy (C_6D_6): $\delta = 23.69$ (quint., 5.7 Hz), 95.37 ppm (quint., 6.4 Hz). ^{19}F NMR spectroscopy (C_6D_6): $\delta = 30.26$ ppm (s). Elemental analysis calcd for $(0.953)C_3H_4F_4N_2Br_2 + (0.047)C_3H_4Br_2O$: C 12.08, H 1.35, N 8.78, F 23.83; found: C 12.12, H 1.30, N 8.93, F 23.53 %.

Theoretical Methods: The molecular structures and harmonic vibrational frequencies were calculated by using second-order many-body perturbation theory[14] (denoted as MP2, but also known as MBPT(2)) and a 6-311 + G(d) basis set. Hessians (energy second derivatives) were calculated for the final equilibrium structures to determine if they were minima (positive definite hessian) or *n*th-order transition states ("*n*" negative eigenvalues). All calculations were performed by using the electronic structure code GAMESS.[20]

X-ray structure determination: The collection, reduction, and processing of X-ray data was described previously.[21] Crystal data for $C_{37}H_{32}Cl_2F_2N_2O_3P_2S$: $M_r = 755.55$, triclinic, space group $P\bar{1}$, $a = 11.8650(12)$, $b = 11.9167(12)$, $c = 14.5180(15)$ Å, $\alpha = 66.755(2)$, $\beta = 68.964(2)$, $\gamma = 71.034(2)°$, $V = 1719.7(3)$ Å^3, $F(000) = 780$, $\rho_{calcd.}$ ($Z = 2$) = 1.459 g cm^{-3}, $\mu = 0.395$ mm^{-1}, approximate crystal dimensions $0.29 \times 0.21 \times 0.05$ mm^3, θ range = 1.58 to 27.49°, index ranges $-15 \le h \le 12$, $-15 \le k \le 12$, $-18 \le l \le 18$, $Mo_{K\alpha}$ ($\lambda = 0.71073$ Å), $T = 133(2)$ K, 10657 measured reflections, of which 7433 ($R_{int} = 0.0487$) were unique, data to parameters ratio = 16.9:1, final *R* indices [$I > 2\sigma(I)$]: $R1 = 0.0731$, $wR2 = 0.1949$, R indices (all data): $R1 = 0.1087$, $wR2 = 0.2102$, GOF on $F^2 = 1.012$.

Crystal data for $C_{37}H_{32}Cl_2F_2N_2O_3P_2S$: $M_r = 755.55$, triclinic, space group $P\bar{1}$, $a = 11.8650(12)$, $b = 11.9167(12)$, $c = 14.5180(15)$ Å, $\alpha = 66.755(2)$, $\beta = 68.964(2)$, $\gamma = 71.034(2)°$, $V = 1719.7(3)$ Å^3, $F(000) = 780$, $\rho_{calcd.}$ ($Z = 2$) = 1.459 g cm^{-3}, $\mu = 0.395$ mm^{-1}, approximate crystal dimensions $0.29 \times 0.21 \times 0.05$ mm^3, θ range = 1.58 to 27.49°, index ranges $-15 \le h \le 12$, $-15 \le k \le 12$, $-18 \le l \le 18$, $Mo_{K\alpha}$ ($\lambda = 0.71073$ Å), $T = 133(2)$ K, 10657 measured reflections, of which 7433 ($R_{int} = 0.0487$) were unique, data to parameters ratio = 16.9:1, final *R* indices [$I > 2\sigma(I)$]: $R1 = 0.0731$, $wR2 = 0.1949$, R indices (all data): $R1 = 0.1087$, $wR2 = 0.2102$, GOF on $F^2 = 1.012$.

CCDC-274108 and -274109 contain the supplementary crystallographic data for this paper. These data can be obtained free of charge from The Cambridge Crystallographic Data Centre via www.ccdc.cam.ac.uk/data_request/cif.

Received: March 15, 2006
Published online: July 6, 2006

Keywords: difluoroamines · fluorine · structure elucidation · sulfamates

[1] a) R. D. Chapman, C. B. Kreutzberger, M. F. Welker, *JANNAF Novel Ingredients for Liquid and Solid Propellants Specialist Session*, Pasadena, CA, 4 April, **1995**; b) R. D. Chapman, R. Y. Yee, R. D. Gilardi, A. A. Pinkerton, *15th Annual Working Group Institute on Synthesis of High Energy Density Materials*, Picatinny Arsenal, NJ, 12–13 June 1996; available from the National Technical Information Service (http://www.ntis.gov/help/ordermethods.asp).

[2] a) R. D. Chapman, M. F. Welker, C. B. Kreutzberger, *J. Org. Chem.* **1998**, *63*, 1566; b) R. D. Chapman, R. D. Gilardi, M. F. Welker, C. B. Kreutzberger, *J. Org. Chem.* **1999**, *64*, 960.

[3] T. Axenrod, X.-P. Guan, J. Sun, L. Qi, R. D. Chapman, R. D. Gilardi, *Tetrahedron Lett.* **2001**, *42*, 2621.

[4] a) K. Baum, *J. Am. Chem. Soc.* **1968**, *90*, 7083; b) W. H. Graham, J. P. Freeman, *J. Org. Chem.* **1969**, *34*, 2589; c) A. V. Fokin, Y. M. Kosyrev, V. A. Makarov, N. P. Novoselov, *Dokl. Akad. Nauk SSSR* **1969**, *186*, 112.

[5] E. W. Lawless, I. C. Smith, *Inorganic High Energy Oxidizers (Syntheses, Structure and Properties)*, Marcel Dekker, New York, NY, **1968**, p. 69.

[6] J. K. Ruff, *Chem. Rev.* **1967**, *67*, 665, and references therein.

[7] J. P. Freeman, A. Kennedy, C. B. Colburn, *J. Am. Chem. Soc.* **1960**, *82*, 5304.

[8] a) V. Grakauskas, K. Baum, *J. Am. Chem. Soc.* **1970**, *92*, 2096; b) R. E. Banks, R. N. Haszeldine, J. P. Lalu, *J. Chem. Soc. C* **1966**, 1514.

[9] a) V. Grakauskas, K. Baum, *J. Am. Chem. Soc.* **1969**, *91*, 1679; b) J. M. J. Lambert, G. M. Alain (Societé Nationale des Poudres et Explosives), DE 2320119, **1973**; c) D. L. Klopotek, G. B. Hobrock, *Inorg. Chem.* **1967**, *6*, 1751.

[10] a) R. C. Petry, J. P. Freeman, *J. Am. Chem. Soc.* **1961**, *83*, 3912; b) W. H. Graham, C. O. Parker, *J. Org. Chem.* **1963**, *28*, 850; c) G. K. S. Prakash, M. Etzkorn, G. A. Olah, K. O. Christe, S. Schneider, A. Vij, *Chem. Commun.* **2002**, 1712.

[11] J. N. Keith, R. J. Douthart, W. K. Sumida, I. J. Solomon in *Advanced Propellant Chemistry* (Ed.: R. T. Holzmann), American Chemical Society, Washington, **1966**, pp. 141–147.

[12] R. D. Shoults, *Development of a Practical Process for the Preparation of gem Difluoramino Compounds. The Difluorosulfamic Acid Reagent*, Rohm and Haas Co. Report S-129, **1967**, NTIS Accession Number AD0380719, available from the National Technical Information Service (http://www.ntis.gov/help/ordermethods.asp).

[13] R. A. Wiesboeck, J. K. Ruff, *Inorg. Chem.* **1965**, *4*, 123.

[14] a) C. Møller, M. S. Plesset, *Phys. Rev.* **1934**, *46*, 618; b) J. A. Pople, J. S. Binkley, R. Seeger, *Int. J. Quantum Chem. Symp.* **1976**, *10*, 1; c) M. J. Frisch, M. Head-Gordon, J. A. Pople, *Chem. Phys. Lett.* **1990**, *166*, 275; d) J. Bartlett, D. M. Silver, *Int. J. Quantum Chem. Symp.* **1975**, *9*, 1927.

[15] a) F. A. Kanda, A. J. King, *J. Am. Chem. Soc.* **1951**, *73*, 2315; b) A. F. Cameron, F. D. Duncanson, *Acta Crystallogr. Sect. B* **1976**, *32*, 1563.

[16] a) V. K. Wadahawan, V. M. Padmanabhan, *Acta Crystallogr. Sect. B* **1972**, *28*, 1903; b) R. Manickkavachagam, R. K. Rajaram, *Z. Kristallogr.* **1984**, *168*, 179; c) A, Meinhart, E. Haussühl, L. Bohatý, E. Tillmanns, *Z. Kristallogr.* **2001**, *216*, 513; d) J. Schreuer, *Z. Kristallogr. New Cryst. Struct.* **1999**, *214*, 305; e) J.

 © 2006 Wiley-VCH Verlag GmbH & Co. KGaA, Weinheim

Schreuer, *Z. Kristallogr. New Cryst. Struct.* **1999**, *214*, 306; f) J. Schreuer, *Z. Kristallogr. New Cryst. Struct.* **1999**, *214*, 307; g) J. Schreuer, *Z. Kristallogr. New Cryst. Struct.* **1999**, *214*, 309; h) M. S. Wickleder, *Z. Anorg. Allg. Chem.* **1999**, *625*, 1794.
[17] L. Pauling, *The nature of the chemical bond*, 3rd ed., Cornell University Press, Ithaca, NY, **1960**, p. 310.
[18] K. O. Christe, W. W. Wilson, C. J. Schack, R. D. Wilson, *Inorg. Synth.* **1986**, *24*, 39.
[19] P. Baumgarten, *Ber. Dtsch. Chem. Ges. B* **1936**, *69*, 1929.
[20] M. W. Schmidt, K. K. Baldridge, J. A. Boatz, S. T. Elbert, M. S. Gordon, J. H. Jensen, S. Koseki, N. Matsunaga, K. A. Nguyen, S. Su, T. L. Windus, *J. Comput. Chem.* **1993**, *14*, 1347.
[21] K. O. Christe, M. Gerken, R. Haiges, S. Schneider, T. Schroer, I. Tsyba, R. Bau, *Inorg. Chem.* **2003**, *42*, 416.

 © 2006 Wiley-VCH Verlag GmbH & Co. KGaA, Weinheim

Nanowires

DOI: 10.1002/anie.200601078

Nanocrystal-Mediated Crystallization of Silicon and Germanium Nanowires in Organic Solvents: The Role of Catalysis and Solid-Phase Seeding**

*Hsing-Yu Tuan, Doh C. Lee, and Brian A. Korgel**

The size-dependent properties, large surface-area-to-volume ratios, dispersibility in solvents, and mechanical flexibility of semiconductor nanowires make them an exciting class of materials.[1–3] Silicon nanowires in particular can be both *n* and *p*-doped and interface well with an insulating oxide and conducting metal silicide and these nanowires might be applied in silicon CMOS (complementary metal oxide semiconductor) circuits or with organic compounds on flexible plastic substrates.[4,5] Germanium is similar to silicon in many respects, but with a higher carrier mobility. Gold-seeded vapor–liquid–solid (VLS) growth is a common route to silicon and germanium nanowire synthesis at low growth temperatures ($\approx$360 °C).[1,3,6–8] Unfortunately, gold traps electrons and holes in both silicon and germanium and poses a serious contamination problem for nanowire integration with silicon CMOSs. Surprisingly few gold alternatives have been investigated for nanowire seeding. Si nanowires have been seeded by chemical vapor deposition (CVD) with Ti particles[9] and Ga droplets,[10] and in organic solvents, Si and Ge nanowires were synthesized using Ni nanocrystals.[11,12] Gold alternatives have been explored more extensively for other semiconductors: Sn for ZnO wires,[13] various metal films for vapor-grown tin oxide nanowires,[14] and low-melting metals such as In and Bi for solution synthesis of Group II–VI,[15,16] III-V[17–19] and Ge nanowires.[20] Herein, many different nanocrystals—Co, Ni, CuS, Mn, Ir, $MnPt_3$, Fe_2O_3, and FePt—are explored as seeds for Si and Ge nanowire synthesis to develop a more general understanding of the role of the seed particles in the nanowire growth process.

Si and Ge nanowires were grown by decomposing silanes or germanes in high temperature (450–500 °C), high pressure (10.3 MPa) supercritical toluene.[21,22] Under these reaction conditions, Au nanocrystals seed nanowires by the "supercritical fluid–liquid–solid" (SFLS) mechanism in which nanowires evolve from a liquid Au:Si (or Au:Ge) eutectic. In combination with Si and Ge, many of the seed materials studied herein do not form liquid eutectics until reaching temperatures well above 500 °C, and are not expected to work for "VLS"-like growth. However, they form solid alloys below 500 °C, perhaps making solid-phase nanowire seeding possible. Figure 1 shows TEM images of the various colloidal nanocrystals used to seed Si and Ge nanowires; their size distributions had standard deviations less than 20% about mean diameters ranging between 4.2 and 10.2 nm. Figure 2 shows the reaction products. All of the nanocrystals seeded Si and Ge nanowires from monophenylsilane (MPS) and diphenylgermane (DPG), but with varying success (summar-

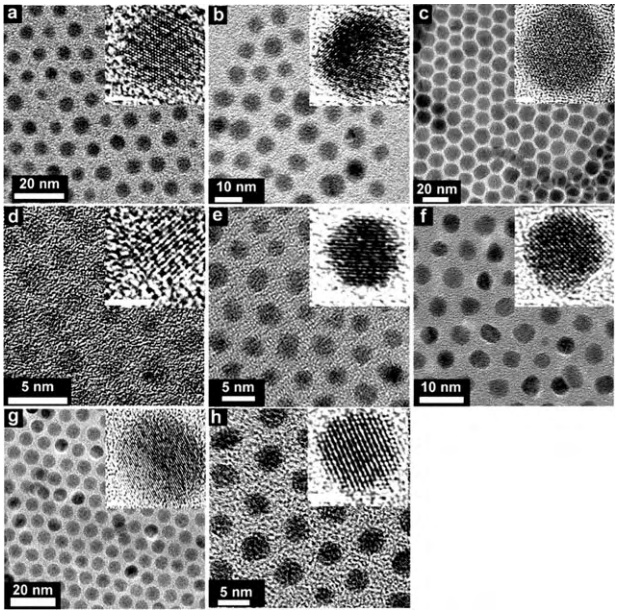


Figure 1. TEM images of metal nanocrystals studied as Si and Ge nanowire seeds: a) Co, b) Ni, c) CuS, d) Mn, e) Ir, f) $MnPt_3$, g) Fe_2O_3 and h) FePt. Insets: magnified images, scale bars 2 nm.

[*] H.-Y. Tuan, D. C. Lee, Prof. B. A. Korgel
Department of Chemical Engineering
Texas Materials Institute
Center for Nano- and Molecular Science and Technology
The University of Texas
Austin, TX 78712-1062 (USA)
Fax: (+1) 512-471-7060
E-mail: korgel@mail.che.utexas.edu

[**] We acknowledge the National Science Foundation, the Robert A. Welch Foundation, the Advanced Materials Research Center in collaboration with International SEMATECH, the Advanced Processing and Prototyping Center (DARPA: HR0011-06-1-0005), and the Office of Naval Research (N00014-05-1-0857) for financial support of this research. We are grateful to Felice Shieh, Cindy Stowell, and Ali Ghezelbash for Co, Ir, and CuS nanocrystals, and to J. P. Zhou for TEM assistance.

Supporting information for this article is available on the WWW under http://www.angewandte.org or from the author.

InterScience
© 2006 Wiley-VCH Verlag GmbH & Co. KGaA, Weinheim

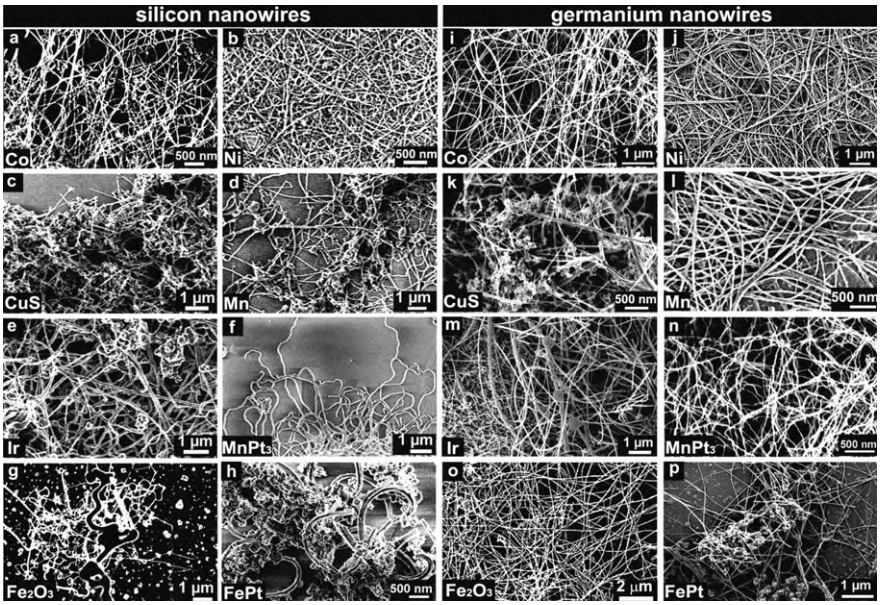


Figure 2. SEM images of a–h) Si and i–p) Ge nanowires synthesized in supercritical toluene from MPS (150 mM, 500 °C, 10.3 MPa) and DPG (80 mM, 460 °C, 10.3 MPa), respectively.

ized in Table 1). In general, straight nanowires are crystalline with few extended defects, whereas curly wires are usually amorphous or polycrystalline.[23] Co nanocrystals gave the highest yield of straight, long (> 10 μm) Si and Ge nanowires (Figure 3). Ni nanocrystals also produced crystalline Si and Ge nanowires with good yield. CuS nanocrystals produced straight crystalline Si nanowires with good yield but slightly shorter lengths (3–10 μm) and Fe_2O_3 nanocrystals produced high quality Ge nanowires with relatively high yield.

All of the nanocrystals produced nanowires at temperatures significantly below their bulk eutectic temperatures (summarized in Table 1). The small size of the seed nanocrystals reduces the eutectic temperature; however, a drop of nearly 350 °C is unlikely.[12] These nanocrystals most likely promote nanowire crystallization from solid-phase seeds. Solid-phase metal-seeded nanowire growth has also been proposed in other systems: Si (Ti,[9] Ni[11]), Ge (Fe,[24] Ni[12]), GaAs (Au),[25] InAs (Au),[26] and ZnSe (Au,[27] Fe[28]) nanowires. Solid-phase seeding is a viable growth mechanism, provided that the seed particles are small enough for rapid saturation by solid-state diffusion and the semiconductor has a high solid solubility in the metal. Co, Ni, Fe, and Cu all form alloys with Si and Ge at the growth temperatures and energy dispersive spectroscopy (EDS) analysis of the seed particles found at the tips of many nanowires revealed silicide and germanides (see Supporting Information for representative data). In the particles located at the tips of nanowires seeded with CuS and Fe_2O_3 nanocrystals, S and O were not observed in significant quantities, indicating that wires probably crystallize from copper silicide and iron germanide phases. Perhaps CuS and Fe_2O_3 are first reduced to Cu and Fe metal in the reaction mixture, prior to nanowire growth. Particles found at the tips of FePt-seeded nanowires showed all three elements—Fe, Pt, and Ge—indicating that nanowire growth probably originates from a ternary Fe:Pt:Ge phase.

Si and Ge nanowires seeded with Ni, Co, Fe_2O_3, and CuS show two predominant growth directions—⟨111⟩ and ⟨110⟩—in nearly equal proportions (Figure 3). Approximately 5% of the nanowires also had ⟨112⟩-oriented growth. This result is different from that for Au-seeded Si and Ge nanowires in organic solvents, which show preferential growth in either the ⟨111⟩ (Si) or ⟨110⟩ (Ge) directions, with only a small proportion of ⟨110⟩ (or ⟨111⟩) and ⟨112⟩ orientations.[22,29] Perhaps the difference in nanowire growth direction relates to the solid-phase

Table 1: Summary of seed nanocrystal composition and selected properties and reaction conditions.

Nanowire	Seed	Nanocrystal diameter [nm]	Reaction temp. [°C][a]	Eutectic temp. [°C][h]	Product description
Si	Co	9.7	500[b]	1200	Long straight wires
Si	Ni	5.6	460	964	Long straight wires
Si	CuS	11.7	500	802[d]	Good yield, shorter wires
Si	Mn	4.7	500	1040	Crystalline wires, low yield
Si	Ir	4.2	500	1470	Amorphous particles & curly wires
Si	$MnPt_3$	5.1	500	N/A	Low yield, mostly curly wires
Si	Fe_2O_3	10.2	500	1200[e]	Amorphous particles & few wires
Si	FePt	4.3	500	N/A	Amorphous particles
Ge	Co	9.7	460[c]	817	Long straight wires
Ge	Ni	5.6	460	762	Long straight wires
Ge	CuS	11.7	460	644[f]	Short curly wires
Ge	Mn	4.7	460	720	Crystalline wires, low yield
Ge	Ir	4.2	460	N/A	Wires & amorphous particles
Ge	$MnPt_3$	5.1	460	N/A	Straight wires with rough surfaces
Ge	Fe_2O_3	10.2	460	838[g]	Long straight wires
Ge	FePt	4.3	460	N/A	Wires & amorphous particles

[a] The optimal synthesis temperature for Si nanowires was approximately 40 °C higher than for Ge nanowires in all cases, indicating slower Si nanowire growth kinetics. [b] The optimum reaction temperature for cobalt-seeded Si nanowires from MPS was approximately 50 °C higher than the optimal synthesis temperature (450 °C) using Au seeds. [c] The optimum reaction temperature for cobalt-seeded Ge nanowires from DPG is approximately 80 °C higher than the optimal synthesis temperature (380 °C) using Au seeds. [d] Value based on Cu:Si phase diagram, because S appears to outgas from the seed particles. [e] Value based on Fe:Si phase diagram, because iron silicide appears to be the seed composition. [f] Value based on Cu:Ge phase diagram, because S appears to outgas from the seed particles. [g] Value based on Fe:Ge phase diagram, because iron germanocide appears to be the seed composition. [h] Ref. [42].

 © 2006 Wiley-VCH Verlag GmbH & Co. KGaA, Weinheim

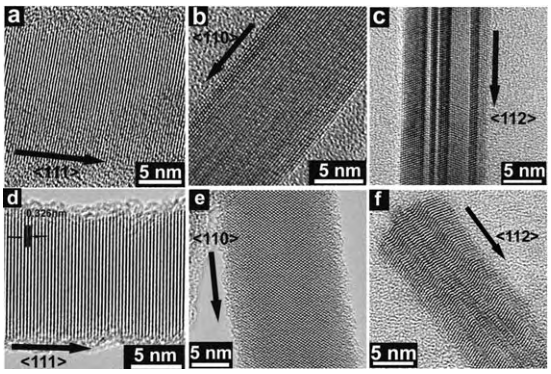


Figure 3. HRTEM images of Si (a–c) and Ge (d–f) nanowires seeded by Co (a–c), Fe_2O_3 (d–e), and CuS (f) showing ⟨110⟩, ⟨111⟩ and ⟨112⟩ growth directions. Approximately 5% of the sample contained ⟨112⟩ oriented nanowires, usually with longitudinal {111} twins, as in (c) and (f). The 0.326 nm lattice spacing agrees with the (111) d-spacing for bulk Ge (0.327 nm).

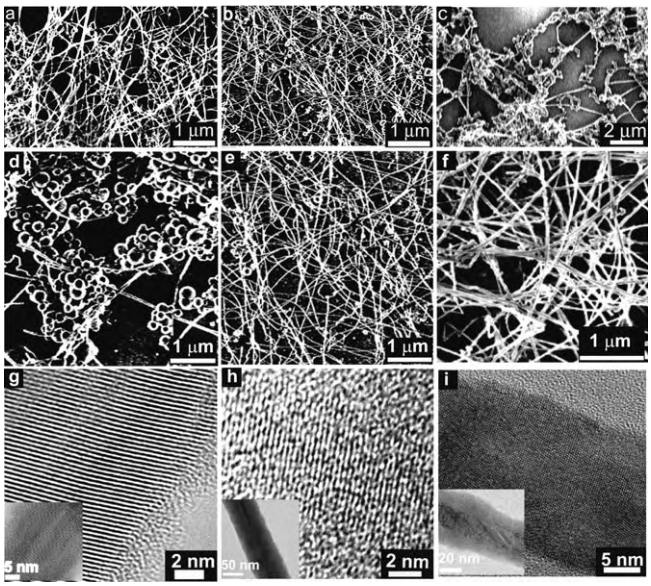


Figure 4. Cobalt-nanocrystal-seeded Si nanowires. HRSEM images of Si nanowires synthesized in supercritical toluene (10.3 MPa) from a) MPS (500 °C), b) trisilane (400 °C), and c) octylsilane (500 °C). HRSEM images of Si nanowires synthesized in supercritical toluene (10.3 MPa) from trisilane at d) 350 °C, e) 400 °C, and f) 450 °C. g–i) TEM images of Si nanowires synthesized in supercritical toluene (10.3 MPa) with g) trisilane (400 °C), h) trisilane (450 °C) and i) octylsilane (500 °C). The nanowires in (h) and (i) are coated with an amorphous shell, as shown more clearly in the low-resolution TEM images in the insets in (h) and (i). The shell material in (h) is amorphous Si and in (i) it is amorphous 3:1 C:Si (by EDS).

nanowire seeding process. However, it is noteworthy that regardless of the metal used to seed the nanowires (i.e., Au, Ni, or Co.), ⟨112⟩-oriented nanowires always tend to have longitudinal {111} twins, as in the wires in Figure 3c and f.

In VLS growth, the metal seed dissolves the semiconductor and recrystallizes it as a nanowire and has a passive role in the precursor decomposition chemistry.[3,6,22] Au does not catalyze reactant decomposition, but simply helps drive crystallization (Au could be called a "crystallization catalyst", but not a catalyst for reactant decomposition). In contrast to Au, the transition metals Ni, Co, and Fe, are catalysts for molecular decomposition reactions. For carbon nanotube (CNT) growth, Fe, Co, and Ni are used as catalysts that enhance reactant decomposition at the seed surface, while also promoting "crystallization" of the nanostructure—for CNTs that is graphitization and tube growth.[30–32] Au-seeded CVD nanowire growth typically uses very reactive precursors, such as silane, and there is generally no need to use catalytic seed metals to promote reactant decomposition. However, sidewall deposition can occur with reactive precursors and lead to substantial diameter tapering over the length of the wire.[33,34] Catalytic seeds might be able to lower the growth temperature and help prevent sidewall deposition. In Au-seeded, solution-phase nanowire growth, many organosilane and organogermane reactants, such as octylsilane, are too unreactive to promote nanowire formation at typical reaction temperatures.[11,22] Trisilane on the other hand is too reactive and forms amorphous Si particles.[22] These Si reactants require a catalytic seed to promote nanowire formation.

Figure 4 shows TEM and SEM images of Si nanowires seeded by Co nanocrystals in supercritical toluene from MPS, trisilane, and octylsilane—all three reactants gave nanowires. The cobalt nanocrystals enhance octylsilane decomposition enough to promote nanowire formation; however, the nanowire quality is only marginal as the nanowires are coated with an amorphous layer with significant carbon content (Figure 4i, 3:1 C:Si by EDS in shell). The cobalt nanocrystals were found to promote Si nanowire formation using trisilane at temperatures as low as 350 °C, although the majority product at this low temperature was amorphous Si colloids (Figure 4d). Cobalt enhances heterogeneous trisilane decomposition relative to homogeneous particle formation. Si nanowires produced with trisilane at 400 °C had very little sidewall deposition and few particulates; slightly higher temperature (450 °C) gave significant sidewall deposition (Figure 4h).

Of the nanocrystals studied, Co gave the highest yield and quality of both Si and Ge nanowires, rivaling Au-seeded reactions (See Supporting Information for an example of Au-seeded Si nanowires). All growth temperatures were well below the bulk eutectic temperatures, indicating solid-phase seeding. Solid-phase seeding can probably occur for any semiconductor with a high solubility in the seed metal; however, the growth temperature must be sufficiently high for fast saturation by solid-state diffusion, which can occur relatively fast in nanometer-diameter seed particles. Cobalt was also found to catalyze silane decomposition to promote Si nanowire growth from octylsilane and trisilane, similar to past studies on Ni nanocrystals.[11,12] In gas-phase reactions, the use of catalytic transition-metal seeds might enable lower temperature reactions for less sidewall deposition and better diameter control. As more seed materials are studied, the solid-phase growth method may become as prevalent as liquid-eutectic seeding, and the use of catalytic seed particles might serve as a general approach for improved diameter control, as it has for carbon nanotube growth.

 © 2006 Wiley-VCH Verlag GmbH & Co. KGaA, Weinheim

Experimental Section

Anhydrous toluene (99.8%, Sigma-Aldrich), monophenylsilane (MPS, 97%, Sigma-Aldrich), *N*-octylsilane ($(C_8H_{17})H_3Si$, Gelest), trisilane (Si_3H_8, Voltaix), and diphenylgermane (DPG, Gelest) were used as received. Co,[35] Ni,[36] CuS,[37] Ir,[38] Mn (Supporting Information), $MnPt_3$, Fe_2O_3,[39] and FePt[40] nanocrystals were prepared by arrested precipitation as described in the literature.

Nanowires were synthesized in semibatch 1 mL or 10 mL Ti grade-2 reactor connected to a high-pressure liquid chromatography (HPLC) pump for pressure control and reactant injection. The reactor was heated in a brass block with temperature monitored by a thermocouple.[22,32,41] A small piece of clean Si wafer was placed in the reactor as a deposition substrate to gather reaction product. The reactor was sealed in a nitrogen-filled glove box, connected to the HPLC pump, and then filled with anhydrous oxygen-free toluene. The reactor was pressurized to 3.4 MPa with toluene and then heated to the reaction temperature. 500 μL of 150 mM MPS in toluene with Si:nanocrystal mole ratios of 50:1 (Co), 100:1 (Ni), 150:1 (CuS), 50:1 (Mn), 50:1 (Ir), 50:1 ($MnPt_3$), 50:1 (Fe_2O_3), and 50:1 (FePt), were injected from a six-way valve injection loop (Valco) at 0.4 mL min^{-1}. For Ge nanowires, 500 μL of 80 mM DPG in toluene were injected with Ge:nanocrystal mole ratios of 100:1 (Co), 100:1 (Ni), 100:1 (CuS), 50:1 (Mn), 20:1 (Ir), 100:1 ($MnPt_3$), 200:1 (Fe_2O_3), and 200:1 (FePt). The reaction pressure was increased to 10.3 MPa with additional toluene. After 10 min, the reactor was immersed in ice-water and cooled to room temperature. The reactor was opened and the deposition substrate removed and stored under nitrogen until the product was characterized by SEM and TEM.

Nanowires were imaged by HRSEM on the deposition substrate without further purification using a LEO 1530 field-emission SEM at 1–3 kV accelerating voltage with working distances ranging between 2–5 mm. For HRTEM and STEM imaging, nanowires were either drop-cast from chloroform dispersions or dry transferred by scratching the deposition substrate onto 200-mesh lacey carbon-coated copper or nickel grids (Electron Microscope Sciences). Images were acquired using 200 kV accelerating voltage on a JEOL 2010F equipped with an Oxford INCA ED spectrometer.

Received: March 20, 2006
Revised: May 1, 2006
Published online: July 5, 2006

Keywords: germanium · nanocrystals · nanowires · silicon · supercritical fluids

[1] J. D. Holmes, K. P. Johnston, R. C. Doty, B. A. Korgel, *Science* **2000**, *287*, 1471.
[2] B. A. Korgel, *Science* **2004**, *303*, 1308.
[3] For a recent review, see M. Law, J. Goldberger, P. Yang, *Annu. Rev. Mater. Res.* **2004**, *34*, 83.
[4] Y. Cui, C. M. Lieber, *Science* **2001**, *291*, 851.
[5] M. C. McAlpine, R. S. Friedman, S. Jin, K. H. Lin, W. U. Wang, C. M. Lieber, *Nano Lett.* **2003**, *3*, 1531.
[6] J. T. Hu, T. W. Odom, C. M. Lieber, *Acc. Chem. Res.* **1999**, *32*, 435.
[7] T. Hanrath, B. A. Korgel, *Adv. Mater.* **2003**, *15*, 437.
[8] D. W. Wang, H. J. Dai, *Angew. Chem.* **2002**, *114*, 4783; *Angew. Chem. Int. Ed.* **2002**, *41*, 4783.
[9] T. I. Kamins, R. S. Williams, D. P. Basile, T. Hesjedal, J. S. Harris, *J. Appl. Phys.* **2001**, *89*, 1008.
[10] M. K. Sunkara, S. Sharma, R. Miranda, G. Lian, E. C. Dickey, *Appl. Phys. Lett.* **2001**, *79*, 1546.
[11] H.-Y. Tuan, D. C. Lee, T. Hanrath, B. A. Korgel, *Nano Lett.* **2005**, *5*, 681.
[12] H.-Y. Tuan, D. C. Lee, T. Hanrath, B. A. Korgel, *Chem. Mater.* **2005**, *17*, 5705.
[13] Y. Ding, P. X. Gao, Z. L. Wang, *J. Am. Chem. Soc.* **2004**, *126*, 2066.
[14] P. Nguyen, H. T. Ng, M. Meyyappan, *Adv. Mater.* **2005**, *17*, 1773.
[15] H. Yu, J. B. Li, R. A. Loomis, P. C. Gibbons, L. W. Wang, W. E. Buhro, *J. Am. Chem. Soc.* **2003**, *125*, 16168.
[16] J. W. Grebinski, K. L. Hull, J. Zhang, T. H. Kosel, M. Kuno, *Chem. Mater.* **2004**, *16*, 5260.
[17] T. J. Trentler, K. M. Hickman, S. C. Goel, A. M. Viano, P. C. Gibbons, W. E. Buhro, *Science* **1995**, *270*, 1791.
[18] S. P. Ahrenkiel, O. I. Micic, A. Miedaner, C. J. Curtis, J. M. Nedeljkovic, A. J. Nozik, *Nano Lett.* **2003**, *3*, 833.
[19] D. D. Fanfair, B. A. Korgel, *Cryst. Growth Des.* **2005**, *5*, 1971.
[20] X. Lu, D. D. Fanfair, K. P. Johnston, B. A. Korgel, *J. Am. Chem. Soc.* **2005**, *127*, 15718.
[21] For a recent review, see P. S. Shah, T. Hanrath, K. P. Johnston, B. A. Korgel, *J. Phys. Chem. B* **2004**, *108*, 9574.
[22] D. C. Lee, T. Hanrath, B. A. Korgel, *Angew. Chem.* **2005**, *117*, 3639; *Angew. Chem. Int. Ed.* **2005**, *44*, 3573.
[23] X. Lu, T. Hanrath, K. P. Johnston, B. A. Korgel, *Nano Lett.* **2003**, *3*, 93.
[24] S. Mathur, H. Shen, V. Sivakov, U. Werner, *Chem. Mater.* **2004**, *16*, 2449.
[25] A. I. Persson, M. W. Larsson, S. Stenstroem, B. J. Ohlsson, L. Samuelson, L. R. Wallenberg, *Nature Mater.* **2004**, *3*, 677.
[26] K. A. Dick, K. Deppert, T. Mrtensson, B. Mandl, L. Samuelson, W. Seifert, *Nano Lett.* **2005**, *5*, 761.
[27] Y. Ohno, T. Shirahama, S. Takeda, A. Ishizumi, Y. Kanemitsu, *Appl. Phys. Lett.* **2005**, *87*, 043105.
[28] A. Colli, S. Hofmann, A. C. Ferrari, C. Ducati, F. Martelli, S. Rubini, S. Cabrini, A. Franciosi, J. Robertson, *Appl. Phys. Lett.* **2005**, *86*, 153103.
[29] T. Hanrath, B. A. Korgel, *Small* **2005**, *1*, 717.
[30] H. J. Dai, J. Kong, C. W. Zhou, N. Franklin, T. Tombler, A. Cassell, S. S. Fan, M. Chapline, *J. Phys. Chem. B* **1999**, *103*, 11246.
[31] D. C. Lee, F. V. Mikulec, B. A. Korgel, *J. Am. Chem. Soc.* **2004**, *126*, 4951.
[32] D. C. Lee, B. A. Korgel, *Mol. Simul.* **2005**, *31*, 637.
[33] H. Adhikari, A. F. Marshall, C. E. D. Chidsey, P. C. McIntyre, *Nano Lett.* **2006**, *6*, 318.
[34] E. Tutuc, S. Guha, J. O. Chu, *Appl. Phys. Lett.* **2006**, *88*, 043113.
[35] V. F. Puntes, D. Zanchet, C. K. Erdonmez, A. P. Alivisatos, *J. Am. Chem. Soc.* **2002**, *124*, 12874.
[36] C. B. Murray, S. Sun, H. Doyle, T. Betley, *MRS Bull.* **2001**, *26*, 985.
[37] A. Ghezelbash, B. A. Korgel, *Langmuir* **2005**, *21*, 9451.
[38] C. A. Stowell, B. A. Korgel, *Nano Lett.* **2005**, *5*, 1203.
[39] T. Hyeon, S. S. Lee, J. Park, Y. Chung, H. B. Na, *J. Am. Chem. Soc.* **2001**, *123*, 12798.
[40] S. Sun, C. B. Murray, D. Weller, L. Folks, A. Moser, *Science* **2000**, *287*, 1989.
[41] T. Hanrath, B. A. Korgel, *J. Am. Chem. Soc.* **2002**, *124*, 1424.
[42] *Binary Alloy Phase Diagrams*, 2nd Ed. (Eds.: B. M. Thaddeus, O. Hiroaki, P. R. Subramanian, K. Linda), ASM International, Materials Park, OH, **1990**.

 © 2006 Wiley-VCH Verlag GmbH & Co. KGaA, Weinheim

Carbon Nanotubes

DOI: 10.1002/anie.200504273

Encapsulation and IR Probing of Cube-Shaped Octasilasesquioxane $H_8Si_8O_{12}$ in Carbon Nanotubes**

*Jiawei Wang, Marina K. Kuimova, Martyn Poliakoff, G. Andrew D. Briggs, and Andrei N. Khlobystov**

Studying the encapsulation of molecules in carbon nanotubes is important because the physical properties of molecules and their chemical reactivity can be controlled by confining them in nanoscopic containers;[1] in turn, the functional properties of single-walled carbon nanotubes (SWNTs), such as the electronic band gap,[2] can be tuned by molecules nested inside. In general, molecules inserted into nanotubes can be divided into two groups. The first group includes small gas molecules whose interactions with the interior and exterior surfaces of nanotubes have been mainly investigated spectroscopically, notably by IR spectroscopy, to provide valuable information about the mechanisms and energy of molecule–nanotube interactions.[3] Nevertheless, it is often difficult to distinguish conclusively between endohedral and exohedral adsorption of such small molecules. The other class of molecules are relatively large, carbon-rich molecular polyhedra, such as fullerenes[4a] and *ortho*-carboranes,[4b] or planar organic compounds, such as derivatives of perylene,[5] for which the use of IR spectroscopy is hindered by the overlap of their absorption bands with those of nanotubes, and whose presence inside nanotubes is usually unambiguously demonstrated by transmission electron microscopy (TEM).

Oligosilasesquioxanes of general formula $(HSiO_{3/2})_{2n}$ ($n = 2, 3, 4,\ldots$)[6,7] have vibrational spectra whose distinct features do not overlap with absorption bands of nanotubes,[7–9] which, in principle, should enable IR, Raman, and neutron-scattering spectroscopies to reveal the mechanism of their interaction with nanotubes. $H_8Si_8O_{12}$, for example, is a cube-shaped molecule with an H atom pointing outwards from each corner of the cube (Figure 1). Since the Si–H bonds are outermost in $H_8Si_8O_{12}$, their stretching vibrations are highly sensitive to the environment around the molecule and could potentially be used to probe the interactions between $H_8Si_8O_{12}$ and nanotubes.

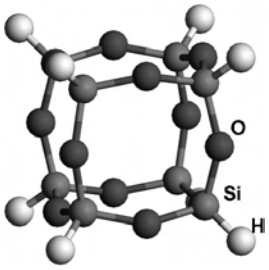


Figure 1. Structural diagram of $H_8Si_8O_{12}$. Selected geometrical parameters:[8] r(Si–H) = 0.148 nm, r(Si–O) = 0.162 nm, α(O-Si-H) = 109.5°, β(O-Si-O) = 109.5°, γ(Si-O-Si) = 148.4°.

Like most other molecular species, $H_8Si_8O_{12}$ is expected to interact with nanotubes through low-directional nonspecific van der Waals forces[10] and, depending on the nanotube diameter, it can experience a significant pressure inside nanotubes,[11] so that the properties of the encapsulated molecules are expected to be altered from those in the bulk crystal or solution phase. The diagonal distance of 0.66 nm between H atoms on the same face of the cube is slightly shorter than the diameter of C_{60} molecules (0.7 nm), which were previously inserted into nanotubes. As the van der Waals radius of an sp^2 carbon atom in the nanotube walls and an H atom in $H_8Si_8O_{12}$ are about 0.15 and 0.12 nm, respectively,[12] it is expected that the smallest tube diameter capable of being filled with octasilasesquioxane would be around 1.2 nm ($= 0.66 + 2 \times 0.15 + 2 \times 0.12$ nm). Because hydrogen atoms of $H_8Si_8O_{12}$ come into direct contact with the nanotube surface when the molecule is lodged inside, the vibrational frequency of the Si–H bonds might be suitable for spectroscopic probing of the interiors of nanotubes to characterize their properties as nanoscopic molecular containers. We have investigated this possibility for SWNTs and multiwalled carbon nanotubes (MWNTs) of different diameters.

We found that $H_8Si_8O_{12}$ can be efficiently inserted into SWNTs with diameters of 1.4–1.5 nm (SWNT-1) and MWNTs with internal diameters of 1.0–3.0 nm and an average diameter of 1.85 nm (MWNT-1) in the gas phase to yield nanotubes filled with $H_8Si_8O_{12}$ molecules, as evidenced by high-resolution TEM (HRTEM) imaging (Figure 2). This observation is in agreement with the fact that the average diameters of SWNT-1 and MWNT-1 used in these experiments are both larger than the estimated minimum diameter of 1.2 nm required for insertion of $H_8Si_8O_{12}$. Unlike in the case of fullerenes, no ordered packing patterns were observed for $H_8Si_8O_{12}$ molecules inside the nanotubes by HRTEM. One reason for this could be related to different orientations of $H_8Si_8O_{12}$ molecules in a nanotube (Figure 2d), which result in different projected shapes of $H_8Si_8O_{12}$ on the viewing plain in TEM and complicate the contrast in electron micrographs.

[*] J. Wang, Dr. M. K. Kuimova,[+] Prof. M. Poliakoff, Dr. A. N. Khlobystov
The School of Chemistry
University of Nottingham
University Park, Nottingham NG72RD (UK)
Fax: (+44) 115-951-3563
E-mail: andrei.khlobystov@nottingham.ac.uk
Prof. G. A. D. Briggs
Department of Materials
University of Oxford
Parks Road, Oxford OX13PH (UK)
[+] current address:
Department of Chemistry
Imperial College London
Exhibition Road, London SW72AZ (UK)

[**] The authors thank the Royal Society, the European Science Foundation (ESF), Research Councils UK (RCUK), EPSRC (GR/S15808/01, GR/S82176/01), and the University of Nottingham for financial support.

Supporting information for this article is available on the WWW under http://www.angewandte.org or from the author.

InterScience
© 2006 Wiley-VCH Verlag GmbH & Co. KGaA, Weinheim

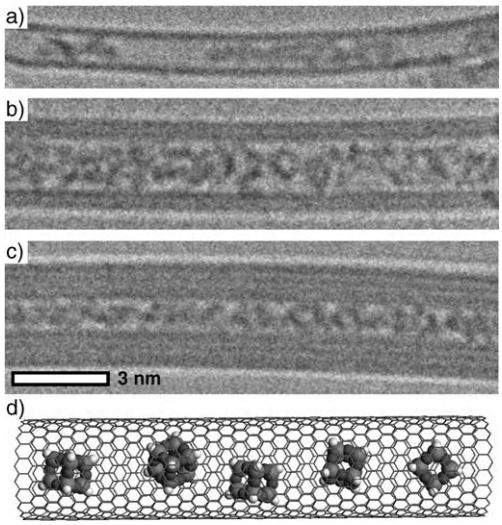


Figure 2. HRTEM images of a) $H_8Si_8O_{12}$@SWNT-1, b) $H_8Si_8O_{12}$@MWNT-1, and c) $H_8Si_8O_{12}$@MWNT-1 with narrow internal diameter (ca. 1.2 nm); d) schematic diagram of $H_8Si_8O_{12}$ encapsulated in a SWNT.

Using supercritical CO_2 ($scCO_2$) as solvent for transporting molecules into carbon nanotubes, a method successfully utilized for insertion of fullerenes,[13] resulted in only partial filling with $H_8Si_8O_{12}$. This can probably be explained by the high affinity of silicon compounds for $scCO_2$,[14] which results in preferential solvation of $H_8Si_8O_{12}$ by CO_2 and thus reduced insertion into the SWNTs. The energy of the interaction of octasilasesquioxanes with the nanotube interior may be lower than that for C_{60} (ca. 3 eV),[15] and this may further reduce the efficiency of filling in supercritical fluids. The filling factor for MWNT-1 in $scCO_2$ appears to be somewhat higher than for SWNT-1 under the same conditions but lower than in the gas phase.

The most striking effect of encapsulation in carbon nanotubes on the vibrational spectra of $H_8Si_8O_{12}$ is a red shift of the ν(Si–H) band, by about $-15\ cm^{-1}$ for SWNT-1 and about $-19\ cm^{-1}$ for MWNT-1 (Figure 3 and Table 1). A shift

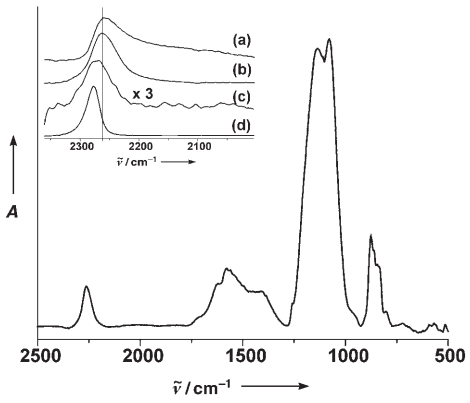


Figure 3. A typical FTIR spectrum of octasilasesquioxane in carbon nanotubes. Inset: ν(Si–H) band for a) $H_8Si_8O_{12}$@MWNT-1, b) $H_8Si_8O_{12}$@SWNT-1, and c) $H_8Si_8O_{12}$@SWNT-2, as compared to the ν(Si–H) band of free octasilasesquioxane dissolved in CCl_4 (d).

Table 1: Characteristics of the ν(Si–H) band for octasilasesquioxane in various environments.

Sample	Nanotube int. diam. [nm]	Peak position [cm^{-1}]	Shift [cm^{-1}][a]	Peak width [cm^{-1}][b]
$H_8Si_8O_{12}$ solution (CCl_4)	–	2277	–	25
$H_8Si_8O_{12}$ solid (KBr)	–	2294, 2300[c]	+17	20
$H_8Si_8O_{12}$@SWNT-1	1.3–1.5	2262	−15	50
$H_8Si_8O_{12}$@MWNT-1	1.0–3.0	2258	−19	>50[d]
$H_8Si_8O_{12}$@SWNT-2	0.8–1.2	2271	−6	40
$H_8Si_8O_{12}$@MWNT-2	5–8	no peak	–	–

[a] Shifts were calculated from the peak maxima relative to $\tilde{\nu}$(Si–H) in CCl_4 solution[8] (uncertainty in peak position $<\pm 2\ cm^{-1}$). [b] Full width at half maximum obtained from Lorentzian curve fit. [c] In CsI pellet three bands were observed: 2274, 2293, 2300 cm^{-1}.[9] [d] The ν(Si–H) band is unsymmetrical.

of opposite sign ($+17\ cm^{-1}$) is observed for $H_8Si_8O_{12}$ in the crystal (Table 1 and Supporting Information), that is, the molecules in $H_8Si_8O_{12}$@SWNT-1 and $H_8Si_8O_{12}$@MWNT-1 are not in a crystal-like state. Inside SWNT-1 with diameters of 1.3–1.5 nm used in our experiments each octasilasesquioxane molecule has only two nearest neighbors because of the geometrical constraint imposed by the nanotube (Figure 2b). In such an arrangement most or all of the H atoms of $H_8Si_8O_{12}$ will point towards the nanotube sidewalls (Figures 4b and c),

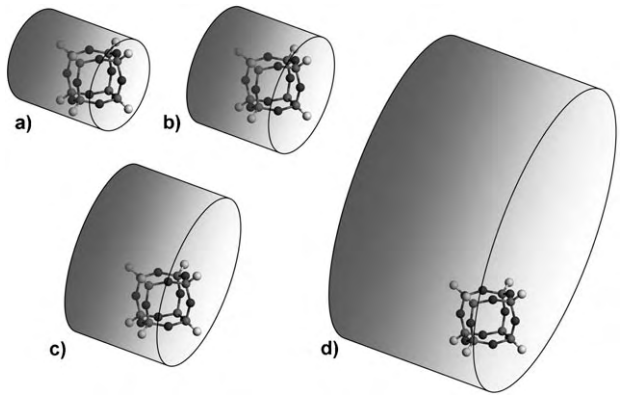


Figure 4. Scaled representation of the average internal diameters of a) SWNT-2, b) SWNT-1, c) MWNT-1, and d) MWNT-2 in relation to the size of $H_8Si_8O_{12}$.

so that $\tilde{\nu}$(Si–H) will be directly affected by any interaction between $H_8Si_8O_{12}$ and the nanotube interior. The most likely explanation for the shift of $\tilde{\nu}$(Si–H) is elongation of the Si–H bonds as a result of dispersion forces acting between $H_8Si_8O_{12}$ and the nanotube. A similar effect was reported for various small molecules such as $(NO)_2$ and CF_4 adsorbed in nanotubes from the gas phase.[16,17]

A twofold broadening of the ν(Si–H) band in nanotubes as compared to solution (Figure 3, Table 1) can be explained by the high degree of disorder inside nanotubes, which is also evidenced by HRTEM imaging (Figure 2). Such disorder creates a distribution of different local environments for $H_8Si_8O_{12}$ in nanotubes, reflected in the shape of the ν(Si–H) band. The distribution of different orientations of $H_8Si_8O_{12}$

 © 2006 Wiley-VCH Verlag GmbH & Co. KGaA, Weinheim

inside MWNT-1 and therefore the width of the band are expected to be sensitive to the internal diameters of nanotubes. We found that the broadening of the ν(Si–H) band for $H_8Si_8O_{12}$@MWNT-1 (Figure 3, spectrum (a) in the inset) is substantially greater than for $H_8Si_8O_{12}$@SWNT-1 (spectrum (b) in the inset). This can be related to the broader spread of internal diameters of MWNT-1 ($d_{NT} = 1.0$–3.0 nm) than of SWNT-1 ($d_{NT} = 1.3$–1.5 nm).

We also attempted insertion of $H_8Si_8O_{12}$ into carbon nanotubes of average diameter smaller than the size of the molecule (ca. 1.0 nm). The filling rate for SWNTs with diameters of 0.8–1.2 nm (SWNT-2), qualitatively estimated from extensive HRTEM imaging, appeared to be lower than for SWNT-1 or MWNT-1, and this resulted in a low intensity of the ν(Si–H) band in the IR spectrum of $H_8Si_8O_{12}$@SWNT-2 (Figure 3, spectrum (c) in the inset). The red shift of the ν(Si–H) peak is only $-6\ cm^{-1}$ in SWNT-2, much smaller than in wider SWNT-1 or MWNT-1. Such a small shift indicates that, in addition to van der Waals dispersive forces, the molecules in narrower nanotubes (Figure 4a) may experience greater compression than in wider nanotubes. The compression effect was previously reported for fullerenes encapsulated in carbon nanotubes of small diameters,[11] and since van der Waals forces are also responsible for the $H_8Si_8O_{12}$–nanotube interaction, a similar effect can be expected for $H_8Si_8O_{12}$ in nanotubes. Such a compression would shorten the Si–H bonds and effectively compensate for their elongation caused by the dispersion interactions and thus suppress the observable red shift of the ν(Si–H) band. The width of the ν(Si–H) band of $H_8Si_8O_{12}$@SWNT-2 is about $40\ cm^{-1}$.

We also explored encapsulation of $H_8Si_8O_{12}$ in carbon nanotubes with diameters greatly exceeding the dimensions of the molecules, but in this case no ν(Si–H) peak was observed in the IR spectra. Open-ended MWNT-2 with internal diameters in the range between 5 and 8 nm was filled with octasilasesquioxane under standard conditions in the gas phase. An $H_8Si_8O_{12}$@MWNT-2 sample was washed with hexane to remove unencapsulated octasilasesquioxane from the nanotube surfaces (in the same way as for all other samples), and this caused complete loss of the ν(Si–H) peak in the IR spectrum, attributed to removal of the molecules from the interior of MWNT-2 by the wash solvent. As the internal diameters of MWNT-2 are substantially larger than the size of $H_8Si_8O_{12}$ (Figure 4d), fewer nanotube carbon atoms are involved in van der Waals interactions per enclosed molecule, and not all sides of the octasilasesquioxane molecules interact with the nanotube, which reduces the efficiency of the nanotube–molecule interactions. Because of the loose geometrical fit of the molecules and MWNT-2, the solvent penetrates into the nanotubes and dissolves and removes $H_8Si_8O_{12}$ from the nanotubes during the washing procedure. This also indicates that in the case of wide-nanotube MWNT-2 it is energetically favorable for $H_8Si_8O_{12}$ to be dissolved in an organic solvent rather than to be encapsulated inside the nanotube.

We have demonstrated that the effectiveness of interactions of $H_8Si_8O_{12}$ with carbon nanotubes depends critically on the internal diameter of the nanotubes. Nanotubes with diameters slightly exceeding the size of the molecules form efficient van der Waals interactions with $H_8Si_8O_{12}$, manifested in a red shift of 15–19 cm^{-1} of the Si–H vibration. Narrow nanotubes with diameters close to the size of the molecules exert pressure on the encapsulated molecules and reduce the shift of the ν(Si–H) band, whereas nanotubes with diameters substantially exceeding the size of the molecules interact weakly with $H_8Si_8O_{12}$ and are unable to retain it. We believe that encapsulation of octasilasesquioxane may be used to quantify the interactions of nanotubes with molecules and to distinguish nanotubes of different internal diameters by using $H_8Si_8O_{12}$ as a spectroscopic probe, by applying the principles outlined in this communication and further quantitative IR analyses which we are planning to carry out.

Experimental Section

$H_8Si_8O_{12}$ was synthesized and purified by an established method.[18] Four types of carbon nanotubes were used for the experiments: SWNT-1 produced by arc-discharge (Aldrich) with diameters of 1.3–1.5 nm after purification,[19] MWNT-1 (Nanocyl) with a distribution of internal diameters of 1.0–3.0 nm, SWNT-2 produced by HiPCO (Carbon Nanotechnologies) with diameters of 0.8–1.2 nm, and MWNT-2 (Aldrich) with internal diameters of 5–8 nm. Prior to filling with $H_8Si_8O_{12}$, SWNTs were oxidized in air at 400 °C for 30 min to open the nanotube caps and partly remove amorphous carbon from their surfaces. MWNTs were treated with 5 M HNO_3 prior to heating in air to ensure that the nanotube ends were open. The mixtures of open-ended nanotubes and $H_8Si_8O_{12}$ were placed in a quartz tube, sealed under a vacuum of 10^{-3} Torr and heated at 175–177 °C for two days[20] or treated in supercritical $scCO_2$ at 50 °C under 15 MPa by using a pressure-cycling filling technique reported previously by us.[13] Following the filling processes, each sample was sonicated in hexane followed by filtration and washing with more hexane to remove unencapsulated $H_8Si_8O_{12}$. Prior to spectroscopic characterizations all samples were analyzed by thermogravimetric analysis (TGA), whereby the absence of weight loss at 126 °C, characteristic of desorption of $H_8Si_8O_{12}$ from the surface of nanotubes, confirmed that $H_8Si_8O_{12}$ is encapsulated in the nanotubes (see the Supporting Information). Nanotube diameter distributions were measured by HRTEM imaging.

Received: December 1, 2005
Revised: May 16, 2006
Published online: July 3, 2006

Keywords: carbon · host–guest systems · nanotubes · silanes · vibrational spectroscopy

[1] a) D. A. Britz, A. N. Khlobystov, K. Porfyrakis, A. Ardavan, G. A. D. Briggs, *Chem. Commun.* **2005**, 37; b) S. Bandow, M. Takizawa, K. Hirahara, M. Yudasaka, S. Iijima, *Chem. Phys. Lett.* **2001**, *337*, 48.
[2] a) L. J. Li, A. N. Khlobystov, J. G. Wiltshire, G. A. D. Briggs, R. J. Nicholas, *Nat. Mater.* **2005**, *4*, 481; b) J. Lee, H. Kim, S. J. Kahng, G. Kim, Y. W. Son, J. Ihm, H. Kato, Z. W. Wang, T. Okazaki, H. Shinohara, Y. Kuk, *Nature* **2002**, *415*, 1005.
[3] D. A. Britz, A. N. Khlobystov, *Chem. Soc. Rev.* **2006**, DOI: 10.1039/B507451G, and references therein.
[4] a) A. N. Khlobystov, D. A. Britz, G. A. D. Briggs, *Acc. Chem. Res.* **2005**, *38*, 901, and references therein; b) D. A. Morgan, J. Sloan, M. L. H. Green, *Chem. Commun.* **2002**, 2442.
[5] Y. Fujita, S. Bandow, S. Iijima, *Chem. Phys. Lett.* **2005**, *413*, 410.

 © 2006 Wiley-VCH Verlag GmbH & Co. KGaA, Weinheim

[6] R. Q. Su, T. E. Müller, J. Procházka, J. A. Lercher, *Adv. Mater.* **2002**, *14*, 1369.
[7] M. Bartsch, P. Bornhauser, G. Calzaferri, R. Imhof, *J. Phys. Chem.* **1994**, *98*, 2817.
[8] C. Marcolli, P. Laine, R. Buhler, G. Calzaferri, J. Tomkinson, *J. Phys. Chem. B* **1997**, *101*, 1171.
[9] A. D. Chomel, U. A. Jayasooriya, F. Babonneau, *Spectrochim. Acta Part A* **2004**, *60*, 1609.
[10] L. A. Girifalco, N. Hodak, R. S. Lee, *Phys. Rev. B* **2000**, *62*, 13104.
[11] M. Yoon, S. Berber, D. Tomanek, *Phys. Rev. B* **2005**, *71*, 155406.
[12] A. Bondi, *J. Phys. Chem.* **1964**, *68*, 441.
[13] A. N. Khlobystov, D. A. Britz, J. Wang, S. A. O'Neil, M. Poliakoff, G. A. D. Briggs, *J. Mater. Chem.* **2004**, *14*, 2852.
[14] T. A. Hoefling, D. A. Newman, R. M. Enick, E. J. Beckman, *J. Supercrit. Fluids* **1993**, *6*, 165.
[15] H. Ulbricht, G. Moos, T. Hertel, *Phys. Rev. Lett.* **2003**, *90*, 095501.
[16] O. Byl, P. Kondratyuk, J. T. Yates, *J. Phys. Chem. B* **2003**, *107*, 4277.
[17] W. L. Yim, O. Byl, J. T. Yates, J. K. Johnson, *J. Am. Chem. Soc.* **2005**, *127*, 3198.
[18] P. A. Agaskar, *Inorg. Chem.* **1991**, *30*, 2707.
[19] A. N. Khlobystov, R. Scipioni, D. Nguyen-Manh, D. A. Britz, D. G. Pettifor, G. A. D. Briggs, S. G. Lyapin, A. Ardavan, *Appl. Phys. Lett.* **2004**, *84*, 792.
[20] The sublimation point of $H_8Si_8O_{12}$ is below 170 °C at atmospheric pressure, and the compound is thermally stable up to 200 °C.

 © 2006 Wiley-VCH Verlag GmbH & Co. KGaA, Weinheim

Copper Sensor

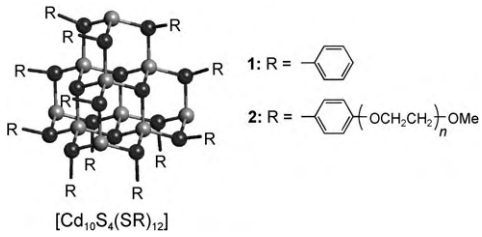
DOI: 10.1002/anie.200601491

Turn-On and Selective Luminescence Sensing of Copper Ions by a Water-Soluble $Cd_{10}S_{16}$ Molecular Cluster**

Katsuaki Konishi and Takayuki Hiratani*

The detection of trace amounts of copper(I) ion is of increasing importance in light of its environmental and biomedical implications. One convenient detection tool is the luminescent chemosensor, whereby the major challenge is to construct sensing systems that exhibit positive responses with high selectivity and sensitivity in water.[1] A variety of fluorescence sensors have been designed by combining an organic fluorophore and a metal-binding chelate,[2] but few examples of "turn-on" sensors that function in aqueous solutions have been reported.

Recently, cadmium chalcogenide nanomaterials have emerged as a novel class of luminescent probes as a result of their unusual photoluminescence properties.[3] These materials are potentially useful for metal-ion sensing, as metal ions, including copper ions, are expected to interact with surface heteroatoms (S, Se, Te) to affect the optical properties of the material. Although the effects of metal ions on photoluminescence properties have been investigated for several nanoclusters and nanorods, only quenching effects have been reported for copper ions.[4,5] Herein, we demonstrate a unique turn-on response of the water-soluble CdS cluster molecule **2** towards copper ions, and highlight its selectivity and sensitivity.



The CdS cluster that we used in this study is a defined and neutral molecule with the general formula $[Cd_{10}S_4(SR)_{12}]$ which has a truncated tetrahedral $Cd_{10}S_{16}$ core and twelve surface substituents (R) attached to the sulfur atoms.[6] We reported recently that clusters capped by lipophilic groups (R = simple alkyl or aryl, such as **1**) show surface-mediated emission at around 600 nm in organic solvents at ambient temperature.[7] To explore the properties of such molecular clusters in aqueous systems, we appended oligo(ethylene glycol) (OEG, $-(OC_2H_4)_nOCH_3$, $n \approx 6$) units to the surface phenyl groups of the phenyl-capped precursor **1** by the thiolate exchange reaction to give **2**. In contrast to **1**, the OEG-modified cluster **2** showed high solubility in water and in organic solvents such as acetonitrile and chloroform.

In HEPES buffer (100 mM, pH 7.0) at 25 °C, **2** (6.7 μM) showed an emission band at 600 nm upon excitation of the cluster at 350 nm. The titration of this solution with $[Cu^I(CH_3CN)_4]PF_6$ resulted in a notable enhancement of photoluminescence along with a slight red shift of the emission maximum to 620 nm (Figure 1a).[8,9] For example, when **2** was mixed with one molar equivalent of Cu^I ion, the intensity at 620 nm and the integrated band area increased by factors of 9.1 and 7.4, respectively. As shown in Figure 1b, the emission intensities at 620 nm increased upon the addition of Cu^I to reach a plateau at $[Cu^I]_0/[\mathbf{2}]_0 \approx 2.0$ with $I/I_0 \approx 12.5$.[10] The nearly linear correlation observed up to $[Cu^I]_0/[\mathbf{2}]_0 = 1.0$ allowed easy detection of Cu^I at nanomolar to micromolar concentrations. Under these conditions the dynamic range and the detection limit were estimated to reach 10 μM and approximately 0.07 μM (≈4 ppb), respectively.

This sharp positive response that was observed was found to be highly specific to Cu^I. As summarized in Figure 2a, no

[*] Prof. Dr. K. Konishi, T. Hiratani
Creative Research Initiative "Sosei" (CRIS) and
Division of Materials Science
Graduate School of Environmental Science, Hokkaido University
North 21 West 10, Sapporo 001-0021 (Japan)
Fax: (+81) 11-706-9290
E-mail: konishi@ees.hokudai.ac.jp

[**] This work was partly supported by a Grant-in-Aid for Scientific Research (B) from the Ministry of Education, Culture, Sports, Science, and Technology of Japan and by the Nagase Science and Technology Foundation. T.H. thanks the JSPS for financial support.

Supporting information for this article is available on the WWW under http://www.angewandte.org or from the author.

 © 2006 Wiley-VCH Verlag GmbH & Co. KGaA, Weinheim

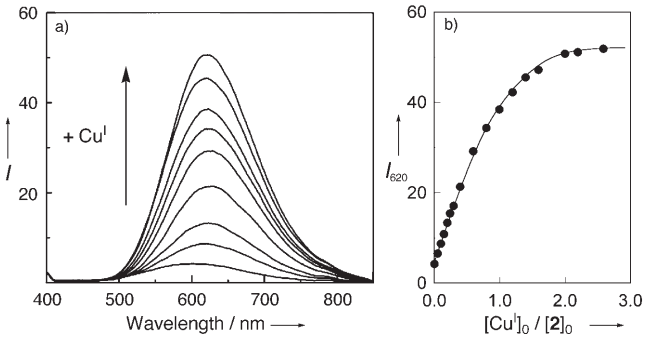


Figure 1. a) Photoluminescence response ($\lambda_{ex}=350$ nm) of **2** (6.7 μM) upon the addition of Cu^{I} (from bottom to top: 0, 0.1, 0.2, 0.4, 0.6, 0.8, 1.0, 1.4, and 2.0 equiv) in HEPES buffer (*N*-(2-hydroxyethyl)piperazine-*N*′-2-ethanesulfonic acid, 100 mM) containing MeCN (2 vol%) at 25 °C; b) plot of the photoluminescence intensity at 620 nm.

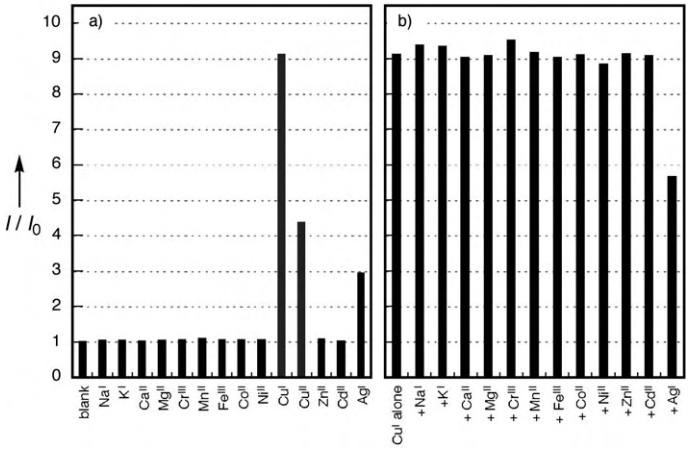


Figure 2. a) Photoluminescence response ($\lambda_{ex}=350$ nm) of **2** (6.7 μM) monitored at 620 nm upon the addition of chloride or nitrate salts of metal ions (1.0 mM for Na^{I}, K^{I}, Ca^{II}, Mg^{II} and 6.7 μM for the other cations); b) emission response of Cu^{I} (6.7 μM) in the presence of equimolar amounts of other cations in HEPES buffer (100 mM) containing MeCN (2 vol%) at 25 °C.

emission enhancements were observed for alkaline (Na, K), alkaline-earth (Mg, Ca), or most other environmentally and biologically relevant metal ions (e.g., Cr^{III}, Mn^{II}, Fe^{III}, Co^{II}, Ni^{II}, Zn^{II}, Cd^{II}). The excellent selectivity for Cu^{I} was further demonstrated by the observation that the emission response to Cu^{I} was not affected by the presence of the above transition-metal ions or of millimolar concentrations of NaCl, KCl, $CaCl_2$, and $MgCl_2$ (Figure 2b). Among the metal ions examined, Ag^{I}, which has the electronic structure $4d^{10}$, induced a less prominent but definite increase in emission intensity ($I/I_0=2.9$ at $[Ag^{I}]_0/[\mathbf{2}]_0=1.0$; Figure 2a). This result suggests that the positive response is specific to the Group 11 d^{10} metal ions.

A positive response was also observed for Cu^{II}, thus revealing the unique ability of **2** to respond to either Cu^{I} or Cu^{II}. It has been reported that the interaction of Cu^{II} with a colloidal CdS results in its reduction to Cu^{I}.[4a,b] A similar redox process appears to occur in the present system. In the ^{1}H NMR spectrum of a mixture of **2** and 1.0 equivalent of $Cu(NO_3)_2$, no paramagnetic features attributable to d^9 Cu^{II} were observed, and the cluster signals were very similar to those of the mixture with diamagnetic Cu^{I}.[11,12] Therefore, the positive emission response to Cu^{II} arises from in situ reduction to Cu^{I}, which again indicates the specificity for monovalent d^{10} ions of the Group 11 elements.

In contrast to the strong increase in emission intensity upon the addition of Cu^{I}, negligible changes were observed in the absorption spectrum of **2**.[11] Isarov and Chrysochoos reported that the metal-displacement reaction of surface Cd by Cu in a colloidal system leads to the emergence of a new absorption band tailing the red region as a result of the formation of Cu_xS species.[4a] In the present case, the absorption onsets were observed at ca. 420 nm and no tailing to the red region was observed throughout the titration. Therefore, as suggested by the results for our colloidal system at low copper-ion concentrations, it is likely that isolated Cu^{I} ions bind to surface sulfur atoms of **2** through simple Cu–S coordination bonds.

To obtain further insight into the adduct between **2** and Cu^{I}, we investigated the complexation stoichiometry by the Job method. As shown in Figure 3, a plot of the amount of the

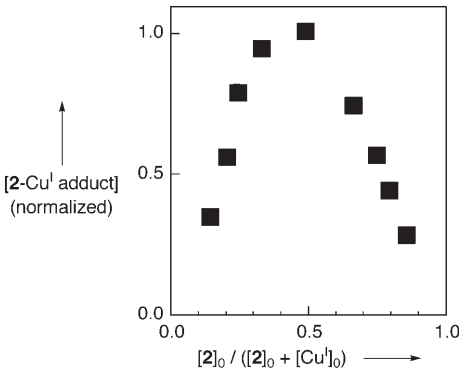


Figure 3. Job plot for the formation of the **2**–Cu^{I} adduct estimated from the emission intensity at 620 nm with $[\mathbf{2}]_0+[Cu^{I}]_0$ maintained at 20 μM.

adduct, as estimated from the emission intensity, versus $[\mathbf{2}]_0/([\mathbf{2}]_0+[Cu^{I}]_0)$ gave a maximum at 0.5, thus indicating 1:1 complexation. However, the simplest one-to-one adduct does not seem to be a major product. Size-exclusion chromatography (SEC) of **2** showed a significant shift of the elution peak towards a higher-molecular-weight region upon the addition of Cu^{I} (Figure 4a,b). Therefore, if the general preference of Group 11 d^{10} ions to form a two-coordinate complex with linear geometry is also considered, **2** and Cu^{I} are likely to assemble through S–Cu–S bridges to form a multicluster/nuclear network with a 1:1 composition $(\mathbf{2}\cdot Cu^{I})_m$, as illustrated schematically in Figure 5.

This conclusion strongly suggests that the formation of Cu^{I}-containing multicluster species $(\mathbf{2}\cdot Cu^{I})_m$ is responsible for the sharp emission response to Cu^{I}. The similarity of the excitation spectral patterns ($\lambda_{em}=610$ nm) before and after the addition of Cu^{I} indicates that the original S-to-Cd transition associated with the emission at 620 nm is almost completely retained after the complexation with Cu^{I}. This

 © 2006 Wiley-VCH Verlag GmbH & Co. KGaA, Weinheim

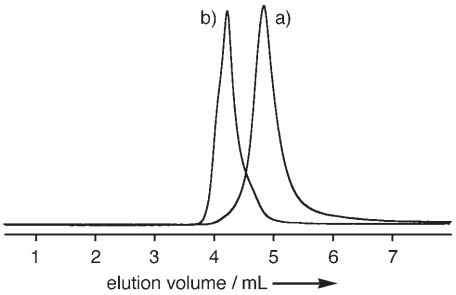


Figure 4. SEC profiles of a) **2** and b) **2**/$[Cu^{I}(CH_3CN)_4]PF_6$ (1:4 molar ratio) monitored at 340 nm with a Shodex OHpak SB802.5HQ instrument with $MeCN/H_2O$ (60/40 v/v) as the eluent.

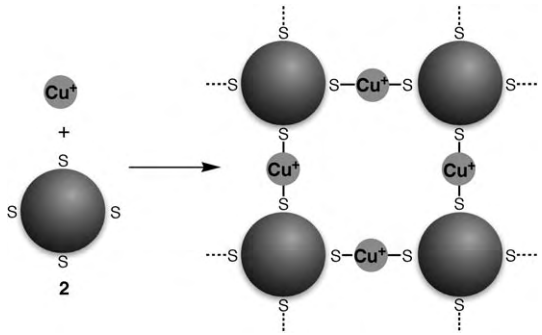


Figure 5. Schematic illustration of a possible network structure of the **2**–Cu^{I} aggregate: $(\mathbf{2}\cdot Cu^{I})_m$. The large spheres represent the clusters.

notion is supported by the above-mentioned absorption profiles, in which no substantial changes were observed upon complexation. Therefore, the observed emission enhancement corresponds to the increase in the quantum yield, which may result from the generation of a new and efficient radiative path involving the bound Cu^{I} ion and/or from the suppression of a nonradiative process. With respect to the latter possibility, we proposed recently that the cluster emission is enhanced when the free motion (rotation) of the surface substituents is suppressed.[7a] A similar mechanism may be involved in the present case, as the formation of S–Cu–S bridges should require the mutual interpenetration of surface aryl units on neighboring clusters, thereby restricting their motion.

In conclusion, we have demonstrated the first CdS-based photoluminescence sensor that shows a turn-on response to copper ions in aqueous solution. Studies on the structures of the aggregate species $(\mathbf{2}\cdot Cu^{I})_m$ as well as their photoluminescence properties are currently underway. Applications for turn-on sensing of small biorelevant molecules are worth further investigation.

Experimental Section

Cluster **2** was prepared by the ligand-exchange reaction of **1**[7] with 4-OEG-modified thiophenol ($HSC_6H_4(OC_2H_4)_nOCH_3$), which was prepared by coupling 4,4′-dihydroxydiphenyl disulfide[13] with the tosylate ester of poly(ethylene glycol) methyl ether ($M_n \approx 350$) followed by $NaBH_4$ reduction. The thiol (2.4 mmol) was added to a solution of **1** (50 mg) in MeCN (0.020 mmol/20 mL), and the mixture was heated at 60 °C for 6 h. After removal of the solvent, the residue was washed copiously with ether to give **2** as a tan solid (113 mg, 95 %). IR spectroscopy showed the complete disappearance of the absorption bands due to the phenyl groups of **1**. From the ^1H NMR spectrum, the average number of ethylene glycol units was estimated to be six. Elemental analysis calcd (%) for $C_{228}H_{372}Cd_{10}S_{16}O_{84}S_{16}$ $(Cd_{10}S_4(SC_6H_4(OC_2H_4)_6OCH_3)_{12})$: C 44.93, H 6.15, S 8.42; found: C 45.04, H 6.09, S 8.61; no nitrogen was found.

Photoluminescence and excitation spectra were recorded with a JASCO FP-6500 spectrofluorometer equipped with a Hamamatsu Photonics R928 photomultiplier tube detector. An optical filter was mounted in front of the detector window to block out light of wavelengths below 360 nm and thus avoid second-order effects of the excitation light.

Received: April 14, 2006
Published online: July 5, 2006

Keywords: cadmium · cluster compounds · copper · luminescence · sensors

[1] a) R. Krämer, *Angew. Chem.* **1998**, *110*, 804; *Angew. Chem. Int. Ed.* **1998**, *37*, 772; b) N. Shao, Y. Zhang, S. Cheung, R. Yang, W. Chan, T. Mo, K. Li, F. Liu, *Anal. Chem.* **2005**, *77*, 7294; c) R. Méallet-Renault, R. Pansu, S. Amigoni-Gerbier, C. Larpent, *Chem. Commun.* **2004**, 2344; d) S. Kaur, S. Kumar, *Chem. Commun.* **2002**, 2840; e) K. Rurack, M. Kollmannsberger, U. Resch-Genger, J. Daub, *J. Am. Chem. Soc.* **2000**, *122*, 968; f) A. Torrado, G. K. Walkup, B. Imperiali, *J. Am. Chem. Soc.* **1998**, *120*, 609.

[2] a) L. Yang, R. McRae, M. M. Henary, R. Patel, B. Lai, S. Vogt, C. J. Fahrni, *Proc. Natl. Adac. Sci. USA* **2005**, *102*, 11179; b) M. Royzen, Z. Dai, J. W. Canary, *J. Am. Chem. Soc.* **2005**, *127*, 1612; c) Z. Xu, Y. Xiao, X. Qian, J. Cui, D. Cui, *Org. Lett.* **2005**, *7*, 889; d) P. Chen, C. He, *J. Am. Chem. Soc.* **2004**, *126*, 728.

[3] A. L. Rogach, D. V. Talapin, H. Weller in *Colloids and Colloid Assemblies* (Ed.: F. Caruso), Wiley-VCH, Weinheim, **2004**, chap. 2.

[4] a) A. V. Isarov, J. Chrysochoos, *Langmuir* **1997**, *13*, 3142; b) Y. Chen, Z. Rosenzweig, *Anal. Chem.* **2002**, *74*, 5132; c) K. M. Gattás-Asfura, R. M. Leblanc, *Chem. Commun.* **2003**, 2684; d) B. Tang, J. Niu, C. Yu, L. Zhuo, J. Ge, *Chem. Commun.* **2005**, 4184; e) M. T. Fernández-Argüelles, W. J. Jin, J. M. Costa-Fernández, R. Pereiro, A. Sanz-Medel, *Anal. Chim. Acta* **2005**, *549*, 20.

[5] Positive responses have been reported for other metal ions: for Zn^{2+}, see ref. [4b]; for Ag^{+}, see: A. Kumar, S. Kumar, *Chem. Lett.* **1996**, 711; L. Spanhel, H. Weller, A. Fojtik, A. Henglein, *Ber. Bunsen-Ges.* **1987**, *91*, 88.

[6] a) R. D. Adams, B. Zhang, C. J. Murphy, L. K. Yeung, *Chem. Commun.* **1999**, 383; b) F. E. Osterloh, D. P. Hewitt, *Chem. Commun.* **2003**, 1700.

[7] a) T. Hiratani, K. Konishi, *Angew. Chem.* **2004**, *116*, 6069; *Angew. Chem. Int. Ed.* **2004**, *43*, 5943; b) K. Konishi, T. Hiratani, *Chem. Lett.* **2006**, 184.

[8] To prevent disproportionation of Cu^{I}, the titration experiments were conducted in the presence of CH_3CN (2 vol %); see: P. Kanau, R. B. Jordan, *Inorg. Chem.* **2001**, *40*, 3879, and ref. [2a].

[9] Similar red shifts upon interaction with copper(I) ion have been reported for CdS colloids (refs. [4a,b]), for which the generation of a new energy level involving copper is suggested.

[10] The strong complexation did not allow determination of the association constant from the titration profiles, but it is estimated to be larger than $10^7\,M^{-1}$.

 © 2006 Wiley-VCH Verlag GmbH & Co. KGaA, Weinheim

[11] See the Supporting Information.
[12] The reduction of Cu^{II} was further supported by the appearance of new ^{1}H NMR signals due to disulfide formed by the oxidative coupling of the surface thiolates.
[13] R. S. Sengar, V. N. Nemykin, P. Basu, *New J. Chem.* **2003**, *27*, 1115.

 © 2006 Wiley-VCH Verlag GmbH & Co. KGaA, Weinheim

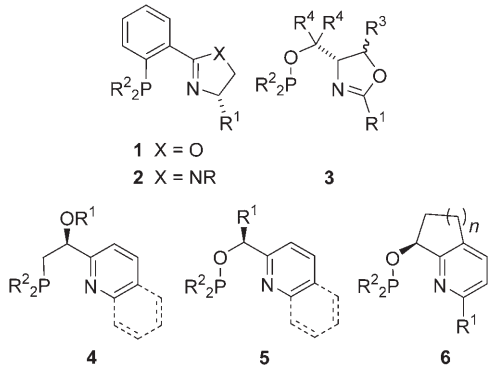
Asymmetric Hydrogenation Catalysts

DOI: 10.1002/anie.200601529

Iridium Catalysts with Bicyclic Pyridine–Phosphinite Ligands: Asymmetric Hydrogenation of Olefins and Furan Derivatives**

*Stefan Kaiser, Sebastian P. Smidt, and Andreas Pfaltz**

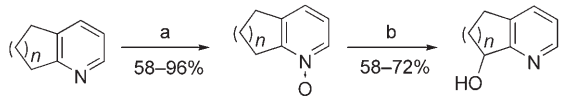
Iridium complexes with chiral N,P ligands have established themselves as efficient catalysts for the asymmetric hydrogenation of olefins, with largely complementary scope to Rh and Ru diphosphane complexes.[1] In contrast to Rh and Ru catalysts, they do not require a coordinating polar group next to the C=C bond. Initial experiments with cationic phosphanyloxazoline (phox)[2] complexes ($[Ir(\mathbf{1})(cod)]^+X^-$) (cod = cyclooctadiene) showed that these catalysts are highly active in the hydrogenation of unfunctionalized tri- and even tetrasubstituted olefins.[3] In this respect, they resemble Crabtree's catalyst, $[(Cy_3P)(pyridine)Ir(cod)]PF_6$ (Cy = cyclohexyl),[4] which provided the stimulus for the development of these catalysts. In these studies, we also found that the choice of solvent and anion is crucial as only in weakly coordinating solvents like dichloromethane or toluene with a virtually non-coordinating anion such as BAr_F (tetrakis[bis-3,5-(trifluoromethyl)phenyl]borate) could high turnover numbers (> 5000) be obtained.[1a,5] Although high enantioselectivities were obtained in the hydrogenation of certain trisubstituted aryl alkenes such as (*E*)-methylstilbene, the application range of Ir-phox catalysts proved to be limited. However, subsequent work has led to new classes of N,P ligands, which have broadened the scope of Ir-catalyzed hydrogenation considerably.[1,6,7]



Among the many structures we investigated, oxazoline-phosphinites such as **3**[1,6a,b] and certain imidazoline analogues[6c] proved to be particularly efficient, giving high enantiomeric excesses with a wide range of unfunctionalized as well as certain functionalized olefins. With the intention of mimicking the coordination sphere of the Crabtree catalysts more closely, we also examined a series of pyridine- and quinoline-derived ligands **4** and **5**.[8] As the results were quite encouraging, we decided to extend our studies to bicyclic analogues of type **6** because we thought that the more rigid conformation imposed by the additional ring could result in even higher enantioselectivities. Here we report the syntheses of a series of pyridyl–phosphinites **6** and their evaluation as ligands for Ir-catalyzed asymmetric hydrogenation.

As shown in the schemes below, ligands of this type are readily accessible from simple, commercially available starting materials via the corresponding pyridyl alcohols. By changing the substituents at the pyridine ring and the P atom, or altering the size of the carbocyclic ring, the steric and electronic properties of these ligands and the coordination geometry can be optimized for a specific substrate.

Ligands with unsubstituted backbones (**6**, $R^1 = H$) were synthesized from commercially available precursors **12–14** via pyridyl alcohols **7–9** (Scheme 1). Oxidation to the corresponding N-oxides **15–17** with aqueous hydrogen peroxide and catalytic amounts of methyltrioxorhenium (MTO),[9] subsequent Boekelheide rearrangement induced by trifluoroacetic anhydride (TFAA), and hydrolysis with aqueous LiOH led to pyridyl alcohols **7–9** in overall yields of 40, 69, and 54%, respectively.[10] Alternatively, **8** could be prepared from 8-hydroxyquinoline by hydrogenation with PtO_2 in CF_3CO_2H. However, the yield of this reaction was only 27%.



Scheme 1. Synthesis of pyridyl alcohols **7–9**: a) 0.5–5 mol% MTO (methyltrioxorhenium), 30% aq. H_2O_2 (2 equiv), CH_2Cl_2, RT; b) TFAA (trifluoroacetic anhydride) (2.5 equiv), CH_2Cl_2, 0°C to RT, 4 h; 2 M LiOH, CH_2Cl_2, RT, 3 h.

The analogous substituted pyridyl alcohols **10** and **11** were synthesized from acetophenone by the five-step sequence

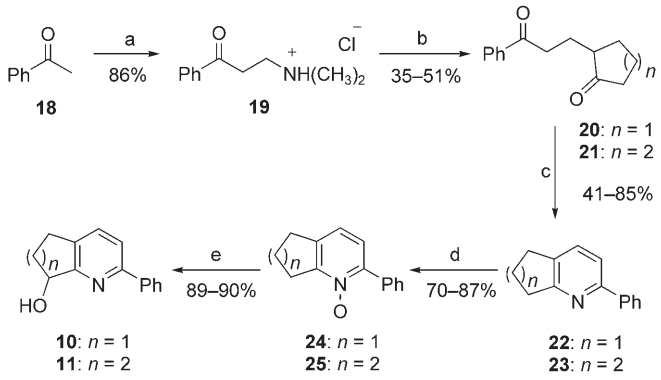
[*] Dr. S. Kaiser, Dr. S. P. Smidt, Prof. Dr. A. Pfaltz
Department of Chemistry
University of Basel
St. Johanns-Ring 19, 4056 Basel (Switzerland)
Fax: (+41) 61-267-1103
E-mail: andreas.pfaltz@unibas.ch

[**] Financial support from the Swiss National Science Foundation and the Federal Commission for Technology and Innovation (KTI) is gratefully acknowledged.

Supporting Information for this article is available on the WWW under http://www.angewandte.org or from the author.

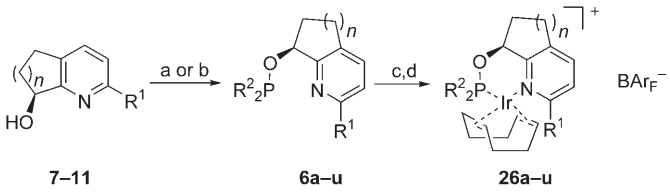
InterScience
© 2006 Wiley-VCH Verlag GmbH & Co. KGaA, Weinheim

shown in Scheme 2 in overall yields of 30 and 10%, respectively.[11] In this case, 3-chloroperbenzoic acid gave better yields of pyridine N-oxides than MTO/H_2O_2.



Scheme 2. Synthesis of pyridyl alcohols **10** and **11**: a) $[H_2C{=}N(CH_3)_2]Cl$ (1 equiv), acetonitrile, reflux, 1 h; b) cyclopentanone morpholine enamine or cyclohexanone pyrrolidine enamine, dioxane, reflux, 16 h; c) HO-NH_3Cl (1 equiv), ethanol, reflux, 3 h; d) *m*-CPBA (1.2 equiv), CH_2Cl_2, 0°C to RT, overnight; e) TFAA (2.5 equiv), CH_2Cl_2, 0°C to RT, 4 h; 2 M LiOH, CH_2Cl_2, RT, 3 h.

The racemic pyridyl alcohols **7**–**11** were resolved by preparative HPLC on a chiral column.[12] This method proved to convenient for preparing ligands on a 0.5 to 5.0-g scale. However, enantioselective routes based on kinetic resolution or asymmetric reduction of the corresponding ketones are available.[13,14] The enantiopure alcohols **7**–**11** were converted into the corresponding phosphinites **6** either by treatment with diaryl (*N*,*N*-diethylamino)phosphane/4,5-dichloroimidazole/NEt_3 in CH_2Cl_2 or by deprotonation with NaH in THF/DMF (9:1) and subsequent treatment with dialkyl chlorophosphane (Scheme 3). The corresponding Ir(cod) complexes

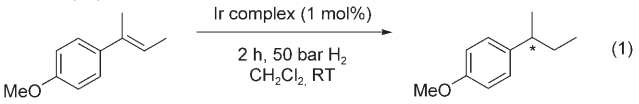


Scheme 3. Synthesis of phosphinite complexes **26a**–**u**: a) Ar_2PNEt_2/4,5-dichloroimidazole/triethylamine (1:1:1, 2 equiv), CH_2Cl_2, 0°C to RT, 1 to 9 d; b) Alk_2PCl (1 equiv), NaH (1.3 equiv), THF/DMF (9:1), 0°C to RT, 1 to 4 d; c) $[Ir(cod)Cl]_2$ (0.5 equiv), CH_2Cl_2, 50°C, 2 h; $NaBAr_F$ (1.3 equiv), RT, 2 min; H_2O, RT, 15 min.

26 were obtained following the standard protocol[3] as orange to red crystalline solids. The absolute configuration of complexes **26c**, **26f**, **26k**, **26o**, **26t**, and **26u** was assigned by X-ray analysis.[13] The absolute configuration of the corresponding phosphinites and pyridyl alcohols was deduced based on these structures.

Complexes **26a**–**u** were evaluated as catalysts in the hydrogenation of a series of alkenes that have previously been used as test substrates.[1] Table 1, which lists a comprehensive data set for alkene **27**, reveals several important trends in the

Table 1: Iridium-catalyzed hydrogenation of (*E*)-2-(4-methoxyphenyl)-2-butene (**27**).[a,b]



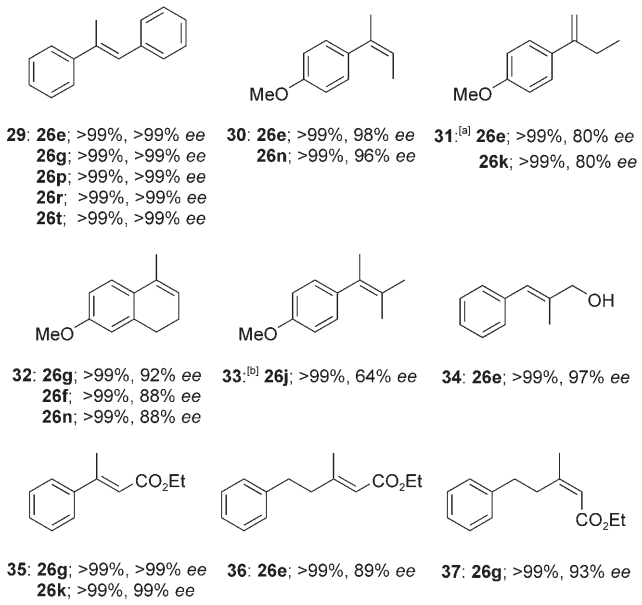
Catalyst	*n*	R^1	R^2	*ee* [%][c]
26a (*R*)	1	H	Ph	78 (*R*)
26b (*R*)	1	H	*o*Tol	74 (*R*)
26c (*R*)	1	H	Cy	68 (*R*)
26d (*R*)	1	H	*t*Bu	72 (*R*)
26e[d] (*R*)	1	Ph	*o*Tol	>99 (*R*)
26f (*R*)	1	Ph	Cy	97 (*R*)
26g (*S*)	1	Ph	*t*Bu	>99 (*S*)
26h (*R*)	2	H	Ph	82 (*R*)
26i (*S*)	2	H	*o*Tol	83 (*S*)
26j (*R*)	2	H	Cy	70 (*R*)
26k (*S*)	2	H	*t*Bu	75 (*S*)
26l (*S*)	2	H	furyl	71 (*S*)
26m[18] (*R*)	2	Me	Ph	86 (*R*)
26n[18] (*R*)	2	Me	*o*Tol	97 (*R*)
26o[18] (*S*)	2	Me	Cy	95 (*S*)
26p[18] (*S*)	2	Me	*t*Bu	97 (*S*)
26q (*S*)	2	Ph	Ph	96 (*S*)
26r (*S*)	2	Ph	*o*Tol	>99 (*S*)
26s (*R*)	2	Ph	Cy	89 (*R*)
26t (*S*)	2	Ph	*t*Bu	96 (*S*)
26u (*S*)	3	H	Ph	82 (*S*)

[a] See Equation (1) for conditions and Refs. [1a, 3] for experimental procedures. [b] Conversion was determined by GC.[3] [c] Determined by chiral HPLC.[3] [d] The diphenylphosphinite analogue formed only catalytically inactive $[IrL_2][BAr_F]$.

observed enantioselectivities. Introduction of a substituent next to the pyridine N atom strongly increases the *ee* obtained (cf. **26b** vs. **26e** and **26i** vs. **26n** and **26r**). For catalysts **26m** and **26q**, which contain a substituted pyridine ring, the enantioselectivities rise substantially when the P-phenyl groups are replaced by *ortho*-tolyl groups, an effect that has also been observed for phox ligands.[3] Di-*tert*-butyl phosphinites (in particular **26g** and **26t**) give better results than the analogous cyclohexyl phosphinites (**26f** and **26s**). For unsubstituted pyridine derivatives **26a**, **26h**, and **26u** the size of the carbocyclic ring seems to have little influence. However, for substituted analogues ($R^1 = Ph$) larger differences are observed between the five- and six-membered ring derivatives (cf. **26g** vs. **26t** and **26f** vs. **26s**). In general, the five-membered ring derivatives induce higher enantioselectivities, although exceptions have been found for other substrates.[15] Three catalysts (**26e**, **26g**, and **26r**) react with essentially 100% enantioselectivity.

Selected results for differently substituted unfunctionalized alkenes **29**–**33**, allylic alcohol **34**, and α,β-unsaturated esters **35**–**37** are listed in Figure 1. A comparison with the results obtained with pyridine- and quinoline-derived ligands **4** and **5** clearly demonstrates that the additional carbocyclic ring improves the enantioselectivity. With the exception of the terminal olefin **31** and the problematic tetrasubstituted alkene **33**, for which no highly selective Ir catalyst has yet been reported,[16] the enantiomeric excesses match or, as in

 © 2006 Wiley-VCH Verlag GmbH & Co. KGaA, Weinheim



29: **26e**; >99%, >99% *ee*
26g; >99%, >99% *ee*
26p; >99%, >99% *ee*
26r; >99%, >99% *ee*
26t; >99%, >99% *ee*

30: **26e**; >99%, 98% *ee*
26n; >99%, 96% *ee*

31:[a] **26e**; >99%, 80% *ee*
26k; >99%, 80% *ee*

32: **26g**; >99%, 92% *ee*
26f; >99%, 88% *ee*
26n; >99%, 88% *ee*

33:[b] **26j**; >99%, 64% *ee*

34: **26e**; >99%, 97% *ee*

35: **26g**; >99%, >99% *ee*
26k; >99%, 99% *ee*

36: **26e**; >99%, 89% *ee*

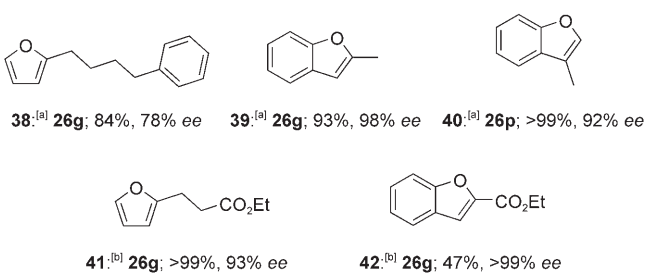
37: **26g**; >99%, 93% *ee*

Figure 1. Selected hydrogenation results; see Table 1 for reaction conditions. [a] 30 min, 1 bar H_2; [b] 2 mol% catalyst.

the case of substrate **30**, surpass the best values reported to date.[1]

Subsequent screening of other potential substrates showed that these catalysts also allow the asymmetric reduction of furan derivatives, a class of substrate for which no efficient enantioselective catalysts were known. In previous studies of furyl-substituted alkenes, we had found that with certain Ir complexes derived from oxazoline–dialkylphosphinite ligands **3**, both the olefinic C=C bond and the furan π system were reduced.[17] The stereoselectivities were, however, moderate. Catalysts **26g** and **26p** proved to be more efficient and induced good to excellent enantioselectivities in the hydrogenation of a series of substituted furans and benzofurans (Figure 2). As expected, the benzene ring of substrates **40** and **42** was not reduced. Ligands with bulky electron-rich $(t\mathrm{Bu})_2$P groups were found to be best suited for this class of substrate. Ligands with cyclohexyl substituents at the P atom gave lower conversion and *ee*, whereas catalysts with analogous diphenylphosphinite ligands showed essentially no activity. Because of the low reactivity of the furan and benzofuran π systems, elevated temperatures and relatively long reaction times were necessary. The benzofuran carboxylate ester **42**, in particular, reacted only sluggishly, albeit with virtually perfect enantioselectivity. Overall, catalysts like **26g** and **26p** open up an attractive enantioselective route to tetrahydrofuran and benzodihydrofuran systems, which are structural motifs found in many natural products and biologically active compounds.

In summary, the results obtained so far indicate a remarkably broad scope for Ir catalysts derived from pyridine–phosphinite ligands **6**. Moreover, we have recently found that complexes **26e**, **26g**, and **26r** are also highly efficient catalysts for the asymmetric hydrogenation of purely alkyl-substituted olefins.[15] Thus, we are confident that these catalysts will find many further applications in asymmetric hydrogenation.



38:[a] **26g**; 84%, 78% *ee*

39:[a] **26g**; 93%, 98% *ee*

40:[a] **26p**; >99%, 92% *ee*

41:[b] **26g**; >99%, 93% *ee*

42:[b] **26g**; 47%, >99% *ee*

Figure 2. Representative hydrogenation results for furan and benzofuran derivatives. [a] 1 mol% catalyst, 50 bar H_2, 24 h, 40°C; [b] 2 mol% catalyst, 100 bar H_2, 24 h, 40°C.

Received: April 18, 2006
Published online: July 5, 2006

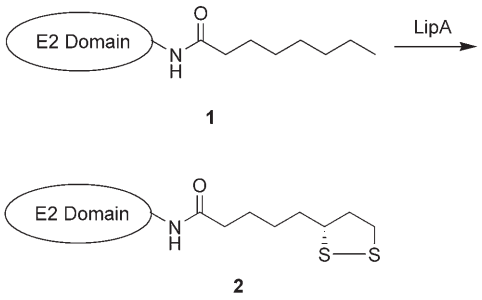
Keywords: asymmetric catalysis · hydrogenation · iridium · ligand design · N,P ligands

[1] a) A. Pfaltz, J. Blankenstein, R. Hilgraf, E. Hörmann, S. McIntyre, F. Menges, M. Schönleber, S. P. Smidt, B. Wüstenberg, N. Zimmermann, *Adv. Synth. Catal.* **2002**, *344*, 33 – 44; b) X. Cui, K. Burgess, *Chem. Rev.* **2005**, *105*, 3272 – 3297; c) K. Källström, I. Munslow, P. G. Andersson, *Chem. Eur. J.* **2006**, *12*, 3194 – 3200.
[2] G. Helmchen, A. Pfaltz, *Acc. Chem. Res.* **2000**, *33*, 336 – 345.
[3] A. Lightfoot, P. Schnider, A. Pfaltz, *Angew. Chem.* **1998**, *110*, 3047 – 3050; *Angew. Chem. Int. Ed.* **1998**, *37*, 2897 – 2899.
[4] R. H. Crabtree, *Acc. Chem. Res.* **1979**, *12*, 331 – 337.
[5] S. P. Smidt, N. Zimmermann, M. Studer, A. Pfaltz, *Chem. Eur. J.* **2004**, *10*, 4685 – 4693.
[6] a) J. Blankenstein, A. Pfaltz, *Angew. Chem.* **2001**, *113*, 4577 – 4579; *Angew. Chem. Int. Ed.* **2001**, *40*, 4445 – 4447; b) F. Menges, A. Pfaltz, *Adv. Synth. Catal.* **2002**, *344*, 40 – 44; c) F. Menges, M. Neuburger, A. Pfaltz, *Org. Lett.* **2002**, *4*, 4713 – 4716; d) S. P. Smidt, F. Menges, A. Pfaltz, *Org. Lett.* **2004**, *6*, 2023 – 2026; e) R. Hilgraf, A. Pfaltz, *Adv. Synth. Catal.* **2005**, *347*, 61 – 77.
[7] For related work from other research groups, see: a) Y. Fan, X. Cui, K. Burgess, M. B. Hall, *J. Am. Chem. Soc.* **2004**, *126*, 16688 – 16689; b) X. Cui, Y. Fan, M. B. Hall, K. Burgess, *Chem. Eur. J.* **2005**, *11*, 6859 – 6868; c) K. Källström, C. Hedberg, P. Brandt, A. Bayer, P. G. Andersson, *J. Am. Chem. Soc.* **2004**, *126*, 14308 – 14309; d) C. Hedberg, K. Källström, P. Brandt, L. K. Hansen, P. G. Andersson, *J. Am. Chem. Soc.* **2006**, *128*, 2995 – 3001; e) D. Liu, W. Tang, X. Zhang, *Org. Lett.* **2004**, *6*, 513 – 516; f) T. Bunlaksananusorn, K. Polborn, P. Knochel, *Angew. Chem.* **2003**, *115*, 4071 – 4073; *Angew. Chem. Int. Ed.* **2003**, *42*, 3941 – 3943; g) T. Focken, G. Raabe, C. Bolm, *Tetrahedron: Asymmetry* **2004**, *15*, 1693 – 1706; h) P. G. Cozzi, F. Menges, S. Kaiser, *Synlett* **2003**, 833 – 836.
[8] a) W. J. Drury III, N. Zimmermann, M. Keenan, M. Hayashi, S. Kaiser, R. Goddard, A. Pfaltz, *Angew. Chem.* **2004**, *116*, 72 – 76; *Angew. Chem. Int. Ed.* **2004**, *43*, 70 – 74; b) for other pyridine-derived N,P ligands, see the review: G. Chelucci, G. Orrù, G. A. Pinna, *Tetrahedron* **2003**, *59*, 9471 – 9515, and ref. [7f].
[9] C. Copéret, H. Adolfsson, T. A. V. Khuong, A. K. Yudin, K. B. Sharpless, *J. Org. Chem.* **1998**, *63*, 1740 – 1741.
[10] a) V. C. Boekelheide, W. J. Linn, *J. Am. Chem. Soc.* **1954**, *76*, 1286 – 1291; b) M. Uchida, S. Morita, M. Chihiro, T. Kanbe, K. Yamasaki, Y. Yabuuchi, K. Nakagawa, *Chem. Pharm. Bull.* **1989**,

 © 2006 Wiley-VCH Verlag GmbH & Co. KGaA, Weinheim

37, 1517 – 1523; c) C. Fontenas, E. Bejan, H. A. Haddou, G. G. A. Balavoine, *Synth. Commun.* **1995**, *25*, 629 – 633.
[11] a) D. Sielemann, R. Keuper, N. Risch, *J. Prakt. Chem.* **1999**, *341*, 487 – 491; b) G. Kinast, L. F. Tietze, *Angew. Chem.* **1976**, *88*, 261 – 262; *Angew. Chem. Int. Ed. Engl.* **1976**, *15*, 239 – 240.
[12] See the Supporting Information; **9** had to be converted into the corresponding diastereomeric (1*S*)-camphanoate before HPLC separation.
[13] S. Kaiser, Dissertation, University of Basel, **2005**.
[14] C. Mazet, S. Roseblade, V. Köhler, A. Pfaltz, *Org. Lett.* **2006**, *8*, 1879 – 1882.
[15] S. Bell, B. Wüstenberg, S. Kaiser, F. Menges, T. Netscher, A. Pfaltz, *Science* **2006**, *311*, 642 – 644.
[16] For highly enantioselective Zr catalysts, see: M. V. Troutman, D. H. Appella, S. L. Buchwald, *J. Am. Chem. Soc.* **1999**, *121*, 4916 – 4917.
[17] B. Wüstenberg, A. Pfaltz, published in: B. Wüstenberg, Dissertation, University of Basel, **2003**.
[18] For preparation of complexes **26m–p** see the Supporting Information.

 © 2006 Wiley-VCH Verlag GmbH & Co. KGaA, Weinheim



Scheme 1. Insertion of sulfur atoms into octanoyl substrates to form lipoyl groups.

Biosynthesis

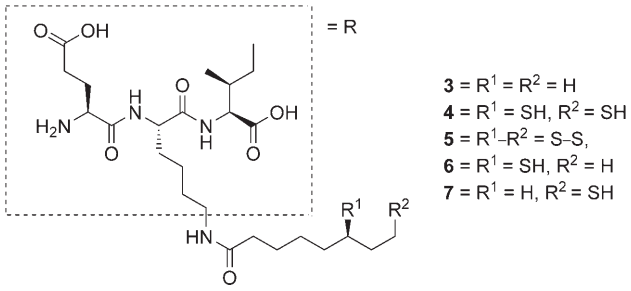
DOI: 10.1002/anie.200601910

Lipoyl Synthase Inserts Sulfur Atoms into an Octanoyl Substrate in a Stepwise Manner**

*Paul Douglas, Marco Kriek, Penny Bryant, and Peter L. Roach**

Lipoyl synthase (LipA) is required for the final step in the biosynthesis of lipoyl groups, the insertion of sulfur atoms at C6 and C8 of octanoyl groups (Scheme 1).[1] The octanoyl groups are found attached through an amide linkage to a lysine residue in a sequence motif that is conserved within a small family of protein domains[2] that include the H-protein of the glycine cleavage system[3] and the E2 subunit of oxoacid dehydrogenases.[4] After attachment of the octanoyl groups,[5–7] the substrates undergo sulfur insertion by LipA,[1] a member of the "radical *S*-adenosyl L-methionine" family.[8] Biochemical studies have shown that it contains two essential [4Fe-4S] clusters[9] and that one of these clusters is used to generate 5′-deoxyadenosyl radicals (Ado•) through the reductive cleavage of S-adenosyl L-methionine (AdoMet). The lipoyl forming reaction requires two hydrogen atoms to be removed from the octanoyl group, one from C6 and the other from C8, so that the overall reaction utilizes two equivalents of AdoMet to form each lipoyl group.[10] LipA has been shown to donate both of the inserted sulfur atoms[11] that were proposed to originate from a [4Fe-4S] cluster.[12] Recently, we reported that a short octanoyl peptide, which corresponds in sequence to the lipoylation site of the E2 subunit, could function as a substrate for LipA.[13] Peptide substrates have now been used to investigate the order of sulfur-insertion steps and hence clarify the structure of a key intermediate on the reaction pathway.

The formation of lipoyl groups was monitored in a reaction by using *Sulfolobus solfataricus* P2 LipA with an octanoyl substrate tripeptide (0.5 mole equiv; **3**,), AdoMet,



and dithionite as a reductant. LipA is not catalytic during assays in vitro, producing substoichiometric quantities of lipoyl products with either octanoyl-protein[10] or octanoyl-peptide substrates.[13] To investigate the formation of any intermediate species, the reaction was stopped by acidification before reaching completion (after 20 min), the precipitated protein was pelleted by centrifugation, and the supernatant analyzed by LCMS. Four peptide species were eluted over the time range from 22 to 25 min (Table 1). The peptide at 24.4 min corresponds to the unreacted octanoyl substrate **3**, whereas new species at 22.4 and 23.4 min correspond to the expected protonated product masses of lipoyl **5** and dihydrolipoyl products **4**, respectively. The final species at 23.2 min coelutes with the dihydrolipoyl product and corresponds to a monothiolated species (either **6** or **7**). Analysis of later time points (up to 2 h) showed that the amount of this monothiolated species decreased with time and that there was a

[*] P. Douglas, Dr. M. Kriek, P. Bryant, Dr. P. L. Roach
School of Chemistry
University of Southampton
Southampton SO171BJ (UK)
Fax: (+44) 2380-596-805
E-mail: plr2@soton.ac.uk

[**] This research was supported by grants from the Royal Society and Engineering and Physical Sciences Research Council to PLR.

Supporting information for this article is available on the WWW under http://www.angewandte.org or from the author.

 © 2006 Wiley-VCH Verlag GmbH & Co. KGaA, Weinheim

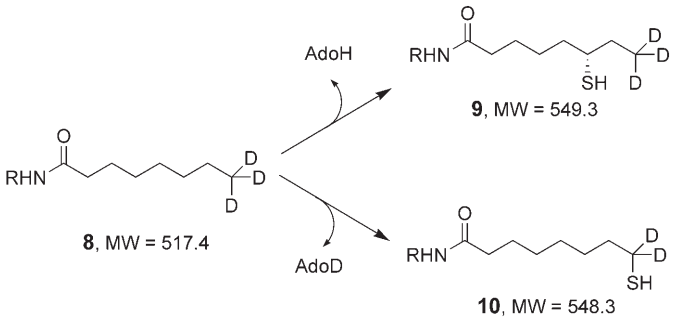
Table 1: LCMS analysis of substrate and product peptides from the LipA reaction.

t_R [min]	Observed mass [m/z]	Calculated mass for MH^+ [Da]	Difference from substrate	Comment
22.4	577.5	577.3	+ 2S−2H	lipoyl product, **5**
23.2	547.3	547.3	+ S	6-thiooctanoyl peptide, **6** or 8-thiooctanoyl peptide, **7**
23.4	579.2	579.3	+ 2S	dihydrolipoyl product, **4**
24.4	515.3	515.3	–	substrate, **3**

concomitant increase in the lipoyl products. This strongly suggests that the monothiolated species represents an intermediate. A similar monothiolation reaction has been observed by mass spectrometry for *E. coli* LipA reacting with an octanoyl protein domain.[10]

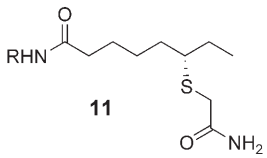
To investigate the nature of the interaction of the monothiolated species with LipA, the assay protocol was modified by using a 5-kDa molecular-weight cut-off filter to remove the LipA. Under these conditions, the proportion of monothiolated species observed by LCMS of the filtrate was greatly reduced (< 10%), indicating that under nondenaturing conditions, the intermediate had remained bound to the native protein and therefore acidic conditions were required for efficient release of the intermediate from LipA. The observation that both of the transferred sulfur atoms originate from the same LipA molecule[11] is also consistent with a tightly bound intermediate that is not in rapid equilibrium with the bulk solution.

If the reaction proceeds by an ordered insertion of sulfur atoms, two potential structures for the monothiolated species can be envisaged: insertion of a sulfur atom at either C6 or C8 of the octanoyl chain. In an effort to identify the order of C–S bond formation, the 8,8,8-trideuterooctanoyl peptide **8** was synthesized and incubated with LipA. With this substrate, two monothiolated peptides that differ in molecular weight could arise from abstraction of a hydrogen atom from C6 or a deuterium atom from C8 (Scheme 2). The results showed the exclusive removal of a hydrogen atom from C6, supporting the formation of a 6-thiooctanoyl intermediate from this substrate (m/z for $MH^+ = 550.3$). Relative to the proteo substrate **3**, the deutero substrate **8** resulted in minute quantities of the lipoyl product. This small amount could not be accurately quantified by using the LCMS data, but the observation is consistent with a large isotope effect on the second sulfur-insertion step.[14]



Scheme 2. Potential outcomes from sulfur insertion into an 8,8,8-trideuterooctanoyl substrate peptide.

The possibility of a mechanism proceeding with a random order of sulfur insertion, biased by the previously observed[14] isotope effect at C8, cannot be excluded by this experiment. This issue was resolved by the spectroscopic determination of the regiochemistry of the initial sulfur insertion. Sufficient material for this analysis was obtained by combining the products from 14 reactions with the proteo-substrate **3**. To ensure the isolation and characterization of the monothiolated peptide without potentially confusing disulfide formation, the crude reaction products were reduced, alkylated with iodoacetamide, and then purified by HPLC. A COSY spectrum facilitated the identification of the signals from protons attached to C6, C7, and C8 of the monothiolated octanoyl group. These spectra indicate unequivocally the exclusive formation of the derivative of the 6-thio intermediate **11** (see Figure 1).



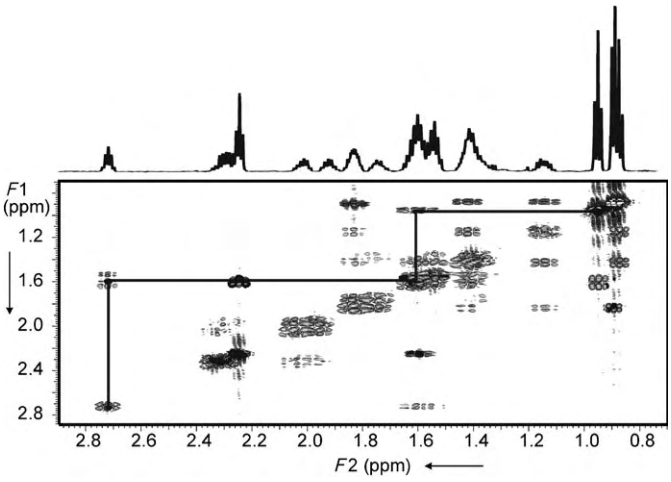


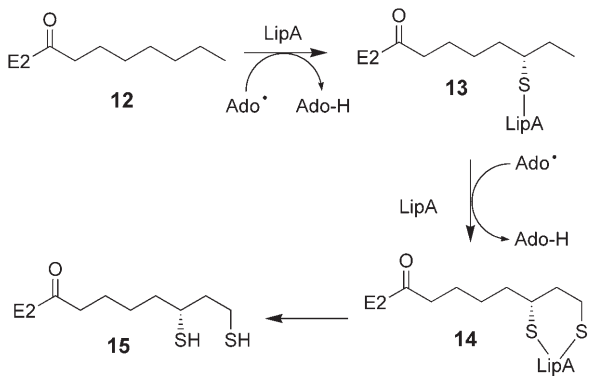
Figure 1. H,H COSY spectrum of the alkylated 6-thio-octanoyl tripeptide **11**. Lines have been added to indicate the key correlations: 0.95 (octanoyl C8 methyl) shows a cross-peak to 1.58 (octanoyl C7 CH_2), which in turn shows a cross-peak to the multiplet at 2.72 (octanoyl C6, CH).

Studies in vivo comparing the efficiency with which deuterium-labeled 6- and 8- thiooctanoic acids were converted into lipoic acid have shown that both can function as precursors, but intriguingly, the 8-thio compound is more efficiently incorporated.[15] Although there may be sufficient flexibility in the active site to accommodate either monothiolated compound, it is clear that when LipA is presented with an octanoyl substrate, the substrate is first converted to

 © 2006 Wiley-VCH Verlag GmbH & Co. KGaA, Weinheim

an enzyme bound 6-thiooctanoyl intermediate, which is subsequently converted to the lipoyl product.

The accumulation of the 6-thiooctanoyl intermediate, together with the observed substantial deuterium isotope effect at C8, is consistent with a mechanism (Scheme 3) in



Scheme 3. Proposed mechanism for lipoyl group formation by LipA. The regiochemistry for the sulfur-insertion steps are shown. The 5′-deoxyadenosyl radicals are derived from the reductive cleavage of S-adenosyl methionine.

which sulfur is first inserted at C6 to form an enzyme bound intermediate **13**. In a subsequent rate determining step, the second sulfur atom is inserted at C8, suggesting an energy profile for the reaction that appears to reflect the relative bond strengths of the primary (C8) and secondary (C6) C–H bonds that must be cleaved to form lipoyl groups.

Received: May 15, 2006
Published online: July 11, 2006

Keywords: biosynthesis · cofactors · enzyme models · insertion · lipoic acid

[1] X. Zhao, J. R. Miller, Y. Jiang, M. A. Marletta, J. E. Cronan, *Chem. Biol.* **2003**, *10*, 1293.
[2] R. N. Perham, *Annu. Rev. Biochem.* **2000**, *69*, 961.
[3] T. J. Vandenboom, K. E. Reed, J. E. Cronan, *J. Bacteriol.* **1991**, *173*, 6411.
[4] L. J. Reed, M. L. Hackert, *J. Biol. Chem.* **1990**, *265*, 8971.
[5] T. W. Morris, K. E. Reed, J. E. Cronan, *J. Bacteriol.* **1995**, *177*, 1.
[6] S. T. Ali, A. J. Moir, P. R. Ashton, P. C. Engel, J. R. Guest, *Mol. Microbiol.* **1990**, *4*, 943.
[7] N. M. Nesbitt, C. Baleanu-Gogonea, R. M. Cicchillo, K. Goodson, D. F. Iwig, J. A. Broadwater, J. A. Haas, B. G. Fox, S. J. Booker, *Protein Expression Purif.* **2005**, *39*, 269.
[8] H. J. Sofia, G. Chen, B. G. Hetzler, J. F. Reyes-Spindola, N. E. Miller, *Nucleic Acids Res.* **2001**, *29*, 1097.
[9] R. M. Cicchillo, K. H. Lee, C. Baleanu-Gogonea, N. M. Nesbitt, C. Krebs, S. J. Booker, *Biochemistry* **2004**, *43*, 11770.
[10] R. M. Cicchillo, D. F. Iwig, A. D. Jones, N. M. Nesbitt, C. Baleanu-Gogonea, M. G. Souder, L. Tu, S. J. Booker, *Biochemistry* **2004**, *43*, 6378.
[11] R. M. Cicchillo, S. J. Booker, *J. Am. Chem. Soc.* **2005**, *127*, 2860.
[12] J. R. Miller, R. W. Busby, S. W. Jordan, J. Cheek, T. F. Henshaw, G. W. Ashley, J. B. Broderick, J. E. Cronan, Jr., M. A. Marletta, *Biochemistry* **2000**, *39*, 15166.
[13] P. Bryant, M. Kriek, R. J. Wood, P. L. Roach, *Anal. Biochem.* **2006**, *351*, 44.
[14] R. J. Parry, *J. Am. Chem. Soc.* **1977**, *99*, 6464.
[15] R. H. White, *J. Am. Chem. Soc.* **1980**, *102*, 6605.

 © 2006 Wiley-VCH Verlag GmbH & Co. KGaA, Weinheim

Biocatalytic Alkene Cleavage

DOI: 10.1002/anie.200601574

Biocatalytic Single-Step Alkene Cleavage from Aryl Alkenes: An Enzymatic Equivalent to Reductive Ozonization**

*Harald Mang, Johannes Gross, Miguel Lara, Christian Goessler, Hans E. Schoemaker, Georg M. Guebitz, and Wolfgang Kroutil**

Driven by the need for mild and selective oxidation methods as well as by increased public awareness of hazards derived from chemical production, environmentally benign oxidation methods have gained increasing importance.[1] Alkene cleavage[2] to give aldehydes or ketones is a very frequently used method in synthetic organic chemistry[3] to 1) introduce oxygen functionalities into molecules, 2) split selectively large compounds, and 3) remove protecting groups.[3g] Among the methods currently available for the chemical oxidative cleavage of alkenes, reductive ozonolysis is considered as the "cleanest".[4] In practice, however, it has several drawbacks, since it depends on special equipment (ozonizer), low temperature (generally −78 °C), and a stoichiometric amount of an additional reducing reagent (e.g. dimethyl sulfide, zinc, hydrogen, phosphines) for reductive workup. Furthermore, special precaution is required, since serious accidents arising from explosions have been reported.[5] Other methods involving metal-based oxidants[6] require (at least) stoichiometric amounts of salts or peroxides and are plagued by limited chemo-, regio-, and stereoselectivity. Over-oxidation of the aldehyde to the corresponding acid as side reaction is in most cases unavoidable. The only catalytic method employing molecular oxygen needs a Co^{II}[7] catalyst, is restricted to isoeugenol-type substrates, and displays moderate chemoselectivity.

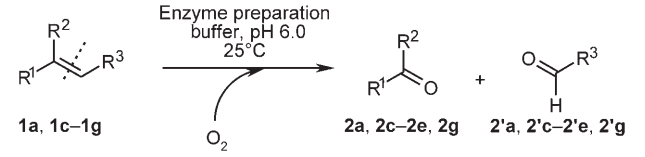
[*] Dr. H. Mang, J. Gross, M. Lara, C. Goessler, Prof. W. Kroutil
Department of Chemistry, Organic and Bioorganic Chemistry
Research Centre Applied Biocatalysis
University of Graz
Heinrichstrasse 28, 8010 Graz (Austria)
Fax: (+43) 316-380-9840
E-mail: wolfgang.kroutil@uni-graz.at
Prof. H. E. Schoemaker
DSM Research, Life Science Products
P.O. Box 18, 6160 MD Geleen (The Netherlands)
Prof. G. M. Guebitz
Institute of Environmental Biotechnology
Research Centre Applied Biocatalysis
University of Technology
Petersgasse 12, 8010 Graz (Austria)

[**] This study was financed by the Austrian Science Fund (FWF Project P18381). Initial experiments were performed within the Research Centre Applied Biocatalysis supported by DSM, FFG, SFG, Province of Styria and City of Graz.

Supporting information for this article is available on the WWW under http://www.angewandte.org or from the author.

As a consequence, novel or improved methods for alkene cleavage are being sought.[6b–e,i,8] Enzymatic alkene cleavage has been observed 1) as a minor (undesired) side-reaction on the analytical scale catalyzed by peroxidases,[9] 2) with a combination of lipoxygenases and hydroperoxide lyases for specific substrates,[10] and 3) on an analytical scale employing molecular oxygen as oxidant using certain mono-[11] or dioxygenases[12] displaying high substrate specificity.[13] To our knowledge, a method for biocatalytic oxidative alkene cleavage has not been developed to date, which can be employed on preparative scale.

In a screening for microorganisms capable of oxidizing alkenes in allylic position, we were not able to identify any hit. Nevertheless, for one fungus, namely *Trametes hirsuta* GFCC047[14] we observed the disappearance of the starting material (*E*)-1-phenyl-1-butene (**1a**; Scheme 1) and the

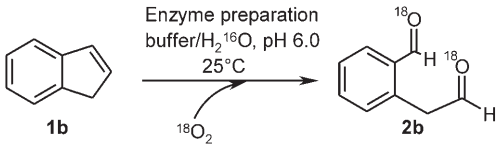


	1a	1c	1d	1e	1f	1g
R^1	Ph	*p*-$MeOC_6H_4$	*p*-$MeOC_6H_4$	Ph	$PhCH_2$	Ph
R^2	H	H	H	H	H	CH_3
R^3	C_2H_5	CH_3	H	H	H	H

Scheme 1. Biocatalytic alkene cleavage employing molecular oxygen. For **1b**→**2b** see Scheme 2.

formation of an unexpected product, which was identified as benzaldehyde. To demonstrate that this is a biocatalyzed reaction, the transformation was repeated with an enzyme preparation inactivated by heat. In this case no reaction was observed, which confirmed our assumption of a biocatalytic reaction. Since biocatalytic conversions in synthetic applications are becoming increasingly important,[15] we aimed to develop a novel biocatalytic procedure for reductive ozonization.

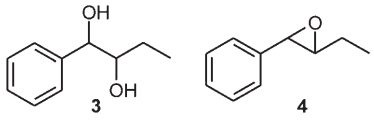
For the identification of the cleavage product(s), a cyclic alkene, such as indene (**1b**; Scheme 2), was envisaged as substrate, since it was expected to give a single product in which both biooxidation cleavage products are present. Thus, transformation of **1b** yielded the corresponding dialdehyde **2b** as shown by GC–MS and comparison with independently synthesized reference material. Indene (**1b**) was also used to elucidate the origin of the two oxygen atoms introduced. By performing the experiments with ^{18}O-labeled molecular oxygen with a cell-free extract, we could show by GC–MS analysis that both oxygen atoms in the two aldehyde frag-



Scheme 2. Biocatalytic alkene cleavage of indene (**1b**) leading to the corresponding dialdehyde.

 © 2006 Wiley-VCH Verlag GmbH & Co. KGaA, Weinheim

ments are labeled. As a blank experiment we performed the experiment in ^{18}O-labeled water using $^{16}O_2$. In this experiment none of the two oxygen atoms was labeled; thus both oxygen atoms originate from molecular O_2 (Scheme 1). Although these experiments are already a strong indication that this is a one-step reaction catalyzed by a dioxygenase,[12] and not a stepwise mechanism as found in the cleavage of β-carotene,[11] possible intermediates in a stepwise transformation of **1a**, such as the diol **3** or the epoxide **4**, were tested. However,



3 **4**

neither **3** nor **4** were transformed to the corresponding aldehyde; thus, neither of these two compounds is an intermediate. Therefore the transformation is a single-step alkene-cleavage reaction catalyzed by an enzyme employing molecular oxygen as the only oxidant (Scheme 2). In contrast to non-enzymatic methods, the reaction can be performed in an aqueous environment at ambient temperature without additional reagents except molecular oxygen.

To achieve high conversion, oxygen saturation, or even better elevated oxygen pressure, is required. To reach such conditions on a one-milliliter scale in parallel for testing, we exploited the catalase activity, which was also present in the enzyme preparation. Thus, a hydrogen peroxide solution was added to the reaction mixture in a GC glass vial (1.5 mL) which was quickly closed with a rubber seal. The hydrogen peroxide was disproportionated by the catalase to yield water and molecular oxygen within seconds giving a theoretical overpressure of approximately 2 bar. Employing this assay with a cell-free extract of *Trametes hirsuta* GFCC047 the conversion of **1a** was increased from 10% to 44% (Table 1, entry 1). An even better substrate was *trans*-anethole (**1c**), which was converted into anisaldehyde (**2c**) at 83% conversion with excellent chemoselectivity (94%, Table 1, entry 3). Most remarkably, no measurable over-oxidation to the corresponding carboxylic acid was observed.

Table 1: Results of the biocatalytic alkene cleavage of various alkenes.

Entry	Substrate[a]	Prod. [%][b]	Chemosel. [%][c]
1	(*E*)-1-phenyl-1-butene (**1a**)	44	72
2	indene (**1b**)	71	88
3	*trans*-anethole (**1c**)	83	94
4	4-methoxystyrene (**1d**)	32	89
5	styrene (**1e**)	25	94
6	allylbenzene (**1f**)	< 0.1	n.a.
7	*o*-methylstyrene	10	> 99
8	*p*-methylstyrene	26	90
9	*p*-aminostyrene	11	> 99
10	*p*-*t*Bu styrene	26	92
11	*m*-chlorostyrene	20	88
12	α-methylstyrene (**1g**)	26	> 99

[a] Conditions: cell-free enzyme preparation of *Trametes hirsuta* GFCC047, performed in GC vials under oxygen pressure, with 6 g L^{-1} substrate concentration, 25 °C, pH 6.0. [b] GC yield, 24 h reaction time, ratio of formed aldehyde/ketone to initial substrate concentration. [c] Ratio of aldehyde/ketone formed to all compounds formed; n.a. not applicable.

Monosubstituted alkenes, such as 4-methoxystyrene (**1d**) are also converted. Substituting the *para*-methoxy moiety of **1d** by hydrogen led only to a slight decrease in activity (styrene (**1e**), Table 1, entry 5). For allyl benzene (**1f**) no conversion was observed, probably because the C=C bond is not conjugated to the aromatic system. It is of note that even a sterically more demanding *ortho*-substituted styrene, such as *o*-methyl styrene (Table 1, entry 7), was converted. With *p*-amino styrene (Table 1, entry 9), the amino group was not touched, and a highly chemoselective alkene cleavage led exclusively to *p*-aminobenzaldehyde with > 99% chemoselectivity. Even ketones are accessible, for instance, the transformation of α-methyl styrene (**1g**) also occurred with absolute chemoselectivity (> 99%) yielding acetophenone (Table 1, entry 12).

To increase the solubility of the substrate in the aqueous phase ethanol can be used as cosolvent up to 25% v/v. The optimum activity is at 15% v/v. In other reactions the substrate concentration was varied, and it can be increased up to 2.7 mol L^{-1} (400 g L^{-1}) for *trans*-anethole (**1c**). The high substrate concentration possible emphasizes the potential of the method for preparative transformations.

For performing the alkene cleavage on a preparative scale, a hydrogenation apparatus (Parr 3910) was adapted to work under oxygen pressure. A constant pressure of 2 bar of molecular oxygen was applied on the reaction mixture. Employing 3 g of lyophilized cells, **1c** was cleaved with 81% conversion within 24 h.

In conclusion, the described novel biocatalytic alkene-cleavage method is a simple, benign, and "green" alternative to chemical methods. It does not require specialized equipment (ozonizer) or chemicals (reducing agents, oxidizing salts) and does not produce any waste. It requires the most innocuous oxidant, namely oxygen. The highest possible achievable atom efficiency[16] for alkene cleavage can only be reached by using molecular oxygen, which is achieved in the biocatalytic method presented. We have demonstrated that the biocatalytic alkene cleavage described extends the repertoire of biocatalytic reactions available for organic synthesis.

Experimental Section

Preparative-scale biocatalytic alkene cleavage under oxygen pressure: Lyophilized cells of *Trametes hirsuta* GFCC047 (3 g) were rehydrated with Bis–Tris buffer (125 mL, 50 mM, pH 6; Bis–Tris = 2,2-bis(hydroxyethyl)iminotris(hydroxymethyl)methane) for 30 min on a rotary shaker (25 °C, 130 rpm). The mixture was placed into the reaction vessel (450 mL) of the "Hydrogenation Apparatus Parr 3910" and *trans*-anethole (**1c**; 0.6 mL, 0.59 g, 3.9 mmol) and EtOH (1.7 mL) were added. The atmosphere was saturated with pure O_2, and then the oxygen pressure was adjusted to 2 bar. After 24 h of agitation at 22 °C under constant oxygen pressure (2 bar), the reaction mixture was extracted with EtOAc (4 × 50 mL) and centrifuged after each extraction step (8000 rpm, 20 min) to achieve phase separation. The cells were removed by filtration from the aqueous solution. The aqueous solution was then extracted with EtOAc (50 mL). The combined organic phase was dried with Na_2SO_4, filtered, and concentrated. A conversion of 81% *p*-anisaldehyde (**2c**) was

 © 2006 Wiley-VCH Verlag GmbH & Co. KGaA, Weinheim

determined by GC analysis. Column chromatography (50 g silica gel, petroleum ether/ethyl acetate 20:1) gave 0.31 g of **2 c** (57% yield of isolated product).

Received: April 21, 2006
Published online: July 20, 2006

Keywords: alkenes · biocatalysis · oxidation · oxygen · ozonolysis

[1] a) *Modern Oxidation Methods* (Ed.: J.-E. Bäckvall), Wiley, Weinheim, **2004**; b) G.-J. ten Brink, I. W. C. E. Arends, R. A. Sheldon, *Chem. Rev.* **2004**, *104*, 4105 – 4123; c) R. Noyori, M. Aoki, K. Sato, *Chem. Commun.* **2003**, 1977 – 1986; d) M. Poliakoff, J. M. Fitzpatrick, T. R. Farren, P. T. Anastas, *Science* **2002**, *297*, 807 – 810; e) K. Sato, M. Hyodo, M. Aoki, X.-Q. Zheng, R. Noyori, *Tetrahedron* **2001**, *57*, 2469 – 2476.

[2] a) F. E. Kühn, R. W. Fischer, W. A. Hermann, T. Weskamp in *Transition Metals for Organic Synthesis*, *Vol. 2* (Eds.: M. Beller, C. Bolm), Wiley-VCH, Weinheim, **2004**, pp. 427 – 436; b) D. G. Lee, T. Chen in *Comprehensive Organic Synthesis*, *Vol. 7* (Eds.: B. M. Trost, I. Fleming), Pergamon, Oxford, **1991**, pp. 541 – 591; c) M. Hudlicky, *Oxidation in Organic Chemistry*, ACS Monograph 186, American Chemical Society, Washington, DC, **1990**.

[3] A selection of recent examples yielding aldehydes: employing ozone: a) I. Paterson, G. J. Florence, A. C. Heimann, A. C. Mackay, *Angew. Chem.* **2005**, *117*, 1154 – 1157; *Angew. Chem. Int. Ed.* **2005**, *44*, 1130 – 1133; b) A. Wrobleski, K. Sahasrabudhe, J. Aube, *J. Am. Chem. Soc.* **2004**, *126*, 5475 – 5481; c) X. Peng, D. Bondar, L. A. Paquette, *Tetrahedron* **2004**, *60*, 9589 – 9598; employing $OsO_4/NaIO_4$: d) T. E. Nielsen, M. Meldal, *Org. Lett.* **2005**, *7*, 2695 – 2698; e) S. Takahashi, K. Souma, R. Hashimoto, H. Koshino, T. Nakata, *J. Org. Chem.* **2004**, *69*, 4509 – 4515; employing $RuCl_3/NaIO_4$: f) L. G. Arini, P. Szeto, D. L. Hughes, R. A. Stockman, *Tetrahedron Lett.* **2004**, *45*, 8371 – 8374; employing $RuCl_3/NaIO_4$ for deprotection: g) B. Alcaide, P. Almendros, J. M. Alonso, *Tetrahedron Lett.* **2003**, *44*, 8693 – 8695.

[4] R. A. Berglund in *Encyclopedia of Reagents for Organic Synthesis*, *Vol. 6* (Ed.: L. A. Paquette), Wiley, New York, **1995**, pp. 3837 – 3843.

[5] a) K. Koike, G. Inoue, T. Fukuda, *J. Chem. Eng. Jpn.* **1999**, *32*, 295 – 299; b) R. A. Ogle, J. L. Schumacher, *Process Saf. Prog.* **1998**, *17*, 127 – 133.

[6] One of the most widely used reagents is $OsO_4/NaIO_4$ (Lemieux–Johnson reagent): a) R. Pappo, D. S. Allen, Jr., R. U. Lemieux, W. S. Johnson, *J. Org. Chem.* **1956**, *21*, 478 – 479; b) W. Yu, Y. Mei, Y. Kang, Z. Hua, Z. Jin, *Org. Lett.* **2004**, *6*, 3217 – 3219; further reagents are: OsO_4/oxone: c) B. R. Travis, R. S. Narayan, B. Borhan, *J. Am. Chem. Soc.* **2002**, *124*, 3824 – 3825; cat. $RuCl_3$/($NaIO_4$ or Oxone): d) D. Yang, C. Zhang, *J. Org. Chem.* **2001**, *66*, 4814 – 4818; ruthenium nanoparticles/$NaIO_4$: e) C.-M. Ho, W.-Y. Yu, C.-M. Che, *Angew. Chem.* **2004**, *116*, 3365 – 3369; *Angew. Chem. Int. Ed.* **2004**, *43*, 3303 – 3307; other ruthenium-derived catalysts: f) V. Kogan, M. M. Quintal, R. Neumann, *Org. Lett.* **2005**, *7*, 5039 – 5042; chromium(VI): g) J. March, *Advanced Organic Chemistry*, Wiley, New York, **1992**, p. 1181; Permanganate: h) D. Arndt, *Manganese Compounds as Oxidizing Agents in Organic Chemistry*, Open Court, LaSalle, IL, **1981**, pp. 241 – 246; i) S. Lai, D. G. Lee, *Synthesis* **2001**, 1645 – 1648; for autooxidation see: j) R. A. Sheldon, J. K. Kochi, *Metal-Catalyzed Oxidation of Organic Compounds*, Academic Press, New York, **1981**; k) Ti-zeolite with hydrogen peroxide: W. Adam, A. Corma, A. Martinez, M. Renz, *Chem. Ber.* **1996**, *129*, 1453 – 1455; peroxotungstate complexes with H_2O_2: l) A. Haimov, H. Cohen, R. Neumann, *J. Am. Chem. Soc.* **2004**, *126*, 11762 – 11763.

[7] R. S. Drago, B. B. Corden, C. W. Barnes, *J. Am. Chem. Soc.* **1986**, *108*, 2453 – 2454.

[8] a) A. G. Shoair, R. Mohamed, *Synth. Commun.* **2006**, *36*, 59 – 64; b) W. P. Griffith, E. Kwong, *Synth. Commun.* **2003**, *33*, 2945 – 2951; c) A. K. Sinha, B. P. Joshi, R. Acharya, *Chem. Lett.* **2003**, *32*, 780 – 781.

[9] Myeloperoxidase and *Coprinus cinereus* peroxidase with electron-deficient styrene derivatives: a) A. Tuynman, J. L. Spelberg, I. M. Kooter, H. E. Schoemaker, R. Wever, *J. Biol. Chem.* **2000**, *275*, 3025 – 3030; Horseradish peroxidase in the presence of phenol as cosubstrate: b) P. R. Ortiz de Montellano, L. A. Grab, *Biochemistry* **1987**, *26*, 5310 – 5314; Horseradish peroxidase with indoles: c) K.-Q. Ling, L. M. Sayre, *Bioorg. Med. Chem.* **2005**, *13*, 3543 – 3551; engineered horseradish peroxidase: d) S.-i. Ozaki, P. R. Ortiz de Montellano, *J. Am. Chem. Soc.* **1995**, *117*, 7056 – 7064; chloroperoxidase from *Caldariomyces fumago* with *tert*-butyl hydroperoxide: e) D. J. Bougioukou, I. Smonou, *Tetrahedron Lett.* **2002**, *43*, 339 – 342; f) D. J. Bougioukou, I. Smonou, *Tetrahedron Lett.* **2002**, *43*, 4511 – 4514; g) M. Takemoto, Y. Iwakiri, Y. Suzuki, K. Tanaka, *Tetrahedron Lett.* **2004**, *45*, 8061 – 8064.

[10] G. Bourel, J.-M. Nicaud, B. Nthangeni, P. Santiago-Gomez, J.-M. Belin, F. Husson, *Enzyme Microb. Technol.* **2004**, *35*, 293 – 299.

[11] Employing β-carotene monooxygenase for epoxidation in a cascade with a hydrolase and further enzymes: M. G. Leuenberger, C. Engeloch-Jarret, W.-D. Woggon, *Angew. Chem.* **2001**, *113*, 2684 – 2687; *Angew. Chem. Int. Ed.* **2001**, *40*, 2614 – 2617.

[12] For reviews see: a) T. D. H. Bugg, *Tetrahedron* **2003**, *59*, 7075 – 7101; b) M. Sono, M. P. Roach, E. D. Coulter, J. H. Dawson, *Chem. Rev.* **1996**, *96*, 2841 – 2888.

[13] Quercetin 2,3-dioxygenase from *Bacillus subtilis*: a) M. R. Schaab, B. M. Barney, W. A. Francisco, *Biochemistry* **2006**, *45*, 1009 – 1016; Quercetin 2,3-dioxygenase from *Aspergillus niger*: b) H.-K. Hund, J. Breuer, F. Lingens, J. Hüttermann, R. Kappl, S. Fetzner, *Eur. J. Biochem.* **1999**, *263*, 871 – 878; indoleamine 2,3-dioxygenase and tryptophan 2,3-dioxygenase from mammals: c) D. H. Munn, M. Zhou, J. T. Attwood, I. Bondarev, S. J. Conway, B. Marshall, C. Brown, A. L. Mellor, *Science* **1998**, *281*, 1191 – 1193, and references therein; a dioxygenase from *Acinetobacter johnsonii* is restricted to 1,3-diones: d) G. D. Straganz, H. Hofer, W. Steiner, B. Nidetzky, *J. Am. Chem. Soc.* **2004**, *126*, 12202 – 12203; e) G. Straganz, A. Glieder, L. Brecker, D. W. Ribbons, W. Steiner, *Biochem. J.* **2003**, *369*, 573 – 581; Lignostilbene-α,β-dioxygenase isozymes cleave various substituted stilbene derivatives: f) S. Kamoda, T. Terada, Y. Saburi, *Biosci. Biotechnol. Biochem.* **1997**, *62*, 2575 – 2576; g) S. Kamoda, M. Samejima, *Agric. Biol. Chem.* **1991**, *55*, 1411 – 1412; h) S. Kamoda, Y. Saburi, *Biosci. Biotechnol. Biochem.* **1993**, *57*, 931 – 934; i) S. Kamoda, T. Terada, Y. Saburi, *Biosci. Biotechnol. Biochem.* **2003**, *67*, 1394 – 1396; j) S. Kamoda, T. Terada, Y. Saburi, *Biosci. Biotechnol. Biochem.* **2005**, *69*, 635 – 637; Heme-dependent oxygenase cleaves double bonds of rubber (poly(*cis*-1,4-isoprene)): k) R. Braaz, P. Fischer, D. Jendrossek, *Appl. Environ. Microbiol.* **2004**, *70*, 7388 – 7395; review on β-diketone cleavage: l) G. Grogan, *Biochem. J.* **2005**, *388*, 721 – 730.

[14] In-house culture collection.

[15] H. E. Schoemaker, D. Mink, M. G. Wubbolts, *Science* **2003**, *299*, 1694 – 1697.

[16] R. A. Sheldon, *Pure Appl. Chem.* **2000**, *72*, 1233 – 1246.

 © 2006 Wiley-VCH Verlag GmbH & Co. KGaA, Weinheim

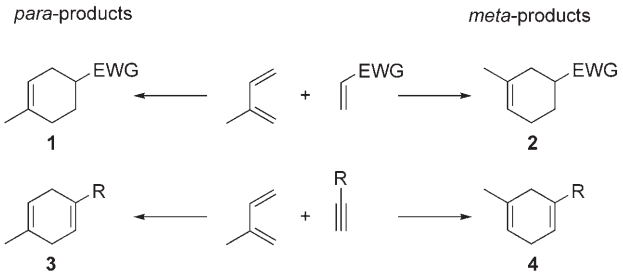
Diels–Alder Reaction

DOI: 10.1002/anie.200601974

meta-Directing Cobalt-Catalyzed Diels–Alder Reactions**

Gerhard Hilt, Judith Janikowski, and Wilfried Hess*

The Diels–Alder reaction has belonged to the arsenal of synthetic organic chemists for decades as can be seen in the large number of applications in natural-product synthesis and of biologically active compounds.[1] The usefulness of the Diels–Alder reaction is based on the cyclic transition state which allows the transfer of the stereochemical information in the starting material *E*- or *Z*-selectively into *cis*- or *trans*-configured products. Furthermore, the regiochemistry of the intermolecular Diels–Alder reaction can be predicted by the Woodward–Hoffmann rules and the therein implied *ortho*/*para* rules.[2] While the *ortho/para*-selectivity of the thermal Diels–Alder reaction allows access to *ortho*- or *para*-substituted products (such as **1**, Scheme 1) the intermolecular reaction is limited to the generation of *para*-substituted products when starting from isoprene, the *meta*-substituted products of type **2** (Scheme 1) can not be accessed. Only the

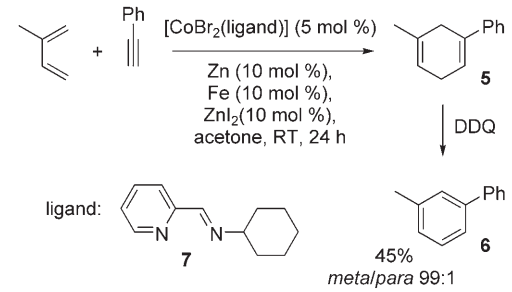


Scheme 1. *para*- and *meta*-Diels–Alder reaction products. EWG = electron-withdrawing group.

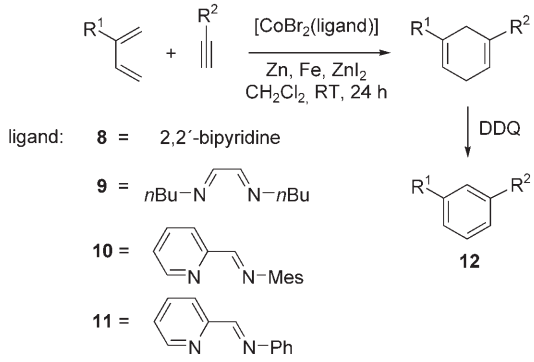
thermal Diels–Alder reaction of alkenyl boron compounds, such as the vinyl-9-borabicyclo[3.3.1]nonane, with unsymmetrical 1,3-dienes, such as isoprene, poses an exception. In this case the regioselective *meta*-directing Diels–Alder reaction generates the product of type **2** in a ratio of *meta*:*para* = 90:10.[3]

To our knowledge an analogous *meta*-directing Diels–Alder reaction to produce **4** starting from a 1,3-diene and an alkyne has not been described. Nevertheless, the *meta*-substituted dihydroaromatic systems **4** have been detected and isolated as side products in transition-metal-catalyzed cycloaddition reactions.[4] In these transition-metal-catalyzed reactions the *para*-substituted product **3** is formed as the major product.

In our investigations of cobalt-catalyzed cyclizations we reported the use of a simple cobalt catalyst system consisting of [$CoBr_2$dppe] (dppe = 1,2-bis(diphenylphosphino)ethane), ZnI_2, Zn, or Bu_4NBH_4 as reducing agent for the Diels–Alder reaction of unactivated starting materials under mild conditions for the production of the *para*-substituted Diels–Alder adducts **3**.[5] Recently, we also identified a simple cobalt catalyst system consisting of [$CoBr_2$(diimine)] (5 Mol %), ZnI_2, Zn, and Fe powder (each 10 Mol %) which performs the cobalt catalyzed Diels–Alder reaction between phenyl acetylene and isoprene, gives very good yields, and forms the *meta*-substituted isomer **5** in excellent regioselectivity. The corresponding aromatic product **6** was then generated by oxidation with 2,3-dichloro-5,6-dicyano-1,4-benzoquinone (DDQ) and its identity determined by NMR spectroscopy. Among several ligands tested the best chemo- and regioselectivity was obtained for cobalt complexes with pyridine donor ligands, such as **7** (Scheme 2) or 2,2′-bipyridine (**8**, Scheme 3) or 1,10-phenanthroline.[6] Also symmetrical aliphatic diimine ligands (**9**) as well as mixed pyridine imine ligands (**10** and **11**) gave good results. In addition, by using a combination of zinc- and iron powder as the reducing agent, the formation of the [2+2+2]-cyclotrimerization product from the alkyne was completely suppressed. The *meta*-



Scheme 2. *meta*-Selective cobalt-catalyzed Diels–Alder reaction.



Scheme 3. Preparative application of the *meta*-selective cobalt-catalyzed Diels–Alder reaction. Mes = 2,4,6-trimethylphenyl, R^1, R^2: see Table 1

[*] Prof. Dr. G. Hilt, J. Janikowski, W. Hess
Fachbereich Chemie
Philipps-Universität Marburg
Hans-Meerwein-Strasse, 35043 Marburg (Germany)
Fax: (+49) 6421-282-5677
E-mail: hilt@chemie.uni-marburg.de

[**] This work was supported by the DFG (Deutsche Forschungsgemeinschaft).

InterScience
© 2006 Wiley-VCH Verlag GmbH & Co. KGaA, Weinheim

substituted product **6** could be isolated in an acceptable yield of 45% and in an almost perfect regioselectivity of 99:1. We recognized that the yield was enhanced in dichloromethane compared to that in acetone. The substitution of the cyclohexyl substituent for aromatic substituents (phenyl- or mesityl-, **10** and **11**) also improved the yield whereas the regioselectivity under these conditions was slightly lower.

In a series of experiments with four selected cobalt complexes aromatic-, aliphatic-, olefinic-, and silyl-functionalized terminal alkynes were converted with isoprene, myrcene and 2-trimethylsilyloxy-1,3-butadiene in dichloromethane (Scheme 3).

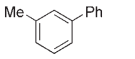
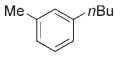
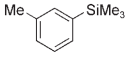
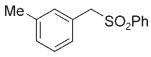
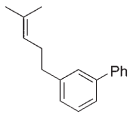
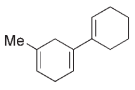
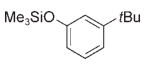
Besides aryl-, alkenyl- and alkyl-substituted alkynes also silyl- and sulfone functionalized terminal alkynes, as well as the non-protected propargylic alcohol, could be successfully converted. The reaction times of the Diels–Alder reactions of the cobalt diimine type ligands are somewhat longer compared to the *para*-directing Diels–Alder reaction with the {Co(dppe)} complex. As the results in Table 1 illustrate the *meta*-substituted products are formed with a high level of regioselectivity and in good to excellent yields. While a single perfect ligand for all reactions was not identified among the four selected ligands, at least one diimine ligand was identified which gave good results for both yield and regioselectivity.

For this new catalyst system we propose that the preformed cobalt(II) complexes are reduced in situ to the corresponding cobalt(I) complexes (neither the zinc powder nor the iron powder are sufficient reducing agents for a further reduction of the cobalt(I) species[7]). We can not rationalize the effect of the iron powder in preventing the formation of the [2+2+2]-cyclotrimerization side product.[8] When one component of the catalyst system is omitted, reduced chemoselectivities or reduced conversions are encountered. In some cases the formation of the 1,3,6-cyclooctatriene side product is observed. Nevertheless, the amount of the [4+2+2]-cycloaddition adduct is barely higher than 10% (GC-analysis) and this by-product can easily be separated by column chromatography.[9]

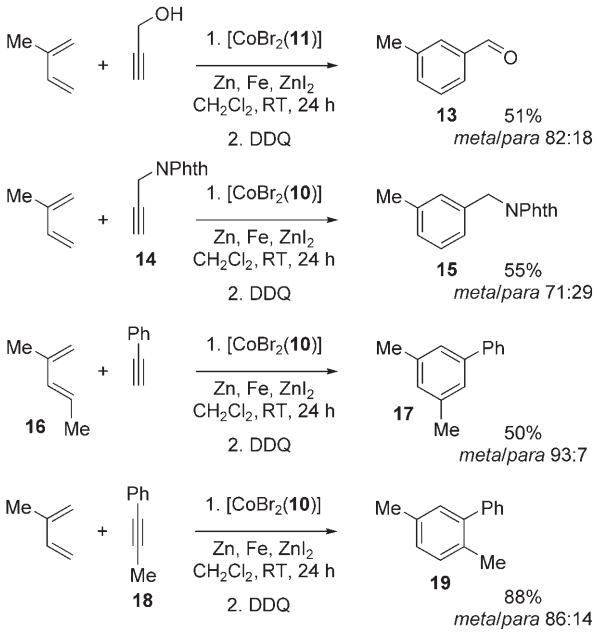
Surprisingly the reaction of the unprotected propargylic alcohol (Scheme 4) with isoprene occurs in relatively good chemo- and regioselectivity. In contrast, the similar reaction with the [$CoBr_2$(dppe)] catalyst could not be realized to date. Nevertheless, the subsequent DDQ oxidation generates the corresponding aldehyde so that in this conversion 2.2 equivalents of DDQ were used to obtain the product **13** in reasonable yields.[10]

Using the cobalt catalysts system [$CoBr_2$(dppe)], ZnI_2, Zn, the propargylic phthalimide **14** reacts with 1,3-dienes giving the cycloaddition products in rather low yields,[11] with the new cobalt diimine system (Scheme 4) **15** could be obtained in yields of up to 55%, a significant increase. The

Table 1: Cobalt-catalyzed Diels–Alder reactions with ligands **8**–**11** (see Scheme 3).[a]

Entry	R^1	R^2	Product (**12**)	Yield (*meta*/*para*)
1 2 3 4	Me	Ph		**8**: 77% (98:2) **9: 90% (97:3)** **10**: 98% (80:20) **11**: 80% (95:5)
5 6 7 8	Me	*n*Bu		**8: 85% (92:8)** **9**: 81% (73:27) **10**: 90% (80:20) **11**: 85% (82:18)
9 10 11 12	Me	$SiMe_3$		**8**: 80% (83:17) **9**: 66% (57:43) **10: 80% (93:7)** **11**: 93% (85:15)
13 14 15 16	Me	CH_2SO_2Ph		**8**: 47% (95:5) **9**: 57% (90:10) **10**: 61% (69:31) **11: 63% (95:5)**
17 18 19 20		Ph		**8**: 67% (97:3) **9**: 75% (96:4) **10: 95% (96:4)** **11**: 53% (95:5)
21 22 23 24	Me			**8**: 88% (82:18)[c] **9**: 88% (85:15)[c] **10**: 80% (87:13)[c] **11: 81% (90:10)**[c]
25 26 27 28	$OSiMe_3$[b]	*t*Bu		**8**: 22% (98:2) **9: 80% (99:1)** **10**: 78% (97:3) **11**: 41% (94:6)

[a] The best results in terms of yield and regioselectivity are highlighted in bold text. [b] For the work-up the silica gel should be deactivated by addition of triethylamine to the eluent. [c] The DDQ oxidation leads to decomposition of the product so that the dihydroaromatic compound was isolated in approximately 95% purity.



Scheme 4. *meta*-Selective Diels–Alder reaction of a higher substituted 1,3-diene and of an internal alkyne; Phth = phthaloyl.

 © 2006 Wiley-VCH Verlag GmbH & Co. KGaA, Weinheim

regioselectivity in this case is diminished and a *meta*/*para* = ratio of 71:29 was observed.

To further illustrate the complementary regioselectivity of the new cobalt catalyst system to that of the *para*-selective [$CoBr_2$(dppe)] system the unsymmetrical 1,3-diene **16** was converted with phenyl acetylene under the new reaction conditions to give the corresponding regioisomeric *meta*-product **17** in good yield and excellent regioselectivity (93:7). Because the reactivity of the higher substituted 1,3-diene **16** is reduced the alkyne trimerization product is isolated in 45% yield. In addition, the cobalt diimine catalyst system also accepts internal unsymmetrical alkynes, such as the 1-phenyl-1-propyne (**18**), and the corresponding aromatic cycloaddition product (**19**) could be obtained in excellent yield (88%) and regioselectivity (86:14) after DDQ oxidation.

Herein we described the first broad application of the *meta*-selective Diels–Alder reaction of non-activated starting materials catalyzed by a new cobalt diimine catalyst system. The dihydroaromatic intermediates can be isolated, but for the determination of the regioisomers a DDQ oxidation was performed to obtain the aromatic products. As we could demonstrate by a variation of the ligands and the reaction conditions regioisomeric Diels–Alder products can be obtained from identical starting materials in good yields and excellent regioselectivities either in favor of the *para*-substituted product ({Co(dppe)} complex) or of the *meta*-substituted product ({Co(diimine)} complex).

Experimental Section

Representative procedure for the *meta*-selective cobalt-catalyzed Diels–Alder reaction (Table 1, entry 2): A solution of [$CoBr_2$(**9**)] (39 mg, 0.1 mmol, 5.0 Mol%), zinc iodide (64 mg, 0.2 mmol, 10.0 Mol%) zinc powder (13 mg, 0.2 mmol, 10.0 Mol%), and iron powder (11 mg, 0.2 mmol, 10.0 Mol%) were briefly heated to boiling in dry dichloromethane (1.0 mL) under nitrogen atmosphere. Then isoprene (136 mg, 2.0 mmol) and phenyl acetylene (204 mg, 2.0 mmol) were added and the suspension was stirred until the starting materials were completely consumed (GC control) at room temperature. Then the suspension was filtered over a small amount of silica gel (eluent: diethyl ether), the solvent was removed in vaccuo, taken up in benzene, and the dihydroaromatic product was oxidized by DDQ (545 mg, 2.4 mmol, 1.2 equiv). After 2 h at room temperature the solution was diluted with diethyl ether (50 mL) and washed with an aqueous sodium hydroxide (10%)/sodium thiosulfate (10%) solution. The solvent was removed in vaccuo and the residue was purified by column chromatography on silica gel (eluent: pentane:CH_2Cl_2 = 100:1).The product was obtained as colorless oil (305 mg, 0.18 mmol, 90%). The analytical data are in accordance with the literature.[12] The ratios of regioisomers were determined by integration of the GC and NMR signals.

Received: May 18, 2006
Published online: July 7, 2006

Keywords: 1,3-dienes · alkynes · cobalt · cycloaddition · regioselectivity

[1] W. Carruthers *Cycloaddition Reactions in Organic Synthesis*, Pergamon, Oxford, **1990**; S. Kobayashi, K. A. Jørgensen *Cycloaddition Reactions in Organic Synthesis*, Wiley-VCH, Weinheim, **2002**; E. J. Corey, *Angew. Chem.* **2002**, *114*, 1724; *Angew. Chem. Int. Ed.* **2002**, *41*, 1650; K. C. Nicolaou, S. A. Snyder, T. Montagnon, G. E. Vassilikogiannakis, *Angew. Chem.* **2002**, *114*, 1743; *Angew. Chem. Int. Ed.* **2002**, *41*, 1668.

[2] K. A. Jørgensen in *Cycloaddition Reactions in Organic Synthesis* (Eds.: S. Kobayashi, K. A. Jørgensen), Wiley-VCH, Weinheim, **2002**, chap. 8, pp. 301–327; I. Fleming *Frontier Orbitals and Organic Chemical Reactions*, Wiley, London, **1977**; R. B. Woodward, R. Hoffmann, *The Conservation of Orbital Symmetry*, VCH, Weinheim, **1970**.

[3] M. A. Silva, S. C. Pellegrinet, J. M. Goodman, *J. Org. Chem.* **2003**, *68*, 4095; M. A. Silva, S. C. Pellegrinet, J. M. Goodman, *Arkivoc* **2003**, 556; S. C. Pellegrinet, M. A. Silva, J. M. Goodman, *J. Am. Chem. Soc.* **2001**, *123*, 8832; Y.-K. Lee, D. A. Singleton, *J. Org. Chem.* **1997**, *62*, 2255; D. A. Singleton, K. Kim, J. P. Martinez, *Tetrahedron Lett.* **1993**, *34*, 3071.

[4] Selected references: R. Z. Dolor, P. Vogel, *J. Mol. Catal.* **1990**, *60*, 59; S.-J. Paik, S. U. Son, Y. K. Chung, *Org. Lett.* **1999**, *1*, 2045.

[5] Selected references: G. Hilt, K. I. Smolko, *Angew. Chem.* **2003**, *115*, 2901; *Angew. Chem. Int. Ed.* **2003**, *42*, 2795; G. Hilt, T. J. Korn, *Tetrahedron Lett.* **2001**, *42*, 2783; G. Hilt, S. Lüers, K. Polborn, *Isr. J. Chem.* **2001**, *41*, 317; G. Hilt, F.-X. du Mesnil, *Tetrahedron Lett.* **2000**, *41*, 6757.

[6] Cobalt complexes of the vitamin B_{12}-type, such as salen-, glyoximato-, or phthalocyanin cobalt complexes are not reactive in the Diels–Alder reaction.

[7] The redox potential of the [$CoBr_2$(**10**)] complex was determined in an electroanalytical investigation. The differential pulse voltamogramms showed a single-electron reduction [Co^{II}/Co^{I}; $E = -560$ mV; Ag/AgCl] within the potential window of the solvent (CH_2Cl_2; 0.1 M Bu_4NClO_4; $E > -1.60$ V). Therefore, a further reduction of the proposed cobalt(I) species seems improbable with the mild reducing agents zinc and iron powder.

[8] G. Hilt, T. Vogler, W. Hess, F. Galbiati, *Chem. Commun.* **2005**, 1474; G. Hilt, W. Hess, T. Vogler, C. Hengst, *J. Organomet. Chem.* 2**005**, 690, 5170.

[9] The results for the optimization of the cobalt-catalyzed [4+2+2]-cycloaddition will be reported elsewhere.

[10] H. D. Becker, A. Bjoerk, E. Adler, *J. Org. Chem.* **1980**, *45*, 1596.

[11] The [$CoBr_2$(dppe)]-catalyzed reaction of the propargylic phthalimide **8** with 2,3-dimethyl-1,3-butadiene generated the cycloaddition products in 36% yield; see: G. Hilt, F. Galbiati, *Synlett* **2005**, 829.

[12] We thank Dr. L. Ackermann, LMU München, for providing the analytical data; see: L. Ackermann, R. Born, *Angew. Chem.* **2005**, *117*, 2497; *Angew. Chem. Int. Ed.* **2005**, *44*, 2444.

 © 2006 Wiley-VCH Verlag GmbH & Co. KGaA, Weinheim

Metalloid Complexes

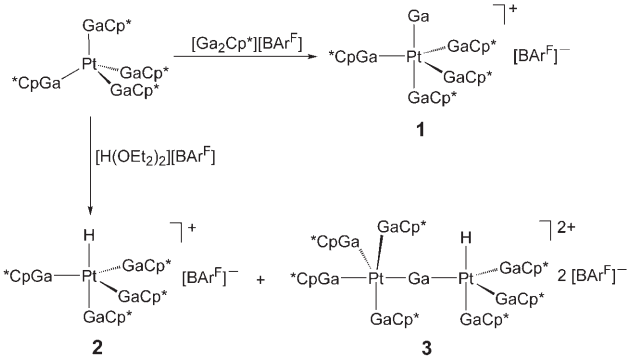
DOI: 10.1002/anie.200601007

"Naked" Ga^+ and In^+ as Pure Acceptor Ligands: Structure and Bonding of $[GaPt(GaCp^*)_4][BAr^F]$**

Beatrice Buchin, Christian Gemel, Thomas Cadenbach, Israel Fernández, Gernot Frenking, and Roland A. Fischer**

Compounds with low-valent Group 13 elements, in particular the series ECp* (E = Al, Ga, In; Cp* = C_5Me_5), are fascinating carbenoid σ-donor ligands for transition-metal–metalloid complexes and clusters.[1] Novel homoleptic metal-rich clusters of the type $[M_a(ECp^*)_b]$ (M = Pd, Pt) were reported in which the mixed-metal cores $\{M_aE_b\}$ were enveloped exclusively by Cp* ligands.[2] Examples of interesting reactivity include Si–H and C–H bond activation at the electron-rich fragments $[M(AlCp^*)_n]$ (M = Fe, Ru, Ni; $n = 3, 4$), as well as an unusual C–C bond cleavage during the rearrangement of $[Cp^*Rh(CH_3)_2(GaCp^*)]$ into the zwitterionic rhodocenium system $[Cp^*Rh\{\eta^5\text{-}C_5Me_4(GaMe_3)\}]$.[3] The σ-donor/π-acceptor properties and the steric demand of ER obviously depend on the nature of the R group. In particular, the π donor Cp* effectively fills the vacant p orbitals of the E atom and therefore diminishes the π acidity of the ligand, whereas in the case of bulky alkyl or aryl R substituents, a substantial π back-donation has been calculated.[4] Moreover, the electrostatic contribution to the overall M–E bond has been shown to be as important as covalent interactions.[5]

What can be said about substituent-free E^+ cations as "ligands"? Complexes of the type $[(L_nM)_aE]$ that exhibit "naked" Group 13 metals are known for $a = 2$–4, but this series is restricted to complexes that bear carbonyl metalate fragments $\{L_nM\}$, whereby E is in the oxidation state +III rather than +I and is located exclusively in M-E-M bridging positions.[6,7] Braunschweig's example of a boron atom in the coordination sphere of Fe, Pt, and Pd fragments exemplifies a novel bonding situation.[8] Complexes of the heavier Group 13 monocations E^+ have not been reported so far, with the noteworthy exception of Tl^+. The "metallophilic" bond to d^8 or d^{10} centers such as Pt^{II}, Pt^0, or Au^I in $[L_nM\text{–}Tl^+]$ is explained by dispersion interactions and long-range polarization effects without covalent contributions.[9] Recently, novel Ga^+- and In^+-transfer reagents, namely $[E_2Cp^*][BAr^F]$ ($BAr^F = B\{C_6H_3(3,5\text{-}CF_3)_2\}_4$), have become available,[10] and thus, we probed the limits of the bonding properties of E^+ ligands to electron-rich $\{L_nPt^0\}$ fragments (Scheme 1).



Scheme 1. Reaction of $[Pt(GaCp^*)_4]$ with $[Ga_2Cp^*][BAr^F]$ and $[H(OEt_2)_2][BAr^F]$.

$[Pt(GaCp^*)_4]$ was treated with an equimolar amount of $[Ga_2Cp^*][BAr^F]$ in fluorobenzene, and the color of the reaction mixture immediately turned deep red. Upon slow diffusion of *n*-hexane into this solution at 25 °C, pale yellow single crystals of $[GaPt(GaCp^*)_4][BAr^F]$ (**1**) were isolated in 94 % yield. The $[GaPt(GaCp^*)_4]^+$ ion of **1** exhibits a slightly distorted trigonal-bipyramidal structure with the Ga^+ ligand in an axial position (Figure 1).[11] The equatorial GaCp*

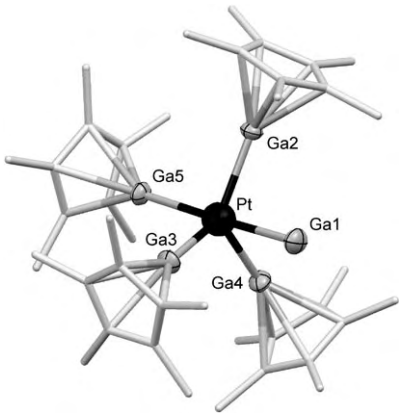


Figure 1. Molecular structure of the cation of **1** (Mercury drawing; hydrogen atoms are omitted). Selected bond lengths [Å] and angles [°]: Pt1-Ga1 2.4593(9), Pt1-Ga2 2.3474(7), Pt1-Ga3 2.3577(8), Pt1-Ga4 2.3515(8), Pt1-Ga5 2.4435(8), $Cp^*_{centroid}$-Ga2 1.910, $Cp^*_{centroid}$-Ga3 1.925, $Cp^*_{centroid}$-Ga4 1.913, $Cp^*_{centroid}$-Ga5 1.942; $Cp^*_{centroid}$-Ga2-Pt1 171.33, $Cp^*_{centroid}$-Ga3-Pt1 163.96, $Cp^*_{centroid}$-Ga4-Pt1 165.81, $Cp^*_{centroid}$-Ga5-Pt1 169.94, Ga1-Pt1-Ga5 176.83(3), Ga1-Pt1-Ga2 82.75(3), Ga1-Pt1-Ga3 84.05(3), Ga1-Pt1-Ga4 82.92(3), Ga2-Pt1-Ga3 112.44(3), Ga2-Pt1-Ga4 121.54(3), Ga3-Pt1-Ga4 121.89(3), Ga2-Pt1-Ga5 96.09(3), Ga3-Pt1-Ga5 99.12(3), Ga4-Pt1-Ga5 95.23(3).

[*] Dr. I. Fernández, Prof. Dr. G. Frenking
Fachbereich Chemie
Philipps-Universität Marburg
Hans-Meerwein-Strasse, 35032 Marburg (Germany)
Fax (+49) 6421-282-5566
E-mail: frenking@chemie.uni-marburg.de
B. Buchin, Dr. C. Gemel, T. Cadenbach, Prof. Dr. R. A. Fischer
Lehrstuhl für Anorganische Chemie II
Organometallics & Materials
Ruhr-Universität Bochum
44780 Bochum (Germany)
Fax: (+49) 234-321-4174
E-mail: roland.fischer@ruhr-uni-bochum.de

[**] Organo Group 13 Complexes of d-Block Elements, XLIV. Part XLIII: A. Kempter, C. Gemel, R. A. Fischer, *Chem. Commun.* **2006**, 1551–1553. $Cp^* = C_5Me_5$; $BAr^F = B\{C_6H_3(3,5\text{-}CF_3)_2\}_4$.

Supporting information for this article is available on the WWW under http://www.angewandte.org or from the author.

 © 2006 Wiley-VCH Verlag GmbH & Co. KGaA, Weinheim

ligands are bent towards the terminal Ga^+ ligand, and the Ga1-Pt-Gax angles ($x = 2, 3, 4$) are closer to 80° than 90°. This property resembles the so-called umbrella effect of classical carbonyl metal hydride complexes $[(CO)_nM{-}H]$.[12] The equatorial Pt–Ga bond lengths average to 2.352 Å and are thus comparable to those of the parent complex $[Pt(GaCp^*)_4]$ (⌀2.335 Å). Interestingly, the Ga1–Pt bond length (2.459(1) Å) is quite close to the value for the axial Cp*Ga5–Pt bond (2.444(1) Å), both bonds being slightly elongated with respect to the equatorial ones.

The η^5-Cp* groups do not exhibit any unusual features. The ^{71}Ga NMR spectrum of **1** revealed only one broad and featureless signal which was centered at $\delta = -640$ ppm ($\delta\nu_{1/2} \approx 2$ kHz), and we could not detect any ^{195}Pt NMR resonance. The solid-state ^{1}H and ^{13}C MAS NMR spectra of **1** exhibit two sets of signals for the GaCp* ligands in the expected ratio of 1:3. In solution, the ^{1}H NMR spectrum of **1** again reveals two singlets at $\delta = 1.81$ and 1.77 ppm, but with relative intensities that are dependent on the concentration of **1** as well as on the temperature, thus indicating dynamic processes and several interacting species. A mixture of pure **1** and $[Pt(GaCp^*)_4]$ in a 2:1 ratio gave a number of distinct signals for coordinated GaCp* groups, but unreacted $[Pt(GaCp^*)_4]$ was not detected. Similarly, the combination of pure GaCp* with **1** (1:1) resulted in several sharp signals in the GaCp* region, but no free GaCp* was observed.

The bonding of the Ga^+ ligand to the closed-shell 18-electron complex $[Pt(GaCp^*)_4]$ is clearly a result of the (soft) Lewis acidic properties of Ga^+ ligand in contrast to the Lewis basic GaCp* ligand. The corresponding protonation of electron-rich transition-metal centers is well-known and was studied by Tolman et al. for the d^{10} complexes $[Ni(PR_3)_4]$ to give $[Ni(PR_3)_4H]^+$.[13] In accordance, a solution of $[Pt(GaCp^*)_4]$ in fluorobenzene immediately turned red when treated with $[H(OEt_2)_2][BAr^F]$.[14a] A mixture of single crystals of **2** and **3** (Scheme 1) was isolated by diffusion of *n*-hexane into the reaction mixture. The ratio of the two products changed in favor of **3** when excess $[H(OEt_2)_2][BAr^F]$ was used. Compound **2** is likely an intermediate on the pathway in formation of the unusual Ga^+-bridged product **3**; the species $[GaPt(GaCp^*)_3]^+$ (Table 1 and Table 2) may also be formed as a result of the release of Cp*H upon protonation. Monitoring of the reactions by NMR spectroscopy revealed complex spectra with a number of very broad, overlapping peaks that indicate H^+-dependent equilibria. To further probe this general principle, we treated $[PtL_4]$ (L = PPh_3, GaCp*) with $Tl[BAr^F]$ and $In[BAr^F]$[14b] as convenient sources of Tl^+ and In^+, respectively. Several products were formed, including orange crystalline $[InPt(PPh_3)_3][BAr^F]$ (**4**), in which the Pt center has a trigonal-pyramidal geometry as a result of elimination of one PPh_3 ligand, and the In^+ ligand is located in the axial position (see the Supporting Information).

To elucidate the bonding situation in the cation of compound **1**, we carried out DFT calculations (BP86/TZ2P) on the model complexes $[GaPt(GaCp)_n]^+$ (**1A**, $n = 4$; **1B**, $n = 3$) and $[EPt(PMe_3)_3]^+$ (**4E**, E = Ga, In; C_s symmetry).[15] The model complexes **1B** and **4E** were included because of their relation to **3** (Scheme 1) and **4**. The nature of the E^+–Pt interactions was investigated with the EDA method (energy decomposition analysis),[15e,f,16] which has previously been used to analyze the Group 13 diyl complexes $[(CO)_nM{-}ER]$ and $[M(ER)_n]$ (M = element of Group 6, 8, or 10).[5,17,18] The relevant data is compiled in Table 1 and Table 2 (see also the Supporting Information).

Table 1: EDA of the model complexes **1A**, **1B**, and **4E** (E = Ga, In) at the BP86/TZ2P level (energy values in kcal mol^{-1}), calculated bond length (Pt–E in Å), and atomic partial charges q(E).

	1A	**1B**	**4Ga**	**4In**
Symmetry	C_s	C_s	C_s	C_s
ΔE_{int}	−81.4	−84.8	−90.7	−73.6
ΔE_{Pauli}	118.5	111.8	124.4	104.2
ΔE_{elstat}[a]	−85.6	−87.6	−104.7	−93.8
	(42.8%)	(44.5%)	(48.6%)	(52.8%)
ΔE_{orb}[a]	−114.2	−110.0	−110.5	−84.0
	(57.2%)	(55.5%)	(51.4%)	(47.2%)
ΔE_{σ}[b]	−69.5	−55.7	−57.3	−43.3
	(60.8%)	(51.0%)	(51.8%)	(51.6%)
ΔE_{π}[b]	−44.8	−53.4	−53.2	−40.8
	(39.2%)	(49.0%)	(48.2%)	(48.4%)
ΔE_{prep}	8.8	3.1	5.9	5.1
ΔE (= $-D_e$)	−72.6	−81.7	−84.8	−68.5
r(Pt–E)	2.494	2.353	2.346	2.565
q(E)	0.21	0.26	0.23	0.30

[a] The percentage values in parentheses give the contributions to the total attractive interactions ($\Delta E_{elstat} + \Delta E_{orb}$). [b] The percentage values in parentheses give the contributions to the total (covalent) orbital interactions ΔE_{orb}.

Table 2: Mulliken population analysis of model complexes **1A**, **1B**, and **4E** (E = Ga, In) at the BP86/TZ2P level. Population of the atomic valence orbitals and polarization functions.

	1A	**1B**	**4Ga**	**4In**
s	1.91	1.87	1.90	1.83
p	0.88	0.76	0.91	0.85
$p_z = p(\sigma)$	0.58	0.37	0.45	0.45
$p_x + p_y = p(\pi)$	0.30	0.38	0.44	0.38
d	0.07	0.07	0.09	0.08
f	0.02	0.02	0.03	0.02

The calculated Ga1–Pt bond length in **1A** (2.494 Å) is slightly larger than that in **1** (2.459(1) Å), which could, in part, be a result of crystal-packing effects, which shorten donor–acceptor bonds in the isolated molecule.[19] The discussion of the bonding situation in the model complexes in terms of interactions between the E^+ ligand and neutral $\{PtL_n\}$ fragment is straightforward since the customary bonding model of closed-shell donor–acceptor interactions can be applied. We also considered the alternative decomposition into E and $[PtL_n]^+$; however, this reaction is less favorable since stabilization by interactions between E^+, solvent molecules, and counterions in a condensed phase is lacking. The EDA results indicate substantial covalent character in the E^+–Pt bond (47–57% fraction of ΔE_{orb}; Table 1). The partitioning of the ΔE_{orb} term into the contributions of the σ and π orbitals reveals strong E^+–Pt π interactions. The ΔE_{π} term contrib-

 © 2006 Wiley-VCH Verlag GmbH & Co. KGaA, Weinheim

utes 39% for **1A** and 49% for **1B** of the total orbital interactions. Hence, the Ga^+–Pt π bonding has nearly the same strength as the Ga^+–Pt σ bonding.

This conclusion is supported by a population analysis, which is given in Table 2. In compound **1B** the population in the p(π) atomic orbitals (AOs) of Ga^+ is nearly as large as in the p(σ) AOs. The p(π) population in Ga^+ is slightly smaller in **1A**, which agrees with the lower π contribution that was given by the EDA results. The occupation of the σ orbitals in Ga^+ (s and p_z) is always greater than 2.0. Interestingly, the Ga^+ ligands in **1A** and **1B** carry only a small partial charge (+0.21 and +0.26, respectively), and the platinum fragment is significantly more positively charged. Hence, the bonding analysis of **1A** and **1B** shows that the Ga^+ ligand serves as both σ acceptor and π acceptor; the electron pair of Ga^+ possesses mainly s character and does not participate in coordinative bonding. This situation is in contrast to GaCp*, which is a rather weak π acceptor and acts as a strong σ donor through pronounced involvement of the lone pair at the Ga atom. Analysis of $[InPt(PMe_3)_3]^+$ (**4In**) as a model for compound **4** indicates the same situation for In^+ in comparison with InCp* (Tables 1 and 2).

The metal fragments $\{PtL_n\}$ in the compounds **1** and **4** are therefore pure donors for E^+. Neither the variation of L (GaCp vs. PMe_3, GaCp* vs. PPh_3) nor variation of the coordination number in $\{PtL_n\}$ ($n = 3$, 4) substantially influences the donor properties. The existence of compound **3** (Scheme 1) in which the Ga^+ ligand occupies a bridging position between two $\{Pt(GaCp^*)_n\}$ donor fragments corroborates this analysis. The D_e value for **1B** (81.7 kcal mol^{-1}) is even larger than that of **1A** (72.6 kcal mol^{-1}, Table 1), thus indicating that the deprotonated derivative of **3**, $[(Cp^*Ga)_4Pt{-}Ga{-}Pt(GaCp^*)_3]^+$, or even the hypothetical symmetric congener $[(Cp^*Ga)_3Pt{-}Ga{-}Pt(GaCp^*)_3]^+$ may exist in the described reaction solutions. We thus suggest that the E^+ ligand is a metal analogue of H^+. This concept matches with the dynamic behavior of **1** in solution, which involves several species from which we could isolate the title complexes in crystalline form. Other interesting species may still await their discovery.

Experimental Section

1: A solution of $[Pt(GaCp^*)_4]$ (100 mg, 0.0985 mol) in fluorobenzene (5 mL) was treated with $[Ga_2Cp^*][BAr^F]$ (112 mg, 0.0985 mol) in fluorobenzene (2 mL). Slow diffusion of *n*-hexane into the reaction mixture at room temperature resulted in pale yellow single crystals of **1**. Yield: 180 mg (94%). Elemental analysis (%) calcd for $C_{72}H_{72}BF_{24}Ga_5Pt$: C 44.40, H 3.73; found: C 43.97, H 3.58.

2, **3**: A solution of $[Pt(GaCp^*)_4]$ (100 mg, 0.0985 mol) and $[H(OEt_2)_2][BAr^F]$ (100 mg, 0.0985 mol) in fluorobenzene (5 mL) was layered with *n*-hexane (15 mL) and allowed to stand at room temperature for 30 h. Single crystals of **2** and **3** formed and were manually separated (typical yields of 20–30% each) and directly analyzed by X-ray diffraction.

4: $[Pt(PPh_3)_4]$ (94 mg, 0.0757 mmol) and $In[BAr^F]$ (74 mg, 0.0757 mmol) were dissolved in fluorobenzene (5 mL). The mixture was stirred for several minutes, until the color of the solution changed to deep red. Slow addition of *n*-hexane gave orange crystals of **4**. Yield: 134 mg (90%). Elemental analysis (%) calcd for $C_{92}H_{62}BF_{25}InP_3Pt$ (**1**·C_6H_5F): C 53.74, H 3.04; found: C 53.02, H 3.77.

Received: March 14, 2006
Revised: April 10, 2006
Published online: July 6, 2006

Keywords: density functional calculations · gallium · Group 13 elements · metalloids · platinum

[1] P. Jutzi, B. Neumann, G. Reumann, H. G. Stammler, *Organometallics* **1998**, *17*, 1305–1314.
[2] a) C. Gemel, T. Steinke, M. Cokoja, A. Kempter, R. A. Fischer, *Eur. J. Inorg. Chem.* **2004**, 4161–4176; b) T. Steinke, C. Gemel, M. Winter, R. A. Fischer, *Chem. Eur. J.* **2005**, *11*, 1636–1646.
[3] a) T. Steinke, M. Cokoja, C. Gemel, A. Kempter, A. Krapp, G. Frenking, U. Zenneck, R. A. Fischer, *Angew. Chem.* **2005**, *117*, 3003–3007; *Angew. Chem. Int. Ed.* **2005**, *44*, 2943–2946; b) T. Steinke, C. Gemel, M. Cokoja, M. Winter, R. A. Fischer, *Angew. Chem.* **2004**, *116*, 2349–2352; *Angew. Chem. Int. Ed.* **2004**, *43*, 2299–2302; c) T. Cadenbach, C. Gemel, R. Schmid, R. A. Fischer, *J. Am. Chem. Soc.* **2005**, *127*, 17068–17078.
[4] a) W. Uhl, M. Benter, S. Melle, W. Saak, G. Frenking, J. Uddin, *Organometallics* **1999**, *18*, 3778–3780; b) J. Weiss, D. Stetzkamp, B. Nuber, R. A. Fischer, C. Boehme, G. Frenking, *Angew. Chem.* **1997**, *109*, 95–97; *Angew. Chem. Int. Ed.* **1999**, *38*, 2830–2850.
[5] a) J. Uddin, C. Boehme, G. Frenking, *Organometallics* **2000**, *19*, 571–582; b) J. Uddin, G. Frenking, *J. Am. Chem. Soc.* **2001**, *123*, 1683–1693.
[6] a) N. A. Compton, R. J. Errington, N. C. Norman, *Adv. Organomet. Chem.* **1990**, *31*, 91–182; b) R. A. Fischer, J. Weiß, *Angew. Chem.* **1999**, *111*, 3002–3022; *Angew. Chem. Int. Ed.* **1999**, *38*, 2830–2850.
[7] a) K. Ueno, T. Watanabe, H. Tobita, H. Ogino, *Organometallics* **2003**, *22*, 4375–4377; b) N. R. Bunn, S. Aldridge, D. L. Kays, N. D. Coombs, A. Rossin, D. J. Willock, J. K. Day, C. Jones, L.-l. Ooi, *Organometallics* **2005**, *24*, 5891–5900; c) H. Braunschweig, G. R. Whittell, *Chem. Eur. J.* **2005**, *11*, 6128–6133.
[8] H. Braunschweig, K. Radacki, D. Rais, F. Seeler, *Angew. Chem.* **2006**, *118*, 1087–1090; *Angew. Chem. Int. Ed.* **2006**, *45*, 1066–1069.
[9] a) J. R. Stork, M. M. Olmstead, A. L. Balch, *J. Am. Chem. Soc.* **2005**, *127*, 6512–6513; b) V. J. Catalano, B. L. Bennett, S. Muratidis, B. C. Noll, *J. Am. Chem. Soc.* **2001**, *123*, 173–174; c) E. J. Fernandez, J. M. Lopez-de-Luzuriaga, M. Monge, M. E. Olmos, J. Perez, A. Laguna, A. A. Mohamed, J. P. Fackler, *J. Am. Chem. Soc.* **2003**, *125*, 2022–2023.
[10] a) B. Buchin, C. Gemel, T. Cadenbach, R. Schmid, R. A. Fischer, *Angew. Chem.* **2006**, *118*, 1091–1093; *Angew. Chem. Int. Ed.* **2006**, *45*, 1074–1076; b) A. H. Cowley, C. L. B. Macdonald, J. S. Silverman, J. D. Gorden, A. Voigt, *Chem. Commun.* **2001**, 175–176; c) $[Al_2Cp^*]^+$ has recently been detected in the gas phase by mass spectrometry: K. Koch, R. Burgert, H. Schnöckel, *Z. Naturforsch. B* **2004**, *59*, 1512–1518; K. Koch, R. Burgert, G. Stösser, H. Schnöckel, *Eur. J. Mass Spectrom.* **2005**, *11*, 469–474.
[11] Crystal structure analysis of **1**: crystal size $0.25 \times 0.20 \times 0.1$ mm, monoclinic, space group $P2_1/c$, $a = 19.637(3)$, $b = 15.543(3)$, $c = 25.475(5)$ Å, $\beta = 95.115(14)°$, $V = 7744(2)$ Å^3, $Z = 4$, $\rho_{calcd} = 1.671$ g cm^{-3}, $2\Theta_{max} = 50.08°$, $\lambda(Mo_{K\alpha}) = 0.71073$ Å, $T = 109(2)$ K. 62970 reflections (13723 unique) were measured on a Oxford Excalibur 2 diffractometer [R(int) = 0.0794]. The structural solution and refinement were done by using the programs SHELXS-97 and SHELXL-97.[20] Final values for $R1$ and $wR2(F^2)$: 0.0701 and 0.1000 (all data). CCDC-601480 contains the supplementary crystallographic data for this paper. These data can be obtained free of charge from The

 © 2006 Wiley-VCH Verlag GmbH & Co. KGaA, Weinheim

Cambridge Crystallographic Data Centre via www.ccdc.cam.ac.uk/data_request/cif.

[12] J. A. Zubieta, J. J. Zuckerman, *Prog. Inorg. Chem.* **1978**, *24*, 251 – 475.

[13] a) C. A. Tolman, *J. Am. Chem. Soc.* **1970**, *92*, 4217 – 4222; b) C. A. Tolman, *Inorg. Chem.* **1972**, *11*, 3128 – 3129.

[14] a) For the synthesis of $[H(OEt_2)_2][BAr^F]$, see: M. Brookhart, B. Grant, A. F. Volpe, Jr., *Organometallics* **1992**, *11*, 3920 – 3922; b) $In[BAr^F]$ is available by quantitative protolysis of InCp* with $[H(OEt_2)_2][BAr^F]$ in CH_2Cl_2; a detailed procedure for the preparation is given in the Supporting Information. Alternatively to $In[BAr^F]$, $[In_2Cp^*][BAr^F]$ can also be used as a source of In^+ ions in this reaction.

[15] a) The geometries of the molecules were first optimized without symmetry constraints (C_1), and the optimized structures had nearly C_s symmetry. Reoptimization of **1A**, **1B**, and **4E** with C_s-symmetry constraints gave structures which were only slightly higher in energy (< 0.2 kcal mol^{-1}) than the C_1 energy minima. The C_s structures were used for the EDA to divide the orbital interactions into σ(a′) and π(a″) contributions. The total π contribution to the ΔE_{orb} term is twice the ΔE_{orb}(a″) value; all calculations were carried out at the BP86 level: b) A. D. Becke, *Phys. Rev. A* **1988**, *38*, 3098 – 3100; c) J. P. Perdew, *Phys. Rev. B* **1986**, *33*, 8822. In this work the basis sets have TZ2P quality, and uncontracted Slater-type orbitals (STOs) were used as basis functions: d) J. G. Snijders, P. Vernooijs, E. J. Baerends, *At. Data Nucl. Data Tables* **1981**, *26*, 483 – 509. An auxiliary set of s, p, d, f, and g STOs was used to fit the molecular densities and to represent the Coulomb and exchange potentials accurately in each SCF cycle: e) J. Krijn, E. J. Baerends, *Fit Functions in the HFS-Method*, Internal Report, Vrije Universiteit Amsterdam, Niederlande, **1984** (in Dutch). All calculations were performed using the program package ADF: f) F. M. Bickelhaupt, E. J. Baerends, *Reviews in Computational Chemistry*, *Vol. 15* (Eds.: K. B. Lipkowitz, D. B. Boyd), Wiley-VCH, New York, **2000**, p. 1; g) G. te Velde, F. M. Bickelhaupt, E. J. Baerends, S. J. A. van Gisbergen, C. Fonseca Guerra, J. G. Snijders, T. Ziegler, *J. Comput. Chem.* **2001**, *22*, 931 – 967. The atomic partial charges were calculated by using the Hirshfeld method: F. L. Hirshfeld, *Theor. Chim. Acta* **1977**, *44*, 129.

[16] a) T. Ziegler, A. Rauk, *Theor. Chim. Acta* **1977**, *46*, 1 – 10; b) K. Morokuma, *J. Chem. Phys.* **1971**, *55*, 1236 – 1244. c) The EDA partitions the instantaneous interaction energy between the bonded fragments ΔE_{int} into three main contributions, namely the Pauli repulsion ΔE_{Pauli}, the quasiclassical electrostatic interaction ΔE_{elstat}, and the orbital (covalent) interaction ΔE_{orb}. The latter term can be divided into the contributions ΔE_σ and ΔE_π for orbitals possessing σ and π symmetry. Further details and a description of the method are found in references [15f,g] and [18].

[17] M. Dörr, G. Frenking, *Z. Anorg. Allg. Chem.* **2002**, *628*, 843 – 850.

[18] For recent reviews about EDA studies of metal–ligand interactions, see: a) G. Frenking, K. Wichmann, N. Fröhlich, C. Loschen, M. Lein, J. Frunzke, V. M. Rayón, *Coord. Chem. Rev.* **2003**, *238–239*, 55 – 82; b) M. Lein, G. Frenking in *Theory and Applications of Computational Chemistry: The First 40 Years* (Eds.: C. E. Dykstra, G. Frenking, K. S. Kim, G. E. Scuseri), Elsevier, Amsterdam, **2005**, pp. 291 – 372.

[19] V. Jonas, G. Frenking, M. T. Reetz, *J. Am. Chem. Soc.* **1994**, *116*, 8741 – 8753.

[20] G. M. Sheldrick, SHELXS-97, Program for the Solution of Crystal Structures, Universität Göttingen, **1997**; G. M. Sheldrick, SHELXL-97, Program for Crystal Structure Refinement, Universität Göttingen, **1997**.

 © 2006 Wiley-VCH Verlag GmbH & Co. KGaA, Weinheim

Chromatography

DOI: 10.1002/anie.200504568

Spherical Particles of Phenylene-Bridged Periodic Mesoporous Organosilica for High-Performance Liquid Chromatography**

*Vivian Rebbin, Rainer Schmidt, and Michael Fröba**

Since the discovery of mesoporous silica materials in 1992,[1,2] much effort has been spent on altering their morphology to obtain spherical particles for use as stationary phases in chromatography. Mesoporous materials offer new opportunities in separation because of their high inner surface areas, narrow pore size distributions, and relatively high stabilities at low and high pH values. Some research groups have developed synthesis procedures for spherical particles of mesoporous silicas,[3–5] but only a few of these materials have the size of 3–10 μm necessary for application in HPLC.[6–13] In most cases, pure silica materials are functionalized in a post-synthetic treatment to produce reversed phases. To date, only two research groups have applied pure silica materials in separation.[8,12]

The introduction of a new class of organic–inorganic hybrid materials, the periodic mesoporous organosilicas (PMOs), in 1999 provided a new possibility:[14–16] various organic moieties could be directly incorporated into pristine mesoporous silicas, without compromising the characteristics of the materials (such as high specific surface areas, narrow pore size distributions, and high degrees of mesopore ordering).[17] Very recently, new synthesis pathways for spherical PMOs (sph-PMOs) have been described.[18–21] However, only one report of the application of a sph-PMO in chromatography has been published; prior to use, the ethylene-bridged sph-PMO material was further functionalized with octadecyl chains to produce a slightly modified reversed phase.[19] Herein, we present the first results for a phenylene-bridged

[*] V. Rebbin, Prof. Dr. M. Fröba
Institute of Inorganic and Analytical Chemistry
Justus Liebig University Giessen
Heinrich-Buff-Ring 58, 35392 Giessen (Germany)
Fax: (+49) 641-993-4109
E-mail: Michael.Fröba@anorg.chemie.uni-giessen.de
R. Schmidt
Institute of Organic Chemistry
Justus Liebig University Giessen
Heinrich-Buff-Ring 58, 35392 Giessen (Germany)

[**] The authors thank M. Jakubowski and S. Pötz for laboratory support, G. Koch, C. Gath, and K. Peppler for the TEM and SEM images, Dr. M. Bertmer (RWTH Aachen) for the ^{2}H NMR spectra, and Prof. Dr. M. Hunger for the ^{29}Si MAS NMR spectra. Special thanks to U. Weißgüttel (Martin Luther University, Halle–Wittenberg) for particle sieving and determination of particle sizes. Financial support from the Justus Liebig University and the Fonds der Chemischen Industrie is gratefully acknowledged.

Supporting information for this article is available on the WWW under http://www.angewandte.org or from the author.

WILEY InterScience DISCOVER SOMETHING GREAT
© 2006 Wiley-VCH Verlag GmbH & Co. KGaA, Weinheim

sph-PMO material used as a stationary phase in HPLC. The separating properties of this material combine those of a normal and a reversed phase.

To better evaluate the properties of the new sph-PMO material, a reference column was packed with a commercially available normal-phase material, and both columns were subjected to the same chromatographic separation tests. According to the supplier, the chosen reference material, Nucleosil 50–10, has a pore diameter of 5 nm and a particle size of 10 μm, which are similar to those of the new sph-PMO. The two materials were first compared on the basis of powder X-ray diffraction (XRD) and nitrogen physisorption measurements (Table 1). Whereas the phenylene-bridged sph-PMO material exhibits a single XRD reflection, indicating an ordering of its pores, the purchased material is amorphous. In nitrogen physisorption measurements, both materials display type-IV isotherms characteristic of mesoporous materials.[22] These measurements reveal that the pore diameter of Nucleosil 50–10 is 8.1 nm (see Supporting Information), in contrast to the information given by the supplier. In addition, the pore size distribution of the sph-PMO material is quite narrow, with a maximum at 5.4 nm, whereas Nucleosil 50–10 exhibits a broad, asymmetric distribution over 5–15 nm.

Table 1: Nitrogen physisorption data for the sph-PMO and Nucleosil 50–10.

	BET specific surface area [$m^2 g^{-1}$]	Pore diameter [nm]	Specific micropore volume [$cm^3 g^{-1}$]	Specific pore volume [$cm^3 g^{-1}$]
Nucleosil 50–10	356	8.1[a]	0.00[b]	0.80[a]
sph-PMO	1180	5.4[a]	0.03[b]	1.12[a]

[a] NLDFT. [b] t method.

The particle size distributions of both materials have a maximum at 10 μm; that of the c material is slightly broader (see Supporting Information). The hybrid character of the sph-PMO material was demonstrated with ^{29}Si MAS NMR spectroscopy. The absence of signals arising from Q species (Q^n: $Si(OSi)_n(OH)_{4-n}$; $n = 2$–4) and the presence of three signals assigned to T species (T^n: $CSi(OSi)_n(OH)_{3-n}$; $n = 1$–3) confirm that none of the Si–C bonds was cleaved during synthesis or extraction (see Supporting Information).

Scanning electron microscopy (SEM) images show that both materials are composed of well-defined spherical particles (Figure 1 a,b). In transmission electron microscopy (TEM) images, the pores can be seen at the particle edges (see Supporting Information).

The surface concentration of silanol functions was determined by ^{2}H NMR spectroscopy (see Supporting Information). Whereas the phenylene-bridged sph-PMO material has only 0.16 silanol groups per nm^2 (which corresponds to 0.26 μmol m^{-2}), Nucleosil 50–10 contains a significantly higher concentration of 4.82 silanol groups per nm^2 (which corresponds to 8 μmol m^{-2}; data from supplier).

All chromatographic tests were first carried out with Nucleosil 50–10, which was chosen as the reference material because of its chemical similarities to the sph-PMO material (with respect to the surface silanol functions). Three test mixtures were selected. Mixture 1 contained benzene, naphthalene, biphenyl, and phenanthrene (Table 2), which were also used in the few reports of chromatographic applications of spherical mesoporous silica particles. Mixture 2, which was chosen for its wide range of log octanol–water partition coefficient ($\log K_{OW}$) values, consisted of the antioxidant butylhydroxytoluene (BHT; 2,6-di-*tert*-butyl-4-methylphenol), the antidegradant sorbic acid, and the sweetener aspartame (L-aspartyl-L-phenylalanine methyl ester; Table 3). Mixture 3 contained coumarin, vanillin, and caffeine, which have $\log K_{OW}$ values (Table 4) that fall within a relatively narrow range and are lower than those of the aromatic molecules of mixture 1. All peaks in the chromatograms of the mixtures were identified on the basis of measurements of the individual components.

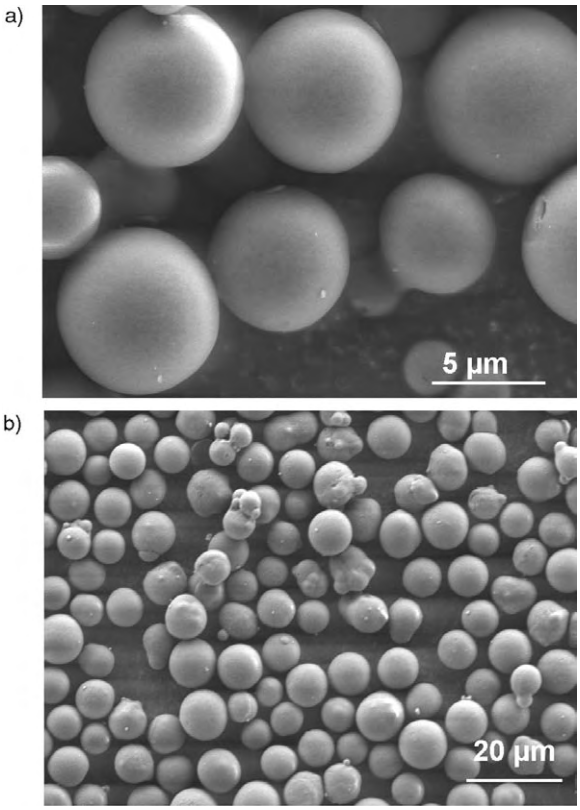
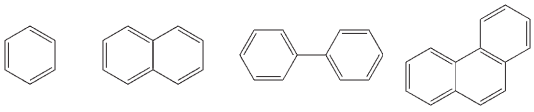


Figure 1. SEM images of spherical particles of a) the sph-PMO and b) Nucleosil 50–10.

Table 2: Structural formulas and $\log K_{OW}$ data for mixture 1.

	Benzene	Naphthalene	Biphenyl	Phenanthrene
Structural formula				
$\log K_{OW}$	1.99	3.17	3.76	4.35

 © 2006 Wiley-VCH Verlag GmbH & Co. KGaA, Weinheim

Table 3: Structural formulas and log K_{OW} data for mixture 2.

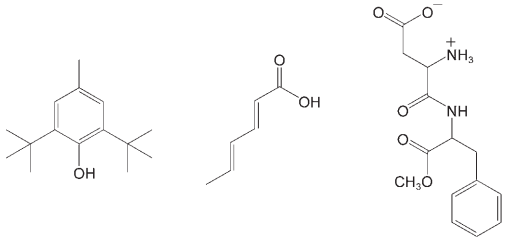
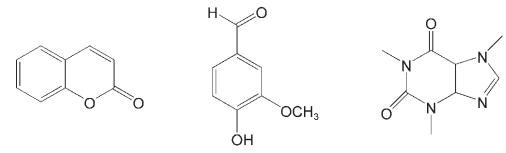
	BHT	Sorbic acid	Aspartame
Structural formula			
log K_{OW}	5.03	1.62	0.07

Table 4: Structural formulas and log K_{OW} data for mixture 3.

	Coumarin	Vanillin	Caffeine
Structural formula			
log K_{OW}	1.51	1.05	0.16

The aromatic compounds of mixture 1 were successfully separated with Nucleosil 50–10, when *n*-hexane was used as the elution solvent at a flow rate of 1 mL min^{-1} (Figure 2).

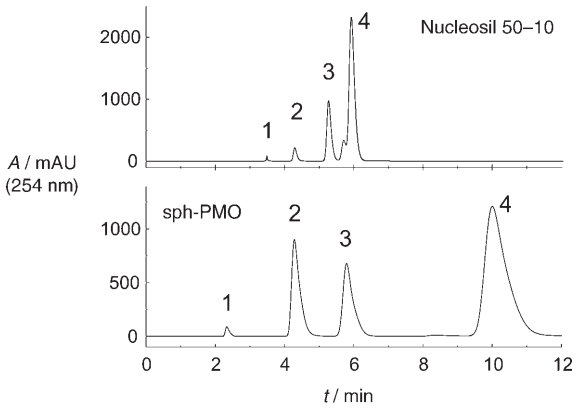


Figure 2. Chromatograms of mixture 1 (benzene (1), naphthalene (2), biphenyl (3), and phenanthrene (4)) separated with *n*-hexane at a flow rate of 1 mL min^{-1} on the Nucleosil 50–10 column or at a flow rate of 2 mL min^{-1} on the sph-PMO column.

More polar solvents and higher flow rates led to co-elution of the substances. In the case of the sph-PMO, it was necessary to increase the flow rate of *n*-hexane to 2 mL min^{-1} to separate the arenes of mixture 1 (Figure 2). The retention sequence remained the same, as expected; however, despite the higher flow rate, the retention times were significantly longer, as a result of the higher specific surface area and smaller pore diameter of the sph-PMO (Table 1). A similar effect was described by Bossière et al. for pure mesoporous silica materials.[12] The large peak widths observed in the sph-PMO chromatogram may result from π–π interactions between the aromatic analytes and the phenylene bridges in the pore walls, which lead to stronger retention. The lower elution strength of *n*-hexane relative to the less-polar surface also leads to peak broadening. Furthermore, peak tailing is observed in the chromatogram of the sph-PMO separation, but not in that of the Nucleosil 50–10 separation. Possible reasons are the longer retention times, larger particle size distribution (the sph-PMO contains a minor fraction of particles with diameters of 10–20 μm), and mixed retention mechanism (based on adsorption to both silanol groups and phenylene bridges) of the sph-PMO, in combination with an elution solvent that is somewhat too nonpolar.

Despite the broader particle size distribution of the sph-PMO material, the plate height of the column filled with the material was 1.2 times lower than that of the Nucleosil 50–10 column, indicating a higher separation efficiency for the sph-PMO. In the first experiments, a slight shift in retention times on the sph-PMO column was observed, but after a few injections, they remained constant. The separation of the individual peaks was not affected. In similar experiments with spherical particles of the mesoporous silica MSU-1, Bossière et al. could not achieve a clear baseline separation of biphenyl and phenanthrene.[12] The separation of naphthalene, biphenyl, and phenanthrene performed by Ma et al. on an unmodified SBA-15 column was also unsuccessful, because an unsuitable elution solvent was chosen.[8] For the separation of polycyclic aromatic hydrocarbons, RP18 columns, which allow an excellent separation of mixtures containing a large number of compounds, are normally used. As the surface of the RP18 stationary phase is almost completely nonpolar, polar solvents, such as methanol and water, are usually used for elution. Because the surface of our new material is more hydrophobic than that of Nucleosil 50–10, the sph-PMO allows better separation of polycyclic aromatic hydrocarbons.

The separation of mixture 2 (BHT, sorbic acid, and aspartame) in 50:50 (v:v) methanol/*tert*-butyl methyl ether (TBME) was more difficult, because of the differing polarities of the components. The best results on the Nucleosil 50–10 column were obtained at a flow rate of 2 mL min^{-1}, but a baseline separation of BHT and sorbic acid was not achieved (Figure 3). Under the same conditions, it was possible to separate all three components of mixture 2 on the sph-PMO column (Figure 3). The resolution of BHT and sorbic acid is significantly higher on the sph-PMO column than on the Nucleosil 50–10 column; However, the tailing of the aspartame peak is more pronounced, probably because of the higher specific surface area of the sph-PMO stationary phase. This problem could be avoided with gradient elution. Overall, the results correspond to our expectations based on the log K_{OW} data for mixture 2.

The most interesting results were obtained for the separation of mixture 3 (coumarin, vanillin, and caffeine). All three components could be cleanly separated on the Nucleosil 50–10 column with 98:2 dichloromethane/methanol at a flow rate of 2 mL min^{-1} (Figure 4). The same conditions led to unacceptable results on the sph-PMO column: the

 © 2006 Wiley-VCH Verlag GmbH & Co. KGaA, Weinheim

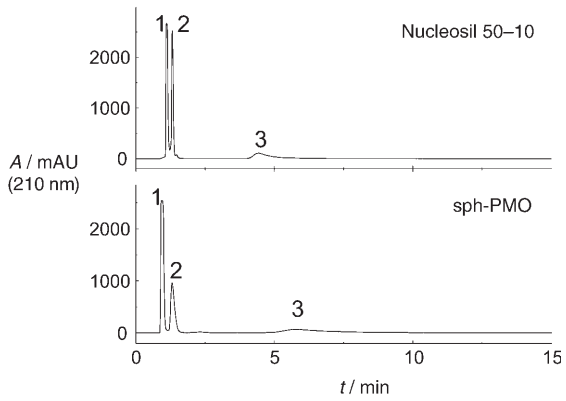


Figure 3. Chromatograms of mixture 2 (BHT (1), sorbic acid (2), and aspartame (3)) separated with 50:50 methanol/TBME at a flow rate of 2 mL min^{-1} on the Nucleosil 50–10 column or on the sph-PMO column.

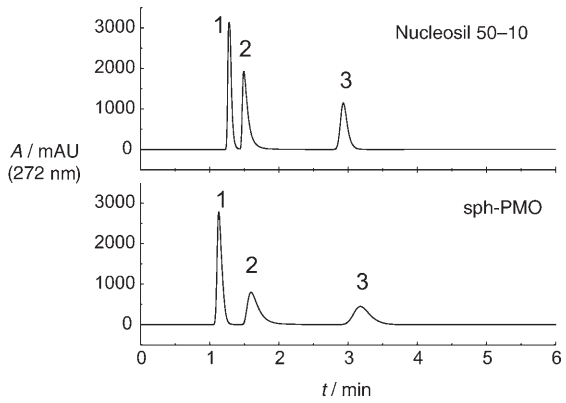


Figure 4. Chromatograms of mixture 3 (coumarin (1), vanillin (2), and caffeine (3)) separated with 98:2 dichloromethane/methanol at a flow rate of 2 mL min^{-1} on the Nucleosil 50–10 column or with 90:10 dichloromethane/methanol on the sph-PMO column.

retention times were too long (over 30 min), and the peaks were broad, with pronounced tailing. An increase in the methanol content to 10% in the elution solvent was necessary to obtain an optimal result. This effect can be explained by considering the large concentration of aromatic groups in the pore wall framework: the hydrophobic phenylene bridges decrease the surface polarity of the sph-PMO compared to that of Nucleosil 50–10, which necessitates the use of a more polar elution solvent.

In summary, we have shown that sph-PMOs are suitable for application in HPLC. The phenylene-bridged sph-PMO exhibits interesting separation properties. In contrast to the normal phase Nucleosil 50–10, the sph-PMO material is able to cleanly separate all three test mixtures, despite the wide range of polarities of the individual analytes. Through the combination of silanol groups and organic bridges in the framework of the sph-PMO material, the properties of a normal and a reversed phase are consolidated in one material. A subsequent grafting of nonpolar groups onto the surface (to form a reversed from a normal phase), which reduces the specific surface area and pore diameter, is no longer necessary. By endcapping the silanol groups in the sph-PMO, it should even be possible to synthesize completely new reversed phases. The use of different organic bridging groups in the synthesis of sph-PMOs should allow the surface properties of the stationary phases to be tuned. In addition, the large specific surface areas of sph-PMOs and their high stabilities towards extreme pH values (below 2 and above 8)[17,20] open up a wide range of interesting applications in separation.

Experimental Section

Methanol, TBME, *n*-hexane, dichloromethane, dioxane, benzene, and carbon tetrachloride (all of HPLC quality), as well as deuterium oxide (> 99.9%) were purchased from Merck. Methanol was distilled and filtered over activated carbon prior to use. TBME was distilled over potassium hydroxide and filtered over silica gel. *n*-Hexane was distilled and filtered over aluminium oxide. All solvents were then filtered over a sinter plate with a pore diameter of 1 μm to remove dust particles. Dioxane and carbon tetrachloride were used as received. Naphthalene (> 90%), biphenyl (> 90%), phenanthrene (< 90%), BHT (> 99%), sorbic acid (> 99%), aspartame (> 99%), coumarin (> 99%), vanillin (> 99%), and caffeine (> 99%) were obtained from Sigma–Aldrich. Nucleosil 50–10 (pore diameter of 5 nm (50 Å); particle diameter of 10 μm) was purchased from Macherey–Nagel.

The sph-PMO was synthesized by dissolving the structure-directing agents Pluronic P123 (0.017 mol) and cetyltrimethylammonium bromide (CTAB; 0.044 mol) in a mixture of hydrochloric acid (1.95 mol), ethanol (14.14 mol), and water (163 mol). The organosilica precursor 1,4-bis(triethoxysilyl)benzene (BTEB) was then added, and the solution was stirred for 30 min. A hydrothermal treatment followed (5 h/80 °C; 12 h/130 °C). The resulting solid was washed with ethanol, and the structure directing agents were removed by solvent extraction with 97:3 v/v ethanol/hydrochloric acid.[20]

Nitrogen physisorption measurements were carried out with a Quantachrome Autosorb 6 analyzer at 77 K. All samples were outgassed for 24 h at 100 °C under vacuum prior to measurement. Specific surface areas were calculated using Brunauer–Emmet–Teller (BET) theory. Mesopore size distributions were calculated from the adsorption branched of the nitrogen isotherms, using nonlocal density functional theory (NLDFT) the micropore volume and the total pore volume were calculated applying the t-method The particle sizes were determined with a Beckmann Coulter Counter LS13320. TEM images were obtained with a Philips CM 30-ST microscope operating at an acceleration voltage of 300 keV. SEM images were acquired with an HREM EDX Leo Gemini 982 microscope. The ^{29}Si MAS NMR spectra were recorded on a Bruker MSL-400 spectrometer (sample spinning frequency of 3.5 kHz; π/2 pulse width of 6 ms; recycle delay of 300 s; 1500 scans). To determine the relative amounts of the different types of silicon sites, the spectra were recorded without cross polarisation. The ^{2}H NMR spectra were recorded (Bruker 200 DBX at 30.7 MHz) after exchanging the hydrogen atoms of the surface silanol groups with deuterium. Sodium 3-trimethylsilyl-[D_4]propionate was used as a standard.

The sph-PMO and Nucleosil 50–10 were each suspended in 50:50 dioxane/carbon tetrachloride and then filled into stainless steel columns (length of 250 mm; inner diameter of 4 mm) under a maximum pressure of 400 bar. HPLC was carried out with a system consisting of a Dionex P680 HPLC pump and a Dionex UVD 170U detector with variable wavelength. The sample was injected through a Rheodyne 7125 valve with a 20 μL sample loop. The optimal wavelength for each experiment was determined by UV/Vis spectrometry.

Received: December 22, 2005
Revised: March 29, 2006
Published online: July 6, 2006

 © 2006 Wiley-VCH Verlag GmbH & Co. KGaA, Weinheim

Keywords: liquid chromatography · organic–inorganic hybrid materials · particles · periodic mesoporous organosilicas

[1] C. T. Kresge, M. E. Leonowicz, W. J. Roth, J. C. Vartuli, J. S. Beck, *Nature* **1992**, *359*, 710.
[2] J. S. Beck, J. C. Vartuli, W. J. Roth, M. E. Leonowicz, C. T. Kresge, K. D. Schmitt, C. T.-W. Chu, D. H. Olson, E. W. Sheppard, S. B. McCullen, J. B. Higginsand, J. L. Schlenker, *J. Am. Chem. Soc.* **1992**, *114*, 1083.
[3] K. Schumacher, M. Grün, K. K. Unger, *Microporous Mesoporous Mater.* **1999**, *27*, 201.
[4] K. Kosuge, T. Murakami, N. Kikukawa, M. Takemori, *Chem. Mater.* **2003**, *15*, 3184.
[5] C. Bossière, A. Labot, E. Prouzet, *Chem. Mater.* **2000**, *12*, 1937.
[6] F. Großmann, V. Ehwald, C. du Fresne von Hohenesche, K. K. Unger, *J. Chromatogr. A* **2001**, *910*, 223.
[7] J. Zhao, F. Gao, Y. Fu, W. Jin, P. Yang, D. Zhao, *Chem. Commun.* **2002**, 752.
[8] Y. Ma, Q. Li, J. Ma, Y. Wu, O. Liu, H. Cheng, *Colloids Surf. A* **2003**, *229*, 1.
[9] M. Mesa, L. Sierra, B. López, A. Ramirez, J.-L. Guth, *Solid State Sci.* **2003**, *5*, 1303.
[10] T. Martin, A. Galarneau, F. DiRenzo, D. Brunel, F. Fajula, *Chem. Mater.* **2004**, *16*, 1725.
[11] K. W. Gallis, J. T. Araujo, K. J. Duff, J. G. Moore, C. C. Landry, *Adv. Mater.* **1999**, *11*, 1452.
[12] C. Bossière, M. Kümmel, M. Persin, A. Larbot, E. Prouzet, *Adv. Funct. Mater.* **2001**, *11*, 129.
[13] C. Thoelen, J. Paul, I. F. J. Vankelevom, P. A. Jacobs, *Tetrahedron: Asymmetry* **2000**, *11*, 4819.
[14] S. Inagaki, S. Guan, Y. Fukushima, T. Ohsuna, O. Terasaki, *J. Am. Chem. Soc.* **1999**, *121*, 9611.
[15] B. J. Melde, B. T. Holland, C. F. Blanford, A. Stein, *Chem. Mater.* **1999**, *11*, 3302.
[16] C. Y. Ishii, T. Asefa, N. Coombs, M. J. MacLachlan, G. A. Ozin, *Chem. Commun.* **1999**, 2539.
[17] F. Hoffmann, M. Cornelius, J. Morell, M. Fröba, *Angew. Chem.* **2006**, *118*, 3290–3326; *Angew. Chem. Int. Ed.* **2006**, *45*, 3216–3251.
[18] V. Rebbin, M. Jakubowski, S. Pötz, M. Fröba, *Microporous Mesoporous Mater.* **2004**, *72*, 99.
[19] D.-J. Kim, J.-S. Chung, W.-S. Ahn, G.-W. Kang, W.-J. Cheong, *Chem. Lett.* **2004**, *33*, 422.
[20] V. Rebbin, M. Jakubowski, S. Pötz, M. Fröba, unpublished results.
[21] M. P. Kapoor, S. Inagaki, *Chem. Lett.* **2004**, *33*, 88.
[22] IUPAC Manual of Symbols and Terminology, Appendix 2, Part 1, *Pure Appl. Chem.* **1972**, *31*, 578.

 © 2006 Wiley-VCH Verlag GmbH & Co. KGaA, Weinheim

Host–Guest Complexes

DOI: 10.1002/anie.200600687

Flying Capsules: Mass Spectrometric Detection of Pyrogallarene and Resorcinarene Hexamers**

*Ngong K. Beyeh, Michael Kogej, Antti Åhman, Kari Rissanen, and Christoph A. Schalley**

The encapsulation of guest molecules into reversibly formed, self-assembling capsules[1] and reactions mediated or even catalyzed[2] by encapsulations mimic biological processes such as substrate recognition in enzymes and its conversion into metabolites. Besides their particular architecture, it is this feature which makes them highly interesting research objects. Pyrogallarenes and resorcinarenes such as **1**–**3** (Scheme 1) were shown to form hexameric capsules in the solid state[3] and in solution[4] through the formation of complex networks of hydrogen bonds. Water molecules are usually involved to complete the network for the resorcinarenes,[5] while pyrogallarenes assemble without the need for water incorporation. Guests such as solvent molecules,[6] quaternary ammonium ions,[7] and cobaltocenium[8] can be encapsulated in the large, approximately 1200 $Å^3$, cavity.

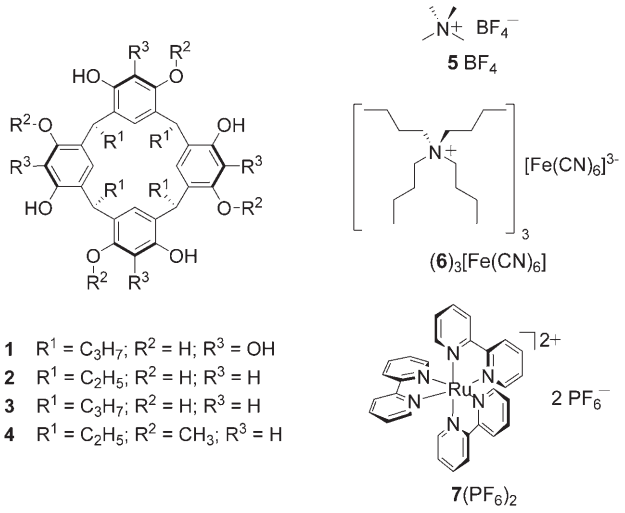
Despite early attempts by Mattay and co-workers,[3b] the hexameric capsules have not been successfully characterized by mass spectrometry[9] as a consequence of three difficulties: 1) It is not always easy to provide the necessary charge without severely interfering with the assembly. This problem can easily be solved for the capsules under study here by using cationic guests encapsulated inside the cavity. 2) Nondestructive desorption of the ions of interest into the gas phase could not be achieved before the advent of electrospray ionization. 3) Finally, the stability of the assembly in the gas phase may

[*] Dipl.-Chem. M. Kogej,[+] Prof. Dr. C. A. Schalley
Institut für Chemie und Biochemie
Freie Universität Berlin
Takustrasse 3, 14195 Berlin (Germany)
Fax: (+49) 30-838-55817
E-mail: schalley@chemie.fu-berlin.de
N. K. Beyeh, A. Åhman, Prof. Dr. K. Rissanen
Nanoscience Center
University of Jyväskylä
P.O. Box 35, 40014 Jyväskylä (Finland)
[+] present address:
Kekulé-Institut für Organische Chemie und Biochemie
Universität Bonn
Gerhard-Domagk-Strasse 1, 53121 Bonn (Germany)

[**] We are grateful for funding from the Deutsche Forschungsgemeinschaft (DFG), the Fonds der Chemischen Industrie (FCI), and the Academy of Finland (AF). C.A.S. acknowledges a Heisenberg fellowship from the DFG and a Dozentenstipendium from the FCI. N.K.B. wishes to thank the Graduate School of Bioorganic and Medicinal Chemistry for financial support. The Deutscher Akademischer Austauschdienst (DAAD) and the AF are thanked for travel grants.

Supporting information for this article is available on the WWW under http://www.angewandte.org or from the author.

WILEY InterScience DISCOVER SOMETHING GREAT
© 2006 Wiley-VCH Verlag GmbH & Co. KGaA, Weinheim



1 $R^1 = C_3H_7$; R^2 = H; R^3 = OH
2 $R^1 = C_2H_5$; R^2 = H; R^3 = H
3 $R^1 = C_3H_7$; R^2 = H; R^3 = H
4 $R^1 = C_2H_5$; $R^2 = CH_3$; R^3 = H

Scheme 1. Hosts **1**–**4** and cationic guests $\mathbf{5}^+$–$\mathbf{7}^{2+}$.

become an issue. However, since hydrogen bonds certainly are strengthened when going from a solution containing acetone and counterions to the gas phase, the capsules under study here will rather increase in stability when transferred into the high vacuum of the mass spectrometer. Following our recently developed protocol for dimeric and tetrameric caspules,[10] we decided to attempt the mass spectrometric characterization of the pyrogallarene and resorcinarene hexamers by using a large enough guest cation with sufficient templating power. Such a guest cation also provides the charge needed for mass spectrometric analysis.

When pyrogallarene **1** (Scheme 1) or resorcinarenes **2** and **3** are ionized with an electrospray ionization (ESI) source in the absence of any guest cation, mass spectra such as that shown in Figure 1a are obtained. Although the exact distributions of ion intensities depend on the ionizing cation (e.g. H^+ or Na^+) and on the nature of the monomers (pyrogallarenes show a greater tendency to form dimers), the overall picture is very similar for all of them: Cluster formation is observed with signal intensities that quickly decrease with increasing cluster size, and no specific formation of hexameric clusters is found.

The use of appropriate (cationic) guests indeed templates capsule formation. Figure 1b shows the mass spectrum of a solution of **1** in $CHCl_3$/acetone (2:1) to which tetramethylammonium tetrafluoroborate (**5**BF_4) was added. Dimers containing $\mathbf{5}^+$ as the guest are observed almost exclusively in the mass spectrum. In line with earlier results,[11] the whole cluster distribution is converted into dimeric capsules $\mathbf{5}^+@\mathbf{1}_2$. Consequently, one might conclude that cations that are large enough will template the formation of hexameric pyrogallarene and resorcinarene capsules. When the tetrabutylammonium ion ($\mathbf{6}^+$) is used (Figure 1c), the observed cluster ions indeed shift to larger cluster sizes, with the hexamer $\mathbf{6}^+@\mathbf{1}_6$ corresponding to one of the most intense cluster signals. However, smaller and larger clusters are also observed, thus indicating that the template effect is not strong enough—possibly because the tetrahedral symmetry of the cation does not match the octahedral interior of the hexameric capsules. Also, quite an intense signal is observed for free $\mathbf{6}^+$ ions, even though the sample mixture contained host monomers and guest cations in a 6:1 ratio.

Consequently, we decided to use $[Ru^{II}(bpy)_3]^{2+}$ ($\mathbf{7}^{2+}$; bpy = 2,2′-bipyridine) as the template—not only because it is a pseudooctahedral metal complex with a shape more congru-

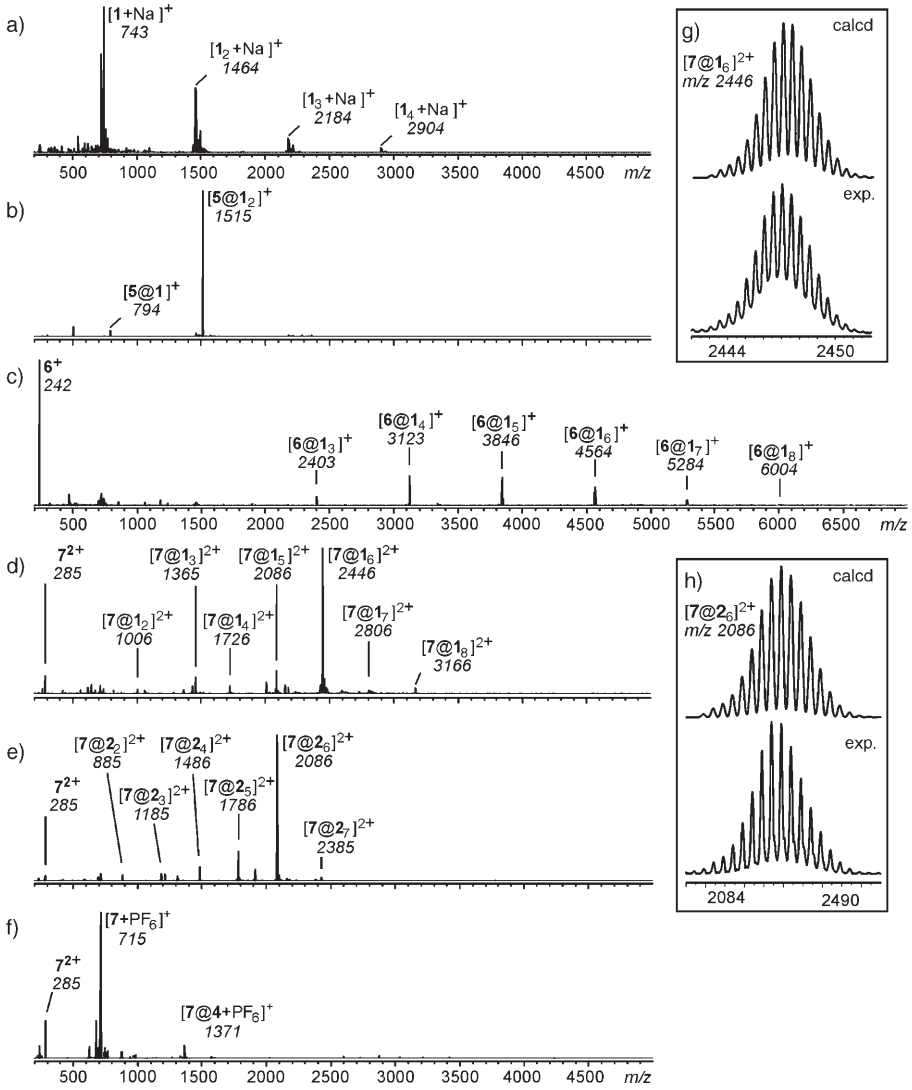


Figure 1. ESI-FTICR mass spectra of a) a 200 μM solution of **1** in $CHCl_3$/acetone (2:1), b) after addition of **5**BF_4, or c) (**6**)$_3$[Fe(CN)$_6$]. d, e) ESI-FTICR mass spectra of the same solution of **1** and **2**, respectively, with **7**$(PF_6)_2$, each optimized for hexamer intensity. f) Control experiment with tetramethylresorcinarene **4**. g,h) Experimental and calculated isotope patterns of the hexamer ions $[\mathbf{7}@\mathbf{1}_6]^{2+}$ and $[\mathbf{7}@\mathbf{2}_6]^{2+}$.

© 2006 Wiley-VCH Verlag GmbH & Co. KGaA, Weinheim

ent to the interior of the hexamer, but also because it is a dication and thus a lower m/z range is needed. The corresponding ESI mass spectra after addition of **1** (Figure 1 d) and **2** (Figure 1 e) with **7**$(PF_6)_2$ to the sample solutions indeed show the hexameric clusters as the by-far dominating signals. The use of softer ionization conditions leads to larger clusters, which indicates that additional pyrogallarene and resorcinarene molecules can bind unspecifically to the hexamer. Under these conditions, pentameric and tetrameric clusters are hardly visible. On the other hand, harsher conditions cause the clusters larger than the hexamers to vanish, while smaller clusters gain in intensity, thus indicating that they are formed from the hexamers through fragmentation involving monomer losses. When the ionization conditions are optimized, as shown in the spectra in Figure 1 d and e, unspecific binding can almost completely be avoided, with fragmentation minimized to only a small extent. Clearly, these experiments show that the formation of hexameric clusters depends on the size and the shape of the guest cation. The ruthenium complex $\mathbf{7}^{2+}$ exerts a more pronounced template effect than tetrabutylammonium $\mathbf{6}^{+}$. The formation of hexamers with $\mathbf{7}^{2+}$ is certainly not just a consequence of the unspecific clustering often typical for electrospray ionization, and we conclude that the hexameric clusters correspond to capsules which contain $\mathbf{7}^{2+}$ as the guest inside their cavity.

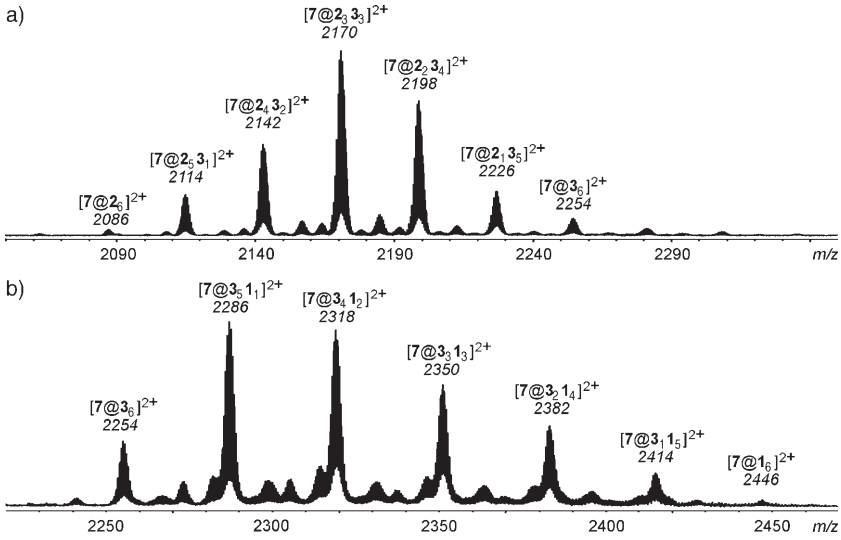


Figure 2. Formation of heterohexamers from 1:1 mixtures of **2** and **3** (top) as well as **1** and **3** (bottom) with $\mathbf{7}^{2+}$ as the guest cation.

A control experiment was performed with tetramethylresorcinarene **4**, since four of the OH groups are blocked by a methyl group and thus cannot participate in the formation of the hydrogen-bonding pattern. No hexameric capsules are observed in the mass spectrum (Figure 1 f), and the most intense signal in this spectrum corresponds to singly charged $\{[Ru(bpy)_3]PF_6\}^+$ at m/z 715, thus indicating that most of the guest salt is present in a free form in the sample solution.

If either **1** and **3** or **2** and **3** are mixed in 1:1 ratios, the mass spectra (Figure 2) reveal the formation of heterohexameric capsules. An intensity distribution close to the statistically expected one is obtained from a mixture of the two resorcinarenes **2** and **3**, while there is some bias towards resorcinarene hexamers in mixtures of resorcinarene **2** and pyrogallarene **1**. The exchange of monomers is too fast to be monitored by mass spectrometry. The equilibrium is reached before the first spectrum can be recorded (ca. 30 s after mixing the two solutions of the homohexamers).

While these experiments taken together are already good evidence for the formation of hexamers with capsular structures, one might of course ask whether the capsular structure is retained during ionization and whether the ions are still capsules in the gas phase. To address this question, tandem MS experiments were conducted with mass-selected $[\mathbf{7}@\mathbf{1}_6]^{2+}$ ions. The whole isotope pattern of this ion was isolated in the analyzer cell of our Fourier-transform ion-cyclotron-resonance (FTICR) mass spectrometer. These ions were irradiated in an infrared multiphoton dissociation (IRMPD) experiment with IR radiation from a CO_2 laser for different time intervals. Fragmentation is induced after a short induction period by an increase in the internal energies of the ions through photon absorption. The series of spectra in Figure 3 clearly show

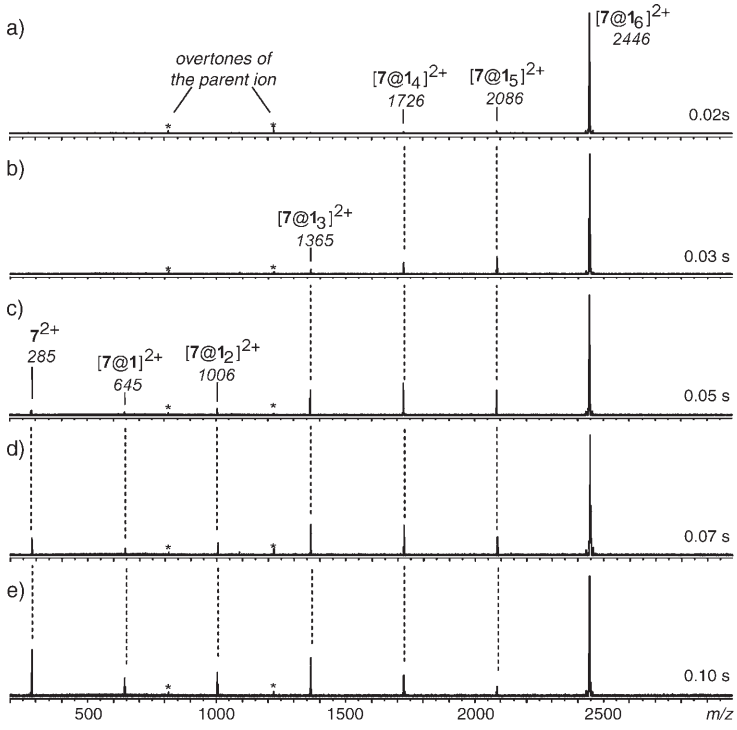


Figure 3. IRMPD experiment with mass-selected $[\mathbf{7}@\mathbf{1}_6]^{2+}$: Longer irradiation times lead to consecutive monomer losses. The formation of free $\mathbf{7}^{2+}$ starts to compete with the loss of additional monomers from the trimer $[\mathbf{7}@\mathbf{1}_3]^{2+}$.

 © 2006 Wiley-VCH Verlag GmbH & Co. KGaA, Weinheim

fragmentation to commence by three consecutive losses of pyrogallarene monomers with signals corresponding to $[\mathbf{7}@\mathbf{1}_5]^{2+}$ and $[\mathbf{7}@\mathbf{1}_4]^{2+}$ becoming visible after 0.02 s and a signal corresponding to $[\mathbf{7}@\mathbf{1}_3]^{2+}$ becoming visible after 0.03 s irradiation. At laser pulse lengths below 0.03 s, no signal corresponding to the free $[Ru(bpy)_3]^{2+}$ ion $\mathbf{7}^{2+}$ is observed, while up to three monomers are already missing in the structure. Only at longer irradiation periods does the signal for bare $\mathbf{7}^{2+}$ arise together with those of $[\mathbf{7}@\mathbf{1}_2]^{2+}$ and $[\mathbf{7}@\mathbf{1}]^{2+}$.

This is exactly the behavior expected for the hexameric capsule. When the cation is encapsulated, the cleavage of hydrogen bonds is necessary, before it can escape. The binding of the guest dication is still strong enough in the hexamer, pentamer, and tetramer, and only pyrogallarene monomers are successively lost from the parent ion. However, when the capsule is already disrupted and the dication is not surrounded by a sufficiently large number of pyrogallarene units, its dissociation from the complex starts to compete with the loss of even more monomers. This argument is even more convincing if one considers that the loss of the first monomer is energetically more demanding than those of the second and third monomers, because a larger number of hydrogen bonds needs to be broken. The barrier for expulsion of the first monomer must thus be higher than those of the consecutive losses.

In turn, a structure in which, for example, the dication interacts with an empty hexamer at the outer periphery (through a correspondingly small interaction area) would at least be expected to show a competition between the loss of monomers from the hexamer and the loss of the complete hexamer, thus giving rise to bare $\mathbf{7}^{2+}$—but this is not observed.

These experiments provide no strict evidence, but give good support to the assignment of a $\mathbf{7}^{2+}$ dication mechanically trapped inside a capsule. In conclusion, the hexameric clusters very likely retain their capsular structure even in the gas phase and do not rearrange their overall architecture during ionization.

Molecular modelling studies[12] on the basis of the X-ray crystallographic data of the pyrogallarene hexamer[3b] provides some insight into the congruence of the size, shape, and symmetry of the host cavity and guest cation (Figure 4). From the molecular model it becomes clear that $\mathbf{7}^{2+}$ fits almost perfectly into the cavity. The periphery of a pyridine ring from the guest cation is directed towards each of the six pyrogallarene monomers. Although the guest is only pseudooctahedral and deviates somewhat from a perfectly octahedral coordination geometry, it nevertheless matches the structure of the hexameric capsular host sufficiently well.

In conclusion, we present for the first time evidence that the hydrogen-bonded pyrogallarene and resorcinarene hexamers can be successfully ionized and transferred into the high-vacuum of a mass spectrometer. The comparison of different guest cations which provide the charge clearly show that the size, shape, and symmetry of the guest are important features for an efficient generation of hexamer ions with a capsule structure. Evidence for a capsular structure even in the gas phase after ionization comes from IRMPD experiments with mass-selected hexamer parent ions. The experimental results are in good agreement with simple molecular modeling calculations. These results not only indicate the stabilizing influence of suitable templating cations, they also point to the remarkable intrinsic softness of electrospray ionization mass spectrometry, which permits their characterization in the gas phase as isolated molecules without the influence of solvents and counterions.

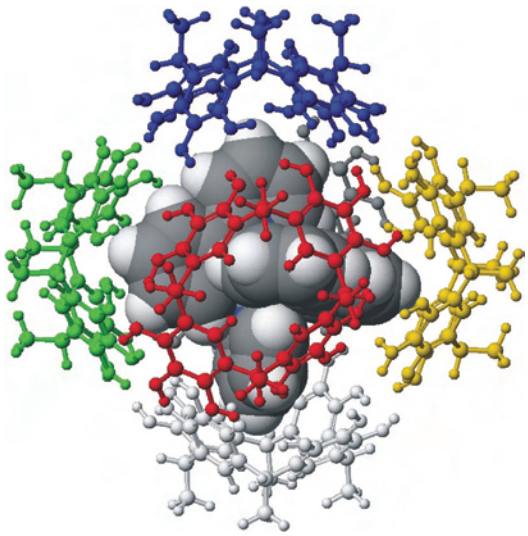


Figure 4. Model of the pyrogallarene hexamer (ball-and-stick representation, each monomer colored differently) and $\mathbf{7}^{2+}$ as the guest (space-filling representation). Alkyl chains at the bottom rim have been simplified as methyl groups.

Received: February 21, 2006
Revised: March 26, 2006
Published online: July 5, 2006

Keywords: mass spectrometry · pyrogallarene · resorcinarene · self-assembly · supramolecular chemistry

[1] a) M. M. Conn, J. Rebek, Jr., *Chem. Rev.* **1997**, *97*, 1647–1668; b) F. Hof, S. L. Craig, C. Nuckolls, J. Rebek, Jr., *Angew. Chem.* **2002**, *114*, 1556–1578; *Angew. Chem. Int. Ed.* **2002**, *41*, 1488–1508.

[2] Examples: a) J. Kang, J. Rebek, Jr., *Nature* **1997**, *385*, 50–52; b) H. Ito, T Kusukawa, M. Fujita, *Chem. Lett.* **2000**, 598–599; c) J. Chen, S. Körner, S. L. Craig, D. M. Rudkevich, J. Rebek, Jr., *Nature* **2002**, *415*, 385–386.

[3] a) L. R. MacGillivray, J. L. Atwood, *Nature* **1997**, *389*, 469–472; b) T. Gerkensmeier, W. Iwanek, C. Agena, R. Fröhlich, S. Kotila, C. Näther, J. Mattay, *Eur. J. Org. Chem.* **1999**, 2257–2262.

[4] a) L. Avram, Y. Cohen, *J. Am. Chem. Soc.* **2002**, *124*, 15148–15149; b) A. Shivanyuk, J. Rebek, Jr., *J. Am. Chem. Soc.* **2003**, *125*, 3432–3433; c) L. Avram, Y. Cohen, *Org. Lett.* **2003**, *5*, 3329–3332.

[5] a) L. Avram, Y. Cohen, *Org. Lett.* **2002**, *4*, 4365–4368; b) L. Avram, Y. Cohen, *Org. Lett.* **2003**, *5*, 1099–1102; c) L. Avram, Y. Cohen, *J. Am. Chem. Soc.* **2005**, *127*, 5714–5719.

[6] a) M. Yamanaka, A. Shivanyuk, J. Rebek, Jr., *J. Am. Chem. Soc.* **2004**, *126*, 2939–2943; b) L. C. Palmer, J. Rebek, Jr., *Org. Lett.* **2005**, *7*, 787–789; c) L. Avram, Y. Cohen, *Org. Lett.* **2006**, *8*, 219–222; hexameric capsules with internally ordered guests:

 © 2006 Wiley-VCH Verlag GmbH & Co. KGaA, Weinheim

J. L. Atwood, L. J. Barbour, A. Jerga, *Proc. Natl. Acad. Sci. USA* **2002**, *99*, 4837 – 4841.
[7] a) L. Avram, Y. Cohen, *J. Am. Chem. Soc.* **2003**, *125*, 16180 – 16181; b) L. Avram, Y. Cohen, *J. Am. Chem. Soc.* **2004**, *126*, 11556 – 11563.
[8] I. E. Philip, A. E. Kaifer, *J. Am. Chem. Soc.* **2002**, *124*, 12678 – 12679.
[9] For a review on mass spectrometric analysis of supramolecules, see: C. A. Schalley, *Mass Spectrom. Rev.* **2001**, *20*, 253 – 309.
[10] a) C. A. Schalley, T. Martín, U. Obst, J. Rebek, Jr., *J. Am. Chem. Soc.* **1999**, *121*, 2133 – 2138; b) C. A. Schalley, R. K. Castellano, M. S. Brody, D. M. Rudkevich, G. Siuzdak, J. Rebek, Jr., *J. Am. Chem. Soc.* **1999**, *121*, 4568 – 4579; c) A. Lützen, A. R. Renslo, C. A. Schalley, B. M. O'Leary, J. Rebek, Jr., *J. Am. Chem. Soc.* **1999**, *121*, 7455 – 7456.
[11] H. Mansikkamäki, M. Nissinen, C. A. Schalley, K. Rissanen, *New J. Chem.* **2003**, *27*, 88 – 97.
[12] CACHE 5.0 für Windows, Fujitsu Ltd. **2001**, Krakau, Poland.

 © 2006 Wiley-VCH Verlag GmbH & Co. KGaA, Weinheim

Protein Modifications

DOI: 10.1002/anie.200600570

Ligation of a Synthetic Peptide to the N Terminus of a Recombinant Protein Using Semisynthetic Protein *trans*-Splicing**

*Christina Ludwig, Martina Pfeiff, Uwe Linne, and Henning D. Mootz**

Our ability to prepare chemically modified proteins with defined covalent structure contributes significantly to the understanding of protein function on the molecular level. Unique biochemical, biophysical, and even cell-based investigations are enabled by the precise introduction of, for example, fluorophores, biophysical probes, unnatural amino acids (aa) with altered side chain or backbone composition, and posttranslational modifications.[1] Several techniques have been used to site-specifically incorporate such synthetic building blocks into proteins.[2] Probably the currently most widely used approach is based on the native chemical ligation (NCL) methodology.[2b] It relies on the chemoselective ligation of two polypeptides, either synthetic or recombinant, one of which bears a C-terminal α-thioester and the other an N-terminal cysteine residue, to give a fully synthetic or an N- or C-terminally modified semisynthetic protein (for reviews see Ref. [3]). Nonetheless, the reaction conditions and the nature of the required functional groups can limit the scope and complicate the practical handling of NCL. Because it is a bimolecular reaction, high reactant concentrations are required. Problems can also be encountered during the preparation of the reactants. In particular, the preparation of peptides or proteins with an α-thioester can be technically demanding. Protein α-thioesters are generated by thiolysis of a fusion construct of the protein of interest with a modified intein.[2e,f] Chemoenzymatic approaches to obtain semisynthetic proteins include reverse proteolysis,[2a,h,i,4] which also requires a peptide with an active ester, and the recently reported use of sortase.[2k] Herein, we show that protein *trans*-splicing can be exploited for the preparation of N-terminally modified semisynthetic proteins. Our approach requires neither an α-thioester at the synthetic peptide nor high reactant concentrations.

Protein splicing describes the autocatalytic removal of an internal protein domain, the intein, from a precursor protein, while the flanking sequences, the N- and C-exteins, are concomitantly linked with a native peptide bond.[5] In protein *trans*-splicing, the intein domain is split into two protein fragments, Int^N and Int^C, which form a complex and fold into the active intein.[6] To use this process for the preparation of semisynthetic proteins, we envisaged expression of the recombinant protein of interest (POI) as C-extein in fusion with an Int^C fragment and chemical synthesis of a polypeptide comprising the N-extein with the desired modification and the Int^N fragment (see Figure 1 A). However, the typical sizes of split intein fragments with about 100–180 amino acids (aa) for the Int^N fragment and about 36–50 aa for the Int^C fragment have restricted their preparation by solid-phase peptide synthesis (SPPS) to the Int^C fragment.[7] Interestingly, a recent genetic investigation on alternative split sites in the *Ssp* DnaB intein showed that an Int^N fragment of only 11 aa and its corresponding 143-aa Int^C counterpart were capable of protein *trans*-splicing in vivo when co-expressed in *E. coli*.[8]

The key question at the beginning of this study was whether the active intein could also be reconstituted from these two fragments in vitro. Because the removed 11 aa of the Int^N fragment correspond to two short β strands that are part of the catalytic pocket,[9] the 143-aa Int^C fragment is most likely prohibited to fold into a compact nativelike structure. While the presence of endogenous chaperones and co-expression of the complementary fragment is likely to have contributed to proper folding in vivo, the isolated fragments would be expected to be more prone to misfolding and aggregation, as has been observed for many split proteins and inteins.[10]

In initial tests, we therefore prepared model intein fusion proteins Trx-Int^N (**1**) and Int^C-His_6 (**2**), which contain thioredoxin (Trx) as the N-extein and a short sequence including a hexahistidine tag (His_6) as the C-extein (see Figure 1 B). Following individual expression of **1** and **2** in *E. coli*, both proteins could be purified from the soluble fraction, suggesting at least partial folding of the Int^C fragment. After **1** and **2** had been mixed in an equimolar ratio

[*] C. Ludwig, M. Pfeiff, Dr. U. Linne, Dr. H. D. Mootz
Philipps-Universität Marburg
Fachbereich Chemie/Biochemie
Hans-Meerwein-Strasse, 35032 Marburg (Germany)
Fax: (+49) 6421-282-2191
E-mail: mootz@chemie.uni-marburg.de

[**] We thank Prof. Mohamed Marahiel for continuous support. This research was funded by the DFG (Emmy Noether grant) and the Fonds der Chemischen Industrie. C.L. is a recipient of a Ph.D. fellowship from the Fonds der Chemischen Industrie.

Supporting information for this article is available on the WWW under http://www.angewandte.org or from the author.

InterScience
© 2006 Wiley-VCH Verlag GmbH & Co. KGaA, Weinheim

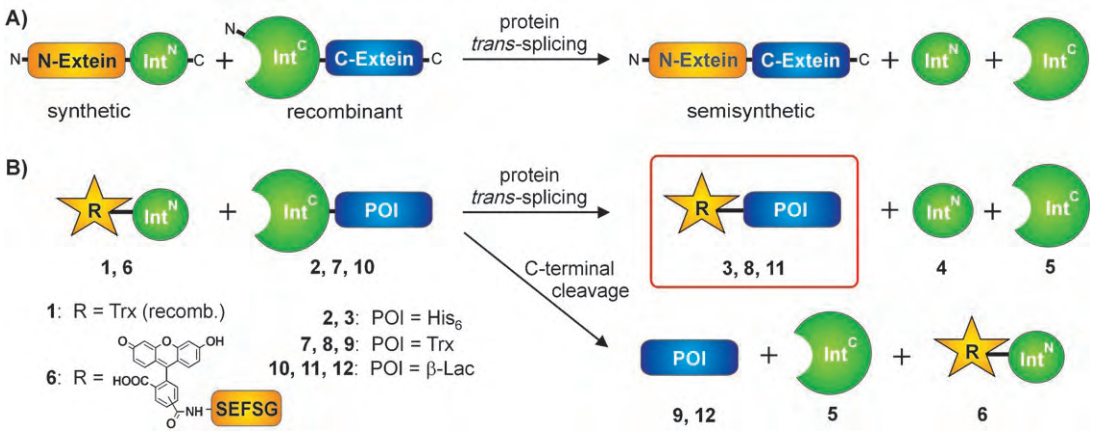


Figure 1. Principle of the approach: A) Protein *trans*-splicing is mediated by N- and C-terminal intein fragments (Int^N and Int^C) and results in ligation of the fused extein sequences with a native peptide bond. B) The group R, which represents the N-extein and may contain chemical modifications, is ligated to the protein of interest (POI). The Int^N fusion constructs can be either a synthetic peptide or a recombinant protein. C-terminal cleavage is a premature release of the POI from the Int^C fragment and occurs as a side reaction. Calculated molecular masses (in Da): **1**: 14798.9, **2**: 18078.5, **3**: 15035.0, **4**: 1320.5, **5**: 16539.0, **6**: 2186.1, **7**: 30212.6, **8**: 14556.1, **9**: 13690.0, **10**: 47252.9, **11**: 31596.7, **12**: 30731.0. βLac = β-lactamase, His_6 = hexahistidine tag, Trx = thioredoxin.

(12 μM in each) and incubated at pH 7.0 and 25 °C, the formation of the expected splice products could be monitored by SDS-PAGE and ESI-TOF MS (see the Supporting Information). A kinetic analysis of the reaction revealed that a splicing yield of about 25% was reached after 40 h. These data indicate that the Int^N and Int^C fragments are surprisingly robust and show that intein activity can be reconstituted in vitro from recombinant protein fragments without further renaturation steps.

Encouraged by these findings, we replaced the recombinant construct **1** with the synthetic peptide 5(6)-carboxyfluorescein- SEF*SG*CISGDSLISLASR (compound **6**, see Figure 1B, the sequence of Int^N is underlined). 5(6)-Carboxyfluorescein-SEF*SG* (abbreviated Fl) represents the N-extein; the two amino acids depicted in italics are native residues flanking the intein. The two C-terminal residues were added to the peptide in analogy to the sequence of **1**. Upon incubation of **6** and Int^C-His_6 (**2**), spontaneous formation of the active intein from the synthetic and recombinant fragments was again observed. The semisynthetic splice product Fl-*SIE*GSRSHHHHHH was detected by UV light on a 20% acrylamide SDS-PAGE gel and by ESI-TOF MS analysis (not shown; $M_{calcd} = 2423.3$ Da, $M_{expt} = 2423.8$ Da). Three native residues of the C-extein were included in all Int^C constructs and are indicated in italics.

We moved on to explore the potential of our approach to prepare semisynthetic proteins. The construct Int^C-Trx-His_6 (**7**), in which the 12-kDa protein Trx represented the C-extein (Figure 1B), was expressed in *E. coli* and purified from the soluble fraction. Incubation of **7** with synthetic peptide **6** yielded the desired semisynthetic protein Fl-Trx-His_6 (**8**) in a time-dependent fashion. Also the intein products of the reaction, Int^N (**4**) and Int^C (**5**), could be identified (see Figure 2A–C).

The general assumption for protein *trans*-splicing is a fast intein fragment association step followed by the rate-determining pseudo-monomolecular reaction of intein folding and protein splicing.[11] In agreement with this model, the kinetic data could be fitted by first-order kinetics. The calculated rate constant of $k = (4.1 \pm 0.2) \times 10^{-5}\ s^{-1}$ is comparable to that determined for the naturally occurring split *Ssp* DnaE

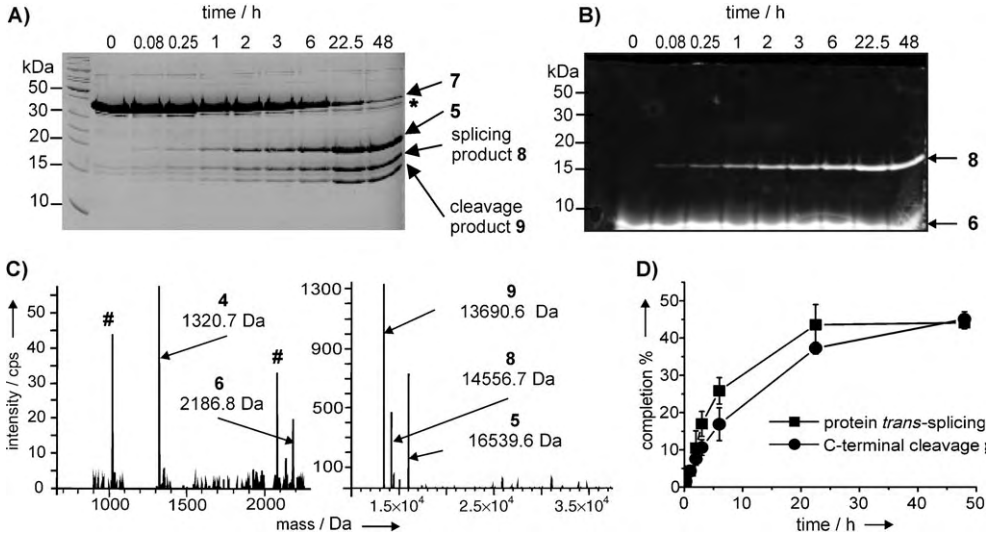


Figure 2. Semisynthetic protein *trans*-splicing. Analysis of the reaction of synthetic peptide **6** (80 μM) with recombinant protein Int^C-Trx-His_6 (**7**) (40 μM) at 25 °C to give semisynthetic Fl-Trx-His_6 (**8**). A, B) Reaction progress monitored on an SDS-PAGE gel using Coomassie staining (A) or UV light (B) (* = impurity protein band). C) ESI-TOF MS analysis of the reaction mixture after 48 h of incubation (mass signals of impurities are marked #). D) Time courses of the protein *trans*-splicing and the C-terminal cleavage reactions.

© 2006 Wiley-VCH Verlag GmbH & Co. KGaA, Weinheim

intein[11] but about 17-fold lower than that reported for the *Ssp* DnaB intein split at the previously known permissive site.[12] The likely explanation for this finding is that the more radical split site employed in this study has a more significant impact on association or folding of the two fragments. Despite these kinetic differences the total achievable yield of protein *trans*-splicing of 40–45% is identical in both cases[12] and lies in the typical range reported for various split inteins.[7a,10c,11–14]

Interestingly, another 40–45% of Int^C-Trx-His_6 (**7**) was transformed into the additional product **9**, which was identified by ESI-TOF MS analysis as the C-extein Trx-His_6 (Figure 2A–C). The formation of **9** by C-terminal cleavage proceeded with a first-order rate constant of $k = (2.1 \pm 0.9) \times 10^{-5}\ s^{-1}$ (Figure 2D). Although undesired, this common side reaction in protein splicing is not problematic as long as the splicing and cleavage products can be separated in a subsequent purification step.[15]

Furthermore, we found that a molar excess of synthetic peptide **6** over protein **7** did not improve the product yields (not shown). The reaction is best performed at a molar ratio of 1:1, which is favorable in economic terms, since only small amounts of the synthetic peptide are consumed. In control reactions using intein fragments with mutations in the key catalytic residues we could confirm that the reaction still proceeds according to the established pathway of protein *trans*-splicing (see the Supporting Information).

To demonstrate the preparative utility of semisynthetic protein *trans*-splicing, we undertook the synthesis, purification, and biochemical characterization of two fluorescein-labeled proteins on a larger scale. For the semisynthesis of Fl-Trx-His_6 (**8**), the above-mentioned **6** and **7** were mixed at equimolar concentrations of 62 μM each in a total volume of 1.5 mL (corresponding to 0.2 mg of peptide and 2.8 mg of protein). The reaction was allowed to proceed for 22 h at 25 °C, at which point about 40% of **7** was converted to the desired product. Pure Fl-Trx-His_6 (**8**) was obtained after anion exchange and a final step of Ni-NTA chromatography (Figure 3A–C) in an overall yield of about 30% (≈0.4 mg). Figure 3D shows that the purified semisynthetic thioredoxin **8** exhibits slightly higher enzymatic activity in an insulin-precipitation assay[16] than the recombinant thioredoxin positive control **1**.

The 30.7-kDa enzyme β-lactamase (βLac) served as the second example. The fusion protein Int^C-βLac-His_6 (**10**, see Figure 1B) was found in the inclusion bodies after expression in *E. coli*. After solubilization in 8 M urea, it was purified using Ni-NTA chromatography under denaturing conditions. Soluble protein was obtained by refolding in a one-step dialysis against assay buffer. Incubation of peptide **6** with **10** at 25 °C (12 μM in each, ≈1.7 mg of protein **10**) for 42 h led to the semisynthetic splice product Fl-βLac-His_6 (**11**) in about 35% yield and similar amounts of the C-terminal cleavage product **12** (see Figure 4A,B). After two-step purification involving anion exchange and Ni-NTA chromatography, pure **11** was obtained in an overall yield of about 30% (≈0.3 mg, Figure 4C).

The enzymatic activity of the semisynthetic protein was assayed photometrically by nitrocefin hydrolysis (Figure 4D) and was indistinguishable from that of an independently

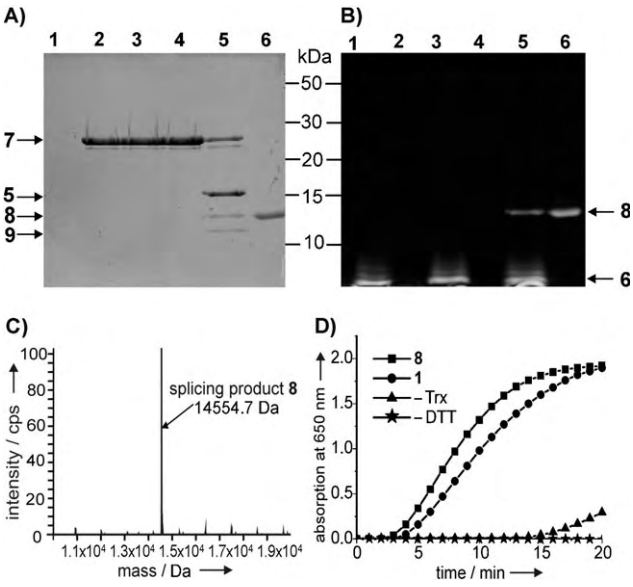


Figure 3. Preparation and characterization of semisynthetic Fl-Trx-His_6 (**8**). A, B) Reaction and purification monitored on a SDS-PAGE gel using Coomassie staining (A) or UV light (B). Lane 1: peptide **6**; lane 2: protein **7**; lane 3: **6** and **7** reacted at 25 °C and each 62 μM at $t = 0$ h; lane 4: protein **7** alone under the same conditions for 22 h; lane 5: same as for lane 3 but at $t = 22$ h; lane 6: purified semisynthetic product **8**. C) ESI-TOF MS of pure product **8**. D) Insulin-precipitation assay of enzymatic activity of semisynthetic **8** in comparison to that of the Trx control construct **1**. Two negative controls, in which either the Trx protein or the substrate DTT were omitted, are included.

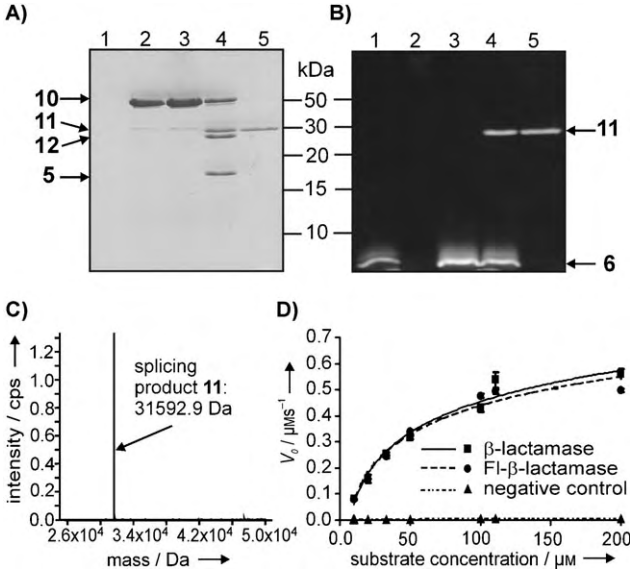


Figure 4. Preparation and characterization of semisynthetic Fl-βLac-His_6 (**11**). Analysis of the reaction and purification on an SDS-PAGE gel using Coomassie staining (A) and UV light (B). Lane 1: peptide **6**; lane 2: protein **10**; lane 3: **6** and **10** each 12 μM and $t = 0$ h; lane 4: **6** and **10** reacted at 25 °C and $t = 42$ h; lane 5: purified semisynthetic Fl-βLac-His_6 (**11**). C) ESI-TOF MS of pure **11** ($M_{calcd} = 31596.7$ Da). D) Enzymatic assay of **11** based on nitrocefin hydrolysis. The construct β-lactamase-His_6 was used as a positive control, construct **7** served as a negative control.

 © 2006 Wiley-VCH Verlag GmbH & Co. KGaA, Weinheim

prepared control construct βLac-His_6 ($K_{M(Fl\text{-}\beta Lac)} = (119.7 \pm 4.2)$ μM; $K_{M(\beta Lac)} = (112.7 \pm 3.3)$ μM; $k_{cat(Fl\text{-}\beta Lac)} = (212 \pm 30)\ s^{-1}$; $k_{cat.(\beta Lac)} = (204 \pm 42)\ s^{-1}$). Thus, both semisynthetic proteins were produced in pure form and good yields, and their catalytic activities remained unaffected by the expression as an intein fusion and the subsequent protein-splicing reaction.

In conclusion, the approach described here is an attractive and easy-to-perform alternative for the preparation of N-terminally modified semisynthetic proteins by protein *trans*-splicing. As a main advantage, the synthesis of an α-thioester peptide, as required for NCL, or other active esters, is avoided. Also the generation of an N-terminal cysteine at the recombinant protein, for example, by treatment with a protease which entails an additional purification step, is circumvented. Efficient reaction progress is obtained at reactant concentrations as low as 10–60 μM due to the inherent affinity of the self-cleaving intein fragments. The amino acid left behind at the ligation junction is a serine, which should generally be better tolerated in the protein of interest than a cysteine in the case of NCL. Our approach has the potential to be generally applicable, because inteins are promiscuous with respect to their fused extein sequences.

Received: February 12, 2006
Published online: July 5, 2006

Keywords: intein · peptides · protein modifications · protein splicing

[1] a) M. E. Hahn, T. W. Muir, *Trends Biochem. Sci.* **2005**, *30*, 26; b) L. Wang, P. G. Schultz, *Angew. Chem.* **2005**, *117*, 34; *Angew. Chem. Int. Ed.* **2005**, *44*, 34.

[2] a) D. Y. Jackson, J. Burnier, C. Quan, M. Stanley, J. Tom, J. A. Wells, *Science* **1994**, *266*, 243; b) P. E. Dawson, T. W. Muir, I. Clark-Lewis, S. B. Kent, *Science* **1994**, *266*, 776; c) H. F. Gaertner, R. E. Offord, R. Cotton, D. Timms, R. Camble, K. Rose, *J. Biol. Chem.* **1994**, *269*, 7224; d) D. A. Erlanson, M. Chytil, G. L. Verdine, *Chem. Biol.* **1996**, *3*, 981; e) T. W. Muir, D. Sondhi, P. A. Cole, *Proc. Natl. Acad. Sci. USA* **1998**, *95*, 6705; f) T. C. Evans, Jr., J. Benner, M. Q. Xu, *Protein Sci.* **1998**, *7*, 2256; g) L. Wang, A. Brock, B. Herberich, P. G. Schultz, *Science* **2001**, *292*, 498; h) N. Wehofsky, N. Koglin, S. Thust, F. Bordusa, *J. Am. Chem. Soc.* **2003**, *125*, 6126; i) Z. Machova, R. von Eggelkraut-Gottanka, N. Wehofsky, F. Bordusa, A. G. Beck-Sickinger, *Angew. Chem.* **2003**, *115*, 5065; *Angew. Chem. Int. Ed.* **2003**, *42*, 4916; j) B. L. Nilsson, R. J. Hondal, M. B. Soellner, R. T. Raines, *J. Am. Chem. Soc.* **2003**, *125*, 5268; k) H. Mao, S. A. Hart, A. Schink, B. A. Pollok, *J. Am. Chem. Soc.* **2004**, *126*, 2670.

[3] a) P. E. Dawson, S. B. Kent, *Annu. Rev. Biochem.* **2000**, *69*, 923; b) T. W. Muir, *Annu. Rev. Biochem.* **2003**, *72*, 249; c) B. L. Nilsson, M. B. Soellner, R. T. Raines, *Annu. Rev. Biophys. Biomol. Struct.* **2005**, *34*, 91.

[4] T. K. Chang, D. Y. Jackson, J. P. Burnier, J. A. Wells, *Proc. Natl. Acad. Sci. USA* **1994**, *91*, 12544.

[5] C. J. Noren, J. Wang, F. B. Perler, *Angew. Chem.* **2000**, *112*, 458; *Angew. Chem. Int. Ed.* **2000**, *39*, 450.

[6] a) H. Wu, Z. Hu, X. Q. Liu, *Proc. Natl. Acad. Sci. USA* **1998**, *95*, 9226; b) H. Paulus, *Annu. Rev. Biochem.* **2000**, *69*, 447.

[7] a) B. M. Lew, K. V. Mills, H. Paulus, *Biopolymers* **1999**, *51*, 355; b) T. C. Evans, Jr., D. Martin, R. Kolly, D. Panne, L. Sun, I. Ghosh, L. Chen, J. Benner, X. Q. Liu, M. Q. Xu, *J. Biol. Chem.* **2000**, *275*, 9091; c) I. Giriat, T. W. Muir, *J. Am. Chem. Soc.* **2003**, *125*, 7180.

[8] W. Sun, J. Yang, X. Q. Liu, *J. Biol. Chem.* **2004**, *279*, 35281.

[9] Y. Ding, M. Q. Xu, I. Ghosh, X. Chen, S. Ferrandon, G. Lesage, Z. Rao, *J. Biol. Chem.* **2003**, *278*, 39133.

[10] a) K. V. Mills, B. M. Lew, S. Jiang, H. Paulus, *Proc. Natl. Acad. Sci. USA* **1998**, *95*, 3543; b) K. Shingledecker, S. Q. Jiang, H. Paulus, *Gene* **1998**, *207*, 187; c) M. W. Southworth, E. Adam, D. Panne, R. Byer, R. Kautz, F. B. Perler, *EMBO J.* **1998**, *17*, 918; d) T. Yamazaki, T. Otomo, N. Oda, Y. Kyogoku, K. Uegaki, N. Ito, Y. Ishino, H. Nakamura, *J. Am. Chem. Soc.* **1998**, *120*, 5591; e) H. Yagi, T. Tsujimoto, T. Yamazaki, M. Yoshida, H. Akutsu, *J. Am. Chem. Soc.* **2004**, *126*, 16632.

[11] D. D. Martin, M. Q. Xu, T. C. Evans, Jr., *Biochemistry* **2001**, *40*, 1393.

[12] S. Brenzel, T. Kurpiers, H. D. Mootz, *Biochemistry* **2006**, *45*, 1571.

[13] H. D. Mootz, T. W. Muir, *J. Am. Chem. Soc.* **2002**, *124*, 9044.

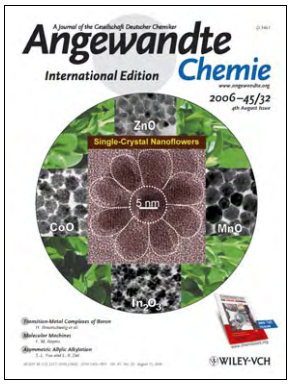
[14] The residual fraction usually remains unreacted for unknown reasons. Misfolding and aggregation are likely explanations.

[15] We believe that the observed C-terminal cleavage reflects incomplete folding of the intein under in vitro conditions, because during co-expression of **1** and **7** in *E. coli* exclusively the protein *trans*-splicing product was formed, whereas also C-terminal cleavage was observed when purified **1** and **7** were incubated in in vitro reactions (see Figure S2 and data not shown). This observation excludes potential sequence constraints as the reason for C-terminal cleavage. Several attempts to eliminate the cleavage reaction by optimizing the reaction conditions, that is, by varying the parameters temperature, salt concentration, nature of reducing agent, and pH (see the Supporting Information), were unsuccessful so far. However, our results show that the Int^N–Int^C complex had formed almost quantitatively, which should be a good starting point for future optimization efforts to drive the reaction exclusively to the splicing product.

[16] A. Holmgren, *J. Biol. Chem.* **1979**, *254*, 9627.

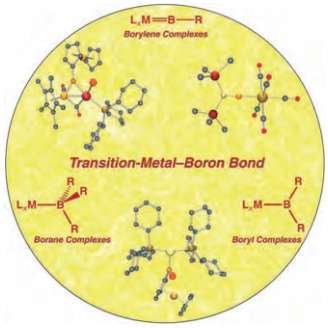
 © 2006 Wiley-VCH Verlag GmbH & Co. KGaA, Weinheim

Cover Picture

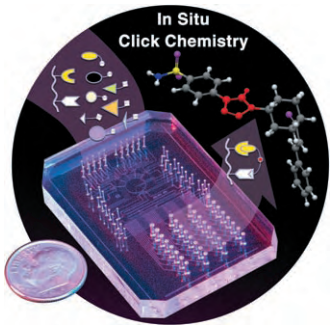


Arun Narayanaswamy, Huifang Xu, Narayan Pradhan, and Xiaogang Peng*

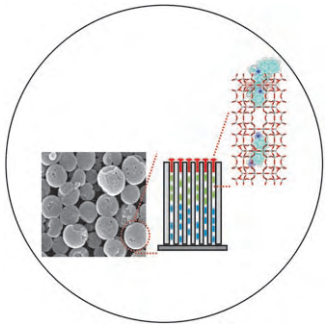
Single-crystal nanoflowers (shown in the cover picture) are grown by a general approach called limited ligand protection (LLP). LLP destabilizes the primary nanoparticles and promotes their three-dimensionally oriented attachment into complex nanostructures. LLP offers a low degree of ligand protection and can be used to yield both nanodots and nanoflowers. For more information see the Communication by X. Peng and co-workers on page 5361 ff.



Boron Ligands
Advances in transition-metal complexes of boron are described in the Review on page 5254 ff. by H. Braunschweig et al. A manifold of new coordination modes and synthetic methods for boron-containing ligands are highlighted.



Lab-on-a-Chip
In their Communication on page 5276 ff., H. R. Tseng, H. C. Kolb, and co-workers present the state-of-the-art of miniaturizing organic synthesis. Inhibitors of bovine carbonic anhydrase II were synthesized and screened in 32 parallel reactions on a microfluidic device.



Monolayers
Dyes in the open channels of monolayers of zeolite L crystals create a hierarchical order. G. Calzaferri et al. describe in the Communication on page 5282 ff. how these materials are the basis for systems where excitation energy is transported in one direction only.

Contents

VIP ***The following Communications have been judged by at least two referees to be "very important papers" and will be published online at www.angewandte.org soon:***

*S. Hiraoka, K. Harano, M. Shiro, Y. Ozawa, N. Yasuda, K. Toriumi, M. Shionoya**
Isostructural Coordination Capsules with a Series of 10 Different d^5–d^{10} Transition-Metal Ions

*J. G. Cordaro, D. Stein, H. Rüegger, H. Grützmacher**
Making the True "CP" Ligand

*N. Shimokhina, A. Bronowska, S. Homans**
Contribution of Ligand Desolvation to Binding Thermodynamics in a Ligand–Protein Interaction

*M. B. Harney, Y. Zhang, L. R. Sita**
Bimolecular Control over Polypropene Stereochemical Microstructure in a Well-Defined Two-State System and a New Fundamental Form: Stereogradient Polypropene

*H. Niu, M. Gao**
Synthesis of Diameter-Tunable CdTe Nanotubes Templated by One-Dimensional Nanowires of Cadmium Thiolate Polymer

*Y. Li, B. S. Lokitz, C. L. McCormick**
Thermally Responsive Vesicles and their Structural "Locking" through Polyelectrolyte Complex Formation

News

Organic Chemistry: Ley and Yoshida awarded ——— **5242**

Inorganic Chemistry: Christe honored ——— **5242**

Books

Nanocrystals Forming Mesoscopic Structures — Marie-Paule Pileni — *reviewed by K. J. Klabunde* ——— **5243**

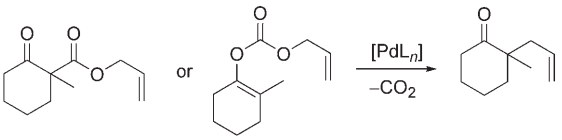
New Theories for Chemistry — Jan C. A. Boeyens — *reviewed by R. Berger* ——— **5243**

Highlights

Asymmetric Catalysis

S.-L. You,* L.-X. Dai ——— **5246 – 5248**

Enantioselective Palladium-Catalyzed Decarboxylative Allylic Alkylations

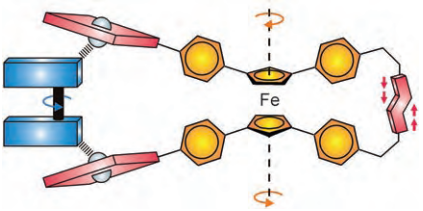


Triple A: Recent developments in palladium-catalyzed decarboxylative asymmetric allylic alkylation (AAA) reactions provide easy access to highly enantioenriched ketones with α-positioned quaternary or tertiary carbon stereocenters under mild conditions.

Molecular Machines

F. M. Raymo* ——— **5249 – 5251**

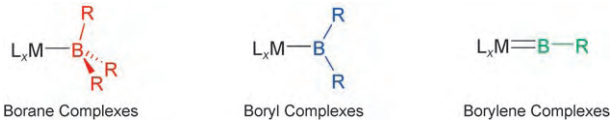
Intermolecular Coupling of Motion under Photochemical Control



An interesting twist: A system in which controlled motion in one part of the molecule is transmitted as rotary motion in a bound guest molecule represents a significant advance toward artificial molecular machines. Light initiates a scissoring motion in the host molecule, a ferrocene unit attached to an azobenzene handle (red) and to two Zn porphyrin units (red squares), which twists the bidentate guest compound (blue part).

© 2006 Wiley-VCH Verlag GmbH & Co. KGaA, Weinheim

Reviews



Glory B! The number and variety of compounds that feature a transition-metal–boron bond have grown significantly in the past fifteen years, and a range of hitherto unknown coordination modes of boron-based ligands have been realized (see scheme). This review article highlights the most useful synthetic strategies for the generation of transition-metal–boron bonds and discusses the most recent and intriguing compounds that have been reported.

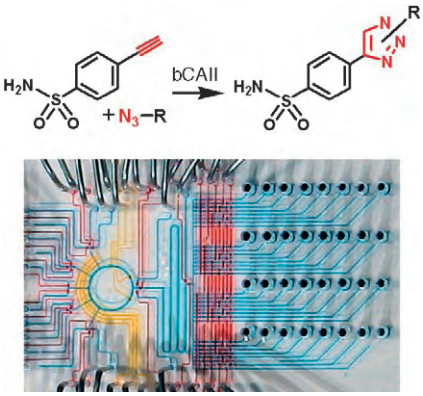
Boron Ligands

H. Braunschweig,* C. Kollann, D. Rais ____ **5254 – 5274**

Transition-Metal Complexes of Boron—New Insights and Novel Coordination Modes

Communications

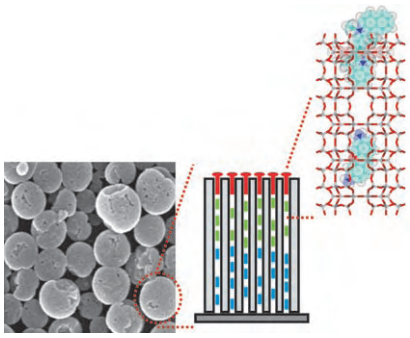
State-of-the-art: Automated chemical reaction circuits have been demonstrated to serve as a miniaturized operation platform for the parallel screening of 32 in situ click chemistry reactions with reduced consumption of reagents. A proof-of-concept study was performed with the bovine carbonic anhydrase II (bCAII) click chemistry system.



Lab-on-a-Chip

J. Wang, G. Sui, V. P. Mocharla, R. J. Lin, M. E. Phelps, H. C. Kolb,* H.-R. Tseng* ____ **5276 – 5281**

Integrated Microfluidics for Parallel Screening of an In Situ Click Chemistry Library



Unidirectional antennas: Dyes in the open channels of the robust monolayers of zeolite L crystals on a glass substrate create a hierarchical order (see picture). Coupling the dye-loaded monolayers to an external acceptor or donor stopcock dye at the channel ends enables electronic excitation energy to be trapped from donor molecules inside the crystal or to inject it to an acceptor inside the channels.

Monolayers

A. Zabala Ruiz, H. Li, G. Calzaferri* ____ **5282 – 5287**

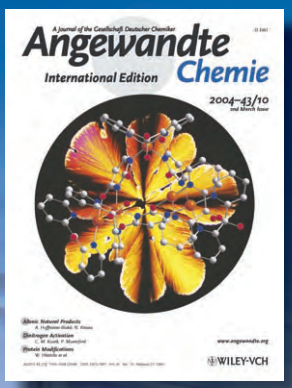
Organizing Supramolecular Functional Dye–Zeolite Crystals

For the USA and Canada:
ANGEWANDTE CHEMIE International Edition (ISSN 1433-7851) is published weekly by Wiley-VCH PO Box 191161, D 69451 Weinheim, Germany. Air freight and mailing in the USA by Publications Expediting Inc. 200 Meacham Ave., Elmont, NY 11003. Periodicals postage paid at Jamaica NY 11431. US POSTMASTER: send address changes to *Angewandte Chemie*, Wiley-VCH, 111 River Street, Hoboken, NJ 07030. Annual subscription price for institutions: US$ 5685/5168 (valid for print and electronic / print or electronic delivery); for individuals who are personal members of a national chemical society prices are available on request. Postage and handling charges included. All prices are subject to local VAT/sales tax.

© 2006 Wiley-VCH Verlag GmbH & Co. KGaA, Weinheim

The best in chemistry –

for more than a hundred years



A Journal of the Gesellschaft Deutscher Chemiker

Angewandte
International Edition **Chemie**

www.angewandte.org

1888: ***The beginning of a success story***

Constant Innovations

- **1962:** *First issue of the International Edition*
- **1976:** *Graphical abstracts*
- **1979:** *Cover pictures*
- **1988:** *Centenary of Angewandte*
- **1989:** *Routine use of color*
- **1991:** *New section: Highlights*
- **1992:** *Computerized editorial tracking system*
- **1995:** *Internet service for readers*
- **1998:** *Regular press service; full-text online*
- **2000:** *New section: Essays; EarlyView: Communications available online ahead of the printed version*
- **2001:** *New section: Minireviews*
- **2002:** *Online submission of manuscripts*
- **2003:** *Weekly publication; new section: News; new layout*
- **2004:** *Backfiles (1962-1997); ManuscriptXpress: Online system for authors and referees*



Angewandte's advisors...

Jean-Marie Lehn
Université Strasbourg
Collège de France

» ***Angewandte Chemie*** *provides timely reviews of great depth and wide interest together with short reports of top quality frontier research. Creative work remains creative wherever it is published! However,* ***Angewandte Chemie*** *brings high visibility while keeping restrain and rigor. Finally, it is also supranational, as science is.* «

Angewandte Chemie International Edition *is a journal of the German Chemical Society (GDCh)*

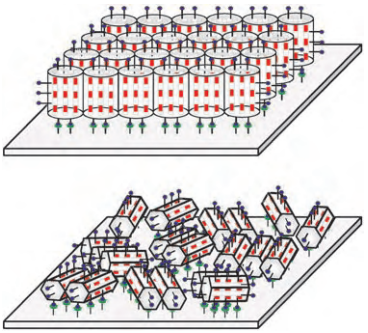
GDCh

WILEY InterScience® DISCOVER SOMETHING GREAT

WILEY-VCH

1851404_gu

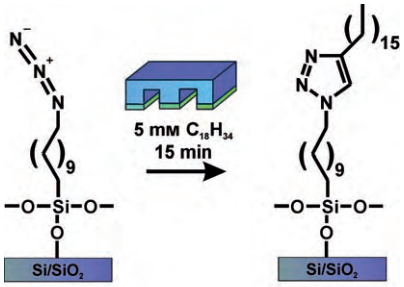
Which way to turn: The tendency of microcrystals to attach to surfaces through their largest faces has resulted in two orientations of zeolite L monolayers on glass. Fluorophore-containing cylindrical and hexagonal columnar zeolite L crystals assemble into vertically and horizontally oriented monolayers, respectively, on glass plates (see pictures). The photoluminescences of the monolayers are highly anisotropic.



Surface Chemistry

J. S. Lee, H. Lim, K. Ha, H. Cheong, K. B. Yoon* ——— **5288 – 5292**

Facile Monolayer Assembly of Fluorophore-Containing Zeolite Rods in Uniform Orientations for Anisotropic Photoluminescence

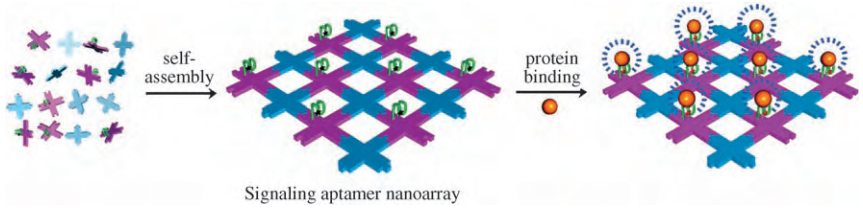


Print and click: "Click" chemistry can be efficiently combined with microcontact printing. Synthesis in the nanoscale confinement between an elastomeric stamp and a reactive substrate leads to the desired product within a short time, without a catalyst, and under ambient conditions. As a result, 1-octadecyne could be printed onto an azido-terminated, self-assembled monolayer on a silicon oxide substrate (see scheme).

Microcontact Printing

D. I. Rozkiewicz, D. Jańczewski, W. Verboom, B. J. Ravoo,* D. N. Reinhoudt* ——— **5292 – 5296**

"Click" Chemistry by Microcontact Printing

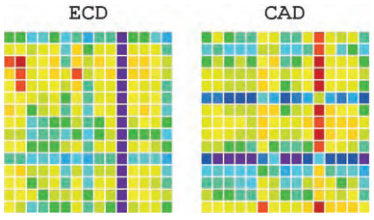


Sticking the tiles: A DNA-tile-directed self-assembly of signaling aptamers into high-density nanoarrays allows subnanomolar detection of protein molecules by using confocal fluorescence microscopy imaging. This water-soluble aptamer microarray provides a novel strategy for developing programmable sensor arrays.

Signaling Aptamer

C. Lin, E. Katilius, Y. Liu, J. Zhang, H. Yan* ——— **5296 – 5301**

Self-Assembled Signaling Aptamer DNA Arrays for Protein Detection



Complementary cleavage: A large-scale (ca. 15 000 spectra) comparison between the cleavage sites and the preferences of collision-activated dissociation (CAD) and electron-capture dissociation (ECD) in tandem mass spectrometry has proved beyond doubt their complementary nature (see picture, red: high, blue: low). The study has also suggested the presence of a preferred N-terminal structure in gas-phase tryptic peptide dications.

Peptide Fragmentation

M. M. Savitski, F. Kjeldsen, M. L. Nielsen, R. A. Zubarev* ——— **5301 – 5303**

Complementary Sequence Preferences of Electron-Capture Dissociation and Vibrational Excitation in Fragmentation of Polypeptide Polycations

© 2006 Wiley-VCH Verlag GmbH & Co. KGaA, Weinheim

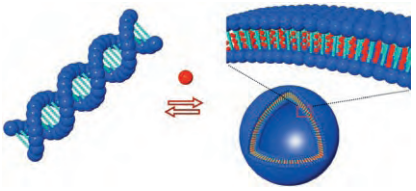
Contents

Intercalations

J.-H. Ryu, H.-J. Kim, Z. Huang, E. Lee, M. Lee* ——— **5304 – 5307**

Self-Assembling Molecular Dumbbells: From Nanohelices to Nanocapsules Triggered by Guest Intercalation

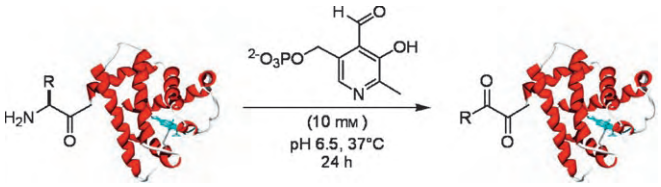
Dumbbells that are not dumb: Dumbbell-shaped molecules based on a hexa-*p*-phenylene derivative self-assemble into well-defined left-handed helical fibers in aqueous solution. These helical nanofibers convert reversibly into hollow nanocapsules by intercalation of aromatic guest molecules (red spheres).



Bioorganic Chemistry

J. M. Gilmore, R. A. Scheck, A. P. Esser-Kahn, N. S. Joshi, M. B. Francis* ——— **5307 – 5311**

N-Terminal Protein Modification through a Biomimetic Transamination Reaction



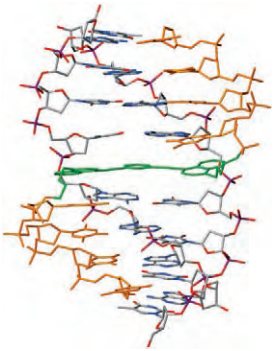
One hit wonder: A biomimetic transamination reaction has been developed that employs pyridoxal-5-phosphate to modify the N terminus of proteins and peptides under mild conditions. This technique introduces a uniquely reactive carbonyl group in a single location (see scheme), thus allowing further elaboration through oxime or hydrazone formation. This modification strategy is also compatible with proteins containing a free cysteine residue.

DNA Recognition

V. V. Filichev,* M. C. Nielsen, N. Bomholt, C. H. Jessen, E. B. Pedersen **5311 – 5315**

High Thermal Stability of 5′-5′-Linked Alternate Hoogsteen Triplexes at Physiological pH

DNA glue: A new alternate-strand linker (shown in green) has been synthesized that can connect two short DNA sequences (5- and 9-mers, yellow) and bind to double-stranded DNA through major-groove interactions at pH 7.2 (see model). The resulting triple helices have high thermal stabilities as shown by melting temperatures exceeding 37 °C at physiological pH values.

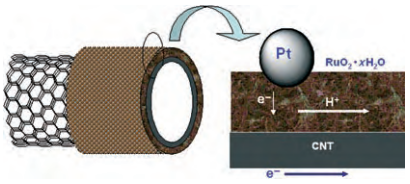


Power Sources

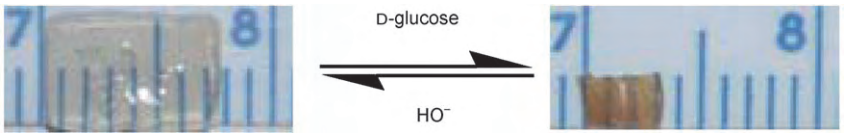
L. Cao, F. Scheiba, C. Roth, F. Schweiger, C. Cremers, U. Stimming, H. Fuess, L. Chen, W. Zhu, X. Qiu* ——— **5315 – 5319**

Novel Nanocomposite Pt/$RuO_2{\cdot}xH_2O$/Carbon Nanotube Catalysts for Direct Methanol Fuel Cells

The perfect combination: $RuO_2{\cdot}xH_2O$ for donating and accepting protons and electrons and carbon nanotubes (CNTs) for compensating the loss of electron conductivity caused by the RuO_2 coating, improving the electrode microstructure, and lowering the electrode resistance. The result: superb performance of the title catalyst for direct electrooxidation of methanol.



© 2006 Wiley-VCH Verlag GmbH & Co. KGaA, Weinheim

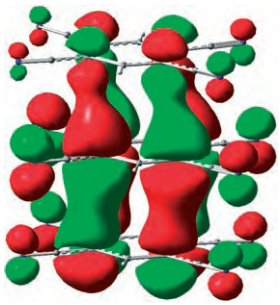


See the shrink: Systematic modification of poly(methyl methacrylate) leads to a chemomechanical polymer that selectively contracts in the presence of glucose at physiological levels in human blood plasma. The polymer also exhibits good reversibility allowing continuous expansion–contraction cycles.

Biosensors

G. K. Samoei, W. Wang, J. O. Escobedo, X. Xu, H.-J. Schneider,* R. L. Cook, R. M. Strongin* ——— **5319 – 5322**

A Chemomechanical Polymer that Functions in Blood Plasma with High Glucose Selectivity



On a reduced charge: The reduction of 1,2,4,5-tetracyanobenzene (TCNB) with tetrakis(dimethylamino)ethylene (TDAE) forms $[TDAE][TCNB]_3 \cdot MeCN$. Characterization reveals that the $[TDAE]^{2+}$ ion is present, and that TCNB is reduced forming diamagnetic $[TCNB]_3^{2-}$. The reduced TCNB units (see picture) are best described as $[TCNB]^{\approx 0.5-}$-$[TCNB]^{\approx 1-}$-$[TCNB]^{\approx 0.5-}$ containing fractionally charged organic species.

Cyanocarbon Compounds

J. D. Bagnato, W. W. Shum, M. Strohmeier, D. M. Grant, A. M. Arif, J. S. Miller* ——— **5322 – 5326**

The Structure of Fractionally Charged Tetracyanobenzene^{n-} Present in $[TCNB]_3^{2-}$

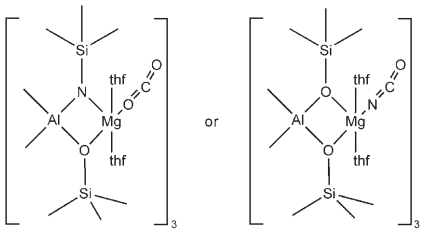


A matter of attraction: A magnet of nominal $V^{II}(TCNB^-)_{1.5}(TCNB^0)_{x-1.5}$-$[V^{-I}(CO)_6]_{0.5} \cdot z$ solvent composition ($T_c = 325$ K) is synthesized and its magnetic properties examined. Its amorphous nature makes it difficult to determine its complex composition and structure. It is a soft ferrimagnet with a coercive field of 7 Oe. The picture shows a sample in a capillary tube being attracted to a magnet at room temperature.

Magnetism

M. L. Taliaferro, M. S. Thorum, J. S. Miller* ——— **5326 – 5331**

Room-Temperature Organic-Based Magnet ($T_c \approx 50\,^\circ C$) Containing Tetracyanobenzene and Hexacarbonylvanadate(−I)



OCO or NCO? The case of irreversible CO_2 coordination to Mg cations has been revisited and reinterpreted as a more straightforward case of reaction of CO_2 with silazanate ligands and formation of coordinated NCO ligands on the basis of DFT calculations, NMR, and chemical-degradation experiments.

Structure Elucidation

H. Phull, D. Alberti, I. Korobkov, S. Gambarotta,* P. H. M. Budzelaar* ——— **5331 – 5334**

Fixation of CO_2 by Magnesium Cations: A Reinterpretation

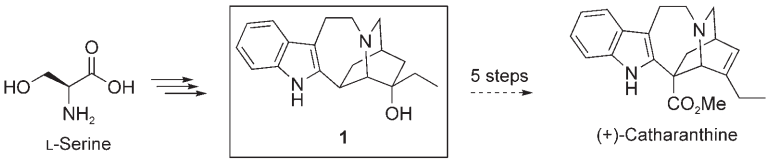
© 2006 Wiley-VCH Verlag GmbH & Co. KGaA, Weinheim

Contents

Natural-Products Synthesis

L. Moisan, P. Thuéry, M. Nicolas, E. Doris,* B. Rousseau —— 5334 – 5336

Formal Synthesis of (+)-Catharanthine



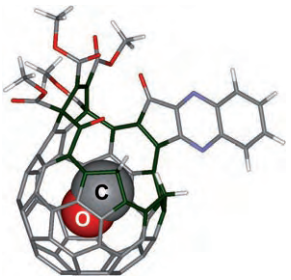
Madagascan periwinkle is the current source of (+)-catharanthine, the crucial building block of the major antitumor agent vinorelbine. In the formal synthesis of this natural product, the key intermediate **1** described by Büchi and co-workers was obtained in virtually optically pure form from L-serine. The strategy presented may be viewed as a general synthetic approach to optically active isoquinuclidines.

Fullerenes

S.-i. Iwamatsu,* C. M. Stanisky, R. J. Cross, M. Saunders, N. Mizorogi, S. Nagase, S. Murata —— 5337 – 5340

Carbon Monoxide Inside an Open-Cage Fullerene

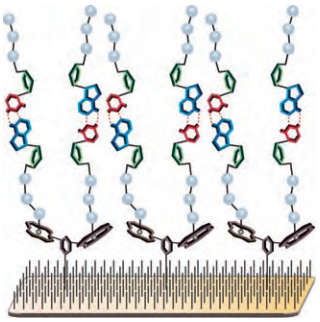
Inside the ball: An endohedral carbon monoxide complex of an open-cage derivative of a [60]fullerene is prepared by insertion of CO through the opening. The incorporation of CO within the C_{60} cage is confirmed by mass spectrometry as well as ^{13}C NMR and IR spectroscopic studies. The product releases CO under ambient conditions to recover a mixture of the endohedral water complex and the empty cage.



Self-Assembly

D. S. Turygin, M. Subat, O. A. Raitman, V. V. Arslanov, B. König,* M. A. Kalinina* —— 5340 – 5344

Cooperative Self-Assembly of Adenosine and Uridine Nucleotides on a 2D Synthetic Template

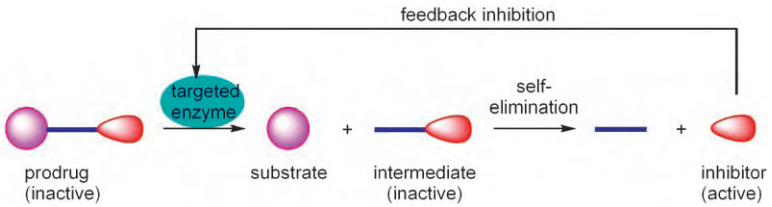


Double plane: Base pairing mediates sterically induced, cooperative self-assembly of complementary nucleotides on a template formed from amphiphilic bis(Zn^{II}–cyclen) derivatives ordered on thiolated surface. Real-time monitoring of binding events proved precise harboring of equal amounts of A and U nucleotides from their arbitrary combinations in solution into planar bilayers (see picture).

Enzyme Inhibition

J. Guo, J. Asong, G.-J. Boons* —— 5345 – 5348

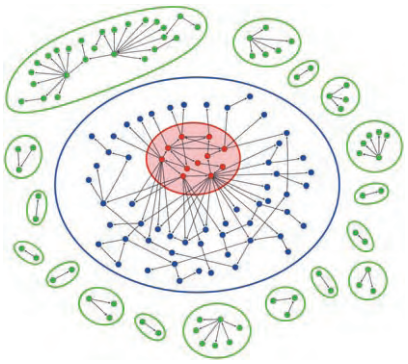
Selective Inhibition of Glycosidases by Feedback Prodrugs



In the loop: A novel concept for the selective inhibition of glycosidases has been developed whereby a glycosidase inhibitor is released by glycosidase-mediated hydrolysis of a prodrug, which subsequently inhibits the glycosidase that initiated the release of the inhibitor.

© 2006 Wiley-VCH Verlag GmbH & Co. KGaA, Weinheim

The fruitful core: Organic syntheses reported in the literature from 1850 to 2004 are analyzed with mathematical tools from network theory and statistical physics. There is a set of substances (the core) from which the majority of other organic compounds can be made (see picture; red: core, blue: periphery, green: islands). Search algorithms are used to identify small optimal sets of maximally useful chemicals.

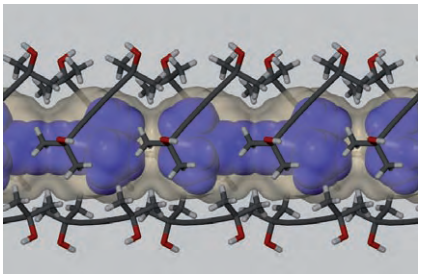


Organic Chemistry

K. J. M. Bishop, R. Klajn, B. A. Grzybowski* ——— **5348 – 5354**

The Core and Most Useful Molecules in Organic Chemistry

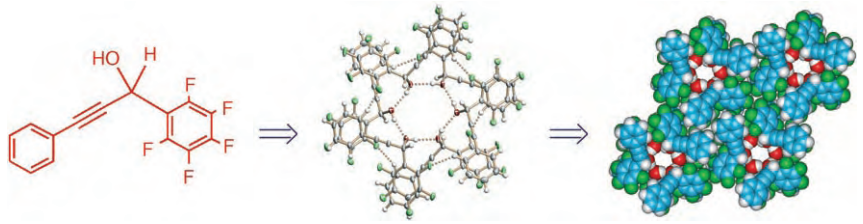
Molecular cannibalism: The concept of self-inclusion in the solid state can be subjective. A host–guest system is prepared in which the same compound (2,7-dimethyl-octa-3,5-diyne-2,7-diol) unequivocally plays both roles simultaneously.



Host–Guest Systems

G. O. Lloyd, J. Alen, M. W. Bredenkamp, E. J. C. de Vries, C. Esterhuysen, L. J. Barbour* ——— **5354 – 5358**

Solid-State Self-Inclusion: The Missing Link



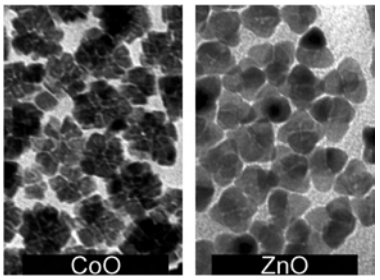
Six pack: A hexameric supramolecular structure with alternating enantiomers is formed in the solid state from propargylic alcohols. These hexamers further assemble to form channels and cages that host solvent molecules. The synergistic cooperation of O–H···O, C–H···F–C, and π–π interactions is important in establishing the supramolecular assembly.

Self-Assembly

M. Hyacinth, M. Chruszcz, K. S. Lee, M. Sabat,* G. Gao, L. Pu* _ **5358 – 5360**

Supramolecular Assemblies of Chiral Propargylic Alcohols

A varied bouquet: Crystalline nanoflowers (see picture) of compounds with different chemical and physical properties, for example, In_2O_3, ZnO, CoO, MnO, and ZnSe, are grown by a new approach, limited ligand protection (LLP). LLP destabilizes the primary nanoparticles and promotes their three-dimensionally oriented attachment into complex nanostructures.



Nanostructures VIP

A. Narayanaswamy, H. Xu, N. Pradhan, X. Peng* ——— **5361 – 5364**

Crystalline Nanoflowers with Different Chemical Compositions and Physical Properties Grown by Limited Ligand Protection

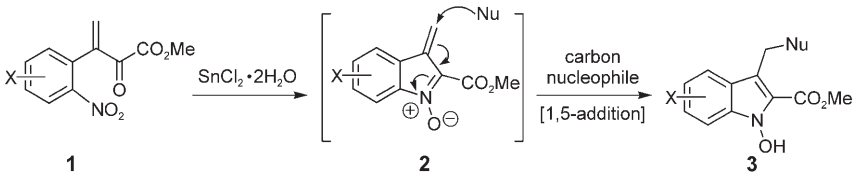
© 2006 Wiley-VCH Verlag GmbH & Co. KGaA, Weinheim

Contents

Synthetic Methods

K. C. Nicolaou,* A. A. Estrada, S. H. Lee, G. C. Freestone ——— **5364 – 5368**

Synthesis of Highly Substituted *N*-Hydroxyindoles through 1,5-Addition of Carbon Nucleophiles to In Situ Generated Unsaturated Nitrones

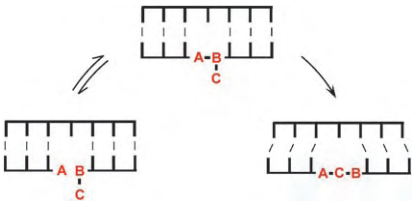


As easy as 1→2→3: Generation (**1**→**2**) and subsequent capture (**2**→**3**) of the reactive α,β-unsaturated nitrone species **2** with silyl enol ethers, silanes, and stannanes leads to a facile and direct entry to a variety of highly substituted *N*-hydroxyindoles **3** through carbon–carbon bond formation.

DNA Catalysis

C. Dose, S. Ficht, O. Seitz* **5369 – 5373**

Reducing Product Inhibition in DNA-Template-Controlled Ligation Reactions

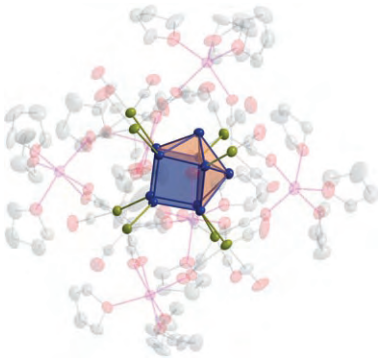


Loosening the zipper: A ligation–rearrangement reaction sequence is the key to signal amplification in chemical DNA-templated ligation reactions. The rearrangement increases the flexibility of the ligation intermediate, thereby reducing the affinity of the rearranged product for the DNA template. A fluorescence-resonant-energy-transfer technique is used for convenient and product-specific real-time detection of product signals.

Cluster Compounds

A. Schnepf,* C. Schenk ——— **5373 – 5376**

$Na_6[Ge_{10}\{Fe(CO)_4\}_8]\cdot 18\,THF$: A Centaur Polyhedron of Germanium Atoms

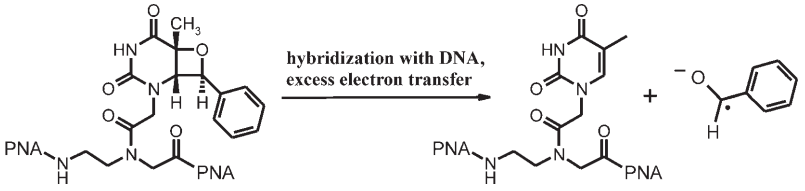


Mythological figure: The reaction of GeBr with $Na_2[Fe(CO)_4]$ yields the polyhedral Ge_{10} cluster compound $Na_6[Ge_{10}\{Fe(CO)_4\}_8]\cdot 18\,THF$. The arrangement of the 10 germanium atoms (blue spheres in figure) in the cluster core can be described as a centaur polyhedron and therefore represents a new structural motif in germanium cluster chemistry.

Electron Transfer

T. Stafforst, U. Diederichsen* ——— **5376 – 5380**

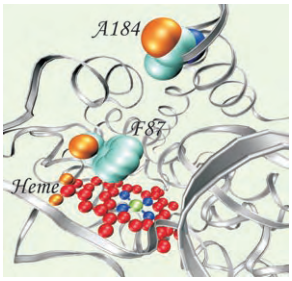
Thymine Oxetanes as Charge Traps for Chemical Monitoring of Nucleic Acid Mediated Transfer of Excess Electrons



Detecting electrons migrating: When incorporated into nucleic acids, thymine oxetanes make it possible to monitor excess-electron transfer with remarkably high quantum yields owing to their favorable redox potentials and fast cyclorevertsion (see scheme; PNA = peptide nucleic acid). In a first experiment, the distance dependence of the charge transfer was investigated and found to be typical for a hopping mechanism.

© 2006 Wiley-VCH Verlag GmbH & Co. KGaA, Weinheim

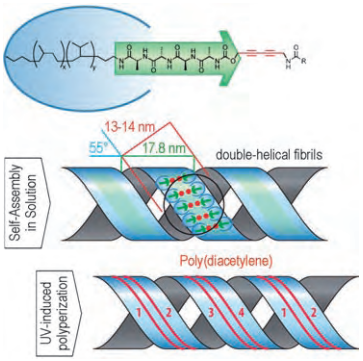
Positively charged: A screening system for the directed evolution of epoxygenases has been developed. Validation reveals that introducing a positively charged amino acid at position 184 (see picture) results in inversion of enantioselectivity in the epoxidation of styrene. The synthetic potential of epoxygenases can now be tailored by methods of directed evolution.



Directed Evolution

K. L. Tee, U. Schwaneberg* **5380 – 5383**

A Screening System for the Directed Evolution of Epoxygenases: Importance of Position 184 in P450 BM3 for Stereoselective Styrene Epoxidation

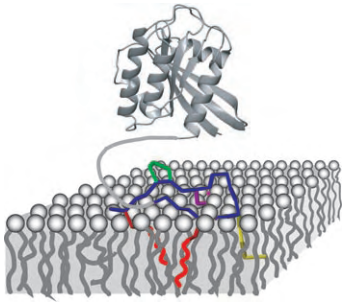


Diacetylene macromonomers functionalized with a β-sheet-forming oligopeptide and a hydrogenated poly(isoprene) coil segment self-assembled into supramolecular polymers with a double-helical, tubular topology and a diameter of a few nanometers. Subsequent "1D topochemical polymerization" affords poly(diacetylene)s with a conjugated backbone and a high degree of biochemically relevant functionalization, as well as a defined hierarchical structure.

Supramolecular Polymers

E. Jahnke, I. Lieberwirth, N. Severin, J. P. Rabe, H. Frauenrath* **5383 – 5386**

Topochemical Polymerization in Supramolecular Polymers of Oligopeptide-Functionalized Diacetylenes



Solid-state NMR spectroscopy was used to determine a structural model of the backbone of the lipid anchor of membrane-bound N-Ras protein. The fully functional lipid-modified protein was obtained by ligating the expressed water-soluble N terminus with a chemically synthesized ^{13}C-labeled lipidated peptide. After the NMR signals had been assigned by correlation experiments, a structural model was calculated from torsion angles derived from ^{1}H and ^{13}C chemical-shift data.

Membrane Proteins

G. Reuther, K.-T. Tan, J. Köhler, C. Nowak, A. Pampel, K. Arnold, J. Kuhlmann, H. Waldmann, D. Huster* **5387 – 5390**

Structural Model of the Membrane-Bound C Terminus of Lipid-Modified Human N-Ras Protein

Sources

Product and Company Directory

You can start the entry for your company in "Sources" in any issue of *Angewandte Chemie*.

If you would like more information, please do not hesitate to contact us.

Wiley-VCH Verlag – Advertising Department
Tel.: 0 62 01 - 60 65 65
Fax: 0 62 01 - 60 65 50
E-Mail: MSchulz@wiley-vch.de

Service

Keywords 5392

Authors 5393

Vacancies A43

Preview 5395

© 2006 Wiley-VCH Verlag GmbH & Co. KGaA, Weinheim



Awarded...

S. V. Ley and J.-i. Yoshida receive Nagoya Medals

The Gold Nagoya Medal has been awarded annually since 1995 in recognition of outstanding achievements in organic chemistry. The Silver Nagoya Medal has been awarded since 1999 to young Japanese chemists for their outstanding contributions in this area.

This year's recipient of the Gold Nagoya Medal is Steven V. Ley (University of Cambridge, Großbritannien) in recognition of his contributions to natural product chemistry and the development of synthetic methods. Indeed, his award lecture on November 9 will focus on "Natural Product Synthesis: A Stimulus for Discovery" and "New Tools for Molecule Makers". In *Angewandte Chemie* last year, he reported the total syntheses of spongistatin 1,[2a] antascomicin B[2b] and 10-hydroxyasimicin.[2c]



S. V. Ley



J.-i. Yoshida

Ley completed his PhD in 1972 at Loughborough University (UK). He then worked as a postdoctoral researcher with L. Paquette at Ohio State University (Columbus, USA) for two years before returning to the UK to join Derek Barton at Imperial College in London. In 1975 he was appointed lecturer there. He climbed the ranks over the following 14 years and was appointed Head of Department in 1989. In 1992 he joined Trinity College at Cambridge University. In 2002, following his two-year presidency of the Royal Society of Chemistry, he was honored as a Commander of the British Empire. He is a member of the Royal Society (London) and the Academy of Medical Sciences.

The Silver Nagoya Medal will be awarded to Jun-ichi Yoshida for his work on the organic chemistry of reactive intermediates, electron-transfer reactions, organometallic chemistry, and microreactors. His award lecture will focus on "Flash Chemistry: Fast Chemical Synthesis in Microsystems". He recently described the Pd-catalyzed convergent synthesis and properties of conjugated dendrimers based on triarylethene branching in *Angewandte Chemie*.[3]

Yoshida was already an assistant professor at the Kyoto Institute of Technology (since 1979) when he completed his PhD in 1981 at Kyoto University under the guidance of M. Kumada. During 1982–83 he worked as a postdoctoral researcher with B. M. Trost at the University of Wisconsin. In 1985 he joined Osaka City University, where he was appointed an associate professor in 1992. Since 1994 he is a full professor at Kyoto University.

K. O. Christe receives Alfred Stock Memorial Prize



K. O. Christe

The German Chemical Society (Gesellschaft Deutscher Chemiker, GDCh) awards the Alfred Stock Memorial Prize in recognition of outstanding experimental studies in the area of inorganic chemistry. On September 18, Karl O. Christe (University of Southern California, Los Angeles, USA) will receive the prize during the 124th Meeting of the Society of German Natural Scientists and Physicians (GDNÄ) in Bremen. His research interests encompass main-group compounds with halogens, polyazide chemistry, and nitroamine chemistry, as well as carbocations and fluorocarbon compounds. His research group recently reported in *Angewandte Chemie* on an energetic ionic liquid[3a] and evidence of linear metal–azido coordination.[3b] Their report on the first structural characterization of binary arsenic(II) and antimony(III) azides featured on the cover of *Chemistry – A European Journal* in 2004.[3c]

Christe completed his PhD in 1961 with J. Goubeau at the Technical University of Stuttgart in collaboration with Hoechst AG. He subsequently moved to the USA and carried out research with A. Pavlath at Stauffer Western Research Laboratory in Richmond (CA) during 1962–67 on commercially interesting inorganic and organic fluoro compounds. During this time, he successfully produced NF_4^+. He then took a position with Rocketdyne, who manufactured synthetic fuels. When Rocketdyne discontinued their efforts in this area in 1994, Christe accepted a position split between the University of Southern California (USC) and the US Air Force Research Laboratory (Edwards Air Force Base). Since 2005 he is active as a researcher at the Loker Hydrocarbon Research Institute at the USC. Christe was a former member of the German and US national teams for fencing and is still active as a fencing coach.

[1] a) M. Ball, M. J. Gaunt, D. F. Hook, A. S. Jessiman, S. Kawahara, P. Orsini, A. Scolaro, A. C. Talbot, H. R. Tanner, S. Yamanoi, S. V. Ley, *Angew. Chem.* **2005**, *117*, 5569; *Angew. Chem. Int. Ed.* **2005**, *44*, 5433; b) D. E. A. Brittain, C. M. Griffiths-Jones, M. R. Linder, M. D. Smith, C. McCusker, J. S. Barlow, R. Akiyama, K. Yasuda, S. V. Ley, *Angew. Chem.* **2005**, *117*, 2792; *Angew. Chem. Int. Ed.* **2005**, *44*, 2732; c) G. L. Nattrass, E. Díez, M. M. McLachlan, D. J. Dixon, S. V. Ley, *Angew. Chem.* **2005**, *117*, 586; *Angew. Chem. Int. Ed.* **2005**, *44*, 580.

[2] K. Itami, K. Tonogaki, T. Nokami, Y. Ohashi, J.-i. Yoshida, *Angew. Chem.* **2006**, *118*, 2464; *Angew. Chem. Int. Ed.* **2006**, *45*, 2404.

[3] a) C. B. Jones, R. Haiges, T. Schroer, K. O. Christe, *Angew. Chem.* **2006**, *118*, 5103; *Angew. Chem. Int. Ed.* **2006**, *45*, 4981; b) R. Haiges, J. A. Boatz, T. Schroer, M. Yousufuddin, K. O. Christe, *Angew. Chem.* **2006**, *118*, 4948; *Angew. Chem. Int. Ed.* **2006**, *45*, 4830; c) R. Haiges, A. Vij, J. A. Boatz, S. Schneider, T. Schroer, M. Gerken, K. O. Christe, *Chem. Eur. J.* **2004**, *10*, 508.

DOI: 10.1002/anie.200602884

WILEY InterScience DISCOVER SOMETHING GREAT
© 2006 Wiley-VCH Verlag GmbH & Co. KGaA, Weinheim

Asymmetric Catalysis

DOI: 10.1002/anie.200601889

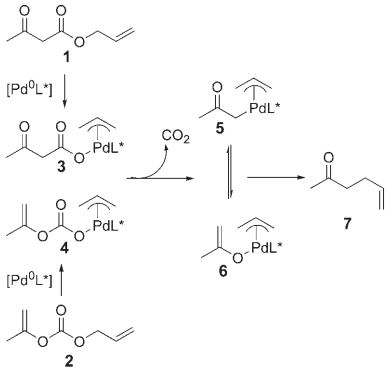
Enantioselective Palladium-Catalyzed Decarboxylative Allylic Alkylations**

Shu-Li You and Li-Xin Dai*

Keywords:
allylic alkylation · asymmetric catalysis · enols · ketones · palladium

Palladium-catalyzed asymmetric allylic alkylation (AAA) has become one of the most efficient ways to construct carbon–carbon bonds with stereocenters.[1] Although a high level of enantioselectivity can be achieved with soft nucleophiles, until recently ketone enolates, which are non-stabilized enolates, have been deemed as poor substrates and have afforded products with low enantioselectivities. It is thought that they attack palladium instead of the π-allyl during the reaction. Recently, studies on palladium-catalyzed decarboxylative AAA reactions (Tsuji protocol) have greatly expanded the scope of the nucleophile, in particular, with ketone enolates.

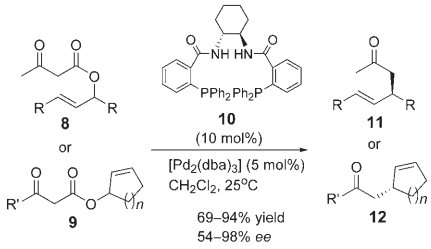
There are two main substrate types for the palladium-catalyzed decarboxylative AAA reaction (Scheme 1). In the presence of palladium(0), allyl β-keto carboxylate **1** can undergo facile oxidative addition to give a metal β-keto carboxylate **3**, which can subsequently undergo decarboxylation (also known as the Carroll rearrangement). Alternatively, vinyl carbonate **2** undergoes oxidative addition to produce palladium vinyl carbonate **4**, which can undergo decarboxylation to give the palladium enolate. Allylic alkylation product **7** is obtained upon reductive elimination or nucleophilic attack on the π-allyl by the enolate.



Scheme 1. The two main substrate types, **1** and **2**, for palladium-catalyzed decarboxylative AAA reactions. L* = chiral ligand.

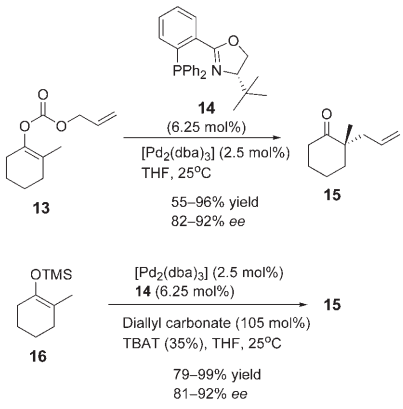
Tsuji and co-workers reported the palladium-catalyzed decarboxylative allylation reaction as early as 1980, when they observed it during their attempts at intramolecular allylic alkylation.[2] Since then, many substrates including β-nitro, cyano, and trifluoromethyl keto acetates have proved suitable therein.[2c–e] However, the asymmetric version of this class of reaction has been less explored until quite recently.

Tunge and Burger recently reported asymmetric palladium-catalyzed decarboxylative allylic alkylations utilizing Trost's ligand **10**.[3] Under optimized conditions, several α-unsubstituted β-keto esters **8** and **9** smoothly underwent the decarboxylative AAA reaction to afford the products in 69–94% yield and with 54–98% *ee* (Scheme 2). A study on cyclic substrates revealed that a larger ring size could lead to higher enantioselectivities.



Scheme 2. Decarboxylation of α-unsubstituted β-keto esters. dba = dibenzylideneacetone.

Stoltz and Behenna observed that decarboxylation of allyl enol carbonate **13** led to formation of a ketone with a quaternary stereocenter at the α-position (Scheme 3).[4] Screening of several ligands revealed that use of the *tert*-butyl-phox ligand **14** resulted in the highest enantioselectivities. A variety of cyclohexanone-derived allyl carbonates could undergo decarboxylation to provide products in high yields (55–96%) and with good enantioselectivities (82–92% *ee*). The reaction between trimethylsilyl enol ethers **16** and diallyl



Scheme 3. Decarboxylation of allyl enol carbonates using ligand **14**. TMS = trimethylsilyl; TBAT = $Bu_4NPh_3SiF_2$.

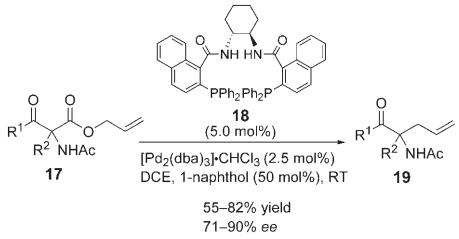
[*] Prof. Dr. S.-L. You, Prof. L.-X. Dai
State Key Laboratory of Organometallic Chemistry
Shanghai Institute of Organic Chemistry
Chinese Academy of Sciences
354 Fenglin Lu
Shanghai 200032 (P.R. China)
Fax: (+86) 21-5492-5087
E-mail: slyou@mail.sioc.ac.cn

[**] We gratefully acknowledge the Chinese Academy of Sciences for generous financial support.

InterScience
© 2006 Wiley-VCH Verlag GmbH & Co. KGaA, Weinheim

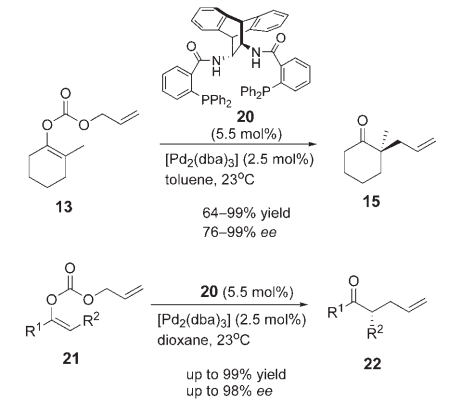
carbonates also proceeded smoothly in the presence of the palladium catalyst and a substoichiometric amount of $Bu_4NPh_3SiF_2$ (TBAT) to give an array of quaternary cycloalkanones **15**.

Murakami and co-workers recently reported that palladium-catalyzed asymmetric decarboxylation of allyl α-acetamido-β-keto carboxylates **17** using Trost's ligand **18** gave optically active γ,δ-unsaturated α-aminoketones **19** with up to 90% *ee* (Scheme 4).[5] They observed that addition of phenol derivatives brought about an enhancement of the enantioselectivity.



Scheme 4. Decarboxylation of allyl α-acetamido-β-keto carboxylates. DCE = 1,1-dichloroethene.

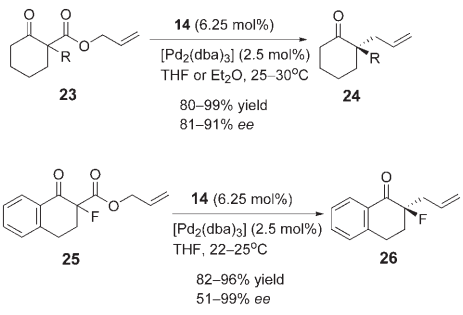
In their search of a process wherein enolate alkylation could be performed under neutral conditions and using a low concentration of enolate, Trost and Xu reported the palladium-catalyzed decarboxylation of allyl enol carbonates (Scheme 5).[6] Using chiral ligand **20**, the reaction was carried out with a wide variety of cyclic ketone-derived substrates **13** under optimized conditions. In general, the monoalkylated ketone products were obtained in good yields (64–99%) with high enantioselectivities (76–99% *ee*). The enol carbonate of 1-tetralone, a substrate often used to prepare ketones with a tertiary carbon center, was somewhat problematic because of potential racemization and the possibility of dialkylation. After screening the reaction conditions, Trost and Xu found that high yields and enantioselectivity could be attained by using dioxane as the solvent instead of toluene, as preferred previously. Following the success with the synthesis of cyclic ketones with tertiary carbon centers, Trost and Xu further expanded the substrate scope to acyclic carbonates **21**.[7] High yields and enantioselectivities were obtained for a wide range of acyclic ketones **22**.



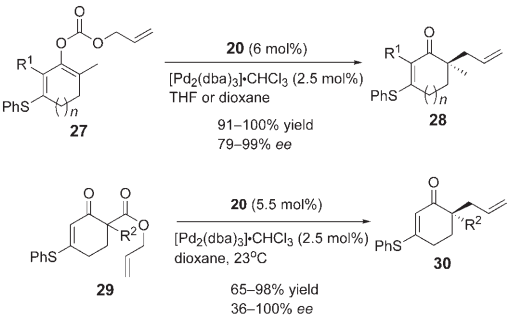
Scheme 5. Decarboxylation of allyl enol carbonates using ligand **20**.

Stoltz and co-workers recently reported a catalytic enantioconvergent synthesis of quaternary stereocenters from racemic β-keto carboxylates **23**.[8] By using ligand **14**, a variety of α-substituted 2-carboxyallyl cyclic ketones **23** were found to undergo decarboxylation and afford ketones **24** with quaternary stereocenters in good yields (80–99%) and with high enantioselectivities (81–91% *ee*; Scheme 6). Meanwhile, Nakamura et al. applied a very similar catalytic system to the decarboxylation of α-fluoro-2-carboxyallyl ketone **25**.[9] In general, high enantioselectivities were obtained for cyclic ketones (>85% *ee*), whereas only moderate enantioselectivities were reported for acyclic ketones (51–55% *ee*). Note that α-fluoro-2-carboxyallyl cyclohexanone was also used as a substrate in the report by Stoltz and co-workers,[8] who obtained the product in 80% yield and with 91% *ee*.

Trost et al. recently developed an efficient synthesis of vinylogous thioesters **28** and **30** by decarboxylation of enol carbonates and β-keto carboxylates (Scheme 7).[10] The products thus obtained are precursors for γ,γ-disubstituted cycloalkenones.



Scheme 6. Decarboxylation of allyl β-keto carboxylates.

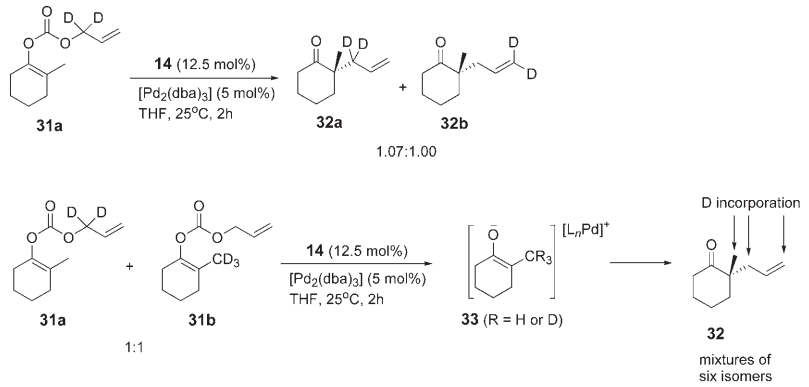


Scheme 7. Decarboxylation of vinylogous thioesters.

The promising synthetic applications of this palladium-catalyzed decarboxylative AAA reaction have triggered extensive mechanistic investigations. As β-keto carboxylates with quaternary stereocenters, such as **23**, **25**, and **29**, smoothly undergo decarboxylative allylation, it suggests that the decarboxylation likely precedes C–C bond formation and that ketone enolates are possibly true intermediates. An interesting mechanistic study was carried out using deuterium-labeled substrates (Scheme 8),[8] concluding the existence of ketone enolates in solution. The reaction of dideuterated carbonate **31a** was performed under decarboxylative allylation conditions, and the deuterium label was almost equally distributed between the termini of the allyl fragment in the products. In a crossover experiment, an equimolar amount of carbonates **31a** and **31b** was subjected to the same reaction conditions. NMR spectroscopic analysis of the product showed deuterium scrambling between the allyl termini as expected. Furthermore, from mass spectrometric analysis of the product mixture it appeared that all six possible products were formed in the reaction, including those derived from crossover reactions. Interpretation of these results suggests that an achiral ketone enolate **33** must exist in solution for some period under the above reaction conditions.

In summary, by tethering the allyl moiety and nucleophile togeth-

 © 2006 Wiley-VCH Verlag GmbH & Co. KGaA, Weinheim



Scheme 8. Mechanistic study using deuterium-labeled enol carbonates **31a**, **b**.

er, the palladium-catalyzed decarboxylative AAA reaction provides a facile means to alkylate relatively hard nucleophiles such as ketone enolates. With appropriate chiral ligands, the reaction can be delivered in high yields and with excellent selectivity. The utilization of neutral conditions and the possibility to prepare products that are not accessible by traditional Tsuji–Trost allylic alkylation warrant its wide applications in organic synthesis.[11]

Published online: July 21, 2006

[1] Reviews: a) B. M. Trost, D. L. Van Vranken, *Chem. Rev.* **1996**, *96*, 395–422; b) B. M. Trost, *Acc. Chem. Res.* **2002**, *35*, 695–705; c) B. M. Trost, M. L. Crawley, *Chem. Rev.* **2003**, *103*, 2921–2943; d) J. A. Tunge, E. C. Burger, *Eur. J. Org. Chem.* **2005**, *9*, 1715–1726.

[2] a) I. Shimizu, T. Yamada, J. Tsuji, *Tetrahedron Lett.* **1980**, *21*, 3199–3202; b) J. Tsuji, I. Minami, I. Shimizu, *Tetrahedron Lett.* **1983**, *24*, 1793–1796; c) J. Tsuji, T. Yamada, I. Minami, M. Yuhara, M. Nisar, I. Shimizu, *J. Org. Chem.* **1987**, *52*, 2988–2995; d) J. Tsuji, I. Minami, *Acc. Chem. Res.* **1987**, *20*, 140–145; e) I. Shimizu, H. Ishii, A. Tasaka, *Chem. Lett.* **1989**, 1127–1128.

[3] E. C. Burger, J. A. Tunge, *Org. Lett.* **2004**, *6*, 4113–4115.

[4] D. C. Behenna, B. M. Stoltz, *J. Am. Chem. Soc.* **2004**, *126*, 15044–15045.

[5] R. Kuwano, N. Ishida, M. Murakami, *Chem. Commun.* **2005**, 3951–3952.

[6] B. M. Trost, J. Xu, *J. Am. Chem. Soc.* **2005**, *127*, 2846–2847.

[7] B. M. Trost, J. Xu, *J. Am. Chem. Soc.* **2005**, *127*, 17180–17181.

[8] J. T. Mohr, D. C. Behenna, A. M. Harned, B. M. Stoltz, *Angew. Chem.* **2005**, *117*, 7084–7087; *Angew. Chem. Int. Ed.* **2005**, *44*, 6924–6927.

[9] M. Nakamura, A. Hajra, K. Endo, E. Nakamura, *Angew. Chem.* **2005**, *117*, 7414–7417; *Angew. Chem. Int. Ed.* **2005**, *44*, 7248–7251.

[10] B. M. Trost, R. N. Bream, J. Xu, *Angew. Chem.* **2006**, *118*, 3181–3184; *Angew. Chem. Int. Ed.* **2006**, *45*, 3109–3112.

[11] After submission of this manuscript, Stoltz and McFadden reported the total synthesis of (+)-dichroanone utilizing a Pd-catalyzed decarboxylative AAA reaction as a key step to install a chiral quaternary carbon center. For details, see: R. M. McFadden, B. M. Stoltz, *J. Am. Chem. Soc.* **2006**, *128*, 7738–7739.

 © 2006 Wiley-VCH Verlag GmbH & Co. KGaA, Weinheim

DOI: 10.1002/anie.200602516

Molecular Machines

Intermolecular Coupling of Motion under Photochemical Control

*Françisco M. Raymo**

Keywords:
chirality · molecular devices · photochromism · supramolecular chemistry

Biology is replete with examples of sophisticated processes that rely on the precise control of motion at the molecular level.[1,2] In these systems, appropriate stimulations induce cascades of programmed molecular motions and regulate crucial biological functions as a result. The cytoplasmic proteins dyneins, kinesins, and myosins, for example, shuttle substrates along linear filaments in response to adenosine triphosphate (ATP).[3] The hydrolysis and synthesis of this particular molecule are in turn correlated to the rotary motion of ATP synthase in response to transmembrane fluxes of ions.[4] Similarly, the hydrolysis of ATP can open and close the cylindrical cavity of chaperonin proteins, controlling the release of entrapped guests.[5]

The complexity of biological processes, based on controlled molecular motions, together with their relevance to cellular functions have stimulated a wealth of investigations aimed at understanding the basic factors that regulate these fascinating systems.[1–5] These fundamental studies have in turn encouraged the identification of viable strategies to control the relative movements of artificial molecular assemblies by external stimuli.[6–9] Clever operating principles and structural designs have emerged as a result in the form of functional nanostructures—molecular machines.[6] Generally, these systems are composed of at least two moving parts, which are covalently, mechanically, or noncovalently connected to each other. The position of one component relative to the other can be controlled reversibly with chemical, electrical, or optical inputs.

Chemically controllable molecular machines are in principle reversible.[6–9] However, the regeneration of their original state often requires the addition of a second chemical input to neutralize the influence of the first. Thus, multiple switching cycles lead to the accumulation of side products. Electrically controllable molecular machines are instead based on interfacial electron transfer.[6–9] Electrochemical oxidation and reduction steps are responsible for their reversible operation. Nonetheless, both processes require the physical contact of the molecular machine with a macroscopic electrode. Optically controllable systems instead do not suffer these limitations.[6–9] In fact, many photochemical processes can simply be reversed by changing the irradiation wavelength. Furthermore, photons can travel through transparent media and reach a molecular target even if this species is not in contact with the irradiation source. Indeed, optical control is emerging as a convenient strategy to operate molecular machines,[10] and numerous photoresponsive systems with diverse structures and functions have recently been developed.[6–10] For example, the relative movements of the interlocked components of photoactive catenanes[11,12] and rotaxanes[13–19] can be controlled with light. Similarly, the unidirectional rotation of one molecular fragment relative to another can be implemented on the basis of the photoinduced isomerizations of overcrowded alkenes.[20]

The controlled motions associated with the photoresponsive molecular machines developed so far involve either the relative movements of two molecular portions integrated within the same structure or the association/dissociation of supramolecular assemblies.[6–10] A recent investigation[21] has taken the design of these functional nanostructures one step further. This clever study demonstrates that the motion of one molecule can be exploited to regulate the movement of another under photochemical control. Indeed, the assistance of supramolecular interactions can be invoked to couple intermolecularly the dynamics of a receptor with those of a complementary substrate. Specifically, compound **1** (Figure 1) combines an azobenzene switch, a ferrocene pivot, and two porphyrin chelators. Irradiation of this molecular assembly with ultraviolet light induces the *trans*→*cis* isomerization of the azobenzene photochrome.[22] This transformation shortens the distance between the two 1,3-phenylene rings of the photochromic fragment, causing a rotation of the two cyclopentadienyl rings of the ferrocene pivot about the main axis of the metallocene.[23] The photoinduced motion alters the separation and relative orientation of the two porphyrin appendages. The overall process is fully reversible, and the original state is regenerated after irradiation with visible light.[24]

The photoinduced and reversible transformations of the receptor **1** can be exploited to regulate the conformation of a complementary substrate.[21] In particular, the bidentate 4,4′-biisoquino-

[*] Prof. F. M. Raymo
Center for Supramolecular Science
Department of Chemistry
University of Miami
1301 Memorial Drive, Coral Gables, FL 33146-0431 (USA)
Fax: (+1) 305-284-4571
E-mail: fraymo@miami.edu

© 2006 Wiley-VCH Verlag GmbH & Co. KGaA, Weinheim

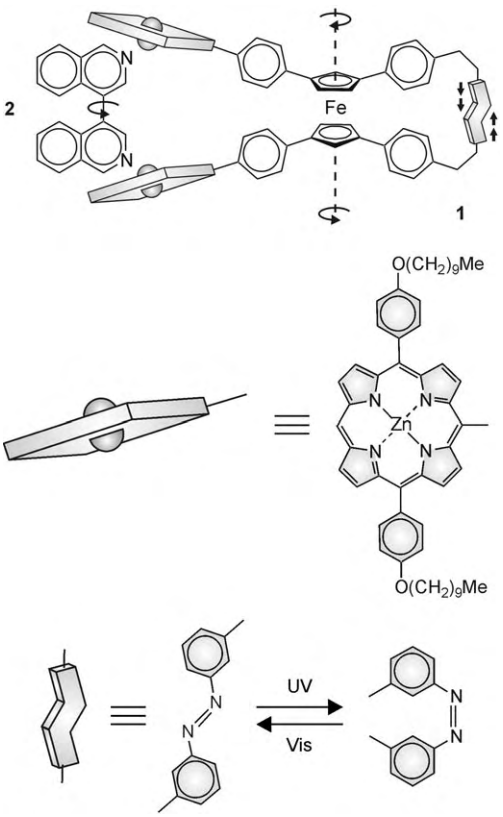


Figure 1. The azobenzene switch of **1** interconverts between *trans* and *cis* forms upon irradiation with UV and visible light. As a result, the two cyclopentadienyl rings of the ferrocene pivot adjust their relative orientation, altering the dihedral angle about the bond that connects the two isoquinoline fragments of the substrate **2** bound in the bis(porphyrin) cleft of **1**.

line **2** (Figure 1) binds the two porphyrin chelators of **1** as a result of N···Zn coordination. In the resulting supramolecular assembly, the photoinduced regulation of the distance between the two porphyrin units controls the dihedral angle about the C–C bond that connects the two isoquinoline fragments. Thus, the geometrical changes associated with the photoisomerization of the azobenzene switch in **1** are coupled intermolecularly to the relative rotation of the two main fragments of **2**.

The photoinduced geometrical modifications of the receptor **1** and the substrate **2** in the corresponding supramolecular assembly translate into profound changes in their chiroptical response.[21] Indeed, the receptor itself is chiral and the *trans* isomer can adopt the two configurations (+)-*trans*-**1** and (−)-*trans*-**1**, as illustrated in Figure 2. The photoisomerization of the azobenzene switch in (+)-*trans*-**1** bound to **2** modulates the intensity of a band at 421 nm in the circular dichroism (CD) spectrum. This band corresponds to an electronic transition centered on the porphyrin chromophores, and increases with the *trans*→*cis* isomerization of the azobenzene switch and decreases with the opposite transformation (Figure 3a). Similarly, the substrate **2** is locked into a chiral conformation upon binding to (+)-*trans*-**1** with the concomitant appearance of a positive band at 307 nm in the CD spectrum. This band decreases with the *trans*→*cis* isomerization of the azobenzene component and increases with the opposite transformation (Figure 3b).[25] The spectra show that the changes in the chiroptical response of the receptor (Figure 3a) parallel those of the substrate (Figure 3b), confirming that the photoinduced motion of the former is coupled to the rotation of the latter.

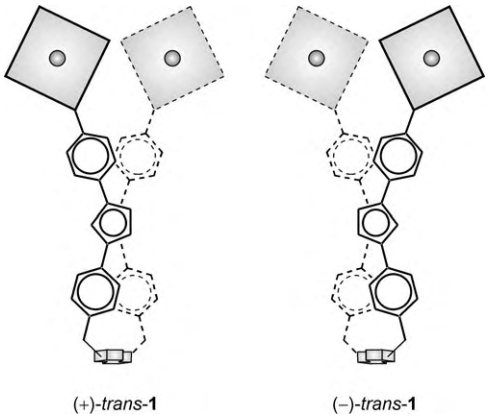


Figure 2. The two enantiomers associated with the *trans* isomer of the receptor **1**.

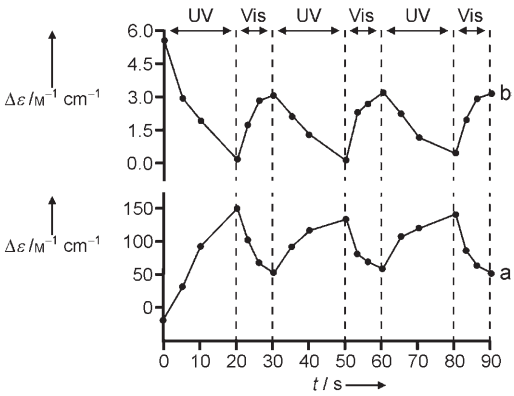


Figure 3. Changes at $\lambda = 421$ (a) and 307 nm (b) in the CD spectrum of the complex between (+)-*trans*-**1** and **2** upon irradiation with UV and visible light (partially reproduced from Ref. [21] with permission).

The analysis of the receptor **1** and substrate **2** demonstrates that their supramolecular association mediates effectively the transfer of dynamic information from one component to the other.[21] This study proves unequivocally that the intermolecular coupling of motion can be designed into artificial molecular machines. In principle, similar mechanisms can further be developed to concatenate the dynamics of more than two moving components. Ultimately, the design of programmed cascades of molecular motions in multicomponent assemblies can certainly be envisaged. It is important to stress, however, that this unique example of artificial molecular machine remains far from the complexity and level of sophistication of its biological counterparts.[1–5] An emerging challenge in this fascinating area of research is indeed the need to identify viable strategies to engineer specific functions in these molecular and supramolecular assemblies. In addition to mimicking the dynamics associated with the many examples of biological systems based on controlled molecular motions, it is essential to learn how their functions can be reproduced. Only then will artificial molecular machines be able to evolve into nanostructured devices with moving molecular components and unique functions and properties.

Published online: July 26, 2006

[1] *Molecular Motors* (Ed.: M. Schliwa), Wiley-VCH, Weinheim, **2003**.
[2] M. Schliwa, G. Woehlke, *Nature* **2003**, *422*, 759.
[3] M. J. A. Tyreman, J. E. Molloy, *IEE Proc. Nanobiotechnol.* **2003**, *150*, 95.
[4] M. Yoshida, E. Muneynki, T. Hisabori, *Nat. Rev. Mol. Cell Biol.* **2001**, *2*, 669.
[5] H. R. Saibil, N. A. Ranson, *Trends Biochem. Sci.* **2002**, *27*, 627.
[6] V. Balzani, A. Credi, F. M. Raymo, J. F. Stoddart, *Angew. Chem.* **2000**, *112*, 3484; *Angew. Chem. Int. Ed.* **2000**, *39*, 3348.

 © 2006 Wiley-VCH Verlag GmbH & Co. KGaA, Weinheim

[7] Special Issue on Molecular Machines (Ed.: J. F. Stoddart): *Acc. Chem. Res.* **2001**, *34*, 409.
[8] V. Balzani, M. Venturi, A. Credi, *Molecular Devices and Machines: A Journey into the Nanoworld*, Wiley-VCH, Weinheim, **2003**.
[9] K. Kinbara, T. Aida, *Chem. Rev.* **2005**, *105*, 1377.
[10] Special Issue on Light-Driven Molecular Machines: *Aust. J. Chem.* **2006**, *59*, 155.
[11] a) A. Livoreil, J.-P. Sauvage, N. Armaroli, V. Balzani, L. Flamigni, B. Ventura, *J. Am. Chem. Soc.* **1997**, *119*, 12114; b) P. Mobian, J.-M. Kern, J.-P. Sauvage, *Angew. Chem.* **2004**, *116*, 2446; *Angew. Chem. Int. Ed.* **2004**, *43*, 2392.
[12] J. V. Hernández, E. R. Kay, D. A. Leigh, *Science* **2004**, *306*, 1532.
[13] a) H. Murakami, A. Kawabuchi, K. Kotoo, M. Kunitake, N. Nakashima, *J. Am. Chem. Soc.* **1997**, *119*, 7605; b) H. Murakami, A. Kawabuchi, R. Matsumoto, T. Ido, N. Nakashima, *J. Am. Chem. Soc.* **2005**, *127*, 15891.
[14] a) N. Armaroli, V. Balzani, J.-P. Collin, P. Gaviña, J.-P. Sauvage, B. Ventura, *J. Am. Chem. Soc.* **1999**, *121*, 4397; b) J.-P. Collin, D. Jouvenot, M. Koizumi, J.-P. Sauvage, *Eur. J. Inorg. Chem.* **2005**, 1850.
[15] a) P. R. Ashton, R. Ballardini, V. Balzani, A. Credi, R. Dress, E. Ishow, C. J. Kleverlaan, O. Kocian, J. A. Preece, N. Spencer, J. F. Stoddart, M. Venturi, S. Wenger, *Chem. Eur. J.* **2000**, *6*, 3558; b) V. Balzani, M. Clemente-León, A. Credi, B. Ferrer, M. Venturi, A. H. Flood, J. F. Stoddart, *Proc. Natl. Acad. Sci. USA* **2006**, *103*, 1178.
[16] I. Willner, V. Pardo-Yssar, E. Katz, K. T. Ranjit, *J. Electroanal. Chem.* **2001**, *497*, 172.
[17] a) A. M. Brouwer, C. Frochot, F. G. Gatti, D. A. Leigh, L. Mottier, F. Paolucci, S. Roffia, G. W. H. Wurpel, *Science* **2001**, *291*, 2124; b) A. Altieri, F. G. Gatti, E. R. Kay, D. A. Leigh, D. Martel, F. Paolucci, A. M. Z. Slawin, J. K. Y. Wong, *J. Am. Chem. Soc.* **2003**, *125*, 8644; c) F. G. Gatti, S. Lent, J. K. Y. Wong, G. Bottari, A. Altieri, M. A. F. Morales, S. J. Teat, C. Frochot, D. A. Leigh, A. M. Brouwer, F. Zerbetto, *Proc. Natl. Acad. Sci. USA* **2003**, *100*, 10.
[18] C. A. Stanier, S. J. Alderman, T. D. W. Claridge, H. L. Anderson, *Angew. Chem.* **2002**, *114*, 1847; *Angew. Chem. Int. Ed.* **2002**, *41*, 1769.
[19] a) Q.-C. Wang, D.-H. Qu, J. Ren, K. Chen, H. Tian, *Angew. Chem.* **2004**, *116*, 2715; *Angew. Chem. Int. Ed.* **2004**, *43*, 2661; b) D.-H. Qu, Q.-C. Wang, H. Tian, *Angew. Chem.* **2005**, *117*, 5430; *Angew. Chem. Int. Ed.* **2005**, *44*, 5296; c) D.-H. Qu, Q.-C. Wang, X. Ma, H. Tian, *Chem. Eur. J.* **2005**, *11*, 5929.
[20] a) N. Koumura, R. W. J. Zijlstra, R. A. van Delden, N. Harada, B. L. Feringa, *Nature* **1999**, *401*, 152; b) M. K. J. ter Wiel, R. A. van Delden, A. Meetsma, B. L. Feringa, *J. Am. Chem. Soc.* **2005**, *127*, 14208; c) R. A. van Delden, M. K. J. ter Wiel, M. M. Pollard, J. Vicario, N. Koumura, B. L. Feringa, *Nature* **2005**, *437*, 1337; d) M. K. J. ter Wiel, R. A. van Delden, A. Meetsma, B. L. Feringa, *Org. Biomol. Chem.* **2005**, *3*, 4071.
[21] T. Muraoka, K. Kinbara, T. Aida, *Nature* **2006**, *440*, 512.
[22] The ratio between the *trans* and *cis* isomers at the photostationary state was 22:78 ($\lambda = 350 \pm 10$ nm).[21]
[23] T. Muraoka, K. Kinbara, Y. Kobayashi, T. Aida, *J. Am. Chem. Soc.* **2003**, *125*, 5612.
[24] The ratio between the *trans* and *cis* isomers at the photostationary state was 63:37 ($\lambda > 420$ nm).[21]
[25] The CD spectrum of the supramolecular assembly was deconvoluted with the aid of model compounds to determine the contribution of the substrate **2**, as the receptor **1** also absorbs at 307 nm.[21]

 © 2006 Wiley-VCH Verlag GmbH & Co. KGaA, Weinheim

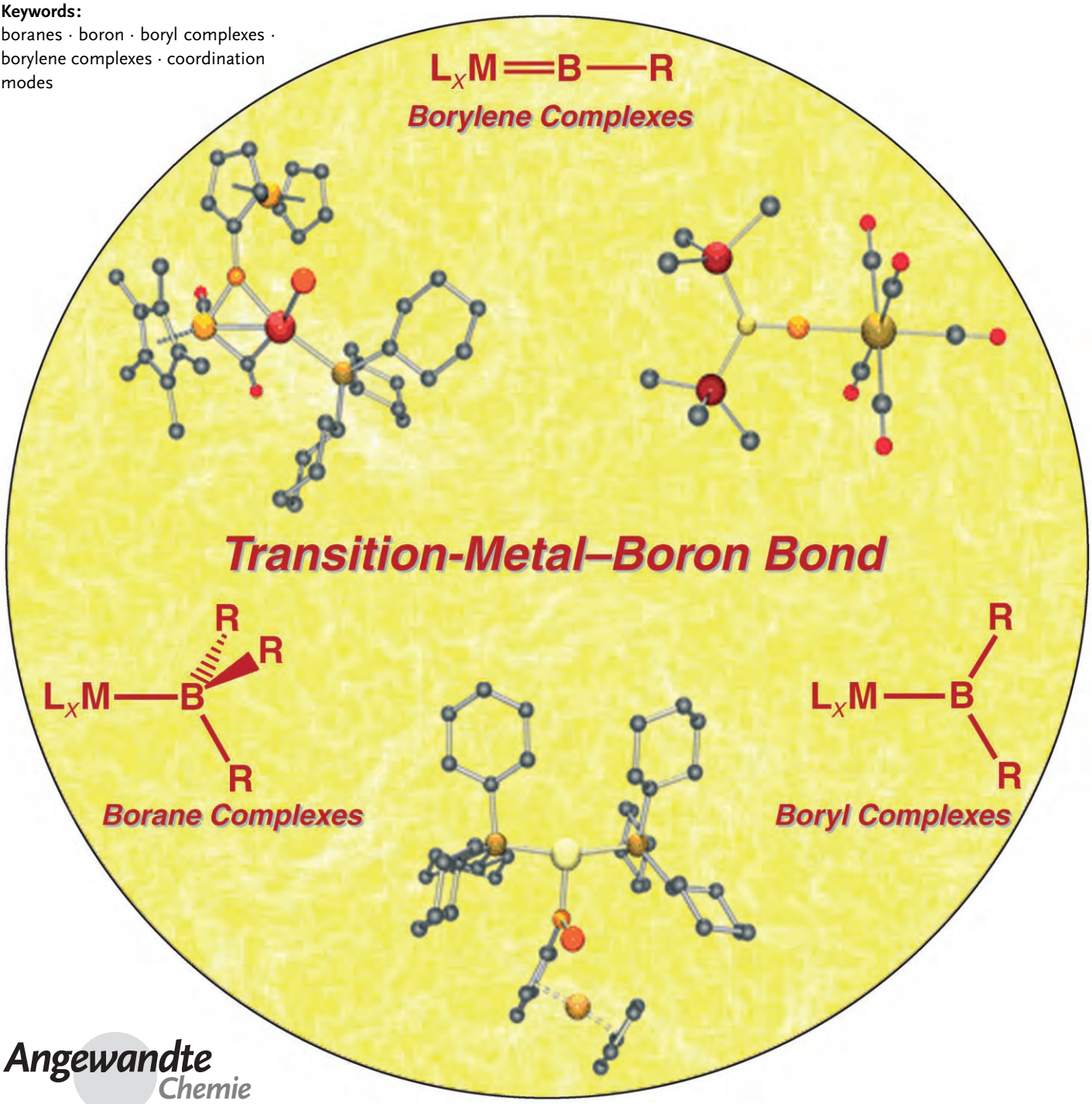
DOI: 10.1002/anie.200600506

Boron Ligands

Transition-Metal Complexes of Boron—New Insights and Novel Coordination Modes

Holger Braunschweig, Carsten Kollann, and Daniela Rais*

Keywords:
boranes · boron · boryl complexes · borylene complexes · coordination modes



© 2006 Wiley-VCH Verlag GmbH & Co. KGaA, Weinheim

Since the publication of the last review in 1998, the transition-metal chemistry of boron has continued to raise unceasing interest. Boryl complexes, representing the most extensive subclass, have remained a focus of intense research, particularly for their implication in the metal-mediated functionalization of organic substrates. Absolute novelties such as borane complexes and terminal borylene complexes have been structurally authenticated. Upon further elaboration of these compounds, the known coordination modes of boron-based ligands have grown considerably. Combined structural and theoretical investigations have contributed to elucidate the fundamental electronic characteristics of the transition-metal–boron bond and are leading to applications of these compounds. The most useful synthetic strategies for the generation of transition-metal–boron bonds are highlighted here, and the most recent and intriguing compounds that have been reported are outlined and discussed.

From the Contents

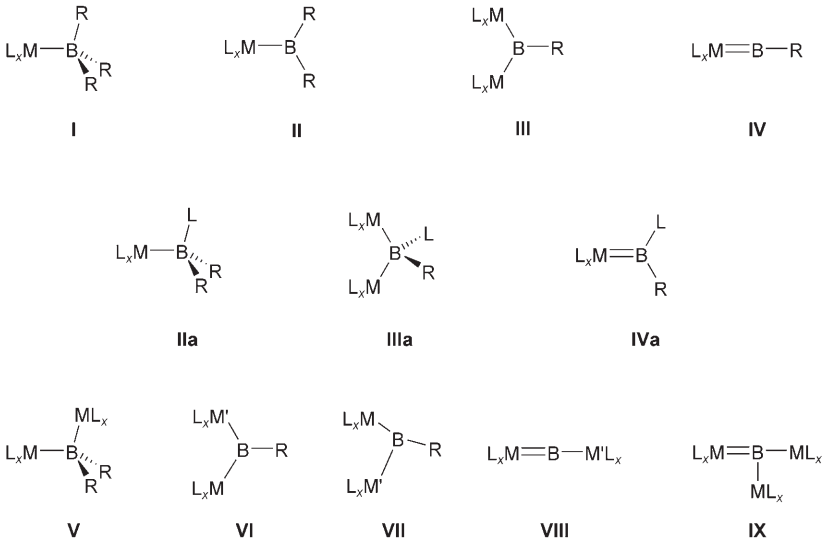
1. Introduction	5255
2. Borane Complexes	5256
3. Boryl Complexes	5258
4. Borylene Complexes	5266
5. Summary and Outlook	5272

1. Introduction

In 1990 the groups of Baker and Marder[1] and Merola[2] reported on various fully characterized iridium complexes that contain a metal-bound BR_2 ligand, thus providing the first structural proof of a transition-metal–boryl compound. These reports defined the starting point of vigorous research on transition-metal complexes of boron, which gradually came to include a growing number of researchers worldwide and still endures today. The broad interest that this class of organometallic compounds has attracted over the past 15 years finds numerous justifications. Transition-metal complexes of boron are characterized by electron-precise two-center, two-electron metal–boron bonds. This classical bonding situation is very well established for transition-metal complexes of related main-group elements such as carbon,[3] and silicon,[4] or the heavier Group 13 elements.[5] For boron, however, evidence for this type of bonding came relatively late, as its combination with transition metals more often results in electron-deficient (that is, non-classical) bonding situations, such as those realized in metallaboranes[6] and transition-metal borides.[7]

Furthermore, boryl complexes are key compounds in the metal-mediated borylation of unsaturated organic substrates[8] and of C–H bonds[9] and, hence, are becoming increasingly important in organic synthesis. In addition to their further synthetic application by cleavage of the boryl group, borylated organic species have more recently found use as building blocks for the synthesis of π-conjugated boron-based materials with potential applications in optoelectronic or sensor devices.[10,11] Finally, coordination to transition metals enables the stabilization of elusive and otherwise labile boron species, thus allowing for detailed study of their properties and reactivity. Transition-metal–borylene complexes, in particular, represent long-standing targets of interest, owing to their close relationship to fundamental organometallic compounds such as carbonyl or carbene complexes.[12]

In the late 1990s we proposed a classification scheme for transition-metal complexes of boron according to the coordination number of the boron atom and the number of metal–boron bonds. As a result, borane (**I**), boryl (**II**), bridging borylene (**III**), and terminal borylene (**IV**) complexes (Scheme 1) were defined.[13] At that time, experimental evidence was restricted to species **II** and **III**, the latter of which, however, being documented by only a handful of examples. Recent years have witnessed not only a broadening of the application of boryl complexes in organic synthesis, but also extension of the possible coordination modes of boron-



Scheme 1. Coordination modes of transition-metal complexes of boron.

[*] Prof. H. Braunschweig, Dr. C. Kollann, Dr. D. Rais
Institut für Anorganische Chemie
Bayerische Julius-Maximilians-Universität Würzburg
Am Hubland, 97074 Würzburg (Germany)
Fax: (+49) 931-888-4623
E-mail: h.braunschweig@mail.uni-wuerzburg.de

 © 2006 Wiley-VCH Verlag GmbH & Co. KGaA, Weinheim

centered ligands. Several examples of borane complexes (**I**) and terminal borylene complexes (**IV**) have been reported, and, depending on the Lewis acidity of the boron center, Lewis base adducts of boryl (**IIa**), bridging borylene (**IIIa**), and terminal borylene complexes (**IVa**) have been realized. Furthermore, unusual coordination modes of boron-based ligands have been reported, including bridging boryl complexes (**V**), hetero-dinuclear (**VI**) and semibridging borylene complexes (**VII**), and compounds that display a "naked" boron atom (that is, without main-group-element substituents) in the coordination sphere of two (**VIII**) or three (**IX**) transition-metal centers.

This article focuses on such recent advances, summarizes new synthetic strategies for transition-metal complexes of boron, and highlights compounds in which new bonding modes of boron-centered ligands are displayed. Comprehensive review articles, particularly on boryl[13,14a,b,d,g] and borylene complexes,[13,14c–h] are available.

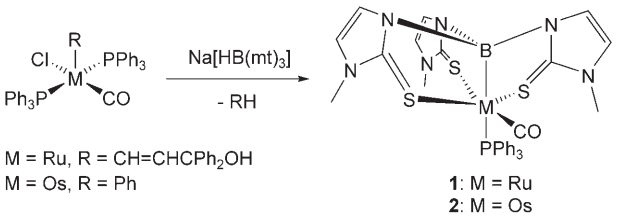
2. Borane Complexes

Borane complexes (**I** in Scheme 1) can be described as Lewis acid–base adducts of acidic boranes BR_3 and basic transition-metal complexes resulting in a fourfold coordination of the boron atom. The first reports on the existence of metal–boron dative bonds[15] were published in the 1960s, but the identity of such compounds was questioned 30 years later.[16]

2.1. Metallaboratranes

Investigation of the coordination chemistry of poly(azolyl)borate ligands led to the first structurally authenticated borane complexes, namely the metallaboratrane derivatives $[M\{B(mt)_3\}(CO)(PPh_3)]$ (**1**: M = Ru, **2**: M = Os; mt = 2-sulfanyl-1-methylimidazole). These compounds were obtained in high yields upon reaction of $[M(R)Cl(CO)(PPh_3)_2]$ (M = Ru, R = CH=CHCPh$_2$OH; M = Os, R = Ph) with $Na[HB(mt)_3]$ (Scheme 2).[17a,b]

The ^{11}B NMR spectroscopic signals for both compounds are in the expected range for fourfold-coordinated boron (**1**: $\delta = 17$ ppm; **2**: $\delta = 12$ ppm). Structural investigations by X-ray diffraction methods indicated tetrahedral geometries for the boron atoms and distorted octahedral coordination for the transition-metal centers. The Ru–B bond length in **1** (2.161(5) Å)[17a] is comparable to that observed in the ruthenium–diboran(4)yl complex $[(\eta^5\text{-}C_5H_5)Ru(CO)_2\{B(NMe_2)BBr(NMe_2)\}]$ (2.173(3) Å),[18] whereas the Os–B bond length in **2** (2.171(8) Å)[17b] is almost as long as the one observed in the osmium–boryl complex $[Os(BO_2C_2H_4)Cl(CO)_2(PPh_3)_2]$ (2.179(7) Å), in which, however, the boryl group is located *trans* to a carbonyl ligand.[17c]



Scheme 2. Synthesis of zero-valent metallaboratranes.

Formation of metallaboratranes is not limited to complexes of formally zero-valent transition metals. Indeed, similar synthetic approaches to the one described in Scheme 2 were subsequently reported for Co^I (**3**),[19a] Rh^I (**4**),[19c] Ir^I (**5**),[19d] and Pt^{II} (**6**)[19b] complexes (Scheme 3). Metallaboratrane structures with the accompanying dative transition-metal–boron interaction appear to be a recurring motif for metals in d^8 and d^{10} electron configuration, whereby the strength of the interaction is additionally determined by geometrical factors and the σ basicity of the metal center. Interestingly, in the iridaboratrane **5**,[19d] which was obtained from the reaction of Vaska's complex with $Na[HB(mt)_3]$, the tris(methimazolyl)borane ligand $B(mt)_3$ adopts an unusual coordination mode in which the Ir–B bond is supported by only two methimazolyl units, while the third sulfur donor remains pendant. This complex therefore provides a strong experimental indication of the inherent stability of the dative metal–boron interaction, which occurs even in the absence of the geometric constraints that the tricyclo[3.3.3.0] cage structures impose.

Very recently, the bimetallic species $[Rh_2\{B(mt)_3\}_2\{\kappa^2\text{-}S,S'\text{-}HB(mt)_3\}]Cl$ (**7**) was reported.[19e] The rhodium centers are coordinated exclusively by poly(methimazolyl)borane ligands and bridged by two sulfur atoms of one $B(mt)_3$ ligand. Compound **7** was obtained when a $CDCl_3$ solution of the

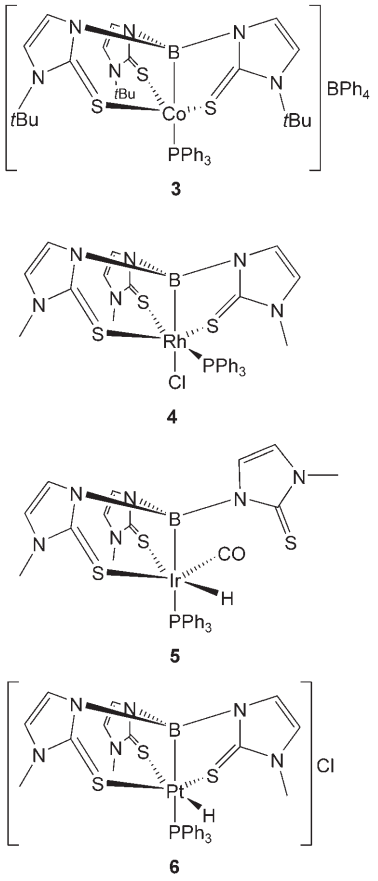


Holger Braunschweig, born in 1961 in Aachen, obtained his Ph.D. and habilitation from the RWTH Aachen with P. Paetzold and then took a postdoctoral position with M. F. Lappert, FRS, at the University of Sussex, Brighton. After two years as Senior Lecturer and Reader at Imperial College he moved to a chair for inorganic chemistry at the Julius-Maximilians-Universität Würzburg in 2002. His research interests are in organometallic synthesis and catalysis in boron chemistry, with a current focus on borametallocenophanes and transition-metal complexes of boron.



Daniela Rais was born in 1973 in Cagliari, Italy, and studied chemistry at the University of Sassari, Italy. After obtaining her Ph.D. from Imperial College, London, under the supervision of Prof. D. M. P. Mingos, FRS, and Dr. R. Vilar, she moved to the University of California at Berkeley for postdoctoral studies in the group of Prof. R. G. Bergman. In 2003 she joined Prof. H. Braunschweig's group as an Alexander von Humboldt fellow to work on the chemistry of transition-metal boryl and borylene complexes.

 © 2006 Wiley-VCH Verlag GmbH & Co. KGaA, Weinheim



3 **4** **5** **6**

Scheme 3. Examples of metallaboratrane compounds of metal centers in positive oxidation states.

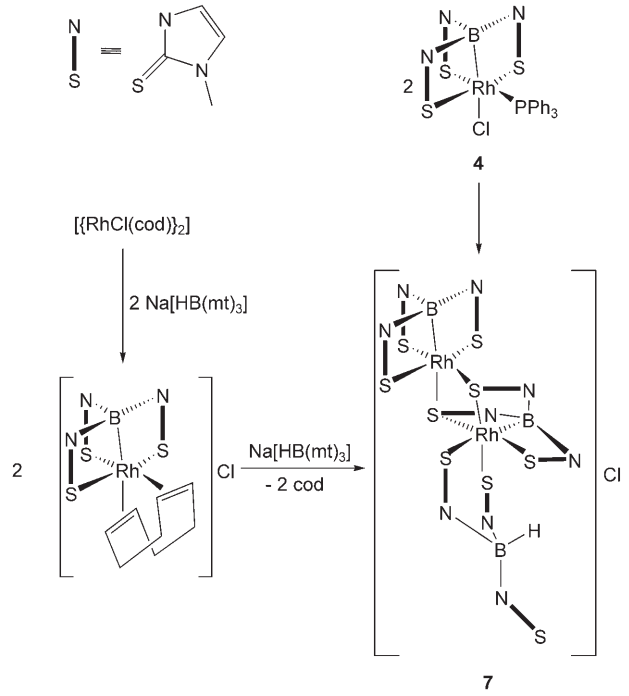
monometallic complex **4** was exposed to air for several days. A systematic approach to **7**, by stepwise reaction of [{RhCl(cod)}$_2$] (cod = 1,5-cyclooctadiene) with Na[HB(mt)$_3$], was subsequently developed (Scheme 4).

2.2. A Particular Case of Borane Complexes: Bridging Boryl Compounds

The large amount of structural data available on transition-metal–boryl complexes indicates a clear preference of the boryl ligand BR_2 for terminal or nearly terminal



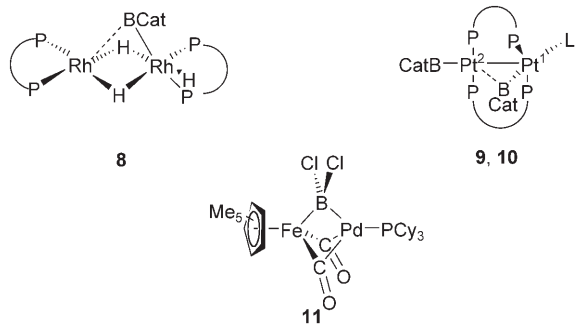
Carsten Kollann, born in 1968 in Marl, Germany, obtained his Ph.D. in 1999 with P. Paetzold at RWTH Aachen. After postdoctoral research with Prof. Dr. J. Caro at the Institut für Angewandte Chemie Berlin–Adlershof (2000–2001), he joined Prof. M. Döring's group at the Forschungszentrum Karlsruhe (2001–2003). Since August 2003 he has been a senior researcher in Prof. H. Braunschweig's group at the Julius-Maximilians-Universität in Würzburg.



4 **7**

Scheme 4. Synthesis of the bimetallic metallaboratrane **7**.

coordination (see Section 3).[13,14a] Indeed, to date, only four complexes that feature a bridging boryl ligand have been reported (Scheme 5). As explained in the following pages, the bridging coordination of the boryl ligands in such complexes relies on the presence of a dative bond between a transition-metal center and a boryl ligand that is σ-bound to another transition-metal center, that is, $L_yM \rightarrow BR_2(M'L_x)$. By virtue of this dative interaction, the compounds that follow can be viewed as particular cases of borane complexes.



8 **9, 10** **11**

Scheme 5. Bridging boryl complexes.

The dimer [(μ-BCat)(μ-H)$_2${Rh(dippe)}{Rh(dippe)(H)}] (**8**; Cat = 1,2-dioxophenylene, dippe = 1,2-bis(diisopropylphosphanyl)ethane), with the rhodium centers in two different oxidation states, was obtained upon reaction of [{Rh(μ-H)(dippe)}$_2$] with two equivalents of HBCat.[20] Structural determination of **8** by X-ray diffraction showed the compound to consist of a Rh^I center that is coordinated to a chelating dippe ligand and two bridging hydride ligands in a

 © 2006 Wiley-VCH Verlag GmbH & Co. KGaA, Weinheim

square-planar arrangement and of an octahedral Rh^{III} center that is bonded to two bridging hydride ligands, one terminal hydride ligand, a chelating dippe ligand, and a σ-bonded BCat ligand. A weak interaction between the boron center and the apical site of the Rh^{I} ion could also be detected with a long Rh^{I}–B distance (2.444(9) Å; Rh^{III}–B distance: 2.057(8) Å).

The reaction of *cis*-[Pt(BCat)$_2$(PPh$_3$)$_2$] with 1.1 equivalents of 1,1-bis(diphenylphosphanyl)methane (dppm) led to the generation of a compound that, on the basis of its spectroscopic data, was tentatively formulated as *cis*-[Pt(BCat)$_2$(dppm)] or, more likely, as *cis*,*cis*-[Pt$_2$(μ-dppm)$_2$(BCat)$_4$].[21] Attempted crystallization led, however, to isolation of small quantities of the two platinum dimers [Pt$_2$(PPh$_3$)(μ-dppm)$_2$(BCat)(μ-BCat)] (**9**) and [Pt$_2$(κ^1-dppm)(μ-dppm)$_2$(BCat)(μ-BCat)] (**10**, Scheme 5). The molecular structures of **9** and **10**, as determined by X-ray diffraction studies, showed very similar atom connectivity in the two compounds and revealed the presence of a BCat group that bridges the two platinum centers in a rather asymmetric fashion, as indicated by the different Pt–B bond lengths (**9**: Pt^1–B 2.12(2), Pt^2–B 2.49(2) Å; **10**: Pt^1–B 2.14(2), Pt^2–B 2.51(2) Å).

The bonding nature of the M-(μ-B)-M systems that were described above was analyzed by DFT calculations,[20] which indicated that in the rhodium complex **8**, the Rh^{I}–(μ-B) interaction can be viewed as σ donation from the filled d_{z^2} orbital of the Rh^{I} center to the empty p orbital of the semibridging boron-based ligand. In the two platinum dimers **9** and **10**, however, the d_{xz} orbital of Pt^2 is responsible for the σ donation into the empty p orbital of the boron atom. The particular d orbital that is utilized in the M–B dative interaction appears, therefore, to depend on the M–M distance. The d_{z^2} orbital is preferred in the presence of the short Rh–Rh distance, and the d_{xz} orbital is preferred for the long Pt–Pt bond.

Very recently, the dinuclear monoboryl complex [(μ-BCl$_2$)(μ-CO)$_2${(η^5-C$_5$Me$_5$)Fe}{Pd(PCy$_3$)}] (**11**, Scheme 5), featuring a symmetrically bridging BR_2 ligand, was obtained.[22] Reaction of the dichloroboryl complex [(η^5-C$_5$Me$_5$)Fe(CO)$_2$(BCl$_2$)] (**25**; Section 3.1) with [Pd(PCy$_3$)$_2$] led to formation of complex **11** with concomitant liberation of tricyclohexylphosphine. The bridging dichloroboryl complex **11** displays a strongly deshielded ^{11}B NMR resonance at $\delta = 72$ ppm, which is shifted only modestly high-field with respect to that of **25** ($\delta = 95$ ppm). Such a low-field value is extremely unusual for a fourfold-coordinated boron atom, particularly when compared to that of the 4-methylpyridine adduct **71** of the dichloroboryl complex [(η^5-C$_5$H$_5$)Fe(CO)$_2$(BCl$_2$)] (**24**, $\delta =$ 19 ppm; Section 3.3).[31]

In the solid state the geometry of the boron center is distorted tetrahedral; the Fe–B (**11a**: 2.095(4) Å; **11b**: 2.078(4) Å—two crystallographically independent molecules are present in the unit cell) and Pd–B bond lengths (**11a**: 2.062(4) Å; **11b**: 2.090(4) Å) are small. The structural parameters that are highlighted above are consistent with a nearly symmetrical bridging mode of the boryl ligand in **11**, thus differentiating this complex from the previously described semibridging catecholboryl species. This difference is a likely consequence of the higher Lewis acidity of the dichloroboryl ligand with respect to that of the catecholboryl group.[20,21] A qualitative description of the bonding in complex **11** was deduced from bonding schemes developed for related carbonyl systems[23] and the aforementioned platinum and rhodium complexes,[20] as well as from preliminary theoretical calculations. Hence, **11** can be formally viewed as resulting from a dative bond from the saturated boryl complex **25** to the {(Cy$_3$P)Pd} fragment and consequent back-donation of the latter into both the out-of-phase combination of the CO π* orbitals and the empty orbital of π symmetry at the boron atom.

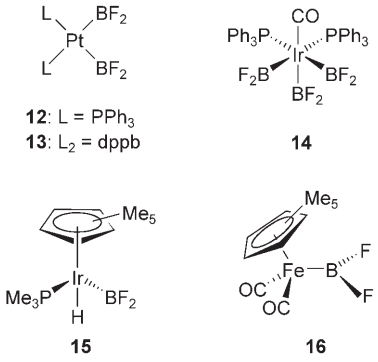
3. Boryl Complexes

Among transition-metal complexes that feature ligands with a single boron atom, boryl compounds (**II** in Scheme 1) are by far the most numerous and comprise more than a hundred examples, most of which were structurally characterized by X-ray diffraction methods.[14] The oxidative addition of B–H, B–B, and B–E bonds (E = main-group element) to low-valent transition-metal complexes is the most common synthetic route to such compounds, and a variety of mono-, bis-, and tris(boryl) complexes were synthesized accordingly. Furthermore, the molecular structures of catalytically important rhodium(hydrido)boryl complexes were also recently determined by neutron diffraction studies.[24] Salt-elimination reactions between anionic transition-metal complexes and haloboranes or halodiboranes(4) represent an alternative important synthetic pathway. The 1,2-dioxophenylene, or catechol, group played a pivotal role in establishing the chemistry of these compounds owing to the widespread use of HBCat in metal-catalyzed hydroborations, and only later was the suitability of other alkoxo- or aminoboranes as starting materials demonstrated. Complexes featuring BR_2 ligands (R = alkyl, aryl, halide) are comparably rare.

3.1. Dihaloboryl Complexes

Only a few structurally authenticated dihaloboryl complexes are known. Oxidative addition of the B–B bond in B_2F_4 to platinum(0) precursors is the key step in the formation of the platinum–difluoroboryl complexes **12** and **13** (Scheme 6).[25] The mechanism that yielded the iridium tris(boryl) compound [Ir(CO)(PPh$_3$)$_2$(BF$_2$)$_3$] (**14**) from the reaction of Vaska's complex, *trans*-[Ir(Cl)CO(PPh$_3$)$_2$], with B_2F_4 is clearly more complex. The authors speculated on a possible sequence of oxidative addition of the B–B bond in B_2F_4 and subsequent σ-bond metathesis between the B–B bond of a second molecule of B_2F_4 and the Ir–Cl bond of the resulting bis(boryl) complex (or these steps in reverse order) as a reasonable reaction pathway.[26] The only example of a difluoroboryl complex to be synthesized by a salt-elimination reaction is [(η^5-C$_5$Me$_5$)Ir(PMe$_3$)(H)(BF$_2$)] (**15**), which was obtained from the reaction of Li[(η^5-C$_5$Me$_5$)Ir(PMe$_3$)H] with BF$_3$·OEt$_2$.[27] Very recently, the iron complex [(η^5-C$_5$Me$_5$)Fe(CO)$_2$(BF$_2$)] (**16**) was unexpectedly obtained as one of the products of the reaction between the mesityloxy(chloro)boryl complex [(η^5-C$_5$Me$_5$)Fe(CO)$_2${B(Cl)OMes}]

 © 2006 Wiley-VCH Verlag GmbH & Co. KGaA, Weinheim



Scheme 6. Mono-, bis-, and tris(difluoroboryl) complexes; dppb = 1,4-bis(diphenylphosphanyl)butane.

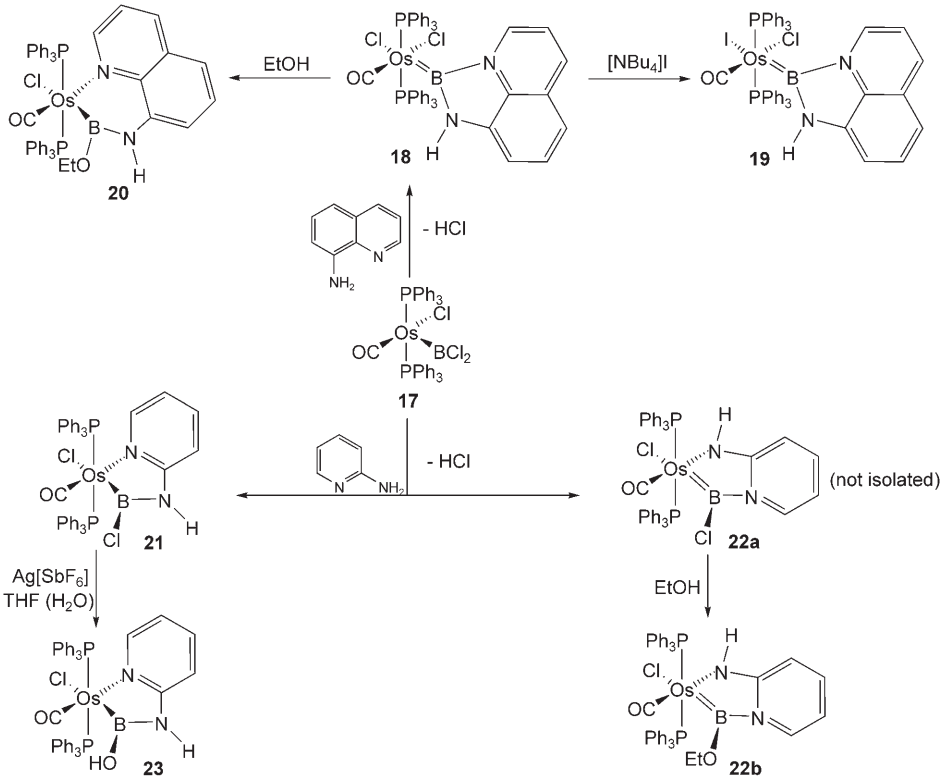
and $Na[BAr^F_4]$ ($Ar^F = 3,5\text{-}(CF_3)_2C_6H_3$), but the mechanism of formation remains unclear (Section 4.1.1.2).[28]

No successful substitution reaction at the boron atom in fluoroboryl complexes is known owing to the high thermodynamic stability of the B–F bond and the low tendency of the fluoride ion to act as a leaving group. In contrast, the osmium–dichloroboryl complex $[Os(Cl)(CO)(PPh_3)_2(BCl_2)]$ (**17**) proved to be a valuable precursor to a number of derivatives upon substitution of its boron-bound chloride ions. Complex **17** was obtained in very good yield by treating $[Os(Ph)Cl(CO)(PPh_3)_2]$ with $HBCl_2{\cdot}OEt_2$ (Scheme 7).[29a]

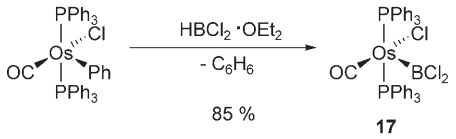
Although complex **17** was not crystallographically characterized in the solid state, its structure was unambiguously established on the basis of its spectroscopic data and the products formed in its reactions with 8-aminoquinoline[29a] and 2-aminopyridine[29b] (Scheme 8).

Reaction of **17** with 8-aminoquinoline led to the isolation of the first base-stabilized borylene complex **18**. Treatment of the sparingly soluble **18** with tetrabutylammonium iodide yielded the corresponding iodo-substituted species **19** upon selective substitution of the osmium-bound chloride *trans* to the boron atom, thus providing evidence for the high *trans* influence of the borylene moiety. The higher solubility of **19** allowed for its complete characterization in solution and its structural characterization in the solid state. The Os–B bond (2.055(8) Å) is shorter than those observed in six-coordinate osmium–boryl complexes, but longer than would be expected for an Os–B double bond with a two-coordinate boron atom. Coordination of the quinoline nitrogen donor is likely to account for the elongated bond and gives rise to resonance structures that feature Os–B single bonds. Similar arguments were invoked to justify the observed elongated bond lengths in base-stabilized silylene complexes, in which the M–Si bond lengths suggest the presence of single bonds rather than double bonds.[4] Complex **19** exhibits a ^{11}B NMR signal at $\delta =$ 52 ppm, which is shifted high-field with respect to donor-free terminal borylene complexes.[14]

Despite its coordination to two nitrogen atoms, the boron center in **18** retains the electrophilic character that was predicted by theoretical studies on terminal borylene complexes.[12] Indeed, reaction with ethanol produced the ethoxyboryl derivative **20** in which the quinoline nitrogen donor coordinates to the osmium center in a position *trans* to the carbonyl ligand. Reaction of **17** with 2-aminopyridine afforded a mixture of two products, **21** and **22a**. Treatment of this mixture with ethanol led to separation of the insoluble amino(chloro)boryl complex **21** from the soluble base-stabilized ethoxyborylene derivative **22b**. Boryl complex **21** showed a remarkable resistance to nucleophilic attack, and did not react even in refluxing ethanol. In the presence of $Ag[SbF_6]$, however, in wet THF the hydroxyboryl complex **23** was obtained and characterized crystallographically.[29b] A direct comparison of the structural data for the base-stabilized ethoxyborylene complex **22b** and the hydroxyboryl



Scheme 8. Reactivity of $[Os(BCl_2)Cl(CO)(PPh_3)_2]$ (**17**).

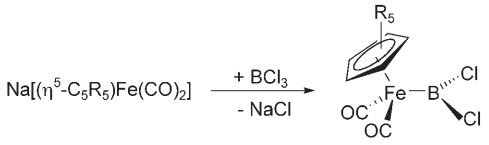


Scheme 7. Synthesis of the dichloroboryl complex **17**.

© 2006 Wiley-VCH Verlag GmbH & Co. KGaA, Weinheim

complex **23** is particularly instructive as the compounds bear the same set of donor atoms at the boron and osmium atoms (**22b**: Os–B 2.066(5) Å, Os-B-O 140.2(4)°; **23**: Os–B 2.085(3) Å, Os-B-O 136.5(2)°). The remarkably small differences in the bond lengths and angles in the two species suggest that the formal distinction between a boryl and a base-stabilized borylene complex is to be considered somewhat artificial. The dichloroboryl complex **17** reacts with other protic nucleophiles such as water, alcohols, and amines to yield the corresponding dihydroxo, dialkoxo, and diamino derivatives.[29c]

The complexes $[(\eta^5\text{-}C_5R_5)Fe(CO)_2(BCl_2)]$ (R = H, **24**; R = Me, **25**) were prepared by a salt-elimination reaction, as shown in Scheme 9.[30a,31] To the best of our knowledge, **24** is



24: R = H
25: R = Me

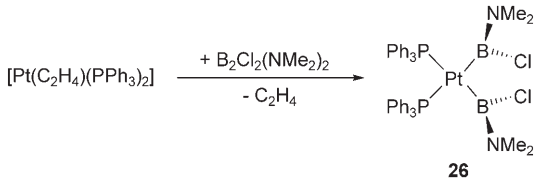
Scheme 9. Synthesis of the boryl complexes **24** and **25**.

the only structurally characterized dichloroboryl complex.[31] The iron–boron bond length (1.942(3) Å) is one of the shortest ever reported for a half-sandwich boryl complex of iron, and is comparable to that in $[(\eta^5\text{-}C_5H_5)Fe(CO)_2(BCat)]$ (1.959(6) Å).[32] In the latter compound, this finding was interpreted as being indicative of substantial Fe–B π back-donation, which is favored by the nearly coplanar arrangement of the C_5H_5(ring centroid)-Fe-B and O-B-O planes (angle of intersection: 7.9°). Indeed, such spatial arrangement allows for favorable π overlap of the HOMO of the transition-metal-complex fragment with the vacant p orbital at the boron atom. Although the relative orientation of this fragment and the boryl ligand precludes an analogous interaction in **24** (angle of intersection: 77.7°), the possibility of π overlap still exists, but in this case with the HOMO−2. As indicated in a recent DFT study on the model compound $[(\eta^5\text{-}C_5H_5)Fe(CO)_2(BO_2C_2H_2)]$,[30b] the π contribution to bonding is very similar for each orientation, thus resulting in a small energy difference (0.025 kcal mol^{-1}) between the two conformers.

3.2. Asymmetric Haloboryl Complexes

3.2.1. Amino(halo)boryl Complexes

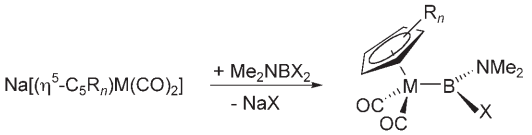
Salt-elimination reactions represent the route of choice for the synthesis of this class of boryl complexes. Two of the very few exceptions are the above-mentioned tethered osmium complex **21** (Section 3.1) and the bis(boryl) complex *cis*-$[(Ph_3P)_2Pt\{B(Cl)NMe_2\}_2]$ (**26**).[21] The latter is obtained by oxidative addition of the B–B bond of bis(dimethylamino)dichlorodiborane(4) to $[(Ph_3P)_2Pt(\eta^2\text{-}H_2C{=}CH_2)]$, accompanied by loss of ethylene (Scheme 10).



26

Scheme 10. Synthesis of the bis(boryl) complex **26**.

Reactions of anionic cyclopentadienyl iron and ruthenium precursors with dimethylamino(dihalo)boranes afforded selective substitution of only one halide atoms to yield the corresponding amino(halo)boryl complexes **27–32** (Scheme 11).[33a,b]

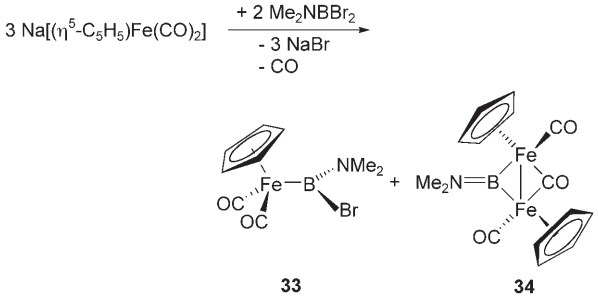


27: M = Fe, X = Cl, $R_n = H_5$
28: M = Fe, X = Cl, $R_n = H_4Me$
29: M = Fe, X = Cl, $R_n = Me_5$
30: M = Fe, X = Br, $R_n = Me_5$
31: M = Ru, X = Cl, $R_n = H_5$
32: M = Ru, X = Br, $R_n = H_5$

Scheme 11. Synthesis of amino(halo)boryl complexes.

The molecular structure of complex **29** was determined by X-ray diffraction methods.[33a] A rather weak π interaction between the iron and boron atoms is indicated by low carbonyl stretching frequencies ($\tilde{\nu}$ = 1988, 1928 cm^{-1}) and by a rather large Fe–B bond length (2.027(5) Å). Reaction of the strong nucleophile $Na[(\eta^5\text{-}C_5H_5)Fe(CO)_2]$ with Me_2NBBr_2, however, produced a 1:1 mixture of the boryl complex $[(\eta^5\text{-}C_5H_5)Fe(CO)_2\{B(Br)NMe_2\}]$ (**33**) and the bridging borylene complex $[(\mu\text{-}BNMe_2)(\mu\text{-}CO)\{(\eta^5\text{-}C_5H_5)Fe(CO)\}_2]$ (**34**, Scheme 12).[33b]

Efficient π donation from the dimethylamino group to the boron center in compounds **27–32** prevented the occurrence of nucleophilic substitution reactions at boron.[33c]



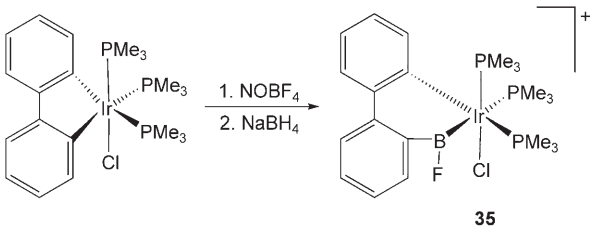
33 **34**

Scheme 12. Reaction of $Na[(\eta^5\text{-}C_5H_5)Fe(CO)_2]$ with Me_2NBBr_2.

 © 2006 Wiley-VCH Verlag GmbH & Co. KGaA, Weinheim

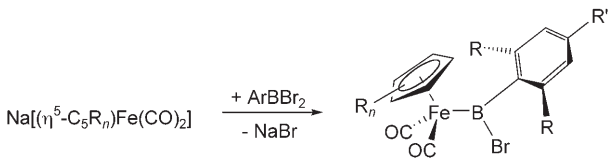
3.2.2. *Aryl(halo)boryl Complexes*

The first report on aryl(halo)boryl complexes dates back to 1993. The cationic, paramagnetic iridium(IV)–boryl compound $[Ir(PMe_3)_3Cl(C_{12}H_8BF)][BPh_4]$ (**35**) was synthesized by reaction of $[Ir(PMe_3)_3Cl(C_{12}H_8)]$ with $NOBF_4$ through formal insertion of "BF" into one of the Ir–C bonds (Scheme 13).[34]



35

Scheme 13. Synthesis of the paramagnetic iridium(IV)–boryl compound **35**.



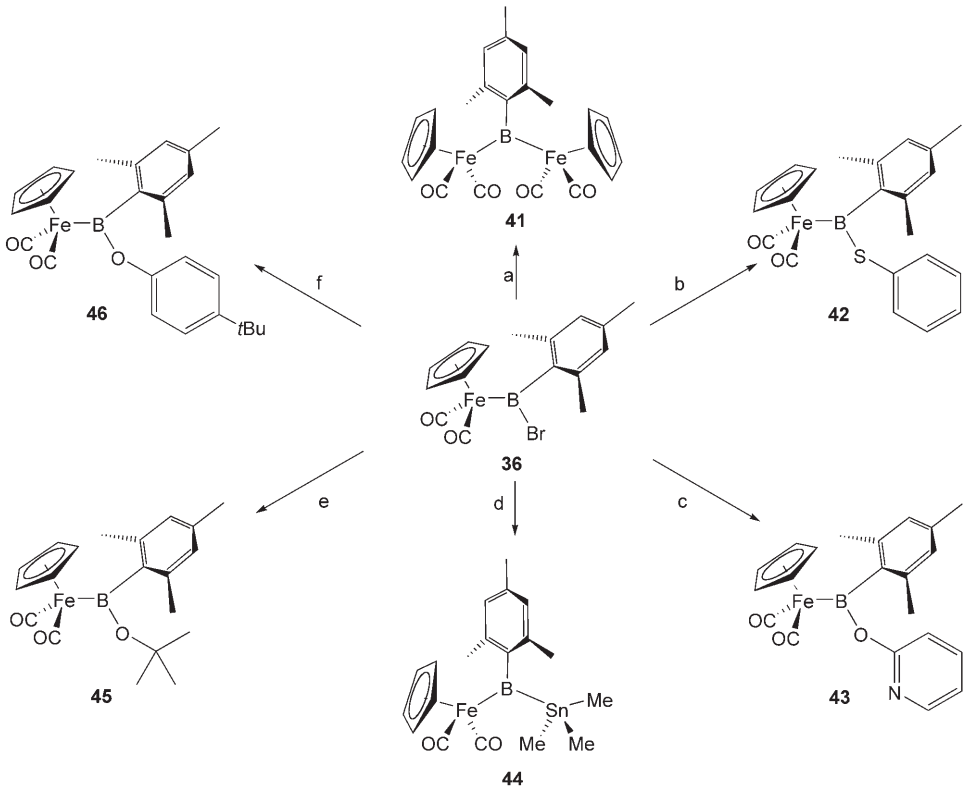
36: R = R' = Me, $R_n = H_5$
37: R = R' = Me, $R_n = H_4Me$
38: R = R' = Me, $R_n = Me_5$
39: R = 2,4,6-*i*$Pr_3C_6H_2$, R' = H, $R_n = Me_5$

Scheme 14. Synthesis of aryl(bromo)boryl complexes **36**–**39**.

A more general means of accessing this class of compounds is provided by salt-elimination reactions, as exemplified by the synthesis of $[(\eta^5\text{-}C_5R_n)Fe(CO)_2\{B(Br)Mes\}]$ ($R_n = H_5$, H_4Me, Me_5; Mes = 2,4,6-$Me_3C_6H_2$), which was accomplished through reaction of equimolar amounts of $MesBBr_2$ and $Na[(\eta^5\text{-}C_5R_n)Fe(CO)_2]$ (Scheme 14).[35b] The phenyl(chloro)boryl iron complex $[(\eta^5\text{-}C_5Me_5)Fe(CO)_2\{B(Cl)Ph\}]$ (**40**) was obtained similarly from the reaction of $PhBCl_2$ with the bulky nucleophile $Na[(\eta^5\text{-}C_5Me_5)Fe(CO)_2]$.[35c]

With the exception of the sterically crowded compound **39**,[35d] all mesityl(bromo)boryl complexes were shown to undergo substitution chemistry at the boron atom.[35] While offering steric protection to the boron center in complexes **36**–**38**, the mesityl group fails to provide sufficient electronic stabilization, thus resulting in the boron atom in **36** that is strongly Lewis acidic and susceptible to nucleophilic attack. Some of its characteristic reactions are shown in Scheme 15. The use of complex **36** in the synthesis of the unsupported bridging borylene complex **41**[35a] and the use of its pentamethylcyclopentadienyl analogue **38** as a precursor to terminal borylene complexes will be discussed in Sections 4.2.1 and 4.1.1.2, respectively.

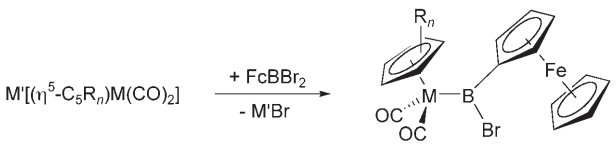
The structures of complexes **36**, **41**, **45**, and **46** were confirmed by X-ray crystallography. The lengthening of the Fe–B bonds in **45** (2.056(2) Å)[35d] and **46** (2.040(2) Å)[35b] as compared with those in the precursor **36** (1.964(5) Å)[35b] clearly results from the replacement of the weak π-donating bromide substituent with the stronger π-donating alkoxo- and aryloxo substituents. Accordingly, lower carbonyl stretching frequencies are observed for **45** (1987 cm^{-1}, 1918 cm^{-1}) and **46** (1997 cm^{-1}, 1933 cm^{-1}) as compared with those of **36** (2016 cm^{-1}, 1926 cm^{-1}).



Scheme 15. Substitution reactions of the mesityl(bromo)boryl complex **36**. Reagents: a) excess $Na[(\eta^5\text{-}C_5H_5)Fe(CO)_2]$; b) NaSPh; c) LiOpy-2; d) excess $LiSnMe_3$; e) KO*t*Bu; f) $NaOC_6H_4$*t*Bu-4.

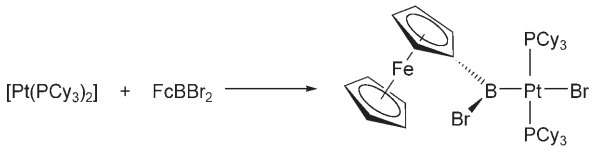
Recently, compounds that feature the ferrocenyl(bromo)boryl ligand, B(Br)Fc, were reported. By employing $FcBBr_2$ as a starting material, salt-elimination reactions with $M'[(\eta^5\text{-}C_5R_n)M(CO)_2]$ (Scheme 16), as well as oxidative addition reactions[36b,c] of the B–Br bond to $[Pt(PCy_3)_2]$ (Scheme 17), led to the generation of the desired boryl compounds.[36a]

© 2006 Wiley-VCH Verlag GmbH & Co. KGaA, Weinheim



47: M' = K, M = Fe, $R_n = H_5$
48: M' = Na, M = Fe, $R_n = Me_5$
49: M' = Na, M = Ru, $R_n = H_5$

Scheme 16. Synthesis of ferrocenyl(bromo)boryl complexes by salt elimination.



50

Scheme 17. Synthesis of **50** by oxidative addition of the B–Br bond.

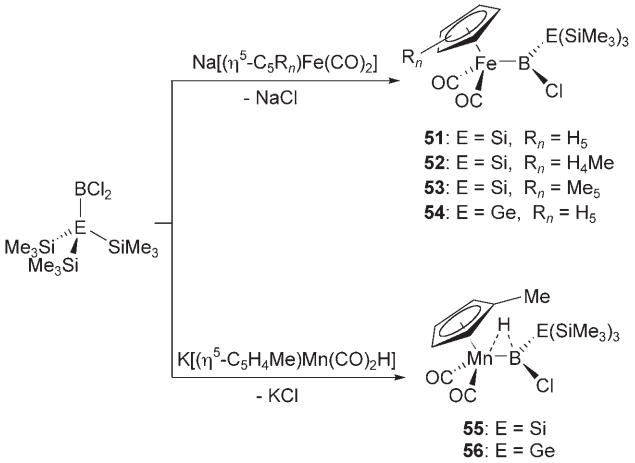
The spectroscopic properties of complexes **47** and **48** are similar to those of the mesityl(bromo)boryl complexes **36**–**38**. Hence, **47** and **48** exhibit ^{11}B NMR signals at $\delta = 99$ and 103 ppm, respectively, which are comparable to that of complex **36** ($\delta = 111$ ppm). In the IR spectra, the carbonyl stretching bands are observed at relatively high wave numbers (**47**: 2015 cm^{-1}, 1955 cm^{-1}; **48**: 2021 cm^{-1}, 1958 cm^{-1}), which are similar to those of **36**–**38**. The iron compounds **47** and **48** were characterized in the solid state by X-ray diffraction methods, and were found to display slightly longer Fe–B bond lengths (**47**: 1.997(2) Å; **48a**: 1.972(3) Å, **48b**: 1.985(3) Å—two crystallographically independent molecules are present in the asymmetric unit of **48**) than that observed in the corresponding mesityl(bromo)boryl complex **36** (1.964(5) Å).

The geometry and electronic properties of ferrocenylboranes have been the subject of structural and theoretical investigations.[37] A characteristic structural feature of ferrocenyl(dibromo)boranes, and of the isoelectronic ferrocenylmethylium cations, is the bending of the BBr_2 unit, or of the exocyclic CR_2 unit, respectively, toward the ferrocenyl iron center.[37a] The degree of substituent bending is indicated by the value of the dip angle α^* ($\alpha^* = 180° - \alpha$, whereby α is defined as the angle formed by the centroid of the cyclopentadienyl ring, the *ipso* carbon atom of the ring, and the boron atom). This observation was interpreted in terms of delocalized orbital interactions that involve the formally empty p orbital at the boron atom, the boron-bound *ipso* carbon atom of one cyclopentadienyl ring, d orbitals at the iron center, and a significant through-space interaction with the remaining cyclopentadienyl ring that is augmented by electrostatic interactions.[37] $FcBBr_2$ exhibits dip angles of 17.7° and 18.9° (for the two crystallographically independent molecules I and II, respectively, in the asymmetric unit),[37a] whereas the structural results for **47** and **48** show significantly smaller α^* values, (**47**: 4.2°; **48**: 8.0°, 7.6°).[36a] Upon coordination of the {B(Br)Fc} unit to the {(η^5-C_5R_5)Fe(CO)$_2$} fragment, any π component of the Fe–B bond is expected to relieve the electronic deficiency of the boron atom. Indeed, the observed α^* values for **47** and **48** might suggest the presence of a modest Fe→B π-back-bonding contribution to the Fe–B bond.

The synthesis of *trans*-[(Cy_3P)$_2$Pt(Br){B(Br)Fc}] (**50**) was accomplished by oxidative addition of a B–Br bond of $FcBBr_2$ to [$Pt(PCy_3)_2$] (Scheme 17).[36a] The X-ray structural determination of **50** revealed the expected square planar coordination geometry around the platinum center, such that the boryl and the bromide ligands adopt a mutually *trans* arrangement. The boryl group is arranged virtually orthogonal to the coordination plane at the platinum center, thus allowing for maximum overlap between the filled platinum d_{xy} orbital and the vacant p orbital at the boron atom.[14a] The Pt–B bond length (1.9963(34) Å) is notably smaller than that found in, for example, *trans*-[(Ph_3P)$_2$Pt(Cl){B(Cl)NMe$_2$}] (2.075(10) Å),[21] thus indicating a less Lewis acidic boron center, and no bending of the boron atom toward the iron center is observed. Both findings support the presence of significant π contribution to the Pt–B bond in **50**.

3.2.3. Silyl- and Germyl(halo)boryl Complexes

Treatment of the extremely bulky, strongly Lewis acidic boranes $(Me_3Si)_3EBCl_2$ (E = Si, Ge) with the anionic iron and manganese complexes Na[(η^5-C_5R_n)Fe(CO)$_2$] and K[(η^5-C_5H_4Me)Mn(CO)$_2$H], afforded the corresponding silyl- and germyl(chloro)boryl complexes **51**–**56** (Scheme 18).[38]



51: E = Si, $R_n = H_5$
52: E = Si, $R_n = H_4Me$
53: E = Si, $R_n = Me_5$
54: E = Ge, $R_n = H_5$

55: E = Si
56: E = Ge

Scheme 18. Synthesis of silyl- and germyl(chloro)boryl complexes by salt-elimination reactions.

A significant spectroscopic feature of these compounds is the strongly deshielded ^{11}B NMR spectroscopic resonances (**51**–**54**: $\delta = 139$–141 ppm; **55**: $\delta = 105$ ppm; **56**: $\delta = 106$ ppm), with respect to, for example, the diphenylboryl complex [(η^5-C_5H_5)Fe(CO)$_2$(BPh_2)][32a] ($\Delta\delta = 20$ ppm) or the aminoboryl complexes **27**–**30** ($\Delta\delta = 80$ ppm).[33] Surprisingly, the carbonyl

 © 2006 Wiley-VCH Verlag GmbH & Co. KGaA, Weinheim

stretching frequencies of the iron complexes **51**–**54** (2008–2009 cm^{-1} and 1956–1957 cm^{-1}) are comparable to those of the corresponding alkyl iron complexes,[39] thus providing no evidence of significant iron–boron π back-donation. The molecular structures of **51**, **54**, and **55** were determined by X-ray diffraction methods. Complexes **51** and **54** are isostructural, with shorter Fe–B bond lengths (**51**: 1.964(8) Å; **54**: 1.985(11) Å) than in the aminoboryl complex **29** (2.027(5) Å).[33a]

Interestingly, the extreme steric bulk of the hypersilyl group $Si(SiMe_3)_3$ is not sufficient to prevent reactions at the boron center. Treatment of **51** with TlF in CH_2Cl_2 afforded the corresponding fluoroboryl complex $[(\eta^5\text{-}C_5H_5)Fe(CO)_2\{B(F)Si(SiMe_3)_3\}]$ (**57**) in 46% yield.[38] The presence of the π-donating fluoride substituent at the boron atom results in a high-field shift of the ^{11}B NMR spectroscopic resonance with respect to that of the starting material (**57**: $\delta = 113$ ppm; **51**: $\delta = 141$ ppm). Such ligand modification, however, barely affects the electronic situation at the iron center as the carbonyl stretching frequencies (**57**: 2001 cm^{-1}, 1946 cm^{-1}) are not significantly different from those of **51**. Accordingly, little variation is observed in the structural parameters of **57** with respect to **51**; the Fe–B bond (1.983(9) Å) is not significantly lengthened with respect to that in **51** (1.964(8) Å).

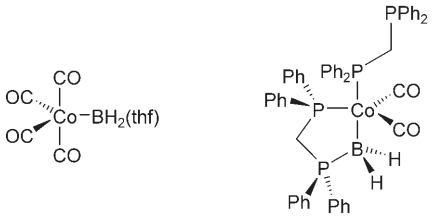
3.2.4. Aryloxy(halo)boryl Complexes

Very recently the synthesis and reactivity of mesityloxy(halo)boryl complexes were reported. Reaction of equimolar amounts of $Na[(\eta^5\text{-}C_5R_n)Fe(CO)_2]$ with $MesOBX_2$ (X = Cl, Br) led to selective substitution of one halide substituent at the boron atom and formation of the desired boryl complexes $[(\eta^5\text{-}C_5R_n)Fe(CO)_2\{B(X)OMes\}]$ (**58**: $R_n = H_5$, X = Cl; **59**: $R_n = H_5$, X = Br; **60**: $R_n = Me_5$, X = Cl).[28] The mesityloxy(halo)boryl complexes are suitable substrates for further substitution chemistry at the boron atom (Scheme 19).

Efforts to abstract the boron-bound halide substituents in **58**–**60** with $Na[BAr^F_4]$ did not lead to cationic borylene complexes (Section 4.1.1.2), but rather to corresponding mesityloxy(fluoro)boryl and difluoroboryl species (**16**).

3.3. Base-stabilized Boryl Complexes

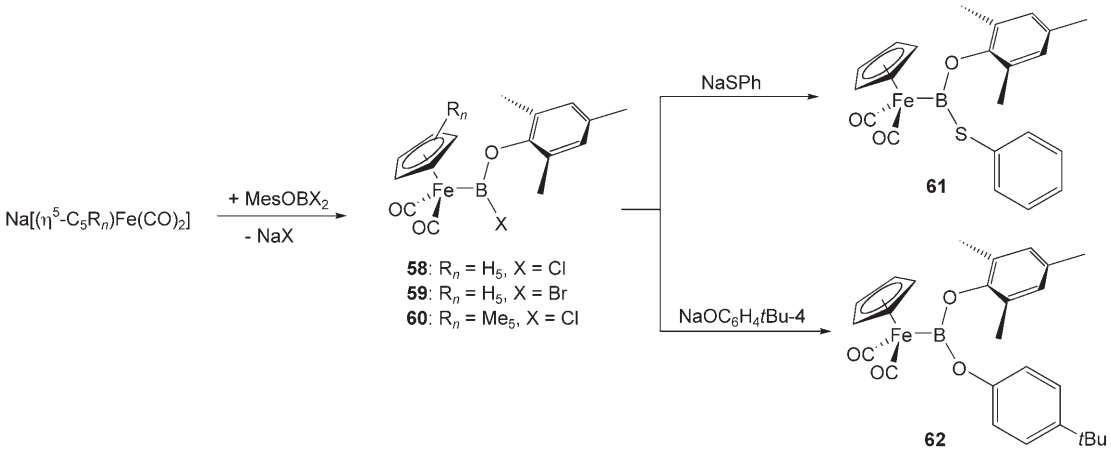
Base-stabilized boryl complexes of the type **IIa** (Scheme 1) are rare compared to the large number of boryl complexes of type **II**. Surprisingly, considering the known tendency of boranes BR_3 to form adducts with Lewis bases, formation of analogous Lewis acid–base adducts by preformed boryl complexes was first reported in 2004. The first reports on base-stabilized boryl compounds date back to 1990,[40] and used borane adducts BH_nX_mL or borates $[BH_4]^-$ as boron sources (Scheme 20).



Scheme 20. Early examples of base-stabilized boryl complexes.

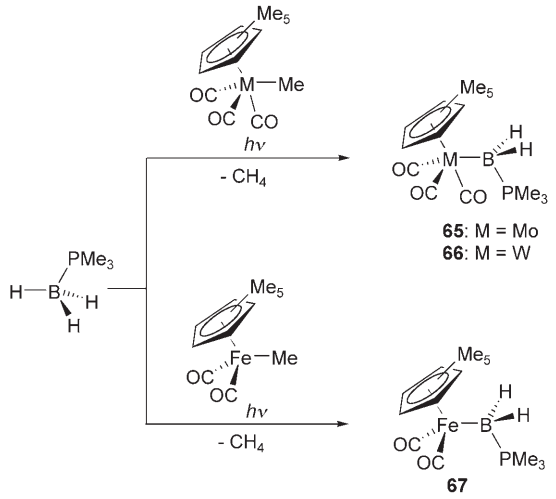
Treatment of $[Co_2(CO)_8]$ with BH_3·thf at low temperatures gave $[Co(CO)_4\{BH_2(thf)\}]$ (**63**).[40] The phosphine adduct **64**, obtained from reaction of $CoCl_2$ with $NaBH_4$ in the presence of CO and dppm, proved to be more stable and could be structurally characterized by X-ray diffraction methods.[41] A more general synthetic route to base-stabilized boryl complexes is represented by photolytic reactions of BH_3·PMe_3 with half-sandwich methyl complexes of molybdenum, tungsten, and iron (Scheme 21).[42a,b]

The yields of these reactions range from moderate (**66**: 49%) to low (**67**: 5%). The analogous cyclopentadienyl derivatives were observed in solution during photolysis, but turned out to be too unstable to be isolated. Alternatively, complex **67** and its ruthenium analogue **68** could be prepared in slightly better yields by salt-elimination reactions according to Scheme 22.[42b]

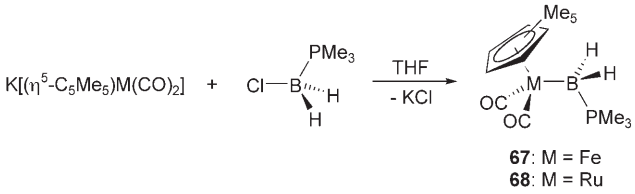


Scheme 19. Synthesis and reactivity of mesityloxy(halo)boryl complexes.

© 2006 Wiley-VCH Verlag GmbH & Co. KGaA, Weinheim



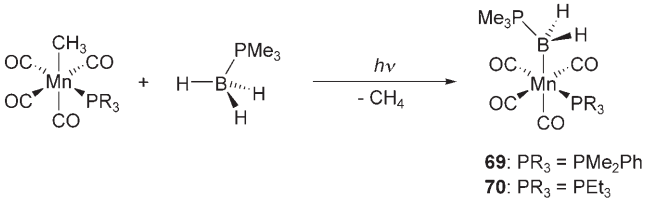
Scheme 21. Photolytic generation of base-stabilized half-sandwich boryl complexes.



Scheme 22. Alternative synthesis of base-stabilized boryl complexes by salt-elimination reactions.

In the ^{11}B NMR spectra, complexes **65**–**68** display resonances ($\delta = -25$ to -29 ppm) expected for a fourfold-coordinated boron center. In the IR spectra, the carbonyl stretching frequencies vary from 1942 cm^{-1} and 1843 cm^{-1} (**65**) to 1951 cm^{-1} and 1883 cm^{-1} (**68**). These values are significantly lower than those of related boryl complexes with a threefold-coordinated boron atom.[13,14] X-ray structural determination of compounds **65**–**68** revealed tetrahedrally coordinated boron atoms with long M–B bonds. On the basis of these data and the lack of M–B π back-donation in the presence of the stabilizing PMe_3 Lewis base at boron, $M^{\delta-}$–$B^{\delta+}$ polarization of the transition-metal–boron single bond was inferred by the authors.

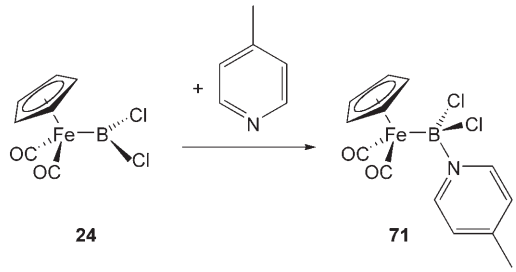
The photolytic methodology that was established with the synthesis of complexes **65**–**67** was subsequently extended to the formation of the base-stabilized boryl complexes of manganese $[Mn(CO)_4(PR_3)\{BH_2(PMe_3)\}]$ (**69**: $PR_3 = PMe_2Ph$; **70**: R = Et; Scheme 23).[42c]



Scheme 23. Photolytic synthesis of base-stabilized boryl complexes of manganese.

The NMR and IR data of **69** and **70** resemble those of complexes **65**–**68**. The dimethylphenylphosphine derivative **69** was structurally characterized by X-ray diffraction methods. The B–Mn bond length (2.314(2) Å) was found to be considerably longer than that in the boryl complex $[Mn(CO)_5(BCat)]$ (2.108(6) Å),[43] thus suggesting a description of the Mn–B linkage as a pure σ bond. The authors proposed that the composition of the compound could be considered as the contact ion pair $[Mn(CO)_4PR_3]^-[BH_2PMe_3]^+$.

Each of the aforementioned base-stabilized boryl complexes was synthesized from base-stabilized borane precursors. In 2004, the synthesis of a base-stabilized boryl compound upon addition of a Lewis base to a preformed boryl complex was reported for the first time. Reaction of the dichloroboryl complex **24** with 4-methylpyridine afforded the corresponding Lewis acid–base adduct $[(\eta^5\text{-}C_5H_5)Fe(CO)_2\{BCl_2(NC_5H_4\text{-}4\text{-}Me)\}]$ (**71**) in nearly quantitative yield (Scheme 24).[31]



Scheme 24. Synthesis of the base-stabilized boryl complex **71**.

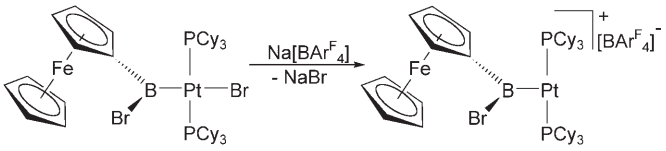
In the ^{11}B NMR spectrum, complex **71** shows a signal at $\delta = 19$ ppm, which is shifted dramatically high-field with respect to that of **24** ($\delta = 90$ ppm), but still deshielded when compared with that of $[(\eta^5\text{-}C_5Me_5)Fe(CO)_2\{BH_2(PMe_3)\}]$ (**67**; $\delta = -25.9$ ppm), owing presumably to the presence of more electronegative substituents at boron. Complex **71** exhibits carbonyl stretching bands at significantly lower frequencies (1976, 1916 cm^{-1}) than those reported for **24** (2026, 1974 cm^{-1}), thus indicating an increase in electron density at the iron center, as caused by breakdown of the Fe–B π interaction through rehybridization at the boron center. The results of a crystal structure analysis of **71** show that the boron atom adopts a tetrahedral geometry and the geometry of the $\{(\eta^5\text{-}C_5H_5)Fe(CO)_2\}$ fragment remains unchanged from that in **24**. The Fe–B (2.1326(14) Å) and B-Cl bonds (average: 1.8814(14) Å) are elongated by 10% and 5.6%, respectively, as a result of coordination of 4-methylpyridine. Such bond lengthening is greater than that expected from rehybridization at boron and lends further support to the presence of a Fe–B π interaction in **24**.

3.4. A Cationic Three-Coordinate Platinum–Boryl Complex

As previously described in Section 3.2.2, the oxidative addition of a B–X bond of haloboranes to low-valent transition-metal compounds represents a viable route to

 © 2006 Wiley-VCH Verlag GmbH & Co. KGaA, Weinheim

boryl complexes[36,44a,c] such as *trans*-$[(Cy_3P)_2Pt(Br)\{B(Br)Fc\}]$ (**50**).[36a] In the solid state, compound **50** displays a rather large Pt–Br bond length (2.6183(8) Å), which provides an indication of the high *trans* influence of the B(Br)Fc group. Indeed, as demonstrated by a number of structural and theoretical studies, the boryl ligand, with its strong σ-donor character, exerts a rather high *trans*-labilizing ability,[45] higher than that of other σ donors such as hydrido[44b,c] and stannyl[44a] groups, or π acceptors like carbon monoxide.[44d] Accordingly, treatment of **50** with $Na[BAr^F_4]$ in CH_2Cl_2 or C_6H_5F led to the facile synthesis of the T-shaped three-coordinate platinum complex *trans*-$[(Cy_3P)_2Pt\{B(Br)Fc\}][BAr^F_4]$ (**72**, Scheme 25).[46]

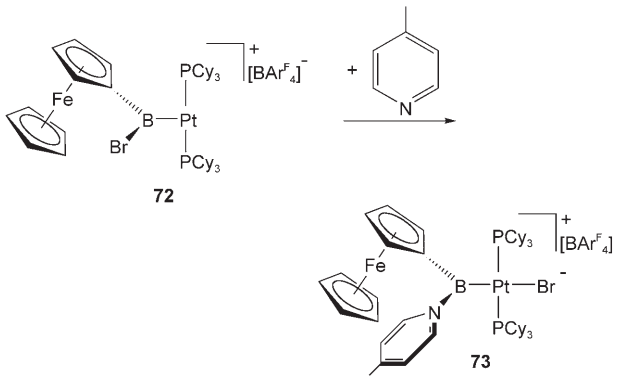


50 72

Scheme 25. Synthesis of the T-shaped three-coordinate platinum–boryl complex **72**.

Despite the highly unsaturated, Lewis acidic nature of the platinum center, no stabilizing interaction of the metal with solvent molecules or with the weakly coordinating $[BAr^F_4]^-$ anion was observed in **72**, neither in the solid state nor in solution. Particularly remarkable is the absence of any efficient agostic interaction between the metal center and the C–H bonds of the cyclohexyl groups in the solid state (shortest Pt···H–C separation: 2.542 Å, Pt···C–H 3.117 Å). Such observations are in agreement with the results of theoretical calculations on 14-electron d^8 ML_3–boryl complexes of the type $[(R_3P)_2Rh(BX_2)]$, which indicate the reluctance of such compounds to bind to C–H bonds in the site *trans* to the boryl group, as a result of the extremely strong *trans* influence of the latter.[47] Interestingly, addition of 4-methylpyridine to a solution of **72** in CD_2Cl_2 yielded the base-stabilized borylene complex *trans*-$[(Cy_3P)_2Pt(Br)\{B(Fc)(NC_5H_4\text{-}4\text{-}Me)\}]$ (**73**), resulting from pyridine coordination at boron and bromide migration from the boron atom to the platinum center (Scheme 26).[46]

Formation of complex **73** bears some resemblance to the generation of the base-stabilized osmium–borylene complex **18**, which was reported by Roper and co-workers (Section 3.1).[29a] Thus, coordination of the Lewis base (intramolecular in **18**, intermolecular in **73**) results in the formation of a strong B–N bond within the borylene moiety and induces a formal halide migration from boron to the coordinatively unsaturated transition-metal center. A slight elongation of the Pt–B bond is observed on going from the boryl complex **72** (1.966(4) Å) to the base-stabilized borylene compound **73** (2.014(5) Å), which contrasts with a conventional description of **73** as possessing a Pt–B double bond. Such ambiguity was already pointed out by Roper, who commented on the "boryl" character of his base-stabilized osmium–borylene complexes (Section 3.1). The same arguments, thus, apply to



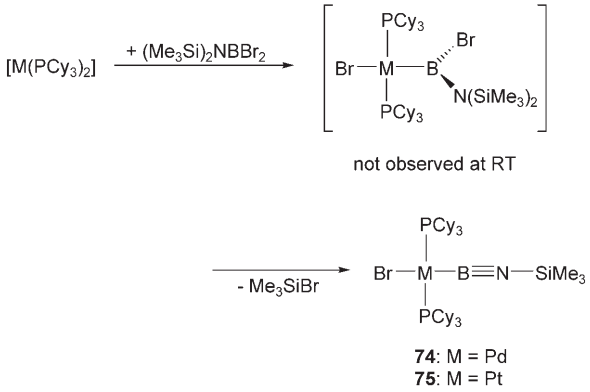
72 73

Scheme 26. Synthesis of the base-stabilized cationic borylene platinum complex **73**.

the base-stabilized platinum–borylene complex **73**. The Pt–Br bond in **73** (2.6057(5) Å) is rather long and comparable to that in the neutral boryl complex **50** (2.6183(8) Å), thus in line with the high *trans* influence of the boron-containing ligand.

3.5. Iminoboryl complexes

Reaction of $(Me_3Si)_2NBBr_2$ with $[M(PCy_3)_2]$ (M = Pd, Pt) at room temperature led to the remarkable isolation of the first transition-metal–iminoboryl complexes *trans*-$[(Cy_3P)_2M(Br)(B{\equiv}NSiMe_3)]$ (**74**: M = Pd, **75**: M = Pt; Scheme 27).[48]



74: M = Pd
75: M = Pt

Scheme 27. Synthesis of iminoboryl complexes **74** and **75**.

Previous results on B–Br bond oxidative addition of $FcBBr_2$ to $[Pt(PCy_3)_2]$[36a] and the reported syntheses of main-group element substituted iminoboranes upon intramolecular Me_3SiX elimination from suitable $R(X)B{=}N(SiMe_3)R'$ precursors,[49] strongly suggest that formation of compounds **74** and **75** occurs by intramolecular elimination of Me_3SiBr from the postulated intermediates *trans*-$[(Cy_3P)_2M(Br)\{B(Br)N(SiMe_3)_2\}]$ (Scheme 27). Since Me_3SiX eliminations from $R(X)B{=}N(SiMe_3)R'$ compounds generally occur at temperatures of 400–500 °C and low pressures,[49] the ease of Me_3SiBr elimination to form **74** and **75** is remarkable. In clear contrast to conventional $RB{\equiv}NR'$ iminoboranes, iminoboryl com-

 © 2006 Wiley-VCH Verlag GmbH & Co. KGaA, Weinheim

plexes **74** and **75** did not show any tendency to oligomerize at elevated temperatures (refluxing toluene) or upon photolysis. The ^{11}B NMR spectra of the complexes show a signal at $\delta =$ 22 ppm for **74** and at $\delta = 26$ ppm for **75**, values that compare well with those of main-group element substituted iminoboranes such as $(Me_3Si)_3SiB{\equiv}NSiMe_3$ ($\delta = 22$ ppm).[50]

The molecular structures of **74** and **75** were determined by X-ray diffraction studies. The B–N bond lengths (**74a**: 1.251(4) Å; **74b**: 1.262(3) Å; **75**: 1.260(4) Å—two crystallographically independent molecules are present in the unit cell of **74**) are very similar and only slightly longer than that reported for $(Me_3Si)_3SiB{\equiv}NtBu$ (1.221(5) Å),[51] hence consistent with the presence of a B–N triple bond. The M–B bonds are short; particularly, that in **74** (**74a**: 1.958(3) Å; **74b**: 1.967(3) Å) is shorter than those reported in palladium–boryl complexes (2.006(9)–2.077(6) Å),[44a,36a] while the Pt–B bond length in **75** (1.960(3) Å) is comparable to the one found in the three-coordinate T-shaped platinum–boryl complex *trans*-$[(Cy_3P)_2Pt\{B(Br)Fc\}][BAr^F{}_4]$ (**72**, 1.966(4) Å).[46] Interestingly, the M–Br bond lengths (**74a**: 2.5531(5) Å; **74b**: 2.5224(5) Å; **75**: 2.5516(4) Å) indicate a weaker *trans* influence of the iminoboryl ligand with respect to that of the B(Br)Fc group (Pt–Br 2.6183(8) Å in *trans*-$[(Cy_3P)_2Pt(Br)\{B(Br)Fc\}]$ (**50**)).[36a] This finding is in line with the reduced p character of the boron-based orbital used in the formation of the M–B σ bond. The reduced p character leads to smaller M–B bond lengths and to a weaker σ donation of the iminoboryl ligand as compared to that of a boryl group,[44c] and the σ-donating ability is further attenuated in **74** and **75** by the presence of the electronegative nitrogen atom.

4. Borylene Complexes

In the course of his ground-breaking work on boron subhalides, Timms reported in 1967 the preparation of fluoroborylene BF from elemental boron and BF_3 at about 2000 °C.[52] In 1984, West and Pachaly generated the silylborylene B–$SiPh_3$ by irradiation of $(Ph_3Si)_3B$ in hydrocarbon matrices at −196 °C.[53] The borylene molecules turned out to be highly reactive species which could only be obtained by applying drastic conditions and could not be isolated as free molecules, but whose formation could be inferred from the nature of the products obtained from trapping experiments.

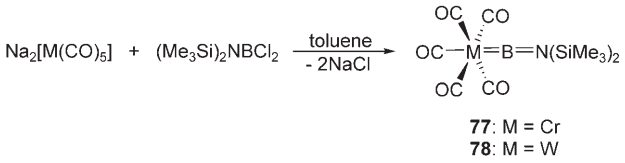
During the past decade, however, it became possible to generate and stabilize borylene moieties in the coordination sphere of various transition metals under standard conditions. DFT studies had predicted the thermodynamic stability of borylene complexes with respect to homolytic dissociation of the metal–boron bond.[12a] Such high thermodynamic stability was explained in terms of the improved σ-donor and π-acceptor properties of the BX molecules in comparison, particularly, to those of the carbonyl ligand. The increased HOMO–LUMO gap within the BX molecule upon metal coordination would improve its kinetic stability. However, the imbalance between σ donation and π acidity was predicted to induce build up of positive charge on BX, thus increasing the likelihood of nucleophilic attack at the coordinated fragment. Accordingly, the presence of sterically demanding and electron-releasing substituents at boron was indicated as a necessary synthetic requisite for the stabilization of the metal-bound BX ligand.

4.1. Terminal Borylene Complexes

4.1.1. Synthesis

4.1.1.1. Synthesis by Salt-Elimination Reactions

The most general synthetic approach to transition-metal terminal borylene complexes is based on the action of dianionic transition-metal carbonylates $M'_2[M(CO)_n]$ on suitable dihaloboranes X_2BR. The resulting double salt-elimination reaction generates species of the type $[(OC)_nM(BR)]$, such as $[(OC)_4Fe{-}B(\eta^5\text{-}C_5Me_5)]$ (**76**)[54] and $[(OC)_5M{=}BN(SiMe_3)_2]$ (**77**: M = Cr, **78**: M = W; Scheme 28),[55] first reported by Cowley and Braunschweig, respectively, in 1998.



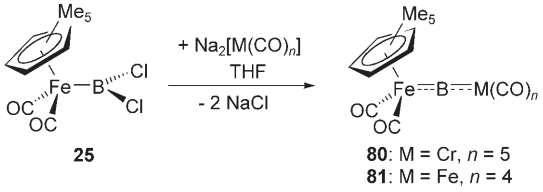
Scheme 28. Synthesis of Group 6 terminal borylene complexes.

A common feature of compounds **76**–**78** is the presence of sterically encumbering and electron-releasing substituents at the boron atom. As pointed out previously, according to theoretical calculations,[12] such substituents are a necessary requisite to alleviate the electron deficiency of the boron atom and to protect it from attack of nucleophiles. In compound **76** this result is achieved by incorporation of boron into a nonclassical polyhedral skeleton, which makes this species a *nido*-pentacarbahexaborane and hence constitutionally very different from compounds **77** and **78**. In solution, the most characteristic feature of the terminal borylene complexes **77** and **78** is a ^{11}B NMR resonance signal at $\delta = 92$ and 87 ppm, respectively, which is considerably low-field-shifted with respect to that of aminoboryl compounds. In the solid state, the structural data for **77** and **78** reveal the presence of a nearly linear M-B-N moiety (M = Cr: 177.4(4)°,[56] M = W: 177.9(5)°),[55] with short B–N (**77**: 1.353(6) Å; **78**: 1.338(8) Å) and M–B bond lengths (M = Cr: 1.996(6) Å, M = W: 2.151(7) Å). Curiously, all attempts at obtaining corresponding complexes $[(OC)_nM(BNR_2)]$ from other aminoboranes X_2BNR_2 were not successful. However, use of the bulky silylborane $Cl_2BSi(SiMe_3)_3$ yielded $[(OC)_5Cr{=}BSi(SiMe_3)_3]$ (**79**), the first terminal borylene complex featuring a coordinatively and electronically unsaturated boron center.[57] The peculiar electronic situation of the boron atom in complex **79** is reflected in a strongly deshielded ^{11}B NMR resonance signal at $\delta = 204$ ppm, as well as in a short Cr–B bond length (1.878(10) Å; **77**: 1.996(6) Å). The elongated $Cr{-}C(O)_{ax}$ bond (1.939(10) Å) indicates the strong *trans* influence of the silylborylene ligand. While steric shielding of the boron center in **79** is undoubtedly provided by

 © 2006 Wiley-VCH Verlag GmbH & Co. KGaA, Weinheim

the $Si(SiMe_3)_3$ group, the absence of any π-donating main-group-element substituent results in a lower thermal stability of **79** as compared to its amino analogue **77**.

In an effort to diversify and broaden the range of available terminal borylene compounds, experimental proof was sought for the possibility of replacing the remaining main-group-element substituent in "conventional" terminal borylene complexes by another transition-metal–ligand fragment. Indeed, the recent realization of the dichloroboryl species $[(\eta^5\text{-}C_5R_5)Fe(CO)_2(BCl_2)]$ (R = H, **24**; R = Me, **25**; Section 3.1) afforded a synthon which could be successfully used in the preparation of compounds that contain a μ_2-bridged boron atom. Thus, a double salt-elimination reaction between **25** and $Na_2[M(CO)_n]$ (M = Cr, $n = 5$; M = Fe, $n = 4$) allowed for the syntheses and structural characterization of $[(\mu_2\text{-}B)\{(\eta^5\text{-}C_5Me_5)Fe(CO)_2\}\{Cr(CO)_5\}]$ (**80**) and $[(\mu_2\text{-}B)\{(\eta^5\text{-}C_5Me_5)Fe(CO)_2\}\{Fe(CO)_4\}]$ (**81**), the first compounds to contain a boron center that is classically bonded solely to transition metals (Scheme 29).[58]



25

80: M = Cr, n = 5
81: M = Fe, n = 4

Scheme 29. Synthesis of the metallaborylene complexes **80** and **81**.

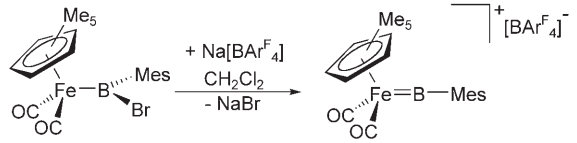
The most striking spectroscopic feature of compounds **80** and **81** in solution is a low-field resonance signal in the ^{11}B NMR spectrum at $\delta = 205$ and 191 ppm, respectively, which is in a region typical of compounds with interstitial boron atoms. The molecular structures of complexes **80** and **81** were determined by single-crystal X-ray diffraction. The structures are characterized by the presence of a linear metal-boron-metal unit (Cr-B-Fe 177.75(11)° and Fe-B-Fe 175.38(12)°), thus confirming the bridging mode of the formally sp-hybridized boron center.

For the bonding interactions that occur between the two metal centers and boron, evaluation of the bond distances, as well as DFT calculations, provide a description in which both metal–boron bonds contain a π component.

4.1.1.2. *Synthesis by Halide Abstraction from Asymmetric Haloboryl Complexes*

An alternative approach to the synthesis of terminal borylene complexes, which employs asymmetric haloboryl species as precursors, was successfully pursued by Aldridge and co-workers. Addition of $Na[BAr^F_4]$ to a solution of the mesityl(bromo)boryl complex $[(\eta^5\text{-}C_5Me_5)Fe(CO)_2\{B(Br)Mes\}]$ (**38**) in dichloromethane afforded the first cationic terminal borylene species $[(\eta^5\text{-}C_5Me_5)Fe(CO)_2(BMes)][BAr^f_4]$ (**82**; Scheme 30) and precipitation of the sparingly soluble NaBr.[59a]

In solution, complex **82** is characterized by the expected strongly low-field-shifted ^{11}B NMR resonance signal ($\delta =$ 145 ppm, **38**: $\delta = 113$ ppm). In the solid state, the linearity of the Fe-B-C unit (178.3(6)°) is accompanied by a very small Fe–B bond length (1.792(8) Å), thus consistent with the presence of a Fe–B double bond. Concerning the bonding interactions within the complex, structural parameters and theoretical calculations support a model in which the covalent portion of the Fe–B bond receives contributions from B→Fe σ donation, as well as from Fe→B π back-donation into one of the two perpendicular vacant p orbitals at the boron atom, while the other orbital is stabilized by π interaction with the mesityl ring.[59a]



38 **82**

Scheme 30. Synthesis of the cationic terminal borylene complex **82**.

In practice, extension of the same protocol to the synthesis of terminal borylene complexes that feature other aryl substituents at boron, differently substituted cyclopentadienyl ligands at iron, or counterions other than the $[BAr^F_4]^-$ anion proved an extremely difficult task. Experimental evidence suggests that steric shielding at both sides of the boron atom is required to ensure stability of the resulting borylene complexes.[59b] However, by analogy with the successful use of amino groups to stabilize the borylene complexes of Group 6 metals, **77** and **78**, use of the π-donating diisopropylamino substituent in place of the mesityl group at boron recently allowed for the isolation of the new cationic complex $[(\eta^5\text{-}C_5H_5)Fe(CO)_2(BNiPr_2)][BAr^F_4]$ (**83**) as a thermally stable colorless oil.[60] Interestingly, treatment of the asymmetric mesityloxyboryl compounds $[(\eta^5\text{-}C_5R_5)Fe(CO)_2\{B(Cl)OMes\}]$ (R = H, **58**; R = Me, **60**) with $Na[BAr^F_4]$ led to the isolation of the corresponding fluoroboryl species $[(\eta^5\text{-}C_5R_5)Fe(CO)_2\{B(F)OMes\}]$ (R = H, Me) as well as the difluoroboryl complex $[(\eta^5\text{-}C_5Me_5)Fe(CO)_2(BF_2)]$ (**16**).[28] Formation of the products is thought to proceed by fluoride abstraction from the $[BAr^F_4]^-$ anion from the putative cationic borylene complexes $[(\eta^5\text{-}C_5R_5)Fe(CO)_2(BOMes)]^+$.[28]

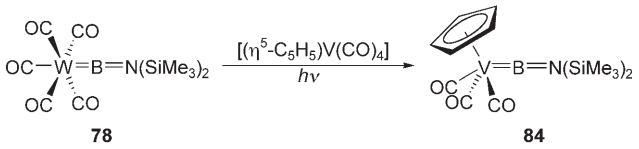
4.1.2. *Reactivity*

4.1.2.1. *Metal-to-Metal Borylene Transfer from $[(OC)_5M{=}BN(SiMe_3)_2]$ (M = Cr, W)*

As demonstrated by the results presented in the previous section, incorporation of the borylene molecule in the coordination sphere of transition metals contributes significantly to the stabilization of this reactive species under standard conditions. The considerable limitations that afflict the established synthetic routes to these interesting compounds, however, prompted an investigation of the potential use of the complexes $[(OC)_5M{=}BN(SiMe_3)_2]$ (**77**: M = Cr, **78**: M = W) as borylene sources under mild conditions. Remarkably, it was found that **77** and **78** are able to transfer the aminoborylene moiety $\{BN(SiMe_3)_2\}$ upon photolysis to suitable borylene acceptors. Hence, photolysis of the tungsten

 © 2006 Wiley-VCH Verlag GmbH & Co. KGaA, Weinheim

compound **78** in the presence of $[(OC)_5Cr(NMe_3)]$ effected the metal-to-metal borylene transfer to form chromium complex **77**.[56] The analogous procedure was performed in the presence of the vanadium precursor $[(\eta^5\text{-}C_5H_5)V(CO)_4]$ (Scheme 31) or the rhenium complex $[(\eta^5\text{-}C_5H_5)Re(CO)_3]$ and led to the generation of the new terminal and bridging borylene species $[(\eta^5\text{-}C_5H_5)(CO)_3V{=}BN(SiMe_3)_2]$ (**84**)[61] and $[\{\mu\text{-}BN(SiMe_3)_2\}\{(\eta^5\text{-}C_5H_5)Re(CO)_2\}_2]$ (**85**), respectively.[56]

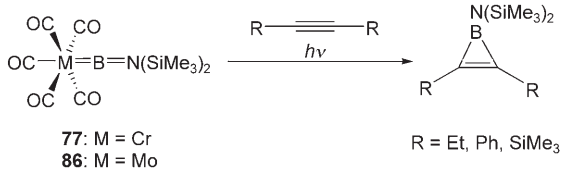


Scheme 31. Formation of the half-sandwich vanadium complex **84** by metal-to-metal borylene transfer.

Importantly, formation of complexes **84** and **85** emphasizes the synthetic significance of the metal-to-metal borylene transfer since all attempts at obtaining these products by more conventional methods, specifically by salt-elimination reactions, had not been successful.[56,61]

4.1.2.2. *Borylene Transfer from $[(OC)_5M{=}BN(SiMe_3)_2]$ (M = Cr, Mo) to Main-Group-Element Compounds*

Further, more recent investigations contributed to broaden the scope of the borylene-transfer reactions by extending the process to include main-group-element borylene acceptors. On the basis of West's observation of the formation of 1-triphenylsilyl-2,3-bis(trimethylsilyl)borirene upon reaction of the photochemically generated triphenylsilylborylene B–$SiPh_3$ at −196 °C with bis(trimethylsilyl)ethyne,[53] photolysis of $[(OC)_5M{=}BN(SiMe_3)_2]$ (**77**: M = Cr, **86**: M = Mo) was performed in the presence of alkynes. These reactions led gratifyingly to the synthesis of a number of borirenes (Scheme 32).[62]



Scheme 32. Synthesis of borirenes by photolytic borylene transfer to alkynes.

Previously reported synthetic routes to these compounds were either limited in scope or laborious and low-yielding.[62] The new method not only confirmed the function of complexes $[(OC)_5M{=}BN(SiMe_3)_2]$ as valuable borylene sources, but also proved to be general with respect to the variety of alkynes that undergo the transformation. Furthermore, this method gave the desired final products in high yield as no boron-containing side products could be detected in the reaction mixtures.

4.1.2.3. *Cationic Terminal Borylene Complexes $[(\eta^5\text{-}C_5Me_5)Fe(CO)_2(BR)][BAr^F{}_4]$ (R = Mes, NiPr$_2$)*

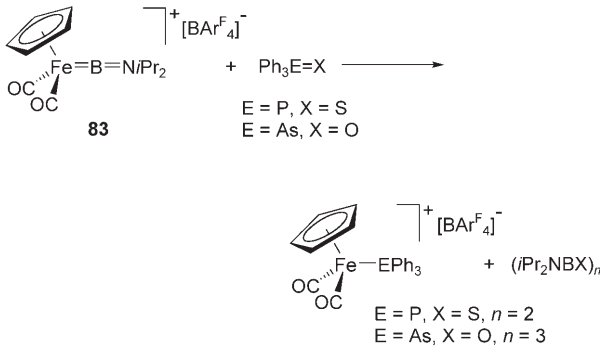
A number of theoretical studies addressed the nature of the M–B bonding interactions in transition-metal–borylene complexes and predicted thermodynamic stability of the linkage but possible kinetic lability owing to the build up of positive charge at the boron atom upon coordination.[12] The reactivity of the cationic terminal borylene $[(\eta^5\text{-}C_5Me_5)Fe(CO)_2(BMes)][BAr^F{}_4]$ (**82**) towards anionic and neutral nucleophiles is representative in this respect. Hence, reaction of **82** with suitable sources of halide anions led to the expected nucleophilic addition at the boron center to yield the corresponding neutral chloro-, bromo-, and iodoboryl complexes.[59b] Furthermore, in the presence of $[PPN]BF_4$ ($[PPN]^+$ = bis(triphenylphosphanylidene)ammonium), fluoride abstraction from the tetrafluoroborate anion occurred with formation of the fluoroboryl compound $[(\eta^5\text{-}C_5Me_5)Fe(CO)_2\{B(F)Mes\}]$. The reactions of complex **82** with $[n\text{Bu}_4N]I$ and $[PPN][BPh_4]$ gave evidence that the iron center can act as an electrophile. In the presence of the iodide nucleophile, addition at the iron center led to formation of $[(\eta^5\text{-}C_5Me_5)Fe(CO)_2I]$ as a minor product and $[(\eta^5\text{-}C_5Me_5)Fe(CO)_2\{B(I)Mes\}]$ as the major product. Reaction with the $[BPh_4]^-$ anion, however, led to the clean formation of the phenyliron derivative $[(\eta^5\text{-}C_5Me_5)Fe(CO)_2Ph]$ along with BPh_3.

The reactivity of **82** towards neutral nucleophiles resulted predominantly in displacement of the borylene moiety.[59b] Thus, addition of CO to a solution of **82** in dichloromethane resulted in the formation of $[(\eta^5\text{-}C_5Me_5)Fe(CO)_3][BAr^F{}_4]$. Analogously, treatment of **82** with 3,3-dimethyl-1-butene or benzophenone led to isolation of $[(\eta^5\text{-}C_5Me_5)Fe(CO)_2(CH_2{=}CHt\text{Bu})][BAr^F{}_4]$ and $[(\eta^5\text{-}C_5Me_5)Fe(CO)_2(\eta^1\text{-}OCPh_2)][BAr^F{}_4]$, respectively. Significant involvement of the dichloromethane solvent in the displacement process and resulting insertion of the BMes moiety into the C–H bond of the solvent molecules was inferred by the authors on the basis of kinetic data. The displacement chemistry is, therefore, thought to be driven by irreversible removal of the BMes ligand. A trapping product from insertion of BMes into the S–S bond of Me_2S_2 was, indeed, isolated.

A broader scope of reactivity appears to be possible for the cationic aminoborylene complex $[(\eta^5\text{-}C_5H_5)Fe(CO)_2(BNi\text{Pr}_2)][BAr^F{}_4]$ (**83**).[60] Hence, reaction of **83** with $Ph_3P{=}S$ or $Ph_3As{=}O$ resulted in the products of net Fe=B bond metathesis, $[i\text{Pr}_2NB(\mu\text{-}S)_2BNi\text{Pr}_2]$ and $(i\text{Pr}_2NBO)_3$,[63] respectively, and formation of the organometallic compounds $[(\eta^5\text{-}C_5H_5)Fe(CO)_2(L)][BAr^F{}_4]$ (L = PPh_3, $AsPh_3$) (Scheme 33).[60]

Isolation and full characterization of the adduct $[(\eta^5\text{-}C_5H_5)Fe(CO)_2\{B(Ni\text{Pr}_2)(OPPh_3)\}][BAr^f{}_4]$, an intermediate in the reaction of **83** with $Ph_3P{=}O$, allowed the authors to suggest a possible mechanism of the reaction. Hence, coordination of $Ph_3E{=}O$ to the Lewis acidic boron atom allows for an addition–substitution pathway to take place, thus yielding the products of overall metathesis chemistry.[60]

 © 2006 Wiley-VCH Verlag GmbH & Co. KGaA, Weinheim



Scheme 33. Metathesis chemistry of the cationic terminal borylene complex **83**.

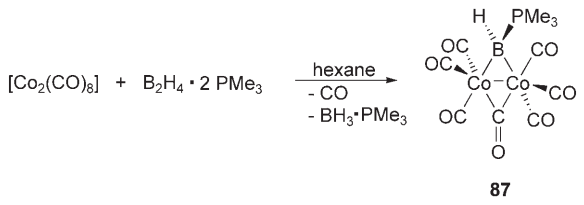
4.2. Bridging Borylene Complexes

At the time of the previous review,[13] the homo-dimetallic manganese and iron compounds $[(\mu\text{-BX})\{(\eta^5\text{-}C_5R_5)\text{Mn}(CO)_2\}_2]$ (X = Cl, *t*Bu, NR'_2, OR″) and $[\{\mu\text{-BN}(SiMe_3)_2\}(\mu\text{-CO})\{(\eta^5\text{-}C_5H_4Me)\text{Fe}(CO)\}_2]$ were the only fully characterized examples of transition-metal complexes that feature the borylene ligand BX. Subsequently, the synthetic routes to similar compounds were optimized, thus resulting in a variety of fully characterized bridging borylene species. Since much of this work has been thoroughly reviewed in previous articles,[14] emphasis is placed in the following section on the most peculiar examples of homo-dinuclear complexes and on the recently obtained first instances of hetero-dinuclear bridging and semibridging borylene complexes, as well as a unique example of a bis(borylene) compound.

4.2.1. Homo-dinuclear Borylene Complexes

Diboranes(4) and, more commonly, dihaloboranes are the traditional boron sources for the synthesis of homo-dinuclear bridging borylene compounds. Reaction of $K[(\eta^5\text{-}C_5H_4Me)\text{Mn}(CO)_2H]$ with $B_2R_2Cl_2$ had granted access to the first series of bridging borylene complexes of manganese. With a different approach, which was also based on the use of diboranes(4), Shimoi and Ogino succeeded in the synthesis of $[\{\mu\text{-BH}(PMe_3)\}(\mu\text{-CO})\{\text{Co}(CO)_3\}_2]$ (**87**; Scheme 34).[64]

Fragmentation of the starting diborane–bis(trimethylphosphine) adduct resulted in liberation of $BH_3{\cdot}PMe_3$ and generation of the parent borylene molecule BH. Stabilization of this extremely reactive species occurred upon coordination to the two cobalt centers and to the remaining PMe_3 molecule to give **87**, a unique example of base-stabilized bridging borylene compound. As in the case of this cobalt species, the borylene bridge in the vast majority of homo-dinuclear borylene compounds is supported by the presence of a metal–metal bond and/or a second bridging ligand.

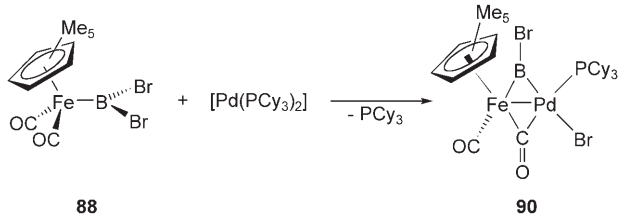


Scheme 34. Synthesis of the base-stabilized bridging borylene complex **87**.

The prototypical reaction of anionic transition-metal compounds with dihaloboranes was exploited by Aldridge and co-workers for the synthesis of $[(\mu\text{-BMes})\{(\eta^5\text{-}C_5H_5)\text{Fe}(CO)\}_2]$ (**41**).[35a] Remarkably, in these species only the reactive mesitylborylene moiety bridges the two iron centers as no liberation of CO occurred during the reaction despite the harsh conditions applied. The Fe–B bond lengths in **41** (2.090(10) Å, 2.091(10) Å) are considerably longer than those found in supported bridging borylene systems,[33a] and the large Fe-B-Fe angle (130.8(5)°) reflects the lack of an Fe–Fe bond.

4.2.2. Hetero-dinuclear Bridging Borylene Complexes

All attempts at preparing hetero-dinuclear bridging borylene compounds from dihaloboranes, by sequential salt-elimination steps with anionic complexes of different transition metals, proved unsuccessful owing to differences in the nucleophilicity of the anions upon changing the metal.[65,59b] By following an alternative strategy, however, the mixed iron–palladium borylene compounds $[(\mu\text{-BX})(\mu\text{-CO})\{(\eta^5\text{-}C_5Me_5)\text{Fe}(CO)\}\{\text{Pd}(Br)(PCy_3)\}]$ (**90**: X = Br, **91**: X = Fc) could recently be obtained. To access these species, the oxidative addition of B–Br bonds to low-valent transition-metal complexes was employed. Specifically, upon reaction of the recently isolated bromoboryl complexes $[(\eta^5\text{-}C_5Me_5)\text{Fe}(CO)_2\{B(Br)X\}]$ (X = Br, **88**;[66] X = Fc, **89**)[36a] with $[\text{Pd}(PCy_3)_2]$, oxidative addition of a B–Br bond to the electron-rich palladium center occurred with liberation of one bulky PCy_3 ligand and formation of the desired hetero-dinuclear bridging borylene complexes (Scheme 35).[66] The



Scheme 35. Synthesis of the hetero-dinuclear bridging borylene complex **90**.

^{11}B NMR spectroscopic data for **90** and **91** ($\delta = 136$ and 118 ppm, respectively) reflect the bridging coordination mode of the bromo- and ferrocenylborylene ligands and display the expected low-field shift of the resonance (compare $\delta = 103$ and 94 ppm for **88** and **89**, respectively), which usually results from an increased number of metal–boron bonds.

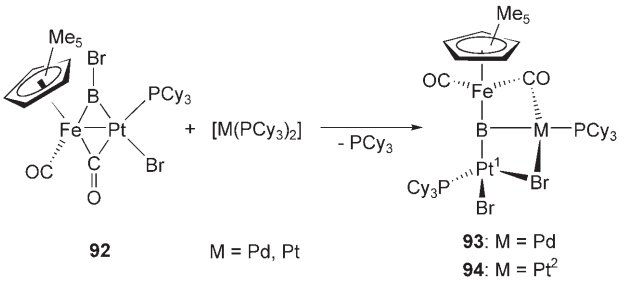
Furthermore, a structural determination of the ferrocenylborylene complex **91** was performed and indicated a *trans* arrangement—likely a result of steric repulsion—of the palladium-bound PCy_3 and BFc groups. Interestingly, the

© 2006 Wiley-VCH Verlag GmbH & Co. KGaA, Weinheim

geometry at the palladium center in bromoborylene complex **90**, as inferred from the spectroscopic data, appears to be different, with a *cis* arrangement of the PCy_3 ligand and the smaller BBr group.

4.2.2.1. Metalloborylenes Stabilized by a Transition-Metal Base

Molecular systems such as the hetero-dinuclear bridging borylene complexes **90** and **91** or the metalloborylene compounds **80** and **81** (Section 4.1.1.1) comprise two different transition-metal fragments linked by boron centers that feature a decreasing number of main-group-element substituents. The possibility of saturating the three classical valencies of boron by linking the boron center to three transition-metal fragments was recently explored and demonstrated by the full characterization of $[(\eta^5\text{-}C_5Me_5)(OC)Fe(\mu\text{-}CO)M(PCy_3)(\mu\text{-}Br)Pt(PCy_3)Br(\mu_3\text{-}B)]$ (**93**: M = Pd, **94**: M = Pt), which feature the unprecedented coordination of boron to three transition-metal centers.[67] As starting point for the build up of the trimetallic systems, the hetero-dinuclear bridging bromoborylene complex $[(\mu\text{-}BBr)(\mu\text{-}CO)\{(\eta^5\text{-}C_5Me_5)Fe(CO)\}\{(Cy_3P)Pt(Br)\}]$ (**92**) was synthesized. Since this platinum analogue of **90**[66] is more stable in solution, the reactivity of the BBr moiety towards low-valent transition-metal complexes could be explored. Hence, reaction of **92** with $[M(PCy_3)_2]$ (M = Pd, Pt) occurred cleanly, thus producing the new compounds $[(\eta^5\text{-}C_5Me_5)(OC)Fe(\mu\text{-}CO)M(PCy_3)(\mu\text{-}Br)Pt(PCy_3)Br(\mu_3\text{-}B)]$ and liberating one equivalent of PCy_3 (Scheme 36).



Scheme 36. Synthesis of the metal-base-stabilized metallaborylene complexes **93** and **94**.

In solution, the ^{11}B NMR resonances of **93** and **94** appear as broad singlets at $\delta = 144$ and 130 ppm, respectively, both being low-field-shifted with respect to those of the precursor **92** ($\delta = 108$ ppm), thus in agreement with the increased number of metal–boron bonds in the products. Accordingly, the ^{31}P NMR spectra of the two compounds display two resonances each, at $\delta = 31.9$ and 32.5 ppm ($^1J_{Pt,P} = 4559$ Hz) for **93** and at $\delta = 31.1$ ($^1J_{Pt,P} = 4703$ Hz) and 57.3 ppm ($^1J_{Pt,P} = 4626$ Hz) for **94**.

The solid-state structures of **93** and **94** display a boron atom surrounded by three transition-metal centers with short Fe–B (**93**: 1.910(4) Å; **94**: 1.903(4) Å) and Pt^1–B bond lengths (**93**: 1.923(4) Å; **94**: 1.938(4) Å). While a trigonal-planar geometry around the boron center might have been expected for a threefold-coordinated, formally sp^2-hybridized boron atom, the structures are characterized by a nearly linear arrangement of the iron, boron, and platinum centers (Fe-B-Pt^1 168.7(2)°, **93**; 167.1(2)°, **94**), thus indicating formal sp hybridization at boron. The iron and platinum arrangement around the boron atom is, therefore, reminiscent of the metallaborylene complexes **80** (Fe-B-Cr 177.75(11)°) and **81** (Fe-B-Fe 175.38(12)°, Scheme 29), with the difference that in **93** and **94**, this arrangement is accompanied by an additional boron–metal interaction. Indeed, a $\{M(PCy_3)\}$ complex fragment (**93**: M = Pd, **94**: M = Pt^2) approaches the central Fe-B-Pt core to make long Pd–B (2.150(4) Å) and Pt^2–B (2.158(4) Å) contacts which are supported by carbonyl and bromide bridges to the outer transition-metal centers.

The resulting description of **93** and **94** metalloborylenes in which the Fe–B=Pt moiety is stabilized by interactions with the Lewis basic complex fragment $\{M(PCy_3)\}$ (M = Pd, Pt), is supported by the results of theoretical calculations which were performed on a model system for complex **93**.[67] Firstly, the likelihood of a dative $\{(PMe_3)Pd\}\rightarrow B$ bond in the system was ascertained by verifying the presence of acceptor orbitals on the hypothetical metalloborylene complex $[(\mu_2\text{-}B)\{(\eta^5\text{-}C_5H_5)Fe(CO)_2\}\{PtBr_2(PMe_3)\}]$ (**95**) and their interactions with the d_{z^2}-type HOMO of an incoming $\{Pd(PMe_3)\}$ complex fragment. Secondly, the changes in the electronic distribution of **95** upon addition of $\{Pd(PMe_3)\}$ were analyzed with Electron Localization Function (ELF) calculations. It was found that the ring attractor between the boron and platinum atoms originally present in **95**, which indicates a partial triple-bond character of the B–Pt bond, converted into a point attractor in the resulting trimetallic system, while the basin of the B–Fe bond stretched to include the palladium center, thus representing a three-center, two-electron Fe-B-Pd bond.

4.2.3. Triply Bridging Borylene Ligands

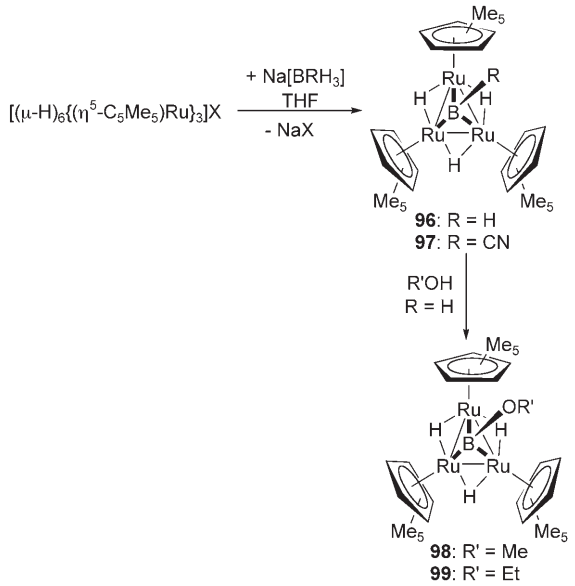
New examples[68] of ruthenium clusters that feature triply bridging borylene ligands were recently reported. Reaction of the cationic cluster $[(\mu\text{-}H)_6\{(\eta^5\text{-}C_5Me_5)Ru\}_3]X$ (X = BF_4, PF_6) with $Na[BRH_3]$ (R = H, CN) resulted in the formation of the neutral species $[\{(\eta^5\text{-}C_5Me_5)Ru\}_3(\mu\text{-}H)_3(\mu_3\text{-}BR)]$ (**96**: R = H, **97**: R = CN; Scheme 37).[69]

Furthermore, the parent borylene compound **96** served as a starting material for the synthesis of the triply bridging alkoxyborylene clusters $[\{(\eta^5\text{-}C_5Me_5)Ru\}_3(\mu\text{-}H)_3(\mu_3\text{-}BOR')]$ (**98**: R′ = Me, **99**: R′ = Et) upon reaction with the corresponding alcohols (Scheme 37). The ^{11}B NMR spectroscopic resonances of the cluster compounds ($\delta = 131$ (**96**), 117 (**97**), 78 (**98**), 88 ppm (**99**)) are in the expected range for transition-metal borylene complexes.

4.2.4. Semibridging Borylene Ligands

A number of theoretical studies have attempted to clarify the salient features of the transition-metal–boron linkage in borylene complexes.[12] As a result, pronounced similarities between the borylene ligand BR and carbon monoxide CO have emerged with respect to their ability to bind synergistically to transition-metal centers.[12a] Such theoretically predicted similarities have gradually found experimental con-

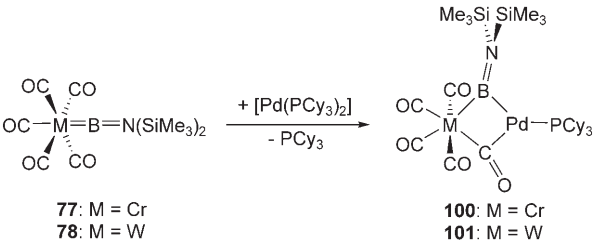
 © 2006 Wiley-VCH Verlag GmbH & Co. KGaA, Weinheim



Scheme 37. Synthesis of ruthenium clusters featuring triply bridging borylene ligands.

firmation. The rich coordination chemistry of the carbonyl ligand, with terminal, symmetrically bridging, semibridging, and triply bridging coordination modes, now finds parallels in borylene chemistry.

As already mentioned, symmetrically bridging borylene complexes represent the most numerous and well-studied class of borylene compounds. Appropriate synthetic routes to their terminal counterparts were subsequently developed, and cluster compounds that feature triply bridging borylene ligands are known (Section 4.2.3). Compounds that feature semibridging borylene ligands represent the most recent accomplishment. The terminal borylene complexes $[(OC)_5M{=}B{=}N(SiMe_3)_2]$ (**77**: M = Cr, **78**: M = W) react cleanly with $[Pd(PCy_3)_2]$ at room temperature to afford the semibridging borylene compounds, $[\{\mu\text{-}BN(SiMe_3)_2\}(\mu\text{-}CO)\{M(CO)_4\}\{Pd(PCy_3)\}]$ (**100**: M = Cr, **101**: M = W; Scheme 38).[70]



Scheme 38. Synthesis of the semibridging borylene complexes **100** and **101**.

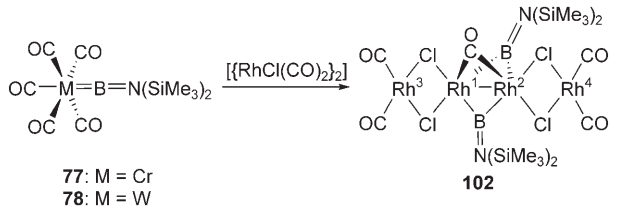
The structural data of the chromium complex **100** reveal a virtually orthogonal orientation of the bis(trimethylsilyl)amino substituent at boron with respect to the plane containing the two transition-metal centers and boron atom (angle between the planes: 85.8°). Such an arrangement differs significantly from that observed in previously reported homodimetallic bridging borylene complexes, for example, $[(\mu\text{-}BNMe_2)\{(\eta^5\text{-}C_5H_5)Mn(CO)_2\}_2]$[71] and $[\{\mu\text{-}BN(SiMe_3)_2\}(\mu\text{-}CO)\{(\eta^5\text{-}C_5H_4Me)Fe(CO)\}_2]$,[33a] for which the structural parameters are in agreement with the presence of a formally sp^2-hybridized boron atom. Accordingly, assuming the same hybridization of the boron atom in **100**, the orthogonal arrangement of the amino substituent would preclude any effective N–B π donation, and should result in considerable elongation of the N–B bond. However, despite the higher coordination number at boron, the B–N bond length (1.377(2) Å) is only slightly larger than that observed in the terminal borylene complex **77** (1.353(6) Å), thus indicating significant double-bond character of the B–N linkage.

A description of the bonding interactions that characterize complexes **100** and **101** can be sketched by invoking the theoretically predicted analogy between borylene and carbon monoxide ligands. The formal donation of electron density by the electronically saturated chromium or tungsten complexes **77** or **78** to the palladium fragment (that is, M→Pd dative bonding) and then π back-donation from the palladium center into the antibonding π* orbitals of the carbonyl and borylene units result in the formation of a pair of noncompensating semibridging ligands by CO and $B{=}N(SiMe_3)_2$, as indicated by the relevant bond angles (Pd-Cr-C(O): 54.21(6)°, Pd-Cr-B: 49.8°, Cr-C-O: 165.5(16)°; Pd-C-O: 115.20(14)°, Cr-B-N: 152.3(13)°, Pd-B-N: 128.74(12)°).[72]

4.2.5. Bis(borylene) Complexes

Until very recently, the formation of the semibridging borylene compounds **100** and **101** represented the only instance of clean thermal (that is, nonphotolytic) reactivity of the terminal borylene complexes **77** and **78**. Compounds **100** and **101** can be viewed as the products of partial transfer of the borylene moiety $BN(SiMe_3)_2$ from the Group 6 metals to the palladium center. Attempts at accomplishing the complete transfer under a variety of conditions were unsuccessful.[73] Interestingly, however, a fast metal-to-metal borylene transfer occurred from $[(OC)_5M{=}BN(SiMe_3)_2]$ (**77**: M = Cr, **78**: M = W) to $[\{RhCl(CO)_2\}_2]$ at room temperature to yield the tetranuclear bis(borylene) complex $[Rh_4\{\mu\text{-}BN(SiMe_3)_2\}_2Cl_4(\mu\text{-}CO)(CO)_4]$ (**102**; Scheme 39).[74]

As revealed by an X-ray diffraction study, the core of the molecule consists of a chain of four rhodium atoms, and the internal metal centers are bridged by two borylene moieties and a carbonyl ligand. The distance between the two central rhodium atoms is small (Rh^1–Rh^2 2.5786(3) Å) and comparable to analogous distances found in dinuclear complexes in



Scheme 39. Synthesis of the tetranuclear bis(borylene) complex **102**.

 © 2006 Wiley-VCH Verlag GmbH & Co. KGaA, Weinheim

which the rhodium atoms are bridged by three carbonyl ligands.[75] The Rh–Rh distances to each Rh terminus, that is, Rh^3–Rh^1 (3.0415(4) Å) and Rh^4–Rh^2 (3.0472(4) Å), are significantly larger. Interestingly, the individual tetramer units aggregate in the solid state to form neutral linear chains through a relatively short intermolecular Rh–Rh contact (3.1833(4) Å). Surprisingly, the ^{11}B NMR signal of compound **102** ($\delta = 74$ ppm) is unusually high-field-shifted with respect to that of the starting materials ($\delta = 92$ ppm, **77**; $\delta = 87$ ppm, **78**). This result is contrary to what could have been expected on account of the increased number of metal–boron bonds in the product.

5. Summary and Outlook

Since the publication of the previous review,[13] a considerable number of new coordination motifs for boron-based ligands have been realized. A variety of metallaboratrane complexes have been synthesized, thus demonstrating that, under appropriate conditions, Lewis acidic boranes do form acid–base adducts with Lewis basic transition-metal fragments. The variety of boryl complexes at hand has increased conspicuously and now includes previously elusive dihaloboryl, asymmetric haloboryl, and iminoboryl complexes. The electronic properties of boryl ligands have been widely investigated, structurally and theoretically. While possessing poor π-accepting abilities, the good σ-donating properties of boryl ligands have been determined to be responsible for their extremely high *trans* influence. This combination of properties has allowed for the unprecedented isolation of the cationic T-shaped three-coordinate platinum–boryl complex *trans*-$[(Cy_3P)_2Pt\{B(Br)Fc\}][BAr^F{}_4]$.

The chemistry of borylene compounds has developed to a great extent. A variety of synthetic methods are now available, and these have extended the range of accessible homo- and hetero-dinuclear, symmetrically bridging and semibridging, mono- and bis(borylene) compounds. The syntheses of neutral as well as cationic terminal borylene complexes, remarkable examples of metallaborylene complexes $[(\mu_2\text{-}B)\{(\eta^5\text{-}C_5Me_5)Fe(CO)_2\}\{M(CO)_n\}]$ (M = Fe, $n = 4$; M = Cr, $n = 5$), as well as transition-metal complexes in which boron is classically bonded to three transition-metal centers have been achieved. Reactivity patterns for these species have started to emerge. Hence, compounds such as $[(OC)_5M{=}BN(SiMe_3)_2]$ (M = Cr, Mo, W) have been shown to transfer the borylene moiety upon photolysis to other transition-metal fragments and to alkynes. The cationic terminal borylene complex $[(\eta^5\text{-}C_5H_5)Fe(CO)_2(BN\mathit{i}Pr_2)][BAr^F{}_4]$ has been reported to undergo metathesis chemistry with $Ph_3P{=}S$ or $Ph_3As{=}O$ to yield $[\mathit{i}Pr_2NB(\mu\text{-}S)_2BN\mathit{i}Pr_2]$ and $(\mathit{i}Pr_2NBO)_3$, respectively. Thanks to numerous theoretical studies the bonding description of these systems is becoming clearer, and as their reactivity is elucidated experimentally, their potential application in stoichiometric or catalytic reactions is likely to emerge shortly.[76]

Received: February 7, 2006
Published online: July 7, 2006

[1] R. T. Baker, D. W. Ovenall, J. C. Calabrese, S. A. Westcott, N. J. Taylor, I. D. Williams, T. B. Marder, *J. Am. Chem. Soc.* **1990**, *112*, 9399 – 9400.
[2] J. R. Knorr, J. S. Merola, *Organometallics* **1990**, *9*, 3008 – 3010.
[3] a) P. J. Davidson, M. F. Lappert, R. Pearce, *Acc. Chem. Res.* **1974**, *7*, 209 – 217; b) E. O. Fischer, *Adv. Organomet. Chem.* **1976**, *14*, 1 – 32; c) R. R. Schrock, *Acc. Chem. Res.* **1979**, *12*, 98 – 104.
[4] a) T. D. Tilley in *Chemistry of Organic Silicon Compounds*, *Vol. 2* (Eds.: S. W. Patai, Z. Rappoport), Wiley, New York, **1989**, pp. 1415 – 1477; b) U. Schubert, *Transition Met. Chem.* **1991**, *16*, 136 – 144; c) C. Zybill, H. Handwerker, H. Friedrich, *Adv. Organomet. Chem.* **1994**, *36*, 229 – 281; d) P. D. Lickiss, *Chem. Soc. Rev.* **1992**, *21*, 271 – 279.
[5] R. A. Fischer, J. Weiss, *Angew. Chem.* **1999**, *111*, 3002 – 3022; *Angew. Chem. Int. Ed.* **1999**, *38*, 2830 – 2850.
[6] T. P. Fehlner in *Electron Deficient Boron and Carbon Clusters* (Eds.: G. A. Olah, K. Wade, R. E. Williams), Wiley, New York, **1991**, pp. 287 – 307.
[7] T. Lundström in *Encyclopedia of Inorganic Chemistry*, *Vol. 1* (Ed.: R. B. King), Wiley, New York, **1994**, pp. 328 – 338.
[8] a) D. Männig, H. Nöth, *Angew. Chem.* **1985**, *97*, 854 – 855; *Angew. Chem. Int. Ed. Engl.* **1985**, *24*, 878 – 879; b) K. Burgess, M. J. Ohlmeyer, *Chem. Rev.* **1991**, *91*, 1179 – 1191; c) H. Wadepohl, *Angew. Chem.* **1997**, *109*, 2547 – 2550; *Angew. Chem. Int. Ed. Engl.* **1997**, *36*, 2441 – 2444; d) I. Beletskaya, A. Pelter, *Tetrahedron* **1997**, *53*, 4957 – 5026; e) T. B. Marder, N. C. Norman, *Top. Catal.* **1998**, *5*, 63 – 73; f) T. Ishiyama, N. Miyaura, *J. Synth. Org. Chem. Jpn.* **1999**, *57*, 503 – 511; g) T. Ishiyama, N. Miyaura, *J. Organomet. Chem.* **2000**, *611*, 392 – 402; h) C. M. Crudden, D. Edwards, *Eur. J. Org. Chem.* **2003**, 4695 – 4712.
[9] a) H. Chen, S. Schlecht, T. C. Semple, J. F. Hartwig, *Science* **2000**, *287*, 1995 – 1997; b) J. Y. Cho, M. K. Tse, D. Holmes, R. E. Maleczka, Jr., M. R. Smith III, *Science* **2002**, *295*, 305 – 308; c) T. Ishiyama, N. Miyaura, *J. Organomet. Chem.* **2003**, *680*, 3 – 11; d) T. Ishiyama, Y. Nobuta, J. F. Hartwig, N. Miyaura, *Chem. Commun.* **2003**, 2924 – 2925; e) D. N. Coventry, A. S. Batsanov, A. E. Goeta, J. A. K. Howard, T. B. Marder, R. N. Perutz, *Chem. Commun.* **2005**, 2172 – 2174; f) J. F. Hartwig, K. S. Cook, M. Hapke, C. D. Incarvito, Y. Fan, C. E. Webster, M. B. Hall, *J. Am. Chem. Soc.* **2005**, *127*, 2538 – 2552; g) G. A. Chotana, M. A. Rak, M. R. Smith III, *J. Am. Chem. Soc.* **2005**, *127*, 10539 – 10544; h) I. A. I. Mkhalid, D. N. Coventry, D. Albesa-Jove, A. S. Batsanov, J. A. K. Howard, R. N. Perutz, T. B. Marder, *Angew. Chem.* **2006**, *118*, 503 – 505; *Angew. Chem. Int. Ed.* **2006**, *45*, 489 – 491.
[10] a) C. D. Entwistle, T. B. Marder, *Angew. Chem.* **2002**, *114*, 3051 – 3056; *Angew. Chem. Int. Ed.* **2002**, *41*, 2927 – 2931; b) C. D. Entwistle, T. B. Marder, *Chem. Mater.* **2004**, *16*, 4574 – 4585.
[11] H. Braunschweig, D. Rais, *Angew. Chem.* **2005**, *117*, 8036 – 8038; *Angew. Chem. Int. Ed.* **2005**, *44*, 7826 – 7828.
[12] a) A. W. Ehlers, E. J. Baerends, F. M. Bickelhaupt, U. Radius, *Chem. Eur. J.* **1998**, *4*, 210 – 221; b) C. Boehme, J. Uddin, G. Frenking, *Coord. Chem. Rev.* **2000**, *197*, 249 – 276.
[13] H. Braunschweig, *Angew. Chem.* **1998**, *110*, 1882 – 1898; *Angew. Chem. Int. Ed.* **1998**, *37*, 1786 – 1801.
[14] a) G. I. Irvine, M. J. G. Lesley, T. B. Marder, N. C. Norman, C. R. Rice, E. G. Robins, W. R. Roper, G. R. Whittell, L. J. Wright, *Chem. Rev.* **1998**, *98*, 2685 – 2722; b) M. R. Smith III, *Prog. Inorg. Chem.* **1999**, *48*, 505 – 567; c) H. Braunschweig, M. Colling, *J. Organomet. Chem.* **2000**, *614–615*, 18 – 26; d) H. Braunschweig, M. Colling, *Coord. Chem. Rev.* **2001**, *223*, 1 – 51; e) H. Braunschweig in *Inorganic Chemistry Highlights* (Eds.: G. Meyer, D. Naumann, L. Wesemann), Wiley-VCH, Weinheim, New York, **2001**, pp. 213 – 218; f) H. Braunschweig, *Adv. Organomet. Chem.* **2004**, *51*, 163 – 192; g) S. Aldridge, D. L. Coombs,

 © 2006 Wiley-VCH Verlag GmbH & Co. KGaA, Weinheim

Coord. Chem. Rev. **2004**, *248*, 535 – 559; h) H. Braunschweig, D. Rais, *Heteroat. Chem.* **2005**, *16*, 566 – 571.

[15] a) D. F. Shriver, *J. Am. Chem. Soc.* **1963**, *85*, 3509 – 3510; b) G. W. Parshall, *J. Am. Chem. Soc.* **1964**, *86*, 361 – 364; c) M. P. Johnson, D. F. Shriver, *J. Am. Chem. Soc.* **1966**, *88*, 301 – 304.

[16] a) H. Braunschweig, T. Wagner, *Chem. Ber.* **1994**, *127*, 1613 – 1614; b) H. Braunschweig, T. Wagner, *Z. Naturforsch. B* **1996**, *51*, 1618 – 1620; c) H. Braunschweig, C. Kollann, *Z. Naturforsch. B* **1999**, *54*, 839 – 842.

[17] a) A. F. Hill, G. R. Owen, A. J. P. White, D. J. Williams, *Angew. Chem.* **1999**, *111*, 2920 – 2923; *Angew. Chem. Int. Ed.* **1999**, *38*, 2759 – 2761; b) M. R. St.-J. Foreman, A. F. Hill, A. J. P. White, D. J. Williams, *Organometallics* **2004**, *23*, 913 – 916; c) C. E. F. Rickard, W. R. Roper, A. Williamson, L. J. Wright, *J. Organomet. Chem.* **2004**, *689*, 1609 – 1616.

[18] H. Braunschweig, M. Koster, R. Wang, *Inorg. Chem.* **1999**, *38*, 415 – 416.

[19] a) D. J. Mihalcik, J. L. White, J. M. Tanski, L. N. Zakharov, G. P. A. Yap, C. D. Incarvito, A. L. Rheingold, D. Rabinovich, *Dalton Trans.* **2004**, 1626 – 1634; b) I. R. Crossley, A. F. Hill, *Organometallics* **2004**, *23*, 5656 – 5658; c) I. R. Crossley, M. R. St.-J. Foreman, A. F. Hill, A. P. J. White, D. J. Williams, *Chem. Commun.* **2005**, 221 – 223; d) I. R. Crossley, A. F. Hill, A. C. Willis, *Organometallics* **2005**, *24*, 1062 – 1064; e) I. R. Crossley, A. F. Hill, E. R. Humphrey, A. C. Willis, *Organometallics* **2005**, *24*, 4083 – 4086.

[20] S. A. Westcott, T. B. Marder, R. T. Baker, R. L. Harlow, J. C. Calabrese, K. C. Lam, Z. Lin, *Polyhedron* **2004**, *23*, 2665 – 2677.

[21] D. Curtis, M. J. G. Lesley, N. C. Norman, A. G. Orpen, J. Starbuck, *J. Chem. Soc. Dalton Trans.* **1999**, 1687 – 1694.

[22] H. Braunschweig, K. Radacki, D. Rais, G. R. Whittell, *Angew. Chem.* **2005**, *117*, 1217 – 1219; *Angew. Chem. Int. Ed.* **2005**, *44*, 1192 – 1194.

[23] For MO calculations and a general scheme applicable to systems featuring "dative" M–M bonds and noncompensating, semi-bridging carbonyl ligands, see: R. D. Barr, T. B. Marder, A. G. Orpen, I. D. Williams, *J. Chem. Soc. Chem. Commun.* **1984**, 112 – 114.

[24] W. H. Lam, S. Shimada, A. S. Batsanov, Z. Lin, T. B. Marder, J. A. Cowan, J. A. K. Howard, S. A. Mason, G. J. McIntyre, *Organometallics* **2003**, *22*, 4557 – 4568.

[25] A. Kerr, T. B. Marder, N. C. Norman, A. G. Orpen, M. J. Quayle, C. R. Rice, P. L. Timms, G. R. Whittell, *Chem. Commun.* **1998**, 319 – 320.

[26] N. Lu, N. C. Norman, A. G. Orpen, M. J. Quayle, P. L. Timms, G. R. Whittell, *J. Chem. Soc. Dalton Trans.* **2000**, 4032 – 4037.

[27] T. H. Peterson, J. T. Golden, R. G. Bergman, *Organometallics* **1999**, *18*, 2005 – 2020.

[28] D. L. Kays, A. Rossin, J. K. Day, L.-L. Ooi, S. Aldridge, *Dalton Trans.* **2006**, 399 – 410.

[29] a) G. J. Irvine, C. E. F. Rickard, W. R. Roper, A. Williamson, L. J. Wright, *Angew. Chem.* **2000**, *112*, 978 – 980; *Angew. Chem. Int. Ed.* **2000**, *39*, 948 – 950; b) C. E. F. Rickard, W. R. Roper, A. Williamson, L. J. Wright, *Organometallics* **2002**, *21*, 4862 – 4872; c) G. R. Clark, G. J. Irvine, W. R. Roper, L. J. Wright, *J. Organomet. Chem.* **2003**, *680*, 81 – 88.

[30] a) S. Aldridge, R. J. Calder, R. E. Baghurst, M. E. Light, M. B. Hursthouse, *J. Organomet. Chem.* **2002**, *649*, 9 – 14; b) A. A. Dickinson, D. J. Willock, R. J. Calder, S. Aldridge, *Organometallics* **2002**, *21*, 1146 – 1157.

[31] H. Braunschweig, K. Radacki, F. Seeler, G. R. Whittell, *Organometallics* **2004**, *23*, 4178 – 4180.

[32] a) J. F. Hartwig, S. Huber, *J. Am. Chem. Soc.* **1993**, *115*, 4908 – 4909; b) K. M. Waltz, C. N. Muhoro, J. F. Hartwig, *Organometallics* **1999**, *18*, 3383 – 3393.

[33] a) H. Braunschweig, C. Kollann, U. Englert, *Eur. J. Inorg. Chem.* **1998**, 465 – 468; b) H. Braunschweig, C. Kollann, K. W. Klinkhammer, *Eur. J. Inorg. Chem.* **1999**, 1523 – 1529; c) H. Braunschweig, C. Kollann, unpublished results.

[34] Z. Lu, C.-H. Jun, S. R. de Gala, M. Sigalas, O. Eisenstein, R. H. Crabtree, *J. Chem. Soc. Chem. Commun.* **1993**, 1877 – 1880.

[35] a) S. Aldridge, D. L. Coombs, C. Jones, *Chem. Commun.* **2002**, 856 – 857; b) D. L. Coombs, S. Aldridge, C. Jones, *J. Chem. Soc. Dalton Trans.* **2002**, 3851 – 3858; c) D. L. Coombs, S. Aldridge, S. J. Coles, M. B. Hursthouse, *Organometallics* **2003**, *22*, 4213 – 4217; d) D. L. Coombs, S. Aldridge, C. Jones, *Appl. Organomet. Chem.* **2003**, *17*, 356 – 360.

[36] a) H. Braunschweig, K. Radacki, D. Rais, F. Seeler, *Organometallics* **2004**, *23*, 5545 – 5549; for other examples of boryl complexes obtained by oxidative addition of a B–X bond, see: b) S.-Y. Onozawa, M. Tanaka, *Organometallics* **2001**, *20*, 2956 – 2958; c) F. E. S. Souza, P. Nguyen, T. B. Marder, A. J. Scott, W. Clegg, *Inorg. Chim. Acta* **2005**, *358*, 1501 – 1509.

[37] a) F. Appel, F. Jäkle, T. Priermeier, R. Schmid, M. Wagner, *Organometallics* **1996**, *15*, 1188 – 1194; b) M. Scheibitz, M. Bolte, J. W. Bats, H.-W. Lerner, I. Nowik, R. H. Herber, A. Krapp, M. Lein, M. C. Holthausen, M. Wagner, *Chem. Eur. J.* **2005**, *11*, 584 – 603.

[38] H. Braunschweig, C. Colling, C. Kollann, U. Englert, *J. Chem. Soc. Dalton Trans.* **2002**, 2289 – 2296.

[39] N. DeLuca, A. Woicicki, *J. Organomet. Chem.* **1980**, *193*, 359 – 378.

[40] J. D. Basil, A. A. Aradi, N. K. Bhattacharyya, N. P. Rath, C. Eigenbrot, T. P. Fehlner, *Inorg. Chem.* **1990**, *29*, 1260 – 1270.

[41] D. J. Elliot, C. J. Levy, R. J. Puddephatt, D. G. Holah, A. H. Hughes, V. R. Magnuson, I. M. Moser, *Inorg. Chem.* **1990**, *29*, 5014 – 5015.

[42] a) Y. Kawano, T. Yasue, M. Shimoi, *J. Am. Chem. Soc.* **1999**, *121*, 11744 – 11750; b) T. Yasue, Y. Kawano, M. Shimoi, *Chem. Lett.* **2000**, 58 – 59; c) T. Yasue, Y. Kawano, M. Shimoi, *Angew. Chem.* **2003**, *115*, 1769 – 1772; *Angew. Chem. Int. Ed.* **2003**, *42*, 1727 – 1730.

[43] K. M. Waltz, H. He, C. N. Muhoro, J. F. Hartwig, *J. Am. Chem. Soc.* **1995**, *117*, 11357 – 11358.

[44] a) S.-Y. Onozawa, Y. Hatanaka, T. Sakakura, S. Shimada, M. Tanaka, *Organometallics* **1996**, *15*, 5450 – 5452; b) C. Dai, G. Stringer, T. B. Marder, R. T. Baker, A. J. Scott, W. Clegg, N. C. Norman, *Can. J. Chem.* **1996**, *74*, 2026 – 2031; c) W. Clegg, F. J. Lawlor, G. Lesley, T. B. Marder, N. C. Norman, A. G. Orpen, M. J. Quayle, G. C. Rice, A. J. Scott, F. E. S. Souza, *J. Organomet. Chem.* **1998**, *550*, 183 – 192; d) C. E. F. Rickard, W. R. Roper, A. Williamson, L. J. Wright, *Organometallics* **1998**, *17*, 4869 – 4874.

[45] a) G. Sivignon, P. Fleurat-Lessard, J.-M. Onno, F. Volatron, *Inorg. Chem.* **2002**, *41*, 6656 – 6661; b) K. C. Lam, W. H. Lam, Z. Lin, T. B. Marder, N. C. Norman, *Inorg. Chem.* **2004**, *43*, 2541 – 2547; c) J. Zhu, Z. Lin, T. B. Marder, *Inorg. Chem.* **2005**, *44*, 9384 – 9390.

[46] H. Braunschweig, K. Radacki, D. Rais, D. Scheschkewitz, *Angew. Chem.* **2005**, *117*, 5796 – 5799; *Angew. Chem. Int. Ed.* **2005**, *44*, 5651 – 5654.

[47] W. H. Lam, K. C. Lam, Z. Lin, S. Shimada, R. N. Perutz, T. B. Marder, *Dalton Trans.* **2004**, 1556 – 1562.

[48] H. Braunschweig, K. Radacki, D. Rais, K. Uttinger, *Angew. Chem.* **2006**, *118*, 169 – 172; *Angew. Chem. Int. Ed.* **2006**, *45*, 162 – 165.

[49] a) P. Paetzold, *Adv. Inorg. Chem.* **1987**, *31*, 123 – 170; b) H. Nöth, *Angew. Chem.* **1988**, *100*, 1664 – 1688; *Angew. Chem. Int. Ed. Engl.* **1988**, *27*, 1603 – 1623; c) P. Paetzold, *Pure Appl. Chem.* **1991**, *63*, 345 – 350; d) P. Paetzold, *Phosphorus Sulfur Silicon Relat. Elem.* **1994**, *93–94*, 39 – 50.

 © 2006 Wiley-VCH Verlag GmbH & Co. KGaA, Weinheim

[50] M. Haase, U. Klingebiel, *Angew. Chem.* **1985**, *97*, 335 – 336; *Angew. Chem. Int. Ed. Engl.* **1985**, *24*, 324.
[51] M. Haase, U. Klingebiel, R. Boese, M. Polk, *Chem. Ber.* **1986**, *119*, 1117 – 1126.
[52] a) P. L. Timms, *J. Am. Chem. Soc.* **1967**, *89*, 1629 – 1632; b) P. L. Timms, *Acc. Chem. Res.* **1973**, *6*, 118 – 123.
[53] B. Pachaly, R. West, *Angew. Chem.* **1984**, *96*, 444 – 445; *Angew. Chem. Int. Ed. Engl.* **1984**, *23*, 454 – 455.
[54] A. H. Cowley, V. Lomelí, A. Voigt, *J. Am. Chem. Soc.* **1998**, *120*, 6401 – 6402.
[55] H. Braunschweig, C. Kollann, U. Englert, *Angew. Chem.* **1998**, *110*, 3355 – 3357; *Angew. Chem. Int. Ed.* **1998**, *37*, 3179 – 3180.
[56] H. Braunschweig, M. Colling, C. Kollann, H. G. Stammler, B. Neumann, *Angew. Chem.* **2001**, *113*, 2359 – 2361; *Angew. Chem. Int. Ed.* **2001**, *40*, 2298 – 2300.
[57] H. Braunschweig, C. Kollann, U. Englert, *Angew. Chem.* **2001**, *113*, 4327 – 4329; *Angew. Chem. Int. Ed.* **2001**, *40*, 4198 – 4200.
[58] H. Braunschweig, K. Radacki, D. Scheschkewitz, G. R. Whittell, *Angew. Chem.* **2005**, *117*, 1685 – 1688; *Angew. Chem. Int. Ed.* **2005**, *44*, 1658 – 1661.
[59] a) D. L. Coombs, S. Aldridge, C. Jones, D. J. Willock, *J. Am. Chem. Soc.* **2003**, *125*, 6356 – 6357; b) D. L. Coombs, S. Aldridge, A. Rossin, C. Jones, D. J. Willock, *Organometallics* **2004**, *23*, 2911 – 2926.
[60] D. L. Kays (née Coombs), J. K. Day, L.-L. Ooi, S. Aldridge, *Angew. Chem.* **2005**, *117*, 7623 – 7626; *Angew. Chem. Int. Ed.* **2005**, *44*, 7457 – 7460.
[61] H. Braunschweig, M. Colling, C. Hu, K. Radacki, *Angew. Chem.* **2003**, *115*, 215 – 218; *Angew. Chem. Int. Ed.* **2003**, *42*, 205 – 208.
[62] H. Braunschweig, T. Herbst, D. Rais, F. Seeler, *Angew. Chem.* **2005**, *117*, 7627 – 7629; *Angew. Chem. Int. Ed.* **2005**, *44*, 7461 – 7463.
[63] Formation of the six-membered B_3O_3 ring in $(i\mathrm{Pr}_2\mathrm{NBO})_3$ and of the four-membered B_2S_2 ring in $[i\mathrm{Pr}_2\mathrm{NB}(\mu\text{-}\mathrm{S})_2\mathrm{B}N i\mathrm{Pr}_2]$ is in agreement with the results described in: J. M. Burke, M. A. Fox, A. E. Goeta, A. K. Hughes, T. B. Marder, *Chem. Commun.* **2000**, 2217 – 2218, on why B_2O_2 rings are rare.
[64] M. Shimoi, S. Ikubo, Y. Kawano, K. Katoh, H. Ogino, *J. Am. Chem. Soc.* **1998**, *120*, 4222 – 4223.
[65] H. Braunschweig, F. Seeler, unpublished results.
[66] H. Braunschweig, K. Radacki, D. Rais, F. Seeler, K. Uttinger, *J. Am. Chem. Soc.* **2005**, *127*, 1386 – 1387.
[67] H. Braunschweig, K. Radacki, D. Rais, F. Seeler, *Angew. Chem.* **2006**, *118*, 1087 – 1090; *Angew. Chem. Int. Ed.* **2006**, *45*, 1066 – 1069.
[68] For earlier examples of compounds featuring a μ_3-BR ligand, see: a) J. Feilong, T. P. Fehlner, A. L. Rheingold, *Angew. Chem.* **1988**, *100*, 400 – 402; *Angew. Chem. Int. Ed. Engl.* **1988**, *27*, 424 – 426; b) X. Lei, M. Shang, T. P. Fehlner, *Inorg. Chem.* **1998**, *37*, 3900 – 3901.
[69] R. Okamura, K.-I. Tada, K. Matsubara, M. Oshima, H. Suzuki, *Organometallics* **2001**, *20*, 4772 – 4774.
[70] H. Braunschweig, D. Rais, K. Uttinger, *Angew. Chem.* **2005**, *117*, 3829 – 3832; *Angew. Chem. Int. Ed.* **2005**, *44*, 3763 – 3766.
[71] H. Braunschweig, T. Wagner, *Angew. Chem.* **1995**, *107*, 904 – 905; *Angew. Chem. Int. Ed. Engl.* **1995**, *34*, 825 – 826.
[72] For a classification scheme of semibridging carbonyl ligands, see: R. H. Crabtree, M. Lavin, *Inorg. Chem.* **1986**, *25*, 805 – 812.
[73] H. Braunschweig, D. Rais, K. Uttinger, unpublished results.
[74] H. Braunschweig, M. Forster, K. Radacki, *Angew. Chem.* **2006**, *118*, 2187 – 2189; *Angew. Chem. Int. Ed.* **2006**, *45*, 2132 – 2134.
[75] B. T. Heaton, C. Jocob, J. T. Sampanthar, *J. Chem. Soc. Dalton Trans.* **1998**, 1403 – 1410.
[76] After submission of this review the following relevant papers on transition-metal borane complexes appeared: a) S. Bontemps, H. Gornitzka, G. Bouhadir, K. Miqueu, D. Bourissou, *Angew. Chem.* **2006**, *118*, 1641 – 1644; *Angew. Chem. Int. Ed.* **2006**, *45*, 1611 – 1614; b) V. K. Landry, J. G. Melnick, D. Buccella, K. Pang, J. C. Ulichny, G. Parkin, *Inorg. Chem.* **2006**, *45*, 2588 – 2597.

 © 2006 Wiley-VCH Verlag GmbH & Co. KGaA, Weinheim

Lab-on-a-Chip

DOI: 10.1002/anie.200601677

Integrated Microfluidics for Parallel Screening of an In Situ Click Chemistry Library**

Jinyi Wang, Guodong Sui, Vani P. Mocharla, Rachel J. Lin, Michael E. Phelps, Hartmuth C. Kolb, and Hsian-Rong Tseng**

Dedicated to Professor Tien-Yau Luh



WILEY InterScience DISCOVER SOMETHING GREAT

© 2006 Wiley-VCH Verlag GmbH & Co. KGaA, Weinheim

There is growing interest in performing chemical reactions in microfluidic devices[1–3] because they offer a variety of advantages over macroscopic reactors, such as reduced consumption of reagents, high surface-area-to-volume ratios, and improved control over mass and heat transfer. Organic reactions[4,5] that involve highly reactive intermediates often exhibit greater selectivities and specificities in microreactors compared to conventional macroscopic synthesis. Many challenges remain, however, in the development of microreactors for 1) multistep syntheses in which the individual steps require a change in solvents, reagents, and conditions, as well as 2) parallel screening in which similar types of reactions are performed using different combinations of reagents. Significant efforts have been devoted to develop functioning modules to improve the performance of microreactors. For example, various valves[6,7] have been demonstrated to isolate distinct regions and prevent cross-contamination from different reactions in a microchip. Elsewhere, different mixing modules[8,9] have been utilized to overcome diffusion-limited mixing in the turbulence-free microfluidic environment. Also, functioning pumps[7,10] that are capable of delivering and metering fluidic components have been successfully integrated with microchannels. With these functioning modules, it becomes feasible to handle complicated chemical and biological processes in microreactors in an automated fashion. In fact, integrated microreactors have been utilized for sequential syntheses of molecular imaging probes,[9] polymerase chain reaction,[11] protein crystallization,[12] and cell culture.[10]

In situ click chemistry is a target-guided synthesis[13–19] method for discovering high-affinity protein ligands by assembling complementary azide and acetylene building blocks inside the binding pockets of the target through 1,3-dipolar cycloaddition.[19–22] The resulting ligands display much higher binding affinities to the target than the individual fragments, and the identification of a hit is as simple as detecting product formation by using analytical instruments, such as LC-MS.[19,21] Recently, this approach was employed to prepare potent inhibitors for acetylcholine esterase (AchE),[19,22,23] bovine carbonic anhydrase II (bCAII),[21] and HIV protease.[24] Typically, in situ click chemistry experiments are conducted in parallel using 96-well microtiter plates. Inevitably, the experimental conditions result in the consumption of significant amounts of the target proteins and reagents, which hampers the broad application of in situ click chemistry screening, especially when target proteins are difficult to obtain. Moreover, the existing approach relies heavily upon manual operation, which limits screening throughput and fidelity. Integrated microfluidics provides an excellent experimental platform for in situ click chemistry screening because it enables parallelization and automation, and, most importantly, the miniaturization allows an economical use of target proteins and click chemistry reagents.

Herein, we describe a new type of microfluidic chemical reaction circuits (Figure 1) that provide an automated platform for the parallel screening of 32 in situ click chemistry reactions, with reduced consumption of target proteins and reagents. We selected the known bCAII click chemistry system[21] for this proof-of-concept study. Acetylenic benzenesulfonamide (**1**; $K_d = 37 \pm 6$ nM) was used as the reactive scaffold (anchor molecule) for screening a library of 20 complementary azides **2**–**21**. In control experiments, we utilized the active-site inhibitor, ethoxazolamide (**22**; $K_d = 0.15 \pm 0.03$ nM), to suppress the in situ click chemistry reactions.

To determine appropriate reaction conditions for this microfluidics-based in situ click chemistry screening, click reactions[21] between acetylene **1** and azide **2** (known to undergo enzyme-induced product formation) were performed under different conditions to ensure minimum use of enzyme and reagents and yet reliable and reproducible LC-MS signals for the identification of hits. The microfluidic screening platform described here utilizes a reaction volume of approximately 4 μL, which corresponds to 19 μg of enzyme, 2.4 nmol of the acetylene, and 3.6 nmol of the azide for each reaction, instead of the 100 μL of reaction mixture (containing 94 μg of enzyme, 6 nmol of acetylene, and 40 nmol of azide) employed in the conventional approach. Overall, 2–12-fold sample economy was achieved.

Our microfluidic chemical reaction circuit comprises four major functional components (Figure 1). A nanoliter-level rotary mixer (component 1; round-shaped loop) with a total volume of about 250 nL is responsible for selective sampling, precise metering,[7] and rotary mixing of nL quantities of reagents—acetylene **1** (80 nL) and azides **2**–**11** (or **12**–**21**; 120 nL) with/without inhibitors **22** (40 nL)—for each screening reaction. A microliter-level chaotic mixer[8] (component 2) combines the reagent solutions from the rotary mixer with μL quantities of bCAII solution in phosphate-buffered saline (PBS, pH 7.4). A homogenous reaction mixture was generated by chaotic mixing inside the 37.8-mm long microchannel (the gray microchannel in the middle section of Figure 1a). The embedded micropatterns (inset in Figure 1a) induce[8] chaotic advection to facilitate mixing within the relatively short microchannel. The micropatterns were 20% longer than theoretically required[25] to ensure

[*] Dr. J. Wang,[+] G. Sui,[+] R. J. Lin, Prof. M. E. Phelps, Prof. Dr. H. C. Kolb, Prof. H.-R. Tseng
Crump Institute for Molecular Imaging
Department of Molecular and Medical Pharmacology
David Geffen School of Medicine at UCLA
700 Westwood Plaza, Los Angeles, CA 90095 (USA)
Fax: (+1) 310-206-8975
E-mail: hartmuth.kolb@siemens.com
hrtseng@mednet.ucla.edu
Dr. V. P. Mocharla,[+] Prof. Dr. H. C. Kolb
Siemens Medical Solutions USA, Inc.
6140 Bristol Parkway, Culver City, CA 90230 (USA)
[+] These authors contributed equally to the work.

[**] This research was supported by the NIH NanoSystems Biology Cancer Center, the DOE-UCLA Institute of Molecular Medicine, the NIH-UCLA Center for In Vivo Imaging in Cancer Biology, and Siemens Medical Solutions USA, Inc. G.S. thanks the UCLA SOMI program for a postdoctoral fellowship. We thank David Twomey for the artwork for the frontispiece.

Supporting information for this article is available on the WWW under http://www.angewandte.org or from the author.

 © 2006 Wiley-VCH Verlag GmbH & Co. KGaA, Weinheim

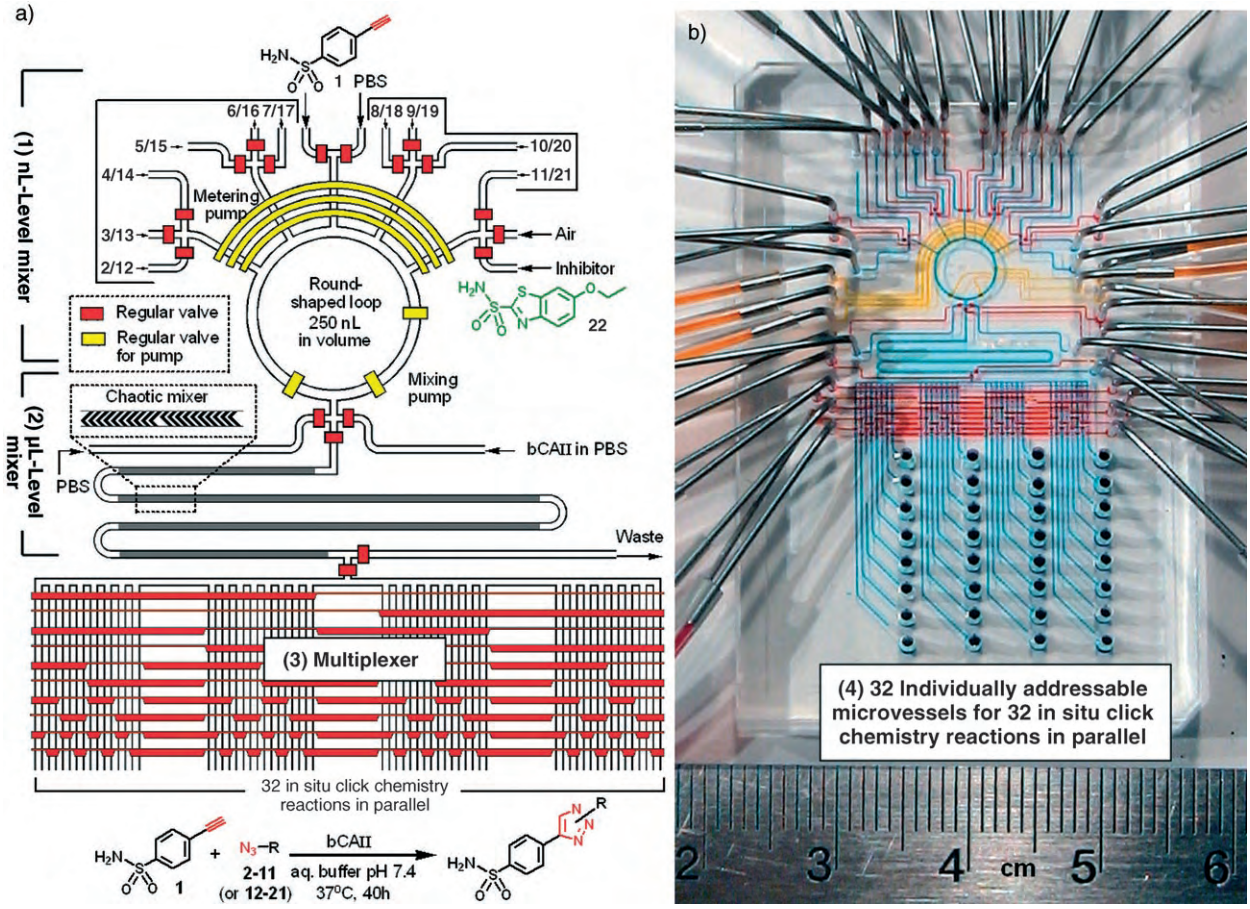


Figure 1. a) Schematic representation of a chemical reaction circuit used for the parallel screening of an in situ click chemistry library. The responsibilities of different valves are illustrated by their colors: red for regular valves (for isolation) and yellow for pump valves (for fluidic metering and circulation). ***n***/***n*** in the nL-level mixer refer to the azides **2**–**11** (or **12**–**21**). b) Optical image of the actual device. The various channels were loaded with food dyes to help visualize the different components of the microfluidic chip: red and yellow as in part (a); blue indicates the fluidic channels. Components (1)–(3) are indicated in part (a), while component (4) is shown in part (b). See text for details.

efficient mixing. Finally, a microfluidic multiplexer[26] (component 3) guides each reaction mixture into one of the 32 individually addressable microvessels (component 4; 1.3 mm in diameter and 6 mm in depth, ca. 8 µL in volume) for storing the reaction mixtures. In situ click chemistry screening of 10 different binary azide/acetylene combinations was performed in parallel by preparing 32 individual reaction mixtures of the following types: 1) ten in situ click chemistry reactions between acetylene **1** and 10 azides in the presence of bCAII; 2) ten control reactions that are performed as in (1), but in the presence of inhibitor **22**, to confirm the active-site specificity of the in situ click chemistry reactions; 3) ten thermal click chemistry reactions performed as in (1), but in the absence of bCAII, to monitor the enzyme-independent reactions; and 4) two "blank" solutions containing only bCAII and PBS solution, respectively. Under these conditions, the entire library of 20 azides **2**–**21** was screened in two batches, first with azides **2**–**11** and then with **12**–**21**. A mixture of DMSO/EtOH (1:4 v/v) was utilized as solvent for all reagents, as it does not damage[27] the PDMS-based microchannels or affect the performance of the embedded valves and pumps. Each in situ click chemistry reaction employed 80 nL of a solution of acetylene **1** (30 mM, 2.4 nmol), 120 nL of a solution of one of the azides **2**–**21** (30 mM, 3.6 nmol), and 3.8 µL of a solution of bCAII (5 mg mL^{-1}, 19 µg) in PBS. For the control reactions, an additional 40 nL of solution of inhibitor **22** (100 mM, 4 nmol) was added. In the thermal reactions, the solutions of bCAII were replaced with PBS.

By means of a computer-controlled interface, multiple steps were programmed in an operation cycle to prepare a single reaction mixture; 32 operation cycles were compiled in sequence to create the entire in situ click chemistry library for a given run. Figure 2 illustrates the four critical steps for the preparation of the reaction mixture, using the inhibitor-containing control reaction between acetylene **1** and azide **2** as an example. First, the metering pumps were used to introduce azide **2**, acetylene **1**, and inhibitor **22** into the mixing loop sequentially (flow rate $\approx$ 10 nL s^{-1}; Figure 2a). PBS solution was then employed to fill the round-shaped loop completely. Second, the reagent solutions were mixed for 15 seconds in the nL-level mixing loop (circulation rate $\approx$ 18 cycle min^{-1}; Figure 2b) using the mixing pumps. Third, PBS solution (flow rate $\approx$ 25 nL s^{-1}) was employed to introduce the 250-nL reagent mixture, along with 3.8 µL of the

 © 2006 Wiley-VCH Verlag GmbH & Co. KGaA, Weinheim

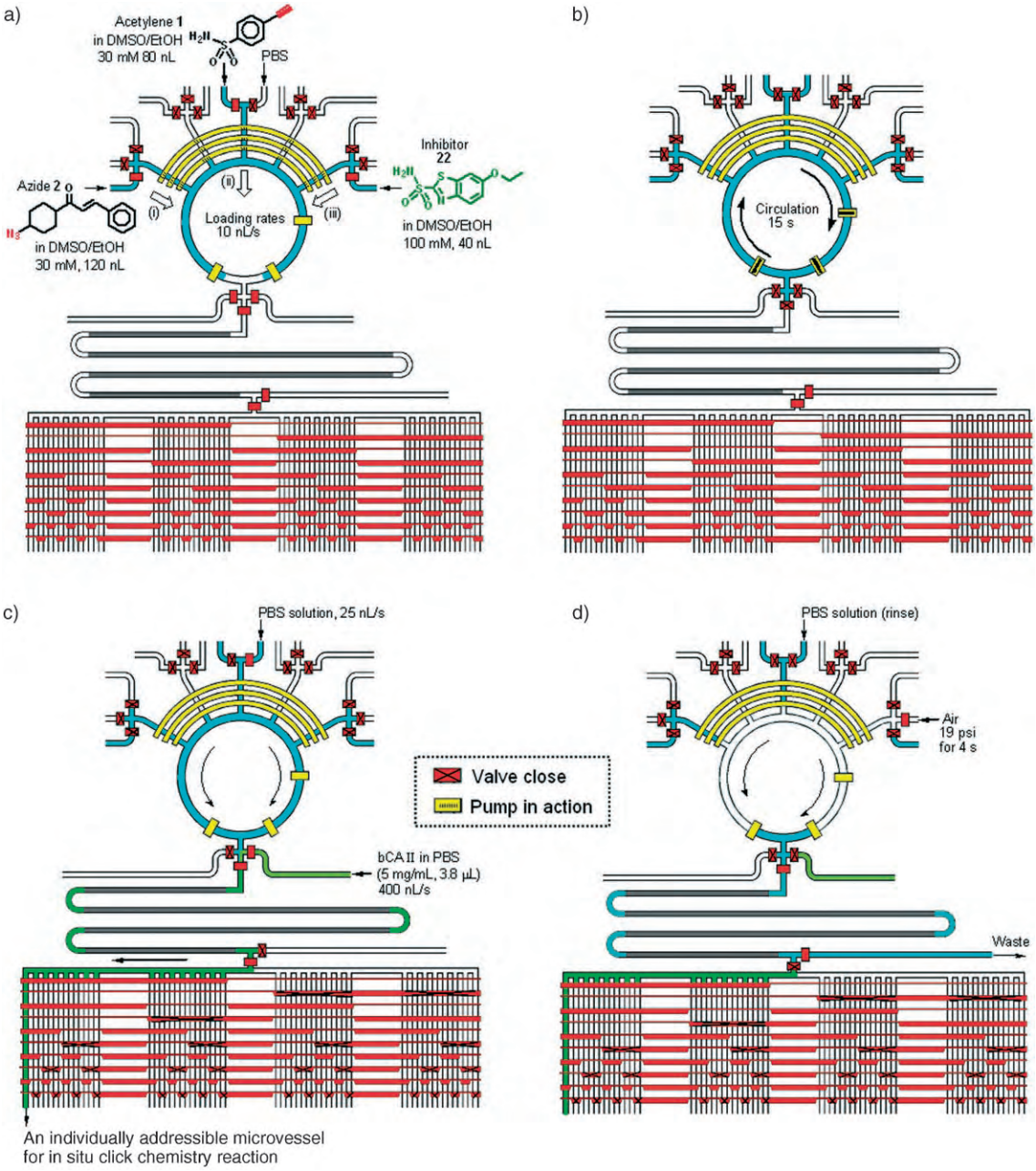


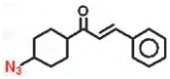
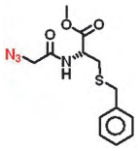
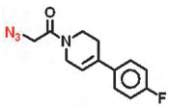
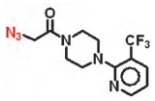
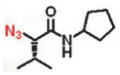
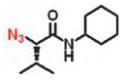
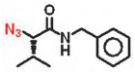
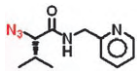
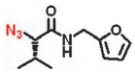
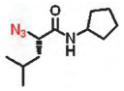
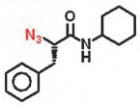
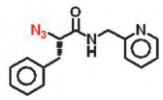
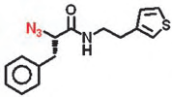
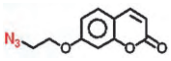
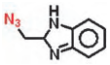
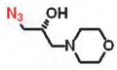
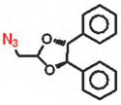
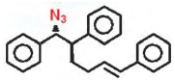
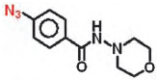
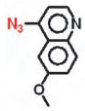
Figure 2. Schematic diagrams that illustrate the four sequential processes for preparing an individual in situ click chemistry mixture in the reaction circuit (this example describes a control experiment, which utilizes the acetylene **1**, azide **2**, and the active-site inhibitor **22**): a) Loading of the reagents in the mixing loop. b) Mixing of the reagent mixture. c) Introduction of the reagent mixture and enzyme into the chaotic mixture and final transportation via the multiplexer into the corresponding microvessel. d) Rinsing and drying of the microchannels.

bCAII solution (flow rate $\approx 400\ nL\,s^{-1}$), into the chaotic mixer (Figure 2c). The microfluidic multiplexer guided the resulting reaction mixture into the corresponding microvessel. Finally, the microchannels were rinsed with PBS solution (2 μL) and then purged with a flow of air to prevent cross-contamination (Figure 2d). The preparation of the entire screening library, which involved 32 operation cycles, took approximately 30 minutes (ca. $57\ s\,cycle^{-1}$). The chemical reaction circuit was then placed in a moisture-regulated incubator at 37 °C for 40 h to complete the reactions.

After incubation, the resulting reaction mixtures were collected from the respective microvessels. Each microvessel was rinsed with MeOH (5 μL × 3), and the rinsing solutions were combined with the original reaction mixtures. For reference purposes, the expected 1,4-disubstituted ("*anti*") triazoles were prepared separately from the corresponding Cu^{I}-catalyzed reactions.[21] The LC-MS analyses indicated that 10 out of the 20 reaction combinations had led to the formation of triazole products in the presence of bCAII. For comparison, all 20 in situ click chemistry reactions were also

 © 2006 Wiley-VCH Verlag GmbH & Co. KGaA, Weinheim

Table 1: Summary of in situ click chemistry screening results between acetylene **1** and azides **2**–**21** obtained using the chemical reaction circuits.

Azide	Result[a]	Azide	Result[a]	Azide	Result[a]	Azide	Result[a]
 **2**	hit (hit)	 **3**	no hit (no hit)	 **4**	hit (hit)	 **5**	no hit (no hit)
 **6**	hit (hit)	 **7**	hit (hit)	 **8**	hit (hit)	 **9**	no hit (no hit)
 **10**	hit (hit)	 **11**	no hit (no hit)	 **12**	hit (hit)	 **13**	no hit (no hit)
 **14**	hit (hit)	 **15**	hit (hit)	 **16**	hit (hit)	 **17**	no hit (no hit)
 **18**	no hit (no hit)	 **19**	no hit (no hit)	 **20**	no hit (no hit)	 **21**	no hit (no hit)

[a] The results obtained for reactions performed in 96-well microtiter plates are indicated in parentheses.

performed in 96-well microtiter plates. The results of the in situ click chemistry screening between acetylene **1** and the 20 azides (**2**–**21**) in the new microfluidic format and the conventional 96-well system are summarized in Table 1 and reveal a very similar outcome.[21] LC-MS analyses of a positive hit identification obtained for the screening reaction between acetylene **1** and azide **2** and its control studies are illustrated in Figure 3, while those obtained for a negative hit identification between acetylene **1** and azide **3** are shown in Figure 4.

Previously, we reported the use of integrated microfluidics for sequential synthesis. [9] Here, we have utilized integrated microfluidics for parallel screening of an in situ click chemistry library. Our results suggest that integrated microfluidics promises to make lead discovery through in situ click chemistry more convenient and reliable, less expensive, and more diverse. Generally, most chemical reactions are performed either sequentially or in parallel. We believe that integrated microfluidics provides chemists a new playing field, where a wide range of chemical reactions can be performed beyond conventional settings, with

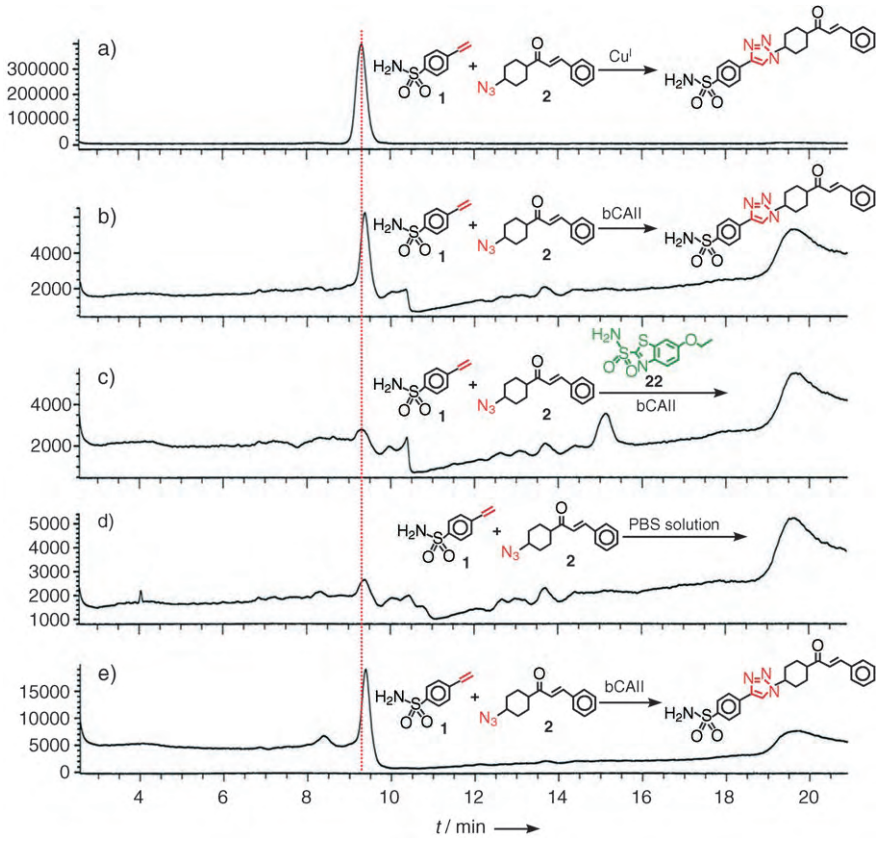


Figure 3. In situ click chemistry reactions between acetylene **1** and azide **2**, analyzed by LC-MS. The triazole product is indicated by the red dashed line. a) Triazole product obtained through Cu^{I}-catalyzed reaction (room temperature, 24 h). b–d) Microchip-based reactions performed at 37 °C for 40 h in the presence of bCAII (b), in the presence of both bCAII and inhibitor **22** (c), and in the absence of bCAII (d). e) Reaction performed at 37 °C for 40 h in a 96-well microtiter plate in the presence of bCAII.

 © 2006 Wiley-VCH Verlag GmbH & Co. KGaA, Weinheim

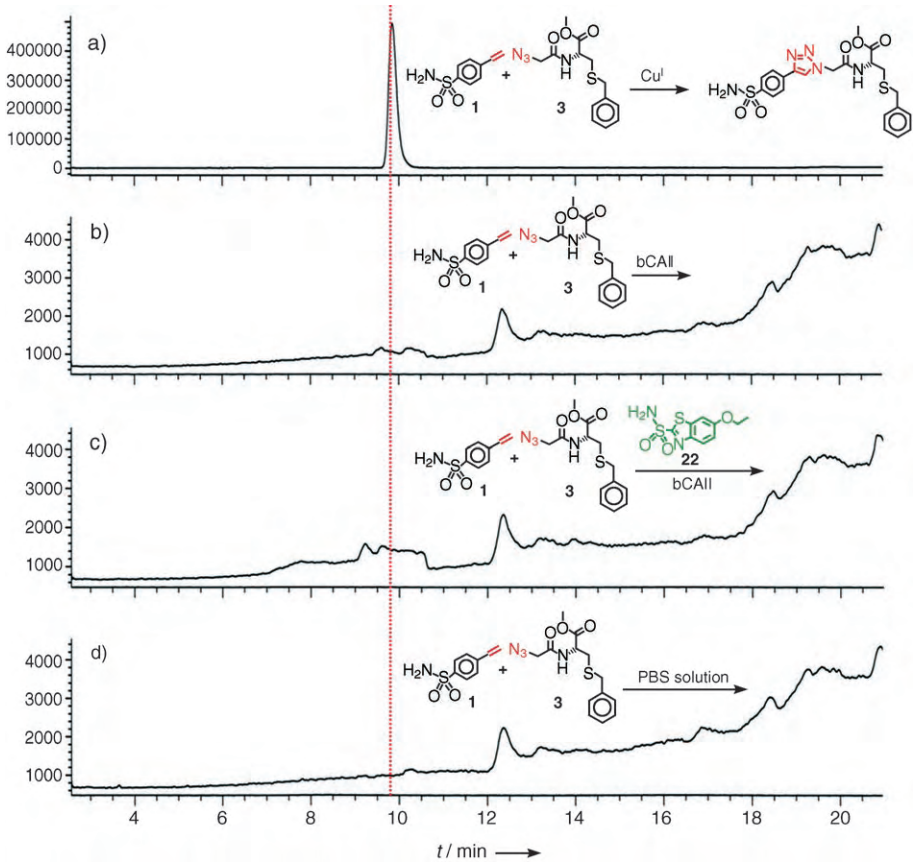


Figure 4. In situ click chemistry reactions between acetylene **1** and azide **3**, analyzed by LC-MS. The triazole product is indicated by the red dashed line. a) Triazole product. b–d) Microchip-based reactions performed at 37 °C for 40 h in the presence of bCAII (b), in the presence of both bCAII and inhibitor **22** (c), and in the absence of bCAII (d).

additional advantages of low reagent consumption, precise control over reaction conditions, faster reaction kinetics, cost efficiency, short design/fabrication processes, and rapid redesign/improvement cycles.

Received: April 28, 2006
Published online: July 6, 2006

Keywords: click chemistry · enzyme catalysis · high-throughput screening · microreactors · parallel synthesis

[1] K. Jahnisch, V. Hessel, H. Lowe, M. Baerns, *Angew. Chem.* **2004**, *116*, 410–451; *Angew. Chem. Int. Ed.* **2004**, *43*, 406–446.
[2] P. Watts, S. J. Haswell, *Chem. Soc. Rev.* **2005**, *34*, 235–246.
[3] G. Jas, A. Kirschning, *Chem. Eur. J.* **2003**, *9*, 5708–5723.
[4] T. Kawaguchi, H. Miyata, K. Ataka, K. Mae, J. Yoshida, *Angew. Chem.* **2005**, *117*, 2465–2468; *Angew. Chem. Int. Ed.* **2005**, *44*, 2413–2416.
[5] D. M. Ratner, E. R. Murphy, M. Jhunjhunwala, D. A. Snyder, K. F. Jensen, P. H. Seeberger, *Chem. Commun.* **2005**, 578–580.
[6] B. J. Kirby, T. J. Shepodd, E. F. Hasselbrink, *J. Chromatogr. A* **2002**, *979*, 147–154.
[7] M. A. Unger, H. P. Chou, T. Thorsen, A. Scherer, S. R. Quake, *Science* **2000**, *288*, 113–116.
[8] A. D. Stroock, S. K. W. Dertinger, A. Ajdari, I. Mezic, H. A. Stone, G. M. Whitesides, *Science* **2002**, *295*, 647–651.
[9] C. C. Lee, G. Sui, A. Elizarov, C. Y. J. Shu, Y. S. Shin, A. N. Dooley, J. Huang, A. Daridon, P. Wyatt, D. Stout, H. C. Kolb, O. N. Witte, N. Satyamurthy, J. R. Heath, M. E. Phelps, S. R. Quake, H. R. Tseng, *Science* **2005**, *310*, 1793–1796.
[10] W. Gu, X. Y. Zhu, N. Futai, B. S. Cho, S. Takayama, *Proc. Natl. Acad. Sci. USA* **2004**, *101*, 15861–15866.
[11] J. Liu, M. Enzelberger, S. Quake, *Electrophoresis* **2002**, *23*, 1531–1536.
[12] C. L. Hansen, M. O. A. Sommer, S. R. Quake, *Proc. Natl. Acad. Sci. USA* **2004**, *101*, 14431–14436.
[13] D. Rideout, *Science* **1986**, *233*, 561–563.
[14] I. Huc, J. M. Lehn, *Proc. Natl. Acad. Sci. USA* **1997**, *94*, 2106–2110.
[15] J. M. Lehn, A. V. Eliseev, *Science* **2001**, *291*, 2331–2332.
[16] O. Ramstrom, J. M. Lehn, *Nat. Rev. Drug Discovery* **2002**, *1*, 26–36.
[17] D. A. Erlanson, A. C. Braisted, D. R. Raphael, M. Randal, R. M. Stroud, E. M. Gordon, J. A. Wells, *Proc. Natl. Acad. Sci. USA* **2000**, *97*, 9367–9372.
[18] K. C. Nicolaou, R. Hughes, S. Y. Cho, N. Winssinger, C. Smethurst, H. Labischinski, R. Endermann, *Angew. Chem.* **2000**, *112*, 3981–3986; *Angew. Chem. Int. Ed.* **2000**, *39*, 3823–3828.
[19] W. G. Lewis, L. G. Green, F. Grynszpan, Z. Radic, P. R. Carlier, P. Taylor, M. G. Finn, K. B. Sharpless, *Angew. Chem.* **2002**, *114*, 1095–1099; *Angew. Chem. Int. Ed.* **2002**, *41*, 1053–1057.
[20] V. D. Bock, H. Hiemstra, J. H. van Maarseveen, *Eur. J. Org. Chem.* **2006**, 51–68.
[21] V. P. Mocharla, B. Colasson, L. V. Lee, S. Roper, K. B. Sharpless, C. H. Wong, H. C. Kolb, *Angew. Chem.* **2005**, *117*, 118–122; *Angew. Chem. Int. Ed.* **2005**, *44*, 116–120.
[22] A. Krasinski, Z. Radic, R. Manetsch, J. Raushel, P. Taylor, K. B. Sharpless, H. C. Kolb, *J. Am. Chem. Soc.* **2005**, *127*, 6686–6692.
[23] R. Manetsch, A. Krasinski, Z. Radic, J. Raushel, P. Taylor, K. B. Sharpless, H. C. Kolb, *J. Am. Chem. Soc.* **2004**, *126*, 12809–12818.
[24] M. Whiting, J. Muldoon, Y.-C. Lin, S. M. Silverman, W. Lindstrom, A. J. Olson, H. C. Kolb, M. G. Finn, K. B. Sharpless, J. H. Elder, V. V. Fokin, *Angew. Chem.* **2006**, *118*, 1463–1467; *Angew. Chem. Int. Ed.* **2006**, *45*, 1435–1439.
[25] Micropatterns of 31.5 mm in length are required to achieve efficient mixing in 200-μm wide microchannels. This length was obtained according to the theoretical model described in Ref. [8].
[26] T. Thorsen, S. J. Maerkl, S. R. Quake, *Science* **2002**, *298*, 580–584.
[27] J. N. Lee, C. Park, G. M. Whitesides, *Anal. Chem.* **2003**, *75*, 6544–6554.

 © 2006 Wiley-VCH Verlag GmbH & Co. KGaA, Weinheim

Monolayers

DOI: 10.1002/anie.200504286

Organizing Supramolecular Functional Dye–Zeolite Crystals**

*Arantzazu Zabala Ruiz, Huanrong Li, and Gion Calzaferri**

Sunlight is absorbed in the antenna system of a green leaf where it is transported by supramolecularly organized chlorophyll molecules for the purpose of energy transformation. The aim of our research is to develop a similar transport of light in an artificial system in which dye-loaded zeolite L crystals adopt the antenna function and to find out if and how this can be used in photoelectronic devices. Organic dye molecules have the tendency to form aggregates even at low concentration. These aggregates are known to generally cause fast thermal relaxation of electronic excitation energy. The main role of the zeolite as a host is to prevent this aggregation and to superimpose a specific organization.[1] We have shown that zeolite L[2] is an ideal host for this purpose. Supramolecular organization of dyes inside the one-dimensional channels of this material has been realized and their communication via stopcock molecules with molecules in the environment with a polymer or a semiconductor as well as solubilization of dye-loaded zeolite L crystals has been demonstrated.[3,4]

We know that in chemical devices a high degree of supramolecular organization is important for attaining the desired macroscopic properties.[5] A possibility for achieving a high level of organization is the controlled assembly of the zeolite crystals into oriented structures and the preparation of monodirectional materials. In the case of cylindrically shaped zeolite L, this implies the alignment of many crystals on a surface, and has the consequence of the alignment of a large number of one-dimensional channels. An overview of the antenna material, of the stopcock-plugged antenna material, and of the desired organization of the zeolite L crystals resulting in monodirectional functional materials is illustrated in Figure 1.

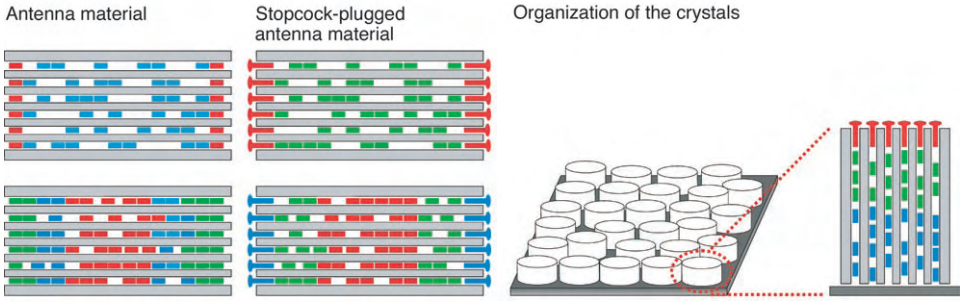


Figure 1. Different stages of organization. Left: Supramolecularly organized dye–zeolite crystals. Middle: Stopcock-plugged dye–zeolite crystals. Right: Organization of supramolecular functional dye–zeolite crystals in oriented monolayers.

The preparation of dense monolayers of zeolite crystals in the nanometer to micrometer size regime was first reported for zeolite A[6] and later considerably improved and also extended to other types of zeolites.[7] As a general rule, we can state that the successful assembly of small zeolite crystals largely depends on the availability of a narrow size distribution and a well-defined morphology. The successful assembly of oriented zeolite L monolayers, which can then be modified to result in organized supramolecular functional materials, offers a new challenge. Table 1 gives an overview of the different ways of preparing such monolayers on a substrate. An underlying principle that has to be respected is that the interaction between the base of the cylindrically shaped zeolite L crystals and the substrate must be stronger or preferably much stronger than that between the coat of the crystals and the substrate and, importantly, any interaction between the zeolite crystals. Working with an excess of crystals, fixing them in the right way to the substrate, and washing away the excess material has, under these conditions, a high chance of leading to the desired material. Subsequent insertion of dye molecules into the channels and the addition of stopcocks is only possible if the channels are not blocked or damaged during the preparation of the monolayer. The procedure leads to materials with exciting properties, for example, to systems where electronic excitation energy is transported in one direction only.

The preparation of zeolite L monolayers was carried out with two types of medium-sized cylindrically shaped zeolite L crystals: 1 μm average length of average aspect ratio (length to diameter ratio) 1.0, and 200 nm average length of average aspect ratio 0.3.[8] Different chemical procedures were followed depending on the reagents used. The incorporation of the dyes and the attachment of stopcock molecules at the channel ends, after calcining the monolayers of oriented zeolite L crystals, led to monodirectional materials. The molecules that have been used as covalent linkers to synthesize the zeolite L monolayers, the dyes that have been

[*] Dipl.-Chem. A. Zabala Ruiz, Dr. H. Li, Prof. Dr. G. Calzaferri
Departement für Chemie und Biochemie
Universität Bern
Freiestrasse 3, 3012 Bern (Switzerland)
Fax: (+41) 31-631-3994
E-mail: gion.calzaferri@iac.unibe.ch

[**] This work was supported by the Schweizerischer Nationalfonds zur Förderung der wissenschaftlichen Forschung (NF 200020-105140) and by the European Comission through the Human Potential Programme (RTN NANOCHANNEL, grant no. HRPN-CT-2002-00323). We would like to thank Dr. D. Pflieger from Clariant for providing some chemicals, Beatrice Frey for the SEM measurements, and Dr. M. Jazdzyk for the C_{60} sample.

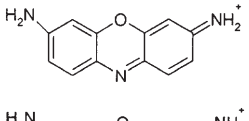
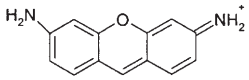
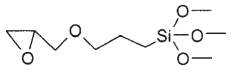
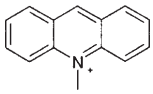
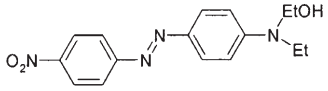
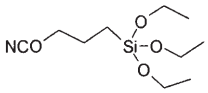
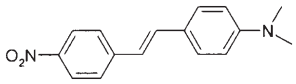
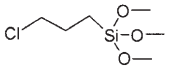
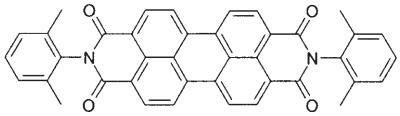
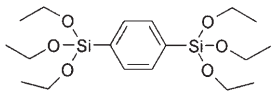
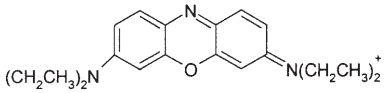
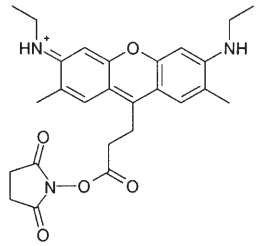
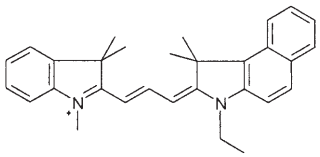
InterScience
© 2006 Wiley-VCH Verlag GmbH & Co. KGaA, Weinheim

Table 1: Procedures for preparing zeolite monolayers.

A	B	C	D
	cleaning the substrate		
–	specific modification of the substrate	specific modification of the zeolite	specific modification of both zeolite and substrate
sedimentation of a calculated amount of zeolite onto the substrate	addition of an excess of zeolite suspended in an appropriate solvent and reaction with the substrate		
fixation of the zeolite crystals—monolayer assembly	migration and bond formation of the zeolite with the substrate monolayer assembly		
–	washing off the excess of zeolite crystals		
–	optional: calcination at 600 °C under O_2 flow		

Different experimental conditions and reagents have been tested for obtaining oriented zeolite L monolayers. Details of the different procedures are reported in the Experimental Section. Based on a previous report,[9] C_{60} was tested as a functional interconnecting covalent linker between the amino-modified zeolite L and the amino-tethered glass plate. The degree of coverage and the homogeneity of the monolayers is acceptable for some applications and the stability is high. It was possible to sonicate the sample for more than ten minutes without damaging the layers. The degree of coverage and close packing as well as the stability obtained with a GOP-TMS linker is unsatisfactory. After a few minutes of sonication all the crystals fell off. The use of PEI as a molecular linker[10] inserted in the channels of zeolite L monolayers, and the stopcock molecules that have been attached are shown in Table 2. The stability of the monolayers was tested before calcination by sonicating the samples in toluene. This test was used because sonication is the best way to clean the monolayers from an excess of crystals. The stability was always considerably improved by the calcination process.

Table 2: Molecules used in this study.[a]

Abbreviation	Structural formula	Abbreviation	Structural formula
Ox^+		C_{60}	
Py^+		GOP-TMS	
$MeAcr^+$		PEI	
DR1		TES-PCN	
DANS		CP-TMS	
DXP		BTESB	
Ox1			
ATTO520		Cy02702	

[a] Left: Dyes inserted in the channels of zeolite L crystals on the monolayer. Right: Covalent linkers that have been used to synthesize the monolayers. Bottom: ATTO520 and Cy02702 are the stopcock molecules that have been attached to the channel ends of the zeolites.

 © 2006 Wiley-VCH Verlag GmbH & Co. KGaA, Weinheim

yielded monolayers of acceptable coverage and homogeneity for some applications. Crystals are bound to each other in some areas, which hinders the formation of a clean monolayer. The monolayer is, however, strongly bound to the glass surface and it was possible to sonicate the sample for more than ten minutes without damaging the layer. The degree of coverage and of close packing is high with TES-PCN. The binding of the crystals to the glass surface is not very strong and sonicating the sample for more than five minutes resulted in a severe loss of crystals. The reaction with CP-TMS consists of two steps:[7b,11] the tethering of CP-TMS to the glass surface and reaction of bare zeolite L with the CP-TMS-tethered glass plates. Both types of zeolite L yielded high quality monolayers. We tested two different ways of promoting the reaction between the zeolite L crystals and the functional groups tethered to the glass surface: reflux and sonication. Figure 2 a shows the SEM images of samples prepared under reflux. The degree of packing and of coverage is good. However, binding the zeolite crystals under sonication results in both the degree of coverage and the packing being significantly higher (Figure 2 b). Carrying out the reaction under sonication turned out to be more convenient and also more successful; it involves considerable less reaction time. This way of treating zeolite L with a surface-modified glass plate was then applied in all other comparable procedures, for example, when using GOP-TMS, TES-PCN, and BTESB. The binding of the zeolite L monolayer and the glass surface through a CP-TMS linker seemed to be strong, and the sample could be sonicated for more than five minutes without any noticeable changes. In the case of a BTESB linker, a procedure that resulted in very good quality monolayers involved first tethering BTESB to the glass surface followed by treating the bare zeolite L crystals with the BTESB-tethered glass plates under sonication. Figure 2 c shows the SEM images of samples prepared by this method. The degree of coverage is high and the degree of close packing is very high. However, the stability of the so-obtained zeolite L monolayers is less good than that obtained following the procedure used for CP-TMS. Sonication of the sample for more than three minutes can cause a great loss of crystals.

The procedures involving TES-PCN, CP-TMS, and BTESB as covalent linkers thus led to closely packed zeolite L monolayers with a very high degree of coverage over the whole plate. The binding of zeolite L crystals onto the TES-PCN/CP-TMS/BTESB-coated glass plate probably proceeds by nucleophilic substitution of the terminal cyanate/chloro/triethoxy groups, respectively, by the surface hydroxy groups on the channel openings of the zeolite L crystals. The strength of the binding between the zeolite monolayer and the glass surface is weak when using TES-PCN and BTESB, whereas it is strong when using CP-TMS. It seems that the nucleophilic substitution of a terminal halide[7c] induces much stronger binding between the zeolite L crystals and the glass surface than the nucleophilic substitution of a terminal cyanate or triethoxy group. The procedures involving C_{60} and PEI as covalent linkers led to zeolite L monolayers with the strongest binding to the glass surface. The binding of amino-modified zeolite L crystals onto the C_{60}-coated glass plate proceeds by amine addition to C_{60}.[9] The binding of GOP-TMS zeolite L crystals onto the GOP-TMS-coated glass plate through PEI proceeds through a nucleophilic ring opening of the epoxy groups tethered on the glass and on the zeolite L surfaces by the amino groups of PEI.[10]

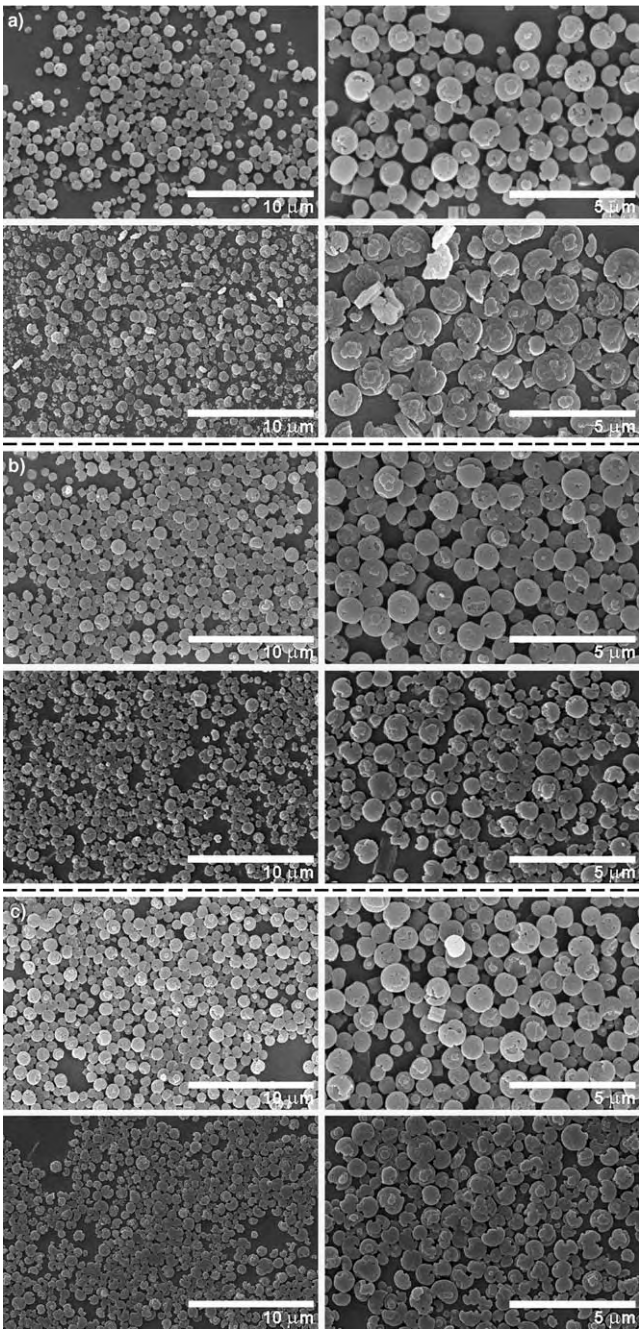


Figure 2. SEM images of zeolite L monolayers after cacination, prepared by using: a) CP-TMS as a covalent linker under reflux, b) CP-TMS under sonication, c) BTESB. Each example contains four images: Upper: 1 μm crystals at two different magnifications. Lower: disc-shaped crystals at two different magnifications.

An important prerequisite for obtaining a high degree of coverage and of close packing is to use a considerable excess of zeolite L crystals when treating them with the modified glass surface. Hence, an underlying principle that has to be

 © 2006 Wiley-VCH Verlag GmbH & Co. KGaA, Weinheim

respected is that the interaction between the base of the crystals and the substrate must be stronger than any other interaction. A process to account for the close-packing phenomenon is surface migration. It can take place if the interaction of zeolite L crystals with the modified glass plate is sufficiently weak at the initial state of the reaction so that migration can take place to form a dense package. In the next step, stronger binding is achieved. On the basis of this, we can understand why sonication is so successful in promoting the reaction during the monolayer assembly process: It helps the zeolite L crystals to rapidly find available sites on the surface by rapid surface migration.

With methods for preparing oriented zeolite L monolayers in hand, it is now possible to modify them by inserting dye molecules. For this purpose materials with CP-TMS and BTESB linkers were calcined to burn away the organic part and to better close the channel openings on the side in contact with the glass plate. Consecutive insertion of dyes was realized by similar procedures as described in references [3a] and [12]. Table 2 shows a representative list of dyes we have inserted to date into the channels of zeolite L crystals organized as monolayers. Figure 3 shows fluorescence microscopy images of two zeolite L monolayers loaded with Py^+ and Ox^+. Strong luminescence of the samples can be observed. This observation also proves that the pores in the zeolite L crystals are still open after the calcination process.

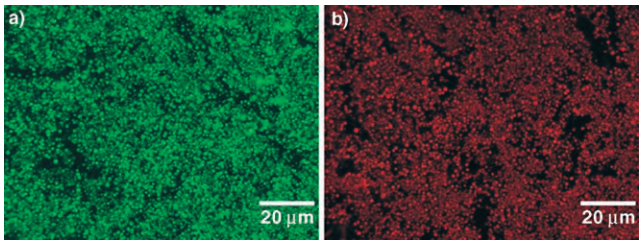


Figure 3. Fluorescence microscopy images of monolayers loaded with one dye: a) Py^+/zeolite L, b) Ox^+/zeolite L.

The consecutive insertion of two different dyes which cannot glide past each other as a result of spatial restrictions is the basis for the preparation of an antenna system capable of efficiently transporting electronic excitation energy. The Py^+/Ox^+ pair is ideal for testing this. The high fluorescence quantum yield and the favorable spectral properties (Figure 4a) of these dyes allow the system to have very efficient Förster-type electronic excitation energy transfer.[13] An oriented Ox^+/Py^+/zeolite L monolayer was prepared by first inserting Py^+ (donors) followed by insertion of Ox^+ (acceptors). The spectra shown in Figure 5a illustrate that considerable energy transfer from the electronically excited Py^+ unit to the Ox^+ moiety occurs after selective excitation of the donor.

Extension beyond the interior of the zeolite crystals is achieved by selectively positioning molecules at the entrances of the zeolite channels.[14] Table 2 shows the two types of stopcock dyes that have been used. The location of the stopcocks allows their use as traps or injectors of electronic excitation energy. We used ATTO520 to act as a donor in a Ox^+/zeolite L monolayer and Cy02702 to act as an acceptor in a Py^+/zeolite L monolayer. In both cases the spectral overlap between the donor emission and the acceptor excitation is considerable (Figure 4), so that energy transfer can occur upon selective excitation of the donor molecule (Figure 5b,c). Figure 5b shows the spectra of an oriented ATTO520/Ox^+/zeolite L monolayer. Figure 5c shows the spectra of an oriented Cy02702/Py^+/zeolite L monolayer.

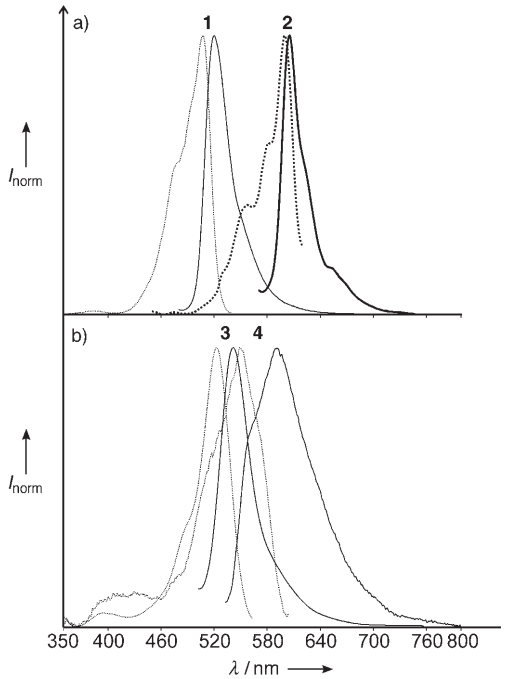


Figure 4. Excitation (dotted) and emission (solid) spectra of the dyes used in this study measured on oriented dye/zeolite L layers on quartz. Spectra have been scaled to the same height at the maxima. a) Py^+/zeolite L (**1**) and Ox^+/zeolite L (**2**). The emission and the excitation spectra of **1** were recorded upon excitation at 460 nm and detection at 560 nm, respectively. Those of **2** were recorded upon excitation at 560 nm and detection at 640 nm, respectively. b) Excitation and emission spectra of ATTO520 (**3**) and Cy02702 (**4**) attached to the zeolite L channel entrances. The emission and the excitation spectra of (**3**) were recorded upon excitation at 460 nm and detection at 600 nm, respectively. Those of **4** were recorded upon excitation at 470 nm and detection at 630 nm.

In conclusion, a new hierarchy of structural order has been reached by organizing supramolecular functional dye–zeolite crystals as oriented monolayers. Different procedures to generate robust monolayers of zeolite L crystals, which have their channels perpendicular to the surface of the substrate, have been described. Subsequent insertion of dyes into the open channel ends was performed and energy transfer was tested. Coupling dye-loaded zeolite monolayers to an external acceptor or donor stopcock dye at the channel ends which trap electronic excitation energy from donor molecules inside the crystal or inject it to an acceptor inside the channels has been demonstrated. These materials are the basis for systems where excitation energy is transported in one direction only, thus largely extending the possibilities to

 © 2006 Wiley-VCH Verlag GmbH & Co. KGaA, Weinheim

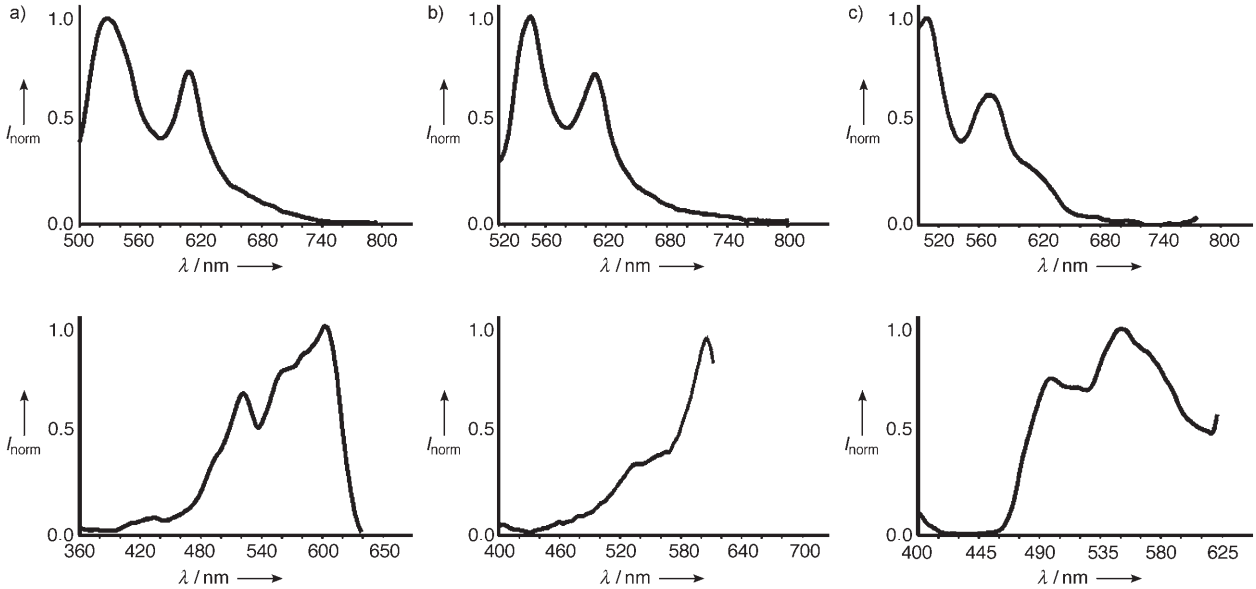


Figure 5. Emission (upper) and excitation spectra (lower) of donor- and acceptor-loaded zeolite L crystals arranged as oriented monolayers on a glass plate. Spectra have been scaled to the same height at the maxima. a) Spectra of a Ox^+/Py^+/zeolite L monolayer. The emission spectrum was recorded after selective excitation of Py^+ at 460 nm and the excitation spectrum was detected at 680 nm, the wavelength at which Ox^+ emits. b) Spectra of an ATTO520/Ox^+/zeolite L monolayer. The emission spectrum was recorded after selective excitation of ATTO520 at 460 nm and the excitation spectrum was detected at 680 nm, the wavelength at which Ox^+ emits. c) Spectra of a Cy02702/Py^+/zeolite L monolayer. The emission spectrum was recorded after selective excitation of Py^+ at 460 nm and the excitation spectrum was detected at 680 nm, the wavelength at which Cy02702 emits.

make use of the quasi 1D electronic excitation energy transport in dye-loaded zeolite L that has recently been observed.[15] The new highly organized robust material offers unique possibilities for developing photonic devices also comprising dye-sensitized solar cells and luminescent solar concentrators.[16,17]

Experimental Section

Materials: Zeolite L crystals of two different sizes (ca. 1×1 μm and 0.3×1 μm) were synthesized and characterized as described previously.[8] Py^+ acetate and Ox^+ perchlorate were synthesized and purified according to Ref. [18]. ATTO520 was purchased from ATTO-TECH GmbH. Cy02702 iodine was obtained from Clariant.[19] APS (purum ≥ 98%), GOP-TMS (purum ≥ 97%), toluene (puriss, absolute, over molecular sieve), ethanol (absolute, 99.8%), methanol (purum), acetonitrile (puriss., 99.5%, over molecular sieve) were obtained from Fluka; PEI (high-molecular weight, water-free), TES-PCN (95%), CP-TMS (≥ 97%), and BTESB (96%) were obtained from Aldrich; the water used was doubly distilled. The substrates were round glass plates (∅ = 10 mm, thickness = 1 mm, TRABOLD, Switzerland).

Preparation of the zeolite L monolayers: C_{60} as a covalent linker: Functionalization of the channel entrances of zeolite L with amino groups was done as described in an earlier report.[20] Typically, two pieces of glass plates supported on a teflon mount were immersed in a solution of APS (50 μL) in toluene (30 mL) in a round-bottomed Schlenk flask and heated at reflux for 1 h under N_2, cooled to RT, and washed with toluene and with copious amounts of ethanol. The APS-tethered glass plates were finally dried for approximately 2 h at 80 °C in air. C_{60} (1 mg) was added to a solution of toluene (15 mL) in a round-bottomed Schlenk flask; a glass plate was then introduced and the mixture was heated at reflux for 24 h under N_2, cooled to RT, and washed with copious amounts of cholorobenzene. An excess of amino-modified zeolite L (between 10 and 11 mg) was added to a solution of toluene (15 mL) in a round-bottomed Schlenk flask and sonicated for 15 min, after which a C_{60}-coated glass substrate was introduced. The mixture was heated at reflux for 5 h under N_2, cooled to RT, and sonicated in fresh toluene for 3 min to remove the physisorbed zeolites. PEI as molecular linker: Zeolite L (50 mg) was suspended in a solution of GOP-TMS (0.1M) in toluene (20 mL) in a round-bottomed Schlenk flask and heated at reflux for 3 h, cooled to RT, and the GOP-TMS-tethered zeolite crystals were washed with ethanol. Two glass plates supported on a teflon mount were then immersed into a solution of GOP-TMS (0.1M) in toluene (20 mL) in a round-bottomed Schlenk flask and the toluene solution was heated at reflux for 3 h, cooled to RT, and then the GOP-TMS-tethered glass plates were washed with toluene. Two GOP-TMS-tethered glass plates were immersed in a solution of PEI (700 mg) in toluene (20 mL) and refluxed for 2 h. The physisorbed PEI was removed by repeatedly washing the plates with hot ethanol and doubly distilled water. An excess of amino-modified zeolite L (15 mg) was added to toluene (15 mL) in a round-bottomed Schlenk flask and sonicated for 15 min after which a GOP-TMS-PEI-coated glass plate was introduced. The mixture was heated at reflux for 3 h under N_2. After cooling the mixture to RT, the opaque glass plates coated with zeolite L were sonicated in fresh toluene for 3 min to remove the physisorbed zeolites. GOP-TMS, TES-PCN, CP-TMS, and BTESB as covalent linkers: Typically, two glass plates supported on a teflon mount were immersed in a solution (20 mL) of ethoxymethoxysilane (0.1M) in toluene in a round-bottomed Schlenk flask and the mixture heated at reflux for 3 h. The ethoxymethoxysilane-tethered glass plates were washed with toluene. An excess of zeolite L (10–13 mg) was added to toluene (10 mL) in a round-bottomed Schlenk flask and sonicated for approximately 40 min. An ethoxymethoxysilane-tethered glass plate was introduced and the mixture heated at reflux for 3 h. The opaque glass plates coated with zeolite L were sonicated in

 © 2006 Wiley-VCH Verlag GmbH & Co. KGaA, Weinheim

fresh toluene for a maximum of 1 min to remove the physisorbed zeolites. Alternatively, an excess of zeolite L (10–13 mg) was added to toluene (10 mL) in a round-bottomed Schlenk flask and sonicated for approximately 40 min. An ethoxymethoxysilane-tethered glass plate was then introduced and sonicated for 15 to 17 min.

Calcination of zeolite L monolayers: The zeolite L monolayer was placed in a closed oven and the temperature was steadily increased up to 600 °C under oxygen where it was kept for 3 h. After calcination, the zeolite L monolayer was dipped in a 0.1 M KNO_3 solution for 30 min.

Functionalization of the zeolite L monolayers: The cationic dyes were inserted into the zeolite L channels by ion exchange from aqueous solutions. A calcined zeolite L monolayer was introduced in an aqueous solution of Py^+ or Ox^+ ions and heated up to 70 °C for 15 h. The zeolite L monolayer was then washed several times with doubly distilled water and with ethanol. Neutral dyes such as DR1 and DANS were inserted from the gas phase by using the single ampoule method.[3,12] The reaction time and temperature were 48 h at 170 °C for DR1 and 24 h at 270 °C for DANS. Attachement of ATTO520 to the channel ends was achieved by treatment of a zeolite L monolayer with a solution of ATTO520 in acetonitrile for 24 h at RT as described in Ref. [14]. For the electrostatic binding of the cationic dye Cy02702, a zeolite L monolayer was treated with a solution of Cy02702 in ethanol for 24 at RT.

Physical measurements: SEM measurements were carried out by means of scanning electron microscopy (Hitachi S-3000N) at an acceleration voltage of 20 kV. A 3-nm gold layer was deposited on top of the samples. Luminescence and excitation spectra were measured at RT in air with a Perkin–Elmer LS 50B instrument with a resolution of 15 nm. For the luminescence microscopy images, an Olympus BX60 microscope equipped with a Kappa CF20DCX air-cooled CCD camera was used. The Py^+/zeolite L monolayer sample was excited from 470 to 490 nm and the fluorescence was detected by using a 520 nm cut-off filter. The Ox^+/zeolite L monolayer sample was excited from 545 to 580 nm and the fluorescence was detected by using a 610 nm cut-off filter. The quality of the zeolite L monolayers was examined by dipping the glass plates coated with zeolite L in fresh toluene and immersing them in an ultrasonic bath (Branson DTH-2510, 130 W, 42 kHz) for several minutes. The glass plates were then investigated using an optical microscope and by SEM.

Received: December 2, 2005
Revised: May 4, 2006
Published online: July 11, 2006

Keywords: energy transfer · FRET (fluorescence resonance energy transfer) · monolayers · supramolecular chemistry · zeolites

[1] a) M. Ganschow, C. Hellriegel, E. Kneuper, M. Wark, C. Thiel, G. Schulz-Ekloff, C. Bräuchle, D. Wöhrle, *Adv. Funct. Mater.* **2004**, *14*, 269; b) G. Schulz-Ekloff, D. Wöhrle, B. van Duffel, R. A. Schoonheydt, *Microporous Mesoporous Mater.* **2002**, *51*, 91; c) J. Caro, F. Marlow, M. Wübbenhorst, *Adv. Mater.* **1994**, *6*, 413.

[2] a) C. Baerlocher, W. M. Meier, D. H. Olson, *Atlas of zeolite Framework Types*, 5th ed., Elsevier, Amsterdam, **2001**; b) T. Ohsuna, B. Slater, F. Gao, J. Yu, Y. Sakamoto, G. Zhu, O. Terasaki, D. E. W. Vaughan, S. Qiu, C. R. Catlow, *Chem. Eur. J.* **2004**, *10*, 5031; c) O. Larlus, V. P. Valtchev, *Chem. Mater.* **2004**, *16*, 3381; d) C. Shaner, D. F. Shantz, *Chem. Mater.* **2005**, *17*, 6192.

[3] a) G. Calzaferri, S. Huber, H. Maas, C. Minkowski, *Angew. Chem.* **2003**, *115*, 3860; *Angew. Chem. Int. Ed.* **2003**, *42*, 3732; b) C. Minkowski, R. Pansu, M. Takano, G. Calzaferri, *Adv. Funct. Mater.* **2006**, *16*, 273.

[4] A. Devaux, Z. Popovic, O. Bossart, L. De Cola, A. Kunzmann, G. Calzaferri, *Microporous Mesoporous Mater.* **2006**, *90*, 69.

[5] F. J. M. Hoeben, A. P. H. J. Schenning, E. W. Meijer, *ChemPhysChem* **2005**, *6*, 2337.

[6] J. Li, K. Pfanner, G. Calzaferri, *J. Phys. Chem.* **1995**, *99*, 2119.

[7] a) P. Lainé, R. Seifert, R. Giovanoli, G. Calzaferri, *New J. Chem.* **1997**, *21*, 453; b) S. Mintova, B. Schoeman, V. Valtchev, J. Sterte, S. Mo, T. Bein, *Adv. Mater.* **1997**, *9*, 585; c) K. Ha, Y.-J. Lee, H. J. Lee, K. B. Yoon, *Adv. Mater.* **2000**, *12*, 1114; d) A. Kulak, Y.-J. Lee, Y. S. Park, K. B. Yoon, *Angew. Chem.* **2000**, *112*, 980; *Angew. Chem. Int. Ed.* **2000**, *39*, 950; e) K. Ha, Y.-J. Lee, D.-Y. Jung, J. H. Lee, K. B. Yoon, *Adv. Mater.* **2000**, *12*, 1614; f) L. Huang, Z. Wang, J. Sun, L. Miao, Q. Li, Y. Yan, D. Zhao, *J. Am. Chem. Soc.* **2000**, *122*, 3530; g) C. Leiggener, G. Calzaferri, *ChemPhysChem* **2004**, *5*, 1593.

[8] a) A. Zabala Ruiz, D. Brühwiler, T. Ban, G. Calzaferri, *Monatsh. Chem.* **2005**, *136*, 77; b) S. Megelski, G. Calzaferri, *Adv. Funct. Mater.* **2001**, *11*, 277.

[9] S. Y. Choi, Y.-J. Lee, Y. S. Park, K. Ha, K. B. Yoon, *J. Am. Chem. Soc.* **2000**, *122*, 5201.

[10] A. Kulak, Y. S. Park, Y.-J. Lee, Y. S. Chun, K. Ha, K. B. Yoon, *J. Am. Chem. Soc.* **2000**, *122*, 9308.

[11] J. S. Lee, K. Ha, Y.-J. Lee, K. B. Yoon, *Adv. Mater.* **2005**, *17*, 837.

[12] a) M. Pauchard, A. Devaux, G. Calzaferri, *Chem. Eur. J.* **2000**, *6*, 3456; b) S. Huber, G. Calzaferri, *ChemPhysChem* **2004**, *5*, 239.

[13] a) T. Förster, *Ann. Phys.* **1948**, *2*, 55; b) T. Förster, *Fluoreszenz organischer Verbindungen*, Vandenhoeck & Ruprecht, Göttingen, **1951**.

[14] a) "Dye Loaded Zeolite Material": G. Calzaferri (DCB, Universität Bern, Switzerland), US Patent 6,932,919 B2, **2005**, Priority Date Nov. 3, 2000, Licenced by Clariant International Ltd; b) H. Maas, G. Calzaferri, *Angew. Chem.* **2002**, *114*, 2389; *Angew. Chem. Int. Ed.* **2002**, *41*, 2284.

[15] C. Minkowski, G. Calzaferri, *Angew. Chem.* **2005**, *117*, 5459; *Angew. Chem. Int. Ed.* **2005**, *44*, 5325.

[16] G. Calzaferri, A. Zabala Ruiz, H. Li, S. Huber (DCB, University Bern, Switzerland), Patentschrift 01266/05, **2005**.

[17] J. S. Batchelder, A. H. Zewail, T. Cole, *Appl. Opt.* **1979**, *18*, 3090.

[18] H. Maas, A. Khatyr, G. Calzaferri, *Microporous Mesoporous Mater.* **2003**, *65*, 233.

[19] S. J. Mason, S. Balasubramanian, *Org. Lett.* **2002**, *4*, 4261.

[20] S. Huber, G. Calzaferri, *Angew. Chem.* **2004**, *116*, 6906; *Angew. Chem. Int. Ed.* **2004**, *43*, 6738.

 © 2006 Wiley-VCH Verlag GmbH & Co. KGaA, Weinheim

Surface Chemistry

DOI: 10.1002/anie.200600075

Facile Monolayer Assembly of Fluorophore-Containing Zeolite Rods in Uniform Orientations for Anisotropic Photoluminescence**

*Jin Seok Lee, Hyunjin Lim, Kwang Ha, Hyeonsik Cheong, and Kyung Byung Yoon**

Microparticles, like atoms, small molecules, and nanoparticles, will someday be used routinely in chemistry and materials science as a class of building blocks. It is therefore necessary to start developing methods for organizing them into larger organized entities and to explore practical applications of the organized entities.[1–4] Thus, zeolite microcrystals have been organized in the form of monolayers on various substrates. For example, Mallouk and co-workers covalently assembled monolayers of zeolite Y mircrocrystals on the surface of SnO_2-coated glass electrodes by using dimethoxysilyl groups as tethers.[5] Yan and Bein similarly assembled monolayers of zeolite A crystals on gold electrodes through trimethoxysilyl tethers.[6] Calzaferri and co-workers assembled monolayers of zeolite A microcrystals on glassy carbon electrodes by using polystyrene as the glue.[7] Tsapatsis and co-workers assembled monolayers of zeolite A crystals on Si substrates through ionic linkages between the substrates and zeolite microcrystals.[8] The research groups of Calzaferri,[9] Tsapatsis,[8] as well as Ban and Takahashi[10] also demonstrated the assembly of a monolayer of zeolite A microcrystals through physical adsorption of the zeolite crystals onto substrates through slow evaporation of droplets of aqueous solutions of zeolite microparticles placed on substrates or by dip-coating the substrates. Similarly, Bein and co-workers demonstrated the aligned growth of zincophosphate crystals on substrates.[11]

[*] J. S. Lee, Dr. K. Ha, Prof. Dr. K. B. Yoon
Center for Microcrystal Assembly
Department of Chemistry
and Program of Integrated Biotechnology
Sogang University
Seoul 121-742 (Korea)
Fax: (+82) 2-706-4269
E-mail: yoonkb@sogang.ac.kr
H. Lim, Prof. Dr. H. Cheong
Department of Physics
Sogang University
Seoul 121-742 (Korea)

[**] We thank the Ministry of Science and Technology (MOST) and Sogang University for supporting this work through the Creative Research Initiatives (CRI) and the Internal Research Fund programs, respectively. H.C. and H.L. also thank the Quantum Photonic Science Research Center supported by the Korea Science and Engineering Foundation.

Supporting information for this article is available on the WWW under http://www.angewandte.org or from the author.

We have developed methods for organizing zeolite microcrystals in the form of uniformly aligned monolayers on various substrates by inducing well-defined molecular linkages between each microcrystal and the substrates.[12–19] The resulting monolayers show high degrees of coverage, high degrees of close packing between the attached crystals, strong binding between the crystals and substrates, and high degrees of uniform orientation of the crystals. The zeolite monolayers have served as supramolecularly organized light-harvesting systems[20,21] and as excellent precursors for the preparation of continuous zeolite films with uniform orientations of the nanopores or nanochannels. The latter property makes the monolayers suitable for application as molecular sieving membranes[22,23] and nonlinear optical films.[24] The assembly of monolayers of zeolite microcrystals has also been regarded as one of the future directions of zeolite research.[25]

In our approaches, the monolayers have mostly been assembled by refluxing solutions of bare or functional-group-tethered zeolite crystals in toluene in the presence of substrates bearing functional groups.[12–18] The solutions were often stirred to keep them dispersed and to give them kinetic energy. More than 24 h were usually required to cover the majority (>90%) of the 4 cm^2 glass plates with closely packed monolayers. High degrees (>98%) of uniform orientation were obtained when the aspect ratios of the zeolite microcrystals were equal to or less than 1. However, the reflux/stirring (RS) method did not produce high coverage and uniform orientation in the case of cylindrical zeolite microcrystals with aspect ratios higher than 1. We recently discovered that sonication of the stacks of bare glass/3-chloropropyl-coated glass (CP-g)/bare glass plates in a toluene solution dispersed with bare zeolite crystals leads to the 4 cm^2 glass plates being fully covered with very tightly packed monolayers of zeolite microcrystals within two minutes.[19] This method was named "sonication with stacking" (SS). We now report that the SS method is also highly effective for assembling cylindrical zeolite crystals with aspect ratios of up to 3 in vertically oriented monolayers, and that the monolayers give anisotropic photoluminescence in a high dichroic ratio, when fluorescent molecules were incorporated in the channels of zeolite L along the channel directions. The crystals self-assembled into horizontally oriented monolayers when the zeolite L crystals had a hexagonal columnar morphology.

Cylindrical zeolite L crystals with dimensions of 1×2–3 μm (diameter × length) and hexagonal columnar zeolite L crystals of 1×4–5 μm (width × length) used in the current study were prepared according to procedures described previously.[26] Pyronin B ions (PyB^+, Figure 1a) were incorporated into the channels of zeolite L crystals by ion exchange of the K^+ ions of the zeolites with PyB^+ ions in water. Since the length of the PyB^+ ion (16.3 Å) is longer than the width of the zeolite L lobe (12.6 Å, Figure 1b), the incorporated PyB^+ ions are likely to be lined up along the direction of the channel (Figure 1c) with a tilt angle of less than 20°.[21] The surfaces of the PyB^+-containing zeolite L [(PyB^+)L] crystals were subsequently treated with (3-aminopropyl)trimethoxysilane (AP-TMS) to tether 3-aminopropyl (AP) groups onto their surfaces and to prevent the egress of the incorporated PyB^+

 InterScience © 2006 Wiley-VCH Verlag GmbH & Co. KGaA, Weinheim

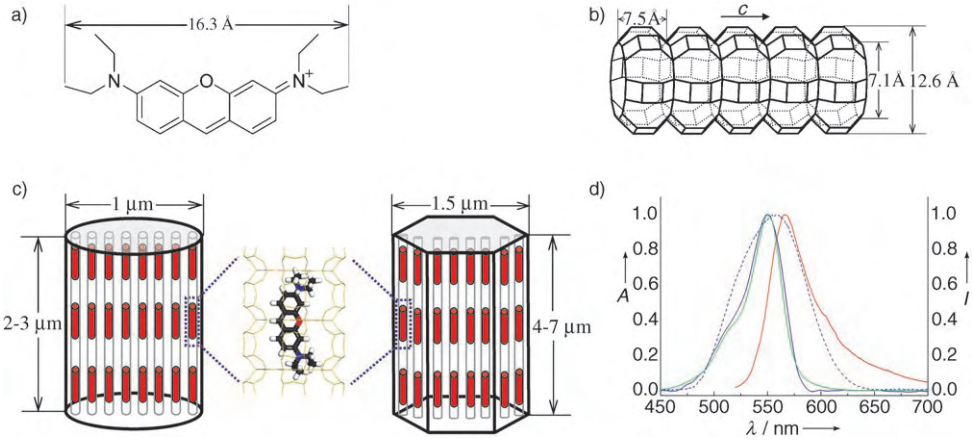


Figure 1. a) Molecular structure of the PyB^+ ion. The estimated length is 16.3 Å. b) The zeolite L channel consists of 7.5 Å long lobes with a pore opening of 7.1 Å. The internal width of a lobe is 12.6 Å, which is smaller than the length of the PyB^+ ion. c) Illustrations of PyB^+-containing cylindrical (left) and hexagonal columnar (right) zeolite L crystals with their dimensions. The red cylinders represent PyB^+ ions positioned in the channel direction. The middle diagram illustrates the imagined position of a PyB^+ ion positioned in the channel direction. d) The diffuse-reflectance spectrum of PyB^+-containing zeolite L crystals (blue dashed curve, $\lambda_{max} = 558$ nm), the excitation spectrum of PyB^+-containing zeolite L crystals dispersed in glycerol (solid blue curve, $\lambda_{max} = 550$ nm), the absorption spectrum of PyB^+ in methanol (green curve, $\lambda_{max} = 551$ nm), and the isotropic fluorescence spectrum of PyB^+-containing zeolite L crystals dispersed in glycerol (red curve, $\lambda_{E_{max}} = 567$ nm).

ions from the channels into the solution (glycerol) during the measurement of the anisotropic photoluminescence. CP-g plates ($1.8 \times 1.8\ cm^2$) were prepared by treating bare glass plates with (3-chloropropyl)trimethoxysilane (CP-TMS). The diffuse-reflectance absorption spectrum of the dry (PyB^+)L crystals and the fluorescence spectra of (PyB^+)L crystals dispersed in glycerol are shown in Figure 1 d.

When cylindrical AP-coated (PyB^+)L (cyl-AP-(PyB^+)L) crystals were attached onto CP-g plates by the SS method over two minutes the crystals self-assembled very tightly and vertically, as shown by scanning electron microscopy (SEM; Figure 2 a). In contrast, hexagonal columnar AP-coated (PyB^+)L (hex-AP-(PyB^+)L) crystals self-assembled horizontally (Figure 2 b). Such a difference in orientation arises from the tendency of the microcrystals to be attached onto substrates through their largest face (Figure 3). Consistent with the SEM images, X-ray diffraction of the monolayers of cyl-AP-(PyB^+)L crystals show signals only from the (00*c*) planes (Figure 2 c), while the monolayers of hex-AP-(PyB^+)L crystals give signals only from the (*a*00) planes (Figure 2 d). The X-ray data revealed that the degrees of uniform orientation on the 4-cm^2 glass plates were higher than 99.9 %.

The degree of close packing and the degree of vertical orientation of cyl-AP-(PyB^+)L crystals decreased significantly when the monolayer assembly was carried out for two minutes by sonication but without interposing the CP-g plates between the bare glass plates (SW method; Figure 2 e). When the RS method was applied instead of the SS and SW methods, the degree of close packing was very poor and the crystals tended to attach onto the CP-g plates horizontally (Figure 2 f), even after reaction for 24 h. The above two results reveal that strong agitation is very important to attach long cylindrical microcrystals vertically and for the remarkable superiority of the SS method over SW and RS methods in terms of coverage, close packing, and uniform orientation during the assembly of a monolayer of long cylindrical microcrystals in the upright position.

The CP-g plate covered with cyl-AP-(PyB^+)L crystals on both sides in vertical orientations is denoted as v-(PyB^+)L-g. The normalized polarized fluorescence spectra obtained from v-(PyB^+)L-g are shown in Figure 4 a. The vertical and horizontal components of the fluorescence spectrum obtained by exciting the v-(PyB^+)L-g stacks with vertically and horizontally polarized laser beams (514.5 nm) are denoted as S_{vVV}, S_{vVH}, S_{vHV}, and S_{vHH}. The subscripts represent the orientation of the zeolite L crystal on the glass, the orientation of the polarized incident light, and the orientation of the polarizer to the detector, respectively.

The corresponding intensities at the maximum-emission wavelengths ($\lambda_{E_{max}}$) are denoted as I_{vVV}, I_{vVH}, I_{vHV}, and I_{vHH}, respectively, with $\lambda_{E_{max}}$ values of 567, 570, 570, and 570 nm, respectively. The $\lambda_{E_{max}}$ value of PyB^+ in glycerol (S_{GL}) was 577 nm, and the corresponding band widths (W_{fwhm}) were 0.18, 0.23, 0.24, 0.23, and 0.16 eV, respectively. Since all the PyB^+ ions residing within the channels are vertically oriented, they are excited only by vertically polarized light and the fluorescence from them must also be vertically polarized. Therefore, the S_{vVH}, S_{vHV}, and S_{vHH} bands are assigned as those arising from randomly oriented PyB^+ ions on the external surfaces. The similarities of the $\lambda_{E_{max}}$ (570 nm) and W_{fwhm} values (ca. 0.23 eV) also support this assignment (see the Supporting Information). The blue shift of the S_{vVV} band relative to those of S_{vVH}, S_{vHV}, and S_{vHH} is attributed to the confinement effect of the ion in the narrow channel.[27]

Figure 4 b shows the anisotropic fluorescence spectra for S_{vVV} and S_{vVH}. The inset shows the angle-dependent change of $I_{v\theta}/I_{vVH}$, where $I_{v\theta}$ represents the intensity of the spectrum of v-(PyB^+)L-g at $\lambda_{E_{max}}$ at various angles (θ) under vertical excitation. The I_{vVV}/I_{vVH} ratio was 8.9:1, which is about double that obtained by Tolbert and co-workers (4.5:1) for polymer-containing mesoporous silica.[28,29] Thus, this current study demonstrates a novel and highly effective way of preparing supramolecularly organized systems that give strongly anisotropic photoluminescence. Figure 4 c shows the anisotropic fluorescence spectra of the S_{vHH} and S_{vHV} components. The inset shows the angle-dependent change of $I_{v\theta}/I_{vHV}$, where $I_{v\theta}$ represents the intensity of the spectrum of v-(PyB^+)L-g at $\lambda_{E_{max}}$ at various values of θ under horizontal excitation.

 © 2006 Wiley-VCH Verlag GmbH & Co. KGaA, Weinheim

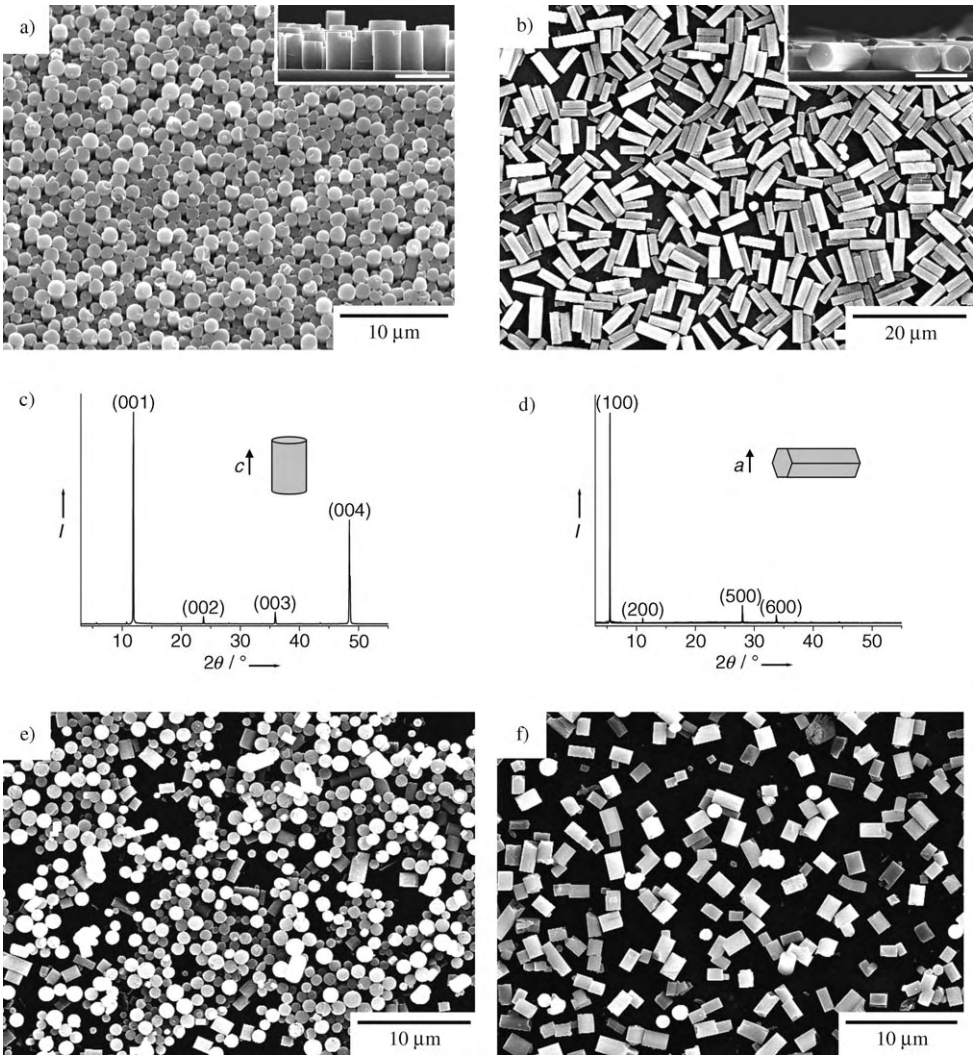


Figure 2. a) SEM image of v-(PyB^+)L-g showing the very tight close packing and vertical orientations of the zeolite L crsytals. The inset shows an SEM image of the cross-section. Scale bar = 2 μm. b) SEM image of h-(PyB^+)L-g. The inset shows an SEM image of the cross-section. Scale bar = 2 μm. c) X-ray diffraction pattern of v-(PyB^+)L-g showing the diffraction lines from (00*c*) planes of zeolite L with $c = 1$, 2, 3, and 4 at $2\theta = 11.9$, 23.8, 35.9, and 48.5°, respectively. d) X-ray diffraction pattern of h-(PyB^+)L-g showing the diffraction lines from (*a*00) planes of zeolite L with $a = 1$, 2, 5, and 6 at $2\theta = 5.5$, 11.1, 28.0, and 33.7°, respectively. The absence of diffraction lines arising from (300) and (400) planes occurs because their intrinsic intensities are very small, that is, 0.7 and 1.5% with respect to the diffraction intensity of the (100) plane. e) SEM image of the monolayer of cyl-AP-(PyB^+)L crystals assembled on CP-g by the SW method for 2 min showing that the poor degrees of close packing and vertical orientation. f) SEM image of the monolayer of cyl-AP-(PyB^+)L crystals assembled on CP-g by the RS method over 24 h.

The I_{vHH}/I_{vHV} ratio was 1.8:1, which is smaller than that of the PyB^+ ion in glycerol (2.8:1, see the Supporting Information). This result may arise as a consequence of faster energy transfer between the external PyB^+ ions as a result of aggregation. Furthermore, the average I_{vVH}/I_{vHV} ratio was 1.8:1. This value indicates that 44% of the value of I_{vVH} arises from energy transfer from intrachannel PyB^+ ions to the external PyB^+ ions. The fact that the W_{fwhm} value of the S_{vVH} band is greater than that of S_{vVV} at longer wavelength regions (Figure 4a) and that $\lambda_{E_{max}}$ is shorter for S_{vVV} than S_{vVH} further support a directional energy transfer. As noted, the direction of energy transfer is opposite to the case reported by Tolbert and co-workers.[28]

The CP-g plate covered with hex-AP-(PyB^+)L crystals on both sides in horizontal orientations is denoted as h-(PyB^+)L-g. The four polarized fluorescence spectra obtained from a stack of three h-(PyB^+)L-g are denoted as S_{hHH}, S_{hHV}, S_{hVH}, and S_{hVV} (see the Supporting Information for spectra). The corresponding intensities at $\lambda_{E_{max}}$ are denoted as I_{hHH}, I_{hHV}, I_{hVH}, and I_{hVV}. The I_{hHH}/I_{hHV} ratio was 3.0:1. The reason for the I_{hHH}/I_{hHV} ratio being about 1/3 of that of I_{vVV}/I_{vVH} (8.9:1) is because the hex-AP-(PyB^+)L crystals are oriented randomly on the glass plane, even though they are all horizontally attached to the glass plane, and the integration of $(\cos\theta)^2$ over the angle range 0–180° gives 1/3. If the hex-AP-(PyB^+)L crystals were uniformly oriented in the x and y directions as well, then the I_{hHH}/I_{hHV} ratio would be approximately 9:1.

Although the assembly of monolayers of zeolite rods in a vertical orientation has been recognized as being important because of the applicability of the aligned zeolite rods to second harmonic generation, molecular sieve membranes, and macroscopic alignments of guest molecules, only a few examples have been reported. Caro et al. developed a method driven by an electric field to vertically orient the related long MFI-type zeolite rods.[30] Chao and co-workers used anodized alumina discs to grow vertical metal-doped aluminophosphate molecular sieves.[31] However, the degrees of close packing and uniform orientation achieved by the above cases cannot compete with those of v-(PyB^+)L-g.

In conclusion, we have described how zeolite L monolayers can be prepared on glass in two orientations. The organized monolayers can be applied as novel supramolecularly organized systems for the demonstration of anisotropic photoluminescence in high dichroic ratios,[32] to study energy-transfer dynamics between internally and externally placed fluorophores,[33,34] and to develop zeolite-based advanced materials. The vertically assembled zeolite L monolayers also have the potential to be transformed into continuous films with one-dimensional channels all oriented perpendicular to the substrate, an arrangement that has been shown to be very difficult to obtain.[35]

 © 2006 Wiley-VCH Verlag GmbH & Co. KGaA, Weinheim

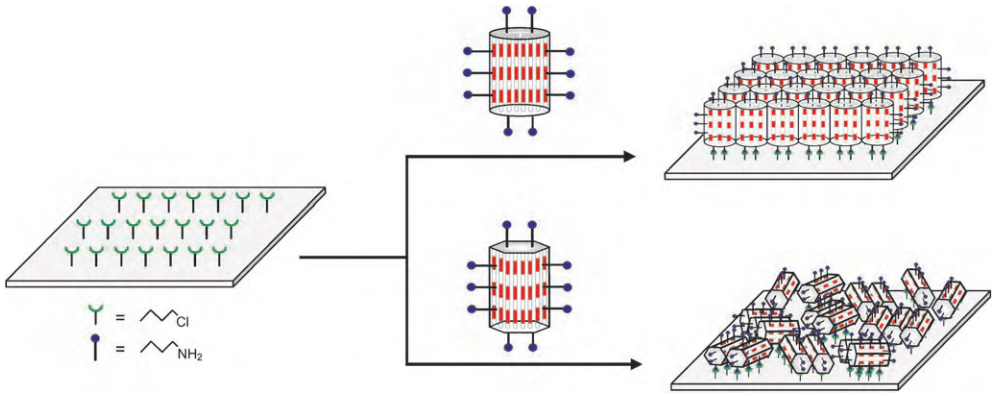


Figure 3. Schematic illustration of the morphology-dependent change of the orientation of zeolite L crystals during assembly of the monolayer by the SS method. While the cyl-AP-(PyB^+)L crystals assemble into a vertically oriented monolayer, the hex-AP-(PyB^+)L crystals assemble into a horizontally oriented monolayer on CP-g plates.

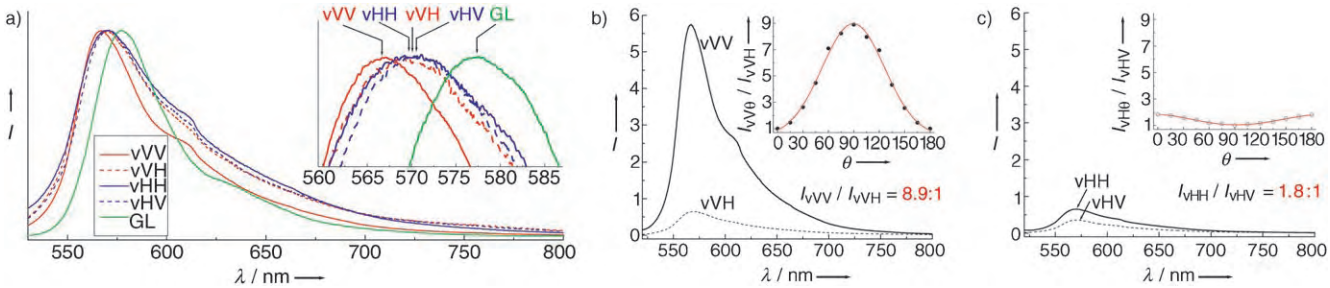


Figure 4. Anisotropic fluorescence spectra and dichroic ratios: a) Normalized anisotropic fluorescence spectra (S_{vVV}, S_{vVH}, S_{vHV}, and S_{vHH}) of v-(PyB^+)L-g and the fluorescence spectrum of the 1 μM solution of PyB^+ ions in glycerol (S_{GL}). The inset shows the peak positions of the spectra. b) S_{vVV} and S_{vVH}. c) S_{vHH} and S_{vHV}. The insets in (b) and (c) show the angle-dependent changes of $I_{vV\theta}/I_{vVH}$ and $I_{vH\theta}/I_{vHV}$, respectively.

Experimental Section

Materials: The cylindrical and hexagonal columnar zeolite L crystals were prepared according to procedures described previously.[26] $PyB^+FeCl_4^-$, AP-TMS, CP-TMS, dimethylsulfoxide (DMSO), and glycerol were purchased from Aldrich and used as received. PyB^+ ions were incorporated into zeolite L crystals (3 g) by aqueous ion exchange of K^+ ions in zeolite L with $PyB^+FeCl_4^-$ (180 mL, 0.1 mM) under reflux (90 min). After rigorously washing the PyB^+-exchanged zeolite L with distilled deionized water, it was further washed with DMSO by soxhlet extraction for more than 24 h until no further $PyB^+FeCl_4^-$ was detected in the DMSO. The washing step with DMSO is highly recommended to rigorously remove the physisorbed $PyB^+FeCl_4^-$ salts from the external surfaces of the zeolite powders. Analysis of the amount of PyB^+ ions according to the method of Minkowski and Calzaferri[36] revealed that the incorporated amount corresponded to 1.7 ions per channel. Although the incorporated amount was rather low, the incorporated PyB^+ ions were aligned with the channel direction as reported by Calzaferri et al.[21] (see the Supporting Information for more evidence). The AP-tethered PyB^+-containing zeolite L crystals and CP-tethered glass (CP-g) plates were prepared according to the standard method developed in our group.[14] v-(PyB^+)L-g and h-(PyB^+)L-g were prepared by the SS method according to the procedure describe in the Supporting Information.[19]

Measurements of anisotropic photoluminescence: The setup used was basically the same as that described in the literature.[29] The layout and the detailed description is given in the Supporting Information. Three v-(PyB^+)L-g or h-(PyB^+)L-g plates were placed horizontally on a stack of five bare glass plates placed horizontally in a glass container ($20 \times 20 \times 10$ mm^3) charged with glycerol as an index-matching fluid. A vertically or horizontally polarized beam ($\lambda = 514.5$ nm) generated from an Ar^+ ion laser (Coherent) was introduced into the stack of v-(PyB^+)L-g or h-(PyB^+)L-g, and the produced fluorescent light was introduced into a spectrometer (Horiba Jobin Yvon, TRIAX 550) equipped with a charge-coupled device (CCD) array (1024×512) detector after passing it through an achromatic $\lambda/2$ plate to rotate the polarization to 0° and a linear polarizer fixed at 0° (horizontal). Care was taken to ascertain that the detection system did not introduce any systematic anisotropy. This was checked by analysis of PyB^+ dissolved in glycerol with circularly polarized laser light and obtaining the ratio of vertically polarized to horizontally polarized luminescence intensity of 1.05:1.

Received: January 8, 2006
Revised: May 17, 2006
Published online: July 11, 2006

Keywords: fluorophores · luminescence · monolayers · zeolites

[1] a) N. B. Bowden, M. Weck, I. S. Choi, G. M. Whitesides, *Acc. Chem. Res.* **2001**, *34*, 231; b) G. A. Ozin, *Chem. Commun.* **2000**, 419.
[2] A. Blanco, E. Chomski, S. Grabtchak, M. Ibisate, S. John, S. W. Leonard, C. Lopez, F. Meseguer, H. Miguez, J. P. Mondia, G. A. Ozin, O. Toader, H. M. van Driel, *Nature* **2000**, *405*, 437.
[3] B. T. Holland, C. F. Blanford, A. Stein, *Science* **1998**, *281*, 538.
[4] J. S. Lee, Y.-J. Lee, E. L. Tae, Y. S. Park, K. B. Yoon, *Science* **2003**, *301*, 818.

 © 2006 Wiley-VCH Verlag GmbH & Co. KGaA, Weinheim

[5] Z. Li, C. Lai, T. E. Mallouk, *Inorg. Chem.* **1989**, *28*, 178.
[6] Y. Yan, T. Bein, *J. Phys. Chem.* **1992**, *96*, 9387.
[7] a) J.-W. Li, K. Pfanner, G. Calzaferri, *J. Phys. Chem.* **1995**, *99*, 12368; b) J.-W. Li, G. Calzaferri, *J. Chem. Soc. Chem. Commun.* **1993**, 1430.
[8] L. C. Boudreau, J. A. Kuck, M. Tsapatsis, *J. Membr. Sci.* **1999**, *152*, 41.
[9] P. Lainé, R. Seifert, R. Giovanoli, G. Calzaferri, *New J. Chem.* **1997**, *21*, 453.
[10] T. Ban, T. Ohwaki, Y. Ohya, Y. Takahashi, *Angew. Chem.* **1999**, *111*, 3590; *Angew. Chem. Int. Ed.* **1999**, *38*, 3324.
[11] a) S. Feng, T. Bein, *Nature* **1994**, *368*, 834; b) S. Feng, T. Bein, *Science* **1994**, *265*, 1839; c) T. Bein, *Chem. Mater.* **1996**, *8*, 1636.
[12] A. Kulak, Y.-J. Lee, Y. S. Park, K. B. Yoon, *Angew. Chem.* **2000**, *112*, 980; *Angew. Chem. Int. Ed.* **2000**, *39*, 950.
[13] S. Y. Choi, Y.-J. Lee, Y. S. Park, K. Ha, K. B. Yoon, *J. Am. Chem. Soc.* **2000**, *122*, 5201.
[14] K. Ha, Y.-J. Lee, H. J. Lee, K. B. Yoon, *Adv. Mater.* **2000**, *12*, 1114.
[15] K. B. Yoon, *Bull. Korean Chem. Soc.* **2006**, *27*, 17.
[16] G. S. Lee, Y.-J. Lee, K. B. Yoon, *J. Am. Chem. Soc.* **2001**, *123*, 9769.
[17] J. S. Park, G. S. Lee, Y.-J. Lee, Y. S. Park, K. B. Yoon, *J. Am. Chem. Soc.* **2002**, *124*, 13366.
[18] J. S. Park, Y.-J. Lee, K. B. Yoon, *J. Am. Chem. Soc.* **2004**, *126*, 1934.
[19] J. S. Lee, K. Ha, Y.-J. Lee, K. B. Yoon, *Adv. Mater.* **2005**, *17*, 837.
[20] G. Calzaferri, O. Bossart, D. Brühwiler, S. Huber, C. Leiggener, M. K. Van Veen, A. Z. Ruiz, *C. R. Chim.* **2006**, *9*, 214.
[21] G. Calzaferri, S. Huber, H. Maas, C. Minkowski, *Angew. Chem.* **2003**, *115*, 3860; *Angew. Chem. Int. Ed.* **2003**, *42*, 3732.
[22] Z. Lai, G. Bonilla, I. Diaz, J. G. Nery, K. Sujaoti, M. A. Amat, E. Kokkoli, O. Terasaki, R. W. Thompson, M. Tsapatsis, D. G. Vlachos, *Science* **2003**, *300*, 456.
[23] G. T. P. Mabande, S. Ghosh, Z. Lai, W. Schwieger, M. Tsapatsis, *Ind. Eng. Chem. Res.* **2005**, *44*, 9086.
[24] H. S. Kim, S. M. Lee, K. Ha, C. Jung, Y.-J. Lee, Y. S. Chun, D. Kim, B. K. Rhee, K. B. Yoon, *J. Am. Chem. Soc.* **2004**, *126*, 673.
[25] T. Bein, *Mater. Res. Soc. Bull.* **2005**, *30*, 713.
[26] Y.-J. Lee, J. S. Lee, K. B. Yoon, *Microporous Mesoporous Mater.* **2005**, *80*, 237.
[27] F. Marquez, C. M. Zicovich-Wilson, A. Corma, E. Palomares, H. Garcia, *J. Phys. Chem. B* **2001**, *105*, 9973.
[28] T.-Q. Nguyen, J. Wu, V. Doan, B. J. Schwartz, S. H. Tolbert, *Science* **2000**, *288*, 652.
[29] J. Wu, A. F. Gross, S. H. Tolbert, *J. Phys. Chem. B* **1999**, *103*, 2374.
[30] J. Caro, G. Finger, J. Kornatowski, J. Richter-Mendau, L. Werner, B. Zibrowius, *Adv. Mater.* **1992**, *4*, 273.
[31] C.-N. Wu, K.-J. Chao, T.-G. Tsai, Y.-H. Chiou, H.-C. Shih, *Adv. Mater.* **1996**, *8*, 1008.
[32] M. Grell, D. D. C. Bradley, *Adv. Mater.* **1999**, *11*, 895.
[33] a) H. Mass, G. Calzaferri, *Angew. Chem.* **2002**, *114*, 2389; *Angew. Chem. Int. Ed.* **2002**, *41*, 2284; b) S. Huber, G. Calzaferri, *ChemPhysChem* **2004**, *5*, 239.
[34] B. J. Schwartz, *Annu. Rev. Phys. Chem.* **2003**, *54*, 141.
[35] M. C. Lovallo, M. Tsapatsis, *Chem. Mater.* **1996**, *8*, 1579.
[36] C. Minkowski, G. Calzaferri, *Angew. Chem.* **2005**, *117*, 5459; *Angew. Chem. Int. Ed.* **2005**, *44*, 5325.

 © 2006 Wiley-VCH Verlag GmbH & Co. KGaA, Weinheim

Microcontact Printing

DOI: 10.1002/anie.200601090

"Click" Chemistry by Microcontact Printing**

Dorota I. Rozkiewicz, Dominik Jańczewski, Willem Verboom, Bart Jan Ravoo, and David N. Reinhoudt**

Microcontact printing (μCP) is commonly used to pattern self-assembled monolayers (SAMs) as etch resists or chemical templates on gold and silicon oxide substrates.[1] However, μCP can also be used for chemical synthesis on gold and silicon oxide in the nanoscale confinement between stamp and substrate. Amines can be printed onto reactive anhydride SAMs.[2] Peptides can be synthesized by printing N-protected amino acids onto an amine SAM.[3] It has been proposed that the confinement of the ink at the interface between the elastomeric stamp and the SAM, in combination with the preorganization of the reactants in the monolayer, facilitates the formation of covalent peptide bonds.[3] Recently, we demonstrated imine formation through the μCP of amines on aldehyde SAMs[4] and applied this chemistry to directing the immobilization of cytophilic proteins.[5] Herein, we present a Huisgen 1,3-dipolar cycloaddition, as a representative example of the Sharpless "click" chemistry,[6] induced without any catalyst by μCP of acetylenes onto azido-terminated SAMs on silicon oxide substrates.

Click chemistry includes a range of reactions that proceed in high yield under ambient conditions, preferably in water, with regioselectivity and a broad tolerance of functional groups.[6] The Cu-catalyzed 1,3-dipolar cycloaddition reaction of azides and acetylenes is known as the "cream of the crop" of all click reactions.[7] This cycloaddition is irreversible and proceeds in quantitative yield without any side products in many solvents, including water. Acetylenes and azides are stable starting materials that do not react among themselves. Azides are known for their ease of introduction, and both azides and acetylenes are tolerant of many other functionalities. The triazole group is a thermally and hydrolytically stable, conjugated linkage. Increasingly, click chemistry is used for the preparation of biological conjugates and the immobilization of biomacromolecules.[8] Triazole formation

[*] D. I. Rozkiewicz, Dr. D. Jańczewski, Dr. W. Verboom, Dr. B. J. Ravoo, Prof. Dr. D. N. Reinhoudt
Laboratory of Supramolecular Chemistry and Technology
MESA+ Institute for Nanotechnology
University of Twente
P.O. Box 217, 7500 AE Enschede (The Netherlands)
Fax: (+31) 53-489-4645
E-mail: b.j.ravoo@utwente.nl
d.n.reinhoudt@utwente.nl

[**] D.N.R. is grateful to Prof. C. Chidsey for discussions. This work was supported by NanoImpuls/NanoNed, the nanotechnology program of the Dutch Ministry of Economic Affairs (grant TTF6329).

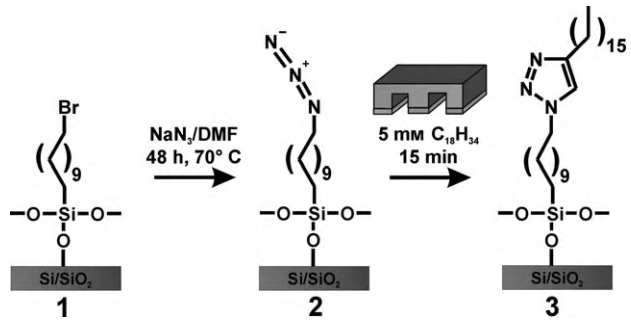
Supporting information for this article is available on the WWW under http://www.angewandte.org or from the author.

WILEY InterScience DISCOVER SOMETHING GREAT
© 2006 Wiley-VCH Verlag GmbH & Co. KGaA, Weinheim

on surfaces was applied for the modification of SAMs on gold substrates,[9] SAMs on silicon oxide,[10] carbon nanotubes,[11] and polymer adhesives.[12] Azido-terminated monolayers were used for the immobilization of substituted acetylenes (including ferrocene and oligonucleotides[9,10,13]) by triazole linkage.

The majority of Huisgen reactions—in particular those that involve electron-rich acetylenes—need a Cu^{I} catalyst, which may accelerate the reaction by a factor of 10^7. The Cu^{I} catalyst is usually generated in situ from Cu^{II} by an excess of reducing agent, such as sodium ascorbate.[7] Here, we show that the high local concentration of reagents in the contact area of the elastomeric stamp and the monolayer surface is sufficient to obtain complete conversion within minutes of contact time, even without a Cu catalyst. In particular, for the immobilization of biomolecules it is advantageous to exclude toxic Cu catalysts.

Azido-terminated SAMs on silicon oxide were prepared by the substitution of a bromo-terminated monolayer with NaN_3.[14] The bromo-terminated SAM was obtained by the immersion of a 1×1-cm piece of silicon wafer (cleaned and activated with piranha solution) in a solution of 11-bromoundecyltrichlorosilane in toluene (0.1%, v/v) for 20 min at 20°C. A saturated solution of NaN_3 in DMF (48 h at 70°C) was used to substitute the bromine for the azido group.[14] The substrate was rinsed with MilliQ water and ethanol and dried with nitrogen. The preparation of the azido-terminated SAMs and the subsequent click chemistry by μCP of acetylenes are outlined in Scheme 1.



Scheme 1. Click chemistry by μCP. **1**: Bromo-terminated SAM on a Si/SiO_2 substrate. **2**: Azido-terminated SAM. **3**: Triazole SAM after μCP of 1-octadecyne onto azido-terminated SAM.

As a first illustration of the potential of μCP of acetylenes on azido-terminated SAMs on a silicon substrate, 1-octadecyne was printed onto azido SAM **2** with a 1×1-cm poly(dimethylsiloxane) (PDMS) stamp with line features of 3×5 μm. The stamp was inked in a solution of 1-octadecyne in ethanol (5 mM) for 1 min, dried with nitrogen, and brought into contact with the substrate SAM **2** for 15 min with a load of 35 g to ensure good contact and constant applied load during the entire printing time. After extensive rinsing with ethanol, the substrate was imaged with atomic force microscopy (AFM). Figure 1 shows the pattern made by printing 1-octadecyne on substrate **2**. Evidently, the 3×5-μm line features of the stamp are reproduced faithfully on the

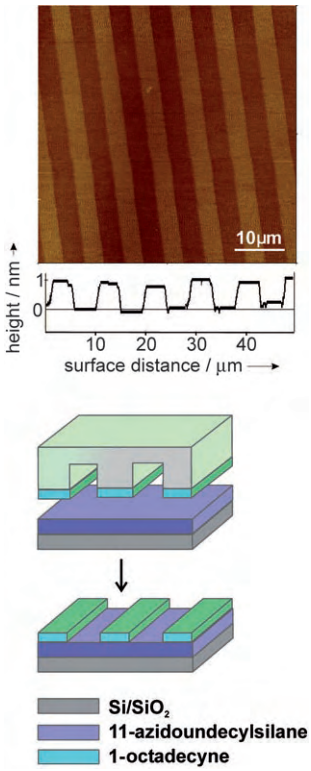


Figure 1. Tapping-mode AFM image (50×50 μm) and line section of a 3×5-μm line pattern obtained by printing 1-octadecyne onto azido-terminated SAM **2** on a silicon oxide substrate.

substrate. The average height of the 3-μm-wide lines in the pattern is approximately 1 nm.

To verify triazole formation on the azido SAM, we compared the reaction between azido SAM **2** and 1-octadecyne induced by μCP and from solution. We used a flat, featureless PDMS stamp to demonstrate triazole formation by μCP. The flat stamp was inked with a solution of 1-octadecyne in ethanol (5 mM) and brought into conformal contact with the azido-terminated SAM for 15 min and with a load of 35 g. After printing, the substrate was rinsed with ethanol and dried with nitrogen. To investigate the reaction with acetylene from solution, the azido-terminated SAM was exposed to a solution of 1-octadecyne in ethanol (5 mM) for 48 h at room temperature. After reaction, the substrate was rinsed with ethanol and dried with nitrogen.

The X-ray photoelectron spectroscopy (XPS) spectrum of bromo-terminated SAM **1** shows a pronounced Br(3d) peak at 70.5 eV (Figure 2). After substitution with NaN_3, the Br(3d) peak disappeared and a N(1s) peak appeared at 400 eV, which confirmed a complete reaction. When 1-octadecyne was introduced over 15 min by μCP using a flat PDMS stamp (**3**) or alternatively in 48 h by reaction from solution (**3***), the intensity of the C(1s) peak increased, while the intensity of the N(1s) peak decreased. The C/N ratio calculated from the elemental composition was 9.7:1 when the triazole monolayer was formed from solution, whereas after printing it was 10.8:1. The theoretical C/N ratio is 10:1. Hence, XPS indicates that the triazole is formed by reaction

 © 2006 Wiley-VCH Verlag GmbH & Co. KGaA, Weinheim

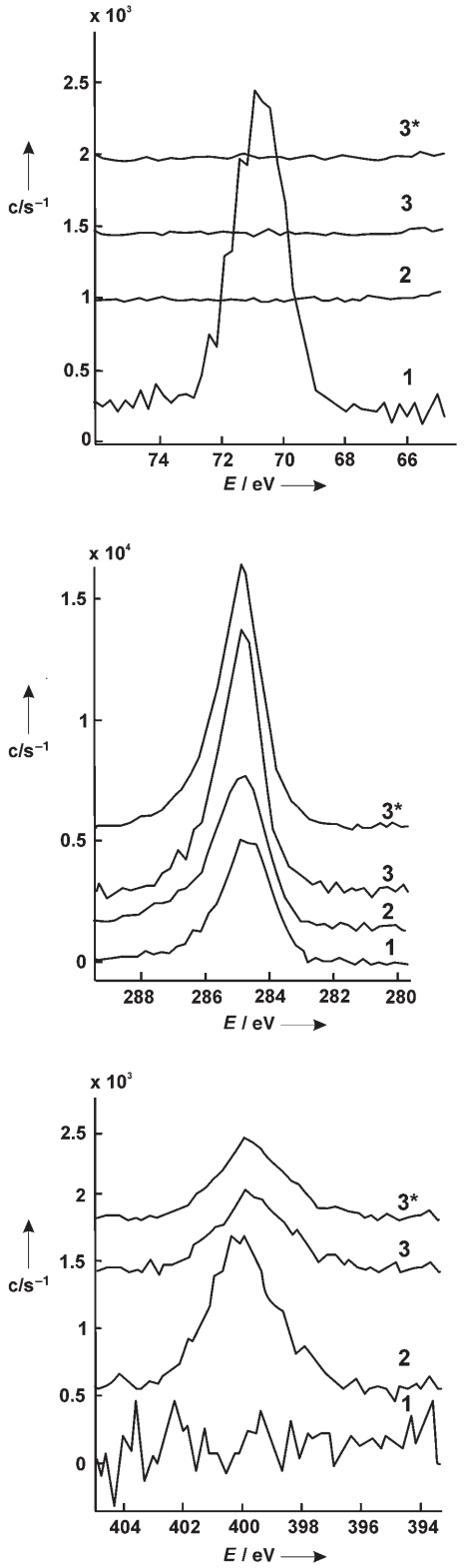


Figure 2. Elemental XPS scans for a) bromine, b) carbon, and c) nitrogen; *E* = binding energy, c = counts. **1**: Bromo-terminated SAM. **2**: Azido-terminated SAM. **3**: Triazole SAM prepared by μCP of 1-octadecyne on SAM **2** for 15 min. **3***: Triazole SAM prepared by reaction from solution of 1-octadecyne with SAM **2** for 48 h.

from solution as well as by using μCP, but the cycloaddition occurs much faster in the latter case.

Grazing-angle infrared spectroscopy (GAIRS) of bromo-terminated SAM **1** revealed the typical methylene bands at 2924 and 2852 cm^{-1} (Figure 3, **1**). After exposure of the

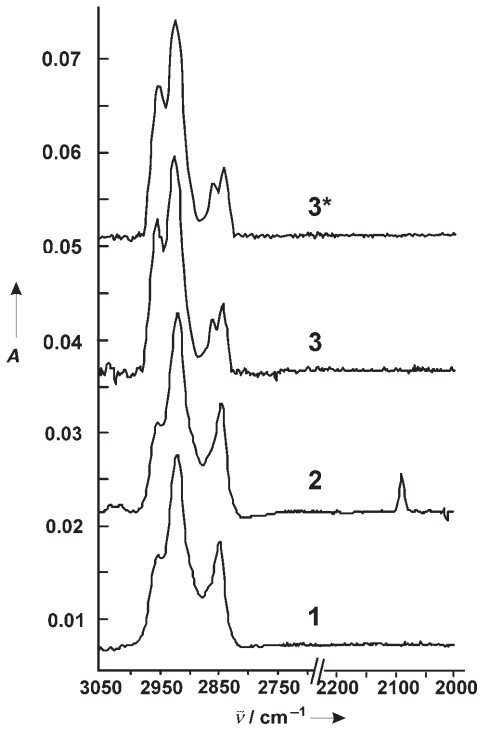


Figure 3. Grazing-angle infrared spectra of functionalized monolayers on a silicon oxide substrate. **1**: Bromo-terminated SAM. **2**: Azido-terminated SAM. **3**: Triazole SAM prepared by μCP of 1-octadecyne on SAM **2** for 15 min. **3***: Triazole SAM prepared by reaction from solution of 1-octadecyne with SAM **2** for 48 h.

bromo-terminated SAM **1** to NaN_3, the azido-terminated monolayer showed an absorption at 2089 cm^{-1} ($\nu_{as}(N_3)$) in addition to the methylene absorption bands (Figure 2a, **2**). When SAM **2** was reacted for 48 h with 1-octadecyne from solution (Figure 3, **3***), the azide peak disappeared and in addition two bands responsible for methyl stretching were visible at 2960 ($\nu_{as}(CH_3)$) and 2871 cm^{-1} ($\nu_s(CH_3)$). The bands at 2935 and 2855 cm^{-1} are the methylene stretching modes. After μCP of 1-octadecyne with a flat PDMS stamp for 15 min (Figure 3, **3**), the GAIR spectrum was identical to that obtained for the reaction conducted from solution. In summary, the cycloaddition reaction is confirmed by the disappearance of the $\nu_{as}(N_3)$ peak and the appearance of the $\nu(CH_3)$ peaks.[9,10]

In addition, the cycloaddition reaction of azido SAM **2** with 1-octadecyne was monitored with ellipsometry. It was found that bromo SAM **1** has a thickness $d = 1.34 \pm 0.08$ nm and azido SAM **2** has $d = 1.48 \pm 0.10$ nm, whereas for triazole SAM **3** $d = 2.10 \pm 0.14$ nm and for triazole SAM **3*** $d = 1.88 \pm 0.17$ nm. Hence, the cycloaddition leads to a significant increase in the thickness of the SAM, consistent with the AFM height scan (Figure 1). The average increase in d (0.5–

 © 2006 Wiley-VCH Verlag GmbH & Co. KGaA, Weinheim

1.0 nm) indicates that the triazole alkyl chain is substantially tilted relative to the substrate surface.

It should be emphasized that the [2+3] cycloaddition of azides and electron-rich acetylenes such as 1-octadecyne is normally very slow in the absence of a Cu^I catalyst. Indeed, Collman et al.[9a] and Lummerstorfer and Hoffmann[10] reported that no reaction occurs between azido SAMs and electron-rich acetylenes such as 1-octyne and ethynyl ferrocene in the absence of a Cu^I catalyst.[15] To scavenge any adventitious metal-ion contamination in solvents, reactants, PDMS stamps, or substrates, the cycloaddition reaction was carried out in the presence of ethylenediaminetetraacetic acid (EDTA, 0.05 mM; see the Supporting Information). No difference was observed in the reaction of the azido SAM with 1-octadecyne, either by μCP or from solution in the presence of EDTA.

Furthermore, to illustrate the power and scope of the triazole click reaction by μCP, fluorescent alkyne LRA (lissamine rhodamine with a terminal acetylene unit) was printed on azido SAM **2** (Figure 4). The synthesis of LRA is described in the Supporting Information. Prior to printing, the PDMS stamp was oxidized with UV/ozone plasma for 30 min to increase the wettability and improve the spreading of the polar ink on the stamp. Directly after oxidation the stamp was inked with a solution of LRA in ethanol (1 mM), dried with nitrogen for 1 min, and brought into conformal contact with azido-terminated SAM **2** on a glass slide for 1 min. The substrate was vigorously rinsed with MilliQ water, sonicated in ethanol for 5 min, and dried with nitrogen. It is evident from the confocal microscopy image in Figure 4 that the 20-μm dot features of the stamp are reproduced faithfully on the substrate and that the ink is distributed homogeneously over the contact area.[16] As fluorescent alkyne LRA is still present on the surface in spite of extensive rinsing and sonication, any type of absorption other than covalent immobilization through triazole formation can be excluded. To scavenge any adventitious metal-ion contamination, μCP of LRA on SAM **2** was also performed in the presence of EDTA (0.05 mM). No change was observed (see the Supporting Information). However, when μCP of LRA was performed on an "inert" SAM of *n*-dodecyltriethoxysilane, no evidence of immobilization of LRA was found (see Supporting Information). We explain the remarkable efficiency of the click reaction of LRA printed on the azido SAM by the high local concentration of the polar ink at the surface of the oxidized PDMS stamp.

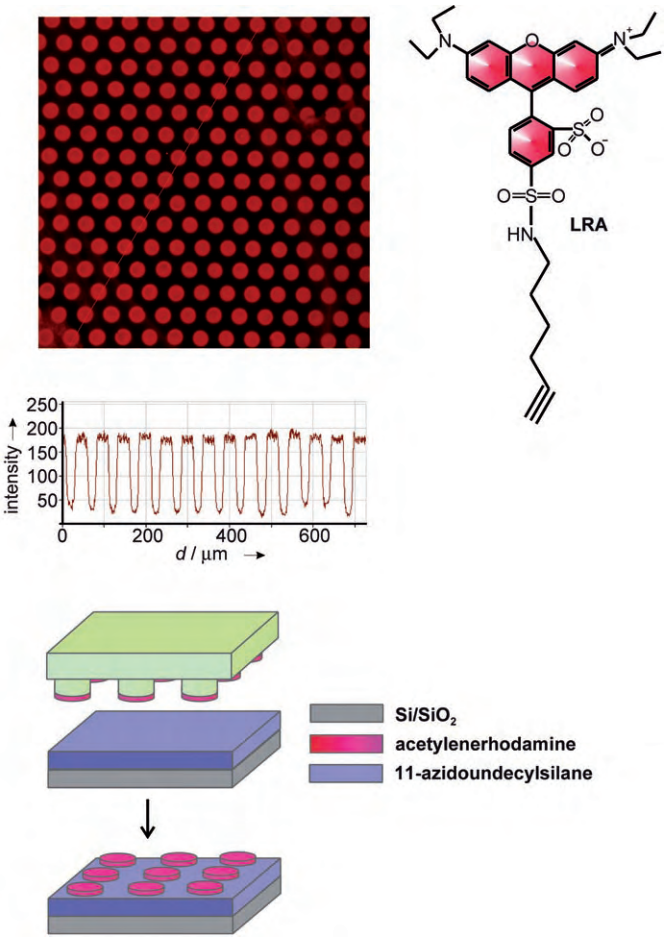


Figure 4. Top: Fluorescence microscopy image (700×700 μm) of LRA printed in 20-μm dots onto azido-terminated SAM **2**. Bottom: Schematic representation of the μCP-induced click reaction between the fluorescent alkyne LRA and the azido-terminated silane SAM on a glass slide.

In conclusion, click chemistry can be applied to the microcontact printing of acetylenes onto azido-terminated SAMs. Synthesis in the nanoscale confinement between a PDMS stamp and a reactive substrate leads to the desired product within a short period of time, without a catalyst, and under mild conditions. We envisage that click chemistry by μCP can be applied using a wide variety of acetylenes and immobilized azides, as well as azides and immobilized acetylenes. In particular, this methodology will be useful for the directed immobilization of (bio)molecules that are modified with either acetylene or azide units. Click chemistry by μCP should serve the development of biological arrays that can be obtained within a short reaction time, under mild reaction conditions with no toxic catalyst required, with high selectivity and quantitative yields, and tolerance for a wide range of functionally complex substances.

Received: March 20, 2006
Published online: July 12, 2006

Keywords: alkynes · azides · cycloaddition · microcontact printing · monolayers

[1] a) A. Kumar, G. M. Whitesides, *Appl. Phys. Lett.* **1993**, *63*, 2002–2004; b) N. L. Jeon, K. Finnie, K. Branshaw, R. G. Nuzzo, *Langmuir* **1997**, *13*, 3382–3391; c) Y. N. Xia, G. M. Whitesides, *Angew. Chem.* **1998**, *110*, 568–594; *Angew. Chem. Int. Ed.* **1998**, *37*, 551–575; d) B. Michel, A. Bernard, A. Bietsch, E. Delamarche, M. Geissler, D. Juncker, H. Kind, J.-P. Renault, H. Rothuizen, H. Schmid, P. Schmidt-Winkel, R. Stutz, H. Wolf, *IBM J. Res. Dev.* **2001**, *45*, 697–719.

[2] a) L. Yan, X.-M. Zhao, G. M. Whitesides, *J. Am. Chem. Soc.* **1998**, *120*, 6179–6180; b) L. Yan, W. T. S. Huck, X.-M. Zhao, G. M. Whitesides, *Langmuir* **1999**, *15*, 1208–1214; c) J. Lahiri, E. Ostuni, G. M. Whitesides, *Langmuir* **1999**, *15*, 2055–2060.

 © 2006 Wiley-VCH Verlag GmbH & Co. KGaA, Weinheim

[3] T. P. Sullivan, M. L. van Poll, P. Y. W. Dankers, W. T. S. Huck, *Angew. Chem.* **2004**, *116*, 4286 – 4289; *Angew. Chem. Int. Ed.* **2004**, *43*, 4190 – 4193.
[4] D. I. Rozkiewicz, B. J. Ravoo, D. N. Reinhoudt, *Langmuir* **2005**, *21*, 6337 – 6343.
[5] D. I. Rozkiewicz, Y. Kraan, M. W. T. Werten, F. A. de Wolf, V. Subramaniam, B. J. Ravoo, D. N. Reinhoudt, *Chem. Eur. J.*, DOI: 10.1002/chem.200501554.
[6] H. C. Kolb, M. G. Finn, K. B. Sharpless, *Angew. Chem.* **2001**, *113*, 2056 – 2075; *Angew. Chem. Int. Ed.* **2001**, *40*, 2004 – 2021.
[7] a) V. V. Rostovtsev, L. G. Green, V. V. Fokin, K. B. Sharpless, *Angew. Chem.* **2002**, *114*, 2708 – 2711; *Angew. Chem. Int. Ed.* **2002**, *41*, 2596 – 2599; b) C. W. Tornøe, C. Christensen, M. Meldal, *J. Org. Chem.* **2002**, *67*, 3057 – 3064; c) V. D. Bock, H. Hiemstra, J. H. van Maarseveen, *Eur. J. Org. Chem.* **2006**, 51 – 68.
[8] a) T. S. Seo, Z. M. Li, H. Ruparel, J. Y. Ju, *J. Org. Chem.* **2003**, *68*, 609 – 612; b) A. J. Link, D. A. Tirrell, *J. Am. Chem. Soc.* **2003**, *125*, 11164 – 11165; c) A. T. Poulin-Kerstien, P. B. Dervan, *J. Am. Chem. Soc.* **2003**, *125*, 15811 – 15821; d) B. Parrish, R. B. Breitenkamp, T. Emrick, *J. Am. Chem. Soc.* **2005**, *127*, 7404 – 7410; e) V. P. Mocharla, B. Colasson, L. V. Lee, S. Röper, K. B. Sharpless, C. H. Wong, H. C. Kolb, *Angew. Chem.* **2005**, *117*, 118 – 122; *Angew. Chem. Int. Ed.* **2005**, *44*, 116 – 120; f) M. Whiting, J. Muldoon, Y.-C. Lin, S. M. Silverman, W. Lindstrom, A. J. Olson, H. C. Kolb, M. G. Finn, K. B. Sharpless, J. H. Elder, V. V. Fokin, *Angew. Chem.* **2006**, *118*, 1463 – 1467; *Angew. Chem. Int. Ed.* **2006**, *45*, 1435 – 1439.
[9] a) J. P. Collman, N. K. Devaraj, C. E. D. Chidsey, *Langmuir* **2004**, *20*, 1051 – 1053; b) J. K. Lee, Y. S. Chi, I. S. Choi, *Langmuir* **2004**, *20*, 3844 – 3847; c) R. Zirbs, F. Kienberger, P. Hinterdorfer, W. H. Binder, *Langmuir* **2005**, *21*, 8414 – 8421; d) N. K. Devaraj, P. H. Dinolfo, C. E. D. Chidsey, J. P. Collman, *J. Am. Chem. Soc.* **2006**, *128*, 1794 – 1795.
[10] T. Lummerstorfer, H. Hoffmann, *J. Phys. Chem. B* **2004**, *108*, 3963 – 3966.
[11] H. Li, F. Cheng, A. M. Duft, A. Adronov, *J. Am. Chem. Soc.* **2005**, *127*, 14518 – 14524.
[12] D. D. Diaz, S. Punna, P. Holzer, A. K. McPherson, K. B. Sharpless, V. V. Fokin, M. G. Finn, *J. Polym. Sci. A* **2004**, *42*, 4392 – 4403.
[13] N. K. Devaraj, G. P. Miller, W. Ebina, B. Kakaradov, J. P. Collman, E. T. Kool, C. E. D. Chidsey, *J. Am. Chem. Soc.* **2005**, *127*, 8600 – 8601.
[14] N. Balachander, C. Sukenik, *Langmuir* **1990**, *6*, 1621 – 1627.
[15] Substitution and addition reactions on SAMs are notoriously sensitive to steric constraints, surface coverage of functional groups, reactant transport limitations, solvation effects, charge, and dipole effects: a) D. G. Kurth, T. Bein, *Langmuir* **1993**, *9*, 2965 – 2973; b) T. P. Sullivan, W. T. S. Huck, *Eur. J. Org. Chem.* **2003**, 17 – 29.
[16] The intensity profile in Figure 4 demonstrates that LRA spreads to the noncontacted area of the substrate. Overinking and ink spreading are common phenomena in μCP.

 © 2006 Wiley-VCH Verlag GmbH & Co. KGaA, Weinheim

Signaling Aptamer

DOI: 10.1002/anie.200600438

Self-Assembled Signaling Aptamer DNA Arrays for Protein Detection**

*Chenxiang Lin, Evaldas Katilius, Yan Liu, Junping Zhang, and Hao Yan**

Herein we report a DNA-tile directed self-assembly of signaling aptamers into high-density nanoarrays for detection of protein molecules. A signaling aptamer for human α-thrombin was created by replacing one nucleotide that is located close to the protein binding site in the aptamer sequence with a fluorescent nucleotide analogue, which generates a significant increase in fluorescence upon binding to thrombin. The signaling aptamer was linked to a DNA tile designed to self-assemble into 2D DNA arrays with ≈27-nm periodic spacing between neighboring aptamers. The high local density of the signaling aptamers displayed on the self-assembled DNA arrays allowed us to detect low concentrations of thrombin protein bound to the arrays by using confocal fluorescence microscope imaging.

This water-soluble, self-assembled signaling aptamer aggregate provides a novel strategy for developing programmable sensors. An important design concept in this work is that the molecular recognition process (protein find-and-bind aptamers) is in solution, but the physical measurement of the recognition is on the surface. The water-soluble signaling aptamer assemblies can lead to more-efficient molecular recognition compared to binding on solid surfaces. After being deposited on solid substrates, each signaling aptamer aggregate collectively gives strong-enough signals that allow the binding events to be read by a fluorescence microscope, which resembles the readout method in microarray technology. Overall, the method described herein involves no surface-chemistry steps, which are common in solid surface-based microarrays, and reveals no reduction in the aptamer-binding efficiency as compared with the unmodified aptamer. Thus, it has the advantage of microarray technology, but avoids its disadvantages.

In recent years, there has been a substantial advancement in the use of DNA as a "smart" material to construct

[*] C. Lin, Dr. E. Katilius, Dr. Y. Liu, Dr. J. Zhang, Prof. Dr. H. Yan
Department of Chemistry and Biochemistry, and
The Biodesign Institute
Arizona State University
Tempe, AZ 85287 (USA)
Fax: (+1) 480-727-2378
E-mail: evaldas@asu.edu
hao.yan@asu.edu

[**] This work has been supported by grants from the NSF and research grants from the Biodesign Institute at ASU to H.Y. and E.K. We thank Prof. Neal Woodbury for helpful discussions. We also thank Prof. Rebekka Wachter for the use of the fluorimeter.

Supporting information for this article is available on the WWW under http://www.angewandte.org or from the author.

WILEY InterScience DISCOVER SOMETHING GREAT
© 2006 Wiley-VCH Verlag GmbH & Co. KGaA, Weinheim

structures with periodical patterns on the nanometer scale.[1–9] Structure formation by using DNA tiles begins with the design of the sequence and chemical synthesis of single-stranded DNA oligonucleotides. When the DNA oligonucleotides are properly annealed together, they self-assemble into DNA branched-junction building blocks or DNA tiles through Watson–Crick base pairing. DNA tiles can carry sticky ends (single-stranded overhangs) that preferentially hybridize to the sticky ends of other DNA tiles, thereby facilitating further assembly into ordered periodic lattices that display designed patterns. Micrometer to millimeter sized 2D DNA-tile lattices containing millions to billions of tiles have been constructed.[10,11] Self-assembled DNA arrays might ultimately offer great opportunities for biomedical applications. For example, self-assembling DNA arrays may be used as templates for the assembly of biomimetic materials. Multiplex biosensing systems could also be built by encoding variable molecular recognition events in a multitile DNA array.

Besides serving as nanosized building blocks, another nonclassical application for nucleic acids has been the discovery of aptamers. Aptamers are short DNA or RNA oligonucleotides that are selected from pools of random sequences based on their ability to bind to other molecules. By using in vitro selection techniques, aptamers that can bind to other nucleic acids, proteins, small organic compounds, and even entire organisms have been identified.[12,13] Some of them exhibit subnanomolar affinities for a variety of protein targets.[14,15] Selection and synthesis in vitro, low molecular weight, and the highly specific molecular recognition of ligands make aptamers appealing for sensing and diagnostic applications as a substitute for antibodies.[16]

Signaling aptamers are aptamer probes that couple target binding to fluorescent-signal generation. This is generally done by introducing a fluorophore in a region of the aptamer that is known to undergo environmental change upon target binding, such as conformational or polarity change, so the molecular-recognition event can be transduced to detectable optical signals. Ellington and co-workers showed that by modifying an ATP binding aptamer with a single fluorescent dye (fluorescein, rhodamine green, or cascade blue), a fluorescence signal increase up to 220% upon the addition of ATP was observed.[17,18] Similarly, Merino and Weeks converted three aptamers into sensor devices by tethering an environmentally sensitive fluorescent group (Bodipy) at an appropriate 2′-ribose position.[19] A variety of other approaches to create signaling aptamers were devised over the years. For example, Stojanovic and Kolpashchikov developed a modular allosteric sensor that combined two aptamers with a connecting stem in which the recognition event in one aptamer was transduced into fluorescence change of a noncovalently attached fluorophore in the other aptamer.[20] Li and co-workers designed "structure-switching" signaling aptamers that showed target binding by the fluorophore-labeled aptamer switching binding partner between quencher-labeled DNA and the target.[21–23] A wide range of fluorescence enhancements of up to 50-fold between the bound and free states had been reported, but very often, depending on the design strategy, the binding affinities for the targets decreased several or even 60-fold when compared with the unmodified aptamers.[17–23]

We have previously shown that by embedding a thrombin-binding-aptamer (TBA) sequence into a linear DNA tile, thrombin can be organized into periodical 1D linear arrays,[24] demonstrating that aptamers keep their molecular-recognition capability when they are introduced into DNA-tile arrays. Herein we demonstrate that signaling aptamers can be organized into micron sized 2D arrays for biosensing applications. Figure 1 schematically illustrates the design of the array based on a two-tile system (A and B tiles) in which the tiles are designed to associate with each other in a periodic fashion to form a 2D nanogrid.[25] In this work, a DNA hairpin–loop (colored green in Figure 1) containing the sequence of the thrombin-binding signaling aptamer is incorporated in the A tile (colored pink), which protrudes out of the tile plane. The periodical spacing between neighboring signaling aptamers is ≈27 nm in the self-assembled array (Figure 1b).

TBA is a well characterized 15-mer DNA aptamer with a consensus sequence of d(GGTTGGTGTGGTTGG) that folds into a unimolecular guanine quadruplex and displays

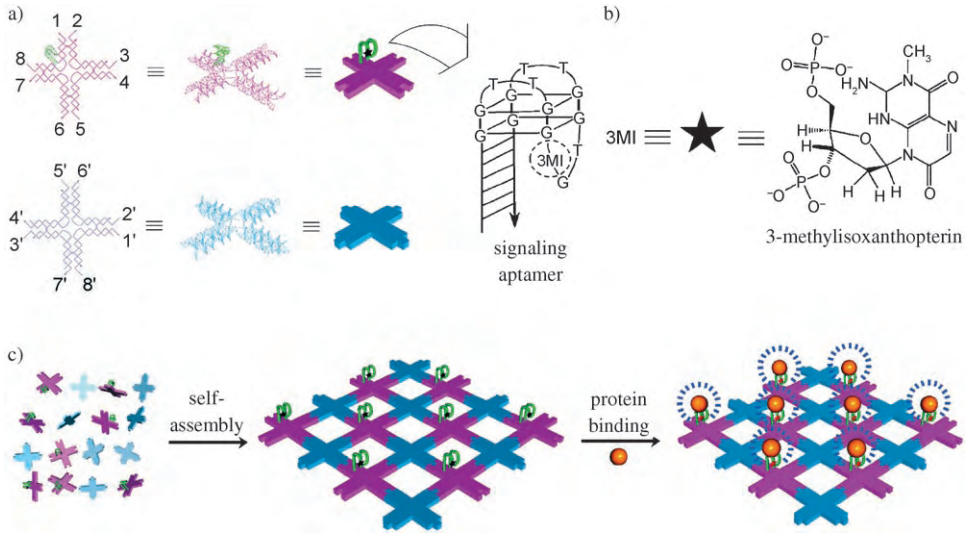


Figure 1. Schematic drawing of the design and operation of the signaling aptamer array created by DNA-tile self-assembly. a) The two tiles of the DNA nanogrid array. Complementary sticky ends are numbered as *n* and *n*′. The pink tile contains the thrombin aptamer sequence (a green loop) in a G-quadruplex structure. At the 7-position, the original dT is substituted by the fluorescent nucleic acid analogue 3 MI. b) The molecular structure of 3 MI. It is also labeled as a black star in the tile without protein. c) The self-assembly of the two-tile system into a 2D array that displays the thrombin-binding aptamer at every other DNA tile. Upon protein binding, the array containing the signaling aptamers "lights up" (labeled as red star).

© 2006 Wiley-VCH Verlag GmbH & Co. KGaA, Weinheim

an approximate 10 nM apparent-dissociation constant to human α-thrombin.[26,27] Herein we used TBA modified with 3-methylisoxanthopterin (3 MI) at position 7 (Figure 1b). The fluorescence quantum yield of 3 MI, a fluorescent guanosine (G) analogue, is highly sensitive to changes in the local environment, in particular to the extent of base-stacking interactions.[28] Crystal-structure analysis[29] of TBA bound to thrombin suggests that dT_7 undergoes significant unstacking from the neighboring bases upon binding to the protein. Therefore, the 3 MI-modified TBA showed a large fluorescence-intensity change upon binding with thrombin (Katilius et al.[34]). 3 MI has a relatively large Stoke shift with excitation and emission maxima at 350 nm and 430 nm, respectively, suitable for fluorescence imaging with a confocal fluorescence microscope. In comparison with other reported signaling aptamers, 3 MI-modified aptamers have the advantage of a decent fluorescence-signal increase upon protein binding, no decrease in binding affinity, and importantly, high resistance to photobleaching.[28]

Fluorescence spectra were measured at two different DNA array concentrations suspended in buffer solution to investigate 3 MI fluorescence-intensity changes as a function of human α-thrombin concentration (Figure 2). With a constant concentration of the DNA arrays equivalent to 1 μM TBA, the thrombin concentration in solution increased from 0 to 1.6 μM, and a twofold increase in the 3 MI fluorescence intensity was observed. The emission peak is also red shifted ≈4 nm from 413 nm to 417 nm. A fit to the "Langmuir model" for the fluorescence-response curve gives an apparent dissociation constant of $\approx 4 \pm 2$ nM. This is obtained by taking into account the depletion in the bulk concentration of protein owing to binding to the aptamer, and with the assumptions of 1) a linear fluorescence response with the concentration of the bound protein, 2) a single binding site for a 1:1 ratio of protein and aptamer, and 3) no interactions between individual binding sites. This dissociation constant shows an ≈2.5-fold increase when compared with the published effective dissociation constant values for TBA, ≈10 nM.[30,31] The detection limit of protein was estimated to be ≈20 nM based on the signal-to-noise (S/N) level.

When the concentration of the DNA array is lowered to 10 nM, as shown in Figure 2c, the addition of human α-thrombin causes ≈60% fluorescence increase at a saturation concentration of ≈30 nM. The detection limit was estimated to be ≈5 nM. The better sensitivity for the lower DNA

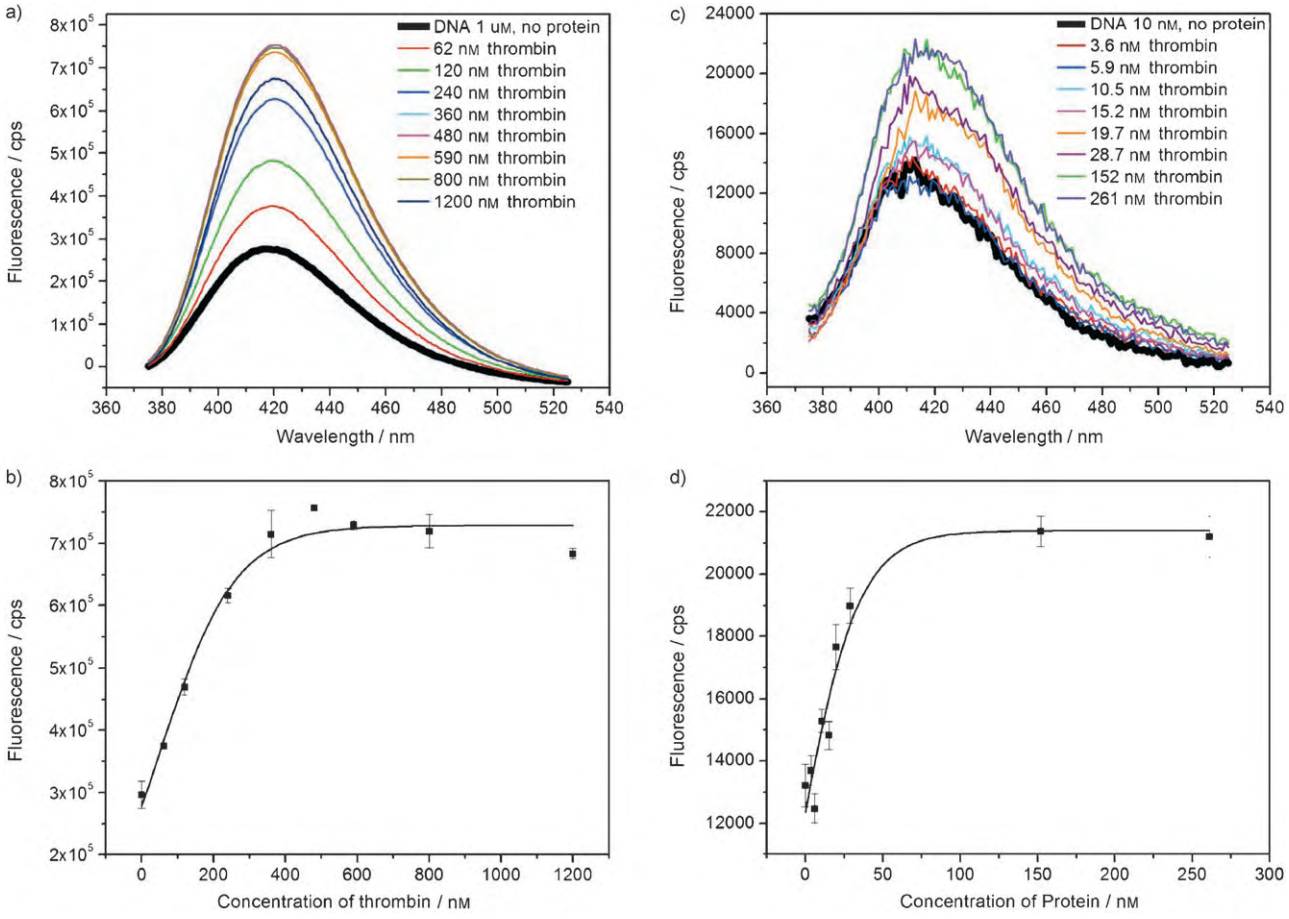


Figure 2. a, c) Fluorescence spectra for the signaling aptamer array with different amounts of thrombin. The aptamer array concentrations are 1 μM (a) and 10 nM (c). Increasing thrombin concentrations were added into the solution as labeled in the Figure legends. b, d) Plots of the fluorescence peak intensity as a function of the thrombin concentration, corresponding to the spectra in (a) and (c). The curves through the data points are fit to Langmuir model. The error bars are estimated from repeating the experiments three times. cps = counts per second.

 © 2006 Wiley-VCH Verlag GmbH & Co. KGaA, Weinheim

nanoarray concentration is due to the lower background signal from the signaling aptamer alone. As the overall signal level decreases, the S/N ratio also decreases significantly. When the concentration of the DNA array is further lowered to 1 nM, the S/N ratio is so low that the signal generated from 6–18 nM thrombin, which should nearly saturate the binding sites, is just buried in the noise (data shown in the Supporting Information). Therefore, the detection limit is difficult to improve for analysis in bulk solutions.

Confocal fluorescence microscopy was used to directly visualize the DNA arrays before and after the addition of the protein (Figure 3). The top image in Figure 3a shows the arrays deposited on the glass slides before addition of the protein. Arrays were assembled and deposited at the effective concentration of 1 μM TBA, some conglomeration of arrays was observed. This is because no terminal tiles were included in the assembly of the arrays and as a result, the final arrays formed are all irregularly shaped with "sticky edges". Therefore, touching of the edges of nearby DNA arrays or even some overlapping or folding of DNA arrays upon binding to the surface is common.[10,11] This phenomenon can also be observed by AFM for the self-assembled signaling aptamer arrays before and after the addition of thrombin (see the Supporting Information). AFM images clearly show the formation of the signaling aptamer array and the protein array. However, scanning across the surface of the AFM tip can scratch some proteins off the array owing to the non-covalent interaction between the protein and aptamer. Therefore, the coverage of the protein on the signaling aptamer array does not reflect the binding efficiency of the protein to the array. It is also notable that smaller domains of the array come together to form larger aggregates which can lead to measurement of the array by fluorescence microscope imaging.

Control experiments were performed to test the specificity of the fluorescence response. First, the common serum protein, bovine-serum albumin (BSA), was added to the arrays instead of α-thrombin and no significant fluorescence-intensity change was observed (Figure 3a). Further addition of 1 μM human β-thrombin and human γ-thrombin to the arrays caused a small increase in the signal intensity, ≈15–20%, which was similar to the observations in solution (see the Supporting Information). Finally, when 1 μM α-thrombin was added, the arrays "light-up" as the fluorescence signal increases significantly (the bottom image in Figure 3a). Immunoglobulin E (IgE) was also used as control and showed no competition in binding to the aptamer (Figure 3b). These experiments show that the fluorescence-signal increase was highly specific to binding of the thrombin protein to the aptamer array.

To further confirm that the fluorescence change was caused by the specific binding of TBA to thrombin, the sequence d(TTTTTT(3 MI)TTTTTTTT) was incorporated into the array instead of the TBA sequence. In this case, the DNA-tile arrays could still self-assemble, but no fluorescence-signal changes were detected before or after addition of the α-thrombin to the solution (Figure 3c). Thus, the self-assembled signaling aptamer array specifically detects the presence of α-thrombin in solution.

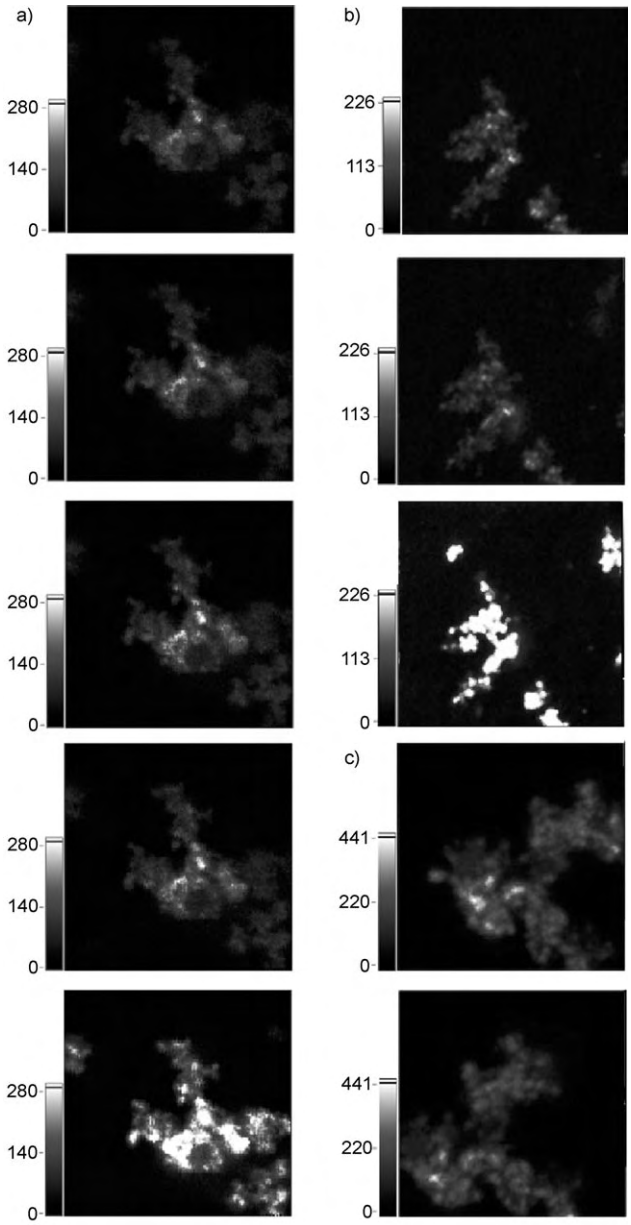


Figure 3. Images of DNA arrays. All images shown are samples containing 1 μM DNA-tile arrays (a–e) in 50×50 μm² scale. a) From top to bottom are the DNA-tile arrays containing thrombin binding aptamer with 3 MI, after addition of 1 μM BSA, after addition of 1 μM human β-thrombin, after the addition of 1 μM human γ-thrombin, and finally after addition of 1 μM human α-thrombin. b) From top to bottom are the DNA-tile arrays without protein, after the addition of 1 μM IgE, and after the addition of 1 μM human α-thrombin. c) Top, DNA-tile array containing a random sequence of DNA loop with 3 MI. Bottom, after the addition of 1 μM α-thrombin to the array.

Fluorescence imaging was also performed on the DNA arrays with an effective concentration of the aptamer of 1 nM (Figure 4). Dilution of the arrays 100 times from 1 μM minimizes their conglomeration, allowing single arrays to be resolved. Imaging of arrays under these conditions showed that most of them exist in sizes ranging from 1–10 μm, as limited by the self-assembly process. An approximate 100% increase in the average fluorescence signal was obtained from

 © 2006 Wiley-VCH Verlag GmbH & Co. KGaA, Weinheim

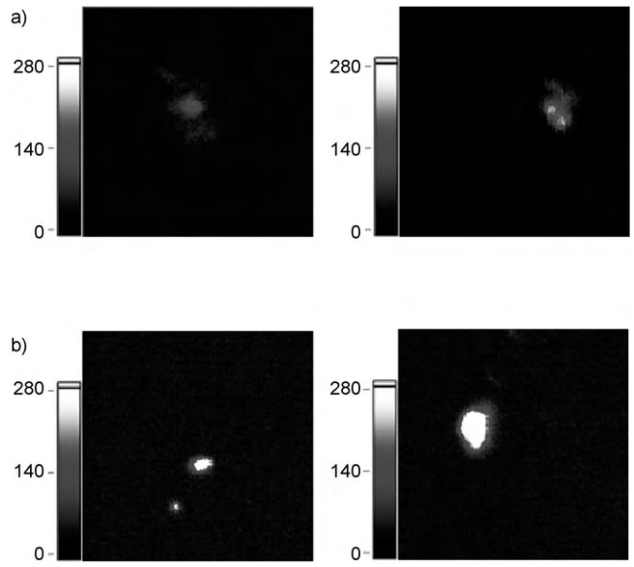


Figure 4. Images of DNA arrays deposited on the slides at low concentration. All images shown are samples containing 1 nM DNA-tile arrays in $25 \times 25\ \mu m^2$ scale. a) Representative samples of single DNA arrays. b) Representative samples of DNA arrays that were preincubated with 1 nM thrombin and then deposited on the slides. Notice a significantly higher fluorescent intensity of the array. The average intensity of arrays before the addition of protein range from 130–190 counts μm^{-2}, whereas the average intensity when 1 nM thrombin is added increases to 300–400 counts μm^{-2}.

images taken in the presence and absence of thrombin protein (Figure 4a and b).

These data may seem contrary to the fluorescene data obtained in solution. with the dissociation constant of $\approx 4 \pm 2$ nM at initial concentrations of the protein and aptamer of 1 nM, the percentage of aptamers binding with protein is expected to be lower than 20%. As a result of this, a maximum 20% increase in the signal is expected based on this calculation. Previous data have indicated the binding of TBA with thrombin maybe very complicated, 1:1, 1:2, 2:1, and 2:2 binding ratios are all possible.[24,32] Therefore, the dissociation constant of 4 nM obtained by fitting the data to the simple Langmuir model may not be accurate. Furthermore, when the aptamers are assembled into nanoarrays, the dissociation of bound protein from the aptamer array is different from that of the individual aptamer molecules in solution. Because of rebinding of the released protein by a nearby aptamer on the array, the dissociation constant may decrease an order of magnitude or more. The data shown in Figure 4 support this argument. This ligand rebinding phenomenon has been examined theoretically on cell-membrane surfaces and macromolecule systems.[33,34] It was pointed out that rebinding can play a major role in the performance of surface-based biosensors. These results show that by incorporating the 3 MI-modified signaling aptamer on DNA nanoarrays and imaging with confocal microscope, we can effectively detect nanomolar and subnanomolar concentration of a target protein in solution.

In summary, we have demonstrated that the DNA-tile directed self-assembly of a signaling aptamer into micron-sized DNA arrays can be used to detect proteins with high specificity and sensitivity at subnanomolar concentrations. However, the strength of the signals that were detected allow us to believe that even picomolar concentrations should be easily detectable if signaling aptamers with higher affinity are selected. This methodology could present future opportunities to construct water-soluble sensor arrays in a programmable fashion. Of course, the use of fluorescent nucleotides as fluorophores for signaling aptamers limits the possibility of multiplexing the assay. Alternatively, different signaling aptamers that are labeled with fluorophores that emit at different wavelengths can be incorporated into the same DNA array (e.g. a multitile system) for multicolor and multicomponent detection.

Received: February 2, 2006
Revised: June 9, 2006
Published online: July 17, 2006

Keywords: DNA arrays · molecular recognition · protein detection · self-assembly · signaling aptamers

[1] N. C. Seeman, *Nature* **2003**, *421*, 427–431.
[2] E. Winfree, F. Liu, L. A. Wenzler, N. C. Seeman, *Nature* **1998**, *394*, 539–544.
[3] T. H. Labean, H. Yan, J. Kopatsch, F. R. Liu, E. Winfree, J. H. Reif, N. C. Seeman, *J. Am. Chem. Soc.* **2000**, *122*, 1848–1860.
[4] C. D. Mao, W. Q. Sun, N. C. Seeman, *J. Am. Chem. Soc.* **1999**, *121*, 5437–5443.
[5] H. Yan, S. H. Park, G. Finkelstein, J. H. Reif, T. H. LaBean, *Science* **2003**, *301*, 1882–1884.
[6] N. Chelyapov, Y. Brun, M. Gopalkrishnan, D. Reishus, B. Shaw, L. Adleman, *J. Am. Chem. Soc.* **2004**, *126*, 13924–13925.
[7] B. Q. Ding, R. J. Sha, N. C. Seeman, *J. Am. Chem. Soc.* **2004**, *126*, 10230–10231.
[8] D. Liu, M. Wang, Z. Deng, R. Walulu, C. Mao, *J. Am. Chem. Soc.* **2004**, *126*, 2324–2325.
[9] Y. Liu, Y. Ke, H. Yan, *J. Am. Chem. Soc.* **2005**, *127*, 17140–17141.
[10] Y. He, Y. Tian, Y. Chen, Z. Deng, A. E. Ribbe, C. Mao, *Angew. Chem.* **2005**, *117*, 6852–6854; *Angew. Chem. Int. Ed.* **2005**, *44*, 6694–6696.
[11] Y. He, Y. Chen, H. Liu, A. E. Ribbe, C. Mao, *J. Am. Chem. Soc.* **2005**, *127*, 12202–12203.
[12] E. N. Brody, M. C. Willis, J. D. Smith, S. Jayasena, D. Zichi, L. Gold, *Mol. Diagn.* **1999**, *4*, 381–388.
[13] R. C. Conrad, L. Giver, Y. Tian, A. D. Ellington, *Comb. Chem.* **1996**, *267*, 336–367.
[14] D. E. Tsai, D. J. Kenan, J. D. Keene, *Proc. Natl. Acad. Sci. USA* **1992**, *89*, 8864–8868.
[15] W. Xu, A. D. Ellington, *Proc. Natl. Acad. Sci. USA* **1996**, *93*, 7475–7480.
[16] M. Rajendran, A. D. Ellington, *Comb. Chem. High Throughput Screening* **2002**, *5*, 263–270.
[17] S. D. Jhaveri, R. Kirby, R. Conrad, E. J. Maglott, M. Bowser, R. T. Kennedy, G. Glick, A. D. Ellington, *J. Am. Chem. Soc.* **2000**, *122*, 2469–2473.
[18] S. Jhaveri, M. Rajendran, A. D. Ellington, *Nat. Biotechnol.* **2000**, *18*, 1293–1297.
[19] E. J. Merino, K. M. Weeks, *J. Am. Chem. Soc.* **2005**, *127*, 12766–12767.
[20] M. N. Stojanovic, D. M. Kolpashchikov, *J. Am. Chem. Soc.* **2004**, *126*, 9266–9270.

 © 2006 Wiley-VCH Verlag GmbH & Co. KGaA, Weinheim

[21] R. Nutiu, Y. Li, *Chem. Eur. J.* **2004**, *10*, 1868 – 1876.
[22] R. Nutiu, Y. F. Li, *J. Am. Chem. Soc.* **2003**, *125*, 4771 – 4778.
[23] R. Nutiu, Y. F. Li, *Angew. Chem.* **2005**, *117*, 1085 – 1089; *Angew. Chem. Int. Ed.* **2005**, *44*, 1061 – 1065.
[24] Y. Liu, C. X. Lin, H. Y. Li, H. Yan, *Angew. Chem.* **2005**, *117*, 4407 – 4412; *Angew. Chem. Int. Ed.* **2005**, *44*, 4333 – 4338.
[25] S. H. Park, P. Yin, Y. Liu, J. H. Reif, T. H. LaBean, H. Yan, *Nano Lett.* **2005**, *5*, 729 – 733.
[26] R. F. Macaya, P. Schultze, F. W. Smith, J. a. Roe, J. Feigon, *Proc. Natl. Acad. Sci. USA* **1993**, *90*, 3745 – 3749.
[27] K. Padmanabhan, K. P. Padmanabhan, J. D. Ferrara, J. E. Sadler, a. Tulinsky, *J. Biol. Chem.* **1993**, *268*, 17651 – 17654.
[28] M. E. Hawkins, *Cell Biochem. Biophys.* **2001**, *34*, 257 – 281.
[29] K. Padmanabhan, A. Tulinsky, *Acta Crystallogr. Sect. D* **1996**, *52*, 272 – 282.
[30] L. C. Bock, L. C. Griffin, J. a. Latham, E. H. Vermaas, J. J. Toole, *Nature* **1992**, *355*, 564 – 566.
[31] N. Hamaguchi, A. Ellington, M. Stanton, *Anal. Biochem.* **2001**, *294*, 126 – 131.
[32] V. Pavlov, Y. Xiao, B. Shlyahovsky, I. Willner, *J. Am. Chem. Soc.* **2004**, *126*, 11768 – 11769;
[33] B. C. Lagerholm, N. Thompson, *Biophys. J.* **1998**, *74*, 1215 – 1228.
[34] M. Gopalakrishnan, K. Forsten-Williams, M. A. Nugent, U. C. Täuber, *Biophys. J.* **2005**, *89*, 3686 – 3700.
[35] E. Katilius, Z. Katiliene, N. W. Woodbury, *J. Am. Chem. Soc.*, submitted.

 © 2006 Wiley-VCH Verlag GmbH & Co. KGaA, Weinheim

Peptide Fragmentation

DOI: 10.1002/anie.200601240

Complementary Sequence Preferences of Electron-Capture Dissociation and Vibrational Excitation in Fragmentation of Polypeptide Polycations**

*Mikhail M. Savitski, Frank Kjeldsen, Michael L. Nielsen, and Roman A. Zubarev**

Electron-capture dissociation (ECD)[1] of polypeptide polycations produces preferential cleavage of the backbone N–C_α bond (*c*, *z* fragments), while fragmentation based on vibrational excitation (VE) of the same ions (for example, collision-activated dissociation (CAD), infrared multiphoton dissociation (IRMPD), or surface-induced dissociation (SID)) gives preferential C–N cleavage (*b*, *y* fragment ions). Both types of fragmentation phenomena show preferences for the context of the amino acids. For example, VE has a strong preference for the N-terminal side of proline and the N-terminal side of aspartic acid.[2] More subtle preferences in CAD have been studied recently on a large data set.[3] Cleavage on the N-terminal side of Pro by ECD are absent because of the tertiary amide nitrogen atom.[1] Preferential cleavage on the C-terminal side of tryptophan has been reported,[4] but in general it has been unclear whether amino acid preferences in ECD are similar to those in CAD.[4] This question has both fundamental and application-related aspects. According to the generally accepted theory,[5] cleavage of C–N bonds by VE are induced by a mobile proton solvated by backbone amides. The presence of a proton at the amide nitrogen atom greatly weakens the amide bond,[5] and can also reduce the strength of other nearby bonds.[6] Thus, cleavage of the amide bond by VE is a local phenomenon with respect to the proton location. Both local[1,7] and nonlocal[8–11] cleavage mechanisms have been suggested for ECD. According to the local ECD model, the N–C_α bond next to the position of the neutralized proton is cleaved. Thus, ECD may be expected to have similar preferences as VE for amino acid contexts (except proline). The practical aspect of this issue is the use of CAD and ECD in tandem mass spectrometry, an important tool for proteomics. Application of two fragmentation methods instead of one is only advantageous if the methods are complementary in terms of sequence preferences.

Some CAD/ECD complementarity has been noticed on a limited data set.[4] Here we report the results of an exhaustive comparison performed on a library containing 14967 pairs of ECD and CAD mass spectra of tryptic peptide dications. The high mass accuracy used (± 3 ppm for molecular mass; ± 20 mDa for fragment masses)[12] ensured unique assignment of the fragments in 99+ % of the cases. Most of the identified fragment ions were singly charged C-terminal products: *y* ions in CAD and *z* ions ($z^\bullet$ and z') in ECD. The distributions of the cases when the y_{m-n} (z_{m-n}) fragment (where *m* is the peptide length) had the highest abundance amongst all the same-type fragments are shown in Figure 1. The striking features are the sharp peak at $n=2$ in the CAD histogram and broader peaks at $n\approx 4$ in both the CAD and ECD histograms. The positions of the maxima are independent of the peptide length and the C-terminal residue (Lys or Arg), and they correlate: 47 % of peptides giving the most abundant z_{m-4} ions by ECD produce y_{m-2} ions as the most abundant fragments by CAD (see inset in Figure 2).

Figure 2 presents statistics on the value $\Delta = n_{ECD} - n_{CAD}$ measured for the same peptide sequences. The distribution has a global maximum at $\Delta = +2$ which reflects the correlation between the peaks at $n_{ECD}=4$ and $n_{CAD}=2$ in Figure 1 (the inset in Figure 2 confirms this correlation). The small local maximum at $\Delta = -1$ corresponds to preferential cleavage at $n_{ECD}=4$ and $n_{CAD}=5$. The local minimum at $\Delta = 0$ means that cleavage by ECD at the same position as by CAD is relatively disfavored, contrary to predictions from the local-

[*] M. M. Savitski, Dr. F. Kjeldsen, M. L. Nielsen, Prof. R. A. Zubarev
Laboratory for Biological and Medical Mass Spectrometry
BMC, Uppsala University
Box 583, 75123 Uppsala (Sweden)
Fax: (+46) 18-471-22-44
E-mail: roman.zubarev@bmms.uu.se

[**] This work was supported by the Knut and Alice Wallenberg Foundation and Wallenberg Consortium North (grant WCN2003-UU/SLU-009 to R.Z. and instrumental grant to R.Z. and Carol Nilsson) as well as the Swedish research council (grants 621-2004-4897, 621-2002-5025 and 621-2003-4877 to R.Z.). Thomas Köcher and Christopher Adams are acknowledged for insightful discussions.

 © 2006 Wiley-VCH Verlag GmbH & Co. KGaA, Weinheim

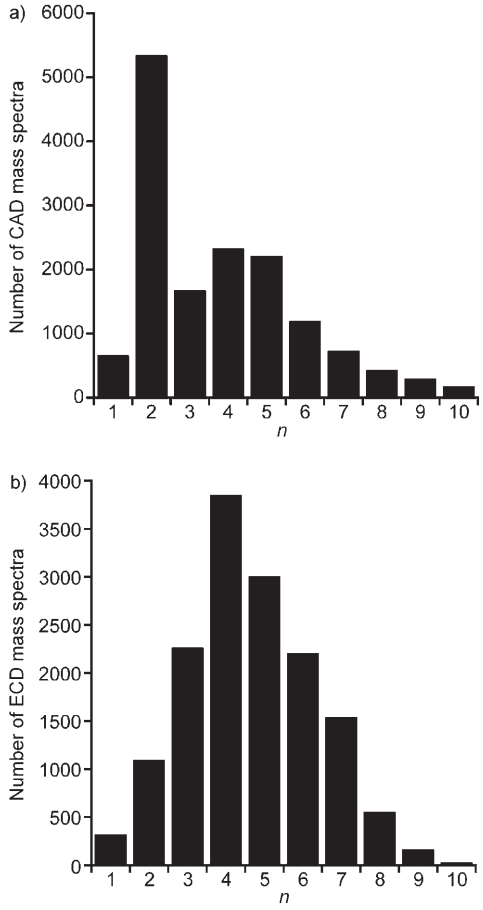


Figure 1. Distributions of tandem mass spectra in which the $(m-n)$th fragment (m is the peptide length) had the highest abundance of all identified C-terminal fragments for tryptic peptide dications fragmented by: a) CAD y'_{m-n} ions; b) ECD z_{m-n} ions (the most abundant of $z^{\cdot}_{m-n}$ and z'_{m-n} species).

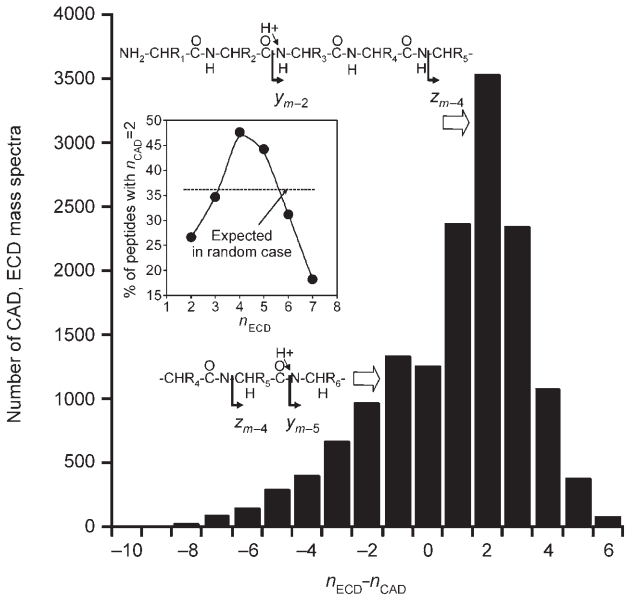


Figure 2. Distribution of the differences $\Delta = n_{ECD} - n_{CAD}$ in the position of the maximum-abundance C-terminal fragment arising from ECD and CAD of the same tryptic peptide dication. Inset: % of peptides with $n_{CAD}=2$ for different n_{ECD}; the value of 36% is expected in a random case. The plot confirms that $n_{ECD}=4$ and $n_{CAD}=2$ are statistically linked.

action ECD mechanism. The preferences for amino acid pairs in ECD and CAD for the same peptide sequences (cleavage positions $n=3$–5) are shown in Figure 3. The abundances of the z_{m-3}, z_{m-4}, and z_{m-5} ion were normalized for each spectrum with respect to the most abundant of these three ions, the same was done for each triplet $(y_{m-3}, y_{m-4}, y_{m-5})$. The CAD and ECD preferences are complementary, with a near-zero correlation of $r=-0.07$. While CAD shows only a small difference between Ile and Leu, cleavages on the N-terminal side of Leu by ECD are much more abundant than for Ile. Furthermore, A–B cleavages in CAD anticorrelate with B–A cleavages, while this feature is much weaker with ECD. Other features of Figure 3 will be discussed in detail in subsequent reports.

The correlated maxima at $n_{ECD}=4$ and $n_{CAD}=2$ in Figure 1 require explanation. The most likely reason for the correlation is the presence of an N-terminal structure that solvates the charge, as in the simulations of Ala_nH^+ ions by Samuelson and Martyna.[13] Such a structure can be further stabilized by neutral hydrogen-bonding interactions. According to the recently suggested nonlocal mechanism,[11] electron capture on the backbone nitrogen atom involved in neutral hydrogen-bonding interactions with the carbonyl group of the fourth residue will induce H· transfer to that carbonyl group. The thus created aminoketyl radical will rapidly relax through cleavage of the N–C_α bond next to the carbonyl group[10,11] to

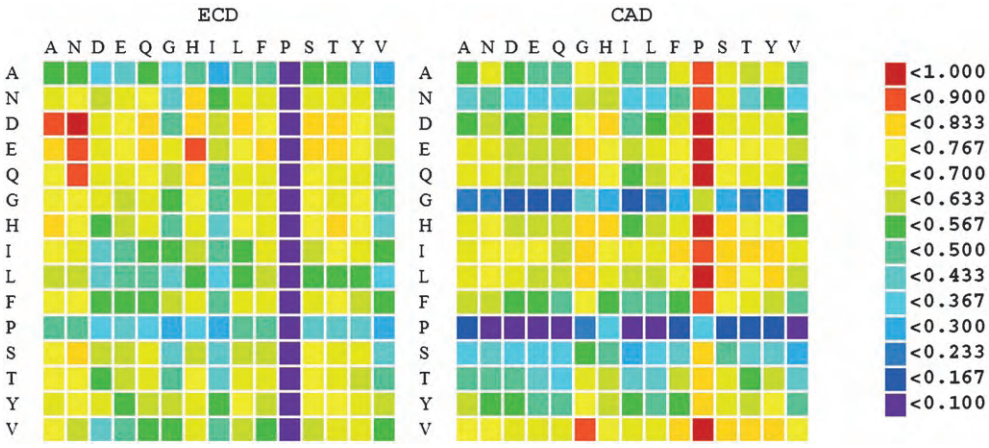


Figure 3. Amino acid pair preferences in ECD (left panel) and CAD (right panel) for C-terminal $(m-n)$th fragments, $n=3.5$. Columns correspond to residue B in an amino acid pair A–B.

© 2006 Wiley-VCH Verlag GmbH & Co. KGaA, Weinheim

give neutral N-terminal c_4 fragments and singly charged z_{m-4} ions, thus accounting for the maximum at $n \approx 4$ in Figure 1b. Vibrational activation of the same structure will result in the solvated proton preferentially attacking the adjacent backbone amide, thus effecting C–N bond cleavage[14] to form y_{m-n} and b_n ions. The maximum peak at $n_{CAD} = 2$ in Figure 1a hints at frequent charge solvation on the second carbonyl group. The enhanced stability of the b_2 ion[14] may additionally increase the cleavage rate for $n_{CAD} = 2$. Vibrational excitation can also unfold the structure and induce proton migration along the backbone.[15] The migrating proton will lead to heterogeneous population of unfolded structures, as suggested by Gaskell and co-workers,[15] which will result in a broad distribution of the C–N cleavage sites (broad maximum in Figure 1a). On the basis of the fraction of peptide sequences that produced y_{m-2} ions by CAD and z_{m-4} by ECD (inset in Figure 2), we estimate that 30 to 40% of all doubly charged tryptic peptides form the N-terminal charge-solvating structure.

Tables similar to those in Figure 3, but created separately for $n = 3$, 4, and 5 (with the intensities still normalized to the most abundant ion in the triplet), vary with n much less for CAD than for ECD. For example, correlation between the CAD tables for $n = 3$ and $n = 4$ is $r_{3,4} = 0.88$, for $n = 4$ and $n = 5$ it is $r_{4,5} = 0.85$, and for $n = 3$ and $n = 5$ it is $r_{3,5} = 0.75$. The corresponding figures for ECD are $r_{3,4} = 0.75$, $r_{4,5} = 0.62$, and $r_{3,5} = 0.47$, that is, sequence preferences for forming z_3 differ markedly from those for z_5. This result is consistent with the presence of a nonrandom secondary N-terminal structure, which is known to affect rates of cleavage by ECD.[11] Since this structure is charge-stabilized, the presence of a strongly basic residue at the N terminus should destabilize it, as the proton will be sequestered by the basic side chain. Consistent with that prediction, peptides with an N-terminal arginine (residue formed in trypsinolysis as a result of a missed cleavage) gave a maximum peak at $n = 1$ instead of $n \approx 4$ in the ECD spectra, and the sharp maximum peak at $n = 2$ in the CAD spectra disappeared.

It was also studied how the proton affinity PA_k of the kth amino acid from the N terminus affected the position n of the most abundant ECD fragment z_{m-n}. A clear anticorrelation was found between PA_k and n, which means that the more basic N terminus sequestered the proton to a higher degree and led to a smaller size of the N-terminal compact structure. The correlation between PA_k and n was equally strong for all cases with $k < 5$, but dropped twofold at $k = 5$ and disappeared at $k > 5$. It was concluded that the N-terminal structure involves four or five residues, in agreement with the size of the complementary part to the most abundant ECD fragment (Figure 1b). The effect of the peptide size on n was only noticeable for $m = 7$, thus indicating that for larger peptides the N-terminal structure is independent of the C-terminal charge.

In summary, this study proves for the first time that preferences for the cleavage site and amino acid context in ECD and CAD are truly complementary. This finding supports nonlocal ECD mechanisms that decouple the proton location and the position of the N–C_α bond that is cleaved. Thus, broader use of ECD in proteomics as a complement to CAD is warranted. The strong indication that an N-terminal charge-solvating structure is a common feature in tryptic peptide dications encourages further investigation, for example, using molecular dynamics simulations.

Experimental Section

Data for Figures 1–3 were collected from the proteomics analysis of lysates of human cell lines and *E. coli* (all samples from Sigma) performed on an LTQ FT mass spectrometer (Thermo) using consecutive ECD and CAD fragmentation of peptides eluting from the analytical column of a nano-LC system (Agilent 1100). The peptides were identified by the Mascot search engine (Matrix Sciences). The details of the experimental procedure and data processing are described in Ref. 12.

Received: March 30, 2006
Revised: June 5, 2006
Published online: July 17, 2006

Keywords: collision-activated dissociation · electron-capture dissociation · ion–electron reactions · mass spectrometry · peptide fragmentation

[1] R. A. Zubarev, N. L. Kelleher, F. W. McLafferty, *J. Am. Chem. Soc.* **1998**, *120*, 3265.
[2] W. Yu, J. E. Vath, M. C. Huberty, S. A. Martin, *Anal. Chem.* **1993**, *65*, 3015.
[3] Y. Y. Huang, J. M. Triscari, G. C. Tseng, L. Pasa-Tolic, M. S. Lipton, R. D. Smith, V. H. Wysocki, *Anal. Chem.* **2005**, *77*, 5800.
[4] N. A. Kruger, R. A. Zubarev, B. K. Carpenter, N. L. Kelleher, D. M. Horn, F. W. McLafferty, *Int. J. Mass Spectrom.* **1999**, *183*, 1.
[5] A. R. Dongre, A. Somogyi, V. H. Wysocki, *J. Mass Spectrom.* **1996**, *31*, 339.
[6] A. Somogyi, V. H. Wysocki, I. Mayer, *J. Am. Soc. Mass Spectrom.* **1994**, *5*, 704.
[7] R. A. Zubarev, K. F. Haselmann, B. Budnik, F. Kjeldsen, F. Jensen, *Eur. J. Mass Spectrom.* **2002**, *8*, 337.
[8] K. Breuker, H. B. Oh, C. Lin, B. K. Carpenter, F. W. McLafferty, *Proc. Natl. Acad. Sci. USA* **2004**, *101*, 14011.
[9] M. Sobczyk, W. Anusiewicz, J. Berdys-Kochanska, A. Sawicka, P. Skurski, J. Simons, *J. Phys. Chem. A* **2005**, *109*, 250.
[10] E. A. Syrstad, F. Turecek, *J. Am. Soc. Mass Spectrom.* **2005**, *16*, 208.
[11] A. Patriksson, C. Adams, F. Kjeldsen, J. Raber, D. van der Spoel, R. A. Zubarev, *Int. J. Mass Spectrom.* **2005**, *248*, 124–135.
[12] M. L. Nielsen, M. M. Savitski, R. A. Zubarev, *Mol. Cell. Proteomics* **2005**, *4*, 835.
[13] S. Samuelson, G. J. Martyna, *J. Phys. Chem. B* **1999**, *103*, 1752.
[14] T. Yalcin, C. Khouw, I. G. Csizmadia, M. R. Peterson, A. G. Harrison, *J. Am. Soc. Mass Spectrom.* **1995**, *6*, 1165.
[15] O. Burlet, C. Y. Yang, S. J. Gaskell, *J. Am. Soc. Mass Spectrom.* **1992**, *3*, 337.

 © 2006 Wiley-VCH Verlag GmbH & Co. KGaA, Weinheim

Intercalations

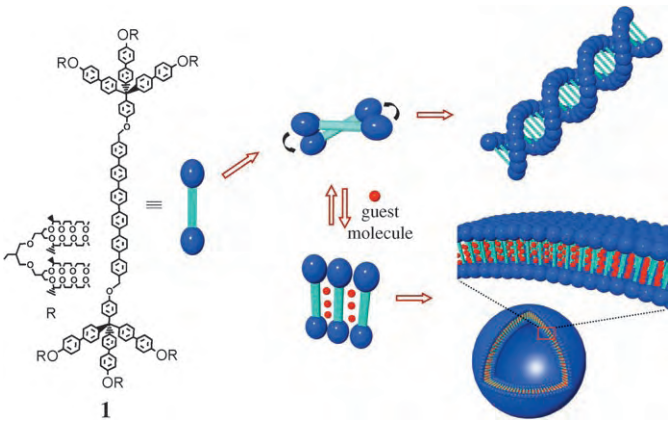
DOI: 10.1002/anie.200600971

Self-Assembling Molecular Dumbbells: From Nanohelices to Nanocapsules Triggered by Guest Intercalation**

*Ja-Hyoung Ryu, Ho-Joong Kim, Zhegang Huang, Eunji Lee, and Myongsoo Lee**

Controlled self-assembly of incompatible molecular components is a challenging topic of interdisciplinary research in chemistry, biology, and materials science.[1] For example, self-assembling molecules consisting of rodlike aromatic and flexible aliphatic segments have proved to be promising scaffolds for well-defined supramolecular structures, such as vesicles, tubules, and twisted ribbons.[2] Precise control of molecular arrangements at the supramolecular level is essential to obtain well-defined nanoscopic architectures with specific shape. Recently, we showed that incorporation of a conjugated rod into an amphiphilic dumbbell-shaped molecular architecture results in the formation of a helical nanostructure consisting of hydrophobic aromatic cores surrounded by hydrophilic flexible segments that are exposed to the aqueous environment.[3] We also showed that rod building blocks in rigid–flexible macrocycles self-assemble into a discrete barrel-like structure with hydrophilic channels.[4]

We present herein the formation of helical strands from the self-assembly of a dumbbell-shaped molecule based on a conjugated rod segment in aqueous solution and reversible transformation between helical strands and nanocages triggered by the addition of aromatic guest molecules (Scheme 1). The dumbbell-shaped molecule **1** consists of a hexa-*para*-phenylene rod and aliphatic polyether dendrons based on a tetrahedral core, which are covalently linked at both ends of the rod segment. To synthesize **1**, aromatic tetrahedral cores containing three oligoether dendrons were prepared according to procedures described previously (Scheme 2).[5] The final dumbbell-shaped molecules were synthesized by using a palladium-catalyzed homocoupling reaction. The resulting compound was characterized by ^{1}H and ^{13}C NMR spectroscopies, elemental analysis, and MALDI-TOF mass spectrometry, the data of which were in full agreement with the structures presented.



Scheme 1. Representation of the reversible transformation of helical fibers into a spherical capsule.

When dissolved in a solvent suitable for the oligoether block such as water, **1** self-assembles into an aggregate structure because of its amphiphilic characteristics. The aggregation behavior of the compound was subsequently studied in aqueous solution by using UV/Vis, fluorescence, and circular dichroism (CD) spectroscopies (see the Supporting Information). The absorption spectrum of **1** in aqueous solution (0.01 wt%) exhibits a broad transition with a maximum at 278 nm and a shoulder at 332 nm arising from the tripodal biphenyl segments and the conjugated rod block, respectively. The fluorescence spectrum of **1** in chloroform (0.01 wt%) excited at 332 nm exhibits two strong emission maxima at 381 and 400 nm. However, the emission maximum in aqueous solution is red-shifted with respect to that observed in chloroform, which is indicative of aggregation of the conjugated rod segments.[6] CD spectra of aqueous solutions of **1** show a positive Cotton effect followed by a negative Cotton effect at higher wavelengths with the CD signal passing through zero near the absorption maximum of the oligo(phenylene) chromophore, thus indicating the formation of a helical superstructure with a preferred handedness.[7]

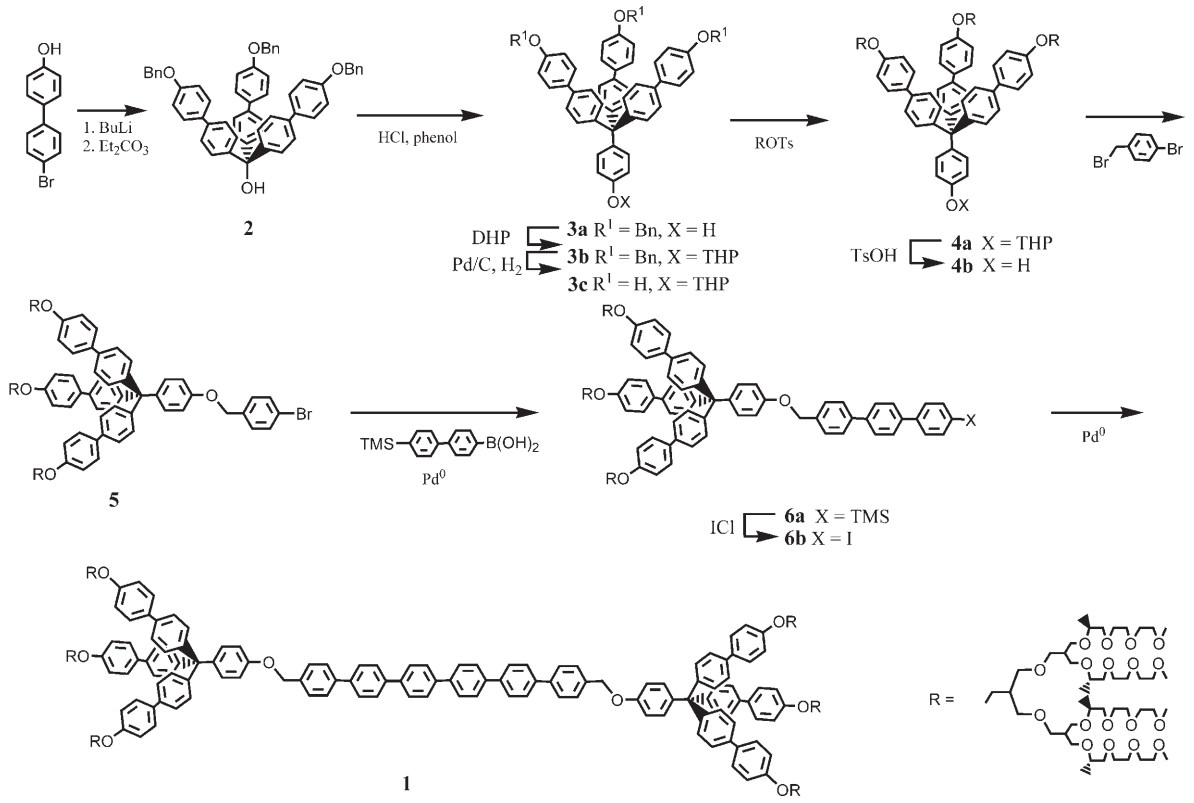
Dynamic light-scattering (DLS) experiments were performed with **1** in aqueous solution to further investigate its aggregation behavior.[8] Analysis of the autocorrelation function with the CONTIN program shows a broad peak corresponding to an average hydrodynamic radius (R_H) of approximately 60 nm. The angular dependence of the apparent diffusion coefficient (D_{app}) was measured, and the gradient of the slope was 0.03, which is consistent with the value predicted for anisotropic objects (see the Supporting Information).[9] The formation of cylindrical micelles was further confirmed by using the Kratky plot, which shows a linear angular dependence on the intensity of the light scattered by the aggregates (see the Supporting Information). In addition to DLS experiments, static light-scattering (SLS) experiments were performed in aqueous solution under the same conditions. The radius of gyration of the aggregates, $R_g = 78$ nm, was obtained from the gradient of the angular dependence of the SLS signal. The ratio R_g/R_H is 1.25, which is evidence of the formation of cylindrical aggregates.[10]

[*] Dr. J.-H. Ryu, H.-J. Kim, Z. Huang, E. Lee, Prof. M. Lee
Center for Supramolecular Nano-Assembly and
Department of Chemistry
Yonsei University
Shinchon 134, Seoul 120-749 (Republic of Korea)
Fax: (+82) 2-393-6096
E-mail: mslee@yonsei.ac.kr

[**] This work was supported by the Creative Research Initiative Program of the Ministry of Science and Technology, Korea. H.J.K., E.L., and Z.H. thank the Seoul Science Fellowship Program.

Supporting information for this article is available on the WWW under http://www.angewandte.org or from the author.

InterScience
© 2006 Wiley-VCH Verlag GmbH & Co. KGaA, Weinheim



Scheme 2. Synthesis of the dumbbell molecule **1**. DHP: dihydropyran, THP: tetrahydropyran, Ts: *para*-toluenesulfonyl, TMS: trimethylsilyl.

Further evidence of the formation of cylindrical aggregates was provided by transmission electron microscopy (TEM; Figure 1). The micrographs, which were negatively

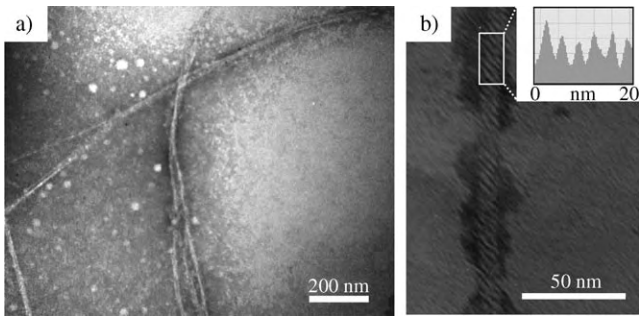


Figure 1. a) TEM image of **1** with negative staining. b) Magnified image; the inset shows the density profile.

stained with a 2 wt% aqueous solution of uranyl acetate, show helical objects with a uniform diameter of about 10 nm and a pitch length of 3.6 nm. When the extended molecular length (9.8 nm in a CPK model) is taken into consideration, the image indicates that the diameter of the elementary cylindrical objects corresponds to one molecular length.

On the basis of these results, we consider that **1** self-assembles into cylindrical micelles in which the rods are aligned perpendicular to the cylinder axis. However, the rod segments stack on top of each other with mutual rotation in the same direction to avoid steric hindrance between the bulky dendritic wedges. Consequently, this stacking of the aromatic rod segments leads to helical objects comprising hydrophobic aromatic cores surrounded by hydrophilic dendritic segments that are exposed to the aqueous environment. This formation process is similar to that of other helical structures of self-assembling molecules that are based on a conjugated rod block.[3,7,11]

Remarkably, these cylindrical objects transformed into spherical objects on adding three equivalents of 4-bromonitrobenzene (Scheme 1) to an aqueous solution of **1**. CONTIN analysis of the correlation functions in DLS experiments of the resulting solution showed R_H to be 70 nm and the SLS results showed R_g to be 73 nm. Thus, the radius of gyration of the mixture solution is nearly identical to the hydrodynamic radius. The measured diameter exceeds the extended molecular length (approximately 10 nm) by a factor of about 14, which also strongly suggests that these aggregates are capsulelike entities rather than simple micelles.[12] In contrast to the results derived for **1**, the gradient of the slope of the angular dependence of the apparent diffusion coefficient (D_{app}) was approximately zero (Figure 2a), which suggests that the self-assembled architecture is spherical.[13] The formation of spherical objects was further confirmed by TEM (Figure 2b), which revealed the presence of spherical objects with an average diameter of about 140 nm. This is in good agreement with the results obtained by DLS and SLS experiments. Atomic force microscopy (AFM) measurements showed that the spherical objects consist of a unilamellar membrane.[14]

 © 2006 Wiley-VCH Verlag GmbH & Co. KGaA, Weinheim

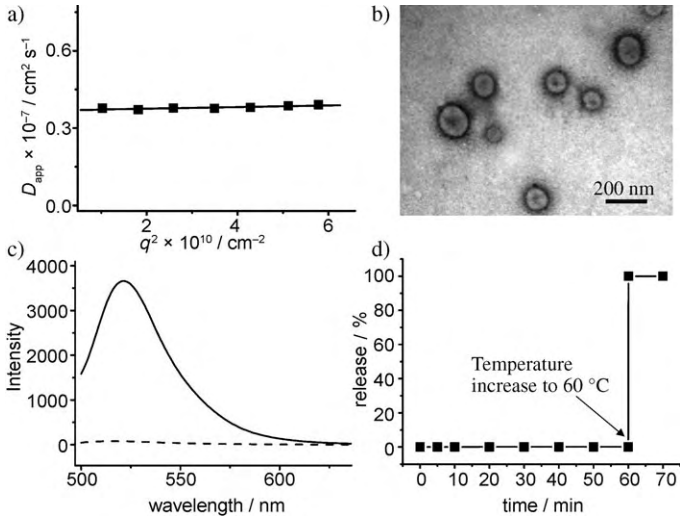


Figure 2. a) Angular dependence of D_{app} (q is the scattering vector); b) TEM image for the spherical capsules with negative staining; c) emission spectra of calcein measured at 25 °C (weak emission) and calcein measured at 60 °C (strong emission) of an aqueous solution of **1** (0.01 wt%) containing three equivalents of 4-bromonitrobenzene; d) release of calcein from the capsule as a function of time.

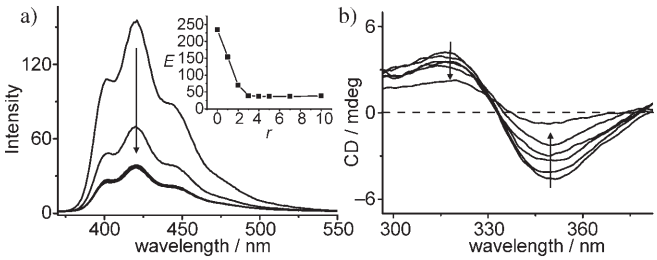


Figure 3. a) Emission spectra of **1** (0.01 wt% aqueous solution, excited at 332 nm) with the addition of 4-bromonitrobenzene. The inset shows the emission intensity at 420 nm (E) as a function of the molar ratio bromonitrobenzene:**1** (r). b) CD spectra of **1** with the addition of bromonitrobenzene (increase in molar ratio from 0 to 1).

Further evidence for the formation of hollow capsules was provided by the encapsulation of the fluorescence dye calcein.[15] Calcein, a hydrophilic fluorescent guest, was encapsulated at a sufficiently high, self-quenching concentration, and free calcein was removed by filtration over a Sephadex column. Release of calcein into solution from the inside of the capsules was accompanied by an increase in fluorescence emission (Figure 2c).[16] As shown in Figure 2d, no leakage of entrapped calcein was observed over periods of 60 min. Heating the calcein-loaded vesicular solution to 60 °C resulted in the rapid and complete release of encapsulated calcein, thus demonstrating that the dye molecules are effectively enveloped within the interior of a capsule.[17] These results show that addition of guest molecules to a solution of **1** leads to the transformation of the helical nanofibers into hollow capsulelike structures.

This unique structural variation on the addition of guest molecules can be rationalized by considering the packing arrangement of the rod segments. With amphiphilic molecular dumbbells in aqueous media, aromatic guest molecules are intercalated between the rod segments through intermolecular interactions, including hydrophobic and π–π interactions. As a result, this intercalation of the guest molecules drives the twisted packing arrangement of the rod segments into a parallel arrangement, which allows more space for guest molecules while maintaining uniform density of the dendron dumbbell ends. This parallel arrangement of the rod segments is responsible for the formation of a cagelike structure. Intercalation of the aromatic substrates within the rod segments was confirmed with 4-bromonitrobenzene as a guest molecule in an aqueous solution of **1** by fluorescence spectroscopy (Figure 3). Upon addition of the guest molecules, the fluorescence intensity of the aqueous rod–coil solution of **1** was suppressed, thus demonstrating that the guest molecules are effectively intercalated between the rod segments.[18]

Consistent with the intensity changes in the emission spectra, the CD intensity decreases rapidly upon addition of up to one equivalent of the guest molecule to give a very small CD signal, which infers the depletion of the twisted arrangement of the rod segments (Figure 3b). Upon removal of the guest molecule by extraction with *n*-hexane, the CD spectrum fully recovered, thus indicating that this structural transformation is reversible.[19] These results demonstrate that the addition of guest molecules into the solution of **1** forces the twisted arrangement of the rod segments into a parallel arrangement that leads to the formation of a capsulelike structure.

In summary, the results described herein demonstrate that the dumbbell-shaped molecules based on a hexa-*p*-phenylene rod and bulky dendritic segments self-assemble into well-defined left-handed helical cylinders with a diameter of approximately the length of one molecule and a pitch of 3.6 nm. Interestingly, the helical structure transforms into a capsulelike structure on addition of guest molecules. This reversible transformation between helical strands and nanocages in response to the addition of guest molecules is attributed to the intercalation of aromatic substrates within the rod segments and subsequent packing change of the rod segments from a twisted to a parallel arrangement to allow more space for guest molecules. This dynamic structural variation triggered by external stimuli may find useful applications in many areas including the development of responsive supramolecular materials.

Received: March 13, 2006
Revised: May 25, 2006
Published online: July 12, 2006

Keywords: host–guest systems · intercalation · nanostructures · nanotechnology · scanning probe microscopy

[1] a) J.-M. Lehn, *Proc. Natl. Acad. Sci. USA* **2002**, *99*, 4763–4768; b) I. Koltover, T. Salditt, J. O. Rädler, C. R. Safinya, *Science* **1998**, *281*, 78–81; c) S. Förster, T. Plantenberg, *Angew. Chem.* **2002**, *114*, 712–739; *Angew. Chem. Int. Ed.* **2002**, *41*, 688–714.

 © 2006 Wiley-VCH Verlag GmbH & Co. KGaA, Weinheim

[2] a) F. J. M. Hoeben, P. Jonkheijm, E. W. Meijer, A. P. H. J. Schenning, *Chem. Rev.* **2005**, *105*, 1491 – 1546; b) M. Lee, B.-K. Cho, W.-C. Zin, *Chem. Rev.* **2001**, *101*, 3879 – 3892.
[3] J. Bae, J.-H. Choi, Y.-S. Yoo, N.-K. Oh, B.-S. Kim, M. Lee, *J. Am. Chem. Soc.* **200**5, 127, 9668 – 9669.
[4] W.-Y. Yang, J.-H. Ahn, Y.-S. Yoo, N.-K. Oh, M. Lee, *Nat. Mater.* **2005**, *4*, 399 – 402.
[5] a) H. W. Gibson, S. H. Lee, P. T. Engen, P. Lecavalier, J. Sze, Y. X. Shen, M. Bheda, *J. Org. Chem.* **1993**, *58*, 3748 – 3756; b) H.-J. Kim, W.-C. Zin, M. Lee, *J. Am. Chem. Soc.* **2004**, *126*, 7009 – 7014.
[6] a) A. Ajayaghosh, S. J. George, *J. Am. Chem. Soc.* **2001**, *123*, 5148 – 5149; b) F. J. M. Hoeben, I. O. Shklyarevskiy, M. J. Pouderoijen, H. Engelkamp, A. P. H. J. Schenning, P. C. M. Christianen, J. C. Maan, E. W. Meijer, *Angew. Chem.* **2006**, *118*, 1254 – 1258; *Angew. Chem. Int. Ed.* **2006**, *45*, 1232 – 1236.
[7] P. Jonkheijm, F. J. M. Hoeben, R. Kleppinger, J. van Herrikhuyzen, A. P. H. J. Schenning, E. W. Meijer, *J. Am. Chem. Soc.* **2003**, *125*, 15 941 – 15 949.
[8] J. F. Gohy, B. G. G. Lohmeijer, A. Alexeev, X. S. Wang, I. Manners, M. A. Winnik, U. S. Schubert, *Chem. Eur. J.* **2004**, *10*, 4315 – 4323.
[9] M. Schmidt, W. H. Stockmayer, *Macromolecules* **1984**, *17*, 509 – 514.
[10] J. Tao, S. Stewart, G. Liu, M. Yang, *Macromolecules* **1997**, *30*, 2738 – 2745.
[11] a) A. P. H. J. Schenning, P. Jonkheijm, E. Peeters, E. W. Meijer, *J. Am. Chem. Soc.* **2001**, *123*, 409 – 416; b) A. Ajayaghosh, C. Vijayakumar, R. Varghese, S. J. George, *Angew. Chem.* **2006**, *118*, 470 – 474; *Angew. Chem. Int. Ed.* **2006**, *45*, 456 – 460.
[12] S. Zhou, C. Burger, B. Chu, M. Sawamura, N. Nagahama, M. Toganoh, U. E. Hackler, H. Isobe, E. Nakamura, *Science* **2001**, *291*, 1944 – 1947.
[13] R. Xu, M. A. Winnik, F. R. Hallett, G. Riess, M. D. Croucher, *Macromolecules* **1991**, *24*, 87 – 93.
[14] AFM measurements showed that when the solution was spread on a silica surface and dried in vacuo, the spherical objects become deformed. This causes the vesicles to appear as circular plates with an average thickness of approximately 20 nm, which is in good agreement with the thickness of two layers of unilamellar vesicles. Y. Tanaka, M. Miyachi, Y. Kobuke, *Angew. Chem.* **1999**, *111*, 565 – 567; *Angew. Chem. Int. Ed.* **1999**, *38*, 504 – 506.
[15] D. H. Thompson, O. V. Gerasimov, J. J. Wheeler, Y. Rui, V. C. Anderson, *Biochim. Biophys. Acta* **1996**, *1279*, 25 – 34.
[16] J. Zhu, R. J. Munn, M. H. Nantz, *J. Am. Chem. Soc.* **2000**, *122*, 2645 – 2646.
[17] At 45 °C, the dumbbell-shaped molecules disassembled so that they were no longer aggregated (see the Supporting Information).
[18] L. Li, C. Tedeschi, D. G. Kurth, H. Möhwald, *Chem. Mater.* **2004**, *16*, 570 – 573.
[19] See the Supporting Information.

 © 2006 Wiley-VCH Verlag GmbH & Co. KGaA, Weinheim

Bioorganic Chemistry

DOI: 10.1002/anie.200600368

N-Terminal Protein Modification through a Biomimetic Transamination Reaction**

*Joshua M. Gilmore, Rebecca A. Scheck, Aaron P. Esser-Kahn, Neel S. Joshi, and Matthew B. Francis**

An important challenge in the field of protein bioconjugation is the development of strategies that can modify a protein once at a single site. Although many bioconjugation reactions can functionalize specific amino acids in aqueous solution,[1] most proteins display multiple copies of the targeted residue on their surface. This commonly results in product mixtures that present the new functionality in multiple locations on the protein surface. As it is one of the rarest amino acids,[2] cysteine is the most commonly targeted residue when site-selective modification is required, but there remain many situations in which the modification of a unique copy of this residue is inconvenient or impossible. To address these limitations, several chemoselective techniques have been developed to target surface-accessible aromatic residues.[3] To complement these methods further, we report herein a biomimetic transamination reaction that can modify the N terminus of proteins and peptides under mild conditions. This technique introduces a uniquely reactive ketone or aldehyde group in a single location, thus allowing further modification through oxime or hydrazone formation. This simple strategy does not require the use of site-directed mutagenesis, and therefore has the potential to introduce virtually any functional group on a wide range of protein substrates.

The unique reactive properties of the N terminus have resulted in several strategies targeting this location to achieve site-selective protein modification. To a limited extent, the lower pK_a value of N-terminal amino groups (relative to lysine side chains) can be used to direct acylation reactions to

[*] J. M. Gilmore,[+] R. A. Scheck,[+] A. P. Esser-Kahn, N. S. Joshi, Prof. M. B. Francis
Department of Chemistry
University of California
Berkeley and Materials Sciences Division
Lawrence Berkeley National Laboratory
Berkeley, CA 94720 (USA)
Fax: (+1) 510-643-3079
E-mail: francis@cchem.berkeley.edu

[+] These authors contributed equally to this work.

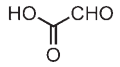
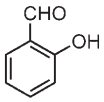
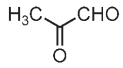
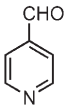
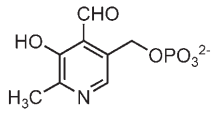
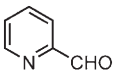
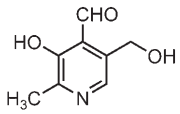
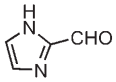
[**] The authors thank the DOE Nanoscale Science and Engineering Technology (NSET) program for financial support, as well as the Department of Chemistry at the University of California, Berkeley, and the Berkeley Chemical Biology Graduate Program. N.S.J. gratefully acknowledges the Saegebarth family for generous fellowship support.

Supporting information for this article is available on the WWW under http://www.angewandte.org or from the author.

© 2006 Wiley-VCH Verlag GmbH & Co. KGaA, Weinheim

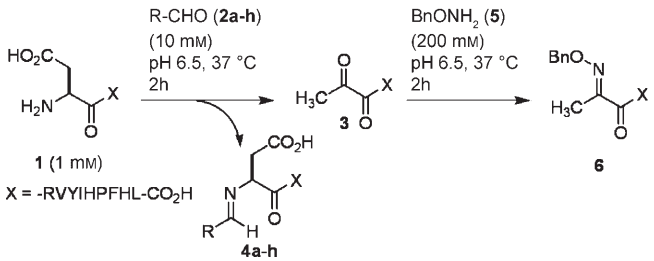
this site through careful control of the reaction pH.[4] However, the large number of competing lysine residues (10–40 on most proteins) limits the selectivity of this reaction in most cases. Alternative strategies have targeted the N terminus in combination with specific amino acid side chains. In particular, the reaction of N-terminal cysteine residues with thioesters has been used with great success, and affords fusion proteins through native chemical ligations.[5] N-terminal cysteine residues have also been modified through thiazolidine formation by using aldehyde reagents.[6] Reactive aldehydes can be formed through periodate oxidation of N-terminal serine and threonine residues,[7] and N-terminal tryptophan residues can be modified through Pictet–Spengler reactions.[8]

Table 1: Modification of angiotensin I (**1**) using aldehyde reagents.[a]

	Aldehyde	**3** [%]	**4a–h** [%]		Aldehyde	**3** [%]	**4a–h** [%]
2a		ca. 10	trace	**2e**		0	25
2b		14	17	**2f**		10	50
2c		65	0	**2g**		trace	>90
2d		0	0	**2h**		20	40

[a] Conditions: 1 mM **1**, 10 mM aldehyde, 50 mM phosphate buffer (pH 6.5), 37 °C, 2 h. Product distributions were determined by ESI-MS.

An alternative strategy that does not depend on the identity of the amino acid side chain can be envisioned through the oxidation of the N-terminal amino group to an imine, followed by hydrolysis to afford a ketone or an aldehyde. This reaction pathway has indeed been demonstrated for the chemospecific functionalization of N termini by using glyoxylic acid, copper(II) salts, 1M pyridine, and 1M HOAc.[9] However, these conditions are too harsh to maintain the folded structure of most proteins, and are therefore more appropriate for sequence-analysis applications. In contrast to these reports, however, initial studies by our research group found that the N-terminal aspartic acid residue of angiotensin I (**1**) unexpectedly decarboxylated to a small extent (ca. 10%) when the peptide was simply treated with glyoxylic acid (**2a**; Scheme 1). The product of the reaction was identified as pyruvamide **3** through subsequent reaction with *O*-benzylhydroxylamine (**5**) to form oxime **6**. Screening experiments indicated that the structure of the aldehyde substitutent strongly influenced the reaction efficiency (Table 1) and that the decarboxylated product was often accompanied by various amounts of imines **4a–h**. Interestingly, pyridoxal-5-phosphate (PLP, **2c**) emerged as the most effective aldehyde, thus affording a 65% conversion of **1** into ketone **3** in 2 h at 37 °C, with no observed imine formation.



Scheme 1. Formation of oxime 6 from the N-terminal aspartic acid residue of angiotensin I (**1**). Bn = benzyl.

Subsequent optimization experiments determined that a 1 mM peptide solution could be modified by using 10 mM PLP in 50 mM phosphate buffer at pH 6.5 and 37 °C (Table 2, entry 1). Consistent with other reactions involving carbonyl condensations,[10] reactions at pH 6.5 afforded the optimal amount of product, although slight variations were still tolerated (Table 2, entries 2–4). An increase in temperature to 65 °C resulted in rapid conversion of **1** into **3** (>95% in 2 h; Table 2, entry 5), although excellent conversion could also be obtained after 24 h at room temperature (Table 2, entry 7). The reaction was found to proceed readily in 2-[4-(2-hydroxyethyl)-1-piperazinyl]ethanesulfonic acid (HEPES), 3-(*N*-morpholine)propanesulfonic acid (MOPS), and phosphate buffers, and, contrary to previous transamination reports,[11] did not require the presence of divalent cations or denaturing organic cosolvents. A variety of Lewis acids were screened to confirm this, and little change in rate or conversion was observed.[12] Moreover, experiments performed in the presence of 10 mM ethylenediaminetetraacetate (EDTA) to sequester any metal ions in the reaction solution resulted in equivalent product yields.

Table 2: Peptide modification using **2c**.[a]

Entry	Peptide	Sequence	pH	*T* [°C]	*t* [h]	Conv [%]
1	**1**	DRYVIHPFHL	6.5	37	1	65
2	**1**	DRYVIHPFHL	5.5	37	1	29
3	**1**	DRYVIHPFHL	7.5	37	1	46
4	**1**	DRYVIHPFHL	8.5	37	1	43
5	**1**	DRYVIHPFHL	6.5	65	2	>95
6	**1**	DRYVIHPFHL	6.5	22	2	55
7	**1**	DRYVIHPFHL	6.5	22	18	88
8	**7**	DNALRAFKYM	6.5	37	2	90
9	**8**	MYKFARLAND	6.5	37	2	71
10	**9**	GLELEEYWKWGDKNYDG	6.5	37	2	43

[a] Conditions for peptides: 1 mM peptide, 10 mM **2c**, 50 mM phosphate buffer. Product distributions were determined by ESI-MS after oxime formation with **5**.

 © 2006 Wiley-VCH Verlag GmbH & Co. KGaA, Weinheim

The most useful feature of this reaction is its selectivity for the N terminus of the peptide. Under the optimized conditions, peptide **7** afforded 90% conversion into the ketone product (Table 2, entry 8). These screening experiments also revealed that the N-terminal residue does not need to be aspartic acid, as peptides bearing N-terminal methionine (**8**) and glycine (**9**) residues still afforded good yields of the desired products. These peptides also provided the singly modified conjugate, despite the presence of internal lysine residues.

In a biological context, PLP is a cofactor that effects a variety of metabolic transformations under enzymatic control, including racemization, elimination, decarboxylation, and transamination.[13] Typically, PLP-mediated reactions first involve condensation of the aldehyde with amino groups on a peptide or protein, thus leading to the formation of imine **4c** (Scheme 2). In the absence of an enzyme, this process could occur with all the amino groups on a particular biomolecule. However, the imine formed with the N terminus has an α proton with a much lower pK_a value, which allows tautomerization to occur uniquely at this site. Hydrolysis of the resulting glyoxyl imine **10** (accompanied by decarboxylation in the case of aspartic acid) yields an aldehyde or ketone specifically at the N terminus. Although in principle this reaction sequence could take place on the N termini of peptides and proteins in living cells, this pathway has not been reported to date. This is likely due to the low concentration of unbound PLP in the cytoplasm.

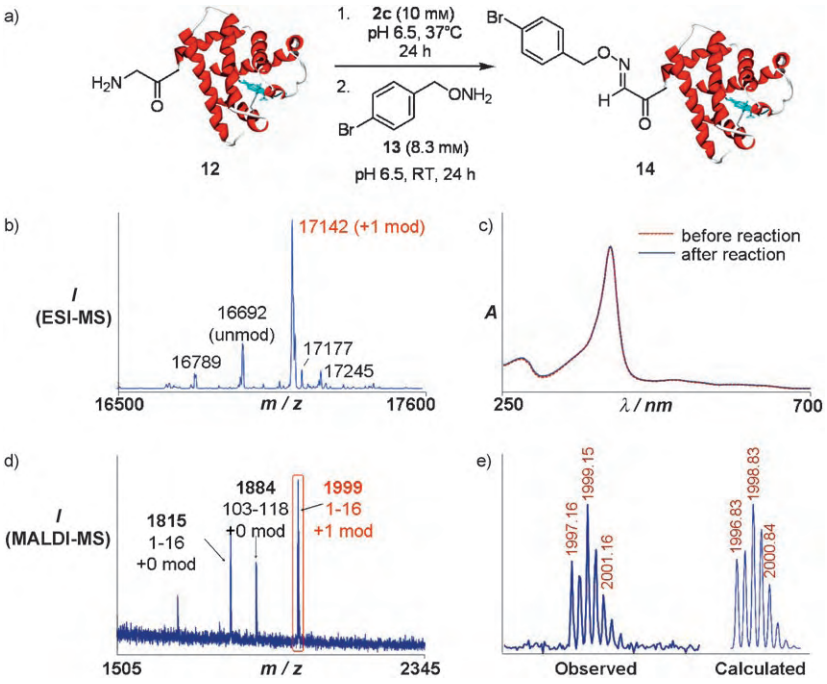
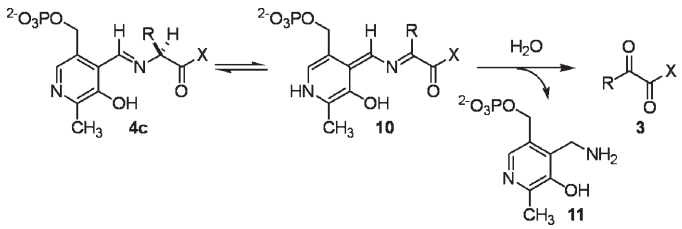


Figure 1. Site-selective protein modification with PLP. a) Myoglobin was treated with **2c** at 37°C for 24 h. After removal of small molecules by gel filtration, oxime **14** was formed after reaction with **13**. b) ESI-LCMS studies indicated that only one modification had occurred. c) UV/Vis spectra of **12** subjected to the reaction conditions in the absence (dotted red) and presence (dashed blue) of **2c**. d) Product **14** was digested with trypsin, and the resulting fragments were analyzed by MALDI-TOF MS. The only modified fragment observed contained the N-terminal residue. e) Predicted (left) and observed (right) isotope patterns for the modified myoglobin peptide fragment shown in (d). All MS values agree with those predicted within 0.01%.



Scheme 2. Formation of pyruvamide **3**.

The development of the reaction for protein targets was initiated with horse heart myoglobin (**12**), which has an N-terminal glycine residue. Optimal conditions for myoglobin modification were found to be 50 μM protein and 10 mM PLP for 20 h at 37°C in 25 mM phosphate buffer (pH 6.5; Figure 1a). Following treatment of the mixture with *p*-bromobenzyloxyamine (**13**), it was determined by ESI-MS that a single product was obtained that corresponded to the expected oxime **14** (Figure 1b). The overall conversion of the reaction was determined to be greater than 75% by ESI-MS and 69% using sodium dodecyl sulfate polyacrylamide gel electrophoresis (SDS-PAGE analysis techniques, see below). Following removal of excess PLP, the absorbance of the heme component was found to be unchanged over the course of the reaction (Figure 1c). This observation provides good evidence that the tertiary structure of the protein was still intact following the modification procedure.

We were able to confirm the site-specificity of this modification after subjecting **14** to a proteolytic digest with trypsin. Analysis of the peptide fragments by MALDI-TOF-MS showed that the reaction had occurred on the N-terminal fragment of the protein (Figure 1d). The bromine atom of **13** provided a useful analysis tag, as the characteristic isotope pattern was specific to the modified fragment and could be observed clearly (Figure 1e). Despite the 17 lysine residues on the protein, no other modified peptides were observed, a result that is consistent with the observation that these residues do not participate in this reaction.

The oxime linkage is well suited for use as a probe or linker in biochemical systems, as it is selective for ketone and aldehyde functionalities, forms in high yield, and is stable under physiological conditions.[14] As an example, the N terminus of myoglobin was fluorescently labeled with chromophore **15**. SDS-PAGE analysis revealed selective labeling of the protein after activation with PLP (Figure 2b, lane 1), whereas no labeling was observed for unactivated myoglobin (lane 2).

This technique can also be used to label proteins when chemistry appropriate for cysteine groups is not available. For example, cysteine 70 in the green fluorescent protein[15] (EGFP, **16a**) is reactive toward maleimide reagents and this protein (in our hands) cannot be expressed in fluorescent

 © 2006 Wiley-VCH Verlag GmbH & Co. KGaA, Weinheim

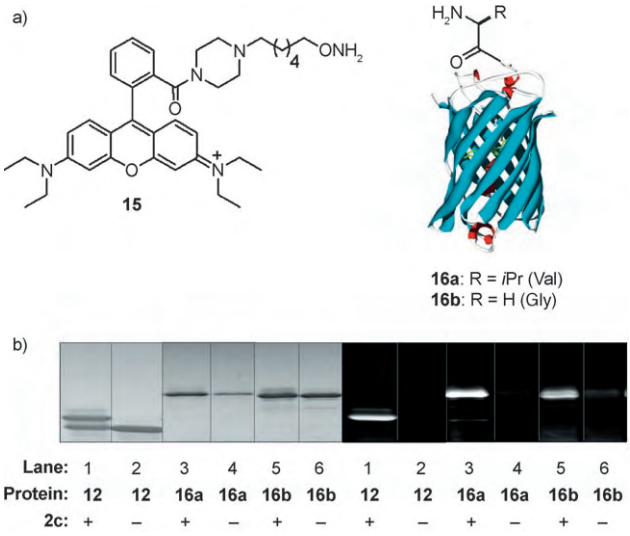


Figure 2. Site-specific chromophore labeling. Proteins possessing N-terminal carbonyl groups introduced by **2c** were labeled with **15**. Reaction success was confirmed by SDS-PAGE analysis using Coomassie staining (left) and fluorescence visualization (right).

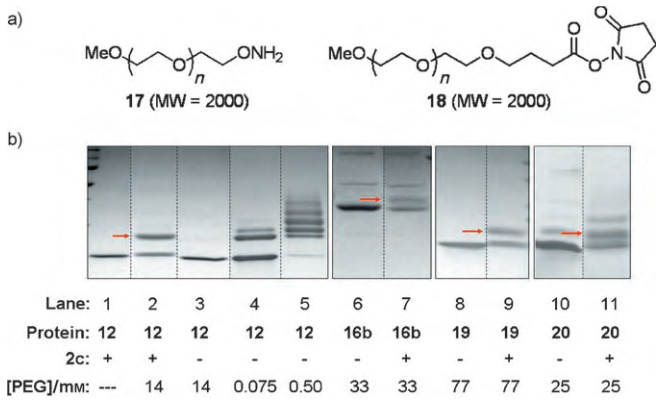


Figure 3. Site-selective attachment of PEG polymers to proteins. a) PEG-alkoxyamine **17** was synthesized and coupled to N-terminal carbonyl groups introduced using **2c**. b) Analysis by SDS-PAGE with Coomassie staining confirmed single-site labeling of the proteins (lanes 1–3, 6–11). The red arrows indicate the shift in the position on the gel caused by the attached PEG polymer. PEG-NHS ester **18** was used to label lysine residues of **12** nonspecifically (lanes 4 and 5). A small portion of thioredoxin (**20**) reacts with the PEG-alkoxyamine without treatment with **2c** (lane 10). This background reaction gives rise to the small portion of doubly labeled product shown in lane 11. Protein **19** is RNase A.

form when this residue has been substituted. Thus, the labeling of other positions on this protein is difficult to achieve by standard mutagenesis techniques. We have found that the N-terminal modification method can overcome this limitation, and results in the attachment of **15** at the N-terminal valine residue of **16a** (Figure 2b, lanes 3 and 4) and at the N-terminal glycine residue of mutant **16b**. Subsequent experiments have confirmed that the internal chromophore retains its fluorescence after modification with PLP.[12]

The attachment of poly(ethylene glycol) (PEG) chains to proteins has been shown to improve circulation lifetime, lower immunogenicity, and confer proteolysis resistance.[16] These conjugates are typically prepared through lysine modification, which results in complex mixtures that exhibit varying levels of efficacy. To avoid this, we have used the two-step strategy outlined above to attach a single polymer chain to the N terminus of proteins.[17,18] Specifically, the aldehyde of PLP-activated myoglobin was treated with various equivalents of the previously reported[19] PEG alkoxyamine **17**. As seen in Figure 3b (lanes 1–3), a single bioconjugate was obtained even when using a large excess of **17**. Using similar conditions, this reaction strategy has also proven effective for EGFP (**16b**, lanes 6 and 7), RNase A (**19**, lanes 8 and 9), and thioredoxin (**20**, lanes 10 and 11). For comparison, PEG-NHS ester **18** yielded a ladder of polymer conjugates for the labeling of **12** (Figure 3b, lanes 4 and 5). Clean conversion to a singly modified protein was not observed under any conditions using this approach.

The shift on the gel caused by polymer attachment provides a useful method for the quantitation of reaction conversion by optical densitometry measurements after Coomassie staining (Table 3). For myoglobin, 69% overall conversion was achieved at 37°C, and for EGFP (**16b**) 53% conversion was obtained. High levels of modification could be obtained for **16a** and **16b** at 55°C. RNase A (**19**) was cleanly modified in 50% conversion at 37°C, as was thioredoxin (**20**) under identical conditions. The large number of disulfide and free thiol groups that proteins **19** and **20** possess render them difficult to modify in a single location by other methods. Finally, initial studies have found that protein G′ (**21**) can be modified to 30% at 41°C, thus indicating that proteins with N-terminal methionine residues are compatible with this technique. Studies to increase the conversion for this important class of substrates are in progress, as are studies to evaluate the compatibility of other N-terminal amino acids.

We anticipate that proteins possessing N-terminal serine, threonine, cysteine, and tryptophan residues will be incompatible with this technique because of known side reactions with aldehydes.[6,8] It is also presumed that N-terminal proline residues will be unreactive. Outside of these limitations, this reaction provides a generally applicable tool for the site-selective labeling of protein targets. Our current efforts use

Table 3: Protein modification using **2c**.[a]

Entry	Protein	N-terminal amino acid	Conc. [μM]	*T* [°C]	Conv. [%]
1	myoglobin (**12**)	glycine	50	37	69
2	GFP-1V (**16a**)	valine	10	55	67
3	GFP-1G (**16b**)	glycine	10	37	41
4	GFP-1G (**16b**)	glycine	10	55	80
5	RNase A(**19**)	lysine	50	37	50
6	thioredoxin (**20**)	glycine	94	37	50
7[b]	protein G′ (**21**)	methionine	33	41	30

[a] Conditions: 10 mM **2c**, 25 mM phosphate buffer, pH 6.5, 18–20 h. Product yields were determined by densitometry after derivitization with **17** and separation by SDS-PAGE (Coomassie stain, see Figure 3). [b] Extent of protein modification was determined by ESI-MS after oxime formation with **5**.

© 2006 Wiley-VCH Verlag GmbH & Co. KGaA, Weinheim

this methodology for the site-specific placement of fluorophores for sensing applications and the dual modification of both protein termini for device integration.

Received: January 27, 2006
Revised: May 27, 2006
Published online: July 17, 2006

Keywords: bioconjugation · bioorganic chemistry · oximes · protein modifications

[1] For an excellent review on protein bioconjugation, see: G. T. Hermanson, *Bioconjugate Techniques*, 1st ed., Academic Press, San Diego, **1996**.
[2] R. F. Doolittle in *Prediction of Protein Structure and the Principles of Protein Conformation* (Ed.: G. D. Fasman), Plenum, New York, **1989**.
[3] a) J. M. Antos, M. B. Francis, *J. Am. Chem. Soc.* **2004**, *126*, 10256; b) N. S. Joshi, L. R. Whitaker, M. B. Francis, *J. Am. Chem. Soc.* **2004**, *126*, 15924; c) J. M. Hooker, E. W. Kovacs, M. B. Francis, *J. Am. Chem. Soc.* **2004**, *126*, 3718–3719; d) S. D. Tilley, M. B. Francis, *J. Am. Chem. Soc.* **2006**, *128*, 1080–1081.
[4] D. P. Baker, E. Y. Lin, K. Lin, M. Pellegrini, R. C. Petter, L. L. Chen, R. M. Arduini, M. Brickelmaier, D. Wen, D. M. Hess, L. Chen, D. Grant, A. Whitty, A. Gill, D. J. Lindner, R. B. Pepinsky, *Bioconj. Chem.* **2006**, *17*(1), 179–188.
[5] a) P. E. Dawson, T. W. Muir, I. Clarklewis, S. B. H. Kent, *Science* **1994**, *266*, 776–779; b) T. W. Muir, *Annu. Rev. Biochem.* **2003**, *72*, 249–289.
[6] J. P. Tam, Q. Yu, Z. Miao, *Biopolymers* **1999**, *51*, 311–332.
[7] a) K. F. Geoghegan, J. G. Stroh, *Bioconjugate Chem.* **1992**, *3*, 138–146; b) J. K. Chen, W. S. Lane, A. W. Brauer, A. Tanaka, S. L. Schreiber, *J. Am. Chem. Soc.* **1993**, *115*, 12591–12592.
[8] X. Li, L. Zhang, S. E. Hall, J. P. Tam, *Tetrahedron Lett.* **2000**, *41*, 4069–4073.
[9] H. B. F. Dixon, *J. Protein Chem.* **1984**, *3*, 99–108.
[10] W. P. Jencks, *J. Am. Chem. Soc.* **1959**, *81*, 475–481.
[11] R. Fields, H. B. F. Dixon, *Methods Enzymol.* **1972**, *25*, 409–419.
[12] See the Supporting Information for details.
[13] For reviews of PLP-mediated reactions, see: a) M. D. Toney, *Arch. Biochem. Biophys*, **2005**, *433*, 279–287; b) A. C. Eliot, J. F. Kirsch, *Annu. Rev. Biochem.* **2004**, *73*, 383–415.
[14] a) M. Calzadilla, T. Cordova, A. Malpica, *J. Phys. Org. Chem.* **1999**, *12*, 708–712; b) S. Rosenberg, S. M. Silver, J. M. Sayer, W. P. Jencks, *J. Am. Chem. Soc.* **1974**, *96*, 7987; see also: c) H. C. Hang, C. R. Bertozzi, *Acc. Chem. Res.* **2001**, *34*, 727–736; d) V. W. Cornish, K. M. Hahn, P. G. Schultz, *J. Am. Chem. Soc.* **1996**, *118*, 8150–8151.
[15] R. Y. Tsien, *Annu. Rev. Biochem.* **1998**, *67*, 509–544.
[16] R. E. Offord, H. F. Gaertner, *Bioconjugate Chem.* **1996**, *7*, 38–44.
[17] For an avidin/biotin-based approach to the site-selective attachment of polymers to proteins, see: D. Bontempo, H. D. Maynard, *J. Am. Chem. Soc.* **2005**, *127*, 6508–6509.
[18] For an alternate strategy that employs solid-phase-assisted synthesis to yield an aminooxy-functionalized protein which has also been used to prepare PEG monoconjugates, see: H. Shao, M. M. Crnogorac, T. Kong, S.-Y. Chen, J. M. Williams, J. M. Tack, V. Gueriguian, E. N. Cagle, M. Carnevali, D. Tumelty, X. Paliard, L. P. Miranda, J. A. Bradburne, G. G. Kochendoerfer, *J. Am. Chem. Soc.* **2005**, *127*, 1350–1351; see also: G. G. Kochendoerfer, *Curr. Opin. Chem. Biol.* **2005**, *9*, 555–560.
[19] T. L. Schlick, Z. Ding, E. W. Kovacs, M. B. Francis, *J. Am. Chem. Soc.* **2005**, *127*, 3718–3723.

 © 2006 Wiley-VCH Verlag GmbH & Co. KGaA, Weinheim

DNA Recognition

DOI: 10.1002/anie.200601127

High Thermal Stability of 5′-5′-Linked Alternate Hoogsteen Triplexes at Physiological pH**

Vyacheslav V. Filichev, Mads C. Nielsen, Niels Bomholt, Carsten H. Jessen, and Erik B. Pedersen*

Sequence-specific recognition, targeting, treatment, and alteration of double-stranded DNA (dsDNA) are topics of considerable interest for the study of mutated or recombined genes.[1] The formation of triple helixes through binding of a single-stranded triplex-forming oligonucleotide (TFO) to a homopurine sequence of dsDNA through major-groove interactions is one of the approaches to generate novel therapeutics on the dsDNA level. The design of a third strand that will bind to the dsDNA under physiological conditions is still challenging. In the parallel binding motif, the sensitivity of C^+·G-C Hoogsteen base pairs to pH must be overcome.[2] The formation of stable secondary structures, such as quadruplexes,[2,3] and the instability of triplexes in the presence of K^+ and Na^+ ions are major limitations for purine-containing TFOs.[2,4] Another limitation for the generation of a TFO is its length, which is supposed to be in the range of 15 to 30 base pairs to ensure target-specificity and binding affinity.[5]

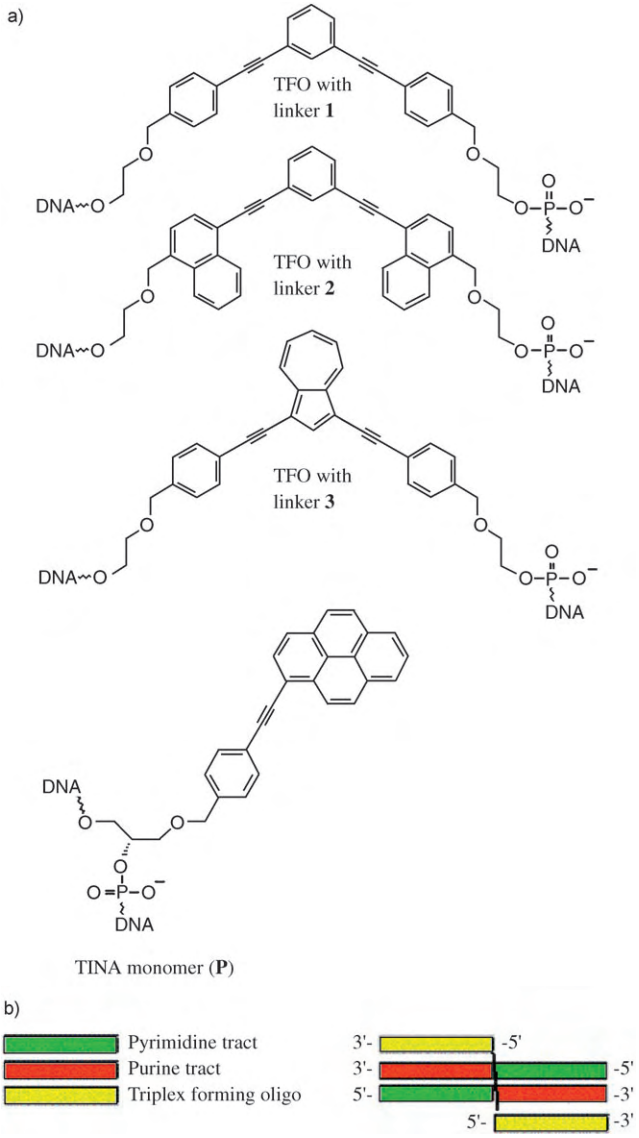
To increase the number of targets, alternate-strand TFOs have been designed, which consist of two sequences with inverted polarity that are linked to each other through an appropriately chosen linker to ensure binding to two adjacent purine tracts on opposite strands of the dsDNA.[6] Most of the sequences have been designed in a 3′-3′ fashion,[7] and only a few examples have been published for the 5′-5′ linkage.[8] A phosphodiester,[6a,7] a short unpaired oligonucleotide sequence,[9] and alkyl chains[10] are usually used as the linkers. However, such linkers do not ensure the stability of the final TFOs under physiological conditions. Attachment of an intercalator at adjacent positions of the alternate-strand TFOs has been used to increase the stability.[11] Recently, we designed an intercalating 5′-5′ linker **1** (Scheme 1) to connect two 8-mer sequences with inverted polarity to generate a Hoogsteen-type triplex, with a considerable increase in the thermal stability.[8b] For further biological evaluation of the alternate-strand TFO containing the bridge **1**, we chose the extensively studied HIV-1 sequence[12] (D1,

[*] Dr. V. V. Filichev, M. C. Nielsen, N. Bomholt, Dr. C. H. Jessen, Prof. E. B. Pedersen
Nucleic Acid Center
Department of Chemistry
University of Southern Denmark
Campusvej 55, 5230 Odense M (Denmark)
Fax: (+45) 6615-8780
E-mail: filichev@chem.sdu.dk

[**] The Nucleic Acid Center is funded by The Danish National Research Foundation for studies on nucleic acid chemical biology.

Supporting information for this article is available on the WWW under http://www.angewandte.org or from the author.

© 2006 Wiley-VCH Verlag GmbH & Co. KGaA, Weinheim



Scheme 1. a) Structures of the monomer of twisted intercalating nucleic acids (**P**, TINA) and linkers for alternate strand TFOs (**1**–**3**). b) Representation of the 5′-5′ alternate-strand triplex concept.

Table 1), which enabled the possibility for the design of alternate-strand triplexes consisting of nine base pairs from one side and five base pairs from another. However, a remarkable drop in the melting temperature (T_m) of the triplex for an alternate-strand TFO possessing linker **1** (ON1/D1, Table 1) from 42.5 °C to less than 5 °C was observed when the pH value of the solution was changed from 6.0 to 7.2. We saw also that the reference 9-mer sequence (ON9), which is the longest part of one of the alternate-strand TFO arms, was unable to bind to dsDNA (D1) at pH 7.2, and a T_m value of 16.0 °C was observed at pH 6.0. This was a result of the presence of a single 5-methylcytosine in the sequence, which is supposed to be less sensitive to pH than cytosine.[13] Increasing the length of one of the strands by three 5-methylcytosine groups in ON2 did not improve the T_m values at neutral pH. As the thermal stability of TFOs should be higher than or in the range of 37 °C to ensure the TFOs have biological activity, we decided to design new 5′-5′ alternate, intercalating linkers for Hoogsteen-type triplexes and also use recently discovered twisted intercalating nucleic acids (TINAs).[14] TINAs possess bulged insertions of (*R*)-1-*O*-[4-(1-pyrenylethynyl)phenylmethyl]glycerol (**P**, Scheme 1) in the middle of homopyrimidine sequences and lead to parallel triplexes with extraordinary thermal stability.[14] Herein, we present novel 5′-5′ alternate-strand Hoogsteen-type oligonucleotides, which can bind to dsDNA at pH 7.2 and possess intercalating linkers. We also report on their combinations with TINA monomer **P**.

We assumed that better π–π interactions with surrounding nucleobases within the complex of TFO/dsDNA and, therefore, increased thermal stabilities could be achieved by increasing the number of fused aromatic rings in the linker **1**. Triple bonds have been considered to be good connectors that provide structural rigidity, twisting ability,[8b,14] and improved intercalation.[15] The two peripheral benzene rings of **1** were replaced by naphthalene rings to give the linker **2** (Scheme 1). The central benzene ring of **1** was also substituted by 1,3-azulene to provide structure **3** (Scheme 1). Models of both linkers in triple helixes were minimized with the AMBER force field in MacroModel 8.0 and the results are presented in Figure 1.[16] As can be seen from these pictures, the naphthalene rings stacked with the nucleic bases of the alternate-strand TFO and they also partially covered purine bases involved in Hoogsteen base pairing (Figure 1 a,c). In contrast to this, the azulene unit was positioned in the middle of the dsDNA part of the triplex, just above the area of Watson–Crick base pairing, partially stacking with both duplex bases (Figure 1 b,d).

The dimethoxytrityl (DMT) protected phosphoramidites of linkers **2** and **3** needed for DNA synthesis were prepared from the corresponding aromatic diols, which were obtained in a Sonogashira Pd^0-catalyzed reaction from 1,3-diethynylbenzene and 2-(4-bromonaphthalen-1-ylmethoxy)ethanol in the case of **2**, and from 1,3-diiodoazulene and 2-(4-iodobenzyloxy)ethanol in the case of **3**.[17] Phosphoramidites were used for the synthesis of TFOs on a DNA synthesizer.[17] The thermal stability of the Hoogsteen-type triplexes was assessed by thermal denaturation experiments. The melting temperatures (T_m, °C) determined as the first derivatives of the melting curves at 260 nm are presented in Table 1. To be sure that the resulting alternate-strand triplexes bind to both purine-rich parts of the dsDNA we checked the thermal stability toward mismatched dsDNA (D2 and D3, Table 1). For comparison, **P** was singly and doubly inserted in a 9-mer (ON11 and ON12, respectively) at the same intercalation sites as in ON5 and ON7. In cases of the coincident melting of the triplexes and duplexes when using a **P** monomer, thermal denaturation was also monitored at 373 nm (T_m values in parentheses in Table 1).

As can be seen from the T_m data in Table 1, the use of linker **2** in the 5′-5′ alternate TFO (ON3) resulted in increased thermal stability ($\Delta T_{m(ON3/D1-ON1/D1)} = +6.5$ °C) at pH 6.0 of the triplex with matched dsDNA (D1) relative to that formed from the TFO with linker **1**. Moreover, a T_m value of 43.5 °C

 © 2006 Wiley-VCH Verlag GmbH & Co. KGaA, Weinheim

Table 1: T_m [°C] data for third-strand melting, taken from UV/melting curves ($\lambda = 260$ nm).[a]

Entry	Sequence	D1 pH 6.0	D1 pH 7.2	D2 pH6.0	D3 pH 6.0
ON1	3′-TT TTT-5′-**1**–5′-TTT T**C**T TTT-3′	42.5	< 5.0	22.5	< 5.0
ON2	3′-TT TTT-5′-**1**–5′-TTT T**C**T TTT **CCC**-3′	44.5	< 5.0	28.5	30.0
ON3	3′-TT TTT-5′-**2**–5′-TTT T**C**T TTT-3′	49.0	43.5	26.0	29.5
ON4	3′-TT TTT-5′-**3**–5′-TTT T**C**T TTT-3′	35.5	< 5.0	20.5	< 5.0
ON5	3′-TT TTT-5′-**1**–5′-TTT T**CTP**TTT-3′	55.5 (55.0)[b]	50.5 (48.5)	44.5	< 5.0
ON6	5′-**P**-3′-TT TTT-5′-**1**–5′-TTT T**C**T TTT-3′	50.0 (50.0)	43.5 (43.5)	32.0	30.5
ON7	3′-TT TTT-5′-**2**–5′-TTT T**CTP**TTT-3′	60.0 (57.5)	50.0 (50.0)	42.5	46.0
ON8	5′-**P**-3′-TT TTT-5′-**2**–5′-TTT T**C**T TTT-3′	54.5 (49.0)	47.5	35.5	36.5
ON9	5′-TTT T**C**T TTT-3′	16.0	< 5.0	n.d.[c]	n.d.
ON10	5′-**2**–5′-TTT T**C**T TTT-3′	41.0	39.0	n.d.	n.d.
ON11	5′-TTT T**CTP**TTT-3′	42.0	35.0	n.d.	n.d.
ON12	5′-**P**TTT T**CTP**TTT-3′	65.5 (58.5)	65.5 (52.5)	50.0 (50.0)	n.d.

[a] $C = 1.5$ μM of ON1–12 and 1.0 μM of each strand of dsDNA (D1–3) in 20 mM sodium cacodylate, 100 mM NaCl, 10 mM $MgCl_2$, pH 6.0 and 7.2; duplex $T_m = 68.0$ (D1: 3′-GGT GAA AAA TTT TCT TTT CCC CCC TGA CC-5′/5′-CCA CTT TTT AAA AGA AAA GGG GGG ACT GG-3′, pH 6.0), 70.0 °C (D2: 3′-GGT GAA AAA *C*TT TCT TTT CCC CCC TGA CC-5′/5′-CCA CTT TTT *G*AA AGA AAA GGG GGG ACT GG-3′, pH 6.0), 70.0 °C (D3: 3′-GGT GACCAA TTT TCT TTT CCC CCC TGA CC-5′/5′-CCA CT*G*GTT AAA AGA AAA GGG GGG ACT GG-3′, pH 6.0) and 68.0 °C (D1, pH 7.2); bases in italics are mismatched to TFOs; **C** is 5-methylcytosine. [b] T_m values determined at 373 nm for **P**-containing sequences are given in parentheses in cases of overlaid triplex and duplex meltings. [c] n.d.–not determined.

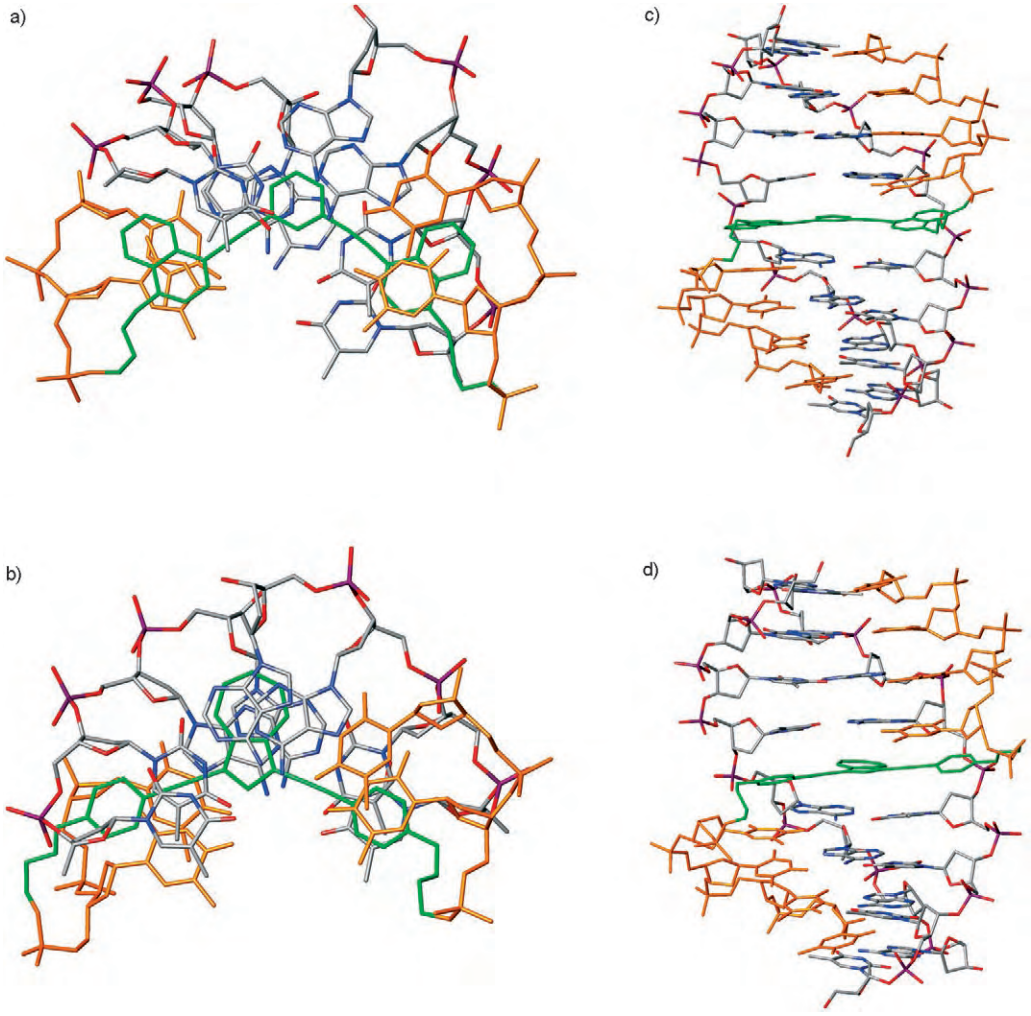


Figure 1. Structures obtained by molecular modeling studies of the triplexes with alternate-strand TFOs in yellow with intercalating linkers **2** (Figure 1 a,c) and **3** (Figure 1 b,d) in green. Top views of the structures are shown in Figure 1 a and b; side views are shown in Figure 1 c and d.

 © 2006 Wiley-VCH Verlag GmbH & Co. KGaA, Weinheim

was detected for ON3/D1 at pH 7.2. In contrast, linker **3** (ON4) lowered the thermal stability of the triplex at pH 6.0 relative to those with **1** and **2**, and no triplex transition was observed at pH 7.2. In cases of binding to mismatched dsDNA (D2 and D3), the considerable drop in the triplex T_m value was observed with linkers **1**–**3** (ON1–ON4) at pH 6.0. The T_m value of the triplex with D1 also increased when the second, shortest arm of the alternate TFO was attached to the linker **2** (ON3 versus ON10). These experiments indicate that both arms of the synthesized alternate-strand TFOs bind to both purine-rich stretches of dsDNA (D1). It could be expected that T_m values for ON10/D1 at pH 6.0 and for the triplex formed between ON3 and the mismatched dsDNA (D3) should be similar. However, a difference of 11.5 °C in the T_m values was observed. We presume that this effect is a result of a different positioning of the intercalator **2** in the dsDNA part of the triplex. The bulky mismatched dangling end of ON3 may force the intercalator **2** into a less favorable position inside the duplex. Interestingly, the replacement of AT base pairing next to the intercalating linker in D1 by GC in D2 gave a large reduction in the T_m values with ON1–ON4, despite the non-interrupting purine sequence in the dsDNA. From these data we can conclude that it is advantageous to use an intercalating linker to connect two alternate strands of the TFO as it leads to a sequence-specific oligonucleotide.

Lower T_m values and a longer time was needed for the formation of a triplex with ON4 containing linker **3** than those required for alternate-strand triplex bridges **1** and **2** (ON1, ON3). Thus, for ON4, keeping the samples for 24 h at 4 °C prior to thermal denaturation was required for the observion of the triplex transition at 260 nm, while samples with TFOs possessing linkers **1** and **2** needed to stand for only 1 h at 5 °C in the same buffer solutions. We suppose that these properties are consequences of placing the azulene ring in linker **3** exactly in the middle of the dsDNA, in the zone where Watson–Crick hydrogen bonds are formed. On the other hand, as can be seen from molecular modeling studies (Figure 1 B), one of the benzene rings of linker **3** does not stack with the TFO bases, because of a difference in the geometry arising from the 1,3-substitution in the 5- and 6-membered rings. For the future design of 5′-5′ Hoogsteen alternate linkers, it can be concluded that structures with increased aromatic surface should cover the area of the TFO bases and purine residues of dsDNA and be connected through a 1,3-disubstituted benzene or similar ring to provide intercalation in the whole system. The importance of the proper intercalation and stacking properties of **2** can also be illustrated by comparison of the thermal stability of triplexes formed between ON1, ON3, and ON4 with D1 at pH 6.0 and 7.2. With ON1 and ON4, the drop in the T_m value was significant when the pH value was increased from 6.0 to 7.2. In contrast, a ΔT_m value of 5.5 °C was observed for the triplex ON3/D1. Double insertion of **P** in a 9-mer gave rise to an extremely stable triplex (ON12/D1) at pH 7.2. This finding is also an indication that the intercalating properties of 5′-5′ alternate linkers in Hoogsteen-type TFOs can be further improved by appropriately chosen modification of structures **1** and **2**. However, the mismatch sensitivity for ON12 was much lower than in the alternate-strand triplex.

To further increase the thermal stabilities of the alternate-strand triplexes at pH 7.2 we prepared several TFOs possessing a TINA monomer (ON5–ON8). The use of inverted thymidine derivatives (3′-O-DMT, 5′-phosphoramidites) in the synthesis of alternate-strand TFOs meant that monomer **P** was linked through secondary hydroxy groups at the 3′-end of the thymidine residue in both ON6 and ON8 at dangling ends (Table 1). Increased thermal stabilities of triplexes possessing **P** in either arm of the TFOs (ON5, ON6 and ON7, ON8) were observed relative to those with ON1 and ON3, respectively. Good discrimination ($\Delta T_m > 10.0$ °C) between matched and mismatched alternate triplexes with **P** insertions (ON5–ON8 with D2 and D3) was observed in all cases at pH 6.0. There is a quite large difference in the thermal stability of the mismatched triplexes ON5/D3 relative to the triplex of ON11/D1 at pH 6.0. This again reflects the increased sensitivity arising from the mismatched dangling end as discussed above. As can be seen, even a single insertion of **P** in the TFOs with linker **1** (ON5, ON6) led to T_m values over 37 °C at pH 7.2. It is interesting to note that at neutral pH the influence of **P** insertion on the thermal stability of the triplexes was larger for TFOs possessing linker **1** than linker **2**. The stabilizing effect coming from linkers **1** and **2** for oligonucleotides with **P** insertion can be illustrated by comparison of the thermal stability of the triplex formed between D1 and ON11 and those with ON5 and ON7 at pH 7.2. In both cases an increase in the T_m value of more than 13.5 °C was observed.

Despite the extraordinary high thermal stability of the triplex with non-alternate ON12 at pH 7.2, the use of alternate-strand TFOs with a single **P** insertion may still be preferred for a more target-specific oriented design, as high binding affinity of nucleic acids is often accompanied by a loss of target specificity.[18] In this regard, alternate-strand triplexes divide the TFO sequence into two or more parts and are proposed to be a new way to achieve specificity.

The triplex stabilities described herein are remarkable, and allows high T_m values to be reached by connection of short homopyrimidine stretches (for example, the 5-mer and 9-mer shown here), which are unable to bind separately to dsDNA at physiological pH values. More importantly, the final T_m values of the systems exceed 37 °C, which gives a possibility to extend the number of gene targets available for biological studies. This result highlights the importance of an appropriate design of intercalating systems for achieving the desired level of stacking interactions within the nucleic acids. Monomer **2** is the first example of a 5′-5′ alternate linker for Hoogsteen-type triplexes, which enables the targeting of dsDNA at pH 7.2. This approach gives a unique opportunity to develop triplex technology since the monomer insertion is compatible with the synthesis of numerous modified oligonucleotides.

Received: March 22, 2006
Revised: May 30, 2006
Published online: July 17, 2006

Keywords: DNA recognition · DNA structures · DNA triplex · helical structures · intercalation

 © 2006 Wiley-VCH Verlag GmbH & Co. KGaA, Weinheim

[1] a) O. Igoucheva, V. Alexeev, K. Yoon, *Curr. Mol. Med.* **2004**, *4*, 445 – 463; b) S. Buchini, C. J. Leumann, *Curr. Opin. Chem. Biol.* **2003**, *7*, 717 – 726.

[2] D. Praseuth, A. L. Guieysse, C. Helene, *Biochim. Biophys. Acta* **1999**, *1489*, 181 – 206.

[3] A. J. Cheng, J. C. Wang, M. W. Van Dyke, *Antisense Nucleic Acid Drug Dev.* **1998**, *8*, 215 – 225.

[4] a) P. Aich, T. J. Thomas, J. S. Lee, *Nucleic Acids Res.* **2000**, *28*, 2307 – 2310; b) S. B. Noonberg, J.-C. Francois, T. Garestier, C. Helene, *Nucleic Acids Res.* **1995**, *23*, 1956 – 1963.

[5] G. E. Plum, D. S. Pilch, S. F. Singleton, K. J. Breslauer, *Annu. Rev. Biophys. Biomol. Struct.* **1995**, *24*, 319 – 350.

[6] a) D. A. Horne, P. B. Dervan, *J. Am. Chem. Soc.* **1990**, *112*, 2435 – 2437; b) S. D. Jayasena, B. H. Johnston, *Biochemistry* **1992**, *31*, 320 – 327.

[7] a) L. De Napoli, G. Di Fabio, A. Messere, D. Montesarchio, A. Pepe, G. Piccalli, M. Varra, *J. Org. Chem.* **1997**, *62*, 9024 – 9030; b) L. De Napoli, G. Di Fabio, A. Messere, D. Montesarchio, G. Piccalli, M. Varra, *Eur. J. Org. Chem.* **1998**, 2119 – 2125.

[8] a) Y. Ueno, A. Ogawa, A. Nakagawa, A. Matsuda, *Bioorg. Med. Chem. Lett.* **1996**, *6*, 2817 – 2822; b) C. H. Jessen, E. B. Pedersen, *Helv. Chim. Acta* **2004**, *87*, 2465 – 2471; c) U. Asseline, V. Roig, N. T. Thuong, *Tetrahedron Lett.* **1998**, *39*, 8991 – 8994.

[9] A. V. Maksimenko, E. M. Volkov, J. R. Bertrand, H. Porumb, C. Malvy, Z. A. Shabarova, M. B. Gottikh, *Eur. J. Biochem.* **2000**, *267*, 3592 – 3603.

[10] a) L. De Napoli, G. Di Fabio, A. Messere, D. Montesarchio, D. Musumeci, G. Piccalli, *Nucleosides Nucleotides* **1999**, *18*, 1639 – 1640; b) S. Hoshika, Y. Ueno, H. Kamiya, A. Matsuda, *Bioorg. Med. Chem. Lett.* **2004**, *14*, 3333 – 3336; c) C. Giancola, L. Petraccone, M. Pieri, L. De Napoli, D. Montesarchio, G. Piccalli, G. Barone, *Int. J. Biol. Macromol.* **2001**, *28*, 387 – 394.

[11] a) J. Amato, A. Galeone, G. Oliviero, L. Mayol, G. Piccialli, M. Varra, *Eur. J. Org. Chem.* **2004**, 2119 – 2125; b) B. Catalanotti, C. Fattorusso, L. Mayol, G. Oliviero, G. Piccialli, M. Varra, *Nucleosides Nucleotides Nucleic Acids* **2003**, *22*, 1069 – 1071; c) T. Miyashita, N. Matsumo, T. Moriguchi, K. Shinozuka, *Tetrahedron Lett.* **2003**, *44*, 7399 – 7402; d) A. T. M. Z. Azam, M. Hasegawa, T. Moriguchi, K. Shinozuka, *Bioorg. Med. Chem. Lett.* **2004**, *14*, 5747 – 5750; e) Y. Ueno, M. Mikawa, S. Hoshika, A. Matsuda, *Bioconjugate Chem.* **2001**, *12*, 635 – 642.

[12] a) C. Giovannangeli, L. Perrouault, C. Escude, T. Nguyen, C. Helene, *Biochemistry* **1996**, *35*, 10539 – 10548; b) C. Giovannangeli, L. Perrouault, C. Escude, S. Gryaznov, C. Helene, *J. Mol. Biol.* **1996**, *261*, 386 – 398.

[13] L. E. Xodo, G. Manzini, F. Quadrifoglio, G. A. van der Marel, J. H. Boom, *Nucleic Acids Res.* **1991**, *19*, 5625 – 5631.

[14] V. V. Filichev, E. B. Pedersen, *J. Am. Chem. Soc.* **2005**, *127*, 14849 – 14858.

[15] a) B. C. Froehler, S. Wadwani, T. J. Terhorst, S. R. Gerrard, *Tetrahedron Lett.* **1992**, *33*, 5307 – 5310; b) J. Sági, A. Szemzö, K. Ébinger, A. Szabolcs, G. Sági, E. Ruff, L. Ötvös, *Tetrahedron Lett.* **1993**, *34*, 2191 – 2194; c) N. Colocci, P. B. Dervan, *J. Am. Chem. Soc.* **1994**, *116*, 785 – 786.

[16] More detailed information about the molecular modeling studies and pictures of the alternative positioning of linkers are given in the Supporting Information.

[17] The synthesis of DMT-protected phosphoramidites of linkers **2** and **3**, their incorporations into DNA, MALDI-TOF analysis of the final TFOs, and details about thermal stability measurements along with the representative first derivatives of the melting curves are described in the Supporting Information.

[18] V. V. Demidov, M. D. Frank-Kamenetskii, *Trends Biochem. Sci.* **2004**, *29*, 62 – 71.

 © 2006 Wiley-VCH Verlag GmbH & Co. KGaA, Weinheim

Power Sources

DOI: 10.1002/anie.200601301

Novel Nanocomposite Pt/$RuO_2 \cdot x H_2O$/Carbon Nanotube Catalysts for Direct Methanol Fuel Cells**

*Lin Cao, Frieder Scheiba, Christina Roth, Franz Schweiger, Carsten Cremers, Ulrich Stimming, Hartmut Fuess, Liquan Chen, Wentao Zhu, and Xinping Qiu**

Two key problems inhibiting the commercialization of direct methanol fuel cells (DMFCs) are the cost of the precious metals employed and the sluggish kinetics and catalyst poisoning by CO or CHO species. Research to solve the first drawback[1–4] focuses on the reduction of precious metal loading, which is achieved by increasing the catalyst's specific surface area and its accessibility. For the second problem, advanced electrocatalyst design relies on the "bifunctional approach",[5–10] in which a second compound such as ruthenium or $RuO_2 \cdot x H_2O$ assists the oxidation of CO or CHO species by adsorption of oxygen-containing species close to the poisoned Pt sites. In contrast to previous work on PtRu alloy catalysts,[11–13] Rolison and co-workers[14,15] emphasized the importance of hydrous ruthenium oxides because the $RuO_2 \cdot x H_2O$ speciation of Ru in nanoscale PtRu blacks shows both high electron and proton conductivity, which results in a much more active catalyst for methanol oxidation. However, direct evidence of the catalytic function of hydrous oxides is very scarce.

Mixed proton–electron conducting materials should be ideal catalyst supports for DMFCs since they allow for low ohmic resistance in both the proton and electron conduction at the same time. As hydrous ruthenium(IV) oxide has been reported to contain liquid or liquid-like regions of water to

[*] Dr. L. Cao, Prof. L. Chen, Prof. W. Zhu, Prof. Dr. X. Qiu
Key Lab of Organic Optoelectronics and Molecular Engineering
Department of Chemistry
Tsinghua University
Beijing, 100084 (P.R. China)
Fax: (+86) 6279-4235
E-mail: qiuxp@mail.tsinghua.edu.cn

F. Scheiba, Dr. C. Roth, Prof. Dr. H. Fuess
Institut für Materialwissenschaften
Technische Universität Darmstadt
64287 Darmstadt (Germany)

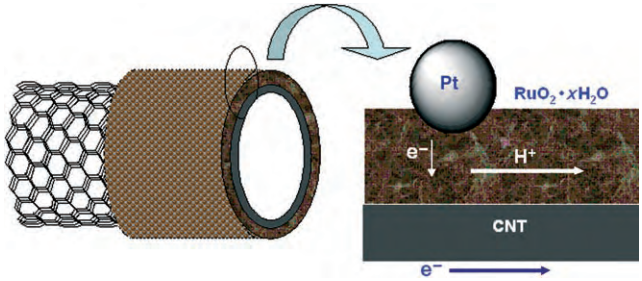
F. Schweiger, Dr. C. Cremers, Prof. Dr. U. Stimming
Abteilung 1: Technik für Energiesysteme und erneuerbare Energien
Bayerisches Zentrum für Angewandte Energieforschung (ZAE)
85748 Garching (Germany)

[**] We are grateful for financial support from the Sino-German Center (GZ 218 (101/6)), the State Key Basic Research Program of the People's Republic of China (2002CB211803), the National Natural Science Foundation of China (90410002), and the Deutsche Forschungsgemeinschaft (Fu 125/41-1 and Sti 74/17).

Supporting Information for this article is available on the WWW under http://www.angewandte.org or from the author.

© 2006 Wiley-VCH Verlag GmbH & Co. KGaA, Weinheim

facilitate proton conduction within an electron-conducting matrix,[16] it appears to be a promising material. To facilitate mass transport in liquid-feed operation and within the mostly thicker electrodes in DMFCs, carbon nanotubes (CNTs) have been chosen as a new support type. CNTs form a porous nanotube micronetwork and therefore show highly electrochemically accessible surface areas. Furthermore, they offer an outstanding electronic conductivity relative to the commonly used Vulcan carbon blacks. A schematic diagram of a novel catalyst design based on the above is given in Scheme 1.



Scheme 1. Schematic diagram of the novel catalyst.

Herein, we describe a composite catalyst combining the properties of hydrous ruthenium oxide in contact with a Pt phase and a new type of carbon support. This novel catalyst design takes into account the problems of CO poisoning, high precious metal loading, and insufficient mass transport in thick electrode layers. The obtained catalyst with 14.8 wt % Pt loading on the support and a Pt:Ru ratio of 1:1 shows superb performance for direct electrooxidation of methanol.

The novel materials were prepared by purifying and pretreating commercial carbon nanotubes (Tsinghua University) in 1 % sodium dodecyl sulfate (SDS) to increase their hydrophilicity. The $RuO_2{\cdot}xH_2O$ coating was obtained by an oxidant-aided co-precipitation technique. The procedure for preparing nanocomposite $Pt/RuO_2{\cdot}xH_2O$/CNT and details of the electrochemical measurements are described in the Experimental Section. Figure 1 shows transmission electron micrographs of platinum nanoparticles decorated on hydrous ruthenium oxide coated SDS-treated carbon nanotubes. As shown in Figure 1 a, the carbon nanotubes exhibit a multiwalled microstructure with an average diameter of about 40 nm. More importantly, however, very high particle densities for platinum and/or $RuO_2{\cdot}0.56H_2O$ were found at all CNT surfaces in the image. Consequently, the surfactant-aided sonication applied for the dispersion of the CNTs combined with the chosen deposition method appears to be a very powerful and effective technique.

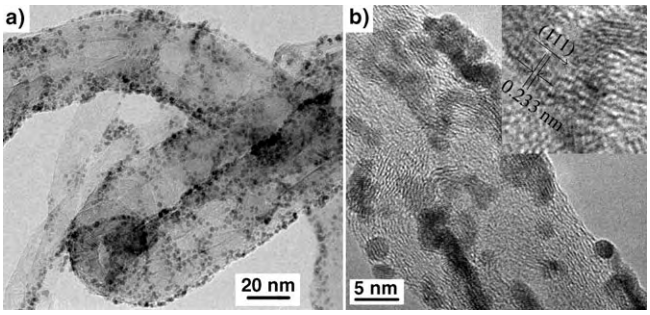


Figure 1. Transmission electron micrographs of $PtRuO_2{\cdot}0.56H_2O$/CNT: a) the multiwalled structure of the carbon nanotubes can be seen in this low-resolution image, with nanoparticles highly dispersed on the tube surface; b) nanoparticles (average diameter of 2.4 nm) show visible lattice planes; from the high-resolution inset a lattice spacing *d* of 0.233 nm can be determined.

The hollow structure of the CNTs (as reported in numerous publications) is not clearly visible from Figure 1 b, probably to the $RuO_2{\cdot}0.56H_2O$ coating. According to the high-resolution TEM image (inset in Figure 1 b) the distance between two adjacent lattice planes (indicated by the *d* spacer in the image) is approximately 0.233 nm. This length is attributed to Pt(111) and is consistent with the results obtained from X-ray diffraction (see the Supporting Information). The average platinum particle size was determined from the TEM images to be about 2.4 nm, which is in the range of, or even smaller than, that reported by other authors.[17] Despite the small size of the platinum particles, particle agglomeration is very rare, probably because of the large number of nucleation centers available on the surface of the $RuO_2{\cdot}0.56H_2O$ coated CNTs. This unique structure appears to provide a suitable support for many uniform platinum particles, thereby favoring the high performance of methanol oxidation, as discussed below.

The $Pt/RuO_2{\cdot}0.56H_2O$/CNT samples were tested for their activity in the electrooxidation of methanol. To investigate the role played by the $RuO_2{\cdot}0.56H_2O$ coating further, a Pt/CNT catalyst with the same Pt-to-CNT ratio was prepared for comparison. In addition, experiments with a carbon-supported binary PtRu catalyst (E-TEK; 20 wt % on Vulcan, Pt:Ru = 1:1) and a carbon-supported Pt catalyst (E-TEK; 20 wt % on Vulcan) were carried out for comparison. Figure 2 shows voltammetric curves recorded for the synthesized and reference catalysts in 1 M CH_3OH + 1 M $HClO_4$ as supporting electrolyte. $Pt/RuO_2{\cdot}0.56H_2O$/CNT displays a 1.5-times higher current density than the PtRu/Vulcan catalyst. Considering that the as-prepared catalyst and PtRu/Vulcan have almost identical Pt loadings, $Pt/RuO_2{\cdot}0.56H_2O$/CNT appears to be significantly more active for methanol oxidation. Furthermore, the onset and peak potentials of $Pt/RuO_2{\cdot}0.56H_2O$/CNT are both lower than those of PtRu/Vulcan, thus indicating a high availability of hydroxide species adsorbed on the surface in the proximity of the active platinum sites that promote the methanol oxidation. Apart from a slight shift to higher potentials for the Vulcan-supported catalyst, the cyclic voltammograms (CVs) of Pt/CNTs and Pt/Vulcan appear almost identical, thus indicating that the promoting effect of the $Pt/RuO_2{\cdot}0.56H_2O$/CNT catalyst is mainly due to the $RuO_2{\cdot}0.56H_2O$ coating on the tubes.

We further hypothesized that the $RuO_2{\cdot}0.56H_2O$ coating can promote methanol oxidation. Indeed, another piece of evidence to support such a bifunctional mechanism is shown in Figure 3. To obtain further insight into the role played by ruthenium and ruthenium oxide in the catalysts, the CV curves of different scanning cycles of the PtRu/Vulcan

 © 2006 Wiley-VCH Verlag GmbH & Co. KGaA, Weinheim

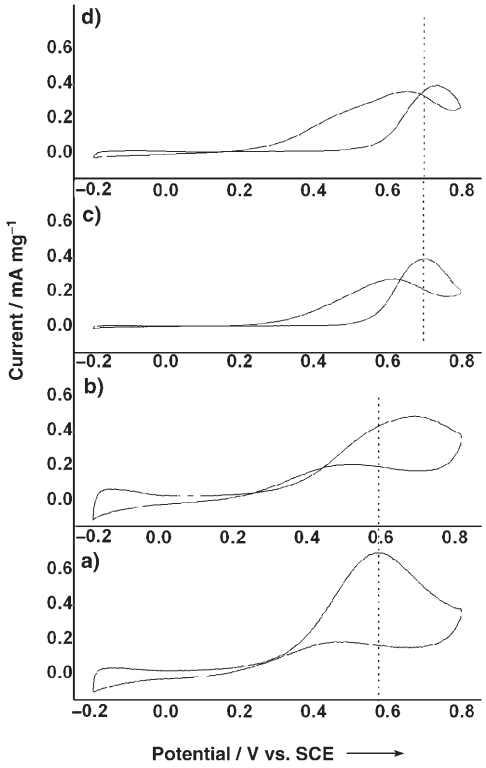


Figure 2. Cyclic voltammograms for Pt/RuO_2·0.56H_2O/CNT (a), PtRu/Vulcan (b), Pt/CNT (c), and Pt/Vulcan (d). See the Experimental Section for further details.

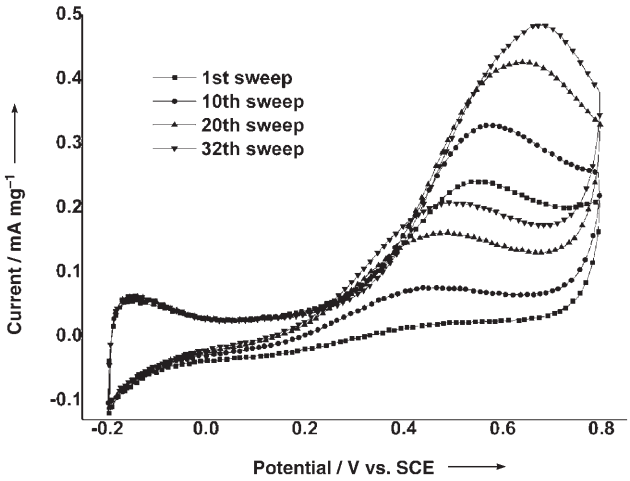


Figure 3. Cyclic voltammograms of different scanning cycles of the PtRu/Vulcan electrode at 25 °C in 1 M CH_3OH + 1 M $HClO_4$ in the potential range −0.2 to 0.8 V vs. SCE with a scan rate of 50 mV s^{-1}.

electrode were recorded. The CV curve for the first cycle shows a rather low methanol oxidation current. High activities are only obtained after 32 sweeps, which can be considered to be due to a kind of electrochemical activation in order to form ruthenium oxide. However, in the case of Pt/RuO_2·0.56H_2O/CNT, only eight scanning cycles are needed for a significant activation. This implies that the PtRu/Vulcan catalyst needs a longer induction period than PtRuO_2·0.56H_2O/CNT to show a good performance for methanol oxidation.

More importantly, as can be seen from Figure 3, even the peak current increases from 242 to 481 mA mg^{-1} after 32 sweeps, whereas the proton adsorption/desorption area (the area between −0.2 and 0.0 V vs. SCE) related to the surface of the Pt particles is almost constant, which implies that the enhancement in activity originates from the hydrous ruthenium oxide formed in PtRu/Vulcan during cycling. We infer that the RuO_2·0.56H_2O component in the PtRuO_2·0.56H_2O/CNT catalyst leads to the reduced activation period and thus to a direct advantage for methanol oxidation. In addition, we also note that the peak potentials for the PtRu/Vulcan catalyst get higher and higher during cycling, which indicates the poorer and poorer electronic conductivity and kinetic characteristics of this catalyst. This can be explained by the low mass transport characteristics and electron conductivity of RuO_2·$x$$H_2O$ relative to PtRu alloy in PtRu/Vulcan owing to the compact microstructure of the former.

As shown in Figure 4, significant differences in the onset potential for CO oxidation between the catalysts containing ruthenium and those of pure platinum are observed, thus illustrating the beneficial role of ruthenium for CO oxidation. Comparison of the CO oxidation curves for the ruthenium-containing catalysts (Figures 4a and c) reveals that the onset

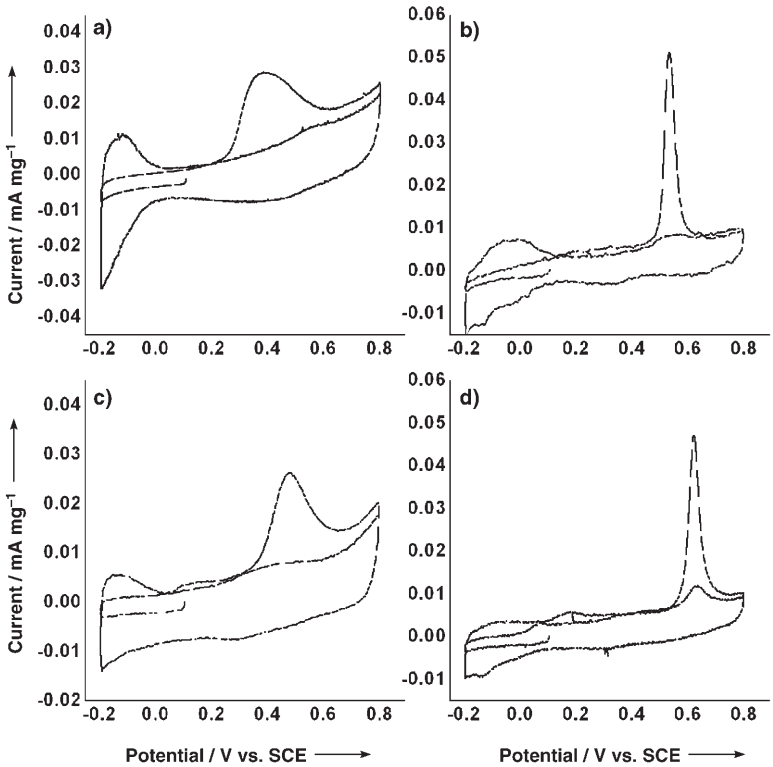


Figure 4. The oxidation of pre-adsorbed CO at 25 °C as measured by CO stripping voltammetry in 1 M $HClO_4$ solution in the potential range −0.2 to 0.8 V vs. SCE at a scan rate of 10 mV s^{-1}: a) PtRuO_2·0.56H_2O/CNT, b) Pt/CNT, c) PtRu/Vulcan, and d) Pt/Vulcan in 1 M $HClO_4$.

 © 2006 Wiley-VCH Verlag GmbH & Co. KGaA, Weinheim

potential for $Pt/RuO_2{\cdot}0.56H_2O/CNT$ is found at even lower potential (223 mV) than that of PtRu/Vulcan (338 mV). This demonstrates that although the ruthenium is present as a hydrous ruthenium oxide phase rather than being alloyed, CO oxidation is promoted even more efficiently, as is also underlined by the higher peak current and the broader peak shape.

Dmowski and co-workers[16] have reported that hydrous ruthenium oxide is, in fact, a nanocomposite consisting of dispersed rutile-like nanocrystals the grain boundaries of which are filled with water. The rutile part of $RuO_2{\cdot}xH_2O$ supports electronic conduction, while the hydrous grain-boundary regions are responsible for the proton transport. Another proposed mechanism is that $RuO_2{\cdot}xH_2O$ can dissociate H_2O. The strength of CO adsorption on the surface of RuO_2 is comparable to that of the bond of the bridging O atoms and unlike that on the metallic Ru surface, where bonding of the O atoms is too strong to allow reaction with CO.[18] Therefore, $RuO_2{\cdot}0.56H_2O$ can easily donate hydroxide species to platinum sites to aid CO oxidation, which leads to the excellent catalytic activity observed. Additionally, the corrected surface areas for Pt of the $Pt/RuO_2{\cdot}0.56H_2O/CNT$ and PtRu/Vulcan catalysts are 90.6 and 63.2 m^2g^{-1}, respectively, assuming that CO adsorption occurs only on Pt. This is another reason why $Pt/RuO_2{\cdot}0.56H_2O/CNT$ shows high activity.

In summary, a $Pt/RuO_2{\cdot}0.56H_2O/CNT$ catalyst has been prepared that shows superb performance for direct methanol electrooxidation. The active material of the catalyst, namely Pt and $RuO_2{\cdot}0.56H_2O$, is deposited in a highly dispersed form on the carbon nanotubes owing to the efficient utilization of their huge specific surface area in combination with the slow Pt reduction and Ru^{3+} oxidation during synthesis. We found that the use of CNTs can improve the microstructure of the electrode and facilitate mass transport, thereby increasing the power output. In addition, the $RuO_2{\cdot}0.56H_2O$ coating can directly donate and accept protons as well as electrons within a short timeframe and therefore supply activated Ru^{III}–OH species for removing strongly adsorbed CO from active Pt sites in an oxygen-transfer step, which results in a lower electrode potential for CO oxidation. Moreover, our studies also testify that the CNTs can compensate the loss of electron conductivity caused by the $RuO_2{\cdot}0.56H_2O$ coating, probably by improving the electrode microstructure because of their rigid structure and lowering the resistance of the electrode. This plays an important role in improving the kinetic characteristics and therefore reveals the suitability of Pt decorated on hydrous RuO_2 with appropriate water content for methanol electrooxidation—it is even more active than the PtRu alloy.

Experimental Section

In the first step, CNTs (0.1 g), coated with sodium dodecyl sulfate, were dissolved in a solution of $RuCl_3$ (0.854 mmol) in water (150 mL) by sonication for 5 min. Then, the pH value was adjusted to 4 by adding sodium hydroxide and appropriate amounts of hydrogen peroxide solution. For the platinum deposition step, the as-prepared $RuO_2{\cdot}xH_2O/CNT$ was added to 50 mL of ethylene glycol with constant stirring for 10 min. Then, 410 μL of 0.2 M $H_2[PtCl_6]$ was added with constant stirring. The resulting slurry was refluxed at 140 °C for 3 h to ensure complete reduction of $H_2[PtCl_6]$. The solid product was then rinsed repeatedly with deionized water. Finally, the product was dried in vacuo at 70 °C for 10 h. The catalyst thus obtained is referred to as $Pt/RuO_2{\cdot}xH_2O/CNT$. Pt particles were also deposited on pure CNTs by the same method without the $RuO_2{\cdot}xH_2O$ deposition step (referred to as Pt/CNT) for comparison. TGA and DSC gave an x value of 0.56 for $Pt/RuO_2{\cdot}xH_2O/CNT$. ICP was used to analyze the Ru and Pt content of the samples; the Pt content was 14.8%, with a Pt:Ru atomic ratio of close to 1:1, which indicates only a small loss of Pt and Ru.

Structural catalyst characterization was carried out by X-ray diffraction (XRD; STOE-STADI P, Ge-monochromated $Cu_{K\alpha}$ radiation) and TEM (Philips CM20, W cathode, 200 kV acceleration voltage). Electrochemical measurements were carried out at 25 °C in a three-electrode cell connected to a Solartron workstation. A gold patch (1×1 cm^2) coated with catalyst ink was used as the working electrode. A saturated calomel electrode (SCE) and Pt gauze were used as reference and counter electrodes, respectively. A solution of 1 M $CH_3OH + 1$ M $HClO_4$ was used as electrolyte. All the reagents used were of analytical grade. Several activation scans were performed until reproducible voltammograms were obtained. Cyclic voltammograms were recorded in the potential range −0.2 to 0.8 V vs. SCE at a scan rate of 50 $mV\,s^{-1}$. Only the last cycles were used for comparison of the catalytic activity of the specified catalysts. The oxidation of pre-adsorbed CO was measured by CO stripping voltammetry in 1 M $HClO_4$ solution at a scan rate of 10 $mV\,s^{-1}$. All the recorded currents are corrected for the weight percentage of the platinum in catalysts.

Received: April 3, 2006
Published online: July 17, 2006

Keywords: fuel cells · methanol · nanotubes · platinum · ruthenium

[1] K. Kordesch, G. Simader, *Fuel Cells and their Applications*, Wiley-VCH, Weinheim, **1996**.
[2] T. S. Ahmadi, Z. L. Wang, T. C. Green, A. Henglein, M. A. El-Sayed, *Science* **1996**, *272*, 1924 – 1926.
[3] H. P. Liang, H. M. Zhang, J. S. Hu, Y. G. Guo, L. J. Wan, C. L. Bai, *Angew. Chem.* **2004**, *116*, 1566 – 1569; *Angew. Chem. Int. Ed.* **2004**, *43*, 1540 – 1543.
[4] H. Wakayama, N. Setoyama, Y. Fukushima, *Adv. Mater.* **2003**, *15*, 742 – 745.
[5] M. Watanabe, S. Motoo, *J. Electroanal. Chem.* **1975**, *60*, 267 – 272.
[6] X. M. Ren, P. Zelenay, S. Thomas, J. Davey, S. Gottesfeld, *J. Power Sources* **2000**, *86*, 111 – 116.
[7] F. Maillard, E. R. Savinova, P. A. Simonov, V. I. Zaikovskii, U. Stimming, *J. Phys. Chem. B* **2004**, *108*, 17893 – 17904.
[8] M. Arenz, K. J. J. Mayrhofer, V. Stamenkovic, B. B. Blizanac, T. Tomoyuki, P. N. Ross, N. M. Markovic, *J. Am. Chem. Soc.* **2005**, *127*, 6819 – 6829.
[9] F. Maillard, G. Q. Lu, A. Wieckowski, U. Stimming, *J. Phys. Chem. B* **2005**, *109*, 16230 – 16243.
[10] Z. G. Chen, X. P. Qiu, B. Lu, S. C. Zhang, W. T. Zhu, L. Q. Chen, *Electrochem. Commun.* **2005**, *7*, 593 – 596.
[11] H. A. Gasteiger, N. Markovic, P. N. Ross, E. J. Cairns, *J. Phys. Chem. B* **1994**, *97*, 12020 – 12029.
[12] A. Kabbabi, R. Faure, R. Durand, B. Beden, F. Hahn, J. M. Leger, C. Lamy, *J. Electroanal. Chem.* **1998**, *444*, 41 – 53.
[13] A. Hamnett, *Catal. Today* **1997**, *38*, 445 – 457.
[14] D. R. Rolison, P. L. Hagans, K. E. Swider, J. W. Long, *Langmuir* **1999**, *15*, 774 – 779.

 © 2006 Wiley-VCH Verlag GmbH & Co. KGaA, Weinheim

[15] J. W. Long, R. M. Stroud, K. E. Swider-Lyons, D. R. Rolison, *J. Phys. Chem. B* **2004**, *108*, 9772 – 9776.
[16] W. Dmowski, T. Egami, K. E. Swider-Lyons, C. T. Love, D. R. Rolison, *J. Phys. Chem. B* **2002**, *106*, 12677 – 12683.
[17] W. H. Lizcano-Valbuena, V. A. Paganin, E. R. Gonzalez, *Eleotrochim. Acta* **2002**, *47*, 3715 – 3722; M. Watanabe, M. Uchida, S. Motoo, *J. Electroanal. Chem.* **1987**, *229*, 395..
[18] H. Over, Y. D. Kim, A. P. Seitsonen, S. Wendt, E. Lundgren, M. Schmid, P. Varga, A. Morgante, G. Ertl, *Science* **2000**, *287*, 1474 – 1476.

 © 2006 Wiley-VCH Verlag GmbH & Co. KGaA, Weinheim

Biosensors

DOI: 10.1002/anie.200601398

A Chemomechanical Polymer that Functions in Blood Plasma with High Glucose Selectivity**

George K. Samoei, Weihua Wang, Jorge O. Escobedo, Xiangyang Xu, Hans-Jörg Schneider, Robert L. Cook, and Robert M. Strongin**

The fabrication of reliable non- or minimally invasive glucose sensors, including those that embody automated insulin-delivery systems, has been a long-term goal of researchers from a variety of disciplines. The foremost challenge is the attainment of materials that are selective for glucose in bodily fluids, wherein a vast number of potential interferences exist.[1]

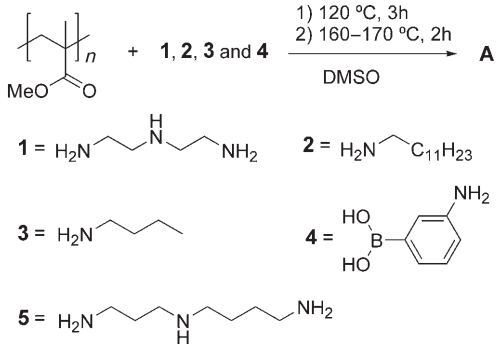
A number of chemomechanical polymers and related hydrogels have been investigated as potentially useful materials for glucose monitoring. Recent examples include glucose oxidase immobilized in hydrogels,[2] functionalized polymers coated on electrodes,[3] a crystalline colloidal array embedded in hydrogel networks,[4] and others.[5]

Few reports, however, describe fully synthetic hydrogel materials that change size in actual biological media in response to glucose. Asher et al. have described a boronic acid containing material that promotes the detection of glucose in tear solution.[4] Lowe and co-workers have reported glucose-induced size changes in a boronic acid functionalized polymer in cell-culture media.[6]

Herein we report a unique hydrogel which exhibits high glucose selectivity over other common blood sugars, such as fructose and galactose. It affords readily seen glucose-promoted size changes in human blood plasma. To the best of our knowledge, this is the first report of a chemomechanical polymer composed entirely of synthetic materials that exhibits a selective, rapid, and reversible size change in the presence of glucose in human blood plasma.

This effort is a start towards creating new materials that do not rely on biological materials for glucose-regulated drug delivery and, moreover, towards understanding new classes of chemomechanical polymers whose properties are highly tunable and amenable to an extensive degree of optimization. In this latter regard, the current study extends prior work, whereby flexible, selective supramolecular binding sites are introduced into pre-existing polymer networks in such a manner as to promote selective and easily seen macroscopic size changes.[7]

The chemomechanical polymer (**A**) is prepared (Scheme 1) by modifying commercial poly(methyl methacrylate) (PMMA; MW 350000 g mol^{-1}) with diethylenetriamine (**1**), dodecylamine (**2**), butylamine (**3**) and 3-aminophenylboronic acid (**4**).



Scheme 1. One-pot synthesis of polymer **A**. DMSO = dimethyl sulfoxide.

Polymer **A** is characterized by elemental analysis, solid-state ^{13}C cross-polarization magic angle spinning (CP-MAS) NMR spectroscopy, and FTIR (see the Supporting Information). Polymer **A** is allowed to swell completely for several hours in water and is then cut into pieces of $8 \times 4 \times 1$ mm^3. The cut polymer is immersed in a solution of glucose (0.005 M, approximating actual human physiological levels) and begins to contract immediately. A significant size change is observed over time (Figure 1). Polymer (**B**) is prepared under conditions identical to those described for **A**, but in the absence of 3-aminophenylboronic acid (**4**). No size change is observed for polymer **B** after immersion in glucose solution for 50 min (Figure 2). This indicates that the glucose-responsive behavior is due to the boronic acid moiety.

Polymer **A** also exhibits reversibility. The contracted polymer swells to its original size within two minutes after

[*] Prof. Dr. H.-J. Schneider
FR Organische Chemie
Universität des Saarlandes
66041 Saarbrücken (Germany)
Fax: (+49) 681-302-3209
E-mail: ch12 hs@rz.uni-sb.de
G. K. Samoei, W. Wang, Dr. J. O. Escobedo, X. Xu, Prof. R. L. Cook, Prof. R. M. Strongin
Department of Chemistry
Louisiana State University
232 Choppin Hall, Baton Rouge, LA 70803 (USA)
Fax: (+1) 225-578-3458
E-mail: rstrong@lsu.edu

[**] We thank the National Institutes of Health for research support through award RO1 EB2044.

Supporting information for this article is available on the WWW under http://www.angewandte.org or from the author.

© 2006 Wiley-VCH Verlag GmbH & Co. KGaA, Weinheim

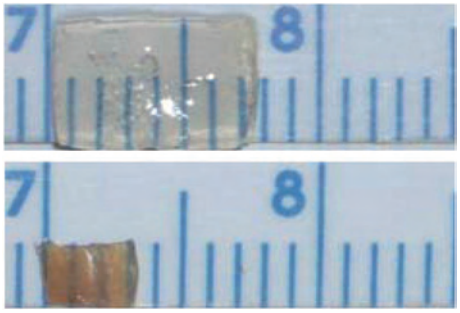


Figure 1. Behavior of polymer **A** in response to glucose. Top: original sample, bottom: after 50 min in a 0.005 M glucose solution.

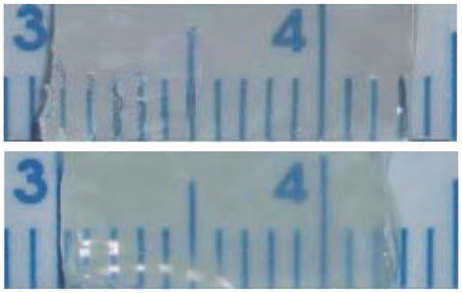


Figure 2. Behavior of polymer **B** in response to glucose. Top: original sample, bottom: after 50 min in a 0.005 M glucose solution.

immersion in a 0.05 M NaOH solution. After it is removed from the NaOH solution and washed with distilled water, the swollen polymer contracts once more when immersed again in a 0.005 M glucose solution (Figure 3).

Further studies also show that polymer **A** is selective for glucose over the other two common blood sugars, fructose and galactose (Figure 4). The error bars in Figure 4 indicate the reproducibility of the glucose-responsive contraction of polymer **A**. Three different batches of polymer **A** were tested on three different days.

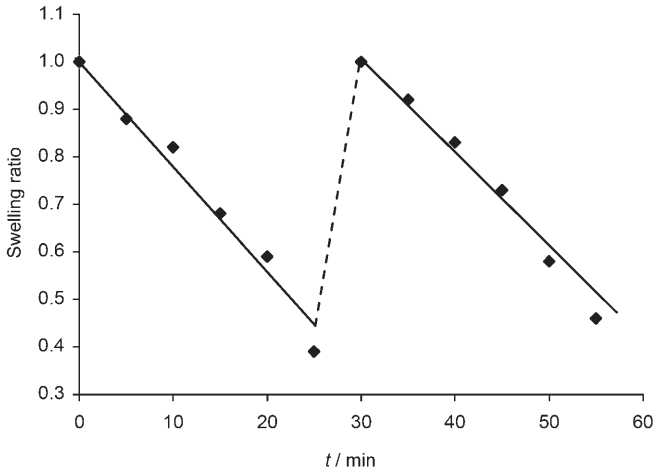


Figure 3. Contraction–expansion of polymer **A** in response to glucose (0.005 M). The polymer was expanded to its initial size between runs by rinsing with 0.05 M NaOH (dashed line). The size of the cut polymer after swelling in water in this experiment is $5\times5\times1$ mm^3.

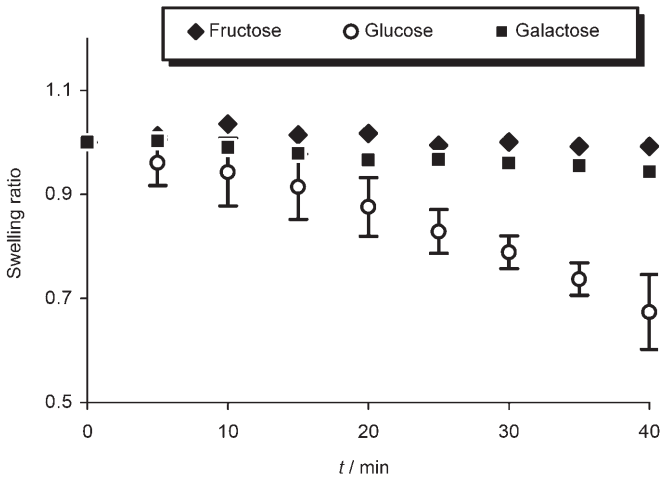


Figure 4. Selective response of polymer **A** to glucose over fructose and galactose. All the three sugars are at the same concentration (0.005 M). The size of the cut polymer after swelling in water in this experiment is $8\times4\times1$ mm^3.

In a commercial sample of human blood plasma, similar glucose responsiveness and reproducibility are observed. A piece of swollen polymer **A** is immersed in a solution of human blood plasma that contains 0.005 M added glucose. The polymer contracts sharply within 5–10 min (Figure 5). No response is observed for galactose and fructose (see the Supporting Information).

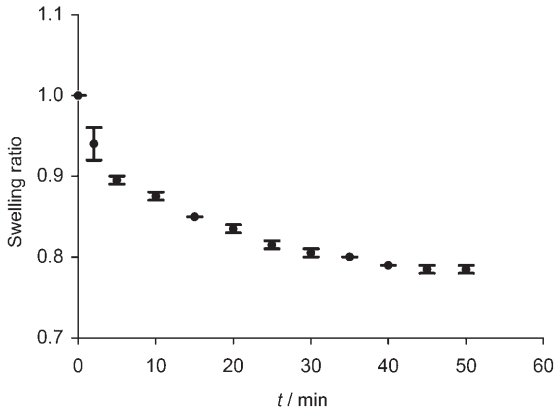


Figure 5. Contraction of polymer **A** in the presence of reconstituted human plasma containing 0.005 M glucose. The size of the cut polymer after swelling in water in this experiment is $8\times7\times1$ mm^3.

Bidentate binding of glucose by two boronic acid moieties is known to occur, in certain cases, selectively over galactose and fructose.[8] Shrinkage has been observed previously in other examples of glucose-induced cross-linkage of boronic acid containing polymers.[9] In our system, the glucose molecule also acts as an additional cross-link (besides the triamine). This results in the expulsion of water and gel shrinkage.

Additionally, sugar-binding-induced H^+ release has been used previously by Arnold et al. (for signal transduction) in a boronic acid containing hydrogel sensor for glucose.[10] In an

 © 2006 Wiley-VCH Verlag GmbH & Co. KGaA, Weinheim

analogous manner, we propose that the presence of emerging cationic charge from water and glucose bound to boron should stabilize the anionic nature of glucose-bound boron, thereby reducing the electrostatic repulsion and solvation by water that would lead to swelling. This may serve as an additional and/or alternative mechanism to glucose cross-linking through bidentate binding to boron.

Conversely, treatment with hydroxide deprotonates the amino groups on the polymer and also adds to boron. The concomitant increase in anionic charges enhances electrostatic repulsion and solvation in the hydrogel, causing it to swell very nearly to its initial size.[11]

Kataoka and co-workers have reported innovative strategies towards synthetic hydrogels that have been proposed as glucose detection/self-regulated insulin-delivery systems.[12,5a] Polymer sensitivity was heightened through rational design of the copolymer structure. In their material, as well as in most other boronic acid containing hydrogels reported to date, the hydrogels were prepared through the polymerization of boronic acid containing monomers. In contrast, our method for the preparation of glucose-responsive hydrogels involves simple modification of commercial PMMA to achieve glucose selectivity as well as a more-rapid equilibration time. Furthermore, the type of macroscopic response (shrinkage or expansion) and the selectivity to a certain stimulus of the hydrogels can be controlled by simply varying modifiers (Table 1).

Table 1: Response (shrinkage or expansion) and selectivity of the hydrogels to a certain stimulus.[a]

Entry	Polymer modifiers	Swelling ratio glucose (0.005 M)	galactose (0.005 M)	fructose (0.005 M)
1	**5**+**2**+**4**	1.70	1.61	1.50
2	**1**+**2**+**4**	1.22	1.25	1.31
3	**1**+**3**+**4**	0.63	0.96	0.93
4	**1**+**2**+**3**+**4**	0.83	0.99	0.97

[a] The size of the cut polymers is $8\times4\times1$ mm^3. Swelling ratios are obtained after 25 min.

When the polymer is modified with the long-alkyl-chain amine, dodecylamine (modifier compound **2**, Scheme 1), it exhibits expansion in all three sugar solutions (Table 1, entries 1 and 2). This may be attributed to steric hindrance of the alkyl chain towards bidentate binding of glucose by two boronic acid moieties. Thus, the binding of sugar molecules enhances the formation of charge on boron atoms and increases the polarity and water content of the polymer, resulting in polymer expansion rather than contraction.

In the case of butylamine (modifier compound **3**, Scheme 1), the smaller butyl chain apparently does not significantly hinder bidentate binding of glucose. The cross-linking of polymer chains by glucose molecules can thereby overcome the effect of charge accumulation (see above), resulting in gel contraction (Table 1, entry 3). Furthermore, when a mixture of dodecylamine and butylamine is used (with half the original amounts each), as in polymer **A** (Table 1, entry 4), the gel contracts but to a lesser extent than when incorporating butylamine alone. This affords additional evidence that dodecyl sterically hinders cross-linking and contraction.

A significant difference in size change is observed when the length of the cross-linker is varied (Table 1, entries 1 and 2). In the presence of the same alkyl amine (dodecyl), the hydrogel with the longer-carbon-chain cross-linker (modifier **5**, Scheme 1) exhibits a greater degree of expansion as compared with the case in which the shorter-carbon-chain cross-linker (**1**) is used. This is attributed to the fact that longer-chain cross-linkers provide wider cavities for the uptake of water.

The optimized polymer **C** (Table 1, entry 3) exhibits the highest degree of selective contraction in the presence of glucose. Importantly, we find that the swelling ratio of polymer **C** exhibits a linear decrease proportional to increasing glucose concentrations (Figure 6).

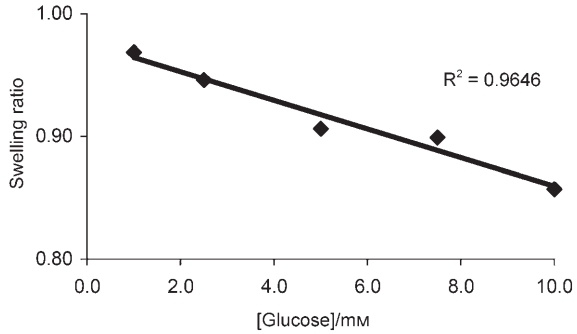


Figure 6. Swelling ratio of polymer **C** in the presence of various concentrations of glucose at 25 °C. The values are the average of three consecutive determinations after 20 min. The size of the cut polymer after swelling in water in this experiment is $14\times7\times1$ mm^3.

Figure 7 shows that polymer **C** serves as a "chemical corkscrew". After contraction triggered by glucose, release of the compound inside the capillary occurs (green ink solution for visualization). This methodology may thus promote the eventual optimization of self-regulating actuators that can work without interfacing to external devices.[7]

In summary, the general synthetic procedure developed[7a] for chemomechanical polymers is highly useful as the recognition groups can be readily introduced and the properties of the polymer can be easily optimized.[7] Current efforts involve further optimization of hydrogel properties through side-chain modification and miniaturization, which is known to enhance the performance of related materials.[7] Many challenges besides achieving glucose selectivity remain before a self-regulated insulin-delivery system can be implemented.[1] These include controlling potential interactions of the deliverable drug with the polymer,[13] response time, biocompatibility, calibration, and the material's lifetime.

Received: April 9, 2006
Revised: May 31, 2006
Published online: July 6, 2006

 © 2006 Wiley-VCH Verlag GmbH & Co. KGaA, Weinheim

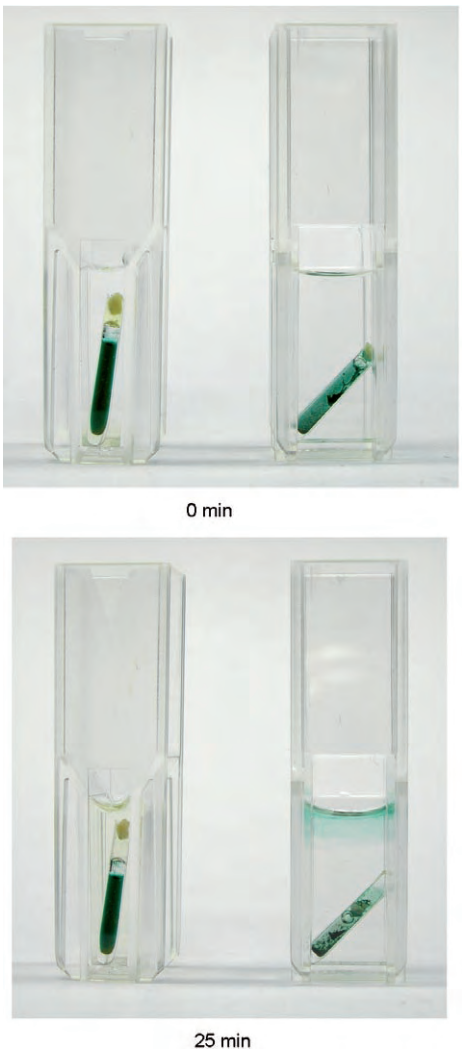


Figure 7. A demonstration with polymer **C** in glucose-regulated chemical delivery. A capillary tube is filled with ink and sealed with swollen polymer **C**. The capillary is immersed in H_2O (control, cuvette on the left in each picture) and in 0.005 M glucose solution. After 25 min, the ink is released only in the glucose solution owing to the contraction of the polymer (right).

Keywords: biosensors · boronic acids · carbohydrates · chemomechanical system · glucose

[1] For a recent review and example, see: a) M. A. Arnold, G. W. Small, *Anal. Chem.* **2005**, *77*, 5429; b) U. Beyer, A. Fleischer, A. Kage, U. Haueter, R. Ehwald, *Biosens. Bioelectron.* **2003**, *18*, 1391, and references therein.
[2] This is a pH-responsive material: D. Kim, K. Seo, K. Park, *J. Biomater. Dent.* **2000**, *16*, 189.
[3] R. Gabai, N. Sallacan, V. Chegel, T. Bourenko, E. Katz, I. Willner, *J. Phys. Chem. B* **2001**, *105*, 8196.
[4] S. A. Asher, V. A. Alexeev, A. C. Sharma, A. V. Goponenko, S. Das, I. K. Lednev, C. S. Wilcox, D. N. Finegold, *J. Am. Chem. Soc.* **2003**, *125*, 3322.
[5] For an example, see: a) K. Kataoka, H. Miyazaki, M. Bunya, T. Okano, Y. Sakurai, *J. Am. Chem. Soc.* **1998**, *120*, 12694; b) Q. Cai, K. Zeng, C. Ruan, T. A. Desai, C. A. Grimes, *Anal. Chem.* **2004**, *76*, 4038; c) J. T. Suri, D. B. Cordes, F. E. Cappuccio, R. A. Wessling, B. Singaram, *Angew. Chem.* **2003**, *115*, 6037; *Angew. Chem. Int. Ed.* **2003**, *42*, 5857; d) E. Kokufata, Y. Q. Zhang, T. Tanaka, *Nature* **1991**, *351*, 302; e) T. Miyata, N. Asami, T. Uragami, *Nature* **1999**, *399*, 766.
[6] M.-C. Lee, S. Kabilian, A. Hussain, X. Yang, J. Blyth, C. R. Lowe, *Anal. Chem.* **2004**, *76*, 5748.
[7] a) H.-J. Schneider, L. Tianjun, N. Lomadze, *Eur. J. Org. Chem.* **2006**, *26*, 677; b) N. Lomadze, H.-J. Schneider, *Tetrahedron* **2005**, *61*, 8694, and references therein.
[8] T. D. James, K. R. A. S. Sandanayake, S. Shinkai, *Angew. Chem.* **1994**, *106*, 2207; *Angew. Chem. Int. Ed. Engl.* **1994**, *33*, 2287.
[9] V. L. Alexeev, S. Das, D. N. Finegold, S. A. Asher, *Clin. Chem.* **2004**, *50*, 2353.
[10] For an example, see: F. H. Arnold, W. G. Zheng, A. S. Michael, *J. Membr. Sci.* **2000**, *167*, 227.
[11] E. Karadag, D. Saraydin, *Turk. J. Chem.* **2001**, *26*, 863.
[12] a) A. Matsumoto, S. Ikeda, A. Harada, K. Kataoka, *Biomacromolecules* **2003**, *4*, 1410; b) A. Matsumoto, R. Yoshida, K. Kataoka, *Biomacromolecules* **2004**, *5*, 1038.
[13] a) K. Nakamura, R. J. Murray, J. I. Joseph, N. A. Peppas, M. Morishita, A. M. Lowman, *J. Controlled Release* **2004**, *95*, 589; b) M. Morishita, T. Goto, N. A. Peppas, J. I. Joseph, M. C. Torjman, C. Munsick, K. Nakamura, T. Yamagata, K. Takayama, A. M. Lowman, *J. Controlled Release* **2004**, *97*, 115.

 © 2006 Wiley-VCH Verlag GmbH & Co. KGaA, Weinheim

Cyanocarbon Compounds

DOI: 10.1002/anie.200601070

The Structure of Fractionally Charged Tetracyanobenzene^{n-} Present in $[TCNB]_3^{2-}$**

*Joshua D. Bagnato, William W. Shum, Mark Strohmeier, David M. Grant, Atta M. Arif, and Joel S. Miller**

Cyanocarbons are electron poor and form numerous Mulliken donor–acceptor complexes,[1] whereas their radical anions are stabilized by charge and spin delocalization, and form numerous stable electron transfer salts. As a consequence of their unpaired electrons and planar topology, these salts enabled the discovery and development of molecule-based materials exhibiting metal-like electrical conductivity,[2]

[*] Dr. J. D. Bagnato, W. W. Shum, Dr. M. Strohmeier, Prof. D. M. Grant, Dr. A. M. Arif, Prof. J. S. Miller
Department of Chemistry
University of Utah
Salt Lake City, UT 84112–0850 (USA)
Fax: (+1) 801-581-8433
E-mail: jsmiller@chem.utah.edu

[**] We thank Jack Simons and Henry S. White for helpful discussions and the continued partial support by the Department of Energy Division of Materials Science (Grant Nos. DE-FG03-93ER45504, and DE-FG03-94ER14452). Computer resources were provided by the Center for High Performance Computing at the University of Utah. $n_{average} \approx 2/3-$, TCNB = Tetracyanobenzene

Supporting information for this article is available on the WWW under http://www.angewandte.org or from the author.

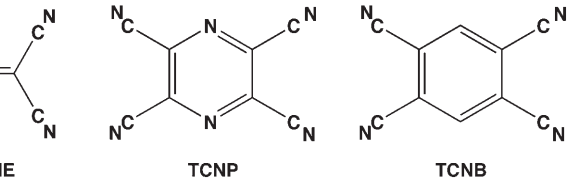
WILEY InterScience DISCOVER SOMETHING GREAT
© 2006 Wiley-VCH Verlag GmbH & Co. KGaA, Weinheim

superconductivity,[3] and ferromagnetic ordering.[4] In particular, the reduction chemistry of numerous cyanocarbons has been studied with the objective of identifying new acceptors to stabilize magnetically ordered molecule-based materials. These include 2,4,6-tricyano-1,3,5-triazine (TCT) and 2,4,6-tricyanobenzene (TCB)[5] in addition to tetracyanoethylene (TCNE)[6] and others.

The reactions of $[V(CO)_6]$ with several cyanocarbon electron acceptors form organic-based magnets. These cyanocarbons include TCNE, TCNQ (7,7,8,8-tetracyano-*p*-quinodimethane), tetracyanopyrazine, and recently, 1,2,4,5-tetracyanobenzene (TCNB), which magnetically order below approximately 400,[7] 56,[8] 200,[9] and 325 K,[10] respectively.

TCNB undergoes a reversible one-electron reduction at −0.64 V versus the saturated calomel electrode (SCE) in MeCN[11] and was reduced with tetrakis(dimethylamino)ethylene (TDAE). TDAE is a strong electron donor with an ionization potential of 6.13 eV,[12] and undergoes two reversible one-electron oxidations to $[TDAE]^+$ and $[TDAE]^{2+}$ at −0.68 and −0.53 V vs. SCE, respectively, in MeCN.[12b]

The reaction of one equivalent of TDAE with two equivalents of TCNB in MeCN led to the isolation of dark green crystals of composition $[TDAE][TCNB]_3 \cdot MeCN$ (**1**).[13] The IR spectrum of **1** exhibits several $\tilde{\nu}_{C\equiv N}$ absorptions with a sharp peak at 2170 cm^{-1} and broad peak at 2130 cm^{-1} (half-width at half-height ≈ 60 cm^{-1}; Figure 1). These absorptions are shifted to lower energy by more than 75 cm^{-1} with respect to the sharp 2245 cm^{-1} $\tilde{\nu}_{C\equiv N}$ absorption observed for TCNB and are thus indicative of its reduction in the formation of **1**.



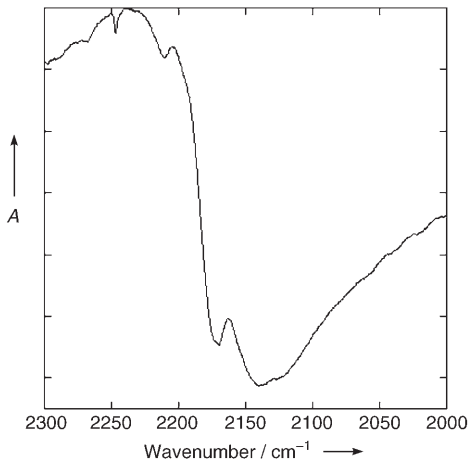


Figure 1. $\tilde{\nu}_{C\equiv N}$ IR (KBr) absorptions for **1** (the peak at 2245 cm^{-1} is due to MeCN).

Single-crystal X-ray diffraction analysis[13] of **1** reveals the presence of $[TDAE]^{2+}$ in addition to three nominally eclipsed TCNB moieties per unit cell (Figure 2), and an acetonitrile of solvation. The oxidation state of $[TDAE]^n$ ($n = 0, 1+, 2+$) is ascertained from both the central C–C bond length, which is 1.36 (for $n = 0$), 1.42 ($n = 1+$), and 1.52 Å ($n = 2+$),[14] owing to a decreasing bond order upon oxidation, and the NCCN dihedral angles that are approximately 26°,[15] ≈ 42°, and ≈ 76° respectively for $n = 0$, $1+$, $2+$,[14] as well as spectroscopic data. The TDAE in **1** has a central C–C bond distance of 1.511(6) Å and an average NCCN dihedral angle of 73.8° characteristic of $[TDAE]^{2+}$. The $[TDAE]^n$ oxidation state can also be distinguished by the IR $\tilde{\nu}_{NCN}$ absorptions that respectively occur at 1340, 1518, and a doublet at 1659/1675 cm^{-1} for $[TDAE]^n$ $n = 0$, $1+$, $2+$.[14] The observed doublet at 1671 and 1648 cm^{-1} (not shown; and the lack of absorptions at ≈ 1340 and ≈ 1518 cm^{-1}) are again consistent with the presence of $[TDAE]^{2+}$. Additionally, **1** is diamagnetic, and the solid-state ^{13}C NMR chemical shift for the TDAE central carbon atoms occurs at δ = 156.4 ppm (relative to tetramethyl silane (TMS) by a secondary external reference to the upfield peak of adamantane at δ = 38.6 ppm) in accord with the previously reported values of δ = 155.7 and 157.2 ppm for $[TDAE]^{2+}$.[16]

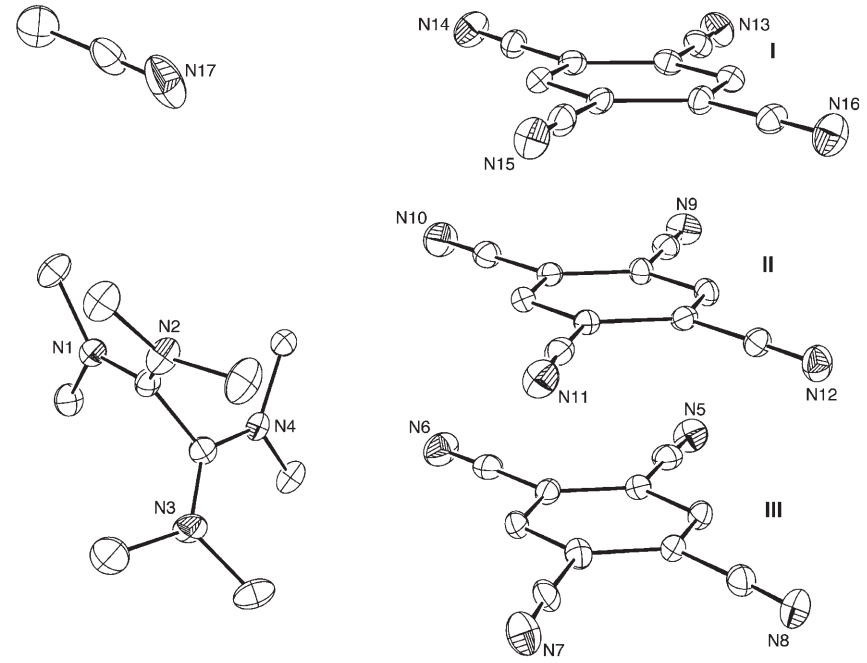


Figure 2. ORTEP plot (thermal ellipsoids set at 30% probability) for **1**. Unlabeled atoms are C.

Each TCNB is planar and each of the 42 atoms in the TCNB triad is unique; hence, all C–C distances are unique (Table 1). Although there are some small fluctuations, the NCC–CCN distances average 1.442 and 1.445 Å for TCNBs (**II** and **III**) (Figure 2, Table 1), while the HC–CCN distances average 1.384 and 1.387 Å for the same TCNBs. Hence, the NCC–CCN distance exceeds the HC–CCN distance by

 © 2006 Wiley-VCH Verlag GmbH & Co. KGaA, Weinheim

Table 1: CC and CN bond lengths observed for **1**.

Moiety in **1**[a]	NCC-CCN [Å]	HC-CCN [Å]	C-CN [Å]	CN [Å]
TCNB **I**	1.446(6)	1.373(6)	1.428(6)	1.151(6)
	1.438(5)	1.390(6)	1.431(6)	1.155(6)
		1.383(6)	1.431(6)	1.165(6)
		1.391(6)	1.431(6)	1.142(6)
TCNB **II**	1.438(5)	1.398(6)	1.430(6)	1.150(6)
	1.452(5)	1.395(6)	1.434(6)	1.149(6)
		1.370(6)	1.421(6)	1.156(6)
		1.384(6)	1.423(6)	1.155(5)
TCNB **III**	1.432(6)	1.381(7)	1.436(6)	1.153(6)
	1.412(6)	1.400(6)	1.430(7)	1.148(6)
		1.397(6)	1.437(7)	1.153(6)
		1.442(6)	1.442(6)	1.148(5)
TCNB **I** Ave	1.442(6)	1.384(8)	1.430(2)	1.153(10)
TCNB **II** Ave	1.445(10)	1.387(13)	1.427(6)	1.153(4)
TCNB **III** Ave	1.422(14)	1.405(26)	1.436(5)	1.151(3)
Ave	1.436(14)	1.392(18)	1.431(6)	1.152(6)

[a] Structure determined at 150(1) K.

0.058 Å. This result is indicative of loss of the aromaticity that is present for $TCNB^0$, which has essentially equivalent NCC–CCN and HC–CCN distances of 1.398 and 1.385 Å,[17] respectively. TCNB **I** has a somewhat longer average NCC–CCN distance of 1.405 Å, and somewhat shorter average HC–CCN distance of 1.426 Å, but these are still less equivalent to that observed for $TCNB^o$. In addition, the average C–CN distance of 1.428 Å is 0.017 Å shorter than that observed for $TCNB^o$, while the C–N distance is 0.085 Å longer. While each TCNB in **1** differs, they are more similar to each other than to $TCNB^0$.

The TCNB units form columns composed of triads, with an average inter-triad separation of 3.6 Å that exceeds the van der Waals separation (> 1.5 Å[18]). The two average intra-triad separations are 3.3 and 3.4 Å, and are below the van der Waals separation. Hence, from structural and charge balance considerations the TCNB units form a trimeric dianion, $[TCNB]_3^{2-}$. The structural differences between the TCNB units are attributed to their different electrostatic environments with respect to the $[TDAE]^{2+}$. Each triad is surrounded by four $[TDAE]^{2+}$ ions. TCNB **II** is closer to all four surrounding $[TDAE]^{2+}$ ions than the TCNB **I** and **III**. TCNB **I** and **III** are close to two $[TDAE]^{2+}$ ions, albeit **III** is slightly closer than **I**. Thus, each TCNB is in a different electrostatic environment, which should effect their charge distributions and structure as observed.

The charge distribution within a trimer was experimentally and computationally investigated to evaluate the importance of the following formal distributions: **a**) $[TCNB]^{1-}$-$[TCNB]^{1-}[TCNB]^0$ {or $[TCNB]^{1-}[TCNB]^0[TCNB]^{1-}$}, **b**) $[TCNB]^0[TCNB]^{2-}[TCNB]^0$ {or $[TCNB]^{2-}[TCNB]^0$-$[TCNB]^0$}, or delocalized **c**) $[TCNB]^{2/3-}[TCNB]^{2/3-}[TCNB]^{2/3-}$, or **d**) $[TCNB]^{1/2-}[TCNB]^{1-}[TCNB]^{1/2-}$. Based upon the reversible first and second one-electron reduction potentials for TCNB,[11] conproportionation of **b** to **a** is disfavored by approximately 1 V; hence, the presence of $[TCNB]^{2-}$ is unlikely.

Localized distributions **a** and **b** should exhibit spectroscopic and structural evidence for the presence of $TCNB^0$. From the above structural data, $TCNB^0$ is not present; however, spectroscopy is a more incisive probe. As noted above, $TCNB^0$ has a characteristic $\tilde{\nu}_{C\equiv N}$ absorption at 2245 cm^{-1} that is not observed[19] and thus is suggestive of distributions **c** or **d**. Likewise, the ^{13}C NMR spectroscopy resonances for CH ($\delta = 139.5$ and 135.2 ppm), *C*CN ($\delta =$ 122.7 ppm), and CN ($\delta = 115.8$ ppm) that occur for $TCNB^0$ (Figure 3) are not observed for **1**, in which these resonances occur at $\delta = 144.8$, 111.8, and 125.5 ppm, respectively.[20] In addition, the two ^1H NMR spectroscopy resonances observed at $\delta = 7.1$ and 6.2 ppm for $TCNB^o$ are not present in **1** for which three resonances occur at $\delta = 5.3$, 6.3, and 8.2 ppm. The observed shifts and the presence of a third ^1H resonance are assumed to arise from the complex chemical environments (six different protons) that are present.

Density functional theory molecular orbital (DFT MO) calculations[21] on $[TCNB]_3^{2-}$ indicate an up field shift of the

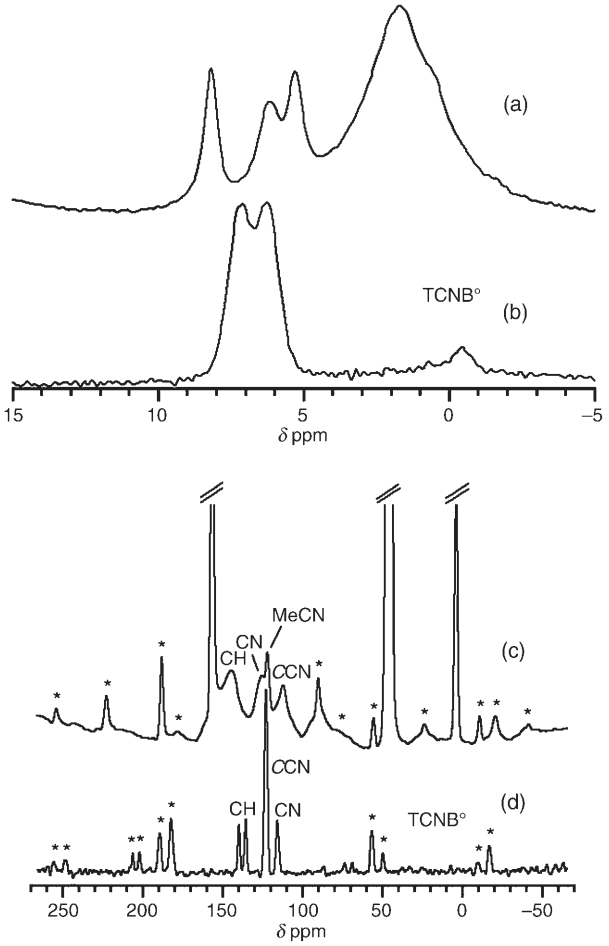
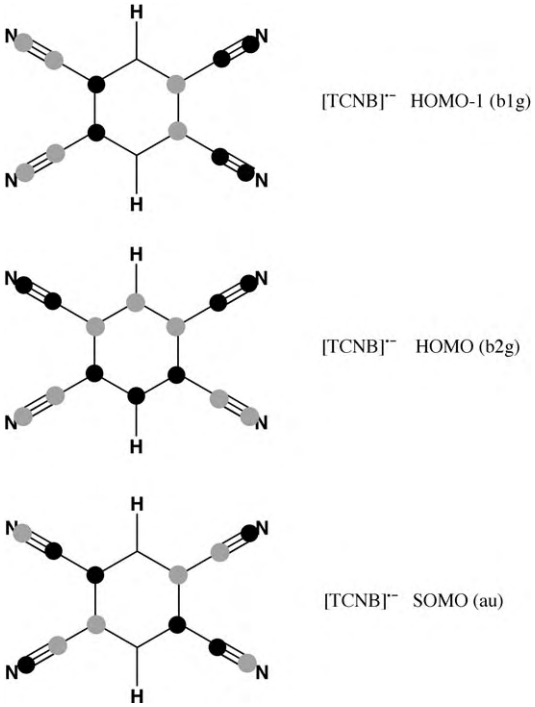


Figure 3. Single pulse magic-angle spinning (MAS) ^1H NMR spectrum for **1** (a) and $TCNB^0$ (b) and cross-polarization (CP)-MAS ^{13}C NMR spectrum for **1** (c) and $TCNB^0$ (d). The ^{13}C and ^1H NMR chemical shift scales are given relative to TMS; spinning sidebands are indicated by asterisks. For the CP-MAS experiments cross polarization from ^1H and TPPM (TPPM = two-pulse phase modulation) ^1H decoupling was used. The spinning speed was 10 kHz in all experiments. Referencing for ^{13}C NMR resonance signals was achieved by a secondary external reference to the upfield peak of adamantane at $\delta = 38.6$ ppm and for ^1H NMR signals to liquid DMSO at $\delta = 2.5$ ppm.

 © 2006 Wiley-VCH Verlag GmbH & Co. KGaA, Weinheim

CH and CN carbon isotropic chemical shifts, whereas the CCN carbon shifts down field as observed in the ^{13}C NMR spectrum.[22] The presence of diamagnetic $[TCNB]^{2-}$ ions is unlikely as MO calculations predict *C*CN to have an isotropic shift of $\delta \approx 68$ ppm, however, there is no resonance observed in this region. As the NMR spectroscopy data does not support the presence of TCNB°, it is in accord with distributions **c** or **d** with each TCNB being fractionally reduced.

The electronic structure of $[TDAE][TCNB]_3 \cdot MeCN$ was calculated by using an ab initio method.[21] Natural bond orbital analysis[21] revealed charge delocalization over all three TCNB units in $[TCNB]_3^{2-}$ in accord with distribution **d**. TCNB has different computed charge distribution, that is, $[TCNB]^{0.25-}[TCNB]^{1.11-}[TCNB]^{0.61-}$.[21] The non-uniform charge distribution is a consequence of the differing electrostatic environments for each TCNB unit, which leads to differences in the contributions from the p_y orbitals (perpendicular to the TCNB plane). The *C*CN p_y orbital contribution of TCNB **II** and TCNB **III** are 12 to 19% and are 5 to 8% higher than TCNB **I**, respectively. Since the electron density is the square of the wavefunction, the orbital contribution qualitatively relates to the charge distribution. The triads form as a result of the delocalized bonding of the $[TCNB]_3^{2-}$ ion. The overlapping of the singly occupied molecular orbital (SOMO) of $[TCNB]^{\bullet -}$ gives the bonding orbital of $[TCNB]_3^{2-}$, the highest occupied molecular orbital (HOMO) of a_u symmetry (Figure 4).



The detailed understanding of multicenter C–C bonding has only recently garnered attention, but is evident for several systems that include dimeric $[TCNE]_2^{2-}$ and the trimeric system reported herein. Related systems that presumably exhibit similar mutlicentered bonding over a trimeric units include examples of $[TCNQ]_3^{2-}$,[23] as well as a extended chains that stabilize metallic conductivity, such as spirobiphenalenyl radicals.[24]

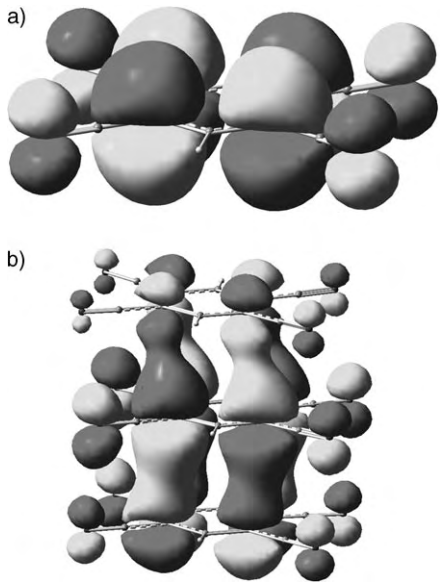


Figure 4. Calculated SOMO for $[TCNB]^{-}$ (a) and HOMO for $[TCNB]_3^{2-}$ (b).

Received: March 17, 2006
Published online: July 17, 2006

Keywords: cyanocarbon compounds · electron transfer · ions · partial charges · structure elucidation

[1] For example, R. S. Mulliken, W. B. Person, *Molecular Complexes: A Lecture and Reprint Volume*, Wiley, New York, **1969**.
[2] For example, *Handbook of Conducting Polymers*, 2nd ed. (Eds.: T. A. Skotheim, R. L. Elsenbaumer, J. R. Reynolds), Marcel Dekker, New York, **1998**; J. R. Ferraro, J. M. Williams, *Introduction to synthetic electrical conductors*, Academic Press, Orlando, **1987**.
[3] For example, J. M. Williams, *Organic Superconductors (Including Fullerenes): Synthesis, Structure, Properties, and Theory*, Prentice Hall, Englewood Cliffs, NJ, **1992**; T. Ishiguro, K. Yamaji, G. Saito, *Organic Superconductors*, Springer, New York, **1998**.
[4] For example, a) V. I. Ovcharenko, R. Z. Sagdeev, *Russ. Chem. Rev.* **1999**, *68*, 345; M. Kinoshita, *Philos. Trans. R. Soc. London Ser. A* **1999**, *357*, 2855; b) J. S. Miller, A. J. Epstein, *Angew. Chem.* **1994**, *111*, 399; *Angew. Chem. Int. Ed. Engl.* **1994**, *33*, 385; J. S. Miller, A. J. Epstein, *Chem. Eng. News* **1995**, *73*(40), 30; c) S. J. Blundell, F. L. Pratt, *J. Phys.: Condens. Matter* **2004**, *16*, R771; J. A. Crayson, J. N. Devine, J. C. Walton, *Tetrahedron* **2000**, *56*, 7829.
[5] R. E. Del Sesto , A. M. Arif, J. J. Novoa, I. Anusiewicz, P. Skurski, J. Simons, B. C. Dunn, E. M. Eyring, J. S. Miller, *J. Org. Chem.* **2003**, *68*, 3367.
[6] J. S. Miller, *Angew. Chem.* **2006**, *118*, 2570; *Angew. Chem. Int. Ed.* **2006**, *45*, 2508.
[7] a) J. M. Manriquez, G. T. Yee, R. S. McLean, A. J. Epstein, J. S. Miller, *Science* **1991**, *252*, 1415; J. S. Miller, G. T. Yee, J. M. Manriquez, A. J. Epstein, in *Proceedings of Nobel Symposium*

 © 2006 Wiley-VCH Verlag GmbH & Co. KGaA, Weinheim

No. NS-81 Conjugated Polymers and Related Materials: The Interconnection of Chemical and Electronic Structure (Eds.: W. R. Salaneck, I. Lundström, B. Rånby), Oxford University Press, Oxford, **1993**, p. 461; b) J. Zhang, P. Zhou, W. B. Brinckerhoff, A. J. Epstein, C. Vazquez, R. S. McLean, J. S. Miller, *ACS Symp. Ser.* **1996**, *644*, 311.

[8] E. B. Vickers, T. D. Selby, M. S. Thorum, M. L. Taliaferro, J. S. Miller, *Inorg. Chem.* **2004**, *43*, 6414.

[9] E. B. Vickers, T. D. Selby, J. S. Miller, *J. Am. Chem. Soc.* **2004**, *126*, 3716.

[10] M. L. Taliaferro, M. S. Thorum, J. S. Miller, *Angew. Chem.* **2006**, *118*, 5452; *Angew. Chem. Int. Ed.* **2006**, *45*, 5326.

[11] M. Moscherosch, E. Waldhor, H. Binder, W. Kaim, J. Fiedler, *Inorg. Chem.* **1995**, *34*, 4326.

[12] a) N. Wiberg, *Angew. Chem.* **1968**, *80*, 809; *Angew. Chem. Int. Ed. Engl.* **1968**, *7*, 766; b) R. Fox, B. M. Foxman, D. Guerrer, J. S. Miller, J. C. Calabrese, A. H. Reis, Jr., *J. Mater. Chem.* **1995**, *6*, 1627.

[13] Elemental analysis (%) calcd for $[TDAE][TCNB]_3 \cdot MeCN$: C 65.02, H 4.29, N 30.69; Found: C 64.82, H 3.98 N 30.39. A $0.23 \times 0.13 \times 0.03$ mm crystal mounted on a glass fiber with traces of a viscous oil was studied at 150(1) K on a Nonius KappaCCD diffractometer [$Mo_{K\alpha}$ ($\lambda = 0.71073$ Å)]. A total of 12534 reflections ($\theta_{max} = 25.07°$) were indexed, integrated, and corrected for Lorentz, polarization, and absorption effects using DENZO-SMN and SCALEPAC. Monoclinic space group $P2_1/c$: $a = 16.0115(7)$, $b = 10.1304(5)$, $c = 24.8810(8)$ Å, $\beta = 96.224(2)°$, $V = 4012.0(3)$ Å^3. $R1 = 0.0850$, $wR2 = 0.2062$, and $S = 1.04$ for 3783 reflections with $I > 2\sigma(I)$, and $R1 = 0.1623$, $wR2 = 0.2493$, and $S = 1.04$ for 7048 unique reflections and 620 parameters. The final difference-Fourier map ranged from -0.306 to 0.449 e Å^3. CCDC-299545 contains the supplementary crystallographic data for this paper. These data can be obtained free of charge from The Cambridge Crystallographic Data Centre via www.ccdc.cam.ac.uk/data_request/cif.

[14] K. I. Pokhodnia, J. Papavassiliou, P. Umek, A. Omerzu, D. Mihailic, *J. Chem. Phys.* **1999**, *110*, 3606.

[15] J. Bruckmann, C. Kruger, H. Borrmann, A. Simon, *Z. Kristallogr.* **1995**, *210*, 521.

[16] M. Strohmeier, D. H. Barich, D. M. Grant, J. S. Miller, R. J. Pugmire, J. Simons, *J. Phys. Chem. A* **2006**, *110*, 7962.

[17] J. Lefebvre, G. Odou, M. Muller, A. Mierzejewski, T. Luty, *Acta Crystallogr. Sect. B* **1989**, *45*, 323.

[18] A. Bondi, *J. Phys. Chem.* **1964**, *68*, 441.

[19] The absorption observed at 2245 cm^{-1} is due to MeCN present in the structure.

[20] Unfortunately, the spread of isotropic shifts for each position in the asymmetric unit of **1** deteriorates the resolution and prevents the measurement of the chemical shift principal values that are an even more sensitive probe of electronic structure.

[21] Electronic structures of TCNB^o, $[TCNB]^{\bullet -}$, and $[TDAE][TCNB]_3 \cdot MeCN$ were calculated by using ab initio Hartree–Fock (HF) method followed by second-order Møller–Plesset (MP2) correlation energy correction (*S1*) with Gaussian type 6-31g(d) basis set. Geometry optimization was performed for both TCNB^o (spin restricted) and $[TCNB]^{\bullet -}$ (spin unrestricted), single-point energy calculation for $[TDAE][TCNB]_3 \cdot MeCN$ (spin restricted) taken from the crystal structure and subsequent natural bond orbital (NBO) analysis (*S1-S1*). DFT calculation for the NMR chemical shift was performed at the B3LYP/D95** level on $[TCNB]_3^{2-}$. C. Møller, M. S. Plesset, *Phys. Rev.* **1934**, *46*, 618; E. D. Glendening, et al. *NBO 5.0* (Theoretical Chemistry Institute, Univerity of Wisconsin, Madison, **2001**. Gaussian 03 (Revision A.1), M. J. Frisch, G. W. Trucks, H. B. Schlegel, G. E. Scuseria, M. A. Robb, J. R. Cheeseman, J. A. Montgomery, Jr., T. Vreven, K. N. Kudin, J. C. Burant, J. M. Millam, S. S. Iyengar, J. Tomasi, V. Barone, B. Mennucci, M. Cossi, G. Scalmani, N. Rega, G. A. Petersson, H. Nakatsuji, M. Hada, M. Ehara, K. Toyota, R. Fukuda, J. Hasegawa, M. Ishida, T. Nakajima, Y. Honda, O. Kitao, H. Nakai, M. Klene, X. Li, J. E. Knox, H. P. Hratchian, J. B. Cross, C. Adamo, J. Jaramillo, R. Gomperts, R. E. Stratmann, O. Yazyev, A. J. Austin, R. Cammi, C. Pomelli, J. W. Ochterski, P. Y. Ayala, K. Morokuma, G. A. Voth, P. Salvador, J. J. Dannenberg, V. G. Zakrzewski, S. Dapprich, A. D. Daniels, M. C. Strain, O. Farkas, D. K. Malick, A. D. Rabuck, K. Raghavachari, J. B. Foresman, J. V. Ortiz, Q. Cui, A. G. Baboul, S. Clifford, J. Cioslowski, B. B. Stefanov, G. Liu, A. Liashenko, P. Piskorz, I. Komaromi, R. L. Martin, D. J. Fox, T. Keith, M. A. Al-Laham, C. Y. Peng, A. Nanayakkara, M. Challacombe, P. M. W. Gill, B. Johnson, W. Chen, M. W. Wong, C. Gonzalez, J. A. Pople, Gaussian, Inc., Pittsburgh, PA, **2003**.

[22] Experimental validation of the assignments could not be achieved due to the low signal to noise ratio.

[23] T. Akutagawa, S. Takeda, T. Hasegawa, T. Nakamura, *J. Am. Chem. Soc.* **2004**, *126*, 291.

[24] M. E. Itkis, X. Chi, A. W. Cordes, R. C. Haddon, *Science* **2002**, *296*, 1443.

 © 2006 Wiley-VCH Verlag GmbH & Co. KGaA, Weinheim

Magnetism

DOI: 10.1002/anie.200600988

Room-Temperature Organic-Based Magnet ($T_c \approx 50\,^{\circ}C$) Containing Tetracyanobenzene and Hexacarbonylvanadate(−I)**

*Michelle L. Taliaferro, Matthew S. Thorum, and Joel S. Miller**

The discovery of the first organic-based magnet, $[Fe(C_5Me_5)_2]^{\bullet+}[TCNE]^{\bullet-}$ (TCNE = tetracyanoethylene),[1] led to the development of several new families of magnetically ordered materials based on unpaired electron spins residing in p orbitals. These include $[Mn^{II}(hfac)_2(NITR)]$ (hfac = hexafluoroacetylactonate; NITR = 2-R-4,4,5,5-tetramethyl-4,5-dihydro-1*H*-imidazolyl-1-oxy-3-oxide)[2] and $[Mn^{III}(porphyrin)]^{+}[TCNE]^{\bullet-}$ [3] based ferrimagnets as well as β-*p*-

[*] M. L. Taliaferro, M. S. Thorum, Prof. J. S. Miller
Department of Chemistry
University of Utah
Salt Lake City, UT 84112-0850 (USA)
Fax: (+1) 801-581-8433
E-mail: jsmiller@chem.utah.edu

[**] We thank Carlos Vazquez (Du Pont), R. Scott McLean (Du Pont), Prasanna S. Ghalsasi, and Elaine B. Vickers for preliminary studies, and Thomas G. Richmond, Richard D. Ernst, Konstantin I. Pokhodnya, Kendric J. Nelson, and Arthur J. Epstein (The Ohio State University) for helpful discussions, and we gratefully acknowledge the continued partial support by the US Department of Energy Division of Materials Science (Grant Nos. DE-FG03-93ER45504 and DE-FG02-01ER45931) and the US Air Force Office of Scientific Research (Grant No. F49620-03-1-0175).

WILEY InterScience DISCOVER SOMETHING GREAT
© 2006 Wiley-VCH Verlag GmbH & Co. KGaA, Weinheim

$NO_2C_6H_4NIT$,[4] [tetrakis(dimethylamino)ethylene][C_{60}],[5] and $NCC_6F_4CS_2N_2$,[6] among others.[3b,7] The reaction of $V(C_6H_6)_2$[8a] and $V(CO)_6$,[8b] albeit by different mechanisms, formed $V[TCNE]_x \cdot z\,CH_2Cl_2$ ($x \approx 2$; $z \approx 0.5$), a disordered room-temperature organic magnet with $T_c \approx 400$ K.[3b] Extended X-ray absorption fine structure (EXAFS) and X-ray absorption near-edge structure (XANES) studies reveal that the vanadium is divalent and surrounded by six nitrogen centers at 2.084(5) Å, Figure 1.[9]

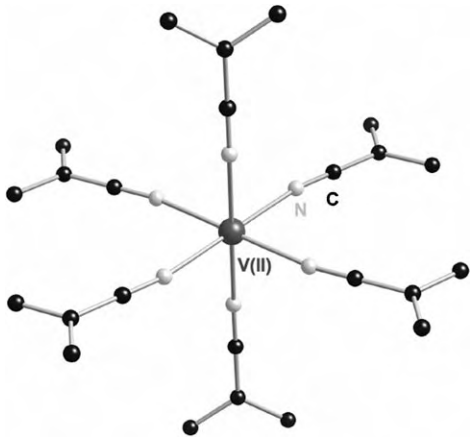
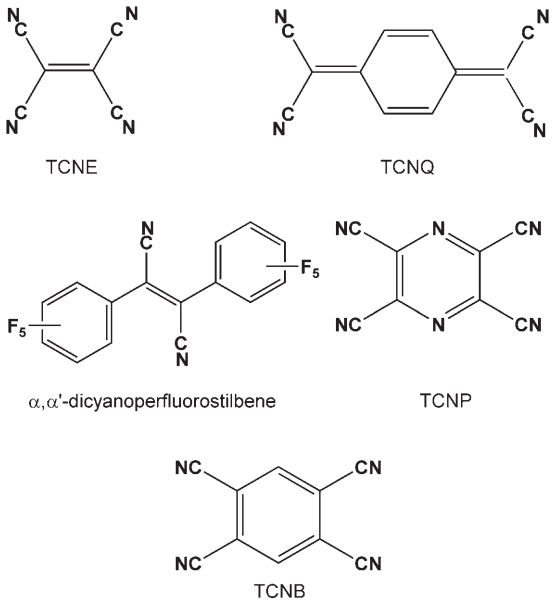


Figure 1. Local structure around each V^{II} site in $V[TCNE]_x$ deduced from XANES and EXAFS studies.

Subsequently, solvent-free thin films of $V[TCNE]_x$ have been prepared by chemical vapor deposition (CVD).[10] Use of trifluoromethylbenzene ($PhCF_3$) as the solvent, which has a slightly enhanced dielectric constant (9.2) with respect to CH_2Cl_2 (8.9),[11] led to an increase in the T_c as well as thermal stability.[12] Magnetotransport studies suggest that the electrons in the valence and conducting bands of $V[TCNE]_x$ are spin polarized,[13] and this material has potential "spintronic" applications.

With the goal of identifying new magnetically ordered organic-based materials, the reaction of $[V(CO)_6]$ with several polynitrile electron acceptors has been studied. To date, V[α,α′-dicyanoperfluorostilbene]$_2$ ($T_c = 205$ K),[14] V-[TCNP]$_2$ (TCNP = tetracyanopyrazine; $T_c = 200$ K),[15] and V[TCNQ]$_2$ (TCNQ = 7,7,8,8-tetracyano-*p*-quinodimethane; $T_c = 56$ K), as well as several 2,5-disubstituted TCNQs[16] are the few reported examples of magnets which are compositionally related to $V[TCNE]_x$. While these structures are unknown, based upon the composition, they are assumed to be similar to $V[TCNE]_x$, Figure 1.

The prototype electron acceptor, TCNE, forms the magnet with the highest T_c. Modification by extension along the central C–C bond, that is, formation of TCNQ, led to a material with a substantial reduction in T_c. In contrast, use of the TCNP electron acceptor, that is, modification of TCNE by extension perpendicular to the central C–C bond leads to a material with only a mild reduction in T_c. Hence, we sought additional examples of electron acceptors with a structure related to TCNP, and preferably one that could be chemically modified or attached to a polymer backbone. Herein, we



report a new, the second, room-temperature organic-based magnet prepared from the reaction of [$V^0(CO)_6$], and 1,2,4,5-tetracyanobenzene (TCNB) as well as a magnet prepared from the reaction of TCNB and [$V^0(PhMe)_2$].

Owing to the high oxidation potential, albeit irreversible, for $[V(CO)_6]$ ($E^{-/o} = +0.88$ V vs. saturated calomel electrode (SCE), in CH_2Cl_2[17]) or the reversible one-electron oxidation for $[V(PhMe)_2]$ ($E^{o/+} \approx -0.30$ V vs. SCE, in CH_2Cl_2[18]) both should not reduce TCNB ($E^{-/o} = -0.64$ V vs. SCE, in MeCN[19]). Nonetheless, immediate reactions occurs forming a dark, amorphous product.

The reaction of two equivalents of TCNB per $[V(CO)_6]$[18,20] in CH_2Cl_2 ($\mathbf{V_{CO}{\cdot}CH_2Cl_2}$) or $PhCF_3$ ($\mathbf{V_{CO}{\cdot}PhCF_3}$) or per $[V(PhMe)_2]$ in CH_2Cl_2[21] ($\mathbf{V_{PhMe}{\cdot}CH_2Cl_2}$) in a dry box, led to the isolation of magnetically ordered materials.[22] $\mathbf{V_{CO}{\cdot}CH_2Cl_2}$, $\mathbf{V_{CO}{\cdot}PhCF_3}$, and $\mathbf{V_{PhMe}{\cdot}CH_2Cl_2}$ exhibit a $\nu_{C\equiv N}$ absorption in at 2158 ± 3 and a shoulder at 2190 ± 4 cm^{-1} (Figure 2). These IR absorptions are lower in energy than that observed for TCNB^o (2245 cm^{-1}) and are indicative of reduced TCNB. The number and broad nature of the $\nu_{C\equiv N}$ absorptions suggest that there are multiple C≡N environments in the material. This situation is also observed for $V[TCNP]_2 \cdot z$ solv. (solv. = solvent)[15] and $V[TCNE]_x \cdot z\,CH_2Cl_2$ ($x \approx 2$; $z \approx 0.5$) that have three absorptions present between 2215 and 2150 cm^{-1}.[3b,8,10]

Unprecedentedly, the materials prepared using $[V(CO)_6]$ additionally have broad absorptions at 1845 ± 4 and 1699 ± 10 cm^{-1}. The assignments of ν_{CO} and $\nu_{\mu\text{-}CO}$, respectively, are indicative of $[V^{-I}(CO)_6]^-$, which has a strong, broad ν_{CO} absorption at approximately 1845 cm^{-1}. Additionally, an absorption at 649 ± 1 cm^{-1} ascribed to ν_{VC} which is also observed for $[V^{-I}(CO)_6]^-$, is present. The presence of $[V^{-I}(CO)_6]^-$ was confirmed by dissolution into MeCN and observation of a solution ν_{CO} absorption at 1860 cm^{-1} that is identical to an authentic sample of $[V^{-I}(CO)_6]^-$. $[V^{-I}(CO)_6]^-$ undoubtedly forms from the disproportionation of $[V^0(CO)_6]$, as has been established from the reaction with several

 © 2006 Wiley-VCH Verlag GmbH & Co. KGaA, Weinheim

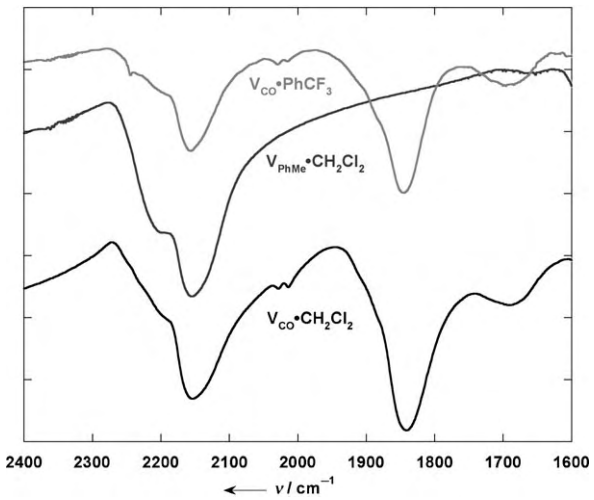


Figure 2. IR spectra of $\mathbf{V_{CO}{\cdot}CH_2Cl_2}$, $\mathbf{V_{CO}{\cdot}PhCF_3}$, and $\mathbf{V_{PhMe}{\cdot}CH_2Cl_2}$ in the range 1600 to 2400 cm^{-1}.

bases.[23] Nonetheless, absorptions in these regions were not observed for the reaction of $[V(CO)_6]$ and TCNE,[3b,8,10] TCNQ,[16] TCNP,[15], and others[14] as CO is facilely lost.[18] Heating the $\mathbf{V_{CO}{\cdot}solv.}$ samples leads to an attenuation of both the $\nu \approx 1845$ and 1699 cm^{-1} absorptions in accord with CO loss, and growth of a peak at $\nu = 2211$ cm^{-1} arising from an increased intensity of the absorption of the band that forms the shoulder.

The 1699 cm^{-1} absorption is assigned to a bridging isocarbonyl, V–C≡O–V. Albeit rare, this linkage has been structurally characterized for $[(OC)_5V^{-I}(\mu\text{-}CO)V^{II}(thf)_4(\mu\text{-}CO)V^{-I}(CO)_5]$,[24a] whose 1684 cm^{-1} absorption is assigned to $\nu_{\mu\text{-}CO}$.[23] Likewise, $[(C_5Me_5)_2V^{II}(\mu\text{-}OC)V^{-I}(CO)_5]$ has a broad absorption at 1708 cm^{-1},[24b] which is in good agreement with the observed values for $\mathbf{V_{CO}{\cdot}solv}$. Hence, the $\mathbf{V_{CO}{\cdot}solv.}$ (**solv.** = CH_2Cl_2, $PhCF_3$) materials are proposed to have $[V^{-I}(CO)_6]^-$ centers with bridging isocarbonyl units. The presence of one ν_{CO} absorption, albeit broad, suggests that the $[V^{-I}(CO)_6]^-$ has high symmetry as $[(C_5Me_5)_2V^{II}(\mu\text{-}OC)V^{-I}(CO)_5]$ and $[(OC)_5V^{-I}(\mu\text{-}CO)V^{II}(thf)_4(\mu\text{-}CO)V^{-I}(CO)_5]$ with a single bridging isocarbonyl have multiple ν_{CO} absorptions.[23,24b]

Thermogravimetric analysis (TGA)[25a] of $\mathbf{V_{CO}{\cdot}CH_2Cl_2}$, $\mathbf{V_{CO}{\cdot}PhCF_3}$, and $\mathbf{V_{CO}{\cdot}CH_2Cl}$ reveal mass-loss events (Figure 3). For $\mathbf{V_{CO}{\cdot}CH_2Cl_2}$ the CO and CH_2Cl_2 losses overlap in temperature and occur below 140 °C, with the shoulder at approximately 100 °C attributed to CO loss. This assignment is supported by the trace for $\mathbf{V_{PhMe}{\cdot}CH_2Cl_2}$ in which this shoulder is not present and the CH_2Cl_2 loss occurs below 100 °C. For $\mathbf{V_{CO}{\cdot}PhCF_3}$ the CO loss occurs below 120 °C, and the $PhCF_3$ loss occurs between 125 and 230 °C. This result is consistent with the lower volatility of $PhCF_3$ (b.p. = 102 °C) with respect to CH_2Cl_2 (b.p. = 40 °C). To confirm the presence of CO and its facile loss, high-resolution mass spectra[25b] as a function of heating were obtained for these samples, and a significant amount CO was detected when the samples were heated to 33 °C.

The composition of $\mathbf{V_{PhMe}{\cdot}CH_2Cl_2}$ was determined from elemental analyses to be $V^{II}[TCNB]_2{\cdot}0.05\,CH_2Cl_2$[26a] consis-

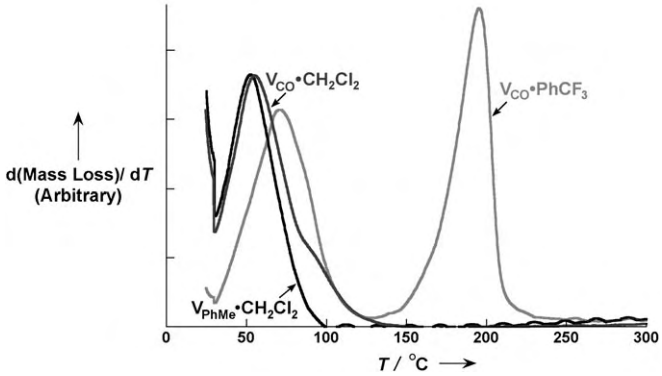
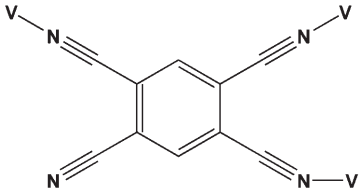


Figure 3. Derivative [d(mass loss)/dT] of the TGA traces for $\mathbf{V_{CO}{\cdot}CH_2Cl_2}$, $\mathbf{V_{CO}{\cdot}PhCF_3}$, and $\mathbf{V_{PhMe}{\cdot}CH_2Cl_2}$.

tent with the reported compositions of other V[A]$_2$-based (A = TCNE,[3b,8] α,α′-dicyanoperfluorostilbene,[14] TCNP,[15] TCNQ[16]) magnets. Hence, $\mathbf{V_{PhMe}{\cdot}CH_2Cl_2}$ is proposed to have a structure similar to V[TCNP]$_2{\cdot}z$solv. (**1**), as it is has a



1

similar composition and it magnetically orders at the same T_c (see below). In contrast, and consistent with the presence of $[V^{-I}(CO)_6]^-$, the composition of $\mathbf{V_{CO}{\cdot}solv.}$ as determined from elemental analyses, is $V^{II}[TCNB]_x[V^{-I}(CO)_y]_{0.5}{\cdot}z$ solv. ($4 > x > 3.5$; $6 > y > 3.2$; $z < 0.4$), with samples of solv. = CH_2Cl_2, $x = 3.8$, $y = 6$, $z = 0.05$,[26b] solv. = $PhCF_3$, $x = 3.8$, $y = 6$, $z = 0.1$ characterized.[26c] This non-stoichiometry and variable stoichiometry has also been observed for V[TCNE]$_x{\cdot}z\,CH_2Cl_2$ ($x \approx 2$; $z \approx 0.5$).[8] Owing to the time delay between their preparation and analysis, CO (and solvent) loss occurs; nonetheless, the elemental-analysis data are consistent with the presence of CO. Hence, from a charge consideration $\mathbf{V_{CO}{\cdot}CH_2Cl_2}$ and $\mathbf{V_{CO}{\cdot}PhCF_3}$ are formulated as $V^{II}[TCNB]^-_{1.5}$-$[TCNB]^0_{x-15}[V^{-I}(CO)_6]_{0.5}{\cdot}z$ solv. The presence of $TCNB^0$, however is not evident from the IR spectra as the $\nu_{C\equiv N}$ absorption expected at 2245 cm^{-1} for $TCNB^0$ is not present. The absence of a $\nu_{C\equiv N}$ absorption suggests that reduced TCNB self-associates to form a complex delocalized anionic species, as recently observed for $[TCNB]_3^{2-}$.[27] TGA analysis of percentage mass losses for the $\mathbf{V_{CO}{\cdot}PhCF_3}$ solv. and CO events, that is, 14.7(3) and 14.3(4) %, respectively (Figure 3), corresponds to the composition of $\mathbf{V_{CO}{\cdot}PhCF_3}$ being V-$[TCNB]_{3.8}[V(CO)_{5.4}]_{0.5}{\cdot}PhCF_3$ suggestive of further loss in transit for elemental-analysized samples. The composition of $\mathbf{V_{CO}{\cdot}CH_2Cl_2}$ is less definitive owing to the overlap of the solv. and CO mass-loss events. The composition of $\mathbf{V_{PhMe}{\cdot}CH_2Cl_2}$ from elemental analysis as well as solv. mass loss in the TGA is V[TCNB]$_2{\cdot}z\,CH_2Cl_2$ $z = 0.7$ and 0.05, respectively.

 © 2006 Wiley-VCH Verlag GmbH & Co. KGaA, Weinheim

Powder diffraction data, like those observed for V-[TCNZ]$_x$ (Z = E, P, Q), indicate that each of these materials is amorphous. Unlike $V^{II}[TCNB]_2 \cdot 0.05\,CH_2Cl_2$, which is compositionally similar to several V[A]$_2$-based magnets, and, as discussed above, is proposed to be structurally similar, $\mathbf{V_{CO}{\cdot}solv.}$ (solv. = CH_2Cl_2, $PhCF_3$) of $V^{II}(TCNB^-)_{1.5}$-$(TCNB^0)_{x-1.5}[V^{-I}(CO)_v]_{0.5}\cdot z$ solv. composition represents a new family of organic-based magnets. The structure of $\mathbf{V_{CO}{\cdot}solv.}$ is elusive and perplexing. Based upon the similarity of the IR spectra with that of V[TCNE]$_x$ in the ν_{CN} region, a similar structure is proposed, containing TCNB radical anions that are nitrile bound to V^{II}. However, the structure is distinct in that $[V^{-I}(CO)_6]^-$ is present, and possesses symmetrical isocarbonyl bridging to the V^{II} center as well as additional TCNB being present. Studies aimed at further elucidating the structure of $\mathbf{V_{CO}{\cdot}solv.}$ are in progress; herein the focus is on its reproducible magnetic ordering.

The 2 to 400 K magnetic susceptibility, $\chi(T)$, was determined on a Quantum Design MPMS-5XL magnetometer, and the 300–370, 315–325, and 190–210 K data can be fit to the Curie–Weiss expression with $\theta = 326$ (for $\mathbf{V_{CO}{\cdot}CH_2Cl_2}$), 308 ($\mathbf{V_{CO}{\cdot}PhCF_3}$), and 188 K ($\mathbf{V_{PhMe}{\cdot}CH_2Cl_2}$), indicative of effective ferromagnetic coupling (Figure 4). At higher temperature, d[$1/\chi(T)$]/dT decreases, indicative of longer range antiferromagnetic coupling. Below θ, $\chi T(T)$ increases to values as high as 17500 emu Oe mol^{-1} for $\mathbf{V_{CO}{\cdot}CH_2Cl_2}$, and $\mathbf{V_{CO}{\cdot}CH_2Cl_2}$, $\mathbf{V_{CO}{\cdot}PhCF_3}$, and $\mathbf{V_{PhMe}{\cdot}CH_2Cl_2}$, reach maxima at $0.64 \pm 0.05\,\theta$ prior to decreasing. The behavior is suggestive of magnetic ordering. The spin-only values of χT of 2.44 (for $\mathbf{V_{CO}{\cdot}CH_2Cl_2}$), 2.44 ($\mathbf{V_{CO}{\cdot}PhCF_3}$), and 2.63 ($\mathbf{V_{PhMe}{\cdot}CH_2Cl_2}$) emu Oe mol^{-1} are significantly exceeded.

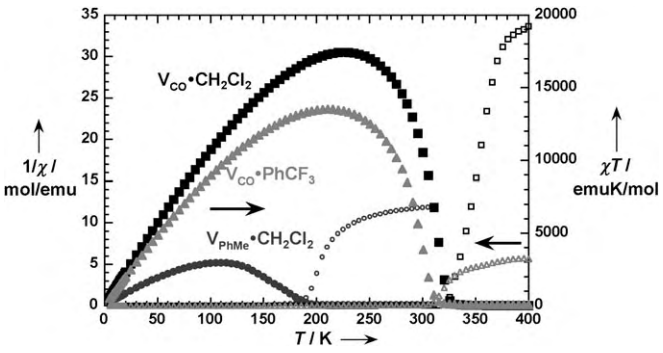


Figure 4. $\chi T(T)$ (filled symbols) and $1/\chi(T)$ (open symbols) for $\mathbf{V_{CO}{\cdot}CH_2Cl_2}$ (■,□), $\mathbf{V_{CO}{\cdot}PhCF_3}$ (▲,△), and $\mathbf{V_{PhMe}{\cdot}CH_2Cl_2}$ (●,○) in a 100 Oe applied field.

The 5 Oe zero-field cooled (ZFC) and field-cooled (FC) magnetization, $M(T)$, have bifurcation temperatures at 311, 306, and 206 K for $\mathbf{V_{CO}{\cdot}CH_2Cl_2}$, $\mathbf{V_{CO}{\cdot}PhCF_3}$, and $\mathbf{V_{PhMe}{\cdot}CH_2Cl_2}$, respectively (Figure 5). Their respective T_c values obtained from an extrapolation of the low-field $M(T)$ to the temperature at which $M(T) \rightarrow 0$ are 325, 305, and 200 K (Figure 5). These T_c values are comparable to θ in accord with mean-field theory.

The 10 K field-dependent magnetization, $M(H)$, shows an immediate increase and reaches saturation at ≤ 75 Oe

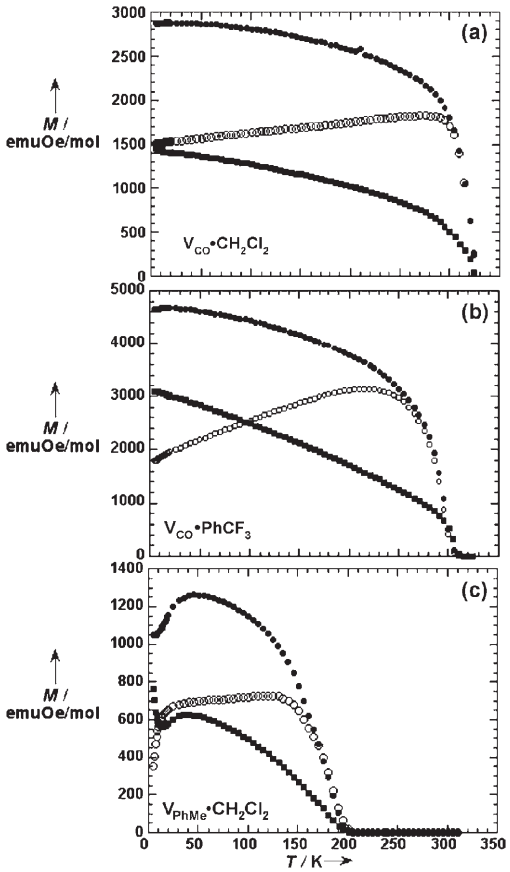


Figure 5. Zero-field (○) and field-cooled (●) (ZFC/FC) as well as remnant magnetization (■) for $\mathbf{V_{CO}{\cdot}CH_2Cl_2}$ (a), $\mathbf{V_{CO}{\cdot}PhCF_3}$ (b), and $\mathbf{V_{PhMe}{\cdot}CH_2Cl_2}$ (c) in a 5 Oe applied field.

(Figure 6). $\mathbf{V_{CO}{\cdot}CH_2Cl_2}$, $\mathbf{V_{CO}{\cdot}PhCF_3}$, and $\mathbf{V_{PhMe}{\cdot}CH_2Cl_2}$, respectively, saturate to 11400, 10700, and 4700 emu Oe mol^{-1} at 50 000 Oe (not shown) For $\mathbf{V_{PhMe}{\cdot}CH_2Cl_2}$ this is 84 % of the expected value of 5585 emu Oe mol^{-1} for $S = 3/2$ V^{II} antiferromagnetically coupled to two $S = 1/2$ $[TCNB]^{\bullet -}$, consistent with the system being a ferrimagnet. In contrast, antiferromagnetic coupling between an $S = 3/2$ V^{II} and 1.5 $S = 1/2$ $[TCNB]^{\bullet -}$ both $\mathbf{V_{CO}{\cdot}CH_2Cl_2}$ and $V_{CO}{\cdot}PhCF_3$ should saturate to 8378 emu Oe mol^{-1}, however approximately 11000 emu Oe mol^{-1} is observed, suggestive of more complex magnetic interactions. Each of these materials has a 7 ± 1 Oe coercive field at 10 and 280 K (Figure 6). These data indicate that they are relatively soft ferrimagnets as reported for V[TCNE]$_2$[8,10] and V[TCNP]$_2$.[15] The remnant magnetization (M_{rem}) is 1860, 3400, and 990 emu Oe mol^{-1} at 10 K for $\mathbf{V_{CO}{\cdot}CH_2Cl_2}$, $\mathbf{V_{CO}{\cdot}PhCF_3}$, and $\mathbf{V_{PhMe}{\cdot}CH_2Cl_2}$ (Figure 6), respectively. The in-phase, $\chi'(T)$, and out-of-phase, $\chi''(T)$, components of ac susceptibility at 10, 100, and 1000 Hz were measured and are consistent with magnetic ordering as a ferrimagnet.

In summary, the reaction of TCNB with $[V^0(CO)_6]$ in CH_2Cl_2 and $PhCF_3$ forms a new compositional family of magnets with T_c values exceeding room temperature and as high as 325 K (≈ 50 °C). The magnets are formulated as

 © 2006 Wiley-VCH Verlag GmbH & Co. KGaA, Weinheim

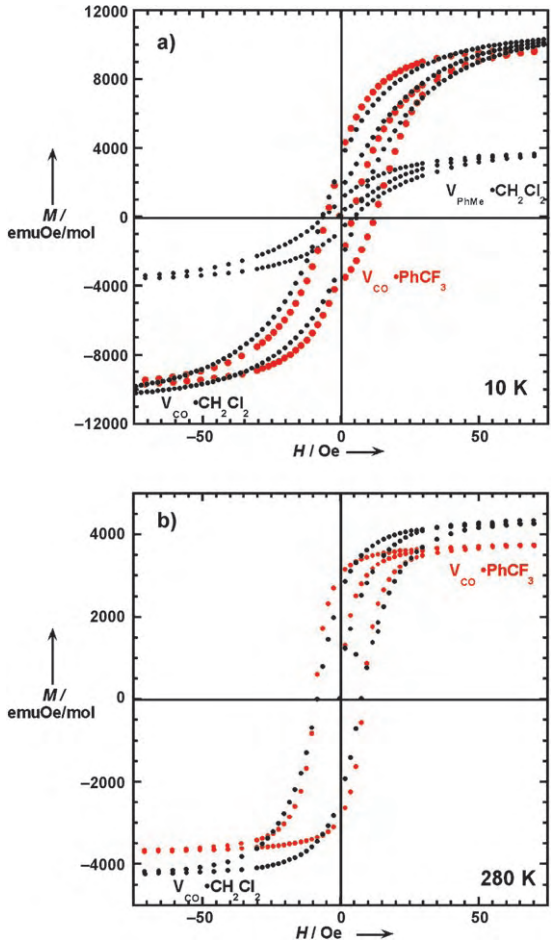


Figure 6. *M*(*H*) showing hysteretic behavior for $\mathbf{V_{CO}{\cdot}CH_2Cl_2}$, $\mathbf{V_{CO}{\cdot}PhCF_3}$, and $\mathbf{V_{PhMe}{\cdot}CH_2Cl_2}$ at 10 K (a) and $\mathbf{V_{CO}{\cdot}CH_2Cl_2}$ and $\mathbf{V_{CO}{\cdot}PhCF_3}$ at 280 K (b).

$V^{II}[TCNB]^{-}_{1.5}[TCNB]^{0}_{x-1.5}[V^{-I}(CO)_6]_{0.5}{\cdot}z$ solv. $(4 > x > 3.5$; solv. $= CH_2Cl_2$, $PhCF_3$), but albeit possessing TCNB and symmetric isocarbonyl bonding of $[V^{-I}(CO)_6]^-$ moieties, its structure is elusive. In contrast, the reaction of TCNB with $[V^0(PhMe)_2]$ in CH_2Cl_2 forms a magnet of V^{II}-$[TCNB]_2{\cdot}z\,CH_2Cl_2$ composition that orders at 200 K. Hence, the addition of diamagnetic TCNB and $[V^{-I}(CO)_6]^-$ moieties unexpectedly and quite surprisingly leads to a 62% increase in T_c (to 325 K; ≈50 °C). Furthermore, the values of the saturation magnetization suggest that the materials are compositionally and structurally even more complex, and this new family of magnets is the focus of studies to resolve these issues. In addition, TCNB, unlike TCNE, possesses hydrogen atoms that could be chemically substituted and perhaps attached to a polymer backbone leading to polymeric magnets.

Received: March 13, 2006
Published online: July 17, 2006

Keywords: cyanocarbon compounds · electron acceptors · electron transfer · organic-based magnets · vanadium

[1] J. S. Miller, J. C. Calabrese, A. J. Epstein, R. W. Bigelow, J. H. Zhang, W. M. Reiff, *J. Chem. Soc. Chem. Commun.* **1986**, 1026; J. S. Miller, J. C. Calabrese, H. Rommelmann, S. Chittipeddi, A. J. Epstein, J. H. Zhang, W. M. Reiff, *J. Am. Chem. Soc.* **1987**, *109*, 769.
[2] A. Caneschi, D. Gatteschi, P. Rey, *Prog. Inorg. Chem.* **1991**, *39*, 331; A. Caneschi, D. Gatteschi, R. Sessoli, P. Rey, *Acc. Chem. Res.* **1989**, *22*, 392.
[3] a) J. S. Miller, J. C. Calabrese, R. S. McLean, A. J. Epstein, *Adv. Mater.* **1992**, *4*, 498; b) J. S. Miller, A. J. Epstein, *Chem. Commun.* **1998**, 1319.
[4] M. Kinoshita, *Philos. Trans. R. Soc. London Ser. A* **1999**, *357*, 2855.
[5] A. Omerzu, D. Arcon, R. Blinc, D. Mihailovic in *Magnetism—Molecules to Materials*, *Vol. 2* (Eds.: J. S. Miller, M. Drillon), Wiley-VCH, Weinheim, **2001**, p. 123.
[6] F. Palacio, G. Antorrena, M. Castro, R. Burriel, J. M. Rawson, N. B. Smith, N. Bricklebank, J. Novoa, C. Ritter, *Phys. Rev. Lett.* **1997**, *79*, 2336; J. M. Rawson, J. Luzon, F. Palacio, *Coord. Chem. Rev.* **2005**, *249*, 2631.
[7] Reviews: S. J. Blundell, F. L. Pratt, *J. Phys. Condens. Matter* **2004**, *16*, R771; V. I. Ovcharenko, R. Z. Sagdeev, *Russ. Chem. Rev.* **1999**, *68*, 345; V. I. Ovcharenko, R. Z. Sagdeev, *Russ. Chem. Rev.* **1999**, *68*, 345; J. S. Miller, A. J. Epstein, *Angew. Chem.* **1994**, *106*, 399; *Angew. Chem. Int. Ed. Engl.* **1994**, *33*, 385.
[8] a) J. M. Manriquez, G. T. Yee, R. S. McLean, A. J. Epstein, J. S. Miller, *Science* **1991**, *252*, 1415; J. S. Miller, G. T. Yee, J. M. Manriquez, A. J. Epstein, in the Proceedings of Nobel Symposium No. NS-81 *Conjugated Polymers and Related Materials: The Interconnection of Chemical and Electronic Structure*, Oxford University Press, **1993**, p. 461; J. S. Miller, G. T. Lee, J. M. Manriquez, A. J. Epstein, *La Chim. La Ind.* **1992**, *74*, 845; b) J. Zhang, P. Zhou, W. B. Brinckerhoff, A. J. Epstein, C. Vazquez, R. S. McLean, J. S. Miller, *ACS Symp. Ser.* **1996**, *644*, 311.
[9] D. Haskel, Z. Islam, J. Lang, C. Kmety, G. Stajer, K. I. Pokhodnya, A. J. Epstein, J. S. Miller, *Phys. Rev. B* **2004**, *70*, 054422.
[10] a) K. I. Pokhodnya, A. J. Epstein, J. S. Miller, *Adv. Mater.* **2000**, *12*, 410; b) K. I. Pokhodnya, D. Pejakovic, A. J. Epstein, J. S. Miller, *Phys. Rev. B* **2001**, *63*, 174408.
[11] *CRC Handbook of Chemistry and Physics*, 85th ed. (Ed.: D. R. Lide), CRC Press, Boca Raton, FL, **2004–2005**, pp. **6**-153–**6**-175.
[12] M. S. Thorum, K. I. Pokhodnya, J. S. Miller, *Polyhedron* **2006**, *27*, 1927.
[13] V. N. Prigodin, N. P. Raju, K. I. Pokhodnya, J. S. Miller, A. J. Epstein, *Adv. Mater.* **2002**, *14*, 1230.
[14] J. P. Fitzgerald, B. B. Kaul, G. T. Yee, *Chem. Commun.* **2000**, 49.
[15] E. B. Vickers, T. D. Selby, J. S. Miller, *J. Am. Chem. Soc.* **2004**, *126*, 3716.
[16] E. B. Vickers, T. D. Selby, M. S. Thorum, M. L. Taliaferro, J. S. Miller, *Inorg. Chem.* **2004**, *43*, 6414.
[17] A. M. Bond, F. A. Cotton, *Inorg. Chem.* **1976**, *15*, 2036.
[18] D. C. Gordon, L. Deakin, A. M. Arif, J. S. Miller, *J. Am. Chem. Soc.* **2000**, *122*, 290.
[19] M. Moscherosch, E. Waldhor, H. Binder, W. Kaim, J. Fiedler, *Inorg. Chem.* **1995**, *34*, 4326.
[20] X. Liu, J. E. Ellis, T. D. Selby, P. Ghalsasi, J. S. Miller, *Inorg. Synth.* **2004**, *34*, 96.
[21] F. Calderazzo, G. Pampaloni, *J. Organomet. Chem.* **1995**, *500*, 47.
[22] A solution of either $[V^0(CO)_6]$ or $[V^0(PhMe)_2]$ (0.150 mmol) in a minimal amount (≈5 mL) of the desired solvent was added dropwise into a stirred suspension of 2 equivalents of TCNB (0.300 mmol, ≈10 mL) under an inert atmosphere of dry nitrogen. The mixture became dark. After stirring for ca.

 © 2006 Wiley-VCH Verlag GmbH & Co. KGaA, Weinheim

20 min, the dark, amorphous precipitate was collected by suction filtration, and dried in vacuo (Yield ≈ 50 %).

[23] T. G. Richmond, Q.-Z. Shi, W. C. Trogler, F. Basolo, *J. Am. Chem. Soc.* **1984**, *106*, 76; W. Heiber, J. Peterhaus, E. Winter, *Chem. Ber.* **1961**, *94*, 2572.

[24] a) M. Schneider, E. Weiss, *J. Organomet. Chem.* **1976**, *121*, 365; b) J. A. Osborne, A. L. Rheingold, W. C. Trogler, *J. Am. Chem. Soc.* **1985**, *107*, 6292.

[25] a) TA Instruments 2050 TGA located in a Dry Box (< 1 ppm O_2); b) CO ($m/z = 27.98833$ amu) was distinguished from N_2 ($m/z = 28.00027$ amu) using a Finnagan MAT95 mass spectrometer.

[26] Elemental analysis (%) calcd for a) $V^{II}(TCNB)_2 \cdot 0.05\,CH_2Cl_2$ ($C_{20.05}H_{4.1}N_8VCl_{0.1}$): C 58.52, H 1.00, N 27.23, V 12.38; Found: C 58.36, H 0.82, N 27.56, V 12.21; b) $V(TCNB)_{3.8}[V(CO)_6]_{0.5} \cdot 0.05\,CH_2Cl_2$ ($C_{41.05}H_{7.7}N_{15.2}V_{1.5}Cl_{0.1}$): C 58.58, H 0.92, N 25.30; Found: C 58.68, H 0.90, N 25.10; c) $V(TCNB)_{3.8}[V(CO)_6]_{0.5} \cdot 0.1\,PhCF_3$ $C_{40.07}H_{8.1}N_{15.2}V_{1.5}F_{0.3}$: C 59.32, H 0.99, N 25.84, V 9.27, F 0.69, O 3.88; Found: C 59.15, H 1.23, N 26.33, V 8.96, F 0.98, O 3.96.

[27] J. D. Bagnato, W. W. Shum, M. Strohmeier, D. M. Grant, A. M. Arif, J. S. Miller, *Angew. Chem.* **2006**, *118*, 5448; *Angew. Chem. Int. Ed.* **2006**, *45*, 5322.

 © 2006 Wiley-VCH Verlag GmbH & Co. KGaA, Weinheim

Structure Elucidation

DOI: 10.1002/anie.200601834

Fixation of CO_2 by Magnesium Cations: A Reinterpretation**

Harminder Phull, Davide Alberti, Ilia Korobkov, Sandro Gambarotta, and Peter H. M. Budzelaar**

Identifying the factors which determine the remarkable variety of bonding modes in the coordination of CO_2 to metal centers[1] is central to controlling electron transfer and ultimately the reactivity.[2–4] In this respect, it seems legitimate to state that d electrons are of critical importance since CO_2 coordination was never observed in d^0- or main-group-metal systems.[1] Furthermore, the CO_2 oxygen atoms do not possess sufficient basicity to form stable adducts with Lewis acids. The sole case of a genuine end-on-bound CO_2 complex[5] involves a very strongly reducing trivalent uranium center, for which it seems likely that partial electron transfer plays a role. Nevertheless, CO_2 is only weakly bound in this complex. As a rule with no exception until very recently, only low- and medium-valent metals have been used for CO_2 coordination. For these reasons, the recent findings[6] describing the robust end-on coordination of CO_2 to magnesium cations with formation of the unprecedented Mg/Al-containing cluster $[\{R_2Al(\mu\text{-}NSiMe_3)(\mu\text{-}OSiMe_3)Mg(thf)_2(\mu\text{-}O_2C)\}_3]\cdot 2\,thf$ (R = Me (**1a**), Et (**1b**)), certainly appear to be a major breakthrough. Not only do compounds **1** represent the first case of CO_2 coordination to a non-transition-metal center in an unprecedented bridging end-on fashion, but also the *irreversible* fixation occurs in THF, the oxygen atom of which is normally regarded as a far better donor than the oxygen atoms of CO_2.

We have revisited the experimental data and, on the basis of additional observations, propose herein that the triatomic units that bridge the magnesium atoms end-on, believed to be CO_2, are in reality isoelectronic NCO anions.

The formation of complexes **1a**,**b** was originally rationalized by assuming the attack of CO_2 at only one silazanate group.[6] It was not explanined why the second silazanate group did not follow the same fate in the presence of excess CO_2. Also, no conclusive evidence was provided for the identification of the bridging imido group generated by the attack of Me_3Al on the intermediate $[Mg(OSiMe_3)\{N(SiMe_3)_2\}]$. The presence of disorder between the imido and silanolate group with equal occupancy was claimed to account for the crystallographic equivalency of the two donor atoms bridging the Al and Mg centers. This interpretation was the only possibility to have the charges balanced within the complex if the triatomic unit bridging the three Mg atoms has to be CO_2. The NMR spectra unexplainably showed *only one resonance* for the silanolate and silylimido groups together.

To our surprise, geometry optimization[7] of the full complex **1a** as well as several simplified model compounds invariably led to fragmentation of the complex and release of CO_2, which thus appears *not* to be strongly bound at all (Figure 1a). This finding in turn made us question the assumptions behind the assignment of the structure of the complex.

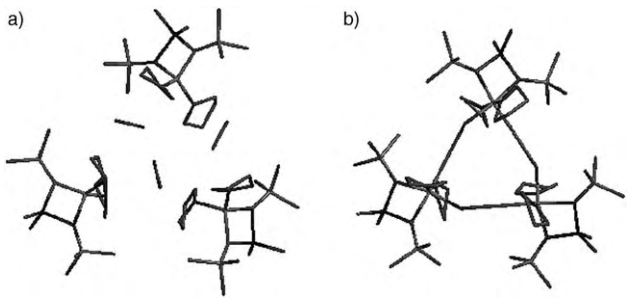


Figure 1. a) Partially optimized structure of **1a**;[7] CO_2 units are dissociating. b) Optimized structure of **1a** with N and O atoms exchanged.

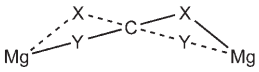
[*] H. Phull, Dr. D. Alberti, I. Korobkov, Prof. S. Gambarotta
Department of Chemistry
University of Ottawa
Ottawa, ON, K1N 6N5 (Canada)
Fax: (+1) 613-562-5170
E-mail: sgambaro@science.uottawa.ca
Prof. P. H. M. Budzelaar
Department of Chemistry
University of Manitoba
Winnipeg, MB, R3T 2N2 (Canada)
Fax: (+1) 204-474-7608
E-mail: budzelaa@cc.umanitoba.ca

[**] This work was supported by the Natural Sciences and Engineering Council of Canada (NSERC).

Supporting information for this article is available on the WWW under http://www.angewandte.org or from the author.

© 2006 Wiley-VCH Verlag GmbH & Co. KGaA, Weinheim

By strictly following the preparation of Chang et al.,[6] we therefore reprepared complex **1a** as air-sensitive, colorless crystals. The crystal structure confirmed the formula [{Me_2Al-(μ-$ESiMe_3$)$_2$Mg(thf)$_2$(μ-E_2C)}$_3$]·1.5 thf (E = O, N, or a combination of both; see the Supporting Information). The lattice molecule of thf gave better refinement when refined with partial occupancy. We found no indication whatsoever for the presence of any sort of disorder involving the two atoms bridging the Mg and Al centers. These two bridging atoms could be best refined as only oxygen atoms of silanolate groups (arbitrarily attributing a 50% nitrogen character to these bridging atoms, in accordance with the silanolate/imido formulation proposed by Chang et al., increased the final convergence factor by 0.7%). Instead, the X-ray structure showed a 50:50 disorder in the three-atom XCY units bridging the Mg atoms (Scheme 1).[8] Each arrangement of the XCY



Scheme 1. Disorder in bridging XCY units.

unit has a bent Mg-X-C geometry and a nearly linear Mg-Y-C geometry; the carbon atoms of the two arrangements coincide. The distinctly different angles around X and Y suggest that they are, in fact, different atoms, as the symmetrical CO_2 molecule would not be expected to prefer very different bond angles at its two oxygen atoms. Assuming that the atoms bridging the Mg and Al centers are all oxygen atoms, electroneutrality requires the XCY units to be NCO. The X-ray data do not allow us to distinguish between N and O assignments for the X and Y atoms; these atoms refine equally well as either N or O, or as a mixture of both. In line with the calculations described below, we refined the X atoms as oxygen and the Y atoms as nitrogen. The negative charge of the bridging unit could well explain the robust coordination to the Mg centers in the presence of a Lewis base such as thf. Indeed, DFT geometry optimization[7] of the N/O-switched molecule and simplified model compounds resulted in geometries very close to the observed one (Figure 1b). In particular, the peculiar bent coordination *at one end only* of "CO_2" is now nicely reproduced.

Calculations were also helpful in explaining the preferential formation of a trimeric structure. The NCO unit prefers a nearly linear geometry at the N atom and a bent geometry at the O atom already in the hypothetical monomeric compound [$Me_2Al(OSiMe_3)_2Mg(thf)_2(NCO)$] (Mg-N-C 163°; [$Me_2Al(OSiMe_3)_2Mg(thf)_2(OCN)$]: Mg-O-C 128°). In a hypothetical dimeric structure, bending at the N atom cannot be avoided, although it remains less than the bending at the O atom ([{$Me_2Al(OSiMe_3)_2Mg(thf)_2(\mu$-NCO)}$_2$]: Mg-N-C 150°, Mg-O-C 123°). Trimer formation, however, fully relieves angle strain by allowing linear coordination at the N atom, as seen in both the X-ray structure and the calculated geometry (Mg-N-C 168°, Mg-O-C 142°).

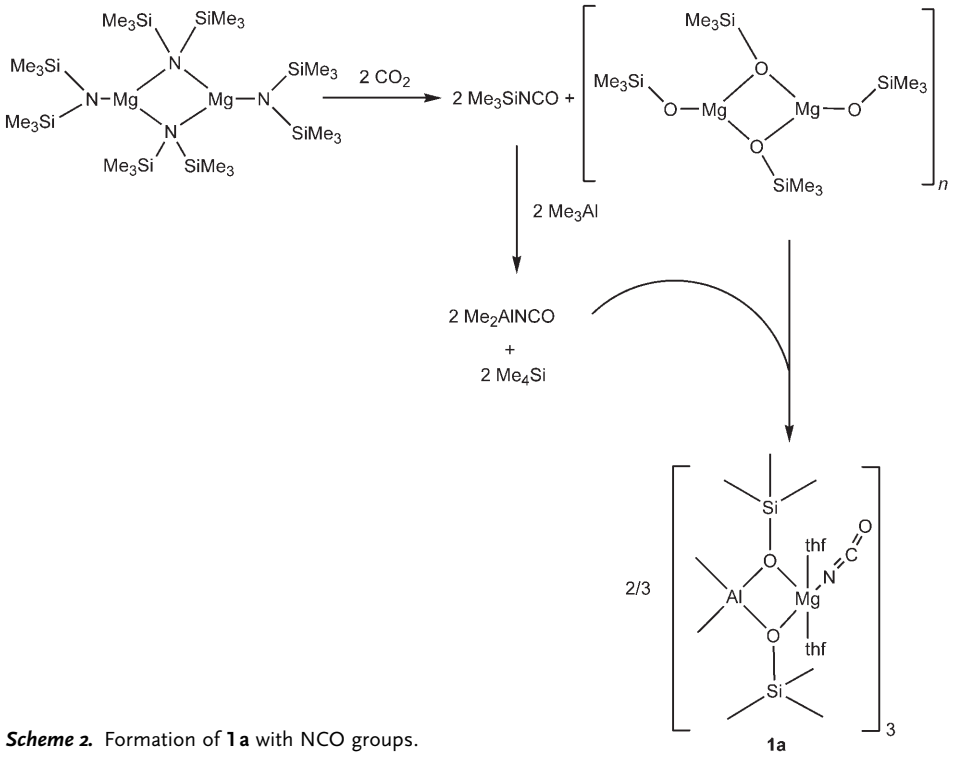
^{1}H NMR spectra of **1a** in [D_8]THF showed only one sharp proton resonance for the silanolate group and one for the Al–CH_3 groups at $\delta = 0.06$ and -0.97 ppm, respectively. Although Me_3Si groups that are bound at either N or O could in principle produce identical chemical shifts in the ^{1}H NMR spectra, this coincidence is much less likely in the ^{13}C NMR spectra, which *also* showed only one resonance each for the Me_3Si and Al–CH_3 groups (at $\delta = 3.21$ and -5.22 ppm, respectively). The ^{29}Si NMR spectrum (in [D_8]toluene) showed only one resonance at $\delta = 14.13$ ppm in the temperature range 355–223 K rather than the two resonances which would be expected if both silanolate and silylimido groups were to be present in the complex. On the other hand, two nonequivalent Me_3Si groups could be expected in principle for a bis(silanolate)-bridged complex (*cis* and *trans* to N of the NCO bridge; see Figure 1b). Indeed, cooling of the solution resulted in splitting of the silanolate resonances in the ^{1}H NMR spectrum, thus giving rise to two singlets at 203 K. The variable-temperature ^{29}Si NMR spectrum showed a far more complex solvent-dependent fluxional behavior for which no straightforward interpretation is possible at this stage. Evidently, a dynamic process, possibly involving opening of the 12-membered {Mg(NCO)}$_3$ ring, exchanges the silanolate groups at higher temperature. Furthermore, there is some indication of further broadening of the signal of the Me groups attached to the Al centers, which might take place at even lower temperatures. Considering that the structure is formed by three different anions ($OSiMe_3$, NCO, Me) which may scramble with different ratios over the two cations and further form mono- and polynuclear structures, a very complex fluxional behavior can be anticipated.

Finally, the ^{14}N NMR spectrum gave a rather broad resonance at $\delta = -304.67$ ppm (the resonance of silazanate groups occurs in the region around $\delta = -338$ ppm) which is in the expected region for the NCO group. In addition, chemical degradation of **1a** with a diluted solution of aqueous KOH at pH 8 and subsequent centrifugation of $Al(OH)_3$ and $Mg(OH)_2$, neutralization with HNO_3, and treatment with $AgNO_3$, afforded a colorless precipitate of Ag(NCO), which showed the characteristic intense resonance at 2176 cm^{-1} in the IR spectrum.

A possible rationalization for the formation of [{$Me_2Al(\mu$-$OSiMe_3)_2Mg(thf)_2(\mu$-OCN)}$_3$]·1.5 thf may consist of the reaction of [{[$(Me_3Si)_2N$]Mg[μ-$N(SiMe_3)_2$]}$_2$][9] with CO_2 to afford Me_3SiNCO (Scheme 2). In turn, Me_3SiNCO reacts with Me_3Al to form the NCO anions which are incorporated into the final trinuclear cluster. In partial support of this speculation, the formation of Me_3SiNCO was clearly observed in the GC–MS of the solution that was obtained from exposure of a solution of [{[$(Me_3Si)_2N$]Mg[μ-$N(SiMe_3)_2$]}$_2$][9] to CO_2. Reaction of Me_3Al with Me_3SiNCO in the stoichiometric ratio 1:1 completely consumed the two starting materials to afford a complex mixture from which, besides Me_4Si (confirmed by GC), no component could be conclusively identified. Nonetheless, the crude reaction mixture that was obtained upon solvent evaporation produced a broad resonance in the ^{14}N NMR spectrum at $\delta = -248$ ppm and a series of four IR absorptions (2255, 2202, 2143, 2065 cm^{-1}), which can only be attributed to Al-coordinated NCO anions.

In conclusion, our observations suggest that, rather than a sensational case of irreversible fixation of CO_2 at magnesium cations, complex **1a** is more reasonably formulated as

 © 2006 Wiley-VCH Verlag GmbH & Co. KGaA, Weinheim



Scheme 2. Formation of **1a** with NCO groups.

the isocyanate derivative $[\{Me_2Al(\mu\text{-}OSiMe_3)_2Mg(thf)_2(\mu\text{-}OCN)\}_3]\cdot 1.5\,thf$.

Experimental Section

All experiments were conducted inside a drybox equipped with a vacuum-line manifold to supply CO_2. Chemical-degradation experiments were carried out in air on samples weighed inside a drybox. All the NMR spectra were recorded on a Varian spectrometer (500 MHz) by using NMR tubes that were prepared inside a drybox and flame sealed.

1a: A solution of $AlMe_3$ (2.0 M in toluene, 2.2 mL, 4.4 mmol) was added dropwise to a solution of $[\{[(Me_3Si)_2N]Mg[\mu\text{-}N(SiMe_3)_2]\}_2]$ (1.5 g, 2.17 mmol) in THF (20 mL). The resulting solution was cooled in an ice bath and stirred for 2 h in an atmosphere of carbon dioxide. The resultant solution was concentrated to a smaller volume (10 mL) and cooled in a freezer. Colorless crystals of **1a** separated upon standing five days (yield: 21%). ^{1}H NMR (500 MHz, $[D_8]$THF, 23 °C): $\delta = -0.97$ (s, 18 H, Al-CH_3), 0.06 (s, 54 H, $OSiMe_3$), 1.78 (m, 30 H, thf), 3.59 ppm (m, 30 H, thf); ^{13}C NMR (125.72 MHz, $[D_8]$THF, 23 °C): $\delta = -5.22$ (Al-CH_3), 3.21 ($OSiMe_3$), 67.65 (thf), 25.21 (thf), 120.98 ppm (NCO); ^{29}Si NMR (99.32 MHz, $[D_8]$THF, 263 K): $\delta =$ 6.96 ppm; ^{29}Si NMR (99.32 MHz, $[D_8]$toluene, 23 °C): $\delta =$ 14.13 ppm; ^{14}N NMR (36.12 MHz, $[D_8]$THF, 23 °C): $\delta = -304.67$ ppm.

Crystal Data for **1a**: $C_{57}H_{132}Al_3Mg_3N_3O_{16.5}Si_6$, $M_r = 1446.07$, orthorhombic, space group *Pbcn*, $a = 12.526(4)$, $b = 25.615(6)$, $c =$ 28.167(6) Å, $V = 9037(5)$ Å^3, $Z = 4$, $\rho_{calcd} = 1.063$ Mg m^{-3}, $T = 213$ K, absorption coefficient 0.194 mm^{-1}, $F(000) = 3144$, 39 407 reflections collected, 4010 independent reflections, GoF = 1.099, $R = 0.0671$ ($I > 2\sigma(I)$), $wR2 = 0.1581$ ($I > 2\sigma(I)$). CCDC-606505 contains the supplementary crystallographic data for this paper. These data can be obtained free of charge from The Cambridge Crystallographic Data Centre via www.ccdc.cam.ac.uk/data_request/cif.

Coordinates for optimized structure of N/O-switched **1a** and simplified model compounds, including a partially dissociated structure for the originally proposed complex **1a**, in *xyz* format and an ORTEP drawing for **1a** with selected bond distances and angles can be found in the Supporting Information.

Received: May 10, 2006
Published online: July 20, 2006

Keywords: aluminum · coordination modes · density functional calculations · isocyanates · magnesium

[1] a) J. C. Calabrese, T. Herskovitz, J. B. Kinney, *J. Am. Chem. Soc.* **1983**, *105*, 5914; b) D. H. Gibson, *Chem. Rev.* **1996**, *96*, 2063; c) A. Behr, *Angew. Chem.* **1988**, *100*, 681; *Angew. Chem. Int. Ed. Engl.* **1988**, *27*, 661; d) X. Yin, J. R. Moss, *Coord. Chem. Rev.* **1999**, *181*, 27; e) D. Walther, M. Ruben, S. Rau, *Coord. Chem. Rev.* **1999**, *182*, 67; f) Y. Tang, L. N. Zakharov, A. L. Rheingold, R. A. Kemp, *Organometallics* **2004**, *23*, 4788; g) K.-C. Yang, C.-C. Chang, C.-S. Yeh, G.-H. Lee, S.-M. Peng, *Organometallics* **2001**, *20*, 126; h) C.-C. Chang, B. Srinivas, M.-L. Wu, W.-H. Chiang, M. Y. Chiang, C.-S. Hsiung, *Organometallics* **1995**, *14*, 5150.

[2] a) D. Min, S. W. Lee, *Inorg. Chem. Commun.* **2002**, *5*, 978; b) L. J. Farrugia, S. Lopinski, P. A. Lovatt, R. D. Peacock, *Inorg. Chem.* **2001**, *40*, 558; c) W. J. Evans, C. A. Seibel, J. W. Ziller, *Inorg. Chem.* **1998**, *37*, 770.

[3] a) T. Tsuda, S.-I. Sanada, T. Saegusa, *J. Organomet. Chem.* **1976**, *116*, C10; b) G. Fachinetti, C. Floriani, A. Chiesi-Villa, C. Guastini, *J. Am. Chem. Soc.* **1979**, *101*, 1767; c) L. J. Procopio, P. J. Carroll, D. H. Berry, *Organometallics* **1993**, *12*, 3087; d) I. Castro-Rodriguez, K. Meyer, *J. Am. Chem. Soc.* **2005**, *127*, 11242; e) D. S. Laitar, P. Müller, J. P. Sadighi, *J. Am. Chem. Soc.* **2005**, *127*, 17196.

[4] a) S. Gambarotta, M. Pasquali, C. Floriani, A. Chiesi-Villa, C. Guastini, *Inorg. Chem.* **1981**, *20*, 1173; b) S. Gambarotta, F. Arena, C. Floriani, A. Gaetani-Manfredotti, *J. Chem. Soc. Chem. Commun.* **1982**, 835; c) S. Gambarotta, F. Arena, C. Floriani, P. F. Zanazzi, *J. Am. Chem. Soc* **1982**, *104*, 5083.

[5] I. Castro-Rodriguez, H. Nakai, L. N. Zakharov, A. L. Rheingold, K. Meyer, *Science* **2004**, *305*, 1757.

[6] C.-C. Chang, M.-C. Liao, T.-H. Chang, S.-M. Peng, G.-H. Lee, *Angew. Chem.* **2005**, *117*, 7584; *Angew. Chem. Int. Ed.* **2005**, *44*, 7418.

[7] Density functional calculations were performed with the TURBOMOLE program (R. Ahlrichs, M. Bär, M. Häser, H. Horn, C. Kölmel, *Chem. Phys. Lett.* **1989**, *162*, 165; O, Treutler, R. Ahlrichs, *J. Chem. Phys.* **1995**, *102*, 346; R. Ahlrichs, et al., Turbomole Version 5, January **2002**; Theoretical Chemistry Group, University of Karlsruhe) in combination with the OPTIMIZE routine of Baker (J. Baker, *J. Comput. Chem.* **1986**, *7*, 385; PQS Version 2.4, **2001**, Parallel Quantum Solutions, Fayetteville, Arkansas, USA; the Baker optimizer is available separately from PQS upon request). All relevant structures were fully optimized at the unrestricted RI-bp86 (K. Eichkorn, F. Weigend, O. Treutler, R. Ahlrichs, *Theor. Chem. Acc.* **1997**, *97*,

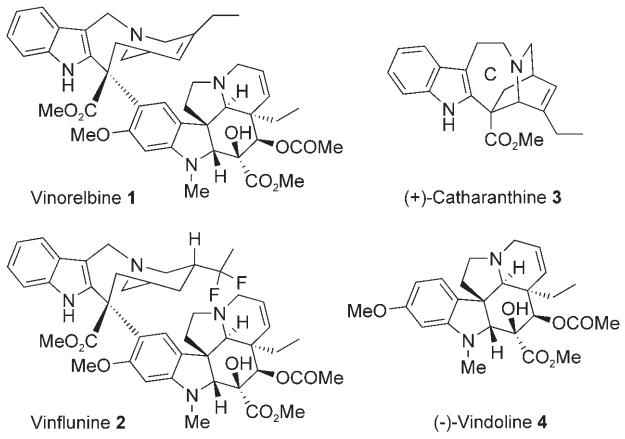
 © 2006 Wiley-VCH Verlag GmbH & Co. KGaA, Weinheim

119; A. D. Becke, *Phys. Rev. A* **1988**, *38*, 3089; J. P. Perdew, *Phys. Rev. B* **1986**, *33*, 8822) and b3-lyp levels (C. Lee, W. Yang, R. G. Parr, *Phys. Rev. B* **1988**, *37*, 785; A. D. Becke, *J. Chem. Phys.* **1993**, *98*, 1372; A. D. Becke, *J. Chem. Phys.* **1993**, *98*, 5648; note that the Turbomole functional "b3-lyp" is not identical to the Gaussian "B3LYP" functional) by employing the standard SV(P) basis sets (A. Schäfer, H. Horn, R. Ahlrichs, *J. Chem. Phys.* **1992**, *97*, 2571).

[8] There was also disorder in some of the thf ligands bound to the Mg centers, which could be refined satisfactorily through partial splitting of the carbon atom positions.

[9] $C_{34}H_{72}Mg_2N_4Si_8$, $M_r = 690.20$, orthorhombic, space group *Pbcn*, $a = 18.040(8)$, $b = 14.888(7)$, $c = 18.038(8)$ Å, $V = 4270(3)$ Å^3, $Z = 4$, $\rho_{calcd} = 1.074\ Mg\,m^{-3}$, $T = 198$ K, absorption coefficient $0.301\ mm^{-1}$, $F(000) = 1520$, 14726 reflections collected, 3599 independent reflections, GoF = 1.039, $R = 0.0439$ ($I > 2\sigma(I)$), $wR2 = 0.1129$ ($I > 2\sigma(I)$).

 © 2006 Wiley-VCH Verlag GmbH & Co. KGaA, Weinheim



Natural-Products Synthesis

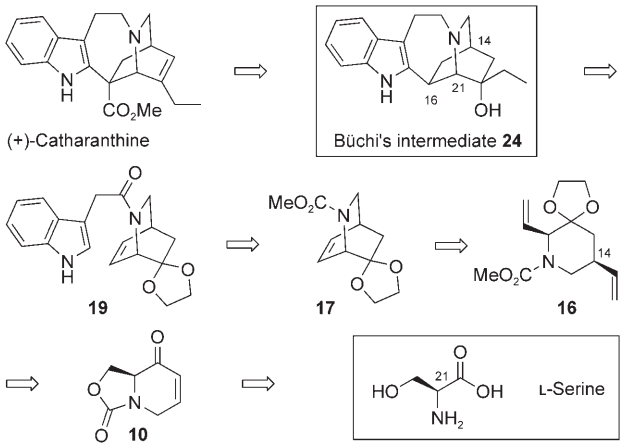
DOI: 10.1002/anie.200601307

Formal Synthesis of (+)-Catharanthine**

Lionel Moisan, Pierre Thuéry, Marc Nicolas, Eric Doris, and Bernard Rousseau*

Since the discovery of vinblastine and vincristine in the late 1950s, vinca alkaloids have become one of the most powerful drug types currently in use for the clinical treatment of cancer. Over the past four decades, synthetic efforts[1] have led to the discovery of the major semisynthetic drugs vinorelbine (**1**)[2] and, more recently, vinflunine (**2**).[3] The industrial synthesis of **1** and **2** relies on the biomimetic coupling of catharanthine (**3**) and vindoline (**4**),[1] two alkaloids that are extracted from the leaves of Madagascan periwinkle (*Catharanthus roseus* L. Don). No enantioselective synthesis has yet been reported for catharanthine, which is found in minute amounts in the plant (about 0.0003 % of the dried leaf mass),[4] although numerous racemic approaches have been developed.[5] (+)-Catharanthine has been prepared only once by resolution.[6] Herein we disclose a new and efficient synthesis of a chiral intermediate for the synthesis of (+)-catharanthine.

Catharanthine (**3**) has three stereocenters, C14, C16, and C21 (see **24** in Scheme 1), which are integrated into the isoquinuclidine skeleton. Its structure is further characterized by the seven-membered C ring, which links the indole subunit to the isoquinuclidine moiety. We chose alcohol **24**, in which each stereocenter is unequivocally defined, as the target compound (Scheme 1). In their elegant total synthesis of (±)-catharanthine, Büchi et al. demonstrated that **24** could be transformed readily into catharanthine by introducing the methoxycarbonyl group at C16 and effecting dehydration of the tertiary alcohol.[5a]



Scheme 1. Retrosynthetic analysis of the key intermediate **24** in the synthesis of (±)-catharanthine by Büchi et al.

In that context, our plan was first to design a route to the optically active isoquinuclidine **17** and to couple it to the indole moiety, as shown retrosynthetically in Scheme 1. Since previously reported attempts to obtain optically active isoquinuclidines analogous to **17** by [4+2] cycloaddition had been unsuccessful,[7] we envisaged that the azabicyclo-[2.2.2]alkene system could be prepared by ring-closing metathesis (RCM) of the *cis*-2,5-dialkenyl *N*-acyl piperidine **16**. The stereocenter C14 would derive from the stereocontrolled

[*] Dr. L. Moisan, Dr. E. Doris, Dr. B. Rousseau
Service de Marquage Moléculaire et de Chimie Bioorganique
DSV/DBJC, CEA/Saclay
91191 Gif-sur-Yvette cedex (France)
Fax: (+33) 169-08-79-91
E-mail: eric.doris@cea.fr
Dr. P. Thuéry
Service de Chimie Moléculaire
DSM/DRECAM, CEA/Saclay
91191 Gif-sur-Yvette cedex (France)
Dr. M. Nicolas
Laboratoires Pierre Fabre
16 rue Jean Rostand, 81600 Gaillac (France)

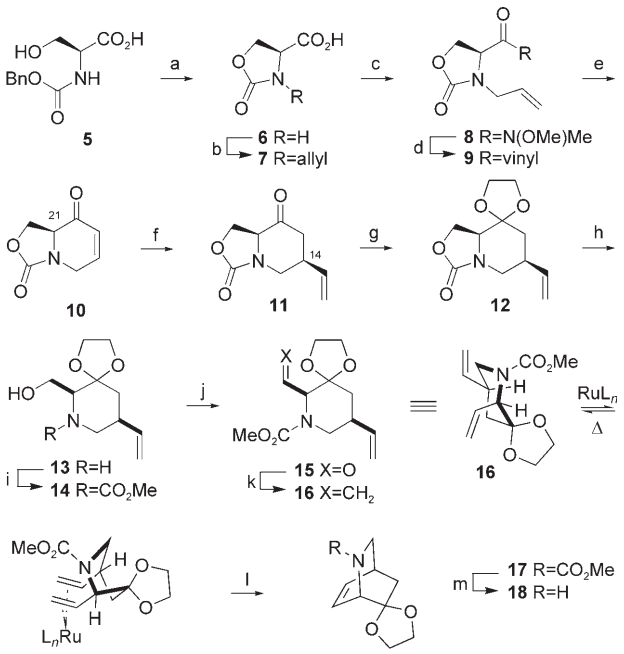
[**] This research is part of a collaboration between "CEA/Direction des Sciences du Vivant" and "Pierre Fabre Médicament".
Supporting information for this article is available on the WWW under http://www.angewandte.org or from the author.

InterScience
© 2006 Wiley-VCH Verlag GmbH & Co. KGaA, Weinheim

Michael addition of a vinyl group to the cyclic enone **10**. Compound **10** could in turn be prepared in five steps starting from protected L-serine, our source of chirality.

Our synthesis started from *N*-benzyloxycarbonyl-L-serine (**5**; Scheme 2). Upon treatment with sodium hydroxide, **5** was converted in 73% yield into oxazolidinone **6**, which was subsequently allylated to give **7** in 61% yield. The conversion of **7** into the corresponding Weinreb amide **8** was carried out in 76% yield under standard EDCI-mediated peptide-coupling conditions. Measurement of the *ee* value of **8** indicated little erosion of the enantiomeric excess (< 5%) over these last three steps.[8] Recrystallization from Et_2O/CH_2Cl_2 provided material of > 99% *ee*. The addition of vinylmagnesium bromide, followed by careful quenching of the reaction with anhydrous acetic anhydride, provided enone **9** in 81% yield. Enone **10** was then obtained in 87% yield by the treatment of **9** with the second-generation Grubbs catalyst (G2).[9] The rapid filtration of crude **10** through a short pad of silica was found to be the most efficient procedure for its purification, as epimerization of the stereogenic center C21 was thus avoided.

With enone **10** in hand, we next had to install the C14 stereocenter by the conjugate addition of vinylmagnesium bromide. The 1,4-nucleophilic attack of the vinyl group proceeded smoothly in the presence of a stoichiometric amount of CuI at −78 °C to afford a 9:1 mixture of diastereomers. As the hydrogen atom at C21 proved to be labile, the carbonyl group of **11** was directly protected to give the corresponding dioxolane **12** in 70% yield (two steps). At this stage, chromatography over silica permitted the isolation of the major diastereomer, whose *cis* configuration was established unambiguously by X-ray crystallographic analysis (Figure 1).[10]



Scheme 2. Synthesis of the optically active isoquinuclidine **18**: a) NaOH, H_2O, room temperature, 73%; b) allyl iodide, NaH, DMF, 61%; c) HN(OMe)Me·HCl, EDCI, DIPEA, CH_2Cl_2, 76%; d) 1) vinylmagnesium bromide, THF, 0 °C; 2) acetic anhydride, 81%; e) G2 (10 mol%), CH_2Cl_2, reflux, 87%; f) vinylmagnesium bromide, CuI, THF, −78 °C; g) ethylene glycol, CH_2Cl_2, TsOH, 70% (2 steps); h) NaOH, H_2O/MeOH, reflux, 18 h; i) $ClCO_2Me$, $NaHCO_3$, THF, 81% (2 steps); j) TPAP, NMO, CH_2Cl_2, 75%; k) Tebbe reagent, Et_2O, −10 °C, 83%; l) G2 (10 mol%), CH_2Cl_2, reflux, 20 h, 84%; m) MeLi, Et_2O, 0 °C, 1 h, 74%. Bn = benzyl, DIPEA = *N*,*N*-diisopropylethylamine, DMF = *N*,*N*-dimethylformamide, EDCI = 1-(3-dimethylaminopropyl)-3-ethylcarboiimide, NMO = *N*-methylmorpholine *N*-oxide, TPAP = tetrapropylammonium perruthenate, Ts = *p*-toluenesulfonyl.

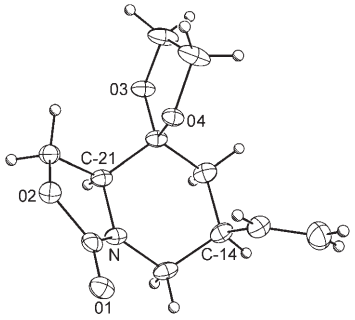


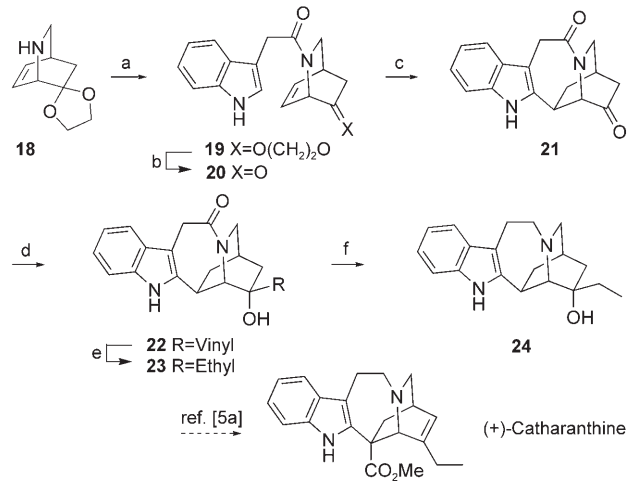
Figure 1. Molecular structure of **12**. Displacement ellipsoids are drawn at the 30% probability level.

We speculate that the observed stereoselectivity of the 1,4-addition could originate from the nitrogen lone-pair electrons, which may direct the *syn* attack of the vinyl group. With the desired *cis* isomer in hand, the second olefinic side chain was introduced. First, the oxazolidinone was hydrolyzed under alkaline conditions followed by protection of the resulting secondary amine as a methyl carbamate. Subsequent TPAP/NMO[11] oxidation of the alcohol provided aldehyde **15** in 75% yield. Finally, the methylenation of **15** occurred in 83% yield in the presence of the Tebbe reagent.

The stage was thus set for the intramolecular alkene metathesis. Despite the prolific use of RCM for the synthesis of bridged azabicyclic structures,[12] no example of the synthesis of azabicyclo[2.2.2]alkene systems has been reported. Indeed, RCM is performed in most cases on *N*-acyl *cis*-2,6-dialkenyl piperidines, as 1,3 allylic strain[13] favors the required axial-like orientation of the alkenyl side chains. In the case of the *N*-acyl *cis*-2,5-dialkenyl piperidine **16**, a less-favored boat conformation is required to bring the substituents at the 2- and the 5-position of the ring into an axial orientation. Nevertheless, upon treatment with the second-generation Grubbs catalyst (10 mol%) in refluxing CH_2Cl_2, piperidine **16** was converted smoothly into isoquinuclidine **17** in 84% yield and with > 99% *ee*.

Isoquinuclidine **17** was next coupled to the indole moiety. First, the secondary nitrogen atom was deprotected with MeLi. The product (**18**) was then treated with 3-indoleacetatic acid in the presence of EDCI (→**19**, 94% yield; Scheme 3), the ketal protecting group removed under acidic conditions (→**20**, 88% yield), and the C ring closed by using the Pd^{II}/Ag^{I} mixed-metal-mediated cyclization developed by Trost and co-workers.[5c] Controlled reduction of the σ C–Pd bond in the resulting intermediate with $NaBH_4$ in MeOH

 © 2006 Wiley-VCH Verlag GmbH & Co. KGaA, Weinheim



Scheme 3. Completion of the synthesis: a) 3-indoleacetic acid, EDCI, CH_2Cl_2, 94%; b) TsOH, H_2O, acetone, reflux, 96 h, 88%; c) 1) $[(CH_3CN)_2PdCl_2]$, $AgBF_4$, CH_3CN, RT→70°C, 18 h; 2) MeOH, $NaBH_4$, 0°C; d) vinylmagnesium bromide, THF, 0°C, 48% (2 steps); e) H_2, PtO_2, THF, room temperature, 70%; f) $AlCl_3$–$LiAlH_4$, THF, 0°C, 77%.

afforded ketone **21** as the major product, together with a small amount of the corresponding alcohol (< 5%). The addition of vinylmagnesium bromide to **21** gave the tertiary alcohol **22** as a single diastereomer. Subsequent hydrogenation over PtO_2 furnished **23** with the desired ethyl side chain in 70% yield. As previously observed by others, a direct introduction of the side chain by using ethylmagnesium bromide was unsuccessful owing to competing reduction of the ketone by hydride transfer from the Grignard reagent.[5a] Finally, the amide was reduced to the corresponding amine with $AlCl_3$–$LiAlH_4$ to give the key intermediate **24**. In our case, the Büchi intermediate **24**, which can be transformed in five steps into (+)-catharanthine, was obtained in virtually optically pure form with greater than 99% *ee*.

In summary, we have disclosed herein the formal synthesis of (+)-catharanthine, the crucial intermediate for the industrial synthesis of the major antitumor drug vinorelbine. Our approach starts from naturally occurring L-serine and is based on two key steps, namely, the stereocontrolled *cis* addition of a vinyl group to the cyclic enone **10** and unprecedented RCM of an *N*-acyl *cis*-2,5-dialkenyl piperidine system. The strategy we have developed to meet this synthetic challenge may be viewed as a general route for the synthesis of optically active isoquinuclidines.

Received: April 3, 2006
Published online: July 17, 2006

Keywords: alkaloids · antitumor agents · metathesis · natural products · synthetic methods

[1] For antitumor bisindole alkaloids from *Catharanthus roseus* L. Don, see: a) *The Alkaloids*, *Vol. 37* (Eds.: A. Brossi, M. Suffness), Academic Press, San Diego, **1990**; b) A. U. Rahman, Z. Iqbal, H. Nasir in *Studies in Natural Products Chemistry*, *Vol. 14* (Ed.: Atta-ur-Rahman), Elsevier, Amsterdam, **1994**, pp. 805–884; for recent achievements in the total synthesis of vinca alkaloids, see: c) S. Yokoshima, T. Ueda, S. Kobayashi, A. Sato, T. Kuboyama, H. Tokuyama, T. Fukuyama, *J. Am. Chem. Soc.* **2002**, *124*, 2137–2139; d) T. Kuboyama, S. Yokoshima, H. Tokuyama, T. Fukuyama, *Proc. Natl. Acad. Sci. USA* **2004**, *101*, 11966–11970.

[2] a) P. Mangeney, R. Z. Andriamialisoa, J.-Y. Lallemand, N. Langlois, Y. Langlois, P. Potier, *Tetrahedron* **1979**, *35*, 2175–2179; b) P. Mangeney, R. Z. Andriamialisoa, N. Langlois, Y. Langlois, P. Potier, *J. Org. Chem.* **1979**, *44*, 3765–3768; c) R. Z. Andriamialisoa, N. Langlois, Y. Langlois, P. Potier, *Tetrahedron* **1980**, *36*, 3053–3060.

[3] a) J. Fahy, A. Duflos, J.-P. Ribet, J.-C. Jacquesy, C. Berrier, M.-P. Jouannetaud, F. Zunino, *J. Am. Chem. Soc.* **1997**, *119*, 8576–8577; b) A. Duflos, A. Kruczynski, J.-M. Barret, *Curr. Med. Chem. Anti-Cancer Agents* **2002**, *2*, 55–70.

[4] M. M. Gupta, D. V. Singh, A. K. Tripathi, R. Pandey, R. K. Verma, S. Singh, A. K. Shasany, S. P. S. Khnuja, *J. Chromatogr. Sci.* **2005**, *43*, 450–453.

[5] a) G. Büchi, P. Kulsa, K. Ogasawara, R. L. Rosati, *J. Am. Chem. Soc.* **1970**, *92*, 999–1005; b) J. P. Kutney, F. Bylsma, *Helv. Chim. Acta* **1975**, *58*, 1672–1689; c) B. M. Trost, S. A. Godleski, J. L. Belletire, *J. Org. Chem.* **1979**, *44*, 2052–2054; d) T. Imanashi, H. Shin, N. Yagi, M. Hanaoka, *Tetrahedron Lett.* **1980**, *21*, 3285–3288; e) C. Marazano, M.-T. Le Goff, J.-L. Fourrey, B. C. Das, *J. Chem. Soc. Chem. Commun.* **1981**, 389–391; f) S. Raucher, B. L. Bray, *J. Org. Chem.* **1985**, *50*, 3237–3239; g) M. Kuehne, W. G. Bornmann, W. G. Earley, I. Marko, *J. Org. Chem.* **1986**, *51*, 2913–2927; h) S. Raucher, B. L. Bray, R. F. Lawrence, *J. Am. Chem. Soc.* **1987**, *109*, 442–446; i) R. J. Sundberg, J. Hong, S. Q. Smith, M. Sabat, *Tetrahedron* **1998**, *54*, 6259–6292; j) M. T. Redding, T. Fukuyama, *Org. Lett.* **1999**, *1*, 973–976.

[6] C. Szantay, H. Bölcskei, E. Gacs-Baitz, *Tetrahedron* **1990**, *46*, 1711–1732.

[7] B. L. Bray, PhD Thesis, Washington University, **1987**.

[8] All *ee* values were determined by HPLC on a chiral phase.

[9] M. Scholl, S. Ding, C. W. Lee, R. H. Grubbs, *Org. Lett.* **1999**, *1*, 953–956.

[10] CCDC-603355 (**12**) contains the supplementary crystallographic data for this paper. These data can be obtained free of charge from The Cambridge Crystallographic Data Centre via www.ccdc.cam.ac.uk/data_request/cif.

[11] S. V. Ley, J. Norman, W. P. Griffith, S. P. Marsden, *Synthesis* **1994**, 639–666.

[12] A. Deiters, S. F. Martin, *Chem. Rev.* **2004**, *104*, 2199–2238.

[13] T. Itoh, N. Yamazaki, C. Kibayashi, *Org. Lett.* **2002**, *4*, 2469–2472.

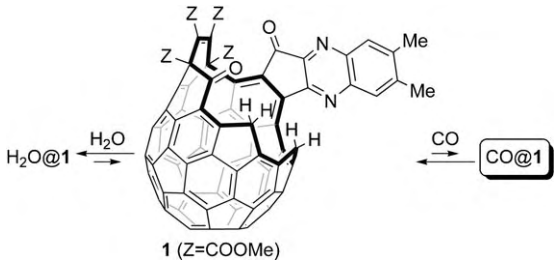
 © 2006 Wiley-VCH Verlag GmbH & Co. KGaA, Weinheim

Fullerenes

DOI: 10.1002/anie.200601241

Carbon Monoxide Inside an Open-Cage Fullerene**

Sho-ichi Iwamatsu, Christopher M. Stanisky, R. James Cross, Martin Saunders, Naomi Mizorogi, Shigeru Nagase, and Shizuaki Murata*



Scheme 1. Open-cage fullerene **1** and its reactivity towards CO and H_2O.

The chemistry of fullerenes that encapsulate molecules or atoms (endohedral fullerenes) has developed extensively in the last decade. A high-pressure, high-temperature method has made it feasible to insert atoms and some small molecules into fullerene cages.[1] However, the yield of the incorporated product obtained by this method is very low. In an attempt to prepare endohedral fullerenes in higher quantities, carbon–carbon bonds of fullerene cages have been cleaved by organic reactions.[2–4] The resulting product, a so-called open-cage fullerene, has an opening that is large enough to insert an atom or a molecule into the cavity of the fullerene.[5–9] Unlike complete endohedral fullerenes, these derivatives can hold and release substrates in a reversible manner. This property offers sensing and storage materials as potential applications.[10] Furthermore, an open moiety can be restored to an intact cage with the inserted chemical species inside. Indeed, pure endohedral $H_2@C_{60}$ was recently synthesized from C_{60} by using this strategy.[6b]

The narrow orifices of previously obtained open-cage derivatives restricted the molecules that could be inserted to helium and hydrogen.[5–8] Recently, we constructed a wide opening on C_{60} by successive cage scissions.[9] The orifice of **1** (Scheme 1) is the largest known to date for a fullerene, and **1** spontaneously encapsulates one water molecule to form $H_2O@\mathbf{1}$.[9a] This result shows that it is possible for atoms or molecules larger than H_2 or He to enter the fullerene cage. Herein, we describe the formation, characterization, and properties of an endohedral carbon monoxide complex, CO@**1**. Although several theoretical studies have been carried out on $CO@C_{60}$,[11,12] the formation of this complex was confirmed only by mass spectrometry.[13]

Carbon monoxide was introduced into **1** by heating a mixture of $H_2O@\mathbf{1}$ and **1** dissolved in 1,1,2,2-tetrachloroethane (TCE) under 9.0 MPa of CO. The signal at $\delta = -11.4$ ppm, characteristic of $H_2O@\mathbf{1}$, disappeared in the ^{1}H NMR spectrum of the reaction mixture,[9a] and the fraction of CO@**1** in the final product reached 84% (see below). By a similar method, $^{13}CO@\mathbf{1}$ was prepared under 3.3 MPa of ^{13}CO (^{13}C content: 99%); the fraction of $^{13}CO@\mathbf{1}$ at the end of the process was 59%. The reaction even proceeded under ambient pressure of CO; however, the final mixture yielded only 20% CO@**1**. For a higher incorporation of CO, it is necessary to carry out the reaction in solution; when the reaction mixture was pressurized as a solid, the conversion into CO@**1** was only 52% even at 9.0 MPa and 150 °C. This low yield may arise from the difficulty in releasing the water molecule of $H_2O@\mathbf{1}$ in the solid state.[9a] Alternatively, CO and/or H_2O might not be able to diffuse through solid **1**.

The product was identified as CO@**1** by electrospray mass spectrometry (ES-MS), ^{1}H NMR, ^{13}C NMR, and IR spectroscopy. In the ES mass spectrum of the product, a series of parent ion peaks was observed around m/z 1200. These peaks correspond to the presence of varying numbers of ^{13}C atoms (Figure 1a). For $^{13}CO@\mathbf{1}$, the series of parent ion peaks shifts to m/z 1201 (Figure 1b). Figure 1c shows the spectrum of the starting material with peaks centered at m/z 1172, which correspond to **1** (peaks corresponding to $H_2O@\mathbf{1}$ were not detected by ES-MS).[9a] It is apparent that the addition of CO causes a decrease in the intensity of the peaks at m/z 1172 and an increase of those at m/z 1200 or 1201. These results are consistent with the formation of the 1:1 complex of CO and **1**.

In the ^{1}H NMR spectrum of CO@**1**, signals associated with H_2O were absent and resonances of methylene protons along the orifice of CO@**1** showed upfield shifts with respect to those of $H_2O@\mathbf{1}$. As shown in Figure 2a, two out of the four methylene-proton signals were observed at $\delta = 3.38$ and 2.86 ppm ($J = 20$ and 19 Hz, respectively, each 1H). The corresponding chemical shifts of $H_2O@\mathbf{1}$ were $\delta = 3.50$ and 2.99 ppm, respectively (Figure 2b). The spectrum of empty **1** showed signals similar to those of $H_2O@\mathbf{1}$ (Figure 2c). Thus, the fraction of CO@**1** present can be estimated by comparing

[*] Dr. S.-i. Iwamatsu, Prof. Dr. S. Murata
Graduate School of Environmental Studies
Nagoya University
Chikusa-ku, Nagoya 464-8601 (Japan)
Fax: (+81) 52-789-4765
E-mail: iwmt@urban.env.nagoya-u.ac.jp
C. M. Stanisky, Prof. Dr. R. J. Cross, Prof. Dr. M. Saunders
Chemistry Department
Yale University
P.O. Box 208107, New Haven, CT 06520-8107 (USA)
N. Mizorogi, Prof. Dr. S. Nagase
Theoretical Molecular Science
Institute for Molecular Science
Myodaiji, Okazaki 444-8585 (Japan)

[**] This research was supported by a Grant-in-Aid for Scientific Research (No.17750124), by the Nanotechnology Support Project from the Ministry of Education, Culture, Sports, Science, and Technology of Japan, and by the US National Science Foundation. C.M.S. acknowledges the JSPS fellowship for foreign researchers. The calculations were performed at the Research Center for Computational Science, Okazaki, Japan.

Supporting information for this article is available on the WWW under http://www.angewandte.org or from the author.

 © 2006 Wiley-VCH Verlag GmbH & Co. KGaA, Weinheim

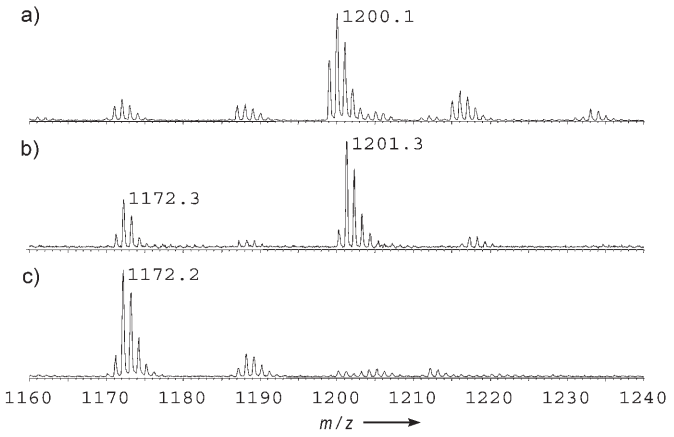


Figure 1. ES mass spectra (negative mode) of a) CO@**1**, b) ^{13}CO@**1**, and c) **1**. Ion peaks of $[M+16]^-$ and $[M+32]^-$ result from oxidation of the samples during measurement (e.g., *m*/*z* 1188 and 1216). These peaks are commonly observed in the spectra of fullerene derivatives.

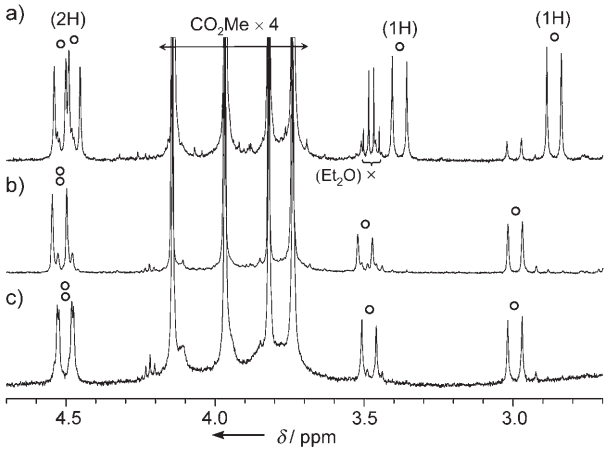


Figure 2. Segments of the ^{1}H NMR spectra (methylene- and methoxy-proton regions) of: a) CO@**1**; b) H_2O@**1**; c) empty **1** (measured in the presence of P_2O_5) in $CDCl_3$.

the ratio of integral values of these signals of CO@**1** with those of H_2O@**1** and **1**.

In the ^{13}C NMR spectrum of CO@**1**, one sharp signal characteristic of CO was observed at $\delta = 174.3$ ppm in $[D_2]$TCE ($\delta = 174.6$ ppm in $CDCl_3$) together with the signals of **1** (Figure 3a). For comparison, the resonance of CO in $CDCl_3$ is 184.6 ppm.[14] The calculated chemical shifts (GIAO-B3LYP/6-31G*) of CO inside **1** and free CO are $\delta =$ 172.3 ppm (average of the three rotational isomers CO@**1**-A, CO@**1**-B, and CO@**1**-C shown in Figure 5; Table 1) and $\delta = 181.3$ ppm, respectively.[15] These results agree well with the observed spectra. Furthermore, atoms and molecules inside fullerenes are known to show upfield shifts because of the magnetic shielding by the fullerene cage.[5–8,16] Thus, the observed upfield shift is clear evidence of the endohedral structure of CO@**1**. In a variable-temperature ^{13}C NMR study of ^{13}CO@**1** in CD_2Cl_2, the CO signal showed slight broadening at −90 °C, which suggests that the encapsulated CO rotates rapidly on the NMR time scale.

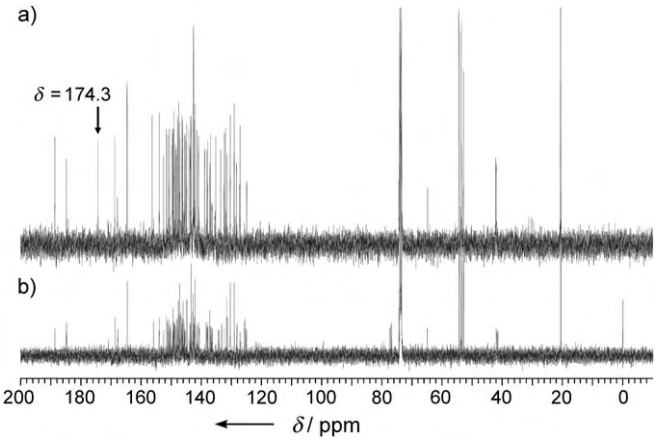


Figure 3. ^{13}C NMR spectra of: a) CO@**1**; b) H_2O@**1** + **1** in $[D_2]$TCE (308 K).

Table 1: Calculated chemical shifts and relative energies of CO@**1** (B3LYP/6-31G*).

Complex	δ(CO) [ppm]	E [kcal mol^{-1}][a]
CO@**1**-A	174.88	+2.7
CO@**1**-B	170.99	+3.8
CO@**1**-C	171.16	+8.1
H_2O@**1**	–	−2.4
CO@C_{60}	–	+8.4[11c]
H_2O@C_{60}	–	−1.5

[a] $E = E$(X@**1**) − [E(X) + E(**1**)], in which E(X@**1**) is the total energy of the complex, and E(X) and E(**1**) are the energies of guest molecule and cage, respectively.

In the IR spectrum of CO@**1**, two CO absorption bands are observed at $\nu = 2125$ and 2112 cm^{-1} (Figure 4), which

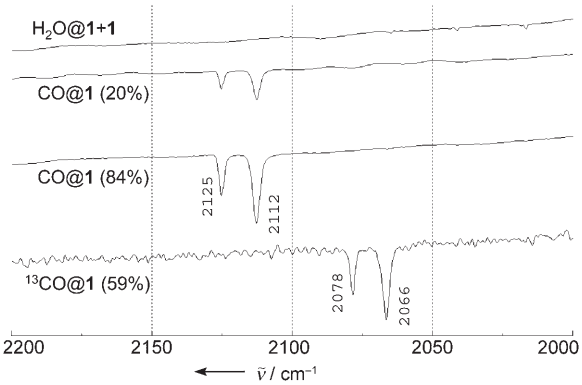


Figure 4. IR spectra of H_2O@**1** + **1**, CO@**1**, and ^{13}CO@**1** (KBr).

differ by −18 and −31 cm^{-1}, respectively, from the CO gas frequency (2143 cm^{-1}). For ^{13}CO@**1**, the corresponding absorptions exhibit clear shifts to lower frequencies ($\tilde{\nu} =$ 2078 and 2066 cm^{-1}; Figure 4), with a uniform ratio of ^{13}CO/^{12}CO ≈ 0.978. This ratio is slightly larger than that calculated for the ^{13}C/^{12}C isotope shift (0.961).[17]

In a related study, carbon monoxide absorbed on the exohedral surface of C_{60} showed two similar absorptions at

 © 2006 Wiley-VCH Verlag GmbH & Co. KGaA, Weinheim

$\tilde{\nu} = 2135$ and $2128\ cm^{-1}$ (at 77 K) arising from CO at the octahedral and tetrahedral sites, respectively, in the crystal lattice.[18] For comparison, carbon monoxide inside single-walled carbon nanotubes absorbs at $\tilde{\nu} = 2135\ cm^{-1}$.[19] The similar but larger shifts of CO@**1** indicate an enhanced interaction between CO and the fullerene cage with respect to that of the exohedral compound. This greater interaction might be due to the shorter distance between the trapped CO and the narrow C_{60} cage. As shown in Figure 4, the intensity ratio of the absorption at $\nu = 2125\ cm^{-1}$ versus that at $\nu = 2112\ cm^{-1}$ is approximately 35:65, independent of the fraction of CO@**1** present. This case contrasts with that of exohedral CO absorptions, in which the ratio is known to be dependent on the equilibrium pressure of CO.[18a] The presence of two absorption bands indicates that there are two distinct orientations for the trapped CO on the IR time scale (picoseconds) whereas there must be rapid interchange between these states on the NMR time scale (milli- to microseconds) to account for the single resonance in the ^{13}C NMR spectrum. In the UV/Vis spectrum, no detectable change was observed between CO@**1** and H_2O@**1** + **1**.

Carbon monoxide absorbed on the exohedral surface of C_{60} is known to disappear under reduced pressure, even at 77 K.[18a] In contrast, CO@**1** was relatively stable under reduced pressure even at ambient temperature. However, it gradually reverts to a mixture of **1** and H_2O@**1** both in solution and in the solid state. A ^1H NMR study on the escape of CO was carried out at 40 °C by using a solution of 2.2 μmol CO@**1** in 0.6 mL $CDCl_3$. In the presence of 9.3 μmol H_2O (ca. 4.2 equiv relative to CO@**1**, analyzed by Karl Fischer titration), the fraction of CO@**1** decreased from 88 to 68, 37, and 7% after 4, 16, and 48 h, respectively. This escape of CO is in contrast to the spontaneous formation of H_2O@**1**, which suggests that H_2O is bound inside the cage more tightly.

To evaluate the rotation of CO in CO@**1**, six rotational isomers were geometrically optimized at the B3LYP/3-21G level.[15] The two lowest-energy geometries and one less-stable geometry were further optimized at the B3LYP/6-31G* level (Figure 5 and Table 1). In the conformation of lowest energy (CO@**1**-A), the CO molecule is aligned towards the opening with the C atom towards the opening. The conformation with the O atom towards the opening (CO@**1**-B) is higher in energy by 1.1 kcal mol^{-1}. Conformations with the CO perpendicular to the opening are even higher in energy but only by about 5.4 kcal mol^{-1} (CO@**1**-C). These results support that CO may rotate rapidly on the NMR time scale but not on the IR time scale, thus giving rise to two or possibly more IR bands. Calculated energies of CO@**1** relative to (CO + **1**) are in the range from +2.7 to +8.1 kcal mol^{-1} (Table 1).[20] The corresponding energy for H_2O@**1** is −2.4 kcal mol^{-1}. The same trend has been reported for CO@C_{60} and H_2O@C_{60} (Table 1).[11c,d] These results suggest that the encapsulation of CO is energetically less favorable than that of H_2O, which is in agreement with the observed instability of CO@**1**.

In summary, we report the formation of an endohedral CO complex of a chemically modified fullerene derivative. The presence of carbon monoxide inside the fullerene cage was confirmed by ES-MS, ^{13}C NMR and IR spectroscopy. Gradual leakage of the CO from CO@**1** contrasts with the spontaneous formation of H_2O@**1**, which suggests that water binds more strongly than CO within **1**. Further investigations are now in progress to construct a library of endohedral complexes of open-cage fullerenes.

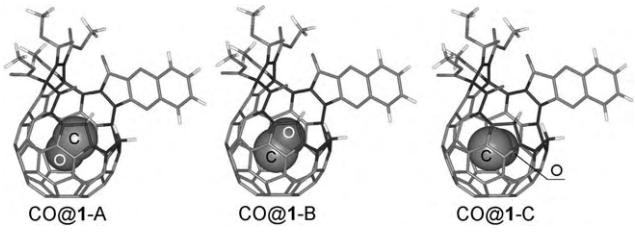


Figure 5. Optimized structures of the rotational isomers of CO@**1** (B3LYP/6-31G*). Carbon monoxide molecules in **1** are shown by the space-filling model.

Experimental Section

CO@**1**: Compound **1** (50 mg) and TCE (10 mL) were loaded into a 50-mL stainless-steel autoclave equipped with an inner glass tube. The reaction vessel was flushed with carbon monoxide three times, charged to 7.5 MPa of CO, and heated at 100 °C for 20 h (the pressure reached 9.0 MPa). After the reaction mixture was allowed to cool, the pressure was released and the solvent was removed in vacuo. The resulting product was centrifuged with Et_2O, and dried in vacuo to give CO@**1** (52 mg, quantitative) as a reddish brown powder. The fraction of CO@**1** present was estimated to be 84% by ^1H NMR spectroscopy. ^1H NMR ($CDCl_3$): $\delta = 8.19$ (s, 1H), 8.03 (s, 1H), 4.51 (d, $J = 20$ Hz, 1H), 4.48 (d, $J = 19$ Hz, 1H), 4.14 (s, 3H), 3.96 (s, 3H), 3.82 (s, 3H), 3.74 (s, 3H), 3.38 (d, $J = 20$ Hz, 1H), 2.86 (d, $J = 19$ Hz, 1H), 2.61 (s, 3H), 2.59 ppm (s, 3H); ^{13}C NMR ([D_2]TCE, 308 K): $\delta =$ 174.30 ppm (CO). Full data are given in the Supporting Information; IR (KBr): $\tilde{\nu} = 2125$, $2112\ cm^{-1}$; UV/Vis (CH_2Cl_2): λ_{max} (ε) = 313 (72000), 351 (68000) nm; ES-MS (negative mode): m/z 1200 $[M]^-$ (100), 1172.

^{13}CO@**1**: Compound **1** (16 mg) and TCE (4 mL) were loaded into a 10-mL stainless-steel autoclave. The reaction vessel was immersed in a dewar of liquid nitrogen and evacuated. A ^{13}CO lecture bottle was connected to the reaction vessel, and approximately 0.9 L of ^{13}CO was condensed into the container. The cooling bath was removed, and the reaction vessel was heated to 100 °C and maintained at that temperature for 20 h (the pressure reached 3.3 MPa). The reaction mixture was allowed to cool, the pressure was released, and the solvent was removed under reduced pressure to give ^{13}CO@**1**. The fraction of ^{13}CO@**1** was estimated to be 59% by ^1H NMR spectroscopy. ^{13}C NMR (CD_2Cl_2): $\delta = 174.92$; IR (KBr): $\tilde{\nu} = 2078$, $2066\ cm^{-1}$; ES-MS (negative mode): m/z 1201 $[M]^-$ (100), 1172.

Received: March 30, 2006
Published online: July 17, 2006

Keywords: cage compounds · fullerenes · host–guest systems · inclusion compounds · nanostructures

[1] "Putting nonmetals into fullerenes": M. Saunders, R. J. Cross in *Endofullerenes: A New Family of Carbon Clusters* (Eds.: T. Akasaka, S. Nagase), Kluwer Academic Publisher, Dordrecht, **2002**, pp. 1–11.
[2] Y. Rubin, *Top. Curr. Chem.* **1999**, *199*, 67–91.
[3] A. Hirsch, M. Brettreich, *Fullerenes: Chemistry and Reactions*, Wiley-VCH, Weinheim, **2005**, pp. 345–358.

 © 2006 Wiley-VCH Verlag GmbH & Co. KGaA, Weinheim

[4] T. Kitagawa, Y. Murata, K. Komatsu, *Fullerene Reactivity—Fullerene Cations and Open-Cage Fullerenes* in *Carbon-Rich Compounds: From Molecules to Materials* (Eds.: M. M. Haley, R. R. Tykwinski), Wiley-VCH, Weinheim, **2006**, pp. 383–420.
[5] Y. Rubin, T. Jarrosson, G.-W. Wang, M. D. Bartberger, K. N. Houk, G. Schick, M. Saunders, R. J. Cross, *Angew. Chem.* **2001**, *113*, 1591–1594; *Angew. Chem. Int. Ed.* **2001**, *40*, 1543–1546.
[6] a) Y. Murata, M. Murata, K. Komatsu, *J. Am. Chem. Soc.* **2003**, *125*, 7152–7153; b) K. Komatsu, M. Murata, Y. Murata, *Science* **2005**, *307*, 238–240.
[7] C. M. Stanisky, R. J. Cross, M. Saunders, M. Murata, Y. Murata, K. Komatsu, *J. Am. Chem. Soc.* **2005**, *127*, 299–302.
[8] S.-i. Iwamatsu, S. Murata, Y. Andoh, M. Minoura, K. Kobayashi, N. Mizorogi, S. Nagase, *J. Org. Chem.* **2005**, *70*, 4820–4825.
[9] a) S.-i. Iwamatsu, T. Uozaki, K. Kobayashi, R. Suyong, S. Nagase, S. Murata, *J. Am. Chem. Soc.* **2004**, *126*, 2668–2669; b) S.-i. Iwamatsu, S. Murata, *Synlett* **2005**, 2117–2129.
[10] a) P. Sozzani, S. Bracco, A. Comotti, L. Ferretti, R. Simonutti, *Angew. Chem.* **2005**, *117*, 1850–1854; *Angew. Chem. Int. Ed.* **2005**, *44*, 1816–1820; b) L. Dobrzañska, G. O. Lloyd, H. G. Raubenheimer, L. J. Barbour, *J. Am. Chem. Soc.* **2005**, *127*, 13134–13135; c) J. A. R. Navarro, E. Barea, J. M. Salas, N. Masciocchi, S. Galli, A. Sironi, C. O. Ania, J. B. Parra, *Inorg. Chem.* **2006**, *45*, 2397–2399.
[11] a) J. Cioslowski, *J. Am. Chem. Soc.* **1991**, *113*, 4139–4141; b) C. I. Williams, M. A. Whitehead, L. Pang, *J. Phys. Chem.* **1993**, *97*, 11652–11656; c) Y. H. Hu, E. Ruckenstein, *J. Chem. Phys.* **2005**, *123*, 144303; d) C. N. Ramachandran, N. Sathyamurthy, *Chem. Phys. Lett.* **2005**, *410*, 348–351.
[12] a) E. H. T. Olthof, A. van der Avoird, P. E. S. Wormer, *J. Chem. Phys.* **1996**, *104*, 832–847; b) J. Hernández-Rojas, A. Ruiz, J. Bretón, J. M. G. Llorente, *Int. J. Quantum Chem.* **1997**, *65*, 655–663.
[13] T. Peres, B. Cao, W. Cui, A. Khong, R. J. Cross, M. Saunders, C. Lifshiz, *Int. J. Mass Spectrom.* **2001**, *210/211*, 241–247.
[14] C. G. Kalodimos, I. P. Gerothanassis, R. Pierattelli, B. Ancian, *Inorg. Chem.* **1999**, *38*, 4283–4293.
[15] Two methyl groups on the quinoxaline moiety in **1** were replaced by two hydrogen atoms in the calculations. Gaussian 03 (Revision C.02): M. J. Frisch et al., see Supporting Information.
[16] a) M. Saunders, R. J. Cross, H. A. Jiménez-Vázquez, R. Shimshi, A. Khong, *Science* **1996**, *271*, 1693–1697; b) Z. Chen, R. B. King, *Chem. Rev.* **2005**, *105*, 3613–3642.
[17] C.-C. Chen, C. M. Lieber, *J. Am. Chem. Soc.* **1992**, *114*, 3141–3142.
[18] a) M. Folman, M. Fastow, Y. Kozirovski, *Langmuir* **1997**, *13*, 1118–1122; b) I. Holleman, G. von Helden, A. van der Avoird, G. Meijer, *J. Chem. Phys.* **1999**, *110*, 2129–2139.
[19] C. Matranga, B. Bockrath, *J. Phys. Chem. B* **2005**, *109*, 4853–4864.
[20] In contrast to the B3LYP results, single-point calculations at the MP2/6-31G(d) level on the optimized geometries of CO@**1** showed stabilizing energies ($E = -12$ to -16 kcal mol^{-1}). Density functional theory (DFT) calculations are known to underestimate the binding energies of the endohedral noble-gas complexes; see a) S. Patchkovskii, W. Thiel, *J. Chem. Phys.* **1997**, *106*, 1796–1799; b) M. Bühl, S. Patchkovskii, W. Thiel, *Chem. Phys. Lett.* **1997**, *275*, 14–18. Experimental verification of the binding energy for CO was not possible due to the contamination of **1** with H_2O@**1** (see reference [8]).

 © 2006 Wiley-VCH Verlag GmbH & Co. KGaA, Weinheim

Self-Assembly

DOI: 10.1002/anie.200600450

Cooperative Self-Assembly of Adenosine and Uridine Nucleotides on a 2D Synthetic Template**

Dmitry S. Turygin, Michael Subat, Oleg A. Raitman, Vladimir V. Arslanov, Burkhard König, and Maria A. Kalinina**

This paper describes a two-dimensional chemical system in which a divalent "template" guides and controls the stepwise and cooperative self-assembly mediated by base pairing of adenosine and uridine nucleotides.

Multiple hydrogen bonding and base pairing constitute one of the most widely studied classes of noncovalent interactions in supramolecular chemistry.[1] The precision with which nature utilizes complementary weak bonding to guide self-assembly of complex structures remains a fascinating challenge for surface chemistry that aims to develop novel approaches to interfacial sensing and nanofabrication.[2] To date, attempts to use base pairing as a basis for planar molecular-recognition systems have focused on self-assembled monolayers (SAMs)[3,4] or Langmuir monolayers[5] that are formed from compounds bearing nucleobases or their synthetic analogues. Although exceptionally useful in the precise vertical alignment of oligo/polynucleotides on solid supports,[6] the SAM-based methods are unsuitable for lateral tailoring of recognition surfaces with different types of bases. This is mostly because of steric hindrance and phase separation of monolayer constituents.[3,7] On the other hand, Langmuir monolayers enable fine-tuning of steric conditions in highly ordered films comprised of different entities at air/water interfaces,[8] but their practical applicability is severely limited. Herein, we use a novel surface-design scheme that combines the advantages of SAM-based and Langmuir-Blodgett (LB) monolayer approaches. This allows for precise harboring of arbitrary combinations of complementary nucleotides in planar films through sterically induced, coop-

[*] M. Subat, Prof. Dr. B. König
Institut für Organische Chemie
Universität Regensburg
Universitätstrasse 31, 93040 Regensburg (Germany)
Fax: (+0049) 941-943-4575
E-mail: burkhard.koenig@chemie.uni-regensburg.de

D. S. Turygin, Dr. O. A. Raitman, Prof. V. V. Arslanov, Prof. M. A. Kalinina
Department of Physical Chemistry of Supramolecular Systems
Frumkin Institute of Physical Chemistry and Electrochemistry RAS
31 Leninsky prospect, Moscow 119991 (Russia)
Fax: (+7) 095-952-53-08
E-mail: pcss_lab@mail.ru

[**] We thank Prof. Bartosz A. Grzybowski for valuable discussion. This work was supported by RFBR (grant no. 05-03-32195).

Supporting information for this article is available on the WWW under http://www.angewandte.org or from the author.

WILEY InterScience DISCOVER SOMETHING GREAT
© 2006 Wiley-VCH Verlag GmbH & Co. KGaA, Weinheim

erative self-assembly on a surface presenting divalent bis-(Zn^{II}–cyclen) complexes.[9–12] These complexes have been previously used for selective recognition of thymidine and uridine bases in polynucleotides and natural DNA.[13] Furthermore, they have a use as highly efficient divalent receptors for thymidine and uridine nucleotides that interact with the bis-cyclic host through simultaneous binding of terminal phosphate and imide groups to complementary macrocyclic fragments.[14] In our system, the selective formation of bis(Zn^{II}–cyclen)-nucleotide aggregates promotes cooperative nucleotide self-assembly on a recognition surface.

We ordered amphiphilic bis(Zn^{II}–cyclen) derivatives (hereafter, Zn^{II}–BC) into a planar matrix through LB transfer of Zn^{II}–BC monolayers from an aqueous subphase onto a gold-coated surface covered with a loosely packed SAM of octanethiol (Figure 1). This simple combination of SAM and

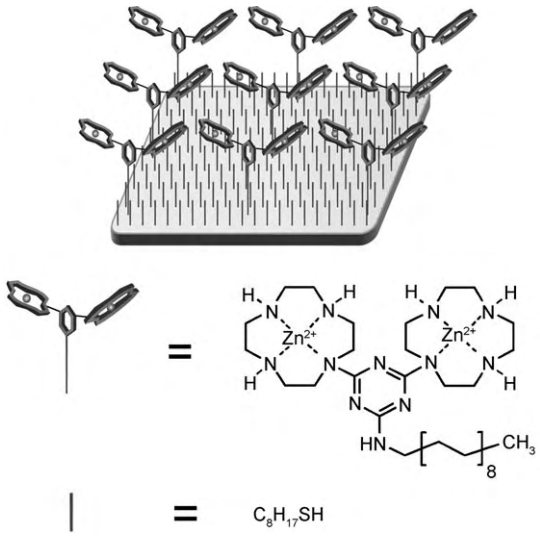


Figure 1. Schematically drawn structure of a SAM-supported monolayer of Zn^{II}–BC on a gold-coated surface.

LB techniques preserves a uniform order of the precursor monolayer and gives a stable, interdigitated bilayer with macrocyclic fragments exposed to the solution. According to our preliminary studies, Zn^{II}–BC immobilized in such a film is capable of binding nucleotide constituents modeled with uracil and an inorganic phosphate dianion while being inactive to adenine or monoanionic phosphates (for details see the Supporting Information).[15] The nucleotide assembly on functionalized SAM/LB plates was investigated in aqueous solutions of monovalent adenosine 5′-mono-, di- or triphosphates (hereafter, 5′-AXPs, where X = M (mono), D (di), or T (tri)) and/or divalent uridine 5′-mono-, di- or triphosphates (5′-UXPs, where X = M (mono), D (di), or T (tri)) at pH 7.5 through surface plasmon resonance (SPR) as a most appropriate tool for real-time monitoring of binding events.

The SPR sensograms in Figure 2 a,b illustrate typical kinetics of the stepwise assembly of 0.02 mM 5′-AXPs and 5′-UXPs for different orders of nucleotide addition (i.e., UTP probing followed by the subsequent addition of ATP and

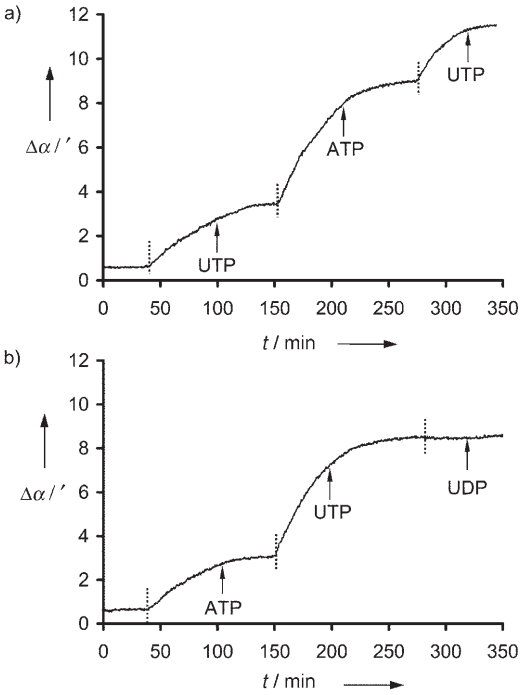


Figure 2. SPR sensograms for stepwise adsorption of a 5′-ATP/5′-UTP binary combination on a SAM-Zn^{II}–BC surface. a) The experiment started by probing with UTP (0.02 mM) followed by subsequent addition of ATP (0.02 mM) and of UTP (0.02 mM), b) the "vice versa" subsequent binding of ATP (0.02 mM) and UTP (0.02 mM) finalized by probing with UDP (0.05 mM); pH 7.5.

UTP (a) and adsorption of ATP, followed by UTP and UDP(b)).

Initially, Zn^{II}–BC surfaces responded slowly to both types of nucleotides. The first-stage binding translated into an SPR maximal response, $\Delta\alpha_1$, that falls within a range of 1.8–2.7 angle min;[16] the absolute values of $\Delta\alpha_1$ increased with the molecular weight of the measured nucleotides.[15] In addition, the kinetics and values of $\Delta\alpha_1$ determined for 5′-AXPs were similar to those measured for similar 5′- UXPs (here, 2.5–2.7 angle min for UTP and ATP).

After the completion of initial adsorption, similar probes of complementary nucleotides (0.02 mM) were added. The kinetics of secondary binding of either 5′-AXP or 5′-UXP at the surface with an already-adsorbed complementary partner was very different from that of initial recognition—the SPR signal increased rapidly and reached its maximal value $\Delta\alpha_2$, which was twice that of $\Delta\alpha_1$. Again, the $\Delta\alpha_2$ value varied from 3.6 to 5.4 angle min in proportion to the nucleotide's molecular weight, and the magnitudes of responses to 5′-AXP and 5′-UXP were similar (5.4 and 5.3 angle min for ATP and UTP, respectively). Importantly, because the magnitude of the SPR signal is proportional to the amount of adsorbed analyte, it appears that the initial binding of one molecule of either monovalent 5′-AXP or divalent 5′-UXP by Zn^{II}–BC film promotes further assembly of not one but two complementary molecules.

Furthermore, when equilibrated after secondary binding, the sensing surfaces were still capable of specific recognition; the films responded to the nucleotides that were comple-

 © 2006 Wiley-VCH Verlag GmbH & Co. KGaA, Weinheim

mentary to the one bound at the second stage (Figure 2a). Moreover, maximal third-stage responses $\Delta\alpha_3$ were close to $\Delta\alpha_1$, that is, the efficiency of final adsorption was comparable with that observed at the initial stage. On the other hand, addition of a nucleotide containing a base similar to that used in second-stage binding caused no significant increase in the SPR signal even at increasing concentrations (Figure 2b). The specificity of the third-stage responses and their absolute values suggest that this stage proceeds with complementary recognition of incoming nucleotides (UTP on Figure 2a) by only half of the potentially available complementary partners already present on the surface (ATP on Figure 2a).

To understand the mechanism of nucleotide assembly, we make several observations related to the inhibition of secondary binding events. Firstly, as illustrated by Figure 3a,

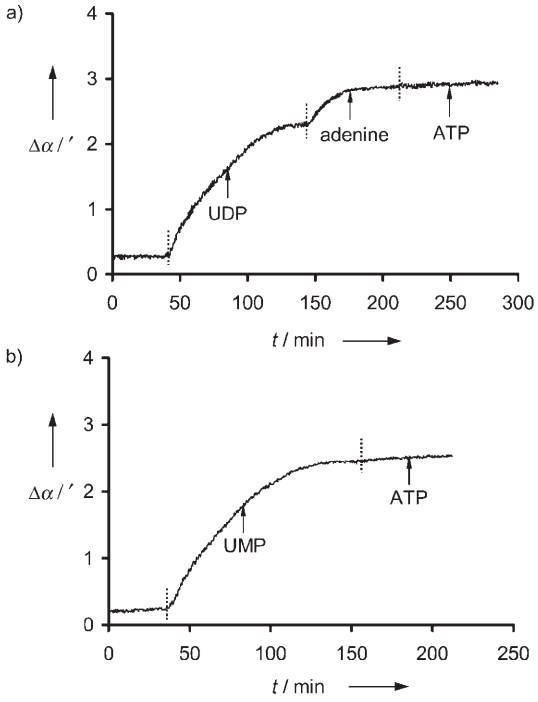


Figure 3. Inhibition of secondary recognition of 5′-ATP at SAM-Zn^{II}–BC sensing film. a) Initial adsorption of 5′-UDP (0.02 mM) at pH 7.5 followed by subsequent addition of adenine (0.05 mM; pH 7.9) and 5′-ATP (0.02 mM), b) the assembly of 5′-UMP (0.02 mM) followed by the probing with 5′-ATP (0.02 mM).

the protective binding of adenine to the Zn^{II}–BC monolayer with initially adsorbed 5′-UDP inhibited further assembly of 5′-ATP on the surface. Importantly, the response, $\Delta\alpha_2$, to adenine (which does not interact itself with Zn^{II}–BC) was almost exactly three-times lower than $\Delta\alpha_1$ for UDP. As adenine's molecular weight is also three-times lower than that of UDP, the registered signal difference corresponds to a 1:1 UDP–adenine binding ratio. The inhibitory effect of this binding on further 5′-AXP recognition suggests that phosphate coordination is the first-stage binding mode even for potentially divalent 5′-UXPs (except for UMP, which is discussed below); moreover, the immobilized nucleotides are well preorganized for the interactions with suitable complementary partners. The effect also points to the mediating role of base pairing in secondary recognition of complementary nucleotides—it is hindered when complementary H-bonding is "switched off".

The secondary recognition of adenosine phosphates was also inhibited by preliminary adsorption of UMP—the smallest divalent nucleotide studied herein (Figure 3b).[18] The distance between cyclic "heads" of Zn^{II}–BC is presumably well matched to UMP's molecular geometry thus allowing for simultaneous intramolecular coordination of phosphate and imide groups to the neighboring macrocycles. The surface with bound UMP becomes inactive with respect to other incoming nucleotides as both macrocyclic moieties in Zn^{II}–BC are occupied and therefore, the UMP nucleobase involved in this divalent binding mode is unavailable for base pairing.

These observations support a mechanism involving stepwise self-assembly of complementary nucleotides at Zn^{II}–BC monolayers (Figure 4). Specifically, irrespective of the nucleotide used, the first binding event is mediated by the coordination of the terminal phosphate to one of the "heads" of the Zn^{II}-BC template (Figure 4a). The geometry of the Zn^{II}–BC molecule prevents simultaneous divalent binding of 5′-UXPs with a distance between the base and terminal phosphate longer than that in 5′-UMP. These first-step interactions, however, cause steric crowding at the opposite Zn^{II}–cyclen, thus shielding the free macrocycle from similar nucleotides and hindering their binding to the same Zn^{II}–BC molecule.

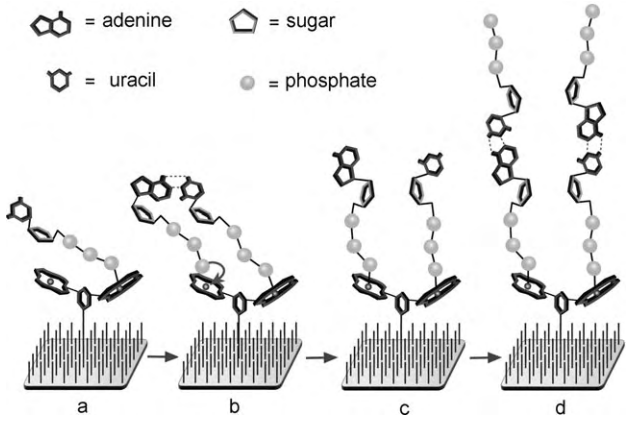


Figure 4. Schematic diagrams illustrating the possible mechanism of the stepwise self-assembly of complementary nucleotides on a SAM-Zn^{II}–BC template (one Zn^{II}–BC unit is shown). a) Phosphate attachment of a nucleotide to the one of Zn^{II}–cyclen units, b) base pairing accompanied by the guiding of terminal phosphate of complementary nucleotide to the opposite Zn^{II}–cyclen, c) firm attachment of the complementary nucleotide to Zn^{II}–BC and dissociation of the base pair, d) base pairing of incoming nucleotides with complementary partners already immobilized on the template.

Incoming complementary nucleotides recognize the already bound partner through base pairing.[19] Nucleotide coupling results in a spatial arrangement of the interacting components that favors simultaneous orientation ("guiding") of the terminal phosphate of a complementary nucleotide to

 © 2006 Wiley-VCH Verlag GmbH & Co. KGaA, Weinheim

the free "head" of the Zn^{II}–BC molecule (Figure 4b). The cooperative action of the template and both nucleotides is, most likely, assisted by base stacking. Although the base stacking interactions stabilize the ordering layer significantly, the energetic contribution of hydrogen bonding is rather small compared with the phosphate-anion coordination. Therefore, dissociation of the base pair, exposing the hydrogen-bond donor and acceptor sites to the solution, is expected to be in equilibrium (Figure 4c). Disengaged bases, in turn, form complementary pairs with other incoming nucleotides.[20] This chain of consecutive interactions results in the formation of a bilayer structure that harbors equal amounts of complementary nucleotides (Figure 4d).

The above mechanism suggests that nucleotide self-assembly is independent from the formation path—that is, stepwise recognition of complementary nucleotides in an arbitrary order as well as their one-step self-assembly from an equimolar mixture should give the same nucleotide pattern on Zn^{II}–BC surfaces. To prove this assumption, we studied both continuous and interrupted adsorption of ATP/UTP equimolar mixtures (0.02 mM of each nucleotide) on Zn^{II}–BC templates. One-step ATP/UTP adsorption translated into a maximal increase in the SPR signal $\Delta\alpha_{\text{one step}} = 9.0$ angle min (data not shown; an SPR curve is given in the Supporting Information). This value is more than twofold greater when compared with $\Delta\alpha = 3.9$ angle min, which was measured for the adsorption of ATP from a solution with a double concentration of nucleotide (0.04 mM).[15] This correlates well to $\Delta\alpha_{\text{multistep}} = 10.4$, which was determined from Figure 2a for the stepwise binding of the ATP/UTP combination.

Figure 5 describes interrupted adsorption of a similar mixture, followed by stepwise surface probing with ATP (0.02 mM) followed by UTP (0.02 mM) solutions. The ATP/UTP mixed solution was replaced by one of ATP (0.02 mM) when $\Delta\alpha$ reached 6.5 angle min greater than $^1/_2\Delta\alpha_{\text{multistep}} \cong 5.2$ angle min. This value assumes that more than half of the nucleotides that constitute the final bilayer were already immobilized on a surface. After the completion of ATP binding, UTP (0.02 mM) was added. We observed almost equal SPR maximal signals for individual solutions; an overall increase in the SPR signal $\Delta\alpha_{\max}$ amounted to 9.4 angle min.

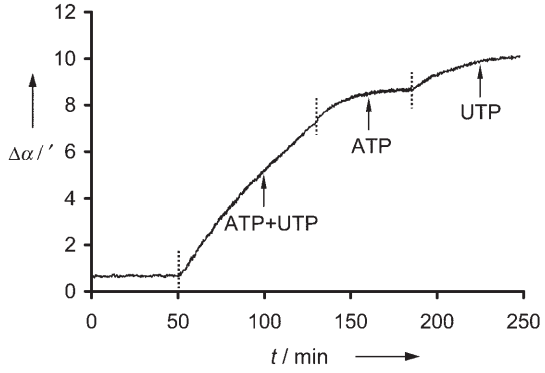


Figure 5. SPR sensogram for the interrupted adsorption of 5′-ATP/5′-UTP equimolar mixture (0.02 mM of each nucleotide) replaced by ATP (0.02 mM) at $\Delta\alpha = 6.5$ angle min and completed with the addition of UTP (0.02 mM).

Close agreement between maximal SPR responses registered for one-step and stepwise modes of assembly indicates that constant amounts of nucleotide bind to the surface irrespective of the procedure used. Some of the differences between $\Delta\alpha_{\text{one step}}$ and $\Delta\alpha_{\text{multistep}}$ may be attributed to steric crowding at the interface in more concentrated mixtures. Such crowding results in the formation of structures that are not-so-rigorously defined, presumably because some base pairs between the nucleotide layer attached to the template and the complementary top layer are uncompleted. Furthermore, equal SPR signals measured in subsequent probing with individual nucleotides in Figure 5 prove the alteration of the binding mode in the course of self-assembly; when the Zn^{II}–BC template is saturated with bound nucleotides and a bottom layer is formed, further completion of the bilayer structure proceeds through 1:1 base recognition.

In summary, we described sterically induced cooperative assembly of complementary nucleotides progressing through the chain of consecutive mono- and divalent interactions on a surface presenting artificial Zn^{II}–BC receptors. We believe that the approach utilized herein might be extended to other types of planar patterns of complementary nucleotides, as well as for the preparation of other artificial systems preorganized for efficient molecular recognition and further bottom-up self-assembly of synthetic molecules containing suitable fragments.

Experimental Section

All nucleotides (adenosine 5′-monophosphate, adenosine 5′-diphosphate disodium salt hydrate, adenosine 5′-triphosphate disodium salt hydrate, uridine 5′-monophosphate disodium salt hydrate, uridine 5′-diphosphate disodium salt hydrate, and uridine 5′-triphosphate trisodium salt hydrate) are of analytical-reagent grade and were obtained from Acros Organics (Belgium). Nucleotides and organic bases (uracil and adenine) were dissolved in water that was deionized to 16 MΩ cm resistivity and preliminarily adjusted to pH 7.5 by the addition of a small amount of sodium hydroxide; these solutions were used for SPR measurements immediately after their preparation.

Platform preparation: TF-1 glass supports covered with a Cr adhesion sublayer (5 nm) and a polycrystalline Au layer (50 nm) supplied by Analytical-μSystem were modified by immersion into an absolute ethanol solution of octanethiol (1 mM) for 2 min. The monolayers of Zn^{II}–BC were spread from 10^{-5} M chlorophorm solution onto basic subphase with pH 8.52, compressed to 17 mN m^{-1}, and vertically transferred (the down-stroke mode of transfer was applied) onto thiolated support at a constant speed of 0.5 mm min^{-1}.

SPR monitoring: The SPR Kretschmann-type spectrometer Biosuplar-2 (Analytical-μSystem; a light-emitting diode light source $\lambda = 670$ nm) equipped with a peristaltic pump (flow rate 0.3 mL min^{-1}) was used for kinetic monitoring; freshly prepared solutions were added in 15 mL portions to the pump vessel when the previous portion was nearly all used. The SPR cell was rinsed with pure water for 15–20 min prior to the addition of each next probe.

Other experimental details are given in the Supporting Information.

Received: February 2, 2006
Revised: April 25, 2006
Published online: July 17, 2006

 © 2006 Wiley-VCH Verlag GmbH & Co. KGaA, Weinheim

Keywords: base pairing cooperativity · macrocycles · nucleobases · self-assembly · thin films

[1] a) L. J. Prins, D. N. Reinhoudt, P. Timmerman, *Angew. Chem.* **2001**, *113*, 2446 – 2492; *Angew. Chem. Int. Ed.* **2001**, *40*, 2382 – 2426; b) J. L. Sessler, J. Jayawickramarajah, *Chem. Commun.* **2005**, *15*, 1939; c) J. Rao, J. Lahiri, R. M. Weis, G. M. Whitesides, *J. Am. Chem. Soc.* **2000**, *122*, 2698.

[2] a) J. D. Badjicä, A. Nelson, S. J. Cantrill, W. B. Turnbull, J. F. Stoddart, *Acc. Chem. Res.* **2005**, *38*, 723; b) J. Huskens, A. Mulder, T. Auletta, C. A. Nijhuis, M. J. W. Ludden, D. N. Reinhoudt, *J. Am. Chem. Soc.* **2004**, *126*, 17050; c) S. J. Metallo, R. S. Kane, R. E. Holmlin, G. M. Whitesides, *J. Am. Chem. Soc.* **2003**, *125*, 4534; d) S. Flink, F. C. J. M. van Veggel, D. N. Reinhoudt, *Adv. Mater.* **2000**, *12*, 1315.

[3] M. Weisser, J. Kalshammer, B. Menges, J. Matsumoto, F. Nakamura, K. Ijiro, M. Shimomura, S. Mittler, *J. Am. Chem. Soc.* **2000**, *122*, 87.

[4] a) A. Sanyal, T. B. Norsten, O. Uzun, V. M. Rotello, *Langmuir* **2004**, *20*, 5958; b) K. Matsuura, Y. Ebara, Y. Okahata, *Langmuir* **1997**, *13*, 814; c) Y. Sato, H. Noda, F. Mizutani, A. Yamakata, M. Osawa, *Anal. Chem.* **2004**, *76*, 5564.

[5] a) M. Weck, R. Fink, H. Ringsdorf, *Langmuir* **1997**, *13*, 3515; b) F. Nakamura, K. Ijiro, M. Shimomura, *Thin Solid Films* **1998**, *327–329*, 603; c) R. Marczak, V. T. Hoang, K. Noworyta, M. E. Zandler, W. Kutner, F. D'Souza, *J. Mater. Chem.* **2002**, *12*, 2123; d) J Chen, A Berman, *Nanotechnology* **2004**, *15*, S303; e) K. Taguchi, K. Ariga, T. Kunitake, *Chem. Lett.* **1995**, 701.

[6] a) N. K. Devaraj, G. P. Miller, W. Ebina, B. Kakaradov, J. P. Collman, E. T. Kool, C. E. D. Chidsey, *J. Am. Chem. Soc.* **2005**, *127*, 8600; b) A. B. Steel, T. M. Herne, M. J. Tarlov, *Anal. Chem.* **1998**, *70*, 4670.

[7] J. C. Love, L. A. Estroff, J. K. Kriebel, R. G. Nuzzo, G. M. Whitesides, *Chem. Rev.* **2005**, *105*, 1103.

[8] K. Ariga, T. Kunitake, *Acc. Chem. Res.* **1998**, *31*, 371.

[9] a) J. D. Chartres, L. F. Lindoy, G. V. Meehan, *Coord. Chem. Rev.* **2001**, *216–217*, 249; b) S. Aoki, A. Jikiba, K. Takeda, E. Kimura, *J. Phys. Org. Chem.* **2004**, *17*, 489.

[10] a) T. Walenzyk, B. Koenig, *Inorg. Chim. Acta* **2005**, *358*, 2269; b) T. Koike, S. Kajitani, I. Nakamura, E. Kimura, M. Shiro, *J. Am. Chem. Soc* **1995**, *117*, 1210.

[11] S. C. Ritter, M. Eiblmaier, V. Michlova, B. Koenig, *Tetrahedron* **2005**, *61*, 5241.

[12] a) T. Koike, M. Takamura, E. Kimura, *J. Am. Chem. Soc.* **1994**, *116*, 8443; b) E. Kimura, E. Kikuta, *J. Biol. Inorg. Chem.* **2000**, *5*, 139; c) R. Cibulka, R. Vasold, B. Koenig, *Chem. Eur. J.* **2004**, *10*, 6223.

[13] a) E. Kinoshita, E. Kinoshita-Kikuta, T. Koike, *Anal. Biochem.* **2005**, *337*, 154; b) E. Kinoshita-Kikuta, E. Kinoshita, T. Koike, *Nucleic Acids Res.* **2002**, *30*, 126; c) E. Kimura, T. Ikeda, S. Aoki, M. Shionoya, *J. Biol. Inorg. Chem.* **1998**, *3*, 259; d) E. Kimura, H. Kitamura, K. Ohtani, T. Koike, *J. Am. Chem. Soc.* **2000**, *122*, 4668.

[14] S. Aoki, E. Kimura, *J. Am. Chem. Soc.* **2000**, *122*, 4542. The authors mentioned an effect of geometrical mismatch on ditopic binding of various U(T)XP's at *meta*- and *para*-xylyl-bis(Zn^{II}–cyclen); *para* isomers with a longer distance between cyclic fragments acted as more efficient divalent receptors than *meta* dimers for the most of investigated nucleotides. However, the *meta* isomer was found to be a more appropriate host for 2′-UMP as the intercycle distance in the *para* isomer was too long for simultaneous coordination of both phosphate and imide groups of the nucleotide.

[15] See the Supporting Information for details of the synthetic procedure for the amphiphilic bis(Zn^{II}–cyclen) derivative, the data for IR, UV/Vis, ^{1}H NMR spectrometry, ^{13}C NMR spectrometry, and MS for the final and intermediate products, the formation procedure for Langmuir monolayers and the LB monolayer of Zn^{II}–BC, and surface pressure–area isotherms. Additionally, cyclic voltammagram (CVA) data on SAM and SAM/Zn^{II}–BC films with an estimated surface coverage and SPR data on the adsorption of other nucleotide combinations that are not described in the main text are also included in the Supporting Information.

[16] Immediate shifts (ones faster than SPR scan) in SPR signals are attributed to the difference in refractive indexes of the analyzed solutions as well as those portions of kinetics curves, which correspond to the rinsing of the SPR cell with water at the end of each stage, were cut from the graphs for clarity. However, the $\Delta\alpha_i$ values that are given account for the "rinsing" decrease in the SPR signal that normally fell within a range of 0.1–0.3 angle min; maximal "rinsing" decrease was observed after first-stage adsorption.

[17] J. Homola, *Anal. Bioanal. Chem.* **2003**, *377*, 528.

[18] The two-stage binding of these nucleotides in reversed order (UMP after ATP) followed the recognition pattern similar to that observed for all other binary combinations—slow initial adsorption of ATP promoted faster and more pronounced responses to UMP (the SPR curve is given in the Supporting Information).

[19] The enthalpic contribution of hydrogen bonds in a single base pair in aqueous solution is too small for stable aggregate formation. However, polarities at interfaces are different from bulk solution. Furthermore, owing to the dramatic change in polarity from the aqueous to the lipid phase, the dielectric constant in the critical recognition zone close to the lipid surface is dramatically lowered with the consequence of drastically enforced electrostatic and hydrogen bond interactions (by a factor of $\approx 10^6$). For an overview and examples, see Ref. [8]; for recent examples applying this effect, see: a) Peptide and protein recognition at mono- and bilayers. Equimolar mixed monolayers of a diglycine and a guanidinium amphiphile were shown to bind free dipeptides by a guanidinium carboxylate interaction and stable antiparallel hydrogen bonds among the peptide chains. K. Ariga, A. Kamino, X. Cha, T. Kunitake, *Langmuir* **1999**, *15*, 3875 – 3885; b) Size matching of amino acid residues in host and guest leads to a certain sequence selectivity for aliphatic peptides. Synthetic bilayers were evenly covered with phosphate anions to bind basic proteins in water at millimolar concentrations. N. Kimzuka, A. Baba, T. Kunitake, *J. Am. Chem. Soc.* **2001**, *123*, 1764 – 1765; c) Matile reported a possible explanation for the cell-permeating activity of arginine-rich protein transduction domains, which have received considerable attention because they transport anionic substrates across membranes. Extensive phase-transfer experiments with liquid and bilayer membranes support their concept of "counteranion scavenging". N. Sakai, S. Matile, *J. Am. Chem. Soc.* **2003**, *125*, 14348 – 14356; d) Koh immobilized BSA on gold surfaces by non-covalent interaction with calix[4]arene derivatives carrying carboxylate groups at their upper rims. The new SAMs were examined with SPR and showed a higher BSA concentration on those surfaces covered with carboxylates rather than those with ester groups. M. Lee, W. G. An, J.-H. Kim, H.-J. Choi, S.-H. Kim, M.-H. Han, K. Koh, *Mater. Sci. Eng. C* **2004**, *24*, 123 – 126; e) Membrane-embedded synthetic receptors showed nanomolar affinities to proteins. R. Zadmard, T. Schrader, *J. Am. Chem. Soc.* **2005**, *127*, 904 – 915; S. Kolusheva, O. Molt, M. Herm, T. Schrader, R. Jelinek, *J. Am. Chem. Soc.* **2005**, *127*, 10000 – 10001.

[20] A major energetic contribution for assembly comes from base-stacking, whereas hydrogen bonding contributes to the selectivity of the process.

 © 2006 Wiley-VCH Verlag GmbH & Co. KGaA, Weinheim

Enzyme Inhibition

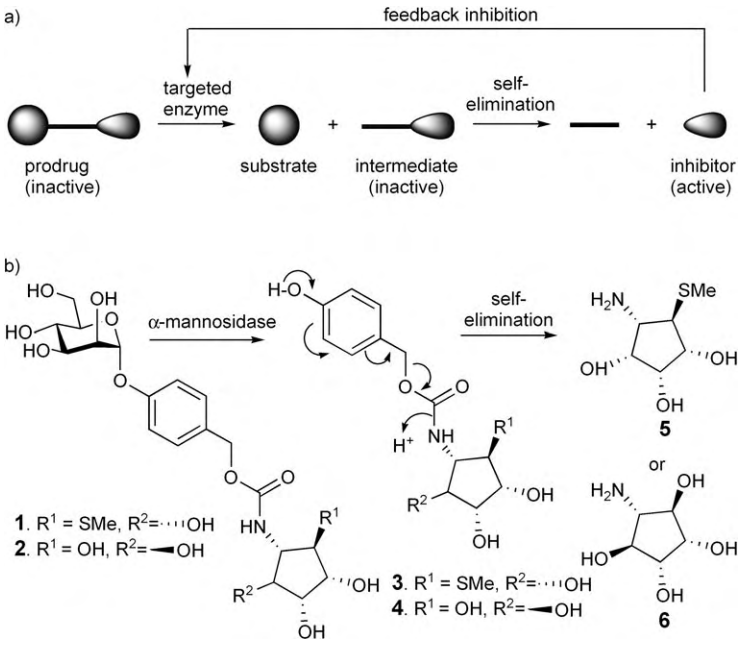
DOI: 10.1002/anie.200600808

Selective Inhibition of Glycosidases by Feedback Prodrugs**

*Jun Guo, Jinkeng Asong, and Geert-Jan Boons**

Protein- and lipid-linked oligosaccharides at the surface of eukaryotic cells are responsible for a wide range of biological processes impacting health and disease.[1–4] Examples of such processes include fertilization, embryogenesis, neuronal development, hormone activities, and the proliferation of cells and their organization into specific tissues. Remarkable changes in cell-surface carbohydrates occur with tumor progression, which appears to be intimately associated with the dreaded state of metastasis.[5–7] Furthermore, carbohydrates of host cells are often employed by pathogens for cell entry. Not surprisingly, compounds that can interfere in the biosynthesis of oligosaccharides are regarded as attractive leads for drug discovery for a wide range of diseases.[8–14] For example, inhibitors of pancreatic α-amylase, such as arcarbose, voglibose, and miglitol, have been introduced for the treatment of diabetes.[15] Furthermore, compounds such as zamamivir and oseltamivir (tamiflu) have been developed as inhibitors of neuramidase for the treatment of the flu.[16–20] Despite these successes, it has been difficult to develop safe and efficacious glycosidase inhibitors for the treatment of many other diseases. A major problem of many natural and synthetic glycosidase inhibitors is that they inhibit other glycosidases, which may lead to serious side effects. More-selective inhibitors may be obtained by carefully designed structure—activity-relationship studies[21–29] in combination with a better understanding of the mechanism of action of glycosidases. This approach is, however, complicated by the fact that of the approximate 100 mammalian glycosidases, only a small number have been cloned and overexpressed.

We report herein a general approach for the design and synthesis of more-selective glycosidase inhibitors based on feedback inhibition. Feedback inhibition is a mechanism in which a biosynthetic pathway regulates itself through inhibition of the first committed step in the pathway by a downstream or final product.[30] Although this type of inhibition is widely used in nature, it has not been exploited for the design and synthesis of selective therapeutics. The feedback-inhibition prodrugs described herein are composed of an inhibitor that is modified by a linker that renders them inactive (Scheme 1a). The linker, in turn, is attached to a glycoside that can be hydrolyzed by a targeted glycosidase. The resulting intermediate is designed in such a way that it will undergo self-fragmentation to release the active inhibitor. Subsequently, the inhibitor inhibits the enzyme that initiated its release. The attraction of this approach is that the inhibitor will only be released at the site of the enzyme. Selectivity is achieved owing to the exquisite selectivity of glycosidases for their substrates. Furthermore, the release of the inhibitor is terminated when a sufficient quantity of the inhibitor is released. The remaining pool of prodrug will, however, be activated when the active enzyme reappears, thereby approximating conditions of continuous infusion.



Scheme 1. a) General strategy for the inhibition of enzymes by a feedback mechanism. b) A feedback inhibitor for mannosidases.

Compound **1** is a prototypic feedback inhibitor that is designed to selectively target α-mannosidases. It is composed of mannostatin A,[10] which is a potent inhibitor of α-mannosidases and has garnered attention as a lead compound for cancer-drug development (Scheme 1b). The amino group of mannostatin A is modified by a 4-hydroxybenzyl carbamate, which in turn is linked to an α-mannoside. The acylation of the amino group of mannostatin A renders the compound inactive for inhibition of mannosidases.[31] However, an α-mannosidase can hydrolyze the glycosidic linkage resulting in the formation of intermediate **3**, which will self-fragment[32] to give mannostatin A (**5**). The active mannostatin A will then inhibit the α-mannosidase that initiated its release, therefore terminating the enzymatic reaction. On the other hand, the enzymatic hydrolysis of compound **2** will release aminocyclopentitetrol **6**, which is not an inhibitor of an α-mannosidase,[33] and therefore this reaction is expected to proceed to completion.

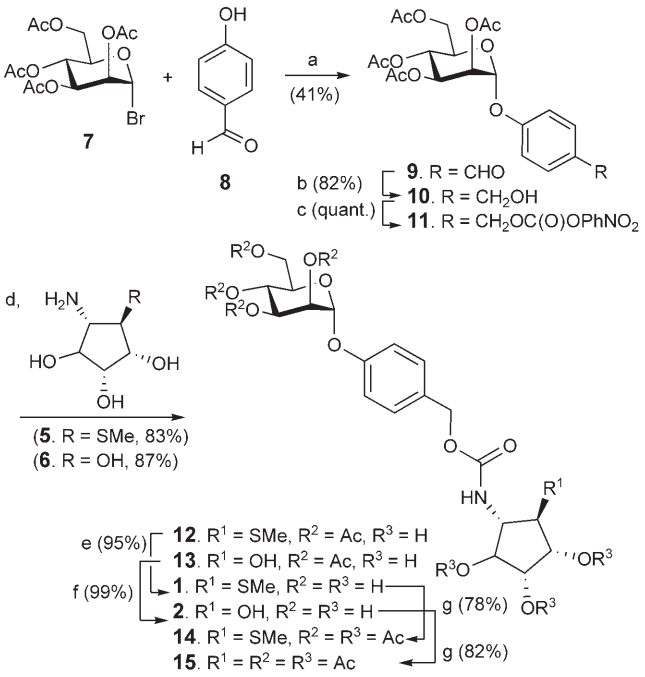
[*] Dr. J. Guo, J. Asong, Prof. G.-J. Boons
Complex Carbohydrate Research Center
University of Georgia
315 Riverbend Road, Athens, GA 30602 (USA)
Fax: (+1) 706-542-4412
E-mail: gjboons@ccrc.uga.edu

[**] This research was supported by the Research Resource Center for Biomedical Complex Carbohydrates (P41-RR-5351) and NCI of NIH (5UO1A91295).

Supporting information for this article is available on the WWW under http://www.angewandte.org or from the author.

© 2006 Wiley-VCH Verlag GmbH & Co. KGaA, Weinheim

The synthesis of compounds **1** and **2** is summarized in Scheme 2. Coupling of 1-bromo-2,3,4,6-tetra-*O*-acetyl-α-D-mannose (**7**) with *p*-hydroxybenzaldehyde (**8**) by using silver(I)oxide as the promoter in refluxing acetonitrile gave



Scheme 2. Reagents and conditions: a) Ag_2O, CH_3CN, Δ, 1 h; b) $NaBH_4$, silica, $CHCl_3$, *i*PrOH; c) *p*-$NO_2PhOCOCl$, pyridine, DCM, 18 h; d) Et_3N, DMF, 18 h; e) NH_3 in MeOH; f) $NH_2NH_2{\cdot}H_2O$, MeOH, 0 °C, 5 h; g) Ac_2O, pyridine. DCM = dichloromethane, DMF = *N*,*N*-dimethylformamide.

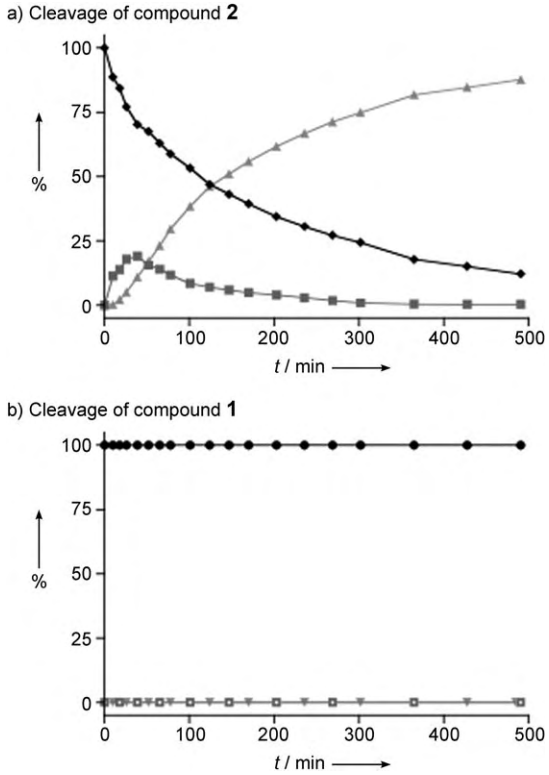


Figure 1. Release of prodrugs **1** and **2** by human lysosomal mannosidase. HLM (20 mU) was added to a solution of **2** (a) and **1** (b) (80 nmol) in deuterated sodium acetate buffer solution (100 mM, pH 5.6, 0.2 mL). The enzymatic cleavage of **1** (●) and **2** (◆) and the formation of the intermediates **3** (□) and **4** (■) and the final products **5** (▼) and **6** (▲), respectively, were monitored by ^{1}H NMR spectroscopy (600 MHz).

9 in a modest yield. The aldehyde moiety of **9** was reduced with $NaBH_4$ to give **10**, which was converted into activated intermediate **11** by reaction with 4-nitrophenyl chloroformate. This compound was immediately reacted with **5**[34] and **6**[35] to afford compounds **12** and **13**, respectively. The acetyl esters of **12** and **13** were cleaved by treatment with ammonia or hydrazine in methanol to give the targeted compounds **1** and **2**, respectively.

The enzymatic cleavage of **1** and **2** by human lysosomal mannosidase (HLM) was monitored by ^{1}H NMR spectroscopy (600 MHz).[36] HLM (20 mU) was added to a solution of **1** or **2** (80 nmol), which were dissolved in a deuterated sodium acetate buffer (100 mM, pH 5.6, 0.2 mL). The progress of the reaction was monitored by the integration of key signals of the starting material, the intermediate, and final product. As can be seen in Figure 1a, HLM hydrolyzed **2** producing intermediate **4**, which self-fragmented to aminocyclopentitetrol **6**. Compound **6** is not an inhibitor of HLM and as a result the enzymatic conversion progressed to completion. On the other hand, virtually no hydrolysis was observed when **1** was treated with HLM (Figure 1b). In this case, the released mannostatin A (**1**) inhibits HLM and terminates further hydrolysis of **1**. Mannostatin A is a potent inhibitor of retaining α-mannosidases (K_i = 90 nM, HLM)[37] and thus, the release of low concentrations of the active compound is sufficient to abolish enzyme activity. Indeed, the addition of 4-methylumbelliferyl-α-D-mannopyranoside did not result in the release of fluorescence methylumbelliferone, demonstrating that the mannosidase was inhibited by the released mannostatin A.

Compounds **1** and **2** were subjected to α-glucosidase, α-fucosidase, and α-galactosidase. As expected, these enzymes did not initiate the release of the compounds **5** and **6**, demonstrating that they have exquisite selectivity for α-mannosidases (data not shown).[41]

Next, the pH dependence of the self-fragmentation of intermediates **3** and **4** was investigated. It is well known that different organelles have different pH values. For example, lysosomes are significantly more acidic than the Golgi apparatus. Golgi mannosidase II has been identified as a target for antimetastatic therapy,[8,38] whereas inhibition of lysosomal mannosidase leads to the phenotype of lysosomal storage disease. It was expected that intermediates **3** and **4** would fragment significantly faster in neutral as opposed to acidic conditions, providing a basis for some selectivity for Golgi mannosidase over the lysosomal mannosidase. Thus, compound **2** (0.4 mM), in deuterated phosphate/citrate buffer solutions (0.2:0.1M) of different pH values, was treated with a large quantity (7 Units mL^{-1}) of Jack Bean α-mannosidase (JBM) to completely convert the prodrug into intermediate **4**.

 © 2006 Wiley-VCH Verlag GmbH & Co. KGaA, Weinheim

Subsequently, the decomposition of **4** was monitored by ^{1}H NMR spectroscopy by integration of key signals of the intermediate and final product. As can be seen in Table 1, the decomposition of **4** is significantly faster at more-basic pH values and elevated temperatures. These results can easily be rationalized by assuming that at a higher pH value, a large proportion of the intermediate is in the phenoxide form, which decomposes significantly faster than the analogous phenol.

Table 1: pH dependence of half-lives upon the self-fragmentation of **2**.[a]

pH	4.0	4.5	5.0	5.5	6.0	6.5
37 °C (min)	480	270	100	45	16	9
25 °C (min)	2800	–	–	–	–	45

[a] Determined by incubating prodrug **2** (80 nmol) and Jack Bean mannosidase (1.4 U) in deuterated 0.2 M phosphate/0.1 M citrate buffer (0.2 mL) at 37 °C or 25 °C in a NMR tube and measuring ^{1}H NMR spectra over time on a 600 MHz spectrometer.

For many applications, compounds such as **1** need to be cell permeable to inhibit intracellular glycosidases. Analysis of fetal calf serum (FCS), which is often used for culturing cells, revealed that it contains a significant amount of mannosidase activity. Thus, these mannosidases can unmask mannostatin A, which can then pass through the cell membrane to inhibit intracellular mannosidases. It was anticipated that *O*-acetylation of **1** and **2** to give **14** and **15**, respectively, would considerably improve the metabolic stability of the prodrug. Furthermore, it has been shown that *O*-acetylation of saccharides can facilitate cellular uptake.[39] Subsequently, intracellular esterases can cleave the acetyl esters revealing the saccharide, which can then interfere in the biosynthesis of oligosaccharides. FCS exhibits only very low levels of esterase activity therefore improving extracellular stability of acetylated carbohydrates. Thus, it was anticipated that compound **14** would be easily taken up by cells, and subsequent deacetylation by intracellular esterases would reveal **1**, which can then be hydrolyzed by an α-manmosidase to initiate the release of mannostatin A. To investigate whether **14** possesses intracellular activity, it was subjected to MDAY-D2 cells and the disappearance of polylactosamine monitored. It is known that the metastatic MDAY-D2 lymphoma cell line overexpresses the enzyme *N*-acetyl glucosaminyltransferase V (GnTV).[8] This enzyme adds an additional β1-6-linked *N*-acetylglucosamine moiety to Asn-linked oligosaccharides, which are subsequently extended by a polylactosamine chain. This increased branching has been observed in human breast, colon, and skin carcinomas and has been correlated with invasive and metastatic potential. Inhibition of the mannose-trimming enzyme, human Golgi α-mannosidase II (HGMII), which acts late in the *N*-glycan processing pathway, provides one route to blocking additional branching of *N*-linked oligosaccharides.[8] In this case, the biosynthetic precursor for GnTV is not formed and hence the polylactosamine chain cannot be appended. Thus, to investigate whether the acetylated prodrugs can inhibit intracellular Golgi mannosidase II, MDAY-D2 lymphoma cells were cultured in the presence of different concentrations of **14** and **15** for two days. Subsequently, the presence of polylactosamine linked to proteins was determined by analyzing cell lysates by Western blotting with a fluorescein-labeled PHA lectin.[40] Interestingly, at a concentration of 1 μM of **14**, a 50 % reduction in fluorescein labeling was observed, whereas compound **15** did not display any inhibitory activity (Figure 2).

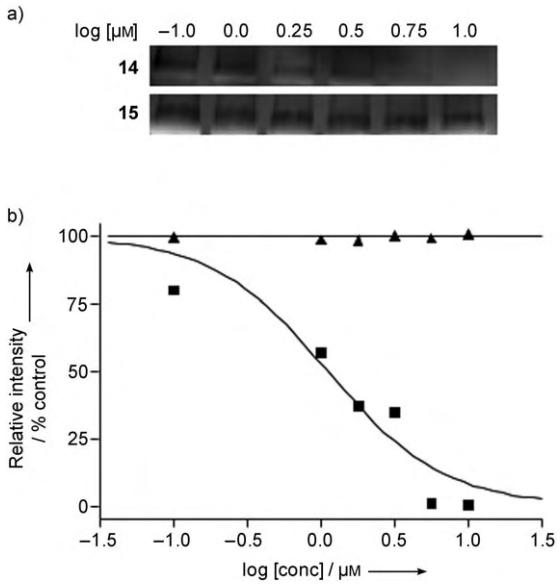


Figure 2. Inhibition of polylactosamine formation by compounds **14** and **15**. MDAY-D2 cells were cultured for 2 days in the absence (control) or presence of different concentrations of compounds **14** (■) or **15** (▲). a) Cellular proteins (10 μg) were subjected to SDS-PAGE and polylactosamine was visualized by using a fluorescein-labeled L-PHA lectin. b) Fluorescence bands were scanned by laser beam densitometry, and the relative intensity depicted.

In conclusion, a feedback prodrug approach in which a glycosidase inhibitor is released by the targeted glycosidase offers an attractive approach for enhancing the selectivity of a glycosidase inhibitor. Another advantage of this type of prodrug is that only the amount of compound required for complete inhibition of the targeted enzyme is released. It is to be expected that chemical modification of a lead compound in combination with a feedback prodrug formulation may make it easier to develop glycosidase inhibitors as safe therapeutics. Furthermore, efforts are underway to modify the linker region of the feedback prodrug, to increase the catalytic efficiency of enzymatic hydrolysis, and to increase the rate of self-fragmentation. Also, the possibility of using feedback prodrugs for other glycosidases, proteases, and kinases is being explored.

Received: March 1, 2006
Revised: May 12, 2006
Published online: July 17, 2006

Keywords: glycosidases · inhibitors · mannosidases · prodrugs · selectivity

 © 2006 Wiley-VCH Verlag GmbH & Co. KGaA, Weinheim

[1] A. Varki, *Glycobiology* **1993**, *3*, 97.
[2] R. A. Dwek, *Chem. Rev.* **1996**, *96*, 683.
[3] T. Kolter, K. Sandhoff, *Angew. Chem.* **1999**, *111*, 1632; *Angew. Chem. Int. Ed.* **1999**, *38*, 1532.
[4] J. W. Dennis, M. Granovsky, C. E. Warren, *BioEssays* **1999**, *21*, 412.
[5] M. M. Fuster, J. D. Esko, *Nat. Rev. Cancer* **2005**, *5*, 526.
[6] D. H. Dube, C. R. Bertozzi, *Nat. Rev. Drug Discovery* **2005**, *4*, 477.
[7] J. W. Dennis, M. Granovsky, C. E. Warren, *Biochim. Biophys. Acta* **1999**, *1473*, 21.
[8] P. E. Goss, M. A. Baker, J. P. Carver, J. W. Dennis, *Clin. Cancer Res.* **1995**, *1*, 935.
[9] V. H. Lillelund, H. H. Jensen, X. F. Liang, M. Bols, *Chem. Rev.* **2002**, *102*, 515.
[10] A. Berecibar, C. Grandjean, A. Siriwardena, *Chem. Rev.* **1999**, *99*, 779.
[11] N. Asano, R. J. Nash, R. J. Molyneux, G. W. J. Fleet, *Tetrahedron: Asymmetry* **2000**, *11*, 1645.
[12] T. D. Heightman, A. T. Vasella, *Angew. Chem.* **1999**, *111*, 794; *Angew. Chem. Int. Ed.* **1999**, *38*, 750.
[13] M. vonItzstein, R. J. Thomson, *Curr. Med. Chem.* **1997**, *4*, 185.
[14] N. Asano, *Glycobiology* **2003**, *13*, 93R.
[15] R. Perfetti, P. S. Barnett, R. Mathur, J. M. Egan, *Diabetes/Metab. Rev.* **1998**, *14*, 207.
[16] M. Von Itzstein, W. Y. Wu, G. B. Kok, M. S. Pegg, J. C. Dyason, B. Jin, T. V. Phan, M. L. Smythe, H. F. White, S. W. Oliver, P. M. Colman, J. N. Varghese, D. M. Ryan, J. M. Woods, R. C. Bethell, V. J. Hotham, J. M. Cameron, C. R. Penn, *Nature* **1993**, *363*, 418.
[17] M. vonItzstein, J. C. Dyason, S. W. Oliver, H. F. White, W. Y. Wu, G. B. Kok, M. S. Pegg, *J. Med. Chem.* **1996**, *39*, 388.
[18] C. U. Kim, W. Lew, M. A. Williams, H. T. Liu, L. J. Zhang, S. Swaminathan, N. Bischofberger, M. S. Chen, D. B. Mendel, C. Y. Tai, W. G. Laver, R. C. Stevens, *J. Am. Chem. Soc.* **1997**, *119*, 681.
[19] W. X. Li, P. A. Escarpe, E. J. Eisenberg, K. C. Cundy, C. Sweet, K. J. Jakeman, J. Merson, W. Lew, M. Williams, L. J. Zhang, C. U. Kim, N. Bischofberger, M. S. Chen, D. B. Mendel, *Antimicrob. Agents Chemother.* **1998**, *42*, 647.
[20] P. Chand, P. L. Kotian, A. Dehghani, Y. El-Kattan, T. H. Lin, T. L. Hutchison, Y. S. Babu, S. Bantia, A. J. Elliott, J. A. Montgomery, *J. Med. Chem.* **2001**, *44*, 4379.
[21] G. Godin, P. Compain, O. R. Martin, K. Ikeda, L. Yu, N. Asano, *Bioorg. Med. Chem. Lett.* **2004**, *14*, 5991.
[22] F. M. Platt, G. R. Neises, R. A. Dwek, T. D. Butters, *J. Biol. Chem.* **1994**, *269*, 8362.
[23] F. M. Platt, G. R. Neises, G. B. Karlsson, R. A. Dwek, T. D. Butters, *J. Biol. Chem.* **1994**, *269*, 27108.
[24] H. S. Overkleeft, G. H. Renkema, J. Neele, P. Vianello, I. O. Hung, A. Strijland, A. M. van der Burg, G. J. Koomen, U. K. Pandit, J. Aerts, *J. Biol. Chem.* **1998**, *273*, 26522.
[25] C. Y. Wu, C. F. Chang, J. S. Y. Chen, C. H. Wong, C. H. Lin, *Angew. Chem.* **2003**, *115*, 5119; *Angew. Chem. Int. Ed.* **2003**, *42*, 4661.
[26] L. L. Johnson, T. A. Houston, *Tetrahedron Lett.* **2002**, *43*, 8905.
[27] I. Robina, A. J. Moreno-Vargas, J. G. Fernandez-Bolanos, J. Fuentes, R. Demange, P. Vogel, *Bioorg. Med. Chem. Lett.* **2001**, *11*, 2555.
[28] R. Lysek, C. Schutz, P. Vogel, *Helv. Chim. Acta* **2005**, *88*, 2788.
[29] T. D. Butters, R. A. Dwek, F. M. Platt, *Curr. Top. Med. Chem.* **2003**, *3*, 561.
[30] A. B. Pardee, G. P. V. Reddy, *Gene* **2003**, *321*, 17.
[31] S. B. King, B. Ganem, *J. Am. Chem. Soc.* **1994**, *116*, 562.
[32] F. M. H. de Groot, W. J. Loos, R. Koekkoek, L. W. A. van Berkom, G. F. Busscher, A. E. Seelen, C. Albrecht, P. de Bruijn, H. W. Scheeren, *J. Org. Chem.* **2001**, *66*, 8815.
[33] S. Ogawa, T. Morikawa, *Bioorg. Med. Chem. Lett.* **2000**, *10*, 1047.
[34] S. Ogawa, Y. M. Yu, *J. Chem. Soc. Chem. Commun.* **1991**, 890.
[35] T. Suami, Y. Sakota, K. Tadano, S. Nishiyam, *Bull. Chem. Soc. Jpn.* **1971**, *44*, 2222.
[36] J. C. Wilson, M. J. Kiefel, D. I. Angus, M. von Itzstein, *Org. Lett.* **1999**, *1*, 443.
[37] B. Li, S. P. Kawatkar, S. George, H. Strachan, R. J. Woods, A. Siriwardena, K. W. Moremen, G. J. Boons, *ChemBioChem* **2004**, *5*, 1220.
[38] A. D. Elbein, *FASEB J.* **1991**, *5*, 3055.
[39] A. K. Sarkar, T. A. Fritz, W. H. Taylor, J. D. Esko, *Proc. Natl. Acad. Sci. USA* **1995**, *92*, 3323.
[40] J. W. Dennis, K. Koch, S. Yousefi, I. Vanderelst, *Cancer Res.* **1990**, *50*, 1867.
[41] Treatment of compound **1** with cell lysate in the presence of the mannosidase inhibitors swainsonine and kifunensine did not lead to significant decomposition, therefore indicating that proteases or other enzymes do not decompose the prodrug.

 © 2006 Wiley-VCH Verlag GmbH & Co. KGaA, Weinheim

Organic Chemistry

DOI: 10.1002/anie.200600881

The Core and Most Useful Molecules in Organic Chemistry**

*Kyle J. M. Bishop, Rafal Klajn, and Bartosz A. Grzybowski**

On the most abstract level, the millions of known chemicals and reactions constituting organic chemistry can be represented as a complex network,[1] in which compounds correspond to nodes and reactions to directed connections between these nodes. We have recently shown[2] that such a network has a scale-free topology similar to that of the World Wide Web and that by analyzing its time evolution, it is possible to derive statistical laws that describe and also predict how and which types of molecules are/will be synthesized. The major limitation of this statistical approach is that it provides information only about the average properties of molecules and the overall network structure—at the same time, it does not tell us how specific chemicals are arranged or what roles they play in the network of chemistry. Herein, we address these important issues with the aim of identifying molecules

[*] K. J. M. Bishop, R. Klajn, Prof. Dr. B. A. Grzybowski
Department of Chemical and Biological Engineering and
Northwestern Institute of Complexity
Northwestern University
2145 Sheridan Rd., Evanston, IL 60208 (USA)
Fax: (+1) 847-491-3728
E-mail: grzybor@northwestern.edu

[**] B.A.G. gratefully acknowledges financial support from the Camille and Henry Dreyfus New Faculty Awards Program, the NSF CAREER, and the 3M Awards. K.J.M.B. was supported by an NSF graduate fellowship.

Supporting information for this article is available on the WWW under http://www.angewandte.org or from the author.

WILEY InterScience DISCOVER SOMETHING GREAT
© 2006 Wiley-VCH Verlag GmbH & Co. KGaA, Weinheim

central to and most useful in organic synthesis. By using mathematical tools from network theory and statistical physics, we demonstrate that 1) there exists a small set of strongly connected, chemically diverse substances (the "core") from which the majority of other known organic compounds (the "periphery") can be made in three or fewer synthetic steps, and that 2) this central structure is surrounded by small "islands" that do not connect either to the core or to the periphery. Furthermore, by defining the usefulness of a compound as proportional to the number of other compounds that can be made from it, we develop Monte Carlo (MC) search algorithms to identify small optimal sets of maximally useful chemicals. Aside from purely scientific interest, the knowledge of such "most useful" collections of compounds should be of practical value to specialty chemical companies, which could use it to optimize product selection and cater for the most diverse group of chemical customers.

Analysis was performed on data stored in the Beilstein Database (BD),[3] which is the largest—albeit not without omissions—repository of organic reactions reported in the literature from 1779 to the present. The data were pruned as described previously[2] to remove catalysts, solvents, substances that participated in no reactions, and reactions that lacked either reactants or products (that is, "half reactions"). Duplicate reactions, that is, reactions with identical reactants and products, were considered only once and were characterized by the date of the earliest publication. This selection procedure left 5.9 million substances and 6.5 million reactions.[4]

The final dataset was converted into a directed network by connecting reactants and products by directed edges (Figure 1a). We implemented and tested several wiring schemes to ascertain that the results of our analysis were not artifacts of the network construction, but captured the true architecture of organic chemistry. The most condensed representation was one in which only the heaviest reactant and the heaviest product of each reaction were retained and connected by a single directed edge. This so-called one-to-one representation is chemically the most intuitive, and it reflects the fact that small reagents usually play only an auxiliary role when transforming larger molecules (Figure 1a, top). At the same time, it excluded some real (albeit rare) connections in the network—for example, in cases when an auxiliary substance (such as a protective group) is more massive than the primary reactant, or when the lighter of two products is the actual synthetic target. These connections were accounted for in an all-inclusive (but clearly redundant) scheme, in which all reactants were connected to all products irrespective of mass (all-to-all; Figure 1a, bottom). Finally, intermediate schemes were also examined in which reactants and products within a given percentage of the mass of the heaviest reactant/product in a reaction were retained and connected (Figure 1a, middle). As all schemes gave qualitatively similar

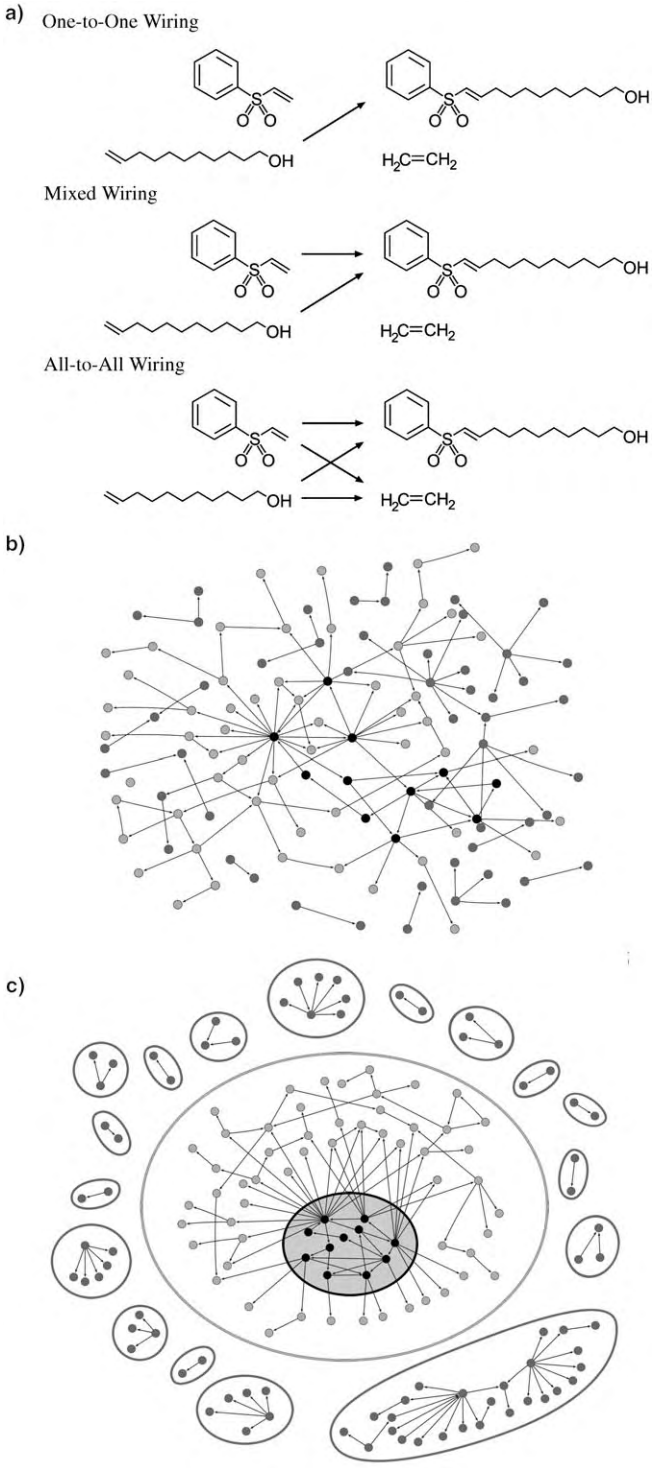


Figure 1. Wiring schemes and network structure. a) Illustration of the three possible wiring schemes as applied to a ruthenium-catalyzed olefin cross-metathesis reaction.[21] In this example, the "mixed-wiring" scheme includes products/reactants within 5% of the heaviest reactant/product; because the molecular weight of phenyl vinyl sulfone is within 2% of that of 10-undecen-1-ol, it is included. On the other hand, ethylene is 91% lighter than (*E*)-11-(phenylsulfonyl)-10-undecen-1-ol and is not wired. b) Schematic representation of the organic-chemistry network based on the reactions reported before 1840. Even with the nodes appropriately color-coded, it is hard to decipher their global roles in this simple network. c) Analysis based on the algorithms described in the text and in the Supporting Information allows identification of the network's major topological components: the core (black), the periphery (light gray), and the islands (dark gray). Although the current (year 2004) organic-chemistry network is several tens of thousands times larger, its qualitative features are similar.

 © 2006 Wiley-VCH Verlag GmbH & Co. KGaA, Weinheim

results, we chose to base our further discussion on the simplest one-to-one network and use other representations only when they illustrate some specific points more clearly.

To identify the core of organic chemistry, we first searched for all strongly connected components (SCCs) present in the network. Mathematically, an SCC of a directed graph is defined as a maximal set of nodes (herein, molecules) such that there exists a path (that is, a sequence of reactions) between any two of these nodes.[5] In our case, an SCC corresponds to a tightly knit "cluster" of molecules all connected by synthetic pathways.[6] Searches performed according to a depth-first search (DFS) algorithm (see the Supporting Information for definitions and algorithmic details) identified all possible SCCs, whose size distribution obeys—with one exception—a power-law relation $f(x) \approx x^{-3.8}$, where $f(x)$ is the frequency of observation of an SCC of size x (Figure 2a). The exception itself is a very notable one and corresponds to an SCC that is thousands of times larger (206993 substances) than the next-largest cluster (79 substances). Although this so-called "giant" SCC contains only 3.5% of all organic substances, these substances are usually more highly connected, are involved in over 35% of known reactions, and give rise to more than 60% ($\approx$3.6 million) of known organic chemicals.[7] For these reasons, this collection of compounds can be considered the "core" of organic chemistry.

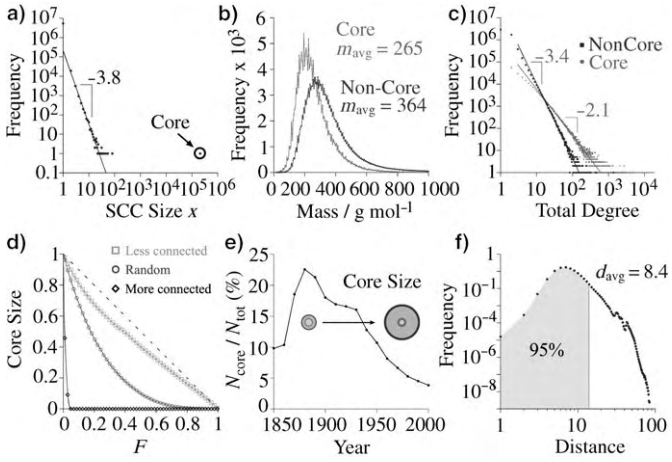


Figure 2. Properties of the core of the organic-chemistry network. The negative numbers give the slopes of the best-fit straight lines. a) Size distribution of the SCCs present in the network. The core corresponds to a giant SCC that is more than three orders of magnitude larger than the next-largest cluster. b) Normalized mass distributions for molecules found in the core and for those outside it. c) Distributions of the total degree (that is, the number of both incoming and outgoing connections) position of the bracketed text of molecules for core and noncore substances. d) Relative size of the core as a function of the fraction F of nodes (and their associated connections) removed. The rate of core "disintegration" depends on the types of nodes that are removed; for example, least-connected nodes (□), highest-connected nodes (◇), or nodes chosen at random (○). e) Evolution of the relative core size from 1850 to 2000. Over the past 125 years, the periphery has been growing larger at the expense of the core. f) Normalized frequency distribution for the synthetic distance (that is, the number of reaction steps) between any two nodes in the core. The average distance between any two molecules in the core is 8.4, and 95% of connections are fewer than 15 steps.

The core has several important characteristics. First, the molecules it contains are on average significantly lighter (average molecular weight, $MW_{avg} = 265\ g\,mol^{-1}$) than those outside it ($MW_{avg} = 364\ g\,mol^{-1}$; Figure 2b), an observation that is perhaps not surprising since, as already stated, the core molecules are precursors of more complex/massive[8] compounds. Second, the core is not simply a collection of highest-connected nodes in the network. Although it does contain the vast majority of such nodes, it also has many poorly connected chemicals (for example, 50% of the nodes have fewer than five connections; Figure 2c). The role of these chemicals is to keep the "traffic" throughout the core open, so that one can connect any two of its members. Third, all of the compounds in the core matter for its integrity and tight-knit structure, in the sense that the removal of any of them shrinks and fragments the core rapidly. Had some molecules been unimportant/redundant, their hypothetical removal would reduce the core size (defined by the number of substances it comprises, N_{core}) only linearly; in other words, if the fraction F of the nodes was removed, N_{core} would decrease by $\Delta N_{core} = N_{core} F$. In reality (Figure 2d), the core shrinks and fragments faster than linearly with F, even if only the lowest-connected nodes are removed.

Although the sizes of both the core and the entire network (N_{tot}) have been growing exponentially with time, the relative core size (N_{core}/N_{tot}) has evolved nonmonotonically (Figure 2e). Until the turn of the twentieth century it slowly increased until, in 1880, it reached 22% of the then known chemical (structural) space; subsequently, it has been steadily decreasing to the present 3.5%. It appears that once chemists have learned how to make and wire the key core molecules, the emphasis has been increasingly on the exploration of the new structural space.

For such an exploration from the core into the periphery to be efficient, the former should contain a diverse set of building blocks—and, indeed, it does. The diversity can be studied either by inspecting the molecules directly (see the Supporting Information) or by topological measures. The latter approach is based on the observation that if two molecules can be connected by a short synthetic pathway (for example, one or two steps) they are likely to be structurally similar (but see reference [9]). If the distance is long, the resemblance between the final and the initial molecules should be, on average, minimal. By performing a set of breadth-first searches (BFSs) starting at each node in the core, we found that the average synthetic distance between core molecules is nine steps and that 95% of all paths are fewer than 15 steps (Figure 2f). While this number might not look high, it is three times larger than the average number of steps needed to make any of the millions of compounds reachable from the core (see below).

We conclude our discussion of the core's properties by noting that it contains the majority of the most important industrial chemicals—of the top 200,[10] over 70% (145) are found in the core. To summarize, the core is compact, wired, yet chemically diverse, and contains important chemicals from which the majority of known organic substances can be made.

The region in the network outside the core can be subdivided into a large periphery, which contains molecules

 © 2006 Wiley-VCH Verlag GmbH & Co. KGaA, Weinheim

that can be synthesized from core substrates, and smaller isolated islands not reachable from the core. Although quantitative details of the subdivision depend on the network-wiring scheme, it can be estimated that the periphery contains at least 3.6 million chemicals, and the islands not more than 1.2 million compounds. A lower bound on the number of island compounds is 270000, as estimated using the all-to-all wiring scheme, which allows identification of islands that are not reachable even by ineffective or "unchemical" reactions, and are thus truly synthetically isolated.

The average distance from the core to any molecule in the periphery is only three steps, and 95% of the peripheral substances lie within seven steps from the core (Figure 3a,b). As one moves away from the core, the average mass and/or complexity[8] of molecules increase linearly with distance (measured in synthetic steps) before leveling off to just over 700 g mol^{-1} after 15 steps (that is, after reaching over 99% of the periphery; Figure 3c). The average "in" and "out" connectivities of compounds in the periphery are both close to unity regardless of their distance from the core. At the same time, there are some molecules that have significant "out" branching, while most molecules (86%) have only one incoming connection (Figure 3d). This property implies that the periphery has a treelike structure (illustrated in Figure 3a). We note that the trees emanating from the various regions of the core do overlap (Figure 3e), thus creating a nontrivial problem of identifying optimal sets of core molecules (see below).

Unconnected to the core/periphery are the molecules in the islands. The islands are generally small (fewer than four molecules on average), and their most connected "hubs" usually correspond to either complex natural products or

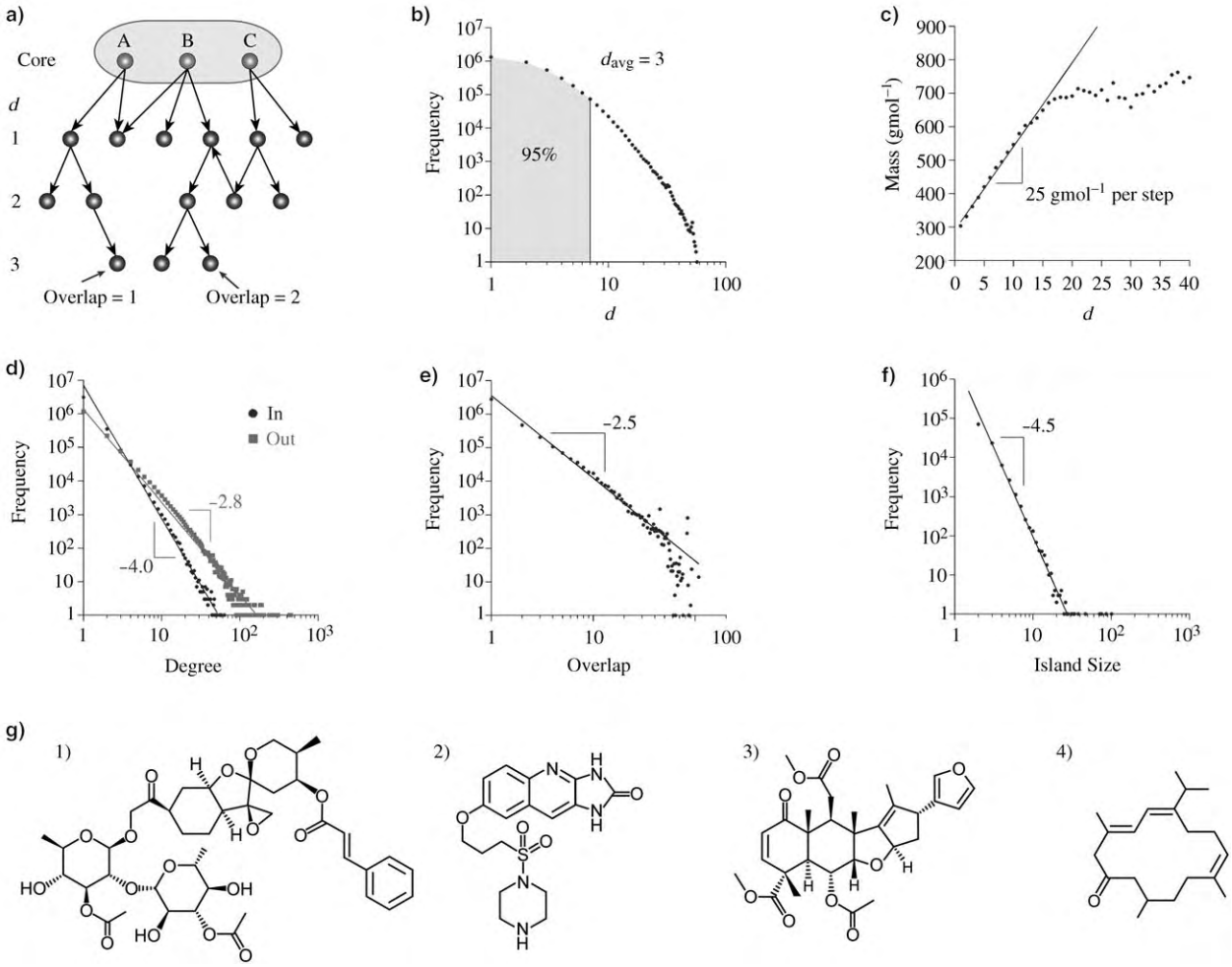


Figure 3. Properties of the network's periphery and islands. a) Schematic illustration of the core (neglecting internal connections) and periphery. The distance *d* from the core represents the shortest synthetic pathway from any node in the core to a given node in the periphery. The "overlap" of a molecule in the periphery is defined as the number of substrates in the core from which the given molecule can be synthesized. b) Number of node in the periphery as a function of their distance from the core. c) Average molecular mass of compounds in the periphery as a function of their distance from the core. d) In and out degree distributions for all molecules in the periphery. In degree is the number of reactions in which a molecule is a product; out degree gives the number of reactions in which a molecule is a substrate. e) Distribution of synthetic overlap for all molecules in the periphery. f) Size distribution of islands found in the all-to-all wired network. The average island includes fewer than three molecules. g) Examples of highly connected island molecules, whose total syntheses have either been reported—1) phyllanthoside[11,12], 2) a phosphodiesterase inhibitor[11,12]—or not described in the literature—3) nimbin[13,14], 4) a diterpenoid from the Caribbean gorgonian *E. calyculata*.[16].

 © 2006 Wiley-VCH Verlag GmbH & Co. KGaA, Weinheim

specialized substances (for example, non-natural isotopes). We wish to emphasize that the fact that these compounds are found in isolated parts of the network does not necessarily mean that they *cannot* be made from the core/periphery substances, but rather that they have *not yet* been connected to them. This could be either 1) because pertinent reactions have not yet been tried and/or deposited in the database, or 2) because achieving a connection to the core is difficult enough to have thwarted previous attempts.

The first scenario is scientifically trivial and reflects the imperfections of the database. Illustrative examples include phyllanthoside, (Figure 3g 1; the 11th most connected hub of the island molecules) and a phosphodiesterase inhibitor (Figure 3g 2; the 81st most connected hub of the island molecules), whose total syntheses from core substances have been reported[11,12] but are not included in the BD. The second scenario is more interesting, as it suggests that an island compound is a challenging synthetic target. For instance, while both nimbin[13,14] (a complex terpenoid from *Melia azadirachta* and an ecdysone 20-monooxygenase inhibitor;[15] Figure 3g 3) and a diterpenoid from the Caribbean gorgonian *Eunicea calyculata*[16] (Figure 3g 4) have been subjects of several chemical studies, no total syntheses of these compounds have been reported.[17]

Aside from satisfying purely scientific curiosity, knowledge of the network's topological structure can be of practical value. Consider a company that manufactures specialty chemicals. While it probably could not supply all the 206993 core compounds, it might be interested in optimizing its limited product line (say, comprising a few hundred compounds) in such a way that the compounds it sells would allow the making of a maximal number of other chemicals. We have developed a simulated annealing MC algorithm that allows such "most useful" sets of molecules to be found.

Briefly, an initial set of desired size M is first chosen from among the most connected core molecules. We note that such a trial solution based on "local" connectivity is not an optimal one, as the trees propagating from the chosen compounds into the periphery often overlap (see Figure 3e). The optimization procedure is based on the Metropolis algorithm frequently used in statistical physics[18,19] for finding global energetic minima of ensembles with very many degrees of freedom. In our case, the energy is replaced by the "usefulness" function defined as $U=(N_{max}-N(M))/N_{max}$, where $N(M)$ is the number of compounds reached from a given set of size M, and N_{max} is the total number of substances in the periphery. With this formulation, U ranges from zero to one and, importantly, is minimal for the optimal set of core substances. For a given set, U is calculated by performing a DFS from each of its nodes into the periphery (see the Supporting Information for details).

At each MC move, a molecule from the current set is exchanged at random, and the values of U for the old and the new sets are compared. If the move is favorable (that is, $\Delta U = U_{new}-U_{old}<0$), it is accepted unconditionally. If, on the other hand, $\Delta U>0$, it is accepted with conditional Boltzmann probability $\exp(-\Delta U/T)$, where T is a control parameter analogous to the "temperature" of the system. During the search, parameter T is decreased exponentially according to $T=T_I\exp(-\log(T_I/T_F)(s/S))$, where T_I and T_F are the initial and final "temperatures", respectively, s is the number of moves taken thus far, and S is the total number of moves in the MC run (typically, millions to tens of millions). This so-called simulated annealing procedure[19] allows the exploration of maximally diverse chemical space in the early stages of the search (when T is high), while preventing the "escape" from the optimal solution ultimately found at low values of T.

Simulations based on this algorithm allowed the identification of most useful sets of various sizes (Figure 4a). The

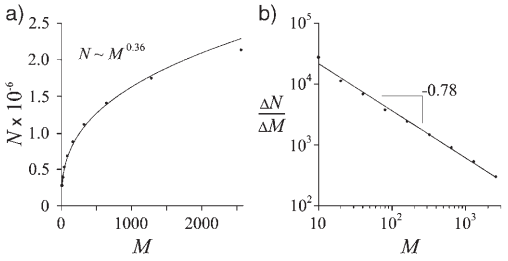


Figure 4. Optimal sets of most useful molecules. a) The number of nodes N reachable from an optimal set of core nodes as a function of the set size M. b) Closely connected to the relationship in (a), the gain rate—defined as the number of new nodes reached (ΔN) per increase in the set size (ΔM)—decreases according to a power law with increasing set size M. This relationship could help chemical companies to find an optimal balance between the costs (likely scales with M) and revenues (likely scales with N) associated with their product line.

number of substances (N) that can be made from M core molecules increases as $N(M)\approx M^{0.36}$. Irrespective of their size, the sets contained diverse and widely applicable chemicals. For example, the set of size $M=300$ (our estimate of a typical offer of a small chemical company) contained common chemicals for various functionalization schemes, heterobifunctional reagents, protective-group-introducing agents, important natural products, biologicals, and more. The specific categories are summarized in Table 1 and the accompanying structures are included in the Supporting Information. We suggest that these most useful compounds should certainly be considered for inclusion in the product line of any fine-chemicals company.[20] In addition, we note that the list reveals certain interesting facts about the functionalities that organic chemists prefer to use in their syntheses.

For instance, although incorporation of a benzoyl moiety can be accomplished through a variety of functional groups (for example, aldehyde, acyl chloride, carboxy, nitrile, anhydride), aromatic aldehydes are the most abundant group of the top-300 core molecules (21 hits) used for this task. This finding can be rationalized based on the fact that benzaldehydes are reactive yet stable. In contrast, the reactivity of benzoic acids, benzoic anhydrides, and nitriles (3, 3, and 0 hits, respectively) is considerably lower, while benzoyl chlorides (8 hits) are too reactive and thus harder to handle. A similar, common-chemical-sense example is that of alkyl halides, which are represented in the core by bromides (9 hits;

 © 2006 Wiley-VCH Verlag GmbH & Co. KGaA, Weinheim

Table 1: Categorization of the optimal set of 300 core substrates.

Compounds[a]	Count	List no.
simple aromatic compounds (32%)		
aromatic aldehydes (+ *3 in category* **)	18	1–18
anilines (+ *1 in* **)	12	19–30
benzoyl chlorides	8	31–38
benzoic acids and their derivatives (+ *1 in* **)	7	39–45
phenols (+ *2 in* **)	6	46–51
α-haloacetophenones	6	52–57
benzyl halides	5	58–62
sulfonyl chlorides	5	63–67
unsubstituted aromatic compounds	4	68–71
chloronitrobenzenes	4	72–75
acetophenones	4	76–79
other reactive di- or polysubstituted benzenes**	4	80–83
other monosubstituted benzenes	13	84–96
simple aliphatic compounds (27%)		
small, bifunctional molecules	13	97–109
simple reagents useful in organic synthesis	12	110–121
very simple small molecules	11	122–132
n-bromoalkanes	9	133–141
aliphatic and heterocyclic amines	7	142–148
α,ω-dibromoalkanes	6	149–154
acyl chlorides	6	155–160
anhydrides	6	161–166
alkyl iodides	5	167–171
other bromides	3	172–174
orthoesters	2	175–176
specialized reagents (23%)		
1,3-dioxoanions or their precursors	16	177–192
protective-group introduction: silyl (8), trityl (3)	11	193–203
Wittig reagents or their precursors	10	204–213
Grignard reagents	6	214–219
α-halo/pseudohaloesters	6	220–225
chlorocarbonates	5	226–230
Michael acceptors	4	231–234
phosphonic chlorides, chlorophosphines	4	235–238
quinones	3	239–241
reagents for peptide synthesis	3	242–244
natural compounds and their building blocks (7%)		
carbohydrates and protected carbohydrates	9	245–253
protected amino acids	6	254–259
DNA building blocks	2	260–261
others (antibiotics, alkaloids, steroids, neurotransmitters)	4	262–265
simple inorganic compounds (2%)	5	266–270
others (10%)	30	271–300

[a] The two stars indicate the category other reactive di- or polysubstituted benzenes.

reactive yet stable) and iodides (5 hits; too reactive), whereas there are 0 hits for chlorides (weakly reactive). Finally, we observe that although nearly all of the "top" compounds are achiral (with the notable exception of natural products), many of them are prochiral (for example, benzaldehydes, 1,3-dicarbonyl compounds) and well-suited for the introduction of chirality through enantioselective addition/substitution reactions.

In summary, we have identified and analyzed major substructures within the network of organic chemical reactions, and shown that the analysis of this network can aid the selection of sets of most useful synthetic substrates. This study and the one preceding it probably exhaust the capabilities of our purely topological approach; the uncovering of more interesting facts about the structure of chemistry will require additional (and downloadable) data, such as detailed structural information, reaction stoichiometries, and yields. With such information at hand, one could look into particular subfields of organic chemistry, select the most efficient pathways, and maybe even draw conclusions about reaction thermodynamics by comparing/studying various cycles/loops in the network. Such analyses, however, will have to rely on databases that report more details about the substances and reactions one wishes to study. We hope that with the rapid progress of information technology such databases will be available in the near future.

Received: March 7, 2006
Revised: May 11, 2006
Published online: July 11, 2006

Keywords: history of science · network theory · organic chemistry · synthetic methods

[1] R. Albert, A. L. Barabasi, *Rev. Mod. Phys.* **2002**, *74*, 47.
[2] M. Fialkowski, K. J. M. Bishop, V. A. Chubukov, C. J. Campbell, B. A. Grzybowski, *Angew. Chem.* **2005**, *117*, 7429; *Angew. Chem. Int. Ed.* **2005**, *44*, 7263.
[3] MDL Crossfire Beilstein Database (see the Supporting Information for details).
[4] Stoichiometry and reaction yields were not considered as they were reported for only a few percent of database entries.
[5] A. V. Aho, J. E. Hopcroft, J. D. Ullman, *Data Structures and Algorithms*, Addison-Wesley, Reading, MA, **1983**.

 © 2006 Wiley-VCH Verlag GmbH & Co. KGaA, Weinheim

[6] Note the importance of directed connections; an undirected network would have no chemical meaning, and the core (that is, the giant SCC) could not be defined.
[7] With the most permissive all-to-all scheme, the percentage is 80%; with the 20-% mixed scheme it is 70%.
[8] Molecular "complexity" scales with molecular mass; see: T. K. Allu, T. I. Oprea, *J. Chem. Inf. Model.* **2005**, *45*, 1237.
[9] We stress that this is true only in a statistical sense, and that ingenious counterexamples can be found where only one synthetic step changes the molecular skeleton extensively (see the elegant tandem and domino reactions shown in the Supporting Information).
[10] March 7, 2005 chemical prices, Chemical Market Reporter, http://www.chemicalmarketreporter.com.
[11] N. A. Meanwell, P. Hewawasam, J. A. Thomas, J. J. K. Wright, J. W. Russell, M. Gamberdella, H. J. Goldenberg, S. M. Seiler, G. B. Zavoico, *J. Med. Chem.* **1993**, *36*, 3251.
[12] A. B. Smith, M. Fukui, H. A. Vaccaro, J. R. Empfield, *J. Am. Chem. Soc.* **1991**, *113*, 2071.
[13] V. Kabaleeswaran, S. S. Rajan, G. Gopalakrishnan, G. Suresh, T. R. Govindachari, *J. Chem. Crystallogr.* **1997**, *27*, 731.
[14] N. S. Narasimhan, *Chem. Ind.* **1957**, 661.
[15] M. J. Mitchell, S. L. Smith, S. Johnson, E. D. Morgan, *Arch. Insect Biochem. Physiol.* **1997**, *35*, 199.
[16] J. H. Shin, W. Fenical, *J. Org. Chem.* **1991**, *56*, 1227.
[17] This fact was verified by cross-checking other literature sources including ChemAbstract and SciFinder.
[18] N. Metropolis, A. Rosenbluth, M. Rosenbluth, A. Teller, E. Teller, *J. Chem. Phys.* **1953**, *21*, 1087.
[19] S. Kirkpatrick, C. D. Gelatt, M. P. Vecchi, *Science* **1983**, *220*, 671.
[20] Inclusion in the "optimal" set is based on the usefulness alone and does not take into account the chemical diversity among the chosen molecules; it is thus possible that some similar chemicals are included (see the Supporting Information). We suggest that for practical/industrial applications, the optimal sets of a few hundred molecules obtained from the usefulness analysis might be further scrutinized for chemical diversity. Alternatively, the usefulness function itself could be modified to simultaneously maximize both the usefulness and the diversity. Such a procedure, however, would be significantly more time-consuming as it would require the analysis of structural details of all molecules in the network.
[21] A. Michrowska, M. Bieniek, M. Kim, R. Klajn, K. Grela, *Tetrahedron* **2003**, *59*, 4525.

 © 2006 Wiley-VCH Verlag GmbH & Co. KGaA, Weinheim

Host–Guest Systems

DOI: 10.1002/anie.200601665

Solid-State Self-Inclusion: The Missing Link**

*Gareth O. Lloyd, Jo Alen, Martin W. Bredenkamp, Elise J. C. de Vries, Catharine Esterhuysen, and Leonard J. Barbour**

Cocrystallization and polymorphism are two of the most well-documented paradigms in the fields of solid-state inclusion chemistry and crystal engineering. Such concepts are often open to interpretation, as evidenced by the recent debate regarding the differences between solvates, pseudopolymorphs, and cocrystals.[1] Self-inclusion (or, alternatively, self-hosting) in the solid state has been suggested by several authors as a distinct paradigm in supramolecular host–guest chemistry.[2] In considering the literature regarding the concept of self-inclusion, it immediately becomes clear that this topic is currently highly subjective. However, in view of the various cases that have been advanced to date as examples of self-inclusion, it is now possible to identify different levels of the phenomenon. Thus, to forestall future disagreement, it is useful to now consolidate the issue in a rational fashion and to supply the "missing piece of the puzzle".

In order of increasing constraints on interpretative freedom, the levels of solid-state self-inclusion can be listed and rationalized as follows (note that the term "molecule" is used loosely and can be substituted by "supramolecule"):

a) Any structure with $Z' = 1$. Each molecule is surrounded by like molecules and is therefore self-included.
b) Any molecular crystal with $Z' > 1$.[3] As with (a), each molecule is surrounded by other molecules of the same kind and the designation of a crystallographically unique molecule as either the host or the guest is arbitrary.[4]
c) Interpenetration or weaving of two or more hydrogen-bonded[5] or coordination[6] frameworks. Each framework "hosts" at least one other and is thus simultaneously both a host and a guest.
d) A molecular crystal in which $Z' > 1$ with the distinction between host and guest justified according to accepted

[*] G. O. Lloyd, Dr. M. W. Bredenkamp, Dr. E. J. C. de Vries, Dr. C. Esterhuysen, Prof. L. J. Barbour
Department of Chemistry
University of Stellenbosch
7602 Matieland (South Africa)
Fax: (+27) 21-808-3849
E-mail: ljb@sun.ac.za
J. Alen
Department of Chemistry
Katholieke Universiteit Leuven
Celestijnenlaan 200F, 3001 Heverlee (Belgium)

[**] We acknowledge the National Research Foundation (South Africa) for financial support and the Central Analytical Facility of the University of Stellenbosch for access to instrumentation.

Supporting information for this article is available on the WWW under http://www.angewandte.org or from the author.

WILEY InterScience DISCOVER SOMETHING GREAT
© 2006 Wiley-VCH Verlag GmbH & Co. KGaA, Weinheim

norms,[7] but without a documented example of the same host framework with another guest.

e) A molecular crystal in which $Z' > 1$ and the identical host framework is precedented by at least one other structure with a different guest.

In discussing the above categories in turn, we concede that it is not always possible to completely eliminate subjectivity as the assignment of "host" and "guest" is generally not immune to the liberties of interpretation. Herein, we adhere to the suggestion by Cram that a host can be identified as a molecule or supramolecular motif that possesses convergent binding sites whereas a guest binds divergently.[7] It should be noted that binding may occur by means of many types of intermolecular interactions, including weak dispersive forces, such as van der Waals contacts.

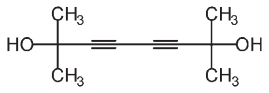
Clearly (a) and (b) are cases of reductio ad absurdum and require no further discussion (namely, because any structure qualifies as self-inclusion under one of these two categories). Although the interpenetrated and interweaved frameworks[5,6] of category (c) host one another, it is not possible to unequivocally distinguish between the host and guest in such systems (for example, the structure of pure selenourea).[2c] On the other hand, identical molecules can be viewed as fulfilling two distinct roles in the structure for (d) and (e). This observation is well illustrated in a report by Bishop and Dance of a self-included alicyclic diol,[2a] in which molecules of the same kind can be assigned as either the host or guest according to Cram. However, this system must be placed in category (d) as there is no evidence that the same host framework can support the inclusion of a different guest.

In isolated examples, it is possible that a system can appear to possess characteristics of more than one category. Indeed, to illustrate the vagaries of interpretation, 4,4-bis(4-hydroxyphenyl)cyclohexanone has been described as forming a self-included structure in accordance with category (d).[2b] However, our interpretation is that the structure consists of interweaved two-dimensional hydrogen-bonded frameworks that conform to category (c).

To the best of our knowledge, no structure that conforms entirely to category (e) has been recognized as such to date. This phenomenon may be either unusual or commonplace: there could be many such systems whose structures were simply not commented on when reported. Indeed, given the obvious potential for disorder, self-inclusion may have been overlooked on many occasions. Of course this kind of inclusion behavior in molecular solids is only to be expected in host molecules that form a series of inclusion compounds that are isostructural with respect to the host packing motif (we suggest use of the term "isoskeletal" to describe this structural phenomenon). Many isoskeletal systems are now known and include host–guest complexes of Dianin's compound,[9] cholic acid,[10] *p-tert*-butylcalix[4]arene,[11] calix[4]arene,[12] hydroquinone,[13] Werner clathrates,[14] cyclodextrins,[15] Bishop's alicyclic diol molecules,[16] and many more. The importance of these types of host is that their structures can generally be predicted on the basis of their demonstrated packing preferences, which facilitates the tailoring of structure[17] as a stated goal of crystal engineering.

Although the structure of hydrated trimesic acid (TMA) almost meets the criteria of category (e), the host framework consists of a supramolecular adduct that incorporates both TMA and water, whereas the guest consists only of TMA.[18] A similar TMA/H_2O framework exists with picric acid as the guest,[18] but there are small differences in the host frameworks between the two structures. Therefore, the hydrated TMA structure can at best be described as water-assisted self-inclusion under category (d). We now report an unequivocal case of true self-inclusion under category (e) as the missing link at the extreme end of the series that represents all the possible levels.

2,7-Dimethyl-octa-3,5-diyne-2,7-diol (**1**) was synthesized as described below. Crystals of $\mathbf{1}_3{\cdot}CCl_4$ (**2**) were grown by slow



evaporation of a solution of **1** in carbon tetrachloride and the structure was determined by single-crystal X-ray diffraction analysis. The binary compound crystallizes in the space group *R3*, and the asymmetric unit consists of one molecule of **1** in a general position and one-third of a molecule of CCl_4 situated on a crystallographic threefold rotation axis. The solid-state adduct can reasonably be categorized as an inclusion compound, with **1** fulfilling the role of the host and the solvent that of the guest. The C–C≡C-C≡C–C spine of the host molecule is slightly curved with four bond angles of approximately 173, 176, 176, and 176°, respectively. The host molecules are arranged in a spiral running parallel to [001] to form an infinite (convergent) channel around the (divergent) solvent guest molecules (Figure 1a). The pitch of the spiral is 6.232(4) Å (namely, the crystallographic *c* axis). Each tube is surrounded by six identical tubes in a hexagonal arrangement and, interestingly, all of the tubes in the crystal spiral in the same direction. The hydroxy groups of **1** are situated on the exterior surfaces of the tubes and each tube is bound to all six of its neighbors by means of six infinite spiral arrangements of O–H···O hydrogen bonds (O···O: 2.733(6) and 2.657(7) Å; Figure 1a). The guest solvent molecules in the channels are packed parallel to [001] within each tube (that is, the intrinsic threefold axis of each guest molecule coincides with that of the host tubule, as shown in Figure 1b). Notably, the linear packing of the guest molecules along [001] is perfectly commensurate with the spiral pitch of the host molecules.

Crystals of $\mathbf{1}_3{\cdot}C_6H_6$ (**3**) were grown from a solution of **1** in benzene. X-ray diffraction analysis reveals that **3** is isoskeletal with respect to **2** and that the guest molecules are similarly included in the channels in a commensurate arrangement (Figure 1c) with a packing periodicity of 6.325(5) Å. The host/guest ratio is also 1:3, and the benzene molecules are disordered about the threefold rotation axis parallel to [001].

Our primary research interest involves engineering porous crystals for gas- or vapor-sorption applications.[11,19] In this regard, we have been successful in either growing suitable crystals of metastable apohost phases by sublima-

 © 2006 Wiley-VCH Verlag GmbH & Co. KGaA, Weinheim

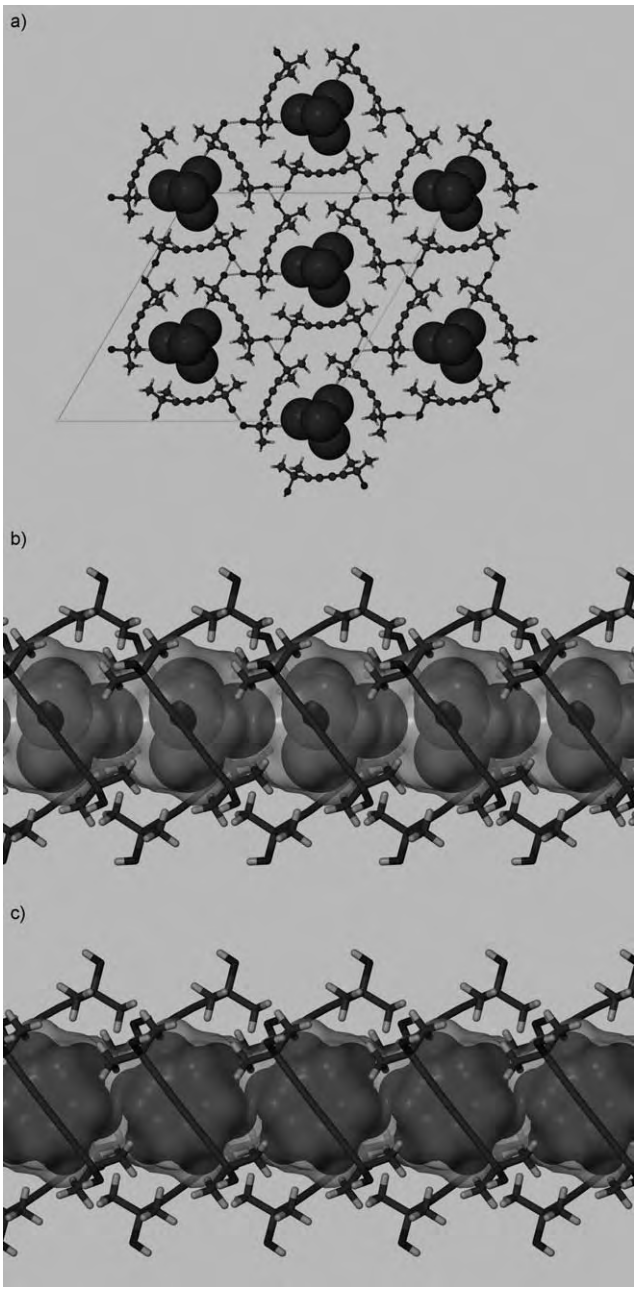


Figure 1. a) Projection of **2** along [00-1] showing the hexagonal arrangement of tubular motifs that consist of spiraling host molecules. The guest molecules are situated in the channels. b) Projection perpendicular to [001] of a tubule in **2** showing the commensurate arrangement of carbon tetrachloride guest molecules within a channel mapped using a spherical probe of radius 1.2 Å. c) A corresponding projection of **3** that shows the benzene guest molecules within a channel (also mapped using a probe of radius 1.2 Å). Hydrogen bonds are shown as fragmented cylinders, guest molecules are shown in a space-filling representation, and host molecules are shown as capped sticks.

tion[11a] and by extracting solvent molecules from guest channels without causing the collapse of the host frameworks.[19] In an attempt to remove the included solvent molecules by gentle heating, crystals of **2** and **3** were subjected to thermogravimetric analysis, which reveals that solvent loss occurs concurrently with sublimation of the host compound (onset temperature (T_{on}) = 63.5 °C). In a separate experiment, crystals were placed under vacuum for several hours, after which their structures were again determined by single-crystal X-ray diffraction analysis. These two studies show that no appreciable solvent loss appears to occur under vacuum conditions and that heating to 70 °C results in guest removal, but only with concomitant disassembly and volatilization of the host framework.

Crystals of pure **1** (**4**) were grown by vacuum sublimation at 70 °C in the hope of forming a guest-free tubular structure. Indeed, single-crystal X-ray diffraction analysis of **4** reveals an isoskeletal arrangement of **1** with respect to the structures of **2** and **3**. The tubular frameworks initially appeared to be devoid of guest molecules. However, difference maps calculated during the latter stages of refinement indicated the presence of appreciable residual electron density within the channels. It was ultimately possible to model a disordered molecule of **1** with its C−C≡C-C≡C−C spine situated on the threefold rotation axis along [001].

It is immediately apparent that the structure of **4** accords completely with category (e) of self-inclusion as delineated above. It is therefore useful in the following discussion to distinguish between the two crystallographically unique cases of **1** according to their respective roles as host $\mathbf{1}_h$ and guest $\mathbf{1}_g$. Space-group symmetry requires the hydroxy and methyl groups of $\mathbf{1}_g$ to be disordered about a threefold axis. Furthermore, application of threefold rotation symmetry to the asymmetric unit yields a molecule of $\mathbf{1}_g$ with a total site occupancy of 0.5. The model employed for $\mathbf{1}_g$ is longer than the crystallographic *c* axis and translation along [001] (that is, $x, y, z+1$) yields a second half-occupancy molecule which overlaps the first (Figure 2a). The nature of the disorder of $\mathbf{1}_g$ with regard to its possible positions along [100] is interesting and warrants further discussion. Close inspection of Figure 1b and c shows that the channels within the host tubules possess bulges and constrictions along [001] with a periodicity equal to the crystallographic *c* axis and that each bulge is occupied by one carbon tetrachloride or benzene guest molecule. However, in **4** the longer guest molecule $\mathbf{1}_g$ spans exactly two bulges and is thus packed with a periodicity of 2*c* along [001] within each channel. As X-ray diffraction analysis only reveals the average structure, it is reasonable to infer from the disordered model that two equally likely possibilities (Figure 2b and c) exist for the end-to-end stacking of $\mathbf{1}_g$ along [001] and that these two arrangements are staggered relative to one another by a distance of *c*.

Evidently the tubular framework persistently observed in structures **2**–**4** is a highly desirable arrangement of **1**, which is most likely due to the stabilizing influence of six infinite hydrogen-bonded spirals that bind each tubule to its nearest neighbors. Indeed, this kind of robust system is well known and **2**–**4** can be considered members of the helical tubuland diol family described by Bishop.[16] Using a probe of radius 1.2 Å to map the contact surface of each channel, we calculate a channel volume of approximately 205(5) Å^3 per repeat unit along the *c* axis. It follows that carbon tetrachloride, benzene, and $\mathbf{1}_g$ occupy the channels with packing coefficients of 0.44, 0.39, and 0.44, respectively. These values are significantly

 © 2006 Wiley-VCH Verlag GmbH & Co. KGaA, Weinheim

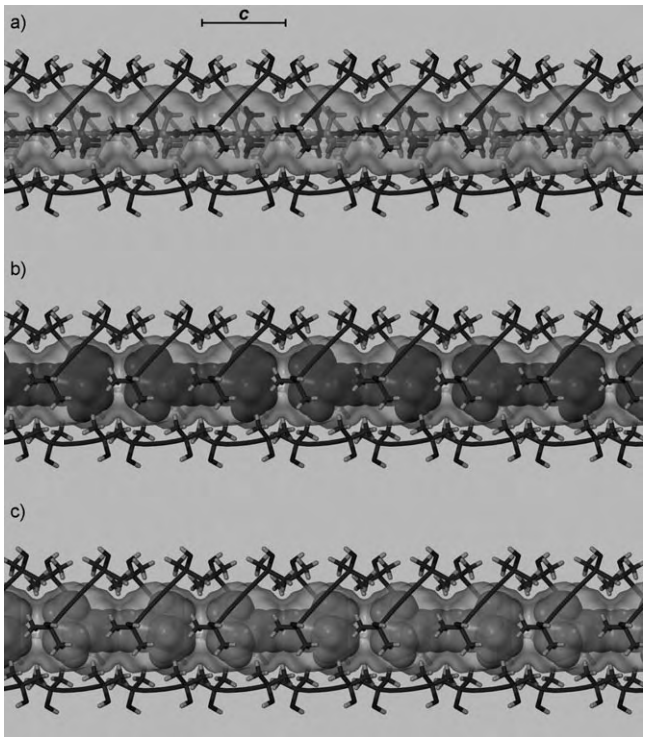


Figure 2. Three identical projections of **4** along [100] that show the two possible arrangements (light and dark) of the included examples of $\mathbf{1}_g$ within each guest-accessible channel formed by $\mathbf{1}_h$. a) An overlay of the guest molecules that indicates the nature of the guest disorder. The length of the crystallographic *c* axis is indicated. b) One distinct linear arrangement of the guest molecules $\mathbf{1}_g$ and c) the alternative arrangement of $\mathbf{1}_g$ within the same channel. The two arrangements are staggered with respect to one another by translation of 6.341(1) Å along [001]. The hydroxy groups of $\mathbf{1}_g$ are threefold disordered about the linear axis of the molecule and are not shown. As both arrangements of $\mathbf{1}_g$ are equally likely, it is presumed that a random arrangement is assumed within each channel and that no synchronization occurs between neighboring channels with regard to periodicity.

lower than packing coefficients normally observed for organic solids (typically 0.60–0.66) and provide further evidence for the overall stability of the host framework.

It is noteworthy that crystals of **4** can also be obtained by slow evaporation of a solution of **1** in dichloromethane.[20] Presumably **1** competes with the solvent molecules for occupancy of the channels. If included, dichloromethane would occupy the channels with a rather low packing coefficient of 0.28, and this poor efficiency may thus be used to rationalize why **1** is included in preference to dichloromethane. On the other hand, benzene is included despite possessing a slightly lower space filling efficiency than **1**. However, in the case of benzene, additional stabilization may be derived from C_{Ar}–H···$\pi_{C\equiv C}$ intermolecular interactions between the guest and host.

We have described the solid-state structures of three different inclusion compounds of **1**, which have in common that they possess tubular arrangements of the host that are virtually superimposable. Remarkably, one of these structures features a host molecule as the guest. Although **4** is composed of a pure substance, the molecule clearly plays two very distinct roles in the structure. A strong case can be made that this distinction is not subjective as at least two other structures can be shown to possess the same host framework with different guests (that is, the host competes for the guest-binding void space). In the vast field of solid-state host–guest chemistry, this observation is unprecedented at the level of interpretative stringency displayed herein. The concept of self-inclusion is an important phenomenon in the field of crystal engineering that relates to porosity as it mitigates against the formation of open structures. The assembly of any porous structure represents a victory by competing factors over the natural proclivity of molecules to close pack. As discussed above, all structures exhibit self-inclusion to a certain extent, and it is the challenge of crystal engineers to understand and control this phenomenon in their quest to form low-density frameworks with minimal self-inclusion.

Experimental Section

2,7-Dimethyl-octa-3,5-diyne-2,7-diol (**1**) was synthesized by the Glaser reaction, in which 2-methylbut-3-yn-2-ol (1 mol) and pyridine (0.25 mol) were heated at 35 °C for 4 h in methanol with 1.2% cuprous chloride as the catalyst and oxygen being passed through. The product was extracted from aqueous ammonium chloride with diethyl ether and recrystallized from benzene in 90% yield (m.p. 127–129 °C). Further purification was achieved by sublimation. Solvated crystals were grown by slow evaporation of a solution of **1** in the relevant solvent, whereas crystals of the pure form were grown by sublimation at 70 °C under vacuum. X-ray diffraction data were collected on a Bruker SMART Apex diffractometer and corrected for Lorentz-polarization effects. Structures were solved by direct methods using SHELXS-97 and expanded/refined on F^2 by difference electron density synthesis using SHELXL-97 and the X-Seed graphical user interface.[21–23]

Received: April 27, 2006
Published online: July 17, 2006

Keywords: crystal engineering · host–guest systems · inclusion compounds · solid-state structures · supramolecular chemistry

[1] a) J. Bernstein, *Chem. Commun.* **2005**, 5007–5012; b) A. Nangia, *Cryst. Growth Des.* **2006**, *6*, 2–4; c) O. Almarsson, M. J. Zaworotko, *Chem. Commun.* **2004**, 1889–1896; d) G. R. Desiraju, *Cryst. Eng. Comm.* **2003**, *5*, 466–467; e) J. D. Dunitz, *Cryst. Eng. Comm.* **2003**, *5*, 506–506; f) K. R. Seddon, *Cryst. Growth Des.* **2004**, *4*, 1087–1087; g) G. R. Desiraju, *Cryst. Growth Des.* **2004**, *4*, 1089–1090; h) J. Bernstein, *Cryst. Growth Des.* **2005**, *5*, 1661–1662; i) D. Braga, F. Grepioni, *Chem. Commun.* **2005**, 3635–3645.

[2] a) K. C. Pich, R. Bishop, D. C. Craig, I. G. Dance, A. D. Rae, M. L. Scudder, *Struct. Chem.* **1993**, *3*, 41–51; b) S. Aitipamula, G. R. Desiraju, M. Jaskólski, A. Nangia, R. Thaimattam, *Cryst. Eng. Comm.* **2003**, *5*, 447–450; c) F. H. Herbstein, *Crystalline Molecular Complexes*, *Vol. 1*, Oxford University Press, Oxford, **2005**.

[3] J. Dalluhn, H.-F. Pröhl, O. Moers, A. Blaschette, P. G. Jones, *Z. Naturforsch. B* **2001**, *56*, 1188–1195.

[4] J. W. Steed, *Cryst. Eng. Comm.* **2003**, *5*, 169–179.

[5] a) B. Moulton, M. J. Zaworotko, *Chem. Rev.* **2001**, *101*, 1629–1658; b) P. J. Langley, J. Hulliger, *Chem. Soc. Rev.* **1999**, *28*, 279–291.

 © 2006 Wiley-VCH Verlag GmbH & Co. KGaA, Weinheim

[6] S. R. Batten, *Cryst. Eng. Comm.* **2001**, *3*, 67 – 73.
[7] D. J. Cram, *Angew. Chem.* **1986**, *98*, 1041 – 1060; *Angew. Chem. Int. Ed. Engl.* **1986**, *25*, 1039 – 1057.
[8] J. S. Rutherford, C. Calvo, *Z. Kristallogr. Kristallgeom. Kristallphys. Kristallchem.* **1969**, *128*, 229 – 258.
[9] P. Finocchiaro, S. Failla, *Comprehensive Supramolecular Chemistry*, *Vol. 6* (Eds.: J. L. Atwood, J. E. D. Davies, D. D. MacNicol, F. Vögtle), Elsevier, Oxford, **1996**, pp. 618 – 627.
[10] M. Miyata, K. Sada, *Comprehensive Supramolecular Chemistry*, Vol. 6 (Eds.: J. L. Atwood, J. E. D. Davies, D. D. MacNicol, F. Vögtle), Elsevier, Oxford, **1996**, pp. 147 – 176.
[11] a) J. L. Atwood, L. J. Barbour, A. Jerga, B. L. Schottel, *Science* **2002**, *298*, 1000 – 1002; b) J. L. Atwood, L. J. Barbour, A. Jerga, *Angew. Chem.* **2004**, *116*, 3008 – 3010; *Angew. Chem. Int. Ed.* **2004**, *43*, 2948 – 2950; c) J. L. Atwood, L. J. Barbour, G. O. Lloyd, P. K. Thallapally, *Chem. Commun.* **2004**, 922 – 923; d) J. L. Atwood, L. J. Barbour, P. K. Thallapally, T. B. Wirsig, *Chem. Commun.* **2005**, 51 – 53.
[12] J. L. Atwood, L. J. Barbour, A. Jerga, *Science* **2002**, *296*, 2367 – 2369.
[13] T. C. W. Mak, B. R. F. Bracke, *Comprehensive Supramolecular Chemistry*, *Vol. 6* (Eds.: J. L. Atwood, J. E. D. Davies, D. D. MacNicol, F. Vögtle), Elsevier, Oxford, **1996**, pp. 23 – 37.
[14] J. Lipkowski, *Comprehensive Supramolecular Chemistry*, *Vol. 6* (Eds.: J. L. Atwood, J. E. D. Davies, D. D. MacNicol, F. Vögtle), Elsevier, Oxford, **1996**, pp. 691 – 714.
[15] K. Harata, *Comprehensive Supramolecular Chemistry*, *Vol. 3* (Eds.: J. L. Atwood, J. E. D. Davies, D. D. MacNicol, F. Vögtle), Elsevier, Oxford, **1996**, pp. 279 – 304.
[16] R. Bishop, *Comprehensive Supramolecular Chemistry*, *Vol. 6* (Eds.: J. L. Atwood, J. E. D. Davies, D. D. MacNicol, F. Vögtle), Elsevier, Oxford, **1996**, pp. 85 – 115.
[17] For example: G. O. Lloyd, M. W. Bredenkamp, L. J. Barbour, *Chem. Commun.* **2005**, 4053 – 4055.
[18] F. H. Herbstein, R. E. Marsh, *Acta Crystallogr. Sect. B* **1977**, *33*, 2358 – 2368.
[19] a) L. J. Barbour, *Chem. Commun.* **2006**, 1163 – 1168; b) L. Dobrzańska, G. O. Lloyd, H. G. Raubenheimer, L. J. Barbour, *J. Am. Chem. Soc.* **2005**, *127*, 13134 – 13135; c) L. Dobrzańska, G. O. Lloyd, H. G. Raubenheimer, L. J. Barbour, *J. Am. Chem. Soc.* **2006**, *128*, 698 – 699.
[20] D. A. Leigh, A. E. Moody, R. G. Pritchard, *Acta Crystallogr. Sect. C* **1994**, *50*, 129 – 131. It is our assessment that this structure was misinterpreted; we believe that the authors assumed the electron density within the tubule to be due to the presence of dichloromethane and they did not attempt to model the guest further.
[21] G. M. Sheldrick, SHELX-97, University of Göttingen, **1997**.
[22] a) L. J. Barbour, *J. Supramol. Chem.* **2001**, *1*, 189 – 191; b) J. L. Atwood, L. J. Barbour, *Cryst. Growth Des.* **2003**, *3*, 3 – 8.
[23] The crystal data, thermoanalytical, and complementary analyses can be found in the Supporting information. CCDC 605735–605737 contain the supplementary crystallographic data for this paper. These data can be obtained free of charge from The Cambridge Crystallographic Data Centre via www.ccdc.cam.ac.uk/data_request/cif.

 © 2006 Wiley-VCH Verlag GmbH & Co. KGaA, Weinheim

Self-Assembly

DOI: 10.1002/anie.200601594

Supramolecular Assemblies of Chiral Propargylic Alcohols**

Marilise Hyacinth, Maksymilian Chruszcz, Ki Sung Lee, Michal Sabat, Ge Gao, and Lin Pu**

Chiral propargylic alcohols are very useful synthetic precursors to many organic compounds.[1] A few propargylic alcohols were also found to form interesting supramolecular structures through intermolecular interactions of the hydroxy groups and the π electrons of the C≡C bonds.[2–4] Another supramolecular interaction based on the quadrupole π–π attraction between an aryl and a perfluoroaryl moiety was used to create new materials for applications in solid-state photopolymerization, liquid crystals, hydrogels, and so forth.[5] We have initiated a program to combine the four functional groups, including the aryl, perfluoroaryl, C≡C, and OH groups, to make the diaryl-substituted chiral propargylic alcohols and to explore their potential in supramolecular chemistry. Herein, we present some of findings that indicate that the presence of the functional groups not only makes the self-assembly of propargylic alcohols possible but it also allows for a finely tuned cooperation of interactions on a scale rarely seen in other supramolecular systems. We show herein that diaryl-substituted chiral propargylic alcohols can form cyclic hexameric supramolecular assemblies as a result of the cooperation between three major intermolecular forces: O–H···O hydrogen bonding, C–H···F–C hydrogen bonding involving organic fluorine atoms, and π–π stacking interactions between the pentafluorophenyl and phenyl rings. We believe that this synergy of intermolecular forces could be utilized in a variety of applications, including molecular recognition and discrimination.

We synthesized the racemic propargylic alcohol *rac*-**1** from the reaction of phenylacetylene with pentafluorobenzaldehyde in the presence of Et_2Zn and HMPA at room

[*] M. Hyacinth, K. S. Lee, Dr. M. Sabat, Dr. G. Gao, Prof. L. Pu
Department of Chemistry
University of Virginia
Charlottesville, VA 22904-4319 (USA)
Fax: (+1) 434-924-3170
E-mail: ms5c@virginia.edu
lp6n@virginia.edu

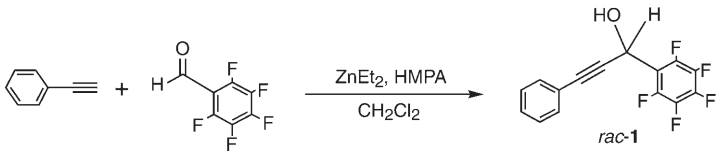
M. Chruszcz
Department of Molecular Physiology and Biological Physics
University of Virginia
Charlottesville, VA 22908 (USA)

[**] We thank Professor Wladek Minor (University of Virginia Medical School) for helpful discussions and the Rigaku/MSC for loan of the RAPID system. Partial support of this work from the National Institute of Health (R01GM58454/R01EB002037) and from the HKL Research Inc. (GI11496) is gratefully acknowledged.

Supporting information for this article is available on the WWW under http://www.angewandte.org or from the author.

InterScience
© 2006 Wiley-VCH Verlag GmbH & Co. KGaA, Weinheim

temperature (Scheme 1). X-ray analysis of the crystals of *rac*-**1** gave a hexameric supramolecular structure that contained alternating *RSRSRS* enantiomers (Figure 1). The crystal structure of *rac*-**1** consists of centrosymmetric hexamers



Scheme 1. Synthesis of the propargylic alcohol *rac*-**1**. HMPA = hexamethyl phosphoramide.

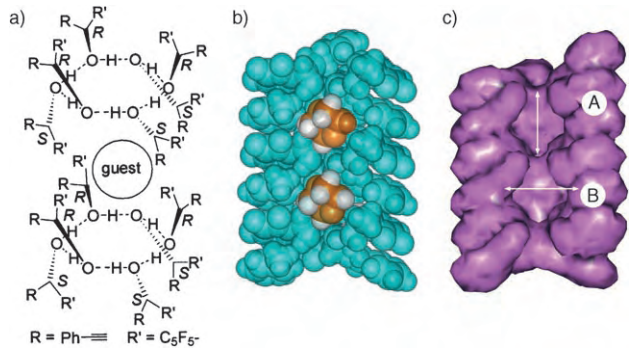


Figure 2. Cages in the crystal structure of *rac*-**1**.

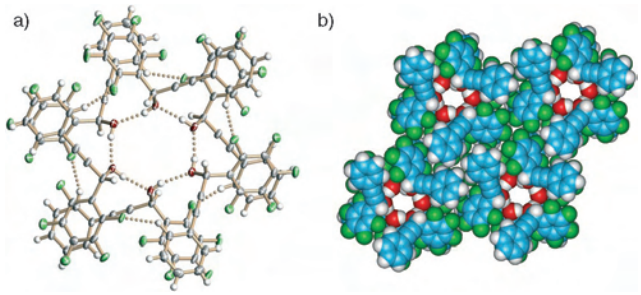
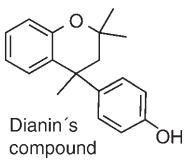


Figure 1. a) The network of O–H···O hydrogen bonds, face-to-face π–π stacking interactions, and C–H···F hydrogen bonds that cooperatively form the hexameric structure of *rac*-**1**. b) Channels formed along the crystallographic *a* axis.

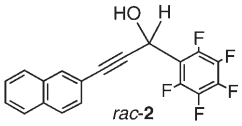
formed by alternating *R* and *S* enantiomers (Figure 1). The hexamers are held together by O–H···O hydrogen bonds with O···O donor–acceptor distances of 2.808, 2.771, and 2.777 Å. The pentafluorophenyl and phenyl rings are almost exactly parallel, with an average separation of 3.52 Å between the ring planes. Additional stabilization comes from a network of C–H···F–C hydrogen bonds between the *ortho* C–H groups of the phenyl ring and the *ortho* C–F groups of the pentafluorophenyl ring, with the C···F separations of 3.25, 3.36, and 3.27 Å comparable with analogous distances found in systems with organic fluorine atoms.[6]

The hexameric structures of *rac*-**1** stack with each other along the unit-cell axis with the alternating parallel phenylethynyl–pentafluorophenyl π–π interaction to form infinite channels. In a hexameric unit of *rac*-**1**, three *R* enantiomers are up and three *S* enantiomers are down (Figure 2a). The two stacking hexamers in a channel generate a cage that can include guest molecules, such as dioxane and dichloromethane. Figure 2b is the cross section of one channel in the crystal structure of *rac*-**1** and shows two cages, with each including a dioxane molecule. Figure 2c gives the dimension of two cages in *rac*-**1**. The diameters A and B are 7.85 and 8.35 Å for each cage, respectively.



The supramolecular assembly of *rac*-**1** is similar to that of Dianin's compound.[7] Dianin's compound was found to be able to host a wide range of organic and inorganic guests, such as glycerol, argon, small carbohydrates, and SF_6. It is useful in the storage and transport of volatile species.

In the same way as the preparation of *rac*-**1**, we also synthesized the racemic compound *rac*-**2** from the addition of



2-ethynylnaphthalene to perfluorobenzaldehyde. The crystal structure of this compound shows the same hexameric channel-like supramolecular structure as *rac*-**1** (Figure 3). The cages inside *rac*-**2** are similar to those of *rac*-**1** (Figure 2c). The diameters A and B are 7.76 and 8.46 Å for each cage in *rac*-**2**, respectively.

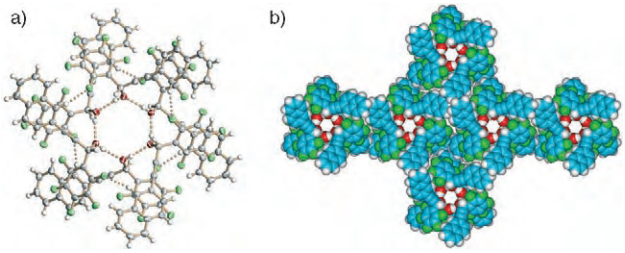
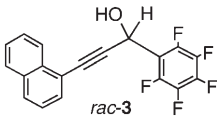


Figure 3. a) The network of O–H···O hydrogen bonds, face-to-face π–π stacking interactions, and C–H···F hydrogen bonds that cooperatively form the hexameric structure of *rac*-**2**. b) Channels formed along the crystallographic *a* axis.

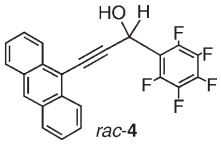
We synthesized the 1-naphthyl-substituted analogue *rac*-**3** to explore the role of the C–H···F–C hydrogen bonds in the supramolecular structures of *rac*-**1** and *rac*-**2**. This compound contains one less C–H group *ortho* to the triple bond than *rac*-**1** and *rac*-**2**, and was thus expected to have less C–H···F–C hydrogen bonds. The X-ray analysis of the single crystal of *rac*-**3** showed no hexameric structure.



© 2006 Wiley-VCH Verlag GmbH & Co. KGaA, Weinheim

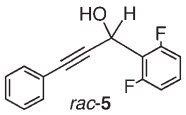
Instead, this compound formed a centrosymmetric *RRSS* tetrameric assembly, stabilized by a network of O–H···O hydrogen bonds in the solid state. No significant C–H···F–C interactions were present in the crystal lattice of *rac*-**3**. Additional stabilization of the tetramer came from the face-to-face π–π stacking interactions involving the naphthylethynyl and pentaflurophenyl units of the adjacent molecules.

We further synthesized the 9-anthrancenyl-substituted compound *rac*-**4**, which contained no C–H group *ortho* to the triple bond. This compound was also unable to form the hexameric structure of *rac*-**1** and *rac*-**2**. Its crystal structure was similar to that of *rac*-**3** with the centrosymmetric *RRSS* tetrameric assembly. Thus, the study of *rac*-**3** and *rac*-**4** demonstrates that the C–F···H–C hydrogen bonds are very important for the hexameric supramolecular structures of *rac*-**1** and *rac*-**2**.



rac-**4**

We synthesized compound *rac*-**5**, which contained a difluorophenyl group in place of the pentafluorophenyl unit in *rac*-**1** and *rac*-**2**, to assess the importance of the π–π attraction of the aryl–perfluorophenyl system. The subsequent structural determination of *rac*-**5** revealed a linear assembly of the opposite enantiomers held together by O–H···O hydrogen bonds rather than the hexameric structure of *rac*-**1** and *rac*-**2**. Some weak C–H···F interactions were also found. However, no apparent stacking forces were observed in this structure.



rac-**5**

Our study of the various diaryl-substituted propargylic alcohols demonstrates that the cooperation of three noncovalent forces, O–H···O hydrogen bonds, aryl–pentafluorobenzene π–π interactions, and C–H···F hydrogen bonds, in *rac*-**1** and *rac*-**2** is crucial for their supramolecular structures. Decreasing any of the forces, as shown in the structures of *rac*-**3**, *rac*-**4**, and *rac*-**5**, leads to a complete disruption of the hexameric channel-like assembly. The supramolecular assembly of *rac*-**1** also exhibits promising host–guest interactions, as evidenced by its complexation with molecules such as dichloromethane and dioxane in the cages between the $(O–H)_6$ planes. Further research is in progress to explore the utility of these structures and functions. We are also preparing the optically active analogues of these compounds by using a catalytic asymmetric synthetic method to construct the optically active supramolecular structures;[8] for example, the combination of (*R*)-**1** with (*S*)-**2** could potentially generate optically active crystals and chiral cages.

Received: April 23, 2006
Published online: July 17, 2006

Keywords: π–π interactions · fluorine · hydrogen bond · propargylic alcohols · supramolecular chemistry

[1] Selected examples: a) *Modern Acetylene Chemistry* (Eds.: P. J. Stang, F. Diederich), VCH, Weinheim, **1995**; b) J. A. Marshall, X. J. Wang, *J. Org. Chem.* **1992**, *57*, 1242–1252; c) M. E. Fox, C. Li, J. P. Marino, Jr., L. E. Overman, *J. Am. Chem. Soc.* **1999**, *121*, 5467–5480; d) A. G. Myers, B. Zheng, *J. Am. Chem. Soc.* **1996**, *118*, 4492–4493; e) B. M. Trost, M. J. Krische, *J. Am. Chem. Soc.* **1999**, *121*, 6131–6141; f) W. R. Roush, R. J. Sciotti, *J. Am. Chem. Soc.* **1994**, *116*, 6457–6458; g) E. J. Corey, K. A. Cimprich, *J. Am. Chem. Soc.* **1994**, *116*, 3151–3152; h) N. K. Anand, E. M. Carreira, *J. Am. Chem. Soc.* **2001**, *123*, 9687–9688; i) L. Pu, *Tetrahedron* **2003**, *59*, 9873–9886.

[2] J. W. Steed, J. L. Atwood, *Supramolecular Chemistry*, Wiley, Chichester, **2000**.

[3] G. R. Desiraju, T. Steiner, *The Weak Hydrogen Bond in Structural Chemistry and Biology*, Oxford University Press, Oxford, **1999**.

[4] a) N. N. L. Madhavi, C. Bilton, J. A. K. Howard, F. H. Allen, A. Nangia, G. R. Desiraju, *New J. Chem.* **2000**, *24*, 1–4; b) C. Bilton, J. A. K. Howard, N. N. L. Manhavi, A. Nangia, G. R. Desiraju, F. H. Allen, C. C. Wilson, *Acta Crystallogr. Sect. B* **2000**, *56*, 1071–1079; c) J. G. Garcia, B. Ramos, A. Rodriguez, *Acta Crystallogr. Sect. C* **1995**, *51*, 2674–2676; d) D. Braga, F. Grepioni, D. Walther, K. Heubach, A. Schmidt, W. Imhof, H. Görls, T. Klettke, *Organometallics* **1997**, *16*, 4910–4919; e) F. H. Allen, J. A. K. Howard, V. J. Hoy, G. R. Desiraju, D. S. Reddy, C. C. Wilson, *J. Am. Chem. Soc.* **1996**, *118*, 4081–4084; f) N. N. L. Madhavi, G. R. Desiraju, C. Bilton, J. A. K. Howard, F. H. Allen, *Acta Crystallogr. Sect. C* **2000**, *56*, 1359–1360; g) R. Banerjee, R. Mondal, J. A. K. Howard, G. R. Desiraju, *Cryst. Growth Des.* **2006**, *6*, 999–1009.

[5] a) C. R. Patrick, G. S. Prosser, *Nature* **1960**, *187*, 1021; b) A. P. West, S. Mecozzi, D. A. Dougherty, *J. Phys. Org. Chem.* **1997**, *10*, 347–350; c) J. H. Williams, J. K. Cockcroft, A. N. Fitch, *Angew. Chem.* **1992**, *104*, 1666–1669; *Angew. Chem. Int. Ed. Engl.* **1992**, *31*, 1655–1657; d) J. H. Williams, *Acc. Chem. Res.* **1993**, *26*, 593–598; e) T. Dahl, *Acta Chem. Scand.* **1994**, *48*, 95–106; f) R. E. Gillard, J. F. Stoddart, A. J. P. White, B. J. Williams, D. J. Williams, *J. Org. Chem.* **1996**, *61*, 4504–4505; g) F. Cozzi, F. Ponizi, R. Annunziata, M. Cinquini, J. S. Siegel, *Angew. Chem.* **1995**, *107*, 1092–1094; *Angew. Chem. Int. Ed. Engl.* **1995**, *34*, 1019–1020; h) G. W. Coates, A. R. Dunn, L. M. Henling, J. W. Ziller, E. B. Lobkovsky, R. H. Grubbs, *J. Am. Chem. Soc.* **1998**, *120*, 3641–3649.

[6] A. Schwarzer, W. Seichter, E. Weber, H. Stoeckli-Evans, M. Losada, J. Hulliger, *CrystEngComm* **2004**, *6*, 567–572.

[7] J. L. Flippen, J. Karle, I. L. Karle, *J. Am. Chem. Soc.* **1970**, *92*, 3749–3655.

[8] G. Gao, R.-G. Xie, L. Pu, *Proc. Natl. Acad. Sci. USA* **2004**, *101*, 5417–5420.

 © 2006 Wiley-VCH Verlag GmbH & Co. KGaA, Weinheim

Nanostructures

DOI: 10.1002/anie.200601553

Crystalline Nanoflowers with Different Chemical Compositions and Physical Properties Grown by Limited Ligand Protection**

*Arun Narayanaswamy, Huifang Xu, Narayan Pradhan, and Xiaogang Peng**

Colloidal nanocrystals with controlled size and shape play a key role in nanotechnology.[1–3] Organometallic[4–6] and related alternative (or so-called greener)[7–10] synthetic methods at elevated temperatures in non-aqueous solvents are the current mainstream strategies for producing high-quality nanocrystals. The ability to control the size and size distribution of nanodots using these strategies is reasonably well developed. Also, advances in the formation of 1D nanocrystals have recently been reported.[5,11–14] These 1D structures offer a unique technical potential that is inaccessible with the corresponding 0D nanocrystals. Reports on the synthesis of complex 3D nanostructures, however, remain uncommon.[15–19] Most of these structures are grown on substrates, are large in size, and/or are polycrystalline. Herein, we demonstrate that, by simply reducing the degree of ligand protection to the domain of limited ligand protection (LLP), the existing mainstream synthetic chemistry for 0D and 1D nanocrystals—more specifically, the greener approaches—can also produce high-quality complex 3D nanostructures, such as crystalline nanoflowers. Unlike the formation of tetrapods of II–VI semiconductors with specific crystal structures,[15,20] we reveal that LLP coupled with 3D oriented attachment can be applied in the preparation of nanocrystals with different compositions, crystal structures, and physical (magnetic and electronic) properties.

The LLP strategy was first applied to the In_2O_3 nanocrystal system, and it was not clear if the 3D oriented attachment caused by LLP would be limited to certain crystal structures and compositions. Herein, we intend to clarify the generality of the LLP strategy. A detailed account of the nanocrystal growth mechanism will be reported separately.[21]

A metal carboxylate (acetate (Ac), myristate (Mt), or stearate (St)) was used as a precursor, and a generic hydrocarbon, such as 1-octadecene (ODE), was used as solvent. Myristic acid (MA) or stearic acid (SA) was optionally used as a free ligand. An alcohol, such as 1-octadecyl alcohol (OA) or decyl alcohol (DA), was often added to either activate the stable precursors or to increase the yield and stability[22] of the oxide nanoflowers. For the ZnSe nanoflowers, an amine, such as 1-octadecyl amine (ODA), was used as an activation reagent and a ligand, and selenium powder dissolved in tributylphosphine was used as a reagent.

The results for the model system of In_2O_3 are briefly summarized in Figure 1, which shows representative transmission electron microscope (TEM) images of the nanostructures formed. When $In(Ac)_3$ is used as the precursor, the extremely short Ac ligands require that a high concentration (2 equiv) of MA be used to stabilize dot-shaped nanocrystals in the domain of sufficient ligand protection (SLP; Figure 1, center panel, top left). If only 1 equivalent of the long-chain fatty acid is present, the system is in the LLP domain. The individual nanodots become unstable and aggregate into 3D nanoflowers (Figure 1, center panel, top right). LLP can also be achieved with indium salts of fatty acids with long hydrocarbon chains, such as $In(Mt)_3$, without addition of free MA (Figure 1, center panel, bottom right). In comparison, the addition of 1 equiv of free MA yields nearly monodisperse nanodots (Figure 1, center panel, bottom left). All four reactions were carried out under the same conditions, with the exception of the types and concentrations of the indium precursors and ligands.

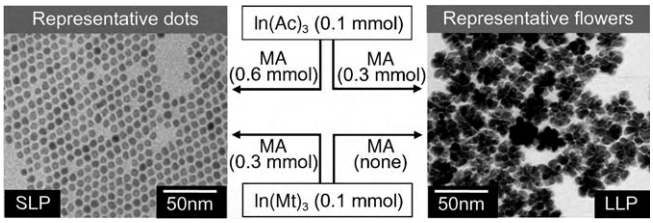


Figure 1. Formation of In_2O_3 nanodots by SLP and nanoflowers by LLP, and representative TEM images of the nanostructures (the size and shape depend on the reaction conditions).

Figure 2 illustrates that a variety of reaction systems can be similarly tuned to either the regular SLP domain or the LLP domain, through the use of metal carboxylates as precursors and the optional addition of a free ligand in a low concentration. This simple approach allows the growth of both nearly monodisperse nanoparticles and nanoflowers without any size sorting.

The size and shape of the 3D nanostructures can be varied in several different ways (Figure 3). The number of primary particles in each 3D ZnO aggregate is similar when MA (Figure 3a) or SA (Figure 3b) is used as the free ligand, but the sizes of the primary particles are different. When a lower concentration of the free fatty acid (MA) is used (Figure 3c), the number of primary particles in each ZnO nanoflower increases dramatically. The primary particles in the CoO nanoflowers formed in the early stages of the reaction (Figure 3e) are pointier and less regular in shape than those found in later stages (Figure 3f).

[*] Dr. A. Narayanaswamy, Dr. N. Pradhan, Dr. X. Peng
Department of Chemistry and Biochemistry
University of Arkansas
Fayetteville, AR 72701 (USA)
Fax: (+1) 479-575-4049
E-mail: xpeng@uark.edu
Dr. H. Xu
Department of Geology and Geophysics
University of Wisconsin
Madison, WI 53706 (USA)

[**] Financial support from the National Science Foundation (X.P.) and Wisconsin Alumni Research Foundation (H.X.) is acknowledged.

Supporting information for this article is available on the WWW under http://www.angewandte.org or from the author.

 © 2006 Wiley-VCH Verlag GmbH & Co. KGaA, Weinheim

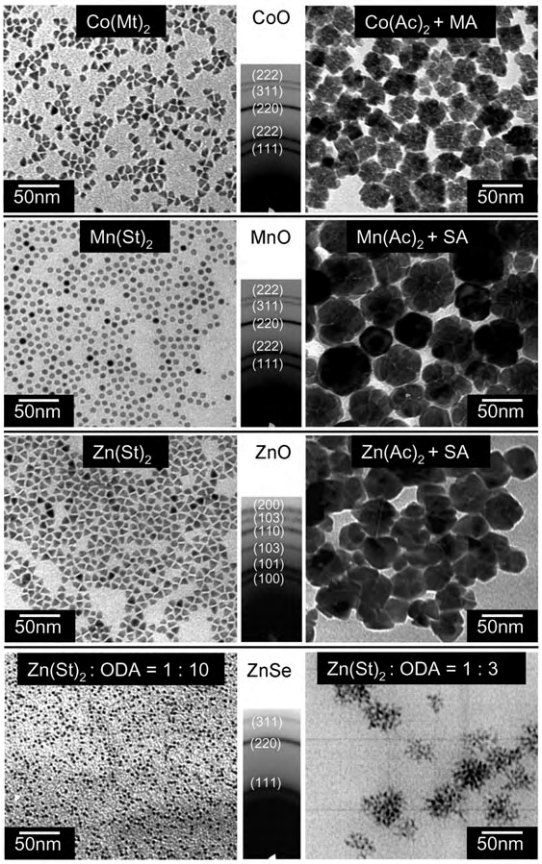


Figure 2. TEM images of the nanoparticles (left) and nanoflowers (right) formed in the CoO, MnO, ZnO, and ZnSe systems, and corresponding selected-area electron diffraction (SAED) patterns (center). The metal precursors and free ligands used in each system are indicated.

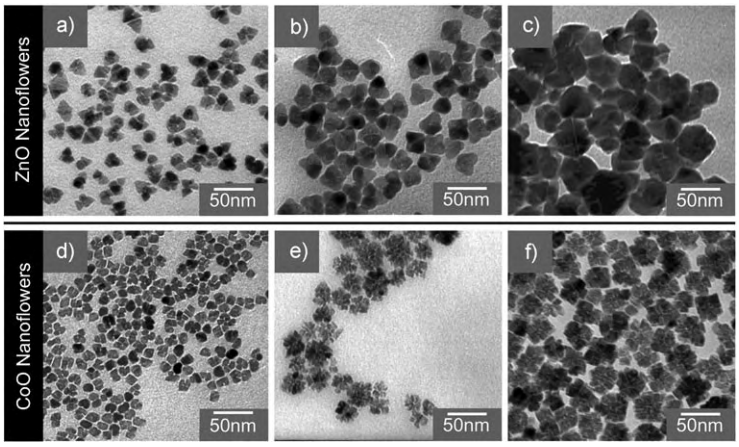


Figure 3. TEM images of the ZnO and CoO nanoflowers formed under different reaction conditions: a) $Zn(Ac)_2$:MA = 1:4, b) $Zn(Ac)_2$:SA = 1:4, c) $Zn(Ac)_2$:MA = 1:1, d) $Co(Ac)_2 \cdot 4H_2O$:MA = 1:2, e) $Co(Ac)_2 \cdot 4H_2O$:SA = 1:2, 5 min after addition of DA, f) $Co(Ac)_2 \cdot 4H_2O$:SA = 1:2, 20 min after addition of DA.

The five types of nanocrystals formed belong to four different crystal structures: bixbyite (cubic) for In_2O_3, rock salt (cubic) for CoO and MnO, wurtzite (hexagonal) for ZnO, and zinc blende (cubic) for ZnSe. The ZnO nanocrystals have an electric dipole moment in the direction of the unique *c* axis of the wurtzite structure. The CoO and MnO nanocrystals have a magnetic dipole. The ratio of cations to anions in In_2O_3 differs from that in the other compounds. Even for the same cation to anion ratio (1:1), the coordination number of the cation differs from case to case, being six in MnO and CoO, and four in ZnO and ZnSe. ZnO and ZnSe are well-known semiconductors.

Although LLP occurs in a variety of systems, there are some noticeable differences among the resulting nanoflowers (Figures 1–3). The primary nanocrystals in the In_2O_3 and ZnSe nanoflowers do not seem to be faceted. The MnO nanoflowers are formed by faceted primary particles, but the primary nanocrystals do not seem to have a fixed morphology. The ZnO nanoflowers are formed by nanopyramid primary particles (Figure 4). The primary nanocrystals in the CoO nanoflowers appear to be cubic. Evidently, the shapes of the primary nanocrystals constituting a nanoflower are not necessarily the same as those of the corresponding individual nanocrystals grown under SLP (Figure 2).

The oriented attachment of the primary nanocrystals to yield nanoflowers was studied by high-resolution (HR)TEM. Oriented attachment refers to the formation of relatively large crystalline structures by the attachment of crystalline primary particles, typically dot-shaped nanocrystals.[23] The 1D oriented attachment of nanodots to form nanorods or nanowires has been well documented, and there is strong evidence that an electric dipole moment is the major driving force.[12–14] Similarly, it has been reported that ferromagnetic nanodots can be self-assembled into 1D nanowires by magnetic dipole–dipole interactions between the primary particles in solution.[24]

Kotov and co-workers clearly demonstrated that, for the 1D oriented attachment of CdTe nanocrystals, it was essential to remove excess ligands in the reaction solution after the formation of the primary CdTe nanodots.[13] Although some reports have suggested that certain 3D nanostructures are formed through 3D oriented attachment in the nanometer regime,[25–27] the evidence is less convincing than in the 1D case. Controlled 3D oriented attachment on the nanoscale through the manipulation of ligand protection has not yet been reported.

HRTEM indicates that 3D oriented attachment occurs, either perfectly (In_2O_3 and CoO) or imperfectly (ZnO and MnO), in the formation of the nanoflowers. The results for the ZnO nanocrystals are particularly interesting. The primary particles of the ZnO nanoflowers are faceted, mainly with a pyramid shape (Figure 4). Stacking faults that may result in local zinc blende-like domains occur in some of the nanopyramids. The imperfection of the 3D oriented attachment[23] can be seen in this case: most of the ZnO nanocrystals attach to form a flower with a common crystallographic orientation, but a small misalignment is observed between some nanocrystals (for example, the 1.5° mismatch between the (100) lattice fringes in the left and right nanocrystals in the center panel of Figure 4). The ZnO nanocrystals attach to each other by sharing several different faces, including their $(00\bar{1})$ faces (Figure 4). Thus, the attachment cannot be caused by an electric-dipole mechanism. As discussed below, the attach-

 © 2006 Wiley-VCH Verlag GmbH & Co. KGaA, Weinheim

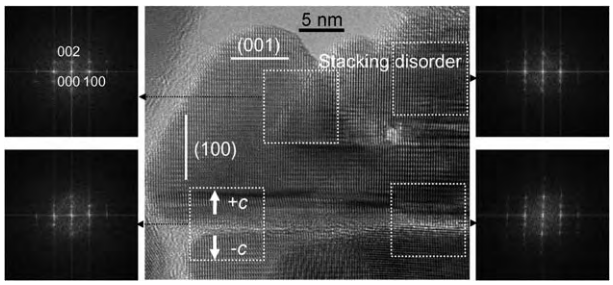


Figure 4. HRTEM image of part of a ZnO nanoflower (center), and fast Fourier transforms (FFTs; left and right) of selected areas (dotted squares) of the HRTEM image. See text for details.

ment of the $(00\bar{1})$ face of one primary nanocrystal to the (001) face of the next to form 1D ZnO nanowires would be expected if the electric dipole, in the direction of the unique *c* axis of the wurtzite structure, were playing a determining role.

Weller and co-workers convincingly showed that ZnO nanorods could be formed by the 1D oriented attachment of spherical nanodots along their *c* axis in an alcohol solution.[12] However, although ZnO nanocrystals have a dipole moment along their *c* axis, 3D oriented attachment can still occur, as shown in Figure 4. In comparison to our experimental conditions, Weller and co-workers used shorter ligands (Ac as the sole ligand) and a significantly lower temperature (60 °C). The very short ligands greatly decreased the distance between primary particles and, thereby, enhanced the dipole interaction between them. The low reaction temperature reduced the thermal energy of the primary particles, allowing them to align their dipole moments during the attachment events.

Significantly more experiments are needed to clarify this interesting system. The attachment of primary particles in one, two, or three dimensions in a controllable fashion is of considerable appeal. Further insight into this system may also help us to understand natural mineralization processes occurring under high-temperature and high-pressure conditions. In these processes, 3D attachment, either perfect or imperfect, should be preferred.

Similar to the electric dipole, the magnetic dipole does not play a determining role in the 3D oriented attachment of the magnetic CoO and MnO nanocrystals. Furthermore, both the CoO and MnO nanoflowers are crystalline in nature, but the MnO nanoflowers show some signs of imperfect oriented attachment (a detailed structural analysis will be published separately).

Although LLP makes individual nanodots unstable, the resulting nanoflowers are generally stable in the reaction solution and are also dispersible in nonpolar solvents after purification. The stability of the nanoflowers is probably a result of their complex surface structure. The ligands bound to surface atoms in the gaps between incompletely fused primary nanocrystals are kinetically "trapped" and, hence, difficult to remove. Similarly, tetrapods and highly branched nanocrystals of CdSe and CdTe were found to be more durable and dispersible than the corresponding nanorods.[15,20,28]

In summary, a unique and general approach, LLP, has been developed for the growth of nearly monodisperse nanostructures through 3D oriented attachment. With LLP, the primary nanocrystals are insufficiently protected, but the resulting 3D nanostructures are stabilized. This principle implies that LLP may be applicable to a broad spectrum of colloidal nanocrystals, without drastically altering the synthetic chemistry established for 0D and 1D nanocrystals in the recent years. Our results indicate that oriented attachment, at least in the 3D case, does not need to be driven by an electric or magnetic dipole moment. A detailed analysis of this issue for the In_2O_3 model system will be published shortly.[21] The complex crystalline nanostructures described herein offer unique nanoarchitectures for the development of high-performance electronic, optoelectronic, and sensing devices. The discovery of the LLP domain in the mainstream synthetic chemistry of high-quality nanocrystals enhances this important materials field. Although 1D oriented attachment has been well documented, the results herein indicate that 3D oriented attachment with LLP may occur more generally in natural mineralization and materials synthesis, especially under relatively vigorous conditions.

Experimental Section

Individual nanocrystals (dots or pyramids) of In_2O_3, ZnO, CoO, and MnO were produced by injecting the corresponding metal salt of a long-chain fatty acid (MA or SA) into a mixture of OA and ODE at 290 °C. In a typical synthesis of ZnO nanocrystals, $Zn(St)_2$ (0.1 mmol) and ODE (4 g) were loaded into a 25-mL three-necked flask, degassed, and heated to 280 °C under an argon atmosphere. OA (0.5 mmol) dissolved in ODE (0.5 g) at 150 °C was then injected into the mixture, and the temperature was decreased to 250 °C. After incubating for 10 min at 250 °C, SA (0.1 mmol) dissolved in ODE (0.5 g) at 120 °C was injected into the reaction mixture. The resulting mixture was incubated for 1 h to yield pyramid-shaped ZnO nanocrystals.

Nanoflowers of In_2O_3, ZnO, CoO, and MnO were formed from the corresponding metal acetates in the presence of MA or SA. In a typical synthesis of ZnO nanoflowers, anhydrous $Zn(Ac)_2$ (0.1 mmol), SA or MA (0.1 mmol), and ODE (4.75 g) were heated to 280 °C under an argon atmosphere. DA (0.75 mmol) in ODE (0.5 g) was then injected into the mixture to yield ZnO nanoflowers. Details of the syntheses of individual nanocrystals and nanoflowers of In_2O_3, CoO, MnO, and ZnSe are given in the Supporting Information.

Received: April 19, 2006
Published online: July 6, 2006

Keywords: crystal growth · ligand protection · nanostructures · oriented attachment · oxides

[1] C. B. Murray, C. R. Kagan, M. G. Bawendi, *Annu. Rev. Mater. Sci.* **2000**, *30*, 545.
[2] M. Yin, C.-K. Wu, Y. Lou, C. Burda, J. T. Koberstein, Y. Zhu, S. O'Brien, *J. Am. Chem. Soc.* **2005**, *127*, 9506.
[3] X. Peng, J. Thessing, *Struct. Bonding (Berlin)* **2005**, *118*, 79.
[4] C. B. Murray, D. J. Norris, M. G. Bawendi, *J. Am. Chem. Soc.* **1993**, *115*, 8706.
[5] X. Peng, U. Manna, W. Yang, J. Wickham, E. Scher, A. Kadavanich, A. P. Alivisatos, *Nature* **2000**, *404*, 59.

 © 2006 Wiley-VCH Verlag GmbH & Co. KGaA, Weinheim

[6] T. Hyeon, S. S. Lee, J. Park, Y. Chung, H. B. Na, *J. Am. Chem. Soc.* **2001**, *123*, 12798.
[7] Z. A. Peng, X. Peng, *J. Am. Chem. Soc.* **2001**, *123*, 183.
[8] W. W. Yu, X. Peng, *Angew. Chem.* **2002**, *114*, 2474; *Angew. Chem. Int. Ed.* **2002**, *41*, 2368.
[9] S. Sun, H. Zeng, *J. Am. Chem. Soc.* **2002**, *124*, 8204.
[10] N. R. Jana, Y. Chen, X. Peng, *Chem. Mater.* **2004**, *16*, 3931.
[11] T. J. Trentler, K. M. Hickman, S. C. Goel, A. M. Viano, P. C. Gibbons, W. E. Buhro, *Science* **1995**, *270*, 1791.
[12] C. Pacholski, A. Kornowski, H. Weller, *Angew. Chem.* **2002**, *114*, 1234; *Angew. Chem. Int. Ed.* **2002**, *41*, 1188.
[13] Z. Tang, N. A. Kotov, M. Giersig, *Science* **2002**, *297*, 237.
[14] K.-S. Cho, D. V. Talapin, W. Gaschler, C. B. Murray, *J. Am. Chem. Soc.* **2005**, *127*, 7140.
[15] L. Manna, D. J. Milliron, A. Meisel, E. C. Scher, A. P. Alivisatos, *Nat. Mater.* **2003**, *2*, 382.
[16] Z. R. Tian, J. A. Voigt, J. Liu, B. McKenzie, M. J. McDermott, M. A. Rodriguez, H. Konishi, H. Xu, *Nat. Mater.* **2003**, *2*, 821.
[17] B. Liu, H. C. Zeng, *J. Am. Chem. Soc.* **2004**, *126*, 8124.
[18] Z. Zhang, H. Sun, X. Shao, D. Li, H. Yu, M. Han, *Adv. Mater.* **2005**, *17*, 42.
[19] J. Chen, T. Herricks, Y. Xia, *Angew. Chem.* **2005**, *117*, 2645; *Angew. Chem. Int. Ed.* **2005**, *44*, 2589.
[20] W. W. Yu, Y. A. Wang, X. Peng, *Chem. Mater.* **2003**, *15*, 4300.
[21] A. Narayanaswamy, H. Xu, N. Pradhan, X. Peng, *J. Am. Chem. Soc.*, in press.
[22] Y. Chen, M. Kim, G. Lian, M. B. Johnson, X. Peng, *J. Am. Chem. Soc.* **2005**, *127*, 13331.
[23] R. L. Penn, J. F. Banfield, *Science* **1998**, *281*, 969.
[24] J. Gao, B. Zhang, X. Zhang, B. Xu, *Angew. Chem.* **2006**, *118*, 1242; *Angew. Chem. Int. Ed.* **2006**, *45*, 1220.
[25] H. G. Yang, H. C. Zeng, *Angew. Chem.* **2004**, *116*, 6056; *Angew. Chem. Int. Ed.* **2004**, *43*, 5930.
[26] D. Zitoun, N. Pinna, N. Frolet, C. Belin, *J. Am. Chem. Soc.* **2005**, *127*, 15034.
[27] V. Tzitzios, D. Niarchos, M. Gjoka, N. Boukos, D. Petridis, *J. Am. Chem. Soc.* **2005**, *127*, 13756.
[28] Z. A. Peng, X. Peng, *J. Am. Chem. Soc.* **2002**, *124*, 3343.

 © 2006 Wiley-VCH Verlag GmbH & Co. KGaA, Weinheim

Synthetic Methods

DOI: 10.1002/anie.200601808

Synthesis of Highly Substituted *N*-Hydroxyindoles through 1,5-Addition of Carbon Nucleophiles to In Situ Generated Unsaturated Nitrones**

K. C. Nicolaou, Anthony A. Estrada, Sang Hyup Lee, and Graeme C. Freestone*

We recently reported a new method for the construction of substituted *N*-hydroxyindoles through trapping of unsaturated nitrones by oxygen, sulfur, and nitrogen nucleophiles.[1] Substituted *N*-hydroxyindoles continue to be of considerable interest to us not only because of our efforts towards the total synthesis of the thiopeptide antibiotic nocathiacin I,[2] whose structure contains such a domain, but also due to the growing interest in their construction as a consequence of the proven biological properties of this unique structural motif.[3,4] Intrigued by the preference of phenolic substrates to react through their carbon, rather than their oxygen, centers,[1] we investigated the behavior of various carbon nucleophiles in that process. Herein, we report our findings in this area which constitute a new method for generating highly substituted *N*-hydroxyindoles through carbon–carbon bond formation involving 1,5-addition[5] to α,β-unsaturated nitrones.

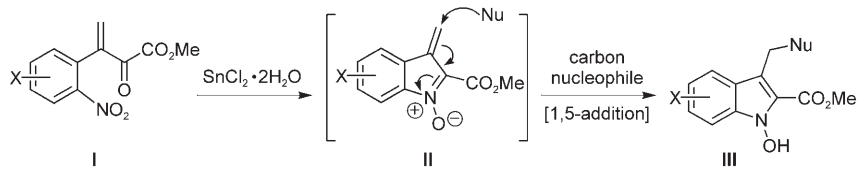
Scheme 1 depicts the transformation involving a $SnCl_2 \cdot 2H_2O$-initiated cascade to facilitate conversion of nitroaromatic α,β-unsaturated ketoesters **I** into α,β-unsaturated nitrones **II**, with subsequent trapping of the latter, rather reactive species by various carbon nucleophiles to afford *N*-hydroxyindoles **III**.[6] To explore this reaction, nitroaromatic α,β-unsaturated ketoesters **3a**–**3e** were prepared from nitroaromatic systems **1a**–**1e** by a two-step process via intermediates **2a**–**2e** in good overall yield (Scheme 2). Bromo-substituted substrate **3a** was then employed in the new process with silyl enol ethers acting as

[*] Prof. Dr. K. C. Nicolaou, A. A. Estrada, Dr. S. H. Lee, Dr. G. C. Freestone
Department of Chemistry and
The Skaggs Institute for Chemical Biology
The Scripps Research Institute
10550 North Torrey Pines Road, La Jolla, CA 92037 (USA)
and
Department of Chemistry and Biochemistry
University of California, San Diego
9500 Gilman Drive, La Jolla, CA 92093 (USA)
Fax: (+1) 858-784-2469
E-mail: kcn@scripps.edu

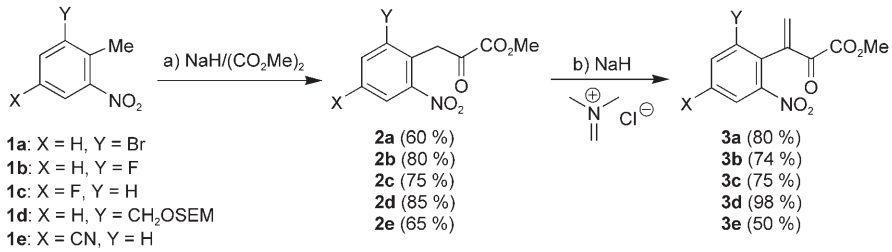
[**] We thank Dr. D. H. Huang, Dr. G. Siuzdak, and Dr. R. Chadha for NMR spectroscopic, mass spectrometric, and X-ray crystallographic assistance, respectively. Financial support for this work was provided by grants from the National Institutes of Health (USA), the National Science Foundation, and the Skaggs Institute for Chemical Biology, and a fellowship from the National Institutes of Health (USA) to A.A.E.

Supporting information for this article is available on the WWW under http://www.angewandte.org or from the author.

WILEY InterScience DISCOVER SOMETHING GREAT
© 2006 Wiley-VCH Verlag GmbH & Co. KGaA, Weinheim



Scheme 1. General path for the construction of 3-substituted *N*-hydroxyindoles (**III**). Nu = carbon nucleophile.



Scheme 2. Synthesis of nitro ketoesters **3a–e**. Reagents and conditions: a) NaH (4.0 equiv), $(CO_2Me)_2$ (5.0 equiv), DMF, 0 °C, 1 h; then 25 °C, 18 h, **2a** (60%), **2b** (80%), **2c** (75%), **2d** (85%), **2e** (65%); b) NaH (1.1 equiv), $CH_2{=}N^+Me_2Cl^-$ (3.0 equiv), THF, 0 °C, 1 h; then 25 °C, 12 h, **3a** (80%), **3b** (74%), **3c** (75%), **3d** (98%), **3e** (50%). DMF = *N*,*N*-dimethylformamide, THF = tetrahydrofuran, SEM = 2-(trimethylsilyl)ethoxymethyl.

carbon nucleophiles under the reductive conditions provided by $SnCl_2{\cdot}2H_2O$ (2.5 equiv) in DME at 40 °C. The results from these experiments are summarized in Table 1. As seen, both cyclic (Table 1, entries 1–3) and acyclic (Table 1, entries 4–10) silyl enol ethers enter the reaction with good yields. The products include *N*-hydroxyindoles substituted at the 3-position with carbon chains containing α-substituted ketones with various groups. These appendages include aliphatic, aromatic, and heteroaromatic ketone functionalities. Of particular interest to pharmaceutical research are the fluoro-substituted compounds, which are also formed in good yields (Table 1, entries 8–10) under these conditions. Furthermore, as a result of their chemical properties, these compounds may serve as viable substrates for further manipulation. By-product **4** (Table 1 and Table 2) is also produced in many of these reactions through an intramolecular Michael addition as previously observed and mechanistically rationalized.[1]

We next tested the possibility of employing silicon- and tin-activated nucleophiles such as allyl silanes and stannanes in the *N*-hydroxyindole-forming reaction. Table 2 summarizes the results of this investigation, further demonstrating the power of this method to construct molecular complexity rapidly and efficiently from simple building blocks. Thus, allyl trimethylsilanes carrying a variety of structural motifs were shown to react smoothly with the α,β-unsaturated nitrone derived from the bromonitroaromatic ketoester **3a** to afford novel *N*-hydroxyindoles (Table 2, entries 1–4). Interestingly, when allyl trimethoxysilane was used (Table 2, entry 5), the methoxy group was transferred to the *N*-hydroxyindole to furnish the corresponding methoxy ether **19** (see Supporting Information) in good yield. In an attempt to complement this result, methoxytrimethylsilane (Table 2, entry 6) was subjected to the reaction conditions and produced, as expected, the same methoxy ether **19**. Further confirmation of the structure of product **19** was obtained by X-ray crystallographic analysis[7] (see Figure 1a). The employment of triethylsilane in the reaction resulted in reduction of the reactive nitrone species, leading to the 3-methyl-substituted product (Table 2, entry 7), while allenyl trimethylsilane furnished an acetylenic compound, **21**, albeit in low yield (20%; Table 2, entry 8). Allyl stannanes (Table 2, entries 9 and 10) also reacted with the nitrone derived from **3a**, leading to the desired products in varying yields. Compound **23** was analyzed by X-ray crystallography[7] (see Figure 1b).

To demonstrate the validity of the proposed method and the generality and scope of the reaction with regards to the nitroaromatic substrate, we explored the employment of substrates **3a–3e** in combination with silyl enol ethers **24** and **25**. Products **5**, **26a–29a**, **8**, and **26b–29b** were formed in moderate to good yields (see Table 3). Of particular interest is the survival of the aromatic nitrile functionality (Table 3, entry 5) under the reductive and nucleophilic conditions employed—an observation that stands as a testament to the mild nature of the process. From Table 3 it can also be seen that the method accommodates various substitution patterns around the aromatic nuclei, including a

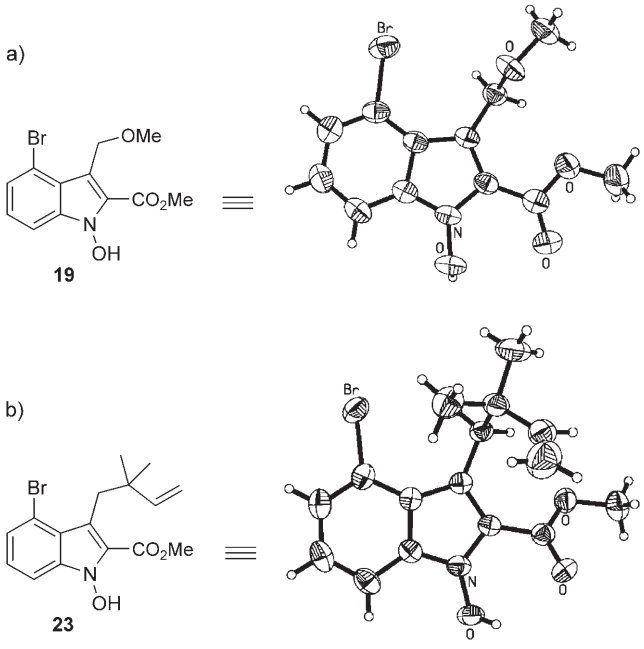
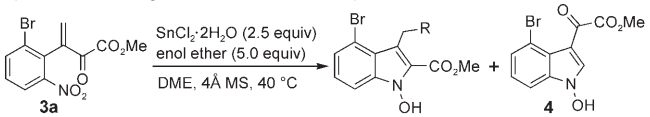
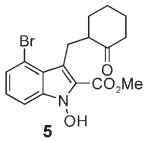
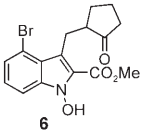
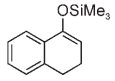
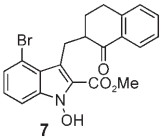
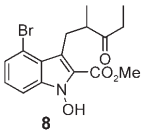
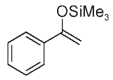
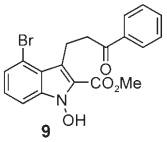
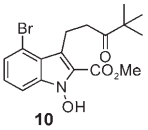
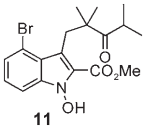
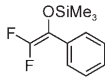
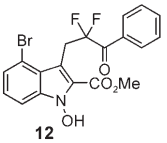
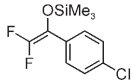
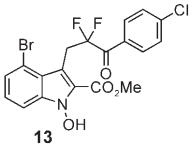
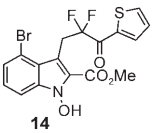


Figure 1. ORTEP drawings of compounds **19** (a) and **23** (b) drawn at the 50% probability level (only heteroatom labels shown).

 © 2006 Wiley-VCH Verlag GmbH & Co. KGaA, Weinheim

Table 1: Synthesis of 3-alkyl-*N*-hydroxyindoles through 1,5-addition of silyl enol ethers to the α,β-unsaturated nitrone derived from **3a**.[a]

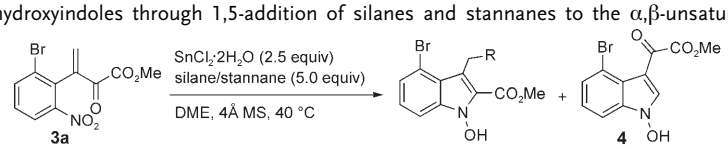


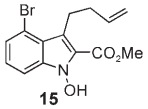
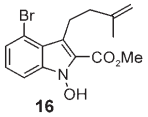
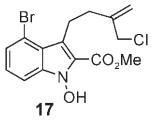
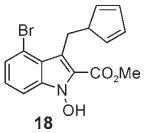
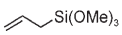
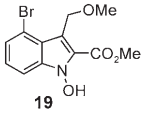
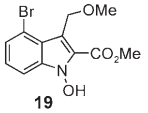
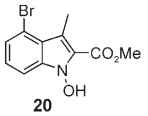
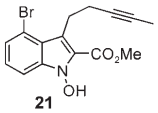
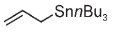
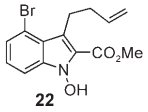
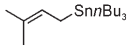
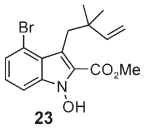
Entry	Enol ether	*t* [h]	Product	Yield [%][b]	Yield (**4**) [%][b]
1		1.5	 **5**	61	17
2		1.5	 **6**	70	17
3		1.2	 **7**	66	11
4		1.0	 **8**	73	10
5		1.3	 **9**	60	10
6		2.0	 **10**	63	10
7		1.0	 **11**	68	15
8		1.5	 **12**	75	[c]
9		1.5	 **13**	75	[c]
10		1.5	 **14**	63	[c]

[a] Reactions were carried out on a scale of 0.06–0.10 mmol in anhydrous 1,2-dimethoxyethane (DME; concentration: 0.12–0.16 M), and the products were purified by preparative TLC (silica gel). [b] Yield of isolated product. [c] Trace amounts not isolated.

© 2006 Wiley-VCH Verlag GmbH & Co. KGaA, Weinheim

Table 2: Synthesis of 3-alkyl-*N*-hydroxyindoles through 1,5-addition of silanes and stannanes to the α,β-unsaturated nitrone derived from **3a**.[a]



Entry	Silane/ stannane	*t* [h]	Product	Yield [%][b]	Yield (**4**) [%][b]
1		2.5	 **15**	57	20
2		1.5	 **16**	61	15
3		3.5	 **17**	50	11
4		15	 **18**	57	15
5		1.5	 **19**	53	12
6	MeO–SiMe$_3$	2.0	 **19**	50	15
7	Et_3SiH	3.5	 **20**	50	16
8		28	 **21**	20	[c]
9		30	 **22**	25	15
10		4.5	 **23**	62	14

[a] Reactions were carried out on a scale of 0.06–0.10 mmol in anhydrous DME (concentration: 0.12–0.16 M), and the products were purified by preparative TLC (silica gel). [b] Yield of isolated product. [c] Trace amounts not isolated.

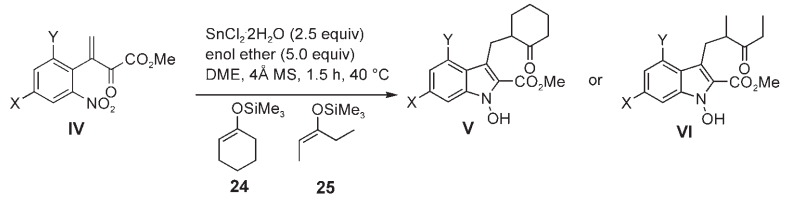
fluorine residue (Table 3, entries 2 and 3), which often exhibits unique pharmacological properties.

Finally, to demonstrate the effect of varying the stoichiometry of the reaction, bromonitroaromatic ketoester **3a** and difluorosilyl enol ether derived from 2,2,2-trifluoroacetophenone[8] were subjected to the standard conditions (Table 1, entry 8), but using 1, 3, 5, or 10 equivalents of the nucleophile. The results (50, 59, 75, and 74% yield, respectively) demonstrate that this method may also be applied to more complex systems where a large excess of the nucleophile may not be acceptable.

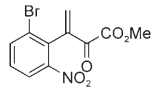
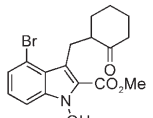
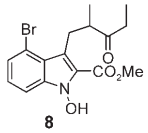
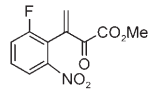
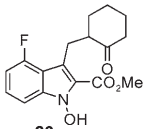
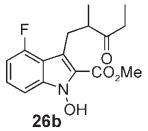
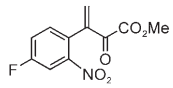
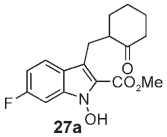
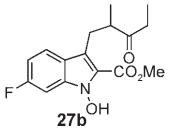
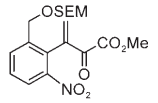
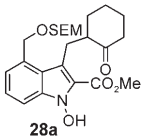
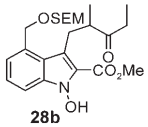
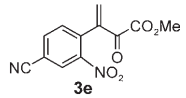
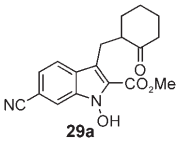
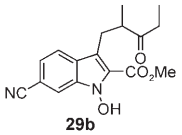
The chemistry described herein expands the repertoire of carbon–carbon bond-forming reactions and provides facile and direct entry to a variety of highly substituted *N*-hydroxyindoles. The method is expected to find applications in chemical synthesis in general and in the construction of

 © 2006 Wiley-VCH Verlag GmbH & Co. KGaA, Weinheim

Table 3: Synthesis of 3-alkyl-*N*-hydroxyindoles through 1,5-addition of silyl enol ethers **24** and **25** to substituted α,β-unsaturated nitrones **IV**.[a,b]



IV 24 25 V VI

Entry	α,β-Unsaturated nitro ketoester	Product **V**	Yield [%][c]	Product **VI**	Yield [%][c]
1	 **3a**	 **5**	61	 **8**	73
2	 **3b**	 **26a**	44	 **26b**	61
3	 **3c**	 **27a**	45	 **27b**	61
4	 **3d**	 **28a**	57	 **28b**	46
5	 **3e**	 **29a**	43	 **29b**	40

[a] Reactions were carried out on a scale of 0.06–0.10 mmol in anhydrous DME (concentration: 0.12–0.16 M), and the products were purified by preparative TLC (silica gel). [b] In each case, a minor by-product corresponding to compound **4** was formed (see Table 1 and Table 2), but not isolated. [c] Yield of isolated product.

molecular complexity and diversity for biological and pharmaceutical purposes in particular.

Received: May 8, 2006
Published online: July 18, 2006

Keywords: *N*-hydroxyindoles · nitrogen heterocycles · silanes · stannanes · synthetic methods

[1] K. C. Nicolaou, S. H. Lee, A. A. Estrada, M. Zak, *Angew. Chem.* **2005**, *117*, 3802–3806; *Angew. Chem. Int. Ed.* **2005**, *44*, 3736–3740.

[2] a) W. Li, J. E. Leet, H. A. Ax, D. R. Gustavson, D. M. Brown, L. Turner, K. Brown, J. Clark, H. Yang, J. Fung-Tomc, K. S. Lam, *J. Antibiot.* **2003**, *56*, 226–231; b) J. E. Leet, W. Li, H. A. Ax, J. A. Matson, S. Huang, R. Huang, J. L. Cantone, D. Drexler, R. A. Dalterio, K. S. Lam, *J. Antibiot.* **2003**, *56*, 232–242; c) K. L. Constantine, L. Mueller, S. Huang, S. Abid, K. S. Lam, W. Li, J. E. Leet, *J. Am. Chem. Soc.* **2002**, *124*, 7284–7285; d) nocathiacin antibiotics: J. E. Leet, H. A. Ax, D. R. Gustavson, D. M. Brown, L. Turner, K. Brown, W. Li, K. S. Lam, WO 2000003722A1 [*Chem. Abstr.* **2000**, *132*, 121531]; e) T. Sasaki, T. Otani, H. Matsumoto, N. Unemi, M. Hamada, T. Takeuchi, M. Hori, *J. Antibiot.* **1998**, *8*, 715–721.

[3] For selected reviews on *N*-hydroxyindoles and their derivatives, see: a) M. Somei, *Adv. Heterocycl. Chem.* **2002**, *82*, 101–155; b) M. Somei, *Heterocycles* **1999**, *50*, 1157–1211; c) R. M. Acheson, *Adv. Heterocycl. Chem.* **1990**, *51*, 105–175.

[4] a) M. Belley, E. Sauer, D. Beaudoin, P. Duspara, L. Trimble, P. Dubé, *Tetrahedron Lett.* **2006**, *47*, 159–162; b) A. Penoni, G. Palmisano, G. Broggini, A. Kadowaki, K. M. Nicholas, *J. Org. Chem.* **2006**, *71*, 823–825; c) A. Wong, J. T. Kuethe, I. W. Davies, *J. Org. Chem.* **2003**, *68*, 9865–9866; d) A. G. Myers, S. B. Herzon, *J. Am. Chem. Soc.* **2003**, *125*, 12080–12081; e) S. Katayama, N. Ae, R. Nagata, *J. Org. Chem.* **2001**, *66*, 3474–3483; f) Z. Wróbel, M. Mąkosza, *Tetrahedron* **1997**, *53*, 5501–5514; g) A. Reissert, H. Heller, *Ber. Dtsch. Chem. Ges.* **1904**, *37*, 4364–4379.

[5] This type of reaction is sometimes referred to as a 1,4-addition.

[6] For a comprehensive review on nitrones, see: P. Merino, *Science of Synthesis, Vol. 27* (Ed.: A. Padwa), Thieme, New York, **2004**, pp. 511–580.

[7] CCDC 603155 (**19**) and 603156 (**23**) contain the supplementary crystallographic data for this paper. These data can be obtained free of charge from The Cambridge Crystallographic Data Centre via www.ccdc.cam.ac.uk/data_request/cif.

[8] a) G. K. S. Prakash, J. Hu, G. A. Olah, *J. Fluorine Chem.* **2001**, *112*, 357–362; b) H. Amii, T. Kobayashi, Y. Hatamoto, K. Uneyama, *Chem. Commun.* **1999**, 1323–1324.

 © 2006 Wiley-VCH Verlag GmbH & Co. KGaA, Weinheim

DNA Catalysis

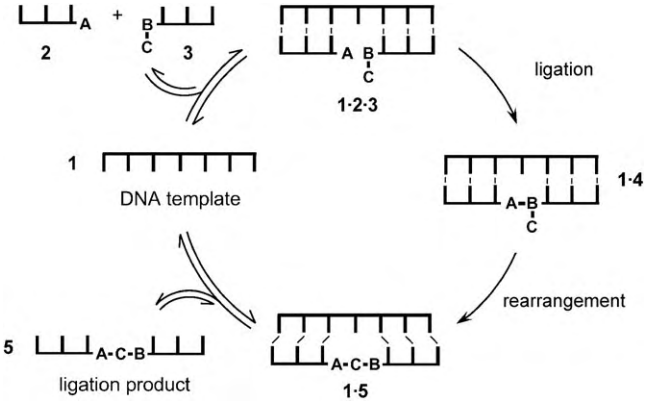
DOI: 10.1002/anie.200600464

Reducing Product Inhibition in DNA-Template-Controlled Ligation Reactions**

*Christian Dose, Simon Ficht, and Oliver Seitz**

Template-directed chemical reactions display features of enzymatic reactions.[1] The binding of reactants allows the alignment of reactive groups to facilitate conversions that would proceed less efficiently when performed in the absence of the template. Templated synthesis has frequently been applied in nucleic acid chemistry, in the construction of nanometer-sized architectures,[2] for the encoding of amplifiable small-molecule libraries,[3] in studies of molecular mechanisms of evolution,[4] to release drugs,[5] and as a diagnostic means of detecting the presence of the nucleic acid template.[6] In contrast to enzymatic reactions, particularly ligation reactions, templates rarely exhibit catalytic turnover since the product usually binds the template with higher affinity than the reactants did before ligation.[7] As a result, stoichiometric amounts of the template are required which is of concern in studies of chemical evolution and in strategies for DNA/RNA detection. Here, we present a potentially general approach to reduce product inhibition in template-controlled ligation reactions. We show that high turnover numbers can be achieved by means of a ligation–rearrangement sequence in which the rearrangement is designed to reduce the template affinity of the initially formed ligation product.

We have explored template-controlled ligation reactions as one of the most powerful methods for the detection of specific DNA sequences.[6a] Chemical ligation methods can discriminate a particular DNA from its single-base mutant by more than 10^3-fold differences in ligation rates.[6c] Conventional methods of chemical oligonucleotide ligation result in only one product molecule per mole of target template. However, amplification of product signals is desired when the DNA or RNA to be detected is present at low concentration. Usually the target segment must span at least 16 nucleotides in order to provide a unique sequence.[8] The high number of cooperatively formed Watson–Crick base pairs poses a problem in the design of catalytic ligation. The challenge is to decrease the DNA affinity of the ligation product without compromising the affinity of the starting compounds for the DNA template or the ligation rate. It has been shown recently that the introduction of a flexible linker at the ligation site helps to lower product inhibition.[7a] As a possible general solution to the problem of product inhibition in DNA-controlled ligation reactions, we propose a two-step ligation–rearrangement sequence (Scheme 1). According to this,



Scheme 1. General scheme of ligation–rearrangement reactions for reducing product inhibition in template-controlled ligations.

hybridization would trigger formation of ligation intermediate **1·4**. We envisioned a subsequent spontaneous rearrangement, which would alter the chain length of the backbone to reduce the template affinity of the rearranged product **5**. As a result, dissociation of product–template duplex **1·5** would be facilitated to liberate template **1** for a further catalytic cycle. To enhance sequence fidelity and as additional means of reducing the template affinity of the ligation product, we planned to perform the ligation opposite to an unpaired nucleobase.[6c]

We have recently introduced native chemical peptide nucleic acid (PNA) ligation,[6b] an extremely rapid and selective reaction[9] that proceeds through a ligation–rearrangement sequence. The design of a ligation architecture that would facilitate dissociation of the product–template duplex was guided by the studies of Egholm, Buchardt, et al., who showed that extension of the aminoethylglycine backbone in PNA by one CH_2 group resulted in destabilization of PNA–DNA duplexes.[10] We assumed that the correct interbase distance would be required not only in seamless base pairing (6 σ bonds) but also in hybridizations involving an abasic site (12 σ bonds). Indeed, the $T_M = 58\,^\circ C$ of a PNA–DNA duplex containing a glycine–glycine unit (interbase distance: 12 σ bonds) as an abasic-site analogue was found to exceed the $T_M = 55\,^\circ C$ measured for a PNA–DNA duplex containing glycine–β-alanine (interbase distance: 13 σ bonds) (Table S1 in the Supporting Information).

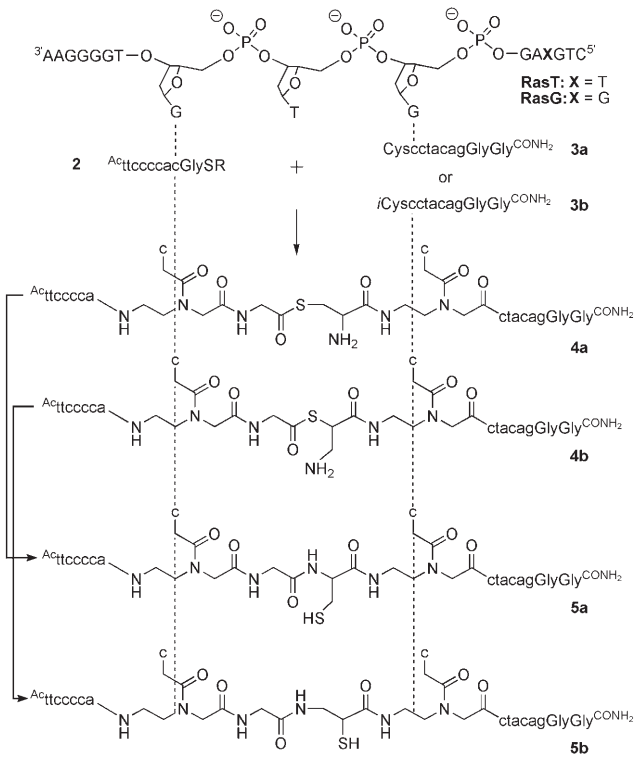
In the previously reported native chemical PNA ligation of PNA–glycine thioester **2** with Cys-PNA **3a**, the thioester intermediate **4a** is formed (Scheme 2).[6b] A subsequent S→N acyl shift leads to contraction of the main chain which is expected to align the nucleobases in product **5a** with an interbase distance of 12 σ bonds, perhaps more favorably than

[*] Dipl.-Ing. C. Dose, Dr. S. Ficht, Prof. Dr. O. Seitz
Institut für Chemie
Humboldt-Universität zu Berlin
Brook-Taylor-Strasse 2, 12489 Berlin (Germany)
Fax: (+49) 30-2093-7266
E-mail: oliver.seitz@chemie.hu-berlin.de

[**] We acknowledge support from Deutsche Forschungsgemeinschaft, Fonds der Chemischen Industrie, and Schering AG. S.F. is grateful for a fellowship from the Grand Duchy of Luxembourg.

Supporting information for this article is available on the WWW under http://www.angewandte.org or from the author.

 © 2006 Wiley-VCH Verlag GmbH & Co. KGaA, Weinheim



Scheme 2. Cys- and *i*Cys-mediated chemical PNA ligation on DNA templates. (R = Bn or $(CH_2)_2SO_3Na$).

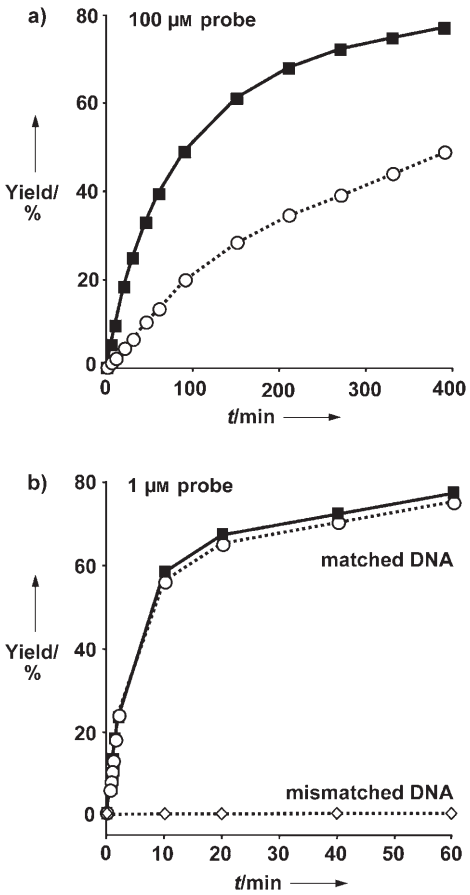


Figure 1. Time courses of the Cys- (■) and *i*Cys-mediated (○) PNA ligation for a) 100 μM **2** and **3** (100 mM Na_2HPO_4, sat. BnSH, pH 7.4, 25 °C) and b) at 1 μM **2** and **3** on matched DNA **RasT** or single-base-mismatched DNA **RasG** (◇, only *i*Cys-mediated ligation shown, 10 mM Na_2HPO_4, 10 mM NaCl, sat. BnSH, pH 7.4, 25 °C).

in thioester intermediate **4a** (interbase distance: 13 σ bonds). To reduce product inhibition, the reaction of thioester **2** with isocysteine(*i*Cys)-PNA **3b** was considered. In *i*Cys-PNA **3b** the positions of the thiol and the amino groups are exchanged.[11] As a result, isocysteine-mediated ligation proceeds by main-chain extension. Here the final product **5b** has an interbase distance of 13 σ bonds and was hence assumed to bind the DNA template less tightly than thioester intermediate **4b**.

The concept was first evaluated by estimating the affinity of PNA probes targeted against the carcinogenic G12V mutation of a 16mer *ras* gene segment. Melting-temperature analysis confirmed that PNA–DNA duplexes containing the final product **5b** of *i*Cys-mediated ligation ($T_M = 53$ °C) are less stable than duplexes that contain the product **5a** of cysteine native chemical ligation ($T_M = 57$ °C). Next studied was the template-independent reaction of Cys-PNA **3a** and *i*Cys-PNA **3b** with PNA-glycine thioester **2** under the conditions of bimolecular native chemical ligation. At 100 μM concentration both Cys- and *i*Cys-mediated ligations proceeded smoothly furnishing product **5a** in 77% yield and **5b** in 49% yield, respectively, after 6.5 h (Figure 1a). Comparison of the initial rates revealed that template-independent bimolecular *i*Cys-mediated PNA ligation is 4.4 times slower than the corresponding Cys-mediated reaction. At a probe concentration of 1 μM, bimolecular ligation was extremely slow (Table S3 in the Supporting Information). Interestingly, Cys and *i*Cys ligations were equally fast when performed on the matched DNA template **RasT** (Figure 1b). In both cases addition of 1 μM template **RasT** led to a dramatic rate enhancement: both **5a** and **5b** were formed in 20% yield after only 90 s reaction time (apparent second-order rate constant: $k_{app} = 2.470\,M^{-1}s^{-1}$). Even higher rate accelerations were obtained with mercaptoethanesulfonate ($k_{app} = 10.820\,M^{-1}s^{-1}$), leading to a 75% yield of ligation product after a reaction time of 5 min (data not shown). Thus, the rate of the *i*Cys- and Cys-mediated PNA ligation is significantly higher than that of alternative chemical reactions for which sequence specificity has been demonstrated[6d–i] and is in the range of the fastest DNA-templated ligations.[12]

The *i*Cys ligation was found to proceed with the same high sequence fidelity (the initial rate on single-base-mismatched DNA **RasG** was 3450-fold slower than on **RasT**) as Cys ligation (Table S2 in the Supporting Information).[6c] It can be concluded that the use of *i*Cys rather than Cys in native chemical PNA ligation reduced the rate of the off-template background reaction without affecting speed and sequence selectivity of the DNA-templated reaction.

The above-discussed features of *i*Cys-mediated ligation were considered to be useful for achieving catalytic turnover. The turnover numbers (TONs) were determined by measuring Cys and *i*Cys ligation at different template/probe ratios. Background signals from reactions in absence of DNA target

 © 2006 Wiley-VCH Verlag GmbH & Co. KGaA, Weinheim

RasT were subtracted in order to ensure that the determined yields were only a result of template-dependent reactions. It was expected that a large excess of ligation probes relative to the template would facilitate the displacement of the ligation product. Indeed, Figure 2 shows that significant turnover

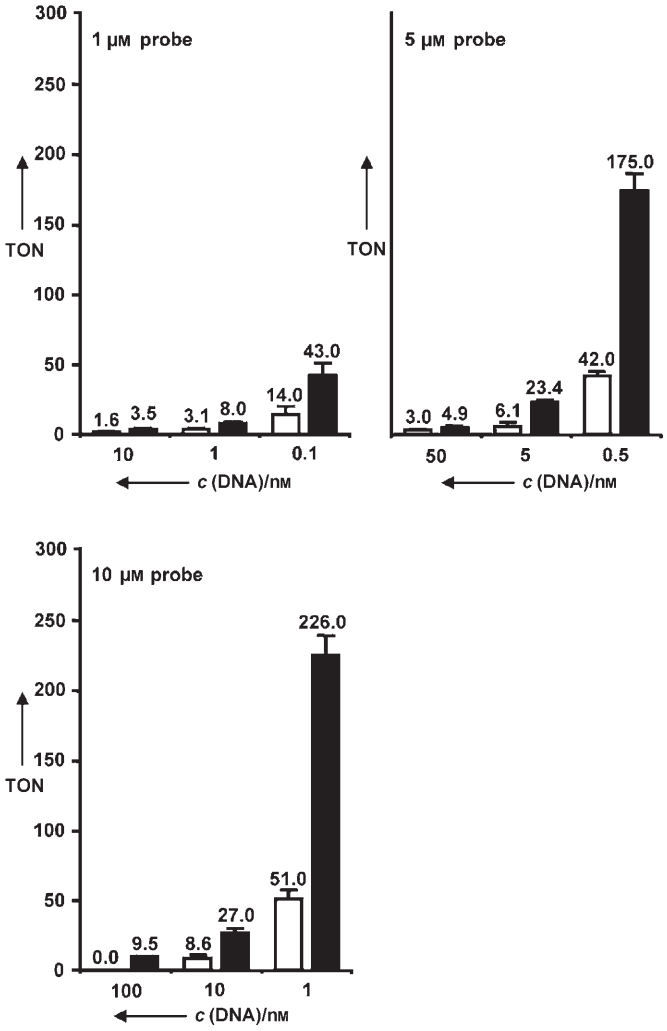


Figure 2. Turnover numbers in Cys- (white bars) and *i*Cys-mediated (black bars) PNA ligations (10 mM Na_2HPO_4, 150 mM NaCl, 10 mM mercaptoethanesulfonic acid (MESNA), pH 7.4, 25 °C, 24 h).

numbers were obtained at low template/probe ratios. For example, at a probe concentration of 1 μM and DNA concentration of 10 nM, *i*Cys ligation yielded a turnover number of 3.5 which improved to 43 for a target concentration of 0.1 nM. Increases of the ligation probe concentration led to further improvements of turnover numbers at any given template/probe ratio. For example, signal amplification in Cys ligation reached 14-fold at 1 μM and 42- and 51-fold at probe concentrations of 5 μM and 10 μM, respectively. However, most noticeable was the observation that in all cases the *i*Cys-mediated chemical ligation provided higher turnover numbers than the Cys-mediated reaction. The highest signal amplification was observed for the *i*Cys ligation with 226 turnovers at a ligation probe concentration of 10 μM and a DNA target concentration of 1 nM; this exceeds turnover numbers reported for alternative methods (vide infra).[7]

The replacement of Cys by *i*Cys has no effect on the stability of probe·DNA complexes; both duplexes **3a·RasT** and **3b·RasT** have a melting temperature of 38 °C. Thus, the remarkable improvement of the turnover numbers observed in isocysteine ligation must be the sole result of the subtle changes of the ligation architecture. The reduced rate of the bimolecular *i*Cys ligation can be explained by the reduced nucleophilicity of the *i*Cys thiol relative to that of the Cys thiol. However, the equal reaction rates of DNA-controlled *i*Cys and Cys ligation suggest that template effects can compensate for the attenuated reactivity of *i*Cys.[13] As a result, DNA-triggered *i*Cys ligation is 43000 times faster than the template-independent reaction, while Cys ligation features rate accelerations of 10000-fold rate accelerations (Table S3 in the Supporting Information). Furthermore, the lower DNA affinity of the *i*Cys-ligation product suggests that the increased flexibility that is provided by a rearrangement that proceeds by main-chain extension helps in facilitating turnover.

In the described work, product signals were quantified by high-pressure liquid chromatography which facilitated the careful analysis of reaction pathways. As fluorescence-based methods enable real-time measurements, they have advantages in terms of ease and speed of detection.[6f] We reckoned that an approach based on fluorescence resonance energy transfer (FRET) between a 6-carboxyfluorescein (FAM) fluorophore in the PNA-glycine thioester **6** and a 5-carboxytetramethylrhodamine (TAMRA) unit in *i*Cys-PNA **7** would enable the specific detection of formed product.[14] HPLC analysis revealed that after 60 min the ligation had proceeded with 52% yield on the matched DNA **Ras2T** and less than 1% yield on the single-base-mismatched template **Ras2G** (Figure S5 in the Supporting Information). The same ligation reaction was analyzed in real time by fluorescence spectroscopy (excitation at 470 nm). Figure 3a shows that the fluorescence spectrum of probes **6** and **7** in the absence of template is dominated by FAM emission at 523 nm. The addition of template **Ras2T** triggered ligation and resulted in a marked change of the fluorescence spectrum characterized by an increase of TAMRA emission (585 nm) and a decrease of FAM emission (523 nm). Melting-temperature analysis for the duplexes **6·Ras2T** ($T_M = 38$ °C) and **7·Ras2T** ($T_M = 36$ °C) confirmed that both PNA probes were aligned on the template at 25 °C. It is noteworthy that adjacent hybridization of two probes that are unable to ligate proved considerably less efficient in inducing fluorescence changes (Figure 3a). Product formation can be monitored by means of the ratio of fluorescence intensities F_{585}/F_{523} or by directly following TAMRA emission at 585 nm (Figure 3b,c). Either method generates a positive signal and, in contrast to other methods that rely on quenchers as leaving groups, is unaffected by hydrolysis. The sequence selectivity of the fluorescence-monitored ligation was high. A comparison of the initial rates, determined by analysis of the increase of F_{585}/F_{523}, revealed that at 25 °C the reaction proceeded 127 times faster on matched DNA **Ras2T** than on mismatched DNA **Ras2G**. Perfect selectivity was obtained at 37 °C. Monitoring of

 © 2006 Wiley-VCH Verlag GmbH & Co. KGaA, Weinheim

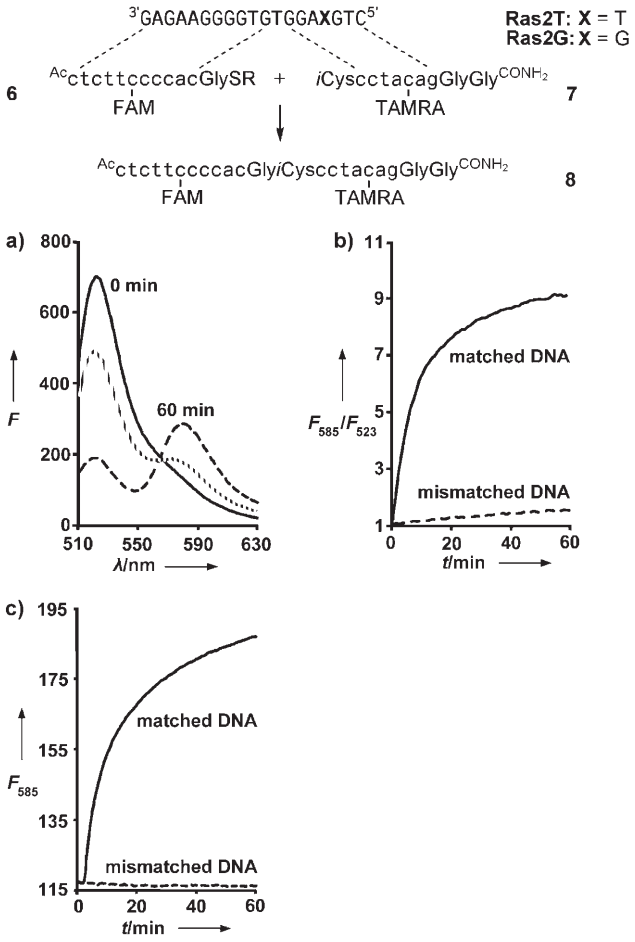


Figure 3. Fluorescence monitoring of the *i*Cys-mediated PNA ligation of PNA probes **6** and **7**. a) Fluorescence spectra before addition of matched DNA **Ras2T** (——) and 60 min after addition (-----). The spectrum of ^{Ac}ctcttc(FAM)cccacGly-OH **9** and **7** after 60 min incubation with **Ras2T** is also shown (•••••). b) Ratio between fluorescence intensities at 585 nm and 523 nm measured for ligations at 25 °C and c) fluorescence intensity at 585 nm for ligations at 37 °C on matched DNA **Ras2T** (——) and mismatched DNA **Ras2G** (-----). (1 μM probes, 10 mM Na_2HPO_4, 150 mM NaCl, 10 mM MESNA, pH 7.4, R = $(CH_2)_2SO_3Na$).

TAMRA emission showed that ligation was not detectable on mismatched template **Ras2G** (Figure 3c).

The presented data demonstrated high single-nucleotide selectivity (3450:1), speed ($k_{app} = 10.820\,M^{-1}s^{-1}$), and rate acceleration (43000-fold) of DNA-template-triggered *i*Cys ligation. We also showed signal amplification (TON = 226) and a convenient means of signal detection by fluorescence spectroscopy. Strategies to reduce product inhibition in template-controlled oligonucleotide reactions have been reported. Kiedrowski et al. introduced a surface-promoted amplification protocol which unlike the present method required successive denaturation–annealing cycles.[15] Albagli et al. used a photoinduced [2+2] cycloaddition for self-replication of oligonucleotide systems.[7c] Lynn and Zhan proposed a DNA ligation of trinucleotides that proceeds by reductive amination and resulted in more than 50 turnovers.[7b] Sequence specificity and fluorescence read-out were not described. Kool et al. introduced a ligation format wherein single-base-mismatched probes coupled 180 times slower than matched probes.[6f] The incorporation of a flexible linker at the ligation site resulted in 12-fold sequence selectivity and 92 turnovers under turnover conditions.[7a] The use of a fluorescence quencher as a leaving group allowed fluorescence-based detection of signals even within living cells. However, fluorescence signaling is not specific for product formation and can arise also from off-target hydrolysis reactions. Krämer, Mokhir, et al. designed a system in which adjacent hybridization of two PNA probes, one bearing a copper complex and the other bearing an ester group, triggered ester hydrolysis. This reaction featured 500-fold rate accelerations on DNA template, 10^2-fold single-nucleotide specificity, and a TON of 5.[6i] Taylor et al. showed the potential for signal amplification in elegant PNA-based systems, in which adjacent hybridization of imidazole- or azide-containing probes prompted deacylation of acyl-quenched fluorogenic probes.[16] Fluorescence signaling was not specific for product formation, and the template-controlled deacylation occurred 36 times faster than the off-template reaction.

In conclusion, we have introduced a new PNA ligation reaction, native chemical isocysteine ligation, and showed significant enhancements of signal amplification over methods based on cysteine ligation and alternative DNA ligation methods. The results demonstrate, for the first time, that the involvement of a flexibility-increasing rearrangement step can reduce product inhibition in template-controlled ligation reactions.

Received: February 3, 2006
Published online: July 17, 2006

Keywords: FRET (fluorescence resonance energy transfer) · native chemical ligation · sequence analysis · single-nucleotide polymorphism · template synthesis

[1] *Templated Organic Synthesis* (Eds.: F. Diederich, P. J. Stang), VCH, Weinheim, **1999**.
[2] a) K. V. Gothelf, A. Thomsen, M. Nielsen, E. Clo, R. S. Brown, *J. Am. Chem. Soc.* **2004**, *126*, 1044–1046; b) L. H. Eckhardt, K. Naumann, W. M. Pankau, M. Rein, M. Schweitzer, N. Windhab, G. von Kiedrowski, *Nature* **2002**, *420*, 286.
[3] a) Z. J. Gartner, B. N. Tse, R. Grubina, J. B. Doyon, T. M. Snyder, D. R. Liu, *Science* **2004**, *305*, 1601–1605; b) X. Li, D. R. Liu, *Angew. Chem.* **2004**, *116*, 4956–4979; *Angew. Chem. Int. Ed.* **2004**, *43*, 4848–4870.
[4] a) L. E. Orgel, *Acc. Chem. Res.* **1995**, *28*, 109–118; b) G. F. Joyce, *Cold Spring Harbor Symposia on Quantitative Biology, Volume LII: Evolution of Catalytic Function*, Cold Spring Harbor Laboratory, **1987**, p. 41–51.
[5] a) Z. C. Ma, J. S. Taylor, *Proc. Natl. Acad. Sci. USA* **2000**, *97*, 11159–11163; b) Q. B. Zhou, S. E. Rokita, *Proc. Natl. Acad. Sci. USA* **2003**, *100*, 15452–15457.
[6] a) A. Mattes, O. Seitz, *Angew. Chem.* **2001**, *113*, 3277–3280; *Angew. Chem. Int. Ed.* **2001**, *40*, 3178–3181; b) S. Ficht, A. Mattes, O. Seitz, *J. Am. Chem. Soc.* **2004**, *126*, 9970–9981; c) S. Ficht, C. Dose, O. Seitz, *ChemBioChem* **2005**, *6*, 2098–2103; d) Y. Z. Xu, E. T. Kool, *Nucleic Acids Res.* **1999**, *27*, 875–881; e) Y. Z. Xu, E. T. Kool, *J. Am. Chem. Soc.* **2000**, *122*, 9040–9041;

 © 2006 Wiley-VCH Verlag GmbH & Co. KGaA, Weinheim

f) Y. Z. Xu, N. B. Karalkar, E. T. Kool, *Nat. Biotechnol.* **2001**, *19*, 148 – 152; g) S. Sando, E. T. Kool, *J. Am. Chem. Soc.* **2002**, *124*, 2096 – 2097; h) J. Brunner, A. Mokhir, R. Krämer, *J. Am. Chem. Soc.* **2003**, *125*, 12410 – 12411; i) I. Boll, R. Krämer, J. Brunner, A. Mokhir, *J. Am. Chem. Soc.* **2005**, *127*, 7849 – 7856; j) P. Hagenbuch, E. Kervio, A. Hochgesand, U. Plutowski, C. Richert, *Angew. Chem.* **2005**, *117*, 6746 – 6750; *Angew. Chem. Int. Ed.* **2005**, *44*, 6588 – 6592.

[7] Template-catalyzed oligonucleotide ligations: a) H. Abe, E. T. Kool, *J. Am. Chem. Soc.* **2004**, *126*, 13980 – 13986; b) Zh.-Y. J. Zhan, D. G. Lynn, *J. Am. Chem. Soc.* **1997**, *119*, 12420 – 12421; c) D. Albagli, R. van Atta, P. Cheng, B. Huan, M. L. Wood, *J. Am. Chem. Soc.* **1999**, *121*, 6954 – 6955.

[8] Q. Liu, D. J. Segal, J. B. Ghiara, C. F. Barbas, *Proc. Natl. Acad. Sci. USA* **1997**, *94*, 5525 – 5530.

[9] P. E. Dawson, T. W. Muir, I. Clark-Lewis, S. B. H. Kent, *Science* **1994**, *266*, 776 – 779.

[10] B. Hyrup, M. Egholm, P. E. Nielsen, P. Wittung, B. Nordén, O. Buchardt, *J. Am. Chem. Soc.* **1994**, *116*, 7964 – 7970.

[11] C. Dose, O. Seitz, *Org. Biomol. Chem.* **2004**, *2*, 59 – 65.

[12] a) I. Saito, Y. Miyauchi, Y. Saito, K. Fujimoto, *Tetrahedron Lett.* **2005**, *46*, 97 – 99; b) S. M. Gryaznov, R. Schultz, S. K. Chaturvedi, R. L. Letsinger, *Nucleic Acids Res.* **1994**, *22*, 2366 – 2369; c) N. I. Sokolova, D. T. Ashirbekova, N. G. Dolinnaya, Z. A. Shabarova, *FEBS Lett.* **1988**, *232*, 153 – 155.

[13] It is conceivable that the template more efficiently stabilizes the transition state of *i*Cys ligation than that of Cys ligation. Equal ligation rates can also be explained if hybridization was rate-determining: a) Z. J. Gartner, M. W. Kanan, D. R. Liu, *Angew. Chem.* **2002**, *114*, 1874 – 1878; *Angew. Chem. Int. Ed.* **2002**, *41*, 1796 – 1800; b) Z. J. Gartner, D. R. Liu, *J. Am. Chem. Soc.* **2001**, *123*, 6961 – 6963. However, PNA hybridization to single-stranded DNA targets has been reported to occur with $k > 10^5\,\text{M}^{-1}\text{s}^{-1}$ while ligation proceeds with $k_{app} = 10^3$–$10^4\,\text{M}^{-1}\text{s}^{-1}$; c) H. Kuhn, V. V. Demidov, J. M. Coull, M. J. Fiandaca, B. D. Gildea, M. D. Frank-Kamenetskii, *J. Am. Chem. Soc.* **2002**, *124*, 1097 – 1103.

[14] The structure of fluorophore-labeled PNA is shown in the Supporting Information. The synthesis will be described elsewhere.

[15] A. Luther, R. Brandsch, G. von Kiedrowski, *Nature* **1998**, *396*, 245 – 248.

[16] a) J. Cai, X. Li, X. Yue, J. S. Taylor, *J. Am. Chem. Soc.* **2004**, *126*, 16324 – 16325; b) J. Cai, X. Li, J. S. Taylor, *Org. Lett.* **2005**, *7*, 751 – 754.

 © 2006 Wiley-VCH Verlag GmbH & Co. KGaA, Weinheim

Cluster Compounds

DOI: 10.1002/anie.200600928

$Na_6[Ge_{10}\{Fe(CO)_4\}_8]\cdot 18\,THF$: A Centaur Polyhedron of Germanium Atoms**

Andreas Schnepf and Christian Schenk*

Metalloid cluster compounds of germanium of the general formula $[Ge_nR_m]$ $(n > m)$[1] contain ligand-bound germanium atoms as well as "naked" germanium atoms that form exclusively Ge–Ge bonds.[2] Various synthetic strategies are known for incorporating naked germanium atoms into metalloid germanium cluster compounds: the reductive elimination of a leaving group XY can provide naked germanium atoms if the X- and Y-bound germanium atoms are further connected only to other germanium atoms in the precursor. This synthetic route was proposed by Sekiguchi et al. for the preparation of the cationic cluster compound $[Ge_{10}(Si\textit{t}Bu_3)_6I]^+$ (**1**).[3] Another synthetic strategy uses the reductive coupling reaction of a substituted germanium(II) halide RGeCl with an adequate reducing agent such as C_8K in the presence of a germanium(II) halide (e.g. $GeCl_2$·dioxane). Thus, Power and co-workers synthesized the metalloid cluster compounds $[Ge_6Ar_2]$ (**2**, $Ar = C_6H_3$-2,6-$Dipp_2$; $Dipp = C_6H_3$-2,6-$i Pr_2$)[4] and $[Ge_5R_4]$ (**3**, $R = CH(SiMe_3)_2$).[5]

We established a third alternative for the preparation of metalloid cluster compounds by using the disproportionation reaction of a molecular germanium(I) halide.[6] Following this synthetic route we were able to synthesize the metalloid cluster compounds $[Ge_8\{N(SiMe_3)_2\}_6]$ (**4**),[7] $[Ge_8\{(O\textit{t}Bu)_2C_6H_3\}_6]$ (**5**),[8] and $[Ge_9\{Si(SiMe_3)_3\}_3]^-$ (**6**).[9]

By using the ternary solvent mixture $N\textit{n}Bu_3$/THF/CH_3CN in the cocondensation reaction[10] of the high-temperature molecule GeBr, we are able to isolate a solution of GeBr from the cocondensation apparatus for the first time. Herein, we report on a first reaction of this GeBr solution with Collman's reagent $Na_2[Fe(CO)_4]$ and formation of the new cluster compound $Na_6[Ge_{10}\{Fe(CO)_4\}_8]\cdot 18\,THF$ (**7**).

The dark red solution of GeBr was treated with Collman's reagent at −40 °C. Slow warming of the reaction mixture to room temperature led to a nearly black reaction solution. Work up of the reaction mixture yielded a dark red diethyl ether extract, from which red crystals of the compound $Na_2[Ge\{Fe(CO)_4\}_3]\cdot 4$ dioxane (**8**) precipitated[11] upon addi-

[*] Dr. A. Schnepf, C. Schenk
Institut für Anorganische Chemie
Universität Karlsruhe (TH)
Engesserstrasse, Geb. 30.45, 76128 Karlsruhe (Germany)
Fax: (+49) 721-608-4854
E-mail: schnepf@chemie.uni-karlsruhe.de

[**] We gratefully acknowledge the financial support of the Deutsche Forschungsgesellschaft. We also thank Prof. Schnöckel for helpful discussions.

Supporting information for this article is available on the WWW under http://www.angewandte.org or from the author.

© 2006 Wiley-VCH Verlag GmbH & Co. KGaA, Weinheim

tion of dioxane. Further work up of the extract yielded another reaction product in the form of black crystals. Recrystallization from THF led to black crystals of the cluster compound **7** which were suitable for X-ray crystal structure analysis. The molecular structure of **7** is shown in Figure 1.

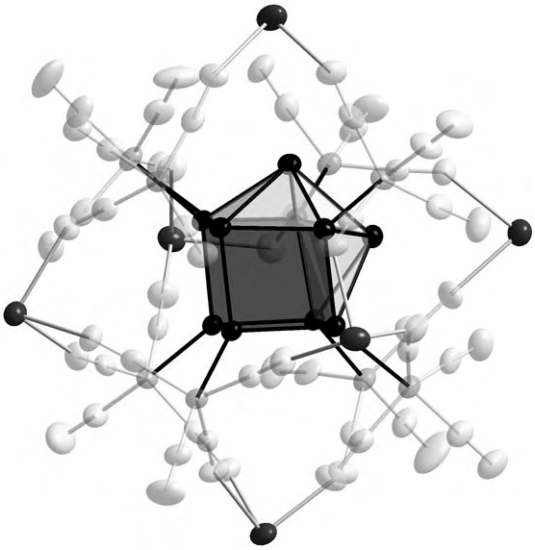


Figure 1. Molecular structure of **7**; THF molecules are omitted for clarity. The central Ge_{10} unit is highlighted by polyhedron illustration. The $\{Fe(CO)_4\}$ units are light-colored, and the six sodium cations are dark-colored.

Cluster compound **7** consists of a Ge_{10} framework in which eight of the ten germanium atoms are each bound to the iron atom of a $\{Fe(CO)_4\}$ ligand (Ge–Fe: 243 pm). The $\{Fe(CO)_4\}$ ligands are further bound to six sodium cations, which are arranged in the form of a distorted octahedron with Na–Na distances between 9 and 11 Å (Figure 1). Each sodium cation is additionally bound to three THF molecules. The cluster core consists of a distorted cubic arrangement of eight $\{GeFe(CO)_4\}$ units. Two of the six rectangular faces are each capped by a naked germanium atom (Ge9 and Ge10, Figure 2). Furthermore, the two capping germanium atoms

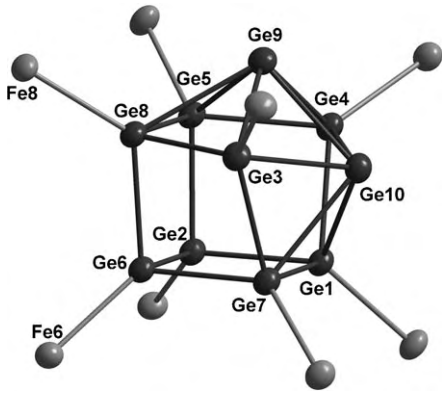


Figure 2. Ge/Fe core of **7**. Selected bond lengths [pm] and angles [°]: Ge6-Fe6 242.21(18), Ge8-Fe8 243.45(16), Ge6-Ge2 249.77(13), Ge6-Ge8 252.63(13), Ge2-Ge1 252.16(14), Ge1-Ge10: 276.47(14); Ge10-Ge9 269.56(14), Ge9-Ge8 274.53(16); Ge8-Ge6-Ge2 91.44(5), Ge8-Ge9-Ge10 100.72(4), Ge9-Ge10-Ge1 99.36(5).

form a direct germanium–germanium bond. Therefore, as in the above-mentioned metalloid germanium cluster compounds, **7** consists of ligand-bound germanium atoms as well as naked germanium atoms.

Since the arrangement of the 10 germanium atoms in the cluster core can also be described as a fusion of two different polyhedra (cube and icosahedron), this arrangement can be called a "centaur polyhedron".[12] In Figure 1 the cubic part (left) is highlighted by a dark-colored polyhedron and the icosahedral part (right) by a light-colored polyhedron. The centaur polyhedron is well-known in solid-state chemistry representing a textbook example for coordination number 10. However, in Group 14 cluster chemistry it is a new structural motif.

The formation of **7** can formally be described, starting from GeBr, by Equation (1).

$$[Ge_{10}Br_{10}] + 8\,Na_2[Fe(CO)_4] \rightarrow Na_6[Ge_{10}\{Fe(CO)_4\}_8] + 10\,NaBr \quad (1)$$

Considering this hypothetical reaction scheme,[13] the average oxidation state of the germanium atoms of **7** can be assigned as +1. Since the oxidation state of the naked germanium atoms should be assigned as zero, the remaining germanium atoms are formally assigned an average oxidation state of +1.25. Consequently, **7** can be described as an internal disproportionation product of GeBr.[14]

Within the Ge_{10} polyhedron the Ge–Ge bond lengths vary between 250 and 276 pm, whereby the germanium atoms with the higher coordination number form the longer Ge–Ge bonds. Thus, the average Ge–Ge bond length for germanium atoms with coordination number four is 252 pm, and the average Ge–Ge bond length of the naked germaniums atoms with coordination number five is 267 pm. This finding corresponds to the same trend observed for Zintl ions, in which the germanium atoms with the higher coordination number also form the longer Ge–Ge bonds. Furthermore, the Ge–Ge bond lengths in **7** are in the same range as in Zintl ions (Ge_5^{2-}: 247–270 pm,[15] Ge_9^{3-}: 257–286 pm,[16] Ge_9^{4-}: 253–296 pm,[17] Ge_{18}^{6-}: 249–284 pm[18]) although the average oxidation state of the germanium atoms is positive in **7** and negative in the Zintl ions.

In contrast, the average Ge–Ge bond lengths in **7** are on average 10 pm larger than those in $[Ge_6\{Cr(CO)_5\}_6]^{2-}$ (**9**),[19] the only other cluster compound in which transition-metal fragments are attached as ligands to the cluster core.[20] These differences may be attributed to the presence of the naked germanium atoms in **7**. Moreover, the difference in formal oxidation state of the germanium atoms in these two compounds is relevant. As described above, the average oxidation state of **7** is +1. Assuming analogous germanium–ligand interactions in **7** and **9**, which is quite realistic as nearly the same Ge–M bond lengths in **7** (243 pm) and **9** (241 pm) are found, a more positive average oxidation state (+1.67) is obtained for cluster compound **9**. Therefore, with respect to the average oxidation state of the germanium atoms, the cluster compound **7** can be classified between the Zintl ions and the octahedral cluster compound **9**. This classification is further supported by the average Ge–Ge bond lengths of these compounds.

 © 2006 Wiley-VCH Verlag GmbH & Co. KGaA, Weinheim

As the Zintl ions[21] and the cluster compound **9** can be described by Wade's rules,[22] the question arises as to whether **7** also fulfills Wade's rules. Assuming that the two electrons of the Ge–Fe bond are supplied by the germanium atom, thus leading to the ideal number of 18 valence electrons for each iron atom, and if the naked germanium atoms further bear a lone pair of electrons, every germanium atom in **7** provides two electrons for cluster bonding. Together with the six electrons of the negative charge of the cluster fragment $[Ge_{10}\{Fe(CO)_4\}_8]^{6-}$, this interpretation leads to 26 electrons for cluster bonding ($2n+6$; $n=10$). For cage compounds with $2n+6$ bonding electrons an *arachno* structure is expected according to Wade's rules, and the structure of **7** can indeed be described as a distorted *arachno* structure. Adding two more germanium atoms would lead to an icosahedral *closo* structure.

The formal description of **7** by Wade's rules points to delocalized bonding electrons within the cluster core. This assumption is supported by preliminary quantum-chemical calculations on the model compound $[Ge_{10}\{Fe(CO)_4\}_8]^{6-}$, for which a structure analogous to **7** was calculated.[23] By using an Ahlrichs–Heinzmann population analysis, SENs (shared electron numbers)[24] of three-center bonding contributions between 0.04 and 0.28 were calculated. In the triangles of the icosahedral part of the centaur polyhedron, an average SEN for the three-center bonding components of 0.28 (e.g. Ge1-Ge7-Ge10: 0.284; Ge3-Ge9-Ge10: 0.283) is found. In contrast, the average SEN for the three-center bonding components in the triangles of the cubic part decreases to 0.07 (e.g. Ge3-Ge6-Ge7: 0.09; Ge8-Ge6-Ge7: 0.06). Thus, the bonding situation of the cluster core changes from "localized" in the cubic part to "delocalized" in the icosahedral part, thus representing a completely new bonding situation in metalloid cluster compounds.

These first results show the synthetic potential of this new metastable solution of GeBr. Furthermore, the average oxidation states of **7** (+1) and **8** (+4) lead to the suggestion that species that have an average oxidation state between one and zero should be present in the reaction solution, and such species may thus contain more "naked" germanium atoms.

Experimental Section

A solution of GeBr (14 mL, 0.29 M in $CH_3CN/THF/nBu_3N$ 2:2:1; 4.06 mmol) at −30 °C was added to $Na_2[Fe(CO)_4]\cdot 1.5\,C_4H_8O_2$ (1.2 g, 3.46 mmol) at −78 °C. The stirred reaction mixture was slowly warmed to room temperature and resulted in a black solution. Removal of the solvent in vacuum yielded a black residue. Extraction with diethyl ether gave a dark red solution from which, after the addition of dioxane and storage at +7°, orange-red crystals of **8** (100 mg, 0.1 mmol, 10%) precipitated. After separation of the crystals and further concentration of the extract, black crystals were formed (ca. 10 mg). Recrystallization of these crystals from THF yielded black crystals of **7**.

Crystal structure data for **8**: $M_r = 974.66\ g\,mol^{-1}$, crystal dimensions $0.3\times0.2\times0.1$ mm, triclinic, space group $P\bar{1}$, $a=10.614(2)$, $b=11.087(2)$, $c=19.205(4)$ Å, $\alpha=103.51(3)$, $\beta=92.17(3)$, $\gamma=114.38(3)°$, $V=1978.4(7)$ Å^3, $Z=2$, $\rho_{calcd}=1.636\ g\,cm^{-3}$, $\mu_{Mo}=1.928\ mm^{-1}$, $2\theta_{max}=51.92°$, 14098 measured, 7203 independent reflections (R(int.) = 0.0343), absorption correction: numerical (min./max. transmission 0.6125/0.9032), $R_1=0.0298$, $wR_2=0.0615$. Stoe IPDS II diffractometer ($Mo_{K\alpha}$ radiation ($\lambda=0.71073$ Å), 120 K).

Crystal structure data for **7**: $M_r = 3504.83\ g\,mol^{-1}$, crystal dimensions $0.4\times0.35\times0.15$ mm, monoclinic, space group $P2(1)/n$, $a=18.557(4)$, $b=27.664(6)$, $c=26.884(5)$ Å, $\beta=92.11(3)°$, $V=13790(10)$ Å^3, $Z=4$, $\rho_{calcd}=1.688\ g\,cm^{-3}$, $\mu_{Mo}=3.055\ mm^{-1}$, $2\theta_{max}=50.24°$, 80226 measured, 23999 independent reflections (R(int.) = 0.0948), absorption correction: numerical (min./max. transmission 0.3549/0.7065), $R_1=0.0735$, $wR_2=0.1623$. Stoe IPDS II diffractometer ($Mo_{K\alpha}$ radiation, ($\lambda=0.71073$ Å), 100 K).

The structures were solved by direct methods and refined against F^2 for all observed reflections. Programs used: SHELXS and SHELXL.[25] CCDC-298741 (**7**) and -298740 (**8**) contain the supplementary crystallographic data for this paper. These data can be obtained free of charge from The Cambridge Crystallographic Data Centre via www.ccdc.cam.ac.uk/data_request/cif.

Received: March 9, 2006
Revised: April 5, 2006
Published online: July 17, 2006

Keywords: centaur polyhedron · cluster compounds · density functional calculations · germanium

[1] A. Schnepf, *Angew. Chem.* **2004**, *116*, 682; *Angew. Chem. Int. Ed.* **2004**, *43*, 664; A. Schnepf, *Coord. Chem. Rev.* **2006**, in press.
[2] According to the original definition from Schnöckel and coworkers, metalloid cluster compounds of germanium contain more germanium–germanium contacts than germanium–ligand contacts and contain germanium atoms (termed "naked" germanium atoms) that participate exclusively in germanium–germanium interactions. As a result of this definition metalloid germanium cluster compounds exhibit the general formula $[Ge_nR_m]$ ($n>m$): A. Purath, R. Köppe, H. Schnöckel, *Angew. Chem.* **1999**, *111*, 3114; *Angew. Chem. Int. Ed.* **1999**, *38*, 2926.
[3] A. Sekiguchi, Y. Ishida, Y. Kabe, M. Ichinohe, *J. Am. Chem. Soc.* **2002**, *124*, 8776.
[4] A. F. Richards, H. Hope, P. P. Power, *Angew. Chem.* **2003**, *115*, 4205; *Angew. Chem. Int. Ed.* **2003**, *42*, 4071.
[5] A. F. Richards, M. Brynda, M. M. Olmstead, P. P. Power, *Organometallics* **2004**, *23*, 2841.
[6] A. Schnepf, *Phosphorus Sulfur Silicon Relat. Elem.* **2004**, *179*, 695.
[7] A. Schnepf, R. Köppe, *Angew. Chem.* **2003**, *115*, 940; *Angew. Chem. Int. Ed.* **2003** *42*, 911.
[8] A. Schnepf, C. Drost, *Dalton Trans.* **2005**, 3277.
[9] A. Schnepf, *Angew. Chem.* **2003**, *115*, 2728; *Angew. Chem. Int. Ed.* **2003**, *42*, 2624.
[10] A. Schnepf, R. Köppe, *Z. Anorg. Allg. Chem.* **2002**, 2914.
[11] Compound **8** is formed from $Na_2[Fe(CO)_4]$ and a germanium halide by metathesis. A suitable germanium halide is $GeBr_4$, the oxidation product of the disproportionation reaction: $GeBr_4 + 3\,Na_2[Fe(CO)_4] \rightarrow Na_2[Ge\{Fe(CO)_4\}_3] + 4\,NaBr$. Therefore, the central germanium atom in **8** can be assigned a formal oxidation state of +4, and thus every iron atom has the ideal value of 18 valence electrons.
[12] Similar to the description of the centaur in Greek mythology (half human, half horse), a polyhedron built through the fusion of two different polyhedrons (here: half cube, half icosahedron) can be called a centaur polyhedron. C. Rocaniere, J. P. Laval, P. Dehaudt, B. Gaudreau, A. Chotard, E. Suard, *J. Solid State Chem.* **2004**, *177*, 1758.
[13] Neither $[Ge_{10}Br_{10}]$ nor any $[(GeBr)_n]$ species have been synthesized so far. However, in analogy to the characterized EX species of Group 13 (E = Ga, Al; X = halogen)[14] the synthetic method

 © 2006 Wiley-VCH Verlag GmbH & Co. KGaA, Weinheim

introduced by us might give access to such germanium subhalides.
[14] A similar situation is known in Group 13 chemistry, in which the cluster compound $[Al_{22}Br_{20}]\cdot 10\,THF$ can also be seen as an internal disproportionation product of AlBr. However, **7** is not a binary compound since the halogen atoms are substituted by the ligand $[Fe(CO)_4]^{2-}$. C. Klemp, M. Bruns, J. Gauss, U. Häussermann, G. Stößer, L. van Wüllen, M. Jansen, H. Schnöckel, *J. Am. Chem. Soc.* **2001**, *123*, 9099; C. Klemp, R. Köppe, E. Weckert, H. Schnöckel, *Angew. Chem.* **1999**, *111*, 1852; *Angew. Chem. Int. Ed.* **1999**, *38*, 1740.
[15] J. Campbell, G. J. Schrobilgen, *Inorg. Chem.* **1997**, *36*, 4078.
[16] T. F. Fässler, U. Schütz, *Inorg. Chem.* **1999**, *38*, 1866.
[17] C. H. E. Belin, J. D. Corbett, A. Cisar, *J. Am. Chem. Soc.* **1977**, *99*, 7163.
[18] L. Xu, S. C. Sevov, *J. Am. Chem. Soc.* **1999**, *121*, 9245.
[19] P. Kircher, G. Huttner, K. Heinze, G. Renner, *Angew. Chem.* **1998**, *110*, 1754; *Angew. Chem. Int. Ed.* **1998**, *37*, 1756.
[20] A great variety of transition-metal-substituted Zintl ions are known. However, in these cluster compounds the transition metal is part of the polyhedron and not a ligand. Thus, these compounds do not belong to the compounds described here. B. Kesanli, J. Fettinger, B. Eichhorn, *Chem. Eur. J.* **2001**, *7*, 5277; B. Kesanli, J. Fettinger, D. R. Gardner, B. Eichhorn, *J. Am. Chem. Soc.* **2002**, *124*, 4779; J. Campbell, H. P. A. Mercier, H. Franke, D. P. Santry, D. A. Dixon, G. J. Schrobilgen, *Inorg. Chem.* **2002**, *41*, 86; L. Yong, S. D. Hoffmann, T. F. Fässler, *Eur. J. Inorg. Chem.* **2005**, 3663.
[21] J. D. Corbett, *Angew. Chem.* **2000**, *112*, 682; *Angew. Chem. Int. Ed.* **2000**, *39*, 670; T. F. Fässler, *Angew. Chem.* **2001**, *113*, 4289; *Angew. Chem. Int. Ed.* **2001**, *40*, 4161; T. F. Fässler, *Coord. Chem. Rev.* **2001**, *215*, 347.
[22] K. Wade, *Adv. Inorg. Chem. Radiochem.* **1976**, *18*, 1.
[23] Quantum-chemical calculations were carried out with the RI-DFT version of the TURBOMOLE program package by employing the Becke–Perdew86 functional. The basis sets were of SVP quality. The electronic structure was analyzed with the Ahlrichs–Heinzmann population analysis as based on occupation numbers. TURBOMOLE: O. Treutler, R. Ahlrichs, *J. Chem. Phys.* **1995**, *102*, 346; BP86 functional: J. P. Perdew, *Phys. Rev. B* **1986**, *33*, 8822; A. D. Becke, *Phys. Rev. A* **1988**, *38*, 3098; RI-DFT: K. Eichkorn, O. Treutler, H. Öhm, M. Häser, R. Ahlrichs, *Chem. Phys. Lett.* **1995**, *240*, 283; SVP: A. Schäfer, H. Horn, R. Ahlrichs, *J. Chem. Phys.* **1992**, *97*, 2571; Ahlrichs–Heinzmann population analysis: E. R. Davidson, *J. Chem. Phys.* **1967**, *46*, 3320; K. R. Roby, *Mol. Phys.* **1974**, *27*, 81; R. Heinzmann, R. Ahlrichs, *Theor. Chim. Acta* **1976**, *42*, 33; C. Erhardt, R. Ahlrichs, *Theor. Chim. Acta* **1985**, *68*, 231.
[24] Shared electron numbers (SENs) for bonds are a reliable measure of the strength of covalent bonding. For example, the SEN for the Ge–Ge single bond in the model compound $R_3Ge–GeR_3$ ($R = NH_2$) is 1.04.
[25] G. M. Sheldrick, SHELXTL, Version 5.1, Bruker AXS, **1998**.

 © 2006 Wiley-VCH Verlag GmbH & Co. KGaA, Weinheim

Electron Transfer

DOI: 10.1002/anie.200600150

Thymine Oxetanes as Charge Traps for Chemical Monitoring of Nucleic Acid Mediated Transfer of Excess Electrons**

*Thorsten Stafforst and Ulf Diederichsen**

Nucleic acid mediated electron transfer in DNA is highly relevant for the understanding of DNA damage and repair.[1] The investigation of the distance and sequence dependence of electron transfer in DNA is necessary to estimate its application as a molecular wire in nanobiotechnology.[2] While principles of hole transfer in DNA were basically elucidated by a combination of modern time-resolved spectroscopy[3] and chemical monitoring,[4] the detailed investigation of the long-range transfer of excess electrons is still problematic owing to the lack of a suitable acceptor system for chemical monitoring. The extensively used cyclobutane pyrimidine dimer (CPD) proved to be unsuitable for chemical monitoring of excess-electron transfer: its redox potential[5] is unfavorable compared to that of thymine ($\Delta G \approx +0.1$ eV), and the cycloreversion rate[6] of the detecting reaction is slow ($\approx 10^6\ s^{-1}$).[7]

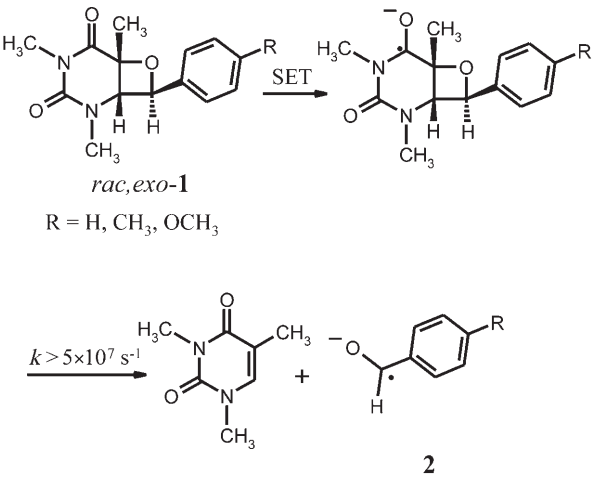
We herein present the synthesis and systematic study of excess-electron transfer of an acceptor system based on a thymine oxetane. These were first introduced as models for a proposed oxetane intermediate in (6–4) photodamage (Scheme 1).[8] It was known from earlier investigations that thymine oxetanes **1** can take up a single electron and react by cycloreversion to give thymine and benzaldehyde radical anions **2**. The cycloreversion rate ($> 5 \times 10^7\ s^{-1}$)[8] determined by transient absorption spectroscopy of the liberated benzaldehyde radical anion **2** is fast, and the energetics compared to those thymine of are favorable [$\Delta G_{\text{thymine}} - \Delta G_{\text{thymine oxetane}} \approx -(0.1\text{–}0.25$ eV)]. Thus we were encouraged to investigate their suitability as charge traps in nucleic acid mediated transfer of excess electrons. In contrast to the detection of guanine oxidation in hole transfer or 5-bromouracil reduction[9] in excess-electron-transfer processes, strand scission is not required for the chemical monitoring of charge transfer through cycloreversion of thymine oxetanes. Thus they can be

[*] Dr. T. Stafforst, Prof. Dr. U. Diederichsen
Institut für Organische und Biomolekulare Chemie
Georg-August-Universität Göttingen
Tammannstrasse 2, 37077 Göttingen (Germany)
Fax: (+49) 551-392-944
E-mail: udieder@gwdg.de

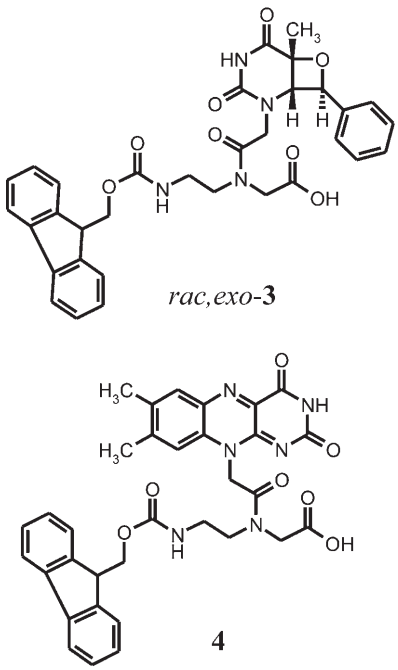
[**] This work was supported by the Volkswagen Foundation and the Deutsche Forschungsgemeinschaft (GRK 782). We are grateful for the fellowship from the Fonds der Chemischen Industrie for T.S.

Supporting information for this article, including the characterization of all oligomers and details concerning excess-electron-transfer experiments, ferrioxalate actinometry, and calculation of the corrected quantum yield $\Phi_{corr.}$, is available on the WWW under http://www.angewandte.org or from the author.

InterScience
© 2006 Wiley-VCH Verlag GmbH & Co. KGaA, Weinheim



Scheme 1. Cycloreversion of thymine oxetanes **1** into *N*,*N*′-dimethylthymine and benzaldehyde radical anions **2** after reductive single-electron transfer (SET). The liberation of **2** was monitored by transient absorption spectroscopy after laser flash photolysis in the presence of various reductive sensitizers.



Scheme 2. Fmoc-protected building blocks **3** and **4** for *N*-(2-aminoethyl)glycine-PNA synthesis. The thymine oxetane moiety was synthesized in *exo* configuration as a racemic mixture by a Paterno–Büchi reaction.

applied in *N*-(2-aminoethyl)glycine-PNA (PNA = peptide nucleic acid),[10] alanyl-PNA,[11] or any other DNA model. Here we describe the properties of oxetane-functionalized *N*-(2-aminoethyl)glycine-PNA and the systematic investigation of excess-electron transfer upon hybridization with DNA with regard to distance dependence.

To incorporate acid-sensitive thymine oxetanes into (2-aminoethyl)glycine-PNA, we synthesized the respective oxetane-functionalized 9-fluorenylmethoxycarbonyl(Fmoc)-protected building block **3** in *exo* configuration (Scheme 2).[12] (2-Aminoethyl)glycine-PNA oligomers were synthesized by means of the Fmoc/benzhydryloxycarbonyl(Bhoc) strategy[13] from commercially available nucleo amino acids. The preparation of building blocks **3** and **4** will be described elsewhere.[14] A protocol was developed to permit the cleavage of the highly acid-sensitive oligomers from Sieberamide resin. All oligomers were purified by preparative HPLC and obtained in yields of 5–10%.

First experiments were performed with the PNA 12mer **5**, in which the large flavin chromophore is placed at the end of the sequence to minimize steric distortion within a DNA/PNA duplex. The thymine oxetane was located two base pairs away from the flavin inside the base stack (Table 1). As reference sequences the 12mer **6**, in which the thymine oxetane is replaced by a thymine, and the 11mer **7**, containing only canonical nucleobases, were synthesized. The antiparallel pairing of these three PNA oligomers with the complementary 11mer DNA **8** (5′-G-C_2-G-C_2-A_5-3′) gave sigmoidal UV-melting curves that showed no hysteresis between cooling and heating. CD spectra of **5**·**8**, **6**·**8**, and **7**·**8** showed temperature-dependent bands at the optical transitions of the

Table 1: Comparison of PNA oligomers **5**–**14** with regard to the UV-melting behavior, kinetic parameters, and HPLC retention times of their complexes with DNA **8** and **15**.[a]

Sequence	DNA	T_{m1}	Hyst.	T_{m2}	$\tau_{1/2}$ [min]	Φ [‰]	t_R [min]
Ac-***flavin***-t_2-***Ox***-t_2-g_2-c-g_2-c-K_2-G-NH_2 (**5**)	**8**	73 °C	1.5 °C	71.5 °C	59 ± 3	5.3	16.04
Ac-***flavin***-t_5-g_2-c-g_2-c-K_2-NH_2 (**6**)	**8**	73 °C	0 °C	73 °C	–	–	13.60
Uro-t_5-g_2-c-g_2-c-K_2-NH_2 (**7**)	**8**	70.5 °C	0 °C	70.5 °C	–	–	12.32
Ac-***flavin***-t-***Ox***-t_7-a-g-c-K_2-G-NH_2 (**9**)	**15**	72 °C	9 °C	63 °C	82.5 ± 4	3.8	16.54
Ac-***flavin***-t_2-***Ox***-t_6-a-g-c-K_2-G-NH_2 (**10**)	**15**	62 °C	5 °C	57 °C	129 ± 6	2.4	16.37
Ac-***flavin***-t_4-***Ox***-t_4-a-g-c-K_2-G-NH_2 (**11**)	**15**	60 °C	2.5 °C	57.5 °C	266 ± 13	1.2	16.32
Ac-***flavin***-t_6-***Ox***-t_2-a-g-c-K_2-G-NH_2 (**12**)	**15**	60 °C	5 °C	55 °C	277 ± 14	1.1	15.96
Ac-***flavin***-t_8-***Ox***-a-g-c-K_2-G-NH_2 (**13**)	**15**	73 °C	14 °C	59 °C	192 ± 10	1.6	15.56
Ac-***flavin***-t_9-a-g-c-K_2-G-NH_2 (**14**)	**15**	89 °C	18 °C	71 °C	–	–	14.05

[a] Ox = thymine oxetane, Ac = Acyl, Uro = N=C[$N(CH_3)_2$]$_2$; T_{m1} = UV-melting temperature (heating), hyst. = $T_{m1} - T_{m2}$ (heating–cooling hysteresis); T_{m2} = UV-melting temperature (cooling); 3 μM PNA plus 3 μM complementary DNA **8** (5′-G-C_2-G-C_2-A_5-3′) or **15** (5′-G-C-T-A_9-3′) in 10 mM NaH_2PO_4 buffer, 0.1 M NaCl, pH 6.9; $\tau_{1/2}$ = half-life in excess-electron transfer experiment; Φ = quantum yield of excess-electron transfer; t_R = retention time from analytical RP-HPLC (Vydac 25 cm, C-4, 5%→40% B in 20 min, B = acetonitrile/water 8:2 + 1‰ trifluoroacetic acid (TFA), A = water + 1‰ TFA); K = lysine, G = glycine.

 © 2006 Wiley-VCH Verlag GmbH & Co. KGaA, Weinheim

nucleobases (265 nm) and the flavin chromophore (373 nm, 450 nm), which are in accordance with the UV-melting behavior. Incorporation of the overhanging flavin chromophore in the oligomer **6·8** was reflected by a slight stabilization of 2.5 °C in the UV-melting temperature compared to that of the nonfunctionalized oligomer **7·8**. These results along with the CD spectra indicate a well-stacked flavin chromophore free of steric distortion. The replacement of one thymine by the thymine oxetane led to no detectable loss in stability and indicates a well-stacked and hydrogen-bonded thymine oxetane/adenine pair without crucial distortion.[15] Although the thymine oxetane was incorporated as a racemic mixture, neither the UV- nor the CD-melting curves of **5·8** show a discrimination for the enantiomers.

In the electron-transfer experiment with a duplex containing PNA **5** and complementary DNA **8**, the dimer was reduced with sodium dithionite in a fluorescence spectrometer and then irradiated at 430 nm (20-nm bandwidth).[16] The reaction was followed by taking samples (each 2.5 % of the total sample volume) for HPLC analysis until 85 % conversion was reached. The obtained photoproduct had the same HPLC retention time as oligomer **6**. The decay of oxetane-PNA **5** was strictly light-dependent and obeyed first-order kinetics (Figure 1). The fluorescence spectrometer was calibrated by ferrioxalate actinometry, and a half-life for **5**, 59 ± 3 min, was calculated which corresponds to a quantum yield of 5.3 ‰.[17] The observed quantum yield was remarkably high—more than 100 times greater than that of the flavin/CPD system for transfer over the same distance (two AT base pairs).[18] No discrimination in the diastereomeric oligomers was observed in the conversion kinetics.

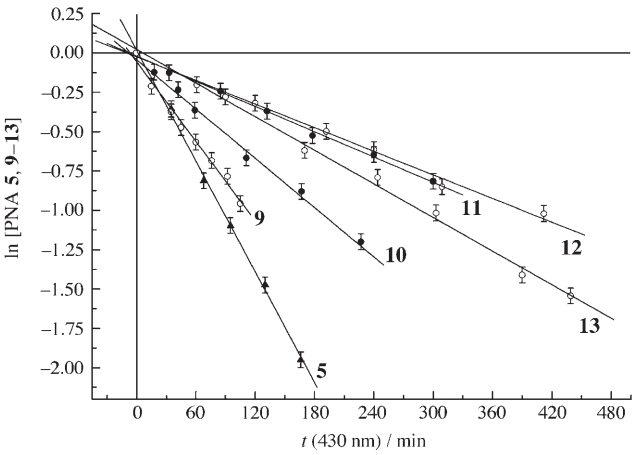


Figure 1. Analysis of the first-order kinetics of excess-electron transfer from the HPLC data for all PNA oligomers: 9 μM PNA **5** plus 15 μM complementary DNA **8** (5′-G-C_2-G-C_2-A_5-3′) or 9 μM of PNA **9–13** plus 15 μM complementary DNA **15** (5′-G-C-T-A_9-3′), each in 10 mM NaH_2PO_4 buffer, 0.1 M NaCl, pH 6.9; t = irradiation time; irradiation under reductive conditions as described. The errors were estimated from the HPLC signal/noise ratio to be roughly 5 %.

To systematically study the charge transfer, we synthesized a series of five oligomers (**9–13**) by varying the distance between the charge donor and the charge acceptor to cover the range d = 6.8–30.6 Å (Table 1). Oligomer **14** was prepared as a reference oligomer lacking the oxetane moiety. Unfortunately, oligomers **9–14** tended to form $(PNA)_2$DNA triple strands upon addition of complementary DNA **15** (5′-G-C-T-A_9-3′), as indicated by the hysteresis of the melting temperatures between cooling and heating. We assume that the typical P-form triple helix[19] forms with antiparallel orientation of the PNA strand in Watson–Crick pairing mode and parallel orientation of the PNA strand in Hoogsteen pairing mode. Only in this way can the PNA strands align with antiparallel orientation and the maximum distance between the thymine oxetane residues be achieved (Figure 2). This is in accordance with the lowest triple-strand stabilization of just 2.5 °C for **11·15**, in which which both thymine oxetanes are incorporated in the same triple base pair. Despite the formation of triple strands, the CD, fluorescence, and UV-melting behavior was as expected. Based on calorimetric data,[20] a melting temperature of 59 °C was proposed for the formation of antiparallel double strand from oligomers **9–13** and the complementary DNA **15**, which is in accordance with the observed melting temperatures T_{m2}.

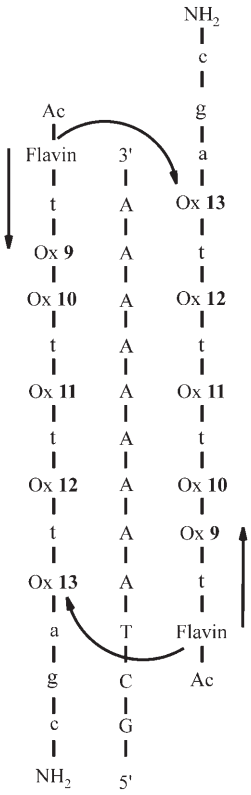


Figure 2. Assumed orientation of all strands as typical for a P-form $(PNA)_2$DNA triple helix; boldface numbers mark the positions at which thymine oxetanes can be incorporated; the directions of intra- and interstrand charge transfer are indicated by the straight and curved arrows, respectively.

The experiments on excess-electron transfer were performed under reductive conditions as described above. The kinetic analysis after HPLC separation yielded a remarkable trend with a weak decrease at d = 6.8–17 Å and a weak increase at d = 17–30.6 Å (Figure 3). The decrease, with an

 © 2006 Wiley-VCH Verlag GmbH & Co. KGaA, Weinheim

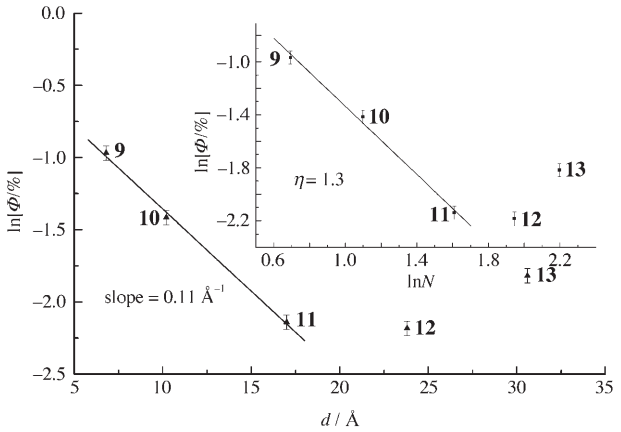


Figure 3. Distance dependence of electron transfer for PNA **9**–**13** + DNA **15**. The quantum yields Φ were determined from half-lives $\tau_{1/2}$ (see the Supporting Information); d = transfer distance; irradiation at 430 nm, after hybridization with complementary DNA **15** and reduction with sodium dithionite; ≈9 μM PNA in 10 mM NaH_2PO_4 buffer, 0.10 M NaCl, pH 6.9. Inset: N = number of transfer steps.

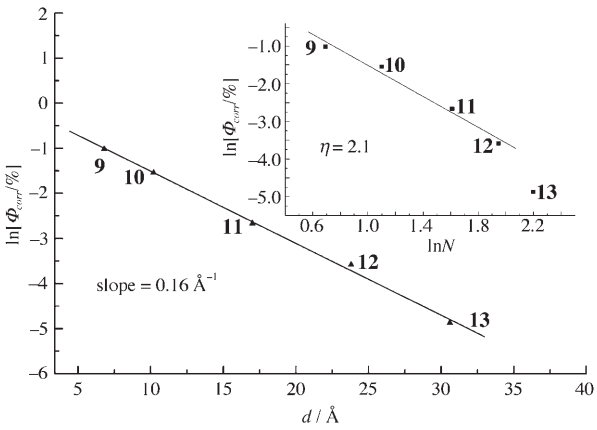


Figure 4. Distance dependence of intrastrand electron transfer for pairing complexes PNA **9**–**13** with DNA **15** after correction of the quantum yields Φ (see the Supporting Information); d = distance of intrastrand transfer; $\Phi_{corr.}$ = corrected quantum yields. Inset: N = number of intrastrand transfer steps.

exponential damping coefficient of 0.11 $Å^{-1}$, was as expected for a charge transfer by a hopping mechanism and is in accordance with literature.[2,4] In contrast, the weak increase for distances larger than 17 Å is assumed to be caused by interstrand charge transfer from the flavin of the opposite PNA strand. With regard to the long transfer distances, each thymine oxetane comes close to the flavin of the opposite strand as a result of the antiparallel orientation of the PNA strands, and therefore, the interstrand charge transfer becomes dominant.

We mathematically eliminated the interstrand fraction of the observed quantum yields Φ to obtain a corrected quantum yield $\Phi_{corr.}$ reflecting only the intrastrand fraction by assuming a P-form triple helix and a hopping mechanism for charge transfer (see the Supporting Information).[21] The plot of the corrected quantum yields resulted in an exponential damping coefficient of 0.16 $Å^{-1}$ and a proportionality coefficient η = 2.1, which are both in accordance with the known weak distance dependence of charge transfer by a hopping mechanism (Figure 4).[2,4]

In summary, the synthesis of thymine oxetane/flavin functionalized *N*-(2-aminoethyl)glycine-PNA by a Fmoc/Bhoc strategy was achieved with consideration of the high acid sensitivity of the oxetane moiety. The thymine oxetane was integrated into the base stack without causing crucial distortion. The photo-induced excess-electron transfer was analyzed by HPLC and proceeded with remarkably high quantum yields, which are in accordance with the favorable energetics and high cycloreversion rate of the thymine oxetane. The systematic investigation of the distance dependence of excess-electron transfer with a series of oligomers was complicated by triple-helix formation but revealed a weak distance dependence over 30 Å in accordance with a hopping mechanism for the charge transfer. From this result, we expect that thymine oxetanes are well suited for chemical monitoring of excess-electron transfer with regard to sequence and direction dependence. A future prospect is the application of time-resolved spectroscopy to the liberated benzaldehyde radical anion **2** for determination of the rates of long-range excess-electron transfer.[22]

Received: January 13, 2006
Published online: July 17, 2006

Keywords: DNA damage · donor–acceptor systems · electron transfer · kinetics · photolysis

[1] a) H. Wagenknecht, *Angew. Chem.* **2003**, *115*, 2558–2565; *Angew. Chem. Int. Ed.* **2003**, *42*, 2454–2460; b) E. M. Boon, A. L. Livingston, N. H. Chmiel, S. S. David, J. K. Barton, *Proc. Natl. Acad. Sci. USA* **2003**, *100*, 12543–12547.
[2] a) E. Katz, I. Willner, *Angew. Chem.* **2004**, *116*, 6166–6235; *Angew. Chem. Int. Ed.* **2004**, *43*, 6042–6108; b) S. Delaney, J. K. Barton, *J. Org. Chem.* **2003**, *68*, 6475–6483; c) D. N. Beratan, J. Onuchic, J. Hoppfield, *Science* **1988**, *241*, 817–820; d) M. Bixon, B. Giese, T. Langenbacher, M. E. Michel-Beyerle, J. Jortner, *Proc. Natl. Acad. Sci. USA* **1999**, *96*, 11713–11716.
[3] a) F. D. Lewis, X. Liu, J. Liu, S. E. Miller, R. T. Hayes, M. R. Wasielewski, *Nature* **2000**, *406*, 51–53; b) F. D. Lewis, J. Liu, X. Zuo, R. T. Hayes, M. R. Wasielewski, *J. Am. Chem. Soc.* **2003**, *125*, 4850–4861.
[4] a) B. Giese, S. Wessely, M. Spormann, U. Lindemann, E. Meggers, M. E. Michel-Beyerle, *Angew. Chem.* **1999**, *111*, 1050–1052; *Angew. Chem. Int. Ed.* **1999**, *38*, 996–998; b) E. Meggers, M. E. Michel-Beyerle, B. Giese, *J. Am. Chem. Soc.* **1998**, *120*, 12950–12955.
[5] M. P. Scannell, G. Prakash, D. E. Falvey, *J. Phys. Chem. A* **1997**, *101*, 4332–4337.
[6] S. Yeh, D. E. Falvey, *J. Am. Chem. Soc.* **1991**, *113*, 8557–8558.
[7] a) B. Giese, B. Carl, T. Carl, T. Carell, C. Behrens, U. Hennecke, O. Schiemann, E. Feresin, *Angew. Chem.* **2004**, *116*, 1884–1887; *Angew. Chem. Int. Ed.* **2004**, *43*, 1848–1851; b) C. Haas, K. Kräling, M. Cichon, N. Rahe, T. Carell, *Angew. Chem.* **2004**, *116*, 1878–1880; *Angew. Chem. Int. Ed.* **2004**, *43*, 1842–1844.
[8] A. Josephs, G. Prakash, D. E. Falvey, *J. Am. Chem. Soc.* **2000**, *122*, 11219–11225.
[9] a) T. Ito, S. E. Rokita, *Angew. Chem.* **2004**, *116*, 1875–1878; *Angew. Chem. Int. Ed.* **2004**, *43*, 1839–1842; b) T. Ito, S. E.

 © 2006 Wiley-VCH Verlag GmbH & Co. KGaA, Weinheim

Rokita, *J. Am. Chem. Soc.* **2003**, *125*, 11480 – 11481; c) P. Kaden, E. Mayer-Enthart, A. Trifinov, T. Fiebig, H. Wagenknecht, *Angew. Chem.* **2005**, *117*, 1662 – 1666; *Angew. Chem. Int. Ed.* **2005**, *44*, 1636 – 1639. Recently, Carell and co-workers demonstrated the application of capillary electrophoresis to detect debromination of DNA hairpins containing 8-bromoguanosine, 8-bromoadenosine, and 5-bromouridine without piperidine-induced strand breaking. A. Manetto, S. Breeger, C. Chatgilialoglu, T. Carell, *Angew. Chem.* **2006**, *118*, 325 – 328; *Angew. Chem. Int. Ed.* **2006**, *45*, 318 – 321.

[10] P. E. Nielsen, M. Egholm, R. H. Berg, O. Buchardt, *Science* **1991**, *254*, 1497 – 1500.

[11] U. Diederichsen, *Angew. Chem.* **1996**, *108*, 458 – 461; *Angew. Chem. Int. Ed. Engl.* **1996**, *35*, 445 – 448.

[12] T. Stafforst, U. Diederichsen, *Chem. Commun.* **2005**, 3430 – 3432.

[13] R. Casale, I. S. Jensen, M. Egholm in *Peptide Nucleic Acids, Protocols and Application* (Eds.: P. E. Nielsen, M. Egholm), Horizon Scientific Press, Norfolk, UK, **1999**, Sec. 2.2, pp. 39 – 50.

[14] T. Stafforst, U. Diederichsen, unpublished results.

[15] In comparison, incorporation of a *cis,syn*-thymine,thymine-CPD causes a decrease of 9 °C in a DNA decamer duplex. J. Taylor, D. S. Garrett, I. R. Brockie, D. L. Svoboda, J. Telser, *Biochemistry* **1990**, *29*, 8858 – 8866.

[16] Reductive conditions were ensured over the whole period (see the Supporting Information). Sodium dithionite should not be used as a reducing agent in combination with irradiation at 365 nm owing to its strong absorbance at $\lambda < 400$ nm ($\lg(\varepsilon_{350nm}) > 3$), which leads to substantial errors in the kinetic analysis. a) R. J. Meyer, E. H. E. Pietsch, A. Kotowski, *Gmelin Handbuch der Anorganischen Chemie, Schwefel Teil B Lieferung 2*, VCH, Weinheim, **1960**, 8th ed., 9S[B]387–396; b) L. Lorenz, R. Samuel, *Z. Phys. Chem. B* **1931**, *14*, 219 – 231.

[17] a) C. G. Hatchard, C. A. Parker, *Proc. R. Soc. London Ser. A* **1956**, *235*, 518 – 536; b) C. A. Parker, *Proc. R. Soc. London Ser. A* **1953**, *232*, 104 – 116.

[18] M. K. Cichon, C. H. Haas, F. Grolle, A. Mees, T. Carell, *J. Am. Chem. Soc.* **2002**, *124*, 13984 – 13985.

[19] L. Betts, J. A. Josey, J. M. Veal, S. R. Jordan, *Science* **1995**, *270*, 1838 – 1841. As in B-DNA, the rise per base pair in P-form $(PNA)_2$DNA triple helices is 3.4 Å and was taken for calculation of transfer distance *d*.

[20] a) K. J. Breslauer, R. Frank, H. Blöcker, L. A. Marky, *Proc. Natl. Acad. Sci. USA* **1986**, *83*, 3746 – 3750; b) J. SantaLucia, H. T. Allawi, P. A. Seneviratne, *Biochemistry* **1996**, *35*, 3555 – 3562.

[21] The correction was made with the following assumptions: Triple strands formed as shown in Figure 2, the interstrand transfer is counted as an additional transfer step, only the shortest transfer route is considered, and the overall transfer efficiency decreases in a quadratic manner with the number of transfer steps (hopping mechanism). Under these assumptions it was not possible to assign any distance dependence to the hopping mechanism. This uncorrected distance dependence is distorted by the participation of interstrand transfer with increasing distance. Therefore, we have chosen a correction that basically affects the results for long-distance transfer and is in accordance with the results for short-distance transfer, the latter of which has shown clearly to obey the hopping mechanism.

[22] Recently, Giese and co-workers presented a similar application of a radical cation in peptide-mediated hole transfer: B. Giese, M. Napp, O. Jasques, H. Boudebous, A. M. Taylor, J. Wirz, *Angew. Chem.* **2005**, *117*, 4141 – 4143; *Angew. Chem. Int. Ed.* **2005**, *44*, 4073 – 4075.

 © 2006 Wiley-VCH Verlag GmbH & Co. KGaA, Weinheim

Directed Evolution

DOI: 10.1002/anie.200600255

A Screening System for the Directed Evolution of Epoxygenases: Importance of Position 184 in P450 BM3 for Stereoselective Styrene Epoxidation**

*Kang Lan Tee and Ulrich Schwaneberg**

Epoxides are important and versatile intermediates in the chemical synthesis of polymers[1] and pharmaceuticals.[2] Styrene oxide and its derivatives are, for instance, key intermediates in the synthesis of antidiabetic agents and dopamine agonists.[3,4] Remarkable progress has been achieved in the chemical synthesis of epoxides through the use of metallosalen compounds[5] and titanium-based complexes.[6] However, challenges remain in the production of chiral epoxides. Enzymatic biotransformations offer attractive alternatives for the production of chiral epoxides through kinetic resolution (epoxide hydrolases) and/or stereospecific oxygenation (monooxygenases and peroxidases). Examples of natural epoxidation catalysts include cytochrome P450,[7] styrene monooxygenase,[8] methane monooxygenase,[9] and microbial organisms.[10]

Directed-evolution experiments have been performed for improving the hydroxylation activities and specificities of monooxygenases.[11] These evolution experiments rely on accurate screening systems with sufficient throughput and sensitivity. For epoxidations, two detection protocols have been developed for screening with 96-well plates, and both rely on the reaction of terminal epoxides with the chromophore 4-(*p*-nitrobenzyl)pyridine (NBP) to form a blue adduct, which can be quantified spectrophotometrically.[12,13] Zocher et al. used this assay to identify epoxide hydrolase activity in *Streptomyces* strains,[14] and Alcalde et al. used it to screen an error-prone library but did not find an improved catalyst variant.[12] These assay systems are a first breakthrough to make the synthetically attractive enzyme class of epoxygenases accessible to directed-evolution methodologies. However, none of these NBP-based assays has yet been reported in a directed-evolution campaign for improving properties of an epoxygenase. One reason might be that the screening

[*] K. L. Tee, Dr. U. Schwaneberg
School of Engineering and Science
International University Bremen
Campus Ring 8, 28759 Bremen (Germany)
Fax: (+49) 421-200-3229
E-mail: u.schwaneberg@iu-bremen.de

[**] This work was supported financially by the Deutsche Bundesstiftung Umwelt. We thank Prof. Frances Arnold for providing the P450 BM3 mutant 139-3, Dr. Danilo Roccatano for helpful discussions, and Prof. Andreas Schmid and Dr. Katja Otto for assistance with GC analysis.

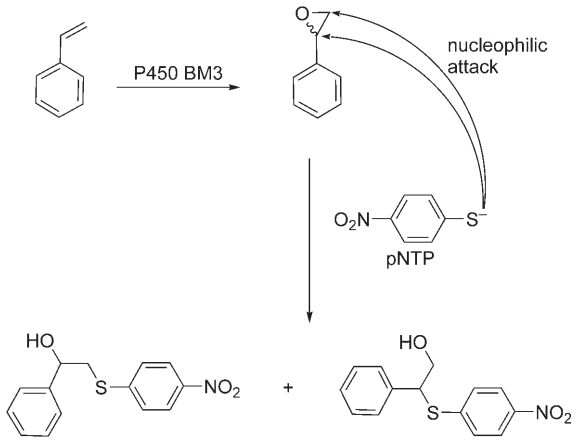
Supporting information for this article is available on the WWW under http://www.angewandte.org or from the author.

WILEY InterScience DISCOVER SOMETHING GREAT
© 2006 Wiley-VCH Verlag GmbH & Co. KGaA, Weinheim

procedure requires heating at high temperatures (70–80 °C) which thus limits assay throughput.[12,13]

Here we report a novel, validated, and product-based screening system using the colorimetric agent *p*-nitrothiophenolate (pNTP) for the directed evolution of epoxygenases. pNTP is a yellow chromophore that reacts with an epoxide through nucleophilic attack, resulting in ring opening and a colorless product.[15] As a model system, we chose styrene and monooxygenase P450 BM3 (BM3).[11] BM3 is a 118-kDa water-soluble monooxygenase isolated from *Bacillus megaterium*; its heme and reductase domains are fused on a single polypeptide chain.[16] It can be expressed in *Escherichia coli* and purified on a preparative scale by a single-step purification method.[17] In addition BM3 has proven to be a versatile catalyst and accepts numerous unnatural substrates including styrene.[7,11]

The reaction principle behind the pNTP assay is shown in Scheme 1: After epoxidation by BM3, the epoxide product is



Scheme 1. Styrene is converted into styrene oxide by P450 BM3, and the reaction can be followed by detection of pNTP.

attacked by the nucleophilic pNTP resulting in a colorless product. The decrease in absorbance can be monitored at 405 nm. The advantage of this assay system is its technical simplicity as it does not require heating and cooling cycles. Additionally a NADPH-cofactor recycling system using isocitrate dehydrogense was implemented in the protocol to reduce screening expenses. However, the pNTP assay does not discriminate between enantiomers. If necessary, the nucleophilicity of the thiolate group can be adjusted by substituents on the arene ring to fit the reactivity of the epoxide. This flexibility should render the pNTP assay suitable for a broad range of epoxides.

We validated the pNTP medium-throughput screening assay for the directed evolution of epoxygenases by optimizing the screening protocol, determining standard deviations, and screening saturation mutagenesis libraries in the 96-well plate format. The 139-3 (V78A, H138Y, T175I, V178I, A184V, H236Q, E252G, R255S, A290V, A295T, L353V) variant of BM3 was used for the development of the pNTP assay since it converts styrene at an initial rate superior to that of the wild-type (WT) enzyme.[7] A styrene concentration of 10 mM was employed in all protocol-optimization steps, in which the amount of lysate used, the shaking speed during the reaction, and the time of pNTP discoloration were optimized. Finally, a remarkably low coefficient of variation (CV) of 8.8% was achieved after the background was subtracted (Figure 1; see

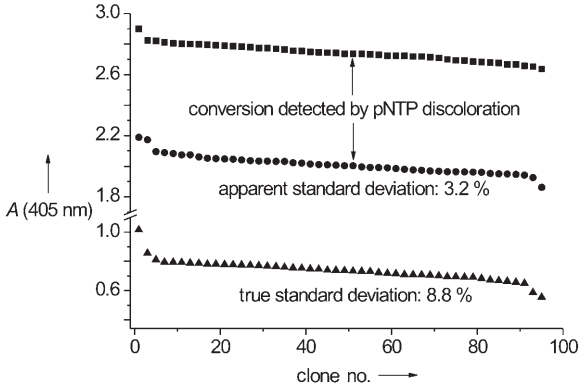


Figure 1. pNTP absorbances for the BM3-catalyzed epoxidation of styrene in a 96-well plate using the protocol optimized for pNTP. ■: Background absorbance due to DH5α without BM3; ●: absorbance after styrene conversion by BM3; ▲: absolute values of calculated absorbance difference based on pNTP discoloration after subtracting the DH5α background.

the Experimental Section). Screening systems with a CV of around 10% have been employed successfully in directed-evolution experiments with BM3.[18] In addition, a calibration curve was prepared employing styrene oxide (0–1 mM) instead of styrene (Figure 2). The cell lysate increased the absorbance from 0 to 0.3, but linearity is maintained within this region and the sensitivity limit of the pNTP assay is approximately 400 μM for styrene oxide. As pNTP discolors slowly over time, the dye should be prepared immediately prior to use.

For creating saturation mutagenesis libraries, the BM3 variant 139-3 was not used because its high extent of uncoupling would make it unsuitable for industrial applica-

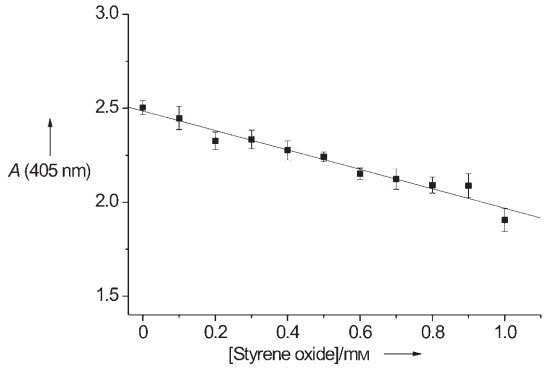


Figure 2. Correlation between styrene oxide concentration and absorbance at 405 nm.

 © 2006 Wiley-VCH Verlag GmbH & Co. KGaA, Weinheim

tions. As an alternative, the BM3 mutant 5F5 (F87A, T235A, R471A, E494K, S1024E) was selected for saturation mutagenesis owing to its high resistance to organic solvents.[19] The standard deviation of the pNTP assay for 5F5 was determined to be 14% under the conditions optimized for 139-3. We generated saturation mutagenesis libraries at two positions previously found mutated in the 139-3 variant (V78 and A184) by using a modified QuikChange protocol. Two plates per position were screened in 96-well format. Beneficial mutants were identified in the A184 mutagenesis library, in contrast to the V78 library. The five most active clones were sequenced, and the following substitutions were found: A184K (twice), A184R (twice), and A184H (once). In all cases the hydrophobic alanine residue had been replaced by a positively charged amino acid. The absorbance changes are 0.24 (5F5) for the parent and 0.53 (A184K), 0.48 (A184R), and 0.67 (A184H) for the mutants after accounting for the background discoloration.

These three mutants together with parent 5F5, WT, and variant 139-3 were purified,[17] normalized by CO measurements, and characterized by determining oxygen consumption rates (Fibox3 oxygen probe; Presens) and styrene oxide formation (chiral GC; dodecane as internal reference).[7]

Table 1 shows the initial kinetic data obtained from oxygen consumption measurements for the conversion of 2 mM styrene. A184K (2.2-fold) and A184R (1.7-fold) are more active than the parent 5F5, while A184H turned out to be an expression mutant after CO normalization. The identified variants have activity improvements of 143–257 min^{-1}, and these results validated the pNTP assay for screening in 96-well format. The uncoupling was determined to be <2% in the parent 5F5 and all 5F5 mutants (A184R, A184K, A184H) using the ABTS assay (see the Supporting Information).[12] Table 1 lists the conversions and enantioselectivities for styrene oxide formation catalyzed by WT, variant 139-3, and 5F5 and 5F5 mutants (A184R, A184K, A184H). All epoxidations were stopped at conversions of 33–42% except the reaction with WT. WT achieved, under comparable conditions (identical amount of BM3 and substrate), a conversion of only 12%. Two additional sets of experiments were conducted to increase conversion (Table 1) by extending reaction time and increasing BM3 concentration. However, in all three experiments a conversion of only 11–14% was achieved with an selectivity of 20% *ee* for the *R* enantiomer. Chiral gas chromatography revealed for all three 5F5 mutants (A184R, A184K, A184H) an exciting and unexpected inversion of enantioselectivity: the 5F5 mutants give preferentially the *S* enantiomer (26.0–27.3% *ee*), whereas the parent 5F5, WT, and variant 139-3 are selective for the *R* enantiomer (Table 1). From these experiments we learn that a positive charge at amino acid residue A184 on the F helix, which is far away from the active site (ca. 18 Å), can modulate the enantioselectivity of styrene epoxidation in BM3. It is, however, difficult to predict whether this inversion was a result of electrostatic effects or long-range conformational changes.

In conclusion, a novel medium-throughput epoxide assay system has been developed and validated for exploiting the synthetic potential of epoxygenases through directed evolution. We demonstrated the ability of the pNTP assay to select more active variants for styrene epoxidation in a mutant library. Upon GC characterization, three investigated mutants showed unexpectedly an inversion of enantioselectivity upon the exchange of a hydrophobic alanine residue (A184) with a positively charged amino acid (R, K, or H).

Table 1: Epoxidation of styrene catalyzed by BM3 and mutants.

Clone	$\nu_{init.,max}$ [min^{-1}][a]	*ee* [%]	Conv. [%][b]	Recov. [%][c]
WT	62±2	19.7±0.1 (*R*)	11.7±0.6	79±3
WT[d]	–	19.7±0.1 (*R*)	14.1±0.2	78±3
WT[e]	–	20.0±1.1 (*R*)	11.0±0.8	79±4
139-3	955±88	6.4±0.3 (*R*)	40.2±0.9	69±2
5F5	217±11	26.6±1.5 (*R*)	36.1±0.4	78±3
5F5A184R	360±27	26.5±0.3 (*S*)	41.6±1.4	75±1
5F5A184K	474±20	27.3±0.5 (*S*)	41.4±0.5	83±2
5F5A184H	199±4	26.0±1.3 (*S*)	32.9±2.0	78±4

[a] Maximum initial rate. [b] Conversion = {*c*(styrene oxide)/[*c*(styrene) + *c*(styrene oxide)]}×100. [c] Styrene + styrene oxide recovered after extraction. [d] Reaction time 2 h. [e] Enzyme concentration 3.2 μM.

Experimental Section

pNTP assay in 96-well format: To prepare cell lysate for the activity assay each cell pellet (400 μL from expression) was resuspended in 200 μL of lysozyme (14000 U, 100 mM Tris, pH 8.0), and the mixture was incubated (37°C, 1 h) and centrifuged. A 50-μL aliquot of the lysed cell supernatant was transferred to a 96-well polypropylene microplate containing 20 μL Tris buffer (100 mM, pH 8.0) and 10 μL styrene (100 mM, dissolved in ethanol). The mixture was incubated for 5 min at room temperature (RT). Reaction was then initiated by the addition of 5 μL NADPH (5 mM) followed by a 10 min incubation (600 rpm, RT). Subsequently, a mixture of 2.5 μL of catalase (19.5 U) and a cofactor recycling system made up of 7.5 μL isocitrate dehydrogenase (0.09 U) and 5 μL D/L-isocitrate acid trisodium salt (50 mM) was added, and the reaction mixture was incubated for additional 50 min. For the colorimetric assay, 95 μL of *p*-nitrothiophenolate (1 mM, 100 mM Tris, pH 8.0) was added to the reaction mixture, which was then shaken (800 rpm, 1 h, RT). The bubbles were removed by flaming before the absorbance was recorded at 405 nm.

To determine the standard deviation, the whole procedure above was repeated using lysed cell supernatant from *E. coli* DH5α lacking the BM3 protein. The apparent standard deviation was based on the absolute absorbance values obtained from the 139-3 mutant plate. The true standard deviation was calculated by subtracting the background absorbance value obtained from the microplate lacking P450 BM3.

Received: January 20, 2006
Revised: April 17, 2006
Published online: July 17, 2006

Keywords: directed evolution · epoxidation · high-throughput screening · monooxygenases · P450

 © 2006 Wiley-VCH Verlag GmbH & Co. KGaA, Weinheim

[1] A. A. Roche, J. Bouchet, S. Bentadjine, *Int. J. Adhes. Adhes.* **2002**, *22*, 431.
[2] O. Takahashi, J. Umezawa, K. Furuhashi, M. Takagi, *Tetrahedron Lett.* **1989**, *30*, 1583.
[3] J. D. Bloom, M. D. Dutia, B. D. Johnson, A. Wissner, M. G. Burns, E. E. Largis, J. A. Dolan, T. H. Claus, *J. Med. Chem.* **1992**, *35*, 3081.
[4] F. R. Pfeiffer, J. W. Wilson, J. Weinstock, G. Y. Kuo, P. A. Chambers, K. G. Holden, R. A. Hahn, J. R. Wardell, A. J. Tobia, P. E. Setler, H. M. Sarau, *J. Med. Chem.* **1982**, *25*, 352.
[5] T. Katsuki, *Curr. Org. Chem.* **2001**, *5*, 663.
[6] T. Katsuki, K. B. Sharpless, *J. Am. Chem. Soc.* **1980**, *102*, 5974.
[7] E. T. Farinas, M. Alcalde, F. H. Arnold, *Tetrahedron* **2004**, *60*, 525.
[8] K. Otto, K. Hofstetter, M. Rothlisberger, B. Witholt, A. Schmid, *J. Bacteriol.* **2004**, *186*, 5292.
[9] S. J. Elliott, M. Zhu, L. Tso, H. H. T. Nguyen, J. H. K. Yip, S. I. Chan, *J. Am. Chem. Soc.* **1997**, *119*, 9949.
[10] A. M. Warhurst, C. A. Fewson, *J. Appl. Bacteriol.* **1994**, *77*, 597.
[11] A. Glieder, E. T. Farinas, F. H. Arnold, *Nat. Biotechnol.* **2002**, *20*, 1135.
[12] M. Alcalde, E. T. Farinas, F. H. Arnold, *J. Biomol. Screening* **2004**, *9*, 141.
[13] F. Zocher, M. M. Enzelberger, U. T. Bornscheuer, B. Hauer, R. D. Schmid, *Anal. Chim. Acta* **1999**, *391*, 345.
[14] F. Zocher, M. M. Enzelberger, U. T. Bornscheuer, B. Hauer, W. Wohlleben, R. D. Schmid, *J. Biotechnol.* **2000**, *77*, 287.
[15] S. C. Agarwal, B. L. Vanduuren, J. J. Solomon, S. A. Kline, *Environ. Sci. Technol.* **1980**, *14*, 1249.
[16] R. T. Ruettinger, L. P. Wen, A. J. Fulco, *J. Biol. Chem.* **1989**, *264*, 10987.
[17] U. Schwaneberg, A. Sprauer, C. Schmidt-Dannert, R. D. Schmid, *J. Chromatogr. A* **1999**, *848*, 149.
[18] T. S. Wong, N. Wu, D. Roccatano, M. Zacharias, U. Schwaneberg, *J. Biomol. Screening* **2005**, *10*, 246.
[19] T. S. Wong, F. H. Arnold, U. Schwaneberg, *Biotechnol. Bioeng.* **2004**, *85*, 351.

 © 2006 Wiley-VCH Verlag GmbH & Co. KGaA, Weinheim

Supramolecular Polymers

DOI: 10.1002/anie.200600610

Topochemical Polymerization in Supramolecular Polymers of Oligopeptide-Functionalized Diacetylenes**

*Eike Jahnke, Ingo Lieberwirth, Nikolai Severin, Jürgen P. Rabe, and Holger Frauenrath**

New generations of synthetic polymers targeting applications at the interface of optoelectronics and the biosciences must "speak the language" of biomaterials and mimic their functioning. They must provide the chemical functionality to interact with biological systems on the molecular level and exhibit a similar ability to form hierarchical structures.[1] Supramolecular self-assembly has proven to be a powerful tool for the preparation of materials with structural features on the nanometer scale.[2] Recently, the self-assembly of oligopeptides through aggregation and formation of β sheets has received increasing attention. This approach has been prompted by research activities in the field of neurodegenerative diseases.[3] Notable examples include the self-assembly of oligopeptides based on amyloids,[4] the formation of organogels from synthetic oligopeptides and their deposition on surfaces,[5] the aggregation of peptidomimetic molecules[6] and PEG conjugates,[7] multiblock copolymers inspired by spider silk,[8] as well as the use of self-assembled oligopeptides in the manufacture of gold nanowires.[9]

Poly(diacetylene)s are optoelectronically active materials. Topochemical polymerizations of diacetylenes are possible whenever the required crystalline order of the monomers is established.[10] They have, for example, been performed in self-assembled mono- or multilayers of diynoic acids and their salts[11] as well as along 1D lamellar structures in self-assembled monolayers on surfaces.[12] Diacetylene-containing

[*] E. Jahnke, Dr. H. Frauenrath
ETH Zürich
Departement Materialien
Wolfgang-Pauli-Strasse 10, HCI H515, 8093 Zürich (Switzerland)
Fax: (+41) 44-633-1390
E-mail: frauenrath@mat.ethz.ch
Dr. I. Lieberwirth
Max-Planck-Institut für Polymerforschung
Ackermannweg 10, 55128 Mainz (Germany)
Dr. N. Severin, Prof. J. P. Rabe
Humboldt-Universität zu Berlin
Institut für Physik
Newtonstrasse 15, 12489 Berlin (Germany)

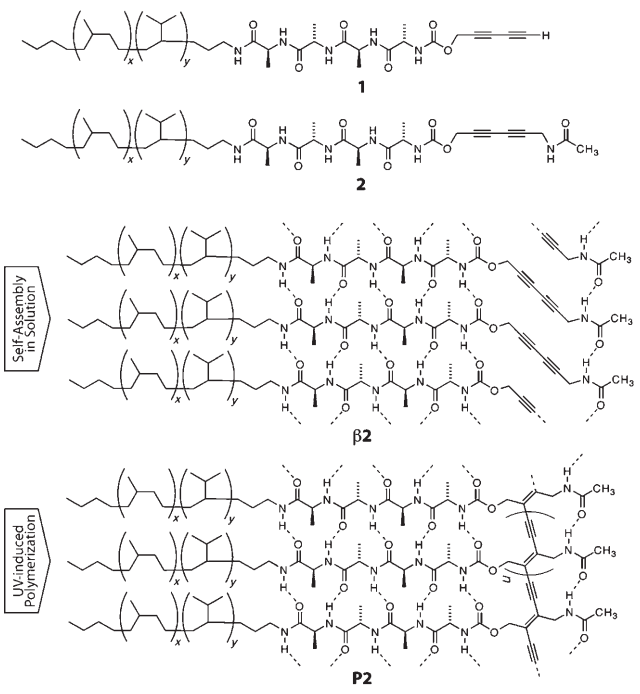
[**] We would like to thank Dr. Heinz Rüegger for the solid-state NMR spectroscopy experiments, Lars Massüger for the X-ray diffraction studies, and Prof. A. Dieter Schlüter for his continuous support. Financial support from the Deutsche Forschungsgemeinschaft (Emmy Noether program, FR 1567/2-1) and the Fonds der Chemischen Industrie (Fonds-Stipendium, E.J.) is gratefully acknowledged.

Supporting information for this article is available on the WWW under http://www.angewandte.org or from the author.

 © 2006 Wiley-VCH Verlag GmbH & Co. KGaA, Weinheim InterScience

lipid amphiphiles with chiral polar head groups, such as phosphatidyl cholines, amino acids, or aldonamides were found to form tubular or helical superstructures in the submicrometer range.[13] Related materials have been used in sensing applications.[14] Finally, diacetylene polymerizations have been carried out in hydrogen-bonded organogels and supramolecular polymers.[15]

Here we describe the use of self-assembled supramolecular polymers consisting of β-sheet-forming oligopeptides as scaffolds for the topochemical polymerization of diacetylenes in solution. Thus, we designed and prepared the macromonomers **1** and **2** which include 1) a hydrogenated poly(isoprene) segment (hPI) as a polydisperse aliphatic coil to provide solubility in organic solvents and prevent global ordering; 2) a tetra(L-alanine) segment to induce anisotropic self-assembly through formation of a β sheet; 3) a diacetylene moiety integrated directly into the hydrogen bonding array without a spacer; and 4) in the case of **2**, an NHAc end group capable of forming hydrogen bonds to promote a parallel arrangement of the molecules. The macromonomer **2** self-assembled into a supramolecular polymer with a double-helical topology which was, then, converted into the corresponding poly(diacetylene) **P2** by UV irradiation (Scheme 1).



Scheme 1. Self-assembly and topochemical polymerization of diacetylenes functionalized with a β-sheet-forming oligopeptide.

1 and **2** were prepared by anionic polymerization of isoprene, high-pressure hydrogenation, stepwise solution-phase peptide synthesis, and acetylene heterocoupling reactions.[16] Solutions of **1** and **2** in CH_2Cl_2 or $CHCl_3$ showed no tendency toward gelation, but ^1H NMR spectra as well as solution-phase IR spectra gave a clear indication of aggregation.[16] In the IR spectrum of **2** (Figure 1), the main amide A (ν_{NH}) band at 3283 cm^{-1}, the predominating amide I (ν_{CO}) band at 1632 cm^{-1}, as well as the amide II and amide III bands were in excellent agreement with a β-sheet structure. A detailed analysis[16] suggested that **2** may form bent or twisted β-sheet structures **β2** with a parallel arrangement of the chains. It is worth noting that, by contrast, the IR spectra of **1** were consistent with a predominantly antiparallel packing of the chains in the β-sheet structure, and a higher proportion of other (unordered) structures.[16] This difference is remarkable given the close structural relationship between **1** and **2**. The NHAc end group in **2** appears to enforce a parallel arrangement of the molecules within the aggregates because, only in this way, can the maximum number of hydrogen bonds be achieved.

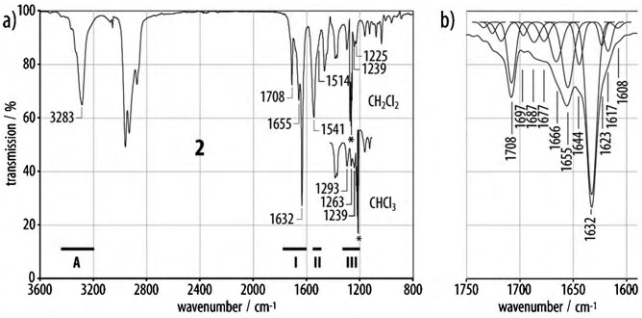


Figure 1. IR spectrum of **2** and assignment of the amide I bands.

Transmission electron microscopy (TEM) images of unstained samples of **2** as well as images obtained after carbon shadowing (Figure 2 a–d) showed remarkably straight fibrillar features which were several micrometers long and, upon qualitative inspection, appeared to have a uniform diameter and height (as concluded from the widths of the carbon shadows). Histographic analyses revealed a bimodal width distribution with two narrow distributions centered around maxima of 6.5(±1.4) nm and 8.7(±2.5) nm. An upper limit for the height of the fibrils was determined to be approximately 1.7(±1.3) nm. This height is about twice the value that is typically expected for an individual β sheet. Nevertheless, the observed fibrils are flat objects—flat ribbons or collapsed tubes—that are preferentially adsorbed flat on the carbon surface. Scanning force microscopy (SFM) images of samples of **2** spin-coated onto highly oriented pyrolytic graphite (HOPG) substrates (Figure 2 e–j) showed similar fibrillar features.[17] The apparent height of the fibrils was 4.7(±0.5) nm according to a histographic analysis, and their widths were estimated to be on the order of 5 nm.[18] Remarkably, the fibrils were consistently found to be right-handed double helices with a pitch of about 17.8(±1.7) nm which were constituted from two flat ribbon-type substructures.[19]

X-ray diffraction studies[16] on solid samples of **2** showed a main meridional reflection at a spacing of 4.59 Å. Electron diffraction studies[16] on multilayer films of **2** revealed a doublet of reflections at 4.76 and 4.59 Å as well as additional reflections at spacings of 8.04 and 4.25 Å. The results were in agreement with the expected β-sheet-type aggregation. Furthermore, they were similar to X-ray data reported for related

 © 2006 Wiley-VCH Verlag GmbH & Co. KGaA, Weinheim

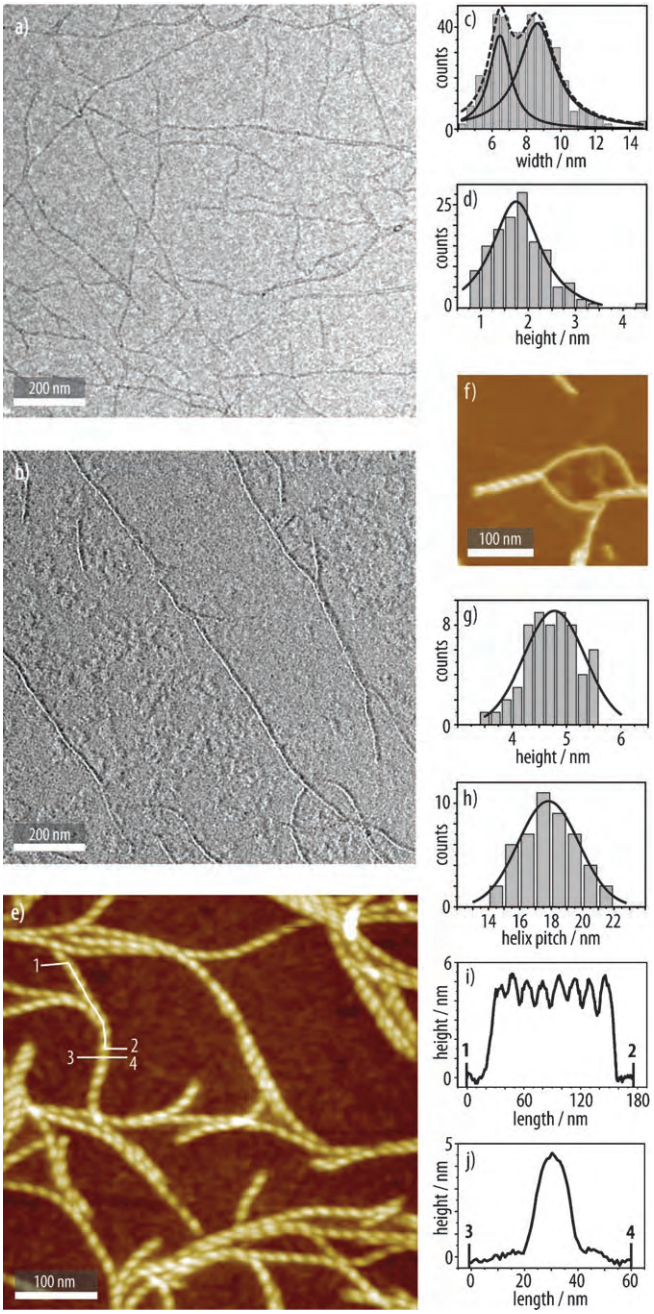


Figure 2. TEM images of samples of **2**: a) unstained and b) after carbon shadowing; histograms showing the c) width and d) height of the fibrils (derived from the TEM images); e,f) SFM images of **2**; g,h) height profiles along and across the fibrils; histograms of the i) height and j) helical pitch (derived from the SFM images).

systems,[8] and closely matched X-ray investigations on helical amyloid fibrils.[4]

On the basis of the above results, we propose as a working hypothesis the following model for the self-assembly of **2** (Figure 3). The observed helix dimensions translate into a ribbon width on the order of 13–14 nm. As the extended length of **2** is about 6.7 nm, we assume that the ribbons are constituted of two parallel β-sheet-type aggregates **β2**. Thus, the oligopeptide would form crystalline cores that would be

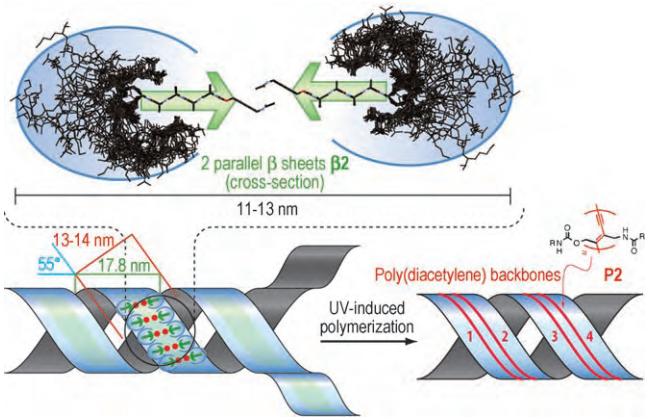


Figure 3. Proposed model for the self-assembly and polymerization of macromonomer **2**; ribbons are formed from two parallel β sheets **β2** (shown in cross-section) and wound into a tubular double-helical aggregate.

embedded into a "cushion" of the coil segments and shielded from the hydrophobic environment. In conclusion, the observed aggregates are to be regarded as well-defined supramolecular polymers with dimensions directly correlated to their molecular constituents rather than as helical micellar or tubular vesicular structures, as have been observed in the case of diacetylene-containing lipid amphiphiles.[13] They are, at the same time, a synthetic example of a "jelly-roll" morphology which has been described in the context of protein superstructures.[20]

Finally, we investigated the polymerizability of the macromonomers **1** and **2** in organic solution. Solutions of the macromonomers in CH_2Cl_2 were degassed in a thermostated quartz Schlenk tube, cooled to 0 °C, and exposed to UV irradiation from a 250 W Ga-doped Hg light source. Solutions of **1** turned only slightly yellow, and the UV spectra[16] showed that the diacetylene functions were consumed probably in the sense of an unspecific cross-linking reaction. By contrast, solutions of **2** attained an intense purple color within less than one minute. The UV spectra of the reaction mixtures showed two strong bands at about 520 nm and 580 nm, which are consistent with the formation of a poly(diacetylene) backbone (Figure 4). Raman spectra as well as solid state CP-MAS ^{13}C NMR spectra provided further evidence for the successful

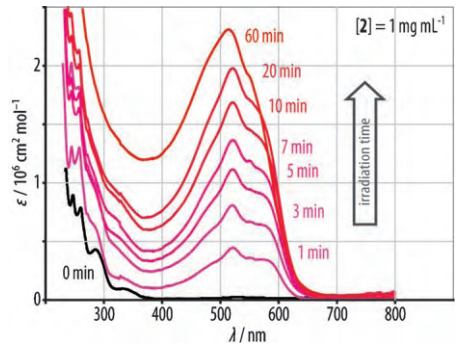


Figure 4. UV spectra of the UV-induced polymerization of **2** in CH_2Cl_2; [**2**] = 1 mg mL^{-1}.

© 2006 Wiley-VCH Verlag GmbH & Co. KGaA, Weinheim

conversion into the poly(diacetylene) **P2**.[16] We attribute the remarkable difference in polymerizability between **1** and **2** to the role of the NHAc end group, which is necessary for the formation of the required parallel β-sheet structures.

In conclusion, we have successfully self-assembled the diacetylene derivative **2** into aggregates with dimensions of a few nanometers. We have, thus, used β-sheet-type hydrogen-bonding networks to obtain a well-defined supramolecular polymer with a double-helical topology. A "1D topochemical polymerization" was then performed and these supramolecular polymers were converted into the poly(diacetylene) **P2**. The obtained poly(diacetylene) features a conjugated backbone, a high degree of functionalization with biochemically relevant substituents, as well as, most importantly, a defined hierarchical structure. It is these properties which may make this system attractive as a platform for optoelectronic applications at the interface with the biosciences.

Received: February 15, 2006
Revised: May 30, 2006
Published online: July 20, 2006

Keywords: β sheets · double helix · hierarchical structures · self-assembly · topochemical polymerization

[1] a) M. Muthukumar, C. K. Ober, E. L. Thomas, *Science* **1997**, *277*, 1225; b) R. Lakes, *Nature* **1993**, *361*, 511.
[2] a) J.-M. Lehn, *Science* **2002**, *295*, 2400; b) G. M. Whitesides, B. Grzybowski, *Science* **2002**, *295*, 2418.
[3] D. J. Selkoe, *Nature* **2003**, *426*, 900.
[4] a) O. S. Makin, L. C. Serpell, *J. Mol. Biol.* **2004**, *335*, 1279; b) M. Sunde, L. C. Serpell, M. Bartlam, P. E. Fraser, M. B. Pepys, C. C. F. Blake, *J. Mol. Biol.* **1997**, *273*, 729; c) J. P. Bond, S. P. Deverin, H. Inouye, O. M. A. El-Agnaf, M. M. Teeter, D. A. Kirschner, *J. Struct. Biol.* **2003**, *141*, 156; d) C. Goldsbury, P. Frey, V. Olivieri, U. Aebi, S. A. Müller, *J. Mol. Biol.* **2005**, *352*, 282; e) C. Goldsbury, J. Kistler, U. Aebi, T. Arvinte, G. J. S. Cooper, *J. Mol. Biol.* **1999**, *285*, 33.
[5] a) A. Aggeli, M. Bell, N. Boden, J. N. Keen, P. F. Knowles, T. C. McLeish, M. Pitkeathly, S. E. Radford, *Nature* **1997**, *386*, 259; b) C. Whitehouse, J. Fang, A. Aggeli, M. Bell, R. Brydson, C. W. G. Fishwick, J. R. Henderson, C. M. Knobler, R. W. Owens, N. H. Thomson, D. A. Smith, N. Boden, *Angew. Chem.* **2005**, *117*, 2001; *Angew. Chem. Int. Ed.* **2005**, *44*, 1965.
[6] H. A. Lashuel, S. R. LaBrenz, L. Woo, L. C. Serpell, J. W. Kelly, *J. Am. Chem. Soc.* **2000**, *122*, 5262.
[7] a) J. M. Smeenk, M. B. J. Otten, J. Thies, D. A. Tirrell, H. G. Stunnenberg, J. C. M. van Hest, *Angew. Chem.* **2005**, *117*, 2004; *Angew. Chem. Int. Ed.* **2005**, *44*, 1968; b) J. H. Collier, P. B. Messersmith, *Adv. Mater.* **2004**, *16*, 907; c) T. S. Burkoth, T. L. S. Benzinger, D. N. M. Jones, K. Hallenga, S. C. Meredith, D. G. Lynn, *J. Am. Chem. Soc.* **1998**, *120*, 7655; d) T. S. Burkoth, T. L. S. Benzinger, V. Urban, D. G. Lynn, S. C. Meredith, P. Thiyagarajan, *J. Am. Chem. Soc.* **1999**, *121*, 7429.
[8] a) O. Rathore, D. Y. Sogah, *J. Am. Chem. Soc.* **2001**, *123*, 5231; b) O. Rathore, D. Y. Sogah, *Macromolecules* **2001**, *34*, 1477; c) J. Yao, D. Xiao, X. Chen, P. Zhou, T. Yu, Z. Shao, *Macromolecules* **2003**, *36*, 7508.
[9] T. Scheibel, R. Parthasarathy, G. Sawicki, X.-M. Lin, H. Jaeger, S. L. Lindquist, *Proc. Natl. Acad. Sci. USA* **2003**, *100*, 4527.
[10] a) G. Wegner, *Z. Naturforsch. B* **1969**, *24*, 824; b) G. Wegner, *Makromol. Chem.* **1972**, *154*, 35.
[11] a) B. Tieke, G. Wegner, D. Naegele, H. Ringsdorf, *Angew. Chem.* **1976**, *88*, 805; *Angew. Chem. Int. Ed. Engl.* **1976**, *15*, 764; b) D. N. Batchelder, S. D. Evans, T. L. Freeman, L. Haeussling, H. Ringsdorf, H. Wolf, *J. Am. Chem. Soc.* **1994**, *116*, 1050; c) K. Kuriyama, H. Kikuchi, T. Kajiyama, *Langmuir* **1996**, *12*, 2283; d) K. E. Huggins, S. Son, S. I. Stupp, *Macromolecules* **1997**, *30*, 5305; e) D. W. Britt, U. G. Hofmann, D. Moebius, S. W. Hell, *Langmuir* **2001**, *17*, 3757.
[12] a) Y. Okawa, M. Aono, *Nature* **2001**, *409*, 683; b) A. Miura, S. De Feyter, M. M. S. Abdel-Mottaleb, A. Gesquiere, P. C. M. Grim, G. Moessner, M. Sieffert, M. Klapper, K. Müllen, F. C. De Schryver, *Langmuir* **2003**, *19*, 6474; c) S. P. Sullivan, A. Schnieders, S. K. Mbugua, T. P. Beebe, *Langmuir* **2005**, *21*, 1322.
[13] a) J. H. Georger, A. Singh, R. R. Price, J. M. Schnur, P. Yager, P. E. Schoen, *J. Am. Chem. Soc.* **1987**, *109*, 6169; b) A. Singh, E. M. Wong, J. M. Schnur, *Langmuir* **2003**, *19*, 1888; c) S. Svenson, P. B. Messersmith, *Langmuir* **1999**, *15*, 4464; d) Q. Cheng, M. Yamamoto, R. C. Stevens, *Langmuir* **2000**, *16*, 5333; e) D. A. Frankel, D. F. O'Brien, *J. Am. Chem. Soc.* **1991**, *113*, 7436; f) J. H. Fuhrhop, P. Blumtritt, C. Lehmann, P. Luger, *J. Am. Chem. Soc.* **1991**, *113*, 7437.
[14] a) S. Okada, S. Peng, W. Spevak, D. Charych, *Acc. Chem. Res.* **1998**, *31*, 229; b) U. Jonas, K. Shah, S. Norvez, D. H. Charych, *J. Am. Chem. Soc.* **1999**, *121*, 4580; c) J.-M. Kim, Y. B. Lee, D. H. Yang, J.-S. Lee, G. S. Lee, D. J. Ahn, *J. Am. Chem. Soc.* **2005**, *127*, 17580.
[15] a) S. Bhattacharya, S. N. G. Acharya, *Chem. Mater.* **1999**, *11*, 3121; b) M. Masuda, T. Hanada, Y. Okada, K. Yase, T. Shimizu, *Macromolecules* **2000**, *33*, 9233; c) M. George, R. G. Weiss, *Chem. Mater.* **2003**, *15*, 2879; d) Z. Yuan, C.-W. Lee, S.-H. Lee, *Angew. Chem.* **2004**, *116*, 4293; *Angew. Chem. Int. Ed.* **2004**, *43*, 4197; e) T. Mori, K. Shimoyama, Y. Fukawa, K. Minagawa, M. Tanaka, *Chem. Lett.* **2005**, *34*, 116.
[16] See the Supporting Information.
[17] In addition to the fibrils, one could observe an ultrathin layer of **2** which was adsorbed onto the HOPG surface.
[18] The apparent height of the fibrils was measured at the maxima of the helical fine structure. The width was estimated from the apparent width of 18 nm after correction for the radius of the SFM tip.
[19] Figure 4c shows the SFM picture recorded after UV irradiation. This irradiation, however, had no influence on the appearance of the fibrils in the SFM images.
[20] a) F. R. Salemme, *Prog. Biophys. Mol. Biol.* **1983**, *42*, 95; b) A. Aggeli, I. A. Nyrkova, M. Bell, R. Harding, L. Carrick, T. C. B. McLeish, A. N. Semenov, N. Boden, *Proc. Natl. Acad. Sci. USA* **2001**, *98*, 11857.

 © 2006 Wiley-VCH Verlag GmbH & Co. KGaA, Weinheim

Membrane Proteins

DOI: 10.1002/anie.200504266

Structural Model of the Membrane-Bound C Terminus of Lipid-Modified Human N-Ras Protein**

*Guido Reuther, Kui-Thong Tan, Julia Köhler, Christine Nowak, André Pampel, Klaus Arnold, Jürgen Kuhlmann, Herbert Waldmann, and Daniel Huster**

Covalent lipid modification is a common posttranslational event relevant for 5–10% of all cellular proteins.[1] In particular, proteins involved in signal transduction are lipidated, providing a hydrophobic anchor that targets these molecules to the membrane.[2] By this mechanism, protein diffusion is constrained to two dimensions, and the probability of interaction with downstream effectors is increased by several orders of magnitude.[3] In spite of the tremendous biological significance of this membrane-binding mechanism, to date no structural data is available for lipidated membrane-bound proteins. Here we report a structural model for the backbone of the membrane-associated lipid-modified C terminus of the Ras protein determined by solid-state magic-angle spinning (MAS) NMR spectroscopy.

Ras is a small GTP-binding protein that plays a key role in cellular signal transduction as a molecular switch regulating cell proliferation and differentiation.[4] Mutations in Ras may lead to uncontrolled cell growth and ultimately cancer. It is known that up to 30% of all human cancers coincide with a mutated form of Ras.[4] The N-Ras isoform is subject to posttranslational lipid modifications on the C terminus (a palmitoyl chain at cysteine (Cys) 181 and a farnesyl chain at Cys186) that anchor the protein in the membrane. A huge amount of structural information has been collected for soluble non-lipid-modified forms of Ras proteins alone and complexed with effector and regulator proteins by X-ray diffraction[5] and solution NMR spectroscopy in the absence of membranes.[6] However, Ras must be at the membrane to be active.[7] The structure of the membrane-bound protein has eluded investigation so far. All members of the Ras family produce distinct biological outputs although they share a homology of $>90\%$ in the N-terminal domain. This suggests that the C terminus of the protein is essential for the biological role of Ras.[8]

Until recently, expression or synthesis protocols for the production of sufficient amounts of lipidated Ras protein and appropriate spectroscopic tools to determine the atomic structure of membrane-associated proteins were not available. For both problems solutions have been found recently. Lipidated proteins can be produced by bioorganic synthesis combining the expressed water-soluble protein with lipophilic chemically synthesized peptides to obtain a fully functional hybrid protein.[9] In this way isotopically labeled amino acids can be introduced into specific positions of the lipidated C terminus. Such a strategy makes it possible to study protein conformation by solid-state NMR spectroscopy, which is a very promising tool for solving the structure of membrane proteins.[10]

For the current study, we synthesized two lipid-modified N-Ras proteins with different ^{13}C-labeling patterns (Figure 1) containing one S-hexadecylated (HD) and one S-farnesylated (Far) Cys.[11] The protein was reconstituted into perdeuterated DMPC membranes and investigated by MAS NMR spectroscopy. In Figure 1 relevant regions of the ^{1}H–^{13}C (a,b)[12] and ^{13}C–^{13}C (c,d)[13] correlation spectra are shown. The alternating labeling pattern precludes most of the signal superposition, and well-resolved peaks are observed. In the ^{1}H–^{13}C spectra all correlation peaks for directly bonded ^{1}H–^{13}C pairs are present. Typical line widths for the Cα and Hα signals are ≈ 1 ppm and ≈ 0.15–0.25 ppm, respectively. This suggests that dipolar couplings are reduced by molecular motion but still sufficiently large to allow for polarization transfer by cross-polarization and proton-driven spin diffusion. ^{13}C–^{13}C correlation spectra show all connectivities within the labeled amino acid, for instance, between Cα and CO (Figure 1c,d). Thus, the complete assignment was possible from this set of MAS NMR experiments. A table containing the assignments and chemical-shift values is given in the Supporting Information.

From empirical analysis it is known that the secondary chemical shift, in other words, the difference between the measured isotropic chemical shift and the corresponding value in the random coil, strongly correlates with protein secondary structure.[14] The program package TALOS[15] was used to determine a model for the backbone structure of the membrane-binding domain of Ras from the isotropic chemical shifts. This program searches a database containing 78 proteins of known X-ray structure for chemical-shift and sequence homology. TALOS finds chemical-shift identities for triplets of amino acids and yields the backbone torsion angles as output. This information provides a basis for calculating a structural model of the molecule in question.[16]

The ^{13}Cα, ^{13}Cβ, ^{13}CO, and ^{1}Hα chemical shifts for the C terminus of the membrane-bound Ras protein determined in

[*] Dipl.-Phys. G. Reuther, Dr. D. Huster
Nachwuchsgruppe "Strukturbiologie von Membranproteinen"
Institut für Biotechnologie
Martin-Luther-Universität Halle-Wittenberg
Kurt-Mothes-Strasse 3, 06120 Halle (Germany)
Fax: (+49) 345-55-27013
E-mail: daniel.huster@biochemtech.uni-halle.de
K.-T. Tan, C. Nowak, Dr. J. Kuhlmann, Prof. Dr. H. Waldmann
Max Planck Institute of Molecular Physiology
Otto-Hahn-Strasse 11, 44227 Dortmund (Germany)
J. Köhler, Dr. A. Pampel
Institute of Experimental Physics II
University of Leipzig
Linnéstrasse 5, 04103 Leipzig (Germany)
Dipl.-Phys. G. Reuther, Prof. Dr. K. Arnold, Dr. D. Huster
Institute of Medical Physics and Biophysics
University of Leipzig
Härtelstrasse 16–18, 04107 Leipzig (Germany)

[**] This work was supported by the DFG (HU 720/5-1; SFB 642).

Supporting information for this article is available on the WWW under http://www.angewandte.org or from the author.

 © 2006 Wiley-VCH Verlag GmbH & Co. KGaA, Weinheim

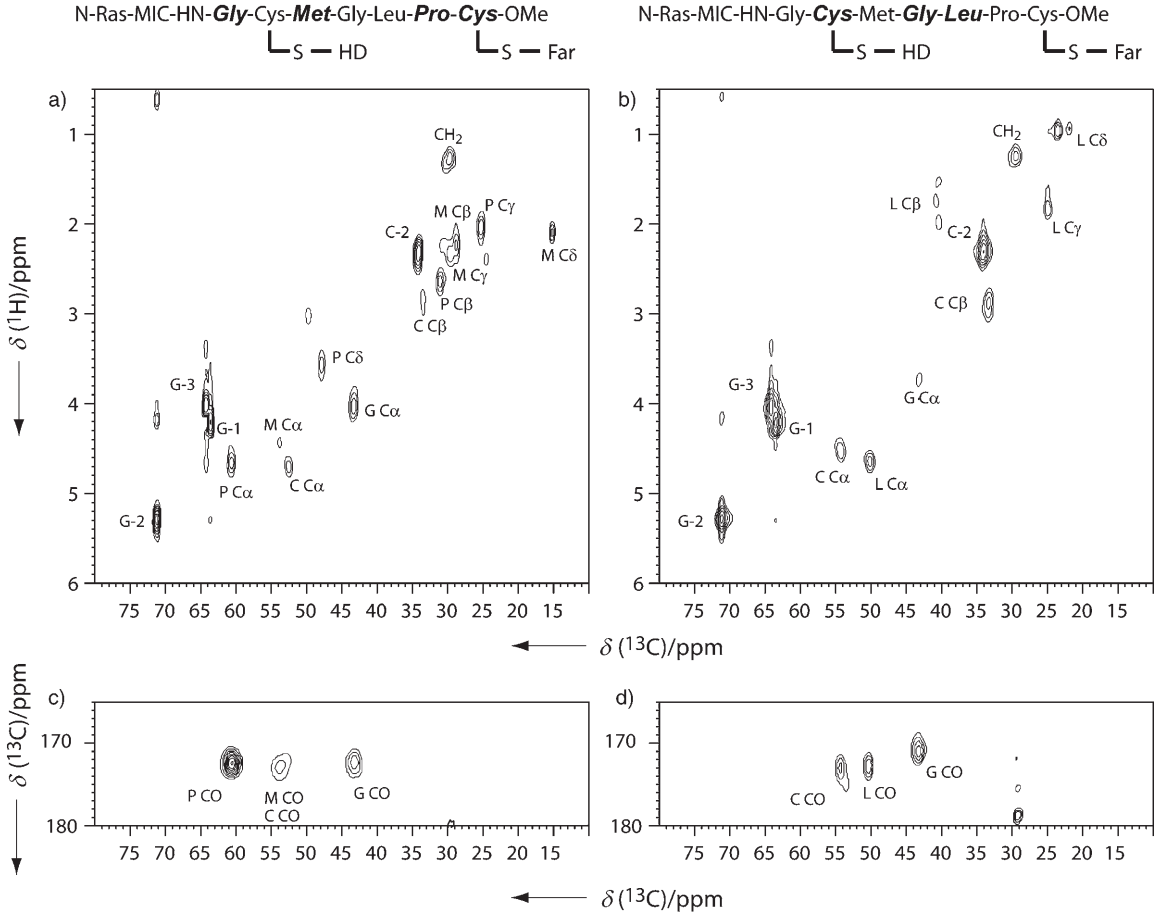


Figure 1. Contour plots of MAS NMR spectra of the lipidated membrane-bound Ras proteins. a, b) The ^{1}H–^{13}C correlation spectra provide different crosspeak patterns depending on the labeling scheme of the protein indicated. $^{13}C/^{15}N$-labeled amino acids are shown in bold italics. In addition to the protein signals, crosspeaks of the non-deuterated glycerol (G) and lipid chain signals (C-2, CH_2) from the membrane are detected. c, d) In the carbonyl region of the ^{13}C–^{13}C correlation spectra six out of seven Cα–CO crosspeaks are resolved.

the MAS NMR experiments provided the input parameters for the structural calculations. The deviations of the observed chemical shifts from those of the random coil increase towards the C terminus of Ras, indicating that the TALOS prediction is also better for the C-terminal amino acids. The backbone torsion angles for the amino acids 181–185 of the C terminus of N-Ras are given in Table 1. Note that no torsion angles for glycine (Gly) 180 and Cys186 could be determined by TALOS because Gly180 is the first and Cys186 the terminal labeled amino acid in the sequence of interest, and TALOS requires the input of chemical-shift data for three consecutive residues. Except for methionine (Met) 182, the determined torsion angles for the backbone geometry were conclusive. For this residue, three equally populated subsets of backbone torsion angles were found.

A simulated annealing protocol was used for structural calculations of the C terminus of the membrane-bound lipidated Ras protein. Because of the ambiguity in the TALOS result for Met182, three families of structural models were calculated. Figure 2 shows the structural model of the lipidated C-terminus of the membrane-bound N-Ras protein derived from solid-state NMR data. The ten backbone models of lowest energy are displayed for the three sets of Met182 torsion angles in the left column. The Cα coordinates of the five amino acid stretch, for which the torsion angles have been predicted, show a root mean square deviation of between 0.51 and 0.63 Å (calculated for 200 structural models). The global fold of the C terminus of the N-Ras protein in the membrane resembles a horseshoe. The

Table 1: Backbone torsions angles of the membrane-binding domain of the lipidated human N-Ras protein.

Residue[a]	Φ	Ψ
Cys181	−135°±20°	151°±17°
Met182[b]	−67°±11°	−22°±25°
	−79°±23°	121°±10°
	51°±5°	45°±7°
Gly183	84°±11°	−12°±13°
Leu184[c]	−83°±14°	141°±22°
Pro185[c]	−63°±8°	147°±9°

[a] For the chemical ligation, the N terminus of Ras is extended by two amino acids. The numbering of the amino acids here follows that of the wild-type protein. [b] For Met182, three sets of torsion angles were found by the TALOS program. [c] The chemical-shift difference between Cβ and Cγ of proline185 indicates a *trans* arrangement of the peptide bond between Leu184 and Pro185 ($\omega = 180°$).[17]

 © 2006 Wiley-VCH Verlag GmbH & Co. KGaA, Weinheim

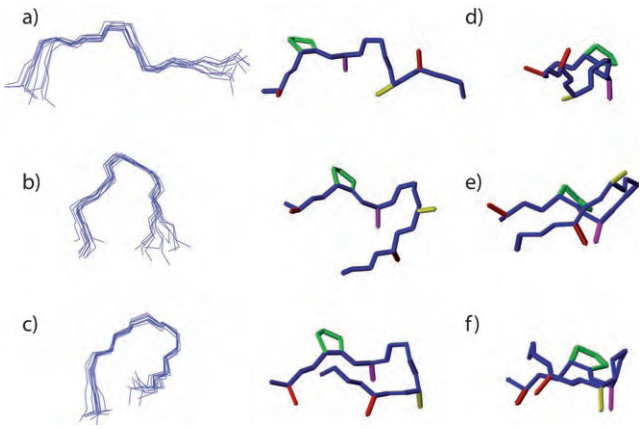


Figure 2. Structural models derived by solid-state NMR spectroscopy for the C terminus of membrane-bound lipidated human N-Ras protein. Three families of structural models are shown. a–c) Superposition of the 10 lowest energy models of the protein backbone. The rmsd for the five amino acids for which TALOS torsion angles are available are: a) 0.56 Å, b) 0.51 Å, and c) 0.63 Å. d–f) Different views of the averaged structural model with the backbone in blue and Pro in green. The Cβ atoms for the Cys, Leu, and Met are shown in red, yellow, and magenta, respectively. The figures were prepared using MOLMOL.[18]

membrane anchor of Ras has no regular α-helical or β-sheet motifs. This is not surprising because the sequence investigated here contains two Gly residues and one proline (Pro) residue, which are well-known turn promoters and helix breakers. As a result of the lack of structural information for Gly180 and Cys186, the ends of the sequence appear disordered in the images.

The TALOS results for Met182 show that the relation between torsion angles and chemical shift is not unique. Therefore, additional spectroscopic information is required to determine the most likely structural model of membrane-bound Ras protein. In previous investigations we studied membrane binding of the lipidated Ras heptapeptide (residues 180–186) by ^{1}H MAS NOESY and neutron diffraction spectroscopy.[19] Strong intermolecular crosspeaks indicated that the hydrophobic side chains (Cys, leucine (Leu), and Met) insert into the membrane interior.[19] The polar five-membered ring of proline points towards the aqueous phase.[20] These results provide additional information for the selection of the most likely of the structural models of the three possible for the membrane-binding domain of N-Ras.

It should be noted that the torsion angle predictions by TALOS do not provide information about the side chains of the protein. However, the tetrahedral geometry of the Cα atom in the backbone determines the direction of the side chain with respect to the protein backbone. This is illustrated in Figure 2. In the middle and right columns, two views of the average backbone conformational model of the Ras membrane-binding domain are shown for each set of Met torsion angles. These structural models also include the Cβ sites. For two of the three models, the hydrophobic side chains point in different directions, which appears a rather unlikely conformation based on thermodynamic considerations and is not in line with the NOEs between Ras peptide side chains and the membrane.[19] Thus one structural model remains, in which the lipidated and hydrophobic side chains point in the same direction, suggesting the orientation of the membrane-binding domain of the protein (Figure 2c, f). In agreement with the hydrophobicity scale[20] in this model Pro would point away from the membrane into the aqueous phase. Therefore, the interaction of the protein with the membrane stabilizes its conformation.

From these results we have constructed a model of the structure of the membrane-bound lipidated N-Ras protein (Figure 3). The membrane topology of the protein is determined by hydrophobic interactions between the lipidated Cys

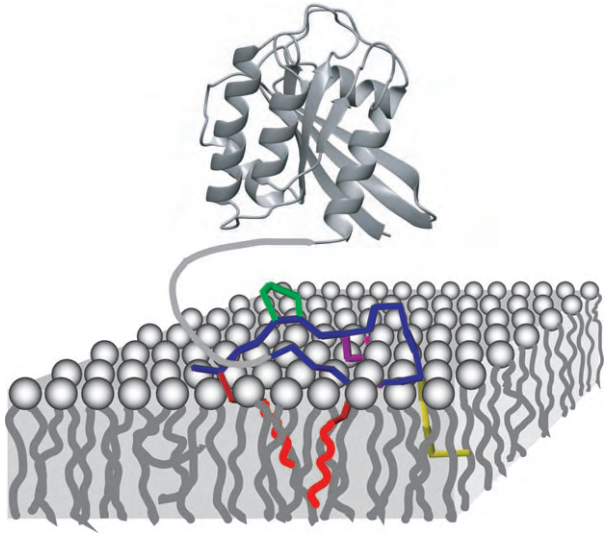


Figure 3. Structural model of the membrane-associated lipid-modified Ras protein (not to scale). The soluble N terminus is connected to the membrane anchor by a flexible linker domain. The conformation of the N terminus (residues 1–166) was adapted from the crystal structure.[5b] The color code is identical to that in Figure 2.

and hydrophobic side chains. Further, hydrogen bonds between the peptide backbone and the phospholipids in the interface region of the membrane are likely to occur. The lipid-binding domain is linked to the GTP-binding N-terminal region of the protein by a linker domain, which is putatively flexible.[6b] In contrast to H-Ras, there is currently no structure available for the N-terminus of N-Ras: however, because of the 92% sequence homology between H-Ras and N-Ras it is assumed that these structures are very similar.

Biological studies have established that all members of the Ras family interact with the same effectors in vitro but generate distinct outputs in vivo, suggesting that the biological difference is most likely imparted by their C termini, which regulate the sorting of Ras proteins into raft and liquid-crystalline membrane domains. Here, two elements direct Ras isoforms to their target structure: first, the primary membrane anchor sequence with two or three hydrophobic modifications (isoprenylation and S-acetylation) for N- and H-Ras or a combination of positively charged amino acids and an isoprene function for K-Ras^{B}. A second "linker domain" motif N-terminally neighboring the membrane anchor sequence defines the association with distinct subcompartments of the membrane by protein–protein interactions.[8] In

 © 2006 Wiley-VCH Verlag GmbH & Co. KGaA, Weinheim

this context, the structural model of the C-terminal membrane-binding domain determined in this work will set a first conformational basis for a more complete understanding of the biological Ras functions in cellular signal transduction.

Finally, it should be emphasized that TALOS represents a database approach, and the structural model derived from this procedure does not meet the criteria of a highly resolved solution NMR structure that is usually determined from 20 or more structural constraints per residue. Nevertheless, the structural model of the Ras membrane anchor determined in this work provides a first approach towards that goal.

Experimental Section

Protein synthesis: The synthesis of the N-Ras lipopeptide with an N-terminal maleimidocaproyl function, a nonhydrolyzable hexadecylated cysteine at the position of the palmitoylable cysteine, and farnesylation and carboxymethylation at the C-terminal cysteine, has been described previously.[9] N-Ras lipoproteins were produced following the published procedure.[11] Briefly, C-terminally truncated wild-type N-Ras (residues 1–181) was expressed in *E. coli* CK600K and purified by diethylaminoethyl (DEAE) ion-exchange chromatography and gel filtration. Coupling with isotopically labeled N-Ras lipopeptides was performed in stoichiometric amounts in 20 mM Tris/Cl, pH 7.4, 5 mM $MgCl_2$ supplemented with the detergent Triton X114. The detergent allowed for convenient separation of lipoprotein product and truncated starting material after completion of the coupling reaction. After removal of Triton X114 from the N-Ras lipoprotein by another DEAE ion-exchange chromatography, the lipoprotein was concentrated and adjusted to 20 mM Tris/Cl, pH 7.4, 5 mM $MgCl_2$, 2 mM dithioerythritol (DTE) by size-exclusion filtration in Amicon concentrators. All protein batches were analyzed by SDS-PAGE and MALDI-TOF mass spectrometry.

Sample preparation: Large unilamellar vesicles of [D_{67}]-DMPC were prepared by extrusion (buffer: 10 mM NaCl, 1 mM $MgCl_2$, 10 mM Hepes, pH 7.4). Aliquots of Ras protein were added to the liposome solution at a protein/lipid molar ratio of 1:150 and incubated at 37° for 4 h. The sample was ultracentrifuged at $\approx 90000 \times g$ for 10 h. Subsequently, the pellet was lyophilized, hydrated to 35 wt% water, and transferred into a 4-mm MAS rotor with Teflon insert. Measurement of the protein concentration in the supernatant after centrifugation revealed that 80–90% of the protein was bound to the liposomes.

NMR spectroscopy: MAS NMR measurements were carried out on a Bruker Avance 750 WB spectrometer operating at a resonance frequency of 188.5 MHz for ^{13}C and 749.8 MHz for ^{1}H. All measurements were conducted at a temperature of 30 °C. NMR spectra were referenced relative to TMS and rereferenced to TSP for the TALOS input.[21] ^{13}C CP MAS spectra were acquired at a MAS frequency of 7 kHz using a ^{1}H excitation pulse length of 4 μs and a CP spin lock field strength of ≈50 kHz (0.7-ms contact time). Spectra were accumulated with a relaxation delay of 2.5–3.2 s. The ^{1}H rf field strength for heteronuclear TPPM decoupling was ≈65 kHz. For the ^{1}H–^{13}C correlation experiments, 256 transients were acquired with a t_1 evolution of 8.5 ms yielding a total experimental time of ≈23 h. The ^{13}C–^{13}C correlation spectra were recorded in ≈80 h with a mixing time of 200 ms, 640 scans per t_1 increment, and an evolution time in the indirect dimension of 2 ms.

Structural calculation: Three families of structural models were calculated by TALOS because ambiguous torsion angles were found for Met 182. The chemical-shift difference between Cβ and Cγ of praline 185 indicated a *trans* arrangement of the peptide bond between Leu 184 and Pro 185.[17] In total, 11 constraints for the backbone conformation were obtained and included in the calculation using the program DYNAMO 3.1.[22] Calculations were performed using a conventional protocol with simulated annealing and torsion-angle dynamics, starting with 200 randomized conformers. More details about the structural calculation are given in the Supporting Information.

Received: December 1, 2005
Revised: May 30, 2006
Published online: July 17, 2006

Keywords: membrane proteins · NMR spectroscopy · Ras proteins · signal transduction

[1] *Lipid Modification of Proteins* (Ed.: M. J. Schlesinger), CRC, Boca Raton, **1993**.
[2] P. J. Casey, *Science* **1995**, *268*, 221–225.
[3] D. Murray, N. Ben-Tal, B. Honig, S. McLaughlin, *Structure* **1997**, *5*, 985–989.
[4] A. Wittinghofer, H. Waldmann, *Angew. Chem.* **2000**, *112*, 4360–4383; *Angew. Chem. Int. Ed.* **2000**, *39*, 4192–4214.
[5] a) M. V. Milburn, L. Tong, A. M. deVos, A. Brünger, Z. Yamaizumi, S. Nishimura, S. H. Kim, *Science* **1990**, *247*, 939–945; b) E. F. Pai, W. Kabsch, U. Krengel, K. C. Holmes, J. John, A. Wittinghofer, *Nature* **1989**, *341*, 209–214.
[6] a) P. J. Kraulis, P. J. Domaille, S. L. Campbell-Burk, T. Van Aken, E. D. Laue, *Biochemistry* **1994**, *33*, 3515–3531; b) R. Thapar, J. G. Williams, S. L. Campbell, *J. Mol. Biol.* **2004**, *343*, 1391–1408.
[7] T. Dudler, M. H. Gelb, *J. Biol. Chem.* **1996**, *271*, 11541–11547.
[8] R. G. Parton, J. F. Hancock, *Trends Cell Biol.* **2004**, *14*, 141–147.
[9] B. Bader, K. Kuhn, D. J. Owen, H. Waldmann, A. Wittinghofer, J. Kuhlmann, *Nature* **2000**, *403*, 223–226.
[10] a) J. Torres, T. J. Stevens, M. Samso, *Trends Biochem. Sci.* **2003**, *28*, 137–144; b) S. Luca, H. Heise, A. Lange, M. Baldus, *Arch. Pharm.* **2005**, *338*, 217–228; c) D. Huster, *Prog. Nucl. Magn. Reson. Spectrosc.* **2005**, *46*, 79–107.
[11] M. Volkert, K. Uwai, A. Tebbe, B. Popkirova, M. Wagner, J. Kuhlmann, H. Waldmann, *J. Am. Chem. Soc.* **2003**, *125*, 12749–12758.
[12] C. W. Lee, R. G. Griffin, *Biophys. J.* **1989**, *55*, 355–358.
[13] N. M. Szeverenyi, M. J. Sullivan, G. E. Maciel, *J. Magn. Reson.* **1982**, *47*, 462–475.
[14] a) D. S. Wishart, B. D. Sykes, *Methods Enzymol.* **1994**, *239*, 363–392; b) S. Spera, A. Bax, *J. Am. Chem. Soc.* **1991**, *113*, 5490–5492; c) H. Saitô, *Magn. Reson. Chem.* **1986**, *24*, 835–852.
[15] G. Cornilescu, F. Delaglio, A. Bax, *J. Biomol. NMR* **1999**, *13*, 289–302.
[16] a) S. Luca, J. F. White, A. K. Sohal, D. V. Filippov, J. H. van Boom, R. Grisshammer, M. Baldus, *Proc. Natl. Acad. Sci. USA* **2003**, *100*, 10706–10711; b) A. T. Petkova, Y. Ishii, J. J. Balbach, O. N. Antzutkin, R. D. Leapman, F. Delaglio, R. Tycko, *Proc. Natl. Acad. Sci. USA* **2002**, *99*, 16742–16747; c) S. Sharpe, W.-M. Yau, R. Tycko, *Biochemistry* **2006**, *45*, 918–933.
[17] S. K. Sarkar, T. D. Kopple, D. L. VanderHart, *J. Am. Chem. Soc.* **1984**, *106*, 3328–3331.
[18] R. Koradi, M. Billeter, K. Wüthrich, *J. Mol. Graphics* **1996**, *14*, 51–55.
[19] a) D. Huster, A. Vogel, C. Katzka, H. A. Scheidt, H. Binder, S. Dante, T. Gutberlet, O. Zschörnig, H. Waldmann, K. Arnold, *J. Am. Chem. Soc.* **2003**, *125*, 4070–4079; b) D. Huster, K. Kuhn, D. Kadereit, H. Waldmann, K. Arnold, *Angew. Chem.* **2001**, *113*, 1083–1085; *Angew. Chem. Int. Ed.* **2001**, *40*, 1056–1058.
[20] W. C. Wimley, S. H. White, *Nat. Struct. Biol.* **1996**, *3*, 842–848.
[21] C. R. Morcombe, K. W. Zilm, *J. Magn. Reson.* **2003**, *162*, 479–486.
[22] G. Kontaxis, F. Delaglio, A. Bax, *Methods Enzymol.* **2005**, *394*, 42–78.

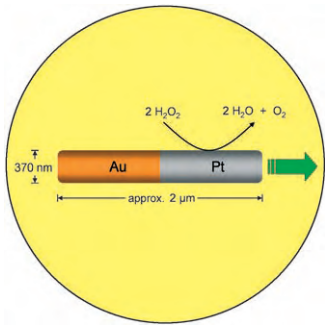
 © 2006 Wiley-VCH Verlag GmbH & Co. KGaA, Weinheim

Cover Picture

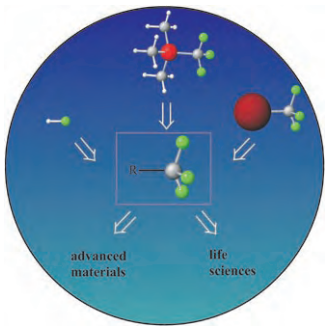


Alois Fürstner,* Michaël D. B. Fenster, Bernhard Fasching, Cédrickx Godbout, and Karin Radkowski

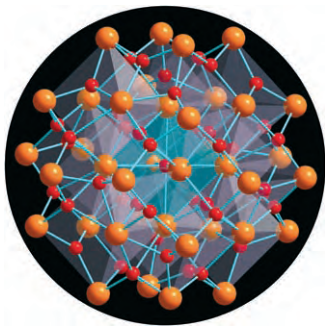
The antimitotic natural product spirastrellolide A is a complicated structure that shows impressive biological effects. Many key issues remain unresolved for this compound, for example its relative and absolute configurations and its biological mode of action. In two Communications on pages 5506 and 5510 ff., Fürstner and co-workers describe the synthesis of all four fragments of spirastrellolide A—initial strides in answering these questions. (Image of cell undergoing mitosis: Conley Rieder.)



Microscopic Machines
Microparticles can move autonomously if they fulfill certain requirements. In their Minireview on page 5420 ff., A. Sen and co-workers discuss the principles of transducing chemical into mechanical energy on the micrometer scale.



Organofluorine Compounds
The biological properties of organic compounds can be fine-tuned by the incorporation of fluorine. But at what point in the synthesis should the fluorine be added? The answers are found in the Review by M. Schlosser on page 5432 ff.



Cluster Compounds
A giant bismuth oxido cluster containing 38 Bi atoms was formed in coordinating solvents. The synthesis and characterization of this cluster, the largest known of its type, are described by E. V. Dikarev et al. in their Communication on p. 5448 ff.

Contents

VIP *The following Communications have been judged by at least two referees to be "very important papers" and will be published online at www.angewandte.org soon:*

*S. Hiraoka, K. Harano, M. Shiro, Y. Ozawa, N. Yasuda, K. Toriumi, M. Shionoya**
Isostructural Coordination Capsules with a Series of 10 Different d^5–d^{10} Transition-Metal Ions

*J. G. Cordaro, D. Stein, H. Rüegger, H. Grützmacher**
Making the True "CP" Ligand

*N. Shimokhina, A. Bronowska, S. Homans**
Contribution of Ligand Desolvation to Binding Thermodynamics in a Ligand–Protein Interaction

*M. B. Harney, Y. Zhang, L. R. Sita**
Bimolecular Control over Polypropene Stereochemical Microstructure in a Well-Defined Two-State System and a New Fundamental Form: Stereogradient Polypropene

*H. Niu, M. Gao**
Synthesis of Diameter-Tunable CdTe Nanotubes Templated by One-Dimensional Nanowires of Cadmium Thiolate Polymer

*Y. Li, B. S. Lokitz, C. L. McCormick**
Thermally Responsive Vesicles and Their Structural "Locking" through Polyelectrolyte Complex Formation

Obituary

Robert Bruce Merrifield (1921–2006) — *B. Gutte* — **5412 – 5413**

Books

Voltage-Gated Ion Channels as Drug Targets — David J. Triggle, Murali Gopalakrishnan, David Rampe, Wei Zheng — *reviewed by P. Reiß, U. Koert* — **5414**

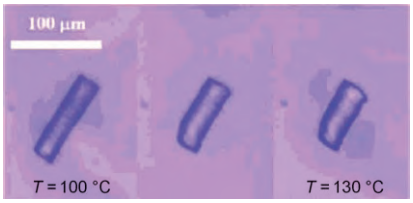
Molecular Modeling Techniques in Material Sciences — Jörg-Rüdiger Hill, Lalitha Subramanian, Amitesh Maiti — *reviewed by R. Q. Snurr* — **5414**

Highlights

Molecular Devices

Y. Yu,* T. Ikeda* — **5416 – 5418**

Soft Actuators Based on Liquid-Crystalline Elastomers



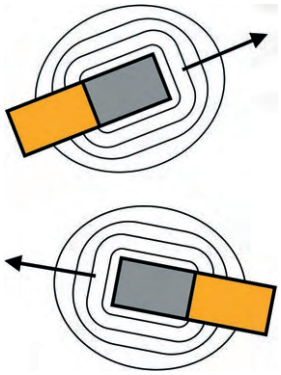
Molecules that twitch: Liquid-crystalline elastomers (LCEs) show promise in applications as soft actuators, with advantages such as large deformations and high-speed, two- (contraction) or three-dimensional (bending) actions. Earlier systems were macroscopic (mm/cm) in size; however, a soft lithography technique called replica molding was recently used to create LCE pillars on the micrometer scale.

Minireviews

Microscopic Machines

W. F. Paxton, S. Sundararajan, T. E. Mallouk, A. Sen* — **5420 – 5429**

Chemical Locomotion



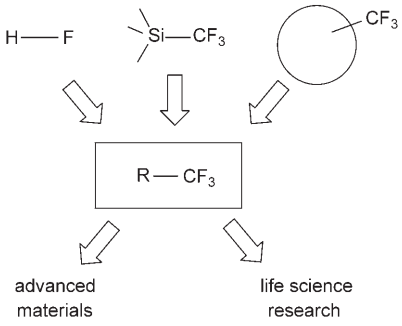
Doing the locomotion! As an alternative to using localized physical interactions and chemical reactions to propel small objects, catalysis can be used to translate the free chemical energy of the surroundings into asymmetric gradients, which result in directed mechanical motion. These approaches and some aspects of converting chemical energy into mechanical energy on the micrometer scale are discussed in the Minireview.

InterScience

© 2006 Wiley-VCH Verlag GmbH & Co. KGaA, Weinheim

Reviews

Doesn't grow on trees: Trifluoromethyl-substituted substances are "unnatural" without exception. To prepare them, one has to choose among principal synthetic strategies: to replace other heteroatoms by fluorine, to transfer the CF_3 entity as a whole from a small precursor to a pre-constructed skeleton, or to start with a CF_3-bearing core compound and to add the missing structural parts, in particular functionality (see scheme).



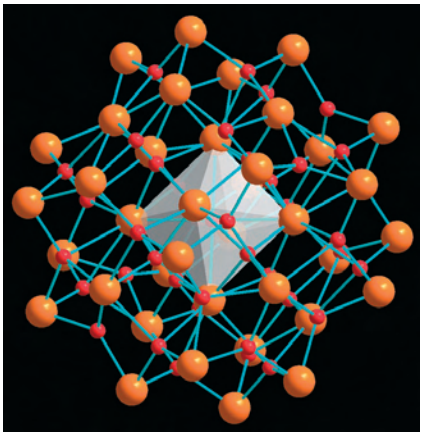
Organofluorine Compounds

M. Schlosser* _____ 5432 – 5446

CF_3-Bearing Aromatic and Heterocyclic Building Blocks

Communications

Aggregation in coordinating solvents: A giant oxido cluster $[Bi_{38}O_{45}(hfac)_{24}]$ (hfac = hexafluoroacetylacetonate), formed in solutions of bismuth oxido diketonate $[Bi_9O_7(hfac)_{13}]$, has been isolated and fully characterized. The $[Bi_{38}O_{45}]^{24+}$ core (see picture: orange Bi, red O; central Bi_6O_9 unit is highlighted) is capped by 24 hfac ligands, has a size larger than 2 nm, and may serve as a model for investigating the chemistry of bismuth oxide nanoparticles.

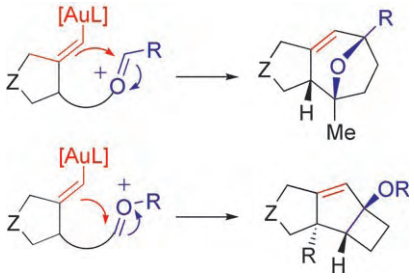


Cluster Compounds

E. V. Dikarev,* H. Zhang, B. Li _____ 5448 – 5451

From a Bismuth Oxido Diketonate to a Giant Bismuth Oxido Cluster

Going for gold: Au^I-catalyzed cyclizations of functionalized enynes lead to the ready assembly of tricyclic carbon skeletons that are present in a number of naturally occurring compounds. An alkenyl gold intermediate is formed in the cyclization of the enynes and can be trapped in 5-*exo-dig* or 6-*endo-dig* Prins reactions to form an additional C–C bond. Z = $C(CO_2Me)_2$, NTs; R = H, Me, *i*Pr.



Cyclization

E. Jiménez-Núñez, C. K. Claverie, C. Nieto-Oberhuber, A. M. Echavarren* _____ 5452 – 5455

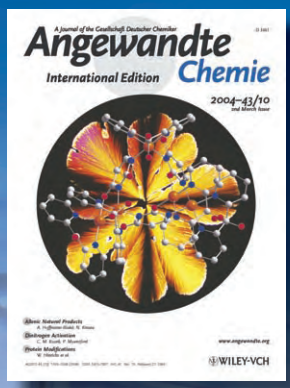
Prins Cyclizations in Au-Catalyzed Reactions of Enynes

For the USA and Canada:
ANGEWANDTE CHEMIE International Edition (ISSN 1433-7851) is published weekly by Wiley-VCH PO Box 191161, D 69451 Weinheim, Germany. Air freight and mailing in the USA by Publications Expediting Inc. 200 Meacham Ave., Elmont, NY 11003. Periodicals postage paid at Jamaica NY 11431. US POSTMASTER: send address changes to *Angewandte Chemie*, Wiley-VCH, 111 River Street, Hoboken, NJ 07030. Annual subscription price for institutions: US$ 5685/5168 (valid for print and electronic / print or electronic delivery); for individuals who are personal members of a national chemical society prices are available on request. Postage and handling charges included. All prices are subject to local VAT/sales tax.

© 2006 Wiley-VCH Verlag GmbH & Co. KGaA, Weinheim

The best in chemistry –

for more than a hundred years



A Journal of the Gesellschaft Deutscher Chemiker

Angewandte
International Edition **Chemie**

www.angewandte.org

1888: ***The beginning of a success story***

Constant Innovations

1962: *First issue of the International Edition*
1976: *Graphical abstracts*
1979: *Cover pictures*
1988: *Centenary of Angewandte*
1989: *Routine use of color*
1991: *New section: Highlights*
1992: *Computerized editorial tracking system*
1995: *Internet service for readers*
1998: *Regular press service; full-text online*
2000: *New section: Essays; EarlyView: Communications available online ahead of the printed version*
2001: *New section: Minireviews*
2002: *Online submission of manuscripts*
2003: *Weekly publication; new section: News; new layout*
2004: *Backfiles (1962-1997); ManuscriptXpress: Online system for authors and referees*



Angewandte's advisors...

Stefan Marcinowski
BASF AG
Ludwigshafen

» In our company ***Angewandte Chemie*** *is seen as an outstanding journal that combines first class performance in publishing innovative chemistry with a high international visibility. With its global recognition* ***Angewandte Chemie*** *functions as a seed cell for innovative technologies to be applied on a commercial basis in the future. «*

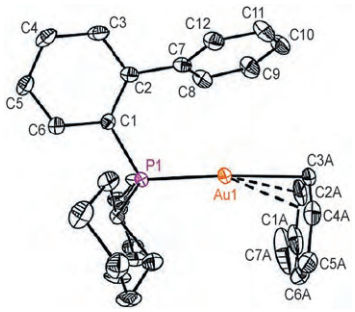
Angewandte Chemie International Edition *is a journal of the German Chemical Society (GDCh)*

GDCh

WILEY InterScience® DISCOVER SOMETHING GREAT

WILEY-VCH

1861404_gu



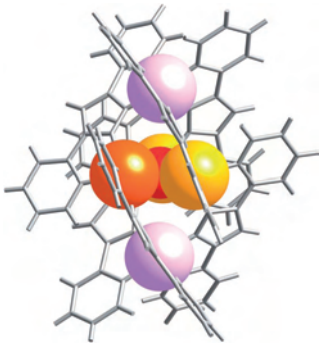
In close contact: The first gold(I) complexes of simple arenes show a separation between the Au center and the mean aromatic plane of 2.20–2.24 Å, which is much shorter than the related silver(I)–arene bonds.

Arene Complexes

E. Herrero-Gómez, C. Nieto-Oberhuber, S. López, J. Benet-Buchholz, A. M. Echavarren* ——— **5455 – 5459**

Cationic η^1/η^2-Gold(I) Complexes of Simple Arenes

An $[Fe^{II}_3O]^{4+}$ core in a candy wrapper: 3,5-Bis(pyridin-2-yl)pyrazolate (L^-) and iron(II) ions undergo homochiral self-assembly into a bis(triple-helical) cluster (see picture), in which a triangular $[Fe^{II}_3O]^{4+}$ core (Fe orange and yellow, O red) is surrounded by two $[Fe^{II}L_3]^-$ units (Fe purple, L^- gray).

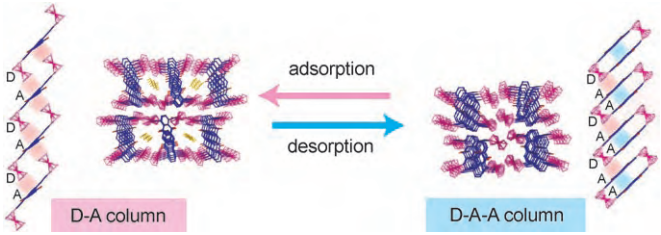


Cluster Compounds

K. Yoneda, K. Adachi, K. Nishio, M. Yamasaki, A. Fuyuhiro, M. Katada, S. Kaizaki,* S. Kawata* ——— **5459 – 5461**

An $[Fe^{II}_3O]^{4+}$ Core Wrapped by Two $[Fe^{II}L_3]^-$ Units

---



Both porous and nonporous structures are formed by crystals of donor–acceptor (D–A) compound 1,4-bis(ferrocenylethynyl)anthraquinone. The guest-incorporating porous and guest-free nonporous structures can interchange instantly and reversibly by desorption and adsorption of guest molecules, which cause alternation of D–A and D–A–A arrangements in the one-dimensional columnar structure (see picture).

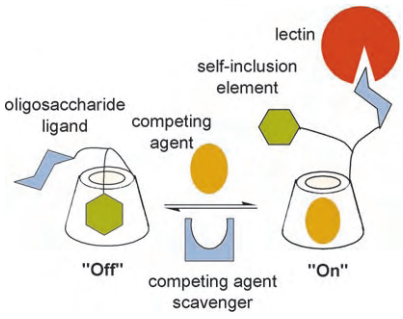
Host–Guest Systems

M. Kondo, M. Murata, H. Nishihara,* E. Nishibori, S. Aoyagi, M. Yoshida, Y. Kinoshita, M. Sakata ——— **5461 – 5464**

Guest-Induced Instant and Reversible Crystal-to-Crystal Transformation of 1,4-Bis(ferrocenylethynyl)anthraquinone

---

The ins and outs of binding: Supramolecular control of carbohydrate–protein interactions has been achieved through the design of β-cyclodextrin (βCD) based conjugates whose conformation is dependent on a reversible self-inclusion process. The accessibility of glycoligands to the lectin binding site is then regulated by allosteric inclusion of effector/antagonist-like molecules in the βCD cavity (see scheme).



Noncovalent Interactions

N. Smiljanic, V. Moreau, D. Yockot, J. M. Benito, J. M. García Fernández,* F. Djedaïni-Pilard* ——— **5465 – 5468**

Supramolecular Control of Oligosaccharide–Protein Interactions: Switchable and Tunable Ligands for Concanavalin A Based on β-Cyclodextrin

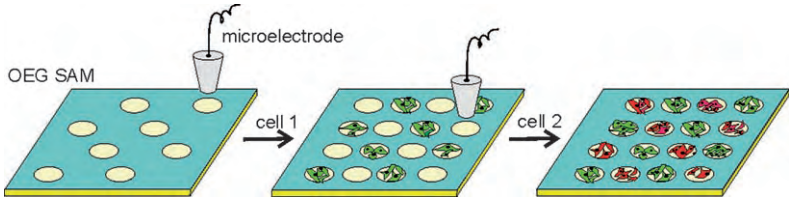
© 2006 Wiley-VCH Verlag GmbH & Co. KGaA, Weinheim

Contents

Attaching Cells

C. Zhao, I. Witte,
G. Wittstock* ——— **5469 – 5471**

Switching On Cell Adhesion with Microelectrodes

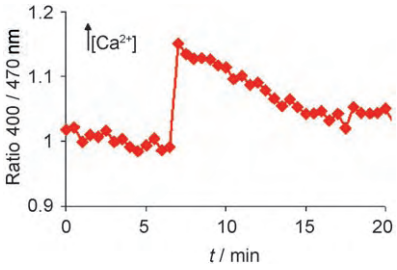


Stick it! A microelectrochemical method was developed for in situ manipulation of the cell-adhesive property of an oligo-(ethylene glycol)-terminated self-assembled monolayer substrate (OEG SAM) and subsequent cell adhesion and growth.

Biosensors

R. M. Sánchez-Martín, M. Cuttle,
S. Mittoo, M. Bradley* ——— **5472 – 5474**

Microsphere-Based Real-Time Calcium Sensing

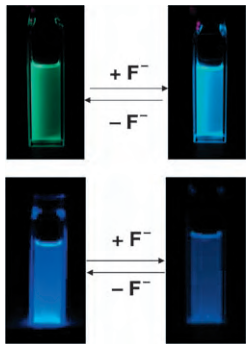


Sensing within the cell: Microspheres (2 μm) covalently loaded with calcium sensors can be delivered efficiently into living cells to analyze the intracellular changes in the concentration of Ca^{2+} ions in real time. The figure shows the real-time ratiometric fluorescent analysis (400/475 nm ratio) of the release of Ca^{2+} ions in cells loaded with the microspheres.

Sensors

X. Y. Liu, D. R. Bai, S. Wang* **5475 – 5478**

Charge-Transfer Emission in Nonplanar Three-Coordinate Organoboron Compounds for Fluorescent Sensing of Fluoride

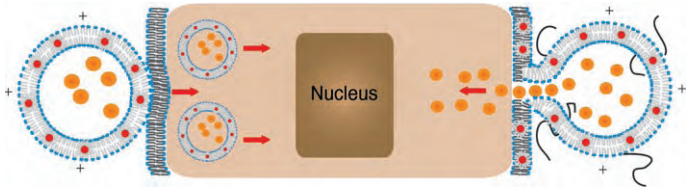


A real turn-on: Two nonplanar three-coordinate boron compounds were synthesized as fluorescent sensors for fluoride that utilize charge-transfer emission. The fluorescence of one of the sensors turns on (see picture) and the other turns off in the presence of fluoride.

Nanobiotechnology

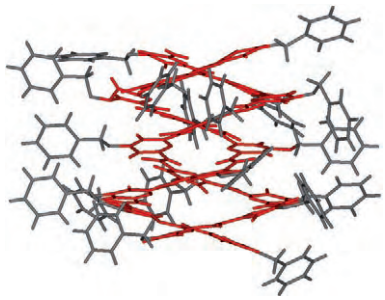
G. Gopalakrishnan, C. Danelon, P. Izewska, M. Prummer, P.-Y. Bolinger, I. Geissbühler, D. Demurtas, J. Dubochet, H. Vogel* ——— **5478 – 5483**

Multifunctional Lipid/Quantum Dot Hybrid Nanocontainers for Controlled Targeting of Live Cells



Hydrophobic quantum dots can be incorporated into the bilayer membrane of lipid vesicles for selective delivery into either plasma membranes or the cytoplasm of living cells (see picture). The cell and lipid membranes can integrate any kind of hydrophobic nanoparticle whose size matches the membrane thickness, thus opening possibilities for their manipulation in nanobiotechnology applications.

© 2006 Wiley-VCH Verlag GmbH & Co. KGaA, Weinheim



Hairy molecules! The numerous benzyloxy side chains sticking out of a helically folded pyridine carboxamide oligomer bring about considerable stabilization to its double-helical conformation. The structure of the duplex was studied both in solution and in the solid state.

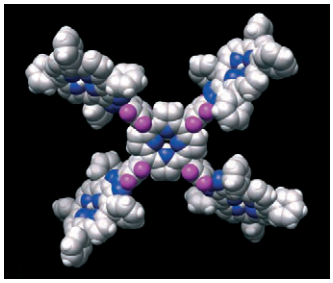
Helical Structures

D. Haldar, H. Jiang, J.-M. Léger, I. Huc* ——— **5483 – 5486**

Interstrand Interactions between Side Chains in a Double-Helical Foldamer

---

An attractive target: Multiple porphyrin systems (see picture for example) are at the center of many synthetic efforts, and efficient strategies for preparing valuable building blocks for these polycycles are much sought after. Herein such a strategy for the synthesis of [1,2,3]triazolo[4,5-*b*]-porphyrin building blocks is presented.

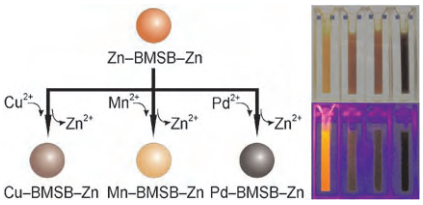


Porphyrins

P. S. S. Lacerda, A. M. G. Silva, A. C. Tomé, M. G. P. M. S. Neves, A. M. S. Silva, J. A. S. Cavaleiro,* A. L. Llamas-Saiz ——— **5487 – 5491**

[1,2,3]Triazolo[4,5-*b*]porphyrins: New Building Blocks for Porphyrinic Materials

---



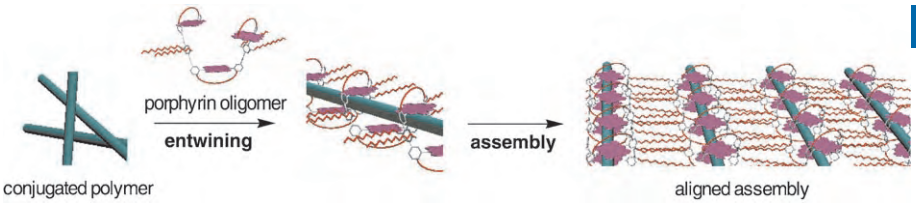
Ion balls: The composition of nano- and microparticles made from infinite coordination polymers can be chemically transformed through ion-exchange reactions without substantially changing the particle size and morphology. This approach is a straightforward and useful way of creating one precursor set of particles whose composition can be controllably transformed into that of a new set of compounds with different properties.

Nano- and Microstructures

M. Oh, C. A. Mirkin* ——— **5492 – 5494**

Ion Exchange as a Way of Controlling the Chemical Compositions of Nano- and Microparticles Made from Infinite Coordination Polymers

---



Straight curls: Conjugated polymers are aligned through the use of twining porphyrin oligomers (twimers), which act as helical "hosts" that twine around and are included within a single conjugated polymer. The resulting composites aggregate into relatively large 2D structures in the solid state and exhibit well-oriented periodic striping.

Porphyrinoids

M. Takeuchi,* C. Fujikoshi, Y. Kubo, K. Kaneko, S. Shinkai* ——— **5494 – 5499**

Conjugated Polymers Complexed with Helical Porphyrin Oligomers Create Micron-Sized Ordered Structures

© 2006 Wiley-VCH Verlag GmbH & Co. KGaA, Weinheim

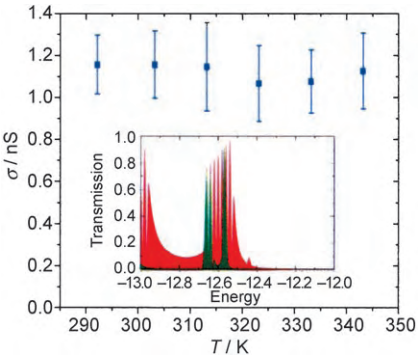
Contents

DNA Conductance

H. van Zalinge, D. J. Schiffrin, A. D. Bates, E. B. Starikov, W. Wenzel, R. J. Nichols* _____ **5499 – 5502**

Variable-Temperature Measurements of the Single-Molecule Conductance of Double-Stranded DNA

A sound result: Calculations have demonstrated a strong influence of acoustic modes on the conductance of double-stranded DNA (transmission spectrum of a duplex in its ideal B-DNA conformation is shown in red, that with deformations along DNA acoustic modes in green). The observed temperature independence of the conductivity at and above room temperature arises from a high overall population of such modes above the Debye temperature.

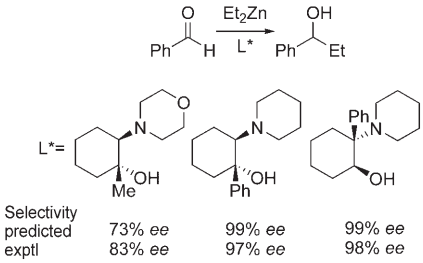


Computational Models

J. C. Ianni, V. Annamalai, P.-W. Phuan, M. Panda, M. C. Kozlowski* **5502 – 5505**

A Priori Theoretical Prediction of Selectivity in Asymmetric Catalysis: Design of Chiral Catalysts by Using Quantum Molecular Interaction Fields

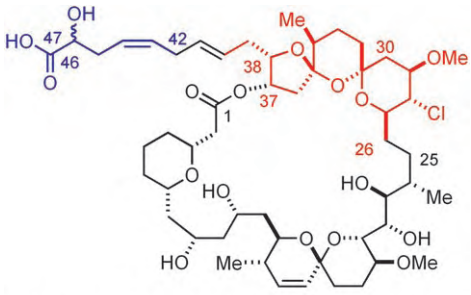
Excellent forecast: The selectivities for a set of chiral catalysts were predicted by methods derived from quantum mechanical molecular interaction fields that were applied to ground-state structures rather than transition-state structures. The predictions for the asymmetric addition of Et_2Zn to PhCHO are in remarkable agreement with the experimental results ($r^2_{pred.} = 0.87$).



Natural Products (1)

A. Fürstner,* M. D. B. Fenster, B. Fasching, C. Godbout, K. Radkowski _ **5506 – 5510**

Toward the Total Synthesis of Spirastrellolide A. Part 1: Strategic Considerations and Preparation of the Southern Domain



one of the possible stereostructures of spirastrelloide A

Natural Products (2)

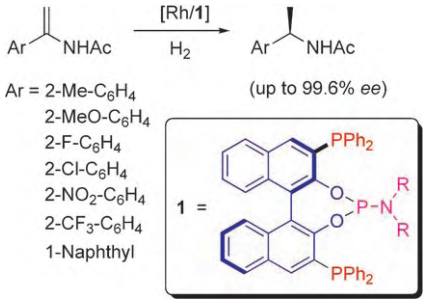
A. Fürstner,* M. D. B. Fenster, B. Fasching, C. Godbout, K. Radkowski _ **5510 – 5515**

Toward the Total Synthesis of Spirastrellolide A. Part 2: Conquest of the Northern Hemisphere

North and South: The unique biological activity of the natural product spirastrellolide A renders it an attractive lead for anticancer agents. The southern hemisphere (C1–C25) and the northern hemisphere (including the chlorinated [5,6,6]-bis-spiroacetal entity and the lateral C42–C47 chain) are prepared by concise and efficient routes. Consequently, the entire carbon framework of this potent phosphatase inhibitor, which contains 21 chiral centers, is prepared in an optically active form, and an important step toward structure determination by total synthesis is achieved.

© 2006 Wiley-VCH Verlag GmbH & Co. KGaA, Weinheim

New couple: A novel combination of phosphine and phosphoramidite groups is applied to the preparation of pseudo-C_2-symmetric triphosphorous bidentate phosphine–phosphoramidite ligands **1**. Unprecedented enantioselectivities toward *ortho*-substituted aryl enamides and a 1-naphthylenamide in Rh-catalyzed hydrogenation reactions are obtained.

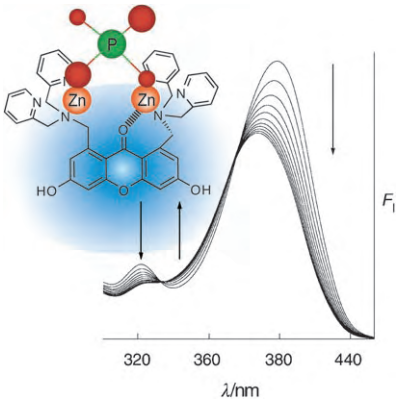


Asymmetric Catalysis

W. Zhang, X. Zhang* ——— **5515 – 5518**

Synthesis of Triphosphorous Bidentate Phosphine–Phosphoramidite Ligands: Application in the Highly Enantioselective Hydrogenation of *ortho*-Substituted Aryl Enamides

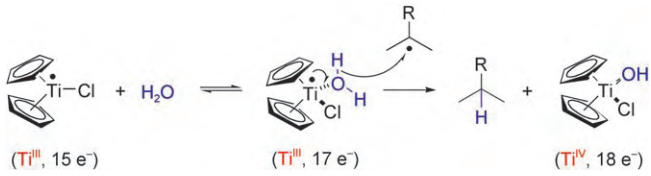
A xanthone-based chemosensor bears two 2,2′-dipicolylamine–zinc(II) sites and displays changes in the excitation spectrum at three wavelengths upon binding phosphates (see picture). These changes in the signals arise from the coordination rearrangement of the xanthone fluorophore around the zinc centers, which modulates the photophysical property of the chemosensor, thus enabling ratiometric fluorescent analysis.



Fluorescent Probes

A. Ojida, H. Nonaka, Y. Miyahara, S.-i. Tamaru, K. Sada, I. Hamachi* ——— **5518 – 5521**

Bis(Dpa-Zn^{II}) Appended Xanthone: Excitation Ratiometric Chemosensor for Phosphate Anions

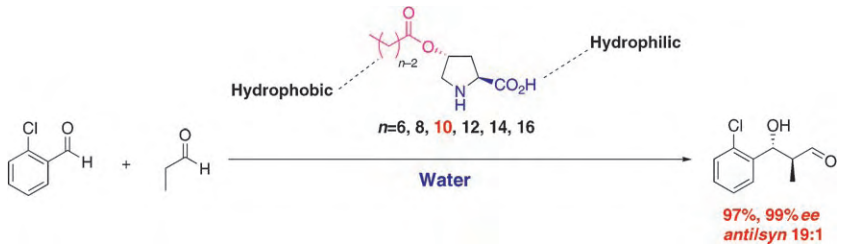


Hydrogen-atom transfer from water to free radicals can be mediated by aqua complexes of titanium(III) (see scheme). Asymmetric epoxidation in combination with $[Cp_2TiCl]/H_2O$-mediated reductive epoxide opening can be viewed as an alternative with complementary stereoselectivity to the hydroboration–epoxidation method for the enantioselective synthesis of anti-Markovnikov alcohols from alkenes.

Free-Radical Chemistry

J. M. Cuerva,* A. G. Campaña, J. Justicia, A. Rosales, J. L. Oller-López, R. Robles, D. J. Cárdenas,* E. Buñuel, J. E. Oltra* ——— **5522 – 5526**

Water: The Ideal Hydrogen-Atom Source in Free-Radical Chemistry Mediated by Ti^{III} and Other Single-Electron-Transfer Metals?



Why not combine the two? The asymmetric direct aldol reaction of two different aldehydes was catalyzed by a combined proline–surfactant organic catalyst in the presence of water. A stable emulsion was formed in the reaction mixture, and the aldols were obtained with excellent diastereo- and enantioselectivities (see scheme).

Organocatalysis

Y. Hayashi,* S. Aratake, T. Okano, J. Takahashi, T. Sumiya, M. Shoji ——— **5527 – 5529**

Combined Proline–Surfactant Organocatalyst for the Highly Diastereo- and Enantioselective Aqueous Direct Cross-Aldol Reaction of Aldehydes

© 2006 Wiley-VCH Verlag GmbH & Co. KGaA, Weinheim

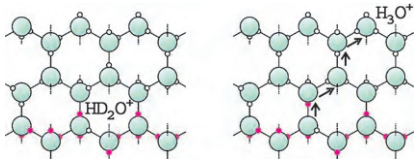
Contents

Proton Transfer

C.-W. Lee, P.-R. Lee, H. Kang* ——— **5529 – 5533**

Protons at Ice Surfaces

Starry, starry ice: A study of proton transfer and H/D exchange in ice films shows that the proton mainly resides at their surface. It can move a short distance by a hopping relay mechanism (see picture) even when molecular motion is virtually frozen. This unique mobility and surface affinity suggest the possibility for proton-catalyzed reactions on cold ice surfaces, such as on interstellar dust particles.



Cycloaddition

Y. Sun, H.-S. Chan, H. Zhao, Z. Lin,* Z. Xie* ——— **5533 – 5536**

Ruthenium-Mediated Coupling/Cycloaddition of the Cyclopentadienyl Ligand in $[\{\eta^5{:}\sigma\text{-}Me_2C(C_5H_4)(C_2B_{10}H_{10})\}Ru(NCCH_3)_2]$ with Alkynes

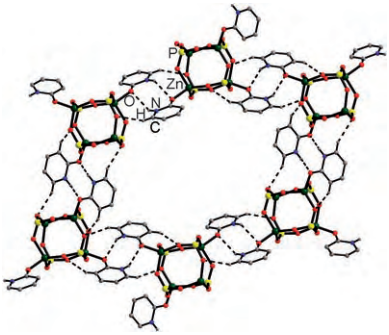


Facile formation of tricycles: Ruthenium-mediated coupling/cycloaddition of a cyclopentadienyl ligand with aromatic alkynes offers a facile route to tricyclic compounds (see scheme). The sterically demanding carborane moiety plays a crucial role in regioselective dimerization of alkynes (to give head-to-tail coupling products) and prevents alkyne trimerization.

Supramolecular Chemistry

R. Murugavel,* S. Kuppuswamy, R. Boomishankar, A. Steiner **5536 – 5540**

Hierarchical Structures Built from a Molecular Zinc Phosphate Core

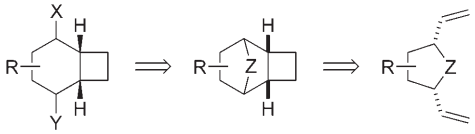


Playing with blocks: Zinc phosphate cubes with molecular structures that resemble the double-four-ring (D4R) secondary building unit of zeolites are prepared. When the appropriate ligands are chosen, the cubes assemble into 1D, 2D (see picture), or 3D supramolecular networks through hydrogen bonds that involve their surface functional groups.

Cyclizations

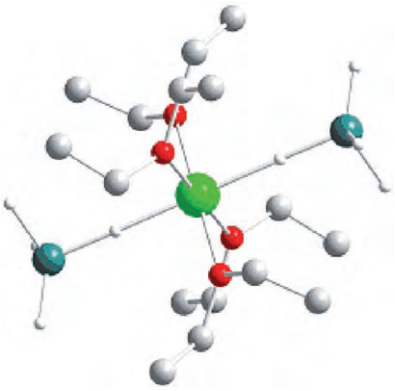
I. Braun, F. Rudroff, M. D. Mihovilovic, T. Bach* ——— **5541 – 5543**

Synthesis of Enantiomerically Pure Bicyclo[4.2.0]octanes by Cu-Catalyzed [2+2] Photocycloaddition and Enantiotopos-Differentiating Ring Opening



Fooling Mother Nature: When the bicyclo[4.2.0]octanes **A** are bridged as in precursors **B** (Z = CO), the otherwise impossible [2+2] photocycloaddition reaction of 1,7-dienes is possible with substrates such as **C**. A subsequent Baeyer–Villiger oxidation serves to desymmetrize substrates **B** and establishes a general approach to enantiomerically pure products **A**.

© 2006 Wiley-VCH Verlag GmbH & Co. KGaA, Weinheim

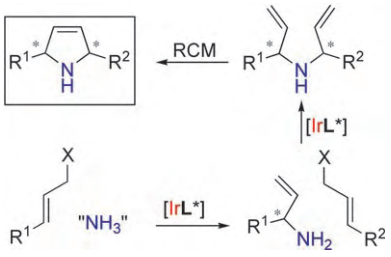


Unknown terrain: $Mg(GaH_4)_2 \cdot 4\,OEt_2$ (see molecular structure; blue Ga, green Mg, red O, gray C, white H) can be regarded as a parent compound for the essentially unexplored group of alkaline-earth tetrahydridogallates. Reaction of $Mg(GaH_4)_2 \cdot 4\,OEt_2$ with *tert*-butyl alcohol leads to $\{Mg(OtBu)[GaH_2(OtBu)_2]\}_2$.

Metal Hydrides

M. Veith,* M. Burkhart, V. Huch ——— **5544 – 5546**

Magnesium Bis(tetrahydridogallate(III)): Structure and Reaction with *tert*-Butyl Alcohol

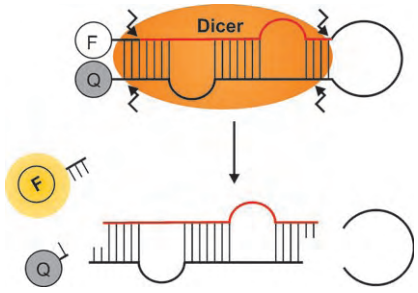


New variants of the iridium-catalyzed allylic substitution allow N-protected and non-protected chiral allylamines to be prepared with high enantio- and regioselectivity. The allylamines are used as nucleophiles in highly diastereoselective, catalyst-controlled allylic aminations. The products are transformed into N-non-protected 2,5-disubstituted 3,4-dehydropyrrolidines by ring-closing metathesis (RCM; see scheme).

Allylic Amination

R. Weihofen, O. Tverskoy, G. Helmchen* ——— **5546 – 5549**

Salt-Free Iridium-Catalyzed Asymmetric Allylic Aminations with *N*,*N*-Diacylamines and *ortho*-Nosylamide as Ammonia Equivalents



Maturation process: Micro RNAs represent a recently (re-)discovered group of regulators of gene expression. Ligands of the inactive precursor RNAs (pre-miRNAs) inhibit the formation of the respective miRNAs. Such ligands could potentially be used as tools in biomedicine. A doubly labeled RNA beacon allows simple screening of potential pre-miRNA binders.

Micro RNAs

B. P. Davies, C. Arenz* —— **5550 – 5552**

A Homogenous Assay for Micro RNA Maturation

Sources

Product and Company Directory

You can start the entry for your company in "Sources" in any issue of *Angewandte Chemie*.

If you would like more information, please do not hesitate to contact us.

Wiley-VCH Verlag – Advertising Department
Tel.: 0 62 01 - 60 65 65
Fax: 0 62 01 - 60 65 50
E-Mail: MSchulz@wiley-vch.de

Service

Keywords ——— *5554*

Authors ——— *5555*

Angewandte's Sister Journals ——— *5556 – 5557*

Preview ——— *5559*

© 2006 Wiley-VCH Verlag GmbH & Co. KGaA, Weinheim

Molecular Devices

DOI: 10.1002/anie.200601760

Soft Actuators Based on Liquid-Crystalline Elastomers

Yanlei Yu and Tomiki Ikeda**

Keywords:
biophysics · elastomers · liquid crystals · lithography · phase transitions

There is a growing interest in the development of artificial muscle-like actuators, which are ideal for the realization of biomimetic movements as they change their shapes and dimensions when a potential is applied. Polymer actuators play a leading role in this field because they provide such advantages as flexibility, light weight, low costs, and quiet operation compliance.[1] Various materials are under current investigation in this field, such as polymer gels,[1] conjugated polymers,[2] carbon nanotubes,[3] and dielectric elastomers,[4] and various chemical and physical stimuli have been applied to induce the responses of these materials, including pH, solvent composition, temperature, electric field, magnetic field, and light. Among these polymer soft actuation materials, gels and conducting polymers are most promising for applications in the field of biomimetic actuation. However, the low elastic modulus and low yield strength of gels provide important limitations for actuator performance, whereas for battery-like conducting polymers faradaic processes involving solid-state dopant diffusion and structural changes limit the rate, cycle life, and energy conversion efficiencies.

[*] Prof. Dr. T. Ikeda
Chemical Resources Laboratory
Tokyo Institute of Technology
R1-11, 4259 Nagatsuta
Midori-ku, Yokohama 226-8503 (Japan)
Fax: (+81) 45-924-5275
E-mail: tikeda@res.titech.ac.jp
Prof. Dr. Y. Yu
Department of Materials Science
Fudan University
220 Handan Road
Shanghai 200433 (China)
Fax: (+86) 21-5566-4576
E-mail: ylyu@fudan.edu.cn

Recently, there has been a growing focus on the study of soft actuation materials based on liquid-crystalline elastomers (LCEs) as a result of their unique combination of the anisotropic features of liquid crystal (LC) phases and the rubber elasticity of polymer networks. In 1997, de Gennes et al. reported theoretical studies on the possibility of using LCEs as artificial muscles.[5] They proposed that a slight drop in the temperature across the isotropic (I)-to-LC transition is able to cause a strong uniaxial deformation of LCEs at nearly constant volume owing to a change in the LC order. Finkelmann and Kundler later reported that nematic LCE (NLCE) films containing polysiloxanes exhibited a spontaneous contraction along the director axis when heated toward the N-to-I phase-transition temperature (Figure 1).[6a] By synthesizing NLCE films through a hydrosilylation reaction of a monofunctional LC compound and a bifunctional LC polyether with poly(methylhydrogensiloxane), a shape change over 300% was obtained.[6b,c] This thermomechanical effect was also observed in side-on NLCE films and fibers that contained polyacrylate.[7a,b]

de Gennes also proposed the possibility of realizing an artificial muscle or actuator from an I–LC–I triblock copolymer.[5b] Accordingly, Li et al. chose side-on LC polymers to construct an LC domain aligned homogeneously throughout the whole sample and synthesized a side-on triblock elastomer by atom-transfer radical polymerization (ATRP). A thermally induced contraction of the elastomer was observed when the LC block underwent the N-to-I phase transition.[7c] In addition, Yusuf et al. investigated the thermomechanical properties of the LCEs swollen in an anisotropic solvent such as low-molecular-weight liquid crystals (LMWLCs).[8]

Recently, photoinduced contractions of LCEs incorporating azobenzene derivatives was achieved upon their irradiation with UV light.[9] This photomechanical effect was ascribed to the decrease in the order parameter caused by a photochemical reaction (*trans*–*cis* isomerization): the rodlike *trans*-azobenzene moieties stabilize the LC alignment, whereas the bent *cis* forms lower the LC order parameter (Figure 2a). Shortly afterwards, we succeeded in achieving a three-dimensional deformation (photoinduced bending) by using azobenzene-containing NLCE films swollen in suitable solvents or heated above their glass-transition temperatures (T_g) in air.[10] In this case, a contraction in the surface region only caused by the limitation of the absorption of photons contributes to the bending (Figure 2b). Other reports on photoinduced bending of LCEs followed subsequently.[11] These photoresponsive LCE materials are promising for applications as high-speed actuators, as the photochemical phase transition of azobenzene-containing LC polymers can be evoked on a timescale of nanoseconds under optimized conditions.[12] By using their deformations, one can convert light

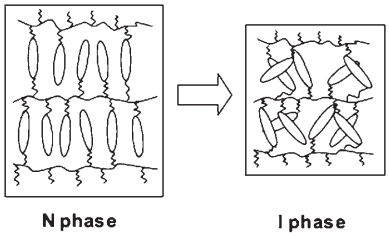


Figure 1. Schematic illustration of the thermally induced contraction in LCEs. N = nematic; I = isotropic.

WILEY InterScience DISCOVER SOMETHING GREAT
© 2006 Wiley-VCH Verlag GmbH & Co. KGaA, Weinheim

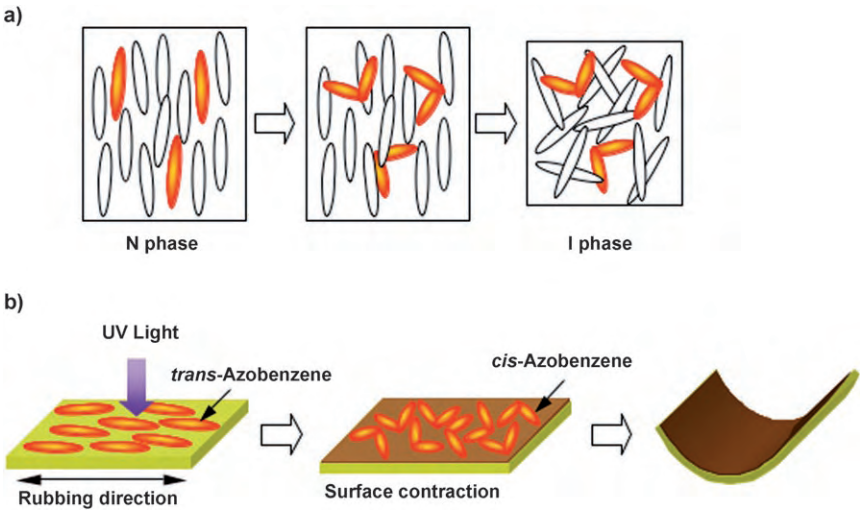


Figure 2. Photomechanical effects of the azobenzene-containing LCEs: a) the photoinduced contraction caused by a photochemical phase transition; b) plausible mechanism of the photoinduced bending behavior.

energy into mechanical power directly. Moreover, as their deformations are driven by light and thus require neither batteries nor controlling devices on the materials themselves, it should be simple to miniaturize the photochemical systems for potential application in driving micromachines and nanomachines.

Another useful property of LCEs is their shape change upon applying electric fields (electromechanical responses) owing to reorientation effects induced by an electric field. Zentel first reported tiny changes of LCEs swollen in LMWLCs under large fields in 1986.[13] Subsequently, Barnes et al. reported a 20% contraction of polydomain elastomers swollen in an isotropic LMWLC.[14] Kishi et al. reported quantitative results on shape changes of swollen polydomain LCEs under a dc electric field ($0.3\ V\,\mu m^{-1}$).[15] Recently, Courty et al. demonstrated a fairly large electromechanical effect in an LCE embedded with carbon nanotubes upon using, however, a large applied field ($1\ V\,\mu m^{-1}$).[16] Yusuf et al. reported measurable shape changes (maximum 13% contraction) in LCEs swollen with an LMWLC under small fields ($0.01–1\ V\,\mu m^{-1}$).[17] Moreover, Zentel et al also investigated electromechanical responses in dry freestanding ferroelectric LCEs[18] and obtained 4% strain in ultrathin films (less than 100-nm thick) at only $1.5\ V\,\mu m^{-1}$.

The studies summarized above fully indicate that LCEs have a high potential to be applied as soft actuators, with such advantages as large deformations and high-speed, two- (contraction) or even three-dimensional (bending) actions. However, all the systems described so far have been macroscopic ones, with sizes in the millimeter/centimeter range. For many applications of stimuli-responsive materials involving LCEs, micro- or nanometer-sized actuators are desirable.

Keller and co-workers recently made an important contribution on creating microsized responsive pillars based on LCE materials by making use of a soft lithography technique called replica molding.[19] Figure 3a illustrates the experimental setup used to prepare the LCE pillars. The soft mold of poly(dimethylsiloxane) with an array of holes 20 μm in diameter and 100 μm in height was first prepared by standard photolithography techniques by using a negative photoresist. Then, the mold was pressed onto the melted monomer mixture, which consisted of a nematic side-on acrylate monomer and a crosslinker. The monomer mixture was slowly cooled to its N phase, and UV-light-induced polymerization was performed under a magnetic field to align the N director parallel to the long axis of

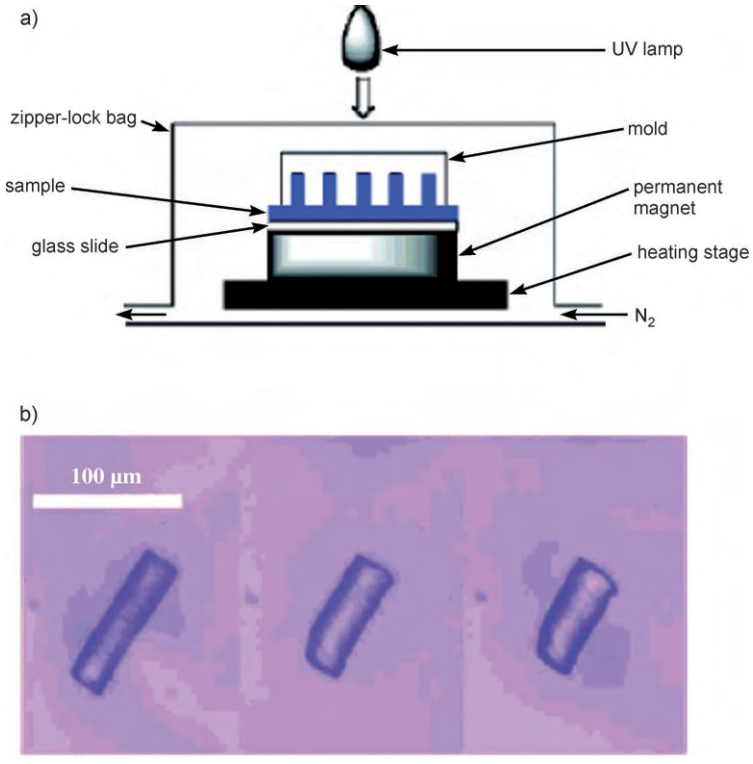


Figure 3. Thermomechanical effects of microsized LCE pillars prepared by a soft lithography technique. a) Experimental setup used to prepare the responsive pillars. b) An isolated pillar (20-μm diameter) heated at various temperatures exhibits 35% contraction along its major axis (from left to right, $T = 100$, 120, and 130 °C).

© 2006 Wiley-VCH Verlag GmbH & Co. KGaA, Weinheim

the pillars. After photopolymerization, the soft mold was peeled off and the side-on LCE pillars were cut off. When heated from an N phase to an I phase, the pillars suspended in silicone oil underwent a contraction on the order of 30–40% (Figure 3b). The contracted pillars could revert to their original size after cooling from the I phase to the N phase. With a decrease in the size of the pillars, this thermal deformation became faster (much less than 1 s) as a result of better thermal exchange with the external medium.

The work described herein summarizes the trend of using LCE materials as muscle-like actuators in response to temperature, light, and electric fields. Particularly, the work by Keller and coworkers constitutes a very important milestone in the field, as they put forward a new concept using a soft lithography technique to prepare micro-sized LCEs. Significant improvements have recently been reported in extreme-UV (EUV) resists.[20] Nested and isolated line resolutions approaching 30 nm and 25 nm, respectively, have been demonstrated. Therefore, we should be able to obtain nanosized LCE actuators with a further endeavor to apply the EUV lithography technique. However, it should be borne in mind that photochemically induced changes in LC orders by incorporating chromophores such as azobenzene into micro- and nanosized LCEs can lead to a faster deformation of the LCEs as compared to thermal deformation.

[1] *Polymer Gels and Networks* (Eds.: Y. Osada, A. R. Khokhlov), Marcel Dekker, New York, **2002**.

[2] a) R. H. Baughman, *Synth. Met.* **1996**, *78*, 339–353; b) E. Smela, *Adv. Mater.* **2003**, *15*, 481–494.

[3] a) R. H. Baughman, C. Cui, A. A. Zakhidov, Z. Iqbal, J. N. Barisci, G. M. Spinks, G. G. Wallace, A. Mazzoldi, D. De Rossi, A. G. Rinzler, O. Jaschinski, S. Roth, M. Kertesz, *Science* **1999**, *284*, 1340–1344; b) Y. Zhang, S. Iijima, *Phys. Rev. Lett.* **1999**, *82*, 3472–3475; c) G. M. Spinks, G. G. Wallace, L. S. Fifield, L. R. Dalton, A. Mazzoldi, D. De Rossi, I. I. Khayrullin, R. H. Baughman, *Adv. Mater.* **2002**, *14*, 1728–1732.

[4] R. Pelrine, R. Kornbluh, Q. Pei, J. Joseph, *Science* **2000**, *287*, 836–839.

[5] a) P.-G. de Gennes, M. Hebert, R. Kant, *Macromol. Symp.* **1997**, *113*, 39–49; b) P.-G. de Gennes, *C. R. Acad. Sci. Ser. IIb* **1997**, *324*, 343.

[6] a) I. Kundler, H. Finkelmann, *Macromol. Chem. Phys.* **1998**, *199*, 677–686; b) S. M. Clarke, A. Hotta, A. R. Tajbakhsh, E. M. Terentjev, *Phys. Rev. E* **2001**, *64*, 061702; c) A. R. Tajbakhsh, E. M. Terentjev, *Eur. Phys. J. E* **2001**, *6*, 181–188.

[7] a) D. L. Thomsen III, P. Keller, J. Naciri, R. Pink, H. Jeon, D. Shenoy, B. R. Ratna, *Macromolecules* **2001**, *34*, 5868–5875; b) J. Naciri, A. Srinivasan, H. Jeon, N. Nikolov, P. Keller, B. R. Ratna, *Macromolecules* **2003**, *36*, 8499–8505; c) M.-H. Li, P. Keller, J. Yang, P.-A. Albouy, *Adv. Mater.* **2004**, *16*, 1922–1925.

[8] a) Y. Yusuf, Y. Sumisaki, S. Kai, *Chem. Phys. Lett.* **2003**, *382*, 198–202; b) Y. Yusuf, Y. Ono, Y. Sumisaki, P. E. Cladis, H. R. Brand, H. Finkelmann, S. Kai, *Phys. Rev. E* **2004**, *69*, 021710; c) Y. Yusuf, P. E. Cladis, H. R. Brand, H. Finkelmann, S. Kai, *Chem. Phys. Lett.* **2004**, *389*, 443–448.

[9] a) H. Finkelmann, E. Nishikawa, G. G. Pereira, M. Warner, *Phys. Rev. Lett.* **2001**, *87*, 015501; b) P. M. Hogan, A. R. Tajbakhsh, E. M. Terentjev, *Phys. Rev. E* **2002**, *65*, 041720; c) J. Cviklinski, A. R. Tajbakhsh, E. M. Terentjev, *Eur. Phys. J. E* **2002**, *9*, 427–434; d) M. Warner, E. Terentjev, *Macromol. Symp.* **2003**, *200*, 81–92; e) M.-H. Li, P. Keller, B. Li, X. Wang, M. Brunet, *Adv. Mater.* **2003**, *15*, 569–572.

[10] a) T. Ikeda, M. Nakano, Y. Yu, O. Tsutsumi, A. Kanazawa, *Adv. Mater.* **2003**, *15*, 201–205; b) Y. Yu, M. Nakano, T. Ikeda, *Nature* **2003**, *425*, 145; c) Y. Yu, M. Nakano, A. Shishido, T. Shiono, T. Ikeda, *Chem. Mater.* **2004**, *16*, 1637–1643; d) Y. Yu, M. Nakano, T. Ikeda, *Pure Appl. Chem.* **2004**, *76*, 1435–1445; e) M. Kondo, Y. Yu, T. Ikeda, *Angew. Chem.* **2006**, *118*, 1406–1410; *Angew. Chem. Int. Ed.* **2006**, *45*, 1378–1382.

[11] a) M. Camacho-Lopez, H. Finkelmann, P. Palffy-Muhoray, M. Shelley, *Nat. Mater.* **2004**, *3*, 307–310; b) K. D. Harris, R. Cuypers, P. Scheibe, C. L. van Oosten, C. W. M. Bastiaansen, J. Lub, D. J. Broer, *J. Mater. Chem.* **2005**, *15*, 5043–5048; c) N. Tabiryan, S. Serak, X. M. Dai, T. Bunning, *Opt. Express* **2005**, *13*, 7442–7448.

[12] a) T. Ikeda, *J. Mater. Chem.* **2003**, *13*, 2037–2057; b) T. Ikeda, O. Tsutsumi, *Science* **1995**, *268*, 1873–1875.

[13] R. Zentel, *Liq. Cryst.* **1986**, *1*, 589–592.

[14] N. R. Barnes, F. J. Davis, G. R. Mitchell, *Mol. Cryst. Liq. Cryst.* **1989**, *168*, 13–25.

[15] R. Kishi, Y. Suzuki, H. Ichijo, O. Hirasa, *Chem. Lett.* **1994**, 2257–2260.

[16] S. Courty, J. Mine, A. R. Tajbakhsh, E. M. Terentjev, *Europhys. Lett.* **2003**, *64*, 654–660.

[17] Y. Yusuf, J.-H. Huh, P. E. Cladis, H. R. Brand, H. Finkelmann, S. Kai, *Phys. Rev. E* **2005**, *71*, 061702.

[18] W. Lehmann, H. Skupin, C. Tolksdorf, E. Gebhard, R. Zentel, P. Kruger, M. Losche, F. Kremer, *Nature* **2001**, *410*, 447–450.

[19] A. Buguin, M.-H. Li, P. Silberzan, B. Ladoux, P. Keller, *J. Am. Chem. Soc.* **2006**, *128*, 1088–1089.

[20] P. P. Naulleau, C. Rammeloo, J. P. Cain, K. Dean, P. Denham, K. A. Goldberg, B. Hoef, B. La Fontaine, A. R. Pawloski, C. Larson, G. Wallraff, *Proc. SPIE-Int. Soc. Opt. Eng.* **2006**, *6151*, 61510Y.

 © 2006 Wiley-VCH Verlag GmbH & Co. KGaA, Weinheim

DOI: 10.1002/anie.200600060

Microscopic Machines

Chemical Locomotion

*Walter F. Paxton, Shakuntala Sundararajan, Thomas E. Mallouk, and Ayusman Sen**

Keywords:
autonomous motion · heterogeneous catalysis · micromotors · molecular devices · nanotechnology

Research into the autonomous motion of artificial nano- and microscale objects provides basic principles to explore possible applications, such as self-assembly of superstructures, roving sensors, and drug delivery. Although the systems described have unique propulsion mechanisms, motility in each case is made possible by the conversion of locally available chemical energy into mechanical energy. The use of catalysts onboard can afford nondissipative systems that are capable of directed motion. Key to the design of nano- and micromotors is the asymmetric placement of the catalyst: its placement in an environment containing a suitable substrate translates into non-uniform consumption of the substrate and distribution of reaction products, which results in the motility of the object. These same principles are exploited in nature to effect autonomous motion.

1. Introduction

Locomotion in macroscale objects is easily achieved by using engines that consume chemical fuel. Directed motion of micro- and nanoscale objects is desirable for many applications, such as self-assembly of superstructures, roving sensors, drug-delivery systems, and useful nanomachinery. The challenge here is to impart energy to an individual object to bring about its autonomous motion. Once this goal is achieved, more complex tasks for application-oriented nano- and micromotors can be envisioned. Conventional approaches to transport and manipulate matter on the small scale use optical trapping methods to address individual or small groups of objects, and external fields that act on an ensemble of small objects. Biomotors and motile bacteria, on the other hand, are able to propel themselves autonomously, independent of external fields and of one another, by harnessing the chemical potential energy available in their environment to produce directed mechanical forces.[1] Several methods of imparting motion to small objects by using localized physical interactions and chemical reactions have been demonstrated in recent years. This Minireview highlights some of these recent developments and discusses the principles and implications of transducing chemical to mechanical energy on the micrometer scale.

[*] W. F. Paxton, S. Sundararajan, Prof. Dr. T. E. Mallouk, Prof. Dr. A. Sen
Department of Chemistry
The Pennsylvania State University
University Park, PA 16802 (USA)
Fax: (+1) 814-865-1543
E-mail: asen@chem.psu.edu

2. Background

In practice, a variety of external fields have been used for colloidal transport in fluids, such as electrophoresis[2] and magnetophoresis[3] for directing the motion of charged and magnetic particles, respectively. Lesser-known modes such as thermophoresis[4] (migration due to a temperature gradient) and diffusiophoresis[5] (migration due to a concentration gradient) have also been used to achieve colloidal transport. The interactions between these externally applied fields and solid–fluid interfaces were discussed by Anderson.[6] While external fields have been used to sort and separate particles based on their response, this type of transport does not afford the flexibility of moving objects independently. In a fundamentally different alternative, optical tweezers have also been used to manipulate colloidal particles with up to nanometer-scale precision using light gradients.[7] However, optical trapping methods require that particles be moved individually or in small groups.[8]

To achieve independent autonomous motion for objects in a given ensemble would require each entity to generate its own field or motive force. For this to occur, each object must convert chemical energy into mechanical energy. Such an

InterScience
© 2006 Wiley-VCH Verlag GmbH & Co. KGaA, Weinheim

object is in essence a chemical locomotor; it harnesses the chemical free energy of locally available reagents in its environment and translates it into motion. However, the relevant laws that govern the motion of small-scale objects are, in practice, different from those encountered in macroscopic processes.[9] The motion of micrometer- and submicrometer-sized objects is dominated by viscous rather than inertial forces (i.e., low Reynolds number).[10,11] Consequently, fluid flow profiles on the microscale are laminar rather than turbulent and viscous drag effectively eliminates any momentum-based "coasting" of a micro- or nanoobject in motion. Moreover, a dramatic increase in surface-to-volume ratios for smaller objects favors surface forces, such as those related to interfacial tension, over body forces.[9,12] Another effect that further complicates the motion of small objects suspended in fluids is the effect of molecule–particle collisions arising from thermal diffusion.[13] Because the thermal diffusion of a small object is inversely proportional to its dimensions, to overcome the effects of Brownian motion becomes a significant challenge as the size of the moving object is scaled down.

Research in chemical locomotion and the related scaling effects is important not only for designing application-oriented nano- and micromotors but also for understanding the interfacial phenomena related to colloidal transport. Synthetic motors may also be used as simplified mimics to probe unanswered questions pertaining to locomotion in natural systems. A case in point is the motile *Synechococcous* cyanobacteria found in a marine environment.[14] Unlike most other motile microorganisms they do not have typical motility-imparting appendages like the flagella or cilia, and the basis of propulsion in these marine bacteria is not yet fully understood. Besides cell motility, there are questions relating to mechanisms of chemotaxis in certain microorganisms whose sensitivity makes them difficult to test. Artificial systems could also be used to study this problem as they can be engineered to be more robust than their natural counterparts and may be subjected to harsher conditions.

3. Biomotors

To aid us in designing chemical locomotors, we can take a cue from naturally occurring motors. A few notable examples are the motor proteins: kinesins, myosins, and dyneins.[15] These linear nanoscale motors move along complementary tracks and perform a variety of functions such as cytokinesis, signal transduction, intracellular trafficking, and locomotion of cellular components. These biomotors have mechanisms in place to convert chemical energy into the desired mechanical output. While each of these biomotors performs a different function, they share a few common features: they hydrolyze adenosine triphosphate (ATP), which is available in the local environment, to obtain energy, their motion is cyclic and reversible, and they operate with high efficiencies that are not commonly encountered in artificial systems.

Natural systems exhibit asymmetry in their design which allows the locally available energy to be expended non-uniformly, resulting in directed mechanical forces. This feature of asymmetrical configuration is evident from the motility of the bacteria *Listeria monocytogenes*, a pathogen that propels itself by polymerizing actin in the host cell.[16] The



Walter F. Paxton received an AAS degree from Ricks College in Rexburg (now Brigham Young University (BYU-Idaho)) in 1998 and graduated from BYU with a BS in Chemistry in 2001. His research interests initially involved exploring the copper-based polymerization of acrylates, and he later became interested in catalytic motors and electrokinetic phenomena. He recently received the American Chemical Society Inorganic Chemistry Young Investigator Award in Nanoscience for his work on catalytic nanomotors.



Thomas E. Mallouk completed his PhD at the University of California, Berkeley. Following a postdoctoral stay at MIT, he joined the University of Texas at Austin in 1985. In 1993 he joined Pennsylvania State University, where he is now DuPont Professor of Materials Chemistry and Physics. His research interests have spanned inorganic self-assembly and the chemistry of porous, lamellar, and nanoscale materials. He is Director of the Penn State MRSEC Center for Nanoscale Science.



Shakuntala Sundararajan was born in Madras, India. She received her MSc in Chemistry from the Indian Institute of Technology in Madras. She is currently working towards her PhD under the guidance of Prof. Ayusman Sen at Pennsylvania State University. Her research interests include investigations of the mechanism of motility in metallic nanorods and the development of applications thereof.



Ayusman Sen was born in Calcutta, India, and completed his PhD at the University of Chicago, where he was first introduced to catalysis. Following a postdoctoral stay at the California Institute of Technology, he joined Pennsylvania State University, where is currently Head of the Chemistry Department. His honors include an Alfred P. Sloan Fellowship and the Paul J. Flory award from IBM, and he is a Fellow of the American Association for the Advancement of Science. His research interests encompass catalysis, organometallic and polymer chemistry, and nanotechnology.

© 2006 Wiley-VCH Verlag GmbH & Co. KGaA, Weinheim

bacterial protein ActA, which catalyzes the polymerization of actin (a protein found in abundance in eukaryotic cells) into polar filaments, is concentrated on one end—the tail—of the cell. The motility-imparting process occurs in a treadmill fashion: polymerization begins at the tail, while ATP-assisted depolymerization occurs at the other end of the polymer filament. Although the polymerization of actin is believed to play a role in cell deformation and motility in a number of eukaryotic systems, the finding that a single bacterial protein ActA was responsible for motility in *Listeria* provided a simple system to investigate the mechanism.[17] Theriot and co-workers demonstrated that this ActA polymerization enzyme can be used to move nonbiological objects up to 2 μm long (polystyrene beads) by functionalizing them asymmetrically with the ActA polymerization enzyme and releasing them in an actin-rich environment.[18]

The efficiency and the myriad functions carried out by biomotors make them ideal models for artificial nanomotors. However, this versatility is based on an increase in structural complexity. Rather than trying to design artificial biomotors, efforts have been made to transpose these in vivo motors to favorable in vitro conditions. Hybrids of biomotors and nano- or microscale inorganic components have been fabricated, thus illustrating that biomotors can function outside their natural environment. For example, the kinesin–microtubule system has been used outside biological systems to transport inorganic components, such as gold nanowires, over immobilized microtubule tracks.[19,20] This configuration has been inverted to transport microtubule filaments functionalized with magnetic nanoparticles over an array of surface-immobilized kinesins.[21]

Another hybrid system was demonstrated by Montemagno and co-workers in which the enzyme ATPase was used to drive the rotation of submicrometer-sized nickel rods in the presence of ATP fuel solution for a few hours (Figure 1).[22]

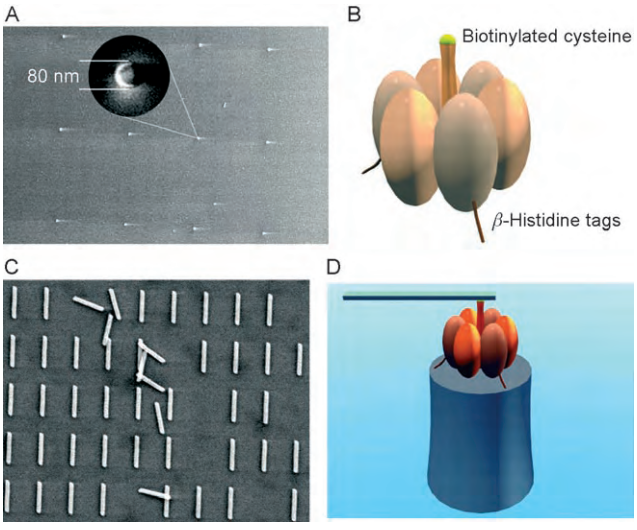


Figure 1. A nanomechanical device (D) powered by an F1-ATPase biomolecular motor and consisting of a Ni post (A; height 200 nm, diameter 80 nm), the F1-ATPase biomolecular motor (B), and a nanopropeller (C; length 750–1400 nm, diameter 150 nm). From Ref. [22].

However, the fraction of functional structures was low as a result of the difficulty in forming ATPase–Ni propeller units that were not pinned down to the underlying substrate. Related approaches have been aimed at fabricating hybrid devices that exploit motile bacteria to drive microscale devices or deliver cargo. Mirkin, Holz, and co-workers demonstrated that surface bound *E. coli* cells exhibit motility and remain live for up to four hours.[23] The feasibility of operating a microbe-powered micromotor based on this method remains to be tested. The precise placement of the bacteria and the prolonged operation of such a device are some of the challenges to this approach. Whitesides and co-workers described another hybrid approach, in which polystyrene beads were attached to photosynthetic unicellular algae (*Chlamydomonas reinhardtii*). They showed that motile microorganisms can be used to move microscale loads.[24]

The problems encountered by Montemagno and others in developing hybrid systems illustrate the intricacies involved in transposing biological motors outside their natural environment, as it is not trivial to mimic in vivo conditions. Even more arduous is replicating biomotors themselves owing to their structural complexity. Besides structural and functional differences, two major themes underlying the operation of biomotors are asymmetry in design and the ability to exploit the supply of locally available high-energy molecules for the transduction of chemical to mechanical energy. Incorporating these ideas of asymmetry and exploiting chemical energy from the environment are keys to the development of autonomously operating synthetic motors.

4. Dissipative Systems

There are a few examples of autonomous motion in chemical systems. The systems discussed in this section involve the lowering of surface free energy due to the interaction between a mobile object and its surrounding medium. A notable example is the selective migration of tin islands on a copper surface.[25] Upon studying the surface alloying of copper–tin at high vacuum, the authors noted that the tin, soon after evaporation on a copper(111) surface, formed islands. Real-time tracking of these tin islands (0.6-μm diameter) using low-energy electron microscopy (LEEM) showed that they migrate selectively over unalloyed copper surfaces to leave behind static bronze features (Figure 2). This selectivity was attributed to the repulsive interaction between moving tin islands and static bronze incorporated on the copper surface.

Another example is that of the spontaneous motion of asymmetric mercury drops when placed in a solution of potassium dichromate and nitric acid.[26] The combination of reactants forms a mercurous chromate product that lowers the surface tension of the reacting mercury surface. Subsequent contact with nitric acid cleanses the surface and exposes fresh mercury for reaction with dichromate. Once set into motion by some spontaneous perturbation of the system, the front of the crescent-shaped drop is constantly exposed to fresh solution while the rear is surrounded by a product-rich environment, thereby maintaining the difference in surface

© 2006 Wiley-VCH Verlag GmbH & Co. KGaA, Weinheim

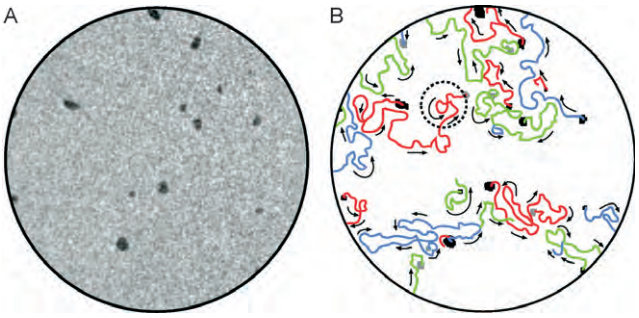


Figure 2. LEEM images (1.5-mm across) of mobile 2D islands on Cu(111). A) Sn islands (dark) formed during Sn deposition on a clean Cu(111) surface (bright background) at 290 K. B) Trajectory plot of migrating Sn islands, demonstrating their tendency to avoid crossing paths. From Ref. [25].

tension between the leading and trailing sides of the moving mercury drop.

Physical processes such as dissolution have also been used to bring about autonomous motion. The motion of camphor solids on a water surface is a well-known example. The dissolution of a scraping of camphor lowers the surface tension of the air–water interface, causing the dissolving "camphor boat" to be propelled over the water surface. An increasing complexity in motion (clockwise, anticlockwise, and unidirectional) has been demonstrated by changing the shape of the piece of camphor.[27] Amphiphilic polymer gels such as poly(*n*-stearyl acrylate) behaved in a similar fashion when they were swollen in tetrahydrofuran and placed on a water surface.[28] As with the case of the dissolving camphor, the swelling solvent has a lower surface tension than water and its spreading at the interface leads to motion of the gel. The hydrophobic alkyl chains of the gel impart to the surface permselective properties, whereby an organic solvent from inside the gel can be ejected whereas water from outside cannot penetrate the gel. The surface of the gel released the swelling solvent and was rendered crystalline soon after it came into contact with water, while the interior responded more slowly. This process set up an osmotic as well as a hydrostatic pressure across the crystalline, permselective skin that allowed a gradual ejection of the organic solvent and resulted in prolonged motion of the gel (Figure 3). When the asymmetry in solvent release was accentuated by covering all but the rear end of the gel, a more directed and prolonged motion was observed.

The above examples of locomotion rely on some chemical or physical process that affects the surface tension at an interface. In the simplest and most general sense, the velocity, v, of the moving objects can be described as a roughly linear function of the interfacial tension gradient ($\nabla\gamma$), such that $v = k\nabla\gamma$, in which k includes geometric parameters and physical properties such as viscosity. Once set into motion, these moving objects are positioned asymmetrically to one side of the interfacial tension gradients responsible for their motion. Because the objects themselves are also the source of these propulsive gradients, these gradients are continually reestablished as the objects move.

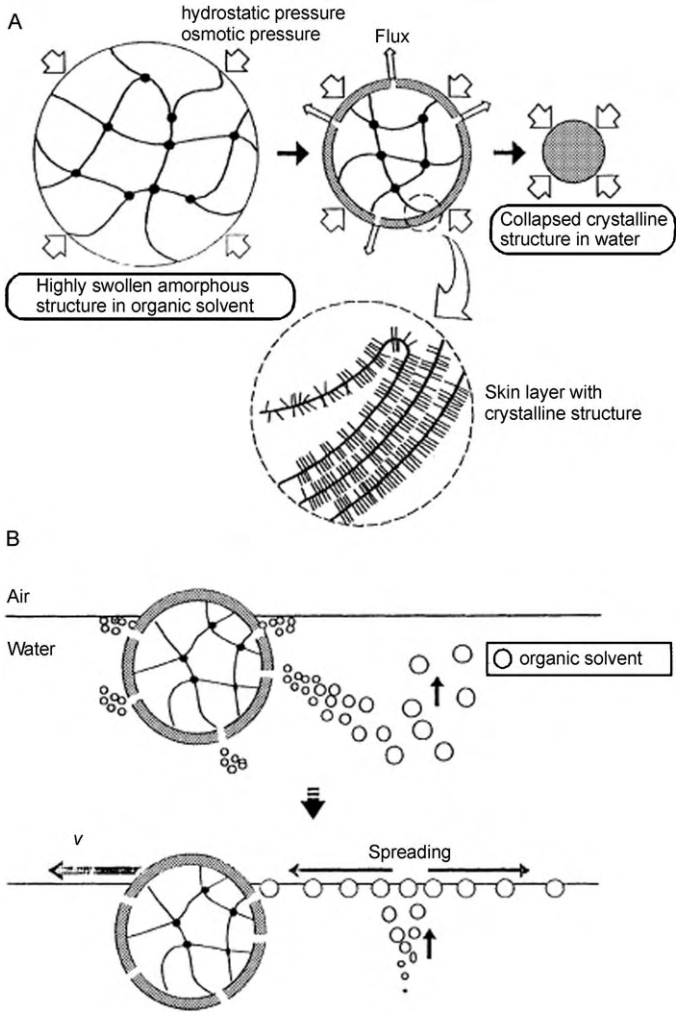


Figure 3. A) Schematic of a solvent-swollen amphiphilic polymer gel. B) The mechanism for its motion due to solvent spreading at the air–water interface. From Ref. [28].

5. Catalytic Systems

Though the synthetic systems described in Section 4 are characterized by simplicity in design, they are all dissipative and hence limited in applicability. Designing application-oriented chemical locomotors requires incorporation of the lessons learned from natural as well as artificial systems, while bearing in mind the limitations presented by the synthetic components used to make them. Many natural systems localize enzymes that act on reagents available in the vicinity, as with the *Listeria* example described in Section 3. From a chemist's perspective, this translates to placement of a catalyst engine on the body of the object where neither engine nor body is consumed when placed in an environment containing the catalyst substrate. The asymmetry in particle design translates into asymmetry in the distribution of reaction products when placed in a suitable "fuel" solution. This use of catalysis and asymmetry would be the most simple and feasible way to power a nanomotor. As discussed in this section, the localized reactions that occur at catalytic sites can

 © 2006 Wiley-VCH Verlag GmbH & Co. KGaA, Weinheim

provide motility through a number of mechanisms, including bubble propulsion, diffusiophoresis, interfacial tension gradients, self-electrophoresis, bioelectrochemical propulsion, and cyclic adsorption/desorption.

5.1. Bubble Propulsion

To our knowledge, Whitesides and co-workers were the first to devise an artificial engine based on a catalyst to move an otherwise inanimate object.[29] The key to their design was the asymmetric placement of platinum on millimeter-sized polydimethylsiloxane (PDMS) structures (Figure 4). When

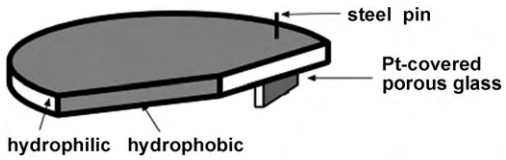


Figure 4. Schematic of a self-propelling object consisting of a PDMS plate (ca. 1–2-mm thick and 9-mm diameter) and a $2\times2\,mm^2$ piece of porous glass filter (covered with platinum by electron beam evaporation) mounted on the PDMS piece with a stainless steel pin. From Ref. [29].

placed in a solution of hydrogen peroxide, the platinum-catalyzed decomposition of hydrogen peroxide to water and oxygen gas led to a jet of bubbles which propelled the objects at the liquid–air interface. This spontaneous motion facilitated the study of self-assembly phenomena by increasing the rate of collisions between objects with both hydrophobic and hydrophilic regions. Close approach of structures resulted in an attractive force arising from the decrease in the total area of the water–air interface, but the force driving the motion of the objects was provided by the catalytic reaction.

Feringa and co-workers described a similar system, which involved the decomposition of hydrogen peroxide by using a manganese-based catalase mimic, rather than platinum, to propel asymmetric silica particles (80-μm diameter).[30] The catalyst was bound to the entire surface of the aminopropyl-modified silica particles by imine linkages. The translational motion of these particles when placed in a solution of hydrogen peroxide was related to the expansion of oxygen bubbles that nucleated on their surface. Although the motor design did not involve localized placement of the catalyst, motility in this case was facilitated by the inhomogeneous distribution of bubble nucleation sites on the asymmetric particle.

5.2. Diffusiophoresis

Besides the generation of bubbles of a gaseous reaction product, such as oxygen, gradients of soluble or nongaseous reaction products themselves are known to induce motion of colloidal particles in solution. In this process of diffusiophoresis, the speed and direction of motion depend on the interaction between the particle surface and the solute, as well as on the magnitude of the solute gradient. A closely related phenomenon is the osmophoresis of a semipermeable vesicle through an osmotic pressure gradient in the surrounding fluid that causes the particle to move to regions of decreasing solute concentration.[31] Both diffusiophoresis and osmophoresis result in fluid transport as a result of concentration gradients of solute and cause motion of particles exposed to such gradients. Although these effects have been described theoretically[6] and demonstrated practically[5] by considering only externally imposed concentration fields, it was proposed by Ajdari and co-workers that this same phenomenon should be observed when the objects themselves are the source of the chemical gradients (Figure 5).[32] This process would occur, for example, if a particle with a catalyst on one side causes an asymmetric distribution of reaction products around the particle.

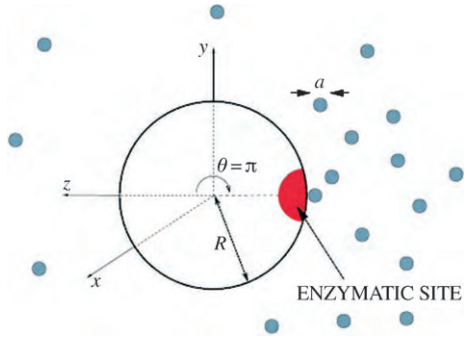


Figure 5. A spherical particle with a spatially defined reaction site. The generation and diffusion of products from this site results in an asymmetric distribution of reaction products around the particle. From Ref. [32].

5.3. Interfacial Tension Gradients

Colloidal particles with catalytic asymmetry can be electrochemically fabricated and indeed exhibit motion when placed in a solution containing a fuel. Prior to the proposal made by Ajdari and co-workers, Paxton et al. reported the autonomous motion of platinum–gold nanorods in aqueous hydrogen peroxide solutions.[33] The rods, with a diameter of 370 nm, consisted of platinum and gold segments, each 1-μm long, and moved at linear speeds of up to 20 $\mu m\,s^{-1}$ (Figure 6). The axial velocity of the rods was related to the rate of the decomposition of hydrogen peroxide, with the rods moving slower in solutions with a lower concentration of hydrogen peroxide. More recently, Fisher et al. have examined the

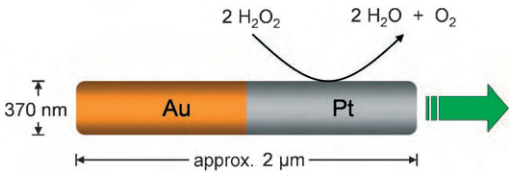


Figure 6. Schematic of an asymmetric Pt–Au nanorod driven by the catalytic decomposition of hydrogen peroxide. From Ref. [33].

© 2006 Wiley-VCH Verlag GmbH & Co. KGaA, Weinheim

motion of these rods at water–organic interfaces to probe the effect of viscosity on rod velocity.[34] Ozin, Manners, and coworkers also reported a similar phenomenon using nickel–gold nanorods, emphasizing the rotational motion imparted to the "nanorotors" induced by the decomposition of hydrogen peroxide.[35]

Rotors of another kind were fabricated lithographically by Catchmark et al.[36] Gold sprockets with a diameter of approximately 150 μm were decorated with platinum on one side of each tooth (Figure 7) to impart catalytic asymmetry to

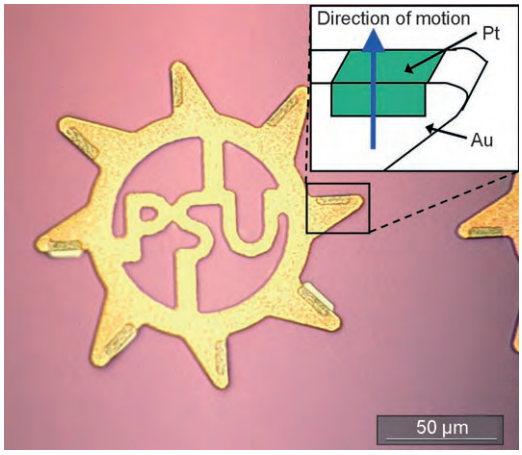


Figure 7. Photograph of a gold gearlike structure with platinum deposited on the tooth regions. The arrow in the inset shows the region where the interfacial tension gradient is formed. From Ref. [39].

the structure and resulted in rotary motion. The linear speed at the circumference of the rotors was 390 $\mu m\,s^{-1}$. Interestingly, the motion of the objects is *towards* the region of high concentration of product (oxygen), rather than away from it, unlike the larger structures described by the groups of Whitesides[29] and Feringa.[30]

In addition to controlling the motion of the systems driven by hydrogen peroxide by geometric design of moving structures, motion may also be controlled magnetically. Kline et al. demonstrated that nanorods, which contain magnetic segments, powered by hydrogen peroxide could be aligned when an external magnetic field is applied.[37] Nickel segments with a length shorter than the segment radius were used to ensure the easy axis of magnetization was orthogonal to the direction of motion (Figure 8). This setup allowed them to show that the motion of the rods was propelled by the decomposition of hydrogen peroxide (and not by attraction to the magnet) and that their direction could be remotely controlled by using relatively weak magnetic fields. This motion is analogous to the behavior of motile bacteria that align themselves with the weak magnetic field of the Earth; in fact, these magnetotactic bacteria have magnetic moments on the same order as that of the nickel-containing rods ($10^{-15}\,A\,m^2$).[38]

Bubbles were generally not observed near the moving objects in any of these examples, demonstrating that bubble propulsion is not responsible for the observed motion and

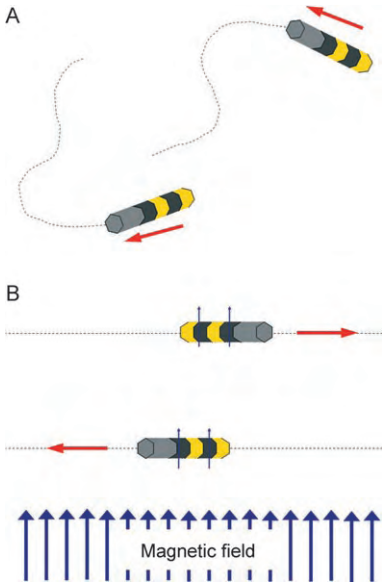


Figure 8. The movement of Pt-Ni-Au-Ni-Au rods in aqueous H_2O_2 without a magnetic field applied (A) and with an applied field (B). Note that rods align perpendicular to the applied magnetic field which results in rod motion about 90 degrees to the applied field. From Ref. [37].

indicating a different propulsion mechanism from that observed by Whitesides[29] and later by Feringa.[30] The motion of these rods was initially attributed to the oxygen concentration gradient emanating from the catalytically active platinum surfaces. Although this process seems a good candidate for a diffusiophoretic mechanism, recent calculations indicated that diffusiophoretic contributions to the motion of these particles would be too small to be the primary driving force and predicted motion in the wrong direction.[39] Instead, it was suggested that the oxygen concentration gradient resulted in an asymmetric interfacial tension gradient around the Pt–Au nanorod that induced a slip velocity at the particle–fluid interface. By solving the convection–diffusion equation to describe the oxygen concentration gradient and by considering the geometric parameters of the nanorods and the surface tension of the bulk solution, the velocity of the Pt–Au nanorods in hydrogen peroxide solutions was reduced to the relationship given in Equation (1), in which S is the surface-normalized oxygen evolu-

$$v \propto \frac{SR^2\gamma}{\eta DL} \qquad (1)$$

tion rate, γ is the surface tension of the bulk solution, D is the rate of diffusion of oxygen away from the rod, and R and L are the geometric radius and length of the nanorods, respectively.

The observed linear relationship between the speed of Pt–Au rods in hydrogen peroxide solutions and the product of the rate of oxygen evolution and surface tension of the bulk solution seemed to confirm this relationship.[33] However, it did not necessarily exclude the possibility of a self-electrophoretic or some other unknown mechanism.

 © 2006 Wiley-VCH Verlag GmbH & Co. KGaA, Weinheim

5.4. Self-Electrophoresis

Self-electrophoresis is the migration of a particle in an electric field that is generated by the particle itself, an idea that was first suggested by Mitchell as a mode of transport for microorganisms.[40] Lammert et al. explored the possibility that a cell with an uneven distribution of ion channels on its surface could self-generate an electric field to propel itself through solution.[41] It was shown that the ability of an object to exhibit self-electrophoresis is directly related to its electrophoretic mobility [Eq. (2)]; v is the velocity of the object

$$v = -\mu E_o \tag{2}$$

undergoing self-electrophoresis, μ is the electrophoretic mobility, and E_o is the magnitude of the self-generated electric field parallel to the cell membrane.

This relationship in fact proved to be useful in ruling out self-electrophoresis as a mechanism for the motility of *Synechococcus* cyanobacteria because these marine bacteria failed to exhibit mobility in their natural environment in the presence of an externally applied field.[42] The motility mechanism of these bacteria is still currently under investigation.[43]

Paxton et al. presented a theoretical analysis for a micrometer-sized conducting particle that produces an electric field as a result of redox chemistry occurring at its two ends.[39] One end of the particle carries out oxidation of species A, which sets up an electron flow to the other end of the particle where reduction of species B occurs. Simultaneously, protons are produced at one end and consumed at the other. As these protons migrate, they drag the fluid with them to cause an observable slip velocity, which propels the particle in the opposite direction (Figure 9). It is evident that the speed of

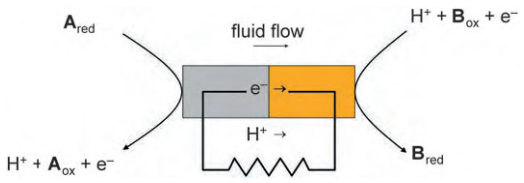


Figure 9. A particle capable of generating its own electric field due to bipolar catalysis. Protons generated when **A** is oxidized on one end migrate along the particle–solution interface and are consumed at the opposite end when **B** is reduced. The ensuing ion flux results in a particle slip velocity relative to the surrounding fluid at the particle–fluid interface. From Ref. [39].

the particle would be dependent not only on the magnitude of the current generated in the particle due to the reaction but also on the conductivity of the surrounding fluid. The Hückel equation was used to demonstrate that an ion current density on the order of 5×10^{-4} mA cm^{-2} would suffice to propel a metallic particle with a zeta potential of -40 mV (conductivity: 10^5 S m^{-1}) at 10 μm s^{-1} in an aqueous medium (conductivity: 10^{-5} S m^{-1}). This current density, J, can be related to the rate of a redox reaction involving n electrons according to the Equation (3), where A is the cross-sectional area of current

$$rate = \frac{JA}{nF} \tag{3}$$

flux and F is Faraday's constant.

5.5. Catalytic Fluid Pumping

An interesting aspect of the work involving hydrogen peroxide and metallic structures relates to immobilization of the catalyst onto a fixed surface. While freely suspended metal nanorods move with respect to the bulk solution, by Galilean invariance an immobilized metal structure in the presence of hydrogen peroxide will induce fluid flows at the interface between the structure and the fluid. Kline et al. demonstrated this fluid-pumping effect on a gold surface patterned with silver—another known catalyst for the decomposition of hydrogen peroxide.[44] When aqueous hydrogen peroxide solution which contained colloidal tracer particles was deposited onto these bimetallic surfaces, the tracers either followed a convection-type fluid flow towards the micrometer-sized silver surface or formed patterns as they were pushed away from the catalyst, depending on the zeta potential of the tracer (Figure 10).

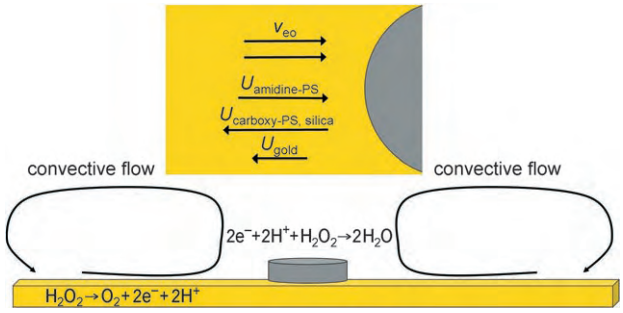


Figure 10. Catalytic fluid pumping on a silver–gold surface. Particles migrate inwards or outwards depending on the zeta potential relative to the zeta potential of the gold substrate. Particles migrating towards the silver catalyst follow electroosmotic convection near the catalyst surface. From Ref. [44].

As in the case of the moving platinum–gold nanorods, the silver catalyst was always in direct electrical contact with the gold. However, when an insulating layer was incorporated between the gold surface and the silver feature, both the convection-driven motion and the pattern formation of the tracers were effectively turned off. The absence of the catalytically driven effect when an insulator separates the two metals is strongly suggestive of an electrokinetic fluid-pumping mechanism resulting from bipolar electrochemistry. It was described that the electric field arises from the silver-catalyzed reduction of hydrogen peroxide and oxidation of hydrogen peroxide on the gold surface, which induces an

© 2006 Wiley-VCH Verlag GmbH & Co. KGaA, Weinheim

electroosmotic flow directed *towards* the silver features. Although particles near the surface–liquid interface are swept inward by this electroosmotic flow, individual particles also experience an electrophoretic force as a result of the catalytically generated electric field, and the direction of this force depends on the zeta potential of the particle. The observed velocity of tracer particles is the sum of the electroosmotic and electrophoretic velocities.

5.6. Bioelectrochemical Propulsion

Bipolar catalysis has also been used to propel the motion of millimeter-scale objects. Mano and Heller described a system based on carbon fibers that exploits two redox-coupled enzymes to induce autonomous motion.[45] An asymmetrically functionalized carbon fiber (0.5–1-cm long; 7-μm wide) was fabricated with one of the ends containing the oxygen-reducing enzyme bilirubin oxidase (BOD) and the other end incorporating glucose oxidase (GOx), which catalyzes the oxidation of glucose to δ-glucono-1,5-lactone. Both enzymes were linked to the carbon fiber using redox polymer bridges to enable efficient electron transport between the enzymes and the conducting fiber (Figure 11). When the fibers were placed at the interface between air and a solution of glucose, they moved in a linear path, with the GOx end forward. This motion was attributed to the difference in surface tension between the two ends caused by the proton flux from anode to cathode. Protons, which are produced in the bipolar oxidation of glucose, are generated at the GOx end and consumed at the BOD end, where cathodic reduction of oxygen takes place to give water. It was proposed that this proton concentration gradient results in surface tension instability and, hence, propulsion of the fiber occurs. To support this hypothesis, they placed an insulating segment between the anode and cathode to prevent the electrochemical reaction and observed no propulsion. Another important observation was that only those fibers at the air–water interface showed mobility. Fibers that were completely immersed in water were immobile, possibly because of the low solubility of oxygen in water.

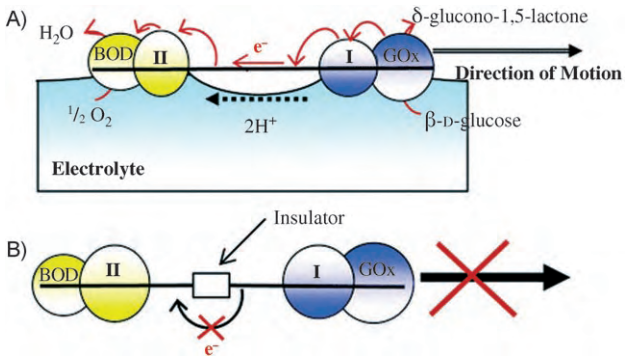


Figure 11. A) A self-propelled bioelectrochemical motor consisting of a carbon fiber functionalized with glucose oxidase (GOx) and redox polymer **I** on one end, and bilirubin oxidase (BOD) and redox polymer **II** on the opposite end. When the fiber is placed on a solution of 10 mM glucose in pH 7 buffer, electrons flow along the path glucose→GOx→**I**→carbon fiber→**II**→BOD→O_2, and the fiber is propelled at the solution–O_2 interface by the ion flow accompanying the flow of electrons. B) The fiber does not move when an insulator is introduced between the two electrocatalytic fiber ends. From Ref. [45].

5.7. Microcantilever-Based Motors

While the examples discussed in this Minireview focus primarily on the motility of unbound objects, transduction of chemical energy to mechanical energy has been achieved in systems such as microcantilevers that are fixed at one end. Microcantilevers find application in the field of sensing, where detection of specific analytes is facilitated by their interaction with a suitably functionalized cantilever.[46] Various modes of signal transduction, such as variations in mass, temperature, and stress, have been employed for sensors based on microcantilever actuation. In the static mode of operation where no driving frequency is applied, the perturbation of the microcantilever due to its interaction with substances in its surroundings is usually detected by means of an optical feedback. Su and Dravid recently described the operation of a catalyst-based cantilever that functions in a cyclic manner.[47] In the presence of UV light, the TiO_2 coated on a cantilever catalyzed the oxidative decomposition of ethanol on its surface, which bent the cantilever as a result of differential stress (Figure 12). Once all the ethanol in the vicinity of the cantilever was consumed by photocatalytic oxidation, the cantilever returned to its original position. The process was repeated when ethanol was reintroduced into the system, allowing the system to function in a cyclic manner, resembling the operation of a combustion engine.

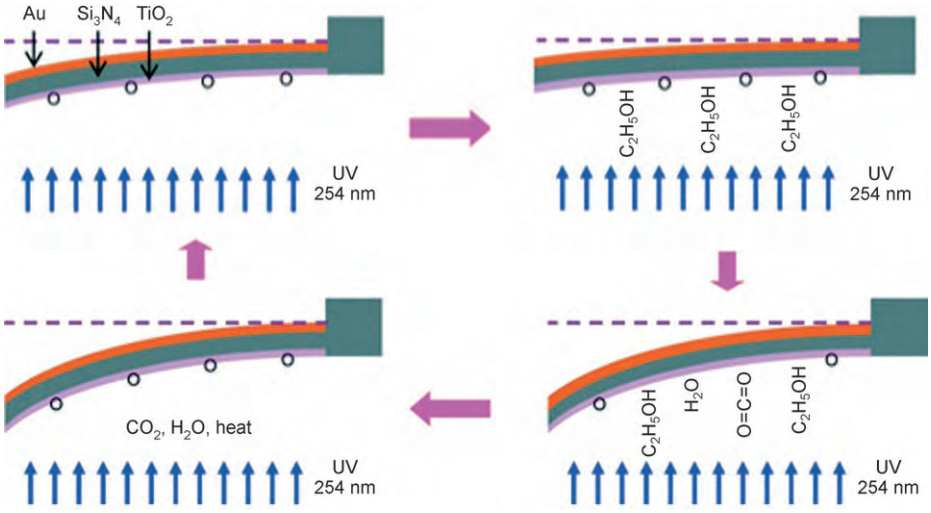


Figure 12. Proposed scheme for ethanol-fuelled photocatalytic microengines based on TiO_2-modified microcantilevers. From Ref. [47].

© 2006 Wiley-VCH Verlag GmbH & Co. KGaA, Weinheim

6. Future Directions and Applications

The small-scale and local conversion of chemical energy into mechanical energy may find use, among other applications, as micropumps and motors for micro- and nanomachinery. As demonstrated by Kline et al., immobilized catalyst systems have the ability to pump fluids without any moving parts.[44] Furthermore, the magnitude of this electrokinetic pumping effect is related to the surface charge on both the moving particles and the substrate in contact with the surrounding fluid. It follows that fluid flow caused by this effect can be modulated by changing the surface charge at solid–fluid interfaces.[48] With appropriate surface chemistry, the properties of the interface may be tuned chemically,[49] electrically,[50] or optically.[51] This catalytically induced electrokinetic phenomenon could find use in microfluidics and lab-on-a-chip applications, where the use of pressure gradients or externally generated electric fields may be difficult or undesirable.

In addition to micropump applications, the ability of particles that are both catalytic and asymmetric to locally convert chemical energy into mechanical energy offers the possibility of designing and controlling micro- and nanoscale machines that can interact with biological systems, such as individual cells. The idea of designing and developing devices that can interact intimately with biological systems at the cellular level is an exciting one and will benefit from addressing two aspects of biocompatibility: one that allows the device to work properly in biological systems, and one that will not interfere in an undesirable way with the biological host. This will require the development of new approaches (or adaptation of current ones) to allow for biocompatible and biologically available materials and fuels.

The examples in this Minireview demonstrate the fulfillment of the minimum requirements for nanoscale machines, namely initiating motion and, to a lesser degree, controlling the direction of that motion at the micro- and nanometer scales. If, in addition to a motor and a director, one could incorporate a device to perform some useful operation such as carrying cargo, entirely new classes of micro- and nanoscale devices may become possible. By incorporating materials that selectively adsorb or desorb a substance upon action of some stimulus from either the immediate environment or a remote source, such devices could be engineered to deliver small-scale amounts of therapeutic agents, or other loads, to specific regions in the human body. In addition, artificial motors could be integrated with biological cells to enhance natural immune responses. For example, synthetic motors attached to leukocytes might increase the rate of movement of these natural defenders especially through capillaries, thus increasing the likelihood that they will find immune-triggering pathogens and may accelerate recovery from or entirely prevent illness.

In charting future directions, two major areas will need to be addressed. First, while we know that catalysts can be used to impart motion to otherwise inanimate objects, we need to more fully understand and develop the mechanisms of chemical-to-mechanical energy transduction. Although some mechanisms of this energy transduction have been discussed here, important work must be done to explore more fully the parameters related to moving small-scale devices, such as the scaling of different mechanisms.

Other mechanisms may also be of interest, such as *Listeria*-mimicking systems propelled by an insertion polymerization mechanism as demonstrated by the motility of ActA-functionalized microspheres in an actin-rich environment.[18] The asymmetric polymerization of monomers at an immobilized metal catalyst will be a biomimetic analogue of the actin-polymerizing *Listeria* system. The ideal system of this type would produce relatively stiff polymer strands at rates equivalent to chains extending by tens of micrometers per second. This corresponds to polymer growth rates on the order of 10^{-5} mol cm^{-2} s^{-1} or site-turnover rates (assuming coverage of about 10^{10} catalyst molecules per cm^2) of approximately 10^5 s^{-1}. The catalyst particle would move by extending a growing polymer chain, akin to the method employed by *Listeria*.[16]

More work must also be done to generalize these phenomena. There are several approaches to convert stored chemical energy into mechanical energy. However, these approaches use a very narrow group of catalytic reactions to convert chemical energy into mechanical energy, which severely limits the usefulness of artificial chemical locomotion at the small scale. Understanding the mechanisms that use asymmetry to induce motion in fluids on the small scale and broadening the class of practical reactions that are capable of utilizing these mechanisms are two key objectives to generalize the phenomena described above. The resulting creative insight and broadened library of reactions will allow tailoring of chemical locomotors to a variety of applications, some of which have been discussed in this Minireview.

We gratefully acknowledge the contributions of our collaborators on this project, in particular Timothy Kline, Jeffrey Catchmark, Paul Lammert, Vincent Crespi, Shyamala Subramanian, Yang Wang, and Darrell Velegol. This work was supported by the Penn State Center for Nanoscale Science, NSF grant DMR-0213623, and NSF-NIRT grant CTS-0506967.

Received: January 6, 2006
Published online: July 31, 2006

[1] M. Shilwa, G. Woehlke, *Nature* **2003**, *422*, 759–765.
[2] *Interfacial Electrokinetics and Electrophoresis* (Ed.: Á. V. Delgado), Marcel Dekker, New York, **2002**.
[3] a) H. Watarai, M. Suwa, Y. Iiguni, *Anal. Bioanal. Chem.* **2004**, *378*, 1693–1699; b) T. M. Vickrey, J. A. Garcia-Ramirez, *Sep. Sci. Technol.* **1980**, *15*, 1297–1304.
[4] a) R. Piazza, *J. Phys.: Condens. Matter* **2004**, *16*, S4195–S4211; b) B. V. Derjaguin, N. V. Churev, V. M. Muller, *Surface Forces* (Engl. transl.), Consultants Bureau, New York, **1987**.
[5] a) H. J. Keh, Y. K. Wei, *Colloid Polym. Sci.* **2000**, *270*, 539–546; b) J. P. Ebel, J. L. Anderson, D. C. Prieve, *Langmuir* **1988**, *4*, 396–406; c) M. M. Lin, D. C. Prieve, *J. Colloid Interface Sci.* **1983**, *95*, 327–339.
[6] J. L. Anderson, *Annu. Rev. Fluid Mech.* **1989**, *21*, 61–99.
[7] a) S. M. Block, *Nature* **1992**, *360*, 493–495; b) A. Ashkin, *IEEE J. Sel. Top. Quantum Electron.* **2000**, *6*, 841–856.

 © 2006 Wiley-VCH Verlag GmbH & Co. KGaA, Weinheim

[8] R. Agarwal, K. Ladavac, Y. Roichman, G. Yu, C. M. Lieber, D. G. Grier, *Opt. Express* **2005**, *13*, 8906 – 8912.
[9] F. W. Went, *Am. Sci.* **1968**, *56*, 400 – 413.
[10] E. M. Purcell, *Am. J. Phys.* **1976**, *45*, 3 – 11.
[11] J. Happell, H. Brenner, *Low Reynolds Number Hydrodynamics*, Prentice Hall, Englewood Cliffs, **1965**.
[12] J. Lee, C.-J. Kim, *Proc. IEEE MEMS Workshop* **1998**, 538 – 543.
[13] A. Einstein, *Investigations on the Theory of Brownian Movement*, Dover, New York, **1956**.
[14] J. B. Waterbury, J. M. Willey, D. G. Franks, F. W. Valois, S. W. Watson, *Science* **1985**, *230*, 74 – 76.
[15] J. J. Schmidt, C. D. Montemagno, *Annu. Rev. Mater. Res.* **2004**, *34*, 315 – 337.
[16] D. Pantaloni, C. L. Clainche, M.-F. Carlier, *Science* **2001**, *292*, 1502 – 1506.
[17] A. Upadhyaya, A. van Oudenaarden, *Curr. Biol.* **2003**, *13*, R734 – R744.
[18] L. A. Cameron, M. J. Footer, A. van Oudenaarden, J. A. Theriot, *Proc. Natl. Acad. Sci. USA* **1999**, *96*, 4908 – 4913.
[19] K. J. Bohm, R. Stracke, P. Muhlig, E. Unger, *Nanotechnology* **2001**, *12*, 238 – 244.
[20] L. Jia, S. G. Moorjani, T. N. Jackson, W. O. Hancock, *Biomed. Microdevices* **2004**, *6*, 67 – 74.
[21] M. Platt, G. Muthukrishnan, W. O. Hancock, M. E. Williams, *J. Am. Chem. Soc.* **2005**, *127*, 15686 – 15687.
[22] R. K. Soong, G. D. Bachand, H. P. Neves, A. G. Olkhovets, H. G. Craighead, C. D. Montemagno, *Science* **2000**, *290*, 1555 – 1558.
[23] S. Rozhok, C. K.-F. Shen, P. H. Littler, Z. Fan, C. Liu, C. A. Mirkin, R. C. Holz, *Small* **2005**, *1*, 445 – 451.
[24] D. B. Weibel, P. Garstecki, D. Ryan, W. R. DiLuzio, M. Mayer, J. E. Seto, G. M. Whitesides, *Proc. Natl. Acad. Sci. USA* **2005**, *102*, 11963 – 11967.
[25] A. K. Schmid, N. C. Bartelt, R. Q. Hwang, *Science* **2000**, *290*, 1561 – 1564.
[26] a) N. Watanabe, K. Kutsumi, O. Sano, *J. Phys. Soc. Jpn.* **1994**, *63*, 2955 – 2963; b) O. Sano, K. Kutsumi, N. Watanabe, *J. Phys. Soc. Jpn.* **1995**, *64*, 1993 – 1999.
[27] a) L. Raleigh, *Proc. R. Soc. London* **1890**, *47*, 364; b) S. Nakata, S. Hiromatsu, H. Kitahata, *J. Phys. Chem. B* **2003**, *107*, 10557 – 10559; c) M. I. Kohira, Y. Hayashima, M. Nagayama, S. Nakata, *Langmuir* **2001**, *17*, 7124 – 7129.
[28] T. Mitsumata, J. P. Gong, Y. Osada, *Polym. Adv. Technol.* **2001**, *12*, 136 – 150.
[29] R. F. Ismagilov, A. Schwartz, N. Bowden, G. M. Whitesides, *Angew. Chem.* **2002**, *114*, 674 – 676; *Angew. Chem. Int. Ed.* **2002**, *41*, 652 – 654.
[30] J. Vicario, R. Eelkema, W. R. Browne, A. Meetsma, R. M. La Crois, B. L. Feringa, *Chem. Commun.* **2005**, 3936 – 3938.
[31] J. L. Anderson, *Phys. Fluids* **1983**, *26*, 2871 – 2879.
[32] R. Golestanian, T. B. Liverpool, A. Ajdari, *Phys. Rev. Lett.* **2005**, *94*, 220801 – 220804.
[33] W. F. Paxton, K. C. Kistler, C. C. Olmeda, A. Sen, S. K. St. Angelo, Y. Cao, T. E. Mallouk, P. E. Lammert, V. H. Crespi, *J. Am. Chem. Soc.* **2004**, *126*, 13424 – 13431.
[34] P. Dhar, T. M. Fischer, Y. Wang, T. E. Mallouk, W. F. Paxton, A. Sen, *Nano Lett.* **2006**, *6*, 66 – 72.
[35] a) S. Fournier-Bidoz, A. C. Arsenault, I. Manners, G. A. Ozin, *Chem. Commun.* **2005**, 441 – 443; b) Review: G. A. Ozin, I. Manners, S. Fournier-Bidoz, A. Arsenault, *Adv. Mater.* **2005**, *17*, 3011 – 3018.
[36] J. M. Catchmark, S. Subramanian, A. Sen, *Small* **2005**, *1*, 202 – 206.
[37] T. R. Kline, W. F. Paxton, T. E. Mallouk, A. Sen, *Angew. Chem.* **2005**, *117*, 754 – 756; *Angew. Chem. Int. Ed.* **2005**, *44*, 744 – 746.
[38] H. Lee, A. M. Purdon, V. Chu, R. M. Westervelt, *Nano Lett.* **2004**, *4*, 995 – 998.
[39] W. F. Paxton, A. Sen, T. E. Mallouk, *Chem. Eur. J.* **2005**, *11*, 6462 – 6470.
[40] P. Mitchell, *FEBS Lett.* **1972**, *28*, 1 – 4.
[41] P. E. Lammert, J. Prost, R. Bruinsma, *J. Theor. Biol.* **1996**, *178*, 387 – 391.
[42] T. P. Pitta, H. C. Berg, *J. Bacteriol.* **1995**, *177*, 5701 – 5703.
[43] B. Brahamsha, *J. Mol. Microbiol. Biotechnol.* **1999**, *1*, 59 – 62.
[44] T. R. Kline, W. F. Paxton, Y. Wang, D. Velegol, T. E. Mallouk, A. Sen, *J. Am. Chem. Soc.* **2005**, *127*, 17150 – 17151.
[45] N. Mano, A. Heller, *J. Am. Chem. Soc.* **2005**, *127*, 11574 – 11575.
[46] a) *Encyclopedia of Nanoscience and Nanotechnology*, *Vol. 1* (Ed.: H. S. Nalwa), American Scientific, Stevenson Ranch, **2004**, pp. 499 – 516; b) R. Raiteri, M. Grattarola, H.-J. Butt, P. Skladal, *Sens. Actuators B* **2001**, *79*, 115 – 126.
[47] M. Su, V. P. Dravid, *Nano Lett.* **2005**, *5*, 2023 – 2028.
[48] T. M. Squires, M. Z. Bazant, *J. Fluid Mech.* **2004**, *509*, 217 – 252.
[49] X. Zhang, R. Bai, *Langmuir* **2003**, *19*, 10703 – 10709.
[50] J. Lahann, S. Mitragotri, T. Tran, H. Kaido, J. Sundaran, S. Hoffer, G. A. Somorjai, R. Langer, *Science* **2003**, *299*, 371 – 374.
[51] D. G. Walter, D. J. Campbell, C. A. Mirkin, *J. Phys. Chem. B* **1999**, *103*, 402 – 405.

© 2006 Wiley-VCH Verlag GmbH & Co. KGaA, Weinheim

M. Schlosser

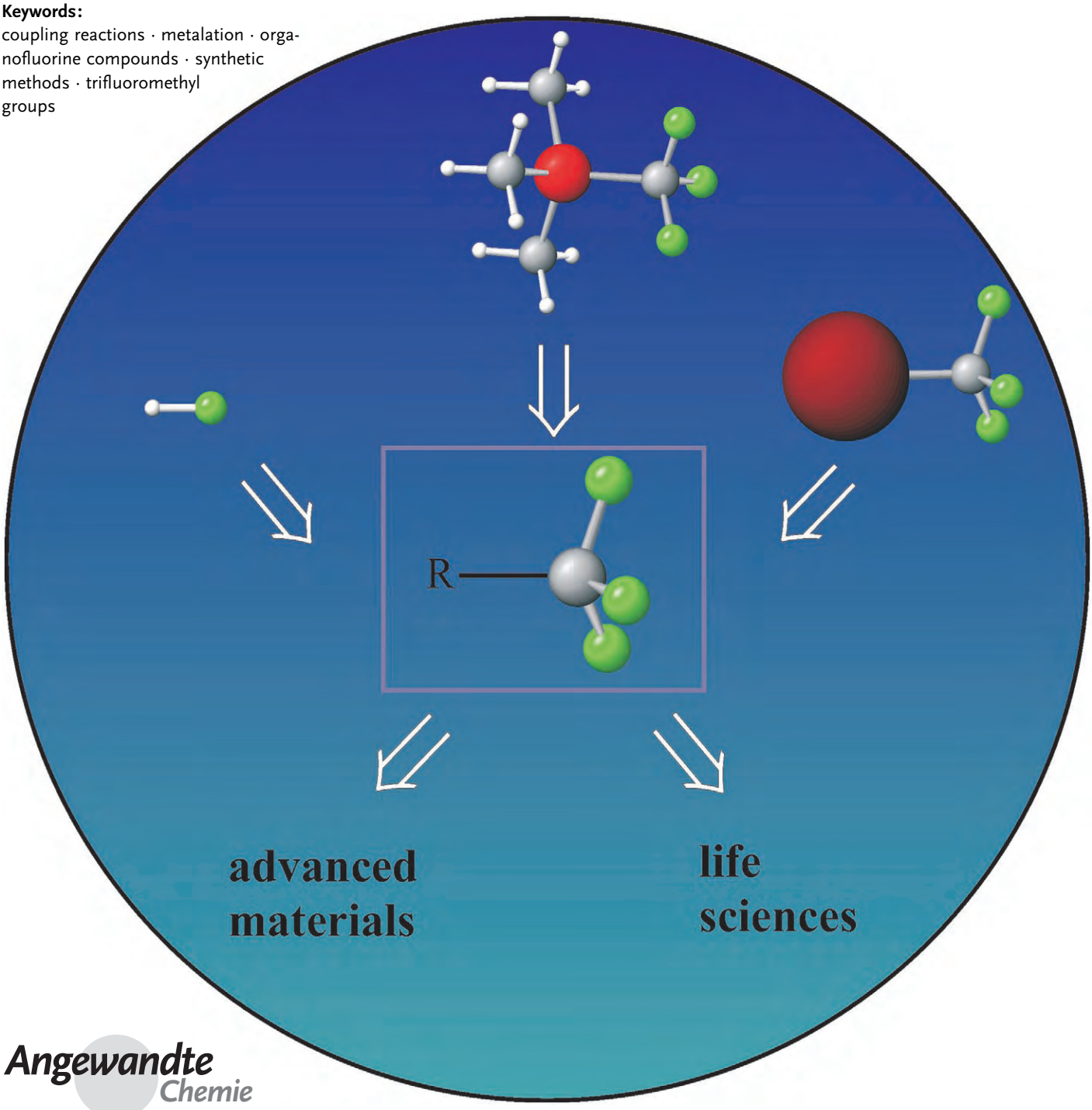
DOI: 10.1002/anie.200600449

Organofluorine Compounds

CF_3-Bearing Aromatic and Heterocyclic Building Blocks

*Manfred Schlosser**

Keywords:
coupling reactions · metalation · organofluorine compounds · synthetic methods · trifluoromethyl groups



© 2006 Wiley-VCH Verlag GmbH & Co. KGaA, Weinheim

Fluorine remains an insiders' tip in the life sciences as it enables the fine-tuning of biological properties. However, the synthesis of fluorine-substituted target compounds is not always trivial. Virtually any fluorine atom attached to an organic backbone has ultimately to be imported from inorganic sources. Crucial for the entire synthetic planning in medicinal and agricultural research is the decision on at what stage and how the halogen will be introduced. Standard technical processes, in particular the displacement of chlorine using anhydrous hydrogen fluoride or potassium fluoride, can hardly be implemented rationally on the laboratory scale. Universal methods that are applicable by both industrial and academic researchers thus have great appeal. If a trifluoromethyl-substituted arene or heterocycle is the target compound, two splendid options exist. The CF_3 group can be delivered packagewise by coupling an appropriate substrate with in situ generated (trifluoromethyl)copper. Alternatively, one may start from a CF_3-substituted arene or heterocycle as a core and complete it with the missing parts of the ultimate structure.

From the Contents

1. Introduction 5433
2. Copper-Mediated Iodo/Trifluoromethyl Displacement 5433
3. (Trifluoromethyl)naphthalenes 5434
4. The Principle of Regiochemically Exhaustive Functionalization 5437
5. Pyridines and Quinolines 5437
6. Pyrimidines and Pyrazoles 5442
7. Indoles 5443
8. Conclusions and Outlook 5443

1. Introduction

Not more than a handful of organofluorine compounds occur in nature, and even those occur just in small amounts.[1] Consequently, any fluorine-containing substance selected for fundamental studies or marketed as a pharmaceutical, agrochemical, or advanced material has to be man-made. This calls for dedicated "methodology", that is, the knowledge of appropriate methods, their critical evaluation, and subordination to an intelligent work plan. Fluorine that is assimilated into organic products generally comes from inorganic sources such as elemental fluorine (either supplied as a nitrogen-diluted gas[2] or electrochemically generated[3]), perchloryl fluoride,[4] heterocyclic *N*-fluoroammonium salts,[5,6] *N*-fluorosulfonamides and -imides,[5,7] hydrogen fluoride,[8] sulfur tetrafluoride[9] and derivatives thereof such as diethylaminosulfur trifluoride (DAST)[10] or analogues,[11] potassium fluoride,[12] or antimony trifluoride.[13] A crucial issue is often to decide whether the fluorine "label" should be introduced into the organic backbone at an early or a late stage of the synthesis sequence. One can avoid this choice if one identifies a commercial material that already comprises the required number of fluorine atoms at the right positions. In fact, hundreds if not thousands of versatile small-molecule modules (most of them with molecular weights in the 100–200 range) are currently listed in the catalogues of specialized suppliers. The present article endeavors to draw attention to the chances offered by this organofluorine pool.

2. Copper-Mediated Iodo/Trifluoromethyl Displacement

The attachment of a trifluoromethyl entity to a carbon skeleton can be accomplished in several ways. For example, trifluoromethyl groups can be effectively connected to secondary and tertiary carbon centers by photolysis of the corresponding alkyl(trifluoromethyl)diazenes (azo compounds), which are easily prepared by the condensation of aliphatic amines with trifluoronitrosomethane.[14] The systematic exploration of this promising method and its practical potential would be worthwhile.

The economically most attractive method is to treat a trichloromethyl precursor compound with anhydrous hydrogen fluoride.[15] Alternatively, any carboxy group can be transformed into a trifluoromethyl unit by using hydrogen fluoride and sulfur tetrafluoride,[16] which is itself a form of stored hydrogen fluoride. Each one of these options suffers from the drawback that it requires expertise in handling with hazardous reagents and dedicated equipment, both unavailable to the average chemist. The fluorodesulfuration of methyl dithiocarboxylates by use of a large excess of amine-complexed hydrogen fluoride in the presence of a mild oxidant such as *N*-bromosuccinimide has been attempted so far only on a small scale.[17]

Trifluoromethyllithium,[18] unlike, for example, dibromofluoromethyllithium,[19] is unstable even at extremely low temperatures owing to instantaneously ensuing elimination and substitution reactions. On the other hand, trifluoromethanide (trifluoromethyl anion) can be readily generated from (trifluoromethyl)trimethylsilane[20] or trifluoromethane (fluoroform)[21] and trapped in situ. Under such conditions, of

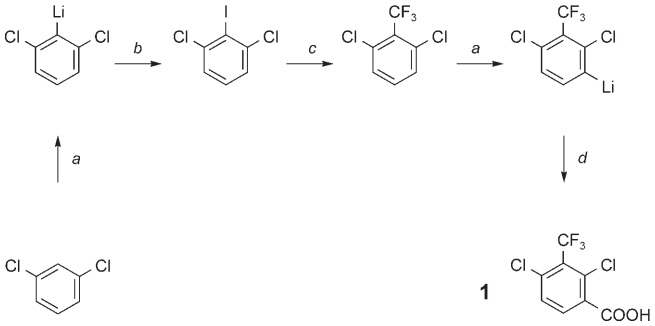
[*] Prof. M. Schlosser
Institut de Chimie moléculaire et biologique
Ecole Polytechnique Fédérale, BCh
1015 Lausanne (Switzerland)
Fax: (+41) 216-939-365
E-mail: manfred.schlosser@epfl.ch
and
Faculté des Sciences
Université, BCh
1015 Lausanne (Switzerland)

© 2006 Wiley-VCH Verlag GmbH & Co. KGaA, Weinheim

course, only highly reactive electrophiles, essentially carbonyl compounds, can be employed successfully.

To combine a trifluoromethyl group with an unsaturated carbon center, the assistance of a transiton element is required. Based on the pioneering work of McLoughlin,[22] Kobayashi,[23] Yagupolskii,[24] Kondo,[25] Burton,[26] and their collaborators, Fuchikami et al.[27] have designed a convenient laboratory procedure that picks up the CF_3 entity integrally ("packagewise") from (trifluoromethyl)trimethylsilane, the so-called Ruppert–Prakash reagent,[20a,28,29] and delivers it through in situ generated (trifluoromethyl)copper to a bromo- or iodo-substituted aromatic condensation partner. This method was fine-tuned in recent years to make it applicable to more challenging substrates, including sterically hindered and heterocyclic ones.[30] For example, 2,6-dichlorobenzotrifluoride was prepared in this way, for the first time, by lithiation and subsequent iodination of 1,3-dichlorobenzene and subsequent treatment with (trifluoromethyl)trimethylsilane in the presence of cuprous iodide and spray-dried potassium fluoride (Scheme 1).[31] The subsequent reaction of this 2,6-dichlorobenzotrifluoride with lithium 2,2,6,6-tetramethylpiperidide (LITMP) and carbon dioxide afforded 2,4-dichloro-3-(trifluoromethyl)benzoic acid (**1**, 71% yield).[31]

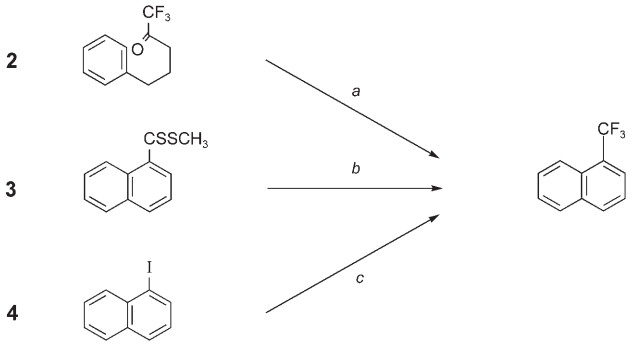
Although the other five dichlorobenzotrifluorides are all commercial compounds, functionalized derivatives thereof were thus far unknown. Site-specific metalation and trapping of the resulting intermediates with a variety of electrophiles open a comfortable entry to new building blocks for life-science-oriented research and thus help combinatorial synthesis to escape from the prison of catalogue chemicals.[31]



Scheme 1. Preparation of 2,6-dichlorobenzotrifluoride by I/CF_3 exchange and subsequent functionalization to 2,4-dichloro-3-(trifluoromethyl)benzoic acid (**1**). Reagents and conditions: a) LITMP in THF at −75 °C; b) elemental iodine; c) $(H_3C)_3SiCF_3$ + KF + CuI in a 1:1 mixture of dimethylformamide and *N*-methylpyrrolidone at +25 °C; d) 1. dry ice, 2. hydrochloric acid.

3. (Trifluoromethyl)naphthalenes

Trifluoromethyl-substituted naphthalenes were among the first targets to reveal the potential of in situ generated (trifluoromethyl)copper. The 1-isomer (Scheme 2) was first prepared by treating 1-naphthoic acid with sulfur tetrafluoride[32] and later by Friedel–Crafts-type cyclization of 1,1,1-trifluoro-5-phenyl-2-pentanone (**2**) to give 4-trifluoromethyl-1,2-dihydronaphthalene,[33] which is subsequently oxidized, as well as by fluorolytic cleavage of xanthogenate **3**.[34] It can also be readily prepared in satisfactory yield (61%) from 1-iodonaphthalene (**4**) and potassium (2-fluorosulfonyl-1,1,2,2-tetrafluoroethoxy)difluoroacetate in the presence of cuprous iodide.[35]



Scheme 2. Three routes to 1-(trifluoromethyl)naphthalene. Reagents and conditions: a) 1. $FeCl_3$ in dichloromethane at +20 °C, 2. dehydrogenation (using an oxidant such as 2,3-dichloro-5,6-dicyano-1,4-benzoquinone; b) *N*-bromosuccinimide and hydrogen fluoride (excess); c) $FSO_2CF_2CF_2OCF_2COOK$ + CuI in dimethylformamide at +45 °C.

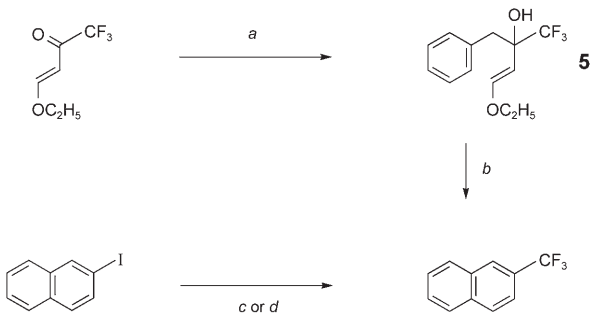
2-(Trifluoromethyl)naphthalene is also accessible by an approach involving C–C coupling and cyclization. The addition of benzylmagnesium bromide to 4-ethoxy-1,1,1-trifluoro-3-buten-2-one and subsequent acid-catalyzed ring closure of the intermediate **5** provides, through elimination of both water and ethanol, the final product in 46% overall yield.[36] However, substitution of iodine by CF_3 transfer from (trifluoromethyl)trimethylsilane[27] or sodium trifluoroacetate[37] appears again to be more straightforward (Scheme 3).

The reagent (trifluoromethyl)trimethylsilane represents a borderline case. Containing just one fluorine-bearing carbon atom along with the three silicon-bound methyl groups, it is not quite an inorganic substance, but at the same time only marginally organic. We wondered whether fully organic starting materials could not provide a more rational and flexible access to fluorinated naphthalenes. In fact, the aryne route to (trifluoromethyl)naphthalenes and congeners[38] proved to be as expedient as the previously explored routes

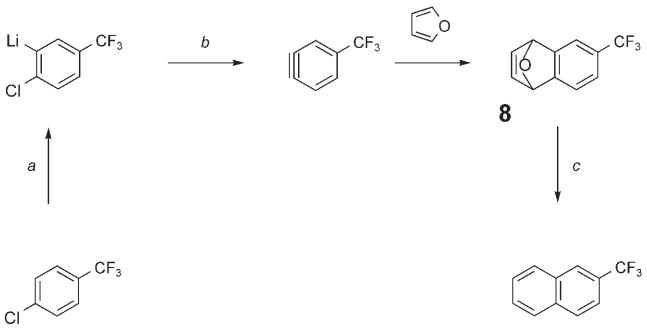


Manfred Schlosser was born in Ludwigshafen (Germany) and studied chemistry with a minor in medicine in Heidelberg, where he received his Ph.D. in 1960 with Georg Wittig. After completing his habilitation in Heidelberg in 1966, he took a position as head physician at the German Cancer Research Center. In 1971, he was appointed to a professorship at the Université de Lausanne and was later affiliated with the Lausanne branch of the ETH. A substantial part of his research efforts are devoted to obtaining a detailed understanding of the chemical reactivity in general and the behavior of organometallic compounds in particular.

 © 2006 Wiley-VCH Verlag GmbH & Co. KGaA, Weinheim

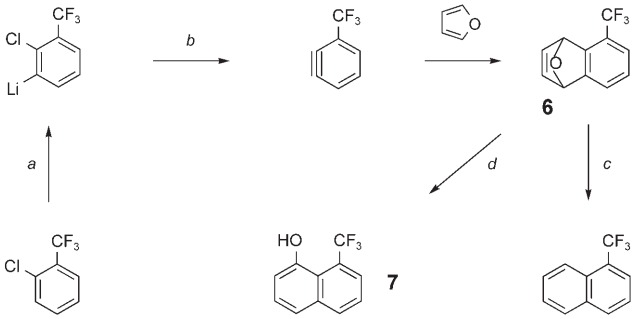


Scheme 3. Cyclization and I/CF_3 displacement routes to 2-(trifluoromethyl)naphthalene. Reagents and conditions: a) benzylmagnesium bromide; b) 4-toluenesulfonic acid in toluene; c) $(H_3C)_3SiCF_3$ + KF + CuI in a 1:1 mixture of *N*,*N*-dimethylformamide and *N*-methylpyrrolidone at +25 °C; d) $NaOOCCF_3$ + CuI in dimethylacetamide at +160 °C.



Scheme 5. The aryne route to 2-(trifluoromethyl)naphthalene. Reagents and conditions: a) butyllithium in THF at −75 °C; b) transfer into furan which is kept at +25 °C; c) titanium tetrachloride and zinc powder in THF.

for the preparation of (trifluoromethoxy)naphthalenes[39] and fluoronaphthalenes.[40] After lithiation of 2-chlorobenzotrifluoride at the position adjacent to Cl,[41] the cold solution (−75 °C) is siphoned through teflon tubing into furan which is kept at ambient temperature. Immediate β elimination of lithium chloride liberates 1,2-didehydro-3-(trifluoromethyl)-benzene, which instantaneously undergoes [4+2] cycloaddition to afford 1,4-epoxy-1,4-dihydro-5-(trifluoromethyl)naphthalene (**6**; 76% yield; Scheme 4).[38] The Diels–Alder



Scheme 4. The aryne route to 1-(trifluoromethyl)-naphthalene and congeners. Reagents and conditions: a) butyllithium in THF at −75 °C; b) transfer into furan which is kept at +25 °C; c) titanium tetrachloride and zinc powder in THF; d) hydrogen chloride in ethanol.

product **6** can be readily deoxygenated by using zinc[39] or low-valent titanium[38] to give 1-(trifluoromethyl)naphthalene (82%), or can be isomerized through acid catalysis to 8-trifluoromethyl-1-naphthol (**7**; 81%; Scheme 4).[38]

Analogously, 4-chlorobenzotrifluoride was fused to furan to give 1,4-epoxy-1,4-dihydro-6-(trifluoromethyl)naphthalene (**8**; 75%).[38] The latter intermediate can again be smoothly reduced to 2-(trifluoromethyl)naphthalene (82%; Scheme 5).[38]

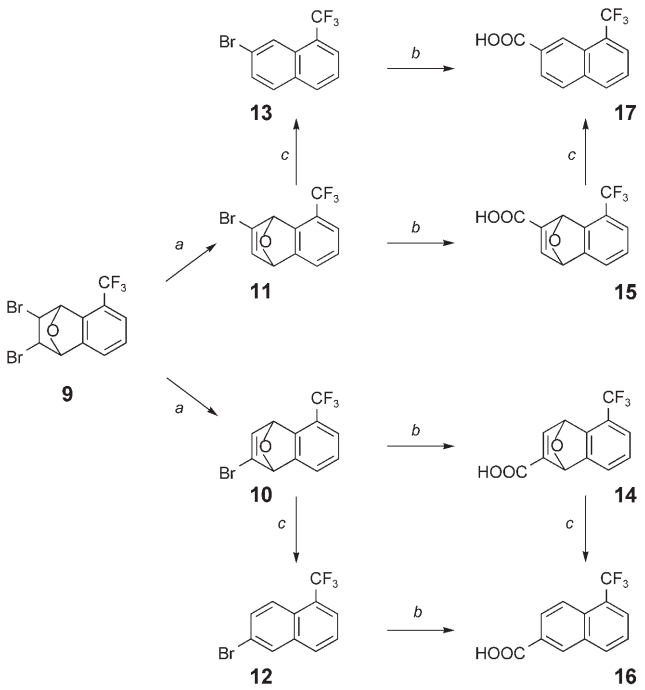
Naphthalenes are "privileged structures" for drug design.[42] Nevertheless, only a small percentage of functionalized congeners that bear additional heterosubstituents such as halogens and trifluoromethyl, trifluoromethoxy, alkoxy, and dialkylamino groups are documented in the chemical literature. This sparsity of representative examples points at practical difficulties with their selective preparation. In fact, monosubstituted naphthalenes consist of seven vacant positions, and electrophiles tend to attack several sites simultaneously. Efforts to overcome this problem are hence welcome.

We first demonstrate how carboxy and other functional groups can be readily introduced into (trifluoromethyl)naphthalene derivatives at selected positions of the ring remote to the CF_3 group. Elemental bromine adds cleanly to the olefinic double bond of cycloadduct **6** if the Balcı high-temperature protocol[43] is applied.[38] Three stereoisomers, the 2-*endo*-3-*exo*, 2-*exo*-3-*exo*, and 2-*exo*-3-*endo* dibromo compounds **9**, are formed in a 1:1:1 ratio and can be separated by column chromatography. When treated with potassium *tert*-butoxide, the former and the latter component give 2- and 3-bromo-1,4-epoxydihydronaphthalene (**10** and **11**), respectively, whereas the *exo*,*exo* isomer produces a 1:1 mixture of these compounds, which again prove to be separable by column chromatography. Halogen/metal permutation and subsequent carboxylation and neutralization provide the epoxynaphthoic acids **14** and **15**, which can be converted into the (trifluoromethyl)naphthoic acids **16** and **17** by deoxygenation.[38] Alternatively, the 2- and 3-bromo-1,4-epoxy-1,4-dihydronaphthalenes (**10** and **11**) may be first deoxygenated (to give compounds **12** and **13**) before being treated with butyllithium and dry ice. The acids **16** and **17** are again the final products (Scheme 6).[38]

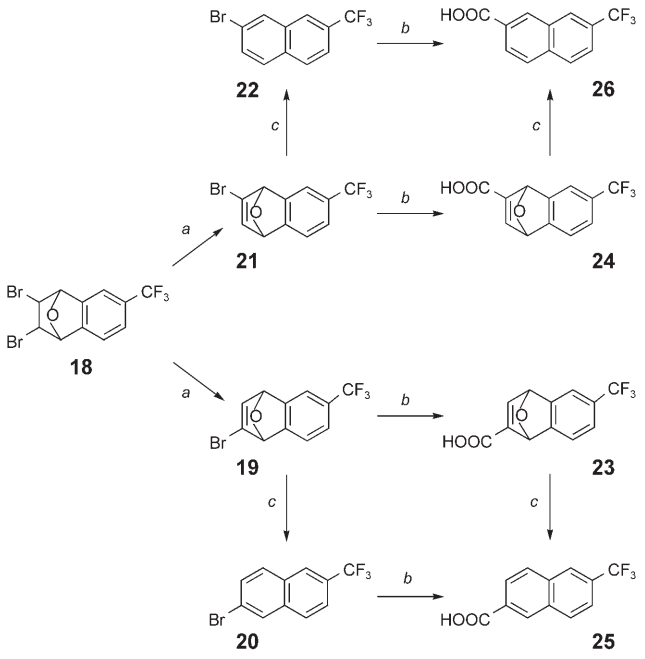
Analogously, the bromo compound **18** was accessed from the epoxydihydronaphthalene **8** (see Scheme 5). It can be readily converted into the dehydrobromination products **19**–**22** and the naphthoic acids **23**–**26**, again in high yields (Scheme 7).[38] Regioisomers and stereoisomers can be chromatographically separated for these reactions as well.

The universality of this approach should be kept in mind. Carbon dioxide is one of the particularly representative reagents for trapping organometallic species. However, the intermediates that are generated by halogen/metal permutation from precursors such as **10**–**13** and **19**–**22** react with all kinds of electrophiles, so that hundreds of other functionalized (trifluoromethyl)naphthalene derivatives can be prepared in the same way.

© 2006 Wiley-VCH Verlag GmbH & Co. KGaA, Weinheim

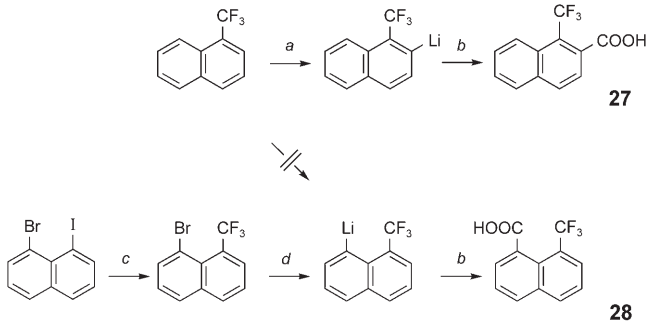


Scheme 6. Preparation of 5- and 8-trifluoromethyl-2-naphthoic acids (**16** and **17**) from 1,4-epoxy-1,4-dihydronaphthalene **6** via intermediates **9** and **10**–**15**. Reagents and conditions: a) potassium *tert*-butoxide in THF at 0 °C; b) 1. butyllithium in THF at −75 °C, 2. excess dry ice, 3. hydrochloric acid; c) titanium tetrachloride and zinc powder in THF at +68 °C (reflux temperature).



Scheme 7. Preparation of 6- and 7-trifluoromethyl-2-naphthoic acids (**25** and **26**) from 1,4-epoxy-1,4-dihydronaphthalene **8** via intermediates **18** and **19**–**24**. Reagents and conditions: a) potassium *tert*-butoxide in THF at 0 °C; b) 1. butyllithium in THF at −75 °C, 2. excess dry ice, 3. hydrochloric acid; c) titanium tetrachloride and zinc powder in THF at +68 °C (reflux temperature).

To add functionality to the CF_3-bearing ring, metalation (hydrogen/metal permutation) is an obvious choice for the key step. Lithium 2,2,6,6-tetramethylpiperidide (LITMP) was found to deprotonate 1-(trifluoromethyl)naphthalene exclusively at the 2-position, though the resulting carboxylic acid **27** was isolated in only moderate yield (27–42 %; Scheme 8).[44]

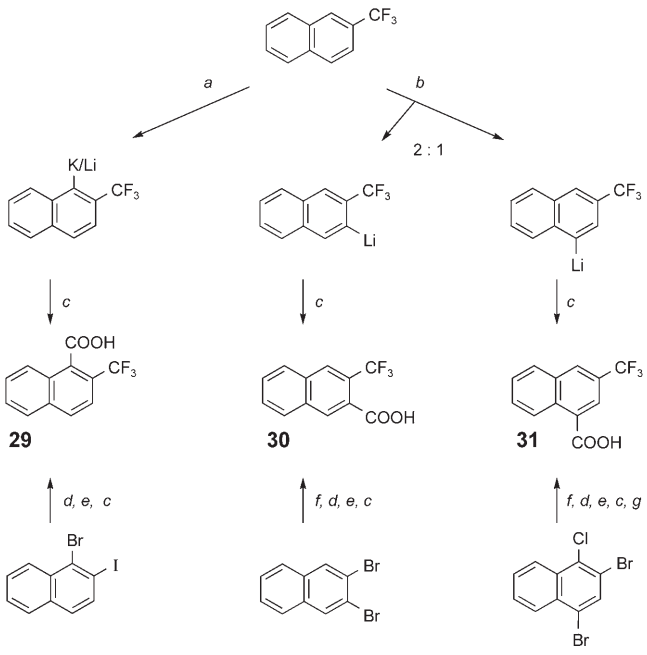


Scheme 8. Selective preparation of 1-trifluoromethyl-2-naphthoic acid (**27**) and 8-trifluoromethyl-1-naphthoic acid (**28**). Reagents and conditions: a) LITMP in THF at −25 °C; b) 1. excess dry ice, 2. hydrochloric acid; c) $(H_3C)_3SiCF_3$ + KF + CuI in a 1:1 mixture of dimethylform amide and *N*-methylpyrrolidone at +25 °C; d) butyllithium in THF at −75 °C.

The absence of the *peri* isomer had to be rigorously demonstrated, as other naphthalene substituents at the 1-position, such as dimethylamino[45] and (dimethylamino)-methyl,[46] activate just the 8-position or, in the case of methoxy,[47] simultaneously the 2- and 8-position. To this end, 8-trifluoromethyl-1-naphthoic acid (**28**) was synthesized from the known compound 1-bromo-8-iodonaphthalene by I/CF_3 displacement and subsequent halogen/metal permutation and carboxylation in 70 % overall yield (Scheme 8). By using this authentic sample as a reference for gas chromatographic analysis, any contamination of acid **27** by its regioisomer **28** could be ruled out (Scheme 8).[44]

2-(Trifluoromethyl)naphthalene is metalated by *tert*-butyllithium in the presence of potassium *tert*-butoxide, one of our superbasic mixed-metal reagents,[48] with complete selectivity at the 1-position as evidenced by the isolation of pure 2-trifluoromethyl-1-naphthoic acid (**29**; 21 %)[44] (Scheme 9). In contrast, simple alkyllithium reagents invariably produce regioisomeric mixtures. Thus, *sec*-butyllithium attacks concomitantly the 3- and 4-position in a 2:1 proportion for a combined yield of 75 %.[44] After carboxylation and neutralization, the main component, 3-trifluoromethyl-2-naphthoic acid (**30**), can be purified by crystallization. The minor product, 3-trifluoromethyl-1-naphthoic acid (**31**), had to be identified by comparison of the retention time with a sample independently prepared from 2,4-dibromo-1-chloronaphthalene (Scheme 9).[44]

 © 2006 Wiley-VCH Verlag GmbH & Co. KGaA, Weinheim

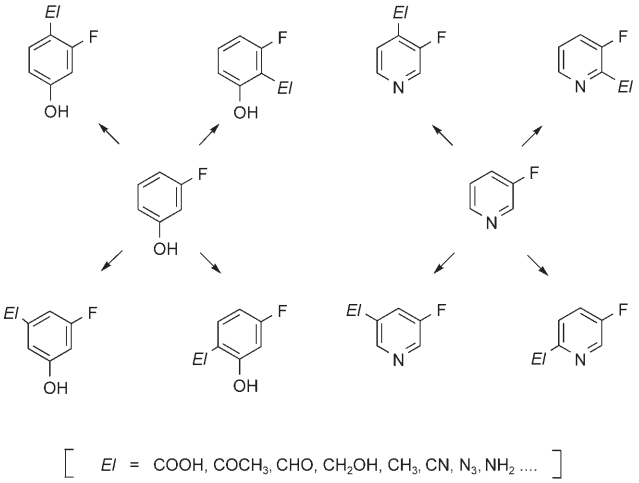


Scheme 9. Both regioselective and unselective metalation of 2-(trifluoromethyl)naphthalene. Reagents and conditions: a) *tert*-butyllithium and potassium *tert*-butoxide in THF at −75 °C; b) *sec*-butyllithium in the presence of *N*,*N*,*N*′,*N*′-tetramethylethylenediamine (TMEDA) in THF at −75 °C; c) 1. excess dry ice, 2. hydrochloric acid; d) $(H_3C)_3SiCF_3$ + KF + CuI in a 1:1 mixture of dimethylformamide and *N*-methylpyrrolidone at +25 °C; e) 1. isopropylmagnesium chloride in THF at 0 °C; f) 1. isopropylmagnesium chloride in THF at −10 °C, 2. elemental iodine; g) ammonium formate and palladium on charcoal in methanol at +25 °C.

4. The Principle of Regiochemically Exhaustive Functionalization

This section marks the transition from arene to heterocyclic chemistry. At the same time it features a new concept which has emerged in the recent years, the commitment to regioisomerically complete ("exhaustive") functionalization of core compounds.

Once a given molecular entity has been unequivocally stipulated as a target of synthesis, there remains only to find the best route leading to that substance in the desired quantity and purity. There are no particular preferences for the methods to be employed beyond economical criteria. A different situation is encountered when one looks for a building block which would improve the bioactivity of a pharmaceutical or agricultural lead compound. At such an exploratory stage, structural diversity is the key issue, and a collection ("library") of as many isosters and analogues as possible is the prime objective. In other words, as long as one has no precise idea about the definitive substituent pattern, it is advisable to make whole families of related structures in order to single out the one that meets the desired criteria optimally. In particular, one would want to access all possible regioisomers to be sure that no hit or new insight is missed. The "toolbox methods"[49,50] have been elaborated to accomplish exactly this task in a rational and reliable manner. Derivatives of 3-fluorophenol and 3-fluoropyridine that carry a given functional group at any of the four vacant positions may serve as typical examples to demonstrate the principle (Scheme 10).[51]



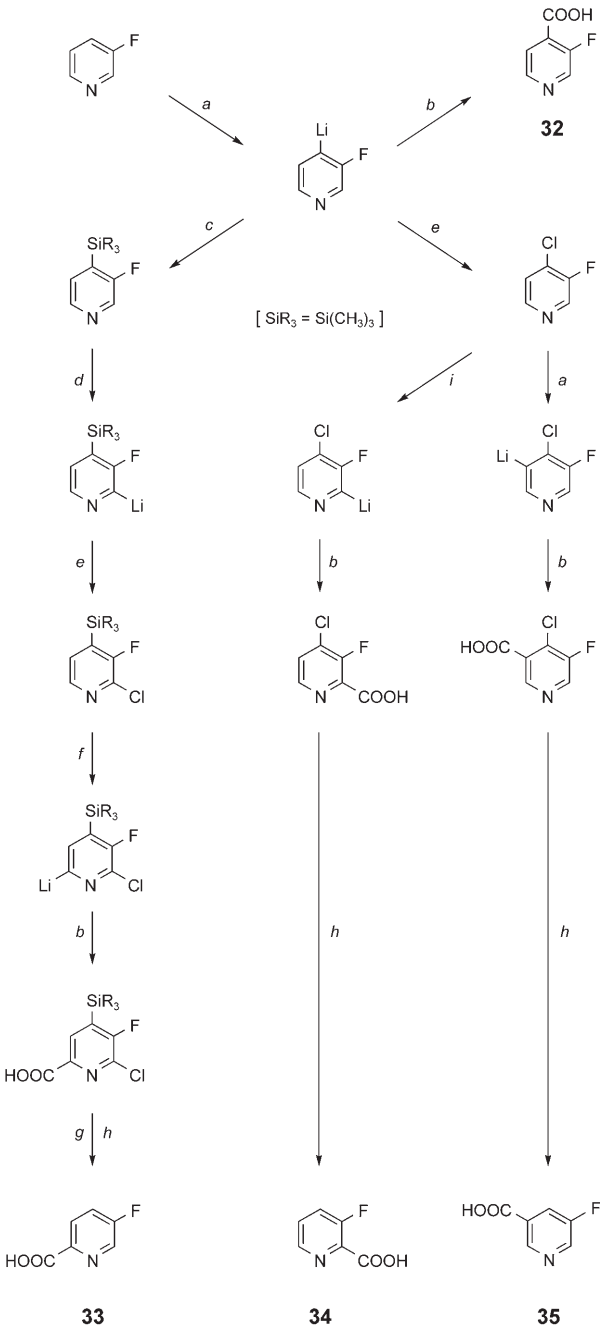
Scheme 10. The principle of "regioisomerically exhaustive functionalization" as applied to 3-fluorophenol and 3-fluoropyridine.

5. Pyridines and Quinolines

The case of 3-pyridine illustrates some of the main options that exist to secure the intended regiochemical flexibility (Scheme 11). The acidity of the various pyridine sites increases with their distance from the nitrogen atom in the ring.[52] Therefore, lithium diisopropylamide (LIDA) and other standard bases deprotonate 3-fluoropyridine at the 4- rather than the 2-position. Subsequent carboxylation furnishes thus 3-fluoropyridine-4-carboxylic acid (**32**; 84 %). The 2-position can be functionalized when the 4-position is blocked by a voluminous and inert trimethylsilyl entity. Quenching the organometallic intermediate, as before, with dry ice affords, after protodesilylation, 3-fluoropyridine-2-carboxylic acid (**34**; 79 % overall yield). Alternatively, one can introduce a second protective group, either a trialkylsilyl group again or a chlorine atom. As the bulky trimethylsilyl substituent silences not only the site to which it is directly attached but also the immediate environment, the 6-position is the only place where a further metalation can occur. This is most effectively brought about with an excess of "Caubère's base" (LIC-LIDMAE), butyllithium in the presence of lithium 2-(dimethylamino)ethoxide (LIDMAE).[53] After carboxylation and removal of the silyl and chlorine substituents, 5-fluoropyridine-2-carboxylic acid (**33**; 26 % overall yield) is obtained.

4-Chloro-3-fluoropyridine, which results from the quenching of the lithiated intermediate with 1,1,2-trichloro-1,2,2-trifluoroethane, represents one of numerous substrates that offer the attractive "reagent-controlled optional site selectivity".[47,54,55] Unlike trialkyl silyl groups, a chlorine atom blocks nothing but the site where it is residing and at the same time activates neighboring sites. Consequently, LIDA deprotonates cleanly the 5-position and thus paves the way to 5-

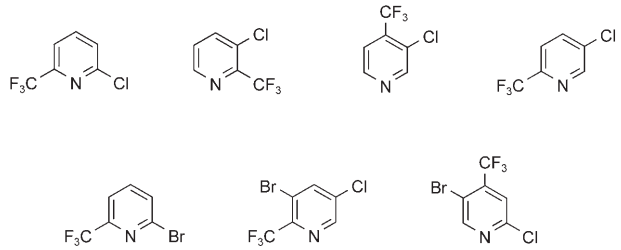
© 2006 Wiley-VCH Verlag GmbH & Co. KGaA, Weinheim



Scheme 11. The regiochemically exhaustive functionalization of 3-fluoropyridine. Reagents and conditions: a) LIDA in THF at −75 °C; b) 1. dry ice, 2. hydrochloric acid; c) chlorotrimethylsilane; d) LITMP in THF at −75 °C; e) 1,1,2-trichloro-1,2,2-trifluoroethane; f) excess butyllithium and LIDMAE in hexanes at −75 °C; g) tetrabutylammonium fluoride (TBAF) hydrate in THF at +25 °C; h) ammonium formate in methanol in the presence of palladium on charcoal at +50 °C; i) LITMP in Et_2O at −75 °C.

fluoropyridine-3-carboxylic acid (**35**; 77% overall yield). In contrast, when the lithiation is carried out with LITMP in diethyl ether, the reagent seeks extra electron density and coordinates to the lone pair of electrons at the nitrogen atom. Therefore, deprotonation takes place at the 2-position this time and provides, after carboxylation and hydrogenolytic reduction, 3-fluoropyridine-2-carboxylic acid (**34**; 63% overall yield; Scheme 11).[51]

2-Chloro-3-, 2-chloro-4-, and 2-chloro-6-(trifluoromethyl)pyridine can be purchased, although at prohibitive prices (20000–25000 €mol^{-1}). To demonstrate the versatility of the method, we prepared 2-chloro-6-(trifluoromethyl)pyridine,[30] 3-chloro-2-(trifluoromethyl)pyridine,[56] 3-chloro-4-(trifluoromethyl)pyridine,[57] 5-chloro-2-(trifluoromethyl)pyridine,[58] 2-bromo-6-(trifluoromethyl)pyridine,[30] 3-bromo-5-chloro-2-(trifluoromethyl)pyridine,[56] and 5-bromo-2-chloro-4-(trifluoromethyl)pyridine[56] by applying the copper-mediated I/CF_3 displacement described above as the key step (Scheme 12). Having sufficient quantities of these enticing materials at hand, we tested several of them as substrates for regiochemically exhaustive functionalizations.

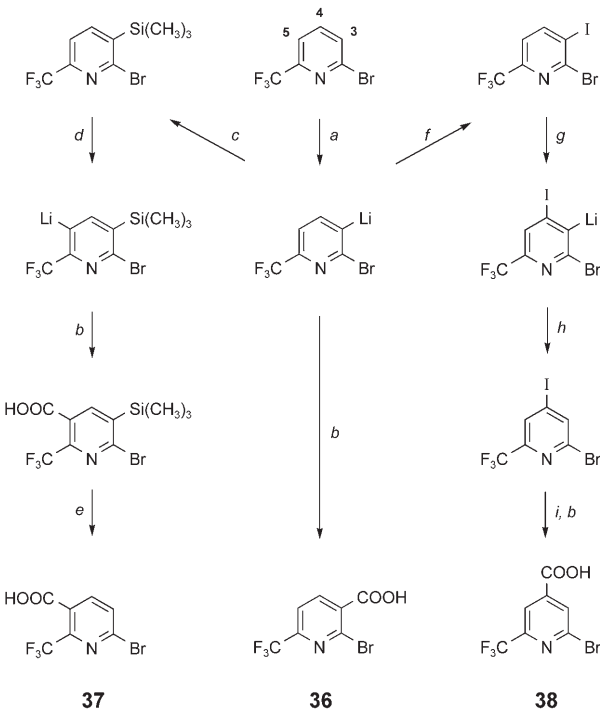


Scheme 12. Chloro- and bromo-substituted (trifluoromethyl)pyridines, all prepared by copper-mediated I/CF_3 displacement.

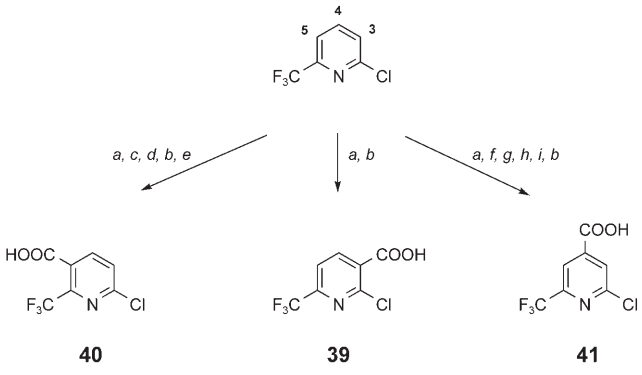
Starting from 2-bromo-6-(trifluoromethyl)pyridine, functionalization at the 3-position to afford, for example, the acid **36** (49%; Scheme 13) can be achieved in a straightforward manner by direct metalation with LIDA carried out at −85 °C[56] (rather than at the usual dry-ice temperature). The metalation is rerouted to the 5-position if the 3-position is protected by a trimethylsilyl group. Carboxylation and protodesilylation give 6-bromo-2-(trifluoromethyl)pyridine3-carboxylic acid (**37**; 42% overall yield).[56] The last isomeric acid **38** (56% overall yield) can be readily accessed by relying on heavy halogen migration.[47,59] When 2-bromo-3-iodo-6-(trifluoromethyl)pyridine is treated with LIDA, a proton is removed from the 4-position, and an exchange of places ensues by which the lithium atom moves to the 3-position and iodine to the 4-position. Neutralization and subsequent halogen/metal permutation between the resulting 2-bromo-4-iodo-6-(trifluoromethyl)pyridine and isopropylmagnesium chloride terminate the reaction sequence (Scheme 13).[56]

Exactly the same methods were used to convert the isologous 2-chloro-6-(trifluoromethyl)pyridine into 2-chloro-6-(trifluoromethyl)pyridine-3-carboxylic acid (**39**; 60% overall yield), 6-chloro-2-(trifluoromethyl)pyridine-3-carboxylic acid (**40**; 79%), and 2-chloro-6-(trifluoromethyl)pyridine-4-carboxylic acid (**41**; 51% overall yield; Scheme 14).[57] The only difference was that the iodine/lithium permutation was performed with lithium tributylmagnesate[60,61] rather than with the less reactive isopropylmagnesium chloride. The single halogen atom at the 2- or 6-position of the acids **37**–**41** is of course prone to replacement by any standard nucleophile.

 © 2006 Wiley-VCH Verlag GmbH & Co. KGaA, Weinheim

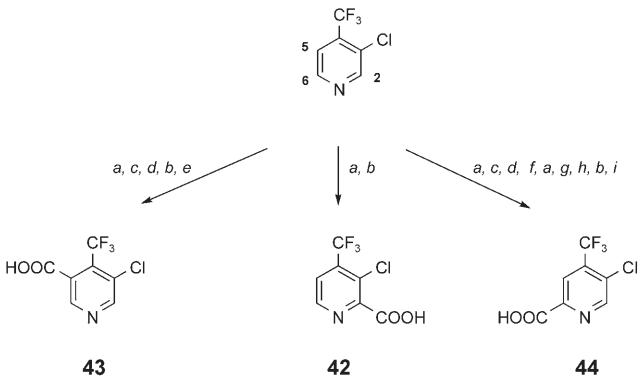


Scheme 13. The regiochemically exhaustive functionalization of 2-bromo-6-(trifluoromethyl)pyridine. Reagents and conditions: a) LIDA in THF at −85 °C; b) 1. excess dry ice, 2. hydrochloric acid; c) chlorotrimethylsilane; d) LITMP in THF at −75 °C; e) TBAF hydrate in refluxing THF; f) elemental iodine; g) LIDA in THF at −75 °C; h) dilute hydrochloric acid; i) isopropylmagnesium chloride in THF at 0 °C.



Scheme 14. The regiochemically exhaustive functionalization of 2-chloro-6-(trifluoromethyl)pyridine. Reagents and conditions: a) LIDA in THF at −85 °C; b) 1. excess dry ice, 2. hydrochloric acid; c) chlorotrimethylsilane; d) LITMP in THF at −75 °C; e) TBAF hydrate in refluxing THF; f) elemental iodine; g) LIDA in THF at −75 °C; h) dilute hydrochloric acid; i) lithium tributylmagnesate in THF at 0 °C.

A similar approach proved successful with 3-chloro-4-(trifluoromethyl)pyridine (Scheme 15).[57] 3-Chloro-4-(trifluoromethyl)pyridine-2-carboxylic acid (**42**; 57 %) was obtained after direct metalation, this time carried out with LITMP in diethyl ether (or THF) at −100 °C, and the isomeric 5-chloro-4-(trifluoromethyl)pyridine-3- and -2-carboxylic acids (**43** and **44**; 61 % and 29 % overall yield, respectively)



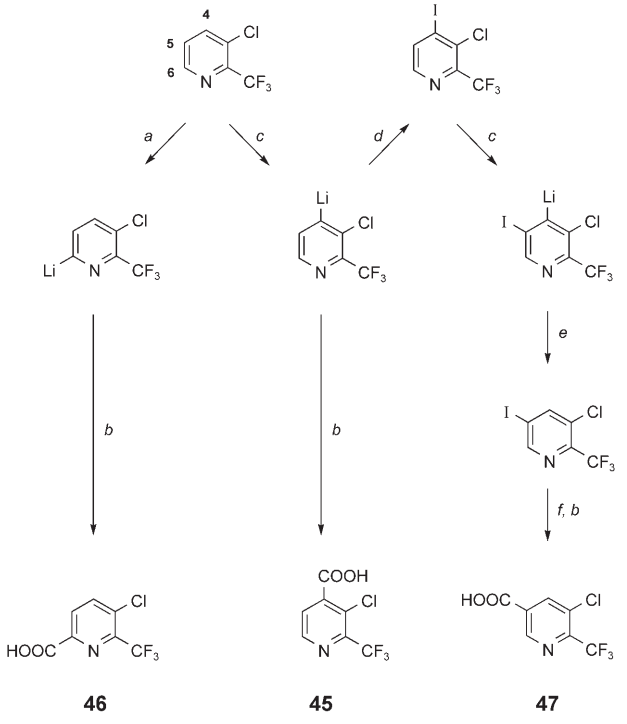
Scheme 15. The regiochemically exhaustive functionalization of 3-chloro-4-(trifluoromethyl)pyridine. Reagents and conditions: a) LITMP in Et_2O or THF at −100 °C; b) 1. excess dry ice, 2. hydrochloric acid; c) chlorotrimethylsilane; d) LITMP in THF at −75 °C; e) aqueous sodium hydroxide at +100 °C; f) elemental iodine; g) dilute hydrochloric acid; h) butyllithium in toluene at −75 °C; i) TBAF hydrate in refluxing THF.

were obtained via 3-chloro-4-trifluoromethyl-2-(trimethylsilyl)pyridine as the common intermediate (Scheme 15).[57]

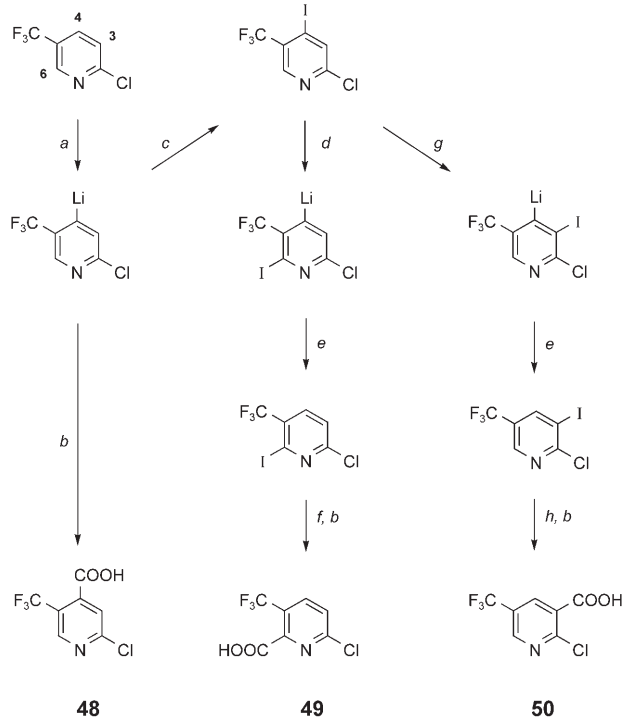
Further examples demonstrate the flexibility of the "toolbox methods",[49] which need only little adaptation to cope with any given situation. 3-Chloro-2-(trifluoromethyl)pyridine does not require silyl protection to steer the metal and subsequently the functional group to the 6-position. When the coordination-sensitive mixture ("Caubère's base") of excess butyllithium and lithium 2-(dimethylamino)ethoxide is employed as the reagent, metalation occurs exclusively there, thus opening an easy entry to 5-chloro-6-(trifluoromethyl)pyridine-2-carboxylic acid (**46**; 26 %).[56] Conversely, standard conditions (for example, LIDA in THF at −75 °C) favor the deprotonation at the most acidic site. This leads directly to the isomeric 3-chloro-2-(trifluoromethyl)pyridine-4-carboxylic acid (**45**; 81 %) and, via 3-chloro-4- and 3-chloro-5-iodo-2-(trifluoromethyl)pyridine (the latter made by LIDA-promoted heavy-halogen migration, analogously as shown in Scheme 13), 5-chloro-6-(trifluoromethyl)pyridine-3-carboxylic acid (**47**; 46 % overall yield; Scheme 16).[56]

Lithium dialkyl amides such as LIDA or LITMP metalate also 2-chloro-5-(trifluoromethyl)pyridine cleanly at the 4-position.[57] Carboxylation and iodination provide directly 2-chloro-5-(trifluoromethyl)pyridine-4-carboxylic acid (**48**; 87 %) and 2-chloro-4-iodo-5-(trifluoromethyl)pyridine (67 %), respectively. The latter compound exhibits a unique kind of optional site selectivity. LIDA causes deprotonation of the 6-position, where the heavy halogen atom is ultimately located, and the lithium atom is accommodated at the 4-position. In contrast, the slim lithium piperidide (LIPIP) attacks the 3-position and thus unleashes the migration of iodine to this site in exchange for lithium. Neutralization, halogen/metal permutation, and carboxylation eventually produce 6-chloro-3-(trifluoromethyl)pyridine-2-carboxylic acid (**49**; 42 % overall yield) and 2-chloro-5-(trifluoromethyl)pyridine-3-carboxylic acid (**50**; 20 % overall yield; Scheme 17).[57]

 © 2006 Wiley-VCH Verlag GmbH & Co. KGaA, Weinheim

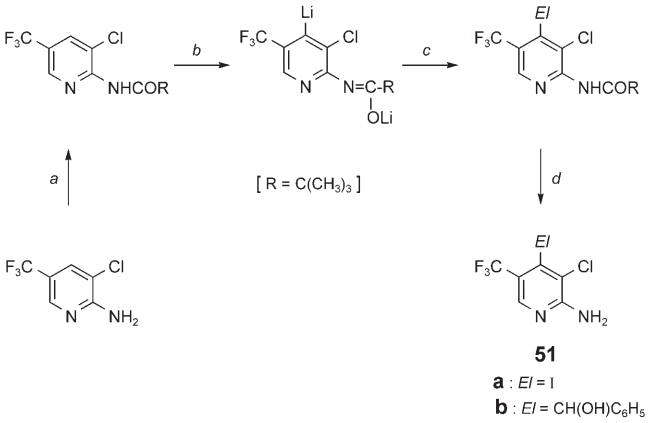


Scheme 16. The regiochemically exhaustive functionalization of 3-chloro-2-(trifluoromethyl)pyridine. Reagents and conditions: a) butyllithium and lithium 2-(dimethylamino)ethoxide in hexanes at −75 °C; b) 1. excess dry ice, 2. hydrochloric acid; c) LIDA in THF at −75 °C; d) elemental iodine; e) dilute hydrochloric acid; f) isopropylmagnesium chloride in THF at 0 °C.



Scheme 17. The regiochemically exhaustive functionalization of 2-chloro-5-(trifluoromethyl)pyridine. Reagents and conditions: a) LIDA in the presence of lithium *N*,*N*-diisopropylcarbamate (1.0 equiv) and lithium bromide (0.1 equiv) in THF at −75 °C; b) 1. excess dry ice, 2. hydrochloric acid; c) elemental iodine; d) LIDA in THF at −75 °C; e) dilute hydrochloric acid; f) isopropylmagnesium chloride in THF at −75 °C; g) lithium piperidide in THF at 0 °C; h) butyllithium in THF at −75 °C.

Smooth metalation of 2-amino-3-chloro-5-(trifluoromethyl)pyridine is achieved by using two equivalents of LIDA, whereby the amino group is acylated beforehand. After electrophilic substitution with elemental iodine or benzaldehyde, the pivaloyl protective group is hydrolytically removed to give 2-amino-3-chloro-4-iodo-5-(trifluoromethyl)pyridine (**51a**; 47 % overall yield) and 2-amino-3-chloro-4-(α-hydroxybenzyl)-5-(trifluoromethyl)pyridine (**51b**; 39 % overall yield; Scheme 18).[56]

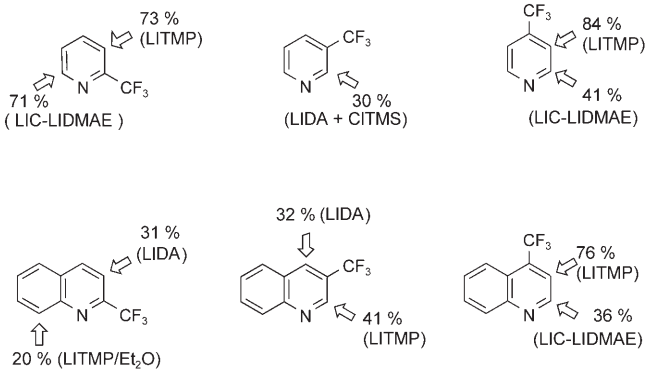


Scheme 18. The site-selective functionalization of 2-amino-3-chloro-5-(trifluoromethyl)pyridine. Reagents and conditions: a) pivaloyl chloride and pyridine in dichloromethane at +40 °C (reflux temperature); b) LIDA (2.0 equiv) in THF at −75 °C; c) 1. elemental iodine or benzaldehyde, 2. dilute hydrochloric acid; d) refluxing 20 % aqueous sulfuric acid.

The preceding half dozen substrates all contained one chlorine or bromine atom in addition to a CF_3 entity. This raises the question whether or not also simple (trifluoromethyl)pyridines can be efficaciously employed in metalation/derivatization sequences. The 3-isomer was problematic because of its extreme susceptibility to nucleophilic (het)aromatic substitution. Even under in situ trapping conditions using chlorotrimethylsilane, not more than 30 % of a product was isolated.[62] The resulting 3-trifluoromethyl-2-(trimethylsilyl)pyridine of course opens the door to subsequent functionalization as the silyl group can be readily replaced not only by a hydrogen atom, but also by bromo, iodo, and often also nitro substituents.[63] 2- and 4-(Trifluoromethyl)pyridine do not cause any problems and even offer reagent-controlled optional site selectivity. Whereas LITMP deprotonates cleanly the 3-positions, Caubère's base (LICLIDMAE) attacks the 6-positions exclusively (Scheme 19).[62] The same reagent lithiates 4-(trifluoromethyl)quinoline at the 2-position whereas LITMP metalates at the 3-position.[62] 3-(Trifluoromethyl)quinoline reacts with LITMP and LIDA (both in THF) at the 2- and 4-position, respectively, and 2-(trifluoromethyl)quinoline reacts with LITMP (in Et_2O) and with LIDA (in THF) at the 8- and 3-

 © 2006 Wiley-VCH Verlag GmbH & Co. KGaA, Weinheim

position, respectively (Scheme 19).[62] The products are usually formed in poor yields since complex formation between the organometallic intermediate and the metalating reagent apparently prevents the reaction from going to completion. From a practical point of view this represents no major drawback as the unconsumed starting material can be recovered and recycled almost quantitatively.

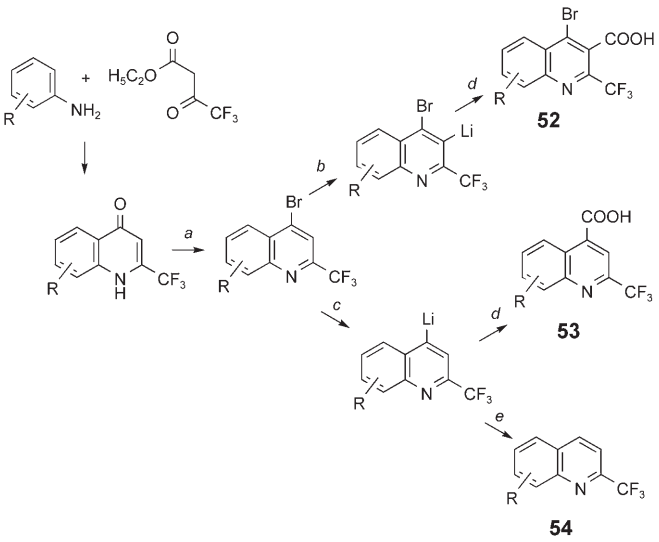


Scheme 19. The direct metalation and subsequent functionalization of 2-, 3-, and 4-trifluoromethyl-substituted pyridines and quinolines. Shown is the yield of the in situ trapping product 3-trifluoromethyl-2-(trimethylsilyl)pyridine (in the center of the upper row) and, in all other cases, the yields of the acids isolated after carboxylation. CITMS = chlorotrimethylsilane, LIDA = lithium diisopropylamide, LIC = butyllithium, LIDMAE = lithium 2-(dimethylamino)ethoxide, LITMP = lithium 2,2,6,6-tetramethylpiperidide.

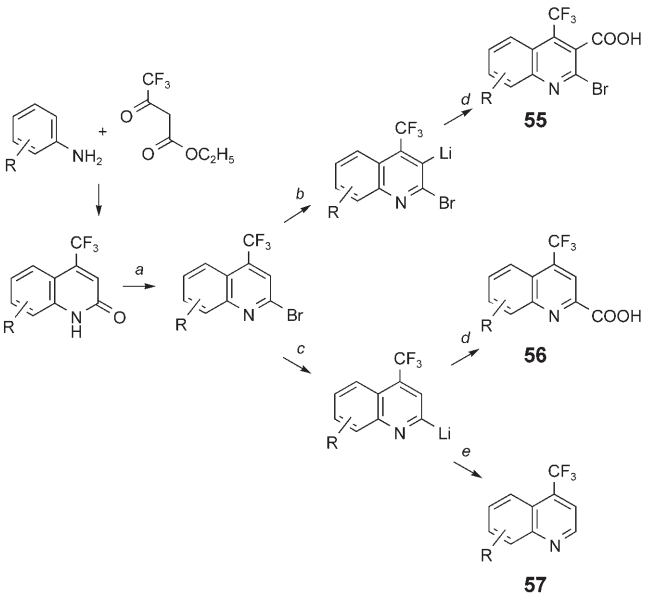
The three (trifluoromethyl)pyridines can be most conveniently prepared from the corresponding iodopyridines,[30] and 3-(trifluoromethyl)quinoline from 3-bromoquinoline by condensation with in situ generated (trifluoromethyl)copper.[23a,b] The two other isomers are readily accessible by the widely applicable and expedient procedure described below.

Ethyl 4,4,4-trifluoroacetoacetate readily combines with a variety of anilines (Scheme 20; R means any substituent) to afford an ethyl β-iminobutanoate ("anil" or rather the tautomeric ethyl β-anilinocrotonate) which can be thermally cyclized to a 2-trifluoromethyl-4(1*H*)-quinolinone. When heated with phosphoric tribromide, it forms a 4-bromo-2-(trifluoromethyl)quinoline, which may be either subjected to a hydrogen/metal permutation (with LIDA) or to a halogen/metal permutation (with butyllithium). Carboxylation of the intermediates produces 4-bromo-2-(trifluoromethyl)quinoline-3-carboxylic acids **52** and 2-(trifluoromethyl)quinoline-4-carboxylic acids **53**, respectively, whereas the treatment of the organometallic species with water gives the unfunctionalized heterocycles **54** (Scheme 20).[64]

The same ethyl 4,4,4-trifluoroacetoacetate and the same anilines can be put together differently by passing through an carboxanilide intermediate to afford the regioisomeric 4-trifluoromethyl-2(1*H*)quinolinones (Scheme 21).[65] In both series, the condensation and subsequent cyclization imply the loss of one molecule of water and one molecule of ethanol. It is solely the detailed reaction protocol that elicits the reaction mechanism. The latter defines the order of elimination and



Scheme 20. 2-Trifluoromethyl-4(1*H*)-quinolinones as precursors to a variety of 2-(trifluoromethyl)quinoline congeners. Reagents and conditions: a) phosphoric tribromide (phosphorus oxybromide) at +150 °C; b) LIDA in THF at −75 °C; c) butyllithium in THF at −75 °C; d) 1. excess dry ice, 2. hydrochloric acid; e) water.



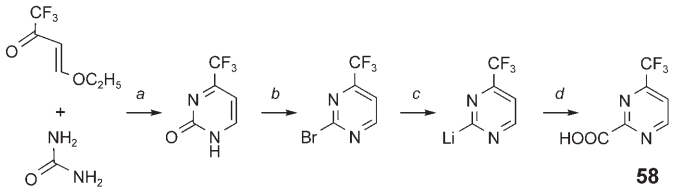
Scheme 21. 4-Trifluoromethyl-2(1*H*)-quinolinones as precursors to a variety of 4-(trifluoromethyl)quinoline congeners. Reagents and conditions: a) phosphoric tribromide (phosphorus oxybromide) at +150 °C; b) LIDA in THF at −75 °C; c) butyllithium in THF at −75 °C; d) 1. excess dry ice, 2. hydrochloric acid; e) water.

thus makes all the difference.[65,66] The 2-bromo-4-(trifluoromethyl)quinolines that are obtained with phosphoric tribromide mark again a bifurcation. The metalation route leads to 2-bromo-4-(trifluoromethyl)quinoline-3-carboxylic acids **55**, and the halogen/metal interconversion route leads to 4-(trifluoromethyl)quinoline-2-carboxylic acids **56** or 4-(trifluoromethyl)quinolines **57** (Scheme 21).[65,66]

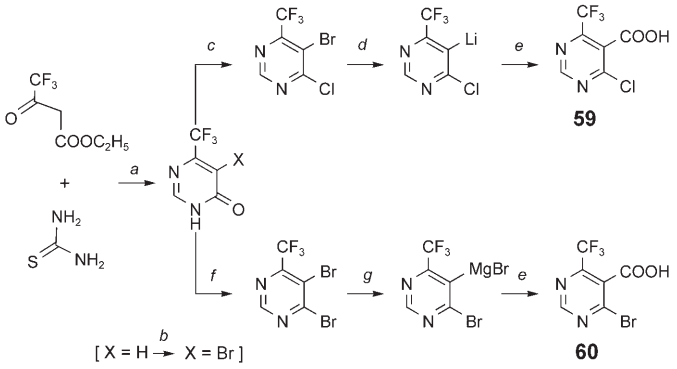
 © 2006 Wiley-VCH Verlag GmbH & Co. KGaA, Weinheim

6. Pyrimidines and Pyrazoles

As pyrimidines are susceptible to nucleophilic addition and subsequent dimerization or oligomerization,[67] metals have to be introduced with caution. Relatively clean halogen/metal permutation can be brought about with 2-bromo-4-(trifluoromethyl)pyrimidine,[68] 5-bromo-4-chloro-6-(trifluoromethyl)pyrimidine,[68] and 4,5-dibromo-6-(trifluoromethyl)-pyrimidine[68] by employing butyllithium or isopropylmagnesium chloride as the exchange reagent. 4-(Trifluoromethyl)-pyrimidine-2-carboxylic acid (**58**; 36%) and 4-chloro- or 4-bromo-6-(trifluoromethyl)pyrimidine-5-carboxylic acid (**59** and **60**; 73 and 54%, respectively) are isolated after carboxylation and neutralization (Schemes 22 and 23).[69]



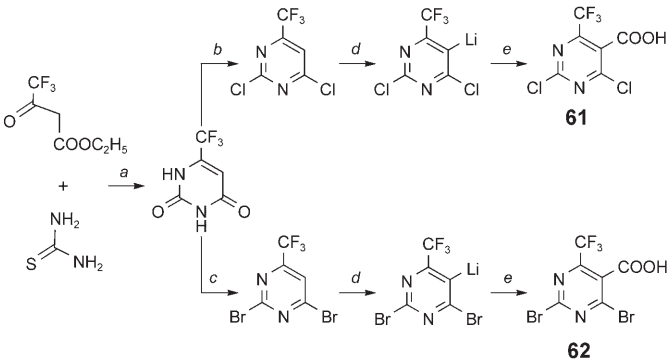
Scheme 22. Bromine/lithium permutation as the key step for the functionalization of 2-bromo-4-(trifluoromethyl)pyrimidine. Reagents and conditions: a) concentrated hydrochloric acid and ethanol for 48 h at +25 °C; b) phosphoric tribromide at +150 °C; c) butyllithium in toluene at −90 °C; d) 1. dry ice, 2. hydrochloric acid.



Scheme 23. Bromine/lithium permutation as the key step for the functionalization of 5-bromo-4-chloro-6-(trifluoromethyl)pyrimidine and 4,5-dibromo-6-(trifluoromethyl)pyrimidine. Reagents and conditions: a) excess hydrogen peroxide at +80 °C; b) bromine in acetic acid +80 °C; c) phosphorus trichloride at +120 °C; d) butyllithium in toluene at −75 °C; e) 1. dry ice, 2. hydrochloric acid; f) phosphoric tribromide at +150 °C; g) isopropylmagnesium chloride in Et_2O at 0 °C.

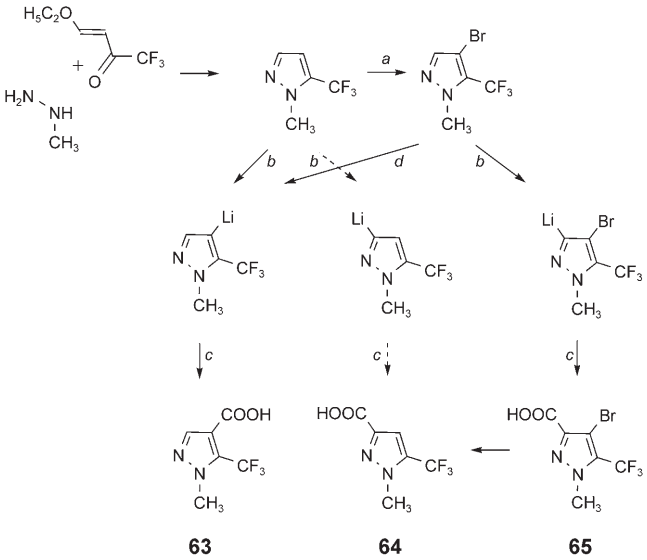
Doubly activated positions are acidic enough to undergo deprotonation already when treated with LITMP. Thus, 2,4-dichloro- and 2,4-dibromo-6-(trifluoromethyl)pyrimidine are smoothly lithiated to afford the acids **61** (79%) and **62** (89%) after carboxylation (Scheme 24).[69]

As previously with quinolines, bromine proves again to be a valuable auxiliary substituent with CF_3-bearing pyrazoles. 1-Methyl-5-(trifluoromethyl)pyrazole, laboriously prepared from 4-ethoxy-1,1,1-trifluoro-3-buten-2-one and methylhydrazine in 26% yield, reacts with butyllithium exclusively at the methyl group.[70] LIDA attacks simultaneously the 3- and 4-positions to give, after carboxylation, about 30% of the 1-methyl-5-(trifluoromethyl)pyrazole-4-carboxylic acid (**63**) and traces (ca. 4%) of the isomeric 3-carboxylic acid **64**. Both products can be selectively prepared by starting from 4-bromo-1-methyl-5-(trifluoromethyl)pyrazoles by halogen/metal permutation with *tert*-butyllithium and subsequent carboxylation (88% of **63**), or by LIDA-promoted metalation, carboxylation (70% of the brominated acid **65**), and subsequent reduction with zinc (93% of acid **64**) (Scheme 25).



Scheme 24. Hydrogen/metal permutation ("metalation") as the key step for the functionalization of 2,4-dichloro- and 2,4-dibromo-6-(trifluoromethyl)pyrimidine. Reagents and conditions: a) sodium ethoxide in refluxing ethanol for 24 h; b) phosphoric trichloride at +120 °C; c) phosphoric tribromide at +150 °C; d) LIDA in THF at −75 °C; e) 1. dry ice, 2. hydrochloric acid.

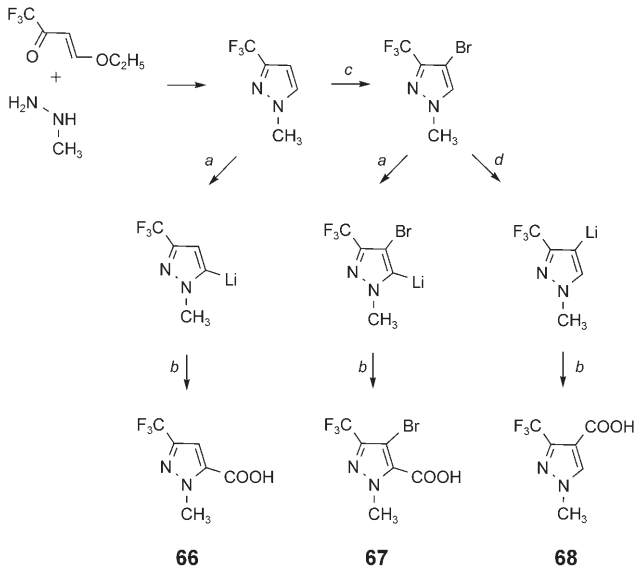
The same starting materials 4-ethoxy-1,1,1-trifluoro-3-buten-2-one and methylhydrazine give, under modified



Scheme 25. Selective functionalization of 1-methyl-5-(trifluoromethyl)-pyrazole at both the 3- and 4-positions. Reagents and conditions: a) elemental bromine and iron powder at +100 °C; b) LIDA in THF at −75 °C; c) 1. excess dry ice, 2. hydrochloric acid; d) *tert*-butyllithium in Et_2O at −75 °C; e) zinc powder in 10% aqueous sodium hydroxide at +25 °C.

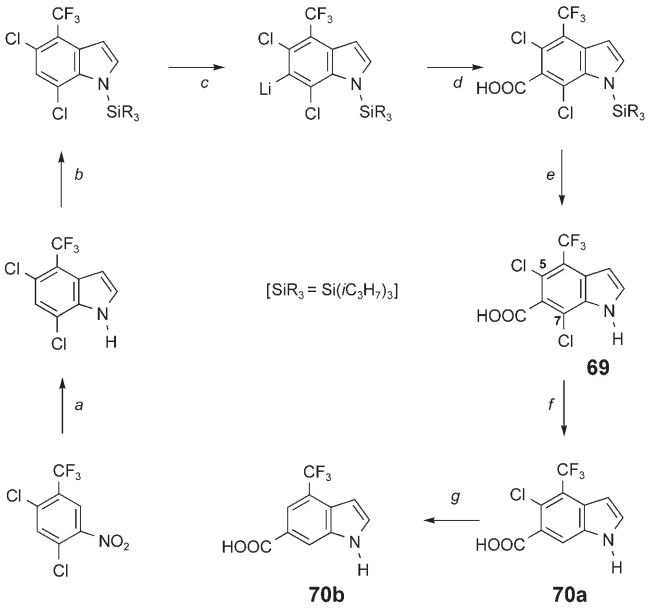
 © 2006 Wiley-VCH Verlag GmbH & Co. KGaA, Weinheim

reaction and work-up conditions, the isomeric 1-methyl-3-(trifluoromethyl)pyrazole, again in moderate yield (49%).[70] Consecutive treatment with LIDA and dry ice produces pure 1-methyl-3-(trifluoromethyl)pyrazole-5-carboxylic acid (**66**; 70%).[70] The same protocol, when applied to the bromination product 4-bromo-1-methyl-3-(trifluoromethyl)pyrazole, furnishes 4-bromo-1-methyl-3-(trifluoromethyl)pyrazole-5-carboxylic acid (**67**; 90%), which can of course be reduced to the bromine-free acid **66**.[70] Finally, the isomeric 1-methyl-3-(trifluoromethyl)pyrazole-4-carboxylic acid (**68**; 85%) is obtained when the 4-bromopyrazole is subjected to a halogen/metal permutation prior to carboxylation (Scheme 26).[70]



Scheme 26. Selective functionalization of 1-methyl-3-(trifluoromethyl)-pyrazole at both the 4- and 5-positions. Reagents and conditions: a) LIDA in THF at −75 °C; b) 1. excess dry ice, 2. hydrochloric acid; c) elemental bromine and iron powder at +100 °C; d) *tert*-butyllithium (2.0 equiv) in THF at −75 °C.

and directs the reagent (butyllithium) to the 6-position. Subsequent carboxylation and protodesilylation afford the 5,7-dichloro-4-(trifluoromethyl)indole-6-carboxylic acid (**69**; 67%). The reductive cleavage of the 7-chlorine atom can be accomplished by catalytic hydrogenation to give 5-chloro-4-(trifluoromethyl)indole-6-carboxylic acid (**70a**; 82%) whereas the elimination of the 5-chlorine atom requires zinc powder[75] in alkaline medium or in concentrated ammonia as the reductant to furnish 4-(trifluoromethyl)indole-6-carboxylic acid (**70b**; 96%; Scheme 27.[73b]



Scheme 27. Metalation as the key step for the functionalization of 5,7-dichloro-4-(trifluoromethyl)indole. Reagents and conditions: a) vinylmagnesium bromide (3.0 equiv); b) triisopropyl trifluoromethanesulfonate; c) butyllithium in THF at −75 °C; d) 1. excess dry ice, 2. hydrochloric acid; e) TBAF hydrate in THF at +25 °C; f) ammonium formate in methanol and in the presence of palladium on charcoal; g) zinc powder in aqueous sodium hydroxide.

7. Indoles

Indoles readily undergo metalation at the 2-position[71] and direct electrophilic substitution at the 3-position.[72] However, there are no universal methods for the selective introduction of substituents onto the six-membered aromatic ring. As a consequence, only few indole derivatives containing a heteroelement and a further functional group in the benzo part are documented so far. We have recently described all twelve fluoroindolecarboxylic acids that meet this criterion.[73] Now we turn to trifluoromethylated analogues.

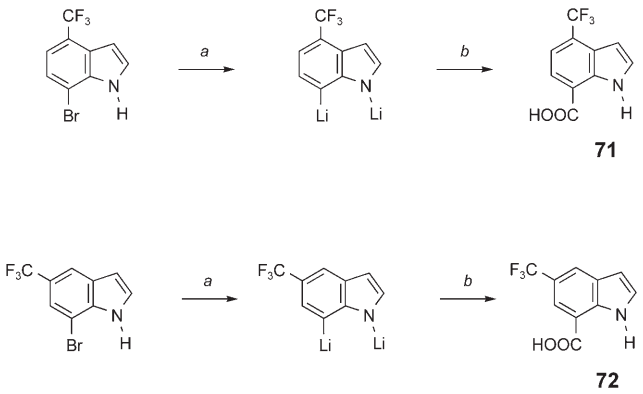
The most convenient synthetic entry to benzo-substituted indoles is the Bartoli cyclization[74] although the yields are generally only moderate if not poor. Thus, treatment of the commercial 2,4-dichloro-5-nitrobenzotrifluoride with an excess of vinylmagnesium bromide produces 5,7-dichloro-4-(trifluoromethyl)indole (84%) in a straightforward way. Attachment of the bulky triisopropylsilyl (TIPS) group protects the heterocyclic part against organometallic attack

One can avoid having to use N-protection if the lithiated intermediate is generated by halogen/metal permutation rather than metalation. It suffices to add 7-bromo-4- or 7-bromo-5-(trifluoromethyl)indole to two equivalents of butyllithium to get in each case an *N,C*-dilithio species which can be cleanly converted into the corresponding 4- or 5-(trifluoromethyl)indole-7-carboxylic acid (**71** and **72**; 61 and 78%, respectively; Scheme 28).[73b]

8. Conclusions and Outlook

The replacement of a hydrogen or halogen atom or of an amino, alkoxy, or alkyl group by a CF_3 group can modulate the physical, chemical, and biological properties of a lead compound in many ways, including alteration of the shape and size[76] of the reference substance, its acidity,[77] its dipole moments and polarizability,[78] its lipophilicity and transport behavior,[79] and its chemical and metabolic stability (or

© 2006 Wiley-VCH Verlag GmbH & Co. KGaA, Weinheim



Scheme 28. Halogen/metal permutation as the key step for the functionalization of 7-bromo-4- and 7-bromo-5-(trifluoromethyl)indole. Reagents and conditions: a) butyllithium in THF at 0 °C; b) 1. excess dry ice, 2. hydrochloric acid.

instability).[80] All this makes the CF_3 unit an attractive structural joker to tailor a specific activity profile.

As organofluorine compounds are not found abundantly in nature, all commercial products have to be made by chemists. One has to prepare them, either by introducing the desired number of fluorine atoms into a prefabricated carbon backbone or by adding the lacking molecular features, in particular functionality, into an inexpensive starting material that already contains the fluorine substituent. The second approach is uniquely advantageous if the objective is to create a great variety of new building blocks for life-science-oriented research.

The symbiotic combination of organofluorine and organometallic chemistry proves exceptionally profitable in this respect. Exhibiting a wider range of effects on neighboring group than individual fluorine atoms do, the trifluoromethyl group facilitates deprotonation not only at adjacent *ortho* positions but, owing to its "altruistic"[81] nature, also at remote *meta* or *para* positions. To pursue the synthetic goals by means of the organometallic approach offers a multitude of benefits.

- There is no regiochemical restriction. In applying the "toolbox methods",[49] any reactive site in a trifluoromethyl-bearing arene or heterocycle can be deactivated in order to direct the metalating reagent to a less reactive position.
- Carbon dioxide is arguably the most popular trapping reagent that is used to quench organometallic intermediates. However, dozens if not hundreds of other electrophiles could serve the same purpose[82] and thus make many new structural patterns readily available. Besides carboxylic acids and their derivatives, carboxaldehydes, ketones, alcohols, phenols, thiols, sulfinic and sulfonic acids, amines, azides, nitriles, phosphines, phosphinous, phosphinic, and phosphonic acids can thus be accessed to quote just a few of the most prominent product classes.
- Organometallic reagents can be easily and safely handled, and an inert atmosphere is generally required only for small-scale (< 50 mmol) reactions. It is rarely necessary to cool to below dry-ice temperatures as even *ortho*-lithiated fluoro-, chloro-, and bromoarenes prove to be amazingly thermoresistant when stabilized by additional electronegative substituents. (For example, 2-bromo-6-(trifluoromethoxy)phenyllithium[39] persists briefly up to a temperature of −25 °C.) As the reactions proceed rapidly and smoothly anyway, they can often be further simplified by contracting several steps into "one-pot" protocols.[83,84]

I am indebted to Drs. Frédéric Bailly, Carla Bobbio, A. Ginanneschi, Elena Marzi, Eric Masson, Marc Marull, Florence Mongin, Levente Ondi, Jean-Noël Volle and, in particular, Fabrice Cottet for outstanding and innovative contributions to the developing area of CF_3 chemistry. Our work was financially supported over a period of several years by the F. Hoffmann–LaRoche AG, Basel, and the Schweizerische Nationalfonds zur Förderung der wissenschaftlichen Forschung, Bern (grants 20-55'303-98, 20-63'584-00, and 20-100'336-02).

Received: February 2, 2006
Published online: July 18, 2006

[1] a) D. B. Harper, D. O'Hagan, *Nat. Prod. Rep.* **1994**, *11*, 123–133 [*Chem. Abstr.* **1994**, *121*, 204996]; b) D. O'Hagan, D. B. Harper, *J. Fluorine Chem.* **1999**, *100*, 127–133.
[2] S. Rozen in *Organo-Fluorine Compounds* (*Houben-Weyl: Methods of Organic Chemistry*, *Vol. E10a*, Thieme, Stuttgart, **2000**), pp. 167–187.
[3] K. Pohmer, A. Bulan in *Organo-Fluorine Compounds* (*Houben-Weyl: Methods of Organic Chemistry*, *Vol. E10a*, Thieme, Stuttgart, **2000**), pp. 305–320.
[4] M. Zupan in *Organo-Fluorine Compounds* (*Houben-Weyl: Methods of Organic Chemistry*, *Vol. E10a*, Thieme, Stuttgart, **2000**), pp. 265–269.
[5] G. G. Furin in *Organo-Fluorine Compounds* (*Houben-Weyl: Methods of Organic Chemistry*, *Vol. E10a*, Thieme, Stuttgart, **2000**), pp. 432–499.
[6] a) S. G. Lal, *J. Org. Chem.* **1993**, *58*, 2791–2796; b) D. P. Matthews, S. C. Miller, E. T. Jarvi, J. S. Sabol, J. R. McCarthy, *Tetrahedron Lett.* **1993**, *34*, 3057–3060; c) R. E. Banks, I. Sharif, R. G. Pritchard, *Acta Crystallogr. Sect. C* **1993**, *49*, 492–495 [*Chem. Abstr.* **1993**, *118*, 223259]; d) R. E. Banks, N. J. Lawrence, A. L. Popplewell, *J. Chem. Soc. Chem. Commun.* **1994**, 343–344; e) P. T. Nyffeler, S. G. Durón, M. D. Burkart, S. P. Vincent, C.-H. Wong, *Angew. Chem.* **2005**, *117*, 196–217; *Angew. Chem. Int. Ed.* **2005**, *44*, 192–212.
[7] a) W. Barnette, *J. Am. Chem. Soc.* **1984**, *106*, 452–454; b) S. H. Lee, J. Schwartz, *J. Am. Chem. Soc.* **1986**, *108*, 2445–2447.
[8] R. Mietchen, D. Peters in *Organo-Fluorine Compounds* (*Houben-Weyl: Methods of Organic Chemistry*, *Vol. E10a*, Thieme, Stuttgart, **2000**), pp. 95–158.
[9] a) G. A. Boswell, W. C. Ripka, *Org. React.* **1974**, *21*, 1–124; b) W. Dmowski in *Organo-Fluorine Compounds* (*Houben-Weyl: Methods of Organic Chemistry*, *Vol. E10a*, Thieme, Stuttgart, **2000**), pp. 321–394.
[10] a) M. Hudlicky, *Org. React.* **1988**, *35*, 513–637; b) M. H. Rock in *Organo-Fluorine Compounds* (*Houben-Weyl: Methods of Organic Chemistry*, *Vol. E10a*, Thieme, Stuttgart, **2000**), pp. 167–187.
[11] a) P. A. Messina, K. C. Mange, W. J. Middleton, *J. Fluorine Chem.* **1989**, *42*, 137–143; b) G. S. Lal, G. P. Pez, R. J. Pasaresi, F. M. Prozonic, *J. Org. Chem.* **1999**, *64*, 7048–7054; c) P. R. Singh, J. M. Shreeve, *Synthesis* **2002**, 2561–2578.

 © 2006 Wiley-VCH Verlag GmbH & Co. KGaA, Weinheim

[12] L. R. Subramanian, G. Siegemund in *Organo-Fluorine Compounds* (*Houben-Weyl: Methods of Organic Chemistry, Vol. E10a*, Thieme, Stuttgart, **2000**), pp. 548 – 596.
[13] L. M. Yagupolskii in *Organo-Fluorine Compounds* (*Houben-Weyl: Methods of Organic Chemistry, Vol. E10a*, Thieme, Stuttgart, **2000**), pp. 509 – 534.
[14] a) P. Gölitz, A. de Meijere, *Angew. Chem.* **1977**, *89*, 892 – 893; *Angew. Chem. Int. Ed. Engl.* **1977**, *16*, 854 – 855; b) V. Hartkopf, A. de Meijere, *Angew. Chem.* **1982**, *94*, 444; *Angew. Chem. Int. Ed. Engl.* **1982**, *21*, 443.
[15] a) P. Osswald, F. Müller, F. Steinhäuser (IG Farben), DRP 575593, **1931**; *Chem. Zbl.* **1933II**, 609; b) J. H. Simons, C. J. Lewis, *J. Am. Chem. Soc.* **1938**, *60*, 492 – 497; c) O. Scherer, *Angew. Chem.* **1939**, *52*, 457 – 459; d) W. A. Sheppard, C. M. Sharts, *Organic Fluorine Chemistry*, Benjamin, New York, **1969**, pp. 71 – 81; e) U. Horn, F. Mutterer, C. D. Weis, *Helv. Chim. Acta* **1976**, *59*, 190 – 211; f) G. A. Olah, J. T. Welch, Y. D. Vankar, M. Nojima, I. Kerekes, J. A. Olah, *J. Org. Chem.* **1979**, *44*, 3872 – 3881; g) R. Nishiyama, K. Fujikawa, I. Yokomichi, T. Yasuhiro, S. Nishimura (Ishihara Sangyo Kasei), Jpn. Kokai Tokkyo Koho JP 55085564, **1978** [*Chem. Abstr.* **1981**, *94*, 47146]; h) T. Fukuhara, N. Yoneda, *Chem. Lett.* **1993**, 509 – 512; i) L. M. Yagupolskii, D. V. Fedyuk, K. I. Petko, V. I. Troitskaya, V. I. Rudyk, V. V. Rudyuk, *J. Fluorine Chem.* **2000**, *106*, 181 – 187.
[16] a) W. R. Hasek, W. C. Smith, V. A. Engelhardt, *J. Am. Chem. Soc.* **1960**, *82*, 543 – 551; b) M. S. Raasch, *J. Org. Chem.* **1962**, *27*, 1406 – 1409; c) D. G. Martin, F. Kagan, *J. Org. Chem.* **1962**, *27*, 3164 – 3168; d) M. P. Mertens, S. E. Saheb, *J. Heterocycl. Chem.* **1965**, *2*, 491 – 491; e) Y. Kobayashi, I. Kumadaki, S. Taguchi, *Chem. Pharm. Bull.* **1969**, *17*, 2335 – 2339.
[17] a) M. Kuroboshi, K. Kanie, T. Hiyama, *Adv. Synth. Catal.* **2001**, *343*, 235 – 250; b) M. Shimizu, T. Hiyama, *Angew. Chem.* **2005**, *117*, 218 – 234; *Angew. Chem. Int. Ed.* **2005**, *44*, 214 – 231.
[18] M. Schlosser, B. Spahić, C. Le Van, *Helv. Chim. Acta* **1975**, *58*, 2586 – 2594.
[19] a) M. Kuroboshi, N. Yamada, Y. Tokebe, T. Hiyama, *Synlett* **1995**, 987 – 988; b) M. Shimizu, N. Yamada, Y. Takebe, T. Hata, M. Kuroboshi, T. Hiyama, *Bull. Soc. Chim. Jpn.* **1998**, *71*, 2903 – 2921.
[20] a) R. Krishnamurti, D. R. Bellew, G. K. S. Prakash, *J. Org. Chem.* **1991**, *56*, 984 – 989; b) J. Wiedemann, T. Heiner, G. Mloston, G. K. S. Prakash, G. A. Olah, *Angew. Chem.* **1998**, *110*, 880 – 881; *Angew. Chem. Int. Ed.* **1998**, *37*, 820 – 821; c) R. P. Singh, J. M. Shreeve, *Tetrahedron* **2000**, *56*, 7613 – 7632.
[21] a) B. Folléas, I. Marek, J.-F. Normant, L. Saint-Jalmes, *Tetrahedron* **2000**, *56*, 275 – 283; b) B. R. Langlois, T. Billard, *Synthesis* **2003**, 185 – 194.
[22] V. C. R. McLoughlin, I. Thrower, *Tetrahedron* **1969**, *25*, 5921 – 5940.
[23] a) Y. Kobayashi, I. Kumadaki, *Tetrahedron Lett.* **1969**, *10*, 4095 – 4096; b) Y. Kobayashi, I. Kumadaki, S. Sato, N. Hara, E. Chikami, *Chem. Pharm. Bull.* **1970**, *18*, 2334 – 2339; c) Y. Kobayashi, I. Kumadaki, A. Ohsawa, T. Yamada, *Chem. Pharm. Bull.* **1972**, *20*, 1839 – 1839; d) Y. Kobayashi, I. Kumadaki, Y. Hanzawa, *Chem. Pharm. Bull.* **1977**, *25*, 3009 – 3012; e) Y. Kobayashi, K. Yamamoto, T. Asai, M. Nakano, I. Kumadaki, *J. Chem. Soc. Perkin Trans. 1* **1980**, 2755 – 2762.
[24] N. V. Konderatenko, E. P. Vechirko, L. M. Yagupolskii, *Synthesis* **1980**, 932 – 933.
[25] a) K. Matsui, E. Tobita, M. Ando, K. Kondo, *Chem. Lett.* **1981**, 1719 – 1720; b) H. Suzuki, Y. Yoshida, A. Osuka, *Chem. Lett.* **1982**, 135 – 136; c) Q.-Y. Chen, S.-W. Wu, *J. Chem. Soc. Chem. Commun.* **1989**, 705 – 706.
[26] a) D. J. Burton, D. M. Wiemers, *J. Am. Chem. Soc.* **1985**, *107*, 5014 – 5015; b) D. M. Wiemers, D. J. Burton, *J. Am. Chem. Soc.* **1986**, *108*, 832 – 834.
[27] H. Urata, T. Fuchikami, *Tetrahedron Lett.* **1991**, *32*, 91 – 94.
[28] a) I. Ruppert, K. Schlich, W. Volbach, *Tetrahedron Lett.* **1984**, *25*, 2195 – 2198; b) G. Pawelke, *J. Fluorine Chem.* **1989**, *42*, 429 – 433.
[29] a) G. K. S. Prakash, R. Krishnamurti, G. A. Olah, *J. Am. Chem. Soc.* **1989**, *111*, 393 – 395; b) G. P. Stahly, D. R. Bell, *J. Org. Chem.* **1989**, *54*, 2873 – 2877; c) V. Broicher, D. Geffken, *Tetrahedron Lett.* **1989**, *30*, 5243 – 5244.
[30] F. Cottet, M. Schlosser, *Eur. J. Org. Chem.* **2002**, 327 – 330.
[31] E. Masson, E. Marzi, F. Cottet, C. Bobbio, M. Schlosser, *Eur. J. Org. Chem.* **2005**, 4393 – 4400.
[32] B. V. Kunshenko, L. A. Alekseeva, L. M. Yagupolskii, *Zh. Org. Khim.* **1972**, *8*, 830 – 834 [*Chem. Abstr.* **1972**, *77*, 19423].
[33] D. Bonnet-Delpon, M. Charpentier-Morize, R. Jacquot, *J. Org. Chem.* **1988**, *53*, 759 – 762.
[34] M. Kuroboshi, T. Hiyama, *Chem. Lett.* **1992**, 827 – 830.
[35] Z.-Y. Long, J.-X Duan, Y.-B. Lin, C. Y. Guo, Q.-Y. Chen, *J. Fluorine Chem.* **1996**, *78*, 177 – 181.
[36] A. H. El-Sagheer, E. E.-D. M. Salem, J. M. Mellor, *Tetrahedron Lett.* **2000**, *41*, 7383 – 7386.
[37] V. P. Le, P. R. Wells, *Aust. J. Chem.* **1992**, *45*, 1057 – 1061.
[38] F. Bailly, F. Cottet, M. Schlosser, *Synthesis* **2005**, 791 – 797.
[39] M. Schlosser, E. Castagnetti, *Eur. J. Org. Chem.* **2001**, 3991 – 3997.
[40] E. Masson, M. Schlosser, *Eur. J. Org. Chem.* **2005**, 4401 – 4405.
[41] F. Mongin, O. Desponds, M. Schlosser, *Tetrahedron Lett.* **1996**, *37*, 2767 – 2770.
[42] "*Topics in Drug Design and Discovery*": A. A. Patchett, R. P. Nargund, *Annu. Rep. Med. Chem.* **2000**, *35*, 289 – 298 [*Chem. Abstr.* **2000**, *133*, 317128].
[43] a) A. Daştan, U. Demir, M. Balcı, *J. Org. Chem.* **1994**, *59*, 6534 – 6538; b) A. Altundaş, A. Daştan, M. M. McKee, M. Balcı, *Tetrahedron* **2000**, *56*, 6115 – 6120; c) A. Daştan, E. Uzundumlu, M. Balcı, *Helv. Chim. Acta* **2002**, *85*, 2729 – 2739.
[44] F. Cottet, E. Castagnetti, M. Schlosser, *Synthesis* **2005**, 798 – 803.
[45] a) J. T. B. H. Jastrzebski, G. van Koten, K. Goubitz, C. Arlen, M. Pfeffer, *J. Organomet. Chem.* **1983**, *246*, C75-C79; b) C. Kiefl, A. Mannscheck, *Synthesis* **1995**, 1033 – 1037.
[46] a) R. L. Gay, C. R. Hauser, *J. Am. Chem. Soc.* **1967**, *89*, 2297 – 2303; b) M. Julia, M. Duteil, J. Y. Lallemand, *J. Organomet. Chem.* **1975**, *102*, 239 – 243; c) Z. Horii, Y. Matsumoto, T. Momose, *Chem. Pharm. Bull.* **1971**, *19*, 1245 – 1256.
[47] M. Schlosser, *Eur. J. Org. Chem.* **2001**, 3975 – 3984, especially 3977–3978.
[48] a) M. Schlosser, S. Strunk, *Tetrahedron Lett.* **1984**, *25*, 741 – 744; b) M. Schlosser, H. Geneste, *Chem. Eur. J.* **1998**, *4*, 1969 – 1973.
[49] M. Schlosser, *Angew. Chem.* **2005**, *117*, 380 – 398; *Angew. Chem. Int. Ed.* **2005**, *44*, 376 – 393.
[50] M. Schlosser, *ACS Symp. Ser.* **2005**, *911*, 218 – 231.
[51] E. Marzi, C. Bobbio, F. Cottet, M. Schlosser, *Eur. J. Org. Chem.* **2005**, 2116 – 2123.
[52] a) I. F. Tupytsin, N. K. Seminova, *Tr. Gos. Inst. Prikl. Khim.* **1962**, *49*, 120 – 132 [*Chem. Abstr.* **1964**, *60*, 6721c]; b) J. A. Zoltewicz, C. L. Smith, *J. Am. Chem. Soc.* **1967**, *89*, 3358 – 3359; c) J. A. Zoltewicz, G. Grahe, C. L. Smith, *J. Am. Chem. Soc.* **1969**, *91*, 5501 – 5505; d) I. F. Tupitsyn, N. N. Zatspina, A. V. Kirova, Y. L. Kaminskii, A. G. Ivanenko, *Reakts. Sposobn. Org. Soedin.* **1973**, *10*, 143 – 162 [*Chem. Abstr.* **1973**, *79*, 114928v].
[53] P. Gros, Y. Fort, P. Caubère, *J. Chem. Soc. Perkin Trans. 1* **1998**, 1685 – 1689.
[54] a) G. Katsoulos, S. Takagishi, M. Schlosser, *Synlett* **1992**, 360 – 362; b) M. Schlosser, F. Faigl, L. Franzini, H. Geneste, G. Katsoulos, G.-f. Zhong, *Pure Appl. Chem.* **1994**, *66*, 1439 – 1446; c) F. Mongin, R. Maggi, M. Schlosser, *Chimia* **1996**, *50*, 650 – 652.
[55] M. Schlosser in *Organometallics in Synthesis: A Manual* (Ed.: M. Schlosser), 2nd ed., Wiley, Chichester, **2002**, pp. 1 – 352, especially 253–259.
[56] F. Cottet, M. Marull, F. Mongin, D. Espinosa, M. Schlosser, *Synthesis* **2004**, 1619 – 1624.

© 2006 Wiley-VCH Verlag GmbH & Co. KGaA, Weinheim

[57] F. Cottet, M. Schlosser, *Eur. J. Org. Chem.* **2004**, 3793 – 3798.
[58] F. Cottet, M. Schlosser, *Tetrahedron* **2004**, *60*, 11 869 – 11 874.
[59] M. Schlosser, T. Rausis, *Eur. J. Org. Chem.* **2004**, 1018 – 1024.
[60] T. Iida, T. Wada, K. Tomimoto, T. Mase, *Tetrahedron Lett.* **2001**, *42*, 4841 – 4844.
[61] A. Inoue, K. Kitagawa, H. Shinokubo, K. Oshima, *J. Org. Chem.* **2001**, *66*, 4333 – 4339.
[62] M. Schlosser, M. Marull, *Eur. J. Org. Chem.* **2003**, 1567 – 1575.
[63] C. Eaborn, *J. Organomet. Chem.* **1975**, *100*, 43 – 57.
[64] M. Marull, M. Schlosser, *Eur. J. Org. Chem.* **2003**, 1576 – 1588.
[65] O. Lefebvre, M. Marull, M. Schlosser, *Eur. J. Org. Chem.* **2003**, 2115 – 2121.
[66] M. Marull, O. Lefebvre, M. Schlosser, *Eur. J. Org. Chem.* **2004**, 54 – 63.
[67] T. J. Kress, *J. Org. Chem.* **1979**, *44*, 2081 – 2082.
[68] L. Ondi, O. Lefebvre, M. Schlosser, *Eur. J. Org. Chem.* **2004**, 3714 – 3718.
[69] M. Schlosser, O. Lefebvre, L. Ondi, *Eur. J. Org. Chem.* **2006**, 1593 – 1598.
[70] M. Schlosser, J.-N. Volle, F. Leroux, K. Schenk, *Eur. J. Org. Chem.* **2002**, 2913 – 2920.
[71] a) D. A. Shirley, P. A. Roussel, *J. Am. Chem. Soc.* **1953**, *75*, 375 – 378; b) R. J. Sundberg, H. R. Russel, *J. Org. Chem.* **1973**, *38*, 3324 – 3330; c) R. J. Sundberg, R. L. Parton, *J. Org. Chem.* **1976**, *41*, 163 – 165; d) I. Hasan, E. R. Marinelli, L.-C. C. Lin, F. W. Fowler, A. B. Levy, *J. Org. Chem.* **1981**, *46*, 157 – 164.
[72] J. A. Joule, K. Mills, G. F. Smith, *Heterocyclic Chemistry*, 3rd ed., Stanley Thornes, Cheltenham, **1998**, pp. 307 – 320.
[73] a) M. Schlosser, A. Ginanneschi, F. Leroux, manuscript in preparation; b) A. Ginanneschi, Dissertation, Ecole Polytechnique Fédérale, Lausanne, **2005**.
[74] G. Bartoli, G. Palmieri, *Tetrahedron Lett.* **1989**, *30*, 2129 – 2132.
[75] a) P. J. Montagne, *Recl. Trav. Chim. Pays-Bas* **1920**, *39*, 483 – 491, 492 – 494; b) M. Tashiro, G. Fukata, *J. Org. Chem.* **1977**, *42*, 835 – 838; c) L. B. Fertel, N. J. O'Reilly, K. M. Callaghan, *J. Org. Chem.* **1993**, *58*, 261 – 263; d) C. Bobbio, M. Schlosser, *J. Org. Chem.* **2005**, *70*, 3039 – 3045.
[76] a) M. Schlosser, D. Michel, *Tetrahedron* **1996**, *52*, 99 – 108; b) M. Schlosser in *Enantiocontrolled Synthesis of Fluoroorganic Compounds: Stereochemical Challenges and Biomedicinal Targets* (Ed.: V. A. Soloshonok), Wiley, Chichester, **1999**, pp. 613 – 659; c) F. Grein, *J. Phys. Chem. A* **2002**, *106*, 3823 – 3827; d) F. Leroux, *ChemBioChem* **2004**, *5*, 644 – 649.
[77] M. Schlosser, *Angew. Chem.* **1998**, *110*, 1538 – 1556; *Angew. Chem. Int. Ed.* **1998**, *37*, 1496 – 1513.
[78] J. D. Dunitz, *ChemBioChem* **2004**, *5*, 614 – 621.
[79] a) B. E. Smart in *Organofluorine Chemistry: Principles and Commercial Applications* (Eds.: R. E. Banks, B. E. Smart, J. C. Tatlow), Plenum, New York, **1994**, pp. 57 – 88, especially 64–65; b) J. C. Biffinger, H. W. Kim, S. G. DiMagno, *ChemBioChem* **2004**, *5*, 622 – 627.
[80] a) F. L. M. Pattison, R. L. Buchanan, F. H. Dean, *Can. J. Chem.* **1965**, *43*, 1700 – 1713; b) J. Fried, D. K. Mitra, M. Nagarajan, M. M. Mehrota, *J. Med. Chem.* **1980**, *23*, 234 – 237; c) P. H. Stern, Y. Tanaka, H. F. DeLuca, N. Ikekawa, Y. Kobayashi, *Mol. Pharmacol.* **1981**, *20*, 460 – 462 [*Chem. Abstr.* **1982**, *96*, 46 392q]; d) K. Bannai, T. Toru, T. Oba, T. Tanaka, N. Okamura, K. Watanabe, A. Hazato, S. Kurozumi, *Tetrahedron* **1983**, *39*, 3807 – 3819; e) J. Fried, E. A. Hallinan, M. J. Szewedo, *J. Am. Chem. Soc.* **1984**, *106*, 3871 – 3872; f) J. G. Dingwall, *Pestic. Sci.* **1994**, *41*, 259 – 267 [*Chem. Abstr.* **1994**, *212*, 127 765a]; lecture held as part of the conference *Fluorine in the Service of Man*, University of Manchester, January 9 – 11, **1995**; g) T. Nakano, M. Makino, Y. Morizawa, Y. Matsumura, *Angew. Chem.* **1996**, *108*, 1082 – 1084; *Angew. Chem. Int. Ed. Engl.* **1996**, *35*, 1019 – 1021; h) S. G. DiMagno, P. H. Dussault, J. A. Schultze, *J. Am. Chem. Soc.* **1996**, *118*, 5312 – 5313; i) P. H. Buist, K. A. Alexopoulos, B. Behrouzian, B. Dawson, B. Black, *J. Chem. Soc. Perkin Trans. 1* **1997**, 2617 – 2624.
[81] a) M. Schlosser, F. Mongin, J. Porwisiak, W. Dmowski, H. H. Büker, N. M. M. Nibbering, *Chem. Eur. J.* **1998**, *4*, 1281 – 1286; b) E. Marzi, F. Mongin, A. Spitaleri, M. Schlosser, *Eur. J. Org. Chem.* **2001**, 2911 – 2915.
[82] M. Schlosser, J. Gorecka, E. Castagnetti, *Eur. J. Org. Chem.* **2003**, 452 – 562.
[83] F. Faigl, M. Schlosser, *Tetrahedron Lett.* **1991**, *32*, 3369 – 3370.
[84] M. Schlosser, G.-f. Zhong, *Tetrahedron Lett.* **1993**, *34*, 5441 – 5444.

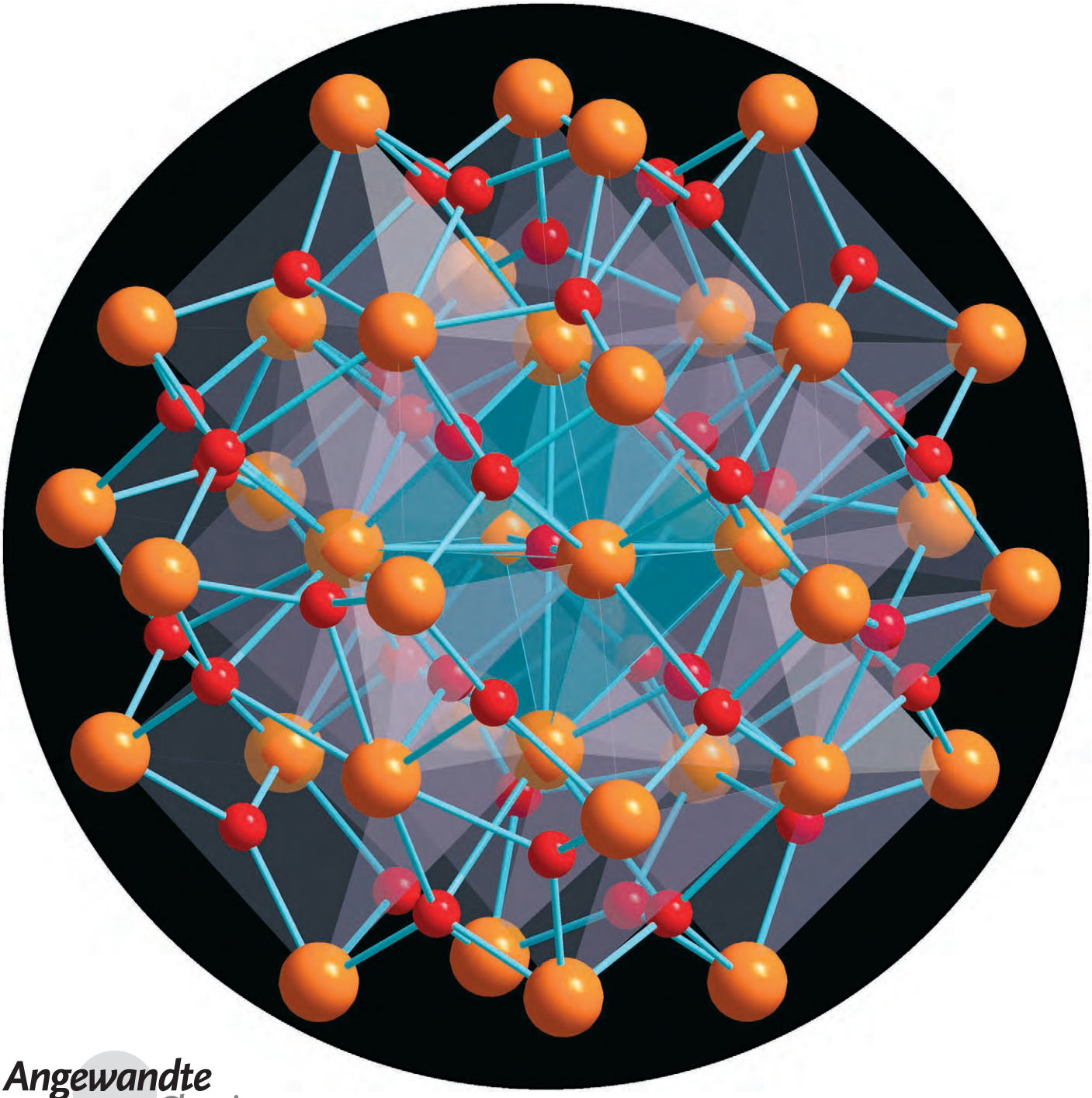
 © 2006 Wiley-VCH Verlag GmbH & Co. KGaA, Weinheim

Cluster Compounds

DOI: 10.1002/anie.200601675

From a Bismuth Oxido Diketonate to a Giant Bismuth Oxido Cluster**

Evgeny V. Dikarev, Haitao Zhang, and Bo Li*



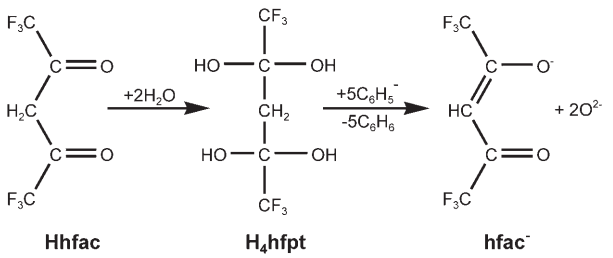
WILEY InterScience DISCOVER SOMETHING GREAT

© 2006 Wiley-VCH Verlag GmbH & Co. KGaA, Weinheim

Homo- and heterometallic oxido alkoxides, diketonates, and carboxylates have attracted considerable attention as precursors for oxide-based materials.[1] Structurally well defined and properly functionalized metal oxido clusters are also used as nanoscale building blocks in the assembly of organic–inorganic hybrid networks.[2] A number of oxido-bridged units obtained from the hydrolysis of medicinally important bismuth compounds (nitrate, salicylate, citrate)[3] indicate that polyoxidobismuth species play an important role in pharmaceuticals as well. Major pathways for introduction of the oxido groups during cluster formation include microhydrolysis, ether elimination, and oxidation.[1c,4] Several bismuth oxido clusters $[Bi_mO_n]^{(3m-2n)+}$ with surface capping ligands such as hydroxide,[5] alkoxides,[6] aryl oxides,[7] siloxides,[8] carboxylates,[9] and phosphonates[10] were isolated recently by using solvolytic methods. In addition, a few heterometallic bismuth compounds in which metal atoms are connected through oxido bridges[8b,11] have also been synthesized by similar approaches.

The common problem associated with hydrolytic pathways is the inherent difficulty of composition control,[4,12] which often results in the formation of mixtures of different species. Herein we report on a new synthetic approach to overcome this problem. We attempted to obtain bismuth oxido clusters using diketonate co-ligands that are known to serve as modifiers to prevent hydrolysis of oxido species[13] and as surface capping groups to stabilize nanoscale building blocks.[14] For this purpose we proposed controlled introduction of oxido centers by using a "non-innocent" fluorinated tetraol, a deprotonated form of which has been hypothesized[15] to generate both oxido and diketonate (β-dik) ligands on decomposition. Thus, the first bismuth oxido diketonate complex $[Bi_9O_7(\beta\text{-dik})_{13}]$ (**1**) was isolated and fully characterized. Moreover, its subsequent aggregation in solution led to a remarkable nanosized molecule, $[Bi_{38}O_{45}(\beta\text{-dik})_{24}]$ (**2**), which contains the largest homometallic bismuth oxido cluster reported to date.

The fluorinated bis(*gem*-diol) 1,1,1,5,5,5-hexafluoropentane-2,2,4,4-tetraol (H_4hfpt) can be instantly obtained[15] by hydration of hexafluoroacetylacetone (Hhfac). We have shown that in the presence of a proton acceptor H_4hfpt acts as a controlled source of both diketonate and oxido groups by undergoing facile cleavage of two C–O bonds (Scheme 1). The first bismuth oxido diketonate was obtained in quantitative yield by reaction of triphenylbismuth with H_4hfpt and Hhfac [Eq. (1)].



Scheme 1.

$$18\,[Bi(C_6H_5)_3] + 7\,H_4\text{hfpt} + 19\,\text{Hhfac} \rightarrow 2\,[Bi_9O_7(\text{hfac})_{13}]\,(\mathbf{1}) + 54\,C_6H_6 \quad (1)$$

The composition of **1** was established by elemental analysis and single-crystal X-ray structure determination. X-ray powder diffraction analysis confirmed the purity of the bulk polycrystalline reaction product and its structural identity with the single crystals.

The crystal structure of **1**[16] features bismuth atoms in two distinctly different chemical and coordination environments (Figure 1). Six bismuth atoms form a slightly distorted octahedron, seven faces of which are centered by oxido groups. The eighth face is unsymmetrically capped with an oxygen atom from one of the diketonate ligands. Three of the

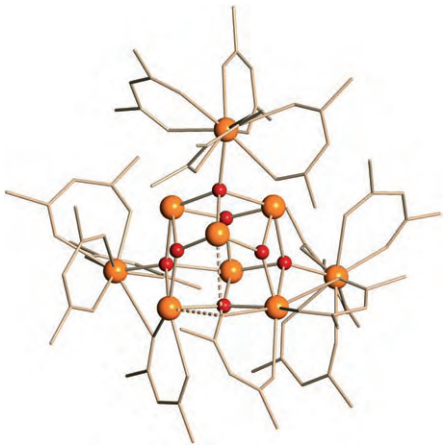


Figure 1. Molecular structure of $[Bi_9O_7(\text{hfac})_{13}]$ (**1**). Only the core bismuth (orange) and oxygen atoms (red) are shown as balls. Fluorine and hydrogen atoms of the β-diketonate ligands are omitted for clarity. Bond lengths [Å]: Bi–O(oxido) 2.091(4)–2.485(4), Bi–O(hfac) 2.193(4)–2.831(5) (see Supporting Information for further details).

seven oxido groups centering the octahedron act as μ_4-bridges to which $Bi(\text{hfac})_x$ ($x = 3$ or 4) arms are attached. This structure directly resembles the oxido alkoxide and oxido silanolate clusters $[Bi_6(\mu_3\text{-O})_4\{\mu_3\text{-OBi(OR)}_4\}_3(\mu_3\text{-OR})]$ ($R = C_6F_5$,[6] $SiMe_3$[8b]) described recently. However, the latter are slightly different in that the eighth face of the Bi_6 core is centered by a μ_3-OR group, and all three arms have four OR ligands coordinated to the bismuth atom.

The structure of **1** helps to explain the behavior of this nonanuclear compound in solution. The molecule remains

[*] Prof. Dr. E. V. Dikarev, H. Zhang, B. Li
Department of Chemistry
University at Albany
Albany, NY 12222 (USA)
Fax: (+1) 518-442-3462
E-mail: dikarev@albany.edu

[**] This work was supported by the American Chemical Society Petroleum Research Fund 44770-AC3.

Supporting information for this article is available on the WWW under http://www.angewandte.org or from the author.

 © 2006 Wiley-VCH Verlag GmbH & Co. KGaA, Weinheim

intact in noncoordinating solvents such as dichloromethane (low solubility) according to NMR spectroscopy (Figure 2a,b) and mass spectrometry. Single peaks observed for both ^{1}H and ^{19}F in the NMR spectra of **1** indicate that the

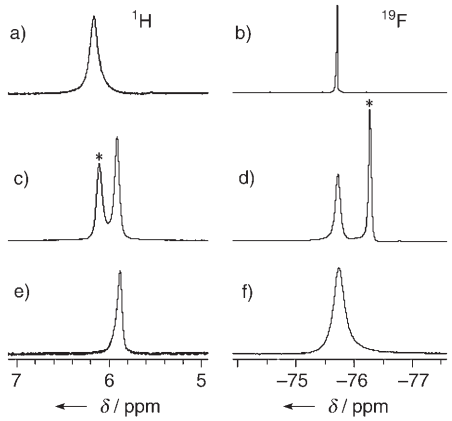


Figure 2. ^{1}H and ^{19}F NMR spectra of **1** in CD_2Cl_2 (a,b), **1** in $(CD_3)_2CO$ (c,d; peaks marked with an asterisk correspond to $[Bi(hfac)_3]$, and **2** in $(CD_3)_2CO$ (e,f) at room temperature.

diketonate ligands exhibit fluxional behavior in solution at room temperature. The solubility of **1** in CH_2Cl_2 is essentially increased by addition of a small amount of Hhfac to the solution, and single crystals of **1** can be grown therefrom by layering with hexanes. On the other hand, in coordinating solvents (acetone, THF, acetonitrile) dissociation of the nonanuclear core molecule occurs, as evidenced by the appearance of two peaks in both ^{1}H and ^{19}F NMR spectra (Figure 2c,d). One peak in each spectrum was identified as corresponding to the solvated form of $[Bi(hfac)_3]$. Mass spectrometric investigation of the acetone solution containing **1** revealed a series of new peaks centered around 5030, 5467, 5903, 6374, 6749, 7250, 7658, and 8062 Da (Figure 3a). These peaks indicate aggregation processes of the Bi–oxido core in acetone, since the molecular mass of the initial $[Bi_9O_7(hfac)_{13}]$ cluster is 4684. After one week, the single group of peaks observed around 12230 Da in the mass spectrum of the above

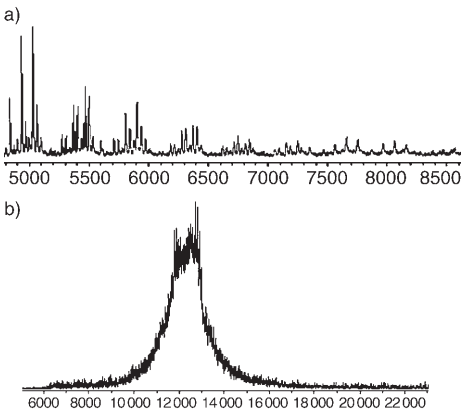


Figure 3. Negative-ion MALDI-TOF mass spectra of **1** in acetone a) immediately on dissolution and b) after one week.

solution (Figure 3b) confirmed that a high-nuclearity species was formed.

The crystal structure of the new oxido diketonate product **2**[16] obtained from solution revealed a giant $[Bi_{38}O_{45}]^{24+}$ core cluster with 24 diketonate groups located on its surface (Figure 4a). The nearly spherical molecule of **2** has a size of

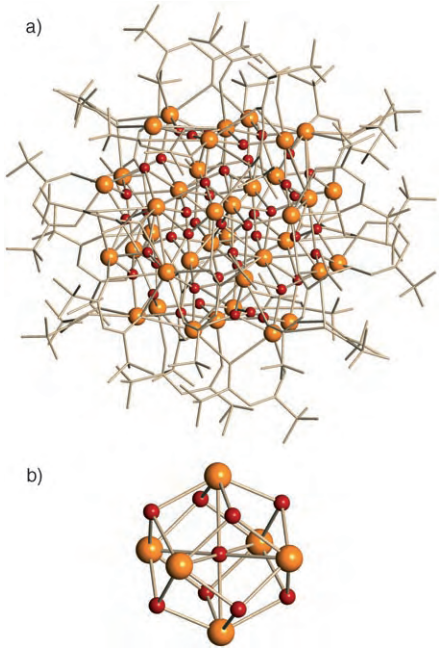


Figure 4. a) Molecular structure of $[Bi_{38}O_{45}(hfac)_{24}]$ (**2**). Only the core bismuth (orange) and oxygen atoms (red) are shown as balls. b) Bi_6O_9 core unit. Bond lengths [Å]: Bi–O(μ_6) 2.52–2.62, Bi–O(μ_4) 2.27–2.47 (see Supporting Information for further details).

about 21 Å and contains the largest known homometallic bismuth oxido cluster. A unit with more bismuth atoms was recently found[8b] in the heterometallic cluster $[Bi_{50}Na_2O_{64}(OH)_2]^{22+}$. Within the bismuth oxido core a central Bi_6 unit can be identified whose metal atoms are connected only to oxido centers. All other 32 bismuth atoms are coordinated to both oxido and diketonate ligands, though eight of those that are directly attached to the μ_4-O atoms of the central core make relatively long (2.69–3.08 Å) contacts with capping groups. The central unit consists of an octahedron of bismuth atoms, each face of which is centered by an oxido ligand (Figure 4b). In addition, a μ_6-O atom, which is unique for homometallic bismuth oxido clusters, resides at the center of the octahedron, on an inversion center. The molecule of **2** has no other symmetry elements. The surface diketonate ligands exhibit some degree of disorder; nevertheless, they could be successfully refined, and the whole structure is thus well ordered.

Alternatively, the structure of the bismuth oxido cluster in **2** can be described as assembled from 13 octahedral edge-sharing Bi_6 units. The arrangement of bismuth atoms is close to an fcc structure in which all of the tetrahedral and some of the octahedral voids are occupied by oxygen atoms. While the basic structural motif in **2** resembles that in β-Bi_2O_3, the

 © 2006 Wiley-VCH Verlag GmbH & Co. KGaA, Weinheim

individual Bi–O bond lengths and Bi-O-Bi bond angles show some significant deviations.

Aggregation of the bismuth oxido cluster occurs on dissociation of $[Bi(hfac)_3]$ from **1** according to Equation (2).

$$45\,[Bi_9O_7(hfac)_{13}] \rightarrow 7\,[Bi_{38}O_{45}(hfac)_{24}]\,(\mathbf{2}) + 139\,[Bi(hfac)_3] \qquad (2)$$

Integration of the NMR spectrum in THF gave a proton ratio for **2**:$[Bi(hfac)_3]$ of 29.8:70.2 (the theoretical value is 28.7:71.3). Such ligand redistribution in polar solvents is a well-known phenomenon[17] for heteroleptic metal β-diketonates. While **2** is insoluble in noncoordinating and aromatic solvents, the striking feature of this giant molecule is its solubility without decomposition in coordinating solvents such as acetone, THF, acetonitrile, DMSO, alcohols, and diethyl ether. Oxido diketonate **2** can be recrystallized from these solutions, for which both ^1H and ^{19}F NMR spectra show single peaks (Figure 2e,f), and the mass spectrum is similar to that shown in Figure 3b.

In conclusion, we have demonstrated that a fluorinated tetraol indeed functions as a source of both diketonate and oxido groups in the presence of a base acting as an irreversible proton sink. This synthetic pathway has been confirmed by the isolation of the first bismuth oxido diketonate $[Bi_9O_7(hfac)_{13}]$ in quantitative yield. Our preliminary results indicate that oxido diketonates of other metals can be obtained by this approach. Importantly, the technique can also be applied to the synthesis of heterometallic oxido diketonates that are immediate precursors for functional oxide materials. We found that in coordinating solvents the nonanuclear oxido diketonate undergoes dissociation of $[Bi(hfac)_3]$ followed by aggregation into the giant oxido cluster $[Bi_{38}O_{45}(hfac)_{24}]$. The latter could serve as a model for studying the chemistry of bismuth oxide nanoparticles. Moreover, the assembly of this molecule shows the way for construction of other nanosized oxido clusters of metals that exhibit a similar coordination environment in their oxido compounds, such as lead and the lanthanides.

Received: April 28, 2006
Revised: May 25, 2006
Published online: July 26, 2006

Keywords: bismuth · cluster compounds · O ligands · oxido ligands

[1] a) L. G. Hubert-Pfalzgraf, *J. Mater. Chem.* **2004**, *14*, 3113; b) L. G. Hubert-Pfalzgraf, *Inorg. Chem. Commun.* **2003**, *6*, 102; c) V. G. Kessler, *Chem. Commun.* **2003**, 1213; d) N. Ya. Turova, E. P. Turevskaya, V. G. Kessler, M. I. Yanovskaya, *J. Sol-Gel Sci. Technol.* **1994**, *2*, 17.

[2] a) G. Fornasieri, L. Rozes, S. Le Calve, B. Alonso, D. Massiot, M. N. Rager, M. Evain, K. Boubekeur, C. Sanchez, *J. Am. Chem. Soc.* **2005**, *127*, 4869; b) U. Schubert, *J. Sol-Gel Sci. Technol.* **2004**, *31*, 19; c) F. R. Kogler, M. Jupa, M. Puchberger, U. Schubert, *J. Mater. Chem.* **2004**, *14*, 3133.

[3] a) K. H. Thompson, C. Orvig, *Science* **2003**, *300*, 936; b) G. G. Briand, N. Burford, *Chem. Rev.* **1999**, *99*, 2601; c) Z. Guo, P. J. Sadler, *Angew. Chem.* **1999**, *111*, 1610; *Angew. Chem. Int. Ed.* **1999**, *38*, 1512; d) P. J. Sadler, H. Li, H. Sun, *Coord. Chem. Rev.* **1999**, *185–186*, 689.

[4] N. Ya. Turova, *Russ. Chem. Rev.* **2004**, *73*, 1041.

[5] J. H. Thurston, D. C. Swenson, L. Messerle, *Chem. Commun.* **2005**, 4228.

[6] K. H. Whitmire, S. Hoppe, O. Sydora, J. L. Jolas, C. M. Jones, *Inorg. Chem.* **2000**, *39*, 85.

[7] L. Liu, L. N. Zakharov, A. L. Rheingold, T. A. Hanna, *Chem. Commun.* **2004**, 1472.

[8] a) D. Mansfeld, M. Mehring, M. Schürmann, *Angew. Chem.* **2005**, *117*, 250; *Angew. Chem. Int. Ed.* **2005**, *44*, 245; b) M. Mehring, D. Mansfeld, S. Paalasmaa, M. Schürmann, *Chem. Eur. J.* **2006**, *12*, 1767.

[9] V. V. Sharutin, I. V. Egorova, O. K. Sharutina, T. K. Ivanenko, N. Yu. Adonin, V. F. Starichenko, M. A. Pushilin, A. V. Gerasimenko, *Russ. J. Coord. Chem.* **2005**, *31*, 2.

[10] M. Mehring, M. Schürmann, *Chem. Commun.* **2001**, 2354.

[11] a) J. W. Pell, W. C. Davis, H. C. zur Loye, *Inorg. Chem.* **1996**, *35*, 5754; b) S. Parola, R. Papiernik, L. G. Hubert-Pfalzgraf, S. Jagner, M. Hakansson, *J. Chem. Soc. Dalton Trans.* **1997**, 4631; c) S. Parola, R. Papiernik, L. G. Hubert-Pfalzgraf, C. Bois, *J. Chem. Soc. Dalton Trans.* **1998**, 737; d) J. H. Thurston, K. H. Whitmire, *Inorg. Chem.* **2003**, *42*, 2014; e) M. Mehring, S. Paalasmaa, M. Schürmann, *Eur. J. Inorg. Chem.* **2005**, 4891.

[12] C. D. Chandler, C. Roger, M. J. Hampden-Smith, *Chem. Rev.* **1993**, *93*, 1205.

[13] a) U. Schubert, *J. Mater. Chem.* **2005**, *15*, 3701; b) L. G. Hubert-Pfalzgraf, H. Guillon, *Appl. Organomet. Chem.* **1998**, *12*, 221; c) T. Kemmitt, M. Daghish, *Inorg. Chem.* **1998**, *37*, 2063; d) F. Ribot, P. Toledano, C. Sanchez, *Chem. Mater.* **1991**, *3*, 759.

[14] U. Schubert, *Chem. Mater.* **2001**, *13*, 3487.

[15] E. Bouwman, K. G. Caulton, G. Christou, K. Folting, C. Gasser, D. N. Hendrickson, J. C. Huffman, E. B. Lobkovsky, J. D. Martin, P. Michel, H.-L. Tsai, Z. Xue, *Inorg. Chem.* **1993**, *32*, 3463.

[16] X-ray crystal data for **1**: $Bi_9C_{65}H_{13}F_{78}O_{33}$, $M_r = 4684.57$, monoclinic, $P2_1/c$, $a = 16.7517(8)$, $b = 25.4542(11)$, $c = 26.0444(12)$ Å, $\beta = 96.8500(10)°$, $V = 11026.1(9)$ Å^3, $Z = 4$. For **2**: $Bi_{38}C_{120}H_{24}F_{144}O_{93}$, $M_r = 13630.63$, monoclinic, $P2_1/n$, $a = 20.4459(12)$, $b = 28.3746(16)$, $c = 21.3740(12)$ Å, $\beta = 93.3470(10)°$, $V = 12378.9(12)$ Å^3, $Z = 2$. See Supporting Information for more details. CCDC 604688 and 604689 (**1** and **2**) contain the supplementary crystallographic data for this paper. These data can be obtained free of charge from The Cambridge Crystallographic Data Centre via www.ccdc.cam.ac.uk/data_request/cif.

[17] a) J. H. Wengrovius, M. F. Garbauskas, E. A. Williams, R. C. Going, P. E. Donahue, J. F. Smith, *J. Am. Chem. Soc.* **1986**, *108*, 982; b) V. G. Kessler, S. Gohil, S. Parola, *Dalton Trans.* **2003**, 544.

 © 2006 Wiley-VCH Verlag GmbH & Co. KGaA, Weinheim

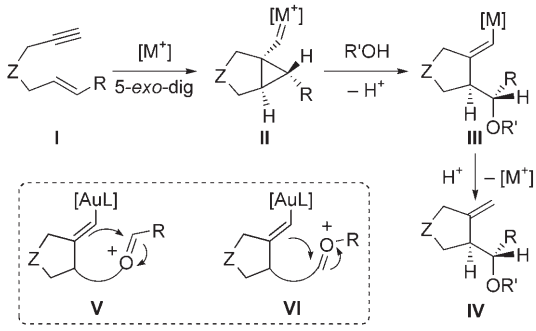
Cyclization

DOI: 10.1002/anie.200601575

Prins Cyclizations in Au-Catalyzed Reactions of Enynes**

*Eloísa Jiménez-Núñez, Christelle K. Claverie, Cristina Nieto-Oberhuber, and Antonio M. Echavarren**

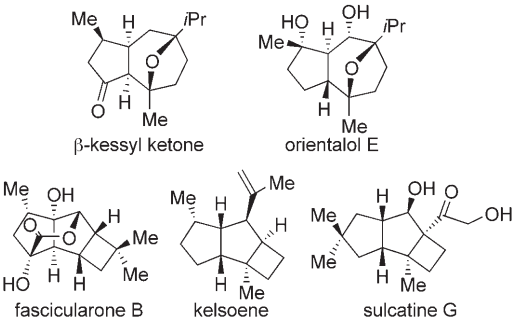
The hydroxy- or alkoxycyclization of enynes **I** catalyzed by electrophilic transition-metal complexes usually takes place through cyclopropyl metal carbenes **II**, which react with nucleophiles R′OH to give intermediates **III** (Scheme 1). The reaction is then terminated by proto-demetalation of the alkenyl metal intermediate **III** to give **IV**.[1,2]



Scheme 1. Different evolution of intermediate **III** by proto-demetalation of the Prins reaction with oxonium cations via **V** or **VI**.

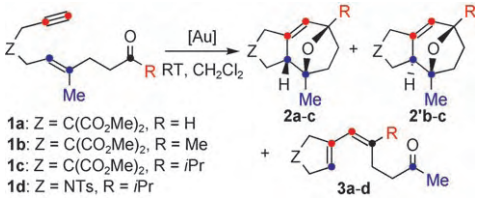
We have now found that in the Au^I-catalyzed cyclization of enynes[3,4] the alkenyl metal intermediate can be trapped with appropriate substituents, as shown in **V** and **VI** in a Prins cyclization. These new cyclizations allow the one-step synthesis of tricyclic skeletons, such as those of β-kessyl ketone[5a] and orientalol E (Scheme 2),[5b] from enynes with carbonyl groups and octahydrocyclobuta[*a*]pentalenes, such as fascicularone B,[6] kelsoene,[7] and sulcatine G,[8] starting from cyclopropyl enynes.

Enynes **1a–c**, bearing a carbonyl group at the alkenyl side chain, are cyclized to give oxatricyclic derivatives **2a–c** and rearranged ketones **3a–c** by using Au^I catalysts (Table 1). The reactions were completed at room temperature in 5–30 min. Aldehyde **1a** gave a mixture of tricycle **2a** (35%) and ketone **3a** (50%) with $[AuCl(PPh_3)]/AgSbF_6$ (catalyst **A**; Table 1, entry 1). Similar results were obtained with $[Au(PPh_3)(MeCN)]SbF_6$ (catalyst **B**) and cationic complex **C**[3] (Table 1, entries 2 and 3). A yield of 58% for **2a** was achieved by using AuCl itself (Table 1, entry 4). In the cyclization of ketones **1b** and **1c**, **2′b**,**c** were obtained as minor isomers, although their formation could be minimized by using Au^I catalysts **B** or **C** (Table 1, entries 6/7 and 10/11). Results with catalysts **A** and **B** were not identical (compare entries 5/6 and 9/10), which suggest that Ag^I may not be innocent in some of these cyclizations.[9] The best yields of **2b–c** were achieved with AuCl (Table 1, entries 8 and 12). Substrate **1d** led only to ketone **3d** (77%; Table 1, entry 13).



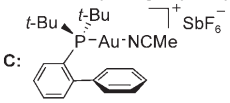
Scheme 2. Representative sesquiterpenes with skeletons accessible by Au-catalyzed cyclizations.

Table 1: Au^I-catalyzed reaction of enynes **1a–d**.[a]



Entry	Enyne	[Au]	2/2′	Yield [%]	2/2′	3	Yield [%]
1	**1a**	**A**	**2a**	35	>50:1	**3a**	50
2	**1a**	**B**	**2a**	36	>50:1	**3a**	34
3	**1a**	**C**	**2a**	29	>50:1	**3a**	50
4	**1a**	AuCl	**2a**	58	>50:1	**3a**	18
5	**1b**	**A**	**2b/2b′**	65	2.3:1	**3b**	9
6	**1b**	**B**	**2b**	47	>50:1	**3b**	44
7	**1b**	**C**	**2b**	47	>50:1	**3b**	52
8	**1b**	AuCl	**2b**	79	>50:1	**3b**	10
9	**1c**	**A**	**2c/2c′**	64	3.4:1	**3c**	22
10	**1c**	**B**	**2c**	49	>50:1	**3c**	45
11	**1c**	**C**	**2c/2c′**	44	26:1	**3c**	39
12	**1c**	AuCl	**2c**	84	>50:1	**3c**	12
13	**1d**	**C**	–	–		**3d**	77

[a] Reactions at 23°C with 3 mol% catalyst for 5–30 min (100% conversion). **A**: $[Au(PPh_3)Cl]/AgSbF_6$, **B**: $[Au(PPh_3)(MeCN)]SbF_6$,



[*] E. Jiménez-Núñez, Dr. C. K. Claverie, C. Nieto-Oberhuber, Prof. Dr. A. M. Echavarren
Institut Catalá d'Investigació Química (ICIQ)
Av. Països Catalans 16
43007 Tarragona (Spain)
Fax: (+34) 977-920-218
E-mail: aechavarren@iciq.es

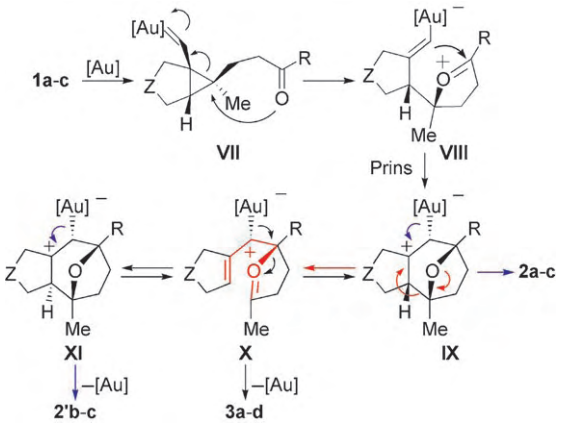
[**] We thank the MEC (project CTQ2004-02869 and predoctoral fellowships to E.J.-N. and C.N.-O.), the AGAUR (postdoctoral fellowship to C.K.C.), and the ICIQ Foundation for financial support. We also thank J. Benet-Buchholz (ICIQ) for the X-ray structures of **2c** and **5**.

Supporting information for this article is available on the WWW under http://www.angewandte.org or from the author.

InterScience
© 2006 Wiley-VCH Verlag GmbH & Co. KGaA, Weinheim

The structures of **2a–d** were assigned by NMR spectroscopic analysis and by the X-ray diffraction determination of **2c**.[10] The *cis* configuration of ketones **3a–d** was based on the coupling constant $^3J = 11.6$ Hz, as observed for **3a** and in NOESY experiments.

The carbonyl group acts as an internal nucleophile in the cyclizations of Table 1, as shown in **VII** (Scheme 3), thus



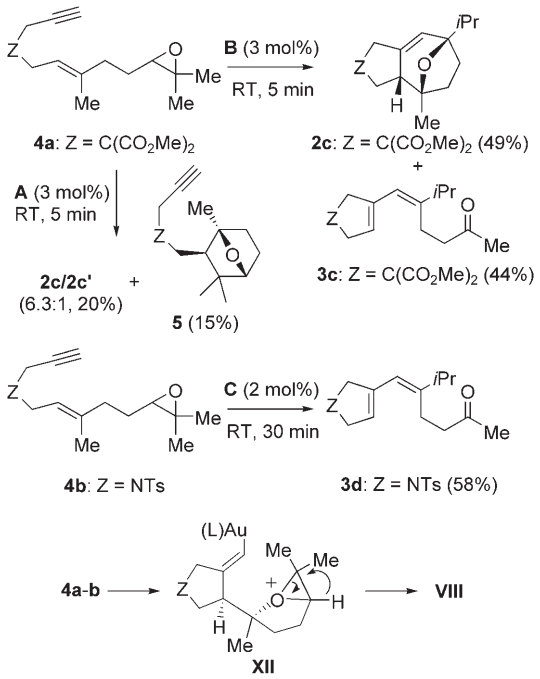
Scheme 3. Proposed mechanism for the cyclization of enynes **1a–c**.

forming oxonium cation **VIII**, which undergoes a Prins reaction[11] to give **IX**. Intermediate **IX** is a substituted 4-tetrahydropyranyl cation, which has been shown to be aromatic.[12] Elimination of the metal fragment forms tricycles **2a–c**. Alternatively, an elimination with fragmentation of the seven-membered ring via **X** leads to carbonyl compounds **3a–d**. Minor epimers **2′b,c** can arise by a competitive 2-oxonia–Cope rearrangement[13] via **X** and **XI**.

The higher selectivity for the formation of tricycles **2a–c** using AuCl as the catalyst (Table 1, entries 4, 8, and 12), relative to the cationic complexes **A–C** could be explained by the faster elimination of the more electron-rich metal center in **IX**, whereas for complexes **A–C** the metal center does not bear a negative charge in intermediates **VIII–XI**.

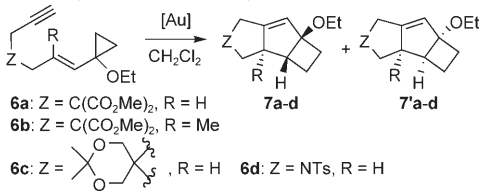
Interestingly, **2c** was also obtained from epoxide **4a** by using catalyst **B** (Scheme 4).[14] On the other hand, the reaction of **4a** with catalyst **A** gave a mixture of **2c/2′c** and oxonorbornane **5**, whose structure was confirmed by X-ray crystallography.[10] Epoxide **4b** reacted with catalyst **C** to give ketone **3d**, a result similar to that from **1d** (Table 1, entry 13). The formation of **2c** and **3c,d** could proceed through intermediates **XII**, which suffer C–O bond cleavage followed by a 1,2-hydrogen shift to form **VIII** (R = *i*Pr). Model epoxides do not isomerize to the corresponding carbonyl compounds under these reaction conditions.[15] We did not observed the direct addition of the ketone or the epoxide to the alkyne in any of these cyclizations.[16]

A related Prins cyclization, which leads to tricycles with an octahydrocyclobuta[*a*]pentalene skeleton (see Scheme 2), was uncovered in the cyclization of cyclopropylenynes **6a–d**[17–19] (Table 2). Thus, the reaction of ethyl ether **6a** with Au^I gave tricycles **7a/7′a** (Table 2, entries 1–3). Interestingly, *syn*-**7′a** was favored with catalyst **C** in the presence of traces of



Scheme 4. Gold-catalyzed reactions of epoxides **4a,b**. Ts = *p*-toluenemethanesulfonate.

Table 2: Au^I-catalyzed reaction of enynes **6a–d**.[a]



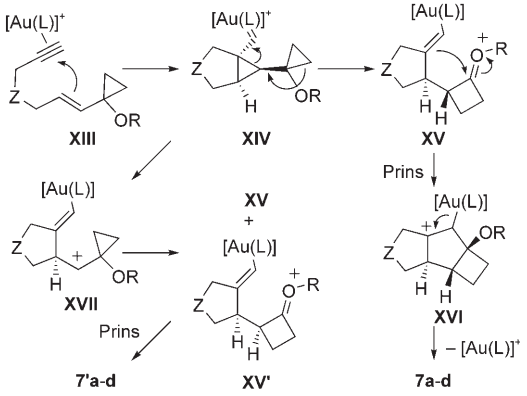
Entry	Enyne	[Au]	*t*	Product (ratio)	Yield [%]
1[a]	**6a**	**C**	5 min	**7a/7′a** (1:1)	88
2[b]	**6a**	**C**	5 min	**7a/7′a** (1:8)	81
3[b,c]	**6a**	**C**	5 min	**7a/7′a** (1:1)	93
4[b,d]	**6a**	AuCl	24 h	**7a/7′a** (30:1)[e]	80[e]
5[a,f]	**6b**	**C**	5 min	**7′b**	44
6[b,f]	**6b**	**C**	5 min	**7b/7′b** (2.5:1)	39
7[b,g]	**6c**	**C**	5 min	**7c/7′c** (3.2:1)	60
8[b,h,d]	**6c**	AuCl	2 h	**7c/7′c** (12:1)	91
9[b,g]	**6d**	**B**	5 min	**7d/7′d** (2:1)	60

[a] Reaction carried out in CH_2Cl_2 ($H_2O \approx 2$ ppm) with 3 mol% catalyst at 23 °C. [b] Reaction with 3–5 mol% water. [c] Reaction with NH_4Cl (2 equiv). [d] Reaction at 0 °C. [e] Average of five runs and determined by ^1H NMR spectroscopic analysis. [f] *E*/*Z* = 1:1. [g] Catalyst = 2 mol%. [h] Catalyst = 12 mol%.

water, whereas the use of AuCl led to the formation of **7a**, although the reaction was relatively slow (Table 2, entries 2 and 4). Low conversions (ca. 20%) were obtained when this reaction was carried out in the presence of 4-Å molecular sieves. Cycloprolylenynes **6b–d** reacted to give tricycles **7b–d** (Table 2, entries 5–9). Cyclobutanones were also formed as minor side products in these reactions.[20,21]

A rationale for the results of Table 2 is provided in Scheme 5. Accordingly, **XIII** forms cyclopropyl metal carbene

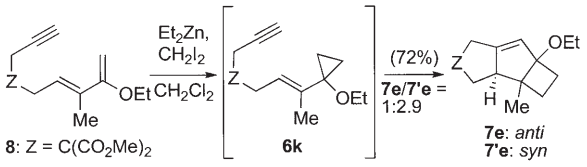
 © 2006 Wiley-VCH Verlag GmbH & Co. KGaA, Weinheim



Scheme 5. Proposed mechanism for the gold-catalyzed reaction of enynes **6a–d**.

XIV, which undergoes ring expansion to form **XV**. The alkenyl gold complex of **XV** could react with the oxonium cation to form **XVI**, which upon demetalation forms tricycles **7a–d** by a Prins reaction.[11] The concerted pathway (**XIV**→**XV**) is favored with AuCl as the catalyst, whereas cationic Au^I complexes apparently favor a nonconcerted reaction via cyclopropyl-stabilized cation **XVII**,[22] which undergoes a non-stereospecific ring expansion to give mixtures of **7a–d**/**7′a–d**.[23] However, as suggested by the dependence of the stereochemical outcome on the amount of water, we cannot exclude a pathway in which water opens intermediate **XIV** to form an alcohol, followed by a pinacol-type expansion. This process would result in an overall retention of configuration to form **XV′**.

Tricycles **7e**/**7′e** were directly obtained when the synthesis of **6k** was attempted by the cyclopropanation of dienyne **8** with the Furukawa reagent[24] (−65→23 °C; Scheme 6). This result is consistent with the mechanistic hypothesis of Scheme 5, in which the nonconcerted pathway is favored with Zn^{II} through intermediates **XV′**, thus leading to *syn*,*cis* diastereomer **7′e** as the major tricycle.



Scheme 6. Direct Zn^{II}-promoted cyclopropanation/cyclization of enyne **8**.

In summary, the alkenyl gold intermediate formed in the cyclization of enynes can be trapped in 5-*exo*-*dig* or 6-*endo*-*dig* Prins reactions to form an additional C–C bond. These Au^I-catalyzed cyclizations of functionalized enynes led to the ready assemblage of tricyclic carbon skeletons that are present in a number of naturally occurring compounds. Thus, for example, tricycle **2c**, which possesses the same skeleton and relative configuration of β-kessyl ketone and orientalol E (Scheme 2), can be obtained in high yield in a single step. The transformation of **1a–d** into ketones **3a–d** represents a new type of skeletal rearrangement of enynes.

Received: April 21, 2006
Published online: July 19, 2006

Keywords: cyclization · enynes · gold · Prins reaction · rearrangements

[1] Reviews of transition-metal-catalyzed reaction of enynes: a) G. C. Lloyd-Jones, *Org. Biomol. Chem.* **2003**, *1*, 215–236; b) C. Aubert, O. Buisine, M. Malacria, *Chem. Rev.* **2002**, *102*, 813–834; c) S. T. Diver, A. Giessert, *Chem. Rev.* **2004**, *104*, 1317–1382; d) A. M. Echavarren, C. Nevado, *Chem. Soc. Rev.* **2004**, *33*, 431–436; e) S. Ma, S. Yu, Z. Gu, *Angew. Chem.* **2006**, *118*, 206–209; *Angew. Chem. Int. Ed.* **2006**, *45*, 200–203; f) C. Nieto-Oberhuber, S. López, E. Jiménez-Núñez, A. M. Echavarren, *Chem. Eur. J.*, DOI: 10.10221/chem.200600174.

[2] a) M. Méndez, M. P. Muñoz, A. M. Echavarren, *J. Am. Chem. Soc.* **2000**, *122*, 11549–11550; b) M. Méndez, M. P. Muñoz, C. Nevado, D. J. Cárdenas, A. M. Echavarren, *J. Am. Chem. Soc.* **2001**, *123*, 10511–10520; c) C. Nevado, D. J. Cárdenas, A. M. Echavarren, *Chem. Eur. J.* **2003**, *9*, 2627–2635; d) C. Nevado, L. Charruault, V. Michelet, C. Nieto-Oberhuber, M. P. Muñoz, M. Méndez, M.-N. Rager, J. P. Genêt, A. M. Echavarren, *Eur. J. Org. Chem.* **2003**, 706–713.

[3] a) C. Nevado, D. J. Cárdenas, A. M. Echavarren, *Chem. Eur. J.* **2003**, *9*, 2627–2635; b) C. Nieto-Oberhuber, M. P. Muñoz, E. Buñuel, C. Nevado, D. J. Cárdenas, A. M. Echavarren, *Angew. Chem.* **2004**, *116*, 2456–2460; *Angew. Chem. Int. Ed.* **2004**, *43*, 2402–2406; c) C. Nieto-Oberhuber, S. López, A. M. Echavarren, *J. Am. Chem. Soc.* **2005**, *127*, 6178–6179; d) C. Nieto-Oberhuber, S. López, M. P. Muñoz, D. J. Cárdenas, E. Buñuel, C. Nevado, A. M. Echavarren, *Angew. Chem.* **2005**, *117*, 6302–6304; *Angew. Chem. Int. Ed.* **2005**, *44*, 6146–6148; e) M. P. Muñoz, J. Adrio, J. C. Carretero; A. M. Echavarren, *Organometallics* **2005**, *24*, 1293–1300; f) C. Nieto-Oberhuber, S. López, M. P. Muñoz, E. Jiménez-Núñez, E. Buñuel, D. J. Cárdenas, A. M. Echavarren, *Chem. Eur. J.* **2006**, *12*, 1694–1702; g) C. Nieto-Oberhuber, M. P. Muñoz, S. López, E. Jiménez-Núñez, C. Nevado, E. Herrero-Gómez, M. Raducan, A. M. Echavarren, *Chem. Eur. J.* **2006**, *12*, 1677–1693.

[4] a) V. Mamane, T. Gress, H. Krause, A. Fürstner, *J. Am. Chem. Soc.* **2004**, *126*, 8654–8655; b) L. Zhang, S. A. Kozmin, *J. Am. Chem. Soc.* **2004**, *126*, 11806–11807; c) M. R. Luzung, J. P. Markham, F. D. Toste, *J. Am. Chem. Soc.* **2004**, *126*, 10858–10859; d) see also: A. S. K. Hashmi, M. C. Blanco, E. Kurpejovic, W. Frey, J. W. Bats, *Adv. Synth. Catal.* **2006**, *348*, 709–713.

[5] a) H. Hikino, Y. Takeshita, H. Hikino, T. Takemoto, S. Ito, *Chem. Pharm. Bull.* **1967**, *15*, 485–489; b) G.-P. Peng, G. Tian, X.-F. Huang, F.-C. Lou, *Phytochemistry* **2003**, *63*, 877–881.

[6] H. Akasaka, Y. Shiono, T. Murayama, M. Ikeda, *Helv. Chim. Acta* **2005**, *88*, 2944–2950.

[7] a) L. Zhang, M. Koreeda, *Org. Lett.* **2002**, *4*, 3755–3758; T. Bach, A. Spiegel, *Synlett* **2002**, 1305–1307.

[8] a) D. G. Taber, K. J. Frankowski, *Org. Lett.* **2005**, *7*, 6417–6421; b) G. Mehta, K. Screenivas, *Tetrahedron Lett.* **2002**, *43*, 3319–3321; c) E. Piers, A. Orellana, *Synthesis* **2001**, 2138–2142; d) S. Fietz-Razavian, S. Schulz, I. Dix, P. G. Jones, *Chem. Commun.* **2001**, 2154–2155.

[9] For an example in which Ag^I catalyzes an additional process, see: C. Nevado, A. M. Echavarren, *Chem. Eur. J.* **2005**, *11*, 3155–3164.

[10] See the Supporting Information for details.

 © 2006 Wiley-VCH Verlag GmbH & Co. KGaA, Weinheim

[11] General references: a) L. E. Overman, L. D. Pennington, *J. Org. Chem.* **2003**, *68*, 7143 – 7157; b) R. Jasti, C. D. Anderson, S. D. Rychnovsky, *J. Am. Chem. Soc.* **2005**, *127*, 9939 – 9945.
[12] R. W. Alder, J. N. Harvey, M. T. Oakley, *J. Am. Chem. Soc.* **2002**, *124*, 4960 – 4961.
[13] S. D. Rychnovsky, S. Marumoto, J. J. Jaber, *Org. Lett.* **2001**, *3*, 3815 – 3818.
[14] For examples in which epoxides were used instead of carbonyl compounds in the Prins reactions, see: a) J. Li, C.-J. Li, *Tetrahedron Lett.* **2001**, *42*, 793 – 796; b) A. P. Dobbs, S. Martinović, *Tetrahedron Lett.* **2002**, *43*, 7055 – 7057.
[15] See also: D. Xing, B. Guan, G. Cai, Z. Fang, L. Yang, Z. Shi, *Org. Lett.* **2006**, *8*, 693 – 696.
[16] a) A. S. K. Hashmi, L. Schwarz, J.-H. Choi, T. M. Frost, *Angew. Chem.* **2000**, *112*, 2382 – 2385; *Angew. Chem. Int. Ed.* **2000**, *39*, 2285 – 2288; b) A. S. K. Hashmi, P. Sinha, *Adv. Synth. Catal.* **2004**, *346*, 432 – 438.
[17] Rh^{I}-catalyzed reaction of cyclopropylenynes: a) P. A. Wender, H. Takahashi, B. Witulski, *J. Am. Chem. Soc.* **1995**, *117*, 4720 – 4721; b) Z.-X. Yu, P. A. Wender, K. N. Houk, *J. Am. Chem. Soc.* **2004**, *126*, 9154 – 9155, and references therein.
[18] Ru^{II}-catalyzed reaction of cyclopropylenynes: a) B. M. Trost, F. D. Toste, H. Shen, *J. Am. Chem. Soc.* **2000**, *122*, 2379 – 2380; b) B. M. Trost, H. C. Shen, D. B. Horne, F. D. Toste, B. G. Steinmetz, C. Korandin, *Chem. Eur. J.* **2005**, *11*, 2577 – 2590.
[19] Ni^{I}-catalyzed cyclization of cyclopropylenynes: G. Zuo, J. Louie, *J. Am. Chem. Soc.* **2005**, *127*, 5798 – 5799.
[20] Reaction of silyloxy analogues of **6a**–**d** led to cyclobutanones by ring expansion of the cyclopropyl ring; details will be published in a full account of these results.
[21] Ring expansion of alkynylcyclopropanols catalyzed by Au^{I}: J. P. Markham, S. T. Staben, F. D. Toste, *J. Am. Chem. Soc.* **2005**, *127*, 9708 – 9709.
[22] J. Casanova, D. R. Kent, W. A. Goddard, J. D. Roberts, *Proc. Natl. Acad. Sci. USA* **2003**, *100*, 15 – 19.
[23] Preliminary DFT calculations show a carbocationic structure for intermediates in which $[Au(L)] = [Au(PH_3)]$, whereas for $[Au(L)] = [AuCl]^-$ the intermediates resemble cyclopropyl gold(I) carbenes, such as **XIV**: D. J. Cárdenas, unpublished results.
[24] J. Furukawa, N. Kawabata, J. Nishimura, *Tetrahedron* **1968**, *24*, 53 – 58.

 © 2006 Wiley-VCH Verlag GmbH & Co. KGaA, Weinheim

Arene Complexes

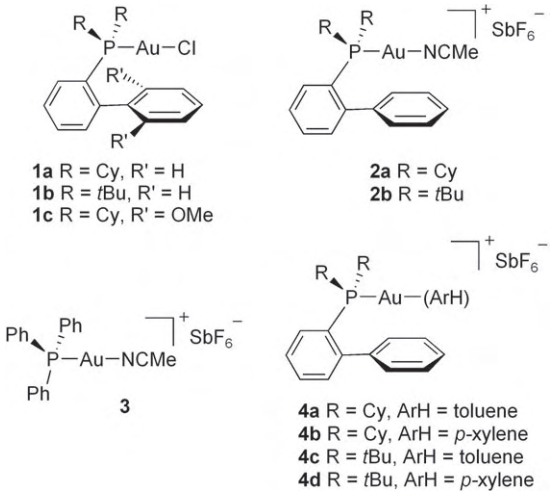
DOI: 10.1002/anie.200601688

Cationic η^1/η^2-Gold(I) Complexes of Simple Arenes**

*Elena Herrero-Gómez, Cristina Nieto-Oberhuber, Salomé López, Jordi Benet-Buchholz, and Antonio M. Echavarren**

Bulky biphenylphosphane ligands have been particularly successful in Pd-catalyzed reactions.[1] These ligands have led to the isolation of new Pd^I complexes, which display unusual Pd–arene interactions and enhanced reactivity in cross-coupling processes.[2]

We have used bulky biphenylphosphanes for the preparation of Au^I complexes **1a–c** (Scheme 1), whose cationic derivatives are very active catalysts that allow for the cyclization of 1,6-enynes substituted at the alkyne function with aryl or alkenyl groups.[3] Instead of preparing the cationic complexes by chloride abstraction with Ag^I salts in situ, we have sought to use stable $[Au(PR_3)(L)]^+A^-$ (L = ligand) complexes with a weakly coordinating ligand that could be replaced by the alkyne functionality of the reacting enyne.



Scheme 1. Neutral and cationic Au^I complexes.

[*] E. Herrero-Gómez, C. Nieto-Oberhuber, Dr. S. López, Dr. J. Benet-Buchholz, Prof. Dr. A. M. Echavarren
Institute of Chemical Research of Catalonia (ICIQ)
Av. Països Catalans 16, 43007 Tarragona (Spain)
Fax: (+34) 977-920-225
E-mail: aechavarren@iciq.es

[**] We thank the MEC (predoctoral fellowships to E.H.-G. and C.N.-O. (CTQ2004-02869) and a Torres Quevedo Contract to S.L.), the AGAUR (2005 SGR 00993), and the ICIQ Foundation for financial support. We also thank E. Escudero-Adán (X-ray diffraction unit, ICIQ).

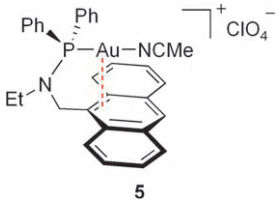
Supporting information for this article is available on the WWW under http://www.angewandte.org or from the author.

© 2006 Wiley-VCH Verlag GmbH & Co. KGaA, Weinheim

Thus, complexes **2a**,**b** with an acetonitrile ligand have been prepared as stable white salts that are particularly active for the alkoxycyclization, skeletal rearrangement,[4–6] and intramolecular cyclopropanation[7] of a variety of enynes.[8] These complexes also catalyze the cyclization of indoles with alkynes.[9] Cationic complex **3** with triphenylphosphane is also an excellent catalyst for the intramolecular cyclopropanation of dienynes.[7,10] Importantly, the use of **2a**,**b** or **3** as catalysts allows reactions to be carried out in the absence of Ag^I, which can lead to unwanted side reactions.[11]

In contrast to Ag^I, whose complexes with arenes have been thoroughly investigated,[12] only three examples in which the Au^I center interacts with an arene have been reported.[13] These have been described by Zhang and co-workers as η^2-arene complexes with an intramolecular interaction with an anthracene unit that is covalently attached to the phosphane ligand. Thus, the Au complex **5** shows the strongest η^2-anthracene–Au^I interaction, with Au···C distances of 2.958 and 3.097 Å,[13b] whereas other anthracene complexes show Au···C close contacts between 3.020 and 3.246 Å.[13]

We wanted to determine if the proximity of the arene ring parallel to the Au–P bonds of complexes **2a**,**b** played any role in stabilizing these complexes by arene–Au interactions. As part of this study, we found that crystallization of **2a**,**b** from toluene or *p*-xylene leads to the isolation of the first Au^I complexes **4a–d** of simple arenes that show η^1/η^2 coordination. Herein, we report the single-crystal structures of Au^I complexes **4a–d**, as well as those of **1a–c**, **2a**,**b**, and **3**.[14]



5

X-ray structures **1a** and **2b**, representative of neutral (**1a–c**) and cationic (**2a**,**b**) complexes,[15–20] are shown in Figure 1. The relevant distances and angles are shown in Tables 1 and 2, respectively.

The Au–P and Au–Cl bond lengths of **1a–c** are around 2.24 and 2.30 Å, respectively, which are similar to those found in $[AuCl(PPh_3)]$[21,22] and related Au^I complexes.[23] The Au–N lengths (around 2.04 Å) in **2a**,**b** and **3** correspond to that found in cationic acetonitrile complex **5** (2.043 Å)[13b] and are slightly longer than that reported for $[Au(NCMe)_2]SbF_6$ (1.96 Å).[24] Cationic complexes **2a**,**b** show a greater bending of the P-Au-NCMe angle (174.43 and 173.06°) than complex **3** (177.10°) with a triphenylphosphane moiety as the ligand.

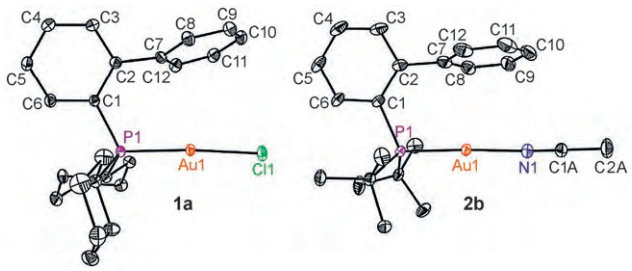


Figure 1. Ortep plots (50%) of complexes **1a** and **2b** (only the complex cation is shown for **2b**). The hydrogen atoms have been omitted for clarity.

Table 1: Selected distances [Å] for **1a–c**, **2a**,**b**, **3**, and **4a–d**.[a]

	Au–P	Au···Cl,N,C2A/C3A/C4A[b]	Au···Ar[c]	Au···C7/C8/C12/O1[d]
1a	2.2364(6)	2.2912(6)		3.15/3.55/3.83
1b	2.254(3)	2.303(4)		3.16/3.40/3.40
1c	2.2378(5)	2.3089(5)		3.27/3.13/3.92/3.27
2a	2.2466(3)	2.0338(9)		3.02/3.25/3.24
2b	2.2539(7)	2.046(2)		3.04/3.28/3.38
3	2.2282(12)	2.038(5)		
4a	2.2459(13)	2.535(6)/2.263(5)/2.689(6)	2.244(5)	3.22/3.10/3.69
4b	2.2400(17)	2.338(7)/2.341(7)	2.229(7)	3.15/3.45/3.33
4c	2.2643(10)	2.299(5)/2.423(5)	2.233(5)	3.03/3.42/3.14
4d A	2.2657(11)	2.300(4)/2.354(4)	2.200(4)	3.04/3.00/3.64
4d B	2.2636(10)	2.308(4)/2.370(4)	2.221(4)	3.04/3.41/3.21

[a] Compound **4d** has two independent molecules (A and B). [b] Distances are from Au to Cl for **1a–c**, to N for **2a**,**b** and **3**, and to C2A/C3A/C4A for **4a–d**. [c] The shortest distance between the Au center and the plane of the complexed arene. [d] These distances are only approximations.

For neutral complexes **1a–c**, the average distance between the Au center and the covering arene ring is 3.15 Å. This distance is slightly shorter in cationic complexes **2a**,**b** (3.03 Å; Figure 2). These values are similar to those found by Zhang et al. for Au–anthracene complexes such as **5**.[13]

In contrast, the arene–Au^I interactions with toluene or *p*-xylene ligands in complexes **4a–d** are considerably stronger

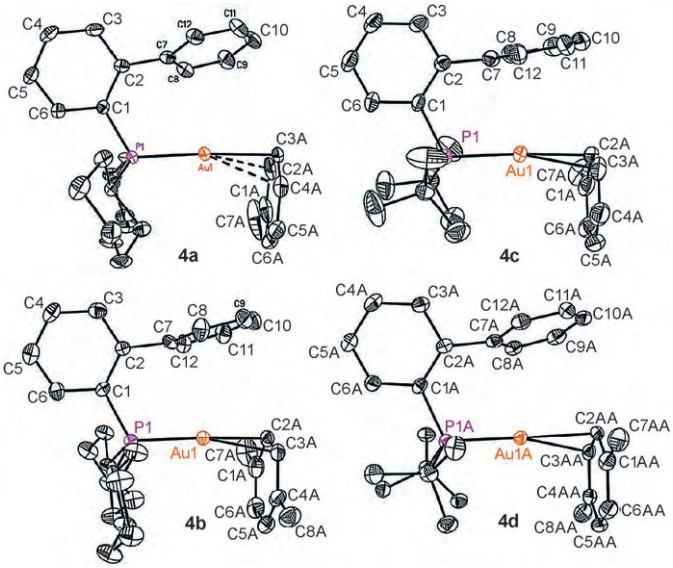


Figure 2. Ortep plots (50%) of the cationic part of the complexes **4a–d**. The hydrogen atoms have been omitted for clarity.

 © 2006 Wiley-VCH Verlag GmbH & Co. KGaA, Weinheim

(Figure 2).[25–29] In all cases, the plane of the aromatic ring forms an angle to the vector of the Au–P bond close to 90° (Table 2). The shortest distances between the Au atom and the plane of the aromatic ring of the π-complexed arenes are

Table 2: Selected angles [°] for **1a–c**, **2a**,**b**, **3**, and **4a–d**.[a]

	P-Au-Cl,N,XA[b]	Au1-P1-C2-C7	C1-C2-C7-C8(C12)	Au ⊥ Ar[c]
1a	175.596(19)	14.2(1)	63.9(3)	
1b	172.56(14)	0.0	87.3	
1c	176.145(18)	18.9(1)	88.7(2) (−99.0(2))	
2a	174.43(3)	9.1(1)	81.90(16)	
2b	173.06(7)	0.0(1)	86.8(3)	
3	177.10(16)			
4a	174.64(16)	7.8(1)	63.5(9)	6.32
4b	171.4 (aprox.)	4.9(1)	77.6(9)	7.21
4c	171.2 (aprox.)	1.7(1)	78.8(6) (−85.9(7))	2.66
4d A	173.7 (aprox.)	0.9(1)	72.6(6)	0.62
4d B	171.9 (aprox.)	3.8(2)	79.8(5)	5.37

[a] Compound **4d** has two independent molecules (A and B). [b] XA is C3A in **4a** and the point centered between C2A and C3A in the rest of molecules. [c] The angle formed between the vector of the Au–P bond and the normal of the aromatic plane C1A–C6A (arene).

2.20–2.24 Å (Table 1). Importantly, these values are markedly shorter than those found for Ag^I–arene complexes (2.41 ± 0.05 Å),[12a] which is probably due to rather large relativistic effects at the Au center.[22] The distances between the Au atom and the covering arene ring for **4a–d** are 3.03–3.22 Å, similar to those found for **1a–c** and **2a**,**b**.

Compound **4a**, which is complexed to toluene, shows a η^1-arene interaction with the shortest atom–atom distance from the Au center to C3A (2.263 Å) and secondary interactions to C2A and C4A (2.535 and 2.689 Å). The Au atom in *p*-xylene complex **4b** shows almost a η^2-arene interaction (2.338 and 2.341 Å with C2A and C3A, respectively). Complex **4c** shows a distorted η^1-arene interaction with the shortest atom–atom distance from the Au center to C2A (2.299 Å) and a secondary interaction to C3A (2.423 Å). Curiously, the Au atom in **4a** is more strongly bonded to the *meta* position of the toluene ring, whereas the strongest interaction in **4c** occurs with the *ortho* position. Complex **4d**, which contains two independent molecules in the crystal packing, shows a distorted η^2-arene interaction with a stronger bond to C2 than to C3. According to the geometrical criteria introduced by Kochi and co-workers,[29] the hapticity of complexes would be $\eta = 1.42$ (**4a**), 1.69 (**4b**), 1.41 (**4c**), and 1.52/1.56 (two independent molecules of **4d**).

The shortest intermolecular Au···Au distance was found for **1a** (5.4 Å), whereas this distance ranges from 7.6 to 9.7 Å for **1b**,**c**, **2a**,**b**, **3**, and **4a–d**, all of which are beyond the accepted contact limit of 3.6 Å for significant aurophilic interactions.[30]

Broad signals were observed in the $^{31}P\{^1H\}$ NMR (202.5 MHz) spectra of the arene–Au^I complexes in CD_2Cl_2 at room temperature, thus indicating a fluxional character of these complexes. The broad resonance around $\delta = 68$ ppm for **4c** leads to a sharp signal at $\delta = 65.70$ ppm upon cooling to 200 K. Addition of water to the solution of **4c** in CD_2Cl_2 leads to a new signal at $\delta = 60.40$ ppm (300 K), which corresponds to the aquo complex. By comparison, the ^{31}P NMR resonance of acetonitrile complex **2b** was observed at $\delta = 60.53$ ppm (300 K).

In summary, we have characterized the first Au^I complexes of simple arenes, which show separation between the Au center and the mean aromatic plane of 2.20–2.24 Å. These Au^I–arene bonds are much shorter than the related Ag^I–arene bonds. Weaker interactions have been found between the Au center and the arene parallel to the P–Au bond.

Experimental Section

X-ray structure determinations: Crystals of **1a** were obtained by slow evaporation of CH_2Cl_2 at room temperature using a synthetic fiber as crystallizing base; crystals of **1b**,**c** and **2a**,**b** were obtained by slow evaporation of CH_2Cl_2 at room temperature; crystals of **3** were obtained by slow evaporation of $CHCl_3$; crystals **4a–d** were obtained by evaporation at room temperature, after heating a solution in an aromatic solvent (toluene or *p*-xylene) of **2a** or **2b**. Although the analyzed crystals are stable under atmospheric conditions, they were prepared under inert conditions and immersed in perfluoropolyether as a protecting oil for manipulation.

Data Collection: Measurements were made on a Bruker-Nonius diffractometer equipped with a APPEX 2 4 K CCD area detector, a FR591 rotating anode with $Mo_{K\alpha}$ radiation, Montel mirrors as a monochromator, and a Kryoflex low-temperature device ($T = -173\,^{\circ}C$). Full-sphere data collection was used with ω and ϕ scans.

Programs used: Data collection Apex2V. 1.0–22 (Bruker-Nonius 2004), data reduction Saint + Version 6.22 (Bruker-Nonius 2001), and absorption correction SADABS V. 2.10 (2003).

Structure solution and refinement: SHELXTL Version 6.10 (Sheldrick, 2000) was used.[31,32]

Received: April 28, 2006
Published online: July 19, 2006

Keywords: π interactions · arene ligands · enynes · gold · phosphanes

[1] a) S. D. Walker, T. E. Border, J. R. Martinelli, S. L. Buchwald, *Angew. Chem.* **2004**, *116*, 1907–1912; *Angew. Chem. Int. Ed.* **2004**, *43*, 1871–1876; b) S. Kaye, J. M. Fox, F. A. Hicks, S. L. Buchwald, *Adv. Synth. Catal.* **2001**, *343*, 789–794.

[2] a) T. E. Barder, *J. Am. Chem. Soc.* **2006**, *128*, 898–904; b) U. Christmann, R. Vilar, A. J. P. White, D. J. Williams, *Chem. Commun.* **2004**, 1294–1295; c) U. Christmann, D. A. Pantazis, J. Benet-Buchholz, J. E. McGrady, F. Maseras, R. Vilar, *J. Am. Chem. Soc.* **2006**, *128*, 6376–6390.

[3] C. Nieto-Oberhuber, S. López, A. M. Echavarren, *J. Am. Chem. Soc.* **2005**, *127*, 6178–6179.

[4] a) C. Nieto-Oberhuber, M. P. Muñoz, E. Buñuel, C. Nevado, D. J. Cárdenas, A. M. Echavarren, *Angew. Chem.* **2004**, *116*, 2456–2460; *Angew. Chem. Int. Ed.* **2004**, *43*, 2402–2406; b) C. Nieto-Oberhuber, M. P. Muñoz, S. López, E. Jiménez-Núñez, C. Nevado, E. Herrero-Gómez, M. Raducan, A. M. Echavarren, *Chem. Eur. J.* **2006**, *12*, 1677–1693.

[5] a) C. Nieto-Oberhuber, S. López, M. P. Muñoz, D. J. Cárdenas, E. Buñuel, C. Nevado, A. M. Echavarren, *Angew. Chem.* **2005**, *117*, 6302–6304; *Angew. Chem. Int. Ed.* **2005**, *44*, 6146–6148; b) C. Nieto-Oberhuber, S. López, E. Jiménez-Núñez, A. M. Echavarren, *Chem. Eur. J.* **2006**, *12*, 5916–5923.

[6] M. P. Muñoz, J. Adrio, J. C. Carretero, A. M. Echavarren, *Organometallics* **2005**, *24*, 1293–1300.

 © 2006 Wiley-VCH Verlag GmbH & Co. KGaA, Weinheim

[7] C. Nieto-Oberhuber, S. López, M. P. Muñoz, E. Jiménez-Núñez, E. Buñuel, D. J. Cárdenas, A. M. Echavarren, *Chem. Eur. J.* **2006**, *12*, 1694 – 1702.

[8] Reviews of transition-metal-catalyzed reaction of enynes: a) G. C. Lloyd-Jones, *Org. Biomol. Chem.* **2003**, *1*, 215 – 236; b) C. Aubert, O. Buisine, M. Malacria, *Chem. Rev.* **2002**, *102*, 813 – 834; c) S. T. Diver, A. Giessert, J. *Chem. Rev.* **2004**, *104*, 1317 – 1382; d) A. M. Echavarren, C. Nevado, *Chem. Soc. Rev.* **2004**, *33*, 431 – 436; e) S. Ma, S. Yu, Z. Gu, *Angew. Chem.* **2006**, *118*, 206 – 209; *Angew. Chem. Int. Ed.* **2006**, *45*, 200 – 203.

[9] C. Ferrer, A. M. Echavarren, *Angew. Chem.* **2006**, *118*, 1123 – 1127; *Angew. Chem. Int. Ed.* **2006**, *45*, 1105 – 1109.

[10] Lead references on the cyclization of enynes with Au^I complexes: a) F. Gagosz, *Org. Lett.* **2005**, *7*, 4129 – 4132; b) V. Mamane, T. Gress, H. Krause, A. Fürstner, *J. Am. Chem. Soc.* **2004**, *126*, 8654 – 8655; c) L. Zhang, S. A. Kozmin, *J. Am. Chem. Soc.* **2004**, *126*, 11806 – 11807; d) M. R. Luzung, J. P. Markham, F. D. Toste, *J. Am. Chem. Soc.* **2004**, *126*, 10858 – 10859.

[11] C. Nevado, A. M. Echavarren, *Chem. Eur. J.* **2005**, *11*, 3155 – 3164.

[12] Leading references: a) S. V. Lindeman, R. Rathore, J. K. Kochi, *Inorg. Chem.* **2000**, *39*, 5707 – 5716; b) M. Munakata, L. P. Wu, G. L. Ning, *Coord. Chem. Rev.* **2000**, *198*, 171 – 203; c) M. Munakata, L. P. Wu, T. Kuroda-Sowa, M. Maekawa, Y. Suenaga, G. L. Ning, T. Kojima, *J. Am. Chem. Soc.* **1998**, *120*, 8610 – 8618; d) K. Ogawa, T. Kitagawa, S. Ishida, K. Komatsu, *Organometallics* **2005**, *24*, 4842 – 4844; e) K. K. Laali, S. Hupertz, A. G. Temu, S. E. Galembeck, *Org. Biomol. Chem.* **2005**, *3*, 2319 – 2326; f) R. Rathore, V. J. Chebny, S. H. Abdelwahed, *J. Am. Chem. Soc.* **2005**, *127*, 8012 – 8023.

[13] a) F.-B. Xu, Q.-S. Li, L.-Z. Wu, X.-B. Leng, Z.-C. Li, X.-S. Zeng, Y. L. Chow, Z.-Z. Zhang, *Organometallics* **2003**, *22*, 633 – 640; b) Q.-S. Li, C.-Q. Wang, R.-Y. Zou, F.-B. Xu, H.-B. Song, X.-J. Wan, Z.-Z. Zhang, *Inorg. Chem.* **2006**, *45*, 1888 – 1890.

[14] The structure of $[Au(PPh_3)(NTf_2)]$ (Tf = trifluoromethanesulfonate) has been reported: N. Mézailles, L. Ricard, F. Gagosz, *Org. Lett.* **2005**, *7*, 4133 – 413; it shows an almost linear arrangement of P-Au-N (174.20(7)°) with a P–Au bond length of 2.2306(7) Å.

[15] Crystal data for **1a** at 100 K: $C_{24}H_{31}Au_1Cl_1P_1$, 582.87 g mol^{-1}, triclinic, $P\bar{1}$, $a = 9.7118(9)$, $b = 9.9657(9)$, $c = 12.1248(12)$ Å, $\alpha = 110.860(2)$, $\beta = 96.215(2)$, $\gamma = 93.468(3)°$, $V = 1083.92(18)$ Å^3, $Z = 2$, $\rho_{calcd} = 1.786$ Mg m^{-3}, $R_1 = 0.0293$ (0.0375), $wR2 = 0.0754$ (0.0786), for 10704 reflections with $I > 2\sigma(I)$ (for 12288 reflections ($R_{int} = 0.0251$) with a total measured of 22170 reflections), goodness-of-fit on $F^2 = 1.027$, largest diff. peak (hole) = 3.426-(−2.170) e Å$^-$.

[16] Crystal data for **1b** at 100 K: $C_{20}H_{27}Au_1Cl_1P_1$, 530.80 g mol^{-1}, orthorhombic, *Pnma*, $a = 18.127(3)$, $b = 10.7748(18)$, $c = 10.6483(16)$ Å, $V = 2079.8(6)$ Å^3, $Z = 4$, $\rho_{calcd} = 1.695$ Mg m^{-3}, $R_1 = 0.1249$ (0.1821), $wR2 = 0.2369$ (0.2628), for 4123 reflections with $I > 2\sigma(I)$ (for 6173 reflections ($R_{int} = 0.0732$) with a total measured of 36777 reflections), goodness-of-fit on $F^2 = 1.205$, largest diff. peak (hole) = 6.868 (−3.855) e Å^{-3}; this structure shows pseudosymmetry; refinement in *Pna*2$_1$ led to $R_1 = 0.1013$ with negative atomic displacement parameters as a result of correlation effects.

[17] Crystal data for **1c** at 100 K: $C_{27}H_{36}Au_1Cl_4P_1O_2$, 762.29 g mol^{-1}, monoclinic, *C*2/c, $a = 29.968(2)$, $b = 10.3999(7)$, $c = 20.0425(14)$ Å, $\beta = 109.644(2)°$, $V = 5883.0(7)$ Å^3, $Z = 8$, $\rho_{calcd} = 1.721$ Mg m^{-3}, $R_1 = 0.0331$ (0.0415), $wR2 = 0.0817$ (0.0868), for 14474 reflections with $I > 2\sigma(I)$ (for 17005 reflections ($R_{int} = 0.0646$) with a total measured of 56899 reflections), goodness-of-fit on $F^2 = 1.024$, largest diff. peak (hole) = 3.020 (−2.245) e Å^{-3}.

[18] Crystal data for **2a** at 100 K: $C_{22}H_{30}Au_1F_6N_1P_1Sb_1$, 772.16 g mol^{-1}, monoclinic, $P2_1/c$, $a = 8.1165(2)$, $b = 22.5583(4)$, $c = 14.3141(3)$ Å, $\beta = 102.0380(10)°$, $V = 2563.20(9)$ Å^3, $Z = 4$, $\rho_{calcd} = 2.001$ Mg m^{-3}, $R_1 = 0.0166$ (0.0378), $wR2 = 0.0197$ (0.0387), for 13337 reflections with $I > 2\sigma(I)$ (for 14489 reflections ($R_{int} = 0.0187$) with a total measured of 50577 reflections), goodness-of-fit on $F^2 = 1.027$, largest diff. peak (hole) = 2.069 (−0.990) e Å^{-3}.

[19] Crystal data for **2b** at 100 K: $C_{31}H_{48}Au_1F_6N_1P_1Sb_1$, 898.39 g mol^{-1}, monoclinic, $P2_1/c$, $a = 14.5077(6)$, $b = 13.8576(7)$, $c = 17.2481(7)$ Å, $\beta = 97.5130(10)°$, $V = 3437.8(3)$ Å^3, $Z = 4$, $\rho_{calcd} = 1.736$ Mg m^{-3}, $R_1 = 0.0430$ (0.1140), $wR2 = 0.0540$ (0.1206), for 16335 reflections with $I > 2\sigma(I)$ (for 19701 reflections ($R_{int} = 0.0515$) with a total measured of 68445 reflections), goodness-of-fit on $F^2 = 1.046$, largest diff. peak (hole) = 7.561 (−4.242) e Å^{-3}.

[20] Crystal data for **3** at 100 K: $C_{20}H_{18}Au_1F_6N_1P_1Sb_1$, 737.04 g mol^{-1}, monoclinic, $P2_1/c$, $a = 11.2737(17)$, $b = 12.1210(19)$, $c = 16.933(3)$ Å, $\beta = 105.290(3)°$, $V = 2232.0(6)$ Å^3, $Z = 4$, $\rho_{calcd} = 2.190$ Mg m^{-3}, $R_1 = 0.0648$ (0.1413), $wR2 = 0.1429$ (0.1815), for 6521 reflections with $I > 2\sigma(I)$ (for 12943 reflections ($R_{int} = 0.1035$) with a total measured of 42796 reflections), goodness-of-fit on $F^2 = 0.998$, largest diff. peak (hole) = 4.169-(−4.437) e Å^{-3}.

[21] N. C. Baenziger, W. E. Bennett, D. M. Soboroff, *Acta Crystallogr. Sect. B* **1976**, *32*, 962 – 963.

[22] For theoretical work on $[AuCl(PH_3)]$: P. Schwerdtfeger, H. L. Hermann, H. Schmidbaur, *Inorg. Chem.* **2003**, *42*, 1334 – 1342.

[23] a) F. Bachechi, A. Burini, R. Galassi, B. R. Pietroni, *J. Chem. Crystallogr.* **2004**, *34*, 743 – 748; b) R. C. Bott, P. C. Healy, G. Smitha, *Aust. J. Chem.* **2004**, *57*, 213 – 218; c) K. Nunokawa, S. Onaka, T. Tatematsu, M. Ito, J. Sakai, *Inorg. Chim. Acta* **2001**, *322*, 56 – 64; d) R. C. Bott, G. A. Bowmaker, R. W. Buckley, P. C. Healy, M. C. S. Perera, *Aust. J. Chem.* **2000**, *53*, 175 – 181; e) T. E. Müller, J. C. Green, D. M. P. Mingos, C. M. McPartlin, C. W. D. J. Williams, T. M. Woodroffe, *J. Organomet. Chem.* **1998**, *551*, 313 – 330; f) M. Bardaji, P. G. Jones, A. Laguna, *Eur. J. Inorg. Chem.* **1998**, 989 – 992; g) K. Angermaier, E. Zeller, H. Schmidbaur, *J. Organomet. Chem.* **1994**, *472*, 371 – 376; h) C. S. W. Harker, E. R. T. Tiekink, *Acta Crystallogr. Sect. C* **1990**, *46*, 1546 – 1547.

[24] H. Willner, J. Schaebs, G. Hwang, F. Mistry, R. Jones, J. Trotter, F. Aubke, *J. Am. Chem. Soc.* **1992**, *114*, 8972 – 8980.

[25] Crystal data for **4a** at 100 K: $C_{31}H_{39}Au_1F_6P_1Sb_1$, 875.31 g mol^{-1}, monoclinic, *Cc*, $a = 10.5275(7)$, $b = 16.2109(11)$, $c = 18.4159(11)$ Å, $\beta = 96.3960(10)°$, $V = 3123.3(4)$ Å^3, $Z = 4$, $\rho_{calcd} = 1.861$ Mg m^{-3}, $R_1 = 0.0364$ (0.0481), $wR2 = 0.0795$ (0.0823), for 9026 reflections with $I > 2\sigma(I)$ (for 9026 reflections ($R_{int} = 0.0656$) with a total measured of 23427 reflections), goodness-of-fit on $F^2 = 0.958$, largest diff. peak (hole) = 2.312-(−1.480) e Å^{-3}.

[26] Crystal data for **4b** at 100 K: $C_{32}H_{41}Au_1F_6P_1Sb_1$, 889.33 g mol^{-1}, orthorhombic, *Pbca*, $a = 17.7639(19)$, $b = 14.9629(15)$, $c = 24.063(3)$ Å, $V = 6396.0(11)$ Å^3, $Z = 8$, $\rho_{calcd} = 1.847$ Mg m^{-3}, $R_1 = 0.0713$ (0.1354), $wR2 = 0.1692$ (0.2045), for 8971 reflections with $I > 2\sigma(I)$ (for 15680 reflections ($R_{int} = 0.1180$) with a total measured of 110187 reflections), goodness-of-fit on $F^2 = 1.027$, largest diff. peak (hole) = 7.329 (−2.613) e Å^{-3}.

[27] Crystal data for **4c** at 273 K: $C_{27}H_{35}Au_1F_6P_1Sb_1$, 823.24 g mol^{-1}, monoclinic, $P2_1/n$, $a = 10.0342(7)$, $b = 25.189(3)$, $c = 11.8275(14)$ Å, $\beta = 95.413(4)°$, $V = 2976.1(6)$ Å^3, $Z = 4$, $\rho_{calcd} = 1.837$ Mg m^{-3}, $R_1 = 0.0546$ (0.1040), $wR2 = 0.1752$ (0.2146), for 7585 reflections with $I > 2\sigma(I)$ (for 14113 reflections ($R_{int} = 0.0509$) with a total measured of 55182 reflections), goodness-of-fit on $F^2 = 1.022$, largest diff. peak (hole) = 3.350-(−1.696) e Å^{-3}; crystals of this compound break down by cooling to lower temperatures probably as a result of a phase transition.

[28] Crystal data for **4d** at 100 K: $C_{60}H_{79}Au_2F_{12}P_2Sb_2$, 1727.60 g mol^{-1}, monoclinic, $P2_1/c$, $a = 25.471(7)$, $b = 13.423(2)$, $c = 18.588(3)$ Å, $\beta = 92.598(9)°$, $V = 6349(2)$ Å^3, $Z = 4$, $\rho_{calcd} = 1.808$ Mg m^{-3}, $R_1 =$

 © 2006 Wiley-VCH Verlag GmbH & Co. KGaA, Weinheim

0.0468 (0.1072), $wR2 = 0.0878$ (0.1040), for 17284 reflections with $I > 2\sigma(I)$ (for 29337 reflections ($R_{int} = 0.0969$) with a total measured of 108860 reflections), goodness-of-fit on $F^2 = 0.930$, largest diff. peak (hole) = 2.749(−2.349) e Å^{-3}.

[29] a) A. V. Vasilyev, S. V. Lindeman, J. K. Kochi, *Chem. Commun.* **2001**, 909–910; b) K. Ogawa, T. Kitagawa, S. Ishida, K. Komatsu, *Organometallics* **2005**, *24*, 4842–4844.

[30] A. L. Balch, M. M. Olmstead, C. Vickery, *Inorg. Chem.* **1999**, *38*, 3494–3499.

[31] G. M. Sheldrick, *SHELXTL Crystallographic System Ver. 5.10*, Bruker AXS, Inc., Madison, Wisconsin, **1998**.

[32] CCDC 605715–605724 contain the supplementary crystallographic data for this paper. These data can be obtained free of charge from The Cambridge Crystallographic Data Centre via www.ccdc.cam.ac.uk/data_request/cif.

 © 2006 Wiley-VCH Verlag GmbH & Co. KGaA, Weinheim

Cluster Compounds

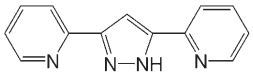
DOI: 10.1002/anie.200602067

An $[Fe^{II}_3O]^{4+}$ Core Wrapped by Two $[Fe^{II}L_3]^-$ Units**

Ko Yoneda, Keiichi Adachi, Kyonosuke Nishio, Mikio Yamasaki, Akira Fuyuhiro, Motomi Katada, Sumio Kaizaki, and Satoshi Kawata**

The spontaneous self-organization of coordination compounds has been studied intensively over the last few decades.[1] One area of particular interest is the assembly of multistranded helicates.[2–5] As most strategies for the synthesis of helicates with high nuclearities make use of long and flexible organic ligands, many linear helicates have been prepared.[3,5] Because of their unique physical and chemical properties, helicates have been used as components of functional materials and devices.[6,7] These applications could experience remarkable development if clusters with novel properties were introduced into the helicates.

There are few examples of cluster helicates, in which metal clusters define the helical axis.[6] However, Saalfrank and co-workers have introduced $[M_3O]^{4+}$ ($M = Mn^{II}$, Zn^{II}, or Cd^{II}) clusters into helicates.[6c] This result prompted us to synthesize a cluster helicate with a similar cluster core. Herein, we report the first pentanuclear bis(triple-helical) complex, $[\{Fe^{II}(\mu\text{-}L)_3\}_2Fe^{II}_3(\mu\text{-}O)]^{2+}$ ($L^- = 3,5$-bis(pyridin-2-yl)pyrazolate), in which an $[Fe^{II}_3O]^{4+}$ core[8] is wrapped by two terminal $[Fe^{II}L_3]^-$ units.



HL

The reaction of HL with $FeCl_2 \cdot 4H_2O$ in the presence of NaNCS under an N_2 atmosphere led to $[\{Fe^{II}(\mu\text{-}L)_3\}_2Fe^{II}_3(\mu\text{-}O)](NCS)_2 \cdot 10H_2O$ (**1**) in 80% yield.[9] The Mössbauer spectrum of **1** at 78 K consists of three quadrupole doublets with relative peak areas of 2:1:2, which correspond to two types of high-spin iron(II) ions (isomer shift (IS) = 1.03 mm s^{-1}, quadrupole splitting (QS) = 3.34 mm s^{-1}; IS = 1.03 mm s^{-1}, QS = 2.81 mm s^{-1}) and one type of low-spin iron(II) ion (IS = 0.46 mm s^{-1}, QS = 0.26 mm s^{-1}), respectively (Figure 1).[10] These Mössbauer data are consistent with the structure determined by X-ray diffraction.

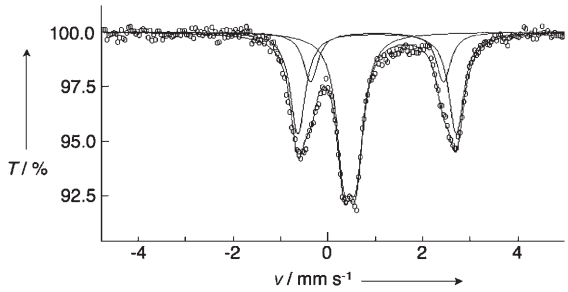


Figure 1. Mössbauer spectrum of a powder sample of **1** at 78 K; T = transmittance, v = velocity; experiment: circles, fit: lines; see text for details.

The structure of the cation of **1** at 93 K is shown in Figure 2.[11] Despite the helical configuration of the cation, which has C_2 point symmetry, the space group of **1** is $I\bar{4}$, and a pair of enantiomers is present in the crystal. The cation consists of six L^- ligands, two iron ions, and an $[Fe^{II}_3O]^{4+}$ core. The core consists of a triangle of three iron ions (Fe(1), Fe(2), and Fe(2*)) with a μ_3-oxygen atom in the center. The Fe-O-Fe angles of the core are 120.9(1) and 118.1(1)°. The remaining two iron ions (Fe(3) and Fe(3*)) take part in terminal triple-stranded $[Fe^{II}L_3]^-$ units. The Fe(3) and Fe(3*) ions, which are

[*] K. Yoneda, Dr. K. Adachi, K. Nishio, Dr. A. Fuyuhiro, Prof. Dr. S. Kaizaki, Prof. Dr. S. Kawata
Department of Chemistry, Graduate School of Science
Osaka University
Toyonaka, Osaka 560-0043 (Japan)
Fax: (+81) 6-6850-5473
E-mail: kaizaki@chem.sci.osaka-u.ac.jp
kawata@chem.sci.osaka-u.ac.jp
Homepage: http://www.chem.sci.osaka-u.ac.jp/lab/kaizaki/
http://www.chem.sci.osaka-u.ac.jp/%7ekawata/
Dr. M. Yamasaki
Single Crystal Structural Analysis Group
Application Laboratories, Rigaku Corporation
Akishima, Tokyo 196-8666 (Japan)
Prof. Dr. M. Katada
Department of Chemistry, Graduate School of Science
Tokyo Metropolitan University
Hachiouji, Tokyo 192-0397 (Japan)

[**] This research was supported by Grants-in-Aid for Scientific Research (Nos. 17350026 and 18550055) and by a Grant-in-Aid for Scientific Research on Priority Areas (No. 434) from the Ministry of Education, Culture, Sports, Science, and Technology of Japan.
$L^- = 3,5$-bis(pyridin-2-yl)pyrazolate.

Supporting information for this article is available on the WWW under http://www.angewandte.org or from the author.

© 2006 Wiley-VCH Verlag GmbH & Co. KGaA, Weinheim

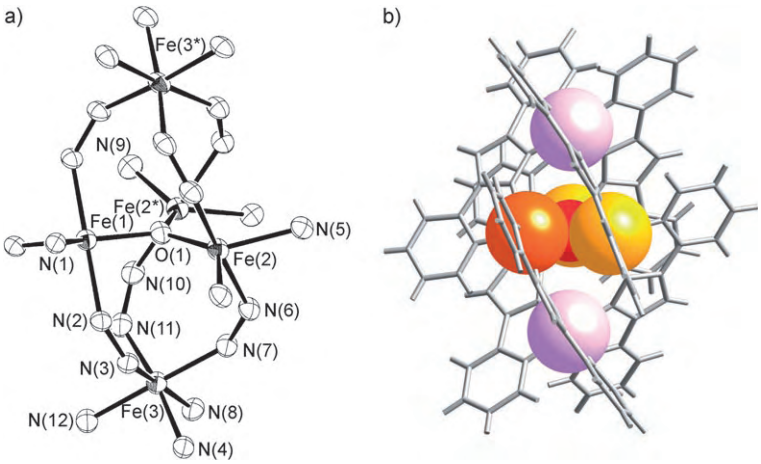


Figure 2. Structure of the $[\{Fe^{II}(\mu\text{-}L)_3\}_2Fe^{II}{}_3(\mu\text{-}O)]^{2+}$ cation of **1**. a) ORTEP representation; displacement ellipsoids set at 50% probability; noncoordinated atoms of the L^- ligands omitted for clarity. b) Ball-and-stick representation; Fe(1) orange, Fe(2)/Fe(2*) yellow, Fe(3)/Fe(3*) purple, O red; C, H, and N gray.

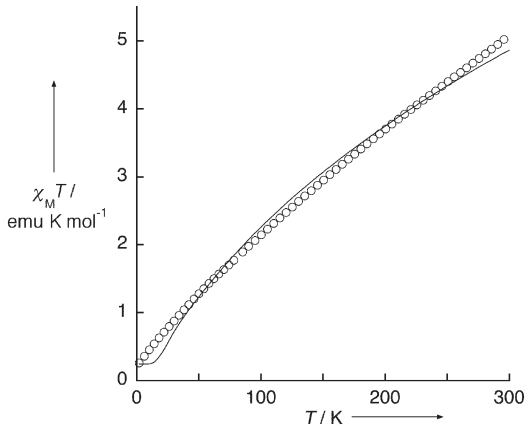


Figure 3. Temperature dependence of $\chi_M T$ for **1**; χ_M = magnetic susceptibility; experiment: circles, fit: line; see text for details.

in the low-spin state ($S=0$), each occupy distorted octahedral coordination environments composed of six nitrogen atoms, two from each of three L^- ligands. Together, the two $[Fe^{II}L_3]^-$ units function as a complex ligand to enclose the $[Fe^{II}{}_3O]^{4+}$ core, like a candy in a wrapper, by using the remaining coordination sites of the L^- ligands. The coordination environments of the Fe(1), Fe(2), and Fe(2*) ions of the core each consist of one O^{2-} ion and four nitrogen atoms from two L^- ligands, which form distorted N_4O trigonal bipyramids (with trigonality indices of $\tau=0.73$ (Fe(1)) and 0.87 (Fe(2)/Fe(2*)).[10] Therefore, it is plausible that the Fe(1) and Fe(2)/Fe(2*) ions are in the high-spin state ($S=2$), consistent with the Mössbauer spectrum. Although many oxo-centered trinuclear iron(III) complexes have been reported,[8,12] to our knowledge, the cation of **1** contains the first example of an oxo-centered trinuclear iron(II) unit. The cation has a pseudo three-fold axis passing through Fe(3) and Fe(3′). Unlike the long organic ligand strands that are generally used for the construction of helicates with high nuclearities, the planar L^- ligand is short and rigid. However, the π stacking of the L^- ligands of the two homochiral $[Fe^{II}L_3]^-$ units leads to bis(triple-helical) strands. The central $[Fe^{II}{}_3O]^{4+}$ core is bound by the remaining coordination sites of these $[Fe^{II}L_3]^-$ units.

The temperature dependence of the magnetic susceptibility (χ_M) of **1** is shown in Figure 3, in the form of a $\chi_M T$ versus T plot. The $\chi_M T$ value at 300 K is approximately 5 emu K mol^{-1} per formula unit, which is smaller than the spin-only value for three high-spin iron(II) ions (9.003 emu K mol^{-1}). Below 300 K, $\chi_M T$ decreases monotonically with decreasing temperature, indicating intramolecular antiferromagnetic coupling. Thus, we fit the essential features of the experimental curve by using the simple triangle model ($H=-2JS_AS_B$),[13] resulting in $J=-29.0$ cm^{-1} and $g=2.29$. Unfortunately, no similar systems with well-characterized Fe^{II}-O-Fe^{II} magnetic interactions are available for comparison with the properties of **1**. However, weak antiferromagnetic interactions have been reported for $[Mn^{III}{}_3(\mu\text{-}O)(O_2CMe)_6(py)_3](py)$ (py = pyridine; $J=-10.9$ cm^{-1}), and ferromagnetic interactions have been reported for $[Mn^{III}{}_3(\mu\text{-}O)(\mu\text{-bamen})_3](ClO_4)\cdot 2H_2O$ (H_2bamen = 1,2-bis(biacetylmonoximeimino)ethane) and $[Mn^{III}{}_3(\mu\text{-}O)(O_2CMe)_3(mpko)_3](ClO_4)\cdot 3CH_2Cl_2$ (Hmpko = methyl 2-pyridyl ketone oxime).[13,14] These findings can be rationalized by noting that the high-spin d^4 manganese(III) ion has an electronic configuration of $(t_{2g})^3(e_g)^1$ in an octahedral field, whereas the high-spin d^6 iron(II) ion has an electronic configuration of $(e'')^3(e')^2(a_1')^1$ in a trigonal bipyramidal field. Unpaired electrons in the e_g or e' orbitals contribute to antiferromagnetic exchange pathways, because the e_g or e' orbitals are involved in σ interactions.

In conclusion, we have shown that L^- and iron(II) ions undergo homochiral self-assembly into a bis(triple-helical) cluster in which an $[Fe^{II}{}_3O]^{4+}$ core is stabilized by bridging two mononuclear $[Fe^{II}L_3]^-$ units. We believe that this synthetic strategy could offer new possibilities for the construction of helicates with unique cluster cores and novel properties.

Received: April 21, 2006
Revised: May 24, 2006
Published online: August 7, 2006

Keywords: bridging ligands · cluster compounds · helical structures · iron · self-assembly

[1] a) S. Kitagawa, R. Kitaura, S. Noro, *Angew. Chem.* **2004**, *116*, 2388; *Angew. Chem. Int. Ed.* **2004**, *43*, 2334; b) J. L. C. Rowsell, O. M. Yaghi, *Angew. Chem.* **2005**, *117*, 4748; *Angew. Chem. Int. Ed.* **2005**, *44*, 4670; c) M. Ruben, J. Rojo, F. J. Romero-Salguero, L. H. Uppadine, J.-M. Lehn, *Angew. Chem.* **2004**, *116*, 3728; *Angew. Chem. Int. Ed.* **2004**, *43*, 3644; d) J.-M. Lehn, *Supramolecular Chemistry-Concepts and Perspectives*, Wiley-VCH, Weinheim, **1995**.
[2] a) M. Albrecht, *Angew. Chem.* **2005**, *117*, 6606; *Angew. Chem. Int. Ed.* **2005**, *44*, 6448; b) M. J. Hannon, L. J. Childs, *Supramol. Chem.* **2004**, *16*, 7; c) J.-M. Lehn, A. Rigault, *Angew. Chem.* **1988**, *100*, 1121; *Angew. Chem. Int. Ed. Engl.* **1988**, *27*, 1095.
[3] M. Albrecht, *Chem. Rev.* **2001**, *101*, 3457.
[4] a) F. E. Hahn, T. Kreickmann, T. Pape, *Dalton Trans.* **2006**, 769; b) J. Garric, J.-M. Léger, I. Huc, *Angew. Chem.* **2005**, *117*, 1990;

 © 2006 Wiley-VCH Verlag GmbH & Co. KGaA, Weinheim

Angew. Chem. Int. Ed. **2005**, *44*, 1954; c) R. Zong, R. Thummel, *Inorg. Chem.* **2005**, *44*, 5984; d) F. E. Hahn, C. S. Isfort, T. Pape, *Angew. Chem.* **2004**, *116*, 4779; *Angew. Chem. Int. Ed.* **2004**, *43*, 4807; e) J. Hamacek, S. Blanc, M. Elhabiri, E. Leize, A. V. Dorsselaer, C. Piguet, A.-M. Albrecht-Gary, *J. Am. Chem. Soc.* **2003**, *125*, 1541; f) L. J. Childs, N. W. Alcock, M. J. Hannon, *Angew. Chem.* **2002**, *114*, 4418; *Angew. Chem. Int. Ed.* **2002**, *41*, 4244; g) J. Hamblin, A. Jackson, N. W. Alcock, M. J. Hannon, *J. Chem. Soc. Dalton Trans.* **2002**, 1635; h) R. W. Saalfrank, S. Trummer, H. Krautscheid, V. Schünemann, A. X. Trautwein, S. Hien, C. Stadler, J. Daub, *Angew. Chem.* **1996**, *108*, 2350; *Angew. Chem. Int. Ed. Engl.* **1996**, *35*, 2206.

[5] a) K. Zeckert, J. Hamacek, J.-M. Senegas, N. Dalla-Favera, S. Floquet, G. Bernardinelli, C. Piguet, *Angew. Chem.* **2005**, *117*, 8168; *Angew. Chem. Int. Ed.* **2005**, *44*, 7954; b) C. J. Matthews, S. T. Onions, G. Morata, L. J. Davis, S. L. Heath, D. J. Price, *Angew. Chem.* **2003**, *115*, 3274; *Angew. Chem. Int. Ed.* **2003**, *42*, 3166.

[6] a) M. Bera, G. Aromí, W. T. Wong, D. Ray, *Chem. Commun.* **2006**, 671; b) M. R. Bermejo, A. M. González-Noya, R. M. Pedrido, M. J. Romero, M. Vázquez, *Angew. Chem.* **2005**, *117*, 4254; *Angew. Chem. Int. Ed.* **2005**, *44*, 4182; c) R. W. Saalfrank, N. Löw, S. Trummer, G. M. Sheldrick, M. Teichert, D. Stalke, *Eur. J. Inorg. Chem.* **1998**, 559.

[7] a) K. Tanaka, A. Tengeiji, T. Kato, N. Toyama, M. Shionoya, *Science* **2003**, *299*, 1212; b) M. Elhabiri, R. Scopelliti, J.-C. G. Bünzli, C. Piguet, *J. Am. Chem. Soc.* **1999**, *121*, 10747.

[8] a) S. Herold, S. J. Lippard, *Inorg. Chem.* **1997**, *36*, 50; b) E. Y. Tshuva, S. J. Lippard, *Chem. Rev.* **2004**, *104*, 987.

[9] An aqueous solution (2 mL) of $FeCl_2 \cdot 4H_2O$ (3.7 mM) was transferred into a glass tube, and then a 1:1 methanol/water mixture (2 mL) of HL (4.5 mM), NaNCS (1.5 mM), and NaOH (4.5 mM) was added without mixing under an N_2 stream. Dark orange crystals began to form at ambient temperature after 2 days. Yield 80%. Elemental analysis (%) calcd for $C_{80}H_{74}N_{26}O_{11}S_2Fe_5$: C 50.05, H 3.94, N 18.97; found: C 49.04, H 3.70, N 19.14. MS (positive ESI; 1:3 CH_3OH/H_2O): *m*/*z*: 811 $[\{Fe^{II}(\mu\text{-}L)_3\}_2Fe^{II}_3(\mu\text{-}O)]^{2+}$.

[10] A. K. Boudalis, J.-M. Clemente-Juan, F. Dahan, J.-P. Tuchagues, *Inorg. Chem.* **2004**, *43*, 1574.

[11] Crystal structure analysis for **1**: The data collection was carried out on a Rigaku RAXIS-RAPID diffractometer with graphite-monochromated $Mo_{K\alpha}$ radiation. The structure was solved by direct methods (Rigaku CrystalStructure, Molecular Structure Corporation) and refined with full-matrix least-squares techniques (SHELXL97[15]). Crystal data: $C_{80}H_{74}N_{26}O_{11}S_2Fe_5$, $T = 93$ K, dark orange, tetragonal, space group $I\bar{4}$, $Z = 1$, $a = 16.897(2)$, $c = 29.980(5)$ Å, $V = 8559(2)$ Å^3, $\rho_{calcd} = 1.489$ g cm^{-3}, $\mu(Mo_{K\alpha}) = 9.51$ cm^{-1}, 50290 reflections collected, $2\theta < 59.9°$, 12349 independent reflections ($R_{int} = 0.026$), 610 parameters, all non-hydrogen atoms anisotropic, all hydrogen atoms in calculated positions, $R_1 = 0.0396$ (for 11207 $F < 4\sigma(F)$), $wR_2 = 0.1243$, Flack parameter = 0.006(10), GOF = 1.062. CCDC-604887 (**1**) contains the supplementary crystallographic data for this paper. These data can be obtained free of charge from The Cambridge Crystallographic Data Centre via www.ccdc.cam.ac.uk/data_request/cif.

[12] A. K. Boudalis, Y. Sanakis, F. Dahan, M. Hendrich, J.-P. Tuchagues, *Inorg. Chem.* **2006**, *45*, 443.

[13] J. B. Vincent, H.-R. Chang, K. Folting, J. C. Huffman, G. Christou, D. N. Hendrickson, *J. Am. Chem. Soc.* **1987**, *109*, 5703.

[14] a) S. G. Sreerama, S. Pal, *Inorg. Chem.* **2002**, *41*, 4843; b) T. C. Stamatatos, D. Foguet-Albiol, C. C. Stoumpos, C. P. Raptopoulou, A. Terzis, W. Wernsdorfer, S. P. Periepes, G. Christou, *J. Am. Chem. Soc.* **2005**, *127*, 15380.

[15] G. M. Sheldrick, SHELXL97, University of Göttingen, Germany, **1997**.

 © 2006 Wiley-VCH Verlag GmbH & Co. KGaA, Weinheim

Host–Guest Systems

DOI: 10.1002/anie.200600933

Guest-Induced Instant and Reversible Crystal-to-Crystal Transformation of 1,4-Bis(ferrocenylethynyl)anthraquinone**

Mio Kondo, Masaki Murata, Hiroshi Nishihara, Eiji Nishibori, Shinobu Aoyagi, Masanori Yoshida, Yusuke Kinoshita, and Makoto Sakata*

For decades, much attention has focused on crystallization from a mixture of electron-donor (D) and -acceptor (A) molecules, forming D- and/or A-stacked column structures that exhibit unique physical properties such as ferromagnetism,[1] strong absorption of Vis/NIR light,[2] and high electronic conductivity.[3] The tendency toward DA stacking in the crystal indicates that D–A conjugated molecules can form network structures which may manifest interesting physical properties. We are interested in the chemistry of a new class of D–A conjugated systems, namely, ferrocenylethynylanthraquinones (FcAq), from two viewpoints: protonation-induced intramolecular electron transfer resulting in valence tautomers,[4] and the construction of D–A stacked nanoporous network structures, which have attracted much recent attention because of great potential for applications such as selective gas adsorption,[5–7] heterogeneous catalysts,[8,9] and molecular recognition.[10,11] In the present study, we found that the new T-shaped FcAq compound 1,4-bis(ferrocenylethynyl)anthraquinone (1,4-Fc_2Aq (**1**); Figure 1a) in the presence of guest solvent molecules forms single crystals, which show instant and reversible crystal-to-crystal transformation on heating or treatment with guest vapors. Recently, several reversible crystal-to-crystal transformations have been reported,[5,12] among which examples accompanying a significant conformational change are few.[13,14] The present study demonstrates an instant and reversible trans-

[*] M. Kondo, Dr. M. Murata, Prof. Dr. H. Nishihara
Department of Chemistry
School of Science
The University of Tokyo
7-3-1 Hongo, Bunkyo-ku, Tokyo 113-0033 (Japan)
Fax: (+81) 358-418-063
E-mail: nisihara@chem.s.u-tokyo.ac.jp
Dr. E. Nishibori, Dr. S. Aoyagi, M. Yoshida, Y. Kinoshita, Prof. Dr. M. Sakata
Department of Applied Physics
Nagoya University
Nagoya 464-8603 (Japan)

[**] The synchrotron radiation experiments were performed at BL02B2 in SPring-8 with the approval of the Japan Synchrotron Radiation Research Institute (JASRI) (proposal nos. 2005A0454-Nb1b-np, 2005B0466, 2006A1595). This work was supported by Grants-in-Aid for Scientific Research (nos. 16047204 (area 434) and 17205007), and by a grant from The 21st Century COE Program for Frontiers in Fundamental Chemistry from MEXT, and CREST, Japan.

Supporting information for this article is available on the WWW under http://www.angewandte.org or from the author.

 © 2006 Wiley-VCH Verlag GmbH & Co. KGaA, Weinheim

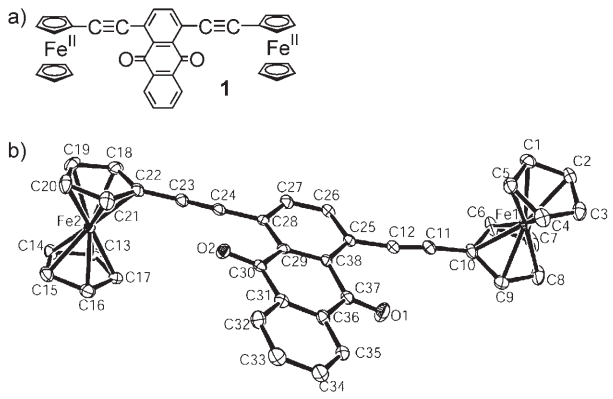


Figure 1. a) Chemical structure of 1,4-Fc_2Aq (**1**); b) ORTEP plot of a 1,4-Fc_2Aq molecule in a crystal of α-**1**·CH_2Cl_2. Hydrogen atoms and disordered guest molecules are omitted for clarity.

formation despite a very large conformational change in the D–A stacked structure, which can be monitored by variable-temperature synchrotron X-ray powder diffraction (VT-XRPD).

We synthesized 1,4-Fc_2Aq (**1**) by Sonogashira cross-coupling of 1,4-dibromoanthraquinone with 1-ethynylferrocene in 33% yield. Crystals of **1** obtained from various solvents were analyzed by single-crystal X-ray diffraction. An ORTEP diagram of a 1,4-Fc_2Aq molecule in a crystal of α-**1**·CH_2Cl_2 is shown in Figure 1b.[15] In most of the structures, inclusion of solvent as guest molecule is observed. The crystal structure of α-**1**·CH_2Cl_2 along the *b* axis is shown in Figure 2a as an example. The crystal was obtained by recrystallization from dichloromethane/hexane at 263 K; under these conditions, a large crystal (25 × 1 × 1 mm) grew within a week (Figure 2d). α-**1**·CH_2Cl_2 has subnanopores with dimensions of 5.7 × 3.5 Å[16] along the *b* axis in which dichloromethane guest molecules are contained with a **1**/CH_2Cl_2 molar ratio of 1:1. An infinite one-dimensional columnar structure is formed along the *b* axis by an alternating arrangement of a π-conjugated spacer and a π–π stacking interaction between Fc (D) and Aq (A) moieties (Figure 3a). The shortest distance between a cyclopentadienyl (Cp) plane of Fc and an Aq plane is 3.44 Å. The Aq and Cp planes form angles of about 45° with the *b* axis. Two kinds of complex columns are almost perpendicular to each other and are arranged alternately to construct the porous framework. Crystallographic data of single crystals with the composition **1**·X (X = guest molecule) obtained by recrystallization from different solvents are

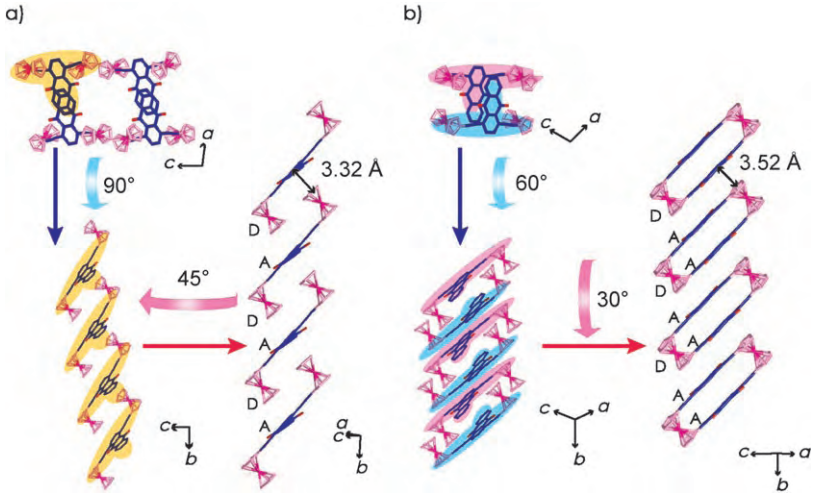


Figure 3. One-dimensional columnar structures of **1**·X (a), and solvent-free **1** (b).

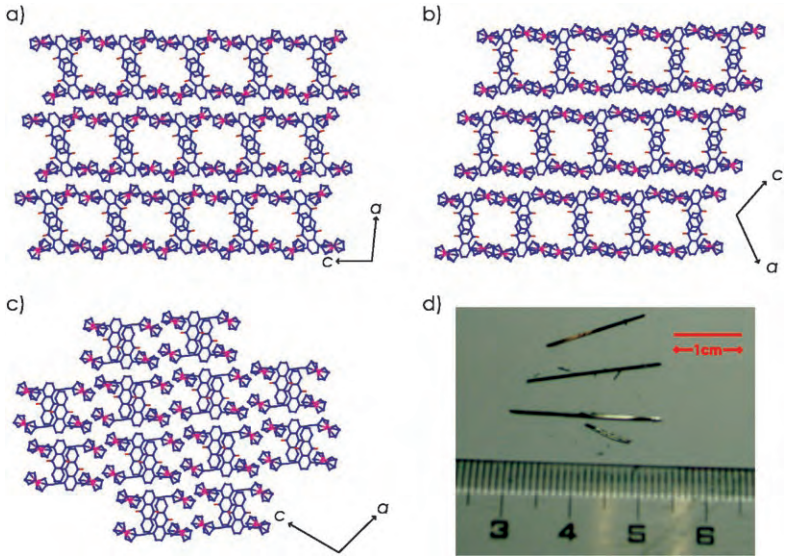


Figure 2. Crystal structures of α-**1**·CH_2Cl_2 along the *b* axis (a), β-**1**·CH_2Cl_2 along the *b* axis (b), solvent-free **1** along the *b* axis (c), and a photograph of α-**1**·CH_2Cl_2 crystals (d). Hydrogen atoms and disordered guest molecules (CH_2Cl_2) are omitted for clarity.

summarized in the Supporting Information.[15] Their crystal structures are similar to that of α-**1**·CH_2Cl_2, but the size of the subnanopores changes according to the size of the included guest molecules. Two types of crystals (α and β phases in Figure 2a and b; see the Supporting Information) were obtained when X was dichloromethane, chloroform, or carbon tetrachloride. The guest molecules in these structures are extremely disordered. The α phase has a shorter plane-to-plane distance between Fc and Aq but a larger dihedral angle ϕ between the Cp ring of ferrocene and the Aq plane (C25–C29, and C38) than the β phase (see the Supporting Information). Because of the balance between these two factors, that is, the shorter distance stabilizing the α phase and the large ϕ destabilizing it, both α and β phases may exist under the same conditions. Only one type of structure was formed when X was a larger guest molecule such as THF, trichloroethylene, or hexane.

Recrystallization of **1** from *o*-dichlorobenzene/hexane at 263 K afforded crystals containing *o*-dichlorobenzene and hexane guests in an ordered arrangement

 © 2006 Wiley-VCH Verlag GmbH & Co. KGaA, Weinheim

(see the Supporting Information). In contrast, when **1** was recrystallized at 293 K from *o*-dichlorobenzene/hexane, crystals without pores and solvent molecules were obtained (Figure 2c).[15] In the solvent-free form, a columnar structure is maintained (Figure 3b), whereas the *syn* conformation of the ferrocene moieties in **1** allows the formation of pairs of adjacent molecules in the crystal and the pattern of the stacking arrangement changes from D–A to D–A–A compared with the porous **1**·X form.

Thermal desorption of the guest molecules in **1**·X was examined by thermogravimetric analysis (TGA). The TG curve indicated desorption of guest molecules at $T_{de} = 346$–380 K without chemical decomposition. The T_{de} values do not correlate with the boiling points of the guest molecules (e.g., the most volatile dichloromethane had high T_{de}), that is, the host–guest interaction affects T_{de} significantly.

To clarify the crystal structure after desorption of guest molecules, the synchrotron X-ray powder diffraction (XRPD) pattern of a sample prepared by heating **1**·THF at 420 K under vacuum for 12 h was measured, and the cell parameters of the sample were determined by the Rietveld method. The XRPD-derived cell parameters were consistent with those of solvent-free **1** (see the Supporting Information). The XRPD patterns of samples of **1**·CH_2Cl_2 from which guests had been desorbed thermally were also the same as those of solvent-free **1**. Thus, it is confirmed that guest desorption causes crystal-to-crystal transformation from **1**·X to solvent-free **1**.

Reversibility of the crystal-to-crystal transformation on guest desorption and adsorption by **1** was studied by variable-temperature XRPD (VT-XRPD). For this measurement, we prepared a vacuum-sealed 1-mm-diameter glass capillary containing a 0.5-mm-diameter capillary filled with frozen THF and a 0.5-mm-diameter capillary packed with powdered solvent-free **1** (Figure 4a). After 3 h at room temperature, the XRPD pattern had completely changed from that of solvent-free **1** to that of **1**·THF (Figure 4b, A→B). Then, THF was frozen at 90 K and the sample was heated from 300 to 400 K. Subsequently, the temperature of the sample capillary T_s was maintained at 300 K, and the temperature of the THF capillary T_g was increased from 90 to 400 K. XRPD patterns were measured at every 50 K with an X-ray exposure time of 5 min for each measurement. On heating a sample of **1**·THF, THF molecules were released, the XRPD pattern of solvent-free **1** emerged, and, at 400 K, the pattern corresponded completely to that of solvent-free **1** (Figure 4b, C). When the capillary was filled with THF vapor by increasing T_g, THF molecules were adsorbed by the host, and XRPD patterns arising from **1**·THF were observed (Figure 4b, D–G). When T_s and T_g were kept at 300 K, guest adsorption was complete within 5 min (see the Supporting Information).

These results indicate rapid and reversible crystal-to-crystal transformation between **1**·THF and solvent-free **1**. In view of the conformational change required, the fast transformation is particularly remarkable.[14] These features are derived from the flexibility of the crystal structure as a result of the D–A interaction, which is weaker than other chemical bonds, and from the higher stability of **1**·THF compared with solvent-free **1** ($\Delta G = -32$ kJ mol^{-1} [17]). Diffuse reflectance

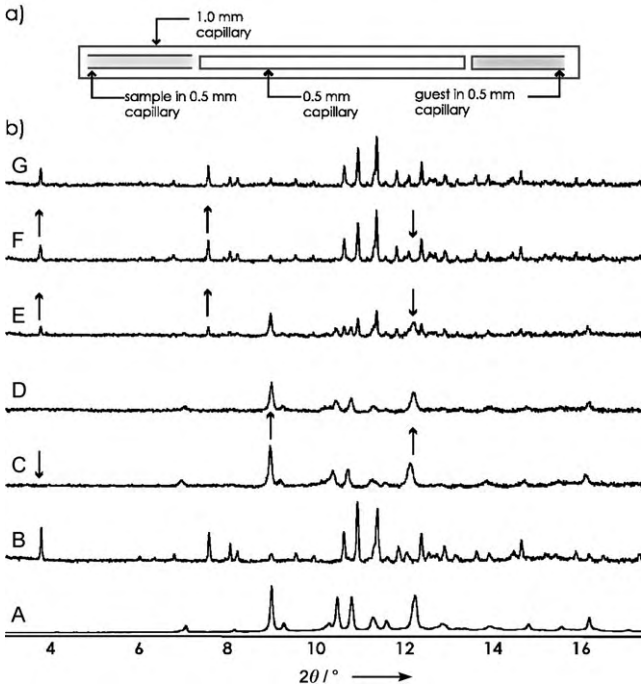


Figure 4. a) Illustration of the capillary used in VT-XRPD experiment. b) XRPD pattern of solvent-free **1** (A) and results of VT-XRPD measurements (B–G). Temperatures of sample (T_s) and guest (T_g) were B: $T_s = 350$, $T_g = 90$ K; C: $T_s = 400$, $T_g = 90$ K; D: $T_s = 300$, $T_g = 200$ K; E: $T_s = 300$, $T_g = 300$ K; F: $T_s = 300$, T_g 350 K; and G: $T_s = 300$, $T_g = 400$ K.

UV/Vis spectra of **1**·THF and solvent-free **1** indicated appearance of a CT band that is not present in the spectrum of **1** in solution and a red shift of the CT band for **1**·THF ($\lambda_{max} = 619$ nm) from that of solvent-free **1** ($\lambda_{max} = 601$ nm; see the Supporting Information). This result suggests stronger D–A interaction in **1**·X, which is consistent with the one-dimensional columnar D–A structure and the shorter Cp–Aq distance compared with that in solvent-free **1**.

In conclusion, the new D–A conjugated compound 1,4-Fc_2Aq (**1**) has been synthesized. Crystals of **1** have either a solvent-incorporating porous structure or a solvent-free nonporous structure, which can be instantly and reversibly interconverted by desorption and adsorption of guest molecules, with alternation of D–A and D–A–A arrangements in the one-dimensional columnar structure. A preliminary study has shown that **1** exhibits protonation-induced intramolecular electron transfer. We are currently investigating the combination of physical property changes resulting from the interaction with acid molecules and the crystal structural transformation.

Experimental Section

1: 1,4-Dibromoanthraquinone (2.42 g, 6.6 mmol) and 1-ethynylferrocene (2.831 g, 13.5 mol) were dispersed in triethylamine (120 mL) and stirred. CuI (136 mg, 0.72 mmol) and [$PdCl_2(PPh_3)_2$] (482 mg, 0.69 mmol) were added. The suspension was heated to reflux for 3 h. The color of the reaction mixture turned from orange to dark red.

 © 2006 Wiley-VCH Verlag GmbH & Co. KGaA, Weinheim

The solvent was removed under vacuum. The residue was dissolved in 100 mL of dichloromethane, washed with water, and then dried over anhydrous Na_2SO_4. The filtrate was subjected to chromatography on an alumina column (activity II–III, 6 × 20 cm) with dichloromethane/hexane (1:3→1:1). The third brown band was collected. The product was recrystallized from dichloromethane/hexane, and black crystals were collected. Yield: 1.3442 g (32.6 %). ^{1}H NMR (400 MHz, $CDCl_3$): δ = 4.34 (t, 4H, J = 1.8 Hz; Cp), 4.35 (s, 10H; Cp), 4.67 (t, 4H, J = 1.8 Hz; Cp), 7.78 (m, 2H; Ph), 7.81 (s, 2H; Ph), 8.34 ppm (s, 2H; Ph). ^{13}C NMR (125 MHz, CD_2Cl_2): δ = 65.4 (Cp), 70.2 (Cp), 70.8 (Cp), 72.4 (Cp), 86.9 (C≡C), 98.1 (C≡C), 123.9 (Aq), 127.4 (Aq), 134,1 (Aq), 134.8 (Aq), 139.0 (Aq), 182.4 ppm (C=O). MS (ESI-TOF-MS): m/z 623.9541; calcd: 624.29 [M^+].

X-ray diffraction measurements: The crystals were mounted in a loop. Data was collected with a Rigaku AFC8 diffractometer with the Rigaku Mercury CCD system equipped with a rotating-anode X-ray generator producing graphite-monochromated $Mo_{K\alpha}$ radiation (λ = 0.7107 Å). An empirical absorption correction using equivalent reflections and Lorentzian polarization were performed with the program Crystal Clear 1.3.5. The structure was solved with the program SHELXS-97[18] and refined against F^2 using SHELXL-97[19] Selected crystallographic data and experimental details are listed in the Supporting Information.

The in situ synchrotron powder diffraction experiment on THF adsorption was performed on a large Debye–Scherrer camera installed at SPring-8 BL02B2 with an imaging plate as detector. The wavelength of the incident X-rays was 1.001 Å. VT-XRPD measurements were performed with a nitrogen gas-flow system.

Received: March 9, 2006
Revised: May 10, 2006
Published online: July 19, 2006

Keywords: donor–acceptor systems · host–guest systems · metallocenes · microporous materials · X-ray diffraction

[1] a) A. Alberola, E. Coronado, J. R. Galán-Mascarós, C. Giménez-Saiz, C. J. Gómez-García, *J. Am. Chem. Soc.* **2003**, *125*, 10774 – 10775; b) K. Mukai, S. Jinno, Y. Shimobe, N. Azuma, M. Taniguchi, Y. Misaki, K. Tanaka, K. Inoue, Y. Hosokoshi, *J. Mater. Chem.* **2003**, *13*, 1614 – 1621; c) T. Matsumoto, T. Kominami, K. Ueda, T. Sugimoto, T. Tada, S. Noguchi, H. Yoshino, K. Murata, M. Shiro, E. Negishi, N. Toyota, S. Endo, K. Takahashi, *Inorg. Chem.* **2002**, *41*, 4763 – 4769; d) G. Wang, C. Slebodnick, R. J. Butcher, M. C. Tam, T. D. Crawford, G. T. Yee, *J. Am. Chem. Soc.* **2004**, *126*, 16890 – 16895; e) H. Nakajima, M. Katsuhara, M. Ashizawa, T. Kawamoto, T. Mori, *Inorg. Chem.* **2004**, *43*, 6075 – 6082.

[2] a) M. Chollet, L. Guerin, N. Uchida, S. Fukaya, H. Shimoda, T. Ishikawa, K. Matsuda, T. Hasegawa, A. Ota, H. Yamochi, G. Saito, R. Tazaki, S. Adachi, S. Koshihara, *Science* **2005**, *307*, 86 – 89; b) H. Nishihara, M. Kurashina, K. Aramaki, K. Kubo, *Synth. Met.* **1999**, *101*, 457 – 458.

[3] a) J. Ferraris, D. O. Cowan, V. Walatka, Jr., J. H. Perlstein, *J. Am. Chem. Soc.* **1973**, *95*, 948 – 949; b) G. Saito, H. Sasaki, T. Aoki, Y. Yoshida, A. Otsuka, H. Yamochi, O. O. Drozdova, K. Yakushi, H. Kitagawa, T. Mitani, *J. Mater. Chem.* **2002**, *12*, 1640 – 1649.

[4] a) M. Murata, H. Nishihara, *Macromolecules Containing Metal and Metal-like Elements, Vol. 2*, Wiley-Interscience, **2003**, chap. 8, p. 135; b) H. Nishihara, *Adv. Inorg. Chem.* **2002**, *226*, 125; c) M. Murata, T. Fujita, M. Yamada, M. Kurihara, H. Nishihara, *Chem. Lett.* **2000**, 1328 – 1329; d) M. Murata, M. Yamada, T. Fujita, K. Kojima, M. Kurihara, K. Kubo, H. Nishihara, *J. Am. Chem. Soc.* **2001**, *123*, 12903 – 12904.

[5] T. K. Maji, K. Uemura, H.-C. Chang, R. Matsuda, S. Kitagawa, *Angew. Chem.* **2004**, *116*, 3331 – 3334; *Angew. Chem. Int. Ed.* **2004**, *43*, 3269 – 3272.

[6] D. N. Dybtsev, H. Chun, S. H. Yoon, D. Kim, K. Kim, *J. Am. Chem. Soc.* **2004**, *126*, 32 – 33.

[7] M. Dincă, J. R. Long, *J. Am. Chem. Soc.* **2005**, *127*, 9376 – 9377.

[8] O. Ohmori, M. Fujita, *Chem. Commun.* **2004**, 1586 – 1587.

[9] J. S. Seo, D. Whang, H. Lee, S. I. Jun, J. Oh, Y. J. Jeon, K. Kim, *Nature* **2000**, *404*, 982 – 986.

[10] R. Matsuda, R. Kitaura, S. Kitagawa, Y. Kubota, R. V. Belosludov, T. C. Kobayashi, H. Sakamoto, T. Chiba, M. Takata, Y. Kawazoe, Y. Mita, *Nature* **2005**, *436*, 238 – 241.

[11] O. Ohmori, M. Kawano, M. Fujita, *J. Am. Chem. Soc.* **2004**, *126*, 16292 – 16293.

[12] a) S. Kitagawa, K. Uemura, *Chem. Soc. Rev.* **2005**, *34*, 109 – 119; b) C-D. Wu, W. Lin, *Angew. Chem.* **2005**, *117*, 1994 – 1997; *Angew. Chem. Int. Ed.* **2005**, *44*, 1958 – 1961; c) T. Pretsch, K. W. Chapman, G. J. Halder, C. J. Kepert, *Chem. Commun.* **2006**, 1857 – 1859; d) C.-L. Chen, A. M. Goforth, M. D. Smith, C.-Y. Su, H.-C. zur Loye, *Angew. Chem.* **2005**, *117*, 6831 – 6835; *Angew. Chem. Int. Ed.* **2005**, *44*, 6673 – 6677.

[13] a) J.-P. Zhang, Y.-Y. Lin, W. X. Zhang, X.-M. Chen, *J. Am. Chem. Soc.* **2005**, *127*, 14162 – 14163; b) S. K. Mäkinen, N. J. Melcer, M. Parvez, G. K. H. Shimizu, *Chem. Eur. J.* **2001**, *7*, 5176 – 5182.

[14] a) C. Hu, U. Englert, *Angew. Chem.* **2005**, *117*, 2321 – 2323; *Angew. Chem. Int. Ed.* **2005**, *44*, 2281 – 2283; b) M. P. Suh, J. W. Ko, H. J. Choi, *J. Am. Chem. Soc.* **2002**, *124*, 10976 – 10977.

[15] CCDC-600337–CCDC-600347 contain the supplementary crystallographic data for this paper. These data can be obtained free of charge from The Cambridge Crystallographic Data Centre via www.ccdc.cam.ac.uk/data request/cif.

[16] The size was determined by considering van der Waals radii of constituent atoms.

[17] Estimated from the DSC measurement.

[18] G. M. Sheldrick, SHELXS-97, Program for crystal structure solution, University of Göttingen, Germany, **1997**.

[19] G. M. Sheldrick, SHELXL-97, Program for crystal structure refinement, University of Göttingen, Germany, **1997**.

 © 2006 Wiley-VCH Verlag GmbH & Co. KGaA, Weinheim

Noncovalent Interactions

DOI: 10.1002/anie.200601123

Supramolecular Control of Oligosaccharide–Protein Interactions: Switchable and Tunable Ligands for Concanavalin A Based on β-Cyclodextrin**

Nicolas Smiljanic, Vincent Moreau, Duplex Yockot, Juan M. Benito, José M. García Fernández, and Florence Djedaïni-Pilard**

Interactions between carbohydrate-binding proteins (lectins) and cell-surface carbohydrate ligands have been shown to be critical for a wide variety of intercellular recognition processes, including cell proliferation, signaling, and recognition.[1] The interaction of a single carbohydrate ligand and a protein molecule is, however, usually too weak to induce a useful biological response. Biological systems commonly engage in multivalent carbohydrate–protein interactions to enhance the affinity. Remarkably, the advantage gained by multiple copies of a ligand is generally more than that predicted for the sum of the individual interactions.[2] This observation was first reported by Lee and Lee and is known as the glycoside cluster effect.[3] Since then it has been speculated that nature uses carbohydrate surface density as an "on/off" switch to regulate biological events involving carbohydrate–protein interactions. However, recent results have indicated that the situation is far more complicated. Architectural and orientational factors as well as secondary interactions in a heterogeneous environment may play a decisive role in the regulation and fine tuning of the binding strength and selectivity of the interaction between a lectin and its putative ligand.[4]

A number of multivalent systems have been reported in which the loading of the saccharide binding epitopes or their overall geometry were varied to get information on the mechanisms involved in the glycoside cluster effect.[5,6] However, none of the reported examples can fully mimic the switching between the "on" and "off" states and the regulation of the binding intensity after an external stimulus. We have now developed a molecular system based on β-cyclodextrin (βCD)[7] that can reproduce this behavior by virtue of allosteric supramolecular interactions with effector/antagonist-like molecules.

Switching of carbohydrate–protein interactions has previously been achieved through chemical modification of the protein with photoisomerizable groups that induce structural perturbations at the protein binding site. In seminal work, Willner prepared chemically modified lectins with reversible photochromic properties and demonstrated the reversible photostimulated "on/off" association and dissociation of monosaccharides.[8] The present study aims at implementing the "reversible structure-dependent binding" strategy by designing conformationally switchable glycoligands that are sensitive to chemical inputs.

Our molecular design is based on the observation that the ability of βCD-centered glycoligands to bind lectins is strongly influenced by the distance between the recognition motif and the βCD scaffold.[9] We conceived that this distance could be modulated by inserting a segment that was able to undergo intramolecular inclusion into the βCD cavity in a reversible manner. Previous results showed that some amino acids grafted on the βCD core form self-inclusion complexes in aqueous solution.[10] Interestingly, this process can be shifted in the presence of a competing guest for βCDs bearing a tyrosinyl residue,[11] thus suggesting that this structural motif could act as a distance-regulating element.

To prove the above concept we have focused on concanavalin A (Con A), a mannose-specific lectin commonly used to probe protein–carbohydrate interactions,[12] and the branched trisaccharide 3,6-di-*O*-(α-D-mannopyranosyl)-α-D-mannopyaranose (Man-tri) as the protein receptor and the sugar ligand, respectively. Con A is known to possess an extended binding site for this trisaccharide, and results in a binding affinity ($\log K = 5.4$) much higher than that encountered for trivalent or even higher-valency mannopyranosides.[1b]

According to our previous work, we attached a succinylamido substituent to the βCD prior to the incorporation of the tyrosine segment or the mannosyl ligand.[13] It was anticipated that this spacer would provide enough flexibility to allow both the self-inclusion process and glycoligand–lectin recognition events in an extended conformation. To confirm this point, compounds **1** and **2**, which differed in the absence or presence of the aromatic amino acid, were prepared. Additionally, conjugate **3**, which possesses two Man-tri units, was synthesized to check how polyvalency could affect both the lectin binding and the self-inclusion phenomena in such a system (Scheme 1).

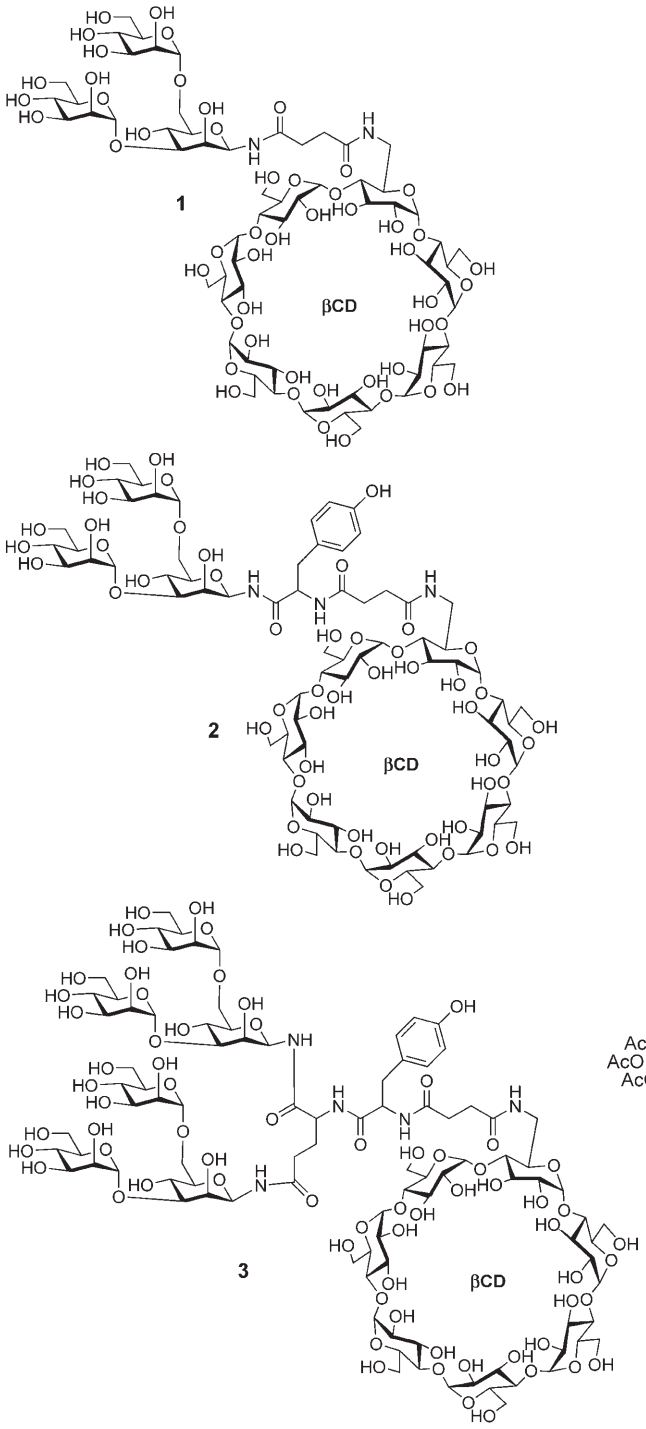
The synthetic strategy to access compounds **1**–**3** follows a convergent approach and makes use of standard peptide-coupling techniques. The synthesis of the per-*O*-esterified Man-tri glycosylamine **4** was achieved by using a simultaneous "double-glycosylation" of 2,4-di-*O*-benzoyl-α-D-mannopyranosyl azide with 2,3,4,6-tetra-*O*-acetyl-α-D-mannopyr-

[*] Dr. J. M. Benito, Dr. J. M. García Fernández
Instituto de Investigaciones Químicas
CSIC – Universidad de Sevilla
Américo Vespucio 49, Isla de la Cartuja, 41092 Sevilla (Spain)
Fax: (+34) 954-460-565
E-mail: jogarcia@iiq.csic.es
Dr. N. Smiljanic, Dr. V. Moreau, Dr. D. Yockot, Prof. F. Djedaïni-Pilard
Laboratoire des Glucides UMR6219
Université Picardie Jules Verne
33, rue St. Leu, 80039 Amiens (France)
Fax: (+33) 322-827-562
E-mail: florence.pilard@u-picardie.fr

[**] This work was supported by the Conseil Régional de Picardie under the scientific IBFBio program and by the Spanish Ministerio de Educación y Ciencia (contract number BQU2003-00937). D.Y. is grateful to the Ministère Gabonais des Finances et des Bourses et Stages for a doctoral fellowship. N.S. is grateful to the Conseil Régional de Picardie for a doctoral fellowship.

Supporting information for this article is available on the WWW under http://www.angewandte.org or from the author.

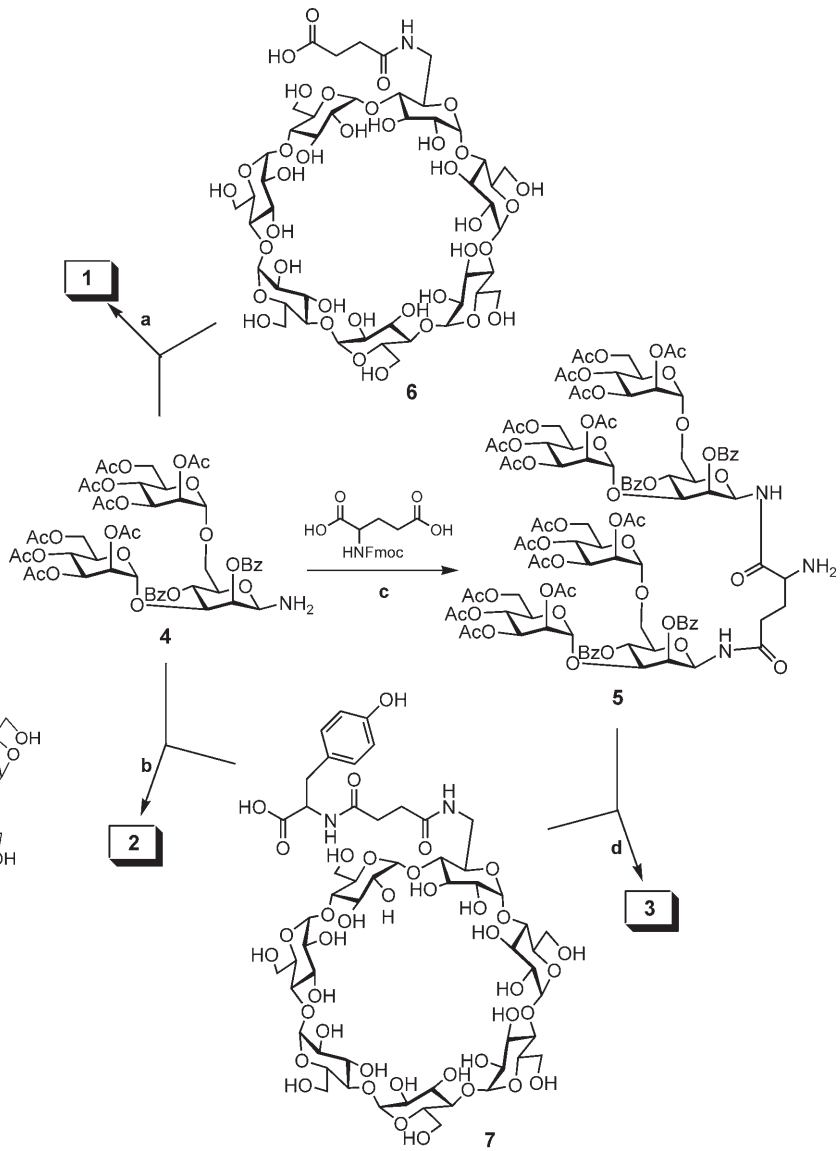
 © 2006 Wiley-VCH Verlag GmbH & Co. KGaA, Weinheim



Scheme 1. Structure of the Man-tri–βCD conjugates evaluated.

anosyl trichloroacetimidate as described previously.[11,14] Reduction of the anomeric azido group to a β-amine was significantly improved by using the "catalytic transfer hydrogenation" method developed by Anwer and Spatola[15] (see the Supporting Information). Amide coupling of the known monofunctionalized βCD derivative **6**[13] and glycosylamine **4** afforded, after deprotection of the corresponding hemiacylated adduct, the succinyl-tethered conjugate **1**. An analogous coupling-deprotection sequence involving **4** and the tyrosinyl-armed precursor **7**[11] provided the elongated analogue **2**. Replacing the trisaccharide precursor by the amine-armed glycodendron **5**, accessible by double peptide coupling of **4** with N-Fmoc-protected glutamic acid and subsequent removal of the carbamate protecting group, afforded the target $(Man\text{-}tri)_2$ conjugate **3** (Scheme 2).

Comparative ^{1}H NMR and T-ROESY experiments on **1**–**3** in D_2O at different concentrations confirmed the formation of intramolecular self-inclusion complexes with the tyrosine-bearing conjugates **2** and **3**, with the aromatic ring placed inside the βCD cavity. These complexes were disrupted in $[D_6]$DMSO solution, thus indicating the reversible character of the self-inclusion process. Addition of adamantane-1-



Scheme 2. Synthesis of the βCD conjugates **1**–**3**. a) DIC, HOBt, iPr$_2$NEt, DMF, 96 h then DMF-MeOH, MeONa (1 M in MeOH), 7 days, (23%); b) Ref. [8]; c) DIC, HOBt, iPr$_2$NEt, DMF, 72 h, then piperidine, DMF, 90 min (76%); d) DIC, HOBt, iPr$_2$NEt, DMF, 72 h then MeOH, NH_3 (7 N in MeOH), 10 days (40%). DIC = diisopropylcarbodiimide, HOBt = 1-hydroxy-1*H*-benzotriazole, Fmoc = 9-fluorenylmethoxycarbonyl, Bz = benzyl.

 © 2006 Wiley-VCH Verlag GmbH & Co. KGaA, Weinheim

carboxylate (AC), known to be an excellent guest for βCD (association constant (K_{ass}) $3.9\times10^4\,M^{-1}$),[16] to solutions of **2** or **3** in D_2O also caused departure of the tyrosine residue from the cavity, with formation of the 1:1 intermolecular inclusion complexes **2**:AC or **3**:AC ($K_{ass}=1.6\times10^4\,M^{-1}$), as deduced from NMR titration experiments.[17]

For evaluation of Con A binding, the enzyme-linked lectin assay (ELLA), a variation on the enzyme-linked immunosorbent assay (ELISA), was implemented.[2b] In agreement with our initial hypothesis, **2** was virtually unrecognized by the lectin at concentrations up to 1 mM, a result which is in stark contrast with data for **1** that lacks the tyrosine segment (IC_{50} 21 μM). Interestingly, a dramatic increase in Con A binding affinity was observed for **2** (IC_{50} 22 μM) in the presence of a threefold molar excess of AC, while that of **1** remained unaffected (Figure 1A). This result strongly supports the scenario depicted in Figure 1B (left-to-right). In the "off" state the epitope is not accessible to the protein binding site because of its conformation, while in the "on" state, the oligosaccharide is fully exposed to interact with the lectin. Switching between these two modes can be controlled by an allosteric supramolecular process at the CD cavity involving AC as a competing guest molecule.

Evaluation of the $(Man\text{-}tri)_2$ conjugate **3** by ELLA indicated that it had an affinity towards the protein receptor ($IC_{50}=3.2$ μM) that was more than sixfold higher than that of **1** or the **2**:AC complex. The Man-tri unit located at the α-substituent of the glutamic acid segment in **3** is probably now fully accessible for binding to Con A, the second one being only partially available to contribute to the glycoside cluster effect because of the energetic cost of disrupting the self-inclusion complex. Accordingly, a gradual increase in activity, up to a factor of three (IC_{50} 1.0 μM), was observed in the presence of increasing proportions of AC (Figure 2A). From this data, a binding isotherm consistent with formation of a 1:1 host/guest ligand was derived. Nonlinear regression analysis (Figure 2B) provided a K_{ass} value of $1.4\times10^4\,M^{-1}$ for the **3**:AC complex, which is about 2.5-fold lower than the value reported for the corresponding complex with βCD, probably because of the presence of the tyrosinyl self-inclusion element.

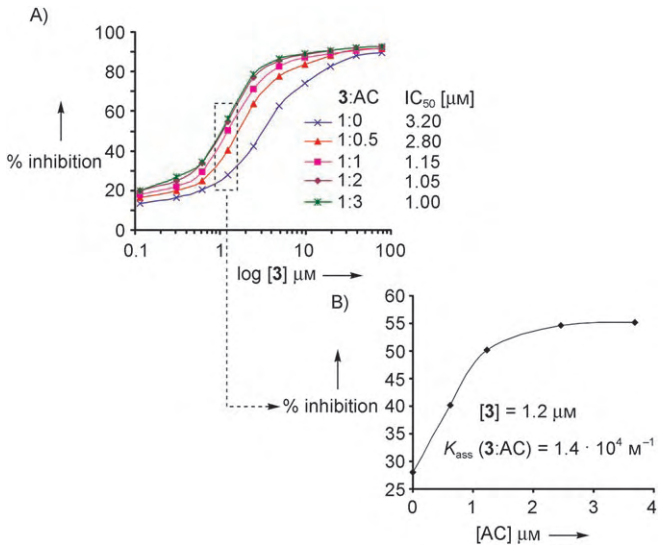


Figure 2. ELLA analysis for **3** in the presence of various concentrations of AC (A) and binding isotherm for the 1:1 **3**:AC complex (B).

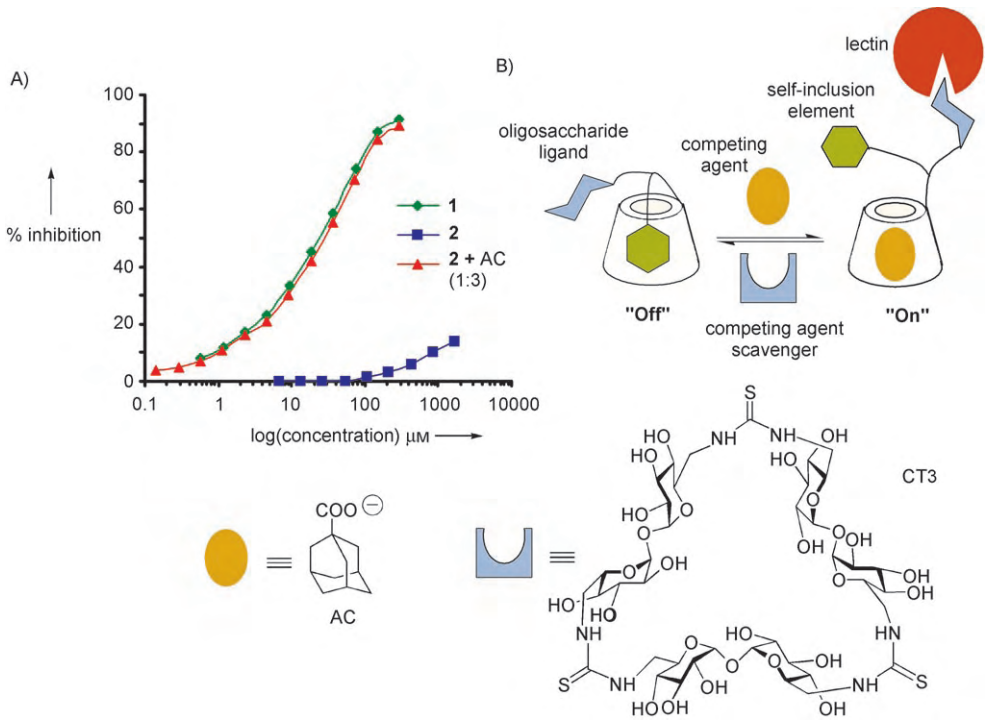


Figure 1. ELLA analysis (% inhibition of the Con A/yeast mannan binding) for **1**, **2**, and **2** + AC (A) and schematic representation of the observed "off/on" switching of carbohydrate–lectin binding through allosteric supramolecular interactions (B).

It is worth mentioning that the presence of a bulky horseradish peroxidase (HRP) label on Con A, to produce a spectrophotometric readout in the ELLA, is supposed to prevent cross-linking processes. These macromolecules likely interact with a single binding site per lectin, with proximity/statistical affinity enhancement mechanisms operating. The above result strongly suggests that both Man-tri groups become fully disposible for protein recruitment after AC stimulation, even under such conditions (microcluster effect[18,19]), which result in an increased biological response, by a biomimetic mechanism.

We hypothesized that the lectin affinity should be

 © 2006 Wiley-VCH Verlag GmbH & Co. KGaA, Weinheim

depleted after addition of an appropriate AC scavenger (Figure 1 B, right-to-left). The trimeric α,α′-trehalose-based receptor CT3, which exhibits a perfect size match and symmetry complementarity with AC ($K_{ass} = 4.6 \times 10^4\ M^{-1}$)[20] was considered a good candidate for this purpose. Addition of 1.5 equivalents of CT3 per mol of effector molecule to AC-activated samples of **2** or **3** led the system back to the initial state—switch "off"—in agreement with the reversible character of the equilibria involved both at the lectin binding site and in the CD cavity.[21]

In summary, our results indicate that reversible tuning and switching of the binding affinity in a model carbohydrate–lectin system is possible through logical design. This work has included the first examples of allosteric activation/deactivation of binding and of the multivalent effect. This switchable, environment-sensitive, supramolecularly mediated carbohydrate–protein recognition offers exciting possibilities to mimic biological processes involving effector/antagonist molecules. Indeed, specific drug delivery using CD conjugates is hampered by the blocking of the protein receptors by unoccupied carriers, which might be avoided by designing switchable systems for which the drug will act as the effector (input "on"). We aim to investigate this possibility, as well as the further supramolecular modulation of multivalent interactions through variations in chemical modification in this and other systems.

Received: March 22, 2006
Revised: June 7, 2006
Published online: July 20, 2006

Keywords: carbohydrates · cyclodextrins · lectins · noncovalent interactions · receptors

[1] a) H.-H. Gabius, H.-C. Siebert, S. André, J. Jiménez-Barbero, H. Rüdiger, *ChemBioChem* **2004**, *5*, 740 – 764; b) T. K. Dam, C. F. Brewer, *Chem. Rev.* **2002**, *102*, 387 – 429; c) C. R. Bertozzi, L. L. Kiessling, *Science* **2001**, *291*, 2357 – 2364.

[2] a) M. Mamen, S.-K. Choi, G. M. Whitesides, *Angew. Chem.* **1998**, *110*, 2908 – 2953; *Angew. Chem. Int. Ed.* **1998**, *37*, 2754 – 2794; b) J. J. Lundquist, E. J. Toone, *Chem. Rev.* **2002**, *102*, 555 – 578.

[3] a) Y. C. Lee, R. T. Lee, *Acc. Chem. Res.* **1995**, *28*, 321 – 327; b) Y. C. Lee, R. T. Lee, *Glycoconjugate J.* **2000**, *17*, 543 – 551.

[4] a) N. Horan, H. Isobe, G. M. Whitesides, D. Kahne, *Proc. Natl. Acad. Sci. USA* **1999**, *96*, 11782 – 11786; b) J. E. Gestwicki, C. W. Cairo, L. E. Strong, K. A. Oetjen, L. L. Kiessling, *J. Am. Chem. Soc.* **2002**, *124*, 14922 – 14933; c) E. K. Soller, E. D. Walter, J. R. Morgan, D. J. Singel, M. J. Cloninger, *J. Am. Chem. Soc.* **2003**, *125*, 8820 – 8826; d) M. Gómez-García, J. M. Benito, J.-X. Yu, K. Chmurski, C. Ortiz Mellet, R. Gutiérrez Gallego, A. Maestre, J. Defaye, J. M. García Fernández, *J. Am. Chem. Soc.* **2005**, *127*, 7970 – 7971; e) L. L. Kiessling, J. E. Gestwicki, L. E. Strong, *Angew. Chem.* **2006**, *118*, 2408 – 2429; *Angew. Chem. Int. Ed.* **2006**, *45*, 2348 – 2368.

[5] a) M. J. Cloninger, *Curr. Opin. Chem. Biol.* **2002**, *6*, 742 – 748; b) W. B. Turnbull, J. F. Stoddart, *Rev. Mol. Biotechnol.* **2002**, *90*, 231 – 255; c) T. K. Lindhorst, *Top. Curr. Chem.* **2002**, *218*, 201 – 235.

[6] For pioneering work on the evaluation of the influence of conformational crowding in carbohydrate–protein binding affinity using dendrimer-centred glycoligands, see: a) D. Page, R. Roy, *Bioconjugate Chem.* **1997**, *8*, 714 – 723; b) P. R. Ashton, E. F. Hounsell, N. Jayaraman, T. M. Nilsen, N. Spencer, J. F. Stoddart, M. Young, *J. Org. Chem.* **1998**, *63*, 3429 – 3437.

[7] Several glycosylated cyclodextrins have been prepared with the aim of combining both the inclusion capabilities of the hydrophobic cavity inherent in the cyclomalto-oligosaccharide structure and the biological receptor binding ability of oligosaccharides; for examples, see: a) C. Ortiz Mellet, J. Defaye, J. M. García Fernández, *Chem. Eur. J.* **2002**, *8*, 1982 – 1990; b) D. A. Fulton, J. F. Stoddart, *Bioconjugate Chem.* **2001**, *12*, 655 – 672; c) A. Vargas-Berenguel, F. Ortega-Caballero, F. Santoyo-González, J. J. García-López, J. J. Giménez-Martínez, L. García-Fuentes, E. Ortiz-Salmerón, *Chem. Eur. J.* **2002**, *8*, 812 – 827; d) T. Yamanoi, N. Yoshida, Y. Oda, E. Akaike, M. Tsutsumida, N. Kobayashi, K. Osumi, K. Yamamoto, K. Fujita, K. Takahashi, K. Hattori, *Bioorg. Med. Chem. Lett.* **2005**, *15*, 1009 – 1013; e) H. Abe, A. Kenmoku, N. Yamaguchi, K. Hattori, *J. Inclusion Phenom. Macrocyclic Chem.* **2002**, *44*, 39 – 47.

[8] I. Willner, *Acc. Chem. Res.* **1997**, *30*, 347 – 356, and references therein.

[9] a) J. M. Benito, M. Gómez-García, C. Ortiz Mellet, I. Baussanne, J. Defaye, J. M. García Fernández, *J. Am. Chem. Soc.* **2004**, *126*, 10355 – 10366; b) I. Baussanne, J. M. Benito, C. Ortiz Mellet, J. M. García Fernández, J. Defaye, *ChemBioChem* **2001**, *2*, 777 – 783.

[10] F. Djedaïni-Pilard, N. Azaroual-Bellanger, M. Gosnat, D. Vernet, B. Perly, *J. Chem. Soc. Perkin Trans. 2* **1995**, 723 – 730.

[11] D. Yockot, V. Moreau, G. Demailly, F. Djedaïni-Pilard, *Org. Biomol. Chem.* **2003**, *1*, 1810 – 1818.

[12] a) J. Bouckaert, T. Hamelryck, L. Wyns, R. Loris, *Curr. Opin. Struct. Biol.* **2001**, *11*, 635 – 643; b) H. Lis, N. Sharon, *Chem. Rev.* **1998**, *98*, 637 – 674.

[13] R. Auzély-Velty, B. Perly, O. Taché, T. Zemb, P. Jéhan, P. Guenot, J.-P. Dalbiez, F. Djedaïni-Pilard, *Carbohydr. Res.* **1999**, *318*, 82 – 90.

[14] N. Smiljanic, S. Halila, V. Moreau, F. Djedaïni-Pilard, *Tetrahedron Lett.* **2003**, *44*, 8999 – 9002.

[15] M. K. Anwer, A. F. Spatola, *Tetrahedron Lett.* **1981**, *22*, 4369 – 4372.

[16] M. V. Rekharsky, Y. Inoue, *Chem. Rev.* **1998**, *98*, 1875 – 1917.

[17] J. Lin, F. Djedaïni-Pilard, P. Guénot, B. Perly, *Supramol. Chem*, **1996**, *7*, 175 – 181.

[18] The terms minicluster (microcluster) and macrocluster effect have been used previously in the literature to refer to the observed increases in lectin-binding affinities for small glycoclusters and large glycopolymers, respectively; see: a) M. S. Quesenberry, R. T. Lee, Y. C. Lee, *Biochemistry* **1997**, *36*, 2724 – 2732; b) J.-Q. Fan, M. S. Quesenberry, K. Takegawa, S. Iwahara, A. Kondo, I. Kato, Y. C. Lee, *J. Biol. Chem.* **1995**, *270*, 17730 – 17735.

[19] For recent evidence on the the existence of an aggregation-independent microcluster effect, see: M. Köhn, J. M. Benito, C. Ortiz Mellet, T. K. Lindhorst, J. M. García Fernández, *ChemBioChem* **2004**, *5*, 771 – 777.

[20] J. M. Benito, J. L. Jiménez Blanco, C. Ortiz Mellet, J. M. García Fernández, *Angew. Chem.* **2002**, *114*, 3826 – 2828; *Angew. Chem. Int. Ed.* **2002**, *41*, 3674 – 3676.

[21] Control ELLA experiments demonstrated that CT3 does not interfere in the binding of the mannosyl ligands **1**–**3** with Con A in the absence of AC. Binding of **1** to Con A was also unaffected by the presence of AC and AC:CT3 in up to threefold excesses. These results strongly support that CT3 triggers the "off" state by a mechanism involving exclusively AC trapping. Consequently, further addition of AC to a CT3-switched-off sample of **2**:AC restored the "on" state in a new cycle, thus confirming the reversibility of both input processes. NMR experiments additionally supported the absence of supramolecular interactions between CT3 and the βCD-centred glycoligands **1**–**3**.

 © 2006 Wiley-VCH Verlag GmbH & Co. KGaA, Weinheim

Attaching Cells

DOI: 10.1002/anie.200601151

Switching On Cell Adhesion with Microelectrodes**

*Chuan Zhao, Irene Witte, and Gunther Wittstock**

Controlling the interfaces between cells and solid substrates is an important theme pertinent to a variety of research applications such as cell biology,[1] tissue engineering,[2] and cell-based sensors and chip devices.[3] In particular, the recent progress in the understanding of the molecular mechanism of cell adhesion has promoted the development of self-assembled monolayer (SAM)-based techniques for precise cell pattering, for example, microcontact printing (μCP).[4] SAMs that are terminated in short oligomers of the ethylene glycol (OEG) unit ($HS(CH_2)_{11}(OCH_2CH_2)_nOH$; $n = 3$–7) were most often used in these studies for resisting the nonspecific adsorption of proteins/cells, and are proven to be the best "nonadsorption" systems that are currently available.[5] However, conventional μCP methods produce static surface stimuli. Once cells are adherent, it is difficult to subsequently alter the matrix environment.[6]

Herein, we described a strategy for the real-time local manipulation of the cell-adhesive property of an OEG-terminated SAM substrate using ultramicroelectrodes (UME), which enables the template-free formation of cellular micropatterns by directing cell adhesion and growth in situ. The strategy is based on our finding that the cytophobic nature of OEG SAMs is rapidly switched to cell adhesive by exposure to some oxidizing agents, such as Br_2, which can be electrogenerated from Br^- in aqueous solution. By scanning a UME as a "pen" closely above the substrate, one can draw a cellular pattern. As illustrated in Figure 1, an OEG-terminated SAM substrate was formed by inserting a gold slide into an OEG-terminated alkanethiol solution for 12 h. Then, a microelectrode with a radius $r_T = 25$ μm (T = tip, of the UME) was brought to 5 μm above the substrate (Figure 1a). A 5 s potential pulse of 1.2 V (compared with an Ag quasi-reference electrode) was applied in a 0.1 M phosphate buffer solution containing 25 mM KBr (pH 7.4). The electrochemically generated Br_2 diffused to the substrate and quickly reacted with the OEG monolayer locally. The modification of the OEG SAM was confirmed by a scanning electrochemical microscopy (SECM) feedback image (Figure 1b). The contrast is based on the permeability difference of the OEG SAM and the Br_2-treated SAM. The bright parts in the image indicate higher reduction currents, corresponding to a higher permeability of the monolayer (see the Supporting Information). The treated substrate was then incubated in extracellular matrix (ECM) protein solutions, for example, fibronectin, fibrinogen etc. Proteins adsorbed exclusively on the electrochemically treated regions (Figure 1c). Figure 1d shows a confocal laser scanning fluorescent micrograph of ECM protein pattern formed after adsorption of a fluorescence-labeled protein (4 h in 100 μg mL^{-1} fibronogen-Alexa 488). During a subsequent seeding of human fibroblast culture on the substrate, the preadsorbed protein promoted the specific attachment of fibroblasts, resulting in the formation of a cellular micropattern on the surface

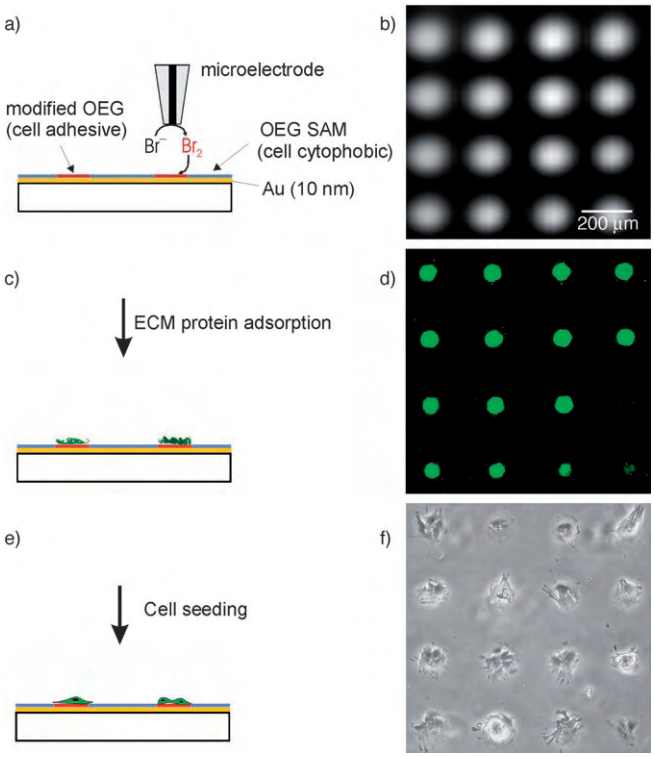


Figure 1. The use of a microelectrode to induce cell adhesion and growth onto an OEG SAM substrate. a) Microelectrochemical modification of the OEG monolayer by electrogenerated Br_2; b) SECM image of the modified OEG substrate; c) site-selective adsorption of fibronogen-Alexa 488 onto a modified region of the monolayer; d) confocal laser scanning fluorescence micrograph after (c); e) attachment of human fibroblasts; f) phase-contrast micrograph of the micropattern 24 h after immersion into the cell culture.

[*] Dr. C. Zhao, Prof. Dr. G. Wittstock
Institut für Chemie und Biologie des Meeres (ICBM)
Fakultät V
Carl von Ossietzky Universität Oldenburg
26111 Oldenburg (Germany)
Fax (+49) 441-798-3684
E-mail: gunther.wittstock@uni-oldenburg.de
Prof. Dr. I. Witte
Institut für Biologie und Umweltwissenschaften (IBU)
Fakultät V
Carl von Ossietzky Universität Oldenburg
26111 Oldenburg (Germany)

[**] We are grateful to our colleagues, Ms. Marita Weerts-Eden and Ms. Elke Frahmann, for help with the cell cultures, and to Ms. Carolina Nunes-Kirchner and Dr. Oleg Sklyar (currently at the European Bioinformatics Institute (UK)) for developing the positioning system on a microscope. We are also thankful to Prof. J. O. Metzger (University of Oldenburg) for the synthesis of OEG thiols. This work is supported by the Deutsche Forschungsgemeinschaft (Wi 1617/6, BioGeoChemistry of Tidal Flats).

Supporting information for this article is available on the WWW under http://www.angewandte.org or from the author.

© 2006 Wiley-VCH Verlag GmbH & Co. KGaA, Weinheim

(Figure 1e,f). Although spots could be formed as a result of holding the microelectrode in a fixed location above the surface, lines could be generated by translating the microelectrode horizontally while producing Br_2 (Figure 2). The

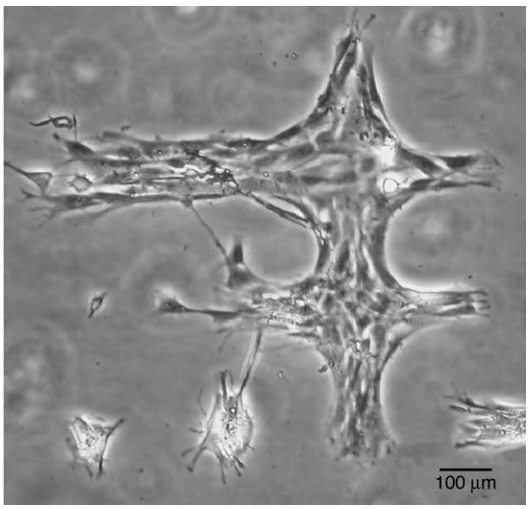


Figure 2. Phase-contrast optical micrograph of the linear cellular pattern fabricated by scanning the microelectrode ($r_T = 25$ µm) at a lateral speed of 5 µm s^{-1}. The microelectrode potential was kept at 1.2 V during "drawing" and at 0 V while not drawing.

size of the patterns depends strongly on the size of the microelectrode.[7] By using advanced approaches for microelectrode fabrication, the smallest pattern size generated by UME could be as low as approximately 50 nm.[8] No restriction exists on larger sizes. The throughput could be increased by the use of microelectrode arrays.

To control cell–substrate interaction dynamically, some groups have reported µCP-based electrochemical methods, such as electrochemically induced immobilization of peptide ligands by a Diels–Alder reaction to activate inert surfaces,[9] or electrochemical desorption of OEG SAMs to induce cell attachment to the SAM-desorbed area.[10] In this study, the UME has also been applied for the modification of prepatterned cellular substrates, which provides an alternative strategy to pattern multiple cell populations by sequentially switching the adhesivity of different regions of the substrate. As illustrated in Figure 3a, the UME was brought above the substrate onto which the first fibroblast population had been previously attached (labeled with a green fluorescent dye). Positioning the UME relative to the first cell pattern was achieved by a positioning system mounted on an inverted microscope. This allowed us to follow the movement of the UME to the desired location. A potential pulse was then applied to open a new region for the adhesion of a second fibroblast population (labeled by a red fluorescent dye, see Figure 3b,c). During this step, the growth of the Br_2 diffusion layer at UME was controlled by adjusting the UME size and potential pulse time to prevent the Br_2 from reaching the prepatterned cells, even though it has been recently reported by Matsue et al. that Br_2 and its subsequent degradation products do little damage to the preexisting cells.[11] Similar to

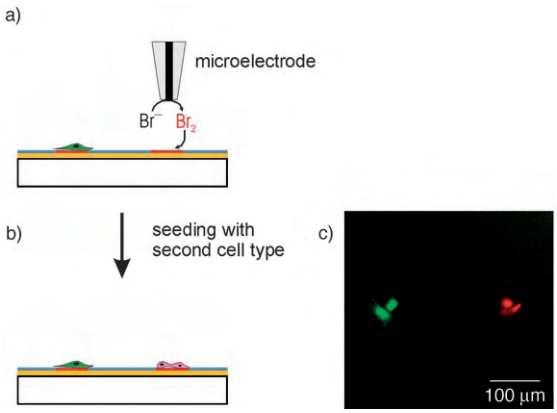


Figure 3. Modification of cellular substrate and formation of multiple cell cocultures by using microelectrodes. a) Microelectrochemical modification of the substrate prepatterned with fibroblasts; b) attachment of a second population of fibroblasts; c) confocal laser scanning fluorescence micrograph of a multiple cell coculture. The second population of fibroblast (red) was introduced onto the sample with the pattern of the first fibroblast population (green).

most lithrography-based methods,[9,12] our method relies on 100% occupancy of the first adhesive area for the first cell population. The second fibroblast population may also attach to the unoccupied region of the first cellular pattern (not shown). Therefore, formation of a confluent monolayer of the first cell population is necessary to obtain a well-defined coculture of different cells on the substrate.

Despite the immense practical importance of the protein/cell resistance effect of OEG SAMs, the underlying mechanisms are not completely clear.[13] Grunze et al. recently summarized the various factors that are critical for the functionality of the monolayer and suggested that only the combination of the three factors, the internal hydrophility, terminal hydrophobicity, and lateral packing density, allows the formation of a SAM that is fully protein/cell resistant.[14] When one of these factors is unfavourable or absent, the overall protein/cell resistance decreases. In this study, the detailed mechanism of the monolayer transformation is still under investigation. X-ray photoelectron spectra show that bromine is not incorporated in the SAM layer, in agreement with the observation that the procedure also works with oxidizers other than bromine. Polarization-modulated infrared reflection–absorption spectroscopy showed that during bromine treatment, the oligoethylene units of the monolayer are lost, whereas degradation of the alkyl part of the SAM takes considerably longer. This is consistent with our observation that bromine treatment of an OEG SAM leads to an increase in the terminal hydrophobicity. A detailed mechanistic study is still in progress.

In conclusion, we have described a simple microelectrochemical method for switching on cell adhesion and growth on OEG SAM substrates in situ. The method could be applied by using basic electrochemical instrumentation that is also employed in neurophysiological experiments (potentiostat, microelectrodes, and positioners). By using a microelectrode as a "pen", the method enables template-free drawing of cellular patterns and in situ modification of a

 © 2006 Wiley-VCH Verlag GmbH & Co. KGaA, Weinheim

prepatterned cellular substrate. As stepwise site-directed introduction of different cell types onto the substrate is possible, the method could also facilitate the formation of micropatterned cocultures and, therefore, contribute to in vitro investigations of multicellular interactions and to tissue engineering. We believe that the application scope will be further enlarged by combining the in situ manipulation function with other microfabrication techniques, for example, microcontact printing that is capable of producing extended and complex patterns of cell culture in a highly parallel way.

Experimental Section

Substrates were prepared by the evaporation of chromium (5 nm) and then gold (10 nm) onto cleaned glass coverslips. The substrate was then immersed in OEG solution (3 mM) in ethanol to form the monolayer. The substrates were rinsed thoroughly with absolute ethanol and dried under a stream of argon.

The microelectrochemical modifications of the monolayer were performed on a Pt UME ($r_T = 25\,\mu m$) mounted on a home-built positioning system which was described previously.[15] A Pt wire as the auxiliary electrode and a silver quasi reference electrode, to which all potentials are referred, completed the electrochemical cell. The working solution was phosphate buffer solution (0.1M; pH 7.4) containing KBr (25 mM). The UME was brought close to the substrate and then a 5 s potential pulse of 1.2 V was imposed to generate Br_2. Electrochemically generated bromine reacts with the monolayer and quickly switched the monolayer from cell resistant to cell adhesive.

After the modification, the substrate was incubated in ECM (100 $\mu g\,mL^{-1}$) proteins fibrinogen-Alexa 488 in phosphate-buffered solution (PBS; phosphate (0.1M), NaCl (0.15M), pH 7.4) for 4 h before the substrate was examined by confocal laser scanning fluorescence microscopy (Leica TCS SP2/AOBS, Leica Microsystems Heidelberg GmbH, Heidelberg, Germany). The dye was excited at a wavelength of 488 nm and the fluorescence was detected with a spectral range of 500–535 nm.

Human fibroblasts grown to confluency were labeled with CellTracker Green (25 μM) for 30 min. After removing the dye and repeated washing with serum-free minimum essential medium (MEM), the cells were trypsinized and resuspended in serum-free culture medium (40000 cells mL^{-1}) and then added onto a patterned monolayer precoated with fibronectin and allowed to attach for 4 h in a CO_2 incubator at 37 °C. The substrate was then transferred to a new culture dish containing complete medium and incubated for 24 h before examined by phase-contrast microscopy.

To prepare cocultures, the UME was then brought to the desired location under the control of the optical microscope and the potential pulse was applied to transform a new region. The substrate was then reseeded with the second population of fibroblasts that were prelabelled with CellTracker Orange at a concentration of 40000 cells mL^{-1}. The substrates were incubated at 37 °C for an additional 2 h before the substrate was examined by confocal laser scanning fluorescence microscopy. The two channels that were used to excite the dyes were 488 nm and 568 nm, and the spectral range of detectors was 500–535 nm (displayed in green) and 555–700 nm (displayed in red), respectively.

Received: March 23, 2006
Published online: July 20, 2006

[1] a) C. S. Chen, M. Mrksich, S. Huang, G. M. Whitesides, D. E. Ingber, *Science* **1997**, *276*, 1425 – 1429; b) A. Brock, E. Chang, C. C. Ho, P. LeDuc, X. Jiang, G. M. Whitesides, D. E. Ingber, *Langmuir* **2003**, *19*, 1611 – 1617.

[2] a) J. Lahann, M. Balcells, T. Rodon, J. Lee, I. S. Choi, K. F. Jensen, R. Langer, *Langmuir* **2002**, *18*, 3632 – 3638; b) M. Yamato, C. Konno, M. Utsumi, A. Kikuchi, T. Okano, *Biomaterials* **2002**, *23*, 561 – 567.

[3] a) B. Straub, E. Meyer, P. Fromherz, *Nat. Biotechnol.* **2001**, *19*, 121 – 124; b) A. Offenhäusser, W. Knoll, *Trends Biotechnol.* **2001**, *19*, 62 – 66.

[4] a) Y. Xia, G. M. Whitesides, *Angew. Chem.* **1998**, *110*, 568 – 594; *Angew. Chem. Int. Ed.* **1998**, *37*, 550 – 574; b) S. Raghavan, C. S. Chen, *Adv. Mater.* **2004**, *16*,1303 – 1313; c) N. Li, A. Tourovskaia, A. Folch, *Crit. Rev. Biomed. Eng.* **2003**, *31*, 423 – 488; d) M. Mrksich, *Chem. Soc. Rev.* **2000**, *29*, 267 – 273.

[5] a) K. L. Prime, G. M. Whitesides, *Science* **1991**, *252*, 1164 – 1167; b) C. Pale-Grosdemagne, E. S. Simon, K. L. Prime, G. M. Whitesides, *J. Am. Chem. Soc.* **1991**, *113*, 12 – 20; c) K. L. Prime, G. M. Whitesides, *J. Am. Chem. Soc.* **1993**, *115*, 10714 – 10721.

[6] a) J. L. Tan, J. Tien, D. M. Pirone, D. S. Gray, K. Bhadriraju, C. S. Chen, *Proc. Natl. Acad. Sci. USA* **2003**, *100*, 1484 – 1489; b) D. T. Chiu, N. L. Jeon, S. Huang, R. Kane, C. J. Wargo, I. S. Choi, D. E. Ingber, *Proc. Natl. Acad. Sci. USA* **2000**, *97*, 2408 – 2413.

[7] a) V. Radtke, J. Heinze, *Z. Phys. Chem* **2004**, *218*, 103 – 121; b) K. Borgwarth, N. Rohde, C. Ricken, M. L. Hallensleben, D. Mandler, J. Heinze, *Adv. Mater.* **1999**, *11*, 1221 – 1226; c) I. Turyan, U. O. Krasovec, B. Orel, T. Saraidorov, R. Reisfeld, D. Mandler, *Adv. Mater.* **2000**, *12*, 330 – 333.

[8] a) F. Forouzan, A. J. Bard, *J. Phys. Chem. B* **1997**, *101*, 10876 – 10879; b) W. Li, J. A. Virtanen, R. M. Penner, *Appl. Phys. Lett.* **1992**, *60*, 1181 – 1183; c) H. Sugimura, T. Uchida, N. Kitamura, H. Masuhara, *J. Phys. Chem.* **1994**, *98*, 4352 – 4357.

[9] a) M. N. Yousaf, B. T. Houseman, M. Mrksich, G. M. Whitesides, *Proc. Natl. Acad. Sci. USA* **2001**, *98*, 5992 – 5996; b) M. N. Houseman, B. T. Yousaf, M. Mrksich, *Angew. Chem.* **2001**, *113*, 1127 – 1130; *Angew. Chem. Int. Ed.* **2001**, *40*, 1093 – 1096.

[10] X. Jiang, R. Ferrigno, M. Mrksich, G. M. Whitesides, *J. Am. Chem. Soc.* **2003**, *125*, 2366 – 2367.

[11] a) H. Kaji, M. Kanada, D. Oyamatsu, T. Matsue, M. Mishizawa, *Langmuir* **2004**, *20*, 16 – 19; b) H. Kaji, K. Tsukidate, T. Matsue, M. Mishizawa, *J. Am. Chem. Soc.* **2004**, *126*, 15026 – 15027.

[12] a) S. N. Bhatia, M. L. Yarmush, M. Toner, *J. Biomed. Mater. Res.* **1997**, *34*, 189 – 199; b) S. N. Bhatia, U. J. Balis, M. L. Yarmush, M. Toner, *Biotechnol. Prog.* **1998**, *14*, 378 – 387; c) S. N. Bhatia, U. J. Balis, M. L. Yarmush, M. Toner, *FASEB J.* **1999**, *13*, 1883 – 1900.

[13] a) H. Wennerstroem, J. Israelachvili, *Nature* **1996**, *379*, 219 – 225; b) P. T. Hammond, S. L. Clark, *Langmuir* **2000**, *16*, 10206 – 10214; c) R. S. Kane, P. Deschatelets, G. M. Whitesides, *Langmuir* **2003**, *19*, 2388 – 2391.

[14] a) S. Herrwerth, W. Eck, S. Reinhardt, M. Grunze, *J. Am. Chem. Soc.* **2003**, *125*, 9359 – 9366; b) R. S. Kane, P. Deschatelets, G. M. Whitesides, *Langmuir* **2003**, *19*, 2388 – 2391.

[15] a) C. Zhao, G. Wittstock, *Anal. Chem.* **2004**, *76*, 3145 – 3154; b) C. Zhao, G. Wittstock, *Biosens. Bioelectron.* **2005**, *20*, 1277 – 1284; c) C. Zhao, G. Wittstock, *Angew. Chem.* **2004**, *116*, 4264 – 4267; *Angew. Chem. Int. Ed.* **2004**, *43*, 4170 – 4172.

Keywords: cell adhesion · electrochemistry · scanning electrochemical microscopy · self-assembled monolayers · surface chemistry

 © 2006 Wiley-VCH Verlag GmbH & Co. KGaA, Weinheim

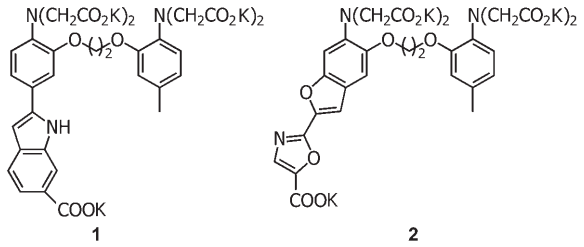
Biosensors

DOI: 10.1002/anie.200601242

Microsphere-Based Real-Time Calcium Sensing**

*Rosario M. Sánchez-Martín, Matt Cuttle, Stifun Mittoo, and Mark Bradley**

Fluorescent sensors for a variety of ions, such as Ca^{2+} and Na^{+}, are among the most useful tools available for studying ion fluxes within the intracellular environment following the modulation or stimulation of a range of complex biological processes. Two widely used fluorescent indicators for Ca^{2+} ions are Indo-1 (**1**) and Fura-2 (**2**), which complex calcium with high affinity ($K_d = 230$ and 145 nM, respectively), and these reagents have allowed numerous investigations into intracellular free Ca^{2+} concentrations following a range of cellular insults.[1–6] However, the pentacarboxylic acid and salts of Indo-1 and Fura-2 (**1** and **2**, respectively; Scheme 1)



Scheme 1. Structures of the commonly used Ca^{2+} sensors salts of Indo-1 and Fura-2 (**1** and **2**, respectively).

are unable to cross cellular membranes, an essential requirement in allowing such molecules to be used within the cellular environment. Thus, several invasive techniques, such as microinjection[7] or electroporation,[8] are routinely used to allow the introduction of the sensor into the cells, which although highly efficient are time-consuming and laborious and can damage the cells. Another established method for the delivery of these probes into cells is the use of cell-permeable acetoxymethyl (AM) ester derivatives, which can freely enter the cell and are subsequently hydrolyzed.[9] However, this method has disadvantages, such as compartmentalization, incomplete AM ester hydrolysis (five ester groups need to be fully cleaved to give the intact sensor), and cellular leakage over time.[10,11] Additionally, these ester derivatives often need to be solubilized in dimethyl sulfoxide (DMSO), which even at low concentrations can be cytotoxic to cells. Another common problem that is encountered with all potential sensors or cellular tags, is dilution and cellular degradation, which results in little or no signal. New approaches to this problem include the use of polymer-particle-based encapsulation[12] and the use of dextran conjugates of ion indicators that give decreased compartmentalization and leakage of sensor but often need to be loaded into cells using membrane-permeabilization reagents, such as Triton X-100.[13]

We recently demonstrated the efficient cellular delivery of amino-functionalized cross-linked polystyrene microspheres (2 μm) into a broad range of cells, including primary cells, and described the efficient fluorescence-activated sorting of cells that contain either single or multiple beads with one or more colors, thereby allowing the "encoding" of multiple cell types and subsequent cellular multiplexing.[14] The delivery of beads into cells, however, has a number of additional potential applications, and herein we show how the beads can be used not only to deliver "cell-impermeable" compounds, such as the acid salt of Indo-1, but how they can be used as a focal point for cellular examination (without cellular dilution taking place), thus allowing calcium fluxes within single live cells to be followed and determined in real time.

To covalently attach the Indo-1 sensor to the microspheres selectively, the original synthesis of this sensor was modified to allow incorporation of a benzyl ester at the indole 6-position while maintaining four ethyl ester functionalities on the coordinating carboxy groups,[15] thereby generating orthogonality between the acid groups that chelate the Ca^{2+} ions and the additional carboxylic acid group required for resin attachment. The synthesis of the novel derivative **7** was carried out in nine steps (see Scheme 2 and the Supporting Information for further details), with hydrogenation of the benzyl ester **7** to give the tetraethylester indolecarboxylic acid ready for coupling onto the aminomethylated microspheres. Subsequent hydrolysis of the ethyl ester gave the microsphere-immobilized sensor **9** (see Scheme 2 and the Supporting Information for further details).

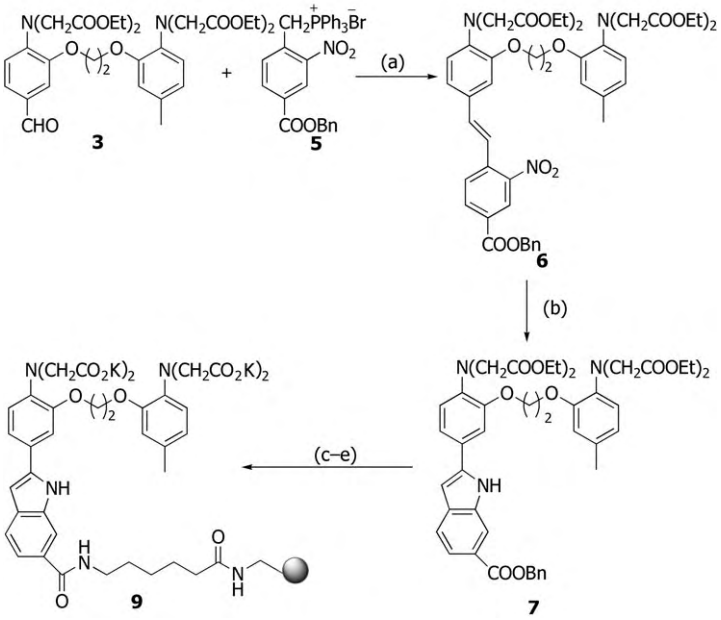
Fluorescence studies were carried out to evaluate how modification and immobilization of the sensor had affected its sensitivity to Ca^{2+} ions by examining the microspheres under a range of concentrations. The emission maximum shifted from 475 nm in Ca^{2+}-free medium to 400 nm when the sensor molecules were saturated with Ca^{2+} ions, as seen for the original Indo-1 sensor. Figure 1 shows the fluorescence emission spectra of **7**. The value of the dissociation constant for this derivative was calculated ($k_d = 226$ nM; details of the determination of the k_d values are given in the Supporting information).[15] Importantly, the sensor had the same fluo-

[*] Dr. R. M. Sánchez-Martín, Prof. M. Bradley
School of Chemistry
University of Edinburgh, Joseph Black building
West Mains Road, Edinburgh EH93JJ (UK)
Fax: (+44) 131-650-6453
E-mail: mark.bradley@ed.ac.uk
Dr. M. Cuttle
School of Biological Sciences
University of Southampton, Bassett Crescent East
Southampton SO167PX (UK)
Dr. S. Mittoo
Activotec
Biomedical Sciences Building
Bassett Crescent East, Southampton SO167PX (UK)

[**] This research was supported by the EPSRC. R.M.S.-M. thanks the Royal Society for a Dorothy Hodgkin Fellowship.

Supporting information for this article is available on the WWW under http://www.angewandte.org or from the author.

InterScience DISCOVER SOMETHING GREAT
© 2006 Wiley-VCH Verlag GmbH & Co. KGaA, Weinheim



Scheme 2. Synthesis and covalent attachment of modified Indo-1 **7** to the microspheres to give the Indo-1-microsphere sensor **9**. Reagents and conditions: a) K_2CO_3, DMF, 100 °C, 3 h (46%); b) $(EtO)_3P$, 160 °C, N_2, overnight (60%); c) H_2, 10% Pd/C, ethanol, 4 h (91%); d) microspheres derivatized with an aminohexanoic acid spacer,[14] HOBt, PyBOP, 4-ethylmorpholine, DMF, room temperature, 16 h (quant.); e) 1 M KOH, 6 h (quant.). DMF = dimethylformamide, PyBOP = (benzotriazol-1-yloxy)tripyrrolidinophosphonium hexafluorophosphate

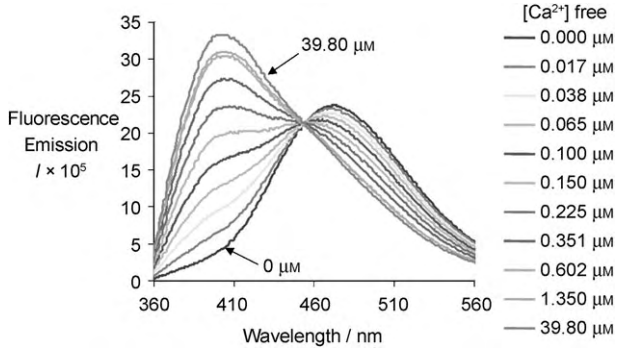


Figure 1. Fluorescence emission spectra (λ_{ex} = 350 nm) for Indo-1 derivative **7** following ester hydrolysis recorded at 22 °C and pH 7.2 as a function of $[Ca^{2+}]$. Solutions of varying $[Ca^{2+}]$ were prepared by mixing together EGTA (10 mM), KCl (100 mM), and MOPS (30 mM) with CaEGTA (10 mM), KCl (100 mM), and MOPS (30 mM) to give $[Ca^{2+}]$ values in the range of 0–39.8 μM. EGTA = ethylene glycol bis(2-aminoethylether)-*N*,*N*,*N*′,*N*′-tetraacetic acid, MOPS = 4-morpholinepropanesulfonic acid.

rescence profile when bound to the microspheres as in solution.

A population of neuronal cells (ND7) were incubated with 2-μm Indo-1-loaded microspheres (0.1 mg mL^{-1}) for 6 hours. Cells containing the beads (ca. 30%) were isolated by fluorescence-activated cell sorting (FACS; see the Supporting Information for details) and were shown by confocal microscopy after 24–72 h of incubation at 37 °C to be healthy and growing with the sensor microspheres inside the cells (Figure 2). The Indo-1-loaded microspheres were found to be nontoxic at all of the concentrations tested, as verified by methylthiazolyldiphenyltetrazolium bromide (MTT)[16] and trypan-blue assays.[17]

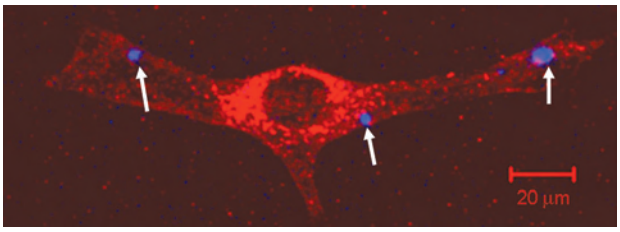


Figure 2. Confocal microscopy image of a single neuronal cell (ND7-immortalized cell line derived from sensory neurons) loaded with Indo-1-microspheres **9** (blue circles) after 24 h of incubation at 37 °C under 5% CO_2 (white arrows indicate the microspheres intracellular location in the cytosol). The cell membrane was stained with a red fluorescent dye (PKH26, Sigma-Aldrich) which allows long term in vitro analysis of live cells.

Intracellular changes in the concentration of free Ca^{2+} ions were detected by microscopy-mediated examination of the Indo-1-labelled microspheres in ND7 cells after stimulation. The measurements were carried out with excitation at 355 nm and with fluorescence emission from the beads monitored at 400 and 470 nm with the levels of free Ca^{2+} ions determined by using the standard ratio method established by Valet and co-workers.[18] Figure 3 shows the results of analysis of cells loaded with microspheres after stimulation of ND7 cells with *N*-methyl-D-aspartate (NMDA) and glutamate (this combination of amino acids is known to active glutamate receptors that gate the flow of Ca^{2+} ions across the membrane of a nerve cell).[19] After approximately six minutes, the average response showed an increase

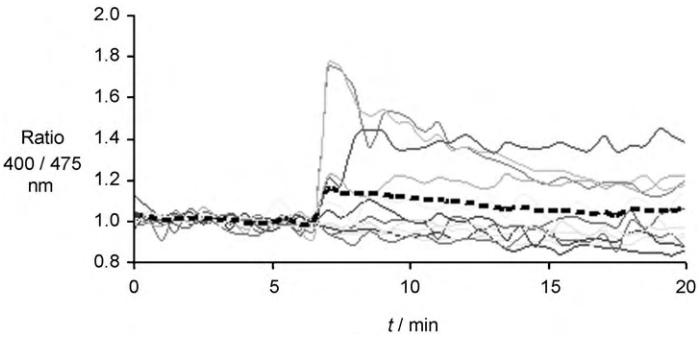


Figure 3. Real-time ratiometric fluorescent analysis (400/475 nm ratio) of the release of Ca^{2+} ions in ND7 cells loaded with Indo-1-microspheres. The cells were incubated with the microspheres for 6 h at 37 °C and under 5% CO_2, sorted (FACS), and regrown for 24 h. Time t = 0 corresponds to the addition of NMDA (10 μM) and glutamate (100 μM) to the microsphere-loaded cells. Each line corresponds to an individual cellular response, while the discontinuous bold line shows the average.

 © 2006 Wiley-VCH Verlag GmbH & Co. KGaA, Weinheim

in free intracellular Ca^{2+} ions, followed by a decrease as a result of receptor desensitization, thus clearly proving that the calcium-sensor-loaded microspheres responded rapidly and with good sensitivity to increases in levels of intracellular Ca^{2+} ions.

A technique has thus been developed in which not only is the acid salt of Indo-1 delivered into cells but it is done so in a manner in which dilution and leakage do not occur. An experiment to demonstrate these advantages was performed in which ND7 cells were incubated with either the microspheres **9** and/or the commercially available Indo-1 AM ester. Both sensors were clearly visible within the cell at $t=0$, although the conventional dye was diffuse. The conventional sensor was lost gradually with time, and only the sensors bound to the microspheres were visible after 18 h of analysis (see the Supporting Information). These results indicate that the sensor-based microspheres avoid the problems conventionally associated with cellular leakage and allow intracellular changes to be followed for long-term studies without having to repeatedly load the cells.

Importantly, these beads are nontoxic to cells (see the Supporting Information), do not disrupt cell physiology, and can be introduced with high efficiency with the "capture" of the sensor beads by the cells that allow cell sorting based on bead content and fluorescence. There is of course a number of questions that relate to the uptake of the beads and their location within the cell. Recent reports in the area of derivatized-nanotube uptake[20,21] and bead uptake[22] suggest that the process is both size and material dependant, whereas cellular location and compartmentalization also depend on the amount of time the particles have been within the cell. However, since spectroscopic changes on the beads are observed following cellular stimulation, the sensors are clearly chemically/biologically accessible and respond to changes in the concentration of intracellular Ca^{2+} ions, thus showing that they are located in the cytosol and not trapped and isolated by a vesicular membrane.

By using these beads, we have shown our ability to measure changes in the concentration of intracellular Ca^{2+} ions in single living cells in real time. The fact that the microspheres are stably retained for several days also allows changes in the concentration of intracellular Ca^{2+} ions to be followed in a single cell for much longer periods of time than using traditional sensors. These results open the door to a range of possible applications, with the microspheres acting as carriers of sensors for other metal ions or pH values and for a range of different biological probes.

Received: March 30, 2006
Published online: July 17, 2006

Keywords: biosensors · fluorescent probes · in vitro sensing · microspheres

[1] O. Eerbeek, E. G. Mik, C. J. Zuurbier, M. van't Loo, C. Donkersloot, C. Ince, *J. Appl. Physiol.* **2004**, *97*, 2042 – 2050.
[2] J. op den Buijs, Z. Miklos, N. A. W. van Riel, C. M. Prestia, O. Szencsi, A. Toth, F. J. van der Vusse, C. Szabo, L. Ligeti, T. Ivanics, *Life Sci.* **2005**, *76*, 1083 – 1098.
[3] L. Chu, J. X. Zhang, I. Norota, M. Endoh, *Br. J. Pharmacol.* **2005**, *144*, 430 – 442.
[4] J. F. Evans, C. L. Shen, S. Pollack, J. F. Aloia, J. K. Yeh, *Endocrinology* **2005**, *146*, 3123 – 3132.
[5] D. Deriu, M. Gassmann, S. Firbank, D. Ristig, C. Lampert, J. Mosbacher, W. Froestl, K. Kaupmann, B. Bettler, M. G. Grutter, *Biochem. J.* **2005**, *386*, 423 – 431.
[6] M. Weber, L. Motin, S. Gaul, F. Beker, R. H. A. Fink, D. J. Adams, *British J. Pharmacol.* **2005**, *144*, 98 – 107.
[7] A. J. Dahlstedt, A. Katz, P. Tavi, H. Westerblad, *J. Physiol.* **2003**, *547*, 395 – 403.
[8] G. R. Bright, N. T. Kuo, D. Chow, S. Burden, C. Dowe, R. J. Przybylski, *Cytometry* **1996**, *24*, 226 – 233.
[9] R. Y. Tsien, *Nature* **1981**, *290*, 527 – 528.
[10] F. Di Virgilio, T. H. Steinberg, S. C. Silverstein, *Cell Calcium* **1990**, *11*, 57 – 62.
[11] M. W. Roe, J. J. Lemasters, B. Herman, *Cell Calcium* **1990**, *11*, 63 – 73.
[12] H. Zhu, M. J. McShane, *J. Am. Chem. Soc.* **2005**, *127*, 13448 – 13449.
[13] M. Beierlein, K. R. Gee, V. V. Martin, W. G. Regehr, *J. Neurophysiol.* **2004**, *92*, 591 – 599.
[14] R. M. Sanchez-Martin, M. Muzerelle, N. Chitkul, S. E. How, S. Mittoo, M. Bradley, *ChemBioChem* **2005**, *6*, 1341 – 1345.
[15] G. Grynkiewicz, M. Poenie, R. Y. Tsien, *J. Biol. Chem.* **1985**, *260*, 3440 – 3450.
[16] T. Mossman, *J. Immunol. Methods* **1983**, *65*, 55 – 63.
[17] H. J. Phillips, J. E. Terryberry, *Exp. Cell Res.* **1957**, *13*, 341 – 347.
[18] G. Valet, A. Raffael, L. Russmann, *Naturwissenschaften* **1985**, *72*, 600 – 602.
[19] J. C. Watkins, D. E. Jane, *Br. J. Pharmacol.* **2006**, *147*, S100 – S108.
[20] D. Pantarotto, R. Singh, D. McCarthy, M. Erhardt, J. P. Briand, M. Prato, K. Kostarelos, A. Bianco, *Angew. Chem.* **2004**, *116*, 5354 – 5358; *Angew. Chem. Int. Ed.* **2004**, *43*, 5242 – 5246.
[21] N. W. S. Kam, Z. Liu, H. Dai, *Angew. Chem. Int. Ed.* **2006**, *118*, 591 – 595; *Angew. Chem. Int. Ed.* **2006**, *45*, 577 – 581.
[22] J. Rejman, V. Oberle, I. S. Zuhorn, D. Hoekstra, *Biochem. J.* **2004**, *377*, 159 – 169.

 © 2006 Wiley-VCH Verlag GmbH & Co. KGaA, Weinheim

Sensors

DOI: 10.1002/anie.200601286

Charge-Transfer Emission in Nonplanar Three-Coordinate Organoboron Compounds for Fluorescent Sensing of Fluoride**

*Xiang Yang Liu, Dong Ren Bai, and Suning Wang**

Three-coordinate organoboron compounds possess an empty p_π orbital on the boron center and hence have a tendency to display intense intramolecular charge-transfer transitions when an appropriate electron donor is present. Such donor–acceptor charge-transfer properties have enabled a number of important applications of three-coordinate boron compounds in materials chemistry such as nonlinear optical materials,[1] charge-transport materials, and emitters in organic light emitting devices (OLEDs).[2] Recently it has been demonstrated by several research groups that three-coordinate boron compounds can also be used as effective colorimetric, fluorescent, or ratiometric sensors for the detection of fluoride by utilizing the empty p_π orbital on the boron center.[3] Selective detection of fluoride is of current interest because of their importance to human health, their impact on the environment, and their association with nerve agents.[4,5] Previously reported fluorescent sensors based on three-coordinate boron compounds operate on the principle that the binding of fluoride to the boron center disrupts or perturbs the p_π–π conjugation between the boron center and the aromatic chromophore, thus inducing a change in fluorescent signal.[3d] Although the donor–acceptor charge-transfer properties of three-coordinate boron compounds have been exploited extensively for applications in nonlinear optics and OLEDs, surprisingly little investigation has been done on their utility in fluorescent sensor applications. Our preliminary investigation indicates that charge-transfer fluorescence of three-coordinate boron compounds can be very sensitive and selective for fluoride, and that "turn-on" fluorescent sensors for fluoride can be made by manipulating the geometry of the donor and acceptor in the molecule.

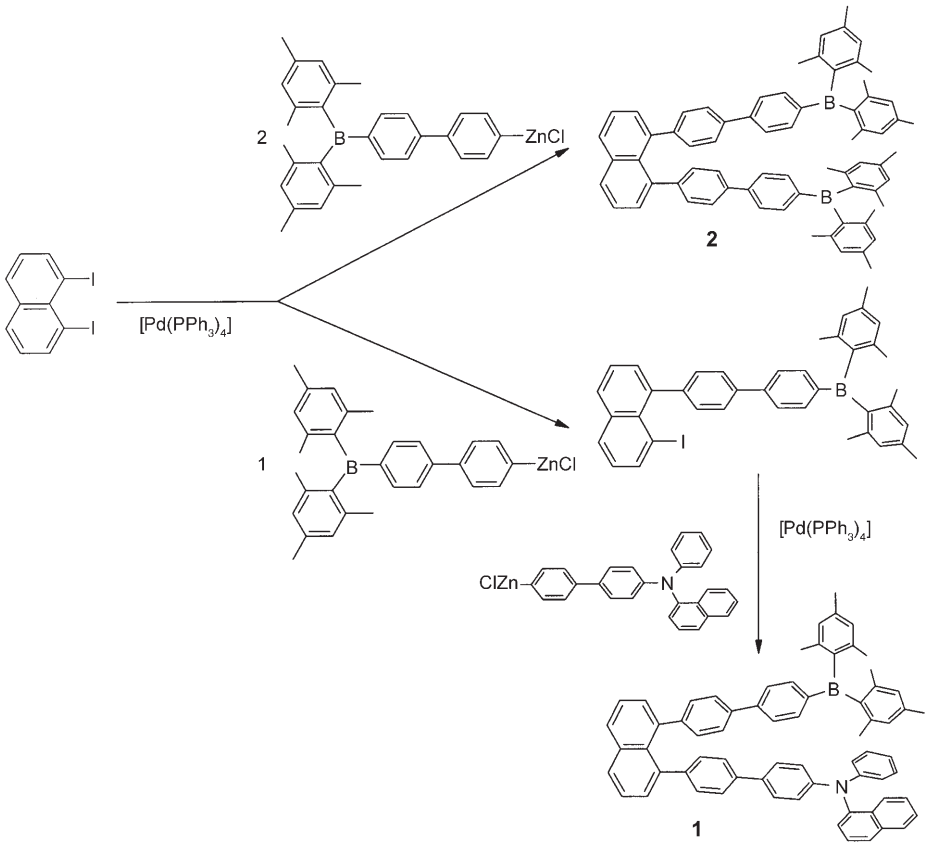
All previously reported three-coordinate boron compounds that produce intense charge-transfer fluorescence are planar conjugated systems,[1–3] an example of which is BNPB, reported by us recently.[2k] BNPB has an N(Ph)(1-naphthyl) donor and a B(mesityl)$_2$ acceptor group that are linked by a 4,4′-biphenyl group (see Scheme 2). BNPB produces intense solvent-dependent fluorescent emission (e.g. $\lambda_{em} = 492$ nm, $\Phi_p = 0.67$ in CH_2Cl_2) originating from the charge transfer between the amino and the boron centers.[2k] We have observed that the addition of fluoride to a solution of BNPB causes fluorescent quenching due to the occupation of the boron p_π orbital by electrons from F^-, which effectively blocks intramolecular charge transfer, thus causing decrease in emission intensity. Direct evidence for F^- binding to the boron center in BNPB comes from our ^{19}F NMR study of a (nBu$_4$N)F solution (TBAF) titrated with BNPB: the spectra revealed distinct ^{19}F chemical shifts for bound and unbound fluoride. We have also established that BNPB binds to fluoride exclusively even in the presence of other halides such as Cl^- or Br^-, which do not cause a significant change in fluorescence when added to the BNPB solution. This high selectivity for F^- by BNPB is consistent with previously reported fluoride sensors based on three-coordinate organoboron compounds in which the boron center is protected by substituent groups at the *ortho* positions.[3] Although BNPB is potentially useful for selective detection of F^-, it is a "turn-off" sensor; that is, fluorescence is quenched in the presence of fluoride. For practical applications, signal detection is more effective in "turn-on" sensors. Even better are "turn-on" sensors that display distinct color changes for fast and efficient sensing.[3f] In our search for "turn-on" organoboron sensors based on intramolecular charge-transfer emission, we synthesized organoboron compound **1** using the procedure shown in Scheme 1. The donor N(Ph)(1-naphthyl) and the acceptor B(mesityl)$_2$ in **1** are linked to two separate biphenyl groups, which are further connected by a naphthalene unit. Thus, the donor and the acceptor groups in **1** have a nonplanar arrangement. Molecule **1** displays solvent-dependent fluorescence ($\lambda_{em} = 504$ nm, $\Phi_p = 0.10$ in CH_2Cl_2), which is characteristic of charge-transfer emission. Molecular orbital calculations (Gaussian 03)[6] confirmed that the HOMO consists indeed of contributions of the aminobiphenyl portion, and the LUMO of the (mesityl)$_2$B(biphenyl) portion. Molecular modeling studies show that the two biphenyl units in **1** are approximately orthogonal to the naphthalene ring, and, as a result, charge transfer from the amine to the boron unit most likely occurs through space rather than through the aromatic linker. In contrast to the behavior of BNPB, whose emission is quenched upon addition of F^-, the emission spectrum of a solution of **1** shifts to a shorter wavelength ($\lambda_{max} = 453$ nm, in CH_2Cl_2) upon addition of TBAF and the emission intensity is drastically enhanced (Figure 1). The color of the emission of **1** changes vividly from green to blue (Figure 1) after addition of F^-. Hence, compound **1** can be described as a "turn-on" sensor for fluoride. A possible explanation for the color change is the presence of dual fluorescent pathways in **1**, that is, charge-transfer emission between the N donor and the B acceptor as well as $\pi^* \rightarrow \pi$ emission localized on the N donor. The binding of F^- to the B center blocks the charge-transfer transition, thus inhibiting the green emission, but the blue emission of the N(Ph)(1-naphthyl)(biphenyl) portion is activated simultaneously (Scheme 2). The closely related molecules 4,4′-bis[(1-naphthyl)(phenyl)amino]biphenyl and 1,8-bis{4-[(1-naphthyl)(phenyl)amino]biphenyl-4′-yl}naphthalene[7] exhibit similar blue emission (see the Supporting

[*] Dr. X. Y. Liu, D. R. Bai, Prof. Dr. S. Wang
Department of Chemistry
Queen's University
Kingston, Ontario, K7L 3N6 (Canada)
Fax: (+1) 613-533-6669
E-mail: wangs@chem.queensu.ca

[**] This work was supported by the Natural Sciences and Engineering Research Council of Canada.

Supporting information for this article is available on the WWW under http://www.angewandte.org or from the author.

 © 2006 Wiley-VCH Verlag GmbH & Co. KGaA, Weinheim



Scheme 1. Synthesis of fluorescent fluoride sensors **1** and **2**.

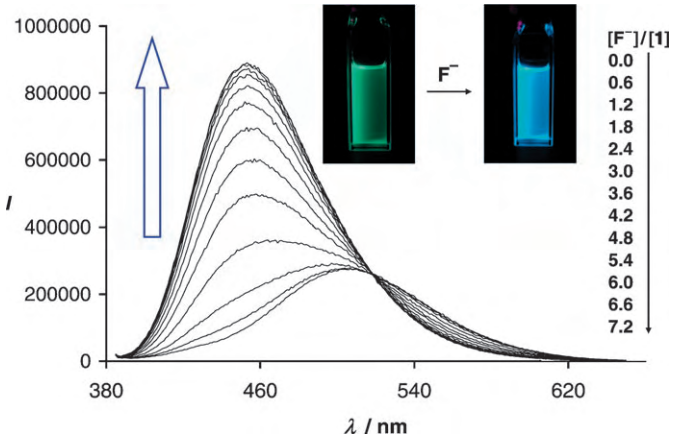
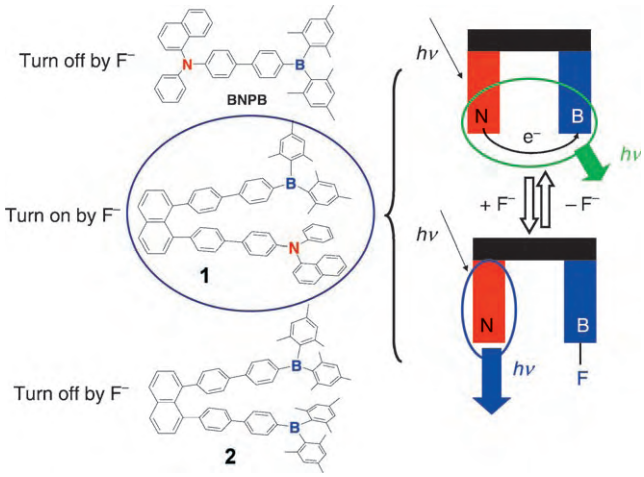


Figure 1. The emission spectra of **1** (7.4×10^{-6} M in CH_2Cl_2) upon addition of TBAF.

Information), which supports the hypothesis that the observed blue emission of F^--bound **1** is indeed from the (phenyl)(1-naphthyl)aminobiphenyl unit. One possible factor that is responsible for the distinct behavior of **1** and BNPB is the difference in their fluorescent quantum efficiencies (0.10 versus 0.67). The emission quantum efficiency of the aminobiphenyl unit in **1** and BNPB is likely between 0.10 and 0.67, and, as a consequence, the quenching of the charge-transfer emission by fluoride leads to an increase in emission intensity for **1**, but a decrease for BNPB. The drastically different emission quantum yields of BNPB and **1** are most likely the consequence of the linker between the donor and the acceptor, namely, a linear aromatic linker versus a nonlinear, nonconjugated linker.

To appreciate the importance of the N(Ph)(1-naphthyl)(biphenyl) group in the "turn-on" sensing of **1**, diboron molecule **2** in which the N(Ph)(1-naphthyl) unit is replaced by $B(mesityl)_2$ was synthesized (Scheme 1). Molecule **2** displays solvent-dependent fluorescence (see the Supporting Information), which is consistent with charge-transfer emission. **2** fluoresces at a much shorter wavelength than **1** and has a much higher quantum efficiency (e.g. $\lambda_{em}=414$ nm, $\Phi_p=0.98$ in CH_2Cl_2). Molecular-orbital calculations (Gaussian03) revealed that the HOMO of **2** consists predominantly of the naphthyl ring whereas the LUMO is dominated by the p_π orbitals of the two boron centers and the biphenyl units. The lowest electronic transition in **2** can be therefore attributed to charge transfer between the naphthyl ring and the two boron centers. The response of **2** to fluoride is in sharp contrast to that of **1**: instead of fluorescent enhancement and a color change, the addition of F^- to a solution of **2** quenches the emission from **2** (Figure 2). **2** is therefore a "turn-off" sensor for fluoride. The behavior of **2** in the presence of F^- resembles that of BNPB, which is not surprising since in both molecules the donor and the acceptor are connected through a linear aromatic linker (biphenyl). The fluorescent quenching of **2** by F^- is due to the occupation of the empty p_π orbital of boron by the F^- ligand—the same operating mechanism as in BNPB. The contrasting fluorescent properties of **2** and its response to fluoride establish unequivocally that the aminobiphenyl unit in **1** is indeed



Scheme 2. Operating principle of "turn-on" and "turn-off" sensors for fluoride.

© 2006 Wiley-VCH Verlag GmbH & Co. KGaA, Weinheim

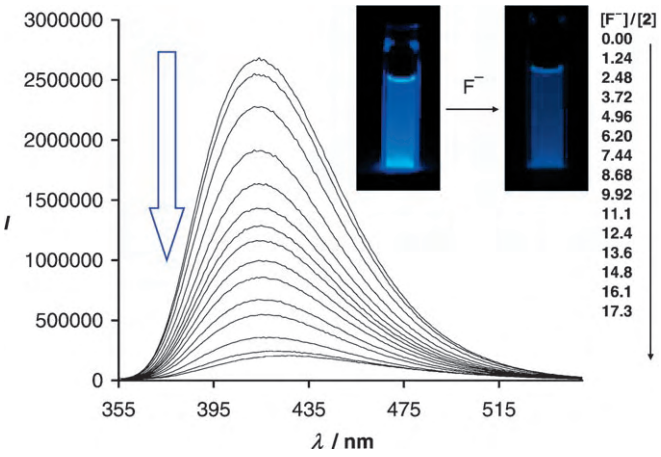


Figure 2. The emission spectra of **2** (9.1×10^{-6} M in CH_2Cl_2) upon the addition of TBAF.

responsible for the fluorescent color change and intensity enhancement of **1** induced by F^-.

The binding of fluoride to **1** and **2** was verified by titration experiments with ^{19}F NMR spectroscopy. The addition of **1** or **2** to a solution containing excess TBAF results in two distinct ^{19}F chemical shifts, which correspond to bound and unbound F^- ions, respectively. Furthermore, the NMR data indicated that **1** forms a 1:1 complex with F^- whereas **2** forms a 1:2 complex. Solé and Gabbai demonstrated that two unsaturated boron groups attached directly to the 1 and 8 positions of naphthalene can capture an F^- ion, which acts as a bridging ligand and results in a complex with an exceptionally large binding constant.[3g] We did not observe any evidence of bridging F^- ligands in the NMR experiments with **2**. Molecular-modeling studies and geometry optimization with the Gaussian 03 program suite showed that the two boron centers in **2** are approximately 10 Å apart, which is too far for an F^- bridge. The binding constants of **1** and **2** with fluoride were determined from the fluorescence titration data (see the Supporting Information for details) to be approximately $4.0\times10^4\,M^{-1}$ and $9.0\times10^8\,M^{-2}$, respectively, which are comparable to previously reported three-coordinate monoboron compounds.[3] (The binding constant of **2** is seemingly large because it is the overall binding constant for two fluoride ions.) The fluorescence spectra of **1** and **2** (Figures 1 and 2) change significantly upon addition of around two equivalents of F^- ions. This corresponds to a detection limit for F^- of between 0.015 and 0.020 mM under the experimental conditions used; thus, **1** and **2** are very sensitive to F^-. Moreover, they do not respond to chloride, bromide, or iodide ions, they can be recovered fully from the titration solution, and the original color and intensity of their fluorescence can be restored fully by adding water to extract the fluoride ions (for organic solvents such as CH_2Cl_2 that are not miscible with water; see the Supporting Information). The use of water to reverse fluoride binding to three-coordinate boron molecules in organic solvents has been noted by Yamaguchi et al.[3c] A large enhancement in the fluorescence of **1** and a drastic quenching of the fluorescence of **2** upon addition of fluoride are also observed in tetrahydrofuran (THF) and *N*,*N*-dimethylformamide (DMF). The disadvantage of using THF or DMF as the solvent is the difficulty of recovering the sensor molecules by using water, as these solvents are water-miscible. When mixed solvents such as THF and H_2O or DMF and H_2O are used for the fluoride titration experiments, no apparent fluorescence change was observed; this observation can be attributed to the formation of hydrogen bonds between fluoride ions and water molecules, which compete with the binding to the boron center.

In summary, we have demonstrated that a nonplanar linker, such as 1,8-bis(4,4′-biphenyl)naphthalene, can be used effectively to bring either two electron acceptor groups (e.g. diaryl boron groups), or an electron donor and an acceptor (e.g. a diaryl amino group and a diaryl boron group) together to form molecules that are stable in water and display distinct fluorescent responses to fluoride. By linking a nitrogen donor and a boron acceptor group in a nonplanar arrangement (as in **1**), it is possible to produce through-space donor–acceptor charge-transfer emission that can be switched off by the addition of fluoride, which in turn activates the fluorescence from the donor chromophore, thus producing a sensitive and selective "turn-on" fluorescent sensor for fluoride. Energy-transfer systems involving three-coordinate boron compounds that exploit dual signaling pathways for the detection of fluoride ions have been reported previously.[3f] Compound **1** demonstrates that dual signal pathways in nonplanar three-coordinate boron compounds can also be modulated by intramolecular charge transfer and exploited effectively for the detection of anions such as fluoride.

Experimental Section

Excitation and emission spectra were recorded on a Photon Technologies International QuantaMaster Model C-60 spectrometer. Fluorescence titrations were carried out by adding stock solutions of TBAF in CH_2Cl_2 to the solutions of **1** or **2** in CH_2Cl_2. Binding constants were obtained by using the fitting methods described by Connors.[8] Elemental analyses were performed by Canadian Microanalytical Service Ltd., Delta, British Columbia, Canada. The Gaussian 03 program suite[6] was used for all molecular-geometry optimization and molecular-orbital calculations. The calculations were carried out at the B3LYP level of theory with 6-311G** as the basis set. 1,8-Diiodonaphthalene[9] and 4-iodo-4′-(1-naphthylphenylamino)biphenyl[10] were synthesized by modified literature methods. The experimental and synthetic details are provided in the Supporting Information.

Received: April 1, 2006
Published online: July 19, 2006

Keywords: boron · charge transfer · fluorescence · fluorides · sensors

[1] a) Z. Yuan, N. J. Taylor, R. Ramachandran, T. B. Marder, *Appl. Organomet. Chem.* **1996**, *10*, 305; b) Z. Yuan, J. C. Collings, N. J. Taylor, T. B. Marder, *J. Solid State Chem.* **2000**, *154*, 5; c) Z. Yuan, N. J. Taylor, T. B. Marder, I. D. Williams, S. K. Kurtz, L. T. Cheng in *Organic Materials for Non-linear Optics, II* (Eds.: R. A. Hann, D. Bloor), The Royal Society of Chemistry, Cambridge, **1991**, p. 190; d) C. D. Entwistle, T. B. Marder, *Angew. Chem.* **2002**, *114*, 3051; *Angew. Chem. Int. Ed.* **2002**, *41*, 2927; e) C. D. Entwistle, T. B. Marder, *Chem. Mater.* **2004**, *16*, 4574; f) Z. Yuan, N. J. Taylor, T. B. Marder, I. D. Williams, S. K. Kurtz, L. T.

 © 2006 Wiley-VCH Verlag GmbH & Co. KGaA, Weinheim

Cheng, *Chem. Commun.* **1990**, 1489; g) Z. Yuan et al., *Chem. Eur. J.* **2006**, *12*, 2758, and Supporting Information thereof; h) R. Stahl, C. Lambert, C. Kaiser, R. Wortmann, R. Jakober, *Chem. Eur. J.* **2006**, *12*, 2358.

[2] a) T. Noda, Y. Shirota, *J. Am. Chem. Soc.* **1998**, *120*, 9714; b) T. Noda, H. Ogawa, Y. Shirota, *Adv. Mater.* **1999**, *11*, 283; c) Y. Shirota, M. Kinoshita, T. Noda, K. Okumoto, T. Ohara, *J. Am. Chem. Soc.* **2000**, *122*, 1102; d) T. Noda, Y. Shirota, *J. Lumin.* **2000**, *87*, 1168; e) M. Kinoshita, H. Kita, Y. Shirota, *Adv. Funct. Mater.* **2002**, *12*, 780; f) H. Kinoshita, K. Okumoto, Y. Shirota, *Chem. Mater.* **2003**, *15*, 1080; g) M. Uchida, Y. Ono, H. Yokoi, T. Nakano, K. Furukawa, *J. Photopolym. Sci. Technol.* **2001**, *14*, 306; h) Y. Shirota, *J. Mater. Chem.* **2000**, *10*, 1, and references therein; i) W. L. Jia, D. R. Bai, T. McCormick, Q. D. Liu, M. Motala, R. Y. Wang, C. Seward, Y. Tao, S. Wang, *Chem. Eur. J.* **2004**, *10*, 994; j) M. Mazzeo, V. Vitale, F. D. Sala, M. Anni, G. Barbarella, L. Favaretto, G. Sotgiu, R. Cingolani, G. Gigli, *Adv. Mater.* **2005**, *17*, 34; k) W. L. Jia, X. D. Feng, D. R. Bai, Z. H. Lu, S. N. Wang, G. Vamvounis, *Chem. Mater.* **2005**, *17*, 164; l) W. L. Jia, M. J. Moran, Y. Y. Yuan, Z. H. Lu, S. N. Wang, *J. Mater. Chem.* **2005**, *15*, 3326.

[3] a) S. Yamaguchi, S. Akiyama, K. Tamao, *J. Am. Chem. Soc.* **2000**, *122*, 6335; b) S. Yamaguchi, T. Shirasaka, K. Tamao, *Org. Lett.* **2000**, *2*, 4129; c) S. Yamaguchi, S. Akiyama, K. Tamao, *J. Am. Chem. Soc.* **2001**, *123*, 11372; d) S. Yamaguchi, T. Shirasaka, S. Akiyama, K. Tamao, *J. Am. Chem. Soc.* **2002**, *124*, 8816; e) H. Shiratori, T. Ohno, K. Nozaki, A. Osuka, *Chem. Commun.* **1999**, 2181; f) Y. Kubo, M. Yamamoto, M. Ikeda, M. Takeuchi, S. Shinkai, S. Yamaguchi, K. Tamao, *Angew. Chem.* **2003**, *115*, 2082; *Angew. Chem. Int. Ed.* **2003**, *42*, 2036; g) S. Solé, F. P. Gabbai, *Chem. Commun.* **2004**, 1284; h) M. Melaimi, F. P. Gabbai, *J. Am. Chem. Soc.* **2005**, *127*, 9680; i) A. Sundararaman, M. Victor, R. Varughese, F. Jäkle, *J. Am. Chem. Soc.* **2005**, *127*, 13748; j) S. Aldridge, C. Bresner, I. A. Fallis, S. J. Coles, M. B. Hursthouse, *Chem. Commun.* **2002**, 740; k) Z. Q. Liu, M. Shi, F. Y. Li, Q. Fang, Z. H. Chen, T. Yi, C. H. Huang, *Org. Lett.* **2005**, *7*, 5481.

[4] a) K. L. Kirk, *Biochemistry of the Halogens and Inorganic Halides*, Plenum, New York, **1991**, p. 58; b) B. L. Riggs, *Bone and Mineral Research*, Annual 2, Elsevier, Amsterdam, **1984**, pp. 366–393; c) A. Wiseman, *Handbook of Experimental Pharmacology XX/2*, Part 2, Springer, Berlin, **1970**, pp. 48–97; d) J. A. Weatherall, *Pharmacology of Fluorides* in *Handbook of Experimental Pharmacology XX/1*, Part 1, Springer, Berlin, **1969**, pp. 141–172; e) R. H. Dreisbuch, *Handbook of Poisoning*, Lange Medical Publishers, Los Altos, CA, **1980**; f) C. R. Cooper, N. Spencer, T. D. James, *Chem. Commun.* **1998**, 1365, and references therein; g) C. B. Black, B. Andrioletti, A. C. Try, C. Ruiperez, J. L. J. Sessler, *J. Am. Chem. Soc.* **1999**, *121*, 10438, and references therein; h) H. Sohn, S. Létant, M. J. Sailor, W. C. Trogler, *J. Am. Chem. Soc.* **2000**, *122*, 5399; i) J. Emsley, *The Sordid Tale of Murder, Fire, and Phosphorus*, *The 13th Element*, Wiley, New York, **2000**.

[5] a) H. E. Katz, *J. Org. Chem.* **1985**, *50*, 5027; b) H. E. Katz, *J. Am. Chem. Soc.* **1986**, *108*, 7640; c) M. T. Reetz, C. M. Niemeyer, K. Harms, *Angew. Chem.* **1991**, *103*, 1517; *Angew. Chem. Int. Ed. Engl.* **1991**, *30*, 1472; d) V. C. Williams, W. E. Piers, W. Clegg, M. R. J. Elsegood, S. Collins, T. B. Marder, *J. Am. Chem. Soc.* **1999**, *121*, 3244.

[6] Gaussian 03, (Revision A.9), Frisch et al., see reference [3] in the Supporting Information.

[7] X. Y. Liu, S. N. Wang, unpublished results.

[8] K. A. Connors, *Binding Constants*, Wiley, New York, p. 1987.

[9] H. O. House, D. G. Koepsell, W. J. Campbell, *J. Org. Chem.* **1972**, *37*, 1003.

[10] B. E. Koene, D. E. Loy, M. E. Thompson, *Chem. Mater.* **1998**, *10*, 2235.

 © 2006 Wiley-VCH Verlag GmbH & Co. KGaA, Weinheim

Nanobiotechnology

DOI: 10.1002/anie.200600545

Multifunctional Lipid/Quantum Dot Hybrid Nanocontainers for Controlled Targeting of Live Cells**

*Gopakumar Gopalakrishnan, Christophe Danelon, Paulina Izewska, Michael Prummer, Pierre-Yves Bolinger, Isabelle Geissbühler, Davide Demurtas, Jacques Dubochet, and Horst Vogel**

Nanocrystal-based organic–inorganic functional hybrid materials with novel, exceptional properties have been explored in recent years because of their potential applications in nanobiotechnology.[1] Viral assembly of inorganic nanoparticles,[2a] and their polypeptide[2b,c] and ligand-receptor-mediated organization[2d] and protein-templated synthesis[2e] are a few examples in this direction. Of utmost interest in this context are lipid molecules because of their unique ability to form a variety of self-organized, supramolecular structures.[3] Although planar and vesicular lipid membranes have been used to compartmentalize and to synthesize nanocrystals in a confined volume,[4] the enormous possibilities of lipid-based, biocompatible nano/microstructures in nanobiotechnology have still to be fully exploited. For example, native and artificial vesicles offer novel possibilities for investigating (bio)chemical reactions and cellular signal transduction processes at the nanometer and attoliter scales.[5] Furthermore, the interaction between specially designed lipid vesicles and mammalian cells (adsorption, fusion, endocytosis)[6a] has been used to deliver DNA and RNA into cells, and has high potential for smart diagnostics, controlled drug delivery, and gene transfer.[4a,6] Inorganic nanoparticles could offer new ways to image native and artificial vesicles and control (bio)chemical reactions therein, if it is possible to selectively position the particles on or within the vesicles.

[*] Dr. G. Gopalakrishnan, Dr. C. Danelon, P. Izewska, Dr. M. Prummer, P.-Y. Bolinger, Dr. I. Geissbühler, Prof. Dr. H. Vogel
Laboratoire de Chimie Physique des Polymères et Membranes
Institut des Sciences et Ingénierie Chimiques (ISIC)
Ecole Polytechnique Fédérale de Lausanne (EPFL)
1015 Lausanne (Switzerland)
Fax: (+41) 21-693-6190
E-mail: horst.vogel@epfl.ch

D. Demurtas, Prof. Dr. J. Dubochet
Laboratoire d'Analyse Ultrastructurale (LAU)
Université de Lausanne (UNIL)
1015 Lausanne (Switzerland)

[**] This work was supported by a grant (no. 4047-057562) from the NRP-47 program of the Swiss National Science Foundation and internal grants from the EPFL. We thank Marc Adrian (LAU, UNIL) for support with electron microscopy, and Ruud Hovius and Jean-Manuel Segura (LCPPM, EPFL) for helpful discussions.

Supporting information for this article is available on the WWW under http://www.angewandte.org or from the author.

WILEY InterScience DISCOVER SOMETHING GREAT
© 2006 Wiley-VCH Verlag GmbH & Co. KGaA, Weinheim

In this context, we investigated quantum dots (QDs), which are inorganic, strongly fluorescent nanoparticles of exceptional photostability, for the in vivo imaging of cellular processes.[7] Notably, coating hydrophobic QDs with phospholipids is a generic method for making them water-soluble[8a] and biocompatible,[8b] which is useful for investigating biochemical reactions in vitro[9a] and when QDs are microinjected into live cells.[9b]

Herein, we report an interesting observation of wide-ranging potential for cellular imaging and manipulation: hydrophobic QDs can be readily incorporated into the bilayer membrane of lipid vesicles. Such lipid/QD hybrid vesicles (HVs) are capable of fusing with live cells, thereby staining a cell's plasma membrane selectively with fluorescent QDs and transferring the vesicle's cargo into the cell.

Figure 1a depicts the steps involved in the fabrication of the HVs. A solution of trioctylphosphine oxide (TOPO) coated CdSe QDs and lipids in chloroform is dried in a vial to form a multilamellar lipid film, from which vesicles are spontaneously formed by hydration under water. We investigated a wide range of phospholipid molecules (different head groups, various alkyl chain lengths, etc.) as well as different established methods of liposome formation (classical swelling, electroswelling).[10] We found that the formation of the HVs is not limited to any particular class of lipid[10c] and/or method of formation. HVs with sizes ranging from 50 nm to a few tens of micrometers can be produced in a controlled manner.

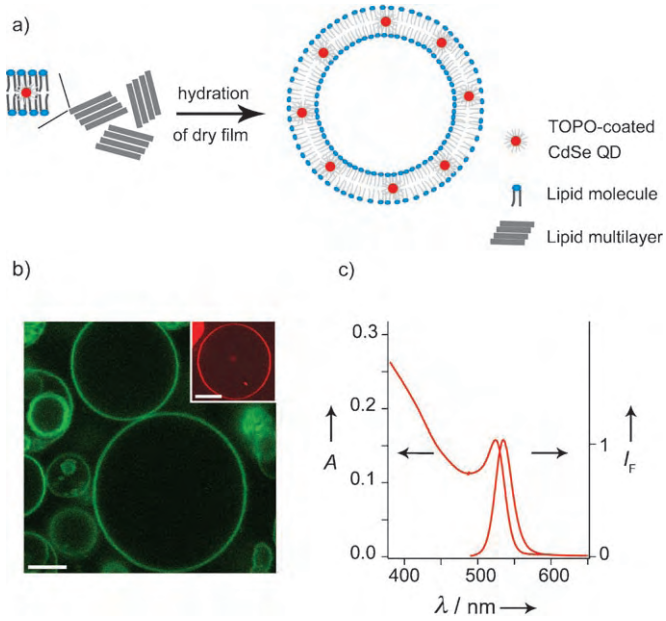


Figure 1. a) Steps involved in the formation of lipid/QD HVs. b) Confocal fluorescence cross-sectional image of HVs made of DMPC by hydration swelling. The inset shows vesicles stained with rhodamine-labeled lipids. Scale bars: 10 μm. c) Typical absorption/emission spectra of the CdSe QDs used in the preparation of HVs. The narrow emission spectrum indicates the uniform size (ca. 3 nm) of the QDs.

For ease of observation by confocal microscopy, we first fabricated giant vesicles (1–50 μm) by classical swelling. Figure 1b shows representative confocal cross sections of vesicles, which appear as clear and sharp fluorescent circles at their perimeters. These images are comparable with those known to result from vesicles stained with fluorescent organic dyes,[10a] which are shown for comparison as the inset of Figure 1b. This result demonstrates that the hydrophobic QDs must be integrated in or attached to the lipid bilayer of the vesicle. A high yield of giant unilamellar vesicles was obtained along with some multilamellar ones, as is usually the case with this approach. Electroswelling[10b] produced more homogeneous unilamellar structures.

Figure 1c shows the absorption and emission spectra of the hydrophobic QDs employed in the production of the HVs. The spectral properties (position of maxima, narrow emission spectrum) indicate a uniform size of about 3 nm of the CdSe QD core;[11a,b] our TOPO/QDs have a size of about 5 nm, which includes the hydrophobic coating. Current limitations that result from photobleaching of organic membrane dyes in acquiring high-resolution images, thin z-sectioning for eventual 3D reconstruction, and longer-term in situ observations could be solved using our HVs. Although core–shell QDs[11c] offer higher photostability compared to core-only QDs, confocal imaging at higher laser power was performed uninterruptedly for hours using our TOPO-coated QDs.[11d] The imaging of vesicles, planar lipid bilayers, and lipid monolayers at the air/water interface can thus be performed for hours, which is of interest for studying phase diagrams and phase separation phenomena in lipid mixtures.[12,13]

Calorimetric measurements revealed the ordered-fluid phase transition temperature T_t of the lipid/QD vesicles at 23.5 °C, which is identical to that for pure DMPC bilayers.[3] This is actually not surprising considering that the lipid/QD molar ratio of our vesicles is 3000:1. Furthermore, we studied the lateral diffusion of QDs in the lipid bilayer above and below the T_t of giant vesicles of DMPC immobilized on a glass plate. Figure 2 shows fluorescence microscopy images of single QDs obtained from the planar membrane region of an immobilized vesicle in contact with a glass support. We observed substantially different diffusion of single QDs within the membrane below and above the T_t of the lipid bilayer. Figure 2a shows single QDs observed at 5 °C ($< T_t$), with the inset giving a single-step photobleaching profile of an individual QD, which proves that the spots are single QDs (see also the movies in the Supporting Information). We calculated the lateral diffusion coefficient D from the mean-square displacements (MSDs) of the diffusing single QDs in the bilayer membrane, as described in Figure 2b and the Supporting Information. In the fluid lipid bilayer at 30 °C, the lateral diffusion of the QDs ($D = 0.3 \times 10^{-8}$ cm^2 s^{-1}) is about ten times slower than that of a lipid molecule ($D = 4 \times 10^{-8}$ cm^2 s^{-1});[12b,c] this reduced diffusion could be a result of the larger size of the QDs compared to lipid molecules. The actual diffusion coefficient might be slightly larger because of a systematic underestimation of fast particles by the single-particle-tracking algorithm.[14] In the fluid membrane phase, 75% of the tracked particles follow the diffusion profile whereas 25% are less mobile.

The tracked single QDs in the ordered bilayer state ($T < T_t$) are nearly immobile, as revealed by the negligibly small

 © 2006 Wiley-VCH Verlag GmbH & Co. KGaA, Weinheim

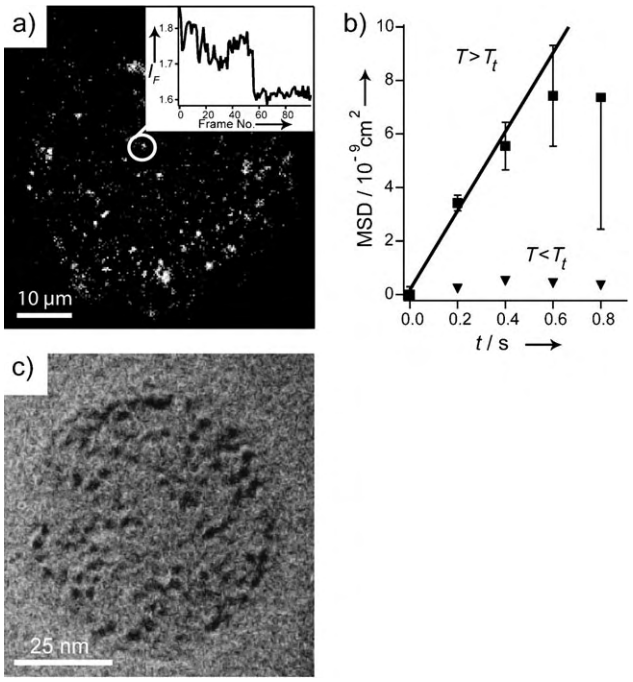


Figure 2. Imaging of single QDs in the bilayer of an immobilized giant vesicle. a) Fluorescence micrograph showing representative images of single QDs in the planar bilayer region attached to a glass surface at 5 °C. The inset shows a photobleaching profile of a single QD. b) Calculated MSD values (mean of three experiments) of the trajectory of single QDs diffusing in a lipid bilayer are plotted as a function of time at 30 °C for a fluid lipid bilayer (top) and at 5 °C for an ordered lipid bilayer (bottom). From the MSD values, it is clear that QDs are immobile in the ordered lipid bilayer. The diffusion coefficient of QDs in the fluid lipid bilayer is calculated from the corresponding slope. (See the Supporting Information for movies of single-molecule experiments and for details of the MSD calculation.) c) Cryo-TEM image of a collapsed HV at ten times higher QD concentration than that used for the confocal microscopy images shown in Figure 1 b. The ca. 3-nm QDs (dark spots) are randomly distributed in the vesicle's lipid bilayer.

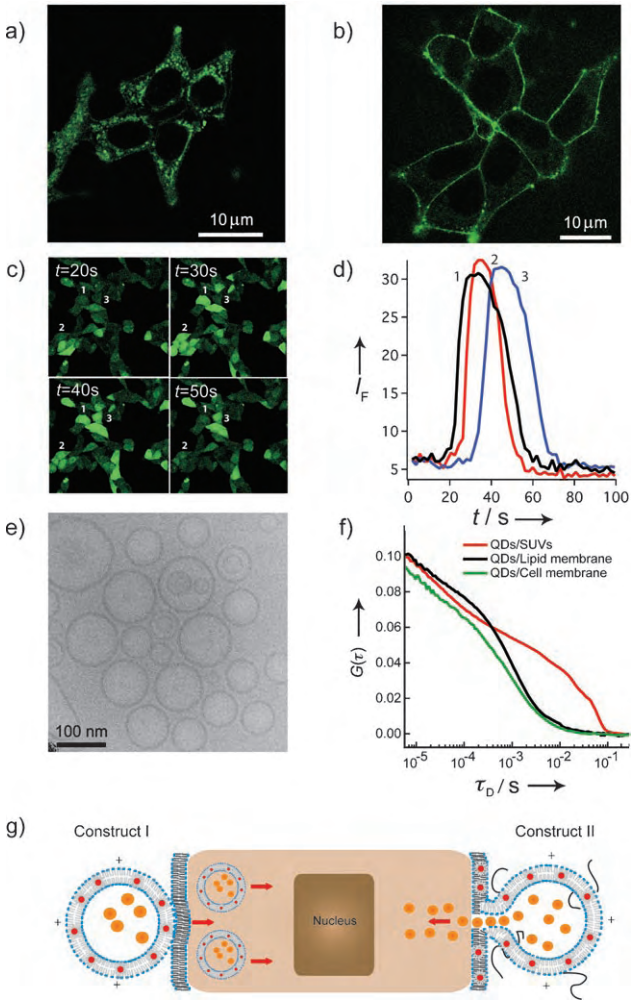


Figure 3. Interaction of HVs with HEK293 cells. a,b) Confocal micrographs of HEK293 cells 30 s after addition of vesicles: a) construct I vesicles are totally internalized into the cells; b) construct II vesicles selectively labeled the cell membrane without internalization into the cytoplasm. c) A series of confocal images (recorded at 300-ms scan rate) showing the fluorescence intensity response of Fluo-3 inside HEK293 cells at different times after fusion with construct II vesicles loaded with 1 mM $CaCl_2$. d) The transient Fluo-3 fluorescence signals of a few representative cells (numbers correspond to numbered cells in (c)). e) Cryo-TEM image of construct II vesicles; the TEM images of construct I vesicles (not shown) are very similar. f) FCS autocorrelation curves showing diffusion times of QDs in different environments. The diffusion time of QDs in the cell plasma membrane observed after the fusion of HVs with the cell (green curve) is nearly identical to that in the lipid bilayer of an immobilized giant HV (black curve). The red curve shows the diffusion of small unilamellar vesicles (SUVs, 20–100 nm; construct II) in solution. g) Cartoon illustrating interactions of construct I and II HVs with living cells. Orange dots in the interior of the HVs represent any deliverable water-soluble molecules.

MSD values. It is important to mention here that the switching of the diffusion properties of the QDs occurs at exactly 23.5 °C, which is identical to the lipid phase transition temperature observed in the calorimetric measurements. These observations show that the QDs are tightly associated with the lipid membrane, because otherwise there would be little or no effect with respect to the membrane state. It has been suggested that hydrophobic QDs could be incorporated into lipid bilayers and thereby achieve efficient phase transfer from organic to aqueous medium,[8a] thus allowing the in vitro study of membrane association by fluorescence resonance energy transfer (FRET).[8b] In spite of these experimental approaches, the prediction of the exact location of the QDs relative to a lipid bilayer remains a difficult task, where artifacts and overinterpretations have to be carefully avoided.[8a] For all the applications discussed herein, it is sufficient to know that the QDs are stably associated with the bilayer, irrespective of whether they are fully or only partially inserted in the lipid bilayer.

The interaction of the lipid/QD vesicles with living cells was tested for two different lipid compositions (Figure 3 a–g). Construct I HVs are designed for transfer into the cell (Figure 3 g). The bilayer of small HVs (20–100 nm; characterized by electron microscopy, as in Figure 3 e) consists of 25 % positively charged lipid (DOTAP), which is known to enhance the cellular internalization,[15] and 75 % DMPC. Lipid/QD hybrid structures were found inside the cytosol within seconds after incubation with cells (Figure 3 a). This

 © 2006 Wiley-VCH Verlag GmbH & Co. KGaA, Weinheim

efficient uptake might allow further targeting of HVs to specific locations inside live cells through prior decoration of the HV surface with specific receptors.[16] Despite the universal use of cationic lipids in DNA transfection experiments,[15a] the exact mechanism of this event is still not clear.[17]

Construct II HVs were designed to fuse with the plasma membrane of a live cell (Figure 3g). This process is usually very difficult to achieve at room temperature.[18] As in the preceding experiment, small HVs (20–100 nm, Figure 3e) are used which now comprise 25% positively charged lipid (DOTAP), 0.5% DPPE-PEG2000, and 74.5% DMPC. Figure 3b shows a confocal image of live cells that were incubated with construct II vesicles. Interestingly, in this case the cell membrane is selectively labeled and no fluorescence was observed in the cytosol even after 1 h of incubation. The mechanism is not yet understood, but we speculate that the membrane-incorporated PEG molecules act as a transient barrier[19] between the cationic liposomal and anionic cellular membranes, thus preventing them from becoming internalized. At this distance (nanometer range), the collective process of electrostatic attraction (resulting from positively charged lipids) and membrane vulnerability (resulting from PE lipids and QDs) triggers the fusion between the membranes.

The appearance of QD fluorescence in the cellular membrane (Figure 3b) could be a consequence of either stable adhesion of intact vesicles on the surface of the plasma membrane or fusion between the bilayer of HVs and the plasma membrane, thus resulting in integration of the QDs into the cell membrane. For a better understanding of the exact event, the HVs were used as nanocontainers filled with aqueous $CaCl_2$ and incubated with cells, which were loaded with Fluo-3 (a fluorescence indicator to measure the Ca^{2+} ion concentration in the cytoplasm). After a certain time lag the cells responded by a transient increase in intracellular Ca^{2+} ion concentration (Figure 3c,d), followed by selective labeling of the plasma membrane (similar to Figure 3b for an experiment without intracellular Fluo-3). The increase in intracellular Ca^{2+} concentration is transient because the Ca^{2+} vesicle cargo released into the living cells becomes accommodated in the endoplasmic reticulum by the cellular machinery. The following control experiments were performed to prove the fusion capability of the HV nanocontainers: 1) on addition of 1 mM $CaCl_2$/phosphate-buffered saline (PBS) without vesicles to the external medium of cells loaded with Fluo-3, the cells did not give an intracellular Ca^{2+} response; 2) addition of HV nanocontainers without a $CaCl_2$ cargo to Fluo-3 loaded cells also did not induce an intracellular Ca^{2+} response. This result shows that the Ca^{2+} ions were not generated inside the cells through any kind of activation of intracellular Ca^{2+} ion stores upon vesicle interaction with the cellular membrane surface, but were delivered into the cell from the nanocontainers by fusion.

Fluorescence correlation spectroscopy (FCS) measurements were performed on the plasma membrane of live cells after incubating them with construct II vesicles to exclude any possibility that nanocontainers are simply adsorbed on the cell membrane, for example, by electrostatic interaction. Figure 3f shows the measured autocorrelation functions (ACFs). The ACFs of QDs in the plasma membrane (green curve) and in the lipid bilayer of immobilized micrometer-sized HVs (black curve) are nearly identical, whereas the ACFs of a solution of small unilamellar vesicles show much slower diffusion (red curve). This finding demonstrates that the QDs reside within the plasma membrane of the cell, and gives additional proof that the observed cell membrane labeling and subsequent Ca^{2+} influx is caused by fusion between the vesicle bilayer and cell membrane. By using this approach, one can potentially carry any water-soluble material that can be enclosed inside the nanocontainers and deliver it into the live cells.

The use of QDs in biological cells always poses concerns about potential cytotoxicity. Unmodified TOPO-coated QDs are toxic to live cells,[20] probably by releasing Cd^{2+} ions into the cell as a result of poor surface coverage. Proper surface coating of QDs seems to avoid direct contact of the QD core with cells.[20] However, in our experiments the lipid/QD vesicles did not show any cytotoxic effects even after three hours of incubation with live cells. This finding indicates, but of course does not prove, that our QDs are well-embedded in the membrane rather than being in the membrane/water interfacial region. The in vivo experiments reported elsewhere using lipid-coated QDs[9b] also did not show any cytotoxic effects in embryonic cells, which suggests that lipid coating is an effective way to make QDs biocompatible.

Our results imply that cell and lipid membranes, and certainly the walls of polymeric vesicles,[21] can integrate any kind of hydrophobic nanoparticles whose size matches the membrane thickness.[10d] The incorporation of, for instance, nanometer-sized magnetic[22a–c] or metallic particles[23a] into the membranes will transform the properties of the cells or vesicles accordingly, and opens up novel possibilities for manipulating them as individuals or in ensembles with wide-ranging applications for nanoscale reactors,[5,24] cellular targeting,[25] targeted drug delivery,[26] contrast agents,[27] etc. The collective magnetic properties offered by the supramolecular membrane systems will add complementary advantages compared to individual, biopolymer-modified, large magnetic nanoparticles.[22d] Another interesting field of investigation in the present context is Au nanoparticles; they are known for their thermal response to radio and photo irradiations, and presently receive great attention in photo/radiotherapy as magnetic particles in hyperthermia-aided diagnostics and treatment.[23b]

In summary, we have described the fabrication of highly controllable organic–inorganic HVs where nanometer-sized particles are confined to 4-nm-thick membranes. The tunable size, switchable physical properties, response to multiple external stimuli, and above all the controlled cell fusion capacity make them very promising tools in nanobiotechnology.

Experimental Section

Lipids: 1,2-Dimyristoyl-*sn*-glycero-3-phosphatidylcholine (DMPC), 1,2-dioleoyl-3-trimethylammonium propane chloride salt (DOTAP), 1,2-distearoyl-*sn*-glycero-3-phosphatidylethanolamine-*N*-[biotinyl-

 © 2006 Wiley-VCH Verlag GmbH & Co. KGaA, Weinheim

(polyethylene glycol 2000)] ammonium salt (DSPE-PEG2000-biotin), and 1,2-dipalmitoyl-*sn*-glycero-3-phosphatidylethanolamine-*N*-[methoxy(polyethylene glycol 2000)] ammonium salt (DPPE-PEG2000) were purchased from Avanti Polar Lipids.

Preparation of hybrid vesicles (HVs): 1) Classical swelling**:** Chloroform solutions of DMPC (1.5 mM, 100 μL), DSPE-PEG2000-biotin (0.6 mM, 5 μL), and CdSe/TOPO QDs (5 μM, 10 μL) were mixed and dried in a vacuum for 4 h in a teflon chamber. The film was then hydrated overnight at 37 °C by incubating with sucrose (0.1 M). 2) Electroswelling: Chloroform solutions of DMPC (1.5 mM, 100 μL), DSPE-PEG2000-biotin (0.6 mM, 5 μL), and CdSe/TOPO QDs (5 μM, 10 μL) were mixed and dried in a vacuum for 4 h on a glass slide coated with indium tin oxide (Sigma). The film was then hydrated at 37 °C by incubating with sucrose (0.1 M) and applying an alternating electric field of 1.2 V/10 Hz during the first 2 h for effective swelling, and then 2.0 V/4 Hz for the next hour for easy detachment of the formed vesicles. 3) Immobilization of HVs for confocal microscopy: Biotinylated HVs in sucrose (0.1 M) were incubated on a glass coverslip, which was pretreated with avidin (0.1 $mg\,mL^{-1}$) in glucose (0.1 M). The glucose solution was used to keep the osmotic pressure balanced while allowing quick settling of sucrose-filled HVs.

Live-cell experiments: 1) Cell culture: Adherent human embryonic kidney cells (HEK293) were cultured in Dulbecco's Modified Eagle Medium (D-MEM; Gibco, Invitrogen, USA), supplemented with 2.2% fetal calf serum (Gibco), in a humidified 5% CO_2 atmosphere at 37 °C. Cells were split at regular intervals. For confocal microscopy, HEK293 cells were seeded into six-well plates (TPP, Trasadingen, Switzerland) containing 25-mm-diameter glass coverslips (Assistent, Germany), in culture medium (2 mL) containing 2.2% fetal calf serum. The cells were grown for 24 h at 37 °C, washed with PBS, and used for further experiments. 2) Cell/construct I vesicles: Chloroform solutions of DMPC (1.5 mM, 75 μL), DOTAP (1.5 mM, 25 μL), and CdSe/TOPO QDs (5 μM, 10 μL) were mixed and dried in a vacuum for 4 h, and the film was hydrated at 40 °C in PBS under vigorous mixing. The solution was then sonified in a bath sonifier for 10 s. This solution (10 μL) of small (20–100 nm) vesicles was added to the cells suspended in PBS (500 μL). 3) Cell/construct II vesicles: Chloroform solutions of DMPC (1.5 mM, 75 μL), DOTAP (1.5 mM, 25 μL), DPPE-PEG2000-PE (0.6 mM, 5 μL), and CdSe/TOPO QDs (5 μM, 10 μL) were mixed and dried in a vacuum for 4 h. The film was hydrated at 40 °C in PBS under vigorous mixing, and the solution was sonified in a bath sonifier for 10 s. This solution (10 μL) of small (20–100 nm) vesicles was added to the cells suspended in PBS (500 μL). 4) Ca^{2+} imaging experiments: For intracellular Ca^{2+} signaling tests, HEK293 cells were grown on sterile microscope coverslips as described above. Cells were loaded with Fluo-3 dye (Molecular Probes, Invitrogen, USA) 24 h after seeding at 37 °C in D-MEM medium containing 2.2% fetal calf serum, by incubation in serum-free D-MEM medium containing Fluo-3 for 30 min at 37 °C. Thereafter, the Fluo-3 containing medium was replaced by D-MEM medium supplemented with 10% fetal calf serum and incubated for 30 min at 37 °C. Subsequently, dye-loaded cells were washed with PBS and subjected to Ca^{2+} imaging. Construct II vesicles were prepared as explained above in $CaCl_2$/PBS (1 mM). A solution (10 μL) of such small (20–100 nm) vesicles loaded with $CaCl_2$ was applied to the cells suspended in PBS (500 μL).

All the fluorescence images were recorded using a Zeiss LSM 510 confocal microscope (Carl Zeiss AG, Germany) with an excitation wavelength of 488 nm and an emission wavelength of > 505 nm.

Received: February 9, 2006
Revised: May 5, 2006
Published online: July 18, 2006

Keywords: lipids · nanoparticles · organic–inorganic hybrid materials · quantum dots · vesicles

[1] a) *Biomineralization: Chemical and Biochemical Perspectives* (Eds.: S. Mann, J. Webb, R. J. P. Williams), VCH, New York, **1989**; b) J. Aizenberg, A. Tkachenko, S. Weiner, L. Addadi, G. Hendler, *Nature* **2001**, *412*, 819; c) T. Douglas, *Science* **2003**, *299*, 1192; d) B. I. Ipe, C. M. Niemeyer, *Angew. Chem.* **2006**, *118*, 519; *Angew. Chem. Int. Ed.* **2006**, *45*, 504; e) C. M. Niemeyer, *Angew. Chem.* **2003**, *115*, 5974; *Angew. Chem. Int. Ed.* **2003**, *42*, 5796.

[2] a) S.-W. Lee, C. Mao, C. E. Flynn, A. M. Belcher, *Science* **2002**, *296*, 892; b) S. R. Whaley, D. S. English, E. L. Hu, P. F. Barbara, A. M. Belcher, *Nature* **2000**, *405*, 665; c) M. S. Wong, J. N. Cha, K.-S. Choi, T. J. Deming, G. D. Stucky, *Nano Lett.* **2002**, *2*, 583; d) M. Bäumle, D. Stamou, J.-M. Segura, R. Hovius, H. Vogel, *Langmuir* **2004**, *20*, 3828; e) T. Douglas, M. Young, *Nature* **1998**, *393*, 152.

[3] a) G. Cevc, D. Marsh, *Phospholipid Bilayers: Physical Principles and Models*, Wiley, New York, **1987**; b) R. B. Gennis, *Biomembranes: Molecular Structure and Function*, Springer, New York, **1989**; c) O. G. Mouritsen, *Life as a Matter of Fat: The Emerging Science of Lipidomics*, Springer, Heidelberg, **2005**.

[4] a) J. H. Collier, P. B. Messersmith, *Annu. Rev. Mater. Res.* **2001**, *31*, 237; b) G. Gopalakrishnan, J.-M. Segura, D. Stamou, C. Gaillard, M. Gjoni, R. Hovius, K. J. Schenk, P. A. Stadelmann, H. Vogel, *Angew. Chem.* **2005**, *117*, 5037; *Angew. Chem. Int. Ed.* **2005**, *44*, 4957.

[5] a) H. Pick, E. L. Schmidt, A.-P. Tairi, E. Ilegems, R. Hovius, H. Vogel, *J. Am. Chem. Soc.* **2005**, *127*, 2908; b) P-Y. Bolinger, D. Stamou, H. Vogel, *J. Am. Chem. Soc.* **2004**, *126*, 8594; c) D. Stamou, C. Duschl, E. Delamarche, H. Vogel, *Angew. Chem.* **2003**, *115*, 5738; *Angew. Chem. Int. Ed.* **2003**, *42*, 5580.

[6] a) R. E. Pagano, J. N. Weinstein, *Annu. Rev. Biophys. Bioeng.* **1978**, *7*, 435; b) G. Gregoriadis, *Trends Biotechnol.* **1995**, *13*, 527; c) V. P. Torchilin, *Nat. Rev.* **2005**, *4*, 145; d) V. P. Torchillin, A. N. Lukyanov, Z. Gao, B. P. Sternberg, *Proc. Natl. Acad. Sci. USA* **2003**, *100*, 6039; e) J. Kunisawa, T. Masuda, K. Katayama, T. Yoshihawa, Y. Tsutsumi, M. Akashi, T. Mayumi, S. Nakagawa, *J. Controlled Release* **2005**, *105*, 344.

[7] a) X. Michalet, F. F. Pinaud, L. A. Bentolila, J. M. Tsay, S. Doose, J. J. Li, G. Sundaresan, A. M. Wu, S. S. Gambhir, S. Weiss, *Science* **2005**, *307*, 538; b) X. Gao, L. Yang, J. A. Petros, F. F. Marshall, J. W. Simons, S. Nie, *Curr. Opin. Biotechnol.* **2005**, *16*, 63.

[8] a) L. Feng, X. Kong, K. Chao, Y. Sun, Q. Zeng, Y. Zhang, *Mater. Chem. Phys.* **2005**, *93*, 310; We cite this report with reservations. 1) The authors claim to show the incorporation of QDs into lipid bilayers by electron and optical microscopy. However, the quality of their electron and optical micrographs does not allow localization of QDs inside or outside the lipid vesicles. 2) From differential scanning calorimetry experiments they claim that increasing amounts of QDs decrease the lipid phase-transition enthalpy, which they took as further proof of QD insertion into lipid bilayers: the reported enthalpy is ca. 0.08 $J\,g^{-1}$, which is orders of magnitude smaller than that typically measured (ca. 35 $J\,g^{-1}$) in lipid systems; b) J. A. Kloepfer, N. Cohen, J. L. Nadeau, *J. Phys. Chem. B* **2004**, *108*, 17042.

[9] a) I. Geissbuehler, R. Hovius, K. L. Martinez, M. Adrian, K. R. Thampi, H. Vogel, *Angew. Chem.* **2005**, *117*, 1412; *Angew. Chem. Int. Ed.* **2005**, *44*, 1388; b) B. Dubertret, P. Skourides, D. J. Norris, V. Noireaux, A. H. Brivanlou, A. Libchaber, *Science* **2002**, *298*, 1759.

[10] a) K. Akashi, H. Miyata, H. Itoh, K. Kinosita, *Biophys. J.* **1996**, *71*, 3242; b) M. I. Angelova, D. S. Dimitrov, *Faraday Discuss. Chem. Soc.* **1986**, *81*, 303; c) The HVs were prepared using saturated lipids such as DLPC, DMPC, DPPC, and DSPC, as well as unsaturated lipids such as DOPC and DOPG using classical swelling and electroswelling. The results imply that HV formation is not limited to any particular class of lipids used;

 © 2006 Wiley-VCH Verlag GmbH & Co. KGaA, Weinheim

d) Larger QDs (ca. 8 nm) were not integrated in the vesicle lipid bilayer under our experimental conditions; this size exclusion of ca. 5 nm is about the thickness of the lipid bilayer.

[11] a) C. B. Murray, D. J. Norris, M. G. Bawendi, *J. Am. Chem. Soc.* **1993**, *115*, 8706; b) Z. A. Peng, X. G. Peng, *J. Am. Chem. Soc.* **2001**, *123*, 183; c) B. O. Dabbousi, J. RodriguezViejo, F. V. Mikulec, J. R. Heine, H. Mattoussi, R. Ober, K. F. Jensen, M. G. Bawendi, *J. Phys. Chem. B* **1997**, *101*, 9463; d) The quantum yield of the QDs was measured by standard methods and found to be 25%.

[12] a) J. Korlach, P. Schwille, W. W. Webb, G. W. Feigenson, *Proc. Natl. Acad. Sci. USA* **1999**, *96*, 8641; b) A. E. Hac, H. M. Seeger, M. Fidorra, T. Heimburg, *Biophys. J.* **2005**, *88*, 317; c) L. A. Bagattoli, S. Sanchez, T. Hazlett, E. Gratton, *Methods Enzymol.* **2003**, *360*, 481.

[13] a) H. Möhwald, *Annu. Rev. Phys. Chem.* **1990**, *41*, 441; b) H. M. McConnell, *Annu. Rev. Phys. Chem.* **1991**, *42*, 171; c) H. M. McConnell, M. Vrljic, *Annu. Rev. Biophys. Biomol. Struct.* **2003**, *32*, 469.

[14] P. H. M. Lommerse, G. A. Blab, L. Cognet, G. S. Harms, B. E. S. Jagalska, H. P. Spaink, T. Schmidt, *Biophys. J.* **2004**, *86*, 69.

[15] a) P. L. Felgner, T. R. Gadek, M. Holm, R. Roman, H. W. Chan, M. Wenz, J. P. Northrop, G. M. Ringold, M. Danielsen, *Proc. Natl. Acad. Sci. USA* **1987**, *84*, 7413; b) I. Wrobel, D. Collins, *Biochim. Biophys. Acta* **1995**, *1235*, 296.

[16] a) K. S. Kawamura, M. Sung, E. Bolewska-Pedyczak, J. Gariépy, *Biochemistry* **2006**, *45*, 1116; b) S. Balayssac, F. Burlina, O. Convert, G. Bolbach, G. Chassaing, O. Lequin, *Biochemistry* **2006**, *45*, 1408.

[17] a) S. Berezhna, S. Schaefer, R. Heintzmann, M. Jahnz, G. Boese, A. Deniz, P. Schwille, *Biochim. Biophys. Acta* **1995**, *1235*, 296; b) A. L. Bailey, P. R. Cullis, *Biochemistry* **1997**, *36*, 1628.

[18] a) E. H. Chen, E. N. Olson, *Science* **2005**, *308*, 369; b) S. J. Scales, M. F. A. Finley, R. H. Scheller, *Science* **2001**, *294*, 1015.

[19] a) B. R. Lentz, *Chem. Phys. Lipids* **1994**, *73*, 91; b) S. W. Hui, T. L. Kuhl, Y. Q. Guo, J. Israelachvili, *Colloids Surf. B* **1999**, *14*, 213.

[20] A. M. Derfus, W. C. W. Chan, S. N. Bhatia, *Nano Lett.* **2004**, *4*, 11.

[21] a) P. Rigler, W. Meier, *J. Am. Chem. Soc.* **2006**, *128*, 367; b) D. E. Discher, A. Eisenberg, *Science* **2002**, *297*, 967.

[22] a) S. Lecommandoux, O. Sandre, F. Chécot, J. R. Hernandez, R. Perzynski, *Adv. Mater.* **2005**, *17*, 712; b) H. Duan, D. Wang, D. G. Kurth, H. Möhwald, *Angew. Chem.* **2004**, *116*, 5757; *Angew. Chem. Int. Ed.* **2004**, *43*, 5639; c) J. Park, K. An, Y. Hwang, J. G. Park, H. J. Noh, J. Y. Kim, J. H. Park, N. M. Hwang, T. Hyeon, *Nat. Mater.* **2004**, *3*, 891; d) A. Ito, M. Shinkai, H. Honda, T. Kobayashi, *J. Biosci. Bioeng.* **2005**, *100*, 1.

[23] a) C. Burda, X. Chen, R. Narayanan, M. A. El-Sayed, *Chem. Rev.* **2005**, *105*, 1025; b) P. Gangopadhyay, S. Gallet, E. Franz, A. Persoons, T. Verbiest, *IEEE Trans. Magn.* **2005**, *41*, 4194.

[24] M. Karlsson, M. Davidson, R. Karlsson, A. Karlsson, J. Bergenholtz, Z. Konkoli, A. Jesorka, T. Lobovkina, J. Hurtig, M. Voinova, O. Orwar, *Annu. Rev. Phys. Chem.* **2004**, *55*, 613.

[25] K. C. Crowder, M. S. Hughes, J. N. Marsh, A. M. Barbieri, R. W. Fuhrhop, G. M. Lanza, S. A. Wickline, *Ultrasound Med. Biol.* **2005**, *31*, 1693.

[26] a) T. M. Allen, P. R. Cullis, *Science* **2004**, *303*, 1818; b) P. Broz, S. M. Benito, C. Saw, P. Burger, H. Heider, M. Pfisterer, S. Marsch, W. Meier, P. J. Hunziker, *J. Controlled Release* **2005**, *102*, 475.

[27] a) G. J. Strijkens, W. J. M. Mulder, R. B. van Heeswijk, P. M. Frederik, P. Bomas, P. C. M. M. Magusin, K. Nicolay, *Magn. Reson. Mater. Phys. Biol. Med.* **2005**, *18*, 186; b) M. S. Martina, J. P. Forlin, C. Menager, O. Clement, G. Barratt, C. Grabielle-Madelmont, F. Gazeau, V. Cabuil, S. Lesieur, *J. Am. Chem. Soc.* **2005**, *127*, 10676.

 © 2006 Wiley-VCH Verlag GmbH & Co. KGaA, Weinheim

Helical Structures

DOI: 10.1002/anie.200600698

Interstrand Interactions between Side Chains in a Double-Helical Foldamer**

*Debasish Haldar, Hua Jiang, Jean-Michel Léger, and Ivan Huc**

Not so long ago the propensity of a polymeric or oligomeric molecular strand to fold into a well-defined conformation in solution was believed to be mainly a property of biopolymers such as proteins and nucleic acids. Recent studies on foldamers[1]—artificial oligomers that also adopt well-defined folded conformations—have led to a fundamental paradigm shift, and biopolymers are now considered to be one of many classes of molecules that fold. Up to now, studies on foldamers have focused on the prime sources of folding, which are main-chain (backbone) conformational preferences and main-chain/main-chain interactions.[1] In peptides and proteins, side-chain/side-chain interactions within and between helices and β sheets are also key to the stabilization of the folded structures,[2] yet their role in the foldamer structure is largely unexplored. Hydrogen bonding between side chains has been incorporated to stabilize some artificial helices.[3] In aromatic structures, interactions between chiral side chains determine helix handedness[4] (unlike in peptides where handedness is induced by side-chain/main-chain interactions), but their nature is not well defined. Even in β peptides—arguably the most studied foldamer family—the helix propensity of side chains has been studied,[5] but examples of direct side-chain/side-chain interactions are rare.[6]

Here, we describe an original example of attractive interactions between side chains in a synthetic foldamer structure. Specifically, we show that interstrand interactions between aromatic side chains can considerably stabilize the double-helical dimers formed by aromatic oligoamides (AOAs) of 2,6-pyridinedicarboxylic acid and 2,6-diaminopyridine. Like many other AOAs,[7] these oligomers adopt very stable single-helical conformations in solution.[8,9] However, the pyridine-derived helices also possess the remarkable

[*] Dr. D. Haldar, Dr. H. Jiang, Dr. I. Huc
Institut Européen de Chimie et Biologie
2 rue Robert Escarpit, 33607 Pessac (France)
Fax: (+33) 540-002-215
E-mail: i.huc@iecb.u-bordeaux.fr
Prof. J.-M. Léger
Laboratoire de Pharmacochimie
146 rue Léo Saignat, 33076 Bordeaux (France)

[**] This work was supported by the Conseil Régional d'Aquitaine, the Centre National de la Recherche Scientifique, the Universities of Bordeaux 1 and Victor Segalen Bordeaux 2, and the Ministère de la Recherche (postdoctoral fellowship to D.H.). We are also grateful to Ms. Bathany and Ms. Grélard for assistance with MS and NMR measurements.

Supporting information for this article is available on the WWW under http://www.angewandte.org or from the author.

 © 2006 Wiley-VCH Verlag GmbH & Co. KGaA, Weinheim

ability to extend like springs and intertwine to form double-helical dimers held by direct noncovalent interactions between the strands (Figure 1).[8,10,11] This is a very rare[12] example of a hybridization motif between two organic strands to form a double helix that is neither derived from naturally occurring multiple helices such as DNA, collagen, or gramicidin A, nor assisted by metal-ion coordination.[13]

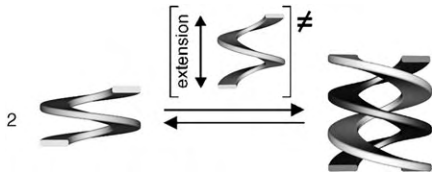
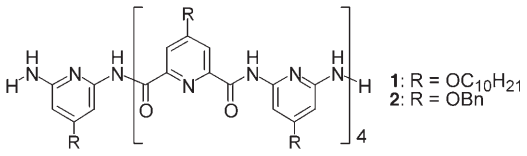


Figure 1. Equilibrium between the single-helical and double-helical structures.

The peculiar hybridization of pyridine carboxamide oligomers to form double helices has been characterized in solution in chlorinated solvents and in the solid state[8,10] and by a computational approach.[11] From these studies, it can be concluded qualitatively that hybridization is driven by intermolecular aromatic stacking, which compensates for the energy cost of extending and doubling the helical pitch of the single-helical monomers. However, numerous aspects of this phenomenon remain unclear. For example, very early on we observed that the presence of 4-decyloxy groups on all pyridine rings leads to a dramatic enhancement of the dimerization constant (K_{dim}). In $CDCl_3$, a heptameric strand comprising three 2,6-pyridinedicarbonyl units and four 2,6-diaminopyridine units shows $K_{dim} = 30\ L\,mol^{-1}$ when it has 4-decyloxy chains on the three 2,6-pyridinedicarbonyl rings only, and $K_{dim} = 6.5 \times 10^4\ L\,mol^{-1}$—a 2000-fold increase—when it has 4-decyloxy chains on all rings![8,10a]

To explain this effect, we proposed that extensive van der Waals interactions between the multiple long side chains of adjacent strands would stabilize the duplex.[8,10a] However this hypothesis could not be verified because 4-decyloxy-substituted oligomers such as nonamer **1** do not crystallize. No



solid-state data about their single- and double-helical conformations are available to compare with the crystal structures of oligomers bearing no side chains[8,10] which show much lower K_{dim} values. We thus undertook the synthesis and structural study of 4-benzyloxy-substituted oligomers such as nonamer **2**. This endeavor was motivated by three assumptions, which all turned out to be valid: 1) the benzyloxy derivatives were expected to be more crystalline; 2) interactions between aromatic benzyloxy chains were expected to be even stronger than those between aliphatic decyloxy chains; and 3) unlike the decyloxy derivatives, the benzyloxy series was expected to be soluble in polar aprotic solvents in which hybridization of pyridinecarboxamide oligomers had not yet been observed.

Nonamer **1**, which has two terminal amine residues, was prepared by hydrogenolysis of the corresponding bisbenzylcarbamate precursor.[10c] Benzyloxy-substituted oligomers including nonamer **2** were prepared from 4-benzyloxy-2,6-diaminopyridine[14] and 4-benzyloxy-2,6-pyridinedicarboxylic acid following schemes similar to those employed in other series.[10a] The synthesis of these compounds will be reported in a full account about the effects of the side chains on oligomer hybridization.

K_{dim} values can be recorded easily by measuring NMR spectra at different concentrations. The single and double helices are in slow exchange on the NMR time scale and give rise to two sets of signals that can be integrated. The assignment of the signals to the two species can be made unambiguously based on: 1) the variation of their intensity with concentration and temperature; 2) the fact that signals of the double helix are shifted upfield because of the ring-current effects associated with intermolecular aromatic stacking; 3) the lower symmetry of the double helix which gives rise to twice as many signals in $CDCl_3$;[8,10] and 4) diffusion coefficients measured by NMR pulsed-gradient spin-echo experiments (diffusion coefficients are about 35% smaller for the double helix than for the corresponding single helix).

The ^1H NMR spectrum of decyloxy-substituted nonamer **1** in $CDCl_3$ at 1 mM shows that this compound is largely hybridized at this concentration but that signals of the single helix are also clearly visible (Figure 2a). A value of $K_{dim} = 6 \times 10^4\ L\,mol^{-1}$ was calculated. In contrast, the spectrum of benzyloxy-substituted nonamer **2** shows signals of the double helix and no signals of the single helix. Spectra recorded in other weakly polar solvents (CD_2Cl_2, $C_2D_2Cl_4$, [D_8]toluene) did not show any detectable amount of the single helix either, even at a dilution of 0.1 mM. The assignment of the observed signals to a double-helical dimer is supported both by diffusion coefficient measurements and by electrospray ionization mass spectra, in which the monomer is barely detected, the dimer dominates, and no higher aggregate is observed. Thus, the benzyloxy nonamer apparently forms considerably more stable dimers than its decyloxy analogue. In the absence of signals for the single helix, no accurate K_{dim}

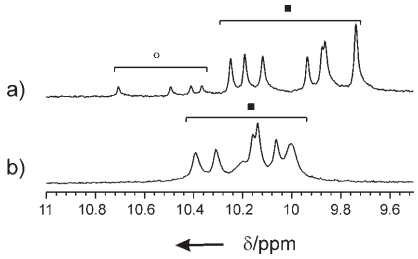


Figure 2. Sections of the ^1H NMR spectra (400 MHz, 25 °C, 1 mM in $CDCl_3$) of a) **1** and b) **2** at showing the amide resonances of the single helix (○) and double helix (■).

 © 2006 Wiley-VCH Verlag GmbH & Co. KGaA, Weinheim

value could be obtained, but it is estimated that K_{dim} is at least 100 times larger for **2** than for **1**. Since these two compounds possess identical main chains, the difference in K_{dim} can be attributed to side-chain effects.

Unlike **1**, the benzyloxy-substituted nonamer **2** is soluble in DMSO and hybridizes in this solvent as well. As shown in Figure 3, its hybridization in DMSO is significant (K_{dim} = 2300 L mol^{-1}) though much weaker than in less polar solvents.

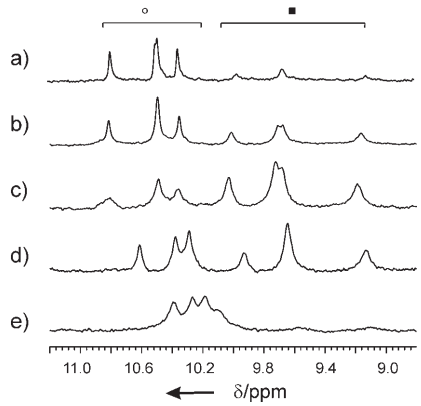


Figure 3. Part of the ^{1}H NMR spectra of nonamer **2** (400 MHz, [D$_6$]DMSO) showing the amide resonances of the single helix (○) and double helix (■): a) 0.12 mM at 25 °C, b) 0.5 mM at 25 °C, c) 4 mM at 25 °C, d) 4 mM at 55 °C, and e) 4 mM at 88 °C.

Thus, the signals of the single helix prevail at low concentration and high temperature. This is the first example of the hybridization of pyridine carboxamide oligomers in this competitive solvent. No hybridization was observed for oligomers having no side chains or with side chains on the pyridinedicarbonyl rings only.[8–10] NMR spectra of **2** recorded in [D$_6$]DMSO at 25 °C, unlike those in CDCl$_3$, show the same number of resonances for the double helix (**2**)$_2$ as for the single helix. This indicates that previously characterized sliding motions within the duplex take place faster in polar solvent and lead to a fast equilibrium between two degenerate duplexes.[8,10]

Clear evidence of interstrand interactions between benzyloxy side chains is found in a crystal structure of nonamer **2**.[15] In view of the very large K_{dim} values of **2** including in the polar solvents (DMSO) that we have often used to grow crystals, we expected the double helix and not the single helix to crystallize. The structure could be solved despite its very large asymmetric unit, which comprise four molecules of **2** entwined in a right-handed and a left-handed double-helical dimer. In fact, the asymmetric unit of **2** appears to be one of the largest all-equal atoms[16] structure solved by ab initio methods.[17]

As shown in Figure 4a,b, the double helix spans two complete helical turns and is one half-turn longer than the longest duplex that we previously described.[8] Since the structure of **2** represents the first X-ray structure of a highly stable duplex with alkoxy substituents on all pyridine rings, we sought for possible structural differences to the structures of oligomers bearing no substituent but could find none. The

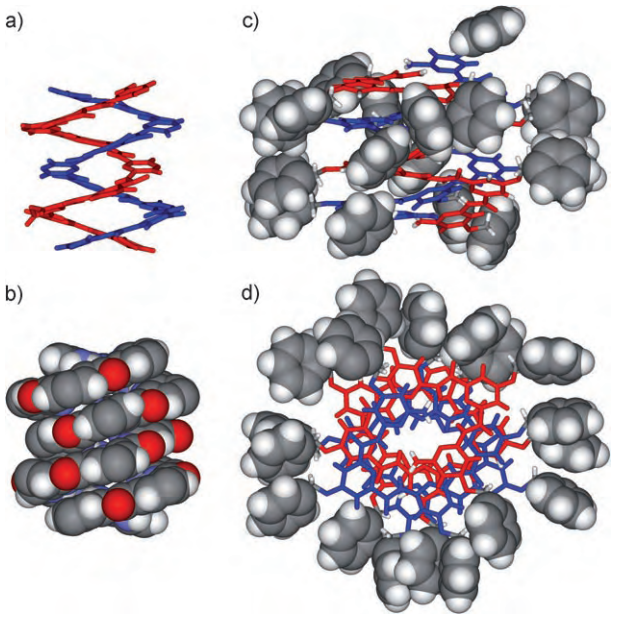


Figure 4. Crystal structure of nonamer **2**. The structures on the left show the double-helical dimer in stick (a) and CPK representations (b). Winding of the two strands produces a three-turn duplex with a pitch of 6.65 Å and with four pyridine–amide units per turn. Benzyloxy groups are omitted for clarity. The stick representation shows that the helical axis of the blue strand is shifted to the right and that of the red strand is shifted to the left. Side view (c) and top view (d) of the dimer showing extensive interstrand aromatic–aromatic interactions between the benzyloxy side chains. The two strands are shown as red and blue sticks and the phenyl rings are represented in CPK. Included solvent molecules are omitted for clarity.

hybridization motif appears in every respect identical to that observed with other oligomers that dimerize more weakly. The two strands are helically shifted by two rings: ring 1 of strand A stacks over ring 3 of strand B and reciprocally. The helix possesses a noncrystallographic C_2 axis along its channel. The helical axes of the two strands are parallel but do not exactly coincide (Figure 4a,b). Contacts between the main chains of the two strands consist essentially of face-to-face aromatic stacking, and of one interstrand bifurcated and presumably weak N–H···N hydrogen bond at one end of the duplex. Some hollows in the helix channel are filled with solvent molecules (H$_2$O, MeOH, or DMSO), but none seems to be engaged in bridging interactions. Other solvent molecules are not involve in direct interactions with the double-helix strands and are simply filling voids in the crystal lattice.

At its periphery, the duplex is surrounded by 18 benzyloxy chains. These are engaged in multiple intraduplex interstrand face-to-face and edge-to-face interactions at various angles (Figure 4c,d). No well-defined motif emerges in the arrangement of these chains and not every benzyl group lies in contact with a benzyl group of the same duplex. In fact, the side chains are also interdigitated (and involved in interduplex interactions) with neighboring molecules. The structure of (**2**)$_2$ may be considered to be a snapshot of one of the many possible conformations of the side chains. Considering the flexibility of the benzyl groups and the mobility of the two

 © 2006 Wiley-VCH Verlag GmbH & Co. KGaA, Weinheim

strands relative to each other in the duplex, numerous side-chain/side-chain interactions are expected in solution and are presumably responsible for the observed stability of $(\mathbf{2})_2$. The strong effect of aryl–aryl interactions between benzyl side chains in $(\mathbf{2})_2$ contrasts with the reported absence of favorable aromatic interactions between β-sheet peptides.[18]

In summary, solution and solid-state data both suggest that interstrand interactions between phenyl rings in the side chains contribute to the very large hybridization constant of **2**. Similar, weaker, interactions between the decyloxy chains of **1** can also be envisaged, but they remain to be demonstrated. The remarkable increase in the dimerization constant as a result of aromatic interactions between side chains opens a new space for designing oligomers with complementary electron-donor and electron-acceptor groups and/or with positive and negative charges leading to cross-hybridization and sequence-selective recognition. More generally, the effects reported here may foster new studies of the role that side chains play in stabilizing foldamer structures.

Received: February 22, 2006
Revised: May 4, 2006
Published online: July 19, 2006

Keywords: helical structures · molecular recognition · supramolecular chemistry

[1] For reviews see: D. J. Hill, M. J. Mio, R. B. Prince, T. S. Hughes, J. S. Moore, *Chem. Rev.* **2001**, *101*, 3893; R. P. Cheng, S. H. Gellman, W. F. DeGrado, *Chem. Rev.* **2001**, *101*, 3219; I. Huc, *Eur. J. Org. Chem.* **2004**, 17; R. P. Cheng, *Curr. Opin. Struct. Biol.* **2004**, *14*, 512; G. Licini, L. J. Prins, P. Scrimin, *Eur. J. Org. Chem.* **2005**, 969; D. Seebach, A. K. Beck, D. J. Bierbaum, *Chem. Biodiversity* **2004**, *1*, 1111.

[2] For example: F. A. Syud, H. E. Stranger, S. H. Gellman, *J. Am. Chem. Soc.* **2001**, *123*, 8667; S. T. Phillips, G. Piersanti, P. A. Bartlett, *Proc. Natl. Acad. Sci. USA* **2005**, *102*, 13737; M. Ramirez-Alvarado, T. Kortemme, F. J. Blanco, L. Serrano, *Bioorg. Med. Chem.* **1999**, *7*, 93.

[3] J. M. Cary, J. S. Moore, *Org. Lett.* **2002**, *4*, 4663; X. Yang, L. Yuan, K. Yamato, A. L. Brown, W. Feng, M. Furukawa, X. C. Zeng, B. Gong, *J. Am. Chem. Soc.* **2004**, *126*, 3148; J. J. L. M. Cornelissen, M. Fischer, N. A. J. M. Sommerdijk, R. J. M. Nolte, *Science* **1998**, *280*, 1427.

[4] R. N. Prince, J. S. Moore, L. Brunsveld, E. W. Meijer, *Chem. Eur. J.* **2001**, *7*, 4150; J. J. van Gorp, J. A. J. Vekemans, E. W. Meijer, *Chem. Commun.* **2004**, 60.

[5] J. A. Kritzer, J. Tirado-Rives, S. A. Hart, J. D. Lear, W. L. Jorgensen, A. Schepartz, *J. Am. Chem. Soc.* **2005**, *127*, 167.

[6] P. Chakraborty, U. Diederichsen, *Chem. Eur. J.* **2005**, *11*, 3208.

[7] Y. Hamuro, S. J. Geib, A. D. Hamilton, *J. Am. Chem. Soc.* **1997**, *119*, 10587; H. Jiang, J.-M. Léger, I. Huc, *J. Am. Chem. Soc.* **2003**, *125*, 3448; V. Maurizot, C. Dolain, Y. Leydet, J.-M. Léger, P. Guionneau, I. Huc, *J. Am. Chem. Soc.* **2004**, *126*, 10049; C. Dolain, J.-M. Léger, N. Delsuc, H. Gornitzka, I. Huc, *Proc. Natl. Acad. Sci. USA* **2005**, *102*, 16146; C. Dolain, H. Jiang, J.-M. Léger, P. Guionneau, I. Huc, *J. Am. Chem. Soc.* **2005**, *127*, 12943; B. Gong, *Chem. Eur. J.* **2001**, *7*, 4337; B. Gong, H. Zeng, J. Zhu, L. Yuan, Y. Han, S. Cheng, M. Furukawa, R. D. Parra, A. Y. Kovalevsky, J. L. Mills, E. Skrzypczak-Jankun, S. Martinovic, R. D. Smith, C. Zheng, T. Szyperski, X. C. Zeng, *Proc. Natl. Acad. Sci. USA* **2002**, *99*, 11583; C. Li, S.-F. Ren, J.-L. Hou, H.-P. Yi, S.-Z. Zhu, X.-K. Jiang; Z.-T. Li, *Angew. Chem.* **2005**, *117*, 5871; *Angew. Chem. Int. Ed.* **2005**, *44*, 5725; Z.-Q. Hu, H.-Y. Hu, C.-F. Chen, *J. Org. Chem.* **2006**, *71*, 1131.

[8] V. Berl, I. Huc, R. Khoury, M. J. Krische, J.-M. Lehn, *Nature* **2000**, *407*, 720.

[9] V. Berl, I. Huc, R. Khoury, J.-M. Lehn, *Chem. Eur. J.* **2001**, *7*, 2798; I. Huc, V. Maurizot, H. Gornitzka, J.-M. Léger, *Chem. Commun.* **2002**, 578; C. Dolain, A. Grélard, M. Laguerre, H. Jiang, V. Maurizot, I. Huc, *Chem. Eur. J.* **2005**, *11*, 6135.

[10] a) V. Berl, I. Huc, R. Khoury, J.-M. Lehn, *Chem. Eur. J.* **2001**, *7*, 2810; b) V. Maurizot, J.-M. Léger, P. Guionneau, I. Huc, *Russ. Chem. Bull.* **2004**, *53*, 1572; c) H. Jiang, V. Maurizot, I. Huc, *Tetrahedron* **2004**, *60*, 10029; d) C. Dolain, C. Zhan, J.-M. Léger, I. Huc, *J. Am. Chem. Soc.* **2005**, *127*, 2400.

[11] A. Acocella, A. Venturini, F. J. Zerbetto, *J. Am. Chem. Soc.* **2004**, *126*, 2362.

[12] See also: Y. Tanaka, H. Katagiri, Y. Furusho, E. Yashima *Angew. Chem.* **2005**, *117*, 3935; *Angew. Chem. Int. Ed.* **2005**, *44*, 3867.

[13] M. Albrecht, *Chem. Rev.* **2001**, *101*, 3457; C. Piguet, G. Bernardinelli, G. Hopfgartner, *Chem. Rev.* **1997**, *97*, 2005.

[14] T. Braxmeier, M. Demarcus, T. Fessmann, S. McAteer, J. D. Kilburn, *Chem. Eur. J.* **2001**, *7*, 1889.

[15] Crystals were obtained by diffusion of MeOH into a DMSO solution. Data were collected on a Rigaku Rapid diffractometer with a MM07 microfocus rotating-anode generator equipped with confocal optics. $(C_{116}H_{93}N_{19}O_{17})_4(C_2H_6SO)_{11}(CH_4O)_7(H_2O)_9$ $M_r = 9346.22$, triclinic, space group $P\bar{1}$, $a = 21.7200(4)$, $b = 24.4279(7)$, $c = 29.4930(6)$ Å, $\alpha = 70.049(6)$, $\beta = 70.624(7)$, $\gamma = 59.770(5)°$, $V = 12459.8(5)$ Å^3, $\lambda = 1.54180$ Å, $T = 163$ K, $Z = 1$, $\rho_{calcd} = 1.246$ Mg m^{-3}, $\mu(Cu_{K\alpha}) = 1.134$ mm^{-1}. 122432 reflections measured, 44237 unique ($R_{int} = 0.095$), 33118 with $I > 2\sigma(I)$, 3062 parameters in final refinement. The final R indices were R_1 ($I > 2\sigma(I)$) = 0.1983, wR_2 (all data) = 0.5047, residual electron density 0.64 e Å^{-3}. CCDC-299073 contains the supplementary crystallographic data for this paper. These data can be obtained free of charge from The Cambridge Crystallographic Data Centre via www.ccdc.cam.ac.uk/data_request/cif.

[16] The structure also contains sulfur atoms, but these are highly disordered and did not help solving the phase problem.

[17] G. Bunkóczi, L. Vértesy, G. M. Sheldrick, *Angew. Chem.* **2005**, *117*, 1364; *Angew. Chem. Int. Ed.* **2005**, *44*, 1340.

[18] D. M. Chung, Y. Dou, P. Baldi, J. S. Nowick, *J. Am. Chem. Soc.* **2005**, *127*, 9998.

 © 2006 Wiley-VCH Verlag GmbH & Co. KGaA, Weinheim

Porphyrins

DOI: 10.1002/anie.200600747

[1,2,3]Triazolo[4,5-*b*]porphyrins: New Building Blocks for Porphyrinic Materials**

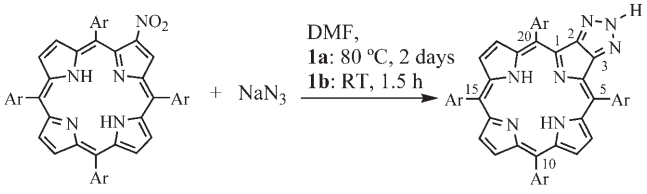
Paula S. S. Lacerda, Ana M. G. Silva, Augusto C. Tomé, Maria G. P. M. S. Neves, Artur M. S. Silva, José A. S. Cavaleiro, and Antonio L. Llamas-Saiz*

Dedicated to Professor Miha Tišler on the occasion of his 80th birthday

There has been a strong interest in recent years in developing multiporphyrin arrays through covalent or noncovalent synthetic methodologies.[1–8] The synthesis of porphyrin-based framework solids is also an active field.[9–12] These multiporphyrinic systems are of interest because of their potential application in a range of areas, such as electronics, materials, catalysis, and medicine.[13–16] In fact, porphyrins are one of the most attractive building blocks for supramolecular systems. They offer a variety of desirable features, such as rigid planar geometry, high stability, intense electronic absorption and emission, a small HOMO–LUMO energy gap, and the ability to tune their optical and redox properties by changing the metal center.[6] During the past decade, various synthetic strategies have been developed to make multiporphyrin oligomers with linear, cyclic, and cross-linked geometries. An elegant and versatile method developed by Osuka and Shimidzu consists of a Ag^{I}-promoted coupling reaction of *meso*-unsubstituted porphyrins.[17] This method allows the preparation of porphyrin arrays in which the constituent porphyrins are connected directly at their *meso* positions without any extra linking atoms. By using this method, Osuka's group prepared a wide range of covalently linked porphyrin arrays,[5] including *meso-meso*-linked linear porphyrin arrays,[18] two-dimensional windmill arrays,[19] three-dimensional gridlike arrays,[20] strapped *meso-meso*-linked diporphyrins,[21] and cyclic arrays.[8,22] Further oxidation of the *meso-meso*-linked porphyrin arrays under strong conditions (DDQ and $Sc(OTf)_3$) provides porphyrin tapes[23,24] and sheets (DDQ = 2,3-dichloro-5,6-dicyano-1,4-benzoquinone, OTf = trifluoromethanesulfonate).[25] These fully conjugated porphyrin systems have planar structures and display drastically red-shifted absorption spectra that reach into the far-IR region, which reflects the extensive π conjugation over the molecules. Other very interesting linear,[26–29] dendritic,[30] and cyclic[31,32] multiporphyrin systems, as well as organometallic porphyrin arrays[33] have been published in recent years. All of these well-defined multiporphyrin arrangements are interesting for application such as molecular photonic and electronic wires. In particular, the cyclic porphyrin arrays are excellent light-harvesting antenna systems that mimic those found in the photosynthetic system.[8,31]

Herein we report the synthesis of the novel heterocyclic system [1,2,3]triazolo[4,5-*b*]porphyrin and its use in the preparation of porphyrinic dimers and pentamers. The 1,2,3-triazoles are an important type of heterocyclic compounds and are being studied by many research groups because of their theoretical interest and synthetic usefulness. They also find numerous applications in industry, in medicine, and as agrochemicals.[34,35] 1,2,3-Triazoles can be synthesized by many approaches;[36] one method involves the reaction of sodium azide with alkenes bearing strongly electron-withdrawing substituents to afford N-unsubstituted 1*H*-1,2,3-triazoles in good yields. We have considered a synthetic route involving the reaction of β-nitro-*meso*-tetraarylporphyrins with sodium azide; in these reactions the porphyrins should behave as nitroalkenes and the formation of triazoloporphyrins was anticipated. Indeed, the [1,2,3]triazolo[4,5-*b*]porphyrins **2** were obtained in moderate to good yields from the reaction of nitroporphyrins **1** with NaN_3. The alkylation and arylation of the triazole moiety allowed easy access to new porphyrinic materials with potentially interesting applications.

[1,2,3]Triazolo[4,5-*b*]porphyrins **2a,b**[37] were prepared by treating β-nitro-*meso*-tetraarylporphyrins **1a,b** with sodium azide in *N*,*N*-dimethylformamide (DMF, Scheme 1). The reaction with porphyrin **1b** occurs at room temperature, and after 1.5 h product **2b** was isolated in 80% yield; the reaction with the less reactive porphyrin **1a** requires stirring at 80 °C for two days to afford **2a** in 30% yield.



1a, Ar = C_6H_5
1b, Ar = C_6F_5

2a, Ar = C_6H_5, 30%
2b, Ar = C_6F_5, 80%

Scheme 1. Synthesis of triazoloporphyrins.

[*] P. S. S. Lacerda, Dr. A. M. G. Silva, Prof. Dr. A. C. Tomé, Prof. Dr. M. G. P. M. S. Neves, Prof. Dr. A. M. S. Silva, Prof. Dr. J. A. S. Cavaleiro
Departamento de Química
Universidade de Aveiro
3810–193 Aveiro (Portugal)
Fax: (+351) 234-370-084
E-mail: jcavaleiro@dq.ua.pt
Prof. Dr. A. L. Llamas-Saiz
Unidad de Rayos X
Laboratorio Integral de Dinámica y Estructura de Biomoléculas José R. Carracido
Edificio CACTUS
Campus Sur
Universidad de Santiago de Compostela
15782 Santiago de Compostela (Spain)

[**] Thanks are due to the University of Aveiro, Fundação para a Ciência e a Tecnologia and FEDER for funding the Organic Chemistry Research Unit. P. S. S. Lacerda and A. M. G. Silva also thank FCT for their doctoral and postdoctoral grants, respectively.

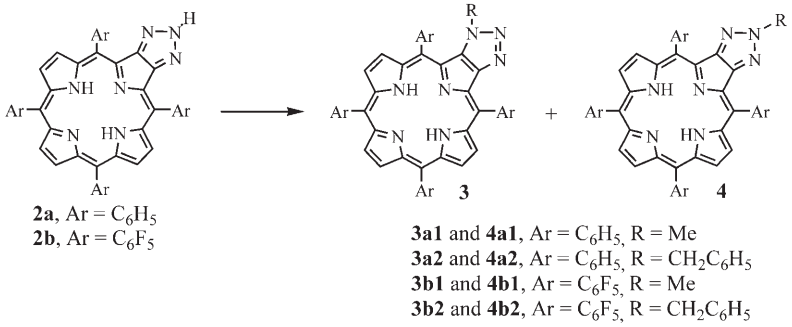
Supporting information (full characterization data of synthesized products) for this article is available on the WWW under http://www.angewandte.org or from the author.

 © 2006 Wiley-VCH Verlag GmbH & Co. KGaA, Weinheim

The structure of compounds **2a,b** was unambiguously established by spectroscopic data from mass spectrometry, as well as UV/Vis and NMR spectroscopy (^{1}H, ^{13}C, ^{19}F, and 2D HSQC and HMBC). The NMR spectra showed the compounds to be C_2-symmetric and the UV/Vis spectra were typical for etio-type porphyrins.[38] The main feature of their ^{1}H NMR spectra is a singlet at low field attributable to the resonance of the triazole NH proton ($\delta = 11.32$ ppm for **2a** and $\delta = 12.38$ ppm for **2b**).

The synthesis of the closely related [1,2,3]triazolo[4,5-*b*]phthalocyanine system was reported recently. However, a completely different synthetic approach was used: 5,6-dicyano-1*H*-benzotriazole was prepared first, and then it was used to synthesize tetra-[39] and monotriazolophthalocyanines.[40] 1*N*-Amination of the latter compound and oxidation of the resulting amino derivative resulted in the generation of a dehydrophthalocyanine, which could be trapped in situ with several dienes to afford the corresponding Diels–Alder adducts.[41]

The N-alkylation and N-arylation of triazoloporphyrins **2** are convenient routes to other porphyrinic derivatives. For example, their methylation and benzylation afford mixtures of the isomeric products **3** and **4** (Scheme 2). The ratio of the two isomers in each reaction can be controlled by the choice of solvent used (Table 1). As an example, N-methylation of **2a** with dimethyl sulfate in boiling acetone favors the formation of the 2-methyl isomer, whereas the main product in toluene is the 1-methyl isomer. A similar effect is observed with porphyrin **2b**.



Scheme 2. N-Methylation and N-benzylation of triazoloporphyrins.

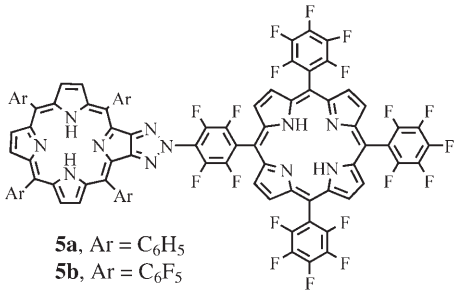
The ^{1}H NMR spectra of compounds **4a1** and **4b1** are similar to those of the corresponding N-unsubstituted precursors, except for the presence of a singlet ascribed to the *N*-methyl group and the absence of the singlet at low field assigned to the NH proton. The ^{1}H NMR spectra of the 1-methyl derivatives **3a1** and **3b1** show clearly that these compounds are not symmetrical. A NOESY spectrum of **3a1** shows space proximity between the methyl group and a phenyl group, thus confirming substitution at triazole N-1. In the ^{1}H NMR spectrum of **3b1** the two protons of the porphyrin nucleus appear as two singlets at $\delta = -3.11$ and -3.06 ppm,which indicates that the macrocycle tautomers are not degenerated.

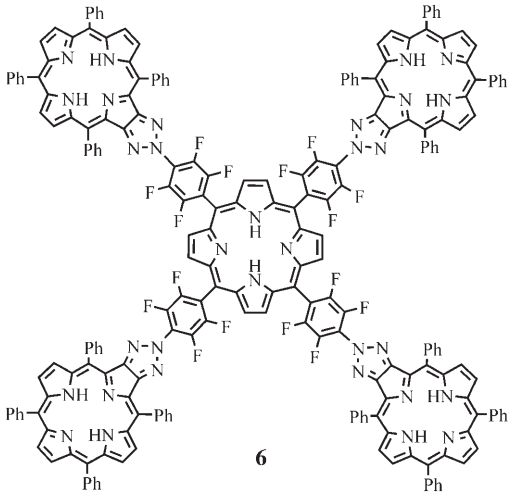
Table 1: Yields of products obtained by N-methylation of **2a** and **2b** in various solvents.

	N-Methylation of **2a**		N-Methylation of **2b**	
Solvent	**3a1**	**4a1**	**3b1**	**4b1**
acetone	34%	59%	10%	80%
toluene	62%	15%	40%	55%

Benzylation of porphyrin **2a** with benzyl bromide in DMF afforded compounds **3a2** (13% yield) and **4a2** (72% yield), along with some precursor **2a** (13%). Under similar conditions, benzylation of **2b** was highly selective; the 2-benzyl isomer was obtained in 90% yield and only a trace amount of the 1-benzyl isomer was present.

The N-arylation of triazoloporphyrins **2** was carried out using 5,10,15,20-tetrakis(pentafluorophenyl)porphyrin (TPFPP) as arylating agent. The reaction of triazoloporphyrin **2a** with an excess of TPFPP (2 equivalents) for 4 h at 80°C afforded dyad **5a** in 57% yield and other minor compounds whose mass and ^{19}F NMR spectra are consistent with further fluorine substitution (triads and tetrads). The formation of dyad **5b** required careful control of the reaction temperature: it was obtained in 30% yield after stirring for 3 days at 60°C, with 35% of the triazoloporphyrin **2b** being recovered. When longer reaction times or higher temperatures were used, the amount of side products increased significantly. When TPFPP was treated with a large excess of triazoloporphyrin **2a** (5 equivalents), the pentamer **6** was obtained in 40% yield as the main product. The reaction occurred smoothly for a period of 22 h and led to the substitution of the four *para*-fluorine atoms of TPFPP by the triazoloporphyrin. Such aromatic nucleophilic substitu-





 © 2006 Wiley-VCH Verlag GmbH & Co. KGaA, Weinheim

tion of the *para*-fluorine on one or more phenyl rings of TPFPP by amines and other nucleophiles is a well-known reaction;[42,43] it has recently been used to prepare galactose–[44] and PEG–porphyrin[45] conjugates (PEG = poly(ethylene glycol)).

The mass, ^{1}H, ^{13}C, and ^{19}F NMR spectra of pentamer **6** are consistent with the proposed structure. The UV/Vis spectrum of **6** shows an etio-type pattern similar to that of the triazoloporphyrin **2a**, but with a bathochromic shift (10 nm) of the Soret band. The electrospray ionization mass spectrum does not show the expected $[M+H]^+$ ion, but rather the peaks corresponding to the multiply charged ions $[M+2H]^{2+}$, $[M+3H]^{3+}$, and $[M+4H]^{4+}$, which result from multiple protonation of the molecule. Deconvolution of the ESIMS spectrum reveals an ion with m/z 3516.190, which corresponds to the monoisotopic mass (3516.035) of the $[M+H]^+$ ion. The simplicity of the NMR spectra of **6** is consistent with the high symmetry of the molecule. The main features of the ^{1}H NMR spectrum are a singlet at $\delta = -2.69$ ppm, assigned to all the NH protons of the five porphyrin nuclei, a singlet at $\delta =$ 8.79 ppm, assigned to the eight β-pyrrolic protons of the antipodal pyrrole rings of the four TPP moieties, a broad singlet at $\delta = 9.02$ ppm, assigned to the sixteen β-pyrrolic protons in the adjacent pyrroles of the four TPP moieties, and a singlet at $\delta = 9.29$ ppm, assigned to the eight β-pyrrolic protons of the TPFPP moiety. The ^{19}F NMR spectrum shows only two double doublets assigned to the *ortho*- and *meta*-fluorine atoms.

Single crystals of **6** were obtained by recrystallization from a mixture of chloroform and methanol. The crystal and molecular structures of **6** were determined by X-ray crystallographic analysis. The crystal is triclinic with space group $P\bar{1}$ and $Z = 2$ (see Experimental Section). The molecules are located around crystallographic inversion centers, and therefore there are two half molecules in the asymmetric unit of the crystal cell. Figure 1 shows an overlay representation of the two molecules with the central porphyrin rings used as a reference. All the peripheral porphyrin moieties in both molecules display the same tautomeric form; however, the positions of the NH protons in the central porphyrin rings are switched. The inner hydrogen atoms could not be found in the difference Fourier synthesis map; nevertheless, their positions were determined unambiguously by considering the significant differences among the bond angles of the nitrogen atoms (110.0(4), 105.6(4), 109.3(4), and 107.0(4)° for N1, N101, N201, and N301, respectively). The situation is the same for the hydrogen atoms defining the tautomeric form of the triazoloporphyrin rings (see Supporting Information for values of the bond angles at the nitrogen atoms). All triazoloporphyrin moieties display the same tautomeric form (Figure 1), which is expected because of the fused triazole ring.

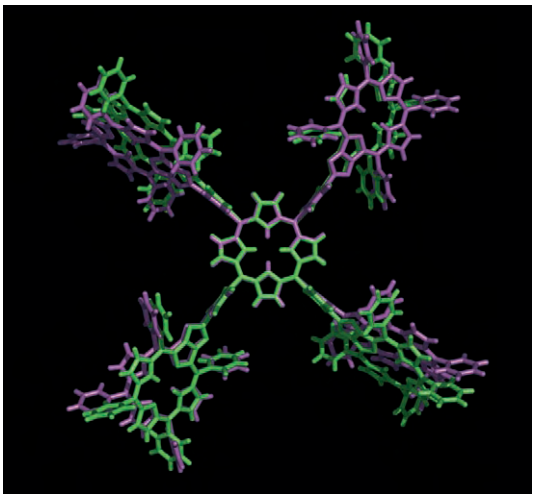


Figure 1. Overlay of the two crystallographically independent molecules of **6** showing the conformational similarities and the different locations of the inner hydrogen atoms in the central porphyrin ring. The same tautomeric form is shown for all triazoloporphyrin substituents. The symmetry-related atoms are included to show the complete molecules.

In conclusion, we have shown that triazoloporphyrins, which can be easily prepared from β-nitroporphyrins, are valuable building blocks for the preparation of novel porphyrinic materials. Currently, we are extending these studies to the synthesis of di(triazolo)porphyrins and their use in the construction of molecular rods.

Experimental Section

5,10,15,20-Tetraphenyl[1,2,3]triazolo[4,5-*b*]porphyrin (**2a**)**:** A solution of **1a** (100.0 mg, 151 μmol) and sodium azide (29.6 mg, 455 μmol, 3 equiv) in DMF (20 mL), under a nitrogen atmosphere, was stirred for 2 days at 80 °C. After cooling to room temperature, the product was precipitated with an aqueous solution of citric acid, filtered, and washed with water. The solid was dissolved in dichloromethane and then washed with water. The organic phase was dried (Na_2SO_4) and then concentrated. The residue was purified by column chromatography (silica gel) using dichloromethane as eluent. Compound **2a** (a pink fraction) was then crystallized from dichloromethane/methanol (30.0 mg, 30 % yield).

5,10,15,20-Tetrakis(pentafluorophenyl)[1,2,3]triazolo[4,5-*b*]porphyrin (**2b**): A solution of **1b** (50 mg, 49 μmol) and sodium azide (3.2 mg, 49 μmol, 1 equiv) in DMF (10 mL), under a nitrogen atmosphere, was stirred at room temperature for 1.5 h. Workup was as described above. The residue was purified by column chromatography (silica gel) using a mixture of dichloromethane/light petroleum (7:3). Compound **2b** was crystallized from dichloromethane/methanol (80 mg, 80 % yield).

Methylation of **2a**: *Reaction in toluene:* To a solution of **2a** (15.9 mg, 24 μmol) and potassium carbonate (10.0 mg, 72 μmol, 3 equiv) in dry toluene (3 mL) was added an excess of dimethyl sulfate (1 drop). This mixture was stirred under a nitrogen atmosphere at 80 °C overnight. After cooling to room temperature, the reaction mixture was evaporated to dryness, and the residue was recovered in dichloromethane, washed with water, and dried (Na_2SO_4), and then the solvent was evaporated. The obtained residue was purified by silica gel column chromatography using a mixture of dichloromethane/light petroleum (1:1) to give two pink fractions. The first fraction was **4a1** (2.5 mg, 15 % yield) and the second was **3a1** (10.0 mg, 62 % yield).

Reaction in acetone: The experimental procedure was similar to that described above, but using acetone as solvent at reflux temperature. The reaction of **2a** (15.0 mg, 23 μmol) gave compound **4a1** in 59 % yield (8.6 mg) and **3a1** in 34 % yield (4.9 mg).

Methylation of **2b**: *Reaction in toluene:* To a solution of **2b** (17.3 mg, 17 μmol) and sodium carbonate (5.4 mg, 51 μmol, 3 equiv) in dry toluene (3 mL) was added an excess of dimethyl sulfate (1 drop). This mixture was stirred for 2 h under a nitrogen atmosphere

 © 2006 Wiley-VCH Verlag GmbH & Co. KGaA, Weinheim

at room temperature. The reaction mixture was then evaporated to dryness, and the residue was recovered in dichloromethane, washed with water, and dried (Na_2SO_4), and finally the solvent was evaporated. The obtained residue was purified by silica gel column chromatography using a mixture of dichloromethane/light petroleum (3:7) to give two brown fractions. The first fraction was **4b1** (9.4 mg, 54% yield) and the second was **3b1** (6.9 mg, 40% yield).

Reaction in acetone: To a solution of **2b** (18.3 mg, 18 μmol) and sodium carbonate (5.7 mg, 54 μmol, 3 equiv) in acetone (5 mL) was added an excess of dimethyl sulfate (1 drop). This mixture was stirred for 2.5 h under a nitrogen atmosphere at room temperature. Workup was the same as described above. Compound **4b1** was obtained in 79% yield (8.6 mg) and **3b1** in 10% yield (2.0 mg).

Benzylation of **2a**: To a solution of **2a** (11.5 mg, 18 μmol) and sodium carbonate (3.7 mg, 35 μmol, 2 equiv) in DMF (2 mL) was added an excess of benzyl bromide (1 drop). This mixture was stirred under a nitrogen atmosphere at room temperature for 2 h. Workup was the same as described above for procedures with DMF. The residue was purified by silica gel column chromatography. Elution with a mixture of dichloromethane/light petroleum (6:4) afforded **4a2** (10.7 mg, 82% yield) followed by **3a2** (1.9 mg, 15% yield).

Benzylation of **2b**: To a solution of **2b** (24.2 mg, 24 μmol) and sodium carbonate (5.0 mg, 48 μmol, 2 equiv) in DMF (2 mL) was added an excess of benzyl bromide (1 drop). This mixture was stirred under a nitrogen atmosphere at room temperature for 2 h. Workup was the same as described above for procedures with DMF. The residue was purified by silica gel column chromatography. Elution with a mixture of dichloromethane/light petroleum (2:8) afforded **4b2** (23.6 mg, 90% yield) followed by a trace amount of **3b2**.

Dyad **5a**: A solution of **2a** (14.9 mg, 23 μmol), TPFPP (44.3 mg, 45 μmol, 2 equiv), and potassium carbonate (6.3 mg, 45 μmol, 2 equiv) in DMF (3 mL) was stirred under a nitrogen atmosphere at 80°C for 4 h. Workup was the same as described above for procedures with DMF. The residue was purified by column chromatography (silica gel) using a gradient of dichloromethane/light petroleum. The first fraction was the precursor TPFPP (2.7 mg, 6%), followed by **5a** (20.7 mg, 57% yield). Other minor fractions were discharged.

Dyad **5b**: A solution of **2b** (20.0 mg, 20 μmol), TPFPP (38.6 mg, 40 μmol, 2 equiv), and sodium carbonate (4.2 mg, 40 μmol, 2 equiv) in DMF (4 mL) was stirred under a nitrogen atmosphere at 60°C for 3 days. Workup was the same as described above for procedures with DMF. The residue was purified by column chromatography (silica gel) using a gradient of dichloromethane/light petroleum. The first fraction was the precursor TPFPP, then **5b** (11.2 mg, 29% yield), and finally the precursor **2b** (7.0 mg, 35%).

Pentamer **6**: A solution of TPFPP (5.9 mg, 6 μmol), **2a** (20.0 mg, 30 μmol, 5 equiv), and potassium carbonate (4.2 mg, 30 μmol, 5 equiv) in DMF (2 mL) was stirred under a nitrogen atmosphere at 80°C for 20 h. Workup was the same as described above for procedures with DMF. The residue was purified by silica gel column chromatography. Using a gradient of dichloromethane/light petroleum, a pink major fraction was eluted, followed by several other fractions, and precursor triazoloporphyrin **2a** (15%). The major product was identified as **6** (40% yield).

Crystal data for **6**: $C_{220}H_{122}F_{16}N_{32}$; triclinic; space group $P\bar{1}$; $a = 23.003(2)$, $b = 23.446(2)$, $c = 25.998(2)$ Å, $\alpha = 63.8390(10)$, $\beta = 83.8860(10)$, $\gamma = 88.325(2)°$, $V = 12511.0(18)$ Å^3, $Z = 2$; $T = 120.0(1)$ K; $M = 3517.51$; $\mu(Mo_{K\alpha}) = 0.065$ mm^{-1}, crystal dimensions $0.38 \times 0.37 \times 0.07$ mm^3, $1.76 \le 2\theta \le 36.20°$. In total 49763 reflections were measured, of which 17325 were independent ($R_{int} = 0.0653$, Friedel pairs merged) and employed for refinement: 2413 parameters, 5208 restraints, $R1 = \Sigma | F_o - F_c | / \Sigma F_o = 0.0536$ $[I > 2\sigma(I)]$, $wR2 = [\Sigma w(F_o^2 - F_c^2)^2 / \Sigma w F_o^4]^{1/2} = 0.1468$ (all data); min./max. difference electron density $-0.22/0.23$ e Å^{-3}. Intensity data were collected with a Bruker SMART CCD X-ray diffractometer with $Mo_{K\alpha}$ radiation ($\lambda = 0.71073$ Å) and a graphite monochromator by performing four ω-scans (0.2° oscillation) at different φ angle settings (0, 90, 180 and 270°). Raw images were integrated using SAINT+,[46] and the resulting intensities were corrected from absorption effects and scaled using SADABS.[47] Crystal cell constants were calculated by global refinement. The structure was solved by direct methods with SHELXD[48] employing real/reciprocal space recycling and peaklist optimization and refined with no intensity cutoff using the block-matrix least-squares refinement implemented in SHELXL97.[49] For block-matrix refinement, the model was split into three blocks containing approximately the same number of parameters. The crystal packing of **6** left a big cavity located around the crystallographic inversion center at the unit-cell origin that is filled with disordered solvent, probably a mixture of chloroform, methanol, and water. The cavity is connected to symmetry equivalent ones through narrower channels in a three-dimensional fashion. The void volume per unit cell is 5194.2 Å^3 (41.3%). Attempts to model solvent molecules into the solvent electron density did not result in an acceptable model. The contribution of the disordered solvent to the scattering factors was taken into account with PLATON/SQUEEZE.[50] A total of 1560 e$^-$ per unit cell was found, corresponding to approximately 26 chloroform molecules per cavity, that is, 13 molecules per each molecule of compound **6**, or even more molecules if the disordered solvent is a mixture of chloroform, methanol, and water. The crystal data reported earlier in this paper are given without the contribution of the disordered solvent. Throughout the refinement, bond length, bond angle, and planarity restraints were imposed because the best diffracting crystal found diffracts only to 1.15 Å resolution. All non-hydrogen atoms were refined anisotropically with suitable rigid bond and similarity restraints. Hydrogen atoms were included as isotropic using a "riding model" in later stages of the refinement. Molecular diagrams have been generated using Pymol.[51]

CCDC-276180 (**6**) contains the supplementary crystallographic data for this paper. These data can be obtained free of charge from The Cambridge Crystallographic Data Centre via www.ccdc.cam.ac.uk/data_request/cif.

Received: February 27, 2006
Revised: June 9, 2006
Published online: July 18, 2006

Keywords: alkylation · arylation · macrocycles · nitrogen heterocycles · porphyrinoids

[1] J. Wojaczynski, L. Latos-Grazynski, *Coord. Chem. Rev.* **2000**, *204*, 113–171.
[2] A. K. Burrell, D. L. Officer, P. G. Plieger, D. C. W. Reid, *Chem. Rev.* **2001**, *101*, 2751–2796.
[3] N. Aratani, A. Tsuda, A. Osuka, *Synlett* **2001**, 1663–1674.
[4] M.-S. Choi, T. Aida, T. Yamazaki, I. Yamazaki, *Chem. Eur. J.* **2002**, *8*, 2667–2678.
[5] D. Kim, A. Osuka, *Acc. Chem. Res.* **2004**, *37*, 735–745.
[6] N. Aratani, A. Takagi, Y. Yanagawa, T. Matsumoto, T. Kawai, Z. S. Yoon, D. Kim, A. Osuka, *Chem. Eur. J.* **2005**, *11*, 3389–3404.
[7] C. M. Drain, I. Goldberg, I. Sylvain, A. Falber, *Top. Curr. Chem.* **2005**, *245*, 55–88.
[8] T. Hori, N. Aratani, A. Takagi, T. Matsumoto, T. Kawai, M.-C. Yoon, Z. S. Yoon, S. Cho, D. Kim, A. Osuka, *Chem. Eur. J.* **2006**, *12*, 1319–1327.
[9] Y. Diskin-Posner, S. Dahal, I. Goldberg, *Angew. Chem.* **2000**, *112*, 1344–1348; *Angew. Chem. Int. Ed.* **2000**, *39*, 1288–1292.
[10] I. Goldberg, *Chem. Eur. J.* **2000**, *6*, 3863–3870.
[11] I. Goldberg, *Chem. Commun.* **2005**, 1243–1254.
[12] M. Vinodu, I. Goldberg, *CrystEngComm* **2005**, *7*, 133–138.
[13] M. Morisue, S. Yamatsu, N. Haruta, Y. Kobuke, *Chem. Eur. J.* **2005**, *11*, 5563–5574.

 © 2006 Wiley-VCH Verlag GmbH & Co. KGaA, Weinheim

[14] S. A. Chavan, W. Maes, L. E. M. Gevers, J. Wahlen, I. F. J. Vankelecom, P. A. Jacobs, W. Dehaen, D. E. De Vos, *Chem. Eur. J.* **2005**, *11*, 6754 – 6762.
[15] D. Bonifazi, G. Accorsi, N. Armaroli, F. Song, A. Palkar, L. Echegoyen, M. Scholl, P. Seiler, B. Jaun, F. Diederich, *Helv. Chim. Acta* **2005**, *88*, 1839 – 1884.
[16] C. M. Drain, G. Bazzan, T. Milic, M. Vinodu, J. C. Goeltz, *Isr. J. Chem.* **2005**, *45*, 255 – 269.
[17] A. Osuka, H. Shimidzu, *Angew. Chem.* **1997**, *109*, 93 – 95; *Angew. Chem. Int. Ed. Engl.* **1997**, *36*, 135 – 137.
[18] N. Aratani, A. Osuka, D. Kim, Y. H. Kim, D. H. Jeong, *Angew. Chem.* **2000**, *112*, 1517 – 1521; *Angew. Chem. Int. Ed.* **2000**, *39*, 1458 – 1462.
[19] A. Nakano, A. Osuka, I. Yamazaki, T. Yamazaki, Y. Nishimura, *Angew. Chem.* **1998**, *110*, 3172 – 3176; *Angew. Chem. Int. Ed.* **1998**, *37*, 3023 – 3027.
[20] A. Nakano, T. Yamazaki, Y. Nishimura, I. Yamazaki, A. Osuka, *Chem. Eur. J.* **2000**, *6*, 3254 – 3271.
[21] N. Yoshida, D. H. Jeong, H. S. Cho, D. Kim, Y. Matsuzaki, K. Tanaka, A. Osuka, *Chem. Eur. J.* **2003**, *9*, 58 – 75.
[22] X. Peng, N. Aratani, A. Takagi, T. Matsumoto, T. Kawai, I.-W. Hwang, T. K. Ahn, D. Kim, A. Osuka, *J. Am. Chem. Soc.* **2004**, *126*, 4468 – 4469.
[23] a) A. Tsuda, H. Furuta, A. Osuka, *Angew. Chem.* **2000**, *112*, 2649 – 2652; *Angew. Chem. Int. Ed.* **2000**, *39*, 2549 – 2552; b) A. Tsuda, H. Furuta, A. Osuka, *J. Am. Chem. Soc.* **2001**, *123*, 10304 – 10321; c) A. Tsuda, A. Osuka, *Science* **2001**, *293*, 79 – 82; d) H. S. Cho, D. H. Jeong, S. Cho, D. Kim, Y. Matsuzaki, K. Tanaka, A. Tsuda, A. Osuka, *J. Am. Chem. Soc.* **2002**, *124*, 14642 – 14654; e) A. Tsuda, Y. Nakamura, A. Osuka, *Chem. Commun.* **2003**, 1096 – 1097.
[24] a) I. M. Blake, A. Krivokapic, M. Katterle, H. L. Anderson, *Chem. Commun.* **2002**, 1662 – 1263; b) D. Bonifazi, M. Scholl, F. Song, L. Echegoyen, G. Accorsi, N. Armaroli, F. Diederich, *Angew. Chem.* **2003**, *115*, 5116 – 5120; *Angew. Chem. Int. Ed.* **2003**, *42*, 4966 – 4970.
[25] Y. Nakamura, N. Aratani, H. Shinokubo, A. Takagi, T. Kawai, T. Matsumoto, Z. S. Yoon, D. Y. Kim, T. K. Ahn, D. Kim, A. Muranaka, N. Kobayashi, A. Osuka, *J. Am. Chem. Soc.* **2006**, *128*, 4119 – 4127.
[26] P. N. Taylor, H. L. Anderson, *J. Am. Chem. Soc.* **1999**, *121,* 11538 – 11545.
[27] T. E. O. Screen, K. B. Lawton, G. S. Wilson, N. Dolney, R. Ispasoiu, T. Goodson III, S. J. Martin, D. D. C. Bradley, H. L. Anderson, *J. Mater. Chem.* **2001**, *11*, 312 – 320.
[28] A. Ambroise, C. Kirmaier, R. W. Wagner, R. S. Loewe, D. F. Bocian, D. Holten, J. S. Lindsey, *J. Org. Chem.* **2002**, *67*, 3811 – 3826.
[29] P. Thamyongkit, J. S. Lindsey *J. Org. Chem.* **2004**, *69*, 5796 – 5799.
[30] W. Maes, J. Vanderhaeghen, S. Smeets, C. V. Asokan, L. M. Van Renterghem, F. E. Du Prez, M. Smet, W. Dehaen, *J. Org. Chem.* **2006**, *71*, 2987 – 2994.
[31] K. Tomizaki, L. Yu, L. Wei, D. F. Bocian, J. S. Lindsey, *J. Org. Chem.* **2003**, *68*, 8199 – 8207.
[32] F. Hajjaj, Z. S. Yoon, M.-C. Yoon, J. Park, A. Satake, D. Kim, Y. Kobuke, *J. Am. Chem. Soc.* **2006**, *128*, 4612 – 4623.
[33] R. D. Hartnell, D. P. Arnold, *Organometallics* **2004**, *23*, 391 – 399.
[34] M. R. Grimmett in *Comprehensive Organic Chemistry*, *Vol. 4* (Eds.: D. H. R. Barton, W. D. Ollis), Pergamon, Oxford, **1979**, p. 357.
[35] H. Wamhoff in *Comprehensive Heterocyclic Chemistry*, *Vol. 5* (Eds.: A. R. Katritzky, C. W. Rees), Pergamon, Oxford, **1984**, Part 4A, p. 669.
[36] "1,2,3-Triazoles": A. C. Tomé in *Science of Synthesis—Houben-Weyl Methods of Molecular Transformations*, *Vol. 13* (Eds.: R. C. Storr, T. L. Gilchrist), Thieme, Stuttgart, **2004**, Chap. 13.
[37] N-Unsubstituted 1,2,3-triazoles exist in two tautomeric forms (1*H*- and 2*H*-) that are in equilibrium both in solution and in the gas phase. For simplification, compounds **2** are represented as 2*H*-triazoles, independently of the predominant tautomer.
[38] "General features of the structure and chemistry of porphyrin compounds" K. M. Smith in *Porphyrins and Metalloporphyrins* (Ed.: K. M. Smith), Elsevier, Amsterdam, **1975**, p. 21.
[39] A. E. Balakirev, V. E. Maizlish, G. P. Shaposhnikov, *Russ. J. Gen. Chem.* **2002**, *72*, 311 – 314.
[40] S. Vagin, A. Frickenschmidt, B. Kammerer, M. Hanack, *Eur. J. Org. Chem.* **2005**, 3271 – 3278.
[41] S. I. Vagin, A. Frickenschmidt, B. Kammerer, M. Hanack, *Chem. Eur. J.* **2005**, *11*, 6568 – 6573.
[42] K. M. Kadish, C. Araullo-McAdams, B. C. Han, M. M. Franzen, *J. Am. Chem. Soc.* **1990**, *112*, 8364 – 8368.
[43] P. Battioni, O. Brigaud, H. Desvaux, D. Mansuy, T. G. Taylor, *Tetrahedron Lett.* **1991**, *32*, 2893 – 2896.
[44] J. P. C. Tomé, M. G. P. M. S. Neves, A. C. Tomé, J. A. S. Cavaleiro, A. F. Mendonça, I. N. Pegado, R. Duarte, M. L. Valdeira, *Bioorg. Med. Chem.* **2005**, *13*, 3878 – 3888.
[45] J.-L. Zhang, J.-S. Huang, C.-M. Che, *Chem. Eur. J.* **2006**, *12*, 3020 – 3031.
[46] SAINT+. Version 6.45. Bruker AXS Inc., Madison, Wisconsin, USA, **2003**.
[47] G. M. Sheldrick, SADABS, Bruker Nonius area detector scaling and absorption correction, Version **2004**/1.
[48] G. M. Sheldrick, H. A. Hauptman, C. M. Weeks, R. Miller, I. Usón, *International Tables for Crystallography*, *Vol. F* (Eds.: E. Arnold, M. Rossmann), Kluwer Academic Publishers, Dordrecht, **2001**, pp. 333 – 351.
[49] a) G. M. Sheldrick, SHELXL-97, Program for Crystal Structure Refinement, Universitat Gottingen, Gottingen, **1997**; b) G. M. Sheldrick, T. R. Schneider, *Methods Enzymol.* **1997**, *277*, 319 – 343.
[50] a) A. L. Spek, *J. Appl. Crystallogr.* **2003**, *36*, 7 – 13; b) P. van der Sluis, A. L. Spek, *Acta Crystallogr. Sect. A* **1990**, *46*, 194 – 201.
[51] "The PyMOL Molecular Graphics System": W. L. DeLano, DeLano Scientific, San Carlos, CA, USA, **2002**. http://www.pymol.org

 © 2006 Wiley-VCH Verlag GmbH & Co. KGaA, Weinheim

Nano- and Microstructures

DOI: 10.1002/anie.200601918

Ion Exchange as a Way of Controlling the Chemical Compositions of Nano- and Microparticles Made from Infinite Coordination Polymers**

*Moonhyun Oh and Chad A. Mirkin**

Micro- and nanosized particles play important roles in many different areas, including catalysis,[1] optics,[2] biosensing,[3] and data storage.[4] Recent advances in this field have made it possible to control many of the chemical and physical properties of these solid-state materials through control over their size, shape, and composition.[5] One important goal in this area is to be able to deliberately interconvert different particle compositions and structures through chemistry that occurs throughout the particle structure in addition to on its surface.[6] There are two ways to effect such transformations, either through a thermally or photochemically induced shape change[6a] or by chemical means that transform the particle from one chemical composition to another.[6b] Even though the latter approach, in principle, can provide a straightforward, economic, and potentially powerful way to access new classes of micro- and nanoparticle materials, very few such approaches have been developed and those that have been realized are quite limited in scope.[6b]

Typically, chemical transformations in the solid state require a high activation energy for the diffusion of small molecules or ions into the solid. Therefore, the reactions are usually slow and involve high temperature and/or pressure.[7] A beautiful demonstration of an exception to this rule is that CdSe can be converted to Ag_2Se in the context of nanosized particles at room temperature.[6b] In contrast, metal–organic coordination polymers are highly porous materials[8,9] that often allow small molecules to move freely within such structures. For this reason, they are typically used for gas storage[9] and catalysis.[8a] Recently, we, and others, have shown how such structures can be transformed into nano- and microparticle materials through controlled precipitation methods.[10,11] We hypothesized that because of the open framework of such structures, the small molecules and ions that comprise such structures should be highly accessible and, in certain cases, susceptible to ion-exchange reactions. Herein, we report a strategy that allows one to transform such particles into new compositions through selective cation-exchange reactions without significantly affecting the size or morphology of the particle (Scheme 1).

We previously reported a synthetic strategy for the preparation of infinite-coordination-polymer particles that consist of metalloligand (bis-metallo-tridentate Schiff base (BMSB)) building blocks and metal interconnecting nodes.[10] These structures form the basis for the studies described herein, and our starting reagents are Zn–BMSB–Zn (**1**) spherical particles suspended in methanol. The approach utilizes two different types of ions, those that are coordinated to the tridentate pockets of the BMSB ligands and those that link the BMSB ligands through the carboxylate groups to form the polymers. When Zn^{2+} is used as the metal ion, it can be readily displaced from the BMSB tridentate pockets but not from the carboxylate sites with a variety of metal ions.

In a typical reaction, we prepared a mixture of Zn–BMSB–Zn microparticles (**1**; average diameter ≈ 1.6 μm) and $Cu(OAc)_2 \cdot H_2O$ in methanol under ambient conditions. The mixture contained Cu^{2+} ions in a slight excess to ensure the replacement of all the Zn^{2+} ions coordinated to the tridentate Schiff base moieties within the particles. Zn–BMSB building blocks are highly fluorescent as are Zn–BMSB–Zn (**1**) particles; however, the product resulting from cation exchange, Cu–BMSB, is not.[10] Therefore, one can easily monitor the particle transformation by optical microscopy (OM) and fluorescence microscopy (FM, Figure 1 a–d, compare the OM and FM images). Within 5 min, most of the fluorescent Zn–BMSB–Zn (**1**) particles had been transformed into the Cu–BMSB–Zn (**2**) particles, and by 60 min the reaction was completed. This transformation could be followed by fluorescence or with the naked eye, as evidenced by a concomitant color change from orange (Zn–BMSB–Zn) to brown (Cu–BMSB–Zn, Figure 1 e).

Further to these optical-property changes, energy-dispersive X-ray (EDX) spectra, inductively coupled plasma (ICP) analyses, and emission spectra that were measured before and after the cation-exchange reaction were consistent with the formation of the Cu–BMSB–Zn (**2**) product. The emission spectrum of the resulting particles reveals complete disappearance of fluorescence, indicating full exchange of two equivalents of Cu^{2+} for the two Zn^{2+} ions contained within the Zn–BMSB building blocks (Figure 1 f). A separate study of the Zn–BMSB monomer shows that one must remove both Zn ions within the Zn–BMSB to quench the fluorescence from this system. Furthermore, an EDX spectrum of the Cu–BMSB–Zn (**2**) particles measured after the cation exchange shows the expected Cu signal in addition to that of Zn (see the Supporting Information). Finally, ICP-analysis data are consistent with a change in the number of metal ions within the particles from three to one Zn^{2+} ion and from zero to two Cu^{2+} ions per repeating unit.[12]

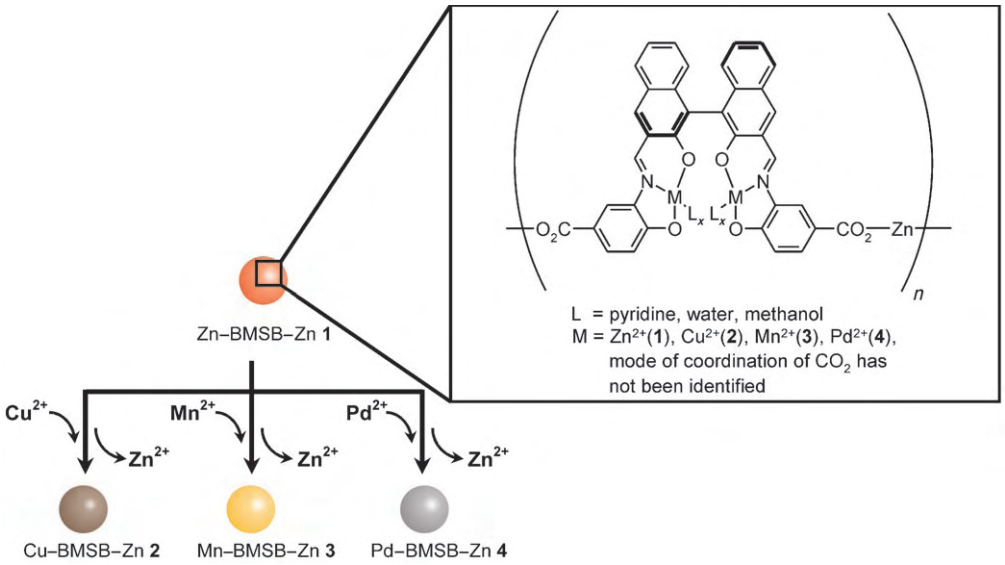
Scanning electron microscopy (SEM) images of initial (Figure 2 a) and cation-exchanged (Figure 2 b) particles show that the size and shape of the particles are preserved after the

[*] Prof. Dr. C. A. Mirkin
Department of Chemistry
and International Institute for Nanotechnology
Northwestern University
2145 Sheridan Road, Evanston, IL, 60208-3113 (USA)
Fax: (+1) 847-467-5123
E-mail: chadnano@northwestern.edu
Prof. Dr. M. Oh
Department of Chemistry
Yonsei University
134 Shinchon-dong, Seodaemun-gu, Seoul 120-749 (Korea)

[**] C.A.M. acknowledges the ONR and NSF-NSEC program for supporting this research.

Supporting information for this article is available on the WWW under http://www.angewandte.org or from the author.

InterScience
© 2006 Wiley-VCH Verlag GmbH & Co. KGaA, Weinheim



Scheme 1. Schematic representation of ion-exchange reactions.

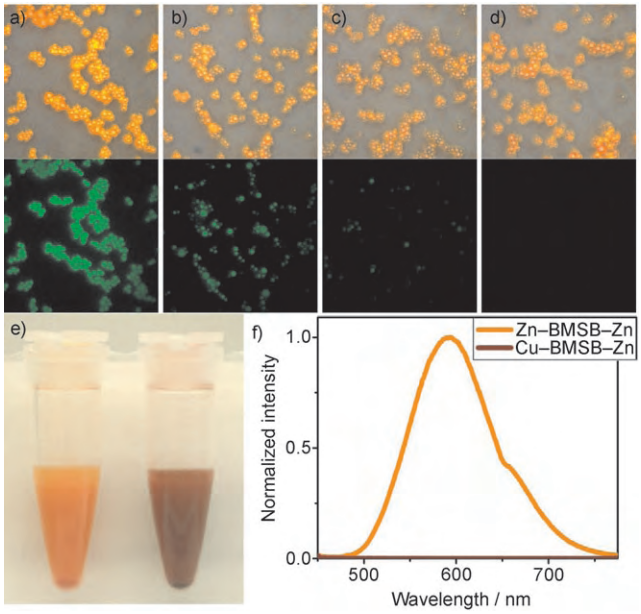


Figure 1. Chemical-transformation reactions from Zn–BMSB–Zn (**1**) to Cu–BMSB–Zn (**2**) microparticles through cation exchange: a–d) time related OM (top) and FM (bottom) images. t = a) 0 min, b) 1 min, c) 5 min, and d) 60 min. e) A photograph showing the color changes (left: **1**, right: **2**) and f) emission spectra obtained by exciting at 420 nm.

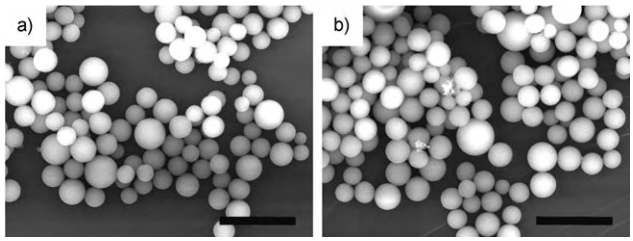


Figure 2. SEM images of spherical microparticles: a) initial Zn–BMSB–Zn (**1**) and b) chemically transformed Cu–BMSB–Zn (**2**). Scale bars = 5 μm.

reaction. From these data, we can conclude that the Cu^{2+} ions only exchange with the Zn^{2+} coordinated to the tridentate Schiff base and not the Zn^{2+} ions that form the interconnecting nodes. When excess Cu^{2+} ions are used in the exchange reaction, the reaction occurs at a faster rate, but results in the same product, Cu–BMSB–Zn (**2**). Under the conditions studied, there is no evidence for the formation of the Cu–BMSB–Cu product, which is a reflection of the difference in binding strength of the two coordination sites.

The cation-exchange reaction rate is size dependent. Indeed, ≈200-nm particles prepared by literature methods[10] undergo a Cu^{2+}-exchange reaction in a few minutes as compared to the hour required to effect it with the micron-scale particles. Again, FM and OM images clearly show the transformation (Figure 3b), with minimal change seen in

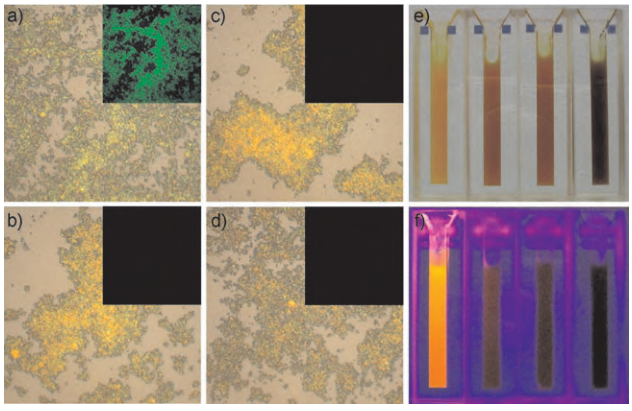


Figure 3. OM and FM (inset) images of spherical nanoparticles: a) initial fluorescent Zn–BMSB–Zn (**1**) and cation-exchanged nonfluorescent products b) Cu–BMSB–Zn (**2**), c) Mn–BMSB–Zn (**3**), and d) Pd–BMSB–Zn (**4**). Digital photographs of a series of nanoparticles (left to right: **1**, **2**, **3**, and **4**): e) without and f) with UV irradiation. The latter shows the starting nanoparticle composition is fluorescent whereas the products are not.

© 2006 Wiley-VCH Verlag GmbH & Co. KGaA, Weinheim

particle size; the average particle sizes measured before (212 nm) and after the cation-exchange reaction (215 nm) by dynamic light scattering (DLS) are nearly identical (see the Supporting Information for size distribution).

We also evaluated the utility of this method for producing additional particle compositions with other metal ions such as Mn^{2+} and Pd^{2+}. We prepared a mixture of Zn–BMSB–Zn (**1**) nanoparticles and $Mn(OAc)_2$ or $Pd(OAc)_2$ in methanol under ambient conditions. In contrast to the process involving Cu^{2+} exchange, excess Mn^{2+} or Pd^{2+} (>20 equiv) must be used to observe significant conversion as measured by fluorescence. The transformations could be followed by fluorescence or with the naked eye (Figure 3). In addition, these nanoparticles, like their Cu^{2+} counterparts, have been characterized by EDX, DLS, and emission spectroscopy (see the Supporting Information).

In conclusion, we have demonstrated that selective cation exchange within the context of nano- and microparticles made from infinite coordination polymers can be used to transform one particle composition into several new ones in a very efficient process. The fast rates of these processes under ambient conditions, which are derived from the porosity of the structures and the labile nature of the Zn-coordination interactions, are unusual (especially when compared to their solid-state counterparts) but extremely useful. These rates provide a way of creating one precursor set of particles that can be deliberately and controllably transformed into a new set of compositions with properties that are derived from the metallated BMSB building blocks.

Received: May 15, 2006
Published online: July 21, 2006

Keywords: chemical transformation · coordination polymers · ion exchange · metalloligands · nanostructures

[1] a) A. T. Bell, *Science* **2003**, *299*, 1688 – 1691; b) S.-W. Kim, M. Kim, W. Y. Lee, T. Hyeon, *J. Am. Chem. Soc.* **2002**, *124*, 7642 – 7643.

[2] a) J. Wang, M. S. Gudiksen, M. X. Duan, Y. Cui, C. M. Lieber, *Science* **2001**, *293*, 1455 – 1457; b) F. Fleischhaker, A. C. Arsenault, V. Kitaev, F. C. Peiris, G. Freymann, I. Manners, R. Zentel, G. A. Ozin, *J. Am. Chem. Soc.* **2005**, *127*, 9318 – 9319.

[3] Y. C. Cao, R. Jin, C. A. Mirkin, *Science* **2002**, *297*, 1536 – 1540.

[4] S. Sun, C. B. Murray, D. Weller, L. Folks, A. Moser, *Science* **2000**, *287*, 1989 – 1992.

[5] a) X. Peng, L. Manna, W. Yang, J. Wickham, E. Scher, A. Kadavanich, A. P. Alivisatos, *Nature* **2000**, *404*, 59 – 61; b) D. Horn, J. Rieger, *Angew. Chem.* **2001**, *113*, 4460 – 4492; *Angew. Chem. Int. Ed.* **2001**, *40*, 4330 – 4361; c) J. Chen, T. Herricks, Y. Xia, *Angew. Chem.* **2005**, *117*, 2645 – 2648; *Angew. Chem. Int. Ed.* **2005**, *44*, 2589 – 2592.

[6] a) R. Jin, Y. Cao, C. M. Mirkin, K. L. Kelly, G. C. Schatz, J. G. Zheng, *Science* **2001**, *294*, 1901 – 1903; b) D. H. Son, S. M. Hughes, Y. Yin, A. P. Alivisatos, *Science* **2004**, *306*, 1009 – 1012.

[7] a) S. Feng, R. Xu, *Acc. Chem. Res.* **2001**, *34*, 239 – 247; b) R. E. Schaak, T. E. Mallouk, *Chem. Mater.* **2002**, *14*, 1455 – 1471.

[8] a) J. S. Seo, D. Whang, H. Lee, S. I. Jun, J. Oh, Y. J. Jeon, K. Kim, *Nature* **2000**, *404*, 982 – 986; b) O. R. Evans, W. Lin, *Acc. Chem. Res.* **2002**, *35*, 511 – 522; c) M. Oh, G. B. Carpenter, D. A. Sweigart, *Acc. Chem. Res.* **2004**, *37*, 1 – 11; d) F. M. Tabellion, S. R. Seidel, A. M. Arif, P. J. Stang, *J. Am. Chem. Soc.* **2001**, *123*, 7740 – 7741; e) B. Moulton, J. Lu, M. J. Zaworotko, *J. Am. Chem. Soc.* **2001**, *123*, 9224 – 9225; f) S.-I. Noro, R. Kitaura, M. Kondo, S. Kitagawa, T. Ishii, H. Matsuzaka, M. Yamashita, *J. Am. Chem. Soc.* **2002**, *124*, 2568 – 2583.

[9] a) O. M. Yaghi, M. O'Keeffe, N. W. Ockwig, H. K. Chae, M. Eddaoudi, J. Kim, *Nature* **2003**, *423*, 705 – 714; b) X. Zhao, B. Xiao, A. J. Fletcher, K. M. Thomas, D. Bradshaw, M. J. Rosseinsky, *Science* **2004**, *306*, 1012 – 1015.

[10] M. Oh, C. A. Mirkin, *Nature* **2005**, *438*, 651 – 654.

[11] X. Sun, S. Dong, E. Wang, *J. Am. Chem. Soc.* **2005**, *127*, 13102 – 13103.

[12] There are inherent difficulties in formulating the exact number of methanol and other guest molecules in the particles. ICP analysis of the starting materials and products from the **1** to **2** conversion ($\approx$210-nm diameter average particle size) shows a decrease in Zn content (from 21.59 to 8.13%) and an increase in Cu content (from 0 to 15.31%) after the cation-exchange reaction.

 © 2006 Wiley-VCH Verlag GmbH & Co. KGaA, Weinheim

Porphyrinoids

DOI: 10.1002/anie.200601493

Conjugated Polymers Complexed with Helical Porphyrin Oligomers Create Micron-Sized Ordered Structures**

Masayuki Takeuchi, Chiaki Fujikoshi, Yohei Kubo, Kenji Kaneko, and Seiji Shinkai**

Recently, oriented polymers and/or polymer nanostructures have attracted a large amount of attention. Of particular interest are structures that consist of conjugated polymers (CPs) because of their potential applications as, for example, electrochemical switches, electric devices, and sensors.[1,2] In

[*] Dr. M. Takeuchi, C. Fujikoshi, Dr. Y. Kubo, Prof. S. Shinkai
Department of Chemistry and Biochemistry
Graduate School of Engineering, Kyushu University
Fukuoka 812-8581 (Japan)
Fax: (+81) 92–802–2823
E-mail: taketcm@mbox.nc.kyushu-u.ac.jp
Prof. K. Kaneko
HVEM Laboratory
Kyushu University
Fukuoka 812-8581 (Japan)

[**] M.T. and C.F. thank Mr. O. Hirata, Mr. S. Tanaka, Mr. M. Shirakawa, Dr. M. Numata, and Dr. N. Fujita for valuable discussions and comments. Y.K. thanks the JSPS Research Fellowship for Young Scientists for financial support. This study was supported partially by a Sumitomo Chemical Award in Synthetic Organic Chemistry (Japan), a Grant-in-Aid for Scientific Research B (17350071), and the 21st Century COE Program (Functional Innovation of Molecular Informatics) of the Ministry of Education, Culture, Science, Sports, and Technology (Japan).

Supporting information for this article is available on the WWW under http://www.angewandte.org or from the author.

WILEY InterScience DISCOVER SOMETHING GREAT
© 2006 Wiley-VCH Verlag GmbH & Co. KGaA, Weinheim

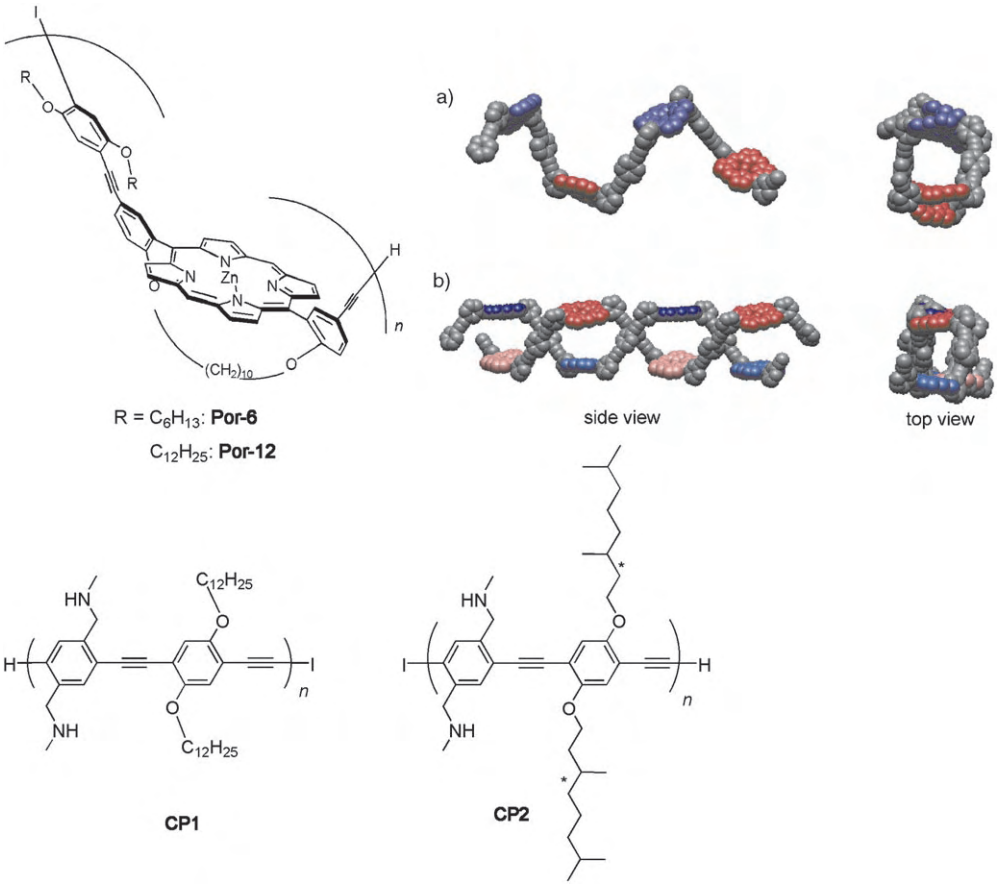
addition to supramolecular assembly schemes,[3–6] a number of approaches, including metastable states enforced by liquid crystalline phases,[7–9] Langmuir monolayers at the air–water interface,[10] incorporation into prealigned host matrixes,[11,12] and rubbing,[13,14] have been utilized to align conjugated polymers, thus leading to some unprecedented and fascinating photophysical functions. From a supramolecular standpoint, we recently proposed a supramolecular bundling approach toward the alignment of CPs. In this approach, aligner molecules, which elicit positive homotropic allosterism, are used to bundle, noncovalently splice, and align CPs to form ordered assemblies of CPs.[15]

Herein, we present a new concept toward the alignment of CPs through the use of twining polymers (twimers) that act as helical "hosts" that would twine around and include within a single conjugated polymer. Furthermore, we wanted these "hosts" to integrate chromogenic groups that could mediate electron or energy transfer to or from the conjugated polymer. Taking these factors into consideration, we designed the oligomeric porphyrins **Por-12** and **Por-6** (Scheme 1). In their energy-minimized states, these oligomers tend to form helical structures in which a coordinative open face of the zinc porphyrin unit (but not a non-coordinative face covered by a decamethylene group[16]) is always turned inwards so that the central metal atom can interact with the included CP. We expected, therefore, that a CP that possesses appropriate ligand groups would become included within this helical strand through coordination with the porphyrinatozinc. We chose to use **CP1** and **CP2**, which bear coordinative amino groups, for the CPs.[15] The R groups in the Por oligomers were introduced to control the spacing between Por/CP composites and to increase their solubility in organic solvents. From studies using various spectroscopic and microscopic techniques, we proposed that the Por oligomers twine around the CP strands and that the resulting composites aggregate into relatively large two-dimensional (2D) structures in the solid state that exhibit well-oriented periodic striping.[17]

We used computational methods (Insight II, Discover) to evaluate whether the porphyrin units in the Por oligomers could be arranged in helical structures. We confirmed that the octamer of the Por series possessed helical turns and a 1D cavity with dimensions of 1.1×1.5 nm, which is adjustable through the oscillation of *meso*-aryl groups (note that Scheme 1a illustrates only the tetramer for the sake of simplicity). Although it is also possible to construct a double strand with a 0.74×1.1 nm 1D cavity, this assembly is quite sterically crowded.

UV/Vis absorption spectra of the complexes formed between the **Por-12** oligomer and **CP1** were measured in $CDCl_3$ at 25 °C.[18] Figure 1a indicates that shifts to longer wavelengths occur for both the Soret (411–420 nm) and Q bands (e.g., 537–550 nm) of **Por-12** with several isosbestic points, thus indicating that the amino groups in **CP1** have coordinated to the Zn^{II} atoms in **Por-12**. A molar ratio plot of A_{550} versus [diamino units in **CP1**]/[porphyrin units in **Por-12**] gives a break point at 1.0 (see the inset of Figure 1a), which suggests that only one of the two amino groups interacts with each porphyrin unit; that is, a single-stranded **Por-12** oligomer could wrap around a single **CP1** chain, probably because the formation of a doubly stranded **Por-12**, in which all of the amino groups interact with porphyrin units (in this case the break point would occur at 0.5), is sterically too crowded (Figure 1c).

When we photoexcited solutions of **Por-12** (0–0.072 mM unit) and **CP1** (0.036 mM unit) in $CDCl_3$



Scheme 1. Chemical structures of the Por oligomers and conjugated polymers used in this study. **CP1**: $M_n = 48\,000$; **CP2**: $M_n = 18\,000$; **Por-12**: $M_n = 12\,000$; **Por-6**: $M_n = 10\,000$ (M_n = number-average molecular mass). Energy-minimized structures of a) single- and b) double-stranded conformations of the Por oligomers. Hydrogen atoms and peripheral alkyl chains have been omitted for clarity.

 © 2006 Wiley-VCH Verlag GmbH & Co. KGaA, Weinheim

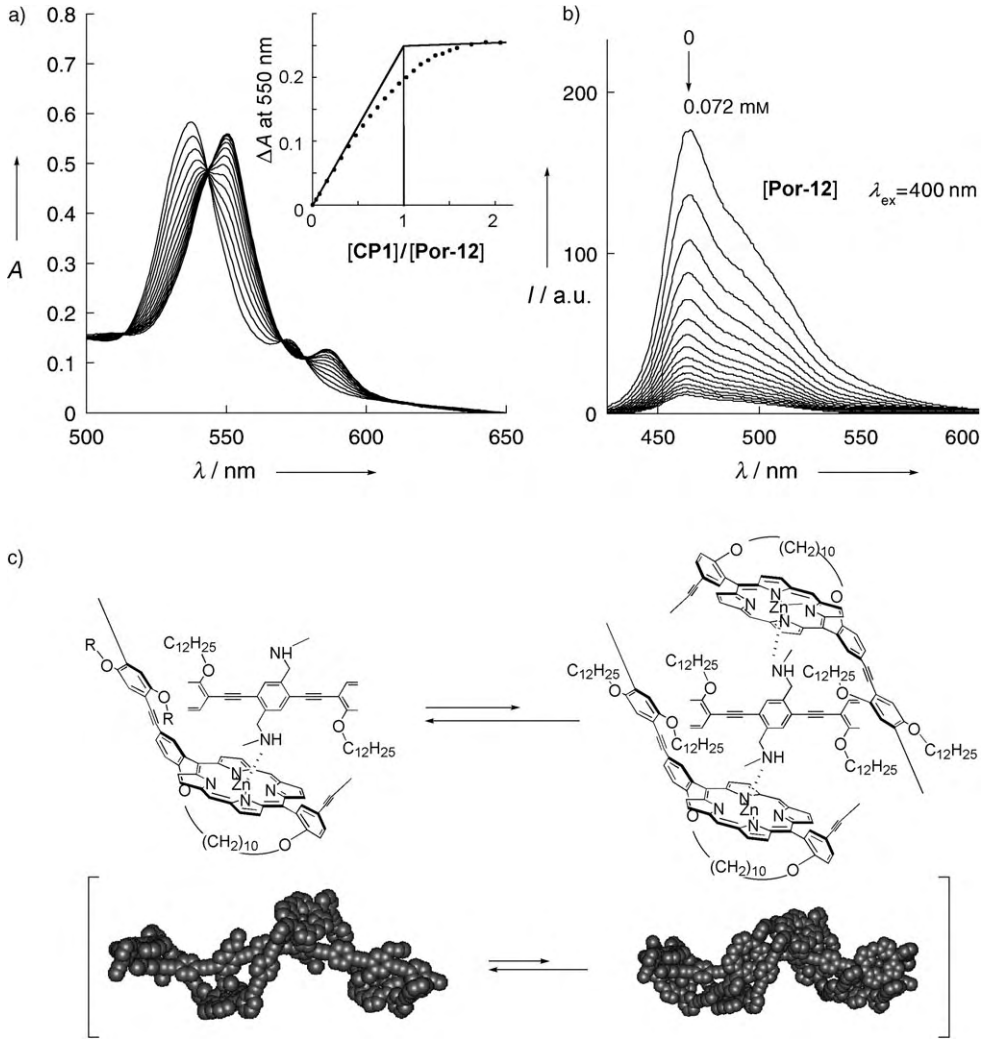


Figure 1. a) UV/Vis spectra of **Por-12** (0.050 mM unit) recorded after the addition of **CP1**. Inset: Plot of the absorbance change at 550 nm of **Por-12** (0.050 mM unit) versus [$\mathbf{CP1}_{unit}$]. b) Fluorescence spectra of **CP1** (0.036 mM unit) recorded in the presence and absence of **Por-12**. c) Schematic illustration of the equilibrium that exists between the singly and doubly complexed **Por-12**/**CP1** composites. Lower scheme of (c) is a schematic representation of the equilibrium that exists between the single- and double-stranded **Por-12**/**CP1** composites; the straps and peripheral alkyl chains have been omitted for clarity. The structures were calculated using Insight II, Discover, software.

at $\lambda_{ex} = 400$ nm (an isosbestic point in the UV/Vis spectrum) at 25 °C, we observed that the emission intensity ($\lambda_{em} =$ 465 nm) of **CP1** decreased upon increasing the **Por-12** concentration (Figure 1 b). At [**Por-12**] = 0.072 mM, the fluorescence intensity of **CP1** decreased to 7 % of its value in the absence of **Por-12**. This finding clearly indicates that the **Por-12** and **CP1** units interact and that efficient energy transfer from **CP1** to **Por-12** probably occurs in their complex as a result of the emission wavelength of **CP1** overlapping considerably with the absorption band of **Por-12**. We obtained a solution-cast film after deposition of a homogeneous solution of **CP1** (0.30 mM unit) in $CDCl_3$ containing 5.0 wt % polystyrene ($M_w = 200000$) on a quartz plate. The emission spectrum of this **CP1** film was broad in comparison with that recorded in dilute solution ([**CP1** unit] = 0.03 mM). This effect probably is due to random aggregation of the polymer main chains in the film.[15] Interestingly, the addition of **Por-12** transformed the broad emission obtained in the solid state into the sharp one similar to that observed for a dilute solution of **CP1** (see the Supporting Information), that is, random aggregates of CP no longer exist. With this experiment, we also confirmed the bathochromic shift of the Q bands of **Por-12** in the solid state, thus indicating that **Por-12** formed the complex with **CP1** (see the Supporting Information). The UV/Vis and emission spectra of the solution-cast film of the composite formed between **Por-12** and **CP1** in $CDCl_3$ suggest that the structure of the composite is maintained in the solid state.

To obtain visual images, we examined the composite formed between **Por-12** and **CP1** in $CDCl_3$ using confocal laser scan microscopy (CLSM), polarized optical microscopy (POM), and high-resolution transmission electron microscopy (HRTEM). From the HRTEM image, we confirmed that the **Por-12**/**CP1** composites grew into large aggregates (several microns in size) that possess stacked sheetlike 2D structures (see below). In a separate study, we confirmed that the aggregates of **Por-12** or **CP1** alone are amorphous[15] and cannot organize into 2D structures as large as that presented in Figures 2 and 3.

We subjected a solution-cast film of the **Por-12**/**CP1** composite, constructed on an indium tin oxide (ITO) glass, to POM observation. In Figure 2, we observe a 2D structure with dimensions greater than 50 μm^2. Very interestingly, this structure exhibits a bright pattern, even between crossed polarizers, thus indicating that this aggregate displays birefringence; that is, **Por-12** and **CP1** assemble into a highly ordered crystalline structure on the micron scale on the ITO glass. When we photoexcited a single large sheetlike aggregate (20 × 120 μm) at 354 nm, the CLSM image displays a blue **CP1** emission (400–440 nm) and a red **Por-12** emission (560–640 nm) in the same morphological domain (see the Supporting Information). It is clear, therefore, that the micron-sized superstructure was assembled through interactions between **Por-12** and **CP1**.

The electron micrographs of the composite provide information regarding how the **Por-12**/**CP1** composite self-organizes. We prepared solution-cast films of the **Por-12**/**CP1** composite on a TEM grid without staining. Figure 3 displays HRTEM images of the aggregate of the **Por-12**/**CP1** composite in which the periodicity of the dark stripes, over a distance

 © 2006 Wiley-VCH Verlag GmbH & Co. KGaA, Weinheim

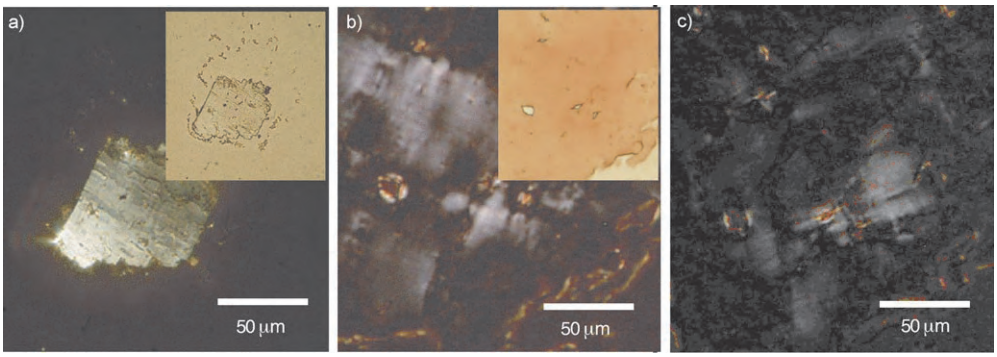


Figure 2. Optical microscopy images of the assemblies of the a) **Por-12/CP1** ([**Por-12**$_{unit}$] = 0.020 mM; [**CP1**$_{unit}$] = 0.036 mM) and b) **Por-12/CP1** ([**Por-12**$_{unit}$] = 0.20 mM; [**CP1**$_{unit}$] = 0.40 mM) composites on ITO as observed between crossed polarizers. c) Optical microscopy image of the assemblies observed after 45° rotation of the sample b). Inset: Images obtained without polarizers. Samples were prepared by drop-casting a solution of the **Por-12/CP1** composite in $CDCl_3$ on the ITO surface and then drying.

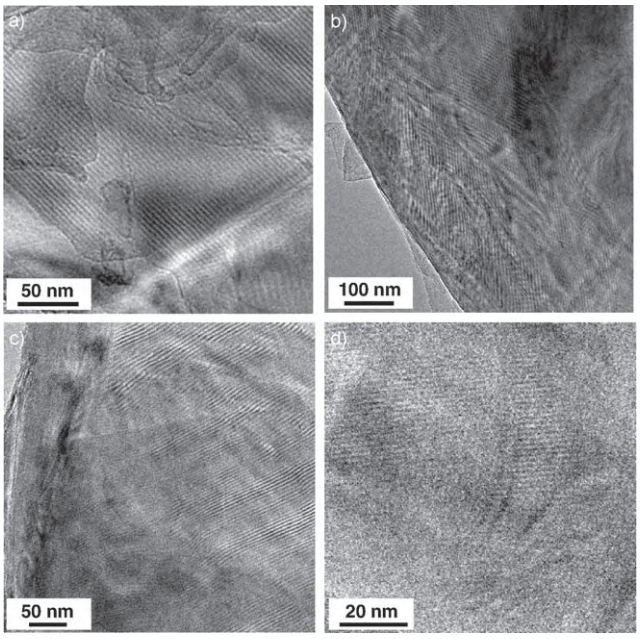


Figure 3. Electron micrographs (no staining) of aggregates of the Por/CP composites. a) HRTEM image of the **Por-12/CP1** composites that display dark and light stripes. The periodicity between the dark stripes is 4.0 nm. b) HRTEM image of a thick plate of **Por-12/CP1** composites. The crossed dark stripes suggest the overlap of a few thin plates that possess striped structures. c) HRTEM image of the **Por-12/CP2** composites. The periodicity between the dark stripes is 4.0 nm. d) HRTEM image of the **Por-6/CP2** composites that display dark and light stripes. The periodicity of the dark stripes is 2.7 nm.

of a few hundred nanometers, was 4.0 nm, as determined from the Fourier-filtered image (Figure 3a). In the image of a thick plate (Figure 3b), we observe crossed dark-stripe contrast, thus indicating that a few thin plates with striped structures were overlapped. We infer that the dark sections in the electron micrographs of the **Por-12/CP1** composites are regions that contain ordered π-stacked layers and/or the heaviest atom (Zn). As mentioned above, the diamino groups in **CP1** coordinate to these Zn^{II} atoms and, therefore, the **CP1** are probably also ordered along these stripes. Given the degree of polymerization of **CP1**, the **Por-12** oligomers must splice **CP1** noncovalently to form such aligned supramolecular assemblies. The addition of trifluoroacetic acid to a solution of the **Por-12/CP1** composite in $CDCl_3$ (namely, to protonate the amino groups of **CP1**) altered the overall morphologies of aggregates of the **Por-12/CP1** composite on the TEM grid from sheetlike to amorphous structures (see the Supporting Information for further details). This phenomenon is due to decomplexation of the **Por-12/CP1** composites into **Por-12** and **CP1**·$n\,H^+$ units in solution, which we confirmed from the appearance of the UV/Vis absorption spectrum of **Por-12** (the value of the λ_{max} value of the Soret band was 412 nm; see Figure 1). Neutralization through treatment of the acidified solution of **Por-12/CP1** in $CDCl_3$ with 1.0 M aqueous NaOH resulted in the Soret band of **Por-12** shifting to 420 nm. Through a process that we ascribe to recomplexation between **Por-12** and **CP1**, TEM analysis clearly indicates that reorganization occurred to form the sheetlike morphologies (see the image given in the Supporting Information). These results indicate that the crystalline sheet structure is constructed from **Por-12/CP1** composites.

Polymer **CP2** also formed complexes with **Por-12** in a manner similar to that occurring between **Por-12** and **CP1**. The UV/Vis and fluorescence spectra support the formation of a composite between **Por-12** and **CP2** (see the Supporting Information). Figure 3c displays a HRTEM micrograph of the aggregates of the **Por-12/CP2** composite; because the striped pattern possesses a 4.0-nm periodicity, it appears that the side chains of **CP2** do not influence the periodicity significantly. The following question arises: What does this distance of 4.0 nm represent? In an attempt to answer this question, we prepared a composite from **Por-6** and **CP2** and its solution-cast film using the same procedure. Interestingly, we observed an HRTEM image that depicts a similar striped structure, but with a distance between stripes of only 2.7 nm (Figure 3d). This result indicates clearly that the distance reflects the length of the alkyl groups of the Por oligomer. In fact, if we assume that partially interdigitated packing of the alkyl groups of Por occurs in the Por/CP composites that were formed through the twining of Por oligomers around the CP, then we estimate the $Zn^{II}\cdots Zn^{II}$ distance between adjacent **Por-12/CP** composites to be 4.0 nm and that for the **Por-6/CP** composites to be 2.7 nm (Figure 4), in which the peripheral alkyl chains are also thought to participate in the packing among the composites but to be indecisive.

From these findings, we propose the following sequential growth mechanism for the preparation of these micron-sized,

 © 2006 Wiley-VCH Verlag GmbH & Co. KGaA, Weinheim

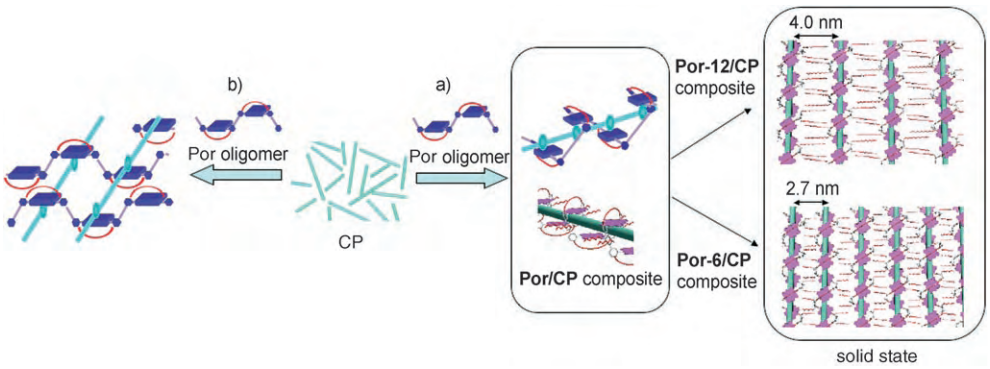


Figure 4. a) Schematic representation of the influence of the peripheral alkyl chains in the Por oligomers on the periodicity of the aligned assemblies. The peripheral alkyl chains in CP entwined within the Por oligomers, which are also considered to participate in the van der Waals packing among the composites in the solid state, have been omitted for clarity. b) Schematic representation of the formation of the crosslinked network structure.

highly ordered assemblies (Figure 4a). In the first step, the Por oligomer, which is preprogrammed for helix formation in the presence of the guest, twines around the CP strand and becomes stabilized through the formation of dative bonds between the porphyrinatozinc and amino units in solution. In the second step on the surface, the composites organize together through attractive van der Waals interactions between the alkyl groups during the solidifying process. In the third step, they construct 2D sheetlike assemblies that display distinctly striped patterns. Other systems that form a crosslinked network structure constructed from the Por oligomer and CP (Figure 4b) could not elucidate the effect of the alkyl chain length in the Por oligomers on the periodicities and the contrast patterns observed in the electron micrographs.[19] It is unlikely that the random crosslinked network structure resulted in the formation of the crystalline assemblies on the ITO glass and the TEM grid during the solidification process.

The assembly/aggregation approach we present herein is also readily applicable for use with nonconjugated, flexible polymers bearing coordinating moieties. For example, poly(4-vinylpyridine) ($M_w = 60\,000$) also complexed with **Por-12** in a manner similar to its assembly with **CP1** through dative bonds, and the stoichiometry between [pyridine units in poly(4-vinylpyridine)] and [porphyrin units in **Por-12**] was clearly determined to be 2:1 (see the Supporting Information). TEM images and electron diffraction patterns indicate clearly that the poly(4-vinylpyridine)/ **Por-12** composites self-organized into crystalline supramolecular assemblies with the periodicity of 5.0 nm that formed stacked thin 2D sheets (see the Supporting Information).

Herein, we have demonstrated that porphyrin oligomers (Por series) form homogeneously dispersed composites with conjugated polymers (**CP1** or **CP2**) and poly-4-vinylpyridine in $CDCl_3$; the resulting micron-sized aggregates on the surface possess highly ordered, crystalline structures.[20] It is quite astonishing that such large, highly ordered assemblies could be created simply by mixing two polymeric components together and then drop-casting on a surface. Modification of the lengths of the alkyl chains in the Por series allows control over the intercomposite spacing. The concepts that we introduce herein are complementary to the techniques that exist currently for the preparation of supramolecular and macromolecular assemblies. Furthermore, our results imply that "molecular programming"—that is, utilizing weak intermolecular interactions that tend to occur through reversible processes in a search for the thermodynamically most stable state—can play crucial roles during such organization processes. This twining association/aggregation event is a rare example of a molecular assembly technique that results in a visually recognizable ordered structure; in this regard, our process is reminiscent of some of the self-assembly and self-organization events that occur in biological systems. The application for other 1D polymeric materials is now under investigation.

Experimental Section

All starting materials and solvents were purchased from Tokyo Kasei Chemicals or Wako Chemicals and used as received. ^{1}H NMR spectra were recorded on a Bruker DRX 600 (600 MHz) spectrometer. Chemical shifts are reported in ppm downfield from tetramethylsilane, the internal standard. Mass-spectral data were obtained using a Perseptive Voyager RP MALDI TOF mass spectrometer and/or a JEOL JMS HX110A high-resolution magnetic sector FAB mass spectrometer. UV/Vis and fluorescence spectra were recorded using Shimadzu UV-2500 PC and Perkin-Elmer LS55 spectrophotometers.

A typical example of sample preparation for TEM and POM measurements: A solution of **CP1** ([**CP1** unit] = 36 μM) and **Por-12** ([**Por-12** unit] = 20 μM) in $CDCl_3$ was prepared. UV/Vis spectroscopy confirmed that the porphyrinatozinc units in **Por-12** had formed complexes quantitatively. This solution was then cast onto a copper TEM grid upon a holey carbon support film or onto the ITO glass.

TEM and HRTEM: The images were acquired using JEOL TEM-2010 (accelerating voltage: 120 kV) and TECNAI-20 FEI (accelerating voltage: 200 kV) microscopes, respectively. The sample solution was placed on a copper TEM grid upon a holey carbon support film. The TEM grid was dried under reduced pressure for 6 h prior to TEM observation.

Received: April 14, 2006
Published online: July 18, 2006

Keywords: alignment · conjugated polymers · porphyrinoids · supramolecular chemistry · twining

[1] a) G. A. Ozin, A. C. Arsenault, *Nanochemistry*, RSC, Cambridge, **2005**; b) D. T. McQuade, A. E. Pullen, T. M. Swager, *Chem. Rev.* **2000**, *100*, 2537–2574.
[2] F. J. M. Hoeben, P. Jonkheijm, E. W. Meijer, A. P. H. J. Shenning, *Chem. Rev.* **2005**, *105*, 1491–1546.
[3] J.-M. Lehn, *Supramoleculer Chemistry*, VCH, New York, *1995*.
[4] S. I. Stupp, V. LeBonheur, K. Walker, L. S. Li, K. E. Huggins, M. Keser, A. Amstutz, *Science* **1997**, *276*, 384–389.

 © 2006 Wiley-VCH Verlag GmbH & Co. KGaA, Weinheim

[5] S. Park, J.-H. Lim, S.-W. Chung, C. A. Mirkin, *Science* **2004**, *303*, 348 – 351.
[6] H. Sirringhaus, P. J. Brown, R. H. Friend, M. M. Nielsen, K. Bechgaard, B. M. W. Langeveld-Voss, A. J. H. Spiering, R. A. J. Janssen, E. W. Meijer, P. Herwig, D. M. de Leeuw, *Nature* **1999**, *401*, 685 – 688.
[7] H. Goto, K. Akagi, H. Shirakawa, *Synth. Met.* **1997**, *84*, 373 – 374.
[8] T. M. Long, T. M. Swager, *J. Am. Chem. Soc.* **2002**, *124*, 3826 – 3827.
[9] K. P. Fritz, G. D. Scholes, *J. Phys. Chem. B* **2004**, *108*, 10141 – 10147.
[10] J. Kim, T. M. Swager, *Nature* **2001**, *411*, 1030 – 1034.
[11] A. Montali, C. Bastiaansen, P. Smith, C. Weder, *Nature* **1998**, *392*, 261 – 264.
[12] W. C. Molenkamp, M. Watanabe, H. Miyata, S. H. Tolbert, *J. Am. Chem. Soc.* **2004**, *126*, 4476 – 4477.
[13] M. Hamaguchi, K. Yoshino, *Appl. Phys. Lett.* **1995**, *67*, 3381 – 3383.
[14] P. Dyreklev, M. Berggren, O. Inganas, M. R. Anderson, O. Wennestrom, T. Hjertberg, *Adv. Mater.* **1995**, *7*, 43 – 45.
[15] Y. Kubo, Y. Kitada, R. Wakabayashi, T. Kishida, M. Ayabe, K. Kaneko, M. Takeuchi, S. Shinkai, *Angew. Chem.* **2006**, *118*, 1578 – 1583; *Angew. Chem. Int. Ed.* **2006**, *45*, 1548 – 1553.
[16] a) A. Osuka, F. Kobayashi, K. Maruyama, *Bull. Chem. Soc. Jpn.* **1991**, *64*, 1213 – 1225; b) N. C. Maiti, M. Ravikanth, *J. Photochem. Photobiol. A* **1996**, *101*, 7 – 10.
[17] C. Kubel, M. J. Mio, J. S. Moore, D. C. Martin, *J. Am. Chem. Soc.* **2002**, *124*, 8605 – 8610.
[18] The spectroscopic data were not as reproducible when we used $CHCl_3$ as the solvent, probably because the amino groups induced decomposition of $CHCl_3$ to generate some acidic species; in contrast, the use of $CDCl_3$, which is somewhat less reactive than $CHCl_3$, resulted in very reproducible data.
[19] Dynamic light scattering (DLS) analysis of a solution of the composite in $CDCl_3$ indicated that by mixing the Por oligomer and CP, somewhat larger assemblies with a high aspect ratio assignable to the Por/CP composite exist in solution (see the Supporting Information). At the present stage, we can not fully rule out the competitive association system (the intersected model) depicted in Figure 4b; however, we infer that the formation of the composite as illustrated in Figure 4a is more likely.
[20] The assemblies of the composites may form a mesophase or organogel; however, we could not observe gelation phenomena under the conditions used and liquid crystalline phases.

 © 2006 Wiley-VCH Verlag GmbH & Co. KGaA, Weinheim

DNA Conductance

DOI: 10.1002/anie.200601263

Variable-Temperature Measurements of the Single-Molecule Conductance of Double-Stranded DNA**

*Harm van Zalinge, David J. Schiffrin, Andrew D. Bates, Evgeni B. Starikov, Wolfgang Wenzel, and Richard J. Nichols**

There has been much interest in the electrical properties of DNA.[1] Recent studies have shown that it is possible to record the current–voltage characteristics of both single-stranded and double-stranded DNA immobilized between metal electrodes in an ambient or aqueous environment.[2–4] As in the case of organic molecular bridges,[5,6] there is also great value in being able to determine the conductance of DNA over a range of temperatures, since this enables charge-transport mechanisms to be investigated. With this aim, we present here a first study of the effect of temperature on the single-molecule conductance (SMC) of double-stranded oligodeoxynucleotides with homogeneous canonical base-pair sequences (adenine–thymine (AT) and guanine–cytosine (GC)).

Each of the DNA duplexes under study here contains 15 canonical nucleotide pairs, and for brevity they are referred to as "$(dA)_{15}$-$(dT)_{15}$" and "$(dG)_{15}$-$(dC)_{15}$", when treated separately, or as "DNA", when described together. The SMC of $(dA)_{15}$-$(dT)_{15}$ and $(dG)_{15}$-$(dC)_{15}$ have been determined over a range between room temperature to about 70 °C by using recently developed STM-based methods.[4,7] These duplexes have been functionalized at their 3′-ends with trimethylene-thiol (C_3) linkers, which help to covalently attach DNA

[*] Dr. H. van Zalinge, Prof. D. J. Schiffrin, Prof. R. J. Nichols
Department of Chemistry
University of Liverpool
Crown Street, Liverpool, L69 7ZD (UK)
Fax: (+44) 151-794-3588
E-mail: vzalinge@liverpool.ac.uk
Dr. A. D. Bates
School of Biological Sciences
University of Liverpool
Liverpool, L69 7ZB (UK)
Dr. E. B. Starikov, Prof. Dr. W. Wenzel
Institut für Nanotechnologie
Forschungszentrum Karlsruhe
Postfach 3640, 70621 Karlsruhe (Germany)

[**] This work was supported by the European Community under contract IST-2001-32152, MINT (Molecular Interconnects for Nanotechnology) and under contract HPRN-CT-2002-00185, SUSANA (Supramolecular Self-Assembly of Interfacial Nanostructures) Research Training Network. Support from the EPSRC under grant EP/C00678X/1 (Mechanisms of Single Molecule Conductance) is also gratefully acknowledged. The work was also supported by a grant from the German National Science Foundation (DFG WE1863/14-1) and through the DASY project of the "Volkswagen Stiftung" foundation.

 © 2006 Wiley-VCH Verlag GmbH & Co. KGaA, Weinheim

strands to gold electrodes; the resistance of these linker chains is known to be relatively low, so they should not contribute significantly to the conductance or its temperature dependence.[5] The SMC values determined over this temperature range are 0.51 ± 0.08 nS and 1.2 ± 0.2 nS for $(dA)_{15}$-$(dT)_{15}$ and $(dG)_{15}$-$(dC)_{15}$, respectively (Figure 1d). It is thus

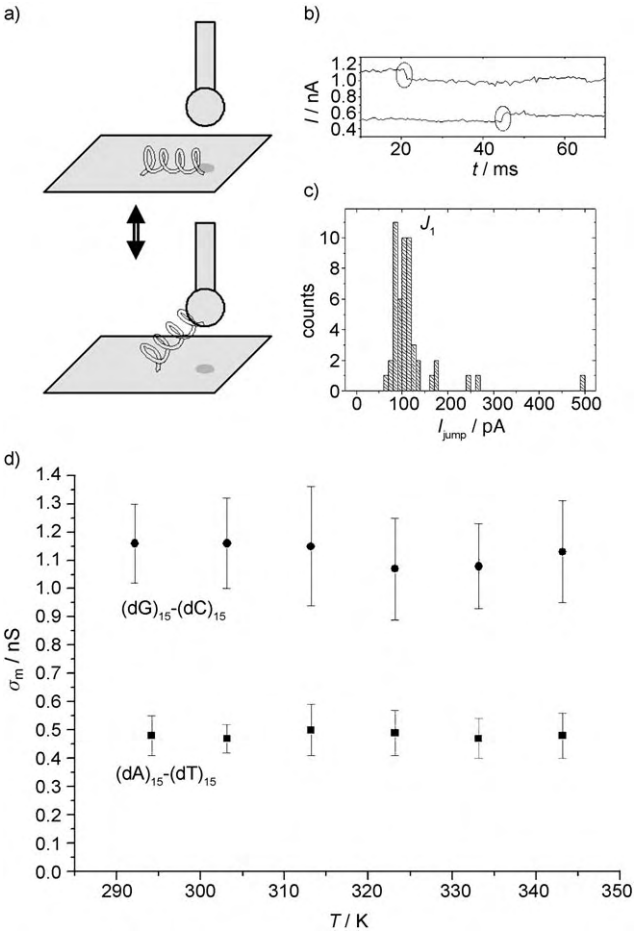


Figure 1. a) The $I(t)$ technique with a fixed gap between the tip and the substrate and a DNA molecule spontaneously bridging the gap. b) Typical $I(t)$ traces. Representative current jumps for this technique are shown in circles. c) The resulting histogram, $J_1 = 102 \pm 16$ pA. All measurements shown are for $(dA)_{15}$-$(dT)_{15}$ at $U_{tip} = 200$ mV in air. d) The SMC as a function of the substrate temperature for both $(dA)_{15}$-$(dT)_{15}$ (■) and $(dG)_{15}$-$(dC)_{15}$ (●). All measurements were performed in air at $U_{tip} = 200$ mV.

evident that $(dG)_{15}$-$(dC)_{15}$ is a better conductor than $(dA)_{15}$-$(dT)_{15}$. Strikingly, along with this, the data do not show (within experimental error) any dependence of the SMC on the temperature, contrary to observations for long homogeneous base sequence DNA in a vacuum.[8] These differences indicate that the medium has a great influence on the temperature dependence of DNA conductance.

The temperature independence recorded here seems to be paradoxical, since there are several theoretically established mechanisms that would predict strong temperature dependence. Firstly, a temperature dependence would be expected for activated charge that hops through DNA in a polaron-like manner. Temperature-dependent conductance may also be expected for DNA in aqueous solutions containing counterions, which are predicted to influence charge transport through a "counterion-gating" mechanism.[9] Moreover, the polaron-like charge transport in DNA is believed to be largely augmented with contributions coming from intramolecular thermal fluctuations.[10,11] Finally, the DNA hydration shell ought to influence the charge transport in a temperature-dependent manner.[12] Thus, our present finding contradicts, at first glance, these theoretical expectations for the temperature dependence of DNA conductance.

In an attempt to explain our surprising experimental result we have carried out a series of DNA conductance calculations by using a completely atomistic approach.[13] With these calculations we can study the influence of the deformations arising from acoustic modes on the valence-band transmission spectrum of $(dA)_{15}$-$(dT)_{15}$ and $(dG)_{15}$-$(dC)_{15}$. On the basis of these data we can ascertain whether the DNA acoustic modes could give rise to the temperature dependence of the conductivity at ambient temperatures. Figure 2a shows that deformation along DNA acoustic modes greatly affects the valence-band transmission for the 26-mer studied in Ref. [2]. The same qualitative conclusion can be drawn for the valence-band transmission in the two 15-mers studied here (Figure 2b and c).

Figure 2b and c show that the area covered by the whole $(dG)_{15}$-$(dC)_{15}$ valence band in the equilibrium conformation is much larger than that of $(dA)_{15}$-$(dT)_{15}$. This area is expected to be approximately proportional to the magnitude of the electrical current flowing through the molecule under study.[14] Closer examination of Figure 2b and c reveals that the DNA acoustic modes significantly suppress the valence-band conduction of $(dG)_{15}$-$(dC)_{15}$, but noticeably improve it for $(dA)_{15}$-$(dT)_{15}$. Even in its improved form the valence-band conduction of $(dA)_{15}$-$(dT)_{15}$ is not as high as that of the $(dG)_{15}$-$(dC)_{15}$ in its equilibrium B-DNA conformation. These results (Figure 2) suggest that DNA valence-band conductance in $(dG)_{15}$-$(dC)_{15}$ is larger than that in $(dA)_{15}$-$(dT)_{15}$, which is in qualitative accordance with the experimentally observed trend (see Figure 1). However, these computations indicate that different acoustic modes for the same sequence give very different valence-band transmission spectra, which might result in a temperature-dependent conductance.

To explain the experimental finding we additionally consider the temperature-dependent population of the acoustic modes through the Debye temperature of the system. By assuming a speed of sound in B-form DNA of 1900 m s^{-1}[15] and a lattice constant of approximately 0.34 nm, the Debye temperature is estimated as 166 K.[16] For this reason, DNA acoustic modes will significantly affect the conductance at low temperatures, but at room and higher temperature this effect will have no noticeable temperature dependence.

In conclusion, we have recorded the SMC of $(dA)_{15}$-$(dT)_{15}$ and $(dG)_{15}$-$(dC)_{15}$ as a function of temperature (from room temperature to about 70 °C). The G-C sequence gives a higher conductance than the equivalent length A-T sequence. This experimental result is consistent with the computations presented here for the valence-band transmission spectra. These computations also predict that the conductance should

 © 2006 Wiley-VCH Verlag GmbH & Co. KGaA, Weinheim

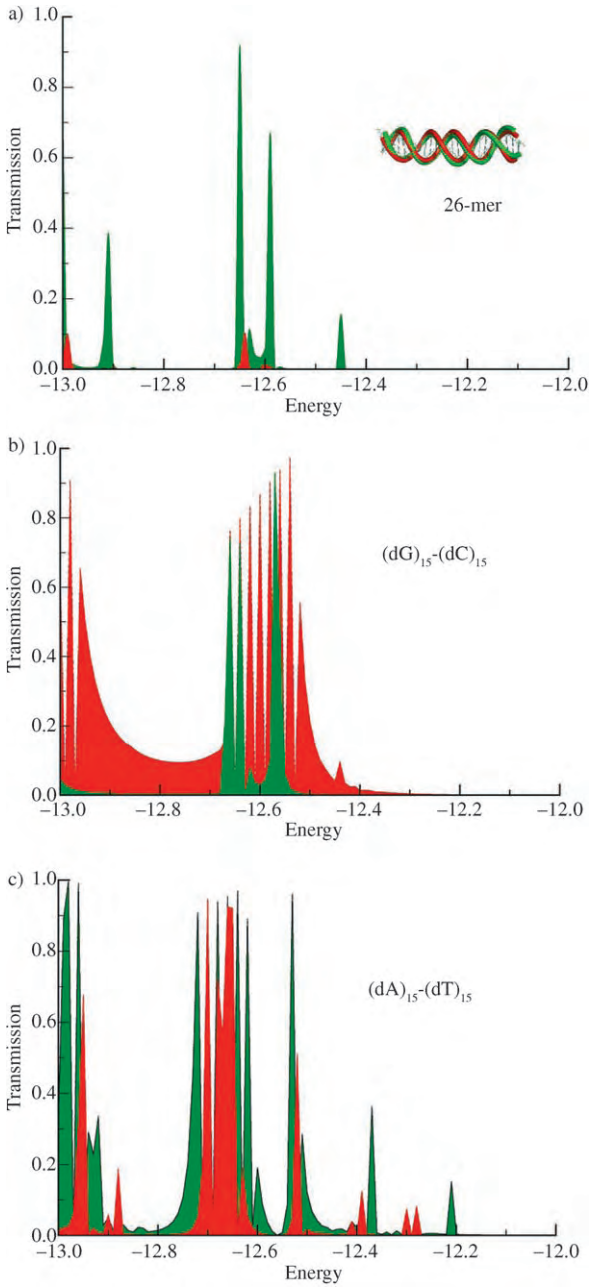


Figure 2. Comparison of the calculated transmission spectra at the upper edge of the valence band for: a) 26-mer duplex studied in Ref. [2] with a trimethylenethiol linker between the 3′-ends and electrodes (inset shows the mode of deformation of the DNA duplex), b) $(dG)_{15}$-$(dC)_{15}$, and c) $(dA)_{15}$-$(dT)_{15}$; the latter two were attached to electrodes directly (without C_3SH linkers) in our calculations. The Fermi level (defined here as halfway between the energies of the highest occupied and lowest unoccupied orbitals at 0 K) is around −12.05 eV for all the graphs. The red spectra correspond to the transmission spectra of the duplexes in their ideal B-DNA conformation, the green ones depict those with deformations along DNA acoustic modes.

be strongly influenced by the acoustic mode. The fact that the Debye temperature of these systems is far below room temperature, means that the contribution from DNA acoustic modes should be essentially temperature-independent, which is in agreement with the experimental observation. Future studies, both theoretical and experimental, of the temperature dependence of DNA conductance and its relationship to other experimental parameters (for example, base sequence, electrolyte concentration, molecular length) are expected to play a key role in establishing DNA conductance mechanisms.

Experimental Section

The experiments were based upon a recently developed technique.[7] The so-called "$I(t)$ technique" is shown schematically in Figure 1a, with temperature control as described by Haiss et al.[5] A gold tip and a gold on glass substrate were employed along with a low coverage of DNA strands. The tunneling current was monitored as a function of time at a fixed tip–substrate separation. Under these conditions events occured in which the DNA strands bridged the gap between the tip and the substrate to form a "molecular wire" (Figure 1b). Examples of both attachment and detachment events for DNA are shown in circles in Figure 1b). These current jumps are associated with current flowing through one or more DNA strands and can be used to calculate the SMC, after statistical analysis of the data. DNA adsorption was achieved by immersion of the gold substrates in aqueous 10 mM sodium phosphate buffer (pH 6.8) with a DNA concentration of ca. 10^{-4} M. The sample was then rinsed with Milli-Q water and gently blown with N_2 to remove excess water. By using these conditions, it was expected that a water film and phosphate counterions would be retained with the DNA sample. Indeed, control experiments at room temperature for fully immersed samples (in an electrochemical STM cell) gave comparable conductance values for a given sequence, thus adding evidence that it is the hydrated sample that is analyzed.

Single-stranded DNA is a much worse conductor than dsDNA and the conductance measured here is consistent with the latter and not the former.[4] Further verification that the double helix was measured in these experiments comes through observation of the frequency of the $I(t)$ jumps. Raising the temperature above the melting temperature (T_M) should show a decreased frequency of such events in the $I(t)$ traces, although the transition should not be sharp since the melting curve is not expected to be sharp.[18] Indeed we saw a much decreased frequency of events with $(dA)_{15}$-$(dT)_{15}$ duplexes bridging the contacts on increasing the temperature from 50 to 70 °C, which is consistent with the melting of the duplex. Such a decrease in the frequency of the current jumps was not observed for a control molecule: nonanedithiol.[5]

The T_M value of $(dG)_{15}$-$(dC)_{15}$ is 76.5 °C, while that of $(dA)_{15}$-$(dT)_{15}$ is 41.9 °C (data supplied by Sigma-Genosys). The highest temperature at which the conductance was measured was 70 ± 2 °C. It may therefore seem paradoxical that molecular conductance for $(dA)_{15}$-$(dT)_{15}$ could still be measured above the quoted melting point. A possible explanation for this observation is that under ambient conditions the electrolyte concentration at the surface is high, since the aqueous film of ambient water/electrolyte is likely to dry at least partially during the temperature ramps. It is well known that a higher ionic strength gives rise to higher melting temperatures.[19]

To compute the conductance behavior of DNA strands, we used a previously established computational method,[13] which employs an all-atom representation for the DNA strands and describes their electronic structure in the framework of an extended Hückel Hamiltonian. To study the influence of DNA acoustic vibrations on its conductive properties, we generated ideal B-DNA conformations for $(dA)_{15}$-$(dT)_{15}$ and $(dG)_{15}$-$(dC)_{15}$, as well as for the DNA duplexes studied elsewhere.[2,3] Deformations were then produced along the three lowest frequency intramolecular vibrational modes for all of these molecules by using an elastic network model.[20] The three vibrations involved are invariant with respect to DNA base composition and sequence, and include bending of DNA double-helical rods

 © 2006 Wiley-VCH Verlag GmbH & Co. KGaA, Weinheim

in the two orthogonal directions perpendicular to the rod axis, as well as a combination of helical twisting and longitudinal stretching/squeezing. Thus, we can consider these modes acoustic ones. Finally, we calculated the energy spectra of charge-transmission probabilities as in Ref. [13] for all the equilibrium and deformed B-DNA conformations.

Received: March 31, 2006
Revised: June 2, 2006
Published online: August 7, 2006

Keywords: conducting materials · DNA · scanning probe microscopy · single-molecule studies

[1] For a recent review, see, for example: "Charge transport in DNA-based devices": D. Porath, G. Cuniberti, R. Di Felice, *Top. Curr. Chem.* **2004**, *237*, 183.
[2] H. Cohen, C. Nogues, R. Naaman, D. Porath, *Proc. Natl. Acad. Sci. USA* **2005**, *102*, 11589.
[3] J. Hihath, B. Q. Xu, P. M. Zhang, N. J. Tao, *Proc. Natl. Acad. Sci. USA* **2005**, *102*, 16979.
[4] H. van Zalinge, D. J. Schiffrin, A. D. Bates, W. Haiss, J. Ulstrup, R. J. Nichols, *ChemPhysChem* **2006**, *7*, 94.
[5] W. Haiss, H. van Zalinge, D. Bethell, J. Ulstrup, D. J. Schiffrin, R. J. Nichols, *Faraday Discuss.* **2006**, *131*, 253.
[6] Y. Selzer, M. A. Cabassi, T. S. Mayer, D. L. Allara, *Nanotechnology* **2004**, *15*, S483.
[7] W. Haiss, R. J. Nichols, H. van Zalinge, S. J. Higgins, D. Bethell, D. J. Schiffrin, *Phys. Chem. Chem. Phys.* **2004**, *6*, 4330.
[8] K. H. Yoo, D. H. Ha, J. O. Lee, J. W. Park, J. Kim, J. J. Kim, H. Y. Lee, T. Kawai, H. Y. Choi, *Phys. Rev. Lett.* **2001**, *86*, 8719.
[9] R. N. Barnett, C. L. Cleveland, A. Joy, U. Landman, G. B. Schuster, *Science* **2001**, *294*, 567.
[10] R. Bruinsma, G. Gruner, M. R. D'Orsogna, J. Rudnick, *Phys. Rev. Lett.* **2000**, *85*, 4393.
[11] R. Gutierrez, S. Mandal, G. Cuniberti, *Nano Lett.* **2005**, *5*, 1093.
[12] A. Hubsch, R. G. Endres, D. L. Cox, R. R. P. Singh, *Phys. Rev. Lett.* **2005**, *94*.
[13] E. B. Starikov, S. Tanaka, N. Kurita, Y. Sengoku, T. Natsume, W. Wenzel, *Eur. Phys. J. E* **2005**, *18*, 437.
[14] S. Datta, *Electronic Transport in Mesoscopic Systems*, Cambridge University Press, Cambridge, **1995**.
[15] M. B. Hakim, S. M. Lindsay, J. Powell, *Biopolymers* **1984**, *23*, 1185.
[16] Interestingly, we note that there is a significant dip in the conductance of assemblies of the gold nanoparticles interlinked by dsDNA at about 200 K (see Ref. [17]), which is close to the Debye temperature estimated here.
[17] S. J. Park, A. A. Lazarides, C. A. Mirkin, P. W. Brazis, C. R. Kannewurf, R. L. Letsinger, *Angew. Chem.* **2000**, *112*, 4003; *Angew. Chem. Int. Ed.* **2000**, *39*, 3845.
[18] R. Owczarzy, *Biophys. Chem.* **2005**, *117*, 207.
[19] R. Owczarzy, Y. You, B. G. Moreira, J. A. Manthey, L. Y. Huang, M. A. Behlke, J. A. Walder, *Biochemistry* **2004**, *43*, 3537.
[20] K. Suhre, Y. H. Sanejouand, *Nucleic Acids Res.* **2004**, *32*, W610.

 © 2006 Wiley-VCH Verlag GmbH & Co. KGaA, Weinheim

Computational Models

DOI: 10.1002/anie.200600329

A Priori Theoretical Prediction of Selectivity in Asymmetric Catalysis: Design of Chiral Catalysts by Using Quantum Molecular Interaction Fields**

*James C. Ianni, Venkatachalam Annamalai, Puay-Wah Phuan, Manoranjan Panda, and Marisa C. Kozlowski**

Much effort has been devoted toward the development of asymmetric catalysts for the synthesis of chiral compounds in pure form.[1] Despite this body of work, the science of asymmetric catalysis remains far from exact, and the process of finding a new catalyst usually requires a large investment of manpower and funding. Therefore, a major goal is the development of more efficient methods for identifying highly selective asymmetric catalysts. In terms of computational methods, the calculation of ground state and transition state energies[2] for metal catalysts is promising.[3] Even so, a detailed knowledge of the reaction mechanism is needed, and many variables must be evaluated requiring extensive time, effort, and resources. This communication illustrates the first example of rapid quantitative structure–selectivity relationship (QSSR) calculations being used to predict the enantioselectivities of new chiral catalysts. Subsequent synthesis and assessment of the new chiral catalysts in the asymmetric addition of Et_2Zn to benzaldehyde (Scheme 1) revealed that the QSSR calculations forecast the experimental results with a high degree of fidelity.

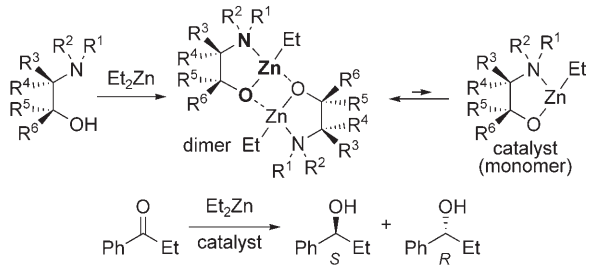
In a prior report[4] we determined that grid-based QSSR methods[5] derived from quantum mechanical molecular interaction fields can be used to generate statistically valid models that correlate enantioselectivities in the addition of Et_2Zn to PhCHO with catalyst geometries obtained from transition structures. The true test of this method lies in predicting the selectivity of catalysts with ligands that have not been tested and for which the experimental results cannot be easily anticipated based on previous results. To this end, we designed **P1**, a cyclohexane with *trans* amino and hydroxy

[*] Dr. J. C. Ianni, V. Annamalai, Dr. P.-W. Phuan, Dr. M. Panda, Prof. M. C. Kozlowski
Roy and Diana Vagelos Laboratories
Department of Chemistry
University of Pennsylvania
Philadelphia, PA 19104-6323 (USA)
Fax: (+1) 215-573-7165
E-mail: marisa@sas.upenn.edu

[**] Financial support of this research was provided by the NIH (GM59945). Computing resources from the NCSA (CHE020059) and the NSF CRIF program (CHE0131132) are acknowledged. We thank Steve Dixon, Giorgio Lauri, and Prof. Kenneth Merz for assistance with the QM-QSAR program. We are grateful to Bill Nugent for supplying the unpublished data for **P3**.

Supporting information for this article is available on the WWW under http://www.angewandte.org or from the author.

WILEY InterScience DISCOVER SOMETHING GREAT
© 2006 Wiley-VCH Verlag GmbH & Co. KGaA, Weinheim



Scheme 1. Generation of the catalyst and the β-aminoalkoxide-catalyzed addition of Et_2Zn to PhCHO.

groups (Figure 1). This type of ligand, with a chiral quaternary alcohol carbon, is not found in the parameterization set **T1**–**T18** used to calibrate the QSSR model.[6] Since syntheses of

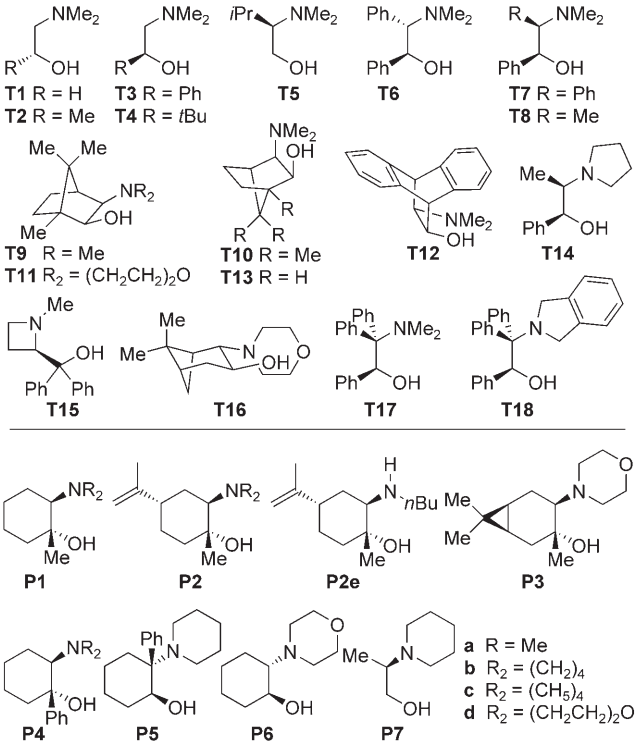


Figure 1. β-Amino alcohols used in parameterization (**T1**–**T18**) and a priori predictions (**P1**–**P7**).

P2[7] and **P3**[8] had been reported, we wished to predict the selectivities of **P1**–**P6**. When the QSSR model based on transition state structures[4] was used to generate predictions, the standard deviations were high and the predictions were found to be dependent on the parameterization set. To solve these problems, further investigation of the QSSR protocol was undertaken.

It is highly desirable to be able to apply a QSSR protocol[5] without knowing the reaction pathway (i.e., the transition structures previously used in the parametrization).[4] We have achieved this here using the catalyst geometries found in the ground state dimers (aligned by N, Zn, O atoms; bold in Scheme 1) of **T1**–**T18**.[6] The geometry around the zinc atom is critical as good QSSR models could not be obtained for the monomers (trigonal at Zn). The dimers (tetrahedral at Zn) likely reflect the interactions encountered during reaction (tetrahedral at Zn). The *syn* zinc dimers were selected as they have been identified crystallographically[9] and in solution[10] for the chiral catalysts.[11] The geometry for the half of the calculated dimer of **T9** (PM3) was quite similar to the reported crystallographic structure (rmsd = 0.23 Å) as well as to other calculated dimers.[10,12] Similarly, the geometry of the half dimer of **T9** matches closely with that portion in calculated transition states.[13]

Use of the QSSR method with these dimers (aligned by N, Zn, O atoms; bold in Scheme 1) provided models that were highly accurate. Notably, these ground state structures were obtained much more readily and with less computational time than the corresponding transition structures. A "leave-two-out" analysis using all 153 combinations of 16 parameterization- and 2 prediction-set elements from **T1**–**T18** indicated a high degree of cross-validation for these internal predictions ($r^2_{cv} = 0.85$, see the Supporting Information). Figure 2 illustrates the grid points (sphere centers) correlated to selectivity for three of the models from this analysis as well as an overlay of all 153 models. The method is robust as the models are relatively unaffected by the constitution of the parameterization set. In addition, these points indicate which portions of the catalyst are most important to the stereoselectivity. For example, the dimethylmethylene bridge of **T9** and **T11** correlates to high selectivity, whereas the phenyl group nearest the hydroxy group in **T6**–**T8** correlates to moderate selectivity.

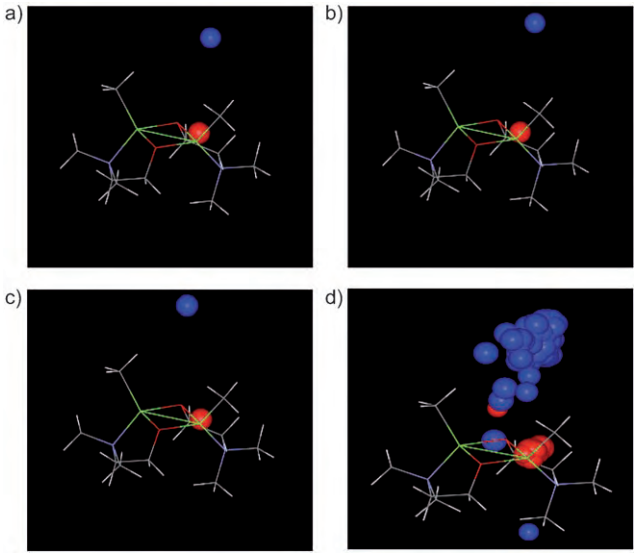


Figure 2. a–c) Several of the models from the "leave-two-out" analyses. d) Superimposed models from all 153 trials. Blue: *ee* value increases with increasing grid-point energy; red: *ee value* decreases.

With this model in hand, we generated predictions for catalysts derived from ligands **P1**–**P6**. In the first analysis (Table 1, single run) with the parameterization set comprising **T1**–**T18**, predicted ΔG values were obtained and translated into enantioselectivity values at 0 °C (273 K). In a second

 © 2006 Wiley-VCH Verlag GmbH & Co. KGaA, Weinheim

Table 1: QSSR a priori predictions for catalysts derived from **P1**–**P7**.

Ligand	Single run[a] ΔG[c]	Single run[a] % *ee*[d]	"Leave-two-out"[b] Mean ΔG[c]	SD ΔG[c]	% *ee*[d]	CI % *ee*[e]	Expt. % *ee*[f]
P1a	1.74	92.3	1.68	0.22	91.5	3.2	–
P1b	0.81	63.5	0.91	0.33	68.8	15.9	–
P1c	1.16	78.9	1.45	0.38	87.2	8.2	89
P1d	0.80	63.0	1.01	0.28	73.2	11.8	83
P2a	1.01	73.1	1.05	0.26	74.9	10.3	67
P2b	0.92	69.3	1.03	0.35	73.9	14.6	70
P2c	1.14	78.5	1.19	0.31	80.2	10.0	87
P2d	1.00	72.7	1.13	0.24	78.0	8.7	81
P2e	0.74	59.2	0.82	0.43	64.1	23.1	48
P3	1.11	77.4	1.26	0.29	82.3	8.4	84
P4a	2.88	99.0	2.68	0.31	98.6	0.8	–
P4b	2.10	96.0	2.01	0.38	95.2	3.2	–
P4c	3.61	99.7	3.77	0.77	99.8	0.3	97
P4d	3.67	99.8	3.78	0.75	99.8	0.2	94
P5	2.71	98.7	2.69	0.16	98.6	0.4	98
P6	0.89	67.6	0.93	0.21	69.8	9.8	59
P7	0.47	41.2	0.55	0.24	50.1	8.0	33

[a] Compounds **T1**–**T18** served as the parameterization set. [b] "Leave-two-out" cross-validating analysis using 16 compounds from **T1**–**T18** as the parameterization set (all 153 combinations). [c] Calculated ΔG in kcal mol^{-1}. [d] Generated from ΔG at 273 K; *S* enantiomer product. [e] 95% confidence interval. [f] From reactions performed at 273 K. *S* enantiomer product.

analysis (Table 1, "leave-two-out") all combinations of 16 parameterization-set elements from **T1**–**T18** were employed, resulting in 153 different models and 153 sets of predicted ΔG values for catalysts derived from **P1**–**P6**. From these data, 95% confidence intervals for the predicted mean *ee* values were generated.

After these predictions were made, we discovered that Singaram et al. had reported the selectivities for catalysts derived from the limonene derivatives **P2.**[14] We were delighted to find a high degree of correlation between the calculated and reported selectivities. The correlation was good even with the conformationally flexible *n*-butyl compound **P2e**. For **P3**, Nugent provided us with unpublished results (84% *ee*) which agreed very well with the QSSR predictions (single 77% *ee*, mean 82% *ee*).[15] To complete our study we synthesized representative examples of the remaining compounds in pure form using the protocol outlined in Scheme 2 for **P4c** and **P5**.[16] We were excited to find that the experimental values for catalysts derived from **P1c**, **P1d**, **P4c**, **P4d**, **P5**, and **P6** (89, 83, 97, 94, 98, 59% *ee*) were in good accord with our predictions (87, 73, 99, 99, 99, 69% *ee*, respectively)[17] and generally fell within the calculated 95% confidence intervals. Notably, in accord with the calculations, a change from a methyl group (**P1**) to a phenyl group (**P4**) at C1 immediately next to the hydroxy group resulted in a dramatic improvement in enantioselectivity largely independent of the substituents on the nitrogen atom. Also in agreement with the calculations, the isopropenyl (**P2**) and cyclopropyl (**P3**) substitution was found to have little effect on the enantioselectivity (cf. **P1d**, **P2d**, **P3**).

To illustrate that the model provides good predictions for poorly selective as well as moderately and highly selective catalysts, further catalysts were screened computationally. Of those, **P7** was predicted to provide low selectivity (50% *ee*) which was borne out in subsequent experiments (33% *ee*). Overall, the agreement between the experimental values and the predictions for a variety of ligands was very good as illustrated in Figure 3 ($r^2_{\text{pred.}} = 0.87$). Based upon these results, the mixture of **P4c** and **P5** obtained during the ligand synthesis (Scheme 2) was also tested and provided the product with very high selectivity (97% *ee*) as predicted by the model. Thus, the quantum QSSR model guided our discovery of this highly enantioselective catalyst system, which can be prepared in two simple steps from commercial materials.

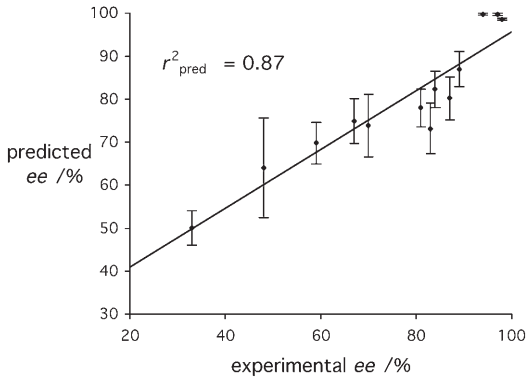
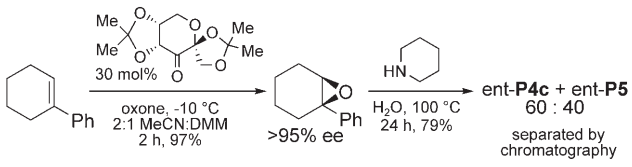


Figure 3. Plot of predicted vs. experimental enantiomeric excesses for catalysts derived from **P1**–**P7**.



Scheme 2. Synthesis of prediction-set β-amino alcohols **P4c** and **P5**. DMM = dimethoxymethane.

Since the initial pioneering theoretical analyses (MP2/6-31G*/Zn//RHF/3-21G/Zn[12] and B3LYP/6-31G*/Zn//RHF/3-21G/Zn[13]) by Yamakawa and Noyori of the asymmetric alkylation of aldehydes, many groups have used various types of transition state calculations employing parameterized force fields (Q2MM[3c]), semiempirical approaches (AM1,[3a] PM3[18]), mixed methods (RHF/LanL2DZ:UFF,[19] RHF/LanL2DZ:MM3[20]), DFT,[21] and post-HF methods (MP2[3b]) to understand or design selective chiral catalysts. Notably, the complexity of the system, the number of relevant structures, and the presence of the zinc atom require considerable computational resources for full ab initio or DFT calculations. For a set of nine catalysts, PM3 performed very well[18] ($r^2_{\text{pred.}} = 0.85$) but was less satisfactory with a more diverse set of catalysts.[19a] Other cases with multiple catalysts that per-

 © 2006 Wiley-VCH Verlag GmbH & Co. KGaA, Weinheim

formed well utilized QM/MM methods[19] ($r^2_{pred.} = 0.43$) and single-point DFT calculations[21] ($r^2_{pred.} = 0.58$). Overall, these calculations were very good in their relative ranking of catalysts and for key transition structure features. The QSSR method identified substituents on the nitrogen atom and on the carbon atom adjacent to the hydroxy group as important to enantioinduction, in agreement with these transition state calculations. In addition, the QSSR method is able to identify other locations at which substitution is advantageous, for example, the distal bridging elements in **T9**–**T13** and the phenyl group in **P5**. Overall, our QSSR method performs as well as or better ($r^2_{pred.} = 0.87$) than other methods, while requiring fewer computational resources since ground states are employed exclusively.

In conclusion, we have shown that grid-based QSSR methods can be used to predict catalyst enantioselectivities with a high degree of accuracy and precision. This method requires knowledge of only the ground state catalyst structure. The empirical models are easily assembled from a small set of ligands and their experimentally measured selectivities such as might be determined in preliminary screening. Relatively quick theoretical calculations provide models that allow a researcher to readily distinguish poorly, moderately, and highly selective catalysts. Within a catalyst series, modifications that result in relatively small changes (i.e., **P2a**–**P2e**) can also be estimated with a good degree of reliability. Studies are underway using this computational method with other reactions, and preliminary results are promising.[22] In addition, the readily prepared catalysts (two steps) that we have discovered are being explored in other transformations.

Received: January 25, 2006

Keywords: asymmetric addition · benzaldehyde · enantioselectivity · structure–activity relationships · zinc

[1] *Comprehensive Asymmetric Catalysis* (Eds.: E. N. Jacobsen, A. Pfaltz, H. Yamamoto), Springer, New York, **1999**.

[2] a) ACS Symposium Series 721*: Transition State Modeling for Catalysis* (Eds.: D. G. Truhlar, K. Morokuma), American Chemical Society, Washington, DC, **1999**; b) S. Niu, M. B. Hall, *Chem. Rev.* **2000**, *100*, 353 – 406.

[3] For the reaction in Scheme 1: designing catalysts using transition state (TS) calculations: a) frozen TS core: A. Vidal-Ferran, A. Moyano, M. A. Pericás, A. Riera, *Tetrahedron Lett.* **1997**, *38*, 8773 – 8776; b) MP2/LanL2DZ//HF/LanL2DZ: M. C. Kozlowski, M. Panda, *J. Org. Chem.* **2003**, *68*, 2061 – 2076. For comments on the complexity of the transition state calculations: c) T. Rasmussen, P.-O. Norrby, *J. Am. Chem. Soc.* **2003**, *125*, 5130 – 5138.

[4] M. C. Kozlowski, S. Dixon, M. Panda, G. Lauri, *J. Am. Chem. Soc.* **2003**, *125*, 6614 – 6615.

[5] For other QSAR applications in enantioselective catalysis see: a) J. D. Oslob, B. Åkermark, P. Helquist, P. O. Norrby, *Organometallics* **1997**, *16*, 3015 – 3021; b) K. B. Lipkowitz, M. J. Pradhan, *J. Org. Chem.* **2003**, *68*, 4648 – 4656; c) S. Alvarez, S. Schefzick, K. Lipkowitz, D. Avnir, *Chem. Eur. J.* **2003**, *9*, 5832 – 5837; d) M. Hoogenraad, G. M. Klaus, N. Elders, S. M. Hooijschuur, B. McKay, A. A. Smith, E. W. Damen, *Tetrahedron: Asymmetry* **2004**, *15*, 519 – 523; e) J. B. van der Linden, E. J. Ras, S. M. Hooijschuur, G. M. Klaus, N. T. Luchters, P. Dani, G. Verspui, A. A. Smith, E. W. P. Damen, B. McKay, M. Hoogenraad, *QSAR Comb. Sci.* **2005**, *24*, 94 – 98; f) S. Sciabola, A. Alex, P. D. Higginson, J. C. Mitchell, M. J. Snowden, I. Morao, *J. Org. Chem.* **2005**, *70*, 9025 – 9027.

[6] Experimental selectivies for **T1**–**T18**: a) M. Kitamura, S. Suga, K. Kawai, R. Noyori, *J. Am. Chem. Soc.* **1986**, *108*, 6071 – 6072; b) L. Pu, H.-B. Yu, *Chem. Rev.* **2001**, *101*, 757, and references therein.

[7] C. T. Goralski, B. Singaram, W. Chrisman, US Patent 6362373B1, **2002**.

[8] a) G. S. Kauffman, G. D. Harris, R. L. Dorow, B. R. P. Stone, R. L. Parsons, Jr., J. A. Pesti, N. A. Magnus, J. M. Fortunak, P. N. Confalone, W. A. Nugent, *Org. Lett.* **2000**, *2*, 3119 – 3121; b) R. L. Parsons, J. M. Fortunak, R. L. Dorow, G. D. Harris, G. S. Kauffman, W. A. Nugent, M. D. Winemiller, T. F. Briggs, B. Xiang, D. B. Collum, *J. Am. Chem. Soc.* **2001**, *123*, 9135 – 9143.

[9] M. Kitamura, S. Okada, S. Suga, R. Noyori, *J. Am. Chem. Soc.* **1989**, *111*, 4028 – 4036.

[10] M. Kitamura, M. Yamakawa, H. Oka, S. Suga, R. Noyori, *Chem. Eur. J.* **1996**, *2*, 1173 – 1181.

[11] With homochiral catalysts, *syn* dimers have been observed experimentally: a) E. Hecht, *Z. Anorg. Allg. Chem.* **2000**, *626*, 2223 – 2227; b) K. Nakano, K. Nozaki, T. Hiyama, *J. Am. Chem. Soc.* **2003**, *125*, 5501 – 5510. With achiral catalysts, *anti* dimers predominate: c) M. R. P. van Vliet, J. T. B. H. Jastrzebski, G. van Koten, K. Vrieze, A. L. Spek, *J. Organomet. Chem.* **1983**, *251*, C17-C21; d) M. R. P. van Vliet, G. van Koten, P. Buysingh, J. T. B. H. Jastrzebski, A. L. Spek, *Organometallics* **1987**, *6*, 537 – 546; e) J. T. B. H. Jastrzebski, J. Boersma, G. van Koten, W. J. J. Smeets, A. L. Spek, *Recl. Trav. Chim. Pays-Bas* **1988**, *107*, 263 – 266; f) M. Kitamura, S. Suga, M. Niwa, R. Noyori, *J. Am. Chem. Soc.* **1995**, *117*, 4832 – 4842.

[12] M. Yamakawa, R. Noyori, *J. Am. Chem. Soc.* **1995**, *117*, 6327 – 6335.

[13] M. Yamakawa, R. Noyori, *Organometallics* **1999**, *18*, 128 – 133.

[14] D. Steiner, S. G. Sethofer, C. T. Goralski, B. Singaram, *Tetrahedron: Asymmetry* **2002**, *13*, 1477 – 1483.

[15] a) W. A. Nugent, personal communication; b) Subsequent to our calculations a report of 81% *ee* for **P3** in this same reaction appeared: S. N. Joshi, S. V. Malhotra, *Tetrahedron: Asymmetry* **2003**, *14*, 1763 – 1766.

[16] See the Supporting Information for further details and full characterization. Epoxidation was accomplished with Shi's protocol (Z. Wang, Y. Tu, M. Frohn, J. Zhang, Y. Shi, *J. Am. Chem. Soc.* **1997**, *119*, 11224 – 11235) and epoxide opening with Singaram's conditions (see reference [14]).

[17] The enantiomers of the predicted catalysts **P1**, **P4**, and **P5** were synthesized and yielded the enantiomer (*R*) opposite to that predicted (*S*).

[18] B. Goldfuss, K. N. Houk, *J. Org. Chem.* **1998**, *63*, 8998 – 9006; C. Jimeno, M. Pastó, A. Riera, M. A. Pericás, *J. Org. Chem.* **2003**, *68*, 3130 – 3138.

[19] a) B. Goldfuss, M. Steigelmann, S. I. Khan, K. N. Houk, *J. Org. Chem.* **2000**, *65*, 77 – 82; b) B. Goldfuss, M. Steigelmann, F. Rominger, *Eur. J. Org. Chem.* **2000**, 1785 – 1792.

[20] J. Vázquez, M. A. Pericás, F. Maseras, A. Lledós, *J. Org. Chem.* **2000**, *65*, 7303 – 7309.

[21] DFT BP86/DN**//PM3 M. Sosa-Rivadeneyra, A. Muñoz-Muñiz, C. Anaya de Parrodi, L. Quintero, E. Juaristi, *J. Org. Chem.* **2003**, *68*, 2369 – 2375.

[22] P.-W. Phuan, J. C. Ianni, M. C. Kozlowski, *J. Am. Chem. Soc.* **2004**, *126*, 15473 – 15479.

 © 2006 Wiley-VCH Verlag GmbH & Co. KGaA, Weinheim

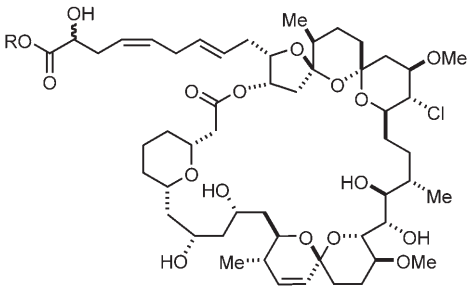
Natural Products (1)

DOI: 10.1002/anie.200601654

Toward the Total Synthesis of Spirastrellolide A. Part 1: Strategic Considerations and Preparation of the Southern Domain**

Alois Fürstner, Michaël D. B. Fenster, Bernhard Fasching, Cédrickx Godbout, and Karin Radkowski*

As part of a program aimed at the discovery of new antimitotic natural products, Andersen and co-workers recently isolated spirastrellolide A (**1**; Scheme 1) from the



1 (R = H)

Scheme 1. One of the 16 possible stereostructures that might represent spirastrellolide A.

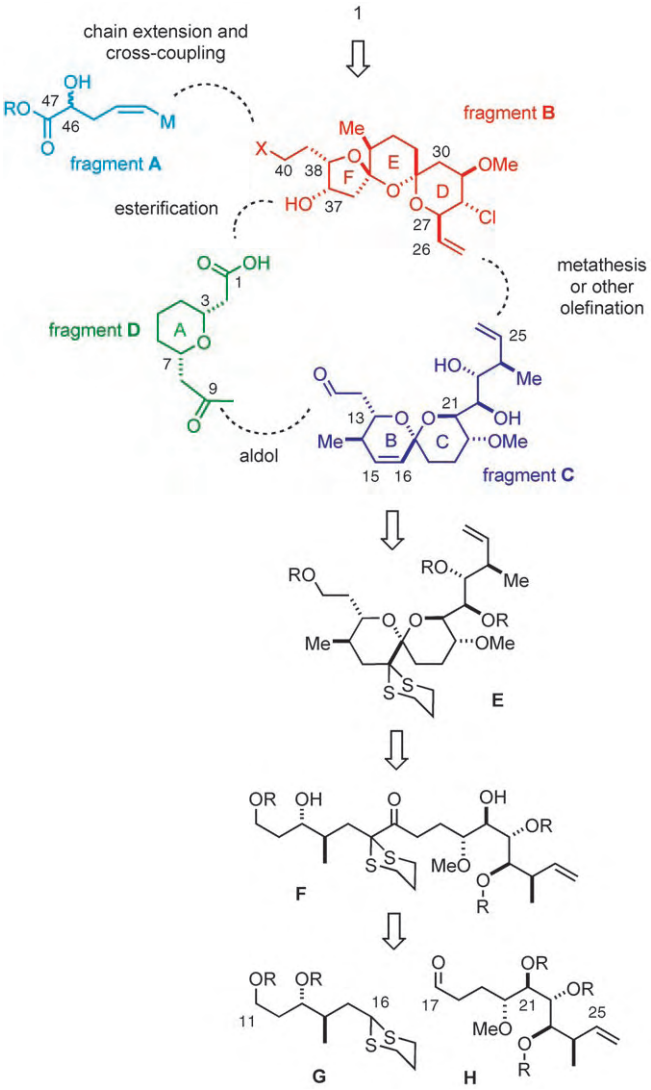
Caribbean sponge *Spirastrella coccinea*.[1] Unlike many other antimitotic macrolides of marine origin, **1** does not affect tubulin polymerization in vitro but was shown to be a very potent ($IC_{50} = 1$ nM) and surprisingly selective inhibitor of protein phosphatase PP2A, with the ability to drive cells directly from the S phase into mitosis before causing cell-cycle arrest.[1,2] In view of the central regulatory role of PP2A, spirastrellolide A represents a potential lead for the development of novel therapeutic agents for the treatment of cancer as well as various neurological and metabolic disorders.[3]

[*] Prof. A. Fürstner, Dr. M. D. B. Fenster, Dipl.-Ing. B. Fasching, Dr. C. Godbout, K. Radkowski
Max-Planck-Institut für Kohlenforschung
45470 Mülheim/Ruhr (Germany)
Fax: (+49) 208-306-2994
E-mail: fuerstner@mpi-muelheim.mpg.de

[**] Generous financial support from the MPG, the Fonds der Chemischen Industrie, the Alexander-von-Humboldt Foundation (fellowship to M.D.B.F.), and the Fonds de Recherche sur la Nature et les Technologies (Québec; fellowship to C.G.) is gratefully acknowledged. We thank Mrs. B. Gabor, Mrs. C. Wirtz, and Dr. R. Mynott for their invaluable help with the structural analysis of several key intermediates.

Supporting information for this article is available on the WWW under http://www.angewandte.org or from the author.

The initial assignment[1] of this intriguing natural product, based on extensive NMR studies of its methyl ester derivative **1a** (R = Me), was corrected shortly after publication.[2] Even the revised structure **1** remains tentative; although it certainly depicts the correct constitution of spirastrellolide A and the proper relative stereochemistry within the individual domains embedded into the complex macrocylic frame, it must be emphasized that the stereochemical relationships between the segments color-coded in Scheme 2 have yet to be determined. Moreover, the absolute stereochemistry of **1** is still unknown.[2]



Scheme 2. Retrosynthetic analysis of spirastrellolide based on disconnections into four stereoclusters of known relative configuration and further analysis of the spiroacetal fragment **C**.

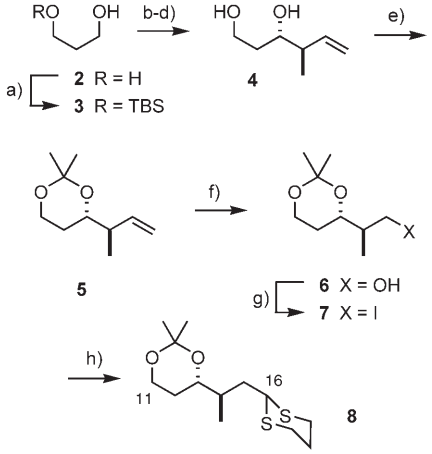
In view of the 16 possible combinations of these stereoclusters, any investigation directed toward this complex natural product, which contains no less than 21 chiral centers, a 38-membered macrolactone, a skipped diene, five pyranose rings, and a tetrahydrofuran moiety which flanks a chlorinated [5,6,6]-bis-spiroacetal entity faces considerable chal-

WILEY InterScience DISCOVER SOMETHING GREAT
© 2006 Wiley-VCH Verlag GmbH & Co. KGaA, Weinheim

lenges.[4] Only a convergent, flexible, and modular approach might eventually be successful; however, any such plot is confined to disconnections at or close to the boundaries of the individual stereoclusters as long as the internal relationship between them has not been established. This notion is reflected in our global retrosynthetic plan depicted in Scheme 2, which envisages cross-coupling, metathesis[5] (or alternative alkene formations), aldol, and esterification transformations for the deconvolution of the target into fragments **A**–**D**. Outlined below is our approach to the fully functional southern C1–C25 domain of spirastrellolide A, whereas the accompanying Communication reports the conquest of the complementary northern hemisphere.[6]

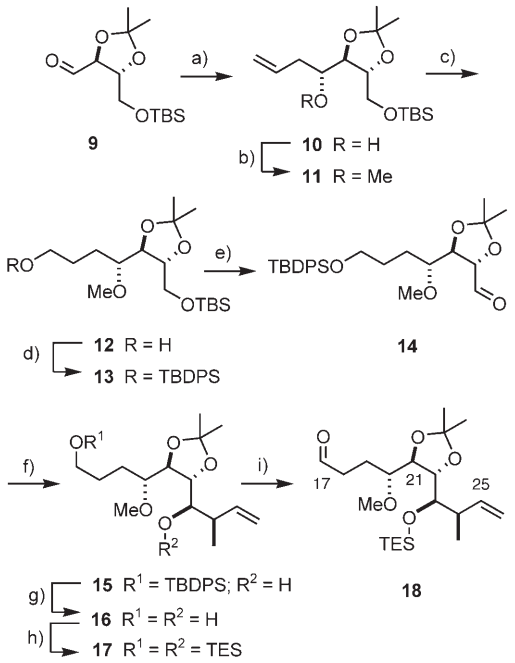
As indicated in Scheme 2, the preparation of the spiroketal segment **C** envisaged a thermodynamic acetalization of a dihydroxyketone precursor **F**. Although it was tempting to have the *Z* alkene at C15/C16 in place at that stage, we opted against this possibility for strategic reasons;[7] rather, we chose to encode this future olefin as a protected carbonyl group (**E**), which in turn facilitates the assembly of the carbon backbone of the spirocyclization precursor **F** from segments **G** and **H**.

To this end, preparation of the required dithiane commenced with monoprotection of 1,3-propanediol **2** followed by oxidation of the resulting product **3** to the corresponding aldehyde (Scheme 3). Brown crotylation[8] and deprotection of the TBS group then gave the known diol **4**[9] (93% *ee*), which was elaborated into acetonide **5** prior to ozonolysis of the double bond followed by reductive work-up with excess $NaBH_4$. The resulting alcohol **6** was converted into iodide **7**, which could be alkylated with lithio-1,3-dithiane at low temperature. To obtain high yields, however, syringe-pump addition of **7** was necessary to minimize elimination of HI. Under these conditions, the route summarized in Scheme 3 was amenable to scale-up and afforded multigram quantities of **8** in high overall yield.



Scheme 3. Preparation of the required dithiane unit. Reagents and conditions: a) TBSCl, Et_3N, CH_2Cl_2 (97%); b) SO_3·pyridine, DMSO, Et_3N, CH_2Cl_2, −78→0°C (95%); c) (+)-[(*E*)-crotyl]B(ipc)$_2$, THF, −78°C (80%; 93% *ee*); d) TBAF, THF (94%); e) 2,2-dimethoxypropane, CSA cat., acetone, MS 4 Å (92%); f) O_3, CH_2Cl_2/MeOH, −78°C, then $NaBH_4$, RT (97%); g) I_2, PPh_3, imidazole, THF, 0°C (97%); h) 1,3-dithiane, *t*BuLi, −78°C, THF/DMPU (10% v/v; 91%). CSA = camphorsulfonic acid, DMPU = 1,3-dimethyl-3,4,5,6-tetrahydro-2(1*H*)-pyrimidinone, DMSO = dimethyl sulfoxide, IPC = isopinocampheyl, MS = molecular sieves, TBS = *tert*-butyldimethylsilyl.

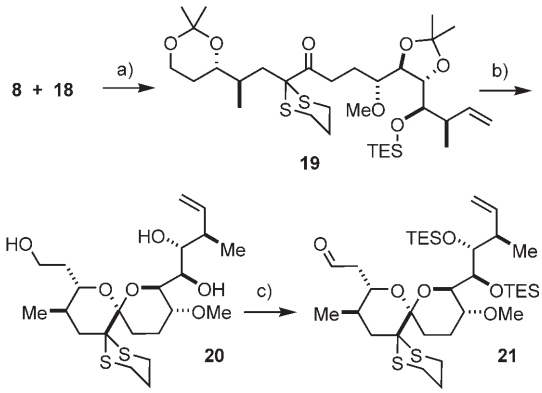
The tartrate-derived aldehyde **9**[10] served as a convenient starting material for the preparation of the C17–C25(26) segment through a "two-directional" synthetic strategy (Scheme 4).[11] A reagent-controlled allylation set the *R* configured secondary alcohol that resides at C20; of the many procedures surveyed, we settled on the classical Brown protocol,[12] which was the only method that reliably gave **10** as a single diastereomer in consistently high yields of up to 81% on a 20-g scale. The symmetry-related chain extension at the C23 terminus of aldehyde **14** derived from **10** by standard protecting-group and oxidation-state management was analogously performed by Brown crotylation,[8] which was once more superior to alternative procedures in terms of scalability and stereoinduction. The terminal TBDPS ether in product **15** thus formed was then cleaved with TBAF; however, all attempts at a selective oxidation of the primary alcohol in the resulting diol **16** remained unsuccessful. Therefore, **16** was bis-silylated with TESCl/imidazole to give **17**, which served as the substrate for a subsequent oxidation with PDC, which nicely remedied the selectivity issue, thus converting only the primary TES ether into the desired aldehyde. Overall, this unambiguous route establishes the challenging stereopentad that extends from C20–C24 and was successful in providing multigram amounts of building block **18**.



Scheme 4. Preparation of the C17–C25(26) segment through a "two-directional" synthetic strategy. Reagents and conditions: a) (+)-Ipc$_2$B-(allyl), Et_2O, −100°C (81%); b) NaH, MeI, THF; c) BH_3·THF, THF, then H_2O_2; d) TBDPSCl, imidazole, CH_2Cl_2 (78%; 3 steps); e) 1. CSA cat., MeOH; 2. SO_3·pyridine, Et_3N, DMSO, CH_2Cl_2; f) (+)-[(*E*)-crotyl]B-(ipc)$_2$, THF, −78°C (56%; 3 steps); g) TBAF, THF; h) TESCl, imidazole, CH_2Cl_2; i) PDC, CH_2Cl_2, 0°C→RT (80%; 3 steps). TBAF = tetra-*n*-butylammonium fluoride, TBDPSCl = *tert*-butyldiphenylsilyl chloride, TES = triethylsilyl, PDC = pyridinium dichromate.

 © 2006 Wiley-VCH Verlag GmbH & Co. KGaA, Weinheim

Envisaging the use of the dithiane ring as a linchpin, **8** was deprotonated with the aid of a mixed organometallic reagent formed from *n*BuLi and $(n\text{Bu})_2\text{Mg}$ in THF.[13] The addition of aldehyde **18** to the resulting anion followed by a Dess–Martin oxidation[14] furnished ketone **19** (Scheme 5). Gratifyingly,

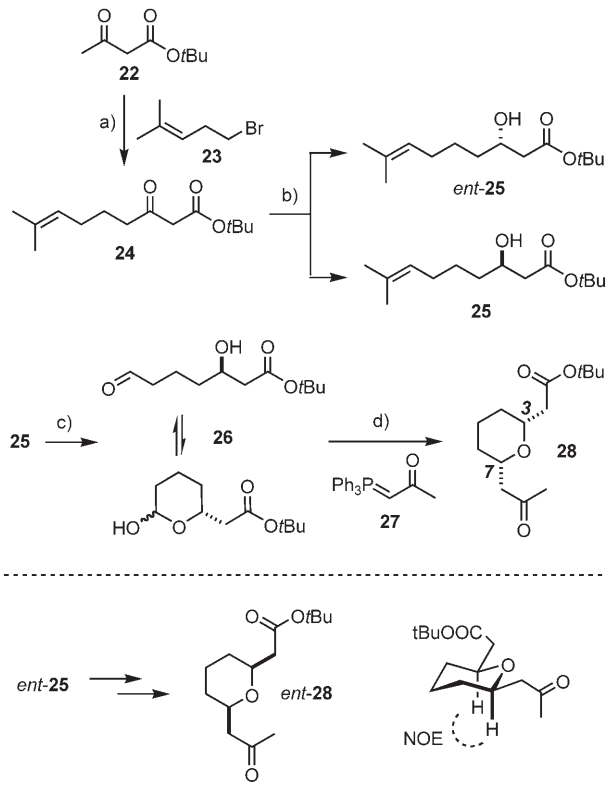


Scheme 5. Preparation of the polyfunctional fragment **21**. Reagents and conditions: a) 1. *n*BuLi/$(n\text{Bu})_2\text{Mg}$ (4:1), THF, RT, then aldehyde **18**, −78 °C; 2. Dess–Martin periodinane, CH_2Cl_2 (69%; 2 steps); b) PTSA (1 equiv), MeOH (87%); c) 1. TESOTf, 2,6-lutidine, CH_2Cl_2; 2. DMSO, $(COCl)_2$, Et_3N, CH_2Cl_2, −40 °C (96%; 2 steps). OTf = triflate, PTSA = *p*-toluenesulfonic acid.

treatment of this compound with PTSA in MeOH engendered cleavage of the isopropylidene acetals followed by spontaneous formation of spiroacetal **20**, which was obtained as a single diastereomer in 87% yield of the isolated product. Extensive 1D and 2D NMR spectroscopic investigations unequivocally established the constitution and stereochemistry of this intricate product, which could be elaborated into aldehyde **21** by the convenient persilylation/selective monooxidation tandem process mentioned above. In this particular case, recourse to Swern oxidation[15] proved optimal, thus delivering the polyfunctional fragment **21** in virtually quantitative yield.

The synthesis of the tetrahydropyran fragment **D** relied on an asymmetric hydrogenation followed by an intramolecular Michael addition to set the two stereocenters at C3 and C7 (Scheme 6). Weiler dianion alkylation[16] of **22** with bromide **23** was followed by a Noyori reduction of the resulting ketoester **24**,[17] which had to be performed in the presence of a catalytic amount of HCl at moderate temperature and hydrogen pressure (5 bar, 40 °C).[18,19] Under these conditions, product **25** was obtained in an almost quantitative yield and excellent optical purity (≥98% *ee*), without any hydrogenation of the trisubstituted olefin or cleavage of the *tert*-butyl ester interfering.

Ozonolysis of the alkene group in **25** and reaction of aldehyde **26** thus formed with the stabilized ylide **27** followed by exposure of the resulting enone to catalytic amounts of CSA in CH_2Cl_2 afforded the Michael addition product **28** in 78% yield over three steps. Compound **28** was readily separated from its C7 isomer (d.r. = 8.5:1), which could be re-equilibrated to give a second crop of **28**. Apprehensive that a similar acid-catalyzed retro-Michael/Michael manifold at

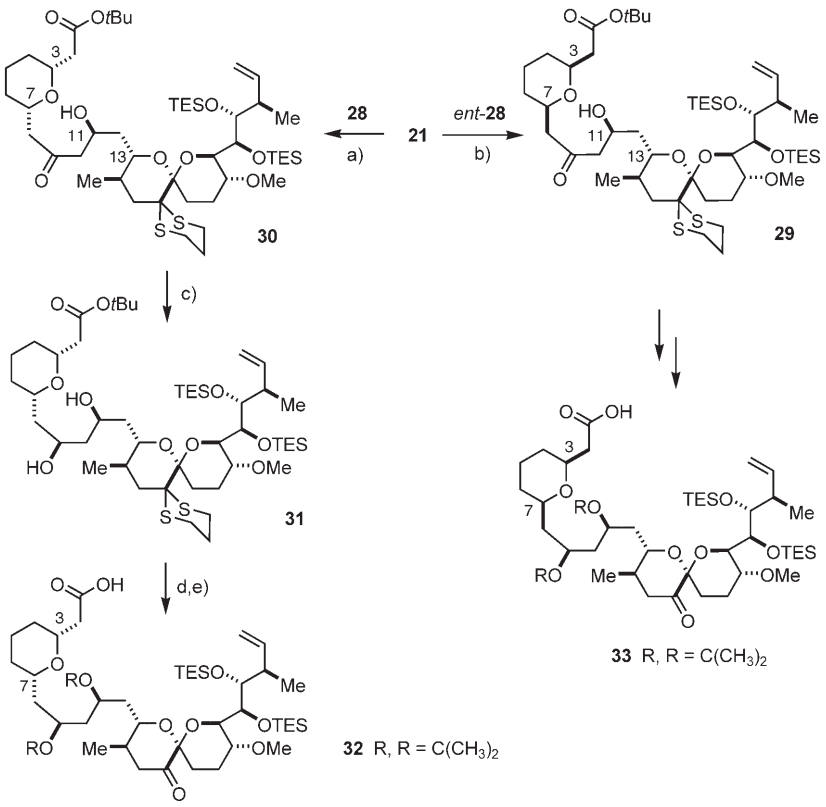


Scheme 6. Preparation of segment **D**. Reagents and conditions: a) NaH, *n*BuLi, then bromide **23**, THF/HMPA (81%); b) $[RuCl_2(\text{binap})]_2{\cdot}NEt_3$ (1 mol%), HCl (2 mol%), H_2 (5 bar), MeOH, 40 °C (95%; 98% *ee*); c) O_3, MeOH, then Me_2S, −78 °C → RT; d) 1. ylide **27**, toluene, reflux; 2. CSA cat., CH_2Cl_2 (78%; 3 steps; d.r. = 8.5:1). binap = (1,1′-binaphthalene)-2,2′-diylbis(diphenylphosphine), HMPA = hexamethyl phosphoramide.

the "ester end" of **28** would engender an erosion in the optical purity of this building block, the enantiomeric excess of **28** was carefully checked but found to be unaltered (98% ee, determined by HPLC). Moreover, the *cis* relationship between C3 and C7 was confirmed by NOE interaction experiments (Scheme 6). Repeating this route with (*S*)-BINAP rather than (*R*)-BINAP as the ligand during the β-ketoester reduction also provided us with multigram quantities of *ent*-**28** in a respectable 60% yield over four readily scalable operations.

Stereoselective aldol reactions of either enantiomer with aldehyde **21** established the required 1,3-*anti* relationship between C13 and C11, as found in the natural product (Scheme 7). Satisfactory solutions for this critical segment coupling were secured when isomer *ent*-**28** was treated with **21** under modified Mukaiyama conditions[20] with $BF_3{\cdot}Et_2O$ as the optimal promoter. $BF_3{\cdot}Et_2O$ should be added slowly to the reaction mixture to avoid complications with the acid-sensitive groups in both reaction partners. This reliable protocol afforded product **29** in 62% yield as a single isomer. In contrast, the reaction that employed the enantiomeric ketone **28** was carried out using the boron–enolate methodology,[21] thus delivering the diastereomeric *anti*-aldol **30** together with its separable C11 isomer in 94% yield of the combined products and a diastereomeric ratio of 4:1.[22]

 © 2006 Wiley-VCH Verlag GmbH & Co. KGaA, Weinheim



Scheme 7. Preparation of two possible diastereomers of the southern hemisphere of spirastrellolide A. Reagents and conditions: a) Cy_2BCl, $(iPr)_2NEt$, CH_2Cl_2, −78 °C (94%; d.r. = 4:1); b) TMSOTf, $(iPr)_2NEt$, CH_2Cl_2, then $BF_3{\cdot}Et_2O$, −78 °C (62%); c) $Me_4NBH(OAc)_3$, MeCN, HOAc, −25 → 0 °C (85%); d) $(CH_3)_2C(OMe)_2$, acetone, PPTS cat. (87%); e) 1. dibal-H, CH_2Cl_2, −78 °C; 2. $NaClO_2$, NaH_2PO_4, 2-methyl-2-butene, *t*BuOH/H_2O (69%; 2 steps). Cy = cyclohexyl, dibal-H = diisobutylaluminum hydride, PPTS = pyridinium *p*-toluenesulfonate, TMS = trimethylsilyl.

The major products of either series were then subjected to a 1,3-*anti* reduction with $Me_4NHB(OAc)_3$ to set the proper stereochemistry at C9 (**30** → **31**),[23] followed by acetonide formation and conversion of the ester terminus into the required acid function by reduction/oxidation (Scheme 7). Not unexpectedly,[24] the dithiane moiety in **31** was concomitantly cleaved by the excess of $NaClO_2$ used in the latter step. This practical maneuver afforded product **32**, which constitutes the properly functionalized southern domain of **1**, in high overall yield. The equally conceivable isomer **33**, characterized by a different internal stereochemical relationship between the A ring and the BC stereocluster, was formed analogously from aldol **29**. Detailed spectroscopic analyses confirmed the structures of these advanced compounds, with the NOE interaction patterns and the acetal resonances in the ^{13}C NMR spectra being particularly diagnostic.[22,25]

In summary, we have devised a concise, efficient, and scalable route to the southern C1–C25 domain of spirastrellolide A (**1**), which was prepared in two possible stereochemical formats. Together with the conquest of the northern hemisphere reported in the accompanying Communication,[6] we are now in a position to tackle the final assembly of this intricate natural product with the hope of unraveling its stereostructure by total synthesis of various conceivable isomers. Progress along these lines will be reported in due course.

Received: April 26, 2006
Published online: July 5, 2006

Keywords: antitumor agents · macrolides · natural products · phosphatase inhibitors · total synthesis

[1] D. E. Williams, M. Roberge, R. Van Soest, R. J. Andersen, *J. Am. Chem. Soc.* **2003**, *125*, 5296 – 5297.
[2] D. E. Williams, M. Lapawa, X. Feng, T. Tarling, M. Roberge, R. J. Andersen, *Org. Lett.* **2004**, *6*, 2607 – 2610.
[3] Recent reviews on phosphatases as targets for medicinal chemistry: a) L. Bialy, H. Waldmann, *Angew. Chem.* **2005**, *117*, 3880 – 3906; *Angew. Chem. Int. Ed.* **2005**, *44*, 3814 – 3839; b) A. McCluskey, A. T. R. Sim, J. A. Sakoff, *J. Med. Chem.* **2002**, *45*, 1151 – 1175; c) R. E. Honkanen, T. Golden, *Curr. Med. Chem.* **2002**, *9*, 2055 – 2075.
[4] For studies toward **1** reported by other groups, see: a) I. Paterson, E. A. Anderson, S. M. Dalby, O. Loiseleur, *Org. Lett.* **2005**, *7*, 4121 – 4224; b) I. Paterson, E. A. Anderson, S. M. Dalby, O. Loiseleur, *Org. Lett.* **2005**, *7*, 4125 – 4128; c) J. Liu, R. P. Hsung, *Org. Lett.* **2005**, *7*, 2273 – 2276; d) Y. Pan, J. K. De Brabander, *Synlett* **2006**, 853 – 856; e) for an approach toward the originally proposed structure, see: I. Paterson, E. A. Anderson, S. M. Dalby, *Synthesis* **2005**, 3225 – 3228.
[5] a) T. M. Trnka, R. H. Grubbs, *Acc. Chem. Res.* **2001**, *34*, 18 – 29; b) A. Fürstner, *Angew. Chem.* **2000**, *112*, 3140 – 3172; *Angew. Chem. Int. Ed.* **2000**, *39*, 3012 – 3043.
[6] A. Fürstner, M. D. B. Fenster, B. Fasching, C. Godbout, K. Radkowski, *Angew. Chem.* **2006**, *118*, 5636 – 5641; *Angew. Chem. Int. Ed.* **2006**, *45*, 5510 – 5515.
[7] Note that a late-stage fragment coupling between the northern and the southern domain at C25/C26 by metathesis (or other suitable olefination reactions) is envisaged (cf. Scheme 2); a selective hydrogenation of this newly formed alkene in the presence of a pre-existing *Z* olefin at C15/C16 might raise serious selectivity issues.
[8] H. C. Brown, K. S. Bhat, *J. Am. Chem. Soc.* **1986**, *108*, 293 – 294.
[9] U. P. Dhokte, V. V. Khau, D. R. Hutchison, M. J. Martinelli, *Tetrahedron Lett.* **1998**, *39*, 8771 – 8774.
[10] H. Iida, N. Yamazaki, C. Kibayashi, *J. Org. Chem.* **1987**, *52*, 3337 – 3342.
[11] a) C. S. Poss, S. L. Schreiber, *Acc. Chem. Res.* **1994**, *27*, 9 – 17; b) for an example from our group, see: A. Fürstner, M. Albert, J. Mlynarski, M. Matheu, E. DeClercq, *J. Am. Chem. Soc.* **2003**, *125*, 13132 – 13142.
[12] a) U. S. Racherla, H. C. Brown, *J. Org. Chem.* **1991**, *56*, 401 – 404; b) U. S. Racherla, Y. Liao, H. C. Brown, *J. Org. Chem.* **1992**, *57*, 6614 – 6617; c) H. C. Brown, P. K. Jadhav, *J. Am. Chem. Soc.* **1983**, *105*, 2092 – 2093.
[13] a) M. Ide, M. Nakata, *Bull. Chem. Soc. Jpn.* **1999**, *72*, 2491 – 2499; b) reviews: D. Seebach, *Synthesis* **1969**, 17 – 36; c) M. Yus, C. Nájera, F. Foubelo, *Tetrahedron* **2003**, *59*, 6147 – 6212; d) A. B.

 © 2006 Wiley-VCH Verlag GmbH & Co. KGaA, Weinheim

Smith, S. M. Condon, J. A. McCauley, *Acc. Chem. Res.* **1998**, *31*, 35 – 46.
[14] S. D. Meyer, S. L. Schreiber, *J. Org. Chem.* **1994**, *59*, 7549 – 7552.
[15] A. J. Mancuso, D. Swern, *Synthesis* **1981**, 165 – 185.
[16] a) L. Weiler, *J. Am. Chem. Soc.* **1970**, *92*, 6702 – 6704; b) S. N. Huckin, L. Weiler, *J. Am. Chem. Soc.* **1974**, *96*, 1082 – 1087.
[17] R. Noyori, T. Okhuma, M. Kitamura, H. Takaya, N. Sayo, H. Kumobayashi, S. Akutagawa, *J. Am. Chem. Soc.* **1987**, *109*, 5856 – 5858.
[18] a) S. A. King, A. S. Thompson, A. O. King, T. R. Verhoeven, *J. Org. Chem.* **1992**, *57*, 6689 – 6691; b) A. Fürstner, T. Dierkes, O. R. Thiel, G. Blanda, *Chem. Eur. J.* **2001**, *7*, 5286 – 5298, and references therein.
[19] Review: T. Ohkuma, R. Noyori in *Comprehensive Asymmetric Catalysis*, *Vol. 1* (Eds.: E. N. Jacobsen, A. Pfaltz, H. Yamamoto), Springer, Berlin, **1999**, pp. 199 – 246.
[20] a) D. A. Evans, M. J. Dart, J. L. Duffy, M. G. Yang, *J. Am. Chem. Soc.* **1996**, *118*, 4322 – 4343; b) review: T. Mukaiyama, *Org. React.* **1982**, *28*, 203 – 331.
[21] For pertinent examples of 1,5-*anti* stereoinduction in boron aldol chemistry as required in the present case, see: a) D. A. Evans, B. Côté, P. J. Coleman, B. T. Connell, *J. Am. Chem. Soc.* **2003**, *125*, 10893 – 10898; b) D. A. Evans, P. J. Coleman, B. Coté, *J. Org. Chem.* **1997**, *62*, 788 – 789; c) I. Paterson, K. R. Gibson, R. M. Oballa, *Tetrahedron Lett.* **1996**, *37*, 8585 – 8588; d) for examples using β-tetrahydropyranyl methyl ketones, see: D. A. Evans, D. M. Fitch, T. E. Smith, V. J. Cee, *J. Am. Chem. Soc.* **2000**, *122*, 10033 – 10046; e) M. T. Crimmins, P. Siliphaivanh, *Org. Lett.* **2003**, *5*, 4641 – 4644; f) S. A. Kozmin, *Org. Lett.* **2001**, *3*, 755 – 758.
[22] A series of control experiments and detailed analyses of the Mosher esters confirmed the proposed stereochemical assignments; details will be reported in a forthcoming report.
[23] D. A. Evans, K. T. Chapman, E. M. Carreira, *J. Am. Chem. Soc.* **1988**, *110*, 3560 – 3578.
[24] T. Ichige, A. Miyake, N. Kanoh, M. Nakata, *Synlett* **2004**, 1686 – 1690.
[25] Comparison of the NMR data of the individual isomers (see the Supporting Information) with the reported data of **1**, however, do not allow us to decide which relative configuration is present in the natural product.

 © 2006 Wiley-VCH Verlag GmbH & Co. KGaA, Weinheim

Natural Products (2)

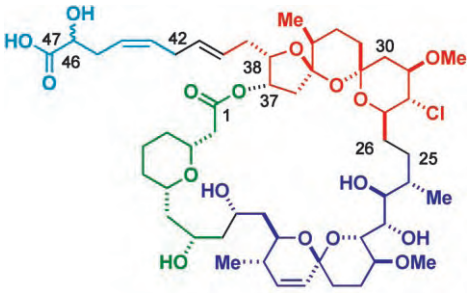
DOI: 10.1002/anie.200601655

Toward the Total Synthesis of Spirastrellolide A. Part 2: Conquest of the Northern Hemisphere**

Alois Fürstner, Michaël D. B. Fenster, Bernhard Fasching, Cédrickx Godbout, and Karin Radkowski*

The novel antimitotic agent spirastrellolide A (**1**), isolated from the Caribbean sponge *Spirastrella coccinea*, is endowed with potent and selective phosphatase inhibitory properties.[1] Although the relative stereochemistry of each individual domain embedded into the macrocyclic frame of this marine natural product has been elucidated by spectroscopic means, the relationship between these stereoclusters remains elusive and the absolute configuration of **1** is equally unknown.[1] Scheme 1 therefore depicts only one of 16 possible isomers that might represent the correct stereostructure of spirastrellolide A.

Intrigued by the exquisite structural complexity of this macrolide and the prospect of contributing to a synthesis-driven mapping of its promising biological profile,[2] we



1

Scheme 1. One of the 16 possible stereostructures that might represent spirastrellolide A. Note that the relative stereochemistry within the color-coded segments has been established, whereas the stereochemical relationship between any pair of them is still unknown.

[*] Prof. A. Fürstner, Dr. M. D. B. Fenster, Dipl.-Ing. B. Fasching, Dr. C. Godbout, K. Radkowski
Max-Planck-Institut für Kohlenforschung
45470 Mülheim/Ruhr (Germany)
Fax: (+49) 208-306-2994
E-mail: fuerstner@mpi-muelheim.mpg.de

[**] Generous financial support from the MPG, the Fonds der Chemischen Industrie, the Alexander-von-Humboldt Foundation (fellowship to M.D.B.F.), and the Fonds de Recherche sur la Nature et les Technologies (Québec; fellowship to C.G.) is gratefully acknowledged. We thank Mrs B. Gabor, Mrs C. Wirtz, and Dr. R. Mynott for their invaluable help with the structural analysis of several key intermediates.

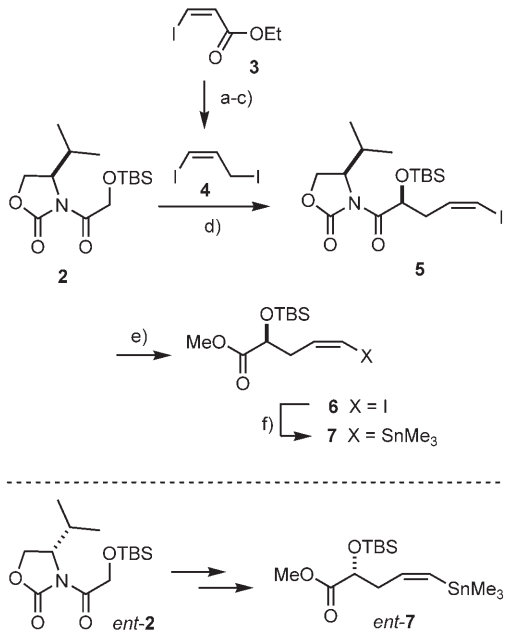
Supporting information for this article is available on the WWW under http://www.angewandte.org or from the author.

WILEY InterScience DISCOVER SOMETHING GREAT
© 2006 Wiley-VCH Verlag GmbH & Co. KGaA, Weinheim

embarked on a program aimed at the development of a flexible access route that must allow the unsolved stereochemical issues to be addressed in an unambiguous yet concise fashion. The preceding Communication outlines the overall strategy and reports the conquest of the southern hemisphere, which extends from C1 to C25 in a fully functional form.[3] Outlined below is the preparation of the complementary northern domain, which consists of the intricate chlorinated [5,6,6]-bis-spiroacetal entity and the lateral chain bearing the remote C46 chiral center of unknown configuration.[4]

In view of the potentially labile character of the skipped *E*,*Z* diene unit, it seems advisable to attach the side chain to the macrocyclic core only in the final stages of the envisaged total synthesis by a methodology that is likely compatible with the displayed array of functional groups. As palladium-catalyzed C–C bond formations should qualify for this purpose, the side-chain surrogate (fragment **A**) was designed as a vinyl stannane amenable to cross-coupling with retention of its *Z* configured double bond.

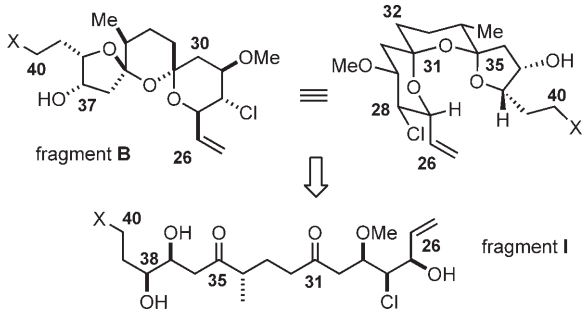
The enantioselective synthesis of **A** was based on the glycolate allylation methodology concurrently reported by Danishefsky and Crimmins (Scheme 2).[5] In the event, allylation of the sodium enolate derived from **2** with the bifunctional reagent **4**[6] effectively delivered compound **5** as a single diastereomer. Removal of the auxiliary furnished methyl ester **6** (> 99 % *ee*) in good yield,[7] which was transformed into stannane **7** by a palladium-catalyzed reaction with hexamethylditin in the presence of the Hünig base.[8]



Scheme 2. Enantioselective synthesis of fragment **A**. Reagents and conditions: a) dibal-H, THF, −78→0 °C (68 %); b) MsCl, Et_3N, CH_2Cl_2, −78 °C→RT; c) $(nBu)_4NI$, acetone (83 %; 2 steps); d) NaHMDS, THF, then iodide **4**, −78→−45 °C (87 %); e) MeOMgBr, MeOH/CH_2Cl_2, 50 °C (73 %); f) Me_6Sn_2, $[Pd(PPh_3)_4]$ (4.5 mol %), $(iPr)_2NEt$ (30 mol %), benzene, reflux (78 %). dibal-H = diisobutyl aluminium hydride, MsCl = methanesulfonyl chloride, NaHMDS = sodium hexamethyldisilazide, TBS = *tert*-butyldimethylsilyl.

This route allowed the convenient preparation of either enantiomer of **A** in multigram quantities from commercially available starting materials.

Inspection of the conspicuous bis-spiroacetal motif[9] embedded into the C26–C40 backbone of spirastrellolide A (fragment **B**) suggests that a thermodynamically controlled cyclization of a suitable acyclic precursor of type **I** should be productive as a result of the reigning double anomeric effect and the all-equatorial disposition of the substituents displayed on this particular structural motif (Scheme 3). Despite such a seemingly favorable arrangement, however, the preparation of this intriguing substructure posed significant challenges that could only be mastered after we had acquired intelligence on its chemical disposition.

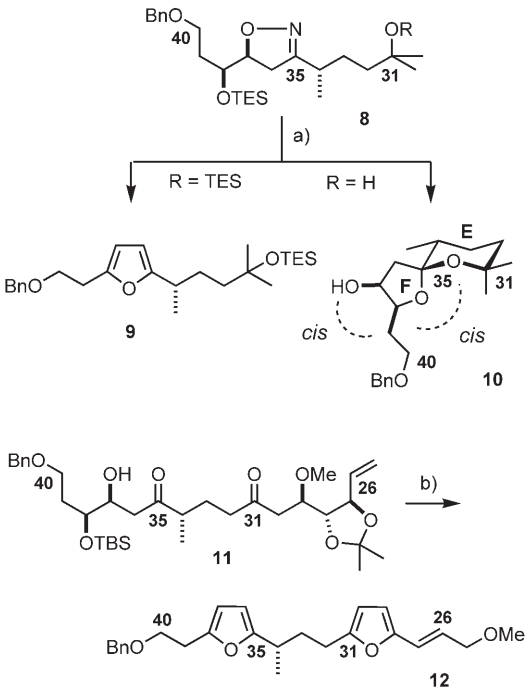


Scheme 3. Unfolding of the [5,6,6]-bis-sprioacetalic entity **B** into a linear precursor **I**; for the segment numbering see Ref. [3].

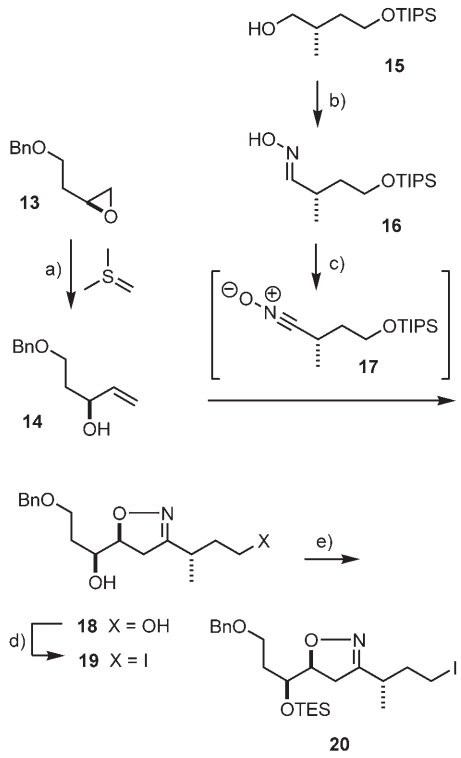
Although a detailed report on our model studies must await a forthcoming full paper, the results summarized in Scheme 4 are representative and illustrate some key observations that provided valuable guidance for the development of the successful route. Specifically, cleavage of the N–O bond in isoxazoline **8a** (R = TES)[10] with $[Mo(CO)_6]$[11] followed by attempted acetalization of the released hydroxy ketone resulted in exclusive aromatization with formation of furan **9**, even though exceptionally mild conditions were chosen. In stark contrast, however, the model gains validity if the seemingly labile TES ether protecting the tertiary alcohol at C31 is removed prior to cyclization. Under identical conditions, the reaction of **8b** (R = H) now delivers the truncated C31–C40 spirocycle **10** in an unoptimized yield of 51 %. The much more elaborate model **11**[10] is similarly instructive: treatment of this particular spirocyclization precursor bearing hydroxy groups yet to be liberated from the isopropylidene acetals with an assortment of Lewis or Bronsted acids under different experimental conditions invariably led to a complex mixture, with the bisfuran **12** being the only product that could be identified.

These results advocate the notion that a free hydroxy group at C31 must be ready to lock the incipient tetrahydrofuran ring; otherwise, aromatization, which is thought to be driven by the release of transannular strain caused by the all-*cis* orientation of the substituents on the five-membered ring (cf. compound **10**), will prevail. Therefore, it is likely that proper phasing of protecting-group cleavage versus acetal formation will be decisive for the success of the synthesis,

 © 2006 Wiley-VCH Verlag GmbH & Co. KGaA, Weinheim



Scheme 4. Model studies concerning the bis-spiroacetal segment. Reagents and conditions: a) 1. $[Mo(CO)_6]$, MeCN/H_2O (5:1), 90 °C; 2. SiO_2 (**9**: 66 %; **10**: 51 %); b) catalytic amounts of CSA, PTSA, TMSOTf, aq. HCl, or $FeCl_3/SiO_2$, in MeOH, acetone, or CH_2Cl_2 (**12**: 5–35 %, see the text). CSA = camphorsulfonic acid, PTSA = *p*-toluenesulfonic acid, TMSOTf = trimethylsilyl triflate.



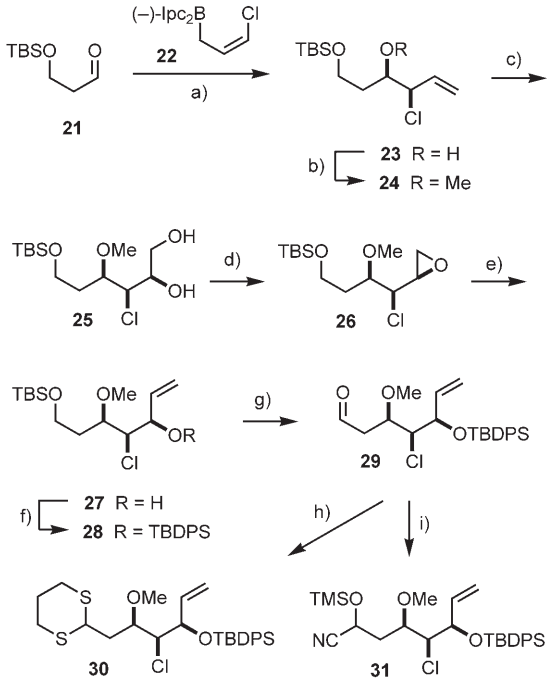
Scheme 5. Preparation of the C32–C40 segment. Reagents and conditions: a) $Me_3S^+ I^-$, *n*BuLi, THF, −10 °C→RT (84 %); b) 1. TPAP, NMO, CH_2Cl_2, MS 4 Å; 2. hydroxyamine hydrochloride, Et_3N, EtOH (78 %; 2 steps); c) 1. *t*BuOCl, −78 °C, CH_2Cl_2, then alkene **14**, EtMgBr, *i*PrOH; 2. TBAF, THF (76 %; 2 steps); d) I_2, imidazole, PPh_3, THF (83 %); e) TESOTf, 2,6-lutidine, THF (92 %). MS = molecular sieves, NMO = *N*-methyl-morpholine-*N*-oxide, TBAF = tetra-*n*-butylammonium fluoride, TES = triethylsilyl, TIPS = triisopropylsilyl, TPAP = tetra-*n*-propylammonium perruthenate.

whereas extensive equilibration must be avoided during attempted spirocyclization. Hence, we concluded that the synthesis of the northern hemisphere should not rely on thermodynamic but rather kinetic control.

In response to this analysis, the convergent route to the cyclization precursor summarized in Schemes 5–8 was designed. Thus, transformation of the known alcohol **15**[12] to oxime **16** followed by exposure to *t*BuOCl[13] at low temperature gave nitrile oxide **17** (Scheme 5), which underwent a smooth 1,3-dipolar cycloaddition[14] with the magnesium salt of alcohol **14** under conditions originally described by Kanemasa et al.[15] The required olefin **14** was conveniently prepared in enantiopure form by hydrolytic kinetic resolution[16] of *rac*-**13** followed by reaction of the resulting optically pure epoxide (*S*)-**13** with dimethylsulfonium methylide.[17] The outcome of the cycloaddition reaction developed by Kanemasa et al.[15] was highly rewarding, thus exclusively furnishing the *syn*-configured 2-isoxazoline **18** in 76 % yield on a multigram scale after fluoride-induced cleavage of the terminal TIPS ether to facilitate purification. Regioselective conversion of the primary hydroxy group in **18** into the corresponding iodide **19** followed by silylation of the remaining secondary alcohol provided the suitably protected C32–C40 surrogate **20** in excellent overall yield. As mentioned above, all steps that led to this valuable building block were scalable and are therefore considered highly adequate.

The preparation of the required coupling partner (Scheme 6) commenced with an asymmetric chloroallylation of aldehyde **21**, a variant of Brown's reliable method developed by Oehlschlager and co-workers.[18] The reaction afforded chlorohydrine **23** in good yield with virtually quantitative *syn* selectivity and respectable optical purity (93 % *ee*) and could be performed on a > 11-g scale, provided that the reagent **22** was generated from freshly prepared (−)-$(ipc)_2$BOMe (icp = isopinocampheyl).[19] Methylation of alcohol **23** followed by asymmetric dihydroxylation[20] of the resulting product **24** gave diol **25**[4] in 73 % yield over both steps. Compound **25** was then converted into epoxide **26** by reaction with tosyl chloride and treatment of the resulting crude sulfonate with K_2CO_3 in MeOH. As in the case of **13** described above, homologation of this epoxide with dimethylsulfonium methylide in THF led to the desired allylic alcohol **27** in 92 % yield, thus attesting to the excellent application profile of this valuable transformation.[17] This particular example is quite challenging because the alkoxide primarily formed upon opening of the oxirane by the nucleophile can undergo an intramolecular nucleophilic substitution of the adjacent chlorine center with formation of a new epoxide ring. This undesirable pathway, however, could be suppressed by using an excess of the sulfur ylide and quenching of the mixture at low temperature after a reaction time of only 10 minutes. Attachment of a TBDPS group to the allylic alcohol in **27**, removal of the more labile primary TBS

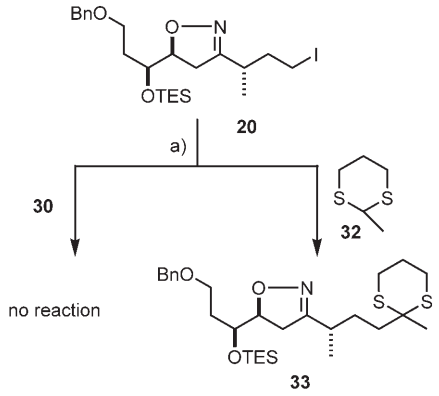
 © 2006 Wiley-VCH Verlag GmbH & Co. KGaA, Weinheim



Scheme 6. Preparation of the C26(25)–C31 segment. Reagents and conditions: a) Et_2O, −78 °C (85%; 93% *ee*); b) Me_3OBF_4, proton sponge (86%); c) [OsO_4] (1 mol%). $K_3Fe(CN)_6$, $(DHQ)_2Pyr$ (2.5 mol%), *t*BuOH/H_2O (85%); d) 1. tosyl chloride, pyridine; 2. K_2CO_3, MeOH (73%; 2 steps); e) $Me_3S^+ I^-$, *n*BuLi, THF, 0 °C (92%); f) TBDPSCl, imidazole (quant.); g) 1. PPTS cat., MeOH (96%); 2. DMSO, $(COCl)_2$, Et_3N, CH_2Cl_2, −78 °C→RT (96%); h) 1,3-propanedithiol, $BF_3{\cdot}Et_2O$, CH_2Cl_2 (86%); i) TMSCN, NMO, CH_2Cl_2 (82%). DMSO = dimethyl sulfoxide, $(DHQ)_2Pyr$ = hydroquinine 2,5-diphenyl-4,6-pyrimidinediyl diether, PPTS = pyridinium *p*-toluene sulfonate, TBDPSCl = *tert*-butyldiphenylsilyl chloride, TMSCN = trimethylsilanecarbonitrile.

ether in **28**, and oxidation of the resulting alcohol afforded aldehyde **29**, which is amenable to "umpolung" alkylation with iodide **20**.

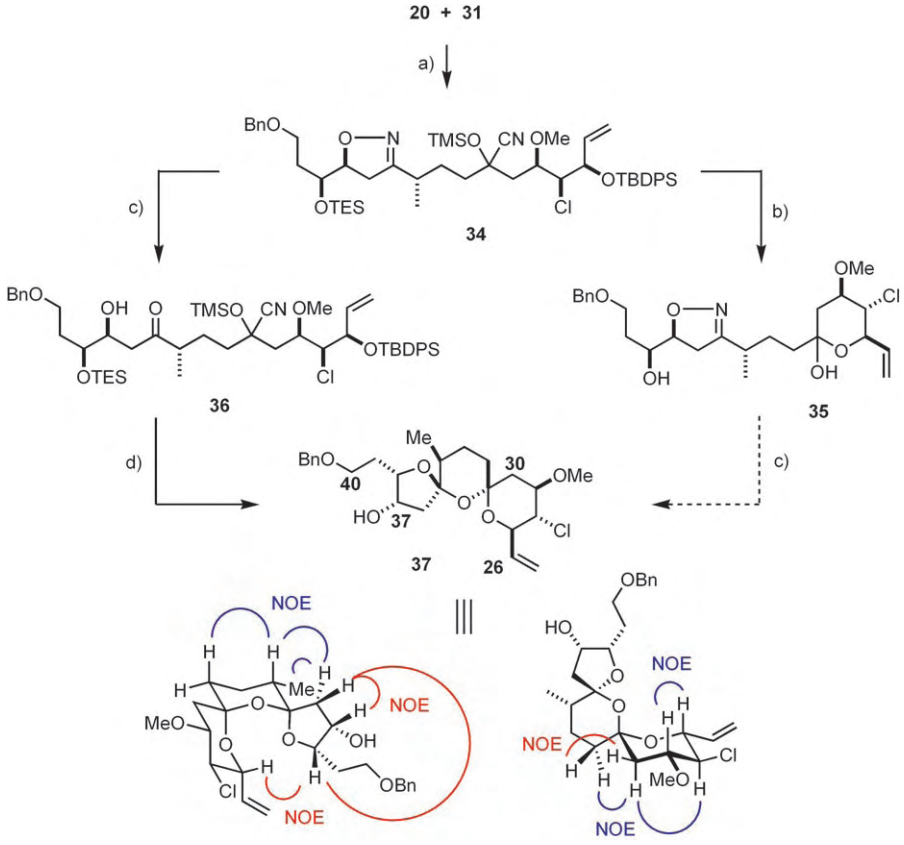
Although a model study (Scheme 7) showed that **20** undergoes a high-yielding alkylation with deprotonated dithiane **32**, all attempts to engage the much more elaborate dithiane **30** (Scheme 6) derived from aldehyde **29** met with failure. Deuteration experiments indicated that it was the deprotonation step that did not occur even though various bases and fairly forcing conditions were applied. Although these puzzling results require further investigation, they must be seen in the light of a report that suggested that tethered olefins can substantially alter the kinetic acidity of a dithiane by through-space orbital interactions ($\pi \rightarrow \sigma^*$ donation).[21] Under this premise, we considered that the use of a cyanohydrin rather than a



Scheme 7. Model study. Reagents and conditions: a) Compound **32**, *n*BuLi, $(n\text{Bu})_2Mg$, THF, RT; then iodide **20**, −78 °C (**33**: 87%).

dithiane might be advantageous for the envisaged "umpolung" alkylation, as the deprotonation step should be easier because of the enolate character of the resulting reactive intermediate.[22]

This plan could be reduced to practice as shown in Scheme 8. Exposure of aldehyde **29** to TMSCN and NMO[23] readily furnished cyanohydrin **31** (Scheme 6), which was deprotonated with LDA at low temperature and treated with iodide **20** to give the desired product **34** in respectable yield



Scheme 8. Assembly of the northern hemisphere of spirastrellolide A. Reagents and conditions: a) LDA, THF, −78 °C (52%); b) TASF, aq. DMF (**35**: 99%); c) [$Mo(CO)_6$], MeCN/H_2O, 90 °C (**36**: 66%); d) 1. TASF, aq. DMF; 2. PPTS cat., CH_2Cl_2 (**37**: 96%; d.r. = 4.1:1.7:1; see text). DMF = dimethylformamide, LDA = lithium diisopropyl amide, TASF = tris(dimethylamino)sulfonium difluorotrimethylsilicate.

© 2006 Wiley-VCH Verlag GmbH & Co. KGaA, Weinheim

(52%; 73% based on recovered starting material)[24] as a single diastereomer.[25] With **34** in hand, the stage was set for the final spirocyclization.

With the information gathered in the model studies in mind (see above), **34** was first subjected to exhaustive desilylation with TASF in aqueous DMF,[26] which resulted in the quantitative formation of hemiacetal **35**. Unfortunately, however, cleavage of the remaining N–O bond in **35** with the aid of $[Mo(CO)_6]$[11] was prohibited by the presence of the free alcohols. Therefore, the order of events was inverted, thus starting with the reductive cleavage of the isoxazoline unit in **34** followed by treatment of the resulting product **36** with TASF,[26] which simultaneously removed the silyl ethers and unmasked the ketone from the cyanohydrin precursor. It was gratifying to see that stirring of the trihydroxy diketone,[27] thus formed with catalytic amounts of PPTS in CH_2Cl_2, triggered an almost quantitative bis-spirocyclization event and delivered the desired product **37** together with two minor isomers in a 96% yield of the combined products with a diastereomeric ratio of 4.1:1.7:1. No furan formation was detected under these conditions. Routine flash chromato graphy allowed the isolation of **37** in respectable 61% yield in analytically pure form; this compound represents the intact and suitably protected northern half of spirastellolide A. Detailed spectroscopic analyses leave no doubt about its constitution and relative configuration. Most characteristic are the strong NOE interactions (indicated in Scheme 8) that reflect the doubly anomeric bis-spiroacetal substructures and the coupling constants that confirm the all-equatorial orientation of the substituents residing on the pyranose rings (see the Supporting Information).

In summary, this investigation outlines a reliable approach to the northern hemisphere of spirastrellolide A (**1**); as the complementary southern domain has also been obtained,[3] the entire carbon frame of this remarkably complex marine macrolide is now covered. Nevertheless, we are well aware that this venture is no more but an auspicious start for the conquest of this challenging natural product because of the as of yet unanswered stereochemical issues delineated in the introduction. Undaunted, however, we are now actively pursuing possible end games with the hope of reaching this monumental target soon.

Received: April 26, 2006

Keywords: cycloaddition · macrolides · natural products · phosphatase inhibitors · total synthesis

[1] a) D. E. Williams, M. Lapawa, X. Feng, T. Tarling, M. Roberge, R. J. Andersen, *Org. Lett.* **2004**, *6*, 2607–2610; b) D. E. Williams, M. Roberge, R. Van Soest, R. J. Andersen, *J. Am. Chem. Soc.* **2003**, *125*, 5296–5297.

[2] For previous syntheses and biological evaluations of phosphatase inhibitors from this group, see: a) A. Fürstner, F. Feyen, H. Prinz, H. Waldmann, *Angew. Chem.* **2003**, *115*, 5519–5522; *Angew. Chem. Int. Ed.* **2003**, *42*, 5361–5364; b) A. Fürstner, F. Feyen, H. Prinz, H. Waldmann, *Tetrahedron* **2004**, *60*, 9543–9558; c) A. Fürstner, J. Ruiz-Caro, H. Prinz, H. Waldmann, *J. Org. Chem.* **2004**, *69*, 459–467; d) A. Fürstner, K. Reinecke, H. Prinz, H. Waldmann, *ChemBioChem* **2004**, *5*, 1575–1579; e) M. Manger, M. Scheck, H. Prinz, J. P. von Kries, T. Langer, K. Saxena, H. Schwalbe, A. Fürstner, J. Rademann, H. Waldmann, *ChemBioChem* **2005**, *6*, 1749–1753.

[3] A. Fürstner, M. D. B. Fenster, B. Fasching, C. Godbout, K. Radkowski, *Angew. Chem.* **2006**, *118*, 5632–5636; *Angew. Chem. Int. Ed.* **2006**, *45*, 5506–5510.

[4] The only other synthesis of the [5,6,6]-bis-spirocyclic entity of **1**: I. Paterson, E. A. Anderson, S. M. Dalby, O. Loiseleur, *Org. Lett.* **2005**, *7*, 4121–4224.

[5] a) M. D. Chappell, S. J. Stachel, C. B. Lee, S. J. Danishefsky, *Org. Lett.* **2000**, *2*, 1633–1636; b) M. T. Crimmins, K. A. Emmitte, J. D. Katz, *Org. Lett.* **2000**, *2*, 2165–2167.

[6] Prepared according to literature precedence: a) S. Ma, X. Lu, Z. Li, *J. Org. Chem.* **1992**, *57*, 709–713; b) E. Piers, J. Renaud, S. J. Rettig, *Synthesis* **1998**, 590–602; c) A. Toró, P. Nowak, P. Deslongchamps, *J. Am. Chem. Soc.* **2000**, *122*, 4526–4527.

[7] D. A. Evans, M. M. Morrissey, R. L. Dorow, *J. Am. Chem. Soc.* **1985**, *107*, 4346–4348; good results were obtained only when the reaction was performed at 50°C; otherwise, a competing attack of MeOMgBr at the carbamate carbonyl group of the substrate is observed, which lowers the yield of **6**.

[8] a) W. J. Scott, J. K. Stille, *J. Am. Chem. Soc.* **1986**, *108*, 3033–3040; b) W. D. Wulff, G. A. Peterson, W. E. Bauta, K.-S. Chan, K. L. Faron, S. R. Gilbertson, R. W. Kaesler, D. C. Young, C. K. Murray, *J. Org. Chem.* **1986**, *51*, 277–279; c) C. D. Vanderwal, D. A. Vosburg, E. J. Sorensen, *Org. Lett.* **2001**, *3*, 4307–4310.

[9] Review on bis-spiroacetal formations: M. A. Brimble, F. A. Farès, *Tetrahedron* **1999**, *55*, 7661–7706.

[10] Details will be reported in a forthcoming full paper.

[11] a) A. Guarna, A. Guidi, A. Goti, A. Brandi, F. De Sarlo, *Synthesis* **1989**, 175–178; b) P. G. Baraldi, A. Barco, S. Benetti, S. Manfredini, D. Simoni, *Synthesis* **1987**, 276–278.

[12] J. W. Bode, E. M. Carreira, *J. Org. Chem.* **2001**, *66*, 6410–6424.

[13] M. J. Mintz, C. Walling, *Org. Synth.* **1969**, *49*, 9–12.

[14] Reviews on the use of 2-isoxazolines as aldol surrogates: a) D. P. Curran, *Adv. Cycloaddit.* **1988**, *1*, 129–189; b) S. Kanemasa, O. Tsuge, *Heterocycles* **1990**, *30*, 719–736.

[15] a) S. Kanemasa, M. Nishiuchi, A. Kamimura, K. Hori, *J. Am. Chem. Soc.* **1994**, *116*, 2324–2339; b) for an optimization and elegant application, see: J. W. Bode, N. Fraefel, D. Muri, E. M. Carreira, *Angew. Chem.* **2001**, *113*, 2128–2131; *Angew. Chem. Int. Ed.* **2001**, *40*, 2082–2085.

[16] S. E. Schaus, B. D. Brandes, J. F. Larrow, M. Tokunaga, K. B. Hansen, A. E. Gould, M. E. Furrow, E. N. Jacobsen, *J. Am. Chem. Soc.* **2002**, *124*, 1307–1315.

[17] L. Alcaraz, J. J. Harnett, C. Mioskowski, J. P. Martel, T. Le Gall, D.-S. Shin, J. R. Falck, *Tetrahedron Lett.* **1994**, *35*, 5449–5452.

[18] a) S. Hu, S. Jayaraman, A. C. Oehlschlager, *J. Org. Chem.* **1998**, *63*, 8843–8849; b) S. Hu, S. Jayaraman, A. C. Oehlschlager, *J. Org. Chem.* **1996**, *61*, 7513–7520.

[19] U. S. Racherla, H. C. Brown, *J. Org. Chem.* **1991**, *56*, 401–404.

[20] H. C. Kolb, M. S. VanNieuwenhze, K. B. Sharpless, *Chem. Rev.* **1994**, *94*, 2483–2547.

[21] A. B. Smith, C. M. Adams, *Acc. Chem. Res.* **2004**, *37*, 365–377.

[22] a) G. Stork, L. Maldonado, *J. Am. Chem. Soc.* **1971**, *93*, 5286–5287; b) G. Stork, L. Maldonado, *J. Am. Chem. Soc.* **1974**, *96*, 5272–5274; c) for applications in natural product synthesis, see: T. Takahashi, H. Nemoto, Y. Kanda, J. Tsuji, Y. Fukazawa, T. Okajima, Y. Fujise, *Tetrahedron* **1987**, *43*, 5499–5520; d) H. Takayanagi, Y. Kitano, Y. Morinaka, *J. Org. Chem.* **1994**, *59*, 2700–2706; e) A. B. Smith, C. Sfouggatakis, D. B. Gotchev, S. Shirakami, D. Bauer, W. Zhu, V. A. Doughty, *Org. Lett.* **2004**, *6*, 3637–3640.

[23] S. S. Kim, G. Rajogopal, D. W. Kim, D. H. Song, *Synth. Commun.* **2004**, *34*, 2973–2980.

 © 2006 Wiley-VCH Verlag GmbH & Co. KGaA, Weinheim

[24] The time for deprotonation must be < 5 minutes; otherwise, significant decomposition of the cyanohydrin part was observed. Likewise, the use of KHMDS as the base and hexamethyl phosphoramide (HMPA) as a cosolvent were detrimental.
[25] The configuration of the cyanohydrin center C31 has not been determined.
[26] a) K. A. Scheidt, H. Chen, B. C. Follows, S. R. Chemler, D. S. Coffey, W. R. Roush, *J. Org. Chem.* **1998**, *63*, 6436 – 6437; b) R. Noyori, I. Nishida, J. Sakata, *J. Am. Chem. Soc.* **1983**, *105*, 1598 – 1608; c) recent application: C. Aïssa, R. Riveiros, J. Ragot, A. Fürstner, *J. Am. Chem. Soc.* **2003**, *125*, 15512 – 15520.
[27] NMR spectroscopic analysis suggests that the compound mainly exists as a pyranoid hemiacetal analogous to that found in **35**.

 © 2006 Wiley-VCH Verlag GmbH & Co. KGaA, Weinheim

Asymmetric Catalysis

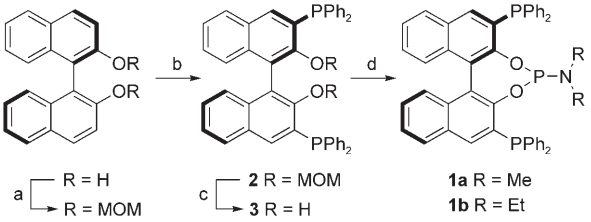
DOI: 10.1002/anie.200601501

Synthesis of Triphosphorous Bidentate Phosphine–Phosphoramidite Ligands: Application in the Highly Enantioselective Hydrogenation of *ortho*-Substituted Aryl Enamides**

*Weicheng Zhang and Xumu Zhang**

The development of new effective chiral ligands is fundamental to asymmetric hydrogenation. Over recent decades, many excellent bisphosphine ligands have been reported for highly enantioselective hydrogenation reactions.[1] However, the modification of a desired structural motif of most bidentate ligands is impeded by multistep synthesis. Recently, this situation has been partially remedied by the emerging monodentate ligands,[2] including phosphoramidites,[3] phosphonites,[4] and phosphites,[5] which have modular structures and can be prepared in one step from chiral binaphthol (BINOL) or its analogues. As part of our continuous interest in exploring new ligands for hydrogenation, we wonder whether the design of new bidentate ligands can benefit from the advantages of modular monodentate ligands for further structural optimization. From a practical viewpoint, ligands should be prepared in a few steps from readily available starting materials. Although various modified BINOL ligands have been utilized for asymmetric catalysis,[6] few efforts have been made to attach the phosphorous group directly at the 3,3′-positions.[7] Inspired by the success of many hybrid C_1-symmetric chelating ligands,[8] we herein report the synthesis and application of a new phosphine–phosphoramidite ligand **1**. To our knowledge, this pseudo-C_2-symmetric triphosphorous bidentate ligand is the first of its class and represents a conceptually new approach to ligand design. Importantly, unprecedented enantioselectivities have been achieved with this new ligand for the hydrogenation of *ortho*-substituted aryl enamides and a 1-naphthylenamide, thereby solving a long-standing problem in the hydrogenation of enamides.

Ligand **1** was synthesized in four steps from (*R*)-BINOL (Scheme 1). Protection of the hydroxy groups of BINOL was



Scheme 1. Ligand synthesis. Reagents and conditions: a) 1. NaH (5 equiv), THF, 0°C; 2. CH_3OCH_2Cl (2.4 equiv), 0°C (98%); b) 1. *n*BuLi, Et_2O/THF, RT; 2. $ClPPh_2$, 0°C (70%); c) HCl (cat.), MeOH, 60°C (79%); d) HMPT or HEPT, toluene, 110°C (88% for **1a**, 80% for **1b**).

followed by double lithiation and subsequent attachment of two identical phosphorous groups at the 3,3′-positions.[9] After removal of the methoxy methyl (MOM) groups of **2** in HCl/MeOH, the desired product **1** was prepared by heating **3** with hexamethylphosphorous triamide (HMPT) or hexaethylphosphorous triamide (HEPT) in toluene at 110°C. As the whole synthesis features a sequential assembly of two types of phosphorous donors onto the chiral BINOL backbone, structural tuning can be achieved by varying the starting R_2PCl reagent and the substitution mode at the central phosphorous donor, thus allowing for the efficient expansion of ligand derivatives. We investigated the effectiveness of the representative member **1** in hydrogenation reactions to demonstrate the potential of this new class of ligand. Thus a [Rh/**1a**] complex was prepared by treating **1a** with $[Rh(cod)_2]BF_4$ (cod = 1,5-cyclooctadiene) in 1:1 molar ratio. As evidenced by NMR spectroscopic analysis, among the three phosphorous donors of **1**, only two form an effective chelation with the Rh center and generate a well-defined complex, thus leaving an uncoordinated free phosphine group.[10] The coordination environment of the [Rh/**1a**] complex based on MM2 calculations is illustrated in Figure 1. Similar to C_2-symmetric bisphosphines, two nonadjacent quadrants (black and gray in Figure 1) are blocked by the equatorial phenyl and the dimethylamino groups, thus creating an effective chiral environment around the transition-metal center.

The catalytic performance of **1** was first tested in the Rh-catalyzed hydrogenation of several standard α-aryl enamides. Initial studies on the [Rh/**1a**] system using the benchmark substrate **4a** showed a strong solvent effect reminiscent of the monodentate ligand systems[3a,c] (Table 1): non-protic solvents, such as CH_2Cl_2 and toluene, give excellent results

[*] W. Zhang, Prof. X. Zhang
Department of Chemistry
The Pennsylvania State University
University Park, PA, 16802 (USA)
Fax: (+1) 814-865-3932
E-mail: xumu@chem.psu.edu

[**] This work was supported by the National Institutes of Health (NIH-GM58832).

Supporting information for this article is available on the WWW under http://www.angewandte.org or from the author.

 © 2006 Wiley-VCH Verlag GmbH & Co. KGaA, Weinheim

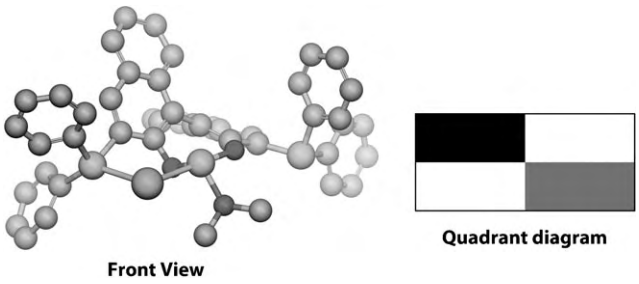
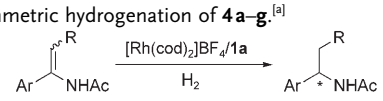


Figure 1. MM2 calculations of the [Rh/**1a**] complex from the CAChe program.

Table 1: Asymmetric hydrogenation of **4a**–**g**.[a]



Entry	Substrate	Ar	R	P_{H_2} [bar]	Solvent	*ee* [%][b] (config.)
1	**4a**	Ph	H	1	CH_2Cl_2	99 (*R*)
2	**4a**	Ph	H	1	toluene	99 (*R*)
3	**4a**	Ph	H	1	THF	97 (*R*)
4	**4a**	Ph	H	1	EtOAc	98 (*R*)
5	**4a**	Ph	H	1	acetone	94 (*R*)
6	**4a**	Ph	H	1	MeOH	91 (*R*)
7	**4a**	Ph	H	5	CH_2Cl_2	98 (*R*)
8	**4a**	Ph	H	10	CH_2Cl_2	97 (*R*)
9[c]	**4a**	Ph	H	1	CH_2Cl_2	98 (*R*)
10	**4b**	3-Me-C_6H_4	H	1	CH_2Cl_2	99 (*R*)
11	**4c**	4-CF_3-C_6H_4	H	1	CH_2Cl_2	99 (*R*)
12	**4d**	4-CF_3-C_6H_4	Me	5	CH_2Cl_2	99 (*R*)
13	**4e**	4-MeO-C_6H_4	Me	5	CH_2Cl_2	96 (*R*)
14	**4f**	2-naphthyl	H	1	CH_2Cl_2	98 (*R*)
15	**4g**	2-naphthyl	Me	5	CH_2Cl_2	97.0 (*R*)

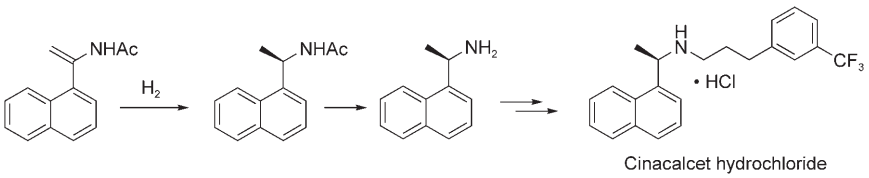
[a] Unless mentioned otherwise, all reactions were carried out with a substrate/catalyst (S/C) ratio of 100:1 at RT for 24 h. In all cases, 100% conversion was achieved. [b] Determined by chiral GC or HPLC. The absolute configuration was assigned by comparison of the observed optical rotation with reported data. [c] S/C = 1000.

(entries 1–2); those with increased polarity tend to lower enantioselectivities (entries 3–5); whereas a further decrease in the enantiomeric excess occurs in the protic solvent MeOH (entry 6). Increasing hydrogen pressure led to a minor deterioration in enantiomeric excess (entries 1, 7, and 8). Compared with monophos, the diphenylphosphine group in **1a** plays an important role in achieving high enantioselectivities as well as high reactivities (entry 9; turnover number (TON) = 1000). Under the established reaction conditions (room temperature, CH_2Cl_2, 1 or 5 bar of H_2), several other enamides were reduced smoothly with high *ee* values were obtained (entries 10–15).

Encouraged by our initial success, we then focused on the hydrogenation of challenging *ortho*-substituted aryl enamides and a 1-naphthylenamide, which are useful synthetic intermediates for pharmaceutical products. For example, the asymmetric hydrogenation of 1-naphthylenamide **4n** leads to (*R*)-1-(1-naphthyl)ethylamine, a key precursor to Cinacalcet hydrochloride for the treatment of hyperparathyroidism and hypercalcemia (Scheme 2).[11] Compared with the hydrogenation of most unhindered aryl enamides, limited progress has been made for those substrates with *ortho* functionalities.[12] Mechanistic studies by Imamoto and co-workers suggested a simultaneous execution of two competitive hydrid insertion pathways, which would account for the low *ee* values observed in the hydrogenation of 2-methoxy- and 2-chloro-substituted phenylenamides with 1,2-bis(alkylmethylphosphino)ethanes (BisP*) and 1,2-bis(alkylmethylphosphino)methanes (miniphos).[12b] To address this challenging problem, we screened commercially available (1*S*,1*S*′,2*R*,2*R*′)-tangphos (L1), (*R*,*R*)-Et-duphos (L2), and the new ligand **1** under the same reaction conditions. As revealed in the screening process, L1 and L2 failed to show high selectivities for most *ortho*-substituted aryl enamides and a 1-naphthylenamide (Table 2). In two extreme cases, a reversal of enantioselectivity was observed with the use of L1 (entries 1 and 7). To our delight, the new ligand **1a**,**b** gave excellent *ee* values. Moreover, further improvement in the hydrogenation of **4h** and **4n** can be achieved by lowering the temperature (0 °C), varying the structure (namely, the use of **1b** instead), or choosing a different solvent (entry 7).

To put our results in another context, we have listed the highest *ee* values reported by other groups using several ligands under a variety of reaction conditions (Table 2). In each case, our results are comparable with or superior to the best results reported so far.[12] These comparative results confirm that the new ligand **1**, which bears a novel combination of phosphine and phosphoramidite groups, is unique in the asymmetric hydrogenation of hindered enamides. Further exploration of the substrate scope is currently ongoing.

To evaluate the potential application of this system in industry, we also studied the hydrogenation of **4n** with [Rh(cod)**1a**]BF_4 at a decreased catalyst loading (TON = 1000) in TFE. It was found that 93% of **4n** was converted into **5n** with 88% *ee* under 80 bar of H_2 within 24 h; furthermore, **5n** was isolated by flash chromatography in 90% yield.[13]

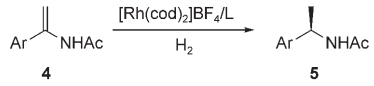


Scheme 2. Asymmetric hydrogenation route to Cinacalcet hydrochloride.

In conclusion, new triphosphorous bidentate phosphine–phosphoramidite ligands have been developed and applied to the highly enantioselective hydrogenation of α-aryl enamides, including *ortho*-substituted aryl enamides and a 1-naphthylenamide. The modular structure and straightforward synthesis of the ligands allows for further systematic modification of the

 © 2006 Wiley-VCH Verlag GmbH & Co. KGaA, Weinheim

Table 2: Ligand screening for the asymmetric hydrogenation of *ortho*-substituted aryl enamides and 1-naphthylenamides **4h–n**.[a]



Entry	Substrate	Ar	*ee* [%] (config.)[b] L1[c]	L2[c]	**1a**[c]	**1b**[c]	The best reported *ee* [%]
1	**4h**	2-Me-C_6H_4	51.8 (*S*)	52.6 (*R*)	84.0 (*R*) 91.0 (*R*)[e]	87.2 (*R*)	74.8[12a]
2	**4i**	2-MeO-C_6H_4	54.4 (*R*)	51.4 (*R*)	99.4 (*R*)	99.0 (*R*)	83.1[12d]
3	**4j**	2-F-C_6H_4	95.8 (*R*)	80.8 (*R*)	99.0 (*R*)	97.0 (*R*)	95.7[12a]
4	**4k**	2-Cl-C_6H_4	9.4 (*R*)	55.6 (*R*)	99.6 (*R*)	98.2 (*R*)	85[12j]
5[d]	**4l**	2-NO_2-C_6H_4	88.0 (−)	85.8 (−)	98.2 (−)	98.2 (−)	–
6[d]	**4m**	2-CF_3-C_6H_4	68.8 (+)	88.4 (+)	93.8 (+)	94.2 (+)	–
7	**4n**	1-naphthyl	74.8 (*S*)	51.8 (*R*)	91.0 (*R*) 92.4 (*R*)[f]	92.8 (*R*) 93.8 (*R*)[g]	91.2[12f]

[a] Unless mentioned otherwise, all reactions were carried out with an S/C ratio of 100:1 in CH_2Cl_2 under 5 bar hydrogen pressure at RT for 24 h. In all cases, 100% conversion was achieved. [b] Determined by chiral GC. The absolute configuration was assigned by comparison of observed optical rotation with literature data. [c] [Rh(nbd)L1]SbF_6 (nbd = 2,5-norbornadiene) , [Rh(cod)L2]BF_4, Rh[(cod)**1a**]BF_4, and Rh[(cod)**1b**]BF_4 were used. [d] Absolution configurations were not determined. [e] $T = 0\,^\circ C$, $P_{H_2} = 25$ bar. [f] $T = 0\,^\circ C$, $P_{H_2} = 50$ bar. [g] 2,2,2-Trifluoroethanol (TFE) was used as solvent.

chiral biaryl backbone and the two types of phosphorous donors. Synthesis and application of analogous triphosphorous bidentate ligands will be reported in due course.

Experimental Section

General procedure for the hydrogenation: A stock solution of [Rh/**1a**] or [Rh/**1b**] complex (2×10^{-3} mol L^{-1}) was prepared by stirring $[Rh(cod)_2]BF_4$ and **1a** or **1b** at a 1:1.1 molar ratio in CH_2Cl_2 at room temperature for 1 h in a nitrogen-filled glovebox. The required amount of catalyst solution (0.5 mL, 0.001 mmol) was transferred by syringe into the vial charged with substrate (0.1 mmol), and the solvent (2.5 mL) was added. All the vials were placed together in a steel autoclave into which hydrogen gas was charged at the desired pressure. After stirring at room temperature for 24 h, the hydrogen was released carefully and the solution was concentrated and subjected to a short column of silica gel to remove the metal complex. The purified solution was analyzed by chiral GC or HPLC to determine the *ee* value.

Received: April 15, 2006
Published online: August 7, 2006

Keywords: asymmetric catalysis · enamides · enantioselectivity · hydrogenation · rhodium

[1] a) *Comprehensive Asymmetric Catalysis I–III* (Eds.: E. N. Jacobsen, A. Pfaltz, H. Yamamoto), Springer, Berlin, **1999**; b) R. Noyori, *Asymmetric Catalysis in Organic Synthesis*, Wiley, New York, **1994**; c) *Catalytic Asymmetric Synthesis* (Ed.: I. Ojima), 2nd ed., Wiley-VCH, New York, **2000**; d) W. Tang, X. Zhang, *Chem. Rev.* **2003**, *103*, 3029.

[2] a) I. V. Komarov, A. Börner, *Angew. Chem.* **2001**, *113*, 1237; *Angew. Chem. Int. Ed.* **2001**, *40*, 1197; b) T. Jerphagnon, J.-L. Renaud, C. Bruneau, *Tetrahedron: Asymmetry* **2004**, *15*, 2101.

[3] a) M. van den Berg, A. J. Minnaard, E. P. Schudde, J. van Esch, A. H. M. de Vries, J. G. de Vries, B. L. Feringa, *J. Am. Chem. Soc.* **2000**, *122*, 11539; b) D. Pena, A. J. Minnaard, J. G. de Vries, B. L. Feringa, *J. Am. Chem. Soc.* **2002**, *124*, 14552; c) M. van den Berg, A. J. Minnaard, R. M. Haak, M. Leeman, E. P. Schedde, A. Meetsma, B. L. Feringa, A. H. M. de Vries, C. E. P. Maljaars, C. E. Williams, D. Hyett, J. A. F. Boogers, H. J. W. Henderickx, J. G. de Vries, *Adv. Synth. Catal.* **2003**, *345*, 308; d) R. Hoen, J. A. F. Boogers, H. Bernsmann, A. J. Minnaard, A. Meetsma, T. D. Tiemersma-Wegman, A. H. M. de Vries, J. G. de Vries, B. L. Feringa, *Angew. Chem.* **2005**, *117*, 4281; *Angew. Chem. Int. Ed.* **2005**, *44*, 4209; e) A.-G. Hu, Y. Fu, J.-H. Xie, H. Zhou, L.-X. Wang, Q.-L. Zhou, *Angew. Chem.* **2002**, *114*, 2454; *Angew. Chem. Int. Ed.* **2002**, *41*, 2348; f) S. Wu, W. Zhang, Z. Zhang, X. Zhang, *Org. Lett.* **2004**, *6*, 3565; g) Y. Liu, K. Ding, *J. Am. Chem. Soc.* **2005**, *127*, 10488.

[4] a) C. Claver, E. Fernandez, A. Gillon, K. Heslop, D. J. Hyett, A. Martorell, A. G. Orpen, P. G. Pringle, *Chem. Commun.* **2000**, 961; b) M. T. Reetz, T. Sell, *Tetrahedron Lett.* **2000**, *41*, 6333.

[5] a) M. T. Reetz, G. Mehler, *Angew. Chem.* **2000**, *112*, 4047; *Angew. Chem. Int. Ed.* **2000**, *39*, 3889; b) M. T. Reetz, A. Meiswinkel, G. Mehler, K. Angermund, M. Graf, W. Thiel, R. Mynott, D. G. Blackmond, *J. Am. Chem. Soc.* **2005**, *127*, 10305.

[6] Y. Chen, S. Yekta, A. K. Yudin, *Chem. Rev.* **2003**, *103*, 3155.

[7] a) J. Li, W. Li, Y. Li, Y. Li, S. Yang, *Org. Prep. Proced. Int.* **1995**, *27*, 685; b) T.-L. Au-Yeung, K.-Y. Chan, R. K. Haynes, I. D. Williams, L. L. Yeung, *Tetrahedron Lett.* **2001**, *42*, 457; c) X. Li, J. B. Hewgley, C. A. Mulrooney, J. Yang, M. C. Kozlowski, *J. Org. Chem.* **2003**, *68*, 5500.

[8] a) H. U. Blaser, W. Brieden, B. Pugin, F. Spindler, M. Studer, A. Togni, *Top. Catal.* **2002**, *19*, 3; b) T. Sturm, W. Weissensteiner, F. Spindler, *Adv. Synth. Catal.* **2003**, *345*, 160; c) N. W. Boaz, S. D. Debenham, E. B. Mackenzie, S. E. Large, *Org. Lett.* **2002**, *4*, 2421; d) N. W. Boaz, E. B. Mackenzie, S. D. Debenham, S. E. Large, Jr. J. A. Ponasik, *J. Org. Chem.* **2005**, *70*, 1872; e) N. W. Boaz, Jr. J. A. Ponasik, S. E. Large, *Tetrahedron: Asymmetry* **2005**, *16*, 2063; f) X.-P. Hu, Z. Zheng, *Org. Lett.* **2004**, *6*, 3585; g) A. Suarez, M. A. Mendez-Rojas, A. Pizzano, *Organometallics* **2002**, *21*, 4611; h) M. Rubio, A. Suarez, E. Alvarez, A. Pizzano, *Chem. Commun.* **2005**, 628; i) S. Vargas, M. Rubio, A. Suarez, D. del Rio, E. Alverez, A. Pizzano, *Organometallics* **2006**, *25*, 961; j) Y. Yan, Y. Chi, X. Zhang, *Tetrahedron: Asymmetry* **2004**, *15*, 2173; k) M. T. Reetz, A. Gosberg, *Tetrahedron: Asymmetry* **1999**, *10*, 2129; l) O. Pamies, M. Dieguez, G. Net, A. Ruiz, C. Claver, *Chem. Commun.* **2000**, 2383; m) S. Deerenberg, O. Pamies, M. Dieguez, C. Claver, P. C. J. Kamer, P. W. N. W. van Leeuwen, *J. Org. Chem.* **2001**, *66*, 7626; n) O. Pamies, M. Dieguez, G. Net, A. Ruiz, C. Claver, *J. Org. Chem.* **2001**, *66*, 8364.

[9] If only one phosphine group is attached to the *ortho* position of the BINOL unit, two diastereomeric phosphine–phosphoramidite ligands will be obtained as a result of the creation of a *P*-stereogenic center; this principle was applied to the preparation of a series of single *ortho*-substituted monodentate ligands, see: M. T. Reetz, J.-A. Ma, R. Goddard, *Angew. Chem.* **2005**, *117*, 416; *Angew. Chem. Int. Ed.* **2005**, *44*, 412.

[10] See the Supporting Information for details.

[11] a) B. C. van Wagenen, S. T. Moe, M. F. Balandrin, E. G. Delmar, E. F. Nemeth, US Patent **2001**, 6211244; b) N. Franceschini,

 © 2006 Wiley-VCH Verlag GmbH & Co. KGaA, Weinheim

M. S. Joy, A. Kshirsagar, *Expert Opin. Invest. Drugs* **2003**, *12*, 1413.

[12] a) M. J. Burk, Y. M. Wang, J. R. Lee, *J. Am. Chem. Soc.* **1996**, *118*, 5142; b) I. D. Gridnev, M. Yasutake, N. Higashi, T. Imamoto, *J. Am. Chem. Soc.* **2001**, *123*, 5268; c) Ref. [3e]; d) A. Ohashi, S.-I. Kikuchi, M. Yasutake, T. Imamoto, *Eur. J. Org. Chem.* **2002**, 2535; e) X. Jia, R. Guo, X. Li, X. Yao, A. S. C. Chan, *Tetrahedron Lett.* **2002**, *43*, 5541; f) M. Bulliard, B. Laboue, S. Roussiasse, PCT Int. Appl. WO 2002012253, **2002**; g) X. Jia, X. Li, L. Xu, Q. Shi, X. Yao, A. S. C. Chan, *J. Org. Chem.* **2003**, *68*, 4539; h) X. Li, X. Jia, G. Lu, T. T.-L. Au-Yeung, K.-H. Lam, T. W. H. Lo, A. S. C. Chan, *Tetrahedron: Asymmetry* **2003**, *14*, 2687; i) H. Huang, Z. Zheng, H. Luo, C. Bai, X. Hu, H. Chen, *J. Org. Chem.* **2004**, *69*, 2355; j) P. Harrison, G. Meek, *Tetrahedron Lett.* **2004**, *45*, 9277.

[13] A small amount of **4n** (7% calculated from ^{1}H NMR spectroscopic analysis) was decomposed into 1-acetonaphthone during hydrogenation.

 © 2006 Wiley-VCH Verlag GmbH & Co. KGaA, Weinheim

Fluorescent Probes

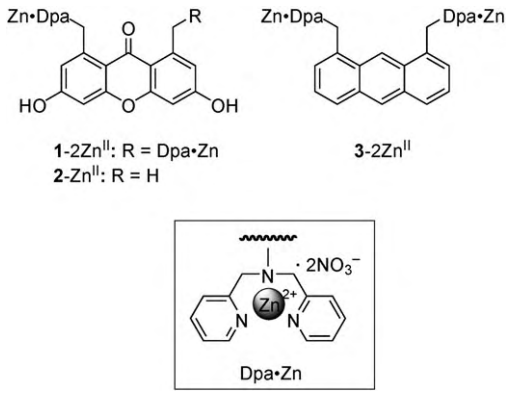
DOI: 10.1002/anie.200601315

Bis(Dpa-Zn^{II}) Appended Xanthone: Excitation Ratiometric Chemosensor for Phosphate Anions

*Akio Ojida, Hiroshi Nonaka, Yoshifumi Miyahara, Shun-ichi Tamaru, Kazuki Sada, and Itaru Hamachi**

The development of molecular-recognition and sensing systems for biologically important anions has received considerable attention in recent years.[1] Among various anions, phosphate derivatives, which include nucleoside pyrophosphates such as adenosine triphosphate (ATP),[2] inorganic pyrophosphate,[3] and phosphoproteins,[4] are significant sensing targets because of their pivotal roles in biological systems. For example, ATP is known not only as a universal energy source but also as an extracellular signaling mediator in many biological processes,[5] and protein phosphorylation is recognized as a ubiquitous regulatory mechanism of signal transduction cascades in living cells.[6] In recent years, several chemosensors that exhibit a rather strong binding affinity for the phosphate derivatives in aqueous medium were reported,[2d,e,3a,c,4] although their bioanalytical application in biological systems has not yet been sufficiently developed.[2e,3c,7]

The detection of a specific anion by using the emission or excitation change at two different wavelengths provides a significant advantage over conventional measurement at a single wavelength because such a dual excitation/emission system enables a ratiometric detection of an analyte, thus allowing precise and quantitative analysis and imaging even in complicated systems. In contrast to the relatively high number of reports of fluorescent ratiometric sensors for cations such as Ca^{II} or Zn^{II},[8] there are few reports of ratiometric anion sensors.[2e,9] Herein, we report a new fluorescent sensory system that is capable of the ratiometric detection of phosphate anions under neutral aqueous conditions. A new chemosensor, **1**–2Zn^{II}, which comprises a xanthone fluorophore that bears two 2,2′-dipicolylamine (Dpa)–zinc(II) moieties as a phosphate-binding site, effects a change in the corresponding fluorescence excitation spectrum at three wavelengths upon binding to phosphate species based on a unique sensing mechanism, that is, a phosphate anion induced coordination rearrangement of the Zn^{II} ions.



The syntheses of the chemosensor **1**–2Zn^{II} and the control monodentate complex **2**–Zn^{II} are described in the Supporting Information.[10] The structure of the binuclear zinc(II) complex **1**–2Zn^{II} with chloride counterions has been investigated by X-ray crystallographic analysis (Figure 1):[11] Complex **1**–2Zn^{II} is a dimeric complex connected by two bridging chloride ions, Cl(1), in the solid state. Interestingly, in the asymmetric half unit, one Zn(1) center coordinates to the carbonyl oxygen atom of the xanthone fluorophore from the upper side of the xanthone ring, in which the Zn(1)–O(1) bond length is 2.18 Å and the C(12)-O(1)-Zn(1) bond angle is 125.07°. The Zn(1) atom is also bound by the three nitrogen atoms of the Dpa unit and by both chloride anions in a square-bipyramidal six-coordinate environment. In contrast, the Zn(2) atom, which is positioned on the lower side of the xanthone ring, is bound to the Dpa unit and the two chloride

[*] Prof. I. Hamachi
Department of Synthetic Chemistry and Biological Chemistry
Graduate School of Engineering, Kyoto University
Katsura Campus, Nishikyo-ku, Kyoto, 615-8510 (Japan)
and
PRESTO (Synthesis and Control, JST)
Fax: (+81) 75-383-2759
E-mail: ihamachi@sbchem.kyoto-u.ac.jp
Dr. A. Ojida, H. Nonaka, Y. Miyahara, Dr. S.-i. Tamaru
Department of Synthetic Chemistry and Biological Chemistry
Graduate School of Engineering, Kyoto University
Katsura Campus, Nishikyo-ku, Kyoto (Japan)
Dr. K. Sada
Department of Chemistry and Biochemistry
Graduate School of Engineering, Kyushu University
Fukuoka, 819-0395 (Japan)

Supporting information for this article is available on the WWW under http://www.angewandte.org or from the author. Dpa = 2,2′-dipicolylamine.

InterScience
© 2006 Wiley-VCH Verlag GmbH & Co. KGaA, Weinheim

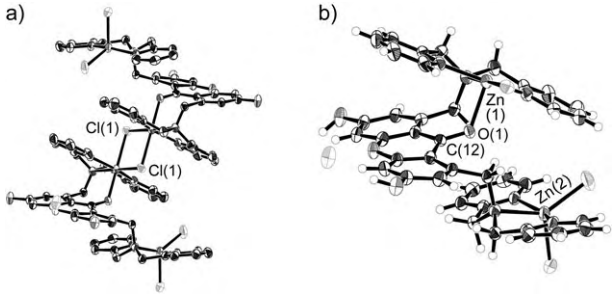


Figure 1. ORTEP drawing of the binuclear Zn^{II} complex [**1**–2 Zn^{II}]Cl_4: a) dimer complex; b) an asymmetric half unit of the complex. Disordered solvent molecules are omitted for clarity.

anions to form a tetragonal-pyramidal five-coordinate environment.

The absorption maximum of **1**–2 Zn^{II} is observed at 397 nm, and when the complex is excited at 397 nm, the emission maximum is 447 nm. The fluorescence quantum yield of **1**–2 Zn^{II} is high ($\Phi = 0.61$) under neutral aqueous conditions (50 mM HEPES, 50 mM NaCl, pH 7.2). Figure 2a shows the excitation spectral response of **1**–2 Zn^{II} upon addition of ATP. The changes in excitation with increasing concentration of ATP occur at three wavelengths (322 (down), 360 (up), and 407 nm (down)) with two isoemission points at 332 and 377 nm (Figure 2b). The plot of the fluorescence intensity at 407 nm (inset) shows saturation behavior with increasing ATP concentration; curve-fitting analysis gives an affinity constant of $4.2 \times 10^5\,M^{-1}$ for ATP. An almost identical affinity value was obtained by the analysis of the intensity ratio R (F at 360 nm/F at 407 nm) within an appropriate detection range ($R_{max}/R_{min} \approx 2$), which indicates that ATP is detected in an excitation ratiometric manner (Figure 2b, inset). The binding of **1**–2 Zn^{II} with ATP was also evaluated by isothermal titration calorimetry (ITC). The ITC data indicate that the binding is an exothermic, entropy-driven process ($\Delta H = -3.83$ kcal mol^{-1} and $T\Delta S = 4.19$ kcal mol^{-1}; see the Supporting Information) and give a binding constant $K_{app} = 7.5 \times 10^5\,M^{-1}$ ($n = 0.83$), which is almost identical to that obtained from the fluorescence titration.

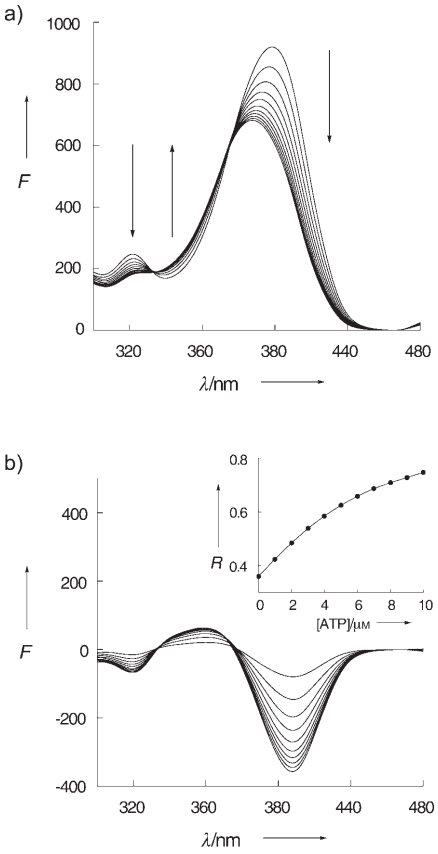


Figure 2. a) Change in the excitation spectrum of **1**–2 Zn^{II}; b) difference spectrum versus the initial state upon addition of ATP. F refers to the fluorescence intensity. Inset: plot of the fluorescence intensity ratio R (F at 360 nm/F at 407 nm; 3 μM **1**–2 Zn^{II} in 50 mM HEPES, 50 mM NaCl, pH 7.2, [ATP] = 0–10 μM, $\lambda_{em} = 480$ nm, 25 °C).

The sensing selectivity of **1**–2 Zn^{II} for various biologically important phosphate species was examined by ratiometric excitation titration (Table 1). The chemosensor **1**–2 Zn^{II} showed strong affinities ($K_{app} > 10^5\,M^{-1}$) towards nucleoside pyrophosphates such as ATP, GTP, and ADP, whereas binding was relatively weak for the HPO_4^{2-} ion and monophosphate derivatives such as AMP. **1**–2 Zn^{II} also sensed a pyrophosphate diester (UDP-Gal) with a weak affinity, and a change in fluorescence was scarcely noticeable with a monophosphodiester (cAMP). A change in fluorescence was not induced upon addition of millimolar concentrations of other anions such as acetate, sulfate, nitrate, and carbonate, thus indicating that **1**–2 Zn^{II} is a selective fluorescent chemosensor for phosphate anions, especially for polyanionic nucleoside pyrophosphate species.[2,12]

Table 1: Apparent binding constants K_{app} of chemosensor **1**–2 Zn^{II} to phosphate species as determined by fluorescence titration.

Anion[a]	K_{app} [M^{-1}][b]	Anion[a]	K_{app} [M^{-1}][b]
ATP	4.2×10^5	HPO_4^{2-}	1.8×10^3
GTP	1.0×10^6	AcO^-	[c]
ADP	2.8×10^5	SO_4^{2-}	[c]
AMP	5.0×10^2	NO_3^-	[c]
cAMP	[c]	HCO_3^-	[c]
UDP-Gal	2.8×10^2		

[a] Phosphate species with sodium counterions. ATP = adenosine-5′-triphosphate, GTP = guanosine-5′-triphosphate, ADP = adenosine-5′-diphosphate, AMP = adenosine-5′-monophosphate, cAMP = adenosine-3′,5′-cyclic monophosphate, UDP-Gal = uridine-5′-diphosphogalactose. [b] Conditions: 50 mM HEPES, 50 mM NaCl, pH 7.2, $\lambda_{em} = 480$ nm, 20 °C. [c] As the fluorescence change was scarcely observed, no binding constant was obtained.

Subsequently, we explored the sensing mechanism of the changes in the excitation spectrum of **1**–2 Zn^{II}. In a UV/Vis titration experiment of the metal-free ligand **1** with Zn^{II} ions in aqueous methanol, a stepwise spectral change occurred during complexation with two equivalents of Zn^{II}. The addition of one equivalent of Zn^{II} induced an absorbance decrease at 328 nm and the concomitant increase of a newly emerged peak at 376 nm with an isosbetic point at 357 nm (Figure 3a), while the subsequent addition of more than one equivalent of Zn^{II} caused an increase at 397 nm and a

 © 2006 Wiley-VCH Verlag GmbH & Co. KGaA, Weinheim

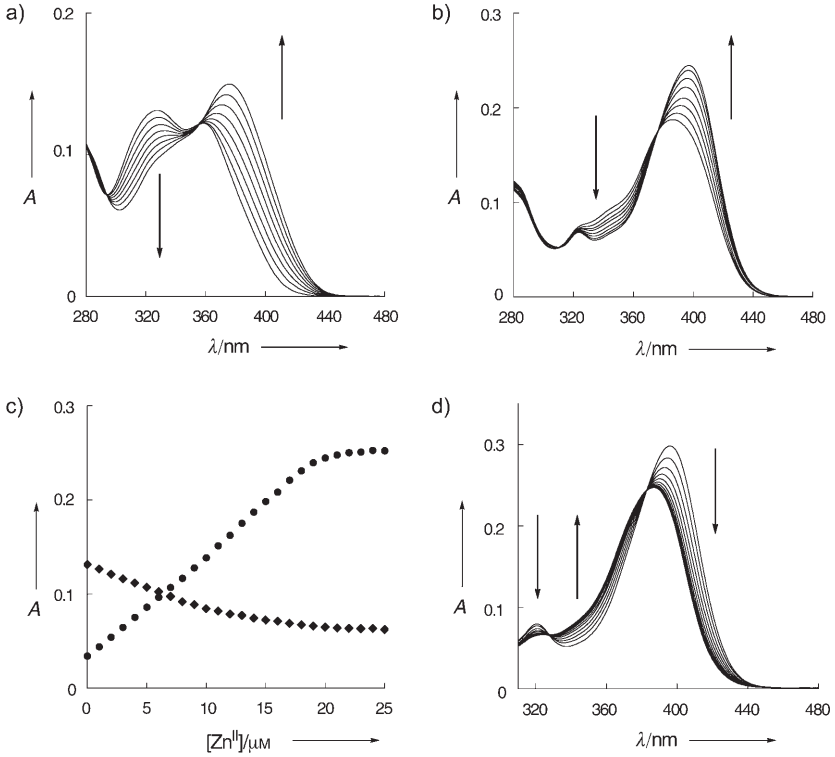


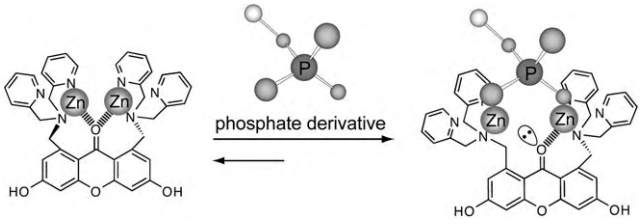
Figure 3. a–c) Zinc(II)-induced change in UV absorption of the ligand **1** (10 μM) upon addition of a) 0–0.7 and b) 1.3–2.0 equivalents of Zn^{II}. c) The plot of the UV absorption at 397 (●) and 328 nm (◆) of **1** (10 μM) in the zinc(II) titration (50 mM HEPES, 50 mM NaCl, pH 7.2/MeOH = 1:1, 25 °C). d) UV spectral change of **1**–2Zn^{II} upon addition of ATP (10 μM **1**–2Zn^{II} in 50 mM HEPES, 50 mM NaCl, pH 7.2, [ATP] = 0–20 μM, 25 °C).

decrease of 335 nm with an isosbetic point at 376 nm (Figure 3b).[13] The observed stepwise change in absorption can be reasonably ascribed to the coordination of both Zn^{II} ions within the molecule to the carbonyl oxygen atom of **1**, which should perturb the electronic properties of the xanthone fluorophore.[14] Interestingly, the absorption spectral change was also induced upon binding of **1**–2Zn^{II} to ATP. As shown in Figure 3d, the absorption maximum of **1**–2Zn^{II} at 397 nm decreases with an isosbestic point at 383 nm upon binding to ATP, the change of which is almost identical to the three signal changes observed in the ATP titration monitored by fluorescence excitation spectroscopy (Figure 2a).

It should be pointed out that the spectral changes induced by ATP absorption are in a direction opposite to the change in UV absorption observed in the process for the complexation of the second Zn^{II} center by **1** (Figure 3b). These results suggest that the excitation spectral change of **1**–2Zn^{II} upon binding to ATP is ascribed to the breaking of the coordinative bond between the xanthone carbonyl oxygen atom to the second Zn^{II} center.

This bond-breaking was also confirmed by a ^{13}C NMR spectroscopic study.[14b] The signal corresponding to the carbonyl carbon atom of the metal-free ligand **1** (10 mM in [D_6]DMSO) shifted downfield from $\delta = 177.9$ to 181.5 ppm in **1**–2Zn^{II}; the latter signal shifted upfield to $\delta = 178.9$ ppm upon adding one equivalent of NaH_2PO_4. A control chemosensor, mononuclear xanthone **2**–Zn^{II}[15] did not change its fluorescence upon adding phosphate species such as ATP or Na_2HPO_4 (data not shown), which suggests that **1**–2Zn^{II} binds to the phosphate anion with both Zn^{II}–Dpa sites as previously reported for the anthracene-type chemosensor **3**–2Zn^{II}.[4c] By combining these results, the excitation ratiometric change of binuclear **1**–2Zn^{II} upon phosphate binding can be reasonably explained as follows: in the resting state, both Zn^{II} centers are coordinated by the carbonyl oxygen atom of the xanthone fluorophore (Scheme 1). When a phosphate derivative is bound, the relatively labile coordination bond between one of Zn^{II} centers and the carbonyl oxygen atom is cleaved by the strong interaction of the metal ion with the phosphate, which results in the excitation change of three signals of the xanthone fluorophore. However, the tight coordination of the carbonyl oxygen atom to the other Zn^{II} center, which is observed in the X-ray crystallographic study of **1**–2Zn^{II}, remains intact in the phosphate complex such that this zinc atom interacts less strongly with the phosphate (Scheme 1).[16]

In conclusion, we have developed a new fluorescence chemosensor, **1**–2Zn^{II}, for phosphate species, which displays excitation change of three signals, thus enabling the ratiometric detection of phosphate species under neutral aqueous conditions. Our experimental data strongly support that the ratiometric excitation change is ascribed to rearrangement of the coordination induced by phosphate binding. We now envision bioanalytical applications of this chemosensor for real-time monitoring of an enzymatic reaction involving nucleoside pyrophosphates in vitro.[2e,3c,7]



Scheme 1. Phosphate anion-induced coordination rearrangement of **1**–2Zn^{II} upon binding to a phosphate derivative.[16]

Received: April 4, 2006
Revised: June 3, 2006
Published online: July 18, 2006

Keywords: anions · coordination modes · fluorescent probes · sensors · zinc

[1] a) R. Martínez-Máñez, F. Sancenón, *Chem. Rev.* **2003**, *103*, 4419–4476; b) S. Aoki, E. Kimura, *Rev. Mol. Biotechnol.* **2002**, *90*, 129–155; c) P. D. Beer, P. A. Gale, *Angew. Chem.* **2001**, *113*, 502–532; *Angew. Chem. Int. Ed.* **2001**, *40*, 486–516; d) L. Fabbrizzi, M. Licchelli, G. Rabaioli, A. Taglietti, *Coord. Chem. Rev.* **2000**, *205*, 865.

 © 2006 Wiley-VCH Verlag GmbH & Co. KGaA, Weinheim

[2] Fluorescent chemosensors for nucleoside pyrophosphates: a) H. Abe, Y. Mawatari, H. Teraoka, K. Fijimoto, M. Inouya, *J. Org. Chem.* **2004**, *69*, 495–504; b) J. Y. Kwon, N. J. Singh, H. N. Kim, S. K. Kim, K. S. Kim, J. Yoon, *J. Am. Chem. Soc.* **2004**, *126*, 8892–8893; c) F. Sancenón, R. Martínez-Máñez, M. J. Seguí, M. A. Miranda, J. Soto, *Angew. Chem.* **2003**, *115*, 671–674; *Angew. Chem. Int. Ed.* **2003**, *42*, 647–650; d) A. Ojida, S.-K. Park, Y. Mito-oka, I. Hamachi, *Tetrahedron Lett.* **2002**, *43*, 6193–6195; e) S. Mizukami, T. Nagano, Y. Urano, A. Odani, K. Kikuchi, *J. Am. Chem. Soc.* **2002**, *124*, 3920–3925; f) S. E. Schneider, S. N. O'Neil, E. V. Anslyn, *J. Am. Chem. Soc.* **2000**, *122*, 542–543; g) H. Fenniri, M. W. Hosseini, J.-M. Lehn, *Helv. Chim. Acta* **1997**, *80*, 786–803; h) M. W. Hosseini, A. J. Blacker, J.-M. Lehn, *J. Am. Chem. Soc.* **1990**, *112*, 3896–3904.

[3] Fluorescent chemosensors for inorganic pyrophosphates: a) D. H. Lee, S. Y. Kim, J.-I. Hong, *Angew. Chem.* **2004**, *116*, 4881–4884; *Angew. Chem. Int. Ed.* **2004**, *43*, 4777–4780; b) L. Fabbrizzi, N. Marcotte, F. Stomeo, A. Taglietti, *Angew. Chem.* **2002**, *114*, 3965–3968; *Angew. Chem. Int. Ed.* **2002**, *41*, 3811–3813; c) D. H. Vance, A. W. Czarnik, *J. Am. Chem. Soc.* **1994**, *116*, 9397–9398.

[4] Fluorescent chemosensors for phosphoproteins/peptides: a) A. Ojida, I. Hamachi, *Bull. Chem. Soc. Jpn.* **2006**, *79*, 35–46; b) A. Ojida, M. Inoue, Y. Mito-oka, H. Tsutsumi, K. Sada, I. Hamachi, *J. Am. Chem. Soc.* **2006**, *128*, 2052–2058; c) A. Ojida, Y. Mito-oka, K. Sada, I. Hamachi, *J. Am. Chem. Soc.* **2004**, *126*, 2454–2463; d) A. Ojida, T. Kohira, I. Hamachi, *Chem. Lett.* **2004**, 1024–1025; e) A. Ojida, M. Inoue, Y. Mito-oka, I. Hamachi, *J. Am. Chem. Soc.* **2003**, *125*, 10184–10185; f) A. Ojida, Y. Mito-oka, M. Inoue, I. Hamachi, *J. Am. Chem. Soc.* **2002**, *124*, 6256–6258.

[5] A. V. Gourine, E. Llaudet, N. Dale, K. M. Spyer, *Nature* **2005**, *436*, 108–111.

[6] S. A. Johnson, T. Hunter, *Nat. Methods* **2005**, *2*, 17–25.

[7] a) J. Wongkongkatep, Y. Miyahara, A. Ojida, I. Hamachi, *Angew. Chem.* **2006**, *118*, 681–684; *Angew. Chem. Int. Ed.* **2006**, *45*, 665–668; b) M. S. Han, D. H. Kim, *Bioorg. Med. Chem. Lett.* **2003**, *13*, 1079–1082.

[8] a) *The Handbook—A Guide to Fluorescent Probes and Labeling Technologies*, *10th ed.* (Ed.: M. T. Z. Spence), Invitrogen, USA, **2005**, chap. 19; b) B. Valeur, I. Leray, *Coord. Chem. Rev.* **2000**, *205*, 3–40.

[9] a) K. Choi, A. D. Hamilton, *Angew. Chem.* **2001**, *113*, 4030–4033; *Angew. Chem. Int. Ed.* **2001**, *40*, 3912–3915; b) J.-H. Liao, C.-T. Chen, J.-M. Fang, *Org. Lett.* **2002**, *4*, 561–564.

[10] a) J. Shi, X. Zhang, D. C. Neckers, *J. Org. Chem.* **1992**, *57*, 4418–4421; b) E. G. Sundholm, *Acta Chem. Scand. Ser. B* **1978**, *32*, 177–181; c) J. B. Hendrickson, M. V. J. Ramsay, T. R. Kelly, *J. Am. Chem. Soc.* **1972**, *94*, 6834–6843.

[11] Crystals of **1**–2 Zn^{II} with chloride counterions grew as colorless prisms by recrystallization from MeOH. A crystal suitable for X-ray crystallography was immersed in cryoprotectant oil (Paratone-N, Hampton Research) directly from the crystal solvent system, to avoid efflorescence, and immediately mounted on a goniometer head by using a CryoLoop (0.2–0.3 mm, Hampton Research) with cooling (120 K). X-ray diffraction data were collected on a Rigaku RAPID-HR diffractometer with a 2D area detector with graphite-monochromatized $Mo_{K\alpha}$ radiation ($\lambda = 0.7107$ Å). Crystal data for [**1**–2 Zn^{II}]Cl_4·*n*MeOH: $C_{39}H_{34}Cl_4N_6O_{10}Zn_2$, $M_r = 1019.30$, monoclinic, space group $P2_1/n$, $a = 12.947(2)$, $b = 12.711(2)$, $c = 27.948(4)$ Å, $V = 4581.2(1)$ Å^3, $\beta = 95.070(6)°$, $Z = 4$, $\rho_{calcd} = 1.478$ g cm^{-3}, $\mu = 1.340$ mm^{-1}, crystal size $0.10 \times 0.10 \times 0.30$ mm^3, 74011 collected, 37732 unique. $R1 = 0.076$ ($I > 2\sigma(I)$), $wR2 = 0.241$ ($I > 3\sigma(I)$), GOF = 1.517. All calculations were performed by using CrystalStructure software package (Rigaku). Direct methods (SIR2002) were used for the structure solution. The structure was refined by a full-matrix least-squares procedure by using observed reflections based on F^2. All non-hydrogen atoms were refined with anisotropic displacement parameters, and hydrogen atoms were placed in idealized positions with isotropic displacement parameters relative to the connected non-hydrogen atoms and refined in riding geometries. CCDC-602702 contains the supplementary crystallographic data for this paper. These data can be obtained free of charge from The Cambridge Crystallographic Data Centre via www.ccdc.cam.ac.uk/data_request/cif.

[12] Artificial receptors for nucleoside pyrophosphates: a) Z. Kejík, K. Záruba, D. Michalík, J. Sebek, J. Dian, S. Pataridis, K. Volka, V. Král, *Chem. Commun.* **2006**, 1533–1535; b) C. Li, M. Numata, M. Takeuchi, S. Shinkai, *Angew. Chem.* **2005**, *117*, 6529–6532; *Angew. Chem. Int. Ed.* **2005**, *44*, 6371–6374; c) S. C. McCleskey, M. J. Griffin, S. E. Schneider, J. T. McDevitt, E. V. Anslyn, *J. Am. Chem. Soc.* **2003**, *125*, 1114–1115; d) V. Janout, B. Jing, I. V. Staina, S. L. Regen, *J. Am. Chem. Soc.* **2003**, *125*, 4436–4437; e) S. M. Butterfield, M. L. Waters, *J. Am. Chem. Soc.* **2003**, *125*, 9580–9581; f) F. Snacenón, A. B. Descalzo, R. Martínez-Mánez, M. A. Miranda, J. Sato, *Angew. Chem.* **2001**, *113*, 2710–2713; *Angew. Chem. Int. Ed.* **2001**, *40*, 2640–2643; g) C. Bazzicalpi, A. Bencini, E. Berni, A. Bianchi, P. Fornasari, C. Giorgi, A. Masotti, P. Paoletti, B. Valtancoli, *J. Phys. Org. Chem.* **2001**, *14*, 432–443; h) K. O. Lara, C. Godoy-Alántar, I. L. Rivera, A. V. Eliseev, A. K. Tatsiminski, *J. Phys. Org. Chem.* **2001**, *14*, 453–462; i) J. A. Aguilar, E. García-Espana, J. A. Guerrero, S. V. Luis, J. M. Llinares, J. F. Miravet, J. A. Ramírez, C. Soriano, *J. Chem. Soc. Chem. Commun.* **1995**, 2235–2239; j) H.-J. Schneider, T. Blatter, B. Palm, U. Pfingstag, V. Rüdinger, I. Theis, *J. Am. Chem. Soc.* **1992**, *114*, 7704–7708.

[13] In the zinc(II) titration of the metal-free ligand **1** (0.5 μM) under the same conditions, the fluorescence emission at 447 nm largely increased ($\lambda_{ex} = 397$ nm), and the change was almost complete upon addition of two equivalents of $Zn(NO_3)_2$. The plot of the emission intensity gave a biphasic titration curve, which was analyzed by nonlinear curve-fitting analysis to estimate the first and second zinc(II) complexation constant to be $> 10^7$ and 1.2×10^7 M^{-1}, respectively.

[14] Study of simultaneous coordination of two Lewis acids with a single carbonyl oxygen atom: a) K. Maruoka, *Pure Appl. Chem.* **2002**, *74*, 123–128; b) N. Asao, S. Kii, H. Hanawa, K. Maruoka, *Tetrahedron Lett.* **1998**, *39*, 3729–3732.

[15] In the zinc(II) titration of the metal-free ligand **2** (10 μM in 50 mM HEPES, 50 mM NaCl, pH 7.2/MeOH 1:1) the UV/Vis spectrum changed in an almost identical manner with that observed in **1** up until the addition of one equivalent of zinc(II) (Figure 3a) with an isosbestic point at 333 nm, thus indicating the coordination of zinc(II) to the carbonyl oxygen atom of the ligand **2**. However, further spectral change was not induced upon addition of an excess amount of zinc(II) ions, as observed in the case of **1** (Figure 3b). These results also support that **1**–2 Zn^{II} forms a complex with coordination between both zinc(II) centers and the carbonyl oxygen atom.

[16] In the binding of **1**–2 Zn^{II} with nucleoside pyrophosphates such as ATP, it was proposed that, unlike the monophosphate species, the two phosphate groups simultaneously interact with the Zn^{II}–Dpa sites of **1**–2 Zn^{II}. This theory was supported by a ^{31}P NMR spectroscopic study, in which the signals corresponding to β and γ phosphate of ATP observed at $\delta = -21.1$ and -8.4 ppm shifted to $\delta = -17.7$ and -4.2 ppm, respectively, upon addition of one equivalent of **1**–2 Zn^{II}, whereas the resonance corresponding to the α-phosphate observed at $\delta = -9.7$ ppm scarcely shifted. Similar shifts were also observed in the case of the two phosphates of ADP upon **1**–2 Zn^{II} binding. Such a multipoint binding mode involving the two phosphate groups may reasonably explain the strong binding affinity of **1**–2 Zn^{II} for nucleoside pyrophosphates.

 © 2006 Wiley-VCH Verlag GmbH & Co. KGaA, Weinheim

Free-Radical Chemistry

DOI: 10.1002/anie.200600831

Water: The Ideal Hydrogen-Atom Source in Free-Radical Chemistry Mediated by Ti^{III} and Other Single-Electron-Transfer Metals?**

Juan M. Cuerva, Araceli G. Campaña, José Justicia, Antonio Rosales, Juan L. Oller-López, Rafael Robles, Diego J. Cárdenas,* Elena Buñuel, and J. Enrique Oltra**

The reactivity of water with both carbanion and carbocation intermediates is well known, but until now it has generally been believed that water is inert towards free radicals.[1] This hypothetical passivity has been attributed to the strong H–OH bond, which, with a bond-dissociation energy of 117.59 ± 0.07 kcal mol^{-1},[2] would impede any potential hydrogen-atom transfer from water. Some years ago, however, we chanced to observe that tertiary radicals were reduced effectively in the presence of bis(cyclopentadienyl)titanium(III) chloride[3] ([Cp_2TiCl]) and water.[4] This observation further facilitated the control of the final step in titanocene-catalyzed radical cyclizations, which are useful for the straightforward synthesis of complex polycyclic terpenoids.[5] However, as, at the time, the idea of water acting as a hydrogen-atom source seemed to be counterintuitive, this phenomenon was rationalized by invoking either the formation and subsequent hydrolysis of alkyl–Ti^{IV} complexes or a virtually intramolecular hydrogen transfer via a quite sophisticated cyclic transition state.[4,5] We now have solid evidence to show that water really can act as a complete hydrogen-atom source rather than as a simple proton donor for radical reductions mediated by Ti^{III} and, presumably, other metals that react by single-electron transfer.

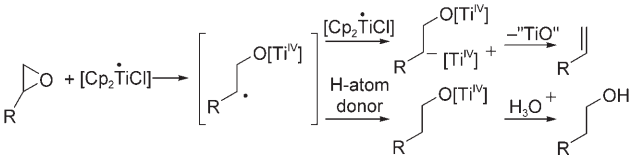
[*] Dr. J. M. Cuerva, A. G. Campaña, Dr. J. Justicia, Dr. A. Rosales, Dr. J. L. Oller-López, Dr. R. Robles, Dr. J. E. Oltra
Departamento de Química Orgánica de la Facultad de Ciencias
Campus Fuentenueva s/n Universidad de Granada
18071 Granada (Spain)
Fax: (+34) 958-248-437
E-mail: jmcuerva@platon.ugr.es
joltra@ugr.es

Dr. D. J. Cárdenas, Dr. E. Buñuel
Departamento de Química Orgánica
C-I. Universidad Autónoma de Madrid
Cantoblanco, 28049 Madrid (Spain)
Fax: (+34) 913-973-966
E-mail: diego.cardenas@uam.es

[**] This research was supported by the "Junta de Andalucía" (PAI group FQM339) and the Spanish Ministry of Education and Science (Projects CTQ2005-08402/BQU and CTQ2004-02040/BQU). We also thank our English colleague Dr. J. Trout for revising our text and the "Centro de Computación Científica-UAM" for computation time.

Supporting information for this article is available on the WWW under http://www.angewandte.org or from the author.

Many highly selective free-radical reactions have been developed and have proved to be very useful in the total synthesis of complex organic compounds owing to the mild conditions required and their compatibility with many functional groups.[6] Within this context, RajanBabu and Nugent introduced a novel concept: homolytic oxirane opening induced by [Cp_2TiCl].[7] This reaction generates the most substituted (i.e., most stable) β-titanoxy radical, which, among other transformations, could be either trapped by a second [Cp_2TiCl] species to provide an alkene (epoxide deoxygenation) by "TiO" elimination or, in the presence of a hydrogen-atom donor such as cyclohexa-1,4-diene (1,4-CHD), reduced to an alcohol with the opposite regiochemistry to that expected from the reduction with metal hydrides (Scheme 1).[7]

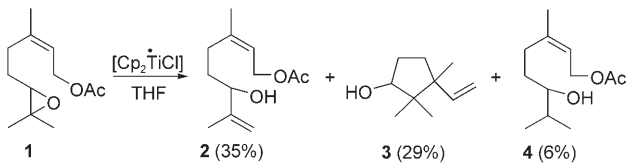


Scheme 1. [Cp_2TiCl]-induced deoxygenation and reductive opening of epoxides by radical chemistry.[7]

Since the development of the first titanocene-catalyzed reaction,[8] [Cp_2TiCl]-mediated processes have become formidable tools in organic synthesis.[9] However, conventional hydrogen-atom donors used in radical chemistry, such as 1,4-CHD, Bu_3SnH, and 2-methylpropan-2-thiol, are toxic, expensive, and/or foul smelling, thus seriously limiting the application of the reaction described by RajanBabu and Nugent and other radical reactions for large-scale preparations.[6] Therefore, the discovery of novel and more convenient hydrogen-atom sources seemed desirable.[10] In this context, we decided to explore the possibility of employing safe and inexpensive water as an ideal hydrogen source in Ti^{III}-mediated radical chemistry; titanocene(III)-promoted homolytic epoxide opening was used as a model process for this study.

We first examined the reaction between 6,7-epoxyneryl acetate (**1**) and an excess of [Cp_2TiCl] (2.5 equiv) in strictly dry THF, that is, under the conditions described by RajanBabu and Nugent for epoxide deoxygenation.[7] In this manner we obtained the allylic alcohol **2** (35% yield of isolated **2**) together with **3** (29%), the product of 5-*exo* cyclization, and minor amounts of the reduction product **4** (6%); neryl acetate (**7**), the expected deoxygenation product, was not detected (Scheme 2).[11]

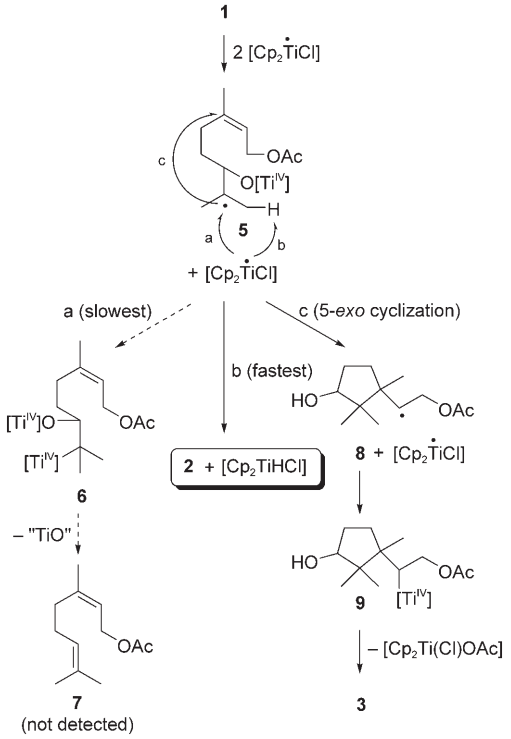
The formation of the major product **2** suggested that a mixed disproportionation had occurred that was slightly



Scheme 2. [Cp_2TiCl]-promoted transformation of **1** in strictly dry THF.

InterScience
© 2006 Wiley-VCH Verlag GmbH & Co. KGaA, Weinheim

faster than the cyclization process to give **3** and much faster than the potential trapping (or two-electron reduction) of the tertiary radical **5** by a second [Cp_2TiCl] species (Scheme 3). Such kinetics would explain why the deoxygenation product **7** was not formed. This behavior, reminiscent of that of bulky bases in the presence of tertiary alkyl halides and sulfonates, might simply be due to steric factors.

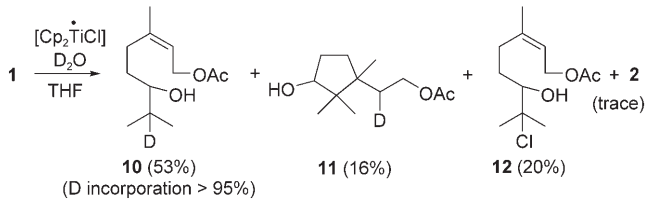


Scheme 3. Mixed disproportionation (b) versus 5-*exo* cyclization (c) and radical trapping of **5** (a).

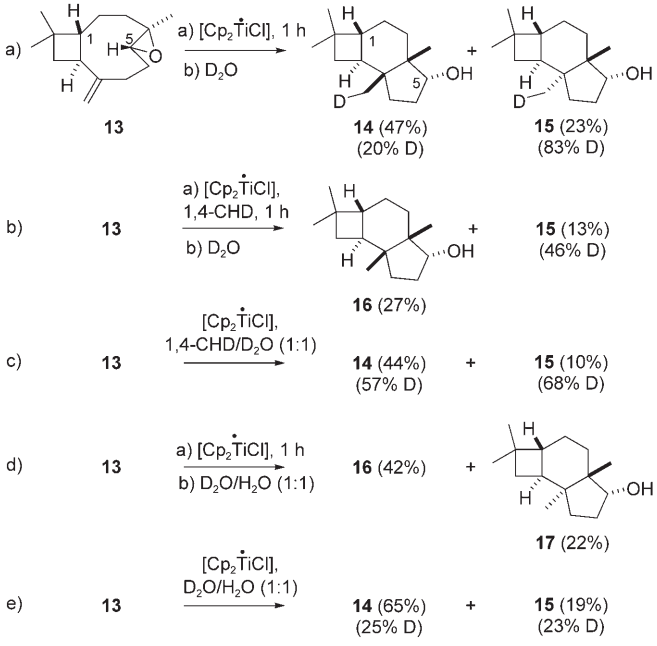
In the light of the above observations, the following experiments clarified the situation considerably. First, when we treated **1** with [Cp_2TiCl] (2.5 equiv) in the presence of D_2O (10 equiv), the reduced derivative **10** became the main product at the expense of the allylic alcohol **2** (Scheme 4). These results indicated that the water-mediated reduction of radical **5** was faster than the mixed-disproportionation process, which in turn had been shown to be much faster than the potential radical trapping by a second [Cp_2TiCl] species. Additionally, when we treated **1** with [Cp_2TiCl] (2.5 equiv) in the presence of an equimolar mixture of D_2O and 1,4-CHD (10 equiv) we obtained **10** with 70% deuterium incorporation. Thus, the transfer of deuterium from D_2O was even faster than that of a hydrogen atom from 1,4-CHD. As these observations on the kinetics of the process ruled out the possibility of **10** being formed by the hydrolysis of an alkyl–Ti^{IV} complex, we considered for the first time the hypothesis that the coordination of water with [Ti^{III}] might diminish the bond-dissociation energy of water to values that allow the transfer of a whole hydrogen atom (or deuterium atom) to the tertiary radical **5**.

The acetate **11** might derive from either the hydrolysis of the alkyl–Ti^{IV} complex **9**, or, more plausibly, deuterium-atom transfer to the secondary radical **8** (see Scheme 3). In the latter case the formation of **9** and the subsequent elimination of [$Cp_2Ti(Cl)OAc$] to give the alkene **3** are avoided. We decided to confirm the possibility of hydrogen-atom transfer from water not only to tertiary but also to primary and secondary radicals. Primary and secondary radicals are generally less hindered sterically than tertiary radicals and therefore can be readily trapped by [Cp_2TiCl] to give alkyl–Ti^{IV} complexes.[7] Thus, hydrogen-atom transfer from water might be masked as the apparent simple hydrolysis of a Ti^{IV} complex. In an attempt to avoid this misleading possibility we chose to investigate the [Cp_2TiCl]-promoted transannular cyclization of caryophyllene oxide (**13**, Scheme 5) because the β-trisubstituted primary radicals formed in the expected 5-*exo*/6-*exo* cyclization (see **18** in Scheme 6) might be sufficiently sterically protected to impede the formation of alkyl–Ti^{IV} complexes.

Thus, we treated the epoxide **13** with [Cp_2TiCl] in strictly dry THF and added D_2O after 1 h, when the starting material had been consumed completely (thin-layer chromatography (TLC) analysis). In this way we obtained the tricyclic alcohol **14** (only 20% incorporation of D) together with its epimer **15** as a minor product (Scheme 5a).[12]



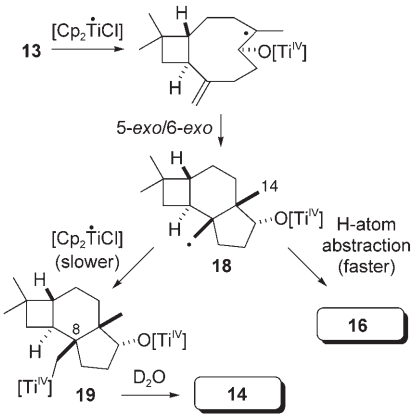
Scheme 4. [Cp_2TiCl]-promoted reductive opening of the epoxide **1** with D_2O as the hydrogen-atom source.



Scheme 5. a)–e) [Cp_2TiCl]-induced transannular cyclization of **13** under different conditions.

 © 2006 Wiley-VCH Verlag GmbH & Co. KGaA, Weinheim

The relatively low proportion of deuterium incorporated into **14** suggested that the coupling of radical **18** with [Cp_2TiCl] to give the alkyl–Ti^{IV} complex **19** was slower than a competing process of hydrogen-atom abstraction from the solvent (THF; formation of **16**; Scheme 6). This result

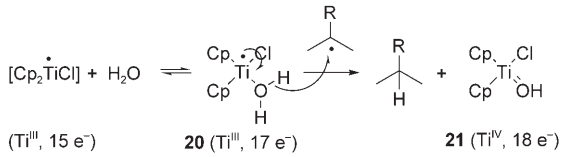


Scheme 6. Competing reactions of the primary radical **18** with [Cp_2TiCl] and hydrogen-atom donors.

prompted us to repeat the experiment in the presence of 1,4-CHD (Scheme 5b), a more efficient hydrogen-atom donor than THF. In this way we obtained alcohol **16** together with **15**, but the deuterated derivative **14** was not detected: a clear indication that hydrogen-atom transfer from 1,4-CHD was faster than radical coupling to [Cp_2TiCl]. Finally, we treated **13** with [Cp_2TiCl] in the presence of an equimolar mixture of D_2O and 1,4-CHD, and thus once more obtained the deuterated derivatives **14** and **15** (Scheme 5c). In this case the incorporation of deuterium into **14** was 57%. Thus, deuterium transfer from D_2O was slightly faster than hydrogen-atom transfer from 1,4-CHD, which in turn had been shown to be much faster than the formation of the alkyl–Ti^{IV} complex **19**. In other words, the [Cp_2TiCl]/water-promoted reduction of the primary radical **18** was faster than the formation of the complex **19**, and consequently 57% of deuterium incorporation into **14** could not be attributed to the hydrolysis of **19**. Moreover, because the radical **18** has no hydrogen atom at the β position, a six-membered cyclic transition state, such as that proposed by some of us in 2002 (see ref. [4]), could not be involved in the process either.

The relatively high deuterium incorporation (83%) into the minor product **15** in the experiment summarized in Scheme 5a shows that a high proportion of an alkyl–Ti^{IV} complex (the C8 epimer of **19**) was formed upon the treatment of **13** with [Cp_2TiCl] in dry THF for 1 h (see ref. [7]). Therefore, we had the opportunity to measure and compare isotope effects. To this end, we treated **13** with [Cp_2TiCl] in dry THF once again and after 1 h added a 1:1 mixture of D_2O and H_2O (Scheme 5d). In this way we obtained the tricyclic isomers **16** and **17**. The deuterated derivative **15** was not detected, which suggests that a large isotope effect exists for the hydrolysis of the Ti^{IV} complex. In contrast, when we treated **13** with [Cp_2TiCl] in the presence of a 1:1 mixture of D_2O and H_2O (Scheme 5e), we obtained, along with **14**, the deuterated derivative **15** with 23% deuterium incorporation. This result corresponds to a K_H/K_D ratio of only 3.35 for the radical-reduction process. Different isotope effects are indicative of different reaction mechanisms; therefore, these results support the conclusion obtained from the kinetics-based evidence that radical reduction in the presence of water and [Cp_2TiCl] does not derive from the hydrolysis of alkyl–Ti^{IV} complexes. Moreover, the magnitude of the isotope effect observed for this reduction of a primary radical (3.35) is virtually the same as that reported for hydrogen-atom transfer from *t*BuSH to the primary 1-nonyl radical ($K_H/K_D = 3.40$).[13]

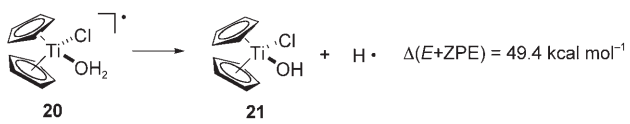
Under these circumstances, the most plausible assumption seemed to be that an aqua complex, such as **20** (Scheme 7),



Scheme 7. Mechanism, Ti oxidation states, and electrons in the metal bonding shell for the hydrogen-atom transfer from water to a free radical via the aqua complex **20**.

might act as an efficient hydrogen-atom donor by means of an inner-sphere, single-electron transfer to the oxygen atom, with concomitant oxidation to a [Ti^{IV}] complex, such as **21**. Finally, **21** might evolve to HCl and stable [$Cp_2Ti{=}O$], which would also explain why the formation of the chlorohydrin **12** (see Scheme 4), presumably by HCl-induced epoxide opening, was only observed in the presence of water.[14]

To check the feasibility of this mechanism, we performed a computational study to determine how the bond-dissociation energy of water might be affected by coordination to [Ti^{III}] in the putative aqua complex **20**. Calculations were performed by using density functional theory (DFT), since high-accuracy ab initio methods are prohibitive for these complexes. The calculated dissociation energy for H_2O at the B3LYP/6-31G(d) level is 108.1 kcal mol^{-1}, which is just slightly lower than the experimental value (117.6 kcal mol^{-1}) and the theoretical value previously calculated at the ab initio G3 level (116 kcal mol^{-1}).[15] Interestingly, homolytic O–H bond dissociation is favored to an extraordinary extent by the coordination of H_2O to [$Cp_2Ti^{III}Cl$]. Thus, at the same DFT level, the calculated reaction energy for O–H dissociation from complex **20** to afford **21** is only 49.4 kcal mol^{-1} (Scheme 8). This dramatic decrease strongly supports the mechanism depicted in Scheme 7. Moreover, comparison of the calculated structures shows that the Ti–O distance is much longer in **20** (2.28 Å) than in **21** (1.86 Å), and thus



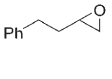
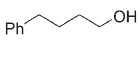
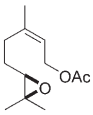
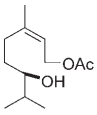
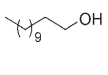
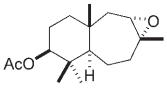
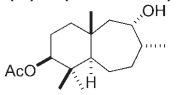
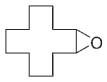
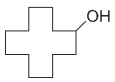
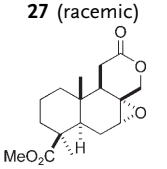
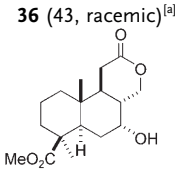
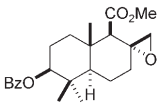
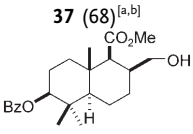
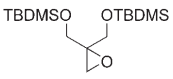
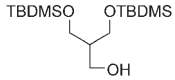
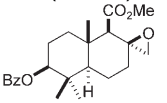
Scheme 8. Calculated reaction energy for the homolytic O–H bond dissociation in the aqua complex **20**.

 © 2006 Wiley-VCH Verlag GmbH & Co. KGaA, Weinheim

confirms that after O–H dissociation the Ti–O bond acquires a certain double-bond character by additional pairing of the electrons of Ti and O.[16]

Epoxides are one of the most versatile functional groups in organic chemistry. Because of the success of methods for asymmetric epoxidation developed by the research groups of Sharpless, Katsuki, Jacobsen, Shi, and others, these compounds have become crucial intermediates for enantioselective synthesis.[17] With valuable mechanistic data in hand, we decided to explore the synthetic usefulness of the $[Cp_2TiCl]/H_2O$ combination for the reductive opening of epoxides, thus avoiding the use of harmful hydrogen-atom donors. To this end we prepared a number of epoxides (**1**, **22**–**30**) and treated them with $[Cp_2TiCl]$ (2.2 equiv) and H_2O (40 equiv) in THF.[18] The results are summarized in Table 1.

Table 1: Reductive opening of epoxides **1** and **22**–**30** mediated by $[Cp_2TiCl]/H_2O$.

Substrate	Product (yield [%])	Substrate	Product (yield [%])
			
22	**31** (78)	**1** (70% *ee*)	(+)-**4** (72, 73% *ee*)[a]
			
23	**32** (85)	**27** (racemic)	**36** (43, racemic)[a]
			
24	**33** (62)[a]	**28**[b]	**37** (68)[a,b]
			
25	**34** (60, racemic)[a]	**29** (racemic)[d]	**38** (81, racemic)
			
26[c]	**35** (60)[a]	**30** (racemic)	**38** (67, racemic)[a]

[a] Besides the main product, minor quantities of by-products, such as chlorohydrins and/or *vic* diols, which are presumably derived from HCl-induced heterolytic epoxide opening, were also detected. [b] Optically pure. [c] TBDMS = *tert*-butyldimethylsilyl. [d] Bz = benzoyl.

Competing deoxygenation is a serious problem when the reductive opening of terminal epoxides is performed with 1,4-CHD.[7] The yields of the alcohol products of the reduction of **22** and **23** (Table 1) revealed that our combination of the titanium reagent and water was not only safer and cheaper but also more efficient than the method of RajanBabu and Nugent[7] for this type of substrate. Additionally, Table 1 shows that our method also worked well with di- and trisubstituted epoxides, and even with the sterically congested substrate **26**, the reaction of which gave the alcohol **35** in an acceptable yield of 60%. Moreover, the $[Cp_2TiCl]/H_2O$-promoted reductive opening of optically active **1**, prepared from nerol with the aid of the chiral ketone described by Wang and Shi,[19] gave the alcohol (+)-**4** (73% *ee*), which suggests that the combination of our process with well-established methods for asymmetric epoxidation could afford a practical two-step procedure for the enantioselective synthesis of anti-Markovnikov alcohols from prochiral alkenes.[20]

Our procedure also showed considerable regio- and stereoselectivity, as was demonstrated in the reduction of the cyclic substrates **27** and **28** to the *cis*-substituted secondary alcohols **36** and **37**, with the incoming hydrogen atom in an *anti* relationship to the OH group. This stereoselectivity is opposite (and complementary) to that observed in the hydroboration–oxidation process.[20] Nevertheless, the reduction of the epimeric spiroepoxides **29** and **30** gave the same product. The formation of **38** from both epimers indicates that for this kind of compound the reaction is stereoselective but not stereospecific. These results can be rationalized readily (and predicted with confidence) by considering that the attack of the bulky aqua complex **20** takes place preferentially at the less hindered face of the intermediate radical formed in each case.

Finally, in a titanocene-catalyzed version of the process the required quantity of the titanocene was decreased by one order of magnitude, but the alcohol products were obtained in slightly lower yields. Thus, the treatment of **22**, **24**, and **25** with a substoichiometric amount of $[Cp_2TiCl]$ (0.2 equiv) and H_2O (8 equiv) in the presence of 2,4,6-collidine hydrochloride as the titanocene-regenerating agent[8] gave the alcohols **31**, **33**, and **34** in yields of 70, 45, and 50%, respectively.

During the course of the study described herein the research group of Wood reported that water could be used as hydrogen-atom source in trialkylborane-mediated variants of the Barton–McCombie reaction and from calculations carried out on the $Me_3Al{\cdot}OH_2$ complex deduced that the observed reaction might be unique to trialkylborane–water ($R_3B{\cdot}OH_2$) systems.[15,21] Our results demonstrate, however, that hydrogen-atom transfer from water can be mediated not only by trialkylboranes but also by Ti^{III} complexes, as we had previously suspected.[4] Furthermore, a careful inspection of the mechanism and electron counts depicted in Scheme 7 suggests that this phenomenon might be more general than expected, and might be mediated by any single-electron-transfer metal with an orbital vacancy to coordinate with H_2O. In this sense, closely related reaction mechanisms might help to explain the hydrogen-atom-donor

 © 2006 Wiley-VCH Verlag GmbH & Co. KGaA, Weinheim

ability of the Mn^{II} aqua complex in the manganese cluster of photosystem II,[22] or the highly exothermic generation of hydrogen by the reaction between sodium and water. In fact, our calculations of the bond-dissociation energy of the O–H bond in the aqua complexes $[Cp_2Zr^{III}(Cl)OH_2]$ and $[Cp_2Hf^{III}(Cl)OH_2]$ provided values of only 25.5 and 13.7 kcal mol^{-1}, respectively. These low values strongly support the hypothesis that hydrogen-atom transfer from water might be mediated by different metals capable of single-electron transfer.

In summary, we have presented theoretical and experimental evidence that indicates that water can act as an efficient hydrogen-atom source in radical reductions mediated by Ti^{III} complexes and, presumably, other metals that react by single-electron transfer. Moreover, this property can be exploited advantageously for the reductive opening of epoxides to provide a mild, safe, inexpensive two-step procedure (complementary to the hydroboration–oxidation method) for the preparation from alkenes of anti-Markovnikov alcohols, even in deuterated form and/or enantioselectively. We are currently studying the hydrogen-atom-transfer ability of other aqua complexes with different transition metals.

Received: March 3, 2006
Published online: July 19, 2006

Keywords: epoxides · hydrogen transfer · radicals · titanium · water

[1] a) D. P. Curran, N. A. Porter, B. Giese, *Stereochemistry of Radical Reactions*, VCH, Weinheim, **1996**, p. 4; b) D. P. Curran in *Comprehensive Organic Synthesis*, *Vol. 4* (Eds.: B. M. Trost, I. Fleming, M. E. Semmelhack), Pergamon, Oxford, **1991**, pp. 715–777.

[2] B. Ruscic, A. F. Wagner, L. B. Harding, R. L. Asher, D. Feller, D. A. Dixon, K. A. Peterson, Y. Song, X. Qian, C.-Y. Ng, J. Liu, W. Chen, D. W. Schwenke, *J. Phys. Chem. A* **2002**, *106*, 2727–2747.

[3] The single-electron-transfer reagent bis(cyclopentadienyl)-titanium(III) chloride can be generated in situ by stirring commercial $[Cp_2TiCl_2]$ with Mn dust in THF, where it exists as a mixture of the mononuclear $[Cp_2TiCl]$ and the dinuclear $[(Cp_2TiCl)_2]$ species; see: R. J. Enemærke, J. Larsen, T. Skrydstrup, K. Daasbjerg, *J. Am. Chem. Soc.* **2004**, *126*, 7853–7864; for the sake of clarity, we represent this complex herein as $[Cp_2TiCl]$.

[4] A. F. Barrero, J. E. Oltra, J. M. Cuerva, A. Rosales, *J. Org. Chem.* **2002**, *67*, 2566–2571.

[5] a) J. Justicia, J. L. Oller-López, A. G. Campaña, J. E. Oltra, J. M. Cuerva, E. Buñuel, D. J. Cárdenas, *J. Am. Chem. Soc.* **2005**, *127*, 14911–14921; b) J. Justicia, J. E. Oltra, J. M. Cuerva, *J. Org. Chem.* **2005**, *70*, 8265–8272; c) J. Justicia, A. Rosales, E. Buñuel, J. L. Oller-López, M. Valdivia, A. Haïdour, J. E. Oltra, A. F. Barrero, D. J. Cárdenas, J. M. Cuerva, *Chem. Eur. J.* **2004**, *10*, 1778–1788; d) A. F. Barrero, A. Rosales, J. M. Cuerva, J. E. Oltra, *Org. Lett.* **2003**, *5*, 1935–1938.

[6] For an excellent overview of contemporary free-radical chemistry, see: *Radicals in Organic Synthesis*, *Vols. 1 and 2* (Eds.: P. Renaud, M. P. Sibi), Wiley-VCH, Weinheim, **2001**.

[7] T. V. RajanBabu, W. A. Nugent, *J. Am. Chem. Soc.* **1994**, *116*, 986–997.

[8] a) A. Gansäuer, M. Pierobon, H. Bluhm, *Angew. Chem.* **1998**, *110*, 107–109; *Angew. Chem. Int. Ed.* **1998**, *37*, 101–103; b) A. Gansäuer, H. Bluhm, *Chem. Commun.* **1998**, 2143–2144; c) A. Gansäuer, H. Bluhm, M. Pierobon, *J. Am. Chem. Soc.* **1998**, *120*, 12849–12859.

[9] For recent reviews, see: a) J. M. Cuerva, J. Justicia, J. L. Oller-López, B. Bazdi, J. E. Oltra, *Mini-Rev. Org. Chem.* **2006**, *3*, 23–35; b) A. Gansäuer, T. Lauterbach, S. Narayan, *Angew. Chem.* **2003**, *115*, 5714–5731; *Angew. Chem. Int. Ed.* **2003**, *42*, 5556–5573; c) A. Gansäuer, B. Rinker in *Titanium and Zirconium in Organic Synthesis* (Ed.: I. Marek), Wiley-VCH, Weinheim, **2002**, pp. 435–450.

[10] The quest for novel hydrogen-atom donors for titanocene-mediated reductive epoxide opening has been the focus of recent research; see: A. Gansäuer, A. Barchuk, D. Fielenbach, *Synthesis* **2004**, 2567–2573.

[11] The results depicted in Scheme 2 suggest that the formation of the minor product **4** and an equimolar amount of **2** (6%) might be the result of a radical–radical disproportionation process. In this aspect, our reaction differs from the reduction of tertiary radicals by SmI_2, in which, in the absence of any proton source, radical–radical disproportionation products were the main components of the mixtures obtained; see: T. Nagashima, A. Rivkin, D. P. Curran, *Can. J. Chem.* **2000**, *78*, 791–799.

[12] The relatively low deuterium incorporation in **14** compared with that in **15** is presumably due to the increased steric hindrance introduced in the radical **18** by the *cis* disposition of the C14 methyl group relative to the adjacent primary radical. This steric hindrance impedes the corresponding radical coupling with bulky $[Cp_2TiCl]$.

[13] W. A. Pryor, K. G. Kneipp, *J. Am. Chem. Soc.* **1971**, *93*, 5584–5586.

[14] Moreover, epoxide **1** was recovered unchanged after treatment with H_2O, $MnCl_2$, and Mn dust in the absence of $[Cp_2TiCl_2]$.

[15] D. A. Spiegel, K. B. Wiberg, L. N. Schacherer, M. R. Medeiros, J. L. Wood, *J. Am. Chem. Soc.* **2005**, *127*, 12513–12515.

[16] Similar double-bond character was observed in the crystal structure of $[Cp_2Ti(OH)Cl]$; see: H. D. Gibson, Y. Ding, M. S. Mashuta, J. F. Richardson, *Acta Crystallogr. Sect. C* **1996**, *52*, 559–560.

[17] W. Carruthers, I. Coldham, *Modern Methods of Organic Synthesis*, 4th ed., Cambridge University Press, Cambridge, **2004**, pp. 337–346.

[18] We tested the reaction with different quantities of water and found that for 2.2 equivalents of $[Cp_2TiCl]$ the best yields of the alcohol were observed with 40 equivalents of H_2O. Detailed experimental procedures and spectroscopic data for all products described herein can be found in the Supporting Information.

[19] Z.-X. Wang, Y. Shi, *J. Org. Chem.* **1998**, *63*, 3099–3104.

[20] Note that alkene epoxidation followed by $[Cp_2TiCl]/H_2O$-mediated epoxide opening might provide a useful (and complementary) alternative to the hydroboration–oxidation method.

[21] For related observations on alcohol–borane systems, see: D. Pozzi, E. M. Scanlan, P. Renaud, *J. Am. Chem. Soc.* **2005**, *127*, 14204–14205.

[22] C. W. Hoganson, G. T. Babcock, *Science* **1997**, *277*, 1953–1956.

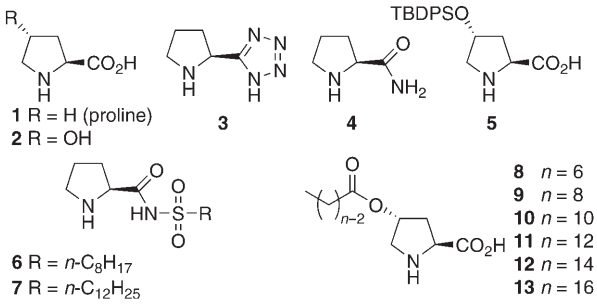
 © 2006 Wiley-VCH Verlag GmbH & Co. KGaA, Weinheim

Organocatalysis

DOI: 10.1002/anie.200601156

Combined Proline–Surfactant Organocatalyst for the Highly Diastereo- and Enantioselective Aqueous Direct Cross-Aldol Reaction of Aldehydes**

Yujiro Hayashi, Seiji Aratake, Tsubasa Okano, Junichi Takahashi, Tatsunobu Sumiya, and Mitsuru Shoji*

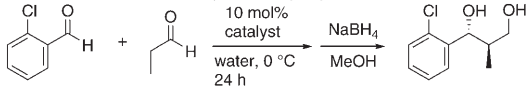


Scheme 1. Organocatalysts examined in this study. TBDPS = *tert*-butyldiphenylsilyl.

As water offers several advantages over organic solvents, reactions in aqueous media have received a great deal of attention in recent years.[1] However, the asymmetric aldol reaction in water has proved very difficult to achieve.[2] While proline has been reported to catalyze aldol reactions efficiently in polar solvents such as dimethyl sulfoxide (DMSO) and *N*,*N*-dimethylformamide (DMF),[3] and while a small amount of water is beneficial in some proline-mediated aldol reactions,[4] only low enantioselectivities have been obtained in water even in the presence of a surfactant.[5] There have been no successful asymmetric aldol reactions performed using organocatalysts in water in the absence of an organic cosolvent or other additives. Recently, we reported that a siloxyproline effectively catalyzes the highly diastereo- and enantioselective aldol reaction of ketones and aldehydes in the presence of water.[6] Barbas and co-workers reported the asymmetric aldol reaction of ketones and aldehydes in water catalyzed by a combination of a diamine and an acid.[7] Herein, we describe how combined proline–surfactant organocatalysis promotes the asymmetric direct aldol reaction of two different aldehydes in the presence of water and no other additives, with high diastereo- and enantioselectivity. The original version of this reaction reported by MacMillan and Northup was carried out in a polar organic solvent under proline catalysis, with introduction of the aldehyde donor by syringe pump.[8]

The reaction of *o*-chlorobenzaldehyde and propanal (5 equiv) was selected as a model and performed in the presence of 18 equivalents of water and several putative organocatalysts (10 mol%, 24 h; see Scheme 1). The aldols were isolated after reduction to the corresponding diols (Table 1). No reaction proceeded when proline (**1**), hydroxyproline (**2**), or proline-tetrazol (**3**)[4a,9] were employed. With siloxyproline,[6,10] two phases were formed as previously described[6] and the aldols were obtained with excellent diastereo- and enantioselectivities. The moderate yield can be ascribed to insufficient mixing of the reagents, as propanal is water-soluble while *o*-chlorobenzaldehyde is not. Emulsions may be the ideal reaction medium for achieving effective mixing, as demonstrated by Kobayashi et al. for several surfactant-combined organometallic catalysts, which promote organic reactions in water or aqueous organic solvents.[2]

Table 1: Effect of the organocatalyst and amount of water on the aldol reaction of *o*-chlorobenzaldehyde and propanal.[a]



Entry	Catalyst	Amount of water [equiv]	Yield [%][b]	*anti*/*syn*[c]	*ee* [%][d]
1	**1**	18	<5	–	–
2	**2**	18	<5	–	–
3	**3**	18	<5	–	–
4	**4**	18	30	2:1	71
5	**5**	18	50	8:1	98
6	**6**	18	14	18:1	96
7	**7**	18	17	20:1	95
8	**8**	18	39	14:1	96
9	**9**	18	57	18:1	97
10	**10**	18	60	20:1	99
11	**11**	18	54	17:1	96
12	**12**	18	15	>20:1	96
13	**13**	18	32	11:1	94
14	**10**	0	71	16:1	97
15	**10**	5	58	17:1	97
16	**10**	54	65	12:1	94
17	**10**	125	58	13:1	95
18[e]	**10**	18	92	19:1	99
19[f]	**10**	18	97	19:1	99

[a] The reaction was conducted with 0.4 mmol of *o*-chlorobenzaldehyde and 2.0 mmol of propanal at 0°C for 24 h. [b] Isolated yield. [c] Determined by ^{1}H NMR spectroscopy. [d] *ee* value of *anti* isomer, determined by chiral HPLC after conversion into the benzoyl ester (see Supporting Information). [e] The reaction was performed for 70 h. [f] The reaction was performed with 15 mmol of *o*-chlorobenzaldehyde and 45 mmol of propanal for 96 h.

[*] Prof. Dr. Y. Hayashi, S. Aratake, T. Okano, J. Takahashi, T. Sumiya, Dr. M. Shoji
Department of Industrial Chemistry
Faculty of Engineering
Tokyo University of Science
Kagurazaka, Shinjuku-ku, Tokyo 162-8601 (Japan)
Fax: (+81) 3-5261-4631
E-mail: hayashi@ci.kagu.tus.ac.jp
Homepage: http://www.ci.kagu.tus.ac.jp/lab/org-chem1/

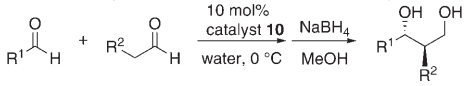
[**] This work was partially supported by the Toray Science Foundation and a Grand-in-Aid for Scientific Research on Priority Areas 16073219 from MEXT.

Supporting information for this article is available on the WWW under http://www.angewandte.org or from the author.

 © 2006 Wiley-VCH Verlag GmbH & Co. KGaA, Weinheim

First, we examined proline *N*-sulfonyl amides **6** and **7** containing long alkyl chains (Scheme 1). Though similar *N*-arylsulfonyl amides are excellent aldol catalysts in organic solvents, as reported by Berkessel et al.[11] and Ley and coworkers,[9] **6** and **7** were found to be poor catalysts: an emulsion did not form in the reaction mixture, and the products were obtained in low yield. Next, we developed the novel catalysts **8**–**13**, which contain both a proline unit and a long alkyl chain and which were easily prepared in large quantities from commercially available L-4-hydroxyproline. An emulsion was formed in the reaction mixture and excellent diastereo- and enantioselectivities were attained using catalysts **8**–**13**, while the chain length dramatically affected the yield. Neither very long nor very short chains were effective, whereas catalyst **10** with a decanoate moiety was found to be the most efficient. The yield was increased to 92% on prolonging the reaction time (70 h). Diastereo- and enantioselectivities decreased slightly as the amount of water in the reaction was increased. The reaction also proceeded efficiently under neat reaction conditions, though slight decreases in diastereo- and enantioselectivities were observed. This result provides evidence that the reaction proceeds in the organic phase, created inside the emulsion when the reaction is performed in the presence of water. Note also that the reaction can be performed on a 15-mmol scale with 3 equivalents of propanal to afford 2.9 g of aldol with 99% *ee* and 19:1 *anti* diastereoselectivity.

Table 2: Enantioselective direct aldehyde cross-aldol reaction in the presence of water.[a]



Entry	R^1	R^2	*t* [h]	Yield [%][b]	*anti*/*syn*[c]	*ee* [%][d]
1	*o*-chlorophenyl	Me	70	92	18:1	99
2	*p*-chlorophenyl	Me	110	90	>20:1	99
3	*p*-fluorophenyl	Me	110	76	>20:1	99
4	phenyl	Me	73	88	>20:1	99
5	2-naphtyl	Me	110	54	>20:1	99
6	1-naphtyl	Me	80	49	>20:1	98
7[e]	*p*-tolyl	Me	68	65	>20:1	99
8	*o*-methoxyphenyl	Me	72	83	20:1	95
9	*p*-methoxyphenyl	Me	70	38	>20:1	97
10	cyclohexyl	Me	118	29	10:1	92
11[f]	2-furyl	Me	68	58	8:1	92
12[e]	*o*-chlorophenyl	*i*Pr	68	61	10:1	73
13[e]	*o*-chlorophenyl	Bn	93	57	14:1	92
14[g]	dimethoxymethyl	Bn	62	35	4:1	93
15[f,g]	ethyl	Me	96	35	10:1	89

[a] Unless otherwise shown, the reactions were conducted with 0.4 mmol of acceptor aldehyde and 2.0 mmol of donor aldehyde and water (130 μL) in the presence of 10 mol% of **10** at 0°C. [b] Isolated yield. [c] Determined by ^{1}H NMR spectroscopy. [d] *ee* value of *anti* isomer (see Supporting Information). [e] 20 mol% of **10** was employed. [f] The reaction was performed at room temperature. [g] 3.8 equiv of water was employed.

The generality of the reaction was also investigated (Table 2). The reaction was highly diastereo- and enantioselective, and hardly any dehydration products were generated in every case investigated. Not only propanal but also isovaleraldehyde and 3-phenylpropanal were successfully employed as the donor. Note the excellent diastereoselectivity obtained in entries 4 and 15 (Table 2), which is in marked contrast to the low d.r. (3:1) reported for the corresponding proline-mediated aldol reactions in DMF.[8] The low yield obtained with aliphatic aldehydes such as cyclohexylcarbaldehyde and propanal can be ascribed to inefficient mixing due to insufficient hydrophobicity of the acceptor aldehydes, as only in these cases was an emulsion not formed. Commercially available aqueous dimethoxyacetaldehyde was also a successful acceptor (Table 2, entry 14). In their procedure using benzaldehyde as the acceptor, MacMillan and Northup employed an excess amount of benzaldehyde (10 equiv) with slow addition of propanal over 16 h.[8] In the present protocol, the nucleophilic aldehyde (5 equiv) was used without slow addition. Although the self-aldol products of propanal were formed (ca. 30%), they could easily be removed by column chromatography. The same predominant enantiomer was formed as with L-proline in DMF,[8] which indicates the involvement of a similar transition state to that reported.

In summary, we have developed a catalytic, direct asymmetric cross-aldol reaction of two different aldehydes in the presence of water, catalyzed by a novel combined proline–surfactant organocatalyst **10**. Neither organic cosolvent nor additional acid is necessary. Though the precise reaction mechanism is not clear at the moment, emulsions seem to offer an ideal reaction environment in the presence of water, in which organic molecules can be assembled through hydrophobic interactions thus enabling the aldol reaction to proceed efficiently.

Experimental Section

General procedure (Table 1, entry 19): *o*-Chlorobenzaldehyde (1.69 mL, 15.0 mmol), and then propanal (3.25 mL, 45 mmol) were added to a mixture of (2*S*,4*R*)-4-decanoyloxypyrrolidine-2-carboxylic acid (**10**; 413 mg, 1.5 mmol) and water (4.9 mL) at 0°C. The reaction mixture was stirred at 0°C for 96 h, then MeOH (60 mL) and $NaBH_4$ (5.67 g, 150 mmol) were added. The reaction mixture was stirred for a further 1 h at 0°C and was then quenched with pH 7.0 phosphate buffer solution. The organic materials were extracted with chloroform three times, and the combined organic extracts were dried over anhydrous Na_2SO_4 and concentrated in vacuo after filtration. Purification by column chromatography (silica gel; hexane/AcOEt 20:1 to 3:1) gave (1*R*,2*R*)-1-(*o*-chlorophenyl)-2-methylpropane-1,3-diol (2.9 g, 14.5 mmol, 97%) as a colorless oil: *anti*/*syn* 19:1 (by ^{1}H NMR spectroscopy of the crude mixture). Enantioselectivity was determined after conversion into the corresponding monobenzoyl ester: 99% *ee* (by HPLC on a Chiralpak AS-H column, $\lambda = 254$ nm,

 © 2006 Wiley-VCH Verlag GmbH & Co. KGaA, Weinheim

*i*PrOH/hexane 1:100, 1.2 mL min^{-1}; $t_R = 15.2$ min (major), 17.2 min (minor)).

Received: March 23, 2006
Revised: June 7, 2006
Published online: July 20, 2006

Keywords: aldol reaction · asymmetric synthesis · green chemistry · organocatalysis · surfactants

[1] a) *Organic Synthesis in Water* (Ed.: P. A. Grieco), Blackie, London, **1998**; b) U. M. Lindstrom, *Chem. Rev.* **2002**, *102*, 2751; c) C.-J. Li, *Chem. Rev.* **2005**, *105*, 3095; d) M. C. Pirrung, *Chem. Eur. J.* **2006**, *12*, 1312.
[2] a) S. Kobayashi, K. Manabe, *Acc. Chem. Res.* **2002**, *35*, 209; b) T. Hamada, K. Manabe, S. Kobayashi, *J. Syn. Org. Chem. Jpn.* **2003**, *61*, 445.
[3] a) B. List, R. A. Lerner, C. F. Barbas III, *J. Am. Chem. Soc.* **2000**, *122*, 2395; for Reviews, see: b) B. List in *Modern Aldol Reactions*, *Vol. 1* (Ed.: R. Mahrwald), Wiley-VCH, Weinheim, **2004**, pp. 161 – 200.
[4] a) H. Torii, M. Nakadai, K. Ishihara, S. Saito, H. Yamamoto, *Angew. Chem.* **2004**, *116*, 2017; *Angew. Chem. Int. Ed.* **2004**, *43*, 1983; b) A. I. Nyberg, A. Usano, P. M. Pihko, *Synlett* **2004**, 1891; c) Z. Tang, Z.-H. Yang, L.-F. Cun, L.-Z. Gong, A.-Q. Mi, Y.-Z. Jiang, *Org. Lett.* **2004**, *6*, 2285; d) J. Casas, H. Sunden, A. Cordova, *Tetrahedron Lett.* **2004**, *45*, 6117; e) D. E. Ward, V. Jheengut, *Tetrahedron Lett.* **2004**, *45*, 8347; f) I. Ibrahem, A. Cordova, *Tetrahedron Lett.* **2005**, *46*, 3363; g) M. Amedjkouh, *Tetrahedron: Asymmetry* **2005**, *16*, 1411; h) P. Dziedzic, W. Zou, J. Hafren, A. Cordova, *Org. Biomol. Chem.* **2006**, *4*, 38; i) P. M. Pihko, K. M. Laurikainen, A. Usano, A. I. Nyberg, J. A. Kaavi, *Tetrahedron* **2006**, *62*, 317.
[5] A. Cordova, W. Notz, C. F. Barbas III, *Chem. Commun.* **2002**, 3024.
[6] Y. Hayashi, T. Sumiya, J. Takahashi, H. Gotoh, T. Urushima, M. Shoji, *Angew. Chem.* **2006**, *118*, 972; *Angew. Chem. Int. Ed.* **2006**, *45*, 958.
[7] N. Mase, Y. Nakai, N. Ohara, H. Yoda, K. Takabe, F. Tanaka, C. F. Barbas III, *J. Am. Chem. Soc.* **2006**, *128*, 734.
[8] A. B. Northup, D. W. C. MacMillan, *J. Am. Chem. Soc.* **2002**, *124*, 6798.
[9] A. J. A. Cobb, D. M. Shaw, D. A. Longbottom, J. B. Gold, S. V. Ley, *Org. Biomol. Chem.* **2005**, *3*, 84.
[10] Y. Hayashi, J. Yamaguchi, K. Hibino, T. Sumiya, T. Urushima, M. Shoji, D. Hashizume, H. Koshino, *Adv. Synth. Catal.* **2004**, *346*, 1435.
[11] A. Berkessel, B. Koch, J. Lex, *Adv. Synth. Catal.* **2004**, *346*, 1141.

 © 2006 Wiley-VCH Verlag GmbH & Co. KGaA, Weinheim

DOI: 10.1002/anie.200601317

Protons at Ice Surfaces**

*Chang-Woo Lee, Poong-Ryul Lee, and Heon Kang**

Ice surfaces play an important role in many chemical processes that occur in nature at low temperatures. Ice particles in the polar stratospheric clouds, for example, catalyze the heterogeneous reactions that lead to the seasonal depletion of the ozone layer,[1] and prebiotic molecules detected in interstellar space are believed to form in the ice mantle of interstellar dust particles.[2,3] The environmental and astrobiological importance of ice reactions has stimulated research on this subject in recent years.[4] A critical issue in the study of ice reactions is the rate of proton transfer. Proton transfer is responsible for a variety of chemical reactions in the aqueous phase, ranging from acid–base neutralization to enzymatic reactions. Proton mobility is anomalously high compared to that of other ions in liquid water. This unique behavior is attributed to a proton relay (Grotthuss) mechanism in which the effective motion of a proton involves a sequence of proton tunnelings along the hydrogen-bonded chain of water molecules.[5–8] This sequential proton transfer is promoted by the rearrangement of hydrogen-bond networks in liquid water in order to accommodate a proton in stable solvation structures.[5–8]

In ice, however, such a large structural rearrangement is impossible due to the fixed geometry of water molecules in the tetrahedral hydrogen-bond structure. Therefore, proton transfer in ice must involve a different mechanism. It is believed that at least two features are essential for this proton transfer.[9] First, the proton transfer should not significantly alter the fixed geometry of water molecules in the tetrahedral lattice. However, in an ice lattice constructed according to the "ice rules", such proton transfers can occur only up to a limited distance. Therefore, the second requirement is that an ice lattice should possess orientational (Bjerrum) defects where the ice rules are violated locally. If these defects move due to reorientation of water molecules, the passage of protons can be extended.

Proton transfer in ice has been studied using various experimental approaches. Electrical conductivity measurements of ice,[9,10] which have a long history, support the proton-transfer mechanism associated with the motion of the Bjerrum defect. The proton mobility in ice deduced from the

[*] C.-W. Lee, P.-R. Lee, Prof. Dr. H. Kang
Department of Chemistry
Seoul National University
Gwanak-gu, Seoul 151-747 (Republic of Korea)
Fax: (+82) 2-889-1568
E-mail: surfion@snu.ac.kr

[**] This work was supported by the Korea Science & Engineering Foundation (R01-2006-000-10019-0). We thank Jung-Hwan Kim for help in conducting experiments.

 © 2006 Wiley-VCH Verlag GmbH & Co. KGaA, Weinheim InterScience

conductivity measurements varies greatly, however, mainly due to the difficulty in controlling and characterizing the space-charge layer formed at the ice/electrode interfaces.[9] More recently, Devlin and co-workers[11,12] studied the H/D isotope exchange of water molecules in ice nanocrystals doped with protons. By identifying water isotopomers by IR spectroscopy, they showed that proton transfer occurs through a combination of proton hopping between adjacent water molecules and thermal rotation of molecules (hop-and-turn process) at temperatures above 125 K.

Cowin et al.[13] have deposited hydronium ions on ice films from low-energy beams and observed that the surface protons are immobile across the films over a fairly wide temperature range (30–190 K), and Park et al.[14] have studied H/D exchange reactions on ice films adsorbed with HCl and have shown that the H/D exchange is facile only at the film surface, while its propagation into the interior is absent or very slow at 90–140 K. These incongruous observations suggest that further study is necessary to understand proton transfer in ice. In particular, these results raise the possibility that protons might behave quite differently at the ice surface and in the interior. The current study examines this puzzling issue.

We carried out experiments with ice films deposited on a Ru(0001) single crystal in an ultrahigh-vacuum chamber by a backfilling method at a water vapor pressure of $(1–5)\times 10^{-8}$ Torr.[15] The temperature of the Ru substrate was varied between 40 and 1500 K by a liquid He cryostat and resistive heating. H_2O, D_2O, and HCl gases were introduced into the chamber through separate leak valves. The ice films were prepared in the form of two different structures.

In structure I, the excess protons were sandwiched between the underlying D_2O layer and the upper H_2O layer. In order to prepare this film, D_2O was deposited on the Ru substrate at a thickness of 2 bilayers (BLs) at 140 K. A small amount of HCl was then deposited on top of the D_2O layer [approx. 0.1 monolayer (ML) by the exposure of 0.1 L; $1\text{ L} = 1\times 10^{-6}$ Torr s] at 140 K. Finally, an H_2O overlayer was deposited to a thickness of 4–12 BLs at temperatures below 100 K. The HCl gas provides excess protons to the film by spontaneous ionization at 140 K,[16,17] and the underlying D_2O layer serves as a spacer to remove any effects of the Ru substrate on the upper layer, since D_2O forms a well-ordered film on Ru(0001) at 140 K without dissociation.[18] It was essential to deposit the upper H_2O layer at low temperature; otherwise the protons remained afloat on the surface during the deposition instead of being buried within the sandwiched layer, as explained below. Diffusional mixing of the H_2O and D_2O layers did not occur during the deposition.[15]

In structure II, the excess protons were placed on the surface of an ice film. To prepare this film, we deposited a 2-BL-thick layer of D_2O on Ru at 140 K, followed by H_2O for a 4- to 12-BL thickness at below 100 K, and finally a small amount (approx. 0.1 ML) of HCl. The thickness of the ice film was estimated from temperature-programmed desorption experiments.

The surface of the ice films was analyzed by reactive-ion scattering (RIS) and low-energy sputtering (LES) using a low-energy Cs^+ beam (10–30 eV). It has been shown[4] that RIS and LES can detect neutral molecules and ions, respectively, at the surface of ice films with a depth resolution of 1 BL. Water isotopomers (H_2O, HDO, and D_2O) and their isotopomeric abundance were measured by RIS, and the proton population was measured by detecting hydronium ions (H_3O^+, H_2DO^+, HD_2O^+, and D_3O^+) by LES.

The results of the RIS and LES measurements with the ice films of structure I (proton-sandwich films) are shown in Figure 1. Apart from reflected Cs^+ primaries at m/z 133, the

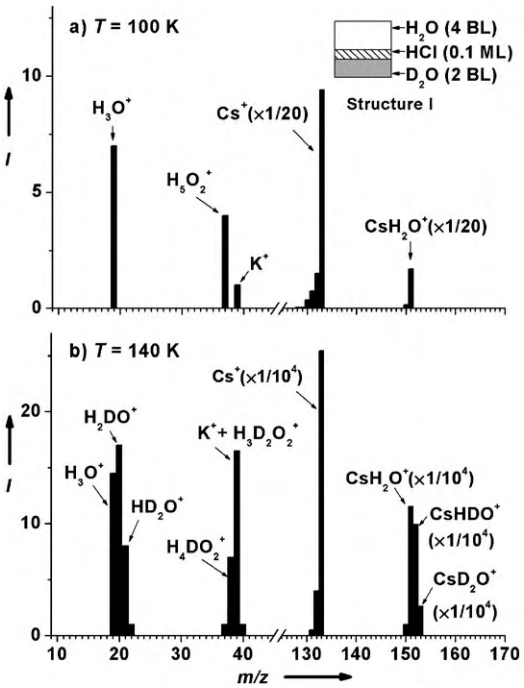


Figure 1. Positive-ion mass spectra measured at the surface of ice films of structure I. The film structure is depicted on the top right. In spectrum (a), the sample temperature was maintained at 100 K during the measurement. In spectrum (b), the temperature was raised to, and maintained at, 140 K for 20 min before the measurement. The Cs^+ and Cs^+–water peak intensities are reduced by the factors indicated. The energy of the incident Cs^+ beam was 30 eV.

mass spectra are characterized by two kinds of peaks. The peaks above m/z 133 are due to RIS, that is, pick-up of surface molecules by the incoming Cs^+. The LES peaks, which are due to the ejection of pre-existing ions at the surface, appear at masses lower than m/z 133. In spectrum (a), the RIS peak at m/z 151 (CsH_2O^+) is due to H_2O molecules at the surface. The LES peaks at m/z 19 and 37 represent the ejection of H_3O^+ and its hydrated cluster ($H_5O_2^+$), respectively. The peak at m/z 39 is due to the reflection of a K^+ impurity in the Cs^+ beam. The H_3O^+ peak indicates that the protons have migrated from the HCl sandwich layer to the surface. This peak is not due to the deposition of residual HCl vapor inside the chamber because it did not appear in the control experiments on pure ice films.

In spectrum (b), the film temperature was raised to 140 K for the measurement. The hydronium ion intensity increased substantially from that measured at 100 K. This indicates enhanced proton transfer to the surface at 140 K. Further, D-

 © 2006 Wiley-VCH Verlag GmbH & Co. KGaA, Weinheim

substituted species appear for hydronium ions (m/z 19–22) and Cs^+–water clusters (m/z 151–153). These deuterated species indicate that the H/D exchange starts at the D_2O/H_2O interface and propagates to the surface. The film becomes crystalline after annealing at 140 K, and this surface morphology change increases the intensity of scattered ions (Cs^+, K^+, and Cs^+–water) by three orders of magnitude in spectrum (b).[15] It has been shown[14] that this morphology change does not significantly alter the LES efficiency for hydronium ions.

Figure 2 shows the variation of LES intensity for hydronium ions as a function of temperature for films of structures I and II. For structure I, the hydronium ion intensity is small and constant in the temperature range 40–125 K, but it then increases noticeably. Below 125 K, the hydronium ion signal contains only H_3O^+ without the D-substituted species. The H_3O^+ signal appears immediately after film deposition and does not increase in intensity with time. Above 125 K, the increase in the hydronium ion signal is mainly due to the D-substituted species ($H_{3-x}D_xO^+$, $x = 1$–3), which suggests a common origin for the proton-transfer enhancement and the H/D exchange process at higher temperatures. At 140 K, the hydronium ion intensity is approximately the same from the surfaces of structures I and II. The same proton population at the two surfaces independent of the initial proton locations suggests that the spatial distribution of protons has reached an equilibrium state as a result of active proton transfer through the films. Above 140 K, water desorption from the surface becomes significant, and this hampers any reliable measurements above this temperature.

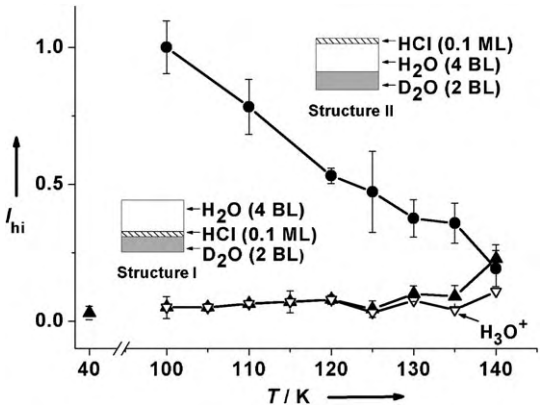


Figure 2. Variation of hydronium ion intensity, I_{hi}, as a function of temperature from films of structures I (▲) and II (●). The hydronium ion intensity is the summation of the intensities of all the isotopomers (H_3O^+, H_2DO^+, HD_2O^+, and D_3O^+). The H_3O^+ intensity of the structure-I film is plotted separately (▽). The scale on the ordinate is normalized against I_{hi} of structure II at 100 K. For measurements between 100 and 140 K, the ice film temperature was increased at the rate of 2 K min^{-1}.

For the structure-II film, the hydronium ion intensity decreases with an increase in temperature. This suggests two possibilities: 1) proton migration from the film surface to the interior at an elevated temperature, or 2) increased hydration of protons at the surface. Desorption of HCl does not occur from the ice surfaces below 140 K.[17] In order to check possibility (1), we performed control experiments that measured the hydronium ion intensity from structure-II films of different thicknesses (4–10 BL) at 140 K. We observed that the surface proton population does not change with film thickness. Further, we continuously exposed these films to a large amount of HCl gas at 140 K in order to measure their HCl uptake curves. The surface proton population became saturated at an HCl exposure of around 2 L; this was independent of film thickness. The results of the control experiments rule out the possibility of continuous proton migration to the film interior. Next, we considered possibility (2). If a proton is fully hydrated at the surface it will occupy a slightly subsurface position relative to the surrounding water molecules. In this situation, the ejection of hydronium ions will be effectively blocked because the LES is a soft-sputtering method that ejects only top-layer species.[4] The stronger bonding between hydronium ions and the ice surface due to hydration will also reduce the LES yield. Thus, we can conclude that protons reside mostly at the film surfaces in hydrated forms.

The Cl^- population was measured at the surface of structure-I films by the LES of negative ions. Cl^- did not appear at the surface until the film temperature reached 140 K, although the proton population at the surface was substantial. This result indicates that the observed proton transfer to the surface is not driven by the electrostatic forces from Cl^-.

The rationale for the propensity of protons to reside at the surface seems straightforward. The excess protons in liquid water prefer to form three-coordinate, planar water structures (commonly called Zundal and Eigen structures).[5–8] In ice, however, all water molecules, including those attached to the excess protons, must be four-coordinate. This bonding requirement destabilizes the protonated molecules and generates a thermodynamic repulsive force that transfers the protons to the surface where water molecules are less coordinated. This thermodynamic tendency for surface residence clearly explains the previous observations[13,14] that protons at ice surfaces are immobile towards the interior.

We further examined the kinetics of vertical proton transfer from the ice interior to the surface by measuring the temporal change in proton population and water isotopomeric distribution at the surface of the structure-I film. Figure 3 shows the results obtained at 130 K. The proton population at the surface rapidly increases to reach a limiting value after 5 min. The H/D exchange of surface water molecules was determined from the $Cs(H_xD_{2-x}O)^+$ ($x = 0$–2) isotopomeric intensities. It occurs more slowly than the proton transfer. The D-enrichment factor of water, defined as $f_{DE} = (([HDO]/2) + [D_2O])/([H_2O] + [HDO] + [D_2O])$, increased up to 0.2, thus indicating the complete isotopic mixing between 4 BLs of H_2O and 1 BL of D_2O. Figure 3 also shows f_{DE} measured in the absence of HCl for an ice film consisting of H_2O and D_2O layers. In this film, the isotopic mixing occurs more slowly than in the structure-I film because it is mostly due to the self-diffusion of water. This shows that the H/D exchange in the structure-I film occurs due to the excess protons.

 © 2006 Wiley-VCH Verlag GmbH & Co. KGaA, Weinheim

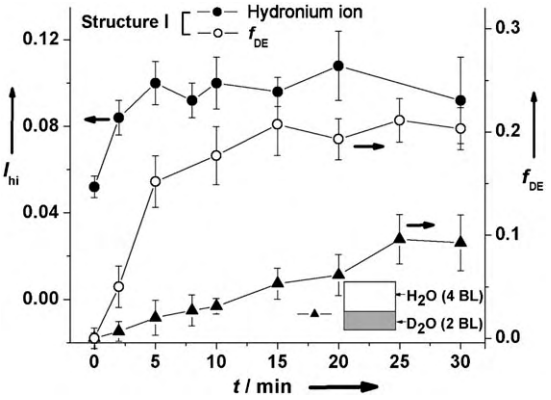


Figure 3. Change in hydronium ion intensity (I_{hi}; ●) and D-enrichment factor in water (f_{DE}; ○) as a function of time for a structure-I film at 130 K. The film structure was the same as that in Figure 2. The hydronium ion intensity includes all isotopomers, and the scale for I_{hi} is the same as that in Figure 2. The scale for f_{DE} is shown along the right ordinate. f_{DE} measured with a pure ice film (its structure is depicted) is also shown (▲). The films were deposited at 100 K and heated to 130 K; the kinetic measurements were then initiated.

Figure 3 shows that the relative speeds of three kinetic processes are in the following order: proton transfer > H/D exchange > self-diffusion. In addition, an extra channel exists for proton transfer that rapidly generates surface H_3O^+ at low temperatures (< 125 K). In the following we will discuss a molecular-level interpretation for these observations using the proton-transfer model depicted in Figure 4. Although this model is configured for a crystalline ice film, key mechanistic features should be applicable to noncrystalline films as well.

The rapid appearance of surface H_3O^+ at 40–125 K suggests the occurrence of sequential proton hopping through the hydrogen-bonded chain, as illustrated in Figure 4b. Such a proton relay does not require molecular reorientation and is therefore feasible even at low temperatures. This mechanism cannot be responsible for proton transfer through bulk ice, however, because the length of a successful proton transfer is limited. Nevertheless, some successful routes may be found across a very thin ice film (only one successful route exists in Figure 4b), through which a specific fraction of protons can be transported.

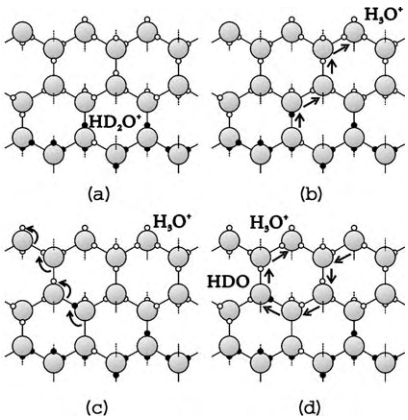


Figure 4. a) A cross-sectional view of a model ice surface with an H_2O layer (2 BLs) on top of a D_2O layer. The small white circles indicate H atoms, and the small black circles indicate D atoms. A hydronium isotopomer ion (HD_2O^+) is initially located at the H_2O/D_2O interface. b) A proton is transferred to the surface by a hopping relay (the arrows) without reorientation of the water molecules. c) Thermally activated rotation of water molecules produces new paths for proton transfer. d) HDO is transported by the recurrence of hop-and-turn processes.

When an ice film is warmed to a temperature above 125 K water molecules gain thermal energy and rotate.[11,12] This creates additional paths for proton hopping (Figure 4c) and therefore more protons can be transferred to the surface. A combined process of molecular reorientation and proton hopping generates an HDO isotopomer (Figure 4d). It should be noted that more D-enriched isotopomers are formed and transported by the recurrence of the hop-and-turn processes. Therefore, the build-up of D-enriched surface species will lag behind the build-up of surface protons, as observed in Figure 3.

To summarize, the detection of hydronium ions at the surface by LES and the asymmetric transport behavior of protons through ice films reveal that protons mainly reside at the ice surface. The surface affinity of a proton is a thermodynamic consequence of the difficulty of embedding protons in the ice lattice with regard to energy. A proton can transfer over a short distance by a hopping relay even at low temperatures (< 125 K) at which the molecular motions are frozen. At higher temperatures, the rate and distance of proton transfer increase due to the hop-and-turn mechanism. This also produces the D-enriched isotopomers. We stress that the present work explicitly demonstrates the occurrence of two types of proton-transfer mechanisms and differentiates their operating ranges and temperatures.

As shown in this study, protons are a unique mobile species in ice films at temperatures at which the motions of molecules and ions are virtually frozen. Proton mobility at the ice surface in the lateral direction is shown to be even higher.[14] With such high mobility and surface affinity, protons can efficiently migrate and protonate molecules on ice surfaces, and are therefore available to catalyze reactions that would otherwise not occur at low temperatures. Indeed, proton-catalyzed reactions have been observed on frozen alcohol films at 100 K.[4] Since hydrogen is the most abundant element in interstellar space, either in neutral or ionized forms, it can be imagined that protons accumulate at the ice surfaces of interstellar dust particles to build up a significant population. Under such circumstances, proton-catalyzed reactions might occur at the surface to form prebiotic organic molecules.[2,3] It is noteworthy that proton-catalyzed reactions are essential for the synthesis of many organic molecules.

Received: April 4, 2006
Published online: July 18, 2006

Keywords: ice · ion beams · proton transport · surface analysis

[1] M. J. Molina, T. L. Tso, L. T. Molina, F. C. Y. Wang, *Science* **1987**, *238*, 1253.
[2] J. M. Greenberg, *Surf. Sci.* **2002**, *500*, 793.

 © 2006 Wiley-VCH Verlag GmbH & Co. KGaA, Weinheim

[3] T. E. Madey, R. E. Johnson, T. M. Orlando, *Surf. Sci.* **2002**, *500*, 838.
[4] H. Kang, *Acc. Chem. Res.* **2005**, *38*, 893.
[5] C. Kobayashi, S. Saito, I. Ohmine, *J. Chem. Phys.* **1988**, *88*, 3086.
[6] N. Agmon, *Chem. Phys. Lett.* **1995**, *244*, 456.
[7] K. Ando, J. T. Hynes, *J. Phys. Chem. B* **1997**, *101*, 10464.
[8] D. Marx, M. E. Tuckerman, J. Hutter, M. Parrinello, *Nature* **1999**, *397*, 601.
[9] V. F. Petrenko, R. W. Whitworth, *Physics of Ice*, Oxford University Press, **1999**, chapters 3 and 4.
[10] G. C. Camplin, J. W. Glen, J. G. Paren, *J. Glaciol.* **1978**, *21*, 123.
[11] P. J. Wooldridge, J. P. Devlin, *J. Chem. Phys.* **1988**, *88*, 3086.
[12] N. Uras-Aytemiz, C. Joyce, J. P. Devlin, *J. Chem. Phys.* **2001**, *115*, 9835.
[13] J. P. Cowin, A. A. Tsekouras, M. J. Iedema, K. Wu, G. B. Ellison, *Nature* **1999**, *398*, 405.
[14] S.-C. Park, K.-H. Jung, H. Kang, *J. Chem. Phys.* **2004**, *121*, 2765.
[15] K.-H. Jung, S.-C. Park, J.-H. Kim, H. Kang, *J. Chem. Phys.* **2004**, *121*, 2758.
[16] J. P. Devlin, N. Uras, J. Sadlej, V. Buch, *Nature* **2002**, *417*, 269.
[17] S.-C. Park, H. Kang, *J. Phys. Chem. B* **2005**, *109*, 5124.
[18] C. Clay, S. Haq, A. Hodgson, *Chem. Phys. Lett.* **2004**, *388*, 89.

 © 2006 Wiley-VCH Verlag GmbH & Co. KGaA, Weinheim

Cycloaddition

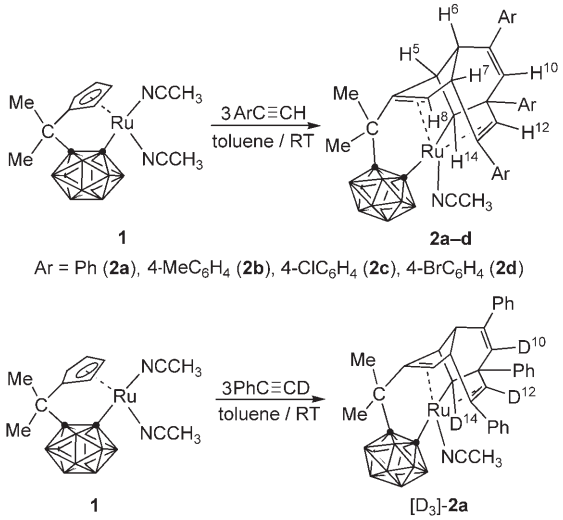
DOI: 10.1002/anie.200601650

Ruthenium-Mediated Coupling/Cycloaddition of the Cyclopentadienyl Ligand in [{η^5:σ-$Me_2C(C_5H_4)(C_2B_{10}H_{10})$}$Ru(NCCH_3)_2$] with Alkynes**

Yi Sun, Hoi-Shan Chan, Haitao Zhao, Zhenyang Lin, and Zuowei Xie**

Cyclopentadienyl and its derivatives (Cp ligands) are among the most extensively utilized π ligands in organometallic chemistry. In most organometallic reactions of transition-metal complexes, the η^5-Cp ligand plays the role of a spectator that stays tightly bound in η^5 fashion to the metal center throughout the course of the reactions.[1] For example, ruthenium half-sandwich complexes [(η^5-C_5R_5)$RuXL_2$] (R = H, Me; X = halide; L_2 = neutral ligands) are very effective catalysts for C–C bond-forming reactions, whereby the CpRu moiety remains intact.[2] Though Cp ligands are usually considered as inert groups, a few examples of C–C activation of Cp have been reported in titanocene,[3–5] cobaltocene, and chromocene complexes.[6] We report herein an unprecedented participation of a Cp in coupling and cycloaddition reactions with alkynes to give tricyclic compounds.

Reaction of [{η^5:σ-$Me_2C(C_5H_4)(C_2B_{10}H_{10})$}$Ru(NCCH_3)_2$] (**1**)[7] with 3 equiv of ArC≡CH in toluene at room temperature afforded unexpected ruthenium complexes bearing a tricyclic moiety [{η^4:σ-$Me_2C(C_{11}H_7Ar_3)(C_2B_{10}H_{10})$}$Ru(NCCH_3)$] (**2a–d**) in 68–76% yields of isolated compounds (Scheme 1).[8] The



Scheme 1. Preparation of **2a–d** and [D_3]-**2a**.

^{1}H NMR spectra of **2a–d** were similar. In addition to multiplets for aromatic protons in the range 7.6–7.2 ppm, two singlets for the Me_2C protons at about 1.5 and 1.3 ppm, and one singlet for CH_3CN protons at about 1.7 ppm, two singlets around 6.2 and 4.9 ppm assignable to vinyl protons H10 and H12, two doublets at about 3.4 and 1.0 ppm attributable to H8 and H14, and three doublets of doublets at approximately 4.8, 3.7, and 3.3 ppm corresponding to H7, H5, and H6, respectively, were observed in all ^{1}H NMR spectra. A characteristic resonance[9] for RuC14H at about −17 ppm was found in the ^{13}C NMR spectra of **2a–d**. All ^{11}B NMR spectra exhibited a 1:1:3 pattern.

When PhC≡CH was replaced by PhC≡CD in the above reaction, [{η^4:σ-$Me_2C(C_{11}H_4D_3Ph_3)(C_2B_{10}H_{10})$}$Ru(NCCH_3)$] ([$D_3$]-**2a**) was isolated in 70% yield with greater than 98% deuterium incorporation (Scheme 1).[8] Its ^{1}H NMR spectrum showed that the resonances corresponding to H10, H12, and H14 had disappeared and one doublet attributable to H5 (instead of one doublet of doublets in **2a**) was observed, while all other signals were identical with those of **2a**. This result indicates that H10, H12, and H14 come from the alkyne.

The molecular structure of **2a** was confirmed by single-crystal X-ray analysis.[10] The Ru atom is σ-bound to C2 and C14, η^2-bound to two double bonds, and coordinated to one CH_3CN molecule in a distorted square-pyramidal geometry

[*] Y. Sun, H.-S. Chan, Prof. Dr. Z. Xie
Department of Chemistry
The Chinese University of Hong Kong
Shatin, N.T., Hong Kong (China)
Fax: (+852) 2603–5057
E-mail: zxie@cuhk.edu.hk
Dr. H. Zhao, Prof. Dr. Z. Lin
Department of Chemistry
The Hong Kong University of Science and Technology
Clear Water Bay, Kowloon, Hong Kong (China)
Fax: (+852) 2358-1594
E-mail: chzlin@ust.hk

[**] This work was supported by grants from the Research Grants Council of The Hong Kong Special Administration Region (Project No. 403805 to Z.X. and 602304 to Z.L.).

Supporting information for this article is available on the WWW under http://www.angewandte.org or from the author.

 © 2006 Wiley-VCH Verlag GmbH & Co. KGaA, Weinheim

with C14 at the axial position (Figure 1). A tricycle containing a five-, a six-, and a seven-membered ring was constructed by coupling/cycloaddition of the Cp ring with three PhC≡CH molecules. The C4–C8/C9–C10/C12–C13 distances of

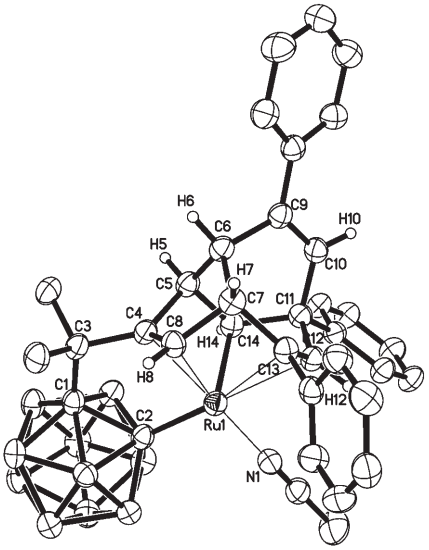
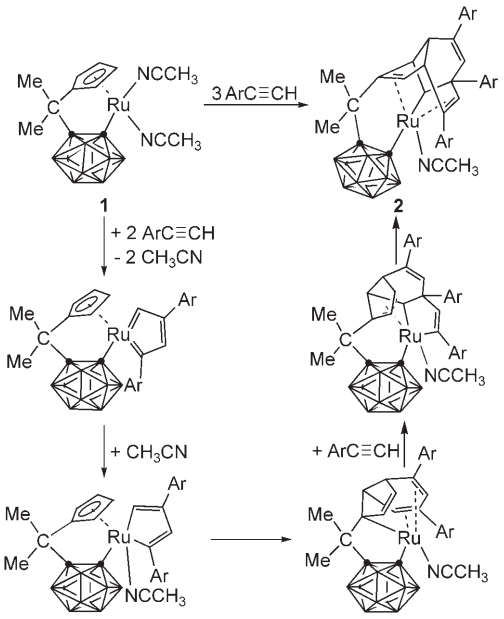


Figure 1. Molecular structure of **2a**. Selected bond lengths [Å]: Ru1–C2 2.115(6), Ru1–C4 2.200(6), Ru1–C8 2.262(8), Ru1–C12 2.337(6), Ru1–C13 2.468(6), Ru1–C14 2.100(6), Ru1–N1 2.098(6), C1–C2 1.740(8), C4–C8 1.417(8), C9–C10 1.349(8), C12–C13 1.387(8).

1.417(8)/1.349(8)/1.387(8) Å are indicative of C=C double bonds. Other C–C distances in the tricyclic framework are typical of single bonds. The Ru1–C2 distance of 2.115(6) Å falls in the range 2.10–2.26 Å observed in $[\{\eta^5{:}\sigma\text{-}Me_2C(C_5H_4)\text{-}(C_2B_{10}H_{10})\}Ru(L_2)]$ (L_2 = Lewis bases).[11] The Ru–C(14) distance of 2.100(6) Å is comparable to those observed in other ruthenium alkyl complexes, for example, 2.273(2) Å in $[(C_5Me_5)\{RuHC(PPh_2NPh)_2\}]$,[9c] 2.211(2) Å in $[(C_5Me_5)Ru(CO)\{\eta^2\text{-}HC(PPh_2NPh)_2\}]$,[9c] 2.142(9) Å in $[Ru(CO)_2\{\sigma,\eta^5\text{-}10\text{-}C(H)(PMe_2Ph)CH_2\text{-}7,8\text{-}C_2B_9H_{10}\}]$,[12a] and 2.293(16) Å in $[RuCH_3(NO)(P\mathit{i}Pr_3)]$.[12b]

The formation of **2a–d** was totally unexpected, and similar reactions have not been observed before in ruthenium chemistry. Therefore, the most interesting feature of these complexes is the mechanism by which they are formed. We considered several possible reaction pathways. The most feasible (Scheme 2) is supported by DFT calculations with the B3LYP hybrid functional in which HCN and acetylene were used as model substrates. Figure 2 shows the energy profile for the pathway, which includes three stages: 1) oxidative coupling of the two acetylene ligands in **PC**, 2) stepwise migration of the newly formed diene unit in **IN2** to the Cp ring, and 3) oxidative coupling between a newly coordinated acetylene and the coordinated double bond of the cyclohexadiene unit in **IN5** followed by reductive elimination.

The first stage begins from bis-acetylene complex **PC** with a small barrier of 10.3 kcal mol^{-1} to complete the oxidative coupling step to give ruthenacycle **IN1**, which is thermodynamically very favorable with a reaction free energy of 35.4 kcal mol^{-1}. Figure 3 shows that **IN1** has a short Ru–C



Scheme 2. Proposed reaction mechanism for the formation of **2**.

bond (1.924 Å), two longer C–C bonds (1.433 Å), and a shorter C–C bond (1.378 Å) in the five-membered ring. Intermediate **IN1** was commonly described as a bis-carbene species and a five-membered aromatic metallole in the literature.[13] On coordination of one nitrile molecule, **IN1** is converted to 18-electron metallacyclopentadiene intermediate **IN2**.[14] This is followed by stepwise migration of the diene unit to the Cp ring with barriers of 14.1 and 24.7 kcal mol^{-1}, respectively, to form 14-electron intermediate **IN4** bearing a five- and a six-membered ring. In the last stage, **IN4** takes up one acetylene molecule to give **IN5**, followed by oxidative coupling between the coordinated acetylene and the coordinated double bond of the cyclohexadiene ring to give **IN6**. Finally, reductive elimination with a very small barrier gives **PR** as the final product.

Our calculations suggest that coordination of a nitrile molecule to bis-carbene intermediate **IN1** to give diene species **IN2** promotes stepwise migration of the diene unit to the Cp ring (Figure 2). We examined the possibility of direct migration starting from **IN1.** The calculations give a barrier of 32.2 kcal mol^{-1}, which is 11.2 kcal mol^{-1} higher than that calculated for the conversion of **IN1** to **IN3**. Clearly, the ruthenium–carbon double-bond character in the five-membered ring of **IN1** prevents direct migration. Conversion of bis-carbene intermediate **IN1** to diene species **IN2** is necessary before migration occurs. Interestingly, a recent computational study showed that direct migration can occur in a titanocene analogue that is an intermediate derived from Cp_2Ti-mediated oxidative coupling of two coordinated acetylene molecules.[15] This is understandable because the intermediate formed is already a metallacyclopentadiene, since a Cp_2Ti fragment does not have orbitals available to make a bis-carbene structure accessible.

We also examined the possibility of acetylene trimerization to form benzene starting from **IN1** by coordinating one more acetylene molecule. Coupling between the coordinated

 © 2006 Wiley-VCH Verlag GmbH & Co. KGaA, Weinheim

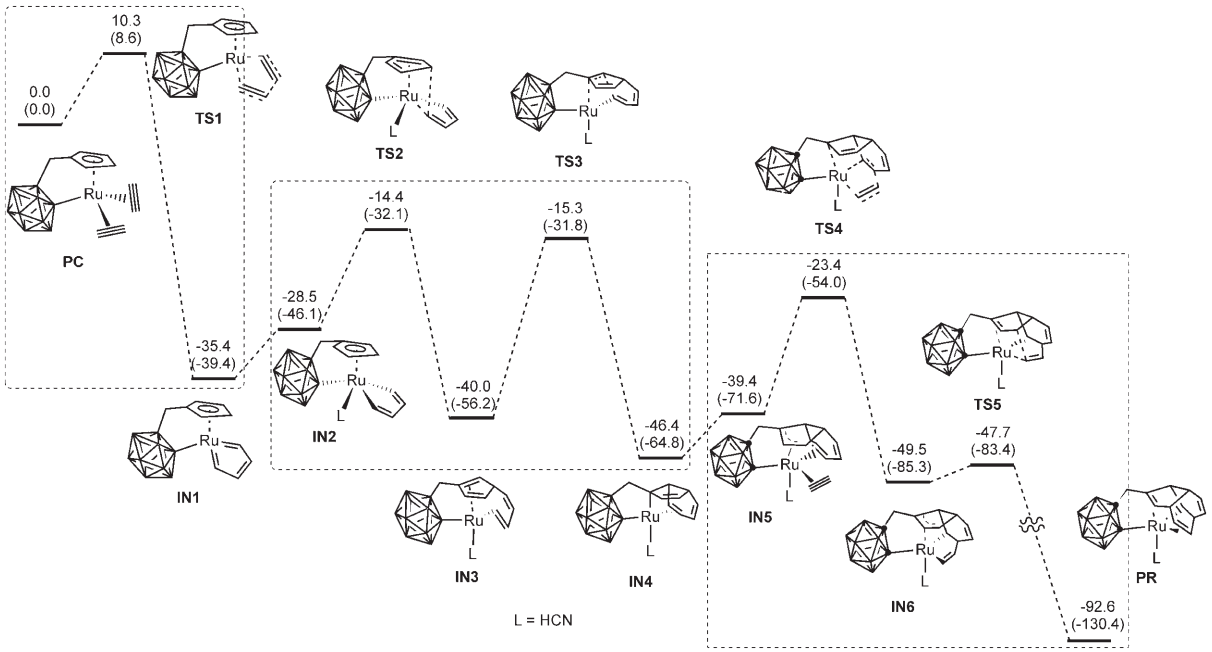


Figure 2. Energy profile of reaction pathway starting from **PC**. The relative free energies and electronic energies (in parentheses) are given in kcal mol^{-1}.

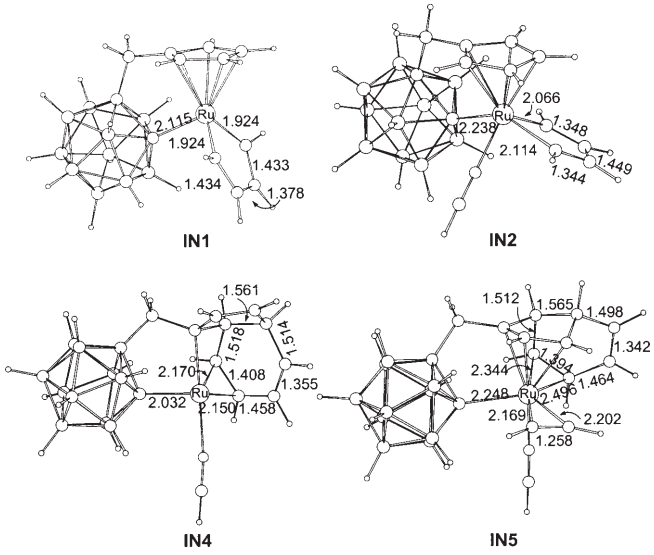


Figure 3. Selected bond lenghts [Å] calculated for intermediates.

acetylene and one of the two metal–carbene bonds was calculated to have a small barrier, consistent with those reported for CpRuCl-mediated cyclotrimerization of acetylenes.[13a,b] The transition state is higher in free energy than **IN1** + acetylene by 9.8 kcal mol^{-1}. The fact that complex **1** does not mediate cyclotrimerization of ArC≡CH can only be explained by steric arguments. Coordination of ArC≡CH to a substituted **IN1**-type intermediate is expected to be less likely in view of the sterically demanding carboranyl moiety in the current system. Even with a possible weak coordination, steric repulsion between the alkyne substituents and the bulky carboranyl moiety would make the transition state for coupling very high in energy, so that trimerization would be unlikely and the current complex differs from other CpRu systems in mediating C–C coupling of unsaturated organic substrates.[2]

The **IN4** structure shown in Figure 3 can be considered as a 14-electron seesaw structure, in which the metal center has a less crowded ligand environment than in **IN1**. Therefore, it can bind an alkyne molecule for further C–C coupling.

Reports on Cp_2Ti-mediated alkyne–Cp coupling can also be found.[3] However, the coupling products are very different from those we observed here. In a theoretical study on Ti-mediated alkyne–Cp coupling,[15] Suresh and Koga also located a Ti^{II} intermediate, which can be derived from **IN5** by replacing the acetylene, L, and carboranyl ligands with an η^5-Cp ligand, and Ru with Ti. Unlike **IN5**, which undergoes C–C coupling (Figure 2), the Ti^{II} intermediate releases a benzene molecule by C–C bond breaking. Apparently, the much greater reducing power of Ti^{II} versus Ru^{II} accounts for the different coupling products. In the cases discussed here, Ti^{II} reduces the organic ligands by breaking their C–C bonds whereas Ru^{II} reduces the organic ligands by coupling them.

In conclusion, ruthenium-mediated coupling/cycloaddition of a Cp ring with aromatic alkynes was reported for the first time and offers a facile route to tricyclic compounds.[16] A possible reaction mechanism was proposed with the help of DFT calculations. This work indicates that the sterically demanding carborane moiety plays a crucial role in regioselective dimerization of alkynes (giving head-to-tail coupling products) and prevention of alkyne trimerization.

Received: April 26, 2006
Published online: July 17, 2006

Keywords: C–C coupling · carboranes · cycloaddition · metallocenes · ruthenium

 © 2006 Wiley-VCH Verlag GmbH & Co. KGaA, Weinheim

[1] a) *Metallocene: Synthesis · Reactivity · Applications* (Eds.: A. Togni, R. L. Halterman), Wiley-VCH, New York, **1998**; b) R. H. Crabtree, *The Organometallic Chemistry of the Transition Metals*, 3rd ed., Wiley-Interscience, New York, **2001**.

[2] a) T. Naota, H. Takaya, S.-I. Murahashi, *Chem. Rev.* **1998**, *98*, 2599; b) B. M. Trost, F. D. Toste, A. B. Pinkerton, *Chem. Rev.* **2001**, *101*, 2067; c) V. Ritleng, C. Sirlin, M. Pfeffer, *Chem. Rev.* **2002**, *102*, 1731; d) B. M. Trost, *Acc. Chem. Res.* **2002**, *35*, 695; e) *Ruthenium Catalysts and Fine Chemistry* (Eds.: C. Bruneau, P. H. Dixneuf), Springer, Berlin, **2004**; f) B. M. Trost, M. U. Frederiksen, M. T. Rudd, *Angew. Chem.* **2005**, *117*, 6788; *Angew. Chem. Int. Ed.* **2005**, *44*, 6630; g) C. Bruneau, P. H. Dixneuf, *Angew. Chem.* **2006**, *118*, 2232; *Angew. Chem. Int. Ed.* **2006**, *45*, 2176; h) C. Fischmeister, C. Bruneau, P. H. Dixneuf in *Ruthenium in Organic Synthesis* (Ed.: S.-I. Murahashi), Wiley-VCH, Weinheim, **2004**, p. 189; i) X. Huang, Z. Lin, *Organometallics* **2003**, *22*, 5478.

[3] a) U. Rosenthal, C. Lefeber, P. Arndt, A. Tillack, W. Baumann, R. Kempe, V. V. Burlakov, *J. Organomet. Chem.* **1995**, *503*, 221; b) A. Tillack, W. Baumann, A. Ohff, C. Lefeber, A. Spannenberg, R. Kempe, U. Rosenthal, *J. Organomet. Chem.* **1996**, *520*, 187; c) D. Thomas, N. Peulecke, V. V. Burlakov, B. Heller, W. Baumann, A. Spannenberg, R. Kempe, U. Rosenthal, R. Beckhaus, *Z. Anorg. Allg. Chem.* **1998**, *624*, 919.

[4] W. E. Crowe, A. T. Vu, *J. Am. Chem. Soc.* **1996**, *118*, 5508.

[5] a) Z. Xi, K. Sato, Y. Gao, J. Lu, T. Takahashi, *J. Am. Chem. Soc.* **2003**, *125*, 9568; b) T. Takahashi, Y. Kuzuba, F. Kong, K. Nakajima, Z. Xi, *J. Am. Chem. Soc.* **2005**, *127*, 17188; for a comment, see also: c) R. Kempe, *Angew. Chem.* **2004**, *116*, 1487; *Angew. Chem. Int. Ed.* **2004**, *43*, 1463.

[6] a) T. L. Dzwiniel, N. Etkin, J. M. Stryker, *J. Am. Chem. Soc.* **1999**, *121*, 10640; b) C. M. Older, J. M. Stryker, *J. Am. Chem. Soc.* **2000**, *122*, 2784; c) T. L. Dzwiniel, J. M. Stryker, *J. Am. Chem. Soc.* **2004**, *126*, 9184; d) K. Kawamura, M. Shang, O. Wiest, T. P. Fehlner, *Inorg. Chem.* **1998**, *37*, 608; e) V. R. Miller, R. Weiss, R. N. Grimes, *J. Am. Chem. Soc.* **1977**, *99*, 5646; f) J. R. Pipal, R. N. Grimes, *Inorg. Chem.* **1978**, *17*, 10.

[7] Y. Sun, H.-S. Chan, P. H. Dixneuf, Z. Xie, *J. Organomet. Chem.* **2006**, *691*, 3071.

[8] Detailed experimental procedures, complete characterization data for complexes **2a**–**d** and [D_3]-**2a**, and computational details are provided in the Supporting Information.

[9] For examples, see: a) M. Lail, B. N. Arrowood, T. B. Gunnoe, *J. Am. Chem. Soc.* **2003**, *125*, 7506; b) M. Lail, T. B. Gunnoe, K. A. Barakat, T. R. Cundari, *Organometallics* **2005**, *24*, 1301; c) C. Bibal, Y. D. Smurnyy, M. Pink, K. G. Caulton, *J. Am. Chem. Soc.* **2005**, *127*, 8944.

[10] Crystal data for **2a**: $C_{36}H_{41}B_{10}NRu$, $M_r = 696.9$, monoclinic, space group $P2_1/c$, $a = 13.734(3)$, $b = 18.414(4)$, $c = 14.171(3)$ Å, $\beta = 104.62(3)°$, $V = 3467.6(12)$ Å^3, $T = 293$ K, $Z = 4$, $\rho_{calcd} = 1.335$ g cm^{-3}, $2\theta_{max} = 50°$, $\mu(Mo_{K\alpha}) = 0.71073$ Å, absorption corrections applied by using ABSCOR,[17a] relative transmission factors in the range 1.000–0.910. A total of 8708 reflections were collected and led to 5264 unique reflections, 5264 of which with $I > 2\sigma(I)$ were considered to be observed, $R_1 = 0.071$, $wR_2(F^2) = 0.149$. The structure was solved by direct methods and refined by full-matrix least-squares techniques on F^2 by using the SHELXTL/PC crystallographic program.[17b] All non-hydrogen atoms were refined anisotropically and all hydrogen atoms were geometrically fixed by using the riding model. CCDC-605516 contains the supplementary crystallographic data for this paper. These data can be obtained free of charge from The Cambridge Crystallographic Data Centre via www.ccdc.cam.ac.uk/data_request/cif.

[11] a) Y. Sun, H.-S. Chan, P. H. Dixneuf, Z. Xie, *Organometallics* **2004**, *23*, 5864; b) Y. Sun, H.-S. Chan, P. H. Dixneuf, Z. Xie, *Organometallics* **2006**, *25*, 2719.

[12] a) S. Anderson, D. F. Mullica, E. L. Sappenfield, F. G. A. Stone, *Organometallics* **1996**, *15*, 1676; b) D. Huang, W. E. Streib, O. Eisenstein, K. G. Caulton, *Organometallics* **2000**, *19*, 1967.

[13] a) Y. Yamamoto, T. Arakawa, R. Ogawa, K. Itoh, *J. Am. Chem. Soc.* **2003**, *125*, 12143; b) K. Kirchner, M. J. Calhorda, R. Schmid, L. F. Veiros, *J. Am. Chem. Soc.* **2003**, *125*, 11721; c) J. Le Paih, F. Monnier, S. Derien, P. H. Dixneuf, E. Clot, O. Eisenstein, *J. Am. Chem. Soc.* **2003**, *125*, 11964.

[14] Such a transformation has been reported: a) M. O. Albers, D. J. A. De Waal, D. C. Liles, D. J. Robinson, E. Singleton, M. B. Wiege, *J. Chem. Soc. Chem. Commun.* **1986**, 1680; b) C. S. Yi, J. R. Torres-Lubian, N. Liu, A. L. Rheingold, I. A. Guzei, *Organometallics* **1998**, *17*, 1257.

[15] C. H. Suresh, N. Koga, *Organometallics* **2006**, *25*, 1924.

[16] For examples of Ti-mediated coupling/cycloaddition of olefin with alkynes, see: a) K. Mach, F. Tureček, H. Antropiusová, V. Hanuš, *Organometallics* **1986**, *5*, 1215; b) B. G. Harvey, C. L. Mayne, A. M. Arif, R. D. Ernst, *J. Am. Chem. Soc.* **2005**, *127*, 16426; c) R. Tomaszewski, I. Hyla-Kryspin, C. L. Mayne, A. M. Arif, R. Gleiter, R. D. Ernst, *J. Am. Chem. Soc.* **1998**, *120*, 2959; d) A. M. Wilson, T. E. Waldman, A. L. Rheingold, R. D. Ernst, *J. Am. Chem. Soc.* **1992**, *114*, 6252.

[17] a) T. Higashi, ABSCOR—An Empirical Absorption Correction Based on Fourier Coefficient Fitting, Rigaku Corp., Tokyo, **1995**; b) G. M. Sheldrick, SHELXTL 5.10 for Windows NT, Structure Determination Software Programs, Bruker Analytical X-ray Systems, Inc., Madison, Wisconsin, USA, **1997**.

 © 2006 Wiley-VCH Verlag GmbH & Co. KGaA, Weinheim

Supramolecular Chemistry

DOI: 10.1002/anie.200601704

Hierarchical Structures Built from a Molecular Zinc Phosphate Core**

Ramaswamy Murugavel, Subramaniam Kuppuswamy, Ramamoorthy Boomishankar, and Alexander Steiner*

Dedicated to Professor Herbert W. Roesky

Assembling hierarchical supramolecular structures through a building-block approach is one of the major challenges in chemistry. In the last few decades, several research groups

[*] Prof. R. Murugavel, S. Kuppuswamy
Department of Chemistry
IIT-Bombay, Powai
Mumbai-400076 (India)
Fax: (+22) 2572-3480
E-mail: rmv@chem.iitb.ac.in
Homepage: http://www.chem.iitb.ac.in/~rmv/
Dr. R. Boomishankar, Dr. A. Steiner
Department of Chemistry
University of Liverpool
Crown Street, Liverpool, L69 7ZD (UK)

[**] Financial support of this work was provided by DST, New Delhi in the form of a Swarnajayanti Fellowship to R.M.

Supporting information for this article is available on the WWW under http://www.angewandte.org or from the author.

WILEY InterScience DISCOVER SOMETHING GREAT
© 2006 Wiley-VCH Verlag GmbH & Co. KGaA, Weinheim

have used a modular approach to assemble superstructures through exploitation of the selective recognition of suitably constructed ligands by various metal ions. An elegant example of this approach is the early work of Lehn and coworkers on the use of neutral polypyridine ligands.[1] More recent work on the use of polycarboxylic acids as multianionic spacer ligands has resulted in the realization of framework solids with exceptional surface areas.[2]

The synthesis of designer silicates and phosphates, on the other hand, is far more difficult. The main reason for this difficulty has been the lack of suitable organic-soluble reactants (or ligands) bearing SiO_4 and PO_4 tetrahedra. This problem was partially overcome in the 1990s with the successful synthesis of kinetically stabilized organosilanetriols containing a Si–N bond, $(R'RN)Si(OH)_3$.[3] These organosilanetriols interact with a variety of main-group and transition-metal ions to produce cages that resemble the secondary building units (SBUs) of zeolites (for example, the double-four-ring (D4R) unit). This approach was later extended to the synthesis of discrete molecular metallophosphonates starting from organophosphonic acids[4] and of metallophosphates starting from organophosphate esters.[5]

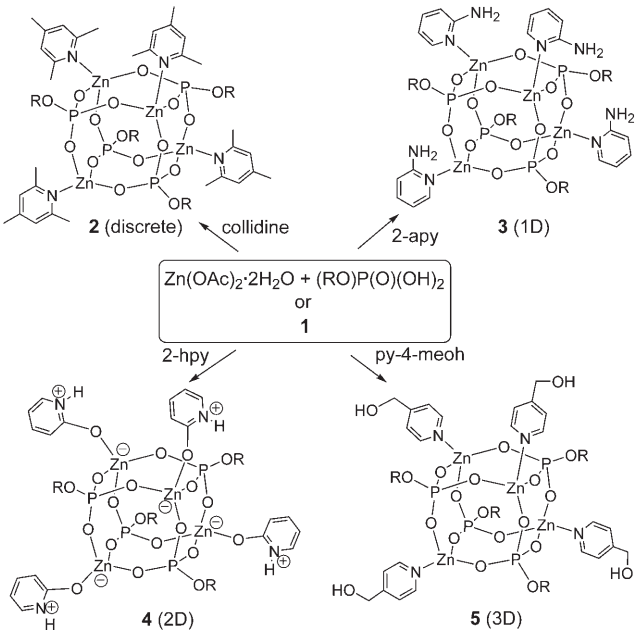
Although organosilanetriols and phosphorus acids have served as ideal starting points for the preparation of a number of SBUs, efforts to covalently link the SBUs into larger structures have met with very little success. For example, the activation of a B–C bond of a borophosphonate cube[6] or of a Ti–O bond of a titanosiloxane[7] (both having D4R cores) has proven to be difficult, even in the presence of phenols, alcohols, or acids. Similar difficulties were encountered when Group 13 element phosphonate cubes were treated with diols or diacids.[8] These results suggest that placing covalent linkages between these types of SBUs to build zeolite analogues would be difficult. In an attempt to rationally assemble metallophosphate superstructures, we have succeeded in not only synthesizing hitherto unknown zinc phosphate cubes, but also in linking them through noncovalent interactions.

Stirring a solution of $Zn(OAc)_2{\cdot}2H_2O$ (Ac = acetyl) and $(RO)P(O)(OH)_2$ (R = 2,6-di(isopropyl)phenyl) in methanol at room temperature produces a precipitate of $[Zn\{O_3P(OR)\}(MeOH)]_n$ [**1**; Eq. (1)]. Rapid loss of methanol

$$Zn(OAc)_2 \cdot 2H_2O + (RO)P(O)(OH)_2 \rightarrow [Zn\{O_3P(OR)\}(MeOH)]_n\,(\mathbf{1}) \quad (1)$$

from the crystals of **1** precludes a single-crystal X-ray structure determination. The fact that **1** is soluble in methanol, acetonitrile, and dimethyl sulfoxide (DMSO) and the observation that compounds **2–5** have tetrameric structures (see below) suggest that **1** is probably composed of discrete molecules, although its powder X-ray diffraction (XRD) pattern resembles that of layered phosphonates such as $[Zn(O_3PPh)(OH_2)]$.[9]

The addition of 2,4,6-trimethylpyridine (collidine) to a solution of **1** leads to the isolation of $[Zn\{O_3P(OR)\}(collidine)]_4$ (**2**; Scheme 1), which has been characterized with analytical and spectroscopic techniques. The IR spectrum of **2** shows strong absorption bands at $\nu = 1190$ (P=O) and 1020 and 920 cm^{-1} (M-O-P asymmetric and symmetric stretching). The presence of a single resonance in the ^{31}P NMR spectrum at $\delta = -4.7$ ppm indicates the presence of only one type of phosphorus atom in the molecule. A single crystal XRD study of **2** revealed that the molecule has a tetrameric cube structure (see below). To our knowledge, **2** is the first metallophosphate with a core composed of tetrahedrally coordinated metal and phosphorus centers that resembles the D4R SBU of zeolites and the cores of metallosiloxanes (such as $[RSiO_3Al]_4$; R = 2,6-*i*$Pr_2C_6H_3$)N($SiMe_3$) and metallophosphonates.[10,11]



Scheme 1. Syntheses of zinc phosphate cubes **2–5** with various substituted pyridine ligands (see the text for details).

In anticipation that the use of a bridging bidentate Lewis base would lead to D4R SBUs that are linked to each other through coordinate bonds, the preparation of **1** was carried out in the presence of ligands such as 4,4′-bipyridine or 1,4-diazabicyclo[2.2.2]octane (DABCO). However, a copious amount of insoluble noncrystalline precipitate was formed in each case, precluding single-crystal XRD studies.

Since neither covalent- nor coordinate-linkage approaches to the preparation of zeolite analogues yielded the desired results, a noncovalent approach was tried. In view of the stable cube complex **2** formed by **1** with collidine, a modified Lewis base approach was used. Additional functional groups, namely NH_2, OH, and CH_2OH, were placed in appropriate positions on the pyridine ring to enhance hydrogen bonding between the D4R cubes, thus resulting in noncovalently linked 1D, 2D, and 3D structures.

Thus, treatment of $Zn(OAc)_2{\cdot}2H_2O$ with $(RO)P(O)(OH)_2$ in the presence of 2-aminopyridine (2-apy), 2-hydroxypyridine (2-hpy), or 4-(hydroxymethyl)pyridine (py-4-meoh) produces $[Zn\{O_3P(OR)\}(2\text{-apy})]_4$ (**3**), $[Zn\{O_3P(OR)\}(2\text{-hpy})]_4$ (**4**), or $[Zn\{O_3P(OR)\}(\text{py-4-meoh})]_4$ (**5**), respectively, in good yield (Scheme 1).[12] Compounds **3–5** were characterized with analytical, spectroscopic, and single-

 © 2006 Wiley-VCH Verlag GmbH & Co. KGaA, Weinheim

crystal XRD[13] studies. The elemental analyses and ^{1}H NMR spectra suggest the formation of a 1:1:1 zinc/phosphate/pyridine complex in each case. The presence of a single sharp resonance at $\delta \approx -4.5$ ppm in the ^{31}P NMR spectrum of each of the compounds demonstrates the presence of only one type of phosphorus atom. Mass-spectrometric analysis did not provide any useful information about the oligomeric structures of the compounds.

As revealed by single-crystal XRD studies, the core structures of **2**–**5** consist of frameworks containing four zinc and four phosphorus atoms at the alternate vertices of a cube (Figure 1). Each of the Zn···P edges of the cube is bridged by a

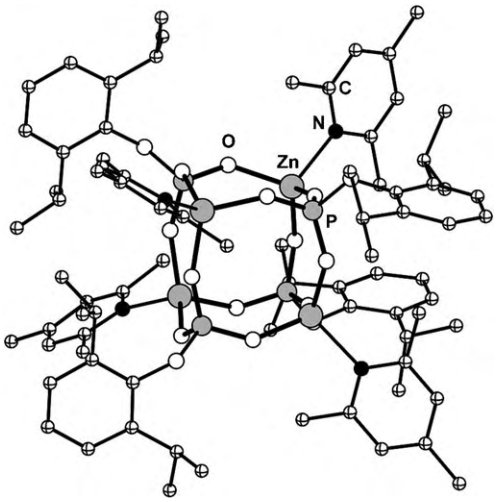


Figure 1. Molecular structure of the zinc phosphate cube **2**; hydrogen atoms are omitted for clarity.

μ_2-oxygen atom, thus resulting in six eight-membered $\{Zn_2O_4P_2\}$ rings, which adopt a crown conformation. The central D4R $\{Zn_4O_{12}P_4\}$ core is enclosed by the bulky aryl oxide ligands on the phosphorus atoms and the Lewis base ligands on the zinc atoms, as shown for **2** in Figure 1.

In **3** and **5**, the nitrogen atoms of the pyridine ligands bind to the Zn^{2+} ions, as expected, while the pendant NH_2 and CH_2OH groups do not interact with the metal centers. On the other hand, the 2-hpy ligand in **4** coordinates to the Zn^{2+} ion through the phenoxide oxygen atom, rather than the pyridine nitrogen atom (Scheme 1); the OH group has undergone a hydrogen-shift during coordination, thus producing a zwitterionic pyridinium phenoxide ligand.

The bond lengths and angles observed for the zinc phosphate cores of **2**–**5** are similar (see the Supporting Information). There are no formal P–O and P=O bonds in **2**–**5**: the average P–O bond lengths are 1.532(3) (**2**), 1.537(2) (**3**), 1.533(2) (**4**), and 1.532(4) Å (**5**). The average Zn–O lengths of 1.916(3) (**2**), 1.923(2) (**3**), 1.919(4) (**4**), and 1.919(2) Å (**5**) are comparable to those observed in several zinc phosphonates and phosphates.[14] The average Zn-O-P angles of 139.9(2) (**2**), 134.3(1) (**3**), 135.4(2) (**4**), and 135.3(1)° (**5**) are smaller than the 180° value expected for a linear edge, thus giving the core a spherical appearance. The bond angles around the zinc and phosphorus atoms do not deviate appreciably from the ideal tetrahedral values. The dimensions of the cores of **2**–**5** can best be understood from the average lengths of the Zn···P edges (3.20 (**2**), 3.18 (**3**), 3.17 (**4**), and 3.17 Å (**5**)), the P···P face diagonals (4.63 (**2**), 4.60 (**3**), 4.64 (**4**), and 4.62 Å (**5**)), the Zn···Zn face diagonals (4.42 (**2**), 4.35 (**3**), 4.32 (**4**), and 4.34 Å (**5**)), and the Zn···P body diagonals (5.53 (**2**), 5.48 (**3**), 5.49 (**4**), and 5.48 Å (**5**)). Thus, the volumes of the inorganic cores of the molecules are roughly 85–90 Å^3, whereas the molecular volumes including the organic substituents are 1700–2200 Å^3.

The most interesting aspect of the zinc phosphate cubes is their ability to assemble through noncovalent interactions, when the appropriate surface functionalities are present, as in **3**–**5**. In the absence of surface functionalities, the tetrameric zinc phosphate clusters in **2** remain discrete. The presence of NH_2 groups in *ortho* positions on the pyridine rings in **3** is the source of intra- and intermolecular N–H···O hydrogen bonds. While each of the four NH_2 groups in **3** forms an intramolecular N–H···O interaction with one of the framework oxygen atoms, two of the NH_2 groups are also involved intermolecular N–H···O interactions with adjacent cubes, thus resulting in a 1D assembly (Figure 2). The intercube distance of 6.812 Å is largely dictated by the strong intermolecular hydrogen bonding.

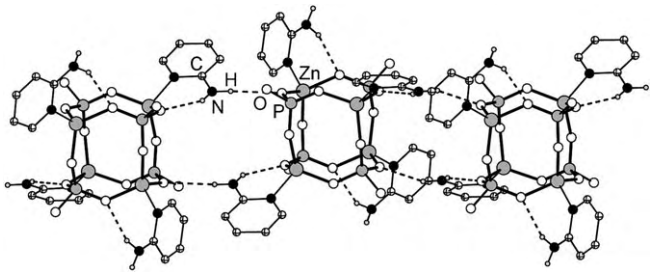


Figure 2. 1D assembly of zinc phosphate cubes in the crystal structure of **3**; dashed lines indicate hydrogen bonds; 2,6-di(isopropyl)phenyl groups and carbon-bound hydrogen atoms are omitted for clarity.

The crystal structure of **4** presents a different type of supramolecular aggregation. As the Zn^{2+} ion is bound to the phenoxide oxygen atom, rather than the pyridine nitrogen atom of the 2-hpy ligand, the NH group is farther away from the framework oxygen centers and hence, prefers intermolecular over intramolecular N–H···O hydrogen bonds. Thus, three of the four NH groups form intermolecular hydrogen bonds with the oxygen atoms of the 2-hpy ligands of three adjacent cubes (Figure 3a). The fourth NH group is content with an intramolecular N–H···O interaction with a framework oxygen atom, as in the case of **3**. The propagation of hydrogen bonds between the cubes occurs through only three terminals, which are oriented approximately 120° from one another in the same plane. Thus, an extended 2D sheet of D4R cubes, which contains hexagonal channels, is formed (Figure 3b). Additional C–H···O hydrogen bonds between pyridine CH groups and framework oxygen centers stabilize the hexagonal arrangement. The average distance of 6.801 Å between the cubes is comparable to that observed for **3**.

It is clear from the crystal structure of **4** that the formation of a 3D structure is hampered by the presence of the single

 © 2006 Wiley-VCH Verlag GmbH & Co. KGaA, Weinheim

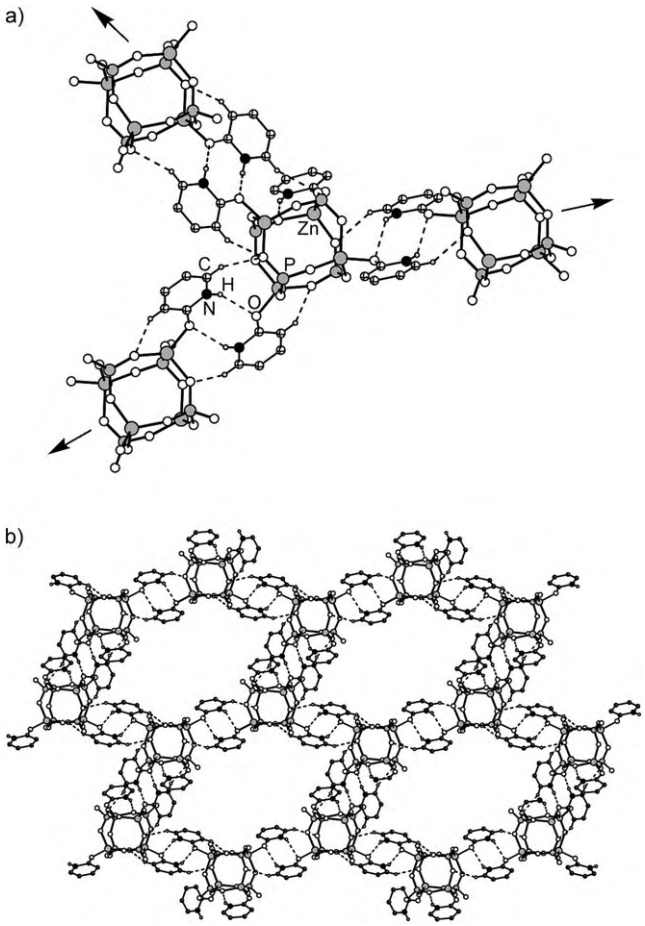


Figure 3. In the crystal structure of **4**, a) each zinc phosphate cube is linked to three others through hydrogen bonding, thus leading to b) a hexagonal 2D assembly; dashed lines indicate hydrogen bonds; 2,6-di(isopropyl)phenyl groups and hydrogen atoms not involved in hydrogen bonding are omitted for clarity.

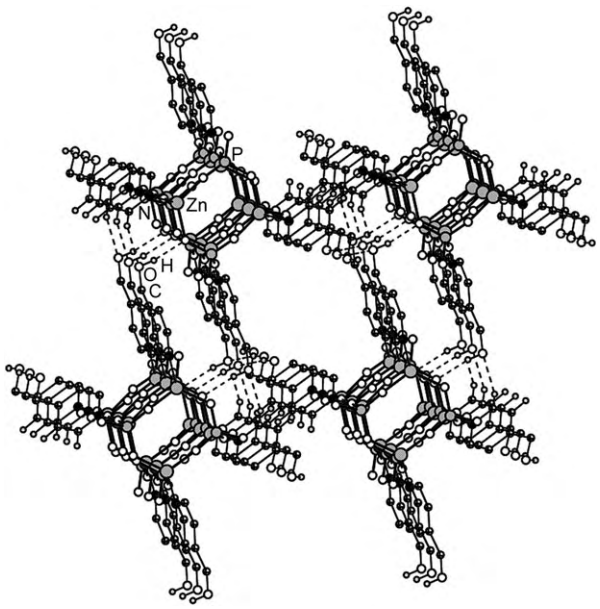


Figure 4. 3D assembly of zinc phosphate cubes in the crystal structure of **5**; dashed lines indicate hydrogen bonds; 2,6-di(isopropyl)phenyl groups and hydrogen atoms not involved in hydrogen bonding are omitted for clarity.

intramolecular N–H···O interaction in each cube. This problem is overcome by introducing a spacer between the functional groups and the pyridine ring. Thus, the OH groups of all four of the py-4-meoh ligands in **5** form exclusively intermolecular hydrogen bonds. As the four OH groups are pointed roughly towards the four corners of a tetrahedron, a 3D supramolecular aggregation results (Figure 4). Two of the four OH groups, which are opposite to one another, form three intermolecular hydrogen bonds each: one with a framework oxygen atom, one with a CH group of a pyridine ring, and one with another OH group. The two remaining OH groups of the cube each form an intermolecular hydrogen bond to an OH group (not shown in Figure 4). Owing to the presence of only intermolecular interactions involving the para CH_2OH groups, the average distance between the cubes in **5** is 10.471 Å, which is much larger than that observed for **2**–**4**.

In conclusion, we have synthesized the first examples of organic-soluble transition-metal phosphates with cores that resemble the D4R SBUs of zeolites. Strategies for arranging these SBUs into either 1D, 2D, or 3D supramolecular structures through noncovalent interactions have also been presented. These studies suggest that it is not only important to have a hydrogen-bond donor on the pyridine ligand, but also to place it in an appropriate position. Furthermore, to build superstructures with higher dimensionalities, it is important to decrease or eliminate intramolecular hydrogen bonds. Note that the reaction of aryl phosphonic acids with metal ions normally leads to the isolation of insoluble layered metal phosphonates. However, when an aryl phosphoric acid (in which an oxygen atom is located between the aryl ring and the phosphorus atom) is used as a reagent herein, discrete organic-soluble clusters are isolated. Finally, the presence of NH, NH_2, or OH groups on the surfaces of clusters **3**–**5** opens up new possibilities for further reactions with metal alkyl reagents (for example, AlR_3) to build dendritic heterometallic superstructures. We are currently investigating these aspects.

Experimental Section

$Zn(OAc)_2{\cdot}2H_2O$ (219 mg, 1 mmol) and 2,6-di(isopropyl)phenylphosphoric acid (258 mg, 1 mmol) were mixed in methanol (30 mL) and warmed to produce a clear solution. The reaction mixture was filtered, concentrated, and left overnight to yield a precipitate of **1**. Compounds **2**–**5** were synthesized in a similar manner, by adding the appropriate substituted pyridine ligand to the reaction mixture.

1: M.p. $>275\,^{\circ}C$; yield: 0.3 g (85%); elemental analysis (%) calcd for $C_{13}H_{21}O_5PZn$ ($M_r = 353.7$): C 44.15, H 5.98; found: C 44.88, H 5.87; ^1H NMR ([D$_6$]acetone, 300 MHz): $\delta = 7.02$ (s, 12H, aryl), 3.77 (sept, 8H, CH; $^3J_{HH} = 6.9$ Hz), 3.65 (br, 4H, OH), 3.30 (s, 12H, CH_3), 1.11 ppm (d, 48H, CH_3); ^{31}P NMR ([D$_6$]acetone, 121 MHz): $\delta = -4.5$ ppm. **2**: M.p. $>275\,^{\circ}C$; yield: 0.3 g (68%); elemental analysis (%) calcd for $C_{80}H_{112}N_4O_{16}P_4Zn_4$ ($M_r = 1771.1$): C 54.24, H 6.37, N 3.16; found: C 52.80, H 6.21, N 2.95; ^1H NMR ([D$_6$]DMSO, 300 MHz): $\delta = 7.02$–6.95 (m, 12H, aryl), 6.85 (s, 8H, aryl), 3.69 (sept, 8H, CH; $^3J_{HH} = 6.6$ Hz), 2.34 (s, 24H, CH_3), 2.20 (s, 12H, CH_3), 1.08 ppm (d, 48H, CH_3); ^{31}P NMR ([D$_6$]DMSO, 121 MHz): $\delta =$

 © 2006 Wiley-VCH Verlag GmbH & Co. KGaA, Weinheim

−4.7 ppm. **3**: M.p. >275 °C; yield: 0.3 g (77 %); elemental analysis (%) calcd for $C_{68}H_{92}N_8O_{16}P_4Zn_4$ (M_r = 1663.0): C 49.11, H 5.57, N 6.73; found: C 48.99, H 5.54, N 6.73; ^{1}H NMR (300 MHz, $CDCl_3$): δ = 7.37–7.51 (m, 8H, aryl), 6.94–7.10 (m, 12H, aryl), 6.37–6.41 (m, 8H, aryl), 5.41 (S, 8H, NH), 3.65 (sept, 8H, CH; $^3J_{HH}$ = 6.9 Hz), 0.98 ppm (d, 48H, CH_3); ^{31}P NMR ([D$_6$]acetone, 121 MHz): δ = −4.9 ppm. **4**: M.p. 257–258 °C, yield: 0. 28 g (68 %), elemental analysis (%) calcd for $C_{68}H_{88}N_4O_{20}P_4Zn_4$ (M_r = 1666.8): C 48.99, H 5.32, N 3.36; found: C 49.39, H 5.62, N 3.44; ^{1}H NMR ([D$_6$]DMSO, 400 MHz): δ = 11.58 (S, 4H, NH), 7.39–7.43 (m, 4H, aryl), 7.35 (dd, 4H, aryl; $^3J_{HH}$ = 5.2 Hz), 6.94–7.02 (m, 12H, aryl), 6.31 (d, 4H, aryl; $^3J_{HH}$ = 9.2 Hz), 6.16 (t, 4H, aryl; $^3J_{HH}$ = 6.4 Hz), 3.68 (sept, 8H, CH; $^3J_{HH}$ = 6.8 Hz), 1.09 ppm (d, 48H, CH_3); ^{31}P NMR ([D$_6$]DMSO, 121 MHz): δ = −4.7 ppm. **5**: M.p. >275 °C; yield: 0.4 g (93 %); elemental analysis (%) calcd for $C_{72}H_{96}P_4O_{20}N_4Zn_4$ (M_r = 1723.0): C 50.18, H 5.61, N 3.25; found: C 50.21, H 5.75, N 3.39; ^{1}H NMR ([D$_6$]DMSO, 400 MHz): δ = 8.22 (s, 8H, aryl), 7.38 (d, 8H, aryl; $^3J_{HH}$ = 4.8 Hz), 6.99 (s, 12H, aryl), 5.55 (t, 4H, OH; $^3J_{HH}$ = 5.2 Hz), 4.58 (d, 8H, CH_2; $^3J_{HH}$ = 5.6 Hz), 3.64 (sept, 8H, CH; $^3J_{HH}$ = 6.4 Hz), 0.98 ppm (d, 48H, CH_3); ^{31}P NMR ([D$_6$]DMSO, 121 MHz): δ = −4.4 ppm.

Received: April 29, 2006
Published online: July 18, 2006

Keywords: cluster compounds · hydrogen bonds · structure elucidation · supramolecular chemistry · zeolite analogues

[1] a) J.-M. Lehn, *Supramolecular Chemistry: Concepts and Perspectives*, VCH, New York, **1995**; b) *Comprehensive Supramolecular Chemistry* (Eds. J. L. Atwood, J. E. D. Davies, D. D. F. MacNicol, J.-M. Lehn), Pergamon, Oxford, **1996**; c) J.-M. Lehn in *Supramolecular Science: Where It Is and Where It Is Going* (Eds.: R. Ungaro, R. F. Dalcanale), Kluwer, Dordrecht, **1996**, pp. 287–304.

[2] Recent reviews: a) C. N. R. Rao, S. Natarajan, R. Vaidhyanathan, *Angew. Chem.* **2004**, *116*, 1490–1521; *Angew. Chem. Int. Ed.* **2004**, *43*, 1466–1496; b) O. M. Yaghi, M. O'Keeffe, N. W. Ockwig, H. K. Chae, M. Eddaoudi, J. Kim, *Nature* **2003**, *423*, 705.

[3] a) R. Murugavel, A. Voigt, M. G. Walawalkar, H. W. Roesky, *Chem. Rev.* **1996**, *96*, 2205–2236; b) V. Chandrasekhar, R. Boomishankar, S. Nagendran, *Chem. Rev.* **2004**, *164*, 5847–5910.

[4] M. G. Walawalkar, H. W. Roesky, R. Murugavel, *Acc. Chem. Res.* **1999**, *32*, 117–126.

[5] a) R. Murugavel, M. G. Walawalkar, M. Dan, H. W. Roesky, C. N. R. Rao, *Acc. Chem. Res.* **2004**, *37*, 763–774; b) R. Pothiraja, M. Sathiyendiran, R. J. Butcher, R. Murugavel, *Inorg. Chem.* **2004**, *43*, 7585–7587; c) R. Pothiraja, M. Sathiyendiran, R. J. Butcher, R. Murugavel, *Inorg. Chem.* **2005**, *44*, 6314–6323; d) C. G. Lugmair, T. D. Tilley, A. L. Rheingold, *Chem. Mater.* **1997**, *9*, 339–348.

[6] M. G. Walawalkar, R. Murugavel, H. W. Roesky, H. G. Schmidt, *Organometallics* **1997**, *16*, 516–518.

[7] R. Murugavel, P. Davis, V. S. Shete, *Inorg. Chem.* **2003**, *42*, 4696–4706.

[8] R. Murugavel, unpublished results.

[9] a) A. Clearfield in *Progress in Inorganic Chemistry*, *Vol. 47* (Ed.: K. D. Karlin), Wiley, New York, **1998**, p. 371; b) K. Segawa, N. Kihara, H. Yamamoto, *J. Mol. Catal.* **1992**, *74*, 213–221; c) A. Clearfield, *J. Mol. Catal.* **1984**, *27*, 251–262; d) G. Alberti, *Acc. Chem. Res.* **1978**, *11*, 163–170; e) G. Cao, H. G. Hong, T. E. Mallouk, *Acc. Chem. Res.* **1992**, *25*, 420–427; f) R. Murugavel, P. Davis, M. G. Walawalkar, *Z. Anorg. Allg. Chem.* **2005**, *631*, 2806–2811.

[10] a) M. L. Montero, I. Usón, H. W. Roesky, *Angew. Chem.* **1994**, *106*, 2198–2200; *Angew. Chem. Int. Ed. Engl.* **1994**, *33*, 2103–2104; b) V. Chandrasekhar, R. Murugavel, A. Voigt, H. W. Roesky, H. G. Schmidt, M. Noltemeyer, *Organometallics* **1996**, *15*, 918–922.

[11] G. Prabusankar, R. Murugavel, R. J. Butcher, *Organometallics* **2005**, *24*, 2124–2128.

[12] Alternatively, compounds **2**–**5** can also be prepared by the addition of the respective substituted pyridine ligand to a methanol solution of **1**. By this route, better yields and good-quality crystals are obtained.

[13] Crystal data for **2**: $C_{80}H_{112}N_4O_{16}P_4Zn_4$, M_r = 1771.1, size = 0.15 × 0.05 × 0.05 mm^3, tetragonal, space group $I4_1/a$, Z = 4, a = 23.722(2), c = 14.608(2) Å, V = 8220(1) Å^3, ρ_{calcd} = 1.431 g cm^{-3}, $\mu(Mo_{K\alpha})$ = 1.298 mm^{-1}, $F(000)$ = 3712, $R_1(I>2\sigma(I))$ = 0.0378, wR_2(all data) = 0.0640, GOF = 0.824. **3**: $C_{68}H_{92}N_8O_{16}P_4Zn_4$, M_r = 1663.0, size = 0.2 × 0.2 × 0.2 mm^3, monoclinic, space group $C2/c$, Z = 4, a = 29.3099(17), b = 14.4890(7), c = 19.9454(14) Å, β = 111.282(5)°, V = 7893(1) Å^3, ρ_{calcd} = 1.399 g cm^{-3}, $\mu(Mo_{K\alpha})$ = 1.348 mm^{-1}, $F(000)$ = 3456, $R_1(I>2\sigma(I))$ = 0.0311, wR_2 = 0.0649, GOF = 0.932. **4**: $C_{68}H_{88}N_4O_{20}P_4Zn_4$, M_r = 1666.8, size = 0.3 × 0.3 × 0.2 mm^3, triclinic, space group $P\bar{1}$, Z = 2, a = 15.384(3), b = 15.421(3), c = 19.551(3) Å, α = 86.45(2), β = 67.62(2), γ = 66.42(2)°, V = 3909(1) Å, ρ_{calcd} = 1.416 g cm^{-3}, $\mu(Mo_{K\alpha})$ = 1.363 mm^{-1}, $F(000)$ = 1728, $R_1(I>2\sigma(I))$ = 0.0529, wR_2 = 0.1241, GOF = 0.934. **5**: $C_{72}H_{96}N_4O_{20}P_4Zn_4$, M_r = 1723.0, size = 0.3 × 0.2 × 0.2 mm^3, monoclinic, space group $C2/c$, Z = 4, a = 24.466(3), b = 14.663(2), c = 23.074(3) Å, β = 104.77(1)°, V = 8004(2) Å, ρ_{calcd} = 1.430 g cm^{-3}, $\mu(Mo_{K\alpha})$ = 1.334 mm^{-1}, $F(000)$ = 3584, $R_1(I>2\sigma(I))$ = 0.0316, wR_2 = 0.0705, GOF = 0.907. CCDC-289557 (**3**), -289558 (**4**), -289559 (**2**), and -289560 (**5**) contain the supplementary crystallographic data for this paper. These data can be obtained free of charge from The Cambridge Crystallographic Data Centre via www.ccdc.cam.ac.uk/data_request/cif.

[14] a) A. Abufarag, H. Vahrenkamp, *Inorg. Chem.* **1995**, *34*, 2207–2216; b) K. Weis, M. Rombach, H. Vahrenkamp, *Inorg. Chem.* **1998**, *37*, 2470–2475; c) J. G. Mao, A. Clearfield, *Inorg. Chem.* **2002**, *41*, 2319–2324; d) F. H. Fry, P. Jensen, C. M. Kepert, L. Spiccia, *Inorg. Chem.* **2003**, *42*, 5637–5644; e) J. C. M. Rivas, R. T. M. Rosales, S. Parsons, *Dalton Trans.* **2003**, 4385–4386; f) Y. Yang, J. Pinkas, M. Noltemeyer, H.-G. Schmidt, H. W. Roesky, *Angew. Chem.* **1999**, *111*, 706–708; *Angew. Chem. Int. Ed.* **1999**, *38*, 664–666; g) A. Clearfield, C. V. K. Sharma, B. Zhang, *Chem. Mater.* **2001**, *13*, 3099–3112; h) V. Chandrasekhar, S. Kingsley, B. Rhatigan, M. K. Lam, A. L. Rheingold, *Inorg. Chem.* **2002**, *41*, 1030–1032.

 © 2006 Wiley-VCH Verlag GmbH & Co. KGaA, Weinheim

Cyclizations

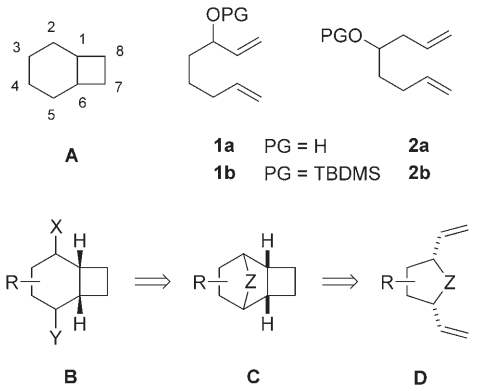
DOI: 10.1002/anie.200600946

Synthesis of Enantiomerically Pure Bicyclo[4.2.0]octanes by Cu-Catalyzed [2+2] Photocycloaddition and Enantiotopos-Differentiating Ring Opening**

*Ingbert Braun, Florian Rudroff, Marko D. Mihovilovic, and Thorsten Bach**

Dedicated to Professor Jochen Mattay on the occasion of his 60th birthday

The wide distribution of bicyclo[4.2.0]octanes in natural products[1] and the inherently difficult synthesis of strained cyclobutanes[2] renders the synthesis of compounds with the general framework **A** (Scheme 1) a challenging task. Quite



Scheme 1. Top: Structures of the bicyclo[4.2.0]octane skeleton **A** and of possible starting materials **1** and **2** for [2+2] photocycloaddition reactions; bottom: retrosynthetic analysis for the synthesis of enantiomerically pure bicyclo[4.2.0]octanes **B**.

clearly, the cyclobutane part invites a photochemical key step, and [2+2] photocycloaddition reactions with cyclohexenones have been studied intensively.[3] In these examples enantiomerically pure products have always been obtained from enantiomerically pure starting materials.[4]

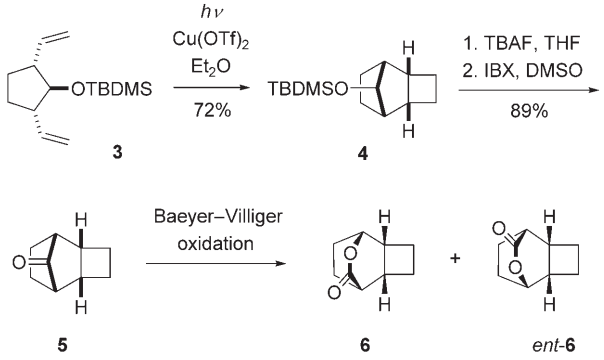
[*] Dipl.-Chem. I. Braun, Prof. Dr. T. Bach
Lehrstuhl für Organische Chemie I
Technische Universität München
Lichtenbergstrasse 4, 85747 Garching (Germany)
Fax: (+49) 89-2891-3315
E-mail: thorsten.bach@ch.tum.de
Dipl.-Ing. F. Rudroff, Prof. Dr. M. D. Mihovilovic
Institut für Angewandte Synthesechemie
Technische Universität Wien
Getreidemarkt 9/163-OC, 1060 Vienna (Austria)

[**] This project was supported by the Deutsche Forschungsgemeinschaft (Ba 1372/11), by the Fonds der Chemischen Industrie, and by the Fond zur Förderung der wissenschaftlichen Forschung Österreich (FWF, P-I19-B10).

The alternative approach by Cu-catalyzed, intramolecular [2+2] photocycloaddition reactions[5] of open-chain 1,7-dienes is not viable. When we attempted [2+2] photocycloaddition reactions of substrates **1** and **2**, there was no indication for the formation of the desired bicyclo[4.2.0]octane. Apparently Cu-catalyzed photocycloaddition reactions require the coordination of both double bonds to the metal atom,[6] which is feasible only for reactions with 1,6-dienes leading to bicyclo[3.2.0]heptanes.

We now propose a retrosynthetic concept (Scheme 1) that encompasses an enantiotopos-differentiating ring-opening reaction of substrates such as **C** (Z = CO) for the synthesis of enantiomerically pure bicyclo[4.2.0]octanes, represented by structure **B**. Because tricyclic compound **C** encompasses both bicyclo[4.2.0]octane and bicyclo[3.2.0]heptane structures, it should be accessible by Cu-catalyzed [2+2] photocycloaddition reaction of diene **D**. Herein, we report the successful application of this concept to a specific example.

We envisioned an enantioselective Baeyer–Villiger oxidation as the enantiotopos-differentiating reaction,[7] which thus requires a carbonyl group as the functional group Z (Scheme 1, **C**, Z = CO). The instability of a 1,3-divinyl-2-cyclopentanone and its undesired photochemical reactions (α-cleavage, oxa-di-π-methane rearrangement) prompted us to incorporate the carbonyl group in protected form (Z = CHOTBDMS, TBDMS = *tert*-butyldimethylsilyl). Accordingly, we attempted a Cu-catalyzed [2+2] photocycloaddition reaction with the readily available[8] diene **3** (Scheme 2). The



Scheme 2. Diastereoselective preparation of ketone **5** and its enantioselective Baeyer–Villiger oxidation.

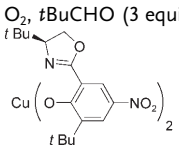
reaction proceeded smoothly, and the desired product **4**[9] was obtained in good yields and with high *endo* diastereoselectivity (*endo*/*exo* > 90:10). As mentioned in previous papers,[10] following the observation of Mattay et al.,[11] the more stable copper(II) trifluoromethanesulfonate ($Cu(OTf)_2$) can be used instead of CuOTf, which facilitates the experimental procedure significantly. Cleavage of the protecting group with tetrabutylammoniumfluoride (TBAF), followed by oxidation with 2-iodoxybenzoic acid (IBX) afforded ketone **5**, which was submitted to different conditions for the Baeyer–Villiger oxidation.

Among the protocols for metal-catalyzed oxidations, the method developed by Bolm et al.[12] gave the best results. The desired product **6**[13] could be obtained with complete

 © 2006 Wiley-VCH Verlag GmbH & Co. KGaA, Weinheim

conversion in 32% *ee* (Table 1, entry 1) and in 72% yield. Significantly higher enantiomeric excesses were achieved with different recombinant *Escherichia coli* whole-cell expression systems of flavin-dependent monooxygenases[14]

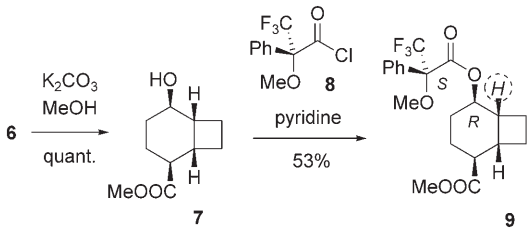
Table 1: Enantioselective Baeyer–Villiger oxidations of substrate **5** under different conditions (cf. Scheme 2).

Entry	Method	Conv. [%]	e.r.[a]	*ee*[b] [%]
1	O_2, *t*BuCHO (3 equiv)  (3 mol%) C_6H_6, RT, 3 d	100	66:34	32
2	$CHMO_{Brevi1}$ (LB_{Amp})[c] 24 °C, 24 h	100	2:98	96
3	$CHMO_{Brachy}$ (LB_{Amp})[c] 24 °C, 24 h	100	4:96	92
4	$CPMO_{Coma}$ (LB_{Amp})[c] 24 °C, 24 h	56	93:7	86
5	$CHMO_{Brevi2}$ (LB_{Amp})[c] 24 °C, 24 h	30	87:13	74

[a] Enantiomeric ratio **6**/*ent*-**6**. Ratios were determined by gas chromatography on a chiral stationary phase (BGB-175: 50% 2,3-diacetyl-6-*tert*-butyldimethylsilylated γ-cyclodextrin). [b] The enantiomeric excess was calculated from the enantomeric ratios. [c] Recombinant *E. coli* strains in Luria–Bertani (LB) media supplemented with ampicillin (Amp) were used. The overexpressed monooxygenases originate from *Brachymonas* ($CHMO_{Brachy}$), *Brevibacterium* ($CHMO_{Brevi1}$, $CHMO_{Brevi2}$), and *Comamonas* ($CPMO_{Coma}$).[17]

(Table 1). In particular, the formation of enantiocomplementary lactone products depending on the enzyme used (entry 2,3 vs. 4,5) is very appealing from a synthetic chemist's point of view. This observation is congruent with the recent identification of two distinct groups (family clusters) of Baeyer–Villiger monooxygenases.[15] Using monooxygenase $CHMO_{Brevi1}$, we obtained predominantly *ent*-**6** (96% *ee*), while $CHMO_{Brevi2}$ and $CPMO_{Coma}$ gave the enantiomeric lactone **6**. So far,[16] monooxygenases producing predominantly enantiomer **6** gave lower conversions and selectivities than monooxygenases with a preference for enantiomer *ent*-**6** (entries 2 and 3, Table 1). Other cyclohexanone monooxygenases ($CHMO_{Arthro}$, $CHMO_{Rhodo1}$, $CHMO_{Rhodo2}$, $CHMO_{Acineto}$) were less successful with regard to the desired enantiotopos differentiation and are not listed in Table 1.

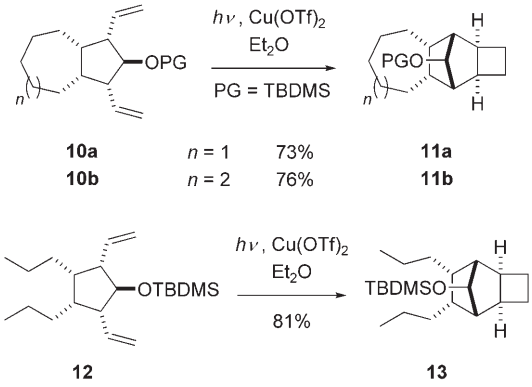
The configuration assignment was conducted by a method described by Mosher et al.[18] for secondary alcohols. Accordingly, δ-lactone **6** and its enantiomer *ent*-**6** underwent quantitative ring-opening to give the methyl δ-hydroxycarboxylates **7** and *ent*-**7**, respectively (Scheme 3), and the free hydroxyl group was acylated with reagent **8**. Owing to the preferred conformation of the resulting Mosher ester, the ^1H NMR chemical shifts for the protons at the α-carbon atoms are differentiated.[18] The *S,R* diastereomer, obtained with an



Scheme 3. Proof of the absolute configuration of lactone **6** by the Mosher ester method.[18]

R-configured alcohol, shows a downfield shift for the proton attached to the larger α-carbon substituent compared to the analogous shift of the *S,S* diastereomer, and vice versa. This chemical-shift difference was observed for the proton on the cyclobutane ring indicated in **9** (Scheme 3). In the ^1H NMR spectrum of the major diastereomer the α protons of the cyclohexyl ring are shifted upfield relative to those of the minor isomer.

It is apparent that many other methods can be employed for the suggested enantiotopos differentiation.[19] The substrates are limited to compounds bearing a mirror plane. Further photocycloaddition reactions, which were shown to proceed in good yields and which led to new substrates for the desymmetrization step, are depicted in Scheme 4. Divinyl-



Scheme 4. Cu-catalyzed [2+2] photocycloaddition reactions leading to the tri- and tetracyclic products **13** and **11**, respectively.

substituted bicyclo[(4+*n*).3.0]alkanes **10a** and **10b** reacted smoothly in good yields and with excellent diastereoselectivities to give products **11**. Pentasubstituted cyclopentane **12** also underwent a [2+2] photocycloaddition reaction to provide the desired tricyclic product **13**. Hence, the introduction of the bridge (Z = CHOTBDMS, Scheme 1) indeed enables the otherwise impossible [2+2] photocycloaddition reaction.

Further investigations in our group currently focus on the development and application of other enantiotopos-differentiating reactions to ketones similar to **5**, and on the variation of the bridge Z in intermediates of type **C**. Saponification of lactone **6** or ester **7** to give the corresponding δ-hydroxycarboxylic acid should facilitate the synthesis of

 © 2006 Wiley-VCH Verlag GmbH & Co. KGaA, Weinheim

enantiomerically pure bicyclo[4.2.0]octane-2-ol and bicyclo-[4.2.0]octane-2-one, which are not accessible from **1a** or **1b**.

Received: March 10, 2006
Revised: May 2, 2006
Published online: July 19, 2006

Keywords: asymmetric synthesis · cycloaddition · enantioselectivity · lactones · oxidation

[1] a) M. Cueto, L. D'Croz, J. L. Mate, A. San-Martin, J. Darias, *Org. Lett.* **2005**, *7*, 415 – 418; b) S. N. Fedorov, O. S. Radchenko, L. K. Shubina, A. I. Kalinovsky, A. V. Gerasimenko, D. Y. Popov, V. A. Stonik, *J. Am. Chem. Soc.* **2001**, *123*, 504 – 505; c) M. Clericuzio, M. Mella, L. Toma, P. V. Finzi, G. Vidari, *Eur. J. Org. Chem.* **2002**, 988 – 994; d) V. U. Ahmad, A. R. Jassbi, *J. Nat. Prod.* **1999**, *62*, 1016 – 1018; e) T. V. Hansen, Y. Stenstrom in *Organic Synthesis: Theory and Applications*, *Vol. 5* (Ed.: T. Hudlicky), Elsevier, Oxford, **2001**, pp. 1 – 38.

[2] Reviews: a) E. Lee-Ruff, G. Mladenova, *Chem. Rev.* **2003**, *103*, 1449 – 1483; b) H. N. C. Wong, P. Margaretha, E. Lee-Ruff, H. Butenschön, G. Mann, H. M. Muchall, L. Fitjer, G. Haufe, Y. Stenstrom, L. K. Syders in *Methoden der Organischen Chemie (Houben-Weyl) 4th* ed., *Vol. E 7e* (Ed.: A. de Meijere), Thieme, Stuttgart, **1997**, pp. 29 – 434.

[3] Reviews: a) P. Margaretha in *Molecular and Supramolecular Photochemistry: Synthetic Organic Photochemistry*, *Vol. 12* (Eds.: A. G. Griesbeck, J. Mattay), Dekker, New York, **2005**, pp. 211 – 237; b) D. I. Schuster in *CRC Handbook of Photochemistry and Photobiology*, 2nd ed. (Eds.: W. M. Horspool, F. Lenci), CRC, Boca Raton, FL, **2004**, pp. 72.1 – 24; c) T. Bach, *Synthesis* **1998**, 683 – 703; d) S. A. Fleming, C. L. Bradford, J. J. Gao in *Molecular and Supramolecular Photochemistry: Synthetic Organic Photochemistry*, *Vol. 1* (Eds.: V. Ramamurthy, K. S. Schanze), Dekker, New York, **1997**, pp. 187 – 243; e) J.-P. Pete, *Adv. Photochem.* **1996**, *21*, 135 – 216; f) J. Mattay, R. Conrads, R. Hoffmann in *Methoden der Organischen Chemie (Houben-Weyl) 4th* ed., *Vol. E 21c* (Eds.: G. Helmchen, R. W. Hoffmann, J. Mulzer, E. Schaumann), Thieme, Stuttgart, **1995**, pp. 3085 – 3132; g) M. T. Crimmins, T. L. Reinhold, *Org. React.* **1993**, *44*, 297 – 583; h) S. W. Baldwin, *Org. Photochem.* **1981**, *5*, 123 – 225.

[4] Examples: a) E. Garcia-Exposito, A. Alvarez-Larena, V. Branchadell, R. M. Ortuno, *J. Org. Chem.* **2004**, *69*, 1120 – 1125; b) A. B. Smith III, N. Kanoh, H. Ishiyama, N. Minakawa, J. D. Rainier, R. A. Hartz, Y. S. Cho, H. F. Cui, W. H. Moser, *J. Am. Chem. Soc.* **2003**, *125*, 8228 – 8237; c) G. Mehta, J. Nandakumar, *Tetrahedron Lett.* **2001**, *42*, 7667 – 7670; d) J. E. Resek, A. I. Meyers, *Synlett* **1995**, 145 – 146; e) A. Abad, M. Arno, M. L. Marin, R. J. Zaragoza, *J. Chem. Soc. Perkin Trans. 1* **1993**, 1861 – 1867.

[5] Reviews: a) G. Salomon, *Tetrahedron* **1983**, *39*, 485 – 575; b) P. Margaretha in *Methoden der Organischen Chemie (Houben-Weyl) 4th* ed., *Vol. E 17e* (Ed.: A. de Meijere), Thieme, Stuttgart **1997**, pp. 159 – 162; c) S. Ghosh in *CRC Handbook of Photochemistry and Photobiology*, 2nd ed. (Eds.: W. M. Horspool, F. Lenci), CRC, Boca Raton, FL, **2004**, pp. 18.1 – 24.

[6] Structural investigations: a) T. Nickel, K.-R. Pörschke, R. Goddard, C. Krüger, *Inorg. Chem.* **1992**, *31*, 4428 – 4430; b) P. H. M. Budzelaar, P. J. J. A. Timmermans, A. Mackor, A. L. Spek, A. J. M. Duisenberg, *Acta Crystallogr. Sect. C* **1987**, *43*, 2298 – 2300.

[7] Reviews: a) C. Bolm, C. Palazzi, O. Beckmann in *Transition Metals for Organic Synthesis, 2nd* ed., *Vol. 2* (Eds.: M. Beller, C. Bolm), Wiley-VCH, Weinheim, **2004**, pp. 267 – 274; b) M. D. Mihovilovic, F. Rudroff, B. Groetzl, *Curr. Org. Chem.* **2004**, *8*, 1057 – 1069.

[8] Prepared from *anti*-norbornenol (P. R. Story, *J. Org. Chem.* **1961**, *26*, 287 – 290) after TBDMS protection (E. J. Corey, A. Venkateswarlu, *J. Am. Chem. Soc.* **1972**, *94*, 6190 – 6191) and ring-opening metathesis (P. Schwab, R. H. Grubbs, J. W. Ziller, *J. Am. Chem. Soc.* **1996**, *118*, 100 – 110).

[9] Analytical data for compound **4**: $R_f = 0.55$ (pentane). IR (neat): $\tilde{\nu} = 2953$ (s, C-H), 2856 (s, C-H), 1471 (s, H-C-H), 1256 (s, Si-C), 1125 (s, C-O), 1060 (s), 907 (s, Si-C), 863 (s, C-O-Si), 835 cm^{-1} (s, Si-C). ^1H NMR (360 MHz, $CDCl_3$): $\delta = 3.77$ (virt. t, $^3J \cong 1.7$ Hz, 1H, H-9), 2.52–2.45 (m, 2H, H-2/5), 2.00–1.93 (m, 4H, H-3/4), 1.88–1.83 (m, 2H, H-1/6), 1.83–1.78 (m, 4H, H-7/8), 0.86 (s, 9H, $C(CH_3)_3$), 0.04 ppm (s, 6H, $Si(CH_3)_2$). ^{13}C NMR (90.6 MHz, $CDCl_3$): $\delta = -4.9$ ($Si(CH_3)_2$), 18.0 ($C(CH_3)_3$), 19.7 (C-3/4), 21.1 (C-7/8), 25.9 ($C(CH_3)_3$), 35.6 (C-2/5), 44.7 (C-1/6), 81.5 ppm (C-9). Elemental analysis (%) calcd for $C_{15}H_{28}OSi$ (252.47): C 71.36, H 11.18, Si 11.12; found: C 71.31, H 11.30 Si, 11.13. HRMS (EI): $[C_{15}H_{28}OSi]^+$: calcd 252.1909, found 252.1906.

[10] a) T. Bach, C. Krüger, K. Harms, *Synthesis* **2000**, 305 – 320; b) T. Bach, A. Spiegel, *Eur. J. Org. Chem.* **2002**, 645 – 654; c) T. Bach, A. Spiegel, *Synlett* **2002**, 1305 – 1307.

[11] K. Langer, J. Mattay, A. Heidbreder, M. Möller, *Liebigs Ann. Chem.* **1992**, 257 – 260.

[12] a) C. Bolm, G. Schlingloff, K. Weickhardt, *Angew. Chem.* **1994**, *106*, 1944 – 1946; *Angew. Chem. Int. Ed. Engl.* **1994**, *33*, 1848 – 1849; b) C. Bolm, G. Schlingloff, F. Bienewald, *J. Mol. Catal. A* **1997**, *117*, 347 – 350.

[13] Analytical data for compound **6**: M.p. 107 °C. $[\alpha]_D^{20} = +66.4$ ($c = 1.05$, $CHCl_3$) IR (KBr): $\tilde{\nu} = 2959$ (m, C-H), 1752 (s, CO), 1006 cm^{-1} (m, C-O). ^1H NMR (360 MHz, $CDCl_3$): $\delta = 4.63$ (ddd, $^3J = 5.5$ Hz, $^3J = 4.2$ Hz, $^3J = 1.5$ Hz, 1H, H-6), 2.87–2.69 (m, 2H, H-2/5), 2.56 (ddd, $^3J = 4.6$ Hz, $^3J = 3.4$ Hz, $^3J = 2.4$ Hz, 1H, H-1), 2.40 (dddd, $^2J = 13.5$ Hz, $^3J = 11.1$ Hz, $^3J = 4.9$ Hz, $^3J = 2.4$ Hz, 1H, H-3), 2.28–2.09 (m, 4H, H-4, H-9/10), 2.00–1.74 ppm (m, 3H, H-3, H-9/10). ^{13}C NMR (90.6 MHz, $CDCl_3$): $\delta = 17.3$ (C-4), 17.9 (C-3), 19.1 (C-10), 21.3 (C-9), 32.2 (C-5), 34.5 (C-2), 38.5 (C-1), 78.9 (C-6), 176.6 ppm (C-8). Elemental analysis (%) calcd for $C_9H_{12}O_2$ (152.19): C 71.03, H 7.95; found: C 70.91, H 8.00. HRMS (EI, $C_9H_{12}O_2$): calcd 152.0837, found 152.0835.

[14] Reviews: a) N. M. Kamerbeek, D. B. Janssen, W. J. H. van Berkel, M. W. Fraaije, *Adv. Synth. Catal.* **2003**, *345*, 667 – 678; b) M. D. Mihovilovic, B. Müller, P. Stanetty, *Eur. J. Org. Chem.* **2002**, 3711 – 3730; c) J. D. Stewart, *Curr. Org. Chem.* **1998**, *2*, 195 – 216; d) S. M. Roberts, P. W. H. Wan, *J. Mol. Catal. B: Enzym.* **1998**, *4*, 111 – 136.

[15] M. D. Mihovilovic, F. Rudroff, B. Grötzl, P. Kapitan, R. Snajdrova, J. Rydz, R. Mach, *Angew. Chem.* **2005**, *117*, 3675 – 3679; *Angew. Chem. Int. Ed.* **2005**, *44*, 3609 – 3613.

[16] Possible optimization: a) M. Bocola, F. Schulz, F. Leca, A. Vogel, M. W. Fraaije, M. T. Reetz, *Adv. Synth. Catal.* **2005**, *347*, 979 – 986; b) M. T. Reetz, B. Brunner, T. Schneider, F. Schulz, C. M. Clouthier, M. M. Kayser, *Angew. Chem.* **2004**, *116*, 4167 – 4170; *Angew. Chem. Int. Ed.* **2004**, *43*, 4075 – 4078.

[17] For details of recombinant expression systems, see a) M. G. Bramucci, P. C. Brzostowicz, K. N. Kostichka, V. Nagarajan, P. E. Rouviere, S. M. Thomas, PCT Int. Appl., WO 2003020890, **2003**; *Chem. Abstr.* **2003**, *138*, 233997; b) P. C. Brzostowicz, K. L. Gibson, S. M. Thomas, M. S. Blasko, P. E. Rouviere, *J. Bacteriol.* **2000**, *182*, 4241 – 4248; c) H. Iwaki, Y. Hasegawa, P. C. K. Lau, S. Wang, M. M. Kayser, *Appl. Environ. Microbiol.* **2002**, *68*, 5681 – 5684.

[18] a) J. A. Dale, H. S. Mosher, *J. Am. Chem. Soc.* **1973**, *95*, 512 – 519; b) I. Ohtani, T. Kusumi, Y. Kashman, H. Kakisawa, *J. Am. Chem. Soc.* **1991**, *113*, 4092 – 4096.

[19] Examples: a) K. Sahasrabudhe, V. Gracias, K. Furness, B. T. Smith, C. E. Katz, D. S. Reddy, J. Aube, *J. Am. Chem. Soc.* **2003**, *125*, 7914 – 7922; b) G. Mehta, D. S. Reddy, *Synlett* **1997**, 612 – 614.

 © 2006 Wiley-VCH Verlag GmbH & Co. KGaA, Weinheim

Metal Hydrides

DOI: 10.1002/anie.200600906

Magnesium Bis(tetrahydridogallate(III)): Structure and Reaction with *tert*-Butyl Alcohol**

Michael Veith, Markus Burkhart, and Volker Huch*

For many years, adducts of the hydrogen compounds of Group 13 elements with other metal hydrides have received considerable attention, because they are considered as important fundamental compounds of these elements, and are also used as reducing agents and hydrogen-transfer agents in inorganic and organic chemistry. Apart from classical representatives such as $MM'H_4$ (M = Li, Na, K, Rb, Cs; M′ = B, Al, Ga, In), there are few examples of compounds of the heavier Group 13 elements, in particular, with electropositive elements other than the alkali metals that provide reliable structure information. $Mg(AlH_4)_2$ was prepared and described by Wiberg and Bauer more than 50 years ago,[1] but was first crystallographically characterized in molecular form as a tetrahydrofuran (THF) adduct by Nöth et al. in 1995.[2] To date, only two representatives have been described for gallium, namely the adduct $(BH_3{\cdot}GaH_3)_8$[3,4] and the amine complex [(pmdeta)ZnCl(GaH_4)] (pmdeta = pentamethyldiethylenetetramine).[5] Herein, we describe the synthesis and complete structure determination of a diethyl ether (OEt_2) adduct of $Mg(GaH_4)_2$, and through its reaction with *tert*-butyl alcohol, give a first glimpse of its reactivity.

$Mg(GaH_4)_2$ is synthesized by the reaction of freshly prepared $LiGaH_4$ [Eq. (1)] with $MgBr_2$ in OEt_2 as solvent, as

$$4\,LiH + GaCl_3 \xrightarrow[-78\,^\circ C]{OEt_2} LiGaH_4 + 3\,LiCl \quad (1)$$

formulated in Equation (2). For the corresponding tetrahydridoaluminates, it has been known for some time that the

$$MgBr_2 + 2\,LiGaH_4 \xrightarrow{OEt_2} Mg(GaH_4)_2 \cdot 4\,OEt_2\,(\mathbf{1}) + 2\,LiBr \quad (2)$$

counterion and donor solvent have a pivotal influence on product formation.[6] Analogously, in the case of the tetrahydridogallates, adept choice of anion and reaction conditions leads not only to $Mg(GaH_4)_2{\cdot}4\,OEt_2$ [**1**; Eq. (2)], but also to $MgBr(GaH_4){\cdot}4\,OEt_2$ [**2**; Eq. (3)]. If chloride, rather than

$$MgBr_2 + LiGaH_4 \xrightarrow{OEt_2} MgBr(GaH_4) \cdot 4\,OEt_2\,(\mathbf{2}) + LiBr \quad (3)$$

bromide, is selected as the counterion, inseparable product mixtures are formed. Direct hydrogenation of $GaCl_3$ with an excess of MgH_2 in THF and OEt_2 does not lead to isolable products either. However, if the bromide counterion is replaced by iodide, the doubly substituted product **1** crystallizes from the reaction solution, even when only one equivalent of $LiGaH_4$ is used.

The two new compounds **1** and **2** are extremely unstable and decompose within a few minutes at room temperature; therefore, only the metal and halogen contents of **1** and **2** could be determined. According to ^1H and ^{13}C NMR spectroscopy, the ratio of OEt_2 molecules to GaH_4 units is 2:1 in **1** and 4:1 in **2**. In the IR spectra of **1** and **2**, two broad vibrational bands attributed to terminal and bridging hydride species occur in the Ga–H stretching region (**1**: $\tilde{\nu}$(Ga-H) = 1863, 1693 cm^{-1}; **2**: $\tilde{\nu}$(Ga-H) = 1833, 1524 cm^{-1}), in agreement with the structural analysis (see below).

The molecular structure of **1**, determined by X-ray diffraction on a single crystal, is shown in Figure 1.[7,8] In the

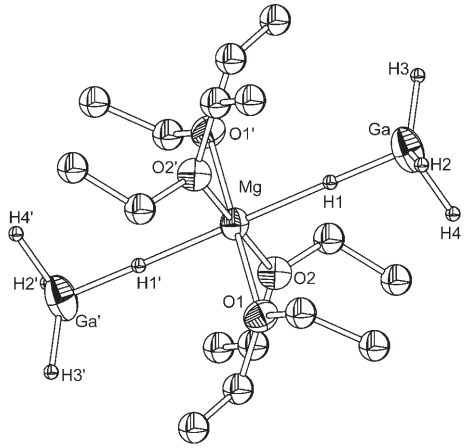


Figure 1. Molecular structure of **1**. Carbon-bound hydrogen atoms and minor disorder components of the ethyl groups are omitted for clarity. Thermal ellipsoids are set at 50% probability. Selected bond lengths [Å] and angles [°]: Mg–O1 2.102(2), Mg–O2 2.103(3), Ga–H1 1.6(1), Ga–H2 1.6(1), Ga–H3 1.5(2), Ga–H4 1.5(2), Mg–H1 1.9(3), Mg···Ga 3.558(1); Mg-H1-Ga 177.0(5), O1-Mg-O2 90.45(1), O1-Mg-O2′ 89.55(1).

case of **2**, only a mixed crystal of approximately 80% **1** and 20% **2** could be isolated. Nevertheless, the molecular structure of **2** was determined, as shown in Figure 2.[7] Molecule **1** is centrosymmetric, with the magnesium atom at the inversion center. The tetrahedral GaH_4 units are connected to the central magnesium atom, in a *trans* orientation, through nearly linear μ^2-hydrogen bridges. The four oxygen atoms of the OEt_2 molecules form a nearly square rhombus and complete the distorted octahedral coordination environment of the magnesium atom. The Mg–O distances are typical for bonds between oxygen donors and magnesium atoms of coordination number 6.[9] The Ga–H bonds in general are shorter for the terminal hydrogen atoms than for the bridging hydrogen atom (Figure 1). Compound **1** is the first structurally characterized alkaline-earth tetrahydridogallate and only the second molecular tetrahydridogallate, in

[*] Prof. Dr. M. Veith, M. Burkhart, Dr. V. Huch
Anorganische Chemie
Universität des Saarlandes
Postfach 15 11 50, 66041 Saarbrücken (Germany)
Fax: (+49) 681-302-3995
E-mail: veith@inm-gmbh.de
Prof. Dr. M. Veith
Leibniz-Institut für Neue Materialien
Im Stadtwald, Geb.10.2.2, 66123 Saarbrücken (Germany)

[**] This work was supported by the DFG within the framework of the SFB 277.

InterScience DISCOVER SOMETHING GREAT
© 2006 Wiley-VCH Verlag GmbH & Co. KGaA, Weinheim

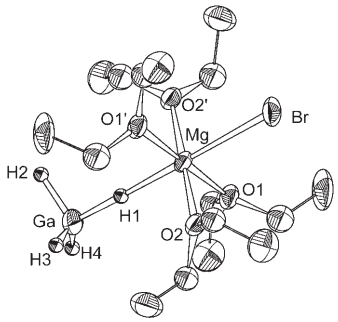


Figure 2. Molecular structure of **2**. Carbon-bound hydrogen atoms are omitted for clarity. Thermal ellipsoids are set at 50% probability. Selected bond lengths [Å] and angles [°]: Mg–O1 2.102(8), Mg–O2 2.109(9), Ga–H1 1.5(1), Ga–H2 1.4(2), Ga–H3 1.4(2), Ga–H4 1.4(2), Mg–H1 2.0(1), Mg–Br 2.87(2), Mg···Ga 3.539(4); Mg-H1-Ga 179.2(5), O1-Mg-O2 89.66(5), O1-Mg-O2′ 90.34(5).

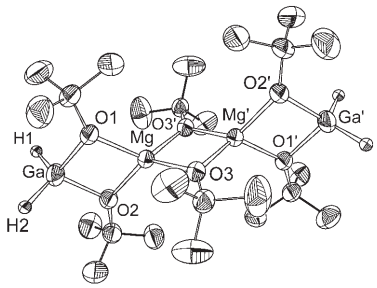


Figure 3. Molecular structure of **3**. Carbon-bound hydrogen atoms are omitted for clarity. Thermal ellipsoids are set at 50% probability. Selected bond lengths [Å] and angles [°]: Mg–O1 1.965(3), Mg–O2 1.987(3), Mg–O3 1.959(3), Mg–O3′ 1.964(3), Ga–O1 1.925(3), Ga–O2 1.909(3), Ga–H1 1.58(9), Ga–H2 1.56(8), Mg···Mg′ 2.922(2), Mg···Ga 2.947(2); Mg′-Mg-Ga 175.91(6), O1-Mg-O2 80.0(1), O3-Mg-O3′ 83.7(1), O1-Ga-O2 83.0(1), Mg-O1-Ga 98.5(1), Mg-O2-Ga 98.3(1), Mg-O3-Mg′ 96.3(1).

addition to $[(pmdeta)ZnCl(GaH_4)]$.[5] Both **1** and $[(pmdeta)ZnCl(GaH_4)]$ have very similar bond lengths, and the M-H-Ga (M = Mg, Zn) angle is almost linear in both cases (**1**: 177.0(5)°; $[(pmdeta)ZnCl(GaH_4)]$: 176.6(2)°). Compound **2** has a relatively long Ga–Br bond,[9] which must be interpreted with caution, however, because of the small fraction of **2** in the mixed crystal with **1**. The Mg···Ga distance in **2** is slightly smaller than in **1**, since the bromide ligand evidently withdraws electron density from the gallium atom. An aluminum compound analogous to **2** with THF ligands instead of the OEt_2 molecules has a similar structure.[2]

When **1** is treated with *tert*-butyl alcohol (*t*BuOH), hydrogen gas is formed, and the hydride ligands should be replaced by O*t*Bu groups, as formulated in Equation (4). However, none of the plausible substitution products "$Mg[GaH_{4-n}(OtBu)_n]_2$" were successfully isolated (regardless of the amount of *t*BuOH used); rather, $\{Mg(OtBu)[GaH_2(OtBu)_2]\}_2$ (**3**) and $[(tBuO)GaH_2]_2$ are obtained. The formation of these products could be explained by a Lewis acid–base dissociation of the hypothetical "$Mg[GaH_2(OtBu)_2]_2$" intermediate [Eq. (5)].

$$Mg(GaH_4)_2 \cdot 4\,OEt_2 + 2\,n\,tBuOH \rightarrow \text{“}Mg[GaH_{4-n}(OtBu)_n]_2\text{”} + 2\,n\,H_2 + 4\,OEt_2 \quad (4)$$

$$\text{“}Mg[GaH_2(OtBu)_2]_2\text{”} \rightarrow {}^1/_2\,[(tBuO)GaH_2]_2 + {}^1/_2\,\{Mg(OtBu)[GaH_2(OtBu)_2]\}_2\ (\mathbf{3}) \quad (5)$$

The known gallane $[(tBuO)GaH_2]_2$[10] can be separated from **3** by sublimation, and **3** can subsequently be recrystallized from toluene. The ^1H NMR spectrum of **3** in solution reveals the presence of two different types of *tert*-butyl groups. According to an X-ray structure analysis,[7,8] the centrosymmetric molecule **3** consists of one Mg_2O_2 and two $GaMgO_2$ four-membered rings; the O*t*Bu groups are bridging and the hydride ligands are terminal (Figure 3). The Ga···Mg···Mg···Ga axis is nearly linear (Ga-Mg-Mg 175.91(6)°). Owing to the absence of bridging hydride ligands, only one band is observed in the Ga-H stretching region of the IR spectrum of **3** ($\tilde{\nu}$(Ga-H) = 1842 cm^{-1}). This band is notably shifted in comparison to that of $[(tBuO)GaH_2]_2$ ($\tilde{\nu}$(Ga-H) = 1906 cm^{-1}),[10] reflecting the different partial charges in the $(\mu\text{-}OtBu)_2GaH_2$ units common to both compounds. The Ga–O bonds are shorter than the Mg–O bonds, in agreement with the smaller ionic radius of four-coordinate Ga^{3+}[11] and the greater steric demands on the magnesium atom. The fact that the hydride ligands in **3** exclusively occupy terminal positions underlines the distinctiveness of the hydride bridges in the starting compound **1**.

Experimental Section

Owing to the extraordinary sensitivity of the compounds towards hydrolysis, all reactions were carried out in a modified Stock vacuum apparatus under nitrogen as inert gas. The solvents were dried over sodium wire and used immediately after distillation. The NMR spectra were recorded on an AC-200-F NMR spectrometer (Bruker), and the IR spectra were recorded on an FTS 165 IR spectrometer (BioRad). LiH and $GaCl_3$ were purchased from Aldrich and used without further purification.

1: A precooled, freshly prepared solution of $LiGaH_4$[12] (0.81 g, 10.0 mmol) in OEt_2 (30 mL) was added dropwise to a solution of $MgBr_2{\cdot}4\,OEt_2$[13] (2.4 g, 5.00 mmol) in OEt_2 (30 mL) over 20 min at −78 °C, and a colorless suspension formed. The reaction was stirred for 30 min at −78 °C. Subsequently, the cooling was removed, and the solution was slowly brought to approximately 0 °C. As soon as the precipitate completely dissolved, the reaction solution was cooled to −30 °C and kept at this temperature for crystallization over 24 h. Yield: 0.98 g colorless crystals, 42%. Elemental analysis (%) calcd for $C_{16}H_{48}Ga_2MgO_4$ (468.31 g mol^{-1}): Ga 29.78, Mg 5.19; found: Ga 29.25, Mg 5.07. M.p.: 5 °C. IR (nujol): $\tilde{\nu}$(Ga-H) = 1863 (br, w), 1693 cm^{-1} (br, w). ^1H NMR (200.13 MHz, C_6D_6, 25 °C): δ = 1.05 (t, 24 H, $^3J(^1H,^1H)$ = 6.8 Hz, OCH_2CH_3), 3.32 (q, 16 H, $^3J(^1H,^1H)$ = 6.8 Hz, OCH_2CH_3), 3.47 ppm (br s, 8 H, Ga*H*). $^{13}C\{^1H\}$ NMR (50.3 MHz, C_6D_6, 25 °C): δ = 65.9, 15.0 ppm.

2: The synthesis was carried out analogously to that of **1**, with $LiGaH_4$ (0.40 g, 5.00 mmol) in OEt_2 (30 mL). Yield: 0.55 g, 23%. Elemental analysis (%) calcd for $C_{16}H_{44}BrGaMgO_4$ (474.46 g mol^{-1}): Br 18.84, Ga 14.70, Mg 5.12; found: Br 17.52, Ga 14.15, Mg 4.93. M.p.: 8 °C. IR (solid): $\tilde{\nu}$(Ga-H) = 1833 (br, w), 1524 cm^{-1} (br, w).

3: A solution of **1** (2.34 g, 5.0 mmol) in OEt_2 (30 mL) was treated dropwise with *tert*-butyl alcohol (1.82 mL, 1.41 g, 19.0 mmol) in OEt_2 (5 mL) over 30 min at −78 °C. Vigorous gas generation ensued. The temperature was slowly raised to room temperature with stirring, and the stirring was subsequently continued for 6 h. After removal of the

 © 2006 Wiley-VCH Verlag GmbH & Co. KGaA, Weinheim

solvent under reduced pressure, fractional sublimation was carried out. First, $[(t\mathrm{BuO})GaH_2]_2$ sublimed at 35 °C, followed by **3** at 130 °C, at 10^{-5} mbar. Yield: 0.423 g, 27 %. By dissolving the product in toluene and cooling to −20 °C, crystals of composition **3**·toluene formed. Elemental analysis (%) calcd for $C_{24}H_{58}Ga_2Mg_2O_6$ (630.78 g mol^{-1}): C 51.51, H 9.20; found: C 49.71, H 8.57. ^{1}H NMR (200.13 MHz, C_6D_6, 25 °C): $\delta = 1.35$ (s, 36 H, $O(CH_3)_3$), 1.39 (s, 18 H, $O(CH_3)_3$), 5.5 ppm (br s, 4 H, Ga*H*). IR (nujol): $\tilde{\nu}$(Ga-H) = 1842 cm^{-1} (br, m).

Received: March 8, 2006
Published online: July 21, 2006

Keywords: gallium · hydrides · magnesium · structure elucidation

[1] E. Wiberg, R. Bauer, *Z. Naturforsch. B* **1950**, *5*, 397 – 398.
[2] H. Nöth, M. Schmidt, A. Treitl, *Chem. Ber.* **1995**, *128*, 999 – 1006.
[3] A. J. Downs, S. Parsons, C. R. Pulham, P. F. Souter, *Angew. Chem.* **1997**, *109*, 910 – 911; *Angew. Chem. Int. Ed. Engl.* **1997**, *36*, 890 – 891.
[4] A. J. Downs, T. M. Greene, E. Johnsen, P. T. Brain, C. A. Morrison, S. Parsons, C. R. Pulham, D. W. H. Rankin, K. Aarset, I. M. Mills, E. M. Page, D. A. Rice, *Inorg. Chem.* **2001**, *40*, 3484 – 3497.
[5] G. A. Koutsantonis, F. C. Lee, C. L. Raston, *J. Chem. Soc. Chem. Commun.* **1994**, 1975 – 1976.
[6] E. C. Ashby, R. D. Schwarz, B. D. James, *Inorg. Chem.* **1970**, *9*, 325 – 332.
[7] All X-ray structural analyses were carried out on a Stoe IPDS diffractometer (Darmstadt), with $Mo_{K\alpha}$ radiation ($\lambda = 0.71073$ Å) at 200(2) K. **1**: colorless rectangular crystals, $0.5 \times 0.4 \times 0.4$ mm^3, $C_{16}H_{48}Ga_2MgO_4$, orthorhombic, space group *Pbca*, $a = 13.523(3)$, $b = 12.419(2)$, $c = 16.395(3)$ Å, $V = 2753.4(9)$ Å^3, $Z = 4$, $\rho_{calcd} = 1.130$ g cm^{-3}, $2\theta_{max} = 48.20°$, 16180 reflections, 2128 independent, solution by direct methods, refinement (against F_o^2) with SHELXL-97,[8] all non-hydrogen atoms refined anisotropically, data/parameters: 2128/118, $R_1 = 0.0517$ ($I > 2\sigma$), $wR_2 = 0.1308$, GooF = 1.063, residual electron density: 0.515/−0.672 e Å^{-3}. The ethyl groups are disordered, such that there are two positions for each of the methylene groups. **2**/4 × **1**: colorless rectangular crystals, $0.3 \times 0.2 \times 0.2$ mm^3, $C_{16}H_{47.2}Br_{0.2}Ga_{1.8}MgO_4$, orthorhombic, space group *Pbca*, $a = 13.515(3)$, $b = 12.418(2)$, $c = 16.303(3)$ Å, $V = 2736.1(9)$ Å^3, $Z = 4$, $\rho_{calcd} = 1.140$ g cm^{-3}, $2\theta_{max} = 48.0°$, 15920 reflections, 2071 independent, solution by direct methods, refinement (against F_o^2) with SHELXL-97,[8] all non-hydrogen atoms refined anisotropically, data/parameters: 2071/133, $R_1 = 0.0632$ ($I > 2\sigma$), $wR_2 = 0.1583$, GooF = 1.11, residual electron density: 0.451/−1.007 e Å^{-3}. Starting with the atomic positions of **1**, a difference Fourier analysis revealed additional electron density between the gallium and magnesium atoms, which was assigned to a bromine atom. Thus, the crystal is a mixed crystal of **1** and **2**, in which **1** is inversion-symmetrically substituted by approximately 20 % **2** (that is, $H_3Ga{-}H{-}Mg{-}Br/Br{-}Mg{-}H{-}GaH_3$). **3**·toluene: colorless crystals, $0.8 \times 0.5 \times 0.4$ mm^3, $C_{31}H_{66}Ga_2Mg_2O_6$, monoclinic, space group $P2_1/n$, $a = 9.297(2)$, $b = 14.004(3)$, $c = 16.324(3)$ Å, $\beta = 103.49(3)°$, $V = 2066.7(7)$ Å^3, $Z = 2$, $\rho_{calcd} = 1.240$ g cm^{-3}, $2\theta_{max} = 48.28°$, 12617 reflections, 3209 independent, solution by direct methods, refinement (against F_o^2) with SHELXL-97,[8] all non-hydrogen atoms refined anisotropically, data/parameters: 3209/276, $R_1 = 0.057$ ($I > 2\sigma$), $wR_2 = 0.158$, residual electron density: 0.921/−0.481 e Å^{-3}. CCDC 601597 (**1**), CCDC 601598 (**2**/4 × **1**), and CCDC 601599 (**3**·toluene) contain the supplementary crystallographic data for this paper. These data can be obtained free of charge from The Cambridge Crystallographic Data Centre via www.ccdc.cam.ac.uk/data_request/cif.
[8] G. M. Sheldrick, SHELXL-97, Program for refinement of crystal structures, Universität Göttingen, **1997**.
[9] N. Metzler, H. Nöth, M. Schmidt, A. Treitl, *Z. Naturforsch. B* **1994**, *49*, 1448 – 1451.
[10] a) H. Nöth, H. Suchy, *Z. Anorg. Allg. Chem.* **1968**, *358*, 44 – 66; b) M. Veith, S. Faber, H. Wolfanger, *Chem. Ber.* **1996**, *129*, 381 – 384.
[11] W. A. Holleman, E. Wiberg, *Lehrbuch der anorganischen Chemie*, 101st ed., W. de Gruyter, Berlin, **1995**, pp. 127.
[12] a) A. E. Shirk, D. F. Shriver, *Inorg. Synth.* **1977**, *17*, 45 – 47; b) A. E. Finholt, A. C. Bond, H. I. Schlesinger, *J. Am. Chem. Soc.* **1947**, *69*, 1199 – 1203.
[13] W. M. Schubert, B. S. Rabinovitch, N. R. Larson, V. A. Sims, *J. Am. Chem. Soc.* **1952**, *74*, 4590 – 4592.

 © 2006 Wiley-VCH Verlag GmbH & Co. KGaA, Weinheim

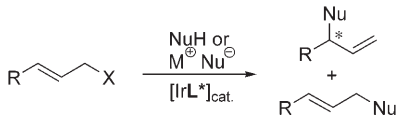
Allylic Amination

DOI: 10.1002/anie.200601472

Salt-Free Iridium-Catalyzed Asymmetric Allylic Aminations with *N,N*-Diacylamines and *ortho*-Nosylamide as Ammonia Equivalents**

*Robert Weihofen, Olena Tverskoy, and Günter Helmchen**

Asymmetric allylic substitutions have been studied with great success over the last few years.[1] With monosubstituted allylic derivatives as substrates (Scheme 1), iridium complexes of



Scheme 1. Iridium-catalyzed allylic substitutions.

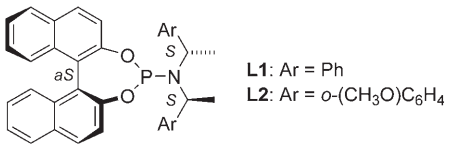
electron-poor ligands seem to be the catalysts of choice for asymmetric allylic alkylations,[2] aminations,[3] and etherifications.[4] Using ligands **L1** and **L2**,[5] regioselectivities of $>95{:}5$ in favor of the branched products and enantioselectivities of up to 99% *ee* have been obtained.

The method appears particularly suited for the synthesis of N-heterocycles. Examples are 2-vinyl-azacycloalkanes,

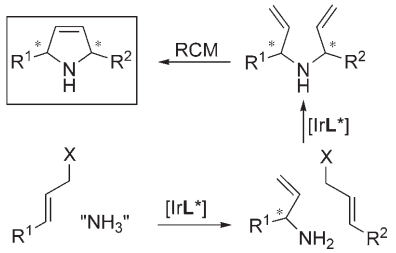
[*] R. Weihofen, O. Tverskoy, Prof. Dr. G. Helmchen
Organisch-Chemisches Institut der Universität Heidelberg
Im Neuenheimer Feld 270, 69120 Heidelberg (Germany)
Fax: (+49) 6221-544-205
E-mail: g.helmchen@oci.uni-heidelberg.de

[**] This work was supported by the Deutsche Forschungsgemeinschaft (SFB 623) and the Fonds der Chemischen Industrie. We thank Prof. K. Ditrich (BASF AG) for enantiomerically pure 1-arylethylamines and Q. Stang for helpful information.

WILEY InterScience DISCOVER SOMETHING GREAT
© 2006 Wiley-VCH Verlag GmbH & Co. KGaA, Weinheim



obtained by intramolecular amination,[3a] and *trans*-2,5-divinylpyrrolidine, prepared by sequential inter- and intramolecular amination.[6] We have now addressed the enantio- and diastereoselective construction of 2,5-disubstituted 3,4-dehydropyrrolidines (Scheme 2), compounds of considerable

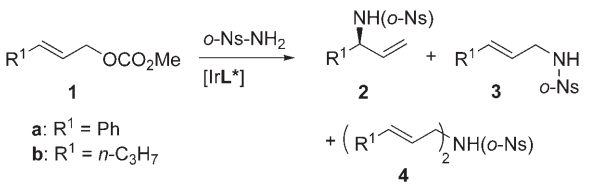


Scheme 2. Synthesis of the four stereoisomeric 2,5-disubstituted 3,4-dehydropyrrolidines by allylic substitution in combination with ring-closing metathesis (RCM).

importance for medicinal chemistry and alkaloid synthesis. We have shown that intramolecular allylic aminations are catalyst rather than substrate controlled.[6] This result means that the configurations of both chirality centers can be controlled at will by the choice of the chirality sense of the chiral ligand (**L***). As 3,4-dehydropyrrolidines are extremely sensitive, our aim was the synthesis of N-unprotected allylamines,[7] that is, we have developed iridium-catalyzed allylic substitutions with ammonia equivalents as nucleophiles.

To date mainly benzylamines have been used as N-nucleophiles. Because of problematic deprotection of the products with methods other than catalytic hydrogenation, we have probed anionic N-nucleophiles, in particular sulfonamides.[8,2b] Deprotection of their reaction products was also not generally successful. Therefore, we have extended this work and present the successful substitutions with *o*-nosylamide (*o*-Ns-NH_2), phthalimide, di-*tert*-butyl imidodicarbonate, *tert*-butyl formylcarbamate, and related compounds. The products were readily transformed into primary amines which allowed us to turn Scheme 2 into reality for the first time.[9]

We have already found that the reaction between *N*-(*o*-Ns)-$NHCH_2Ph$ and carbonate **1a** (ligand: **L2**) was fast, however, gave exclusively the linear product **3** (Scheme 3).[8] Subsequently, careful monitoring revealed that the branched



Scheme 3. Iridium-catalyzed allylic substitutions with *o*-nosylamide.

product **2a** was initially formed, but rearranged to the more stable **3**. It was also discovered that the parent compound *o*-Ns-NH_2 reacted with kinetic control to give the branched, chiral product with excellent selectivity (Table 1). The

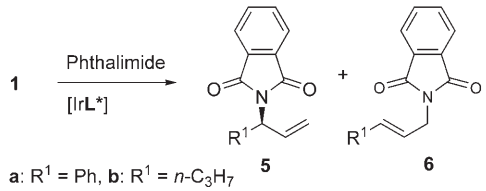
Table 1: Iridium-catalyzed allylic substitution with *o*-nosylamide according to Scheme 3.[a]

Entry	Substrate	Ligand	Additive[b]	*t* [h][c]	Yield [%][d]	**2**:**3**:**4**[e]	*ee* [%][f]
1	**1a**	**L1**	–	24	60	93:7:1	94
2	**1a**	**L2**	–	12	64	95:5:1	95
3	**1a**	**L2**	NEt_3	3	92	90:10:1	96
4	**1b**	**L1**	NEt_3	18	85	92:4:4	93
5	**1b**	**L2**	–	4	84	84:8:8	90
6	**1b**	**L2**	NEt_3	2.5	94	93:3:4	94

[a] Reactions were carried out as described in the Experimental Section. [b] 1 equiv. [c] Reaction time. [d] Combined yield of isolated **2**, **3**, and **4**. [e] Determined by ^{1}H NMR spectroscopy and/or isolation. [f] Determined by HPLC on a chiral column (Daicel Chiralcel AD-H, 250×4.6 mm, 5 μm with guard cartridge AD-H 10×4 mm, 5 μm, *n*-hexane/*i*PrOH 9:1, flow = 0.5 mL min^{-1}, room temperature): t_R[(−)-**2a**] = 52.2 min, t_R[(+)-**2a**] = 54.9 min (major), t_R[(+)-**2b**] = 28.8 min (major), t_R[(−)-**2b**] = 31.7 min.

reaction proceeds directly with *o*-Ns-NH_2 ("salt-free" conditions) because the liberated methyl carbonate or methoxide is acting as base (Table 1, entries 1, 2, and 5). The addition of NEt_3 led to improved reaction rate, yield, and enantiomeric excess (Table 1, entries 3 and 6), regioselectivity was lowered with **1a** (entry 3) or increased with **1b** (Table 1, entry 6).[10]

Experiments with carboxamides as prenucleophiles were not successful to date. However, excellent results were obtained with *N*,*N*-diacylamines. Thus, the iridium-catalyzed allylic substitution with phthalimide (Scheme 4, Table 2) gave



Scheme 4. Substitutions with phthalimide.

regioselectivity ≥ 90:10 in favor of the branched products and ≥ 96% ee with **1a** and **1b** as substrates. Additional base for deprotonation of the prenucleophile was not required. With potassium phthalimide no reaction was possible, presumably because of its very low solubility in THF (Table 2, entry 2). Results very similar to those with phthalimide were obtained with succinimide as prenucleophile.[11]

The prenucleophile $HN(Boc)_2$ ((Boc = 1,1-dimethylethoxycarbonyl) is electronically similar to phthalimide; however, it is sterically more demanding and more soluble than phthalimide. It has been successfully used in palladium-catalyzed allylic substitutions.[12] In contrast to phthalimide, it reacted very slowly under salt-free conditions. With substrate **1a** a best yield of 51% was reached, however, regioselectivity

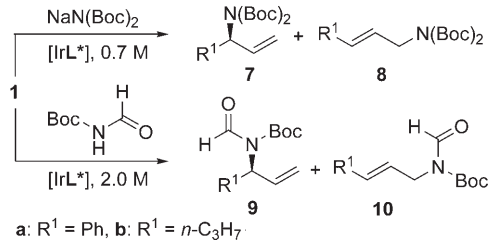
 © 2006 Wiley-VCH Verlag GmbH & Co. KGaA, Weinheim

Table 2: Iridium-catalyzed allylic substitutions according to Schemes 4 and 5.[a]

Entry	Substrate	Ligand	NuH or NuM	*t*[h][b]	Products	Yield [%][c]	b:l[d]	*ee* [%][e]
1	**1a**	**L1**	Phth	18	**5a**+**6a**	66	93:7	96
2	**1a**	**L1**	KPhth	–	–	–	–	–
3	**1a**	**L2**	Phth	2.5	**5a**+**6a**	95	96:4	98
4[f]	**1b**	**L1**	Phth	18	**5b**+**6b**	86	90:10	95
5	**1b**	**L2**	Phth	2.5	**5b**+**6b**	82	94:6	96
6[f,g]	**1a**	**L1**	$NaN(Boc)_2$	18	**7a**+**8a**	80	97:3	97.5
7	**1a**	**L2**	$NaN(Boc)_2$	0.7	**7a**+**8a**	80	97:3	99
8	**1b**	**L1**	$NaN(Boc)_2$	18	**7b**+**8b**	86	92:8	96(−)
9	**1b**	**L2**	$NaN(Boc)_2$	0.7	**7b**+**8b**	86	96:4	99
10	**1a**	**L1**	HN(Boc)(CHO)	18	**9a**+**10a**	86	97:3	97.5
11	**1a**	**L2**	HN(Boc)(CHO)	0.7	**9a**+**10a**	96	98:2	98.5
12[f]	**1b**	**L1**	HN(Boc)(CHO)	24	**9b**+**10b**	98	92:8	97(+)
13	**1b**	**L2**	HN(Boc)(CHO)	1	**9b**+**10b**	98	97:3	96

[a] See Experimental Section; $NaN(Boc)_2$ was used as suspension in THF (1.0 mL). [b] Reaction time. [c] Yield of the combined isolated products. [d] Branched (b) and linear (l) substitution products; determined by ^{1}H NMR spectroscopy. [e] Determined by HPLC on a chiral column (Daicel columns, 250×4.6 mm, 5 μm with guard cartridge, 10×4 mm, 5 μm, flow = 0.5 mL min^{-1}, room temperature); **5a** (Chiralcel OD-H, *n*-hexane/*i*PrOH 95:5): t_R[(+)-**5a**] = 18.4 min, t_R[(−)-**5a**] = 22.0 min (major); **5b** (Chiralcel OJ-H, *n*-hexane/*i*PrOH 98.5:1.5): t_R[(+)-**5b**] = 18.0 min, t_R[(−)-**5b**] = 19.1 min (major); **7a** (Chiralcel OJ-H, *n*-hexane/*i*PrOH 99.5:0.5): t_R[(+)-**7a**] = 11.3 min, t_R[(−)-**7a**] = 13.0 min (major). The *ee* values of products **7b** and **9b** were determined after transformation into **12** (see Scheme 6); **12** (Chiralcel OD-H, *n*-hexane/*i*PrOH 99:1): t_R[(−)-**12**] = 11.0 min (major), t_R[(+)-**12**] = 12.7 min; **9a** (Chiralcel OJ-H, *n*-hexane/*i*PrOH 95:5): t_R[(−)-**9a**] = 14.3 min (major), t_R[(+)-**9a**] = 28.2 min. [f] 5 mmol scale. [g] 1.1 Equivalents of nucleophile were used.

was very high (branch:linear (b:l) = 99:1). Finally, complete conversion (yield 80%) and excellent selectivity were obtained with the sodium salt $NaN(Boc)_2$ (Scheme 5 and Table 2, entries 6–9).[13] Selectivities as well as rates were again slightly higher with ligand **L2** than ligand **L1**.

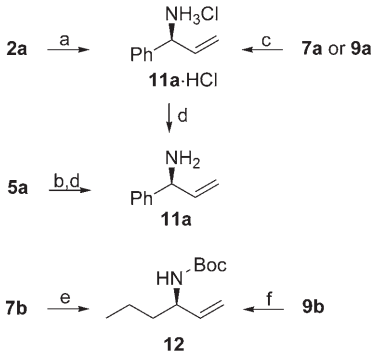


Scheme 5. Substitutions with Boc- and formyl-protected *tert*-butyl carbamate.

To make N-Boc derivatives available by substitution under salt-free conditions, we probed the new prenucleophile HN(Boc)(CHO), which was expected to be more acidic than $HNBoc_2$. This readily available compound[14] indeed gave excellent results with respect to yield as well as regio-and enantioselectivity (Table 2, entries 10–13).

N-Nosyl-amides can be deprotected under mild and specific conditions with thiols.[15] This situation is also true for **2a** (Scheme 6), except that purification of the amine **11a** by flash chromatography was difficult, but its hydrochloride **11a**·HCl could be conveniently isolated by chromatography on silica gel. Deprotection of the phthalimide derivative **5a**, to give the primary amine **11a**, with 1,2-diaminoethane in refluxing ethanol proceeded with excellent yield (Scheme 6).[16] The Boc-protected amines **7a** and **9a** were hydrolyzed to give hydrochloride **11a**·HCl, which was converted into the volatile free amine **11a** (Scheme 6).[17]

With primary allylamines available, the preparation of unsymmetrically substituted 2,5-disubstituted 3,4-dehydropyrroles could be addressed (Scheme 7). The reaction of the amine (*S*)-**11a** with carbonate **1b** was first carried out using ligand **L2**. The substitution product (*S*,*R*)-**13** was obtained in 80% yield. Analysis of crude product by GC-MS indicated as side products approximately 3% of the diastereomer (*S*,*S*)-**13** and only about 1% of the linear substitution product. The corresponding reaction using ligand *ent*-**L2** proceeded with essentially identical selectivity to give the diastereomer (*S*,*S*)-**13**. This result demonstrates that the steric course of the allylic amination is controlled by the catalyst rather than the substrate.

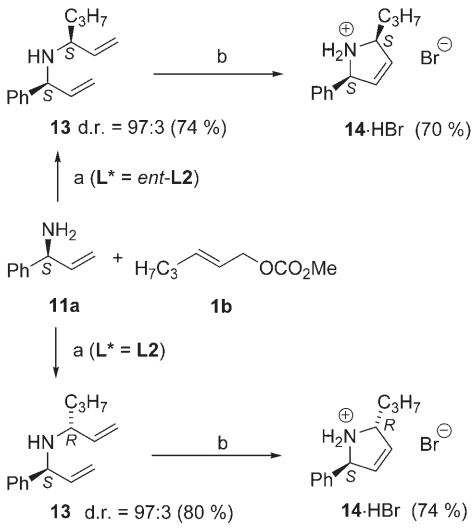


Scheme 6. Deprotection of substitution products. a) 1. PhSH, K_2CO_3, DMF, 60°C, 5 h; 2. 6 N HCl, column chromatography, 94%; b) 1. $H_2N(CH_2)_2NH_2$, EtOH, reflux; 2. 6 N HCl, column chromatography, 94%; c) 5% HCl in MeOH, 60°C, 89%; d) 6 N KOH (10 equiv), Et_2O or Dowex MWA-1, CH_2Cl_2/MeOH 9:1, quant.; e) TFA (1.5 equiv), CH_2Cl_2, 96%; f) cat. KOH, MeOH, 97%.

Ring-closing metathesis (RCM)[18] required protection of the nitrogen by salt formation. With the hydrobromide (*S*,*S*)-**13**·HBr the reaction proceeded at 80°C within 4 h to give *cis*-**14**·HBr without any by-products. The reaction of the corresponding hydrochloride (**13**·HCl) was accompanied by partial decomposition.

In conclusion, we have developed new variants of the iridium-catalyzed allylic substitution, allowing the preparation of conveniently N-protected or non-protected chiral allylic amines, which were used as nucleophiles in highly

 © 2006 Wiley-VCH Verlag GmbH & Co. KGaA, Weinheim



Scheme 7. Enantioselective synthesis of 2,5-disubstituted 3,4-dehydropyrroles. a) [{Ir(cod)Cl}$_2$] (2 mol%), **L*** (4 mol%), TBD (8 mol%), THF, room temperature, 12 h; b) 1. HBr/CH_3CO_2H; 2. Grubbs II catalyst (6 mol%), 1,2-dichloroethane (0.03 M), reflux, 4 h; cod = cyclooctadiene, TBD = 1,5,7-triazabicyclo[4.4.0]-unedec-5-one.

diastereoselective, catalyst-controlled allylic aminations. The products were subjected to ring-closing metathesis to give non-protected 2,5-disubstituted 3,4-dehydropyrrolidines.

Experimental Section

General procedures: Success with the following procedures requires dry THF (< 35 μg of H_2O/mL, Karl Fischer titration).

Under argon, TBD (0.08 mmol) was added to a solution of [{Ir(cod)Cl}$_2$](0.02 mmol) and **L*** (0.04 mmol) in dry THF (0.5 mL). After stirring for 2 h at room temperature the allylic carbonate **1** (1.0 mmol) was added, and the mixture was stirred for 5 min at room temperature. Then the prenucleophile (1.2 mmol) and, when required, NEt_3 (1 mmol) were added and the mixture was stirred until thin-layer chromatography (TLC) indicated complete conversion. The reaction mixture was concentrated in vacuo and the residue subjected to flash chromatography. The content of branched and linear product was determined by ^{1}H NMR spectroscopy and/or isolation of both products by flash chromatography on silica.

Received: April 13, 2006
Published online: July 20, 2006

Keywords: allylic amination · enantioselectivity · iridium · pyrrolidines · ring-closing metathesis

[1] a) B. M. Trost, C. Lee in *Catalytic Asymmetric Synthesis*, 2nd ed. (Ed.: I. Ojima), Wiley, New York, **2000**, p. 593; b) A. Pfaltz, M. Lautens in *Comprehensive Asymmetric Catalysis I–III* (Eds.: E. N. Jacobsen, A. Pfaltz, H. Yamamoto), Springer, Berlin, **1999**, p. 833; c) B. M. Trost, M. L. Crawley, *Chem. Rev.* **2003**, *103*, 2921.

[2] a) B. Bartels, G. Helmchen, *Chem. Commun.* **1999**, 741; b) B. Bartels, C. Garcia-Yebra, F. Rominger, G. Helmchen, *Eur. J. Inorg. Chem.* **2002**, 2569; c) G. Lipowsky, N. Miller, G. Helmchen, *Angew. Chem.* **2004**, *116*, 4695; *Angew. Chem. Int. Ed.* **2004**, *43*, 4595; d) G. Lipowsky, G. Helmchen, *Chem. Commun.* **2004**, 116; e) D. Polet, A. Alexakis, *Org. Lett.* **2004**, *6*, 3529; f) K. Tissot-Croset, D. Polet, A. Alexakis, *Angew. Chem.* **2004**, *116*, 2480; *Angew. Chem. Int. Ed.* **2004**, *43*, 2426.

[3] a) C. Welter, O. Koch, G. Lipowsky, G. Helmchen, *Chem. Commun.* **2004**, 896; b) A. Leitner, C. Shu, J. F. Hartwig, *Proc. Natl. Acad. Sci. USA* **2004**, *101*, 5830; c) C. Shu, A. Leitner, J. F. Hartwig, *Angew. Chem.* **2004**, *116*, 4901; *Angew. Chem. Int. Ed.* **2004**, *43*, 4797; d) A. Leitner, C. Shu, J. F. Hartwig, *Org. Lett.* **2005**, *7*, 1093; e) D. Polet, A. Alexakis, *Org. Lett.* **2005**, *7*, 1621; f) C. Welter, R. Moreno, S. Streif, G. Helmchen, *Org. Biomol. Chem.* **2005**, *3*, 3266.

[4] a) F. Lopez, T. Ohmura, J. F. Hartwig, *J. Am. Chem. Soc.* **2003**, *125*, 3426; b) C. Shu, J. F. Hartwig, *Angew. Chem.* **2004**, *116*, 4898; *Angew. Chem. Int. Ed.* **2004**, *43*, 4794.

[5] a) **L1**: B. L. Feringa, *Acc. Chem. Res.* **2000**, *33*, 346; b) **L2**: K. Tissot-Croset, D. Polet, S. Gille, C. Hawner, A. Alexakis, *Synthesis* **2004**, 2586.

[6] C. Welter, A. Dahnz, B. Brunner, S. Streiff, P. Dübon, G. Helmchen, *Org. Lett.* **2005**, *7*, 1239.

[7] For further asymmetric syntheses of amines with a stereogenic center in α-position to N see: a) J. A. Ellman, T. D. Owens, T. P. Tang, *Acc. Chem. Res.* **2002**, *35*, 984; b) D. Enders, U. Reinhold, *Tetrahedron: Asymmetry* **1997**, *8*, 1895; c) M. Johannsen, K. A. Jørgensen, *Chem. Rev.* **1998**, *98*, 1689.

[8] R. Weihofen, Axel Dahnz, O. Tverskoy, G. Helmchen, *Chem. Commun.* **2005**, 3541.

[9] P. A. Evans et al. have prepared corresponding *N*-tosyl derivatives by stereoconservative Rh-catalyzed allylic substitution at enantioenriched derivatives of allylic alcohols, which does not constitute an asymmetric synthesis. Surveys: a) D. K. Leahy, P. A. Evans in *Modern Rhodium-Catalyzed Organic Reactions* (Ed.: P. A. Evans), Wiley, New York, **2005**, p. 191; b) P. A. Evans, J. E. Robinson, *Org. Lett.* **1999**, *1*, 1929.

[10] The absolute configurations of the products described herein were as anticipated (Ref. [8]); for independent determinations see a) M. Atobe, N. Yamazaki, C. Kibayashi, *J. Org. Chem.* **2004**, *69*, 5595; b) M. Alcón, M. Canas, M. Poch, A. Moyano, M. A. Pericàs, A. Riera, *Tetrahedron Lett.* **1994**, *35*, 1589.

[11] For substrate **1a** (in combination with **L2**) a reaction time of 2.5 h was required to give the substitution product in 87% yield with 98% *ee* and a regioselectivity of 96:4.

[12] a) R. D. Connell, T. Rein, B. Åkermark, P. Helquist, *J. Org. Chem.* **1988**, *53*, 3845; b) D. A. Evans, K. R. Campos, J. S. Tedrow, F. E. Michael, M. R. Gagné, *J. Am. Chem. Soc.* **2000**, *122*, 7905.

[13] Similar results were obtained with $NaN(CHO)_2$, which has previously been used in Pd-catalyzed allylic substitutions (Y. Wang, K. Ding, *J. Org. Chem.* **2001**, *66*, 3238).

[14] To our knowledge, this compound has not been previously described. We prepared it according to a general procedure (Y. Lin, S. A. Lang, Jr, *Synthesis* **1980**, 119) in 88% yield.

[15] a) T. Fukuyama, C.-K. Jow, M. Cheung, *Tetrahedron Lett.* **1995**, *36*, 6373; b) T. Fukuyama, M. Cheung, C.-K. Jow, Y. Hidai, T. Kan, *Tetrahedron Lett.* **1997**, *38*, 5831.

[16] O. Kanie, S. C. Crawley, M. M. Palcic, O. Hindsgaul, *Carbohydr. Res.* **1993**, *243*, 139.

[17] The *ee* values of the free amines were determined and found to agree, within the range of precision, with those of the protected precursors.

[18] *Handbook of Metathesis* (Ed.: R. H. Grubbs), Wiley, New York, **2003**.

 © 2006 Wiley-VCH Verlag GmbH & Co. KGaA, Weinheim

Micro RNAs

DOI: 10.1002/anie.200601332

A Homogenous Assay for Micro RNA Maturation**

*Brian P. Davies and Christoph Arenz**

Recent insights into the mechanisms of gene regulation on the transcriptional and post-transcriptional levels may very well expand the arsenal of present therapeutic strategies. Current biomedical research concerns itself, in particular, with gene regulation by hormones, cellular signal cascades, and transcription factors. By manipulating protein-mediated pathways, such as with enzyme inhibitors or receptor agonists or antagonists, it is often possible to reduce or suppress pathological processes.[1] There are many reasons why an intervention at the RNA level, however, could also be advantageous. Of particular interest in this respect are the so-called micro RNAs (miRNAs) whose role in the cellular regulation of gene expression has been underestimated for a long time. MiRNAs are short, double-stranded, regulatory RNA molecules of approximately 21 base pairs in length and of endogenous origin. They are cleaved from their inactive hairpin precursor molecules, the pre-miRNAs, by the enzyme Dicer (Figure 1).[2] Dicer is a nuclease that is specific for double-stranded RNA. The mature miRNAs, in the form of RNA–protein complexes, can block the messenger RNA and thus inhibit protein translation. Many aspects of miRNA-mediated gene regulation remain unclear, in particular the identity and number of mRNAs regulated by the respective miRNAs. The amount of evidence is ever increasing, however, that various diseases, especially many types of cancer, are associated with specifically modified cellular miRNA expression patterns.[3] It therefore makes sense to consider miRNAs as target molecules for new therapeutic approaches.[4]

We are therefore interested in the possibility of manipulation of gene regulation by inhibiting the Dicer-mediated maturation of miRNAs. This could be accomplished, for example, by blocking the respective inactive pre-miRNAs with specific ligands. Although RNAs contain appropriate target structures for the binding of small molecules,[5] a rational design of selective RNA ligands is extremely difficult.[6] Herein we present for the first time a homogenous, fluorescence-based Dicer assay that allows easy screening of libraries of potential pre-miRNA ligands and therefore potential inhibitors of miRNA maturation.

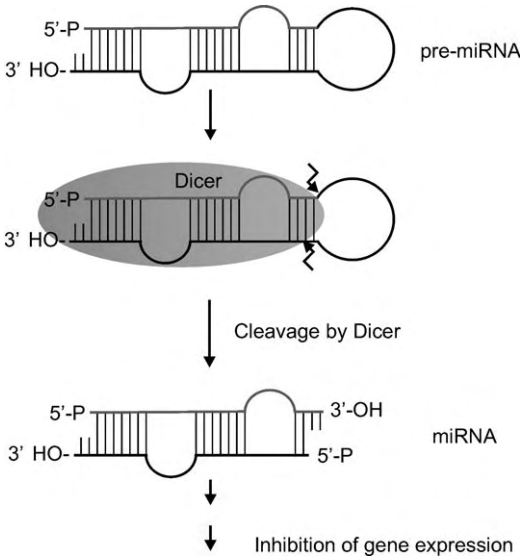


Figure 1. Formation of miRNAs from the inactive pre-miRNAs by the ribonuclease Dicer.

Drawing on previously known DNA- and RNA-based fluorescence assays, we first planned the synthesis of a doubly-labeled pre-miRNA beacon containing a 5′-fluorescence emitter (F) and a 3′-fluorescence quencher (Q)[7] Intramolecular base pairing would bring these groups into close proximity to one another, leading to quenching of the fluorescence most likely through collisional quenching. The Dicer-mediated hydrolysis of the pre-miRNA would result in a dissociation of the fluorescence emitter and quencher, and thus a Dicer-dependent increase in the fluorescence. In analogy to common assay designs for protease inhibitors,[8] the presence of a dicer inhibitor or ligand of the pre-miRNA would instead show a lack of fluorescence increase (Figure 2).

In selecting an appropriate target structure for establishing a homogenous miRNA assay, we decided upon a doubly labeled pre-let-7 RNA from *Drosophila melanogaster*.[9] The respective let-7 miRNA is considered one of the most studied miRNAs and was the first miRNA shown to be cleaved from a longer RNA strand by Dicer.[9] The beacon was formed by ligating two halves of the labeled pre-let-7 RNA partial strands by using T4 RNA ligase. The 5′-terminal half containing a 5′-fluorescein was ligated together with the respective 3′-dabcyl labeled half, which also contained a 5′-phosphate.

Dicer can cleave hairpin RNA molecules in two ways: Natural pre-miRNAs with a typical 3′-overhang of two nucleotides are cleaved preferentially through hydrolysis of two phosphodiester bonds located 21–23 nucleotides from the helical end.[10] In the absence of the 3′-terminal overhang, however, the substrate is cleaved several nucleotides further away from the helical end. This results in the cleavage of a total of four phosphodiester bonds instead of only two. The respective one to three nucleotide terminal fragments are thus removed.[11] To allow the fluorophore and quencher to

[*] B. P. Davies, Prof. Dr. C. Arenz
Humboldt Universität zu Berlin
Institut für Chemie
Brook-Taylor-Strasse 2, 12489 Berlin (Germany)
Fax: (+49) 30-2093-6947
E-mail: christoph.arenz@chemie.hu-berlin.de

[**] This work was funded by the Fonds der Chemischen Industrie and by the Innovationsfond der Humboldt Universität zu Berlin.

Supporting information for this article is available on the WWW under http://www.angewandte.org or from the author.

InterScience
© 2006 Wiley-VCH Verlag GmbH & Co. KGaA, Weinheim

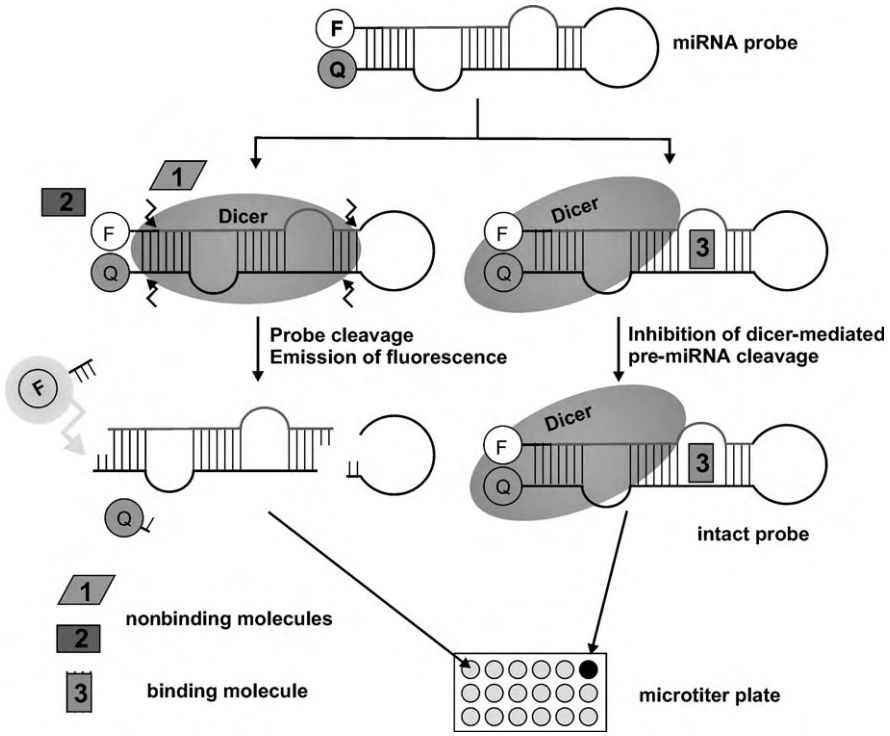


Figure 2. A homogenous assay for miRNA maturation. Left: the doubly labeled RNA beacon is hydrolyzed by Dicer leading to a fluorescence increase. Right: no fluorescence increase is seen in the presence of a pre-miRNA ligand.

dissociate more easily upon hydrolysis, our beacon contains no 3′-overhang as in natural pre-miRNAs. The ligation product showed no significant fluorescence in comparison to the fluorescein-labeled 5′-partial strand. Upon incubation of the beacon with recombinant Dicer, however, both a concentration- and time-dependent fluorescence increase of 3- to 10-fold were seen depending on reaction conditions (Figure 3). Furthermore, the control experiment containing heat denatured Dicer showed no fluorescence increase. After completion of the reaction, the RNA was precipitated and, when necessary, protein was removed by using a phenol extraction. Electrophoretic- and mass-spectrometric analyses of the pellet showed the presence of the expected ≈22 mer RNA.

To show the applicability of the reaction for high-throughput screening, all further experiments were carried out in commercially available 96-well microtiter plates. As the next step we wanted to see if cell lysate could be used as the enzyme source instead of the purified recombinant Dicer enzyme. This would have the advantage of performing the homogenous assay under more realistic conditions as Dicer interacts with other proteins such as transactivating response binding protein (TRBP) in its cellular surroundings. TRBP increases not only the Dicer-mediated RNA hydrolysis in vitro, but is essential for the correct cellular function of the miRNAs.[12] A possible unspecific hydrolysis by other RNAses was avoided by the addition of RNAse inhibitor to the reaction mixture. As expected, the addition of 10% HEK 293 cell lysate to our beacon led to a particularly fast increase in the fluorescence, which was otherwise unaffected by different concentrations of RNAse inhibitor. The addition of RNAse inhibitor did not affect the hydrolytic activity of the recombinant Dicer either. The selectivity of the RNAse inhibitor may be explained by the fact that Dicer belongs to the type III family of RNAses, which is distinct from the type I family of RNAses, like RNAse A. Previous heating of the cell lysate or the addition of erbium III chloride, an inhibitor of Dicer,[13] leads to retention of the fluorescence on the baseline.[14]

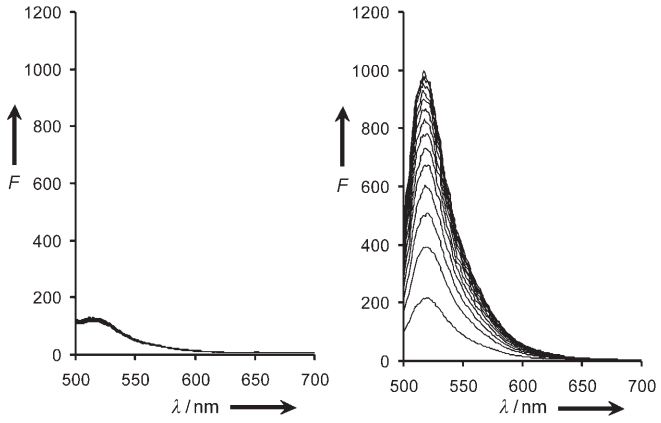


Figure 3. Incubation of the pre-miRNA beacon with heat denatured Dicer (left) and with native recombinant Dicer (right). The fluorescence was measured in 10 min increments.

To answer the question if our beacon is in principle suitable for identifying inhibitors of miRNA maturation, the reaction was also performed in the presence of various potential pre-miRNA ligands. The aminoglycoside antibiotic, kanamycin, binds preferentially to bacterial ribosomal 70S RNA.[15] At a concentration of 100 μM, kanamycin showed an approximate 40% reduction in the fluorescence increase when compared with the reference reaction. As Dicer inherently binds pre-miRNA, we synthesized three dodecapeptides derived from the amino acid sequence of Dicer as potential binders of pre-let-7 RNA (see the Supporting Information).[15] At a concentration of 100 μM, peptide S117 and S417 showed only moderate inhibition of 10–20% (see the Supporting Information). Peptide S186, however, showed an inhibition of approximately 85% at this concentration (Figure 4). When the same peptide was tested at 10 μM and 1 μM concentrations, an inhibition of the fluorescence increase of 30% and 10%, respectively, could be seen.[16] Interestingly, the observed inhibition for all ligands tested was less when the cell lysate was used as the Dicer source instead of the recombinant Dicer enzyme. This can be most likely

 © 2006 Wiley-VCH Verlag GmbH & Co. KGaA, Weinheim

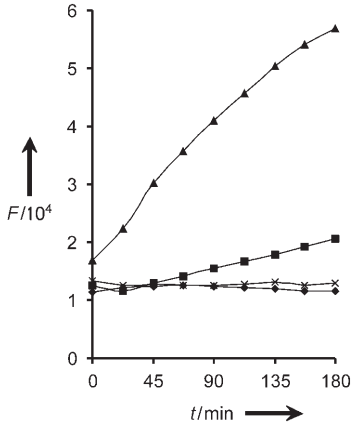


Figure 4. Fluorescence increase of the pre-let7 upon addition of recombinant dicer with (■) and without (▲) 100 μM peptide S186. An inhibition of pre-let-7 processing of approximately 85% is observed. Controls: 10 μM $ErCl_3$ (◆)and heat-inactivated dicer enzyme plus peptide S186 (×).

attributed to a reduction in the active concentration of the ligand because of unspecific binding to cellular nucleic acids.

Small, regulatory, RNA molecules represent potential target structures for future compounds. We present a concept with which the function of regulatory miRNAs can be manipulated by blocking their respective inactive precursors. With our doubly labeled pre-let-7 RNA beacon we have succeeded in establishing the first homogenous fluorescence assay for Dicer. This beacon is suitable for identifying potential inhibitors of miRNA maturation. According to our calculations, the cost of the RNA beacon can be estimated at just under five cents (Euro) per well in a 96-well plate (100-μL reaction volume). The cost would be reduced accordingly with the use of 384- or 1536-well plates. This would allow the screening of larger libraries of compounds. The search for pre-miRNA ligands able to block the miRNA maturation is still in the early stages. Future research has to answer, in particular, the question of selectivity of pre-miRNA ligands.

Experimental Section

Assay conditions: Option 1. 50 nM pre-miRNA beacon, 150 mM NaCl, 20 mM Tris-HCl (Tris = tris(hydroxymethyl)aminomethane; pH 7.4), 2.5 mM $MgCl_2$, 1 mM DTT, and 5–25 U mL^{-1} recombinant Dicer (Stratagene/Genlantis).

Option 2. As above, but with 10% HEK 293 cell lysate (corresponds to a protein concentration of 10–25 μg in the assay).

Received: April 4, 2006
Published online: July 21, 2006

Keywords: enzyme catalysis · fluorescence assay · gene expression · micro RNAs · RNA recognition

[1] K. Hinterding, D. Alonso-Diaz, H. Waldmann, *Angew. Chem.* **1998**, *110*, 716–780; *Angew. Chem. Int. Ed.* **1998**, *37*, 688–749.
[2] For current reviews, see: a) E. J. Sontheimer, R. W. Carthew, *Cell* **2005**, *122*, 9–12; b) C. M. Croce, G. A. Calin, *Cell* **2005**, *122*, 6–7.
[3] For recent examples, see: a) G. A. Calin et al., *N. Engl. J. Med.* **2005**, *353*, 1793–1801; b) P. M. Voorhoeve, C. le Sage, M. Schrier, A. J. Gillis, H. Stoop, R. Nagel, Y. P. Liu, J. van Duijse, J. Drost, A. Griekspoor, E. Zlotorynski, N. Yabuta, G. De Vita, H. Nojima, L. H. Looijenga, R. Agami, *Cell* **2006**, *124*, 1169–1181; c) N. Yanaihara, N. Caplen, E. Bowman, M. Seike, K. Kumamoto, M. Yi, R. M. Stephens, A. Okamoto, J. Yokota, T. Tanaka, G. A. Calin, C. G. Liu, C. M. Croce, C. C. Harris, *Cancer Cell* **2006**, *9*, 189–198.
[4] M. P. Czech, *N. Engl. J. Med.* **2006**, *354*, 1194–1195.
[5] For an overview, see: a) T. Hermann, E. Westhof, *Curr. Opin. Biotechnol.* **1998**, *9*, 66–73; b) Q. Vicens, E. Westhof, *ChemBioChem* **2003**, *4*, 1018–1023.
[6] T. Hermann, E. Westhof, *Comb. Chem. High Throughput Screening* **2000**, *3*, 219–234.
[7] a) W. Tan, X. Fang, J. Li, X. Liu, *Chem. Eur. J.* **2000**, *6*, 1107–1111; b) A. Jenne, W. Gmelin, N. Raffler, M. Famulok, *Angew. Chem.* **1999**, *111*, 1383–1386; *Angew. Chem. Int. Ed.* **1999**, *38*, 1300–1303.
[8] E. D. Matayoshi, G. T. Wang, G. A. Krafft, J. Erickson, *Science* **1990**, *247*, 954–958.
[9] G. Hutvagner, J. McLachlan, A. E. Pasquinelli, E. Balint, T. Tuschl, P. D. Zamore, *Science* **2001**, *293*, 834–838.
[10] H. Zhang, F. A. Kolb, L. Jaskiewicz, E. Westhof, W. Filipowicz, *Cell* **2004**, *118*, 57–68.
[11] A. Vermeulen, L. Behlen, A. Reynolds, A. Wolfson, W. S. Marshall, J. Karpilow, A. Khvorova, *RNA* **2005**, *11*, 674–682.
[12] A. D. Haase, L. Jaskiewicz, H. Zhang, S. Laine, R. Sack, A. Gatignol, W. Filipowicz, *EMBO Rep.* **2005**, *6*, 961–967.
[13] I. J. Macrae, K. Zhou, F. Li, A. Repic, A. N. Brooks, W. Z. Cande, P. D. Adams, J. A. Doudna, *Science* **2006**, *311*, 195–198.
[14] Incubation with dicer antibody (Ambion) did not lead to an inhibition of fluorescence increase, neither with the lysate nor with the purified recombinant enzyme.
[15] a) A. Okuyama, N. Tanaka, T. Komai, *J. Antibiot.* **1975**, *28*, 903–905; b) H. Wang, Y. Tor, *Angew. Chem.* **1998**, *110*, 117–120; *Angew. Chem. Int. Ed.* **1998**, *37*, 109–111.
[16] For the sequence of the peptides, see the Supporting Information.

 © 2006 Wiley-VCH Verlag GmbH & Co. KGaA, Weinheim